2005-01-01

Digital Image Processing

Jonathan Blackledge
Technological University Dublin, jonathan.blackledge@tudublin.ie

DIGITAL IMAGE PROCESSING

Mathematical and Computational Methods

"You British asses, who expect to hear ever some new thing, I have nothing to tell, but what I fear may be a true thing. For Tait[1] comes with his plummet and his line, quick to detect your old stuff, now dressed in what you call a fine popular lecture."

James Clerk Maxwell, 1868

"Talking of education, people have now a-days" (he said) "got a strange opinion that every thing should be taught by lectures. Now, I cannot see that lectures can do so much good as reading the books from which the lectures are taken. I know nothing that can be best taught by lectures, except where experiments are to be shown. You may teach chymestry by lectures - You might teach making of shoes by lectures!"

Samuel Johnson, 1766

DEDICATION

To all those students with whom I had the good fortune to work and, in using the material herein, taught me how to teach it

[1] An experimentalist and close colleague of Maxwell

ABOUT THE AUTHOR

Jonathan Blackledge graduated in physics from Imperial College and music from the Royal College of Music, London, in 1980 and obtained a Doctorate in theoretical physics from the same university in 1983. He was appointed as Research Fellow of Physics at Kings College, London from 1983 to 1988 specializing in inverse problems in electromagnetism and acoustics. During this period, he worked on a number of industrial research contracts undertaking theoretical and computational work on the applications of inverse scattering theory for the analysis of signals and images.

In 1988, he joined the Applied Mathematics and Computing Group at Cranfield University as Lecturer and later, as Senior Lecturer and Head of Group where he promoted postgraduate teaching and research in applied, engineering and industrial mathematics in areas which included computer aided engineering, digital signal processing and computer graphics. In 1994, he was appointed Professor of Applied Mathematics and Computing and Head of the Department of Mathematical Sciences at De Montfort University where he established the Institute of Simulation Sciences. He is currently Professor of Digital Signal Processing and Communications Technology in the Department of Electronics and Electrical Engineering at Loughborough University, England and Professor of Computer Science in the Department of Computer Science at the University of the Western Cape, South Africa. He is also a co-founder and Director of a group of companies specializing in communications technology and financial analysis based in London and New York.

Professor Blackledge has published over one hundred scientific and engineering research papers and technical reports for industry, six industrial software systems, fifteen patents, ten books and has been supervisor to sixty research (PhD) graduates. He lectures widely to a variety of audiences composed of mathematicians, computer scientists, engineers and technologists in areas that include cryptology, communications technology and the use of artificial intelligence in process engineering, financial analysis and risk management. His current research interests include computational geometry and computer graphics, image analysis, nonlinear dynamical systems modelling and computer network security, working in both an academic and commercial context. He holds Fellowships with England's leading scientific and engineering Institutes and Societies including the Institute of Physics, the Institute of Mathematics and its Applications, the Institution of Electrical Engineers, the Institution of Mechanical Engineers, the British Computer Society, the Royal Statistical Society and the Institue of Directors. He is a Chartered Physicist, Chartered Mathematician, Chartered Electrical Engineer, Chartered Mechanical Engineer, Chartered Statistician and a Chartered Information Technology Professional. He has an additional interest in music for which he holds a Fellowship of the Royal Schools of Music, London.

DIGITAL IMAGE PROCESSING
Mathematical and Computational Methods

JONATHAN M. BLACKLEDGE†

Professor of Digital Signal Processing and Communications Technology,
Department of Electronic and Electrical Engineering,
Loughborough University, England

Horwood Publishing
Chichester, West Sussex

---

†*Professor of Computer Science, Department of Computer Science,*
University of the Western Cape, Republic of South Africa.

HORWOOD PUBLISHING LIMITED
Coll House, Westergate, Chichester, West Sussex, PO20 3QL, England.
First published in 2005.

ISBN 1-898563-49-7
British Library Cataloguing in Publishing Data
A catalogue record of this book is available from the British Library.

Typeset in LaTeX, the TeXnicCenter graphical user interface and the stylefile of the Institute of Mathematics and its Applications.

Printed and bound in Great Britain by Antony Rowe Limited.

Foreword

Newspapers and the popular scientific press today publish many examples of highly impressive images. These images range, for example, from those showing regions of star birth in the distant Universe to the extent of the stratospheric ozone depletion over Antarctica in springtime, and to those regions of the human brain affected by Alzheimer's disease. Processed digitally to generate spectacular images, often in false colour, they all make an immediate and deep impact on the viewer's imagination and understanding.

Professor Jonathan Blackledge's erudite but very useful new treatise *Digital Image Processing: Mathematical and Computational Methods* explains both the underlying theory and the techniques used to produce such images in considerable detail. It also provides many valuable example problems - and their solutions - so that the reader can test his/her grasp of the physical, mathematical and numerical aspects of the particular topics and methods discussed. As such, this magnum opus complements the author's earlier work *Digital Signal Processing*. Both books are a wonderful resource for students who wish to make their careers in this fascinating and rapidly developing field which has an ever increasing number of areas of application.

The strengths of this large book lie in:

- excellent explanatory introduction to the subject;
- thorough treatment of the theoretical foundations, dealing with both electromagnetic and acoustic wave scattering and allied techniques;
- comprehensive discussion of all the basic principles, the mathematical transforms (e.g. the Fourier and Radon transforms), their interrelationships and, in particular, Born scattering theory and its application to imaging systems modelling;
- discussion in detail - including the assumptions and limitations - of optical imaging, seismic imaging, medical imaging (using ultrasound), X-ray computer aided tomography, tomography when the wavelength of the probing radiation is of the same order as the dimensions of the scatterer, Synthetic Aperture Radar (airborne or spaceborne), digital watermarking and holography;
- detail devoted to the methods of implementation of the analytical schemes in various case studies and also as numerical packages (especially in C/C++);
- coverage of deconvolution, de-blurring (or sharpening) an image, maximum entropy techniques, Bayesian estimators, techniques for enhancing the dynamic range of an image, methods of filtering images and techniques for noise reduction;
- discussion of thresholding, techniques for detecting edges in an image and for contrast stretching, stochastic scattering (random walk models) and models for characterizing an image statistically;

- investigation of fractal images, fractal dimension segmentation, image texture, the coding and storing of large quantities of data, and image compression such as JPEG;
- valuable summary of the important results obtained in each Chapter given at its end;
- suggestions for further reading at the end of each Chapter.

I warmly commend this text to all readers, and trust that they will find it to be invaluable.

Professor Michael J Rycroft
Visiting Professor at the International Space University, Strasbourg, France, and at Cranfield University, England.

In 2003 Jonathan Blackledge published *Digital Signal Processing*, a book based on material developed by him for the first semester of the MSc course in *Digital Systems Engineering* offered by the Department of Electronic and Electrical Engineering at Loughborough University. The content of the present text forms the basis of the second semester of that course, and it completes an authoritative and comprehensive account of the subject. The requisite mathematical and computational techniques are covered in satisfying detail, but the really significant feature is the way in which the fundamental physics underlying the generation of data is consistently and thoroughly explored. This is not simply a transcript of a course of lectures aiming to describe the methods used to process images but a painstaking study of the principles involved, together with a generous supply of wide-ranging examples and tutorial problems (all provided with detailed model answers). The aim, in the author's own words, has been to 'encourage the reader to design some example software solutions for digital image processing' and to 'develop a small digital image processing library that can be developed further and tailored to his/her learning and/or research interests'. That aim has been most satisfactorily achieved. Digital image processing is, of course, a most rapidly changing and developing field, but this book promises to remain a standard and essential guide to its fundamental ideas and techniques for a considerable time to come.

Professor Roy F Hoskins
Visiting Professor, Loughborough University, England

Preface

Digital Image Processing complements *Digital Signal Processing* (Horwood Publishing 2003) which was based on teaching material developed for the MSc programme in *Digital Systems Engineering* at Loughborough University. *Digital Image Processing* extends this material further by exploring the characteristics of imaging systems, the computational techniques used to process digital images and the interpretation of the information which an image conveys through an understanding of the physical processes that occur.

Many excellent image processing systems, software libraries and packages are currently available for low-level general applications whereas others have been designed for specific applications. Users can process images using either a command line language (e.g. the MATLAB[2] image processing toolbox) or a graphical user interface (e.g. Adobe Photoshop) to improve the general quality and fidelity of a digital image and/or to achieve results conveying specific aspects of its information content (feature extraction). This can be accomplished without the user having a thorough understanding of the computational methods involved or how and why such methods have evolved, e.g. the application of a particular filter. For those who are only interested in using a particular processing system to 'get the job done' working in a commercial environment for example, application of a specific commercial package or packages with an appropriate selection of image processing options is all that is required. However, for those who wish to contribute to the future development of such systems and/or develop their own 'home-spun' versions for research purposes, a deeper understanding of the mathematical and computational techniques is, by necessity, required.

This work provides a study of the computational methods that are used to process images, but in such a way that there is a direct link (where possible) between the process that is used, the data to which it is applied and, most of all, the 'physics' that underpins the generation of the data. In order to do this, it is necessary to spend some time discussing the principles of how waves and wavefields propagate and interact with objects whose images are required. Depending on the wavelength of the field, the interactions that occur are usually in the form of some scattered wavefield. Hence, after a review of the mathematical and computational background to the subject given in Part I (which includes material on vector fields, the 2D Fourier transform and the 2D FIR filter), we provide an introduction to the field equations and wave equations used to model different types of wavefields and the scattering theory needed to develop appropriate models for the images that these wavefields produce in terms of the information on the imaged object that they convey. We formulate some of the analytical methods and results that are required to compute a scattered wavefield and provide details on the equations that are used in later chapters. Some of this material is based on a previous work published by the author, namely, *Quantitative Coherent Imaging* (Academic Press, 1989), which was concerned with the principles of interpreting the structure and material properties of objects by the way in which they scatter electromagnetic and

[2]High-level technical computing language by MathWorks Inc.

acoustic radiation with the aim of exploring the theory, methods and some of the applications of incoherent and coherent imaging systems.

Having established the principal theoretical background to modelling an imaging system, we look at a range of imaging techniques which are classified into two main types, namely, incoherent and coherent imaging. In Part II, incoherent optical systems are studied and an introduction given to the method of projection tomography where it is assumed that the probe (i.e. the radiation field) used to interrogate an object can be described in terms of a sequence of rays traceable through the object and 'back-projected'. Part II includes a study of coherent imaging methods and investigates the principles of coherent optics, the imaging of layered media, diffraction tomography and synthetic aperture imaging. Both electromagnetic and acoustic imaging systems are discussed. In the case of diffraction tomography for example, the aim is to interpret the internal structure and composition of an object by the way in which it diffracts electromagnetic or acoustic radiation. Two types of diffraction tomography are discussed where the object is illuminated/insonified with a wavefield oscillating at a fixed frequency (Continuous Wave or CW case) or with a short pulse of radiation. In the material on synthetic aperture imaging, attention is focused on the use of Radar for imaging the surface of the Earth and a model presented to describe the scattering of a pulse of frequency modulated microwave radiation by the ground. This material also includes a case study which develops a solution to the so called 'sea spikes' problem.

In the 'light' of the preceding material, Part III introduces the basis of digital image processing including the problem of image restoration, image reconstruction and image enhancement. The methods discussed are all related in one form or another to the physical principles presented in Parts I and II and forms the basis for Part IV of this work which studies the principles of pattern recognition and computer vision. This includes an introduction to statistical modelling and analysis, an extended chapter on fractal images and fractal image processing, and a chapter on data coding and image compression, including fractal image compression.

The author has attempted to provide the reader with the mathematical methods required for image analysis which are then used to develop models and algorithms for processing digital images and, finally, to encourage the reader to design some example software solutions for Digital Image Processing (DIP). In this way, the reader is invited to develop a small DIP library that can then be developed further and tailored to his/her learning and/or research interests. This is accomplished by the inclusion of a series of tutorial problems which are given at the end of each Part with model answers provided in Appendix A. These problems include theoretical, computational and programming exercises in the C programming language.

The emphasis throughout is on the mathematical foundations of the subject which are common to a variety of imaging systems and methods. In some cases, examples have been provided to illustrate the conversion of a computational algorithm into a computer program. Either pseudo code, C or MATLAB code is used for this purpose. The book has been designed to serve the reader with enough formal detail for him/her to acquire a firm foundation on which to

build. References to other important texts and/or key scientific papers are included at the end of each chapter or within the text for this purpose.

The material presented in this book is based on the lecture notes and supplementary material developed by the author as part of an advanced taught MSc programme in 'Digital Signal Processing'. This programme was originally established at Cranfield University in 1990 and modified at De Montfort University in 1994. The programmes are still operating at these universities and the material has been used by more than 500 graduates since its creation and development in the early 1990s. The material was enhanced and developed further when the author moved to the Department of Electronic and Electrical Engineering at Loughborough University in 2003, and now forms part of the department's post-graduate teaching and learning activities. The original MSc programme was based on taught components covering a period of eight months and consisting of two semesters, each semester, being composed of four modules; the third semester focused on a minor research project. The material in this work covers the second semester and is 'index-linked' through this teaching programme to the publication *Digital Signal Processing* (Horwood, 2003) which covers the first semester. The classification of this work into four parts reflects the four modules given in the second semester. It has been necessary to include some of the material published previously with the view of revising some of the principal themes such as those concerned with the properties and computational methods associated with the Fourier transform. This has been done for reasons of completeness and to provide the reader with an account of the field that does not necessarily require significant reference to previous publications (by the author or otherwise).

An attempt has been made to cut through much of the jargon characterizing different fields of research in imaging science presenting an account of the fundamental physical principles common to nearly all imaging systems. This is done by illustrating the similarity of the underlying mathematical models used to process data on a wavefield in a variety of applications. The approach has been to unify the principles of different imaging systems and to provide a course text covering the theoretical foundations of imaging science in an integrated and complete form.

Finally, while every effort has been made by the author and publisher to provide a work that is free from error, it is inevitable that in a first edition, typing errors or 'typos' and 'bugs' will occur. If the reader starts to suffer from a lack of comprehension over certain aspects of the material (due to errors or otherwise) then he/she should not assume that there is something wrong with him/herself as the fault may lie with the author and his imaging system!

Professor Jonathan M Blackledge
Department of Electronic and Electrical Engineering, Loughborough University.

Acknowledgements

The material presented has been used by numerous postgraduate students studying for their MSc and PhD degrees under the supervision of the author who would like to acknowledge their valuable and challenging critical appraisal of the work over many years. This book has been written for future students but with the help and guidance of past students in mind and it is to them that this work is dedicated. The author would like to acknowledge the support of Loughborough University (Department of Electronic and Electrical Engineering) and, in particular, Prof Peter Smith (Head of Department) and Dr S Datta (Head of the Applied Signal Processing Group) for their help and guidance.

Much of the material was originally conceived at Cranfield University in the early 1990s in the Applied Mathematics and Computing Group for the advanced MSc programme, *Software Solutions for Digital Signal and Image Processing*, first established by the author in 1990. The principal course text at that time was *Quantitative Coherent Image* (Academic Press, 1989) written by the author. In turn, this book was based on the author's research undertaken during the time he spent as a Research Fellow at King's College, London University. The author would like to thank all those colleagues with whom he collaborated at King's College and Cranfield University, in particular, Prof R Burge, Prof M Pratt, Dr P Sherar and in particlar, Prof R Hoskins, for editing the manuscipt. The material was developed further while the author was based at De Montfort University for the advanced MSc programmes provided by the Imaging Research Centre, for the industrial short course programme and for the induction programmes given as part of the Institute of Mathematics and its Applications conference series in Image Processing held at De Montfort University in 1998 and 2001. The author would like to thank the following for their collaboration and support: Dr M Turner, Dr A Evans, Dr P Andrews, Prof N Phillips, Prof H Bjelkhagen and in paticular, Prof M Rycroft, for his help and advice.

Some of the material and case studies given are based on work undertaken by the author's research students including the following: Dr A Aburas, Dr A Ahmed, Dr S De Souza, Dr D Doubovitski, Dr M Fayed, Dr E Fowler, Dr K Mahmoud, Dr K Mazharov, Dr S Mikhailov, Dr A Onsalou, Dr N Ptitsyn, Dr S Purahoo, Dr D Sapounas, Dr H Tassignon, Dr D Topiwala and Dr W Zorski. The funding for some of the research projects undertaken by the author and his research students was secured through overseas initiatives pioneered by Prof Brian Foxon to whom he (and the students) are very grateful. Finally, the author would like to thank all those organizations and industries that have provided funding for the development of his teaching and research activities over the years including the Engineering and Physical Sciences Research Council, the Defense Evaluation and Research Agency (Royal Signals and Radar Establishment), the UK Ministry of Defence, the International Science and Technology Council, British Coal (Geophysics Unit), British Gas, British Petroleum, British Aerospace, Oxford Instruments, Microsharp, Marconi, Microsoft, the Chimera Partnership and British Intelligence.

Notation

Alphabetical

$A(\mathbf{k})$	Amplitude spectrum
$\mathbf{A}$	Magnetic vector potential
$\mathbf{b}$	Microscopic magnetic field
$\mathbf{B}$	Magnetic field density
c	Wavespeed
c_0	Wavespeed of free space (e.g. speed of light)
c_{nm}	Complex coefficients (e.g. complex 2D Fourier series)
c_L	longitudinal (compression) wave speed
c_R	Rotational (shear) wave speed
D	Fractal dimension, scale size of an object or Diffusivity
$\mathbf{D}$	Electric displacement
1D	One-Dimensional
2D	Two-Dimensional
3D	Three-Dimensional
$\mathbf{e}$	Microscopic electric field
$\mathbf{E}$	Macroscopic electric field
$f(\mathbf{r})$	Arbitrary real (or complex) function (typically the object function or system input)
$\mid f(\mathbf{r}) \mid$	modulus of complex variable or function f
$\|f(\mathbf{r})\|$	Norm (e.g. a Euclidean L_2-norm) of a continuous function f
f_{ij}	2D discrete function (in real space)
$\|f_{ij}\|$	Norm (e.g. a Euclidean ℓ_2-norm) of a discrete function (e.g. 2D array or matrix) f_{ij}
$F(\mathbf{k})$	Complex spectrum of function $f(\mathbf{r})$
F_r	Real component of spectrum
F_i	Imaginary component of spectrum
F_{ij}	Discrete complex spectrum of discrete function f_{ij}
$g(\mathbf{r} \mid \mathbf{r}_0, k)$	Time independent Green function
$G(\mathbf{r} \mid \mathbf{r}_0, t \mid t_0)$	Time dependent Green function
G	Gradient function
$\mathrm{Im}[f]$	Imaginary part of complex variable or function f
H	Hurst exponent
$\mathbf{H}$	Macroscopic magnetic field
$\mathcal{H}$	Hausdorff space
$\mathbf{I}$	Unit dyad
$\mathbf{j}$	Charge density
k	Wavenumber ($= 2\pi/\lambda$)
k_x	Spacial frequency in the x-direction
k_y	Spacial frequency in the y-direction
$\mathbf{k}$	Wave vector $= \hat{\mathbf{x}}k_x + \hat{\mathbf{y}}k_y$
$n(\mathbf{r})$	Noise function
n_{ij}	Discrete noise function

$\hat{\mathbf{n}}$	Unit vector
N_{ij}	Noise spectrum
$O(x, y)$	Object function
$\widetilde{O}$	Fourier transform of object function
$p(\mathbf{r})$	Instrument function, or Point Spread Function
$p(\mathbf{r}, t)$	Acoustic pressure field
p_{ij}	Discrete Point Spread Function
$P(\mathbf{k})$	Optical Transfer Function [Fourier transform of $p(\mathbf{r})$]
P_{ij}	Discrete Optical Transfer Function (DFT of p_{ij})
$P(x)$	Probability density function (also denoted by $\Pr[x(t)]$)
$P(a \mid b)$	Conditional probability of obtaining a given b
$P(z, \theta)$	Projection function
$P(\mathbf{k})$	Power spectrum ($=\mid F(\mathbf{k}) \mid^2$)
P_s	Scattered pressure wavefield,
$\widetilde{P}_s$	Fourier transform of scattered pressure wavefield
$\widetilde{P}$	Fourier transform of projection function, or characteristic function
$\Pr[x(t)]$	Probability occurrence of x in $x(t)$
q	Fourier dimension
$\mathrm{Re}[f]$	Real part of complex variable or function f
$\mathbf{r}$	General position vector in a 2D or 3D space (depending on the context)
$d^2\mathbf{r}$	Surface element $dxdy$
$d^3\mathbf{r}$	Volume element $dxdydz$
$s(\mathbf{r})$	Real or complex (analytic) image
$\mathrm{s}(\mathbf{r}, t)$	Displacement vector
s_{ij}	Discrete real or complex image
S	Surface
$\mathrm{sinc}(x)$	Sinc function ($= \sin(x)/x$)
t	Time
$\mathbf{T}(\mathbf{r}, t)$	Material stress tensor
$u(\mathbf{r}, t)$	Solution to a partial differential equation (e.g. a wavefield)
u_i	Incident wavefield
$\mathbf{v}$	Velocity field
v_{ij}	Value of a pixel at ij
V	Volume
$\mathbf{V}$	Fourier transform of velocity field
x, y	General independent variables
z	Complex number of the form $a + ib$ or spatial variable
z^*	Complex conjugate $a - ib$ of a complex number $a + ib$
z_0	Free space wave impedance
Z	Impedance
$\in$	In (e.g. $x \in [a, b)$ is equivalent to $a \leq x < b$)
$\forall$	Forall (e.g. $f(t) = 0, \quad \forall t \in (a, b]$)

Greek

α	Chirping parameter, or first Lamé parameter
β	Second Lamé parameter, or angle, or spectral exponent
γ	General scattering function
γ_a	Scattering function due to parameter a
$\Gamma(q)$	Gamma function $= \int_0^\infty x^{q-1}e^{-x}dx$
δ^n	n-dimensional Dirac delta function
δ_{ij}	Kronecker delta
ϵ	Permittivity
ϵ_0	Permittivity of free space
κ	Compressibility
κ_0	Ambient (homogeneous) compressibility
ζ	Bulk viscosity
η	Shear viscosity
θ	Phase, angle
$\theta(G)$	Angle of gradient
λ	Wavelength, or Lagrange multiplier
σ	Conductivity, or standard deviation of a stochastic function
μ	Permeability
μ_0	Permeability of free space
ϕ	Longitudinal velocity potential
Φ	Acoustic dilatation
ρ	Charge density, or material density
ρ_0	Ambient (homogeneous) material density
σ^2	Variance
ω	Angular frequency

Operators

$\hat{D}$	Homogeneous linear differential operator
$\hat{B}$	Back-projection
$\det \begin{pmatrix} a & b \\ c & d \end{pmatrix}$	Determinant of $A = ab - dc$
$\hat{F}_1$	One dimensional Fourier transform
$\hat{F}_1^{-1}$	One dimensional inverse Fourier transform
$\hat{F}_2$	Two dimensional Fourier transform
$\hat{F}_2^{-1}$	Two dimensional inverse Fourier transform
$\hat{H}$	Hilbert transform
$\hat{L}$	Inhomogeneous linear differential operator
$\hat{R}$	Radon transform
$\hat{R}^{-1}$	Inverse Radon transform
$\otimes$	1D or 3D convolution operation - continuous or discrete, causal or otherwise (depending on the context specified)
$\otimes\otimes$	2D convolution operation - continuous or discrete, causal or otherwise (depending on the context specified)
$\odot$	1D correlation operation - continuous or discrete, causal or otherwise (depending on the context specified)
$\odot\odot$	2D correlation operation - continuous or discrete, causal or otherwise (depending on the context specified)
$\Longleftrightarrow$	Transformation into Fourier space
$\longleftrightarrow$	Transformation into some transform space (as defined)
$\vee$, $\wedge$	Logical AND and OR set operators
$\oplus$, $\ominus$	Morphological erosion and dilation operators
$\circ$, $\bullet$	Morphological opening and closing operator
$\triangleright\, \triangleleft$, $\triangleleft\, \triangleright$	Morphological thinning and thickening operators
$\langle \cdot \rangle$	Expected or mean value for $\cdot$
$\begin{pmatrix} n \\ k \end{pmatrix}$	Binomial coefficient $\frac{n!}{k!(n-k)!}$
∇^2	Laplacian operator

Glossary

Mathematical and Statistical

AC	Arithmetic Coder
ACF	Autocorrelation Function
AM	Amplitude Modulations (the amplitude envelope)
BHPF	Butterworth High Pass Filter
BLPF	Butterworth Low Pass Filter
BL	Band Limited
CDP	Common Depth Point
COTF	Coherent Optical Transfer Function
DC	Direct Current - Zero Frequency Component
DCT	Discrete Cosine Transform
DFT	Discrete Fourier Transform
FT	Fourier Transform
FFT	Fast Fourier Transform
FM	Frequency Modulation
FIR	Finite Impulse Response
HPF	High Pass Filter
IDFT	Inverse Discrete Fourier Transform
IFS	Iterated Function System
IRF	Impulse Response Function
IOTF	Incoherent Optical Transfer Function
IPSF	Intensity Point Spread Function
LPF	Low Pass Filter
MAP	Maximum *a Posteriori*
MEM	Maximum Entropy Method
ML	Maximum Likelihood
MTF	Modulation Transfer Function
OTF	Optical Transfer Function
PCTF	Phase Coherent Transfer Function
PDE	Partial Differential Equation
PDF	Probability Distribution or Density Function
PIFS	Partitioned Iterated Function System
PSE	Power Spectrum Equalization
PSF	Point Spread Function
PSDF	Power Spectral Distribution or Density Function
PSNR	Peak Signal-to-Noise ratio
PTF	Phase Transfer Function
RSF	Random Scaling Fractal
SNR	Signal-to-Noise Ratio
TF	Transfer Function

Computer Science

B-Scan	Brightness-mode Scan
CASE	Computer Aided Software Engineering
CD	Compact Disc
CPU	Central Processing Unit
DSP	Digital Signal Processing
DIP	Digital Image Processing
GUI	Graphical User Interface
I/O	Input/Output
IT	Information Technology
PCNG	Pseudo Chaotic Number Generator
PRNG	Pseudo Random Number Generator
RAM	Random Access Memory

Organizational and Standards

ART	Arithmetic Reconstruction Tomography
CT	Computed Tomography
CAT	Computer Aided Tomography
CW	Continuous Wave
DSR	Dynamic Spatial Reconstruction
ECT	Emission Computed Tomography
EM	Electromagnetic
ERS-1	Earth Resources Satellite (of the European Space Agency)
HH	Horizontal-Horizontal polarization field
HV	Horizontal-Vertical polarization field
JPEG	Joint Photographic Expert Group
LZ77, LZ78	Lempel and Ziv Substitution Coders
MPEG	Motion Picture Experts Group
MR	Magnetic Resonance
MATLAB	Highlevel technical computing language by MathWorks Inc.
PIN	Personal Identity Number
Radar	Radio Detection and Ranging
RAR	Real Aperture Radar
RCS	Radar Cross Section
SAR	Synthetic Aperture Radar
SAS	Synthetic Aperture Sonar
UCT	Ultrasonic Computer Tomography
VV	Vertical-Vertical polarization field
VH	Vertical-Horizontal polarization field

Contents

Introduction

Of the five senses that human beings and most other animals have, the visual system, is arguably the most important and dominant. Compared with the local areas of the brain used to process signals from our sensors for smell, taste, hearing and touch, the area required for processing the input from our eyes is larger by some 30% and is located toward the back of the brain. Thus, the development in our understanding of the world is, in one respect, determined by the evolution of our ability to generate images of that world. It is the visual system which, coupled with appropriate training, provides us with the concept of dimension. Our three-dimensional perception of the world gives the optimal interpretation required for the survival of our species and other animals. In other words, we learn most through sight - 'a picture paints a thousand words (ten thousand if you like)'. This three-dimensional interpretation comes from a sensor that only provides two-dimensional information, albeit in stereo.

The images that we acquire and train our brain to interpret are resolution limited; there is a limit to the spatial resolution of the information that our eyes provide. This is determined by the size of the aperture through which the image is formed and the wavelength of the electromanetic radiation field (light) that generates the input. In general, the resolution R of an image is given by

$$R \sim \frac{D}{\lambda}$$

where D is the diameter of the aperture and λ is the wavelength of the wavefield. The information we acquire (in terms of the resolution available) through our own imaging system is determined by the size of our eyes (the pupil) and the wavelength of light. Thus, our imaging sensors are limited by the frequency band of the electromagnetic radiation that they can detect, i.e. the visual spectrum. It is interesting to ask why our visual system should be based on such a limited portion of the available electromagnetic spectrum (from blue light through green to red light) with wavelengths λ of the order of 10^{-7}m which is such a tiny percentage of that spectrum (from gamma rays $\lambda \sim 10^{-12}$m through to radio waves $\lambda \sim 10^{3}$m) One answer may be based on an interesting relationship between the visual spectrum and the temperature of the surface of the Sun. As with all stars and most radiating bodies, energy is radiated at different frequencies or wavelengths and by varying amounts. An important model for describing a wavelength dependent energy spectrum was first derived by Max Planck in the early part of the twentieth century. Planck's radiation

law gives a spectrum with a well defined maximum corresponding to a specific wavelength. This law, expressed in terms of energy per unit range of wavelength E_λ, is given by

$$E_\lambda = \frac{8\pi ch}{\lambda^5[\exp(ch/\lambda kT) - 1]}$$

where c is the speed of light, h is Planck's constant, k is the Boltzmann constant and T is temperature in ^oK. Now, the wavelength λ_m at which E_λ is a maximum occurs when

$$\frac{\partial E_\lambda}{\partial \lambda} = 0$$

or when

$$\left(1 - \frac{x}{5}\right) e^x = 1, \quad \text{where} \quad x = \frac{ch}{\lambda kT}$$

whose solution is

$$\frac{ch}{\lambda_m kT} = 4.9651$$

which is trivial to compute numerically using the iteration $x_{n+1} = 5[1 - \exp(-x_n)]$ with $x_0 > 0$. Taking the surface temperature T of the Sun to be approximately 6000^oK, the above result yields a value for λ_m of approximately 4.7×10^{-7} metres[1] which is in the green region of the visible spectrum, i.e. in the middle of the visible spectrum where the eye is most sensitive. Is this relationship purely coincidental or could it be a product of evolution? In other words, is the fact that we 'see' in the visible spectrum due to the chance that we have evolved on a planet that is orbiting a yellow Sun which radiates more energy at the wavelength of green light than any other wavelength?

It is interesting to consider what a species such as ourselves would image, had we evolved on a suitable planet orbiting a hotter or cooler sun. In the latter case, and based on the discussion above, such a species might interpret the world through images based on the emission of infrared radiation. If so, then their image interpretation would be radically different from our own. Common objects that we take for granted would not necessarily be based on features with well-defined edges, because infrared radiation scatters from larger scale objects than light waves. Moreover, the emission of infrared radiation from such objects tends to saturate the image, i.e. the emission of infrared red radiation from a body tends to dominate the scattering of this radiation by the body, the process of thermal diffusion being more significant than infrared diffraction. Now, edge recognition is particularly important in the human visual system. This aspect of our image understanding is one of the reasons why early mathematical developments 'focused' on geometry in which lines, curves and circles were contemplated - hypothetical 'elements' which have evolved from imaging objects through the scattering of waves in the visible spectrum. It is thus interesting to ponder whether the value of π would exist to a species that had evolved the same degree of intelligence as ourselves but with an imaging system based on the detection of infrared radiation due to their sun being cooler than our own. It is similar to asking the question: If the frequency spectrum

[1]Using the values: $c = 3 \times 10^8$ metres/sec, $h = 6.62 \times 10^{-34}$ joule sec and $k = 1.38 \times 10^{-23}$ joules/degree.

at which we hear, was shifted by 50% above or below middle C, would the instruments of the orchestra exist along with the techniques that have been developed to play them? Such arguments are central to the reasoning of the great eighteenth century Prussian philosopher, Immanual Kant, who was one the first to propose that human understanding, learning and development is limited by the bandwidth of our senses. Since the time of Kant, developments in science and technology have provided images using a wide range of frequencies, based on observations through detectors that transform the data back into the visible spectrum, which is not the same as actually 'seeing' in a different spectrum.

Imaging Science

In recent years, there has been a rapid advance in the science and technology of information processing and analysis. Most of the early research and development was stimulated by the need for military intelligence, the 'space race' and the cold war. It is now important in all physical and biological sciences. Many important developments have occurred in information science since the 1940s, due to a dramatic increase in the speed, power and availability of digital computers which carry out high speed calculations on incoming data samples. One area of information technology which has consequently grown rapidly is imaging science. This area has become increasingly important because of the growing demand to obtain information about the structure, composition and characteristics of different materials. The use of imaging science for medicine, remote sensing, astronomy and space exploration, to name but a few, is now common place.

Many imaging techniques have been developed using different types of radiation over a wide range of frequencies. In each case, the underlying principle that is used to construct, model and analyse an image is similar and in many cases requires solutions to the so called 'inverse problem'. In simple terms, and in the context of imaging science, the inverse problem is concerned with evaluating the structure of an object by observing how it modifies certain properties of a probe, i.e. the field of radiation used to interrogate an object. This usually involves finding a method of inverting certain integral equations. The exact form of integral equation depends upon the details of the model used to describe the interaction between the probe and the object. This book is concerned with the variety of mathematical models and reconstruction methods which are used to provide detailed quantitative information about the structure and material properties of an object by the way in which it scatters radiation. Some examples of the imaging systems to which this material applies are as follows: Remote sensing (optical, infrared, microwave); Astronomy (optical, X-ray, radio, ultraviolet); Radiology (X-ray radiography, X-ray tomography, emission tomography, ultrasonic imaging, nuclear medicine, magnetic resonance imaging); Microscopy (optical, electron, scanning transmission mode); Civilian and military reconnaissance (real aperture radar, synthetic aperture radar, high resolution optical and infrared imaging); Non-destructive testing (ultrasonic imaging, mm microwave imaging, teraHertz imaging, X-ray

imaging); Seismic prospecting (seismic reflection imaging, seismic tomography, vibro-seismic imaging); Industrial tomography (acoustic tomography, capacitance tomography, nuclear tomographic imaging); Computer vision (pattern recognition, automatic inspection, computer integrated manufacturing, biometrics, digital watermarking). In addition to the above, many other applications exist which involve the construction, processing and analysis of one-, two- and three-dimensional signals.

Signals and Images

A large proportion of information comes in the form of electrical waveforms or signals. Information can also be encoded in two-dimensional signals or images, certain processes being required to provide useful information. The subject which is concerned with the theory and applications of these processes for the analysis and interpretation of signals and images is signal and image processing. The only basic difference between signal processing and image processing is the dimension. There are other more subtle differences which stem from the nature of the mathematical techniques used in each case. Nevertheless, many of the equations and transforms used to process signals can be applied directly to images: single integrals become double integrals and single sums become double sums for example, making the mathematics appear more complicated although conveying the same basic principles and ideas.

Electrical waveforms are usually analogue signals, and methods of processing them were once performed and, to a lesser extent, still are performed using analogue computers. Another way of processing and analysing signals can be obtained by converting them into a set of numbers or digits. This is known as digital conversion and signals of this type are called digital signals. Each number of a digital signal is a sample of the original analogue signal providing it has been sampled adequately. Digital conversion can also be carried out on images. This method provides a two-dimensional array of numbers or a digital image, in which the individual samples or picture elements are referred to as pixels. Digital signals can be stored easily (on a CD, memory chip and so on) and can be processed numerically using a digital computer. This has led to a close association between digital image processing and many other fields of interest including computer graphics, machine vision, optics, non-destructive evaluation, robotics, artificial intelligence and computer science. The issue of simulating the human visual system on a digital computer and emulating its capability for decision-making based on feature extraction and pattern recognition is major problem and is likely to remain so for some time.

Many techniques developed for processing and interpreting signals with applications ranging from telecommunications to the analysis of economic time series are adopted for image processing. We can think of an image as being a two-dimensional signal, and digital image processing in terms of two-dimensional signal processing. Some images are built up from sets of signals and, in some applications, image processing amounts to processing each signal before it is used to construct the final image. Hence, signal processing can be considered to be an essential pre-processing stage. Some special cases also arise

where the image is separable and can be processed digitally by operating on each column and each row separately.

Image Formation

There are two principal types of images that are formed from the radiation used to image an object, namely electromagnetic (EM) images and acoustic images. Some imaging methodologies make use of such physical properties of a material as its capacitance, inductance and resistance. When mechanical radiation is used to image an object that is to a good approximation, incompressible, the image that is obtained is based on the characteristics of so called elastic wavefields. In order to study the way images are formed and interpret their properties, the physics of EM and acoustic waves and their interaction with matter must be understood.

Most imaging systems can be divided into two distinct classes: incoherent imaging and coherent imaging. Coherent images are usually of two types, either fully or partially coherent. The basic difference between incoherent and coherent images is determined by a single parameter called the phase. Coherent imaging is based on recording spatial and/or temporal variations in both the amplitude and phase of a scattered wavefield as a function of time or space (partially coherent) or of both time and space (fully coherent). Incoherent imaging is based on recording fluctuations in just the intensity of the scattered field which may be an intensity value based on short time integration. Coherent imaging systems utilize relatively low frequency radiation (i.e. frequencies in the range of 10-10^{10} Hz). At these frequencies it is technically possible to record the time-history of the scattered field. Examples include seismic imaging ($1 - 10^2$Hz), sonar and radio imaging ($10^3 - 10^4$Hz), ultrasonic imaging ($\sim 10^6$Hz) and microwave imaging ($10^9 - 10^{10}$Hz). Many time-resolved coherent or partially coherent images are formed using a 'pulse-echo' type experiment. Typically, a pulse of EM or acoustic radiation is emitted and interacts with an object at a distance. The interaction sets up a 'back-scattered' field whose time history is recorded - a signal providing time resolved amplitude and phase information. Modelling this back-scattered field is important in the physical interpretation of an image, i.e. image understanding.

Coherent images are also generated from Continuous Wave (CW) fields with a narrow-band spectrum (e.g. laser optics) when the phase shift rather than the phase itself associated with the emission/transmission/reflection of the radiation can be detected, i.e. constructive and destructive interference patterns.

Incoherent images are time-averaged intensity distributions of very high frequency wavefields such as light ($\sim 10^{14}$ Hz), X-rays ($\sim 10^{18}$ Hz) and γ-rays ($\sim 10^{20}$ Hz). They are formed by recording the intensity of a CW or pulsed field over a given interval of time. The amplitude and phase variations of the wavefield as a function of time are not recorded: the phase variations or phase shift is not recorded either. In this case, the frequency of the radiation is too high for the time variations of the wavefield to be measured. The photograph is a well known example of an incoherent image.

If a wavefield is denoted by $u(x, y, z, t)$ which is taken to have both amplitude $A(x, y, z, t)$ and phase $\theta(x, y, z, t)$ information say, then u can be written in the form

$$u = A \exp(i\theta).$$

With this simple wavefield model in mind, an incoherent (time integrated) image $I_{\text{incoherent}}$ taken at a point in space z_0 say, is given by

$$I_{\text{incoherent}}(x, y) = \int_0^T \mid u(x, y, z_0, t) \mid^2 dt$$

where T is the exposure time. Here, information on the phase function is lost. Partially coherent (time resolved) image data D recorded at (z_0, y_0) say is given by

$$D_{\text{coherent}}(x, t) = \text{Re}[u(x, y_0, z_0, t)] = A(x, y_0, z_0, t) \cos\theta(x, y_0, z_0, t)$$

where both the amplitude and phase contribute to the recording (as a function of time). Here, signals are recorded at different positions and then 'staked' together to construct the image.

Coherent and incoherent imaging systems record and process information related to the spectral characteristics of an object. It is important to realize that the characteristic spectrum of an imaged object is not necessarily that of the object itself but rather the result of a physical interaction between the incident wavefield and the object. Many images provide information on the structure of an object according to the way in which it scatters radiation. They do not necessarily provide information about the properties of the material from which the object is composed. Different properties of a material can scatter certain types of radiation in a variety of ways. By using this effect to provide information on the material properties as well as the structure of an object, a quantitative interpretation of the object is obtained. This is known as quantitative imaging and attempts to provide a physical interpretation of the imaged object to be formulated.

Image Information

Besides varying in space or time (or both), image data may contain random or unpredictable features known as noise. Such an image will generally contain information that can be extracted by processing the data in an appropriate way. The meaning of 'information' in a signal or image can vary considerably from one application to the next and needs to be defined carefully in the context of an application via some suitable mathematical or computational model. In practice, the extraction of information usually requires some degree of user input which affects the performance of the algorithm being executed, from selecting the parameters of a filter to training an Artificial Neural Network for example. Methods of automation are often desirable but not always possible.

To extract useful information from a signal or image a mathematical model for the data must be established. There is one overall governing equation that

is used extensively for this purpose. This equation is given by

$$data \;=\; (instrument\ function)\ convolved\ (information) \;+\; noise$$

The *instrument function* describes the way in which an imaging instrument responds to an input. It has a variety of names which depend on the context in which the above equation is used. In signal analysis the instrument function describes the way in which information is spread about an impulse or spike. In this case the instrument function is usually referred to as the impulse response function. In image analysis it describes how information is spread about a point and is therefore known as the point spread function or PSF. *Convolution* is a mathematical operation that can be thought of as smearing, smoothing or blurring the information which is determined by the characteristics of the *instrument function*. It is therefore sometimes referred to as a 'smoothing' or 'blurring function'. In addition to this effect, data can be perturbed by a whole range of external and unwanted disturbances which gives rise to the *noise* term. The introduction of the imaging equation at this point has been done to introduce the reader to one of the more important underlying models of imaging science. We shall provide extensive detail on the 'origins of the imaging equation' for different imaging systems and establish relationships between the term *information* and the physical parameters that control the behaviour of electromagnetic and acoustic wavefields.

There are two basic problems fundamental to imaging science in general which, in light of the equation above, can be summarized as follows:

(i) Given the *data* together with an estimate of the *instrument function* and a valid statistical model for the *noise*, recover the *information*.

(ii) By employing suitable physical models, interpret the *information* that is recovered.

Problems (i) and (ii) above are the basis for a variety of applications. Examples include the analysis and interpretation of speech signals, imaging the surface of the Earth with Radar, active and passive sonar, investigating the internal structure and composition of the earth using seismic waves and using ultrasound to determine the pathological state of human tissues. In each case, the act of recording the relevant data involves setting up an experiment with a given *instrument function* and certain *noise* statistics. In both cases, the problem is to recover and interpret the information in the *data*.

The information in the data generated by a scatter imaging system is related to the way in which the radiation is scattered by the imaged object. To interpret this information, we must establish a mathematical model for the scattering mechanism that takes place. The behaviour of the scattered field is compounded in a characteristic function which depends on the type and material properties of the object. This function is known generally as the *object function* and our fundamental imaging equation can be written in the form

$$data \;=\; (point\ spread\ function)\ convolved\ (object\ function) \;+\; noise$$

This equation is known as the imaging equation. It is based on a mathematical description for a the wavefield that is the result of single or weak scattering

alone in which multiple scattering is (assumed to be) negligible. This basis for the imaging equation is explored in Part II. The exact form of the *point spread function* depends upon the type and properties of the imaging system whereas the form of the *object function* depends upon the type of physical interaction that takes place. In this book, emphasis is placed on finding a mathematical expression for the *object function* in terms of a more fundamental set of material parameters. Two principal cases are considered:

1. Electromagnetic imaging, where the probe is an electromagnetic wavefield and the material parameters are the permittivity, permeability and conductivity.

2. Acoustic imaging, where the probe is an acoustic wavefield and the material parameters are the density, compressibility and the viscosity.

In both cases, the basic problem is the same and involves:

(i) designing an algorithm to compute the object function given appropriate data on the scattered field, knowledge of the point spread function and noise statistics;

(ii) finding a way to recover the appropriate set of material parameters from the object function.

Both (i) and (ii) above are inverse problems. The recovery of the object function from the data is an inverse problem which is known generally as deconvolution. In one way or another, deconvolution (together with convolution and correlation) are common to all imaging systems. It is the basis for the large majority of the reconstruction methods that are presented in this book and is discussed at length in Part III.

Image Analysis

The analysis of an image can be classified into four principal categories: (i) resolution; (ii) distortion; (iii) fuzziness; (iv) noise. Resolution is determined primarily by experimental parameters such as the wavelength of the radiation that is used to probe an object and scattered by it. Two other important parameters that affect the resolution are the size of the aperture used to measure the scattered field and the beam-width of the wavefield used to probe the object. In terms of the imaging equation, the resolution of an image is determined by the spread (the local spatial extent) of the point spread function. In contrast to resolution, distortion and fuzziness are determined by the type of physical model used to design the data processing algorithm. These effects are associated with two distinct physical aspects of the imaging system. Distortion is related to the geometry of the system and, in particular, the type of model that is used to describe the propagation of the probe from the source to scatterer and from the scatterer to detector. If an inversion algorithm that is based on a model for the probe that is inaccurate, is used to invert data, then distortion will occur. The amount of distortion depends on how well the theoretical model describes the characteristics of the probe. In turn, this is determined

by the accuracy of the point spread function. Image fuzziness is related to the physical model used to describe the type and material properties of a scatterer. Fuzziness occurs when the physical model used to design an inversion algorithm fails to describe all the properties of the material and hence the variety of scattering that can occur. The degree of image fuzziness is determined by the accuracy of the mathematical model adopted for the object function and can lead to errors in the way an image is interpreted. The noise in an image is a combination of effects due to a whole range of unwanted disturbances and interference. In practice, because the noise is multifaceted, it is not possible to define it uniquely. For this reason, models are used to construct a suitable probability density function for the noise which is statistically compatible with the experiment. In general, noise accounts for all the non-ideal effects that may occur in an imaging system including multiple scattering events.

In terms of the imaging equation, i.e.

$$Image \;=\; (point\ spread\ function)\ convolved\ (object\ function) \;+\; noise$$

we can summarize resolution, distortion, image fuzziness and noise in the following way:

Resolution is determined by the spread of the point spread function.

Distortion is determined by the accuracy of the mathematical model for the point spread function.

Fuzziness is determined by the accuracy of the mathematical model for the object function.

Noise is determined by the accuracy of the convolution model for the data.

The aim of an imaging system is to obtain data on the scattered field which provides an image with minimal noise, fuzziness, distortion and maximum resolution.

By studying the physics of each imaging system and using 'suitable' approximations and mathematical models, one can formulate the imaging equation directly rather than introducing it via the phenomenological approach used here. This approach provides a mathematical description of the point spread function and the object function which is a central theme of this work.

The convolution operation is a direct consequence of using a linear systems theory approach. This is demonstrated in Parts I and II where it is shown that the convolution operation is fundamental to the solution of inhomogeneous wave equations using a Green function. For example, linear systems theory is used in the study of Fourier optics which is based on two fundamental results:

(i) The wavefield generated by light scattering in the 'object plane' is, in the 'far field' (i.e. a long way from the object plane), given by the Fourier transform of the object function.

(ii) In the focal plane of a well corrected lens, the field pattern can be taken to be given by the inverse Fourier transform[2] of the input.

[2]A lens can be taken to perform either a forward or inverse Fourier transform - it's all the

Suppose the object plane is denoted by the function $f(x, y)$, then from (i) above we can say that the scattered field is given by $F(k_x, k_y) = \hat{F}_2[f(x, y)]$ where $\hat{F}_2$ denotes the 2D Fourier transform operator and k_x, k_y are the spatial frequencies. Further, suppose that in the far field, we now introduce an aperture with an area denoted by P. This aperture will allow only a limited portion of the wavefield $F(k_x, k_y)$ to pass through, a portion that is given by PF (i.e. the aperture becomes a spatial filter). If a well corrected lens is then placed behind the aperture, then, from point (ii) above, the field pattern in the focal plane will be given by $F_2^{-1}[PF]$ where F_2^{-1} denotes the inverse 2D Fourier transform operator. Now, using the convolution theorem,

$$F_2^{-1}[P(k_x, k_y)F(k_x, k_y)] = p(x, y) \otimes\otimes f(x, y)$$

where $\otimes\otimes$ denotes the 2D convolution operation. This principle is the basic physical model for the way in which the reader is imaging this text, one of whose aims is to explain how points (i) and (ii) above come to be.

In general, the functions f, p and the noise n will have both amplitude and phase information and can therefore be written in the form $A_f \exp(i\theta_f)$, $A_p \exp(i\theta_p)$ and $A_n \exp(i\theta_n)$ where A is the amplitude and θ is the phase of the respective functions. As discussed earlier, the difference between these imaging systems is determined by whether or not the image contains information which is phase related. In terms of the imaging equation, a coherent image is given by

$$I_{\text{coherent}} = \mid p \otimes\otimes f + n \mid^2$$

whereas an incoherent image is given by

$$I_{\text{incoherent}} = \mid p \mid^2 \otimes\otimes \mid f \mid^2 + \mid n \mid^2 .$$

Note that, in an incoherent image, there is no information on the phase of the functions p, f or n 'encoded' in the image whereas, in a coherent image, the phase information of the functions p and f is 'mixed' together through the convolution operation and additive noise. Also, note that, in the former case, the data can be of the form $p \otimes\otimes f + n$ when the image is based on detecting time resolved signals and it is a matter of convention as to whether an image is constructed from the amplitude modulations $\mid p \otimes\otimes f + n \mid$ or the intensity modulations $\mid p \otimes\otimes f + n \mid^2$. The phase 'mixing' that occurs in a coherent image yields an effect that is a characteristic of all coherent images and is called 'speckle'. A speckle pattern is most easily observed by looking at the scattering of laser light from a (rough on the scale of a wavelength) surface. It is a pattern that has a characteristic statistical distribution of grey levels; thus, coherent images can usually be classified in terms of this unique distribution unlike incoherent images which have a wide range of different distributions. An example of an incoherent and coherent image of approximately the same region is given in Figure 1 which shows an optical image (overhead high resolution photograph) of a region of Northamptonshire (just south-west of the town of Northampton), England, showing both urban (e.g. the village of Wootton) and rural features.

---

same to a lens!

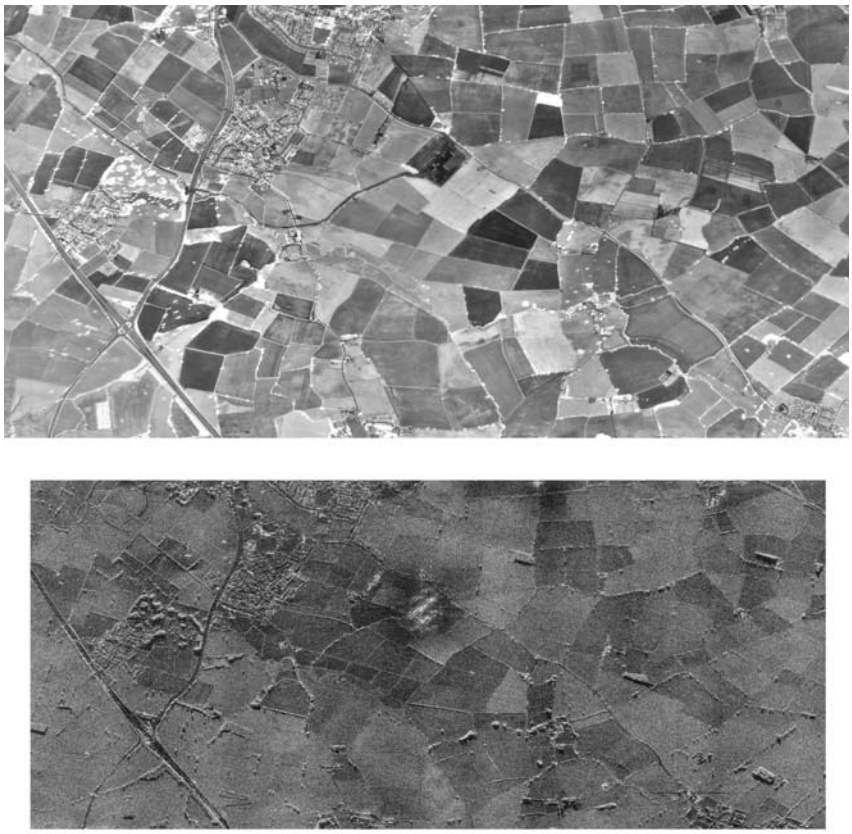

Figure 1: An incoherent optical image (above) and a coherent (Synthetic Aperture Radar) image of the same region of Northamptonshire, England.

The major road in the bottom left hand corner of this image is the M1 Motorway (which runs from London to Leeds, Yorkshire) in the locality of Junction 15. Figure 1 also shows a 'microwave photograph' of the same area taken with an X-band (2.8cm wavelength) Synthetic Aperture (airborne) Radar or SAR using vertical polarization. In contrast to the optical image, the SAR image is dominated by what, at first sight, looks like noise and arguably is noise, but noise of a special and quantifiable physical type, namely, speckle.

Digital Image Processing

A digital image can be considered to be visual display of a matrix of (integer) numbers whose value determines a particular shade of grey (for grey level images) or a specific colour (for colour images). A grey level image can be

represented by a function of two variables, $f(x, y)$ say, which gives a number $z = f(x, y)$ corresponding to a grey level at a point (x, y). A grey level digital image can therefore be considered to be a discrete function

$$f_{ij} \quad \text{where} \quad f_{ij} \equiv f(x_i, y_i).$$

Here, f_{ij} is the value of the function at $x = x_i$ and $y = y_i$; defines a two-dimensional array or matrix of numbers, i.e.

$$f_{ij} = \begin{pmatrix} f_{11} & f_{12} & \cdots & f_{1n} \\ f_{21} & f_{22} & \cdots & f_{2n} \\ \vdots & \vdots & \ddots & \vdots \\ f_{n1} & f_{n2} & \cdots & f_{nn} \end{pmatrix}$$

which is taken to be an accurate representation of $f(x, y)$. The range of values which f_{ij} is given defines the 'depth' of the image. As with any real image (i.e. a real data field), there must be a brightest and darkest point or point set in the data which corresponds to the minimum and maximum values of the matrix respectively and, hence, f_{ij} is bounded. If a real image is taken to be a map of the intensity of light at a particular point, then it must be described by a non-negative function and we can therefore impose the the condition

$$f_{ij} \geq 0 \quad \forall \quad i, j.$$

The process of converting $f(x, y)$ into f_{ij} is called digitization or A-to-D (Analogue-to-Digital) conversion, or spatial quantization, where the analogue image is sampled providing a matrix of discrete values typically on a rectangular grid. There are two elements to digitization: (i) sampling or spatial quantization; (ii) grey level or luminance quantization as illustrated below:

Analogue Image

$\downarrow$

Sampling (Spatial Quantization)

$\downarrow$

Grey Level (Luminance Quantization)

$\downarrow$

Digital Image

Spatial quantization gives rise to an array of numbers which can be taken to be an approximation to the original image, i.e. f_{ij} approximates $f(x, y)$. A fundamental question which then arises is how well does f_{ij} approximate $f(x, y)$? If n^2 samples are taken at regular intervals (uniform sampling) within a bounded square, then clearly, the approximation will improve as n increases. If enough samples are taken, a spatially quantized image is as good as the original. However, the precise answer to the above question is compounded in a theorem called the 'sampling theorem' which states that an analogue signal

can be reconstructed exactly from its digital form as long as the sampling frequency (i.e. samples per linear measure) is at least twice that of the highest frequency or 'Nyquist' frequency present in the signal, i.e.

$$sampling\ interval\ \leq\ \frac{1}{Nyquist\ frequency}$$

where

$$Nyquist\ frequency\ =\ 2 \times (Maximum\ frequency)$$

This 'sampling at twice the maximum frequency rule' is usually attributed to the work of Shannon in the 1940s and is known as the 'Shannon Sampling Theorem'. The theorem is concerned with the number of samples needed to recover the original analogue signal and not with the adequacy of the digitization of any particular type of process or presentation. For an image $f(x, y)$ in which the sampling must be undertaken in both the x and y directions with sampling intervals given by Δx and Δy, respectively, then

$$\Delta \leq \frac{1}{K_x} \quad \text{and} \quad \Delta y \leq \frac{1}{K_y}$$

where K_x and K_y are the Nyquist frequencies in the x and y directions respectively. The 'readability' of an image depends on the total number of pixels (picture elements) that are used to represent the image. Digital images which are composed of only a few pixels appear 'boxy'. This is shown in Figure 2 which illustrates the effect of sampling an image with fewer and fewer pixels. Failure to sample an analogue image correctly (i.e. at the Nyquist frequency) leads to an effect known as aliasing. This effect leads to low frequency features distorting a digital image resulting from the under sampling of high frequency features in the analogue image.

The next step in the generation of a digital image is luminance quantization where each pixel is assigned a discrete value, i.e. level of greyness or luminance. The number of steps in the scale available for assignment is called the pixel depth (in bits). Too little depth results in inaccurate representations and loss of information as well as false contours. The number of shades of grey that can be present is related to the number of bits n by 2^n. A grey tone is then assigned to each value, for example, 0=black, 1=dark grey, 2=light grey, 3=white, could represent the scale assignment for a 2 bit depth image which would result from $2^2 = 4$ shades of grey. A special case arises when images are considered using just 1 bit and binary image processing becomes applicable which, being based on 1's and 0's, is very fast. Binary image processing is often used in image segmentation (e.g. edge detection) and pattern recognition where one of the main tasks is to binarize an image into a data field with a valid information content for the pattern recognition task that is to be applied. Figure 3 shows the effect of changing the luminance quantization of an image using 4, 3, 2 and 1 bits.

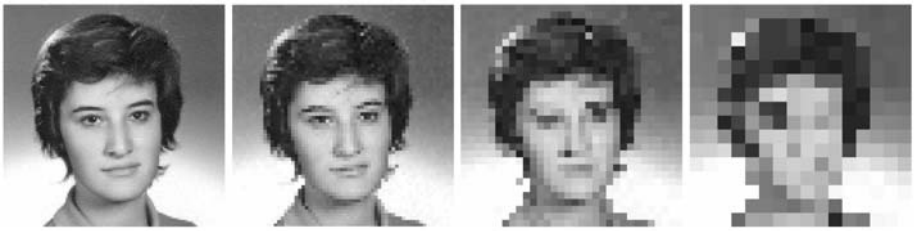

Figure 2: A digital image sampled using (from left to right) 128×128, 64×64, 32×32 and 16×16 pixels.

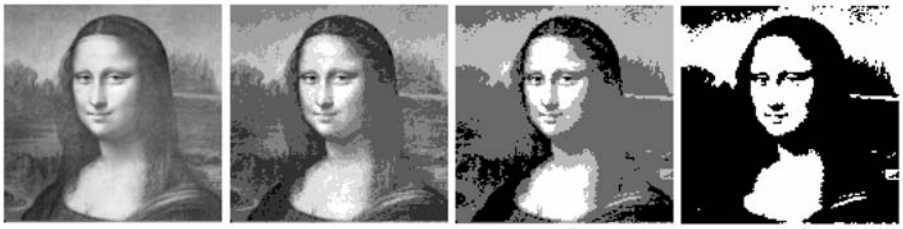

Figure 3: A 128×128 image with luminance quantization using (from left to right) 4, 3, 2 and 1 bits.

In addition to grey levels, colours can be assigned in the same basic way. Any colour can be assigned to any chosen value. In some cases, colour coding a digital image in a predetermined way can provide useful information. This allows the interpreter to observe features with greater clarity, increasing the visual performance of the imaging system such as in infrared imaging for example, where a colour code is designed to distinguish between different temperatures. Whether a digital image is displayed as a matrix of grey levels or colour coded, a satisfactory picture representation ultimately depends upon the details and contrasts in the image. A matrix of say 256×256 pixels with a depth of eight bits is often satisfactory, where 8 bits provide 2^8 or 256 shades of grey, and requires 64 kilobytes of memory. Better image quality can of course be obtained with a larger matrix of pixels. However, more pixels and greater depth increase the storage requirements, data transfer and processing time. Techniques for data compression are therefore of value not only for storing and transmitting images but in some cases for processing images in 'compression space'. It is important to note that, while a digital image can be thought of in terms of an integer data field, the processing of a digital image is usually based on

floating point arithmetic. A floating point field can of course be quantized for display purposes and analysis at any point in a single process or sequence of processes. However, each process is taken to operate on the floating point field and not the quantized field.

Digital image processing (DIP) utilizes a number of mathematical techniques. The essential subject areas are computational linear algebra, integral transforms, statistics and other techniques of numerical analysis (numerical methods for differentiation and integration for example). Many DIP algorithms can be written in terms of a matrix equation or a set of matrix equations and, hence, computational methods in linear algebra become an important aspect of the subject. Integral transforms and, in particular, the discrete forms of these transforms, form the basis for a wide range of processing methods. These include the discrete Fourier transform, the discrete correlation and convolution sums, the discrete cosine transform and the discrete wavelet transform. The statistical significance of image data plays a vital role from the suppression of noise to feature extraction and statistical pattern recognition. Many DIP algorithms can be classified in terms of a digital filter. There are two principal types: (i) moving window filters and (ii) transform space filters. Moving window filters are usually non-recursive filters which are normally linear processes that operate on the image data directly. Transform space filters operate on the data by first performing an appropriate transform on the image, processing the transformed data and then inverting the result.

Image processing is a very demanding task for 'standard' serial computers. Simple processes (point processes) such as the multiplication of each pixel by a constant takes n^2 operations for an $n \times n$ image. The total number of operations required increases rapidly with the size of the image. Parallel computing and distributed array processing is therefore essential for rapid or real-time image processing. Ideally, an image processing engine would be composed of an array of sub-processors - one per pixel. Using this type of approach the processing time depends very little on the size of the image. Parallel image processing engines have been available for some time, but they are comparatively expensive and specialist machines. However, valuable image processing can usually be carried out on conventional serial computers especially with the ever increasing performance of the central processors and memory capacity. Nevertheless, virtual memory is still useful as it allows images to be processed whose storage requirements may exceed the internal memory of the computer.

Fundamental Problems

There are three distinct and fundamental problems which are common to most areas of image processing:

(i) image restoration and reconstruction;

(ii) pattern recognition;

(iii) image understanding.

The restoration/reconstruction problem is concerned with the recovery of information encoded in an image. This is an inverse problem compounded by the performance of a process known as deconvolution. Pattern recognition is usually concerned with processing data obtained after deconvolution or if deconvolution is not required. It typically involves the manipulation of data to improve the 'readability' of an image and to identify areas of geometric and/or textural significance. In particular, we are interested in converting a digital image into a form from which geometric and/or statistically significant features can be recognized and interpreted by man or machine; the latter case is significantly more difficult, and is in general, as yet, an unsolved problem. There are a number of techniques that can be classified under the general heading of 'pattern recognition' which form one of three basic categories: (i) image enhancement; (ii) noise reduction; (iii) segmentation. Image enhancement is concerned with improving the 'readability' of an image. Noise reduction algorithms eliminate uncorrelated features from an image while preserving the resolution of the data. Image segmentation identifies meaningful features in an image based on some measure of (local) pixel similarity and discontinuity which includes the detection of self-similar features when a model for an image is used that assumes self-similar structures (i.e. fractal images)

Pattern recognition identifies physical features in an image leading to our third categorization which is concerned with physical interpretation. The physical interpretation of an image is difficult to quantify because objectives and expectations of this aspect of DIP are inextricably related to the design and applications of a particular imaging system. We interpret an image in terms of the 'physical properties' of the radiation field from which an image has been derived and deduce information on the structure and material properties of an imaged object.

Although image processing can accomplish many tasks and produce exceptionally spectacular results, it is a computer based subject that still conforms to the basic rule of computing, namely, *rubbish in gives rubbish out*. There are a number of case studies in which poor quality imaging systems have been the focus of image processing applications that have attempted to do the impossible, i.e. get something from nothing. A good example of this was the Hubble space telescope which, after its initial launch, provided images whose resolution was significantly less than that for which the system had been designed. This was found to be due to calibration errors associated with the manufacture of the primary reflector, i.e. total quality management! It was originally thought that image restoration and reconstruction methods might be applied using data provided by the telescope. However, because the deconvolution problem was ill-posed with numerical solutions that were at best, ill-conditioned, together with the fact that the point spread function of the Hubble images was non-stationary, the problem became intractable, irrespective of the computer processing power. Hence, NASA was forced to use the space shuttle to install the compensating optics required to bring the Hubble images into focus rather than rely on digital image processing methods alone.

About this Book

This book establishes the underlying physical principles linking different imaging methods and systems. In each case, it shows how, starting with an appropriate physical model, a solution for the scattered field can be obtained which provides mathematical expressions for the point spread function and the object function.

Part I is devoted to the essential mathematical and computational background to the subject required to comprehend the rest of the work. Part II discusses the application of the scattering theory to different imaging systems. Part III covers methods of digital image processing including the problem of deconvolving the data to recover the object function and methods of image enhancement. In Part IV, image segmentation, feature extraction and pattern recognition are used to interpret the information content of an image and apply decision criteria, including an introduction to statistical image processing and the application of fractal or self-affine models for image interpretation.

To illustrate the principal results, a number of different imaging methods are introduced. They include optical imaging, seismic imaging and medical imaging with ultrasound, two related imaging methods known as projection tomography and diffraction tomography and also a method of imaging the surface of the earth using microwaves called Synthetic Aperture Radar or SAR. In each case, the physical principles involved are discussed with examples illustrating the phenomena that occur and used to interpret the structure and physical state of an object.

This book introduces some of the software functions essential for routine DIP and encourages readers to design and test their own 'software solutions' to a range of DIP problems given at the end of Parts I-IV. These questions relate to algorithms discussed, the solution being compounded in the 'resolution' of a given program. Some questions relate to methods of testing code and help readers investigate the characteristics and performance of a given DIP algorithm. This is done by synthesizing specific test data for which certain characteristics are expected when processed by a given method. This approach is consistent with the modular nature of image processing software and the way in which it is designed for research and development. Methods of interfacing the software through a graphical user interface is not addressed; the book is concerned with the fundamentals forming the computational basis of an image processing package, irrespective of the character and sophistication of the user interface.

The software provided is designed to illustrate the conversion of a given DIP algorithm into code using either pseudo code, C or MATLAB m-code. MATLAB has a number of 'toolboxes' including a DIP toolbox that provides a range of facilities for I/O, format conversion, display and image processes. This toolbox has been used to provide illustrative examples of image processing and in some cases, the m-code used for that processing. The MATLAB DIP toolbox provides a valuable resource for rapid prototyping using m-code and is ideal for research and development. However, in this book, emphasis is placed on developing 'software solutions' from scratch in C/C++. Software is provided

as solutions to programming questions given at the end of each of the four main parts of the book. The software has been included to help readers to build their own prototype DIP library. Prototype I/O and a graphics utilities based on an X-windows environment are provided in Appendix D, functions that are used in some of the software solutions that are provided in Appendix A. Readers are free to use the code provided, modify it and restructure it to suit their own interests. No warranties are made, expressed or implied that the software is error free or consistent with any particular standard, or that it will meet the requirements for any particular application. The software has been designed for students undertaking primarily postgraduate programmes in DSP for which this work has been written together with its companion text *Digital Signal Processing*, J M Blackledge, Horwood, 2003. In *Digital Signal Processing*, graphics utilities were designed using Borland C++ and software development was assumed to be undertaken using a DOS/Windows operating system on a PC. In this work, the utilities have been designed for software development using *unix* or *linux* and the graphics functions available under X-windows, so that students gain experience of working with two different but equally important operating environments.

In order to reduce the length of this book, graphics has been used sparingly, particularly with regard to illustrating the full range of image processing techniques that are discussed. Rather, readers themselves are encouraged to study the effect of applying an image processing algorithm in practice in order to familiarize themselves with the output associated with a specific function using m-code or C-code or a mixture of both as undertaken in this work.

Finally, references to other important texts and/or key scientific papers which have both academic and historical value are included at the end of each chapter or occasionally within the text. In some special cases, Internet based references are provided but this has been done sparingly as Internet materials and data change rapidly and can, in any case, usually be accessed effectively using a good search engine together with an appropriate set of key words. Thus, it is left to the reader to supplement the 'learning curve' derived (or otherwise) from reading this book with the wealth of information and data that the Internet provides.

Summary of Important Results

The imaging equation

$$image \;=\; (point\ spread\ function)\ convolved\ (object\ function) \;+\; noise$$

Principles of Fourier optics

(i) In the far field, the scattered radiation pattern is given by the Fourier transform of the object function that best describes the scatterer(s).

(ii) In the focal plane of a well corrected lens, the field pattern is given by the (inverse) Fourier transform of the input wavefield.

Image restoration and reconstruction

Concerned with processes that aim to recover the information contained in the data. These 'processes' are usually directly or indirectly related to the problem of deconvolution (the inverse of convolution). Many types of degraded images can be restored but image processing cannot fully restore all degradation.

Image Enhancement

Concerned with processes whose goal is to improve the 'quality' or 'readability' of an image in some way, i.e. to emphasize features of particular importance or relevance.

Pattern Recognition

Concerned with the identification or interpretation of an image. It aims to extract deterministic or statistically significant information (usually at a high level) that an image conveys.

Image Understanding

Attempts to interpret an image in terms of the 'physics' of the imaging system.

Model for an incoherent image

$$I = \mid p \mid^2 \otimes\otimes \mid f \mid^2 + \mid n \mid^2$$

where $\mid p \mid^2$ is the intensity point spread function, f is the object function and n is the noise field.

Model for a coherent image

$$I = \mid p \otimes\otimes f + n \mid^2$$

where p is the point spread function

Amplitude and phase functions

In general, p, f and n may have both amplitude and phase contributions, e.g.

$$f = A_f \exp(i\theta_f).$$

In a coherent image $\mid f \mid^2 = A^2$ and, hence, the phase information on the object function is lost in an incoherent image.

Speckle

Speckle is a characteristic of coherent images and results from constructive and destructive interference of wave fronts. This is represented mathematically

by the phase information of the object function being 'mixed' with the point spread function (via the convolution operation).

Fundamental problems

In terms of the imaging equation, DIP involves finding solutions to the following problems:

(i) recovering the object function from the data;

(ii) detecting meaningful patterns in the object function;

(iii) interpreting the object function in terms of the 'physics' of the imaging system and the environment in which it operates.

Resolution A characteristic of the point spread function.

Distortion Determined by the accuracy of the mathematical model for the point spread function.

Fuzziness Determined by the accuracy of the mathematical model for the object function.

Noise Determined by the accuracy of the convolution model for the data.

Golden rule of digital image processing *Rubbish in gives rubbish out.*

Further Reading

- Rosenfeld A and Kak A C, *Digital Picture Processing*, Academic Press, 1980.
- Huang T S (Ed), *Two-dimensional Digital Signal Processing*, Topics in Applied Physics, Vol 43, Springer-Verlag, 1981.
- Bates R H T an McDonnal M J, *Image Restoration and Reconstruction*, oxford Science Publications, 1986.
- Gonzalez R C and Wintz P, *Digital Image Processing*, Addison-Wesley, 1987.
- Lim J S, *Two-Dimensional Signal and Image Processing*, Prentice-Hall, 1990.
- Marion A, *An Introduction to Image Processing*, Chapman and Hall, 1991.
- Russ J C, *The Image Processing Handbook*, CRC Press, 1995.
- Jähne B, *Digital Image Processing*, Springer, 1995.

- Blackledge J M (Ed.) *Image Processing I: Mathematical Methods and Applications*, Oxford University Press, 1997.
- Blackledge J M and Turner M J (Eds.) *Image Processing II: Mathematical Methods, Algorithms and Applications*, Horwood Publishing Series: Mathematics and Applications, 1999.
- Blackledge J M and Turner M J (Eds.) *Image Processing III: Mathematical Methods, Algorithms and Applications*, Horwood Publishing Series: Mathematics and Applications, 2001.

Part I

Mathematical and Computational Background

Chapter 1

Vector Fields

Vector fields have an algebra and calculus that is used extensively in multi-dimensional field theory. The essential elements of vector calculus are the operators grad, div and curl, surface and volume integrals and theorems associated with these integrals such as the divergence theorem.

The operators grad, div and curl were originally investigated by the British (Scottish) physicist, James Clerk Maxwell, in the 1860s to characterize the properties of electric and magnetic fields and were first used in Maxwell's equations. These equations unified the theories of electricity and magnetism and introduced the 'physics' of electromagnetism and, in particular, electromagnetic radiation. Surface and volume integrals and the divergence theorem are used in many areas of vector field theory. They are used extensively for modelling the propagation and scattering of electromagnetic and acoustic waves, e.g. Kirchhoff's theory for the diffraction of light which forms the basis of optical imaging theory.

This chapter provides a brief resumé of vector fields and vector calculus covering those aspects of the subject that are specific to material that is used later on in this book.

1.1 Scalar Fields

Consider the scalar field $u(x, y, z)$ where x, y, z are rectangular (Cartesian) coordinates. Suppose that $x \to x + dx$, $y \to y + dy$ and $z \to z + dz$. How does the field u change? i.e. what is

$$du = u(x + dx, y + dy, z + dz) - u(x, y, z)?$$

Using Taylor's theorem,

$$u(x + dx, y + dy, z + dz) = u(x, y, z) + \frac{\partial u}{\partial x}dx + \frac{\partial u}{\partial y}dy + \frac{\partial u}{\partial z}dz + ...$$

and neglecting $O(dx^2, dxdy, ...)$ we get

$$du = \frac{\partial u}{\partial x}dx + \frac{\partial u}{\partial y}dy + \frac{\partial u}{\partial z}dz.$$

Now, let us introduce the following definitions:

$$d\mathbf{r} = \hat{\mathbf{x}}dx + \hat{\mathbf{y}}dy + \hat{\mathbf{z}}dz$$

and

$$\nabla = \hat{\mathbf{x}}\frac{\partial}{\partial x} + \hat{\mathbf{y}}\frac{\partial}{\partial y} + \hat{\mathbf{z}}\frac{\partial}{\partial z}$$

where $\hat{\mathbf{x}}, \hat{\mathbf{y}}$ and $\hat{\mathbf{z}}$ are unit vectors in the x, y and z directions, respectively. We can then write,

$$du = \nabla u \cdot d\mathbf{r}$$

where $\nabla \equiv$ grad is the 'gradient' operator.

Some example properties of the gradient operator are

$$\nabla(u+v) = \hat{\mathbf{x}}\frac{\partial}{\partial x}(u+v)+... = \hat{\mathbf{x}}\left(\frac{\partial u}{\partial x} + \frac{\partial v}{\partial x}\right)+... = \left(\hat{\mathbf{x}}\frac{\partial u}{\partial x} + ...\right)+\left(\hat{\mathbf{x}}\frac{\partial v}{\partial x} + ...\right)$$

$$= \nabla u + \nabla v$$

and

$$\nabla(uv) = \hat{\mathbf{x}}\frac{\partial}{\partial x}(uv)+... = \hat{\mathbf{x}}\left(u\frac{\partial v}{\partial x} + v\frac{\partial u}{\partial x}\right)+... = u\left(\hat{\mathbf{x}}\frac{\partial v}{\partial x} + ...\right)+v\left(\hat{\mathbf{x}}\frac{\partial u}{\partial x} + ...\right)$$

$$= u\nabla v + v\nabla u.$$

Note that ∇ operates in the same way as ordinary differentiation with respect to sums and products.

Spherically Symmetric Scalar Fields

Let

$$u = u(r); \quad r = \sqrt{x^2 + y^2 + z^2},$$

then

$$\frac{\partial u}{\partial x} = \frac{du}{dr}\frac{\partial r}{\partial x}, \quad \frac{\partial u}{\partial y} = \frac{du}{dr}\frac{\partial r}{\partial y}, \quad \frac{\partial u}{\partial z} = \frac{du}{dr}\frac{\partial r}{\partial z}.$$

Now,

$$\frac{\partial r}{\partial x} = \frac{\partial}{\partial x}(x^2 + y^2 + z^2)^{\frac{1}{2}} = \frac{1}{2}(x^2 + y^2 + z^2)^{-\frac{1}{2}}2x = \frac{x}{r}.$$

Similarly,

$$\frac{\partial r}{\partial y} = \frac{y}{r} \quad \text{and} \quad \frac{\partial r}{\partial z} = \frac{z}{r}.$$

Hence,

$$\nabla u = \hat{\mathbf{x}}\frac{du}{dr}\frac{x}{r} + \hat{\mathbf{y}}\frac{du}{dr}\frac{y}{r} + \hat{\mathbf{z}}\frac{du}{dr}\frac{z}{r} = \frac{\mathbf{r}}{r}\frac{du}{dr}; \quad \mathbf{r} = \hat{\mathbf{x}}x + \hat{\mathbf{y}}y + \hat{\mathbf{z}}z$$

or

$$\nabla u = \hat{\mathbf{n}}\frac{du}{dr}; \quad \hat{\mathbf{n}} = \frac{\mathbf{r}}{r}$$

where $\hat{\mathbf{n}}$ is a unit vector pointing in the direction of $\mathbf{r}$.

1.2 Vector Fields

A vector field is a vector function of position, e.g.

$$\hat{\mathbf{x}}F_x(x,y,z) + \hat{\mathbf{y}}F_y(x,y,z) + \hat{\mathbf{z}}F_z(x,y,z)$$

and the notation $\mathbf{F}(\mathbf{r})$ is used to represent a vector field, i.e.

$$\mathbf{F}(\mathbf{r}) = \hat{\mathbf{x}}F_x(\mathbf{r}) + \hat{\mathbf{y}}F_y(\mathbf{r}) + \hat{\mathbf{z}}F_z(\mathbf{r}); \quad \mathbf{r} = \hat{\mathbf{x}}x + \hat{\mathbf{y}}y + \hat{\mathbf{z}}z.$$

1.2.1 First Order Differential Operators

Consider the gradient operator

$$\nabla = \hat{\mathbf{x}}\frac{\partial}{\partial x} + \hat{\mathbf{y}}\frac{\partial}{\partial y} + \hat{\mathbf{z}}\frac{\partial}{\partial z},$$

then

$$\nabla u = \hat{\mathbf{x}}\frac{\partial u}{\partial x} + \hat{\mathbf{y}}\frac{\partial u}{\partial y} + \hat{\mathbf{z}}\frac{\partial u}{\partial z}$$

is a vector field and

$$\nabla\mathbf{F} = \left(\hat{\mathbf{x}}\frac{\partial}{\partial x} + \hat{\mathbf{y}}\frac{\partial}{\partial y} + \hat{\mathbf{z}}\frac{\partial}{\partial z}\right)(\hat{\mathbf{x}}F_x + \hat{\mathbf{y}}F_y + \hat{\mathbf{z}}F_z)$$

is a dyadic field.

We can define two other ways of combining ∇ with a vector field $\mathbf{F}$ in terms of the dot product

$$\nabla\cdot\mathbf{F} = \left(\hat{\mathbf{x}}\frac{\partial}{\partial x} + \hat{\mathbf{y}}\frac{\partial}{\partial y} + \hat{\mathbf{z}}\frac{\partial}{\partial z}\right)\cdot(\hat{\mathbf{x}}F_x + \hat{\mathbf{y}}F_y + \hat{\mathbf{z}}F_z)$$

and the cross product

$$\nabla\times\mathbf{F} = \left(\hat{\mathbf{x}}\frac{\partial}{\partial x} + \hat{\mathbf{y}}\frac{\partial}{\partial y} + \hat{\mathbf{z}}\frac{\partial}{\partial z}\right)\times(\hat{\mathbf{x}}F_x + \hat{\mathbf{y}}F_y + \hat{\mathbf{z}}F_z).$$

Expanding the first result,

$$\begin{aligned}\nabla\cdot\mathbf{F} = {}& \hat{\mathbf{x}}\cdot\hat{\mathbf{x}}\frac{\partial F_x}{\partial x} + \hat{\mathbf{x}}\cdot\hat{\mathbf{y}}\frac{\partial F_y}{\partial x} + \hat{\mathbf{x}}\cdot\hat{\mathbf{z}}\frac{\partial F_z}{\partial x}\\ &+\hat{\mathbf{y}}\cdot\hat{\mathbf{x}}\frac{\partial F_x}{\partial y} + \hat{\mathbf{y}}\cdot\hat{\mathbf{y}}\frac{\partial F_y}{\partial y} + \hat{\mathbf{y}}\cdot\hat{\mathbf{z}}\frac{\partial F_z}{\partial y}\\ &+\hat{\mathbf{z}}\cdot\hat{\mathbf{x}}\frac{\partial F_x}{\partial z} + \hat{\mathbf{z}}\cdot\hat{\mathbf{y}}\frac{\partial F_y}{\partial z} + \hat{\mathbf{z}}\cdot\hat{\mathbf{z}}\frac{\partial F_z}{\partial z}.\end{aligned}$$

Now, since

$$\hat{\mathbf{x}}\cdot\hat{\mathbf{x}} = \hat{\mathbf{y}}\cdot\hat{\mathbf{y}} = \hat{\mathbf{z}}\cdot\hat{\mathbf{z}} = 1$$

with all other dot products being zero, we get

$$\nabla\cdot\mathbf{F} = \frac{\partial F_x}{\partial x} + \frac{\partial F_y}{\partial y} + \frac{\partial F_z}{\partial z}.$$

The operator $\nabla\cdot$ is called the divergence of the field and is also written as div, i.e.

$$\nabla\cdot \equiv \text{div}$$

Expanding $\nabla \times \mathbf{F}$, we have

$$\begin{aligned}\nabla \times \mathbf{F} = \hat{\mathbf{x}} \times \hat{\mathbf{x}}\frac{\partial F_x}{\partial x} + \hat{\mathbf{x}} \times \hat{\mathbf{y}}\frac{\partial F_y}{\partial x} + \hat{\mathbf{x}} \times \hat{\mathbf{z}}\frac{\partial F_z}{\partial x}\\ +\hat{\mathbf{y}} \times \hat{\mathbf{x}}\frac{\partial F_x}{\partial y} + \hat{\mathbf{y}} \times \hat{\mathbf{y}}\frac{\partial F_y}{\partial y} + \hat{\mathbf{y}} \times \hat{\mathbf{z}}\frac{\partial F_z}{\partial y}\\ +\hat{\mathbf{z}} \times \hat{\mathbf{x}}\frac{\partial F_x}{\partial z} + \hat{\mathbf{z}} \times \hat{\mathbf{y}}\frac{\partial F_y}{\partial z} + \hat{\mathbf{z}} \times \hat{\mathbf{z}}\frac{\partial F_z}{\partial z}.\end{aligned}$$

For vector products,

$$\hat{\mathbf{x}} \times \hat{\mathbf{y}} = \hat{\mathbf{z}}, \quad \hat{\mathbf{y}} \times \hat{\mathbf{z}} = \hat{\mathbf{x}}, \quad \hat{\mathbf{z}} \times \hat{\mathbf{x}} = \hat{\mathbf{y}}, \hat{\mathbf{y}} \times \hat{\mathbf{x}} = -\hat{\mathbf{z}}, \quad \hat{\mathbf{z}} \times \hat{\mathbf{y}} = -\hat{\mathbf{x}}, \quad \hat{\mathbf{x}} \times \hat{\mathbf{z}} = -\hat{\mathbf{y}}$$

and

$$\hat{\mathbf{x}} \times \hat{\mathbf{x}} = \hat{\mathbf{y}} \times \hat{\mathbf{y}} = \hat{\mathbf{z}} \times \hat{\mathbf{z}} = 0.$$

Hence,

$$\begin{aligned}\nabla \times \mathbf{F} &= \hat{\mathbf{z}}\frac{\partial F_y}{\partial x} - \hat{\mathbf{y}}\frac{\partial F_z}{\partial x} - \hat{\mathbf{z}}\frac{\partial F_x}{\partial y} + \hat{\mathbf{x}}\frac{\partial F_z}{\partial y} + \hat{\mathbf{y}}\frac{\partial F_x}{\partial z} - \hat{\mathbf{x}}\frac{\partial F_y}{\partial z}\\ &= \hat{\mathbf{x}}\left(\frac{\partial F_z}{\partial y} - \frac{\partial F_y}{\partial z}\right) + \hat{\mathbf{y}}\left(\frac{\partial F_x}{\partial z} - \frac{\partial F_z}{\partial x}\right) + \hat{\mathbf{z}}\left(\frac{\partial F_y}{\partial x} - \frac{\partial F_x}{\partial y}\right)\\ &= \begin{vmatrix} \hat{\mathbf{x}} & \hat{\mathbf{y}} & \hat{\mathbf{z}} \\ \frac{\partial}{\partial x} & \frac{\partial}{\partial y} & \frac{\partial}{\partial z} \\ F_x & F_y & F_z \end{vmatrix}.\end{aligned}$$

The operator $\nabla\times$ is called the curl of the vector field $\mathbf{F}$, i.e.

$$\nabla\times \equiv \text{curl}$$

1.2.2 Second Order Differential Operators

The operator $\nabla \cdot (\nabla u)$ is an example of a second order differential operator where

$$\nabla \cdot (\nabla u) \equiv \nabla^2 u = \frac{\partial^2 u}{\partial x^2} + \frac{\partial^2 u}{\partial y^2} + \frac{\partial^2 u}{\partial z^2}.$$

The operator ∇^2 is called the Laplacian.

There are many results that can be derived for second order operators but the following are three of the more important that are used later on in this work.

(i) $\nabla \times (\nabla u) = 0$

(ii) $\nabla \cdot (\nabla \times \mathbf{F}) = 0$

(iii) $\nabla \times (\nabla \times \mathbf{F}) = \nabla(\nabla \cdot \mathbf{F}) - \nabla^2\mathbf{F}$

1.3 The Divergence Theorem

Let V be a closed volume with surface S in which a surface element dS is characterized by an outward unit normal $\hat{\mathbf{n}}$ which is perpendicular to this surface element. If

$$\mathbf{F}(x,y,z) = \hat{\mathbf{x}}F_x(x,y,z) + \hat{\mathbf{y}}F_y(x,y,z) + \hat{\mathbf{z}}F_z(x,y,z)$$

where F_x, F_y and F_z have continuous first partial derivatives, then

$$\oint_S \mathbf{F}\cdot\hat{\mathbf{n}}dS = \int_V \nabla\cdot\mathbf{F}dV$$

where $\oint_S$ denotes the 'closed surface' integral (i.e. integration over the entire surface that encloses the volume V) and $\int_V$ denotes the volume integral.

Simple Proof

We want to prove that

$$\oint_S \mathbf{F}\cdot\hat{\mathbf{n}}dS = \int_V \left(\frac{\partial F_x}{\partial x} + \frac{\partial F_y}{\partial y} + \frac{\partial F_z}{\partial z}\right) dxdydz.$$

Consider the integral

$$\int_V \frac{\partial F_z}{\partial z}dxdydz$$

evaluated over a small rectangular volume with its axis of rotation in the z-direction and with top and bottom surfaces located at z_2 and z_1, respectively. In this case,

$$\int_V \frac{\partial F_z}{\partial z}dxdydz = \int\int [F_z(x,y,z)]_{z_1}^{z_2}\,dxdy = \int\int [F_z(x,y,z_2) - F_z(x,y,z_1)]dxdy.$$

The last integral can be written in the form

$$\oint_S F_z(x,y,z)\hat{\mathbf{n}}\cdot\hat{\mathbf{z}}dS$$

because, when $\hat{\mathbf{n}} = \hat{\mathbf{z}}$, the integral is over the top surface of the rectangle. When $\hat{\mathbf{n}} = -\hat{\mathbf{z}}$, the integral is over the bottom surface and, when $\hat{\mathbf{n}} \neq \hat{\mathbf{z}}$, the dot product is zero and hence the surface integral is zero. Thus, we have

$$\int_V \frac{\partial F_z}{\partial z}dxdydz = \oint_S F_z\hat{\mathbf{n}}\cdot\hat{\mathbf{z}}dS.$$

By a similar argument,

$$\int_V \frac{\partial F_y}{\partial y}dxdydz = \oint_S F_y\hat{\mathbf{n}}\cdot\hat{\mathbf{y}}dS$$

and

$$\int_V \frac{\partial F_x}{\partial x} dxdydz = \oint_S F_x \hat{\mathbf{n}} \cdot \hat{\mathbf{x}} dS.$$

Combining these results, we get

$$\int_V \left(\frac{\partial F_x}{\partial x} + \frac{\partial F_y}{\partial y} + \frac{\partial F_z}{\partial z} \right) dxdydz = \oint_S (\hat{\mathbf{x}} F_x + \hat{\mathbf{y}} F_y + \hat{\mathbf{z}} F_z) \cdot \hat{\mathbf{n}} dS$$

or

$$\int_V \nabla \cdot \mathbf{F} dV = \oint_S \mathbf{F} \cdot \hat{\mathbf{n}} dS.$$

An important 'by-product' of the divergence theorem are Green's identities (known collectively as Green's theorem). For two scalar fields u and v with continuous first and second partial derivatives, Green's first identity is

$$\int_V (u\nabla^2 v + \nabla u \cdot \nabla v) dV = \oint_S u \nabla v \cdot \hat{\mathbf{n}} dS$$

and Green's second identity is

$$\int_V (u\nabla^2 v - v\nabla^2 u) dV = \oint_S (u\nabla v - v\nabla u) \cdot \hat{\mathbf{n}} dS.$$

1.4 Summary of Important Results

Scalar fields

$$du(x, y, z) = \nabla u(x, y, z) \cdot d\mathbf{r}$$

where

$$d\mathbf{r} = \hat{\mathbf{x}} dx + \hat{\mathbf{y}} dy + \hat{\mathbf{z}} dz$$

and

$$\nabla \equiv \hat{\mathbf{x}} \frac{\partial}{\partial x} + \hat{\mathbf{y}} \frac{\partial}{\partial y} + \hat{\mathbf{z}} \frac{\partial}{\partial z}$$

Vector fields

$$\nabla \cdot \mathbf{F} = \frac{\partial F_x}{\partial x} + \frac{\partial F_y}{\partial y} + \frac{\partial F_z}{\partial z}$$

$$\nabla \times \mathbf{F} = \begin{vmatrix} \hat{\mathbf{x}} & \hat{\mathbf{y}} & \hat{\mathbf{z}} \\ \frac{\partial}{\partial x} & \frac{\partial}{\partial y} & \frac{\partial}{\partial z} \\ F_x & F_y & F_z \end{vmatrix}$$

$$\nabla \times \nabla \times \mathbf{F} = \nabla(\nabla \cdot \mathbf{F}) - \nabla^2 \mathbf{F}$$

Laplacian operator

$$\nabla^2 u(\mathbf{r}) = \left(\frac{\partial^2}{\partial x^2} + \frac{\partial^2}{\partial y^2} + \frac{\partial^2}{\partial z^2} \right) u(x, y, z)$$

The divergence theorem

$$\int_V \nabla \cdot \mathbf{F} dV = \oint_S \mathbf{F} \cdot \hat{\mathbf{n}} dS$$

Green's theorem

$$\int_V (u\nabla^2 v + \nabla u \cdot \nabla v) dV = \oint_S u \nabla v \cdot \hat{\mathbf{n}} dS$$

and

$$\int_V (u\nabla^2 v - v\nabla^2 u) dV = \oint_S (u\nabla v - v\nabla u) \cdot \hat{\mathbf{n}} dS$$

1.5 Further Reading

There are many text books covering vector analysis and vector calculus that have been published over the years. The following are some examples.

- Phillips H B, *Vector Analysis*, Wiley, 1933.
- Craig H V, *Vector and Tensor Analysis*, McGraw-Hill, 1943.
- Marder L, *Vector Analysis*, Allen and Unwin, 1970.
- Spiegel M R, *Vector Analysis*, McGraw-Hill, 1974.
- Matthews P C, *Vector Calculus*, Springer, 1997.

Chapter 2

2D Fourier Theory

The Fourier transform in two-dimensions has many of the same properties as the Fourier transform in one-dimension and can be studied in terms of both the classical approach (starting with the Fourier series) or in terms of a generalized formalism (which relies implicitly on the properties of the delta function). In this chapter, we consider the complex Fourier series in 2D from which definitions of the Fourier transform and the discrete Fourier transform are derived. Important properties of this transform are then considered together with the computational procedures used for applying it in discrete form as used for processing digital images. The Fourier transform is the 'work-horse' for a significant number of methods in signal and image processing and has been discussed at length in Chapters 3 and 4 of the companion work to this book, namely, Blackledge J M, *Digital Signal Processing*, Horwood, 2003. Here, we extend this material further, introducing the reader to the use of the Fourier transform in two-dimensions.

2.1 The 2D Complex Fourier Series

A Fourier series is just one of a number of linear series which can be used to 'model' a piecewise continuous function $f(x,y)$. In general, we may consider the function f to be composed of a linear sum of 'basis functions' B_{nm} and coefficients c_{nm}, i.e.

$$f(x,y) = \sum_n \sum_m c_{nm} B_{nm}(x,y)$$

where the range of the summation will vary depending on the characteristics of the basis functions and/or coefficients.

A complex Fourier series is one in which the basis functions are of the form

$$B_{nm}(x) = \exp(inx)\exp(imy)$$

where

$$\sum_n \sum_m \equiv \sum_{n=-\infty}^{\infty} \sum_{m=-\infty}^{\infty}.$$

The problem is then reduced to finding the coefficients c_{nm}. This series is basic to all Fourier theory and is used to model signals and images which are periodic. Let us first consider a periodicity of 2π where $-\pi \leq x \leq \pi$ and $-\pi \leq y \leq \pi$. To find the coefficients c_{nm}, we multiply both sides of the equation

$$f(x,y) = \sum_n \sum_m c_{nm} \exp(inx) \exp(imy)$$

by $\exp(-ipx)\exp(-iqy)$ and integrate over x and y from $-\pi$ to π giving

$$\int_{-\pi}^{\pi} \int_{-\pi}^{\pi} f(x,y) \exp(-ipx) \exp(-iqy) dxdy$$

$$= \sum_n \sum_m c_{nm} \int_{-\pi}^{\pi} \exp[i(n-p)x] dx \int_{-\pi}^{\pi} \exp[i(m-q)y] dy.$$

The integral on the RHS is given by

$$(2\pi)^2 \frac{\sin \pi(n-p)}{\pi(n-p)} \frac{\sin \pi(m-q)}{\pi(m-q)} = \begin{cases} (2\pi)^2, & n = p \quad \text{and} \quad m = q; \\ 0, & \text{otherwise.} \end{cases}$$

Thus, all terms on the RHS vanish except for the case when $n = p$ and $m = q$ and we can therefore write

$$c_{nm} = \frac{1}{(2\pi)^2} \int_{-\pi}^{\pi} \int_{-\pi}^{\pi} f(x,y) \exp(-inx) \exp(-imy) dxdy$$

which provides an expression for computing the coefficients of this particular series and has been derived by exploiting the orthogonality of the function $\exp(inx)\exp(imy)$.

In order to derive an expression for the coefficients c_{nm} in the case when $f(x,y)$ has a general period $2L$ say (i.e. $-L \leq x \leq L$; $-L \leq y \leq L$) we consider

$$f(x,y) = \sum_n \sum_m c_{nm} \exp(inx\pi/L) \exp(imy\pi/L).$$

As before, to find the coefficients c_{nm}, we multiply both sides of equation above by $\exp(-ipx\pi/L)\exp(-iqy\pi/L)$ and integrate over x and y from $-L$ to L, i.e.

$$\int_{-L}^{L} \int_{-L}^{L} f(x,y) \exp(-ipx\pi/L) \exp(-iqy\pi/L) dxdy$$

$$= \sum_n \sum_m c_{nm} \int_{-L}^{L} \int_{-L}^{L} \exp[i(n-p)x\pi/L] \exp[i(m-q)y\pi/L] dxdy.$$

The integral on the RHS is equal to

$$= (2L)^2 \frac{\sin \pi(n-p)}{\pi(n-p)} \frac{\sin \pi(m-q)}{\pi(m-q)} = \begin{cases} (2L)^2, & n = p \quad \text{and} \quad m = q; \\ 0, & \text{otherwise} \end{cases}$$

and all terms on the RHS vanish except for the case when $n = m$ and $p = q$ leaving us with the result

$$c_{nm} = \frac{1}{(2L)^2} \int_{-L}^{L} \int_{-L}^{L} f(x,y) \exp(-inx\pi/L) \exp(-imy\pi/L) dxdy.$$

Thus, the complex Fourier series for a 2D signal with a period of $2L$ is

$$f(x,y) = \sum_n \sum_m c_{nm} \exp(inx\pi/L) \exp(imy\pi/L)$$

where

$$c_{nm} = \frac{1}{(2L)^2} \int_{-L}^{L} \int_{-L}^{L} f(x,y) \exp(-inx\pi/L) \exp(-imy\pi/L) dxdy.$$

Having derived an expression for the 2D complex Fourier series, let us now consider a specific example by computing the series for a 2D 'square wave' signal with a period of 2π, i.e.

$$f(x,y) = f_x(x) f_y(y)$$

where

$$f_x(x) = \begin{cases} -1, & -\pi \leq x < 0; \\ 1, & 0 \leq x \leq \pi. \end{cases}$$

$$f_y(y) = \begin{cases} -1, & -\pi \leq y < 0; \\ 1, & 0 \leq y \leq \pi. \end{cases}$$

and

$$f(x + 2\pi, y + 2\pi) = f(x,y).$$

The complex Fourier coefficients are given by

$$c_{nm} = \frac{1}{2\pi} \int_{-\pi}^{\pi} f_x(x) \exp(-inx) dx \frac{1}{2\pi} \int_{-\pi}^{\pi} f_y(y) \exp(-imy) dy$$

and computing the integral over $f_x(x)$ gives

$$-\frac{1}{2\pi} \int_{-\pi}^{0} \exp(-inx) dx + \frac{1}{2\pi} \int_{0}^{\pi} \exp(-inx) dx$$

$$= \frac{1}{in\pi}[1 - \cos(n\pi)] = \frac{1}{in\pi}[1 - (-1)^n].$$

The integral over $f_y(y)$ is of same form and thus,

$$c_{nm} = \frac{1}{in\pi}[1 - (-1)^n]\frac{1}{im\pi}[1 - (-1)^m]$$

and

$$f(x,y) = \left(\sum_n \frac{1}{n\pi}[1 - (-1)^n]\sin(nx) - i\sum_n \frac{1}{n\pi}[1 - (-1)^n]\cos(nx)\right)$$

$$\times \left(\sum_m \frac{1}{m\pi}[1 - (-1)^m \sin(my) - i\sum_m \frac{1}{n\pi}[1 - (-1)^m \cos(my)\right)$$

$$= \sum_{n=1}^{\infty} \frac{2}{n\pi}[1 - (-1)^n]\sin(nx) \sum_{m=1}^{\infty} \frac{2}{m\pi}[1 - (-1)^m]\sin(my)$$

$$= \frac{16}{\pi^2}\left(\sin x + \frac{\sin 3x}{3} + \frac{\sin 5x}{5} + ...\right)\left(\sin y + \frac{\sin 3y}{3} + \frac{\sin 5y}{5} + ...\right).$$

Note that the series has 'zeros' when $x = 0, \pm\pi$ and when $y = 0, \pm\pi$ where $f(x,y)$ is discontinuous. The term $\frac{16}{\pi^2}\sin x \sin y$ is the 'fundamental' and the other terms are the 'harmonics'. We need many harmonics (i.e. terms in the series) to obtain a good fit to the discontinuities associated with the 2D square wave signal (i.e. the 'sharp corners'). In other words, the Fourier series representation of an 'on-off' type signal such as a square wave requires many terms to represent it accurately. Truncation of the series leads to 'ringing' in which $f(x,y)$ is approximated by a function that is dominated by the sinusoidal characteristics of the series. The generalization of this effect is called the Gibbs' phenomenon. As a general rule of thumb (a rule that is important in all aspect of image processing) discontinuous or 'sharp' features in a image (e.g. a high definition line) require many Fourier coefficients to be represented accurately whereas smooth features in an image require fewer Fourier coefficients. Hence, one way of smoothing an image is to reduce the number of Fourier coefficients used to represent it. This is the basis for low pass filtering.

2.2 The 2D Delta Function

In two dimensions, the delta function may be defined and used in the same way as the delta function in 1D which is discussed extensively in Blackledge J M, *Digital Signal Processing*, Horwood, 2003 (Chapter 2). In order to distinguish between different dimensions, it is common to label the 2D delta function with the superscript 2. Similarly, the superscript 3 is used to denote a 3D delta function. The dimension of any position vector associated with the delta function is then inferred from the value of this superscript. Further, the 2D delta function is a separable function and in Cartesian coordinates, we can written as

$$\delta^2(\mathbf{r} - \mathbf{r}_0) = \delta(x - x_0)\delta(y - y_0)$$

where

$$\mathbf{r} = \hat{\mathbf{x}}x + \hat{\mathbf{y}}y, \quad \mathbf{r}_0 = \hat{\mathbf{x}}x_0 + \hat{\mathbf{y}}y_0$$

and $\hat{\mathbf{x}}$ and $\hat{\mathbf{y}}$ are unit vectors pointing in the x and y directions, respectively. In 3D, we have

$$\delta^3(\mathbf{r} - \mathbf{r}_0) = \delta(x - x_0)\delta(y - y_0)\delta(z - z_0)$$

where

$$\mathbf{r} = \hat{\mathbf{x}}x + \hat{\mathbf{y}}y + \hat{\mathbf{z}}z$$

and

$$\mathbf{r}_0 = \hat{\mathbf{x}}x_0 + \hat{\mathbf{y}}y_0 + \hat{\mathbf{z}}z_0.$$

The 2D delta function may be defined (symbolically) as the function

$$\delta^2(\mathbf{r} - \mathbf{r}_0) = \begin{cases} 0, & \mathbf{r} \neq \mathbf{r}_0; \\ \infty, & \mathbf{r} = \mathbf{r}_0 \end{cases}$$

for which (fundamental property and strictly consistent definition)

$$\int_{-\infty}^{\infty} f(\mathbf{r})\delta^2(\mathbf{r} - \mathbf{r}_0)d^2\mathbf{r} = f(\mathbf{r}_0).$$

If S defines a 2D finite region of space (i.e. a surface), then

$$\int_S f(\mathbf{r})\delta^2(\mathbf{r} - \mathbf{r}_0)d^2\mathbf{r} = f(\mathbf{r}_0), \quad \mathbf{r}_0 \in S$$

where $\in$ signifies that the position vector $\mathbf{r}_0$ is 'in' the region of space denoted by S. If $\mathbf{r}_0$ is 'not in' S (the notation for this statement being $\mathbf{r}_0 \notin S$), then the above integral in zero, i.e.

$$\int_S f(\mathbf{r})\delta^2(\mathbf{r} - \mathbf{r}_0)d^2\mathbf{r} = 0, \quad \mathbf{r}_0 \notin S.$$

Because the delta function is so highly discontinuous and is not a 'proper function', it is often useful to define it in terms of the limit of a continuous or 'proper' function. A number of 'auxiliary functions' can be used for this purpose. However, there is one function that is particularly important in this respect and in the theory of signal and image processing in general, namely, the sinc function given by [1]

$$\text{sinc}(x) = \frac{\sin(x)}{x}.$$

Using the sinc function, we can construct the following auxiliary function:

$$\delta(X, x) = \frac{X}{\pi}\,\text{sinc}(Xx)$$

[1] Some authors define $\text{sinc}(x) = \text{sinc}(\pi x)/(\pi x)$

where $X > 0$ is a constant. This function has its maximum value at $x = 0$ where $\text{sinc}(0) = 1$ and $\delta(X, x) = X/\pi$. As the value of X increases, the sinc function contracts (its 'first zeros' that occur when $x = \pm\pi/X$ move toward the origin at $x = 0$ as X increases in value) and the value or amplitude of $\delta(X, x)$ increases. Eventually, as X approaches infinity, we can 'imagine' that the sinc function contracts to a single spike at $x = 0$ (at least within the resolving power of our imagination!) where $\delta(X, x)$ is infinitely large. Hence, we can consider the result

$$\delta(x) = \lim_{X\to\infty} \delta(X, x)$$

and on noting that

$$\delta(X, x) = \frac{1}{2\pi} \int_{-X}^{X} \exp(ikx)dk,$$

we have

$$\delta(x) = \frac{1}{2\pi} \int_{-\infty}^{\infty} \exp(ikx)dk.$$

This is the integral representation for a delta function. In 2D, we have

$$\delta(x)\delta(y) = \frac{1}{(2\pi)^2} \int_{-\infty}^{\infty} \exp(ik_x x)dk_x \int_{-\infty}^{\infty} \exp(ik_y y)dk_y$$

or alternatively, using vector notation

$$\delta^2(\mathbf{r}) = \frac{1}{(2\pi)^2} \int_{-\infty}^{\infty} \exp(i\mathbf{k}\cdot\mathbf{r})d^2\mathbf{r}$$

where

$$\mathbf{k} = \hat{\mathbf{x}}k_x + \hat{\mathbf{y}}k_y.$$

Similarly, in 3D, we have

$$\delta^3(\mathbf{r}) = \frac{1}{(2\pi)^3} \int_{-\infty}^{\infty} \exp(i\mathbf{k}\cdot\mathbf{r})d^3\mathbf{r}$$

where

$$\mathbf{k} = \hat{\mathbf{x}}k_x + \hat{\mathbf{y}}k_y + \hat{\mathbf{z}}k_z.$$

In terms of a 'physical picture' for the delta function, the contraction of a sinc-based auxiliary function to an infinitely high and infinitely thin spike is adequate. However, mathematically it is still unsatisfactory because we are 'imagining' the contraction of a continuous function to a discontinuous function. In other words, the limit

$$\delta(x) = \lim_{X\to\infty} \delta(X, x)$$

does not actually define a function with the properties of the δ-function. Instead, we should consider the result

$$\lim_{X\to\infty} \int_{-\infty}^{\infty} \delta(X,x) f(x) dx = \int_{-\infty}^{\infty} \delta(x-x_0) f(x) dx = f(x_0).$$

In other words, the whole problem is overcome if we recognize the generalized shifting or sampling property of the delta function, i.e.

$$\int_{-\infty}^{\infty} f(\mathbf{r}) \delta^n(\mathbf{r}-\mathbf{r}_0) d^n\mathbf{r} = f(\mathbf{r}_0), \quad n = 1,2,3$$

to be a fundamental result, rather than attempting to define the delta function itself. In other words, we define the delta function in terms of the role that it plays in a mathematical operation rather than in terms of what it actually is. Thus, one should always bear in mind that, strictly speaking, the delta function is not really a function even though it is referred to as one and can be written as one using the notation δ. It is actually just one of infinitely many different distributions. However, its shifting property is unique and this is the principal reason why it has such a wide range of applications.

2.3 The 2D Fourier Transform

If we let $c_{nm} = F_{nm}/(2L)^2$, then the complex Fourier series can be written as

$$f(x,y) = \frac{1}{(2L)^2} \sum_n \sum_m F_{nm} \exp(inx\pi/L) \exp(iny\pi/L)$$

where

$$F_{nm} = \int_{-L}^{L} \int_{-L}^{L} f(x,y) \exp(-inx\pi/L) \exp(-imy\pi/L) dxdy.$$

Now, let $k_n = n\pi/L, \quad k_m = m\pi/L$ and $\Delta k_n = \pi/L$ and $\Delta k_m = \pi/L$ so that we can write

$$f(x,y) = \frac{1}{(2\pi)^2} \sum_n \sum_m F_{nm} \exp(ik_n x) \exp(ik_m y) \Delta k_n \Delta k_m,$$

$$F_{nm} = \int_{-L}^{L} \int_{-L}^{L} f(x,y) \exp(-ik_n x) \exp(-ik_m y) dxdy.$$

Then, in the limit as $L \to \infty$, we have

$$f(x,y) = \frac{1}{(2\pi)^2} \int_{-\infty}^{\infty} \int_{-\infty}^{\infty} F(k_x,k_y) \exp(ik_x x) \exp(ik_y y) dk_x dk_y$$

$$F(k_x, k_y) = \int_{-\infty}^{\infty} \int_{-\infty}^{\infty} f(x, y) \exp(-ik_x x) \exp(-ik_y y) dx dy.$$

Here, $F(k_x, k_y)$ is the 2D Fourier transform of $f(x, y)$ where f is a non-periodic function (i.e. a function where $-\infty < x < \infty, \quad -\infty < y < \infty$). Using vector notation, where

$$\mathbf{r} = \hat{\mathbf{x}}x + \hat{\mathbf{y}}y \quad \text{and} \quad \mathbf{k} = \hat{\mathbf{x}}k_x + \hat{\mathbf{y}}k_y,$$

the 2D Fourier transform can be written as

$$F(\mathbf{k}) = \hat{F}_2[f(\mathbf{r})] = \int_{-\infty}^{\infty} f(\mathbf{r}) \exp(-i\mathbf{k} \cdot \mathbf{r}) d^2\mathbf{r}$$

where $\hat{F}_2$ denotes the 2D Fourier transform operator. The parameters k_x and k_y are the spatial frequencies of the function (in cycles per metre). Observe that in Cartesian coordinates, the Fourier transform of a two-dimensional function can be obtained by generating the one-dimensional transform in x and y separately, i.e.

$$F(k_x, k_y) = \int_{-\infty}^{\infty} f(x, k_y) \exp(-ik_x x) dx = \int_{-\infty}^{\infty} f(k_x, y) \exp(-ik_y y) dy.$$

Hence, if $f(x, y)$ is separable so that we can write

$$f(x, y) = f_1(x) f_2(y)$$

then the Fourier transform is also separable, i.e.

$$F(k_x, k_y) = F_1(k_x) F_2(k_y).$$

The inverse Fourier transform in 2D can be derived by multiplying $F(\mathbf{k})$ by $\exp(i\mathbf{k} \cdot \mathbf{r}')$ and integrating over $\mathbf{k}$, giving

$$\int_{-\infty}^{\infty} F(\mathbf{k}) \exp(i\mathbf{k} \cdot \mathbf{r}') d^2\mathbf{k} = \int_{-\infty}^{\infty} d^2\mathbf{r} f(\mathbf{r}) \int_{-\infty}^{\infty} \exp[i\mathbf{k} \cdot (\mathbf{r}' - \mathbf{r})] d^2\mathbf{k}$$

$$= \int_{-\infty}^{\infty} d^2\mathbf{r} f(\mathbf{r}) (2\pi)^2 \delta^2(\mathbf{r}' - \mathbf{r}) = (2\pi)^2 f(\mathbf{r}')$$

where we have used the integral representation for the 2D delta function, i.e.

$$\delta^2(\mathbf{r}) = \frac{1}{(2\pi)^2} \int_{-\infty}^{\infty} \exp(i\mathbf{k} \cdot \mathbf{r}) d^2\mathbf{k}$$

and the sampling property of the delta function, namely

$$\int_{-\infty}^{\infty} f(\mathbf{r}) \delta^2(\mathbf{r}' - \mathbf{r}) d^2\mathbf{r} = f(\mathbf{r}').$$

Hence,

$$f(\mathbf{r}) = \hat{F}_2^{-1}[F(\mathbf{k})] = \frac{1}{(2\pi)^2} \int_{-\infty}^{\infty} F(\mathbf{k}) \exp(i\mathbf{k} \cdot \mathbf{r}) d^2\mathbf{k}$$

where $\hat{F}_2^{-1}$ denotes the inverse 2D Fourier transform.

2.4 Physical Representation

The Fourier transform of a function provides a physical representation of the frequency content of the function. From a mathematical point of view, any basis function can, in principle, be used to define a series as can the kernel of an integral transform - depending upon its use. What makes the Fourier transform so important is that it 'reflects' the way in which wavefields arise in nature, i.e. from the linear superposition of cosinusoidal waves of different amplitude and frequency. With regard to the transform

$$F(k_x, k_y) = \int_{-\infty}^{\infty} \int_{-\infty}^{\infty} f(x, y) \exp(-ik_x x) \exp(-ik_y y) dx dy,$$

x and y are taken to be distances measured in metres and k_x and k_y are the spatial frequencies in cycles per metre. The independent variable $r = \sqrt{x^2 + y^2}$ is a measure of a point on the 2D plane from the centre of the plane. The variable $k = \sqrt{k_2^2 + k_y^2}$ is the wavenumber and is related to the wavelength λ of a wavefield by

$$k = \frac{2\pi}{\lambda}.$$

2.5 The Spectrum

The Fourier transform of a function defines its spectrum which can be written in the form

$$F(\mathbf{k}) = F_r(\mathbf{k}) + iF_i(\mathbf{k})$$

where $F_r = \mathrm{Re}[F]$ and $F_i = \mathrm{Im}[F]$. If, $f(\mathbf{r})$ is real, then

$$F_r(\mathbf{k}) = \int_{-\infty}^{\infty} f(\mathbf{r}) \cos(i\mathbf{k} \cdot \mathbf{r}) d^2\mathbf{r}$$

and

$$F_i(\mathbf{k}) = \int_{-\infty}^{\infty} f(\mathbf{r}) \sin(i\mathbf{k} \cdot \mathbf{r}) d^2\mathbf{r}.$$

The spectrum is therefore a complex function which can be written in the form

$$F(\mathbf{k}) = A(\mathbf{k}) \exp[i\theta(\mathbf{k})]$$

where

$$A(\mathbf{k}) =\mid F(\mathbf{k}) \mid= \sqrt{F_r^2 + F_i^2}$$

and

$$\theta(\mathbf{k}) = \tan^{-1}\left(\frac{F_i}{F_r}\right).$$

Here, F defines the Complex Spectrum, A is the Amplitude Spectrum, θ is the Phase Spectrum and

$$P(\mathbf{k}) =\mid F(\mathbf{k}) \mid^2$$

defines the so called Power Spectrum.

A special case occurs when $\mathbf{k} = \mathbf{0}$ and

$$F(\mathbf{0}) = \int_{-\infty}^{\infty} f(\mathbf{r}) d^2\mathbf{r}.$$

The value of F in this case is called DC (after Direct Current) or zero frequency value.

2.6 Definitions and Notation

There are two principal definitions of the 2D Fourier transform pair given by

$$F(\mathbf{k}) = \int_{-\infty}^{\infty} f(\mathbf{r}) \exp(-i\mathbf{k}\cdot\mathbf{r}) d^2\mathbf{r},$$

$$f(\mathbf{r}) = \frac{1}{(2\pi)^2} \int_{-\infty}^{\infty} F(\mathbf{k}) \exp(i\mathbf{k}\cdot\mathbf{r}) d^2\mathbf{k}$$

and

$$F(\mathbf{k}) = \frac{1}{2\pi} \int_{-\infty}^{\infty} f(\mathbf{r}) \exp(-i\mathbf{k}\cdot\mathbf{r}) d^2\mathbf{r},$$

$$f(\mathbf{r}) = \frac{1}{2\pi} \int_{-\infty}^{\infty} F(\mathbf{k}) \exp(i\mathbf{k}\cdot\mathbf{r}) d^2\mathbf{k}.$$

It is also a matter of convention that F is called the Fourier transform of f with $-i$ in the exponential and that f is the inverse Fourier transform of F with $+i$ in the exponential.

In general, if a function is denoted by some 'lower case' letter such as f, then the function obtained by taking its Fourier transform is denoted by the associated 'upper case' letter F. If a function is denoted by some upper case letter such as F, then the function obtained by taking its Fourier transform is denoted by introducing a 'tilde' $\widetilde{F}$.

Although ultimately a personal choice, in optics a kernel of the form $\exp(\pm 2\pi i \mathbf{u}\cdot\mathbf{r})$ is often used with the Fourier transform pair being given by

$$F(\mathbf{u}) = \int_{-\infty}^{\infty} \exp(-i2\pi\mathbf{u}\cdot\mathbf{r}) f(\mathbf{r}) d^2\mathbf{r},$$

$$f(\mathbf{r}) = \int_{-\infty}^{\infty} \exp(i2\pi\mathbf{u}\cdot\mathbf{r}) F(\mathbf{u}) d^2\mathbf{u}.$$

This is for the following reasons:

(i) Continued use is made of the wavenumber given by $2\pi/\lambda$, where λ is the wavelength of light, and, since it is common practice to express results in terms of the wavelength itself (rather than the wavenumber), the factor of 2π is unavoidable.

(ii) For the type of equations and functions that occur in optics, this kernel leads to results with less constants and factors of π.

(iii) The scaling symmetry of the forward and inverse Fourier transforms provided using this definition of the Fourier transform gives the best possible comparison with the Fourier transforming properties of a lens for example, i.e. the intensity of light passing through a lens is not scaled according the direction in which it travels through the lens.

However, in this text, the first definition of the Fourier transform pair is used throughout so that it can be applied in the study of different imaging systems including optics in a manner that is consistent.

To avoid constantly having to write Fourier integrals, it is common to make use of the symbolic form

$$f(\mathbf{r}) \Longleftrightarrow F(\mathbf{k})$$

which means that F is the Fourier transform of f and that f is the inverse Fourier transform of F. This notation is useful when we want to indicate the relationship between a process (defined by some mathematical operation) on f in 'real-space' or 'image- space' and the effect of this operation on F in 'Fourier-space' of '$\mathbf{k}$-space'. For example, the gradient of the function f is compounded in the relationship

$$\nabla f(\mathbf{r}) \Longleftrightarrow i\mathbf{k}F(\mathbf{k})$$

and the Laplacean of f yields

$$\nabla^2 f(\mathbf{r}) \Longleftrightarrow -k^2 F(\mathbf{k}).$$

2.7 Some Important Results

As with the 1D Fourier transform, there are a number of analytical results compounded in the computation of $F(\mathbf{k})$ given a function $f(\mathbf{r})$ for which there are a number of published tables. The difficulty or otherwise of these computations

usually depends on the functional complexity of $f(\mathbf{r})$. However, there are two important results which frequently occur in imaging and optics, for example, and are therefore provided here for the sake of completeness.

The 2D Fourier transform of a 'box' function

The box function is given by

$$f(x,y) = \begin{cases} 1, & \mid x \mid \leq \frac{a}{2} \quad \text{and} \quad \mid y \mid \leq \frac{b}{2}; \\ 0, & \text{otherwise.} \end{cases}$$

and

$$F(k_x,k_y) = \int_{-\frac{a}{2}}^{\frac{a}{2}} \exp(-2\pi i k_x x)dx \int_{\frac{b}{2}}^{-\frac{b}{2}} \exp(-2\pi i k_y y)dy$$

$$= ab\,\mathrm{sinc}(\pi k_x a)\,\mathrm{sinc}(\pi k_y b).$$

The 2D Fourier transform of a Gaussian function

The 2D Gaussian function can be defined as (ignoring scaling)

$$f(x,y) = \exp\left(-\frac{r^2}{a^2}\right), \quad \text{where} \quad r^2 = x^2 + y^2.$$

Then,

$$F(k_x,k_y) = \int_{-\infty}^{\infty} \exp\left(-\frac{x^2}{a^2}\right)\exp(-ik_x x)dx \int_{-\infty}^{\infty} \exp\left(-\frac{y^2}{a^2}\right)\exp(-ik_y y)dy$$

$$= \frac{\pi}{a}\exp(-k^2/4a), \quad \text{where} \quad k^2 = k_x^2 + k_y^2.$$

The 2D Fourier Transform of Rotationally Symmetric Functions

If the function $f(x,y)$ is rotationally symmetric, then we can write

$$f(x,y) \equiv f(r), \quad \text{where} \quad r = \sqrt{x^2+y^2}.$$

In this case, the 2D Fourier transform is also rotationally symmetric and can be written as a transform of a single variable; the result is known as the Hankel transform. Using polar coordinates:

$$x = r\cos\theta; \quad y = r\sin\theta; \quad k_x = k\cos\phi; \quad k_y = k\sin\phi$$

where

$$k = \sqrt{k_x^2 + k_y^2}.$$

We can then write

$$F(\omega,\phi) = \int_0^\infty \int_{-\pi}^{\pi} f(r)\exp[-ikr(\cos\theta\cos\phi + \sin\theta\sin\phi)]d\theta r dr$$

$$= \int_0^\infty \left(\int_{-\pi}^{\pi} \exp[-ikr\cos(\theta-\phi)]d\theta \right) f(r) r dr.$$

The integral in the brackets can be written as

$$\int_{-\pi}^{\pi} \exp[-ikr\cos(\theta-\phi)]d\theta = 2\pi J_0(kr)$$

where J_0 is the zero order Bessel function of the first kind. Hence

$$F(k) = 2\pi \int_0^\infty f(r) J_0(kr) r dr$$

This integral transform is a (zero-order) Hankel or Fourier-Bessel transform. Note that if

$$f(r) = \delta(r-a)$$

where δ is a delta function, then

$$F(k) = 2\pi a J_0(ka),$$

i.e. the 2D Fourier transform of an 'infinitely thin ring' is given by the zero order Bessel function (ignoring scaling constants).

An important result which will be used later in this work is the 2D Fourier transform of the 2D 'tophat' or 'circular disc' function given by

$$f(r) = \begin{cases} 1, & r \le a; \\ 0, & \text{otherwise.} \end{cases}$$

In this case,

$$F(k) = 2\pi \int_0^a J_0(kr) r dr.$$

Let

$$\xi = kr \quad \text{and} \quad r = \frac{\xi}{k},$$

then

$$F(k) = \frac{2\pi}{k^2} \int_0^{ka} J_0(\xi)\xi d\xi.$$

Now,

$$\int_0^x J_0(\xi)\xi d\xi = xJ_1(x)$$

where J_1 is the first order Bessel function of the first kind. Hence,

$$F(k) = \frac{2\pi}{k^2} kaJ_1(ka) = \frac{2\pi a}{k} J_1(ka)$$

or

$$F(k) = 2\pi a^2 \left(\frac{J_1(ka)}{ka}\right)$$

The function $J_1(x)/x$ is the 'jinc' function which, in image processing, plays an equivalent role to the sinc function in signal processing. Note that at $k = 0$, $F(k) = 2\pi a^2$. The function is a circularly symmetric spectrum composed of a central lobe surrounded by a sequence of concentric rings separated by the positions at which the Bessel function approaches zero. The pattern is a well known result of Fraunhofer diffraction theory. The square modulus of $F(k)$ describes the intensity pattern produced by the diffraction of light by a circular aperture under the assumption that the thickness of the aperture is much smaller than the wavelength of light. This result was first derived by the Astronomer Royal, George Airy, in 1835.

2.8 Some Important Theorems

The following collection of results are important in the Fourier analysis of images and are listed here for completeness with regard to later work.

The Addition Theorem

$$f(\mathbf{r}) + g(\mathbf{r}) \Longleftrightarrow F(\mathbf{k}) + G(\mathbf{k})$$

The Similarity Theorem

$$f(a\mathbf{r}) \Longleftrightarrow \frac{1}{a} F\left(\frac{\mathbf{k}}{a}\right), \quad a > 0$$

where a is a constant.

The Shift Theorem

$$f(\mathbf{r} - \mathbf{a}) \Longleftrightarrow \exp(-i\mathbf{k} \cdot \mathbf{a}) F(\mathbf{k})$$

Parseval's Theorem

$$\int_{-\infty}^{\infty} f(\mathbf{r}) g^*(\mathbf{r}) d^2\mathbf{r} = \frac{1}{(2\pi)^2} \int_{-\infty}^{\infty} F(\mathbf{k}) G^*(\mathbf{k}) d^2\mathbf{k}$$

2.9 Convolution and Correlation

The convolution process and the convolution theorem are absolutely fundamental to the theory of imaging and image processing in general. In 1D, the convolution integral is defined as

$$f(x) \otimes g(x) = \int_{-\infty}^{\infty} f(y)g(x-y)dy$$

where the symbol $\otimes$ is taken to denote the convolution integral given above. Note that some authors write the RHS of the above equation as $(f \otimes g)(x)$ to stress that the convolution operation produces an output that is a function of x. In 2D, we have

$$f(\mathbf{r}) \otimes \otimes g(\mathbf{r}) = \int_{-\infty}^{\infty} f(\mathbf{r}')g(\mathbf{r}-\mathbf{r}')d^2\mathbf{r}'$$

where the symbol $\otimes\otimes$ denotes the 2D convolution integral. Similarly, the correlation integral - which is also known as cross-correlation - of two 2D functions f and g is defined by the operation

$$f(\mathbf{r}) \odot \odot g(\mathbf{r}) = \int_{-\infty}^{\infty} f(\mathbf{r}')g(\mathbf{r}'-\mathbf{r})d^2\mathbf{r}'.$$

This is a very similar operation to convolution except that the function g is not reversed (i.e. g is a function of $\mathbf{r}'-\mathbf{r}$ and not $\mathbf{r}-\mathbf{r}'$). Note that for real functions f and g,

$$f(\mathbf{r}) \otimes \otimes g(\mathbf{r}) = f(\mathbf{r}) \odot \odot g(-\mathbf{r}).$$

Physically, the convolution process describes the 'blurring' or 'smearing' of one function by another. Convolution integrals arise in a wide range of applications. They are fundamental to the description of images and image formation. As shall be shown later on in this work, the Green function is fundamental to modelling image formation processes because of its ability to provides a completely general solution to a variety of inhomogeneous wave equations, a solution that is compounded in the convolution integral. Further, an important component of image processing is often concerned with solving an inverse problem known as deconvolution which is the inverse of deconvolution and forms the basis for image restoration and reconstruction techniques.

2.10 Convolution and Correlation Theorems

2.10.1 The Convolution Theorem

The convolution theorem (together with related theorems) is one of the most important results of Fourier theory which is that the convolution of two func-

tions in real space is the same as the product of their respective Fourier transforms in Fourier space, i.e.

$$f(\mathbf{r}) \otimes \otimes g(\mathbf{r}) \Longleftrightarrow F(\mathbf{k})G(\mathbf{k}).$$

This theorem is sometimes referred to as the Faltung theorem from the German word 'Faltung' meaning 'folding'. The theorem also holds (apart from scaling), if the roles are reversed, i.e. the convolution of two complex spectra in Fourier space is equal to the product of these functions in real space or

$$f(\mathbf{r})g(\mathbf{r}) \Longleftrightarrow \frac{1}{(2\pi)^2} F(\mathbf{k}) \otimes G(\mathbf{k}).$$

This result is known as the product theorem.

2.10.2 The Correlation Theorem

In the case of the correlation integral, the correlation theorem takes the form

$$f(\mathbf{r}) \odot \odot g(\mathbf{r}) \Longleftrightarrow F(\mathbf{k})G^*(\mathbf{k}).$$

Note that this result implies that

$$f(\mathbf{r}) \odot \odot g(\mathbf{r}) \neq g(\mathbf{r}) \odot \odot f(\mathbf{r})$$

since

$$F(\mathbf{k})G^*(\mathbf{k}) \neq F^*(\mathbf{k})G(\mathbf{k}).$$

Also note that if $g = f$ then we arrive at the autocorrelation theorem, i.e.

$$f(\mathbf{r}) \odot \odot f(\mathbf{r}) \Longleftrightarrow \mid F(\mathbf{k}) \mid^2 .$$

This theorem has a unique feature which is that information about the phase of F is missing from the power spectrum $\mid F \mid^2$, in contrast to the autoconvolution integral in which

$$f(\mathbf{r}) \otimes \otimes f(\mathbf{r}) \Longleftrightarrow [F(\mathbf{k})]^2$$

where information on the phase spectrum is retained. Hence, the correlation of a function f with itself contains no information about the phase of the Fourier components of f, and is consequently unchanged if the phase changes.

2.10.3 Some Important Properties

There are some particularly important properties of the convolution integral, all of which can be derived using the convolution theorem. They are as follows:

Convolution is commutative

$$f \otimes \otimes g = g \otimes \otimes f$$

Convolution is associative

$$f \otimes \otimes (g \otimes \otimes h) = (f \otimes \otimes g) \otimes \otimes h$$

Multiple convolutions can therefore be carried out in any order.

Convolution is distributive

$$f \otimes\otimes (g + h) = f \otimes\otimes g + f \otimes\otimes h$$

The derivative of a convolution is

$$\nabla(f \otimes\otimes g) = f \otimes\otimes \nabla g = g \otimes\otimes \nabla f$$

The Laplacian of a convolution is

$$\nabla^2(f \otimes\otimes g) = f \otimes\otimes \nabla^2 g = g \otimes\otimes \nabla^2 f$$

2.11 Other Integral Transforms

An integral transform $F(u)$ of a function $f(x)$ has the general form

$$F(u) = \int f(x)K(x, u)dx$$

where K is the kernel. The Fourier and Hankel (Fourier-Bessel) transforms discussed so far are just special cases of this general form.

2.11.1 The Fresnel Transform

Another integral transform which is discussed in this work (in the study on 'Fresnel diffraction') is the Fresnel transform given by

$$F(x) = \int_{-\infty}^{\infty} f(x') \exp[ik(x - x')^2]dx'$$

where k is a real constant. The inverse relationship is

$$f(x') = \int_{-\infty}^{\infty} F(x) \exp[-ik(x - x')^2]dx.$$

2.11.2 The Abel Transform

The Abel transform is given by

$$F(x) = 2 \int_{x}^{\infty} \frac{f(r)rdr}{(r^2 - x^2)^{\frac{1}{2}}}$$

where typically, x is a rectangular coordinate and r is a radial coordinate. This transform is a special case (the case when f is radially symmetric) of the Radon transform

$$F(r, \theta) = \int_{-\infty}^{\infty} f(r)\delta(r - x\cos\theta - y\sin\theta)dxdy$$

which forms the theoretical basis for a method of imaging called projection tomography and is discussed later on in this work. The inverse Abel transform is

$$f(r) = -\frac{1}{\pi}\int_r^\infty \frac{1}{(x^2-r^2)^{\frac{1}{2}}}\frac{dF(x)}{dx}dx.$$

2.12 Discussion

As with signal processing, there are a number of different integral transforms that are used to process images. These transforms are often compounded in terms of some filter or sequential filter processes. However, there are some transforms such as the Hankel, Fresnel, Radon and Abel transforms that are unique to image processing. Equally so, there are transforms and filters that are usually only applicable for processing signals and/or signal analysis, e.g. the z-transform and the Infinite Impulse Response (IIR) filter[2]. The IIR filter is not of any significance in image processing. This is because images are rarely, if ever, formed from some 'feed-back' process. Whereas in some signal analysis problems, initial conditions are applicable, leading to applications of the Laplace transform for example, in image analysis, initial conditions are not relevant. Thus, some integral transforms are specific only to signal analysis or image analysis but not both. Those transforms which do apply to both include the Fourier transform, the cosine transform (used in image compression for example), the wavelet transform (multi-resolution analysis) and of course, the convolution and correlation integrals. As integral transforms, they are applied in the development of image analysis models and in discrete form, they provide a range of image processing algorithms. However, as in signal analysis, of all the transforms available, the Fourier transform provides us with the principal link between methods of processing an image and the 'physics' through which the image has been generated and the information it coveys. In this sense, the Fourier transform 'reigns supreme'.

2.13 Summary of Important Results

2D complex Fourier series

$$f(x,y) = \sum_n \sum_m c_{nm} \exp(inx\pi/L)\exp(imy\pi/L)$$

where

$$c_{nm} = \frac{1}{(2L)^2}\int_{-L}^{L}\int_{-L}^{L} f(x,y)\exp(-inx\pi/L)\exp(-imy\pi/L)dxdy.$$

[2]see Blackledge J M, *Digital Signal Processing*, Horwood, 2003.

2D Fourier transform pair

$$F(k_x, k_y) = \int_{-\infty}^{\infty}\int_{-\infty}^{\infty} f(x,y)\exp(-ik_x x)\exp(-ik_y y)dxdy,$$

$$f(x,y) = \frac{1}{(2\pi)^2}\int_{-\infty}^{\infty}\int_{-\infty}^{\infty} F(k_x, k_y)\exp(ik_x x)\exp(ik_y y)dk_x dk_y.$$

Integral representation of the 2D delta function

$$\delta^2(\mathbf{r}) \equiv \delta(x)\delta(y) = \frac{1}{(2\pi)^2}\int_{-\infty}^{\infty}\exp(i\mathbf{k}\cdot\mathbf{r})d^2\mathbf{k}$$

The convolution integral

$$f(\mathbf{r}) \otimes \otimes g(\mathbf{r}) = \int_{-\infty}^{\infty} f(\mathbf{r}')g(\mathbf{r}-\mathbf{r}')d^2\mathbf{r}'$$

The correlation integral

$$f(\mathbf{r}) \odot \odot g(\mathbf{r}) = \int_{-\infty}^{\infty} f(\mathbf{r}')g(\mathbf{r}'-\mathbf{r})d^2\mathbf{r}'$$

The convolution theorem

$$f(\mathbf{r}) \otimes \otimes g(\mathbf{r}) \Longleftrightarrow F(\mathbf{k})G(\mathbf{k})$$

The correlation theorem

$$f(\mathbf{r}) \odot \odot g(\mathbf{r}) \Longleftrightarrow F(\mathbf{k})G^*(\mathbf{k})$$

The autocorrelation theorem

$$f(\mathbf{r}) \odot \odot f(\mathbf{r}) \Longleftrightarrow \mid F(\mathbf{k}) \mid^2$$

2.14 Further Reading

- Lighthill M J, *An Introduction to Fourier Analysis and Generalized Functions*, Cambridge University Press, 1960.
- Papoulis A, *The Fourier Integral and its Applications*, McGraw-Hill, 1962.
- Bracewell R N, *The Fourier Transform and its Applications*, McGraw-Hill, 1978.
- Dudgeon D E and Mersereau R M, *Multidimensional Digital Signal Processing*, Prentice-Hall, 1983.
- Gonzalez R C and Wintz P, *Digital Image Processing*, Addison-Wesley, 1987.
- Lim J S, *Two-dimensional Signal and Image Processing*, Prentice-Hall, 1990.
- Kraniauskas P, *Transforms in Signals and Systems*, Addison-Wesley, 1992.

Chapter 3

The 2D DFT, FFT and FIR Filter

The application of Fourier theory to processing digital images requires that the 2D Fourier integral is discretized and algorithms designed that make explicit use of the Discrete Fourier Transform (DFT). In this Chapter, we review the DFT and the Fast Fourier Transform (FFT) which provides a method for computing the DFT with less multiplications and additions than required when computing a DFT directly. This chapter also discusses the computational background to the Finite Impulse Response (FIR) filter which is, in effect, a discrete convolution or convolution sum.

3.1 The Discrete Fourier Transform

The complex Fourier series is given by

$$f(x,y) = \frac{1}{(2L)^2} \sum_n \sum_m F_{nm} \exp(inx\pi/L) \exp(imy\pi/L)$$

where

$$F_{nm} = \int_{-L}^{L} \int_{-L}^{L} f(x,y) \exp(-inx\pi/L) \exp(-imy\pi/L) dxdy$$

over the range $[-L, L]$. Consider the case where $f(x,y)$ is uniformly sampled at points $x_{00}, x_{01}, x_{02}, ..., x_{0(N-1)}$; $x_{10}, x_{11}, x_{12}, ..., x_{1(N-1)}$ etc. giving the discrete function or 2D vector (a matrix)

$$f_{pq} \equiv f(x_p, y_q); \quad p = 0, 1, 2, ..., N-1; \quad q = 0, 1, 2, ..., N-1$$

with sampling intervals Δx and Δy. Now, $x_p = p\Delta x$, $y_q = q\Delta y$ and with $N = 2L/\Delta x = 2L/\Delta y$ we have[1]

$$f_{pq} = \frac{1}{N^2} \sum_n \sum_m F_{nm} \exp(i2\pi np/N) \exp(i2\pi mq/N)$$

[1] with $f_{pq} \equiv f_{pq}/(\Delta x \Delta y)$ and $F_{nm} \equiv F_{nm}/(\Delta x \Delta y)$

and

$$F_{nm} = \sum_p \sum_q f_{pq} \exp(-i2\pi np/N) \exp(-i2\pi mq/N)$$

where the summations are over N points, i.e.

$$\sum_n \sum_m \equiv \sum_{n=0}^{N-1} \sum_{m=0}^{N-1}$$

providing the 'standard form' of the transform in which the first value of the 2D array F_{nm} occurs at F_{00}. This is the the so called DC level which corresponds to the zero frequency component. This transform, can also be cast in terms of its 'optical form' where

$$\sum_n \sum_m \equiv \sum_{n=-N/2}^{(N/2)-1} \sum_{m=-N/2}^{(N/2)-1}.$$

Here, the DC level occurs at the centre of the array F_{nm}, i.e. at the point $(N/2{+}1, \quad N/2{+}1)$. The optical form of the DFT produces a more familiar form of output which places the zero frequency component in the centre of the plane. This type of output is usually referred to as the 'optical form' because this is the way a spectrum is produced optically (e.g. an optical diffraction pattern). It is consistent with analysis undertaken using the Fourier transform and is also consistent with the use of the discrete Fourier transform for simulating optical systems in which a lens (which can be taken to perform a Fourier transform) generates a spectrum in the 'image plane' where the DC level or zero frequency occurs in the centre of the plane. The difference between the standard and optical forms does not present any particular problem because placing the zero frequency component in the center of the array can be achieved by a simple rearrangement or 'shift' of the output of a DFT computed using the standard form.

The Fourier transform pair is given by

$$F(k_x, k_y) = \int_{-\infty}^{\infty} \int_{-\infty}^{\infty} f(x, y) \exp(-ik_x x) \exp(-ik_y y) dx dy,$$

$$f(x, y) = \frac{1}{(2\pi)^2} \int_{-\infty}^{\infty} \int_{-\infty}^{\infty} F(k_x, k_y) \exp(ik_x x) \exp(ik_y y) dk_x dk_y$$

and the discrete Fourier transform pair is given by

$$F_{nm} = \sum_p \sum_q f_{pq} \exp(-i2\pi np/N) \exp(-i2\pi mq/N),$$

$$f_{pq} = \frac{1}{N^2} \sum_n \sum_m F_{nm} \exp(i2\pi np/N) \exp(i2\pi mq/N).$$

In order to establish the relationship between these transforms (one continuous and one discrete), we consider the discretization of the Fourier transform pair to obtain

$$F(k_n, k_m) = \sum_p \sum_q f(x_p, x_q) \exp(-ik_n x_p) \exp(-ik_m x_q) \Delta x \Delta y$$

$$f(x_p, y_q) = \frac{1}{(2\pi)^2} \sum_n \sum_m F(k_n, k_m) \exp(ik_n x_p) \exp(ik_m x_q) \Delta k_n \Delta k_m$$

where Δx, Δy, Δk_n and Δk_m are the sampling intervals. Now, with $k_n = n\Delta k_x$, $k_m = m\Delta k_y$, $x_p = p\Delta x$ and $y_q = q\Delta y$, by inspection (i.e. comparing the results above with the discrete Fourier transform pair) we see that

$$\Delta k_x \Delta x = \frac{2\pi}{N} \quad \text{and} \quad \Delta k_y \Delta y = \frac{2\pi}{N}.$$

Thus, in terms of the discrete Fourier transform, the interval Δk_x between the numbers F_{nm} (for constant n) is related to the interval Δx between the numbers f_{pq} (for constant p) by

$$\Delta k_x = \frac{2\pi}{N\Delta x}$$

and the interval Δk_y between the numbers F_{nm} (for constant m) is related to the interval Δy between the numbers f_{pq} (for constant q) by

$$\Delta k_y = \frac{2\pi}{N\Delta y}.$$

3.2 The Sampling Theorem

When a digital image is generated from an analogue image, an array of numbers is obtained which is assumed to be a accurate numerical representation of the original analogue image. The conversion is called digitization. When conversion takes place, it is a normally a requirement that all the information in the original analogue image is retained in digital form. To do this, the analogue image must be sampled at the correct rate. So what is the correct rate? The answer to this question is provided by the sampling theorem. In 2D, this theorem states that if $f(x, y)$ is bandlimited and has a complex spectrum $F(k_x, k_y)$, $\mid k_x \mid \leq K_x$, $\mid k_y \mid \leq K_y$, then it is fully specified by values spaced at regular intervals in the x- and y-directions given by

$$\Delta x \leq \frac{\pi}{K_x}, \quad \text{and} \quad \Delta y \leq \frac{\pi}{K_y}$$

respectively. The parameters K_x/π of K_y/π are the 'Nyquist frequencies'. If the bandwidth of the image is uniform and omni-directional, then the sampling interval in any direction is given by

$$\Delta \leq \frac{\pi}{K}$$

where

$$K = \sqrt{K_x^2 + K_y^2}.$$

To convert an analogue image into a digital image with no loss of information, one must choose a sampling rate that is at least equal to the Nyquist frequency of the image. To show why this is the case, the 2D 'comb function' must first be introduced. This function describes an array of delta functions which, in the Cartesian plane is given by

$$\text{comb}(x, y) = \sum_{n=-\infty}^{\infty} \sum_{m=-\infty}^{\infty} \delta(x - nX)\delta(y - mY).$$

Here, each delta function is taken to be equally spaced apart by a fixed length X in the x-direction and Y in the y-direction respectively.

The sampling a 2D function can be described mathematically by multiplying it by this comb function. Thus, if $f(x, y)$ is the bandlimited function and $g(x, y)$ is the sampling function, then we can write

$$g(x, y) = \text{comb}(x, y)f(x, y).$$

The sampling theorem is obtain by analyzing the spectrum of the sampling function $g(x, y)$. To do this, we are required to consider the Fourier transform of the 2D comb function.

3.2.1 Fourier Transform of the Comb Function

The evaluation of $\hat{F}_2[\text{comb}(x, y)]$ is important generally and is crucial to the proof of the sampling theorem to follow. Using the definition of $\text{comb}(x, y)$, we can write

$$\int_{-\infty}^{\infty} \int_{-\infty}^{\infty} \text{comb}(x, y) \exp(-ik_x x) \exp(-ik_y y) dx dy$$

$$= \int_{-\infty}^{\infty} \int_{-\infty}^{\infty} \sum_{n=-\infty}^{\infty} \sum_{m=-\infty}^{\infty} \delta(x - nX)\delta(y - mY) \exp(-ik_x x) \exp(-ik_y y) dx dy$$

$$= \sum_{n=-\infty}^{\infty} \sum_{m=-\infty}^{\infty} \int_{-\infty}^{\infty} \int_{-\infty}^{\infty} \delta(x - nX)\delta(y - mY) \exp(-ik_x x) \exp(-ik_y y) dx dy$$

$$= \sum_{n=-\infty}^{\infty} \sum_{m=-\infty}^{\infty} \exp(-ik_x nX) \exp(-ik_y mY).$$

Hence, using the product theorem, the spectrum of the product $\text{comb}(x, y)f(x, y)$ is given by

$$\frac{1}{(2\pi)^2} F(k_x, k_y) \otimes\otimes \sum_{n=-\infty}^{\infty} \sum_{m=-\infty}^{\infty} \exp(-ik_x nX) \exp(-ik_y mY).$$

Although valid, the above result is not in itself very useful. The 'key' to proving the sampling theorem comes from expressing $\text{comb}(x, y)$ as a complex Fourier series (not a transform). This can be done, because although a special case, the comb function is just a periodic function and, thus, a Fourier series representation can be used. Hence, we consider writing the comb function in terms of a complex Fourier series given by

$$\text{comb}(x, y) = \sum_{n=-\infty}^{\infty} \sum_{m=-\infty}^{\infty} c_{nm} \exp(i2\pi nx/X) \exp(i2\pi my/Y)$$

where the coefficients c_{nm} are obtained by computing the integral

$$c_{nm} = \frac{1}{XY} \int_{-X/2}^{X/2} \int_{-Y/2}^{Y/2} \text{comb}(x, y) \exp(-i2\pi nx/X) \exp(-2\pi my/Y) dxdy.$$

Substituting the definition for the comb function into the equation above and noting that $\text{comb}(x, y) = \delta(x)\delta(y)$ when $x \in [-X/2, X/2]$ and $y \in [-Y/2, Y/2]$, we get

$$c_{nm} = \frac{1}{XY} \int_{-X/2}^{X/2} \int_{-Y/2}^{Y/2} \delta(x)\delta(y) \exp(-i2\pi nx/X) \exp(-2i\pi my/Y) dxdy = \frac{1}{XY}.$$

Hence, we can represent the comb function by the complex Fourier series

$$\text{comb}(x, y) = \frac{1}{XY} \sum_{n=-\infty}^{\infty} \sum_{m=-\infty}^{\infty} \exp(i2\pi nx/X) \exp(i2\pi my/Y).$$

Consequently, the Fourier transform of the comb function can be written as

$$\int_{-\infty}^{\infty} \int_{-\infty}^{\infty} \frac{dxdy}{XY} \sum_{n=-\infty}^{\infty} \sum_{m=-\infty}^{\infty} \exp(i2\pi nx/X) \exp(i2\pi my/Y) \exp(-ik_x x) \exp(-ik_y y)$$

$$= \frac{1}{XY} \sum_{n=-\infty}^{\infty} \sum_{m=-\infty}^{\infty} \int_{-\infty}^{\infty} \int_{-\infty}^{\infty} \exp[-ix(k_x - 2\pi n/X)] \exp[-iy(k_y - 2\pi m/Y)] dxdy$$

$$= \frac{4\pi^2}{XY} \sum_{n=-\infty}^{\infty} \sum_{m=-\infty}^{\infty} \delta(k_x - 2\pi n/X)\delta(k_y - 2\pi m/Y).$$

We have therefore obtained the fundamental and important result (crucial to the proof of the sampling theorem)

$$\sum_{n=-\infty}^{\infty} \sum_{m=-\infty}^{\infty} \delta(x - nX)\delta(y - mY) \Longleftrightarrow$$

$$\frac{4\pi^2}{XY} \sum_{n=-\infty}^{\infty} \sum_{m=-\infty}^{\infty} \delta(k_x - 2\pi n/X)\delta(k_y - 2\pi m/Y).$$

3.2.2 Proof of the Sampling Theorem

Suppose we sample a 2D function at regular intervals (Δx, Δy). The sampling function $g(x, y)$ is then given by

$$g(x,y) = f(x,y) \sum_{n=-\infty}^{\infty} \sum_{m=-\infty}^{\infty} \delta(x - n\Delta x)\delta(y - m\Delta y).$$

Using the product theorem, in Fourier space, this equation becomes

$$G(k_x, k_y) = F(k_x, k_y) \otimes\otimes \frac{2\pi}{\Delta x}\frac{2\pi}{\Delta y} \sum_{n=-\infty}^{\infty} \sum_{m=-\infty}^{\infty} \delta(k_x - 2\pi n/\Delta x)\delta(k_y - 2\pi m/\Delta y)$$

$$= \frac{2\pi}{\Delta x}\frac{2\pi}{\Delta y} \sum_{n=-\infty}^{\infty} \sum_{m=-\infty}^{\infty} F(k_x - 2\pi n/\Delta x, k_y - 2\pi m/\Delta y).$$

This result demonstrates that sampling the function f, creates a new spectrum G which is a periodic replica of the spectrum F spaced at regular intervals $\pm 2\pi/\Delta x, \pm 4\pi/\Delta x, \pm 6\pi/\Delta x$ in the x-direction and $\pm 2\pi/\Delta y, \pm 4\pi/\Delta y, \pm 6\pi/\Delta y$ in the y-direction. Since F is a bandlimited function, the total width of the spectrum is $K_x - (-K_x) = 2K_x$ and $K_y - (-K_y) = 2K_y$ in the x- and y-directions respectively, i.e. the bandwidth of F. Thus, if $2\pi/\Delta x < 2K_x$, $2\pi/\Delta y < 2K_y$, then the replicated spectra will overlap leading to aliasing. To ensure that aliasing does not occur, we require that

$$\frac{2\pi}{\Delta x} \geq 2K_x, \quad \frac{2\pi}{\Delta y} \geq 2K_y$$

or a sampling rate where

$$\Delta x \leq \frac{\pi}{K_x}, \quad \Delta y \leq \frac{\pi}{K_y}.$$

A digital image that has been sampled according to the conditions

$$\Delta x = \frac{\pi}{K_x}, \quad \Delta y = \frac{\pi}{K_y}$$

is called a Nyquist sampled image where K_x/π and K_y/π are Nyquist frequencies (equal to twice the frequency bandwidth of the image). This is the optimum sampling interval required to avoid aliasing and to recover the information of an analogue image in digital form. It is the fundamental result used in all A-to-D (Analogue-to-Digital) conversion schemes.

3.2.3 Sinc Interpolation

If the conditions given above provide the necessary sampling rate that is required to convert an analogue image into a digital image without loss of information, then one should be able to recover the analogue signal from the digital

signal also without loss of information (i.e. undertake D-to-A or Digital-to-Analogue conversion). Assuming that f has been sampled at the Nyquist frequency, the only difference between g and f is that the spectrum of g consists of F repeated at regular interval $2\pi n/\Delta x$ and $2\pi m/\Delta y$; $\quad n = \pm 1, \pm 2, \pm 3, ..., \pm\infty$. Thus, f can be obtained from g by retaining just the part of G for values of $\mid k_x \mid$ and $\mid k_y \mid$ less than or equal to K_x and K_y, respectively, and setting all other values in the spectrum to zero, i.e.

$$F(k_x, k_y) = G(k_x, k_y)$$

provided we set

$$G(k_x, k_y) = 0 \quad \forall \mid k_x \mid > K_x \quad \text{and} \quad \mid k_y \mid > K_y.$$

We can describe this process mathematically by multiplying G with the Tophat function

$$H(k_x, k_y) = \begin{cases} 1, & \mid k_x \mid \leq K_x, \mid k_y \mid \leq K_y; \\ 0, & \text{otherwise.} \end{cases}$$

Thus, F is related to G by the equation

$$F(k_x, k_y) = H(k_x, k_y)G(k_x, k_y).$$

Using the convolution theorem, we then obtain

$$f(x, y) = 4K_xK_y \operatorname{sinc}(K_x x) \operatorname{sinc}(K_y y) \otimes\otimes g(x, y).$$

This result describes the restoration of a continuous function $f(x, y)$ from a sampling function $g(x, y)$ and therefore demonstrates that a function can be interpolated by convolving it with the appropriate sinc functions. This is known as sinc interpolation. In practice, a sampled function can be sinc interpolated by 'zero padding' its complex spectrum (see Section 3.6.2).

3.3 The Discrete Spectrum of a Digital Image

The DFT of an image is given by

$$F_{pq} = \sum_{n=0}^{N-1} \sum_{m=0}^{N-1} f_{nm} \exp(-2\pi inp/N) \exp(-2\pi imq/N).$$

This result yields some important definitions for the spectral characteristics of an image which are as follows:

Complex Spectrum

$$F_{nm} = G_{nm} + iH_{nm}$$

where $G_{nm} = \mathrm{Re}[F_{nm}]$ and $H_{nm} = \mathrm{Im}[F_{nm}]$

Amplitude Spectrum

$$\mid F_{nm} \mid = \sqrt{G_{nm}^2 + H_{nm}^2}$$

Phase Spectrum

$$\phi_{nm} = \tan^{-1}\left(\frac{H_{nm}}{G_{nm}}\right)$$

Power Spectrum

$$\mid F_{nm} \mid^2 = G_{nm}^2 + H_{nm}^2$$

Although these definitions are common, methods of displaying a 2D spectrum vary from one application to the next. The real and imaginary parts (typically the positive half-space) of a spectrum can be displayed as a grey level or colour map or alternatively the amplitude or power spectrum can be displayed as a digital image, the latter case being more common. This requires that the spectrum (a floating point array) is quantized into an 8-bit integer array.

Because an image is usually taken to be a positive function, its DC level is typically very much larger than the other frequency components and tends to 'swamp' the detailed characteristics available over the rest of the spectrum. It can therefore become difficult to observe and 'analyse' a grey level or colour coded display of the spectrum. To overcome this problem, the DC component can be omitted by setting it to zero or assigning it to the value of its nearest neighbour for example, after the DFT has been computed. Alternatively, a spectrum can be presented based on a logarithmic scale, i.e. by generating a display of[2]

$$\ln(1+ \mid F_{nm} \mid^2)$$

for example, or

$$\log_{10}(1+ \mid F_{nm} \mid^2).$$

The latter case provides a decibel scale analysis of the power spectrum.

3.3.1 Frequency Aliasing

A source of inaccuracy in computing the DFT is due to under sampling which causes frequency aliasing. Under sampling causes high frequency components in the original image to be mistaken for low frequency components in the digitized image. The low frequencies are 'aliases' of the high frequencies. The solution to this problem is to sample the original (analogue) image at rate equal to twice the highest frequency it contains - the Nyquist frequency (see Section 3.2.2). In practice, the highest frequency in an image is not usually known exactly, and either a theoretical upper limit is used or the image is low pass filtered to impose a limit.

3.3.2 Spectral Leakage

The DFT is an approximation to the Fourier transform of the continuous image from which a digital image is obtained. This approximation is subject to a number of effects caused by the nature of the sampling process. One important effect is due to the fact that an image is of finite support, i.e. it is a data field with fixed boundaries or edges. This leads to 'spectral leakage' which, in turn,

[2] 1 is added so that the output is guaranteed to be positive

generates errors in the values of the spectral components that are computed. To examine the effect of this, let us consider a digital $N \times N$ image f_{ij} which is a Nyquist sampled version of the analogue image $f(x, y)$. The N^2 point DFT can be taken to be a square 'windowed' Fourier transform of $f(x, y)$ given by

$$F_{nm} \sim \int_{-N/2}^{N/2} \int_{-N/2}^{N/2} f(x,y) \exp(-ik_n x) \exp(-ik_m y) dxdy$$

$$= \int_{-\infty}^{\infty} \int_{-\infty}^{\infty} f(x,y) w(x,y) \exp(-ik_n x) \exp(-ik_m y) dxdy$$

where w is the 'box' function

$$w(x,y) = \begin{cases} 1, & \mid x \mid \leq \frac{N}{2} \quad \text{and} \quad \mid y \mid \leq \frac{N}{2}; \\ 0, & \text{otherwise.} \end{cases}$$

Using the product theorem

$$F_{nm} \sim \frac{N^2}{(2\pi)^2} \int_{-\infty}^{\infty} \int_{-\infty}^{\infty} F(k_n - k_x, k_m - k_y) \text{sinc}(k_x N/2) \text{sinc}(k_y N/2) dk_x dk_y.$$

This result demonstrates that the discrete spectrum F_{nm} obtained by computing the DFT of a $N \times N$ image is not given by $F(k_n, k_m)$ but by the convolution of $F(k_n, k_y)$ with a sinc function. Thus, each spectral component F_{nm} is an approximation to $F(k_n, k_m)$ which depends on the influence of the sinc function associated with one sample 'bin' on the next sample 'bin'. The sinc function 'leaks' from one bin to the next producing errors in the values of the neighbouring spectral components causing 'spectral leakage'. However, note that

$$F_{nm} \to F(k_n, k_m) \quad \text{as} \quad N \to \infty$$

because

$$\lim_{N \to \infty} \frac{N}{2\pi} \text{sinc}(k_x N/2) \frac{N}{2\pi} \text{sinc}(k_y N/2) = \delta(k_x, k_y)$$

and

$$\int_{-\infty}^{\infty} \int_{-\infty}^{\infty} F(k_n - k_x, k_m - k_y) \delta(k_x, k_y) dk_x dk_y = F(k_n, k_m).$$

Hence, as the size of the digital image increases, the extent of the spectral leakage decreases.

The DFT assumes that the digital image is just one period of an infinitely periodic function and, if the values at the opposite edges of the image are not the same, then these edge discontinuities introduce spurious frequencies into the spectrum. These spurious frequencies may or may not be troublesome, depending on the purpose to which the spectrum is to be put. However, they can be reduced by 'tapering' the image toward its boundaries, so producing 'soft' rather than 'hard' edges. These tapers can be generated by designing a variety of functions called 'windows' which are multiplied by the image before computing the DFT.

3.4 The Fast Fourier Transform

The Fast Fourier Transform or FFT is an algorithm for computing the DFT with fewer additions and multiplications. In this section, we consider the background to the FFT for processing a 1D array or signal and then apply the same method for processing a 2D array or image using this 1D FFT. The DFT (in standard form) of an N-point vector is given by

$$F_m = \sum_{n=0}^{N-1} f_n \exp(-2\pi inm/N)$$

How much computation is involved in computing the DFT of N points? If we write

$$W_N = \exp(-2\pi i/N)$$

then

$$F_m = W_N^{nm} f_n.$$

This result is a matrix equation which can be written in the form

$$\begin{pmatrix} F_0 \\ F_1 \\ \vdots \\ F_{N-1} \end{pmatrix} = \begin{pmatrix} W_N^{00} & W_N^{01} & \dots & W_N^{0(N-1)} \\ W_N^{10} & W_N^{11} & ... & W_N^{1(N-1)} \\ \vdots & \vdots & \ddots & \vdots \\ W_N^{(N-1)0} & W_N^{(N-1)1} & \dots & W_N^{(N-1)(N-1)} \end{pmatrix} \begin{pmatrix} f_0 \\ f_1 \\ \vdots \\ f_{(N-1)} \end{pmatrix}$$

In this form, we see that the DFT is essentially computed by multiplying an N-point vector f_n by a matrix of coefficients given by a (complex) constant W_N to the power of nm. This requires $N \times N$ multiplications. Thus, for example, to compute the DFT of 1000 points requires 10^6 multiplications!

3.4.1 Basic Ideas

By applying a simple but very elegant trick, a N-point DFT can be written in terms of two $\frac{N}{2}$-point DFT's. The FFT algorithm is based on repeating this trick again and again until a single point DFT is obtained. The basic idea is compounded in the following result:

$$\sum_{n=0}^{N-1} f_n \exp(-2\pi inm/N)$$

$$= \sum_{n=0}^{(N/2)-1} f_{2n} \exp[-2\pi i(2n)m/N] + \sum_{n=0}^{(N/2)-1} f_{2n+1} \exp[-2\pi i(2n+1)m/N] =$$

$$\sum_{n=0}^{(N/2)-1} f_{2n} \exp[-2\pi inm/(N/2)] + \exp(-2\pi im/N) \sum_{n=0}^{(N/2)-1} f_{2n+1} \exp[-2\pi inm/(N/2)]$$

$$= \sum_{n=0}^{(N/2)-1} f_{2n} W_{N/2}^{nm} + W_N^m \sum_{n=0}^{(N/2)-1} f_{2n+1} W_{N/2}^{nm}.$$

Fundamental Result

The result above leads to the fundamental result:

$$\begin{gathered}\text{DFT of N-point array} \\ = \text{DFT of even components} + W_N^m \times \text{ DFT of odd components.}\end{gathered}$$

Using the subscripts e and o to represent odd and even components, respectively, we can write this result in the form

$$F_m = F_m^e + W_N^m F_m^o.$$

The important thing to note here is that the evaluation of F_m^e and F_m^o is over $N/2$ points - the $N/2$ even components and the $N/2$ odd components of the original N - point array. To compute F_m^e and F_m^o we only need half the number of multiplications that are required to compute F_m.

Repeating the Trick: The Successive Doubling Method

Because the form of the expressions for F_m^e and F_m^o is identical to the form of the original N-point DFT, we can repeat the idea and decompose F_m^e and F_m^o into even and odd parts producing a total four $\frac{N}{4}$-point DFT's as illustrated below.

$$\begin{array}{ccc} & F_m & \\ & \Downarrow & \\ F_m^e & + & W_N^m F_m^o \\ \Downarrow & \Downarrow & \Downarrow \\ F_m^{ee} + W_{N/2}^m F_m^{eo} & + & W_N^m \times (F_m^{oe} + W_{N/2}^m F_m^{oo}) \end{array}$$

We can continue subdividing the data into odd and even components until we get down to the DFT of a single point. However, because the data are subdivided into odd and even components of equal length we require an initial array of size $N = 2^k, k = 1, 2, 3, 4, ...$

Some Simple Examples

Consider the 2 point FFT with data (f_0, f_1). Then

$$F_m = \sum_{n=0}^{1} f_n W_2^{nm} = W_1^0 f_0 + W_2^m W_1^0 f_1 = f_0 + \exp(i\pi m) f_1$$

so that

$$F_0 = f_0 + f_1$$

and

$$F_1 = f_0 + \exp(i\pi) f_1 = f_0 - f_1.$$

Now consider the 4 point FFT operating on the data (f_0, f_1, f_2, f_3). Here,

$$F_m = \sum_{n=0}^{3} f_n W_4^{nm} = \sum_{n=0}^{1} f_{2n} W_2^{nm} + W_4^m \sum_{n=0}^{1} f_{2n+1} W_2^{nm}$$
$$= f_0 + W_2^m f_2 + W_4^m (f_1 + W_2^m f_3).$$

Thus,

$$F_0 = f_0 + f_1 + f_2 + f_3,$$
$$F_1 = f_0 + f_2 W_2 + f_1 W_4 + f_3 W_4 W_2,$$
$$F_2 = f_0 + f_2 W_2^2 + f_1 W_4^2 + f_3 W_4^2 W_2^2,$$

and

$$F_3 = f_0 + f_2 W_2^3 + f_1 W_4^3 + f_3 W_4^3 W_2^3.$$

Further, certain values of W_N^m are simple, for example,

$$W_2^0 = 1, \quad W_2^1 = -1, \quad W_4^0 = 1, \quad W_4^1, \quad W_4^2 = -1, \quad W_4^3 = -i.$$

Also, if we let $k = n + N/2$, then

$$\exp\left(\frac{2\pi i k}{N}\right) = \exp\left(\frac{2\pi i (n + N/2)}{N}\right) = \exp\left(\frac{2\pi i n}{N}\right) \exp(\pi i) = -\exp\left(\frac{2\pi i n}{N}\right)$$

and thus,

$$W_N^{(n+N/2)} = -W_N^n.$$

3.4.2 Bit Reversal

Consider the 8-point array

$$f_0, f_1, f_2, f_3, f_4, f_5, f_6, f_7$$

and consider the decomposition of this array into even and odd components as given below.

	Even arguments	Odd arguments	
	f_0, f_2, f_4, f_6	f_1, f_3, f_5, f_7	
Even	Odd	Even	Odd
f_0, f_4	f_2, f_6	f_1, f_5	f_3, f_7

To use the successive doubling method, the input array must first be expressed in the form

$$f_0, f_4, f_2, f_6, f_1, f_5, f_3, f_7.$$

The general procedure for re-ordering an input array follows a simple bit-reversal rule where the position of an element of the original array f_i is expressed in binary form. The bits are then reversed to obtain the position of this element in the re-ordered array as illustrated below.

Original Argument	Original Array	Bit-reversed Argument	Re-ordered Array
000	f_0	000	f_0
001	f_1	100	f_4
010	f_2	010	f_2
011	f_3	110	f_6
100	f_4	001	f_1
101	f_5	101	f_5
110	f_6	011	f_3
111	f_7	111	f_7

If the FFT algorithm is applied to an array in its natural order, then the output is bit-reversed. Bit-reversal of the output is then required to obtain the correct order. Thus, bit reversal can be applied either before or after the computations commence. The effect of applying this method is to reduce the number of multiplications from $O(N^2)$ to $O(N \log N)$ which, for relatively small array sizes, considerably reduces the time taken to perform a DFT.

The method discussed above depends on using array sizes of 2^n and is therefore a Base-2 algorithm. It is natural to ask why this method cannot be extended, i.e. instead of decomposing the original array into two arrays (based on the odd and even components of the original) why not decompose it into three or four arrays and repeat the process accordingly leading to Base-3 and Base-4 algorithms. The problem with this approach is that, although it can lead to slightly fewer operations, the reordering of the data required to establish an appropriate output is significantly more complicated than bit reversal. The extra effort that is required to establish a re-ordering algorithm tends to outweigh the reduction in the processing time from adopting a Base-3 or Base-4 approach.

3.4.3 The FFT in C

The following code is a C (void) function called FFT1D which computes the DFT of a complex input with real and imaginary parts using the method described above. In this case, the arrays are re-ordered on both input and output so that the DFT appears in optical forms in which the DC or zero frequency component occurs at $n/2 + 1$, where n is the size of the array. The algorithm performs either a forward or an inverse DFT using the switch sign. If *sign=-1*, then the forward DFT is computed and, if *sign=1*, then the inverse DFT is computed.

```
#include <math.h>

void FFT1D( float a[], float b[], int n, int sign )
{
  int l,l1,l2,j,jj,i,ii,k,nh,nm;
  float *cr, *ci;
```

```
  float den,p,q;
  float ur,ui,vr,vi,wr,wi,urtemp;
  double pi,x;

/* FUNCTION: This function computes the DFT of a complex
             array whose real and imaginary parts are a and b
             respectively using the successive doubling method.

   NOTES:    The function returns the real (a) and
             imaginary (b) parts of the DFT.

             The size of the arrays n must be an int power of 2

             Zero frequency occurs at n/2+1.

             By convention, the forward Fourier transform is
             obtained when sign=-1 and the inverse Fourier
             transform is obtained when sign=1.

    If the input is purely real then the imaginary part
    (i.e. array b) must be set to zero.

 I/O and PARAMETERS

 Input: a - real part of signal/spectrum
        b - imaginary part of signal/spectrum
        n - size of signal

 Output: a - real part of spectrum/signal
         b - imaginary part of spectrum/signal

 EXTERNAL FUNCTIONS: None

 INTERNAL FUNCTIONS: None */

  /* Allocate space for work arrays. */

  cr = (float *) calloc( n+1, sizeof( float ) );
  ci = (float *) calloc( n+1, sizeof( float ) );

  /* Compute scaling paremeter (den) */

  if ( sign < 0 )
    den=1.0;
  else
    den=n;
```

```
  /* Setup constants required for computation. */

  pi = 4.0 * atan( 1.0 );
  p = n;
  q = log( p ) / log( 2.0 );
  k = q;
  nh = n * 0.5;
  nm = n-1;

  /* Generate switched arrays - switch positive/negative
     half spaces to negative/positive half spaces respectively. */

  for ( i=nh+1, j=1; i<=n; i++, j++ )
    {
    cr[j] = a[i];
    ci[j] = b[i];
    }

  for ( i=1; i<=nh; i++, j++ )
    {
    cr[j] = a[i];
    ci[j] = b[i];
    }

  /* Reorder data, i.e. perform 'bit-reversal'. */

  for ( i=1, j=1; i<=nm; i++ )
    {
    if ( i < j )
      {
      vr = cr[j];
      vi = ci[j];
      cr[j] = cr[i];
      ci[j] = ci[i];
      cr[i] = vr;
      ci[i] = vi;
      }

    jj = nh;
    while ( jj < j )
      {
      j -= jj;
      jj = jj * 0.5;
      }

    j += jj;
    }
```

```
  /* Do fast transform computations. */

  for ( l=1; l<=k; l++ )
    {
    l1 = ldexp( 1.0, l );
    x = (2 * pi * (double) sign) / l1;
    wr = cos( x );
    wi = sin( x );
    l2 = l1 * 0.5;
    ur = 1.0;
    ui = 0.0;

    for ( j=1; j<=l2; j++ )
      {

      for ( i=j; i<=n; i+=l1 )
        {
        ii = i + l2;
        vr = (cr[ii] * ur) - (ci[ii] * ui);
        vi = (cr[ii] * ui) + (ci[ii] * ur);
        cr[ii] = cr[i] - vr;
        ci[ii] = ci[i] - vi;
        cr[i] = cr[i] + vr;
        ci[i] = ci[i] + vi;
        }

      urtemp = ur;
      ur = (ur * wr) - (ui * wi);
      ui = (urtemp * wi) + (ui * wr);
      }
    }

 /*  Scale */

  for ( i=1; i<=n; i++ )
    {
    cr[i] = cr[i] / den;
    ci[i] = ci[i] / den;
    }

  /* Reverse half-spaces - write out data in 'optical form'. */

  for ( i=nh+1, j=1; i<=n; i++, j++ )
    {
    a[j] = cr[i];
    b[j] = ci[i];
```

```
    }

  for ( i=1; i<=nh; i++, j++ )
    {
    a[j] = cr[i];
    b[j] = ci[i];
    }

  /* Free space from work arrays. */

  free( cr );
  free( ci );
}
```

3.4.4 The 2D FFT

The 2D DFT pair are given by

$$F_{nm} = \sum_p \sum_q f_{pq} \exp(-i2\pi np/N) \exp(-i2\pi mq/N),$$

$$f_{pq} = \frac{1}{N^2} \sum_n \sum_m F_{nm} \exp(i2\pi np/N) \exp(i2\pi mq/N).$$

If we write the DFT in the form

$$F_{nm} = \sum_p \left(\sum_q f_{pq} \exp(-i2\pi np/N) \right) \exp(-i2\pi mq/N)$$

then it is immediately clear that we can compute the 2D DFT by first computing the set of 1D DFTs for all of the rows of the matrix f_{pq} and then computing the set of 1D DFTs for all of the columns of the matrix output from the first process. Thus, to obtain the DFT of a 2D array, we simply compute the 1D DFT of each row and then each column or, alternatively, each column and then each row. This result follows from the fact that, in Cartesian coordinates, the 2D Fourier transform is separable and thus can be computed by successive passes of the 1D transform.

The following code is a C (void) function called FFT2D which computes the 2D DFT of a complex $n \times n$ matrix with real and imaginary parts using the function FFT1D and the method discussed above. The algorithm performs either a forward or an inverse DFT using the switch sign. If *sign=-1*, then the forward DFT is computed and, if *sign=1*, then the inverse DFT is computed. The DC component occurs at $(1 + n/2, 1 + n/2)$.

```
void FFT2D( float **a, float **b, int n, int sign )
{
  float  *aa, *bb;
```

```
  int i, j;


/* FUNCTION: This subroutine computes the DFT of a 2D array with
             real and imaginary parts a and b respectively.

   NOTE: This function computes the 'optical' transform
         where the zero frequency occurs at (n/2+1,n/2+1).

   I/O and PARAMETERS

   Input: a - real part of image/spectrum
          b - imaginary part of image/spectrum
          n - image size (=n x n where n=2**k; k-integer)
          sign = -1 gives forward Fourier transform
               =  1 gives inverse Fourier transform

   Output: a - real part of spectrum/image
           b - imaginary part of spectrum/image

           EXTERNAL FUCTIONS: FFT1D

           INTERNAL FUNCTIONS: None */

/* Allocate space for internal matrices. */

  for (i=0; i<n; i++)

      {
      c[i] = (float*) malloc(n*sizeof(float));

    d[i] = (float*) malloc(n*sizeof(float));
      }
/* Allocate space for work arrays. */

  aa = (float *) malloc( (n+1)*sizeof( float ) );
  bb = (float *) malloc( (n+1)*sizeof( float ) );

/* Use subroutine FFT1D to generate a 2D FFT by computing
   the 1D FFT of the columns and rows separately.          */

/* Put columns into single-dimension array and call FFT1D.  */

  for ( i=0; i<n; i++ )
    {
    for ( j=0; j<n; j++ )
      {
```

```
      aa[j+1] = a[i][j];
      bb[j+1] = b[i][j];
      }

    FFT1D( aa, bb, n, sign);

    for ( j=0; j<n; j++)
      {
      c[i][j] = aa[j+1];
      d[i][j] = bb[j+1];
      }
    }

/* Put rows into single-dimension array and call FFT1D. */

  for ( j=0; j<n; j++ )
    {
    for ( i=0; i<n; i++ )
      {
      aa[i+1] = c[i][j];
      bb[i+1] = d[i][j];
      }

    FFT1D( aa, bb, n, sign );
    for ( i=0; i<n; i++)
      {
      a[i][j] = aa[i+1];
      b[i][j] = bb[i+1];
      }
    }

/* Free space from work arrays.    */

  free( aa );
  free( bb );

/* Free space from internal matrices.  */

  for (i=0; i<n; i++)
  {
     free(c[i]);
     free(d[i]);
  }

}
```

3.5 The Imaging Equation and Convolution in 2D

The fundamental imaging equation for $x \in [-X, X], \quad y \in [-Y, Y]$ is given by

$$s = p \otimes\otimes f + n$$

$$= \int_{-X}^{X} \int_{-Y}^{Y} p(x - x', y - y') f(x', y') dx' dy' + n(x, y).$$

Here, p is the point spread function which describes the way in which information on the object function f is 'spread out' as a result of recording the data. It is a characteristic of the imaging instrument which represents the response of the imaging system to a point source in the object plane and is a deterministic function. The object function f describes the object that is being imaged (its surface or internal structure, for example). The noise n is a non-deterministic function which can at best be described in terms of some statistical distribution. It is a stochastic function which is a consequence of all of the external disturbances that occur during the recording process. The operation $\otimes\otimes$, which denotes 2D convolution, describes the blurring process that occurs when an image is taken. This equation assumes that the imaging system can be described by a stationary process in which the point spread function remains the same over the image domain, i.e. it is spatially invariant. The equation also assumes that the scattering process (e.g. light scattering from a surface) that produces the image is dominated by single scattering events.

For a digital image, we consider a discrete 2D array of space or of space and time and consider the discrete imaging equation given by

$$s_{ij} = p_{ij} \otimes\otimes f_{ij} + n_{ij} = \sum_n \sum_m p_{i-n,j-m} f_{nm} + n_{ij}$$

where

$$\sum_n \equiv \sum_{n=-N}^{N} \quad \text{and} \quad \sum_m \equiv \sum_{m=-M}^{M}.$$

Here, the digital image is taken to of size $2N \times 2M$.

3.6 The Finite Impulse Response Filter

The Finite Impulse Response or FIR filter is that process defined by

$$s_{nm} = \sum_i \sum_j p_{n-i,m-j} f_{ij}$$

which is just a discrete convolution sum. In discrete terms, the FIR filter p_{ij} performs the role of the point spread function in the imaging equation. However, the filter has more general applications other than the role it plays in describing the point spread function, and its computational aspects need to be considered.

3.6.1 The FIR Filter in 1D

In order to introduce the FIR filter, it is of value to first consider the operational characteristic of this filter in 1D.

The FIR Convolution Filter

In 1D, the discrete convolution operation (the convolution sum) can be written in the form (since the convolution process is commutative)

$$s_j = \sum_{i=-N}^{N} p_i f_{j-i}$$

where, in 1D (i.e. for signal processing), the function p_i is the 'impulse response function'.

To illustration the nature of this process, consider the case when p_i and f_i are vectors with just 3 elements, i.e.

$$\mathbf{p} = (p_{-1}, p_0, p_1)^T,$$
$$\mathbf{f} = (f_{-1}, f_0, f_1)^T,$$

and where

$$f_{-2} = 0, \quad \text{and} \quad f_2 = 0.$$

Then,

for $j = -1$:

$$s_{-1} = \sum_{i=-1}^{1} p_i f_{-1-i} = p_{-1}f_0 + p_0 f_{-1} + p_1 f_{-2} = p_{-1}f_0 + p_0 f_{-1},$$

for $j = 0$:

$$s_0 = \sum_{i=-1}^{1} p_i f_{-i} = p_{-1}f_1 + p_0 f_0 + p_1 f_{-1},$$

for $j = 1$:

$$s_1 = \sum_{i=-1}^{1} p_i f_{1-i} = p_{-1}f_2 + p_0 f_1 + p_1 f_0 = p_0 f_1 + p_1 f_0.$$

Clearly, this result can be written in matrix form as

$$\begin{pmatrix} s_1 \\ s_0 \\ s_1 \end{pmatrix} = \begin{pmatrix} f_0 & f_{-1} & 0 \\ f_1 & f_0 & f_{-1} \\ 0 & f_1 & f_0 \end{pmatrix} \begin{pmatrix} p_{-1} \\ p_0 \\ p_1 \end{pmatrix}.$$

Now consider the convolution sum defined as

$$s_j = \sum_{i=-N}^{N} p_{j-i} f_i.$$

With

$$\mathbf{p} = (p_{-1}, p_0, p_1)^T, \quad p_{-2} = p_2 = 0$$

and

$$\mathbf{f} = (f_{-1}, f_0, f_1)^T$$

we have

for $j = -1$:

$$s_{-1} = \sum_{i=-1}^{1} p_{-1-i} f_i = p_0 f_{-1} + p_{-1} f_0 + p_{-2} f_1 = p_0 f_{-1} + p_{-1} f_0,$$

for $j = 0$:

$$s_0 = \sum_{i=-1}^{1} p_{-i} f_i = p_1 f_{-1} + p_0 f_0 + p_{-1} f_1,$$

for $j = 1$:

$$s_1 = \sum_{i=-1}^{1} p_{1-i} f_i = p_2 f_{-1} + p_1 f_0 + p_0 f_1 = p_1 f_0 + p_0 f_1.$$

In matrix form, this result becomes

$$\begin{pmatrix} s_{-1} \\ s_0 \\ s_1 \end{pmatrix} = \begin{pmatrix} p_0 & p_{-1} & 0 \\ p_1 & p_0 & p_{-1} \\ 0 & p_1 & p_0 \end{pmatrix} \begin{pmatrix} f_{-1} \\ f_0 \\ f_1 \end{pmatrix}.$$

Note that

$$\begin{pmatrix} p_0 & p_{-1} & 0 \\ p_1 & p_0 & p_{-1} \\ 0 & p_1 & p_0 \end{pmatrix} \begin{pmatrix} f_{-1} \\ f_0 \\ f_1 \end{pmatrix} = \begin{pmatrix} f_0 & f_{-1} & 0 \\ f_1 & f_0 & f_{-1} \\ 0 & f_1 & f_0 \end{pmatrix} \begin{pmatrix} p_{-1} \\ p_0 \\ p_1 \end{pmatrix}$$

and in general that

$$\sum_{i=-N}^{N} p_i f_{j-i} = \sum_{i=-N}^{N} p_{j-i} f_i$$

which shows that the discrete convolution sum is commutative. However, the latter definition of a convolution sum is better to work with because it ensures that the matrix is filled with elements relating to the impulse response function p_i, i.e.

$$\mathbf{s} = P\mathbf{f}.$$

Clearly, if $\mathbf{f}$ is an $(2N+1)^{\text{th}}$ order vector and $\mathbf{p}$ contains just three elements say, then the convolution sum can be written in the form

$$\begin{pmatrix} s_{-N} \\ \vdots \\ s_{-1} \\ s_0 \\ s_1 \\ \vdots \\ s_N \end{pmatrix} = \begin{pmatrix} \ddots & & & & & & \\ & \ddots & & & & & \\ & p_1 & p_0 & p_{-1} & & & \\ & & p_1 & p_0 & p_{-1} & & \\ & & & p_1 & p_0 & p_{-1} & \\ & & & & & \ddots & \\ & & & & & & \ddots \end{pmatrix} \begin{pmatrix} f_{-N} \\ \vdots \\ f_{-1} \\ f_0 \\ f_1 \\ \vdots \\ f_N \end{pmatrix}.$$

Here, P is a tridiagonal matrix. In general, the bandwidth of the matrix is determined by the number of elements of the impulse response function.

Useful Visualization of the Discrete Convolution Process

Another way of interpreting the discrete convolution process which is useful visually is in terms of the of two streams of numbers sliding along each other where at each location in the stream, the appropriate numbers are multiplied and the results added together. In terms of the matrix above we have:

$$\begin{array}{cc} \vdots & \\ f_{-4} & \\ f_{-3} & p_1 \\ f_{-2} & p_0 \quad (= s_{-2}) \\ f_{-1} & p_{-1} \\ f_0 & \\ f_1 & \\ f_2 & p_1 \\ f_3 & p_0 \quad (= s_3) \\ f_4 & p_{-1} \\ \vdots & \end{array}$$

In general, if

$$\mathbf{f} = \begin{pmatrix} f_{-N} \\ \vdots \\ f_{-1} \\ f_0 \\ f_1 \\ \vdots \\ f_N \end{pmatrix} \quad \text{and} \quad \mathbf{p} = \begin{pmatrix} p_{-N} \\ \vdots \\ p_{-1} \\ p_0 \\ p_1 \\ \vdots \\ p_N \end{pmatrix}$$

then

$$\begin{array}{cc} \vdots & \\ f_{-4} & \\ f_{-3} & \vdots \\ f_{-2} & p_1 \\ f_{-1} & p_0 \quad (= s_{-1}) \\ f_0 & p_{-1} \\ f_1 & \vdots \\ f_2 & \\ f_3 & \\ f_4 & \\ \vdots & \end{array}$$

Note that the order of the elements of $\mathbf{p}$ is reversed with respect to $\mathbf{f}$.

On Notation and Jargon

The vector $\mathbf{p}$ is sometimes called the **kernel**, a term taken from the 'Kernel' of an integral equation of the type

$$s(t) = \int K(t,\tau) f(\tau) d\tau$$

where K is the Kernel. Visualizing a discrete convolution in the form discussed above leads to $\mathbf{p}$ being referred to as a 'window' since we can think of this process in terms of looking at the data f_i through a window of coefficients p_i. As we slide the stream of coefficients p_i along the data f_i, we see the data in the form of the output s_i which is the running weighted average of the original data f_i. Because the window moves over the data it is often referred to as a 'moving window'.

The FIR Correlation Filter

The discrete correlation operation (the correlation sum) can be written in the form

$$s_j = \sum_{i=-N}^{N} p_i f_{i-j}.$$

Compared with the convolution sum, the subscript on f is reversed (i.e. f_{j-i} becomes f_{i-j}). Consider the case, when p_i and f_i are vectors with just 3 elements:

$$\mathbf{p} = (p_{-1}, p_0, p_1)^T,$$
$$\mathbf{f} = (f_{-1}, f_0, f_1)^T, \quad f_{-2} = f_2 = 0.$$

For $j = -1$:

$$s_{-1} = \sum_{i=-1}^{1} p_i f_{i+1} = p_{-1} f_0 + p_0 f_1 + p_1 f_2 = p_{-1} f_0 + p_0 f_1,$$

for $j = 0$:

$$s_0 = \sum_{i=-1}^{1} p_i f_i = p_{-1}f_{-1} + p_0 f_0 + p_1 f_1,$$

for $j = 1$:

$$s_1 = \sum_{i=-1}^{1} p_i f_{i-1} = p_{-1}f_{-2} + p_0 f_{-1} + p_1 f_0 = p_0 f_{-1} + p_1 f_0.$$

This result can be written in matrix form as

$$\begin{pmatrix} s_1 \\ s_0 \\ s_1 \end{pmatrix} = \begin{pmatrix} f_0 & f_1 & 0 \\ f_{-1} & f_0 & f_1 \\ 0 & f_{-1} & f_0 \end{pmatrix} \begin{pmatrix} p_{-1} \\ p_0 \\ p_1 \end{pmatrix}.$$

Now consider the correlation sum defined as

$$s_j = \sum_{i=-N}^{N} p_{i-j} f_i.$$

With

$$\mathbf{p} = (p_{-1}, p_0, p_1)^T, \quad p_{-2} = p_2 = 0$$

and

$$\mathbf{f} = (f_{-1}, f_0, f_1)^T$$

we have

for $j = -1$:

$$s_{-1} = \sum_{i=-1}^{1} p_{i+1} f_i = p_0 f_{-1} + p_1 f_0 + p_2 f_1 = p_0 f_{-1} + p_1 f_0,$$

for $j = 0$:

$$s_0 = \sum_{i=-1}^{1} p_i f_i = p_{-1}f_{-1} + p_0 f_0 + p_1 f_1,$$

for $j = 1$:

$$s_1 = \sum_{i=-1}^{1} p_{i-1} f_i = p_{-2}f_{-1} + p_{-1}f_0 + p_0 f_1 = p_{-1}f_0 + p_0 f_1$$

and in matrix form, the result becomes

$$\begin{pmatrix} s_{-1} \\ s_0 \\ s_1 \end{pmatrix} = \begin{pmatrix} p_0 & p_1 & 0 \\ p_{-1} & p_0 & p_1 \\ 0 & p_{-1} & p_0 \end{pmatrix} \begin{pmatrix} f_{-1} \\ f_0 \\ f_1 \end{pmatrix}.$$

Note that

$$\begin{pmatrix} p_0 & p_1 & 0 \\ p_{-1} & p_0 & p_1 \\ 0 & p_{-1} & p_0 \end{pmatrix} \begin{pmatrix} f_{-1} \\ f_0 \\ f_1 \end{pmatrix} \neq \begin{pmatrix} f_0 & f_1 & 0 \\ f_{-1} & f_0 & f_1 \\ 0 & f_{-1} & f_0 \end{pmatrix} \begin{pmatrix} p_{-1} \\ p_0 \\ p_1 \end{pmatrix}$$

and in general

$$\sum_{i=-N}^{N} p_i f_{i-j} \neq \sum_{i=-N}^{N} p_{i-j} f_i$$

illustrating that, unlike the convolution sum, the correlation sum is not commutative. As with the discrete convolution sum, the latter definition of a correlation sum is better to work with because it ensures that the matrix is filled with elements relating to the impulse response function p_i so that we can write

$$\mathbf{s} = P\mathbf{f}.$$

If $\mathbf{f}$ is an $(2N+1)^{\text{th}}$ order vector and $\mathbf{p}$ contains just three elements say, then the correlation sum can be written in the form

$$\begin{pmatrix} s_{-N} \\ \vdots \\ s_{-1} \\ s_0 \\ s_1 \\ \vdots \\ s_N \end{pmatrix} = \begin{pmatrix} \ddots & & & & & & & \\ & \ddots & & & & & & \\ & p_{-1} & p_0 & p_1 & & & & \\ & & p_{-1} & p_0 & p_1 & & & \\ & & & p_{-1} & p_0 & p_1 & & \\ & & & & & \ddots & & \\ & & & & & & \ddots & \end{pmatrix} \begin{pmatrix} f_{-N} \\ \vdots \\ f_{-1} \\ f_0 \\ f_1 \\ \vdots \\ f_N \end{pmatrix}.$$

Useful Visualization of the Discrete Correlation Process

A useful way of visualizing the discrete correlation process is in terms of the two streams of numbers sliding along each other where, at each location in the stream, the appropriate numbers are multiplied and the results added together. In terms of the matrix equation above we have:

$$\begin{array}{cc} \vdots & \\ f_{-4} & \\ f_{-3} & p_{-1} \\ f_{-2} & p_0 \quad (= s_{-2}) \\ f_{-1} & p_1 \\ f_0 & \\ f_1 & \\ f_2 & p_{-1} \\ f_3 & p_0 \quad (= s_3) \\ f_4 & p_1 \\ \vdots & \end{array}$$

In general, if

$$\mathbf{f} = \begin{pmatrix} f_{-N} \\ \vdots \\ f_{-1} \\ f_0 \\ f_1 \\ \vdots \\ f_N \end{pmatrix} \quad \text{and} \quad \mathbf{p} = \begin{pmatrix} p_{-N} \\ \vdots \\ p_{-1} \\ p_0 \\ p_1 \\ \vdots \\ p_N \end{pmatrix}$$

then

$$\begin{array}{cc} \vdots & \\ f_{-4} & \\ f_{-3} & \\ f_{-2} & \vdots \\ f_{-1} & p_{-1} \\ f_0 & p_0 \quad (= s_0) \\ f_1 & p_1 \\ f_2 & \vdots \\ f_3 & \\ f_4 & \\ \vdots & \end{array}$$

Note that, unlike convolution, the order of the elements of $\mathbf{p}$ is preserved with respect to $\mathbf{f}$. If the impulse response function is symmetric, then the convolution and correlation sums are identical (for real data). The jargon associated with the discrete convolution process is also used in the case of discrete correlation. Correlation is also the principal basis for matched filtering which is of primary importance in pattern recognition (i.e. matching a pattern in an image with an existing template) - see Chapter 16.

3.6.2 Computational Methods

A problem arises in computing the FIR filter (convolution or correlation) at the ends of the array f_i. For example, if $\mathbf{p}$ is a 5×1 kernel, then at the end of the data stream we have

$$\begin{array}{cc} \vdots & \\ f_{N-3} & p_{-2} \\ f_{N-2} & p_{-1} \\ f_{N-1} & p_0 \\ f_N & p_1 \\ & p_2 \end{array}$$

In the computation of s_{N-1} there is no number associated with the data f_i with which to multiply p_2. Similarly, in the computation of s_N we have

$$\begin{array}{cc} \vdots & \\ f_{N-3} & \\ f_{N-2} & p_{-2} \\ f_{N-1} & p_{-1} \\ f_N & p_0 \\ & p_1 \\ & p_2 \end{array}$$

Here, there are no numbers associated with the array f_i with which to multiply p_1 and p_2. The same situation occurs at the other end of the array f_i. Hence, at both ends of the data, the moving window 'runs out' of data for computing the convolution sum. There are a number of ways of solving this problem including zero padding, endpoint extension and wrapping.

Zero Padding

Zero padding assumes that the data is zero beyond the ends of the array, i.e.

$$f_{\pm N\pm 1} = f_{\pm N\pm 2} = f_{\pm N\pm 2} = ... = 0.$$

This method was applied in the previous Sections to introduce the FIR filter.

Endpoint Extension

Endpoint extension assumes that the data beyond the ends of the array takes on the value of the end points of the array, i.e. the extrapolated data is equal in value to end points:

$$f_{N+1} = f_{N+2} = f_{N+3} = ... = f_N$$

and

$$f_{-N-1} = f_{-N-2} = f_{-N-3} = ... = f_{-N}.$$

This method is sometimes known as the 'constant continuation method'.

Wrapping

The wrapping technique assumes that the array is wrapped back on itself so that

$$f_{N+1} = f_{-N}; \quad f_{N+2} = f_{-N+1}; \quad f_{N+3} = f_{-N+2}; \quad \text{etc.}$$

and

$$f_{-N-1} = f_N; \quad f_{-N-2} = f_{N-1}; \quad f_{-N-3} = f_{N-2}; \quad \text{etc.}$$

These methods are used in different circumstances but the endpoint extension technique is probably one of the most widely used.

3.6.3 Moving Window Filters

The FIR filter is just one example of a moving window filter in which the computational process is a convolution. There are a range of filters that can be designed in which various processes are repeatedly applied to the windowed data.

The moving average filter computes the average value of a set of samples within a predetermined window.

Example For a 3×1 window:

$$\begin{array}{ll} \vdots & \\ f_i & \\ f_{i+1} & s_{i+1} = (f_i + f_{i+1} + f_{i+2})/3 \\ f_{i+2} & s_{i+2} = (f_{i+1} + f_{i+2} + f_{i+3})/3 \\ f_{i+3} & s_{i+3} = (f_{i+2} + f_{i+3} + f_{i+4})/3 \\ f_{i+4} & \\ \vdots & \end{array}$$

As the window moves over the data, the average of the samples 'seen' within the window is computed; hence the term 'moving average filter'. In mathematical terms, we can express this type of processing in the form

$$s_i = \frac{1}{M} \sum_{j \in w(i)} f_j$$

where $w(i)$ is the window located at i over which the average of the data samples is computed and M is the total number of samples in w. Note that the moving average filter is just an FIR of the form

$$s_i = \sum_{i=-N}^{N} p_{j-i} f_i$$

with

$$\mathbf{p} = \frac{1}{M}(1, 1, 1, ..., 1)$$

so that for a 3×1 kernel

$$\mathbf{p} = \frac{1}{3}(1, 1, 1)$$

and for a 5×1 kernel

$$\mathbf{p} = \frac{1}{5}(1, 1, 1, 1, 1).$$

This filter can be used to smooth a signal, a feature which can be taken to include the reduction of noise. Note that this filter, is in effect, the convolution of an input with a tophat function; the spectral response is therefore a sinc function.

3.6.4 The 2D FIR Filter

Computing the 2D FIR filter follows the same principles as those associated with the 1D filter. To illustrate this, consider the 3×3 kernel

$$\begin{pmatrix} p_{00} & p_{01} & p_{02} \\ p_{10} & p_{11} & p_{12} \\ p_{20} & p_{21} & p_{22} \end{pmatrix} \longrightarrow \begin{pmatrix} p_{22} & p_{21} & p_{20} \\ p_{12} & p_{11} & p_{10} \\ p_{02} & p_{01} & p_{00} \end{pmatrix}$$

where we have interchanged the rows and columns of the above matrix in order to compute the convolution process in which the kernel is reversed (as in the case of the 1D convolution process). Now consider the 8×8 digital image given below:

$$\begin{pmatrix} f_{00} & f_{01} & f_{02} & f_{03} & f_{04} & f_{05} & f_{06} & f_{07} \\ f_{10} & f_{11} & f_{12} & f_{13} & f_{14} & f_{15} & f_{16} & f_{17} \\ f_{20} & f_{21} & f_{22} & f_{23} & f_{24} & f_{25} & f_{26} & f_{27} \\ f_{30} & f_{31} & f_{32} & f_{33} & f_{34} & f_{35} & f_{36} & f_{37} \\ f_{40} & f_{41} & f_{42} & f_{43} & f_{44} & f_{45} & f_{46} & f_{47} \\ f_{50} & f_{51} & f_{52} & f_{53} & f_{54} & f_{55} & f_{56} & f_{57} \\ f_{60} & f_{61} & f_{62} & f_{63} & f_{64} & f_{65} & f_{66} & f_{67} \\ f_{70} & f_{71} & f_{72} & f_{73} & f_{74} & f_{75} & f_{76} & f_{77} \end{pmatrix}$$

Suppose we wish to compute the output s_{ij} of this FIR filter at the position of the element f_{11}. Then

$$s_{11} = p_{22}f_{00}+p_{21}f_{01}+p_{20}f_{02}+p_{12}f_{10}+p_{11}f_{11}+p_{10}f_{12}+p_{02}f_{20}+p_{01}f_{21}+p_{00}f_{22}.$$

Now suppose we compute the output of this filter at the position of the element f_{54}, then

$$s_{54} = p_{22}f_{43} + p_{21}f_{44} + p_{20}f_{45} + ...$$

The output at all other positions follows the same principle which involves moving a 3×3 window with elements p_{ij} over the image and at each position computing the output by multiplying the adjacent element together and adding the results together.

In the case of a 2D discrete correlation, when the FIR filter is defined as

$$s_{nm} = \sum_i \sum_j p_{i-n,j-m} f_{ij}$$

the kernel is not reversed but the process described above is applied in an identical manner using the kernel

$$\begin{pmatrix} p_{00} & p_{01} & p_{02} \\ p_{10} & p_{11} & p_{12} \\ p_{20} & p_{21} & p_{22} \end{pmatrix}$$

To compute the 2D FIR filter, padding is required at the edges of the image. As with digital signals, one can apply techniques that include zero padding, end point extension or wrapping, but zero padding is most common in the majority of image processing systems. In the case of zero padding, the image is given a

'frame' of zeros. With end point extension, the image is given a frame consisting of data based on the first and last pixel value of each row and column; a block of data is formed at the corners of the image based on the pixel value at each corner.

Depending on the values of p_{ij} used, the output obtained from application of an FIR filter (convolution or correlation) will contain positive, negative or positive and negative values. For signal processing, in which the input to and the output from, an FIR filter are usually expected to be bi-polar (i.e. a floating point stream with positive and negative values), this is not an issue. However, in terms of displaying a digital image of a data field with positive and negative values, a choice needs to be made on how the data should be modified to comply with the condition that $f_{ij} \geq 0 \ \ \forall \ \ i, j$, where f_{ij} is a matrix composed of integers. There are several possibilities. The first is to ignore all the negative components and set them to zero, normalize and apply 8-bit quantization for example (see Introduction). The second is to rescale the data by adding the value of the largest negative data point(s) to the data field and then normalize and quantize in the usual way. The third option is to compute the absolute values of the data, and then normalize and quantize in the usual way.

The issue of generating negative data values when applying processes to an intensity image is quite common. In some cases, the condition $f_{ij} \geq 0 \ \ \forall \ \ i, j$ is used to pre-condition the data prior to an iteration when the output from each iteration may contain negative data. In other cases, this condition is the basis for the method of application, e.g. maximum entropy reconstruction.

3.6.5 The 2D FIR Filter and the 2D FFT

The implementation of the FIR filter directly is computationally advantageous when the size of the kernel is small compared to the image. For a kernel of size $M \times M$ say and an image of size $N \times N$ where $N > M$, the number of multiplications are or the order of $N^2 \times M^2$. When M approaches N and the number of multiplication approaches N^4, it is computationally more efficient to implement the FFT algoithm to perform the convolution operation (where the number of multiplications is approximately $N^3 \log N$). To perform this operation, the kernel is required to be zero padded. In other words, the kernel is padded out with zeros (i.e. framed by zeros) until the size of the array is equal to the size of the image to which the convolution operation is to be applied.

3.7 Origin of the Imaging Equation

The convolution process is fundamental to both general methods of processing a digital image but also in terms of the physical models we use to describe the way in which images are formed.

By studying the 'physics' of an imaging system and using appropriate approximations and geometries, one can formulate the imaging equation

$$s = p \otimes \otimes f + n$$

directly. This approach provides a mathematical description of the point spread function and the object function in terms of fundamental physical parameters, which is required in order to understand the information that an image conveys and hence the most appropriate processing methods that should be applied. The mathematical apparatus required for undertaking this task is the basis for the chapters that follow which look at the use of the Green function for determining a scattered wavefield and discuss the field equations and wave equations used to model electromagnetic and acoustic imaging systems. This principle is illustrated in Figure 3.1.

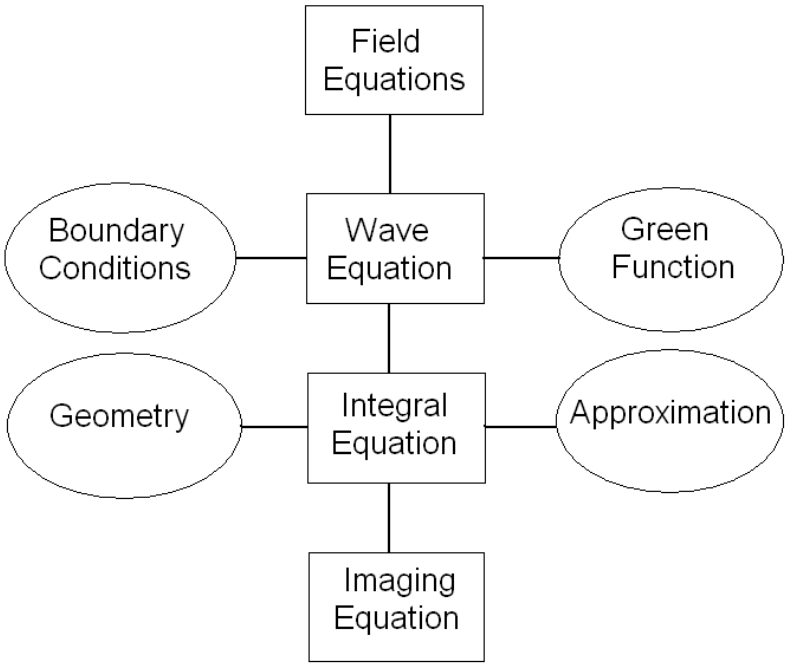

Figure 3.1: Schematic diagram illustrating the principles of modelling an imaging system by deriving the imaging equation from the field equations: From the field equations we derive an inhomogeneous wave equation. Using the Green function together with appropriate boundary condition, we derive an integral equation. From this integral equation, given the geometry of the imaging system and certain approximations (primarily the single scattering or Born approximation) we derive the imaging equation with expressions for the point spread function and the object function in terms of the system parameters and field variables, respectively.

3.8 Summary of Important Results

The 2D discrete Fourier transform pair

$$f_{pq} = \frac{1}{N^2} \sum_n \sum_m F_{nm} \exp(i2\pi np/N) \exp(i2\pi mq/N),$$

$$F_{nm} = \sum_p \sum_q f_{pq} \exp(-i2\pi np/N) \exp(-i2\pi mq/N).$$

Principle of the (base-2) FFT

DFT of N-point array
= DFT of even components + $W_N^m \times$ DFT of odd components.

Bit reversal

Reversal of the binary number representation of the position of an element in an array which is used to reorder the data before application of the principle above.

2D DFT

The 2D DFT of an array f_{nm} can be generated by computing the 1D DFT of all the rows and then all the columns (or visa versa).

1D FFT C function

```
void FFT1D(float a[ ], float b[ ], int n, int sign)
```

where *a* and *b* are the real and imaginary parts respectively, *n* is the array size (an integer power of 2) and *sign* is a switch to control the computation of the forward DFT (*sign=-1*) or inverse DFT (*sign=1*).

2D FFT C function

```
void FFT2D(float **a, float **b, int n, int sign)
```

The FIR filter

For an input digital image f_{ij} of size $N \times N$, the output of an FIR filter s_{nm} is given by

$$s_{nm} = p_{nm} \otimes \otimes f_{nm} = \sum_{i=0}^{N-1} \sum_{j=0}^{N-1} p_{n-i,m-j} f_{ij}$$

for the convolution FIR filter and

$$s_{nm} = \sum_{i=0}^{N-1} \sum_{j=0}^{N-1} p_{i-n,j-m} f_{ij}$$

for the correlation FIR filter where p_{ij} is the FIR filter or kernel.

Zero padding

Computing the FIR filter by padding the input data with zeros.

End point extension

Computing the FIR filter by padding the input data with the values of those elements at the edge of the image.

FIR filtering using an FFT

Computing the FIR filter by zero padding the kernel to the array size of the input data and using the convolution theorem to employ an FFT.

Computational efficiency

For kernels that are small compared to the input, the FIR filter is efficiently computed by direct application. For kernels whose arrays are of similar size to the input data, the FIR is computed most efficiently by application of the FFT.

Moving window filtering

Filtering or processing the input data by application of some process applied to a sample of data over a window that moves over the input data one element at a time.

3.9 Further Reading

- Brigham E O, *The Fast Fourier Transform*, Prentice-Hall, 1974.
- Elliot D F and Rao K R, *Fast Transforms, Algorithms, Analysis and Applications*, Academic Press, 1982.
- Brigham E O, *The Fast Fourier Transform and its Applications*, Prentice-Hall, 1988.
- Blahut R E, *Fast Algorithms for Digital Signal Processing*, Addison-Wesley, 1985.
- Burrus C S and Parks T W, *DFT/FFT and Convolution Algorithms*, Wiley, 1985.

- Lawrence Marple, S *Digital Spectral Estimation*, Prentice-Hall, 1986.
- Press W H et al, *Numerical Recipes*, Cambridge University Press, 1986.
- Gonzalez R C and Wintz P, *Digital Image Processing*, Addison-Wesley, 1987.
- Lim J S, *Two-dimensional Signal and Image Processing*, Prentice-Hall, 1990.
- DeVries P L, *A First Course in Computational Physics*, Wiley, 1994.

Chapter 4

Field and Wave Equations

This Chapter is concerned with the equations used to describe the fields that are measured in an imaging system and their relationship with the material variables with which these fields interact. The field equations determine the physical characteristics and behaviour of a particular type of field. Two types of fields are important in imaging: the electromagnetic field and the acoustic field. The primary purpose of this Chapter is to introduce and discuss the electromagnetic and acoustic field equations which are employed in later chapters (Chapters 7 - 11 for example). From these results, we derive equations (wave equations or equations of propagation) which describe the propagation of different wavefields through various types of materials or media.

4.1 The Langevin Equation

The propagation of a wavefield can be modelled by various different wave equations depending upon the type of field, the supporting material and its physical state. In general, however, if the supporting material is assumed to be a linear medium, the scalar field $u(\mathbf{r}, t)$ obeys a partial integro-differential equation of the form

$$\hat{D}^{(1)} u(\mathbf{r}, t) = -s(\mathbf{r}, t)$$

where

$$\hat{D}^{(1)} = \hat{D}^{(0)} + \hat{L}$$

For a vector field $\mathbf{u}(\mathbf{r}, t)$,

$$\hat{D}^{(1)} \mathbf{u}(\mathbf{r}, t) = -\mathbf{s}(\mathbf{r}, t)$$

This is the Langevin equation where $\hat{D}^{(0)}$ and $\hat{L}$ are linear operators: $\hat{D}^{(0)}$ is associated with the homogeneous portion of the medium, $\hat{L}$ is, in general, an integro-differential scattering operator, and s is a source function which describes the emission of the incident field from a given source. The operator $\hat{L}$ models the interaction of the incident field with the differential or local

scattering from material inhomogeneities. The operator $\hat{D}^{(1)}$ has the general form

$$\hat{D}^{(1)} \equiv \hat{D}^{(1)}\left(\nabla, \nabla^2, ...; 1, \frac{\partial}{\partial t}, \frac{\partial^2}{\partial t^2}, ...\right).$$

The source function s is, in general, given by

$$s = p \otimes f$$

where f is the probe field, p is a filter weighting function for the emitted field and $\otimes$ is taken to denote the convolution over three-dimensional space and time. From this general formalism, one can consider a variety of scalar wave equations governing the propagation of different types of wavefields supported by different isotropic media. Two cases arise that are based on: (i) a rigorous derivation of the Langevin from a set of fundamental field equations; (ii) the proposition of a Langevin equation (a phenomenological model) whose characteristics (e.g. the phase velocity) are confirmed experimentally.

The wave equation that is used to model a wavefield determines the underlying physical model for a (scatter) imaging system. This includes aspects such as the resolution of the image (e.g. the wavelength or bandwidth of the probe), the accuracy of the spatial mapping of the scatter generating parameters in an image (e.g. the level of distortion as determined by the propagation model) and image fuzziness. A fuzzy image is an image which, although attempting to display a specific scatter generating parameter, fails to achieve this because the scattered wavefield that has been measured and processed is corrupted by some other interaction that has not been included on the original model (i.e. the wave equation). Thus, all scatter-imaging techniques are highly model dependent since the reconstruction algorithm is determined by the wave equation which characterizes the medium, in particular, the model associated with the operator $\hat{L}$. An inappropriate choice of wave equation results in image fuzziness. Scatter imaging demands appropriate modelling of the scattering dynamics, even if the computations are approximate. An inexact model will lead to a fuzzy image whereas an approximate computation may lead to poor resolution. Distortion, due to poor propagator models which are compounded in the operator $\hat{D}^{(0)}$ and its associated (free-space) Green function, is a common artifact in many imaging systems and poor physical modelling manifests some form of distortion in most imaging methods. A general criticism, common to many imaging systems, is that emphasis is often placed on a significant amount of computation for image reconstruction and processing. This can provide good, or at least, enhanced resolution but at the expense of developing accurate models for the propagation of a wavefield through the medium that generates the scattered field from which an image is generated and interpreted. This leads to images which are well resolved but may be badly distorted and fuzzy.

In this chapter, we start by considering Maxwell's equations which provide a unified theoretical framework for the interaction of electromagnetic waves with matter. In the case of the macroscopic form of these equations, we introduce material parameters such as the permittivity, the permeability and the conductivity. The elastic and acoustic field equations are then studied. An elastic

field describes the characteristics of 'mechanical radiation' when a material is solid and incompressible. The acoustic field equations relate the acoustic field variables (such as the pressure and velocity fields) to material parameters including the density, compressibility and viscosity. These are used to model the propagation and scattering of an acoustic wavefield when the material is a compressible solid, liquid or gas. In each case, the material is taken to be isotropic.

The field equations presented provide the fundamental basis for modelling electromagnetic and acoustic imaging systems. In each case, it is shown how the field equations can (under certain conditions and approximations) be decoupled to provide a governing inhomogeneous wave equation whose complexity increases according to the number of material parameters that are considered. General methods of solving such equations are then addressed in Part II using the Green function method which is discussed in the following Chapter.

4.2 Maxwell's Equations

We shall now consider Maxwell's equations and study the electromagnetic wavefields and wave equations that arise from these equations. We first consider these equations in their microscopic form (for individual charged particles) and go on to consider the macroscopic form of Maxwell's equations (for the case when there are many particles per cubic wavelength) and briefly study the propagation of monochromatic electromagnetic waves in homogeneous media. The macroscopic form of Maxwell's equations is then used to construct inhomogeneous wave equations in a form that are suitable for applying the solutions methods discussed in Chapter 5.

The motions of electrons (and other charged particles) give rise to electric and magnetic fields. These fields are described by the following equations which are a complete mathematical descriptions for the physical laws quoted [1].

Coulomb's law

$$\nabla \cdot \mathbf{e} = 4\pi\rho \tag{4.1}$$

Faraday's law of induction

$$\nabla \times \mathbf{e} = -\frac{1}{c}\frac{\partial \mathbf{b}}{\partial t} \tag{4.2}$$

No free magnetic monopoles exist

$$\nabla \cdot \mathbf{b} = 0 \tag{4.3}$$

Modified (by Maxwell) Ampere's law

$$\nabla \times \mathbf{b} = \frac{1}{c}\frac{\partial \mathbf{e}}{\partial t} + \frac{4\pi}{c}\mathbf{j} \tag{4.4}$$

[1] For CGS units.

where $\mathbf{e}$ is the electric field, $\mathbf{b}$ is the magnetic field, $\mathbf{j}$ is the current density, ρ is the charge density and $c \simeq 3 \times 10^8$ ms^{-1} is the speed of light. These microscopic Maxwell's equations are used to predict the pointwise electric $\mathbf{e}$ and magnetic $\mathbf{b}$ fields given the charge and current densities (ρ and $\mathbf{j}$ respectively).

By including a modification to Ampere's law, i.e. the inclusion of the 'displacement current' term $\partial\mathbf{e}/\partial(ct)$, Maxwell (see Figure 4.1) provided a unification of electricity and magnetism compounded in the equations above.

Figure 4.1: James Clerk Maxwell

4.2.1 Linearity of Maxwell's Equations

Maxwell's equations are linear because if

$$\rho_1, \quad \mathbf{j}_1 \rightarrow \mathbf{e}_1, \quad \mathbf{b}_1$$

and

$$\rho_2, \quad \mathbf{j}_2 \rightarrow \mathbf{e}_2, \quad \mathbf{b}_2$$

then

$$\rho_1 + \rho_2, \quad \mathbf{j}_1 + \mathbf{j}_2 \rightarrow \mathbf{e}_1 + \mathbf{e}_2, \quad \mathbf{b}_1 + \mathbf{b}_2$$

where $\rightarrow$ means 'produces'. This is because the operators $\nabla\cdot$, $\nabla\times$ and the time derivatives are all linear operators.

4.2.2 Solution to Maxwell's Equations

The solution to these equations is based on exploiting the properties of vector calculus and, in particular, identities involving the curl.

Taking the curl of equation (4.2), we have

$$\nabla \times \nabla \times \mathbf{e} = -\frac{1}{c}\nabla \times \frac{\partial \mathbf{b}}{\partial t}$$

and using the identity (see Chapter 1)

$$\nabla \times \nabla \times \mathbf{e} = \nabla(\nabla \cdot \mathbf{e}) - \nabla^2 \mathbf{e}$$

together with equations (4.1) and (4.4), we get

$$\nabla(4\pi\rho) - \nabla^2 \mathbf{e} = -\frac{1}{c}\frac{\partial}{\partial t}\left(\frac{1}{c}\frac{\partial \mathbf{e}}{\partial t} + \frac{4\pi}{c}\mathbf{j}\right)$$

or, after rearranging,

$$\nabla^2 \mathbf{e} - \frac{1}{c^2}\frac{\partial^2 \mathbf{e}}{\partial t^2} = 4\pi\nabla\rho + \frac{4\pi}{c^2}\frac{\partial \mathbf{j}}{\partial t}. \tag{4.5}$$

Taking the curl of equation (4.4), using the identity above, equations (4.2) and (4.3) and rearranging the result gives

$$\nabla^2 \mathbf{b} - \frac{1}{c^2}\frac{\partial^2 \mathbf{b}}{\partial t^2} = -\frac{4\pi}{c}\nabla \times \mathbf{j}. \tag{4.6}$$

Equations (4.5) and (4.6) are inhomogeneous wave equations for $\mathbf{e}$ and $\mathbf{b}$. These equations are related or coupled to the vector field $\mathbf{j}$ (which is related to $\mathbf{b}$). If we define a region of free space where $\rho = 0$ and $\mathbf{j} = 0$, then both $\mathbf{e}$ and $\mathbf{b}$ satisfy the equation

$$\nabla^2 \mathbf{f} - \frac{1}{c^2}\frac{\partial^2 \mathbf{f}}{\partial t^2} = 0.$$

This is the homogeneous wave equation. One possible solution of this equation (in Cartesian coordinates) is

$$f_x = p(z - ct); \quad f_y = 0, \quad f_z = 0$$

which describes a wave or distribution p moving along z at velocity c. Thus, we have shown that in free space when

$$\nabla \cdot \mathbf{e} = 0, \qquad \nabla \cdot \mathbf{b} = 0,$$

$$\nabla \times \mathbf{e} = -\frac{1}{c}\frac{\partial \mathbf{b}}{\partial t}, \qquad \nabla \times \mathbf{b} = \frac{1}{c}\frac{\partial \mathbf{e}}{\partial t}.$$

Maxwell's equations describe the propagation of an electric and magnetic (or electromagnetic field) in terms of a wave traveling at the speed of light (see front cover). After developing the origins of the vector calculus, Maxwell derived the wave equations for an electromagnetic field in a paper entitled *A Dynamical Theory of the Electromagnetic Field*, first published in 1865 and arguably one of the greatest intellectual achievements in the history of physics.

4.3 General Solution to Maxwell's (Microscopic) Equations

The solution to Maxwell's equation in free space is specific to the charge density and current density being zero. We now investigate a method of solution for the general case. The basic method of solving Maxwell's equations (i.e. finding $\mathbf{e}$ and $\mathbf{b}$ given ρ and $\mathbf{j}$) involves the following:

(i) Expressing $\mathbf{e}$ and $\mathbf{b}$ in terms of two other fields U and $\mathbf{A}$.

(ii) Obtaining two separate equations for U and $\mathbf{A}$.

(iii) Solving these equations for U and $\mathbf{A}$ from which $\mathbf{e}$ and $\mathbf{b}$ can then be computed.

For any vector field $\mathbf{A}$

$$\nabla \cdot \nabla \times \mathbf{A} = 0.$$

Hence, if we write

$$\mathbf{b} = \nabla \times \mathbf{A} \tag{4.7}$$

then equation (4.3) remains unchanged. Equation (4.2) can then be written as

$$\nabla \times \mathbf{e} = -\frac{1}{c}\frac{\partial}{\partial t}\nabla \times \mathbf{A}$$

or

$$\nabla \times \left(\mathbf{e} + \frac{1}{c}\frac{\partial \mathbf{A}}{\partial t}\right) = 0.$$

The field $\mathbf{A}$ is called the Magnetic Vector Potential. For any scalar field U

$$\nabla \times \nabla U = 0$$

and thus equation (4.2) is satisfied if we write

$$\pm \nabla U = \mathbf{e} + \frac{1}{c}\frac{\partial \mathbf{A}}{\partial t}$$

or

$$\mathbf{e} = -\nabla U - \frac{1}{c}\frac{\partial \mathbf{A}}{\partial t} \tag{4.8}$$

where the minus sign is taken by convention. U is called the Electric Scalar Potential.

Substituting equation (4.8) into Maxwell's equation (4.1) gives

$$\nabla \cdot \left(\nabla U + \frac{1}{c}\frac{\partial \mathbf{A}}{\partial t}\right) = -4\pi\rho$$

or

$$\nabla^2 U + \frac{1}{c}\frac{\partial}{\partial t}\nabla \cdot \mathbf{A} = -4\pi\rho. \tag{4.9}$$

Substituting equations (4.7) and (4.8) into Maxwell's equation (4.4) gives

$$\nabla \times \nabla \times \mathbf{A} + \frac{1}{c}\frac{\partial}{\partial t}\left(\nabla U + \frac{1}{c}\frac{\partial \mathbf{A}}{\partial t}\right) = \frac{4\pi}{c}\mathbf{j}$$

Finally, using the identity

$$\nabla \times \nabla \times \mathbf{A} = \nabla(\nabla \cdot \mathbf{A}) - \nabla^2 \mathbf{A}$$

we can write

$$\nabla^2 \mathbf{A} - \frac{1}{c^2}\frac{\partial^2 \mathbf{A}}{\partial t^2} - \nabla\left(\nabla \cdot \mathbf{A} + \frac{1}{c}\frac{\partial U}{\partial t}\right) = -\frac{4\pi}{c}\mathbf{j} \tag{4.10}$$

If we could solve equations (4.9) and (4.10) above for U and $\mathbf{A}$ then $\mathbf{e}$ and $\mathbf{b}$ could be computed. The problem here, is that equations (4.9) and (4.10) are coupled. They can be decoupled by applying a technique known as a 'gauge transformation' called the Lorentz gauge transformation, after Lorentz who was among the first to consider it as an approach to solving these equations. The idea is based on noting that equations (4.7) and (4.8) are unchanged if we let

$$\mathbf{A} \to \mathbf{A} + \nabla X$$

and

$$U \to U - \frac{1}{c}\frac{\partial X}{\partial t}$$

since $\nabla \times \nabla X = 0$. If this gauge function X is taken to satisfy the homogeneous wave equation

$$\nabla^2 X - \frac{1}{c^2}\frac{\partial^2 X}{\partial t^2} = 0$$

then

$$\nabla \cdot \mathbf{A} + \frac{1}{c}\frac{\partial U}{\partial t} = 0 \tag{4.11}$$

which is called the Lorentz condition. With equation (4.11), equations (4.9) and (4.10) become

$$\nabla^2 U - \frac{1}{c^2}\frac{\partial^2 U}{\partial t^2} = -4\pi\rho \tag{4.12}$$

and

$$\nabla^2 \mathbf{A} - \frac{1}{c^2}\frac{\partial^2 \mathbf{A}}{\partial t^2} = -\frac{4\pi}{c}\mathbf{j}$$

respectively. These equations are non-coupled inhomogeneous wave equations whose solution (using the Green function) will be considered in the following Chapter.

4.4 The Macroscopic Maxwell's Equations

The microscopic form of Maxwell's equations tells us how individual charged particles and electromagnetic fields interact. When there are many particles

per cubic wavelength, the electromagnetic radiation 'sees' only a macroscopic average. The medium is then described by its dielectric parameters: the permittivity ϵ, the magnetic permeability μ and the conductivity σ.

Simple averaging of the quantities over a small volume V, e.g.

$$\mathbf{E}(\mathbf{r},t) = \frac{1}{V}\int_V \mathbf{e}(\mathbf{r}',t)d^3\mathbf{r}', \quad \mathbf{B}(\mathbf{r},t) = \frac{1}{V}\int_V \mathbf{b}(\mathbf{r}',t)d^3\mathbf{r}'$$

leads to the following, but not very useful, macroscopic form of Maxwell's equations:

$$\nabla\cdot\mathbf{E} = 4\pi\rho_{\text{macro}}, \quad \nabla\times\mathbf{E} = -\frac{1}{c}\frac{\partial\mathbf{B}}{\partial t},$$
$$\nabla\cdot\mathbf{B} = 0, \quad \nabla\times\mathbf{B} = \frac{1}{c}\frac{\partial\mathbf{E}}{\partial t} + \frac{4\pi}{c}\mathbf{j}_{\text{macro}}.$$

However, both ρ_{macro} and $\mathbf{j}_{\text{macro}}$ can be split into two terms due to free and bound electrons, i.e. we can write

$$\rho_{\text{macro}} = \rho_{\text{bound}} + \rho_{\text{free}}$$

and

$$\mathbf{j}_{\text{macro}} = \mathbf{j}_{\text{bound}} + \mathbf{j}_{\text{free}}.$$

By *bound*, we mean that the electrons are bound to the nucleus to constitute an atom. If we introduce an electric polarization $\mathbf{P}$ of the medium to represent the average dipole moment per unit volume given by

$$\mathbf{P} = -Ne\mathbf{s}$$

where $\mathbf{s}$ is the average vector between bound electrons and nuclei, e is the charge of an electron and N is the average number of electrons per unit volume, then we can define the charge density of bound electrons as

$$\rho_{\text{bound}} = -\nabla\cdot\mathbf{P}$$

and the current density of bound electrons in the form

$$\mathbf{j}_{\text{bound}} = \frac{\partial\mathbf{P}}{\partial t} + c\nabla\times\mathbf{M}$$

where $\mathbf{M}$ is the magnetization vector. At optical frequencies, $\mathbf{M} = 0$ (in the absence of a strong applied magnetic field). Further, we now define the following:

(i) the displacement vector given by $\mathbf{D} = \mathbf{E} + 4\pi\mathbf{P}$;

(ii) the magnetic field strength given by $\mathbf{H} = \mathbf{B} - 4\pi\mathbf{M}$.

From these definitions, we obtain a useful macroscopic form of Maxwell's equations given by

$$\nabla\cdot\mathbf{D} = 4\pi\rho_{\text{free}}, \quad \nabla\times\mathbf{E} = -\frac{1}{c}\frac{\partial\mathbf{B}}{\partial t}$$
$$\nabla\cdot\mathbf{B} = 0, \quad \nabla\times\mathbf{H} = \frac{1}{c}\frac{\partial\mathbf{D}}{\partial t} + \frac{4\pi}{c}\mathbf{j}_{\text{free}}$$

These equations are valid for media which are: (i) non-isotropic; (ii) inhomogeneous.

4.5 EM Waves in a Homogeneous Medium

Having derived Maxwell's equation in macroscopic form, let us now consider the type of solutions they provide for a specific case. Suppose we illuminate a homogeneous material with monochromatic radiation of angular frequency ω. What are the possible solutions of Maxwell's equations in the material? i.e. what waves exist in the medium?

4.5.1 Linear Medium

Assume that all the macroscopic vectors oscillate sinusoidally at angular frequency ω (this is true, in general, only for high frequency, weak fields). Define vector amplitudes $\mathbf{E}(\mathbf{r},t) = \mathbf{E}(\mathbf{r},\omega)\exp(-i\omega t)$, $\mathbf{B}(\mathbf{r},t) = \mathbf{B}(\mathbf{r},\omega)\exp(-i\omega t)$ and so on[2], so that Maxwell's equations can be written in the form

$$\nabla \cdot \mathbf{D} = 4\pi\rho \tag{4.13}$$

$$\nabla \times \mathbf{E} = \frac{i\omega}{c}\mathbf{B} \tag{4.14}$$

$$\nabla \cdot \mathbf{B} = 0 \tag{4.15}$$

$$\nabla \times \mathbf{H} = -\frac{i\omega}{c}\mathbf{D} + \frac{4\pi}{c}\mathbf{j} \tag{4.16}$$

where ρ and $\mathbf{j}$ are taken to be the free charge density and the free current density, respectively.

Let

$$\mathbf{P} = \chi_e\mathbf{E}, \quad \mathbf{M} = \chi_m\mathbf{H} \quad \text{and} \quad \mathbf{j} = \sigma\mathbf{E}$$

where χ_e is the electric susceptibility, χ_m is the magnetic susceptibility and σ is the conductivity, each of which may be tensors. Note that, in general, this linearity may not occur and $\mathbf{P}$ could be of the form

$$\mathbf{P} = \chi_e\mathbf{E}(1 + a_1\mathbf{E} + a_2\mathbf{E}^2 + ...).$$

Here $a_1, a_2, ...$ are constant coefficients which would introduce a nonlinear optical material and nonlinear optical effects for example. Note that the effect of introducing monochromatic radiation (i.e. a wavefield oscillating at one single frequency ω) is to replace the time derivatives in Maxwell's equations with $i\omega$ which significantly helps in the algebra required to derive the solutions that follow.

4.5.2 Isotropic Medium

Let χ_e, χ_m and σ be complex scalars (not tensors) and let us define the following:

(i) the dielectric constant given by $\epsilon = 1 + 4\pi\chi_e$;

[2]Strictly speaking $\mathbf{E}(\mathbf{r},\omega)$, $\mathbf{B}(\mathbf{r},\omega)$, etc. should be given a different notation but, in the context of the equations that follow, it is implied that all dependent variables are functions of $\mathbf{r}$ and ω and not $\mathbf{r}$ and t.

(ii) the magnetic permeability given by $\mu = 1 + 4\pi\chi_m$

so that we can write

$$\mathbf{D} = \epsilon\mathbf{E} \tag{4.17}$$

and

$$\mathbf{B} = \mu\mathbf{H}. \tag{4.18}$$

Taking the divergence of equation (4.16) and noting that $\nabla \cdot \nabla \times \mathbf{H} = 0$, we have

$$-i\omega\nabla \cdot \mathbf{D} + 4\pi\nabla \cdot \mathbf{j} = 0.$$

Hence, from equation (4.13) we get

$$\rho = -\frac{i}{\omega}\nabla \cdot \mathbf{j} = -\frac{i}{\omega}\nabla \cdot (\sigma\mathbf{E}). \tag{4.19}$$

Substituting equations (4.17), (4.18) and (4.19) into Maxwell's equation (4.13)-(4.16), we obtain the following time independent equations for the complex vector amplitudes:

$$\nabla \cdot \left(\epsilon + \frac{i4\pi\sigma}{\omega}\right)\mathbf{E} = 0, \quad \nabla \times \mathbf{E} = \frac{i\omega\mu}{c}\mathbf{H},$$

$$\nabla \cdot (\mu\mathbf{H}) = 0, \quad \nabla \times \mathbf{H} = -\frac{i\omega}{c}\left(\epsilon + \frac{i4\pi\sigma}{\omega}\right)\mathbf{E}.$$

These equations apply to a linear, isotropic but inhomogeneous medium, i.e. ϵ, μ and σ may be functions of position. Note that, for any vector $\mathbf{X}$ and scalar a,

$$\nabla \cdot (a\mathbf{X}) = \nabla a \cdot \mathbf{X} + a\nabla \cdot \mathbf{X} \neq a\nabla \cdot \mathbf{X}, \quad \text{unless} \quad \nabla a = 0.$$

4.5.3 Homogeneous Medium

For a homogeneous medium (where ϵ, μ and σ are constants, the previous set of equations reduces to

$$\nabla \cdot \mathbf{E} = 0, \quad \nabla \times \mathbf{E} = \frac{i\omega\mu}{c}\mathbf{H},$$

$$\nabla \cdot \mathbf{H} = 0, \quad \nabla \times \mathbf{H} = -\frac{i\omega}{c}\left(\epsilon + \frac{i4\pi\sigma}{\omega}\right)\mathbf{E}.$$

4.5.4 Plane Wave Solutions

Let

$$\mathbf{E} = \mathbf{E}_0 \exp(i\mathbf{k}_c \cdot \mathbf{r}) \qquad \mathbf{H} = \mathbf{H}_0 \exp(i\mathbf{k}_c \cdot \mathbf{r})$$

where $\mathbf{k}_c$ is the complex wave number. Noting that

$$\nabla \cdot [\mathbf{C} \exp(i\mathbf{k}_c \cdot \mathbf{r})] = i\mathbf{k}_c \cdot \mathbf{C} \exp(i\mathbf{k}_c \cdot \mathbf{r})$$

and

$$\nabla \times [\mathbf{C} \exp(i\mathbf{k}_c \cdot \mathbf{r})] = i\mathbf{k}_c \times \mathbf{C} \exp(i\mathbf{k}_c \cdot \mathbf{r})$$

we obtain

$$\mathbf{k}_c \cdot \mathbf{E}_0 = 0, \quad \mathbf{k}_c \cdot \mathbf{H}_0 = 0, \tag{4.20}$$

$$\mathbf{k}_c \times \mathbf{E}_0 = \frac{\mu\omega}{c}\mathbf{H}_0, \tag{4.21}$$

$$\mathbf{k}_c \times \mathbf{H}_0 = -\frac{\omega}{c}\left(\epsilon + \frac{i4\pi\sigma}{\omega}\right)\mathbf{E}_0. \tag{4.22}$$

Equations (4.20) are referred to as the transversality conditions. Substituting equation (4.21) into equation (4.22) yields

$$\frac{c}{\mu\omega}\mathbf{k}_c \times (\mathbf{k}_c \times \mathbf{E}_0) = -\frac{\omega}{c}\left(\epsilon + \frac{i4\pi\sigma}{\omega}\right)\mathbf{E}_0.$$

Using the identity

$$\mathbf{A} \times (\mathbf{B} \times \mathbf{C}) = (\mathbf{A} \cdot \mathbf{C})\mathbf{B} - (\mathbf{A} \cdot \mathbf{B})\mathbf{C}$$

we can write this result in the form

$$(\mathbf{k}_c \cdot \mathbf{E}_0)\mathbf{k}_c - (\mathbf{k}_c \cdot \mathbf{k}_c)\mathbf{E}_0 = -\frac{\mu\omega^2}{c^2}\left(\epsilon + \frac{i4\pi\sigma}{\omega}\right)\mathbf{E}_0$$

or, since $\mathbf{k}_c \cdot \mathbf{E}_0 = 0$, as

$$\mathbf{k}_c \cdot \mathbf{k}_c = n_c^2 k_0^2 \tag{4.23}$$

where

$$k_0 = \frac{2\pi}{\lambda} = \frac{\omega}{c}$$

and

$$n_c^2 = \epsilon\mu + \frac{i4\pi\mu\sigma}{\omega}.$$

Here, n_c is called the complex refractive index. Let

$$n_c = n + i\kappa$$

and

$$\mathbf{k}_c = \mathbf{k} + i\mathbf{a}$$

where n is the refractive index, κ is the extinction index, $\mathbf{k}$ is the wavenumber and $\mathbf{a}$ is the attenuation vector. Substituting these expressions into equation (4.23) and equating the real and imaginary parts gives

$$k^2 - a^2 = k_0^2(n^2 - \kappa^2) \tag{4.24}$$

and

$$\mathbf{k} \cdot \mathbf{a} = k_0^2 n\kappa. \tag{4.25}$$

Thus, plane wave solutions exist of the form

$$\mathbf{E} = \mathbf{E}_0 \exp(i\mathbf{k}_c \cdot \mathbf{r}); \quad \mathbf{H} = \mathbf{H}_0 \exp(i\mathbf{k}_c \cdot \mathbf{r})$$

where, from equation (4.23),

$$|\ \mathbf{k}_c\ | = n_c k_0, \mathbf{k}_c \cdot \mathbf{E}_0 = 0$$

and

$$\mathbf{H}_0 = \frac{1}{\mu k_0}\mathbf{k}_c \times \mathbf{E}_0.$$

4.5.5 Non-absorbing Media ($\kappa = 0$)

Equations (4.24) and (4.25) reduce to

$$k^2 - a^2 = n^2 k_0^2 > 0$$

and

$$\mathbf{k} \cdot \mathbf{a} = 0.$$

Two kinds of waves are possible:

(i) Real vector waves where $\mathbf{a} = 0, \quad \mathbf{k}_c = \mathbf{k}, \quad | \mathbf{k} | = k_0 n$ and

$$\mathbf{E}(\mathbf{r}, \omega) = \mathbf{E}_0(\mathbf{r}, \omega) \exp(i\mathbf{k} \cdot \mathbf{r})$$

or

$$\mathbf{E}(\mathbf{r}, t) = \mathbf{E}_0(\mathbf{r}, t) \exp[i(\mathbf{k} \cdot \mathbf{r} - \omega t)].$$

This is like a free space plane wave. The velocity of propagation is $\omega/k = c/n$ and the wavelength, is λ/n. Both amplitude and phase are constant and perpendicular to $\mathbf{k}$, i.e. the wave is homogeneous. Since $\mathbf{k} \cdot \mathbf{E}_0 = 0$, the real and imaginary parts of $\mathbf{E}$ are perpendicular to $\mathbf{k}$. $\mathbf{H}$ is also perpendicular to $\mathbf{k}$ and Re[$\mathbf{E}$] is perpendicular to Re[$\mathbf{H}$].

(ii) Complex wave vector where $\mathbf{k}$ is perpendicular to $\mathbf{a}$ so that $\mathbf{k} \cdot \mathbf{a} = 0$ and

$$\mathbf{E}(\mathbf{r}, t) = \mathbf{E}_0(\mathbf{r}, t) \exp(-\mathbf{a} \cdot \mathbf{r}) \exp[i(\mathbf{k} \cdot \mathbf{r} - \omega t)]$$

which propagates along $\mathbf{k}$ with velocity $\omega/k < c/n$. The amplitude is constant over planes perpendicular to $\mathbf{a}$ and the phase is constant over planes perpendicular to $\mathbf{k}$ - the wave is homogeneous.

4.5.6 Absorbing Media ($\kappa > 0$, $\mathbf{k} \cdot \mathbf{a} \neq 0$)

(i) Homogeneous wave: $\mathbf{k}$ and $\mathbf{a}$ are in the same direction,

$$\mathbf{k} = n\mathbf{k}_0, \quad \mathbf{a} = \kappa \mathbf{k}_0$$

and

$$\mathbf{E}(\mathbf{r}, t) = \mathbf{E}_0(\mathbf{r}, \omega) \exp(-\kappa \mathbf{k}_0 \cdot \mathbf{r}) \exp[i(n\mathbf{k}_0 \cdot \mathbf{r} - \omega t)].$$

This wave propagates along $\mathbf{k}_0$ at velocity c/n, with wavelength λ_0/n and decreases exponentially along the direction of propagation. Both amplitude and phase are constant and perpendicular to $\mathbf{k}_0$ and both $\mathbf{E}$ and $\mathbf{H}$ are perpendicular to $\mathbf{k}_0$. Re[$\mathbf{E}$] is not perpendicular to Re[$\mathbf{H}$].

(ii) Inhomogeneous wave: $\mathbf{k}$ and $\mathbf{a}$ are not in the same direction. There is constant phase perpendicular to $\mathbf{k}$ and constant amplitude perpendicular to $\mathbf{a}$. Since $\mathbf{a}$ has a component along $\mathbf{k}$, there is a decrease of amplitude along $\mathbf{k}$.

4.6 EM Waves in an Inhomogeneous Medium

In the previous Section, we considered the EM waves that can occur in a homogeneous material that is linear and isotropic by studying Maxwell's equations for monochromatic propagation. We now turn our attention to developing wave equations for a medium that is linear, isotropic and inhomogeneous using Maxwell's equations in the form[3]

$$\nabla \cdot \epsilon \mathbf{E} = \rho, \tag{4.26}$$

$$\nabla \cdot \mu \mathbf{H} = 0, \tag{4.27}$$

$$\nabla \times \mathbf{E} = -\mu \frac{\partial \mathbf{H}}{\partial t}, \tag{4.28}$$

and

$$\nabla \times \mathbf{H} = \epsilon \frac{\partial \mathbf{E}}{\partial t} + \mathbf{j}. \tag{4.29}$$

where $\mathbf{E}(\mathbf{r}, t)$ is the electric field (volts/metre), $\mathbf{H}(\mathbf{r}, t)$ is the magnetic field (amperes/metre), $\mathbf{j}(\mathbf{r}, t)$ is the current density (amperes/metre^2), $\rho(\mathbf{r}, t)$ is the charge density (charge/metre^2), $\epsilon(\mathbf{r})$ is the permittivity (farads/metre) and $\mu(\mathbf{r})$ is the permeability (henries/metre). The values of ϵ and μ in a vacuum (denoted by ϵ_0 and μ_0, respectively) are $\epsilon_0 = 8.854 \times 10^{-12}$ farads/metre and $\mu_0 = 4\pi \times 10^{-7}$ henries/metre. In electromagnetic imaging problems there are two important physical models to consider, based on whether a material is either conductive or non-conductive.

4.6.1 Conductive Materials

In this case, the medium is assumed to be a good conductor. A current is induced which depends on the magnitude of the electric field and the conductivity σ (siemens/metre) of the material from which the object is composed. The relationship between the electric field and the current density is given by Ohm's law

$$\mathbf{j} = \sigma \mathbf{E} \tag{4.30}$$

A good conductor is one where σ is large. By taking the divergence of equation (4.29) and noting that

$$\nabla \cdot (\nabla \times \mathbf{H}) = 0$$

we obtain (using equation (4.26) for constant ϵ)

$$\frac{\partial \rho}{\partial t} + \frac{\sigma}{\epsilon} \rho = 0.$$

The solution to this equation is

$$\rho(t) = \rho_0 \exp(-\sigma t/\epsilon), \quad \text{where} \quad \rho_0 = \rho(t = 0).$$

This solution shows that the charge density decays exponentially with time. Typical values of ϵ are $\sim 10^{-12} - 10^{-10}$ farads/metre. Hence, provided σ is

[3]For SI units.

not too small, the dissipation of charge is very rapid. It is therefore physically reasonable to set the charge density to zero and, for problems involving the interaction of electromagnetic waves with good conductors, equation (4.26) can be approximated by

$$\nabla \cdot \epsilon \mathbf{E} = 0 \tag{4.31}$$

and equation (4.29) becomes

$$\nabla \times \mathbf{H} = \epsilon \frac{\partial \mathbf{E}}{\partial t} + \sigma \mathbf{E}.$$

Note that, in imaging problems, the material may not necessarily be conductive throughout but may be a varying dielectric with distributed conductive elements. For example, in imaging the surface of the Earth using microwave radiation (Synthetic Aperture Radar), the electromagnetic scattering model is based on a 'ground truth' that is predominantly a dielectric (dry ground surfaces and dry vegetation for example) with distributed conductors (e.g. metallic objects on a dry ground surface, the sea and to a lesser extent rivers and lakes).

4.6.2 Non-conductive Dielectrics

In this case, it is assumed that the conductivity of the medium is negligible and no current can flow, and hence

$$\mathbf{j} = 0$$

and equation (4.29) is just

$$\nabla \times \mathbf{H} = \epsilon \frac{\partial \mathbf{E}}{\partial t}.$$

Also, if the conductivity is zero then $\rho = \rho_0$ and if $\rho_0 = 0$ then equation (4.26) becomes

$$\nabla \cdot \epsilon \mathbf{E} = 0.$$

The issues of when a material is a conductor or a dielectric is compounded in the relative importance of the terms j and $\epsilon(\partial \mathbf{E}/\partial t)$ in equation (4.29). Let us consider the electric and magnetic fields to be monochromatic waves, so that equation (4.29) becomes (with $\mathbf{j} = \sigma \mathbf{E}$)

$$\nabla \times \mathbf{H}(\mathbf{r}, \omega) = (i\omega\epsilon + \sigma)\mathbf{E}(\mathbf{r}, \omega).$$

The relative importance of the terms on the right hand side of equation (4.29) is then determined by the magnitudes of σ and $\omega\epsilon$. If

$$\frac{\sigma}{\omega\epsilon} >> 1$$

then conduction currents dominate and the medium is a conductor. If

$$\frac{\sigma}{\omega\epsilon} << 1$$

then displacement currents dominate and the material behaves as a dielectric. When

$$\frac{\sigma}{\omega\epsilon} \sim 1$$

the material is a quasi-conductor; some types of semi-conductor fall into this category. Note that the ratio $\sigma/\omega\epsilon$ is frequency dependent and that, consequently, a conductor at one frequency may be a dielectric at another. For example, copper has a conductivity of 5.8×10^7 siemens/metre and $\epsilon \simeq 9 \times 10^{-12}$ farads/metre so that

$$\frac{\sigma}{\omega\epsilon} \sim \frac{10^{18}}{\omega}.$$

Up to a frequency of 10^{16}Hz (the frequency of ultraviolet light) $\sigma/\omega\epsilon >> 1$, and copper is a conductor. At a frequency of 10^{20}Hz (the frequency of X-rays), however, $\sigma/\omega\epsilon << 1$ and copper behaves as a dielectric. This is why X-rays travel distances of many wavelengths in copper. An insulator has a conductivity in the order of 10^{-15} siemens/metre and a permittivity of the order of 10^{-11} farads/metre, which gives

$$\frac{\omega\epsilon}{\sigma} \sim 10^4\omega$$

so the conduction current is negligible at all frequencies.

4.6.3 EM Wave Equation

In many electromagnetic imaging systems, the field that is measured is the electric field. It is therefore appropriate to use a wave equation which describes the behaviour of the electric field. This can be obtained by decoupling Maxwell's equations for the magnetic field $\mathbf{H}$. Starting with equation (4.28), we divide through by μ and take the curl of the resulting equation. This gives

$$\nabla \times \left(\frac{1}{\mu}\nabla \times \mathbf{E}\right) = -\frac{\partial}{\partial t}\nabla \times \mathbf{H}.$$

By taking the derivative with respect to time t of equation (4.29) and using Ohm's law - equation (4.30) - we obtain

$$\frac{\partial}{\partial t}(\nabla \times \mathbf{H}) = \epsilon\frac{\partial^2\mathbf{E}}{\partial t^2} + \sigma\frac{\partial\mathbf{E}}{\partial t}.$$

From the previous equation we can then write

$$\nabla \times \left(\frac{1}{\mu}\nabla \times \mathbf{E}\right) = -\epsilon\frac{\partial^2\mathbf{E}}{\partial t^2} - \sigma\frac{\partial\mathbf{E}}{\partial t} \tag{4.32}$$

Expanding the first term, multiplying through by μ and noting that

$$\mu\nabla\left(\frac{1}{\mu}\right) = -\nabla \ln \mu$$

we get

$$\nabla \times \nabla \times \mathbf{E} + \epsilon\mu\frac{\partial^2\mathbf{E}}{\partial t^2} + \sigma\mu\frac{\partial\mathbf{E}}{\partial t} = (\nabla \ln \mu) \times \nabla \times \mathbf{E}.$$

Expanding equation (4.31) we have

$$\epsilon\nabla \cdot \mathbf{E} + \mathbf{E} \cdot \nabla\epsilon = 0$$

or

$$\nabla \cdot \mathbf{E} = -\mathbf{E} \cdot \nabla \ln \epsilon.$$

Hence, using the vector identity

$$\nabla \times \nabla \times \mathbf{E} = -\nabla^2 \mathbf{E} + \nabla(\nabla \cdot \mathbf{E})$$

we obtain the following wave equation for the electric field

$$\nabla^2 \mathbf{E} - \epsilon\mu \frac{\partial^2 \mathbf{E}}{\partial t^2} - \sigma\mu \frac{\partial \mathbf{E}}{\partial t} = -\nabla(\mathbf{E} \cdot \nabla \ln \epsilon) - (\nabla \ln \mu) \times \nabla \times \mathbf{E}.$$

This equation is inhomogeneous in ϵ, μ and σ. Solutions to this equation provide information on the behaviour of the electric field in a fluctuating conductive dielectric environment. In electromagnetic imaging problems, interest focuses on the behaviour of the scattered EM wavefield generated by variations in the material parameters ϵ, μ and σ. In this context, ϵ, μ and σ are sometimes referred to as the electromagnetic scatter generating parameters. In electromagnetic imaging, the problem is to reconstruct these parameters by measuring certain properties of the scattered electric field. This is a three parameter inverse problem which requires us to first solve for the electric field $\mathbf{E}$ given ϵ, μ and σ.

4.6.4 Inhomogeneous EM Wave Equations

In order to solve the wave equation derived in the last section using the most appropriate analytical methods for imaging science (i.e. Green function solutions which are discussed in the following Chapter), it must be re-cast in the form of the Langevin equation

$$(\nabla^2 + k^2)\mathbf{E} = -\hat{L}\mathbf{E}$$

where $\hat{L}$ is an inhomogeneous differential operator. Starting with equation (4.32), by adding

$$\epsilon_0 \frac{\partial^2 \mathbf{E}}{\partial t^2} - \frac{1}{\mu_0} \nabla \times \nabla \times \mathbf{E}$$

to both sides of this equation and re-arranging, we can write

$$\nabla \times \nabla \times \mathbf{E} + \epsilon_0\mu_0 \frac{\partial^2 \mathbf{E}}{\partial t^2} = -\epsilon_0\mu_0\gamma_\epsilon \frac{\partial^2 \mathbf{E}}{\partial t^2} - \mu_0\sigma \frac{\partial \mathbf{E}}{\partial t} + \nabla \times (\gamma_\mu \nabla \times \mathbf{E})$$

where

$$\gamma_\epsilon = \frac{\epsilon - \epsilon_0}{\epsilon_0} \quad \text{and} \quad \gamma_\mu = \frac{\mu - \mu_0}{\mu}.$$

We can then use the result (valid for $\rho \sim 0$)

$$\begin{aligned} \nabla \times \nabla \times \mathbf{E} &= -\nabla^2 \mathbf{E} + \nabla(\nabla \cdot \mathbf{E}) \\ &= -\nabla^2 \mathbf{E} - \nabla(\mathbf{E} \cdot \nabla \ln \epsilon) \end{aligned}$$

so that the above wave equation can be written as

$$\nabla^2\mathbf{E} - \epsilon_0\mu_0\frac{\partial\mathbf{E}}{\partial t^2} = \mu_0\epsilon_0\gamma_\epsilon\frac{\partial^2\mathbf{E}}{\partial t^2} + \mu_0\sigma\frac{\partial\mathbf{E}}{\partial t} - \nabla(\mathbf{E}\cdot\nabla\ln\epsilon) - \nabla\times(\gamma_\mu\nabla\times\mathbf{E}).$$

Finally, introducing the Fourier transform

$$\mathbf{E}(\mathbf{r},t) = \frac{1}{2\pi}\int_{-\infty}^{\infty}\widetilde{\mathbf{E}}(\mathbf{r},\omega)\exp(i\omega t)d\omega,$$

we can write the above wave equation in the time independent form

$$(\nabla^2 + k^2)\widetilde{\mathbf{E}} = -k^2\gamma_\epsilon\widetilde{\mathbf{E}} + ikz_0\sigma\widetilde{\mathbf{E}} - \nabla(\widetilde{\mathbf{E}}\cdot\nabla\ln\epsilon) - \nabla\times(\gamma_\mu\nabla\times\widetilde{\mathbf{E}})$$

where

$$k = \frac{\omega}{c_0}, \quad c_0 = \frac{1}{\sqrt{\epsilon_0\mu_0}} \quad \text{and} \quad z_0 = \mu_0 c_0.$$

The parameter z_0 is the free space wave impedance and is approximately equal to 376.6 ohms. The constant c_0 is the velocity at which electromagnetic waves propagate in a perfect vacuum. In electromagnetic imaging, the fundamental problem is to obtain images of the parameters γ_ϵ, γ_μ and the conductivity σ.

4.7 Elastic Field Equations

The propagation and scattering of acoustic radiation in a non-compressible solid is characterized by the elastic field equations. For a stationary isotropic material, the governing equation of motion for an elastic field is given by

$$\rho\frac{\partial^2\mathbf{s}}{\partial t^2} = \nabla\cdot\mathbf{T}$$

where $\mathbf{s}(\mathbf{r},t)$ is the displacement vector (metres), $\rho(\mathbf{r})$ is the material density (mass per unit volume) and $\mathbf{T}(\mathbf{r},t)$ is the material stress tensor (force per unit volume). The material stress tensor is determined by two parameters known as the first and second elastic Lamé parameters (α and β, respectively), whose dimensions are force×time/volume, and is given by

$$\mathbf{T}(\mathbf{r},t) = \alpha(\mathbf{r})\mathbf{I}\nabla\cdot\mathbf{s}(\mathbf{r},t) + \beta(\mathbf{r})[\nabla s(\mathbf{r},t) + \mathbf{s}(\mathbf{r},t)\nabla]$$

where $\mathbf{I}$ $(= \hat{\mathbf{x}}\hat{\mathbf{x}} + \hat{\mathbf{y}}\hat{\mathbf{y}} + \hat{\mathbf{z}}\hat{\mathbf{z}})$ is the unit dyad and

$$[\nabla\mathbf{s} + \mathbf{s}\nabla] = \nabla\mathbf{s} + \nabla\mathbf{s}^\dagger$$

where $\nabla\mathbf{s}^\dagger$ denotes the transposition of the dyadic field $\nabla\mathbf{s}$.

4.8 Inhomogeneous Elastic Wave Equation

Consider an inhomogeneous elastic material embedded in a homogeneous medium with material constants ρ_0, α_0 and β_0. By adding

$$\rho_0 \frac{\partial^2 \mathbf{s}}{\partial t^2} - \nabla \cdot [\alpha_0 \mathbf{I} \nabla \cdot \mathbf{s} + \beta_0 (\nabla \mathbf{s} + \mathbf{s} \nabla)]$$

to both sides of the equation

$$\rho \frac{\partial^2 \mathbf{s}}{\partial t^2} = \nabla \cdot [\alpha \mathbf{I} \nabla \cdot \mathbf{s} + \beta (\nabla \mathbf{s} + \mathbf{s} \nabla)]$$

and using the results

$$\nabla^2 \mathbf{s} = \nabla(\nabla \cdot \mathbf{s}) - \nabla \times \nabla \times \mathbf{s}, \quad \nabla \mathbf{s} + \mathbf{s} \nabla = 2 \nabla \mathbf{s} + \mathbf{I} \times \nabla \times \mathbf{s} \quad \text{and} \quad \nabla \cdot \mathbf{I} \equiv \nabla$$

we obtain

$$(1 + \gamma_\rho) \frac{1}{c_L^2} \frac{\partial^2 \mathbf{s}}{\partial t^2} = \left(\nabla \nabla \cdot + \nabla \gamma_\alpha \nabla \cdot \quad - \frac{c_R^2}{c_L^2} \nabla \times \nabla \times \right) \mathbf{s} + \nabla \cdot [\gamma_\beta (\nabla \mathbf{s} + \mathbf{s} \nabla)]$$

where γ_α, γ_β and γ_ρ are functions of the elastic field defined by

$$\gamma_\alpha(\mathbf{r}) = \frac{\alpha(\mathbf{r}) - \alpha_0}{\alpha_0 + 2\beta_0}, \quad \gamma_\beta(\mathbf{r}) = \frac{\beta(\mathbf{r}) - \beta_0}{\alpha_0 + 2\beta_0} \quad \text{and} \quad \gamma_\rho(\mathbf{r}) = \frac{\rho(\mathbf{r}) - \rho_0}{\rho_0}$$

and the constants c_L and c_R are the longitudinal and rotational wave speeds respectively, given by

$$c_L^2 = \frac{\alpha_0 + 2\beta_0}{\rho_0} \quad \text{and} \quad c_R^2 = \frac{\beta_0}{\rho_0}, \quad c_L > c_R.$$

The displacement vector $\mathbf{s}$ consists of both longitudinal and rotational components. We can write this vector in terms of two potentials u and $\mathbf{w}$ as

$$\mathbf{s} = \nabla u + \nabla \times \mathbf{w}.$$

Here, u is the longitudinal displacement potential for which $\nabla \times \nabla u = 0$. The first term is the longitudinal or compression wave and the second term describes the shear wave. In general, an elastic wavefield is composed of both compression and shear waves. In order to simplify the problem and work with a single-component wave equation, we consider the case when the shear component is negligible. In an imaging system in which the shear component is not measured, this is a reasonable assumption. However, this case assumes that mode coupling between the compression and shear waves, which can affect the shear wave component that is measured, is negligible. This is a reasonable assumption when the elastic material is weakly inhomogeneous. Thus, substituting the equation $\mathbf{s} = \nabla u$ into the above equation for $\mathbf{s}$, we have

$$\left(\nabla^2 - \frac{1}{c_L^2} \frac{\partial^2}{\partial t^2} \right) \nabla u = \nabla(\gamma_\alpha \nabla^2 u) + 2 \nabla \cdot (\gamma_\beta \nabla \nabla u) + \frac{\gamma_\rho}{c_L} \frac{\partial^2}{\partial t^2} \nabla u.$$

Applying the divergence operator to each term, then gives

$$\left(\nabla^2 - \frac{1}{c_L^2}\frac{\partial^2}{\partial t^2}\right) e = (\gamma_\alpha + 2\gamma_\beta)\nabla\nabla^2 u + 2\nabla(\gamma_\alpha + 2\gamma_\beta)\cdot\nabla\nabla^2 u$$

$$+\nabla^2\gamma_\alpha\nabla^2 u + \frac{1}{c_L^2}\frac{\partial^2}{\partial t^2}\nabla\cdot\gamma_\rho\nabla u + \nabla\nabla\gamma_\beta : \nabla\nabla u$$

where

$$e(\mathbf{r},t) = \nabla^2 u(\mathbf{r},t)$$

and : denotes the tensor product. The wavefield e is the elastic dilatation. The quantitative imaging problem in this case is, on the basis of this elastic wave equation, is to obtain a reconstruction of the parameters γ_ρ, γ_α and γ_β from measurements of the field $e(\mathbf{r},t)$. As with the electromagnetic case, this is a three parameter problem. Finally, introducing the Fourier transforms

$$e(\mathbf{r},t) = \int_{-\infty}^{\infty} E(\mathbf{r},\omega)\exp(-i\omega t)dt$$

and

$$u(\mathbf{r},t) = \int_{-\infty}^{\infty} U(\mathbf{r},\omega)\exp(-i\omega t)dt,$$

we arrive at the inhomogeneous wave equation

$$\left(\nabla^2 + \frac{\omega^2}{c_L^2}\right) E = (\gamma_\alpha + 2\gamma_\beta)\nabla^2\nabla^2 U + 2\nabla(\gamma_\alpha + 2\gamma_\beta)\cdot\nabla\nabla^2 U$$

$$+\nabla^2\gamma_\alpha\nabla^2 U + \frac{\omega^2}{c_L^2}\nabla\cdot\gamma_\rho\nabla U + \nabla\nabla\gamma_\beta : \nabla\nabla U.$$

4.9 Acoustic Field Equations

The acoustic field equations are obtained by linearizing the hydrodynamic equations of motion and may be written in the form

$$\nabla\cdot\mathbf{v} = \kappa\frac{\partial p}{\partial t} \tag{4.33}$$

$$\nabla p = \rho\frac{\partial \mathbf{v}}{\partial t} - \nabla\cdot\mathbf{T} \tag{4.34}$$

where $\mathbf{v}(\mathbf{r},t)$ is the velocity field (length/time), $p(\mathbf{r},t)$ is the pressure field (force/area), $\mathbf{T}(\mathbf{r},t)$ is the material stress tensor (force/volume), $\rho(\mathbf{r})$ is the density (mass/volume) and $\kappa(\mathbf{r})$ is the compressibility (area/force). Compared with the elastic field equation, we now have another material parameter, namely, the compressibility. It is assumed that the material to which these equations comply is adiabatic. The first equation comes from the law of

conservation of mass and the second equation is a consequence of the law of conservation of momentum. For compressional waves alone, the material stress tensor is given by

$$\mathbf{T} = \mathbf{I}\alpha\nabla\cdot\mathbf{v} + 2\beta\nabla\mathbf{v}$$

where $\mathbf{v}$ is taken to be given by ∇u, u being the longitudinal velocity potential. The parameters α and β are related to the bulk ζ and shear η viscosities of a material by the equations

$$\alpha = \zeta - \frac{2}{3}\eta$$

and

$$\beta = \eta$$

When the viscosity is zero (i.e. when $\zeta = \eta = 0$) we are left with the following acoustic field equations:

$$\nabla\cdot\mathbf{v} = \kappa\frac{\partial p}{\partial t} \tag{4.35}$$

$$\nabla p = \rho\frac{\partial \mathbf{v}}{\partial t} \tag{4.36}$$

As in previous cases, it is assumed that ρ, κ, α and β are both isotropic and time invariant.

4.9.1 Acoustic Wave Equation

By decoupling the field equations (4.35) and (4.36) for $\mathbf{v}$, a scalar wave equation for the pressure p can be obtained. This is accomplished by dividing equation (4.36) by ρ and taking the divergence of each term, giving

$$\frac{\partial}{\partial t}\nabla\cdot\mathbf{v} = \nabla\cdot\left(\frac{1}{\rho}\nabla p\right)$$

Differentiating equation (4.35) with respect to time t then gives

$$\frac{\partial}{\partial t}\nabla\cdot\mathbf{v} = \kappa\frac{\partial^2 p}{\partial t^2}.$$

Hence, we can write

$$\nabla\cdot\left(\frac{1}{\rho}\nabla p\right) - \kappa\frac{\partial^2 p}{\partial t^2} = 0 \tag{4.37}$$

or, after expanding the first term,

$$\nabla^2 p - \kappa\rho\frac{\partial^2 p}{\partial t^2} = \nabla\ln\rho\cdot\nabla p.$$

This wave equation is based on a physical model where it is assumed that the propagation and scattering of acoustic waves is only due to variations in the compressibility and density. When fluctuations in the bulk and shear viscosities are present, an additional source of scattering occurs. In this case the appropriate wave equation is obtained by decoupling equations (4.33) and (4.34) for p, giving

$$\nabla\left(\frac{1}{\kappa}\nabla\cdot\mathbf{v}\right) = \rho\frac{\partial^2\mathbf{v}}{\partial t^2} - \frac{\partial}{\partial t}\left[\nabla(\alpha\nabla\cdot\mathbf{v}) + 2\nabla\cdot(\beta\nabla\mathbf{v})\right]. \tag{4.38}$$

4.9.2 Inhomogeneous Acoustic Wave Equations

As with electromagnetic problems, in acoustic imaging, we need to develop inhomogeneous wave equations of the form

$$(\nabla^2 + k^2)u = -\hat{L}u$$

or

$$(\nabla^2 + k^2)\mathbf{u} = -\hat{L}\mathbf{u}$$

depending on whether we need to solve for the pressure wavefield p or the velocity wavefield $\mathbf{v}$, respectively.

Non-viscous Medium

Consider the case when the viscosity of the material is zero. By adding

$$\kappa_0 \frac{\partial^2 p}{\partial t^2} - \frac{1}{\rho_0}\nabla \cdot \nabla p$$

to both sides of equation (4.37), we can write

$$\nabla^2 p - \frac{1}{c_0^2}\frac{\partial^2 p}{\partial t^2} = \gamma_\kappa \frac{1}{c_0^2}\frac{\partial^2 p}{\partial t^2} + \nabla \cdot (\gamma_\rho \nabla p)$$

where

$$\gamma_\kappa = \frac{\kappa - \kappa_0}{\kappa_0}, \quad \gamma_\rho = \frac{\rho - \rho_0}{\rho} \quad \text{and} \quad c_0 = \frac{1}{\sqrt{\rho_0 \kappa_0}}.$$

Here, c_0 is the velocity at which acoustic waves propagate in a homogeneous material with a density ρ_0 and compressibility κ_0. If we then introduce the Fourier transform

$$p(\mathbf{r}, t) = \frac{1}{2\pi}\int_{-\infty}^{\infty} P(\mathbf{r}, \omega)\exp(i\omega t)dt$$

then the above wave equation becomes

$$(\nabla^2 + k^2)P = -k^2\gamma_\kappa P + \nabla \cdot (\gamma_\rho \nabla P)$$

where $k = \omega/c_0$. The inverse scattering problem posed by this equation involves reconstructing γ_κ and γ_ρ by measuring appropriate properties of the scattered pressure field. This is a two parameter reconstruction problem.

Viscous Medium

The problem becomes a little more complicated when we consider an inhomogeneous viscous material. In this case, by adding

$$\frac{\partial}{\partial t}[\nabla(\alpha_0 \nabla \cdot \mathbf{v}) + 2\nabla \cdot (\beta_0 \nabla \mathbf{v})] - \rho_0 \frac{\partial^2 \mathbf{v}}{\partial t^2} - \nabla\left(\frac{1}{\kappa_0}\nabla \cdot \mathbf{v}\right)$$

to both sides of equation (4.38) and noting that for compression waves only

$$\nabla(\nabla \cdot \mathbf{v}) = \nabla^2 \mathbf{v}$$

since $\mathbf{v} = \nabla u$ and $\nabla \times \nabla u = 0$, we obtain the wave equation

$$\left(1 + \tau_0 \frac{\partial}{\partial t}\right) \nabla^2 \mathbf{v} - \frac{1}{c_0^2} \frac{\partial^2 \mathbf{v}}{\partial t^2} = \gamma_\rho \frac{1}{c_0^2} \frac{\partial^2 \mathbf{v}}{\partial t^2} + \nabla(\gamma_\kappa \nabla \cdot \mathbf{v})$$

$$-\tau \frac{\partial}{\partial t}\left(\nabla(\gamma_\alpha \nabla \cdot \mathbf{v}) + 2\nabla \cdot (\gamma_\beta \nabla \mathbf{v})\right) \tag{4.39}$$

where

$$\gamma_\kappa = \frac{\kappa - \kappa_0}{\kappa}, \quad \gamma_\rho = \frac{\rho - \rho_0}{\rho_0}, \quad \gamma_\alpha = \frac{\alpha - \alpha_0}{\alpha_0 + 2\beta_0}$$

$$\gamma_\beta = \frac{\beta - \beta_0}{\alpha_0 + 2\beta_0}, \quad c_0 = \frac{1}{\sqrt{\rho_0 \kappa_0}} \quad \text{and} \quad \tau_0 = \kappa_0(\alpha_0 + 2\beta_0).$$

The parameter τ_0 is known as the relaxation time and may be written in the form

$$\tau_0 = \frac{\alpha_0 + 2\beta_0}{\rho_0 c_0^2}$$

and the quantity

$$\alpha_0 + 2\beta_0 = \zeta_0 + \frac{4}{3}\eta_0$$

is the compressional viscosity. Introducing the Fourier transform

$$\mathbf{v}(\mathbf{r}, t) = \frac{1}{2\pi} \int_{-\infty}^{\infty} \mathbf{V}(\mathbf{r}, \omega) \exp(i\omega t) dt,$$

equation (4.39) can be written as

$$(1 + i\omega\tau)\nabla^2 \mathbf{V} + k^2 \mathbf{V} = -k^2 \gamma_\rho \mathbf{V} + \nabla(\gamma_\kappa \nabla \cdot \mathbf{V})$$

$$-i\omega\tau[\nabla(\gamma_\lambda \nabla \cdot \mathbf{V}) + 2\nabla \cdot (\gamma_\beta \nabla \mathbf{V})].$$

If we then use the relationship

$$\omega\tau = k\ell$$

where ℓ is the relaxation length ($= \tau/c_0$) and divide through by $1 + ik\ell$, we obtain

$$(\nabla^2 + \xi^2)\mathbf{V} = -\xi^2 \gamma_\rho \mathbf{V} + \frac{1}{1 + ik\ell} \nabla(\gamma_\kappa \nabla \cdot \mathbf{V})$$

$$-\frac{ik\ell}{1 + ik\ell}[\nabla(\gamma_\lambda \nabla \cdot \mathbf{V}) + 2\nabla \cdot (\gamma_\beta \nabla \mathbf{V})]$$

where

$$\xi = \frac{k}{\sqrt{1 + ik\ell}}.$$

Finally, we can obtain a scalar wave equation by substituting $\mathbf{V}$ for ∇u and taking the divergence of each term to obtain

$$(\nabla^2 + \xi^2)U = -\hat{L}u$$

where

$$\hat{L}u = \xi^2 \nabla \cdot (\gamma_\rho \nabla u) - \frac{1}{1 + ik\ell} \nabla^2 (\gamma_\kappa \nabla^2 u)$$

$$+ \frac{ik\ell}{1 + ik\ell} \Big(\nabla^2 (\gamma_\alpha \nabla^2 u) + 2\nabla \cdot [\nabla \cdot (\gamma_\beta \nabla \nabla u)] \Big)$$

and

$$U = \nabla^2 u.$$

The field U is the acoustic dilatation. It represents the fractional change in the volume of a material due to the disturbance of an acoustic wave. The imaging problem posed by the wave equation above involves finding inverse solutions for the four acoustic scatter generating parameters $\gamma_\rho, \gamma_\kappa, \gamma_\alpha$ and γ_β. This is a four parameter reconstruction problem.

Any spatial or temporal inhomogeneity in the acoustic properties of a medium will scatter acoustic radiation. Thus, fluctuations in the density, compressibility, shear and bulk viscosity will produce scattering of different directional behaviours and can therefore, in principle, be characterized by their own directional scattering properties. A small density fluctuation (with regard to the wavelength of the field) within an otherwise homogeneous medium will exhibit a differential displacement amplitude when exposed to the oscillatory forces within an acoustic field. This motion is essentially equivalent to an oscillating particle in an otherwise stationary medium. Hence, a density fluctuation is basically a dipole source of sound emission (or scattering), exhibiting a non-isotropic directivity pattern with an intensity that depends on a differential force, i.e. the acoustic pressure gradient ∇p.

A fluctuation in compressibility will expand and contract quite differently to its surroundings when exposed to an acoustic field and is equivalent to a pulsating object within an otherwise stationary medium. Thus, a compressibility fluctuation is essentially a monopole source of sound emission which gives rise to isotropic scattering. This isotropic directivity pattern has an intensity dependence related to the acceleration of the source boundaries by the acoustic pressure, and is thus determined by the second time derivative $\partial^2 p / \partial t^2$.

An additional source of acoustic scattering occurs with any variation in the viscosity of the medium which is a measure of the absorption of a wave by the medium. A small fluctuation in the viscosity produces a local change in the amplitude of the wavefront of a passing acoustic disturbance. This is equivalent to a small vibrating membrane within an otherwise stationary medium. Thus, a viscosity fluctuation represents a sound source having a relatively complicated directivity pattern (multi-pole scattering) but predominantly along the forward and backward directions of the acoustic wave vector with an intensity related to the vibrational velocity.

4.10 Discussion

This Chapter has been concerned with investigating the field equations for the electromagnetic, elastic and acoustic fields. In each case, it has been shown how these equations can be reduced or decoupled to provide a linear inhomogeneous scalar wave equation (a Langevin equation) of the form

$$(\nabla^2 + k^2)\mathbf{u}(\mathbf{r}, k) = -\hat{L}\mathbf{u}$$

where $\hat{L}$ is an inhomogeneous linear differential operator which involves the 'scatter generating parameter' sets $(\gamma_\epsilon, \gamma_\mu, \sigma)$ for the electromagnetic case (where the material may be composed of 'good conductors'), $(\gamma_\rho, \gamma_\alpha, \gamma_\beta)$ for the elastic case and $(\gamma_\rho, \gamma_\kappa, \gamma_\alpha, \gamma_\beta)$ for the case of an acoustic field. The difference between the last two cases is determined by whether or not the material is compressible. Note that, in the case of acoustics, the field equations are a result of linearizing the hydrodynamic equations of motion whereas, in electromagnetism, the field equations are linear. Thus in acoustics, it is possible to incur a number of nonlinear effects that are not considered here. In electromagnetism, nonlinear behaviour can occur as a result of the polarization vector having a nonlinear relationship with the electric field vector. Also note that the wave equations derived here for the elastic and acoustic fields assume that the shear wave component is negligible. This is not always the case, particularly when elastic wavefields propagate through solids (seismic waves for example). The wave equations derived here are the result of trying to find a balance between developing a physical model that is relatively complete but 'simple' enough for the 'forward problem' (solving for the wavefield $\mathbf{u}$ given $\hat{L}$) and the 'inverse problem' (solving for the material parameter sets given $\mathbf{u}$) to become tractable using the analytical methods discussed in the following chapter - such is the nature of physics!

4.11 Summary of Important Results

The Langevin equation

$$\hat{D}^{(1)}u(\mathbf{r}, t) = -s(\mathbf{r}, t)$$

where

$$\hat{D}^{(1)} = \hat{D}^{(0)} + \hat{L}$$

$D^{(0)}$ is the homogeneous differential operator and $\hat{L}$ is the inhomogeneous operator.

Maxwell's (microscopic) equations in CGS units

$$\nabla \cdot \mathbf{e} = \rho$$

$$\nabla \cdot \mathbf{b} = 0$$

$$\nabla \times \mathbf{e} = -\frac{1}{c}\frac{\partial \mathbf{b}}{\partial t}$$

$$\nabla \times \mathbf{b} = \frac{1}{c}\frac{\partial \mathbf{e}}{\partial t} + \frac{\mathbf{j}}{c}$$

where $\mathbf{e}(\mathbf{r}, t)$ is the (microscopic) electric field generated by a point charge, $\mathbf{b}(\mathbf{r}, t)$ is the (microscopic) magnetic field, $\rho(\mathbf{r}, t)$ is the charge density, $\mathbf{j}(\mathbf{r}, t)$ is the current density and c is the speed of light.

Maxwell's (macroscopic) equations in SI units

$$\nabla \cdot \epsilon \mathbf{E} = \rho$$

$$\nabla \cdot \mu \mathbf{H} = 0$$

$$\nabla \times \mathbf{E} = -\mu \frac{\partial \mathbf{H}}{\partial t}$$

$$\nabla \times \mathbf{H} = \epsilon \frac{\partial \mathbf{E}}{\partial t} + \mathbf{j}$$

where $\mathbf{E}(\mathbf{r}, t)$ is the (macroscopic) electric field (volts/metre), $\mathbf{H}(\mathbf{r}, t)$ is the (macroscopic) magnetic field (amperes/metre), $\mathbf{j}(\mathbf{r}, t)$ is the current density (amperes/metre^2), $\rho(\mathbf{r}, t)$ is the charge density (charge/metre^2), $\epsilon(\mathbf{r})$ is the permittivity (farads/metre) and $\mu(\mathbf{r})$ is the permeability (henries/metre).

Ohm's law

$$\mathbf{j} = \sigma \mathbf{E}$$

where σ is the conductivity in siemens/metre.

Charge decay rate

$$\rho(t) = \rho_0 \exp(-\sigma t/\epsilon)$$

Elastic field equation

$$\rho \frac{\partial^2 \mathbf{s}}{\partial t^2} = \nabla \cdot \mathbf{T}$$

where $\mathbf{s}(\mathbf{r}, t)$ is the displacement vector (metres), $\rho(\mathbf{r})$ is the material density (mass per unit volume) and $\mathbf{T}(\mathbf{r}, t)$ is the material stress tensor (force per unit volume).

Acoustic field equations

$$\nabla \cdot \mathbf{v} = \kappa \frac{\partial p}{\partial t}$$

$$\nabla p = \rho \frac{\partial \mathbf{v}}{\partial t} - \nabla \cdot \mathbf{T}$$

where $\mathbf{v}(\mathbf{r}, t)$ is the velocity field (length/time), $p(\mathbf{r}, t)$ is the pressure field (force/area), $\mathbf{T}(\mathbf{r}, t)$ is the material stress tensor (force/volume), $\rho(\mathbf{r})$ is the density (mass/volume) and $\kappa(\mathbf{r})$ is the compressibility (area/force).

Inhomogeneous wave equation for EM waves in a conductive dielectric

$$(\nabla^2 + k^2)\widetilde{\mathbf{E}} = -\hat{L}\widetilde{\mathbf{E}}$$

where

$$\hat{L}\widetilde{\mathbf{E}} = k^2\gamma_\epsilon\widetilde{\mathbf{E}} - ikz_0\sigma\widetilde{\mathbf{E}} + \nabla(\mathbf{E}\cdot\nabla\ln\epsilon) + \nabla\times(\gamma_\mu\nabla\times\widetilde{\mathbf{E}});$$

$$\gamma_\epsilon = \frac{\epsilon-\epsilon_0}{\epsilon_0}, \quad \gamma_\mu = \frac{\mu-\mu_0}{\mu}$$

$\widetilde{\mathbf{E}}(\mathbf{r},\omega)$ - Electric field (Fourier transform of)

ϵ - Permittivity

μ - Permeability

σ - Conductivity

Inhomogeneous wave equation for a compressional elastic wavefield in a non-compressible solid

$$\left(\nabla^2 + \frac{\omega^2}{c_L^2}\right)E = \hat{L}U$$

where

$$\hat{L}U = (\gamma_\alpha + 2\gamma_\beta)\nabla^2\nabla^2 U + 2\nabla(\gamma_\alpha + 2\gamma_\beta)\cdot\nabla\nabla^2 U$$

$$+\nabla^2\gamma_\alpha\nabla^2 U + \frac{\omega^2}{c_L^2}\nabla\cdot\gamma_\rho\nabla U + \nabla\nabla\gamma_\beta : \nabla\nabla U,$$

$$\gamma_\rho = \frac{\rho-\rho_0}{\rho_0}, \quad \gamma_\alpha = \frac{\lambda-\lambda_0}{\lambda_0+2\mu_0} \quad \text{and} \quad \gamma_\beta = \frac{\mu-\mu_0}{\lambda_0+2\mu_0}.$$

$e(\mathbf{r},\omega) = \nabla^2 u(\mathbf{r},\omega)$ - elastic dilatation (Fourier transform of)

ρ - Density

α, β - First and second Lamé parameters, respectively

Inhomogeneous wave equation for an acoustic pressure field propagating in a non-viscous compressible medium

$$(\nabla^2 + k^2)P = -\hat{L}P$$

where

$$\hat{L}P = k^2\gamma_\kappa P - \nabla\cdot(\gamma_\rho\nabla P),$$

$$\gamma_\kappa = \frac{\kappa-\kappa_0}{\kappa_0}, \quad \gamma_\rho = \frac{\rho-\rho_0}{\rho}.$$

$p(\mathbf{r},\omega)$ - Pressure field (Fourier transform of)

κ - Compressibility

ρ - Density

Inhomogeneous wave equation for a compressional acoustic wavefield propagating in a viscous compressible material

$$(\nabla^2 + \xi^2)U = -\hat{L}u$$

where

$$\hat{L}u = \xi^2 \nabla \cdot (\gamma_\rho \nabla u) - \frac{1}{1 + ik\ell} \nabla^2 (\gamma_\kappa \nabla^2 u)$$

$$+ \frac{ik\ell}{1 + ik\ell} \Big(\nabla^2 (\gamma_\alpha \nabla^2 u) + 2\nabla \cdot [\nabla \cdot (\nabla \gamma_\beta \nabla \nabla u)] \Big),$$

$$\gamma_\kappa = \frac{\kappa - \kappa_0}{\kappa}, \quad \gamma_\rho = \frac{\rho - \rho_0}{\rho_0},$$

$$\gamma_\alpha = \frac{\alpha - \alpha_0}{\alpha_0 + 2\beta_0}, \quad \gamma_\beta = \frac{\beta - \beta_0}{\alpha_0 + 2\beta_0}$$

and

$$\xi = \frac{k}{\sqrt{1 + ik\ell}}.$$

$u(\mathbf{r}, \omega)$ - Longitudinal velocity potential (Fourier transform of)

$U = \nabla^2 u$ - Acoustic dilatation

κ - Compressibility

ρ - Density

α, β - First and second Lamé parameters, respectively

ℓ - Relaxation length

4.12 Further Reading

- Webster A G, *Partial Differential Equations of Mathematical Physics*, Stechert, 1933
- Stratton J A, *Electromagnetic Thoery*, McGraw-Hill, 1941.
- Morse P M and Feshbach H, *Methods of Theoretical Physics*, McGraw-Hill, 1953.

  Atkin R H, *Theoretical Electromagnetism*, Heinemann, 1962.
- Morse P M and Ingard K U, *Theoretical Acoustics, McGraw-Hill*, 1968.
- Butkov E, *Mathematical Physics*, Addison-Wesley, 1973.

- Bleaney B I and Bleaney B, *Electricity and Magnetism*, Oxford University Press, 1976.
- Sander K F and Reed G A L, *Transmission and Propagation of Electromagnetic Waves*, 1986.
- Evans G A, Blackledge, J M and Yardley P, *Analytical Solutions to Partial Differential Equations*, Springer, 1999.

Chapter 5

Green Functions

5.1 Overview

Green functions[1] are named after the mathematician and physicist George Green born in Nottingham in 1793 who 'invented' the Green function in 1828. This invention is developed in an essay entitled *Mathematical Analysis to the Theories of Electricity and Magnetism* originally published in Nottingham in 1828 and reprinted by the George Green Memorial Committee to mark the bicentenary of the birth of George Green in 1993 when he was finally given the recognition he deserved.

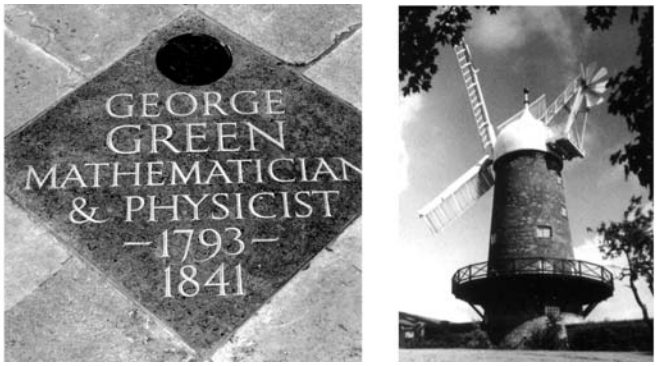

Figure 5.1: George Green memorial stone in Westminster Abbey, London (left) and Green's windmill (right) in Sneinton (now a suburb of Nottingham), originally built by his father and restored in the 1970s.

[1]It has been a tradition for most authors to use the term Green's functions rather than Green functions. Here, we break with tradition and use the term Green function(s) in the same way as authors traditionally refer to Bessel or Hankel functions, for example.

The Green function is a powerful mathematical tool rather than a physical concept and was successfully applied to classical electromagnetism and acoustics in the late Nineteenth Century. More recently, the Green function has been the working tool of calculations in particle physics, condensed matter and solid state physics, quantum mechanics and many other topics of applied mathematics and mathematical physics. Just as the Green function revolutionized classical field theory in the nineteenth century (hydrodynamics, electrostatics and magnetism) so it revolutionized quantum field theory in the mid-Twentieth Century through the introduction of quantum Green functions. This provided the essential link between the theories of quantum electrodynamics in the 1940s and 1950s and has played a major role in theoretical physics ever since. It is interesting to note that the work of Richard Feynman in the 1950s which led to the development of the Feynman diagram was based on the Green function. In fact, the Feynman diagram can be considered to be a pictorial representation of a Green function (a Green function associated with wave operators) - what Feynman referred to as a 'propagator'.

The Green function remains the single most powerful tool we have for solving partial differential equations and hence for solving problems in theoretical and mathematical physics in general (since most physical laws can be cast in terms of differential equations - arguably Isaac Newton's greatest legacy!). This tool is all the more enigmatic in that the work of George Green was neglected for nearly thirty years after his death in 1841. To this day no one knows what he looked like (there are no paintings or photographs of him) or how and why he developed his completely original ideas. His work was rediscovered and popularized in the latter part of the Nineteenth Century primarily by William Thomson (later Lord Kelvin).

George Green was the son of a prosperous Nottingham miller, also called George Green, and spent most of his early life helping with the family business which centred on a windmill originally built by his father and restored in the 1970s (see Figure 5.1). It is in this windmill that we may suppose he might of have done much of his original work. Only in 1829, on the death of his father, did he become wealthy enough to devote the remaining years of his life to mathematics; at the age of forty, he enrolled as an undergraduate at Cambridge University, England. However, his most influential work (Green functions and Green's theorems) was produced before he had the benefit (or otherwise) of a university education.

Green functions are used mainly to solve certain types of linear inhomogeneous partial differential equations (although homogeneous partial differential equations can also be solved using this approach). In principle, the Green function technique can be applied to any linear constant coefficient inhomogeneous partial differential equation (scalar or vector) in any number of independent variables, although in practice difficulties can arise in computing the Green function analytically. In fact, Green functions provide more than just a 'solution', for they transform a partial differential equation representation of a physical problem into a integral equation representation of the same problem which is entirely general and complete. The kernel of the integral equation is composed (completely or partly) of the Green function associated with the par-

tial differential equation. This is why Green function solutions are one of the most powerful analytical tools we have for solving partial differential equations, equations that arise in areas of physics such as electromagnetism (Maxwell's equations), wave mechanics (elastic wave equation), optics (Helmholtz equation), quantum mechanics (Schrödinger and Dirac equations), fluid dynamics (fluid equations of motion), relativistic particle dynamics (Klein-Gordon equation) and general relativity (Einstein equations) to name but a few.

The following points provide the reader with a brief history of the essential developments in (mathematical) physics since the early Nineteenth Century in order to illustrate the way in which Green functions have come to play a central role.

- Early 19th Century: Green function 'invented' in 1828, providing general solutions to the Laplace and Poisson equations - equations which represented the 'best models' for electricity and magnetism at this time.
- Mid 19th Century: Partial Differential Equations (PDEs) start to rule the underlying models associated with physical problems leading to the mechanics and dynamics of a continuum supporting 'fields' (e.g. Maxwell's equations developed in the early 1860s).
- Late 19th Century: PDEs lead to classical field theory and Green functions used for the first time to solve problems in classical field theory (hydrodynamics, electrostatics, magnetism, electromagnetism and optics).
- Early 20th Century: Early developments in 'old' quantum mechanics based on discrete states of (microscopic) matter, the idea of a 'quantum' being originally proposed by Max Planck in 1901.
- 1920s - 1930s: Development of 'new' quantum mechanics, based on conventional solutions to PDEs, e.g. Schrödinger and Dirac equations.
- 1940s - 1950s: Development of quantum field theory, a field theory based on Green function solutions (i.e. quantum Green functions).
- 1950s -1960s: Development of quantum electrodynamics using Green functions (Feynman diagrams) and the use of Green functions to describe the many-body interactions of condensed matter physics.
- 1960s - 1970s: Unification of electromagnetism and the weak force based on the use of Green functions to model intermediate vector bosons.
- 1970s - date: Development of string theory based on multi-dimensional and multi-modal Green functions.

In high energy particle physics, Green functions have been and continue to be used to model the interactions of elementary particles. The basic principle is very similar to that of active image systems in which: (i) matter is probed with high energy particle (typically proton) beams and the effect of this interaction measured; (ii) from the measured data, a model is developed

to interpret what type of interaction has occurred. Particle beam experiments are based on two principal types: (i) 'Beam-Dump' experiments in which a particle beam is 'focused' on to a 'lump' of matter (the basis of particle physics since Rutherford's work of 1910 to confirm the basic model for an atom); (ii) 'Beam-Beam' experiments in which two particle beams (travelling in opposite directions) are 'focused' on to each other. Beam-Beam experiments were first developed in the mid 1970s and led to the confirmation of intermediate vector bosons and hence the validation of a unification theory for electromagnetic and weak forces. These experiments were based on advances in technology which, in effect, eliminated the need to solve the multiple scattering problem that had been worked on extensively over the 1950s and 1960s using Green functions.

The use of Green functions for solving problems in engineering has accompanied their use and applications in high energy nuclear and mathematical physics. In particular, Grenn functions have been used to solve inverse problems with applications that include telecommunications, optics, astronomy, remote sensing, seismic prospecting, non-destructive evaluation (acoustic and electromagnetic), Radar, Sonar, microscopy, etc. The governing principle is the same in each case:

(i) Interrogate a material with a wavefield (electron, electromagnetic, acoustic).

(ii) Measure the way in which the wavefield interacts with the material.

(iii) Interpret the distribution and/or type of material from these measurements, i.e. solve the inverse problem.

Considerable investment in intellectual labour associated with solving inverse problems in imaging has occurred since the late 1970s. In England, and in addition to other scientific journals and specialized conferences, this influenced the introduction of a new journal by the Institute of Physics, namely, the Journal of Inverse Problems which first appeared in 1984. With regard to the application of Green functions, the inverse (scattering) problem is typically based on first defining the (scattering) problem in terms of the solution to a linear inhomogeneous PDE of the type[2]

$$\hat{D}u(\mathbf{r},t) = \hat{L}u(\mathbf{r},t)$$

where u is the wavefield (which is taken to include the scattered wavefield), $\hat{D}$ is a homogeneous differential operator and $\hat{L}$ is an inhomogeneous differential operator. The forward scattering problem can then be defined as follows:

$$\text{Given } \hat{D} \text{ and } \hat{L} \text{ compute } u(\mathbf{r},t).$$

The inverse scattering problem is then defined as:

$$\text{Given } u(\mathbf{r},t) \text{ compute the inhomogeneous characteristics of } \hat{L}.$$

An appropriate Green function solution (if available) allows us to write (without loss of generality)

$$u(\mathbf{r},t) = \hat{I}\hat{L}u(\mathbf{r},t)$$

[2] $\mathbf{r}$ is the multi-dimensional space vector and t denotes time.

where $\hat{I}$ is an integral operator that incorporates the Green function.

Inverse scattering problems are, in general, concerned with the inversion of integral equations of this type. However, the technique is not limited to wave equations alone, but can be applied to a wide range of inhomogeneous partial differential equations including those associated with diffusion problems (the diffusion equation), transport phenomena (the Föcker-Planck equation) and static problems (e.g. the Poisson equation).

Why are Green functions relevant to imaging and image processing? It is because light (and sound) obeys a wave equation and, by deriving a Green function for this equation, we can calculate the response of an optical system at a point of measurement (e.g. a photographic plate or charge couple device camera) to a disturbance at some source (a laser or some illuminated object). Further, many problems in image processing revolve around the recovery of information that has been degraded or lost in the passage of a signal through optical instruments. Green functions give us a very general way of thinking about this process. If we have a good physical model for an imaging process, then we have a better chance of extracting valuable information by reversing the process.

5.2 Introduction to the Green Function

In this Chapter, we provide an introduction to the Green function method. The material focuses attention on Green function solutions to the wave equation. In addition to imaging theory, this reflects the role that the Green function has played in quantum field theory and wave mechanics in general over the past 50 years. It is an area in which Green functions have and continue to play a central part especially with regard to Green functions for the wave equation. However, for completeness, we also consider Green function solutions to the diffusion equation and the Poisson and Laplace equations. Here, we are concerned with the use of 'Free Space' Green functions which provide a general solution in the infinite domain or over a finite domain to which boundary conditions can then be applied.

By way of a short introduction to help the reader understand the principle of using Green functions we now consider two short examples. The first example is based on considering point sources to generate a solution to an ordinary differential equation and is based on a 'qualitative analysis'. The second example makes specific use of the delta function and its properties to develop a solution which is based on a more systematic analysis - as used throughout this Chapter.

Example 1: Consider the following inhomogeneous ordinary differential equation

$$\hat{D}u(x) = f(x) \tag{5.1}$$

where $\hat{D}$ is a linear differential operator and $f(x)$ is a given function (the source term), the solution being required on the interval $0 \leq x \leq a$ where a is some constant.

Instead of considering $f(x)$ as a continuous source function, let us approximate it by a set of source functions $f(\xi_1), f(\xi_2), ..., f(\xi_n)$ acting at the points $x = \xi_1, x = \xi_2, ..., x = \xi_n$, all for $x \in [0, a]$. Now define the function $g(x, \xi_i)$ to be the solution to equation (5.1) due to a source acting at ξ_i. The solution due to the single effect of this point source is given by $g(x, \xi_i)f(\xi_i)$. The solution for $u(x)$ is then obtained by summing the results for all the n source terms acting over the interval $0 \leq x \leq a$, and takes the form

$$u(x) = \sum_{i=1}^{n} g(x, \xi_i) f(\xi_i).$$

As n becomes larger so that the number of point source functions $f(\xi_i)$ increases, a better and better approximation to $f(x)$ is obtained. In the limit as $n \to \infty$, $|\xi_i - \xi_{i+1}| \to 0 \ \forall i$ and the summation in the equation above may be replaced by an integral to give the required solution to equation (5.1) in the form

$$u(x) = \int_0^a g(x, \xi) f(\xi) d\xi.$$

The function $g(x, \xi)$ is called the Green function of the problem.

The Green function is usually denoted by g and G, but the notation changes from author to author. They are usually written in the form $g(x, \xi)$ (as in this example), or $g(\mid x - \xi \mid)$, or $g(x \mid \xi)$ (as used throughout this Chapter).

Similar results to the one given above may be obtained for linear partial differential equations. For example, the solution of the Poisson equation in two dimensions, i.e.

$$\nabla^2 u(x, y) = f(x, y); \quad x \in [0, a], \quad y \in [0, b]$$

may be written as

$$u(x, y) = \int_0^a \int_0^b g(x, y; \xi, \eta) f(\xi, \eta) d\xi d\eta$$

where $g(x, y; \xi, \eta)$ is the Green function of the problem.

The approach to developing a Green function solution discussed in this example is based on considering point sources to provide a set of elementary results and then summing up the results to give the required solution. In optics and acoustics, this principle is often referred to as Huygens' principle. It allows the optical or acoustic field generated by a given source to be computed by considering the field generated from a single point on the source and then summing up the field generated from a large collection of such points. In this sense, the principle behind a Green function solution is effectively the same as Huygens' principle, i.e. find the solution to the problem for a single point and then integrate over all such points.

A point source can be described by a delta function and the relationship between the delta function and the Green function is fundamental. By way

of a short introduction to the use of the delta function for solving partial differential equations using Green functions, we consider the following example which, in comparison with the example given above, provides a more complete form of analysis to develop a Green function solution for the one-dimensional inhomogeneous wave equation.

Example 2: Consider the inhomogeneous wave equation

$$\left(\frac{\partial^2}{\partial x^2} + k^2\right) u(x,k) = f(x) \tag{5.2}$$

where k (the wavenumber) is a constant and $f(x)$ is the source term, the solution being required over all space $x \in (-\infty, \infty)$ subject to the conditions that u and $\partial u/\partial x$ are zero at $\pm\infty$. This equation describes the behaviour of 'steady waves' (with constant wavelength $\lambda = 2\pi/k$) generated by a source $f(x)$. With reference to the Example 1, we are considering the case where

$$\hat{D} = \frac{\partial^2}{\partial x^2} + k^2.$$

Let us define the Green function as being the solution to equation (5.2) when the source term is replaced by a point source or delta function at a point x_0 say, giving the equation

$$\left(\frac{\partial^2}{\partial x^2} + k^2\right) g(x \mid x_0, k) = \delta(x - x_0) \tag{5.3}$$

where δ has the following fundamental property

$$\int_{-\infty}^{\infty} u(x)\delta(x - x_0)dx = u(x_0).$$

Pre-multiplying equation (5.2) by g gives

$$g\left(\frac{\partial^2}{\partial x^2} + k^2\right) u = gf$$

and pre-multiplying equation (5.3) by u gives

$$u\left(\frac{\partial^2}{\partial x^2} + k^2\right) g = u\delta(x - x_0).$$

Subtracting the two results and integrating over all space, we obtain

$$\int_{-\infty}^{\infty} \left(g\frac{\partial^2 u}{\partial x^2} - u\frac{\partial^2 g}{\partial x^2}\right) dx = \int_{-\infty}^{\infty} fgdx - \int_{-\infty}^{\infty} u\delta(x - x_0)dx.$$

Using the generalized sampling property of the delta function given above and rearranging the result, we obtain

$$u(x_0, k) = \int_{-\infty}^{\infty} fgdx - \int_{-\infty}^{\infty} \left(g\frac{\partial^2 u}{\partial x^2} - u\frac{\partial^2 g}{\partial x^2}\right) dx.$$

Evaluating the second integral on the right-hand side,

$$\int_{-\infty}^{\infty}\left(g\frac{\partial^2 u}{\partial x^2}-u\frac{\partial^2 g}{\partial x^2}\right)dx=\int_{-\infty}^{\infty}\left[\frac{\partial}{\partial x}\left(g\frac{\partial u}{\partial x}\right)-\frac{\partial g}{\partial x}\frac{\partial u}{\partial x}-\frac{\partial}{\partial x}\left(u\frac{\partial g}{\partial x}\right)+\frac{\partial u}{\partial x}\frac{\partial g}{\partial x}\right]dx$$

$$=\int_{-\infty}^{\infty}\frac{\partial}{\partial x}\left(g\frac{\partial u}{\partial x}\right)dx-\int_{-\infty}^{\infty}\frac{\partial}{\partial x}\left(u\frac{\partial g}{\partial x}\right)dx=\left[g\frac{\partial u}{\partial x}\right]_{-\infty}^{\infty}-\left[u\frac{\partial g}{\partial x}\right]_{-\infty}^{\infty}=0$$

provided u and $\partial u/\partial x$ are zero at $x=\pm\infty$. With these conditions, we obtain the Green function solution to equation (5.2.2) in the form

$$u(x_0,k)=\int_{-\infty}^{\infty}f(x)g(x\mid x_0,k)dx.$$

Physically the Green function associated with wavefield problems, as in this example, represents the way in which a wave propagates from one point in space to another. For this reason, Grenn functions are sometimes referred to as propagators. In this case, the Green function is a function of the 'path length' between x and x_0, irrespective of whether $x>x_0$ or $x<x_0$. The path length is given by $\mid x-x_0\mid$ and the Green function is a function of this path length which is why, using the notation $x\mid x_0\equiv\mid x-x_0\mid$, we write $g(x\mid x_0)$. Note that the solution for u is a convolution (since $x\mid x_0=x_0\mid x$), the convolution of the source function $f(x)$ with the Green function $g(\mid x\mid)$. In general, we can consider the solution to an equation of the type

$$\hat{D}u(x)=f(x)$$

to be given by

$$u(x)=g(\mid x\mid)\otimes f(x)$$

where $\otimes$ denotes the convolution operation and g is the solution to the equation

$$\hat{D}u(x)=\delta(x-x_0).$$

Such a solution is of little value unless the Green function can be computed and, in the following Section, this problem is addressed.

5.3 The Time Independent Wave Operator

In this Section, we shall concentrate on the computation of Green functions for the time-independent wave equation in one-, two- and three-dimensions. The solution is over all space and the Green function is not constrained to any particular boundary conditions (except those at $\pm\infty$). It is therefore referred to as a free space Green function. Green functions of this type are used in a wide range of physical problems related to the propagation and interaction of waves with matter. They are one of the most important functions in mathematical physics because of the way they allow partial differential equations that describe

the interaction of wavefields with matter to be solved. Physically, these Green functions represent the way in which a wave propagates from one point source to another.

The type of equations that we are forced to consider with regard to the 'physics' of imaging systems, and the analytical techniques that have been developed to cope with them, nearly always originate in some way from the properties of the Green function that is used. A good understanding of these functions is therefore required if the basic elements of imaging theory are to be understood.

5.3.1 The One-dimensional Green Function

We start by reconsidering Example 2 given in the Section 5.2 which, through the application of the sampling property of the delta function together with some relatively simple analysis, demonstrated that the solution to the inhomogeneous wave equation

$$\left(\frac{\partial^2}{\partial x^2} + k^2\right) u(x,k) = f(x)$$

for constant k and $x \in (-\infty, \infty)$ subject to the boundary conditions

$$u(x,k) \mid_{\pm\infty} = 0 \quad \text{and} \quad \left[\frac{\partial}{\partial x} u(x,k)\right]_{\pm\infty} = 0$$

is given by

$$u(x_0,k) = \int_{-\infty}^{\infty} f(x) g(x \mid x_0, k) dx$$

where g is the Green function given by the solution to the equation

$$\left(\frac{\partial^2}{\partial x^2} + k^2\right) g(x \mid x_0, k) = -\delta(x - x_0) \tag{5.4}$$

subject to $g(x|x_0,k)|_{\pm\infty} = 0$ and $[\partial g(x|x_0,k)/\partial x]_{\pm\infty} = 0$. We shall now discuss the evaluation of the Green function for this case. Note that, here, the Green function is defined for $-\delta$ on the right hand side instead of δ as used previously. This is for convenience only in the computations that follow; it does not affect the analysis but does reduces the number of negative signs that accompany the calculation. For this reason, many authors define the Green function with $-\delta$, a definition which is used throughout the rest of this Chapter.

The solution for the Green function is based on employing the properties of the Fourier transform. Writing $X = \mid x - x_0 \mid$, we express g and δ as Fourier transforms, i.e.

$$g(X,k) = \frac{1}{2\pi} \int_{-\infty}^{\infty} G(u,k) \exp(iuX) du \tag{5.5}$$

and

$$\delta(X) = \frac{1}{2\pi} \int_{-\infty}^{\infty} \exp(iuX) du.$$

Substituting these expressions into equation (5.4) and differentiating gives

$$\frac{1}{2\pi}\int_{-\infty}^{\infty}(-u^2+k^2)G(u,k)\exp(iuX)du = -\frac{1}{2\pi}\int_{-\infty}^{\infty}\exp(iuX)du$$

from which it follows that

$$G(u,k) = \frac{1}{u^2-k^2}.$$

Substituting this result back into equation (5.5), we obtain

$$g(X,k) = \frac{1}{2\pi}\int_{-\infty}^{\infty}\frac{\exp(iuX)}{u^2-k^2}du = \frac{1}{2\pi}\int_{-\infty}^{\infty}\frac{\exp(iuX)}{(u-k)(u+k)}du.$$

The problem is therefore reduced to that of evaluating the above integral. This can be done using Cauchy's integral formula,

$$\oint_C f(z)dz = 2\pi i \times (\text{sum of the residues enclosed by } C)$$

where C is the contour defining the path of integration. In order to evaluate the integral explicitly using this formula, we must consider the singular nature or poles of the integrand at $z=-k$ and $z=k$. For now, let us consider a contour which encloses both poles. The residue at $z=k$ is given by $\exp(ikX)/(2k)$ and at $z=-k$ by $-\exp(-ikX)/(2k)$. Hence the Green function is given by

$$g(X,k) = 2\pi i\left(\frac{\exp(ikX)}{4\pi k} - \frac{\exp(-ikX)}{4\pi k}\right) = -\frac{\sin(kX)}{k}.$$

This Green function represents the propagation of waves travelling away from the point disturbance at $x=x_0$, or 'outgoing waves', and also waves traveling toward the point disturbance, or 'incoming waves'. Since x and x_0 are points along a line, we can consider the result to be the sum of waves travelling to the left of $\delta(x-x_0)$ in which $x<x_0$ and to the right of $\delta(x-x_0)$ where $x>x_0$. In most applications it is convenient to consider the Green function for outgoing or (more rarely) incoming waves, but not both. Here, the Green function for a incoming waves is given by

$$g(x \mid x_0,k) = -\frac{i}{2k}\exp(-ik \mid x-x_0 \mid)$$

and for outgoing waves is

$$g(x \mid x_0,k) = \frac{i}{2k}\exp(ik \mid x-x_0 \mid).$$

5.3.2 The Two-dimensional Green Function

A Green function in two- and three-dimensions is synonymous with the source-observer system illustrated in Figure 5.2. If the position of the source is denoted by $\mathbf{r}_0$ and the position of the observer by $\mathbf{r}$, then the Green function is written as a function of $\mid \mathbf{r} - \mathbf{r}_0 \mid$ where in Cartesian coordinates,

$$\mid \mathbf{r} - \mathbf{r}_0 \mid = \sqrt{(x - x_0)^2 + (y - y_0)^2}.$$

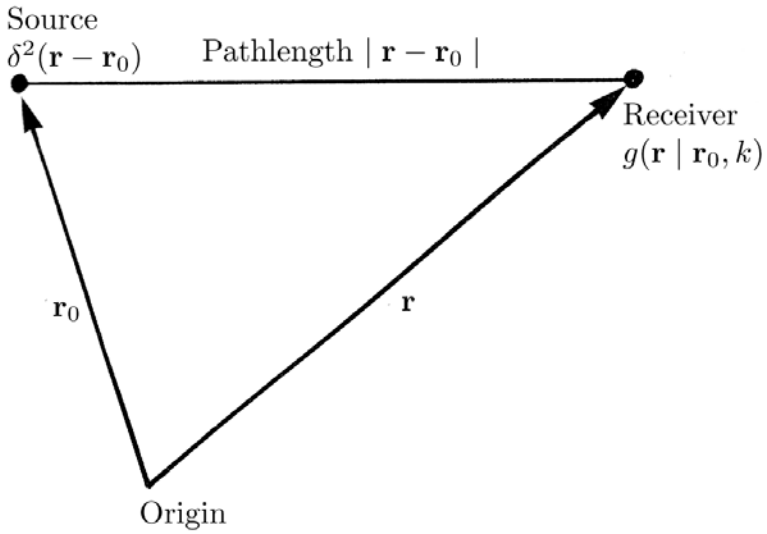

Figure 5.2: Source-observer geometry used to defined the Green function which is a function of the 'pathlength' $\mid \mathbf{r} - \mathbf{r}_0 \mid$.

When the functional dependence of the Green function is declared, instead of writing $g(\mid \mathbf{r} - \mathbf{r}_0 \mid)$, which is messy, it is more convenient to write $g(\mathbf{r}, \mathbf{r}_0)$ or $g(\mathbf{r} \mid \mathbf{r}_0)$. Here, the latter notation is used throughout, i.e.

$$g(\mathbf{r} \mid \mathbf{r}_0) \equiv g(\mid \mathbf{r} - \mathbf{r}_0 \mid).$$

In two dimensions, the same method can be used to obtain the (free space) Green function as that used to solve the one-dimensional case, i.e. to solve the equation

$$(\nabla^2 + k^2) g(\mathbf{r} \mid \mathbf{r}_0, k) = -\delta^2(\mathbf{r} - \mathbf{r}_0)$$

where

$$\mathbf{r} = \hat{\mathbf{x}} x + \hat{\mathbf{y}} y, \quad \mathbf{r}_0 = \hat{\mathbf{x}} x_0 + \hat{\mathbf{y}} y_0,$$

and

$$\nabla^2 = \frac{\partial^2}{\partial x^2} + \frac{\partial^2}{\partial y^2}.$$

Note that

$$\delta^2(\mathbf{r} - \mathbf{r}_0) \equiv \delta(x - x_0)\delta(y - y_0).$$

Also note that g is a function of the path length $\mid \mathbf{r} - \mathbf{r}_0 \mid$. Writing $\mathbf{R} = \mathbf{r} - \mathbf{r}_0$ and using the same technique as before, namely the one used to derive an integral representation of the one-dimensional Green function, we obtain

$$g(R,k) = \frac{1}{(2\pi)^2} \int_{-\infty}^{\infty} \frac{\exp(i\mathbf{u}\cdot\mathbf{R})}{u^2 - k^2} d^2\mathbf{u}.$$

In polar coordinates this result becomes

$$g(R,k) = \frac{1}{(2\pi)^2} \int_0^{\pi} \int_{-\infty}^{\infty} \frac{\exp(iuR\cos\theta)}{u^2 - k^2} u\,du\,d\theta.$$

Integrating over u first and using Cauchy's residue theorem, we have

$$\oint_C \frac{z\exp(izR\cos\theta)}{(z+k)(z-k)} dz = i\pi\exp(ikR\cos\theta)$$

where the contour of integration C has been chosen to enclose just one of the poles at $z = k$. This provides an expression for the 'outgoing' Green function in which the wave propagates away from the point disturbance at $\mathbf{r}_0$. A solution for the pole at $z = -k$ would provide a solution which represents a wavefield converging on $\mathbf{r}_0$. The 'outgoing' Green function is usually the most physically significant result (except for an implosion for example). Thus, the (outgoing) Green function can be written in the form

$$g(R,k) = \frac{i}{4\pi} \int_0^{\pi} \exp(ikR\cos\theta) d\theta.$$

Writing the Green function in this form allows us to employ the result

$$H_0^{(1)}(kR) = \frac{1}{\pi} \int_0^{\pi} \exp(ikR\cos\theta) d\theta$$

where $H_0^{(1)}$ is the Hankel function (of the first kind and of order zero). This is the integral representation for the Hankel transform and it can be used to write the two-dimensional Green function as

$$g(\mathbf{r} \mid \mathbf{r}_0, k) = \frac{i}{4} H_0^{(1)}(k \mid \mathbf{r} - \mathbf{r}_0 \mid).$$

A useful form of this function can be obtained by employing the asymptotic approximation

$$H_0^{(1)}(kR) \simeq \sqrt{\frac{2}{\pi}} \exp(-i\pi/4) \frac{\exp(-ikR)}{\sqrt{kR}}$$

which is valid when

$$kR >> 1.$$

This condition means that the wavelength of the wave originating from $\mathbf{r}_0$ is very small compared with the distance between $\mathbf{r}_0$ and $\mathbf{r}$, which is physically reasonable in many cases, and so a two-dimensional Green function of the following form can be used:

$$g(\mathbf{r} \mid \mathbf{r}_0, k) = \frac{1}{\sqrt{8\pi}} \exp(i\pi/4) \frac{\exp(ik \mid \mathbf{r} - \mathbf{r}_0 \mid)}{\sqrt{k \mid \mathbf{r} - \mathbf{r}_0 \mid}}, \quad k \mid \mathbf{r} - \mathbf{r}_0 \mid >> 1.$$

5.3.3 The Three-dimensional Green Function

In three dimensions, the free space Green function is given by the solution to the equation

$$(\bigtriangledown^2 + k^2) g(\mathbf{r} \mid \mathbf{r}_0, k) = -\delta^3(\mathbf{r} - \mathbf{r}_0)$$

where

$$\mathbf{r} = \hat{\mathbf{x}}x + \hat{\mathbf{y}}y + \hat{\mathbf{z}}z, \quad \mathbf{r}_0 = \hat{\mathbf{x}}x_0 + \hat{\mathbf{y}}y_0 + \hat{\mathbf{z}}z_0,$$
$$\delta^3(\mathbf{r} - \mathbf{r}_0) \equiv \delta(x - x_0)\delta(y - y_0)\delta(z - z_0)$$

and

$$\bigtriangledown^2 = \frac{\partial^2}{\partial x^2} + \frac{\partial^2}{\partial y^2} + \frac{\partial^2}{\partial z^2}.$$

In this case, following the same procedure as before,

$$g(R, k) = \frac{1}{(2\pi)^3} \int_{-\infty}^{\infty} \frac{\exp(i\mathbf{u} \cdot \mathbf{R})}{u^2 - k^2} d^3\mathbf{u}.$$

It proves convenient to evaluate this integral using spherical polar coordinates which gives

$$g(R, k) = \frac{1}{(2\pi)^3} \int_0^{2\pi} d\phi \int_{-1}^{1} d(\cos\theta) \int_0^{\infty} \frac{\exp(iuR\cos\theta) u^2}{u^2 - k^2} du.$$

Integrating over ϕ and θ we then obtain

$$g(R, k) = \frac{1}{2\pi^2 R} \int_0^{\infty} \frac{u \sin(uR)}{u^2 - k^2} du.$$

Since the integrand is an even function we may extend the integration to include the interval $-\infty$ to 0 by writing

$$g(R, k) = \frac{1}{4\pi^2 R} \int_{-\infty}^{\infty} \frac{u \sin(uR)}{u^2 - k^2} du.$$

This is done in anticipation of using Cauchy's residue theorem to evaluate the contour integral

$$\oint_C \frac{z\exp(izR)}{(z-k)(z+k)}dz$$

which has simple poles at $z = \pm k$. Choosing the contour C to enclose the pole at $z = k$ (the 'outgoing' case), the residue is

$$\frac{\exp(ikR)}{2}$$

and, thus, the 'outgoing' Green becomes

$$g(\mathbf{r} \mid \mathbf{r}_0, k) = \frac{1}{4\pi \mid \mathbf{r} - \mathbf{r}_0 \mid} \exp(ik \mid \mathbf{r} - \mathbf{r}_0 \mid).$$

We see that in one-, two- and three dimensions the Green function is singular. The precise nature of the singularity changes from one dimension to the next. In three dimensions, the Green function is spatially singular when $\mathbf{r} = \mathbf{r}_0$, whereas in one dimension the singularity occurs when $k = 0$. In two dimensions, a singularity occurs when either $k = 0$ or $\mathbf{r} = \mathbf{r}_0$. An example of this two-dimensional Green function is observed when a small stone falls vertically into a large pool of water. The symmetrical expanding wavefront represents the result of applying a short impulse to the surface of the water. What is observed is a good approximation to a Hankel function! There are relatively few examples in nature which are characteristic of an ingoing Green function since most impulses produce wavefields that propagate away from the point of disturbance. However, there are some notable exceptions, one of which relates to the development of the Plutonium fission bomb first used in 1945. Figure 5.3 shows the implosion generated by the 'device' shown in Figure 5.4 (left), the effect being illustrated in Figure 5.4 (right). This was the first plutonium fission bomb designed using conventional charges to compress a plutonium core at the centre of the device.

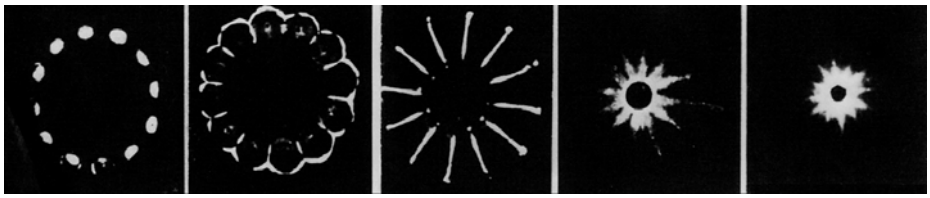

Figure 5.3: Example of a 3D 'ingoing' Green function (recorded in the plane over five time frames) - an implosion.

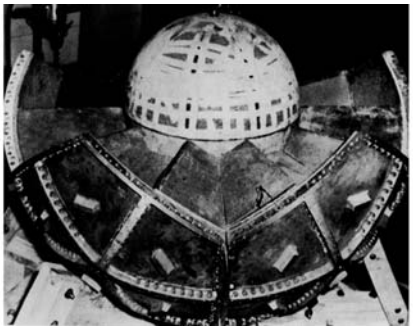

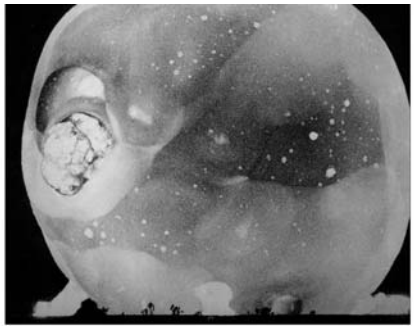

Figure 5.4: The device (above left) used to produce the implosion shown in Figure 5.3 and its 'output' (above right), i.e. a 3D 'outgoing' Green function - an explosion.

In addition to the derivation of the 3D Green function given above, the function can be derived in a more physically intuitive way. Imagine a point source of radiation with a wavenumber k which gives out a stream of waves, moving radially outwards. If the distance from the source is R, then we should expect to be able to describe the wavefield (taken to be of unit amplitude) as $\exp(ikR)$ in the usual way. However, in 3D, the intensity of the field should obey an inverse square law and vary as $1/R^2$. But the intensity of the wavefield is proportional to the modulus squared and so the amplitude of the wavefield must be proportional to $1/R$ and hence the amplitude of the field should be

$$\frac{\exp(ikR)}{R}$$

which is the correct form of the Green function, up to a numerical factor (i.e. $1/4\pi$). Finally, if the source is taken to be at $\mathbf{r}_0$ and the field is measured at $\mathbf{r}$, then R must be given in terms of the 'path length' $\mid \mathbf{r} - \mathbf{r}_0 \mid$.

5.3.4 Asymptotic Forms

Although the Green functions for the inhomogeneous wave equation can be computed in the manner already discussed, their algebraic form is not always easy, useful or indeed necessary to work with. This is because the geometry of many imaging systems justifies an approximation. For this reason, it is now appropriate to consider the form of the Green function when the field generated by a point source is moved away from that source, i.e. when the magnitude of $\mathbf{r}_0$ becomes increasingly larger than the magnitude of $\mathbf{r}$. There are two approximations which are important in this respect which are often referred to as the Fraunhofer and Fresnel approximations. These approximations are usually associated with the applications of Green functions in optics (in which both Fraunhofer and Fresnel undertook their original work) but are, in fact, of general applicability.

The Fraunhofer Approximation

In one-dimension, we note that

$$|x - x_0| = \begin{cases} x_0 - x, & x_0 > x; \\ x - x_0, & x > x_0. \end{cases}$$

so that the Green function for a left-travelling wave for example can be written as

$$g(x \mid x_0, k) = \frac{i}{2k} \exp(ikx_0) \exp(-ikx), \quad x_0 > x$$

and

$$g(x \mid x_0, k) = \frac{i}{2k} \exp(-ikx_0) \exp(ikx), \quad x_0 < x$$

for a right-travelling wave.

In two- and three-dimensions, we expand the path length between the source and observer in terms of their respective coordinates. To start with, let us look at the result in two dimensions. In this case,

$$\mid \mathbf{r} - \mathbf{r}_0 \mid = \sqrt{r_0^2 + r^2 - 2\mathbf{r} \cdot \mathbf{r}_0} = r_0 \left(1 - \frac{2\mathbf{r} \cdot \mathbf{r}_0}{r_0^2} + \frac{r^2}{r_0^2}\right)^{\frac{1}{2}}$$

where $\mathbf{r} = \hat{\mathbf{x}}x + \hat{\mathbf{y}}y$, $r = \mid \mathbf{r} \mid$ and $r_0 = \mid \mathbf{r}_0 \mid$. A binomial expansion of this result gives

$$\mid \mathbf{r} - \mathbf{r}_0 \mid = r_0 \left(1 - \frac{\mathbf{r} \cdot \mathbf{r}_0}{r_0^2} + \frac{r^2}{2r_0^2} + ...\right) \tag{5.6}$$

which under the condition

$$\frac{r}{r_0} << 1$$

reduces to

$$\mid \mathbf{r} - \mathbf{r}_0 \mid \simeq r_0 - \hat{\mathbf{n}}_0 \cdot \mathbf{r}$$

where

$$\hat{\mathbf{n}}_0 = \frac{\mathbf{r}_0}{r_0}.$$

It is sufficient to let

$$\frac{1}{\mid \mathbf{r} - \mathbf{r}_0 \mid} \simeq \frac{1}{r_0}, \quad r_0 >> r$$

because small changes in $\hat{\mathbf{n}} \cdot \mathbf{r}$ compared to r_0 are not significant in an expression of this type. However, with the exponential function

$$\exp[ik(r_0 - \hat{\mathbf{n}}_0 \cdot \mathbf{r})]$$

a relatively small change in the value of $r_0 - \hat{\mathbf{n}}_0 \cdot \mathbf{r}$ compared to r_0 will still cause this term to oscillate rapidly, particularly if the value of k is large. We therefore write

$$\exp(ik \mid \mathbf{r} - \mathbf{r}_0 \mid) = \exp(ikr_0) \exp(-ik\hat{\mathbf{n}}_0 \cdot \mathbf{r}).$$

The asymptotic form of the two dimensional Green function is then given by

$$g(\mathbf{r} \mid \mathbf{r}_0, k) = \frac{\exp(i\pi/4)}{\sqrt{8\pi}} \frac{1}{\sqrt{kr_0}} \exp(ikr_0) \exp(-ik\hat{\mathbf{n}}_0 \cdot \mathbf{r}), \quad kr_0 >> 1.$$

In three dimensions, the result is (using exactly the same arguments as in the two dimensional case)

$$g(\mathbf{r} \mid \mathbf{r}_0, k) = \frac{1}{4\pi r_0} \exp(ikr_0) \exp(-ik\hat{\mathbf{n}}_0 \cdot \mathbf{r})$$

where

$$\mathbf{r} = \hat{\mathbf{x}}x + \hat{\mathbf{y}}y + \hat{\mathbf{z}}z.$$

When we observe the field described by a Green function at large distances (i.e. the wavefield generated by a point source a long distance away), it behaves like a plane wave $\exp(-ik\hat{\mathbf{n}}_0 \cdot \mathbf{r})$. Approximating the Green function in this way provides a description for the wave in what is commonly referred to as the far field or Fraunhofer zone (or plane). This approximation is often referred to as the Fraunhofer approximation in physical optics. In this zone, the wave front which reaches the observer is a plane wave front because, in effect, the divergence of the field is so small. Observations of a field in this zone are said to be in the Fourier plane because they lead to equations that involve a Fourier transform as shall be shown later. This is the basis for Fraunhofer diffraction theory which is important in applications such as X-ray crystallography, electromagnetic and acoustic imaging and, of course, modern optics.

The Fresnel Approximation

When the source is brought closer to the observer, the wavefront ceases to be a plane wavefront. In this case, the Fraunhofer approximation is inadequate and another approximation for the Green function must be used. This is known as the Fresnel approximation and is based on incorporating the next term in the binomial expansion of $\mid \mathbf{r} - \mathbf{r}_0 \mid$, namely the quadratic term $r^2/2r_0^2$ in equation (5.6). In this case, it is assumed that $r^2/r_0^2 << 1$ rather than $r/r_0 << 1$ so that all the terms in the binomial expansion of $\mid \mathbf{r} - \mathbf{r}_0 \mid$ that occur after the quadratic term can be neglected. As before, $\mid \mathbf{r} - \mathbf{r}_0 \mid^{-1}$ is approximated by $1/r_0$ but the exponential term now possesses an additional feature, namely a 'quadratic phase factor'. In this case, the two and three-dimensional Green functions are given by

$$g(\mathbf{r} \mid \mathbf{r}_0, k) = \frac{\exp(i\pi/4)}{\sqrt{8\pi}} \frac{\exp(ikr_0)}{\sqrt{kr_0}} \exp(-ik\hat{\mathbf{n}}_0 \cdot \mathbf{r}) \exp(ir^2/2r_0), \quad kr_0 >> 1$$

and

$$g(\mathbf{r} \mid \mathbf{r}_0, k) = \frac{\exp(ikr_0)}{4\pi r_0} \exp(-ik\hat{\mathbf{n}}_0 \cdot \mathbf{r}) \exp(ir^2/2r_0)$$

respectively. This type of approximation is used in the study of systems (optical systems for example) in which the divergence of the field is a measurable quantity. This is important in imaging systems such as Synthetic Aperture

Radar, the application of Fresnel- or zone-plates for example, and Fresnel optics in general. If the source is moved even closer to the observer then neither the Fraunhofer nor the Fresnel approximations will apply. In such cases, it is usually easier to retain the Green function in full rather than consider another term in the binomial expansion of the path length. Analysis of a wavefield that is produced when a non-asymptotic form of the Green function is used is referred to as near field analysis. Thus, the Green function solution to two- and three-dimensional wave type partial differential equations usually falls into one of the three categories:

(i) near field analysis;

(ii) intermediate field (Fresnel zone) analysis;

(iii) far field (Fraunhofer zone of Fourier plane) analysis.

These 'zones' are characterized by the geometry of the 'wavefront' as illustrated in Figure 5.6.

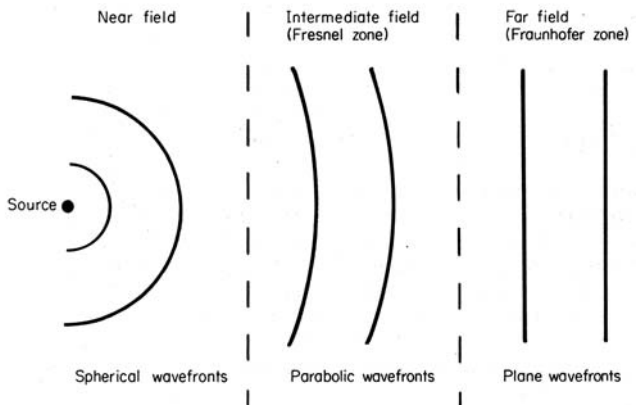

Figure 5.5: Characteristic wavefronts in the near, intermediate and far fields

In practice the far field approximation is much easier to use. This is because it leads to solutions that can be written in terms of a Fourier transform which is a relatively easy transform to work with and invert. Using the Fresnel approximation leads to solutions which involve a class of integral known as the Fresnel integral. The nonlinear behaviour of this integral, because of the quadratic phase factor, makes it more difficult to evaluate compared with the Fourier integral. There are relatively few applications in wavefield theory which require a full near field analysis. This is fortunate, because near field analysis presents some formidable analytical and computational problems.

5.4 Wavefields Generated by Sources

Now that we have studied Green functions for the inhomogeneous time-independent wave equation, in this Section we turn our attention to the more general problem of developing a solution for the wavefield $u(\mathbf{r}, k)$ generated by an arbitrary and time independent source function $f(\mathbf{r})$. This study is a prelude to the work discussed in the following Chapter which provides an introduction to scattering theory in which the source function is not $f(\mathbf{r})$ but $f(\mathbf{r})u(\mathbf{r}, k)$ or $k^2 f(\mathbf{r})u(\mathbf{r}, k)$. Working in three dimensions, our aim is to solve

$$(\nabla^2 + k^2)u(\mathbf{r}, k) = -f(\mathbf{r}), \quad \mathbf{r} \in V$$

for u where V is the volume of the source function which is of compact support (occupies a finite region of space V) . Outside of this region, it is assumed that the source function is zero. Note that we define the source term as $-f$ rather than $+f$. This is done so that there is consistency with the definition of the Green function which is defined in terms of $-\delta$ by convention. We start by writing the equation for a Green function, i.e.

$$(\nabla^2 + k^2)g(\mathbf{r} \mid \mathbf{r}_0, k) = -\delta^3(\mathbf{r} - \mathbf{r}_0).$$

If we now multiply both sides of the first equation by g and both sides of the second equation by u, then by subtracting the two results we obtain

$$g\nabla^2 u - u\nabla^2 g = -gf + u\delta^3.$$

By integrating the last equation over all space, we can exploit the result

$$\int_{-\infty}^{\infty} u(\mathbf{r}, k)\delta^3(\mathbf{r} - \mathbf{r}_0)d^3\mathbf{r} = u(\mathbf{r}_0, k)$$

and therefore write (noting that $\mathbf{r} \in V$)

$$u(\mathbf{r}_0, k) = \int_V f(\mathbf{r})g(\mathbf{r} \mid \mathbf{r}_0, k)d^3\mathbf{r}$$

$$+ \int_V [g(\mathbf{r} \mid \mathbf{r}_0, k)\nabla^2 u(\mathbf{r}, k) - u(\mathbf{r}, k)\nabla^2 g(\mathbf{r} \mid \mathbf{r}_0, k)]d^3\mathbf{r}.$$

We see that this expression is not a 'proper solution' for u because u occurs on both the left and right hand sides. What we require is a solution for u in terms of known quantities on the right hand side of the above equation. To this end, we can simplify the second term by using Green theorem (see Chapter 1)

$$\int_V (g\nabla^2 u - u\nabla^2 g)d^3\mathbf{r} = \oint_S (g\nabla u - u\nabla g) \cdot \hat{\mathbf{n}} d^2\mathbf{r}.$$

Here, S defines the surface enclosing the volume V and $d^2\mathbf{r}$ is an element of this surface. The unit vector $\hat{\mathbf{n}}$ points out of the surface and is perpendicular to the surface element $d^2\mathbf{r}$. Green's theorem is a special but important consequence of Gauss' divergence theorem as shown below.

5.4.1 Green's Theorem

Let u and g be any two piecewise continuous functions of position and S be a surface enclosing a volume V. If u, g and their first and second partial derivatives are single-valued and continuous within and on S, then

$$\int_V (g\nabla^2 u - u\nabla^2 g)d^3\mathbf{r} = \oint_S \left(g\frac{\partial u}{\partial \hat{\mathbf{n}}} - u\frac{\partial g}{\partial \hat{\mathbf{n}}} \right) d^2\mathbf{r}$$

where $\partial/\partial\hat{\mathbf{n}}$ is a partial derivative in the outward normal direction on S.

The proof of this result stems from noting that since

$$\nabla \cdot (g\nabla u) = \nabla g \cdot \nabla u + g\nabla^2 u$$

and

$$\nabla \cdot (u\nabla g) = \nabla u \cdot \nabla g + u\nabla^2 g$$

then

$$\int_V \nabla \cdot (g\nabla u - u\nabla g)d^3\mathbf{r} = \int_V (g\nabla^2 u - u\nabla^2 g)d^3\mathbf{r}.$$

But from Gauss' theorem

$$\int_V \nabla \cdot \mathbf{F} d^3\mathbf{r} = \oint_S \mathbf{F} \cdot \hat{\mathbf{n}} d^2\mathbf{r}$$

for any vector $\mathbf{F}$. Hence,

$$\int_V \nabla \cdot (g\nabla^2 u - u\nabla^2 g)d^3\mathbf{r} = \oint_S (g\nabla u - u\nabla g) \cdot \hat{\mathbf{n}} d^2\mathbf{r}$$

which provides the basic result, a result that can be written in an alternative (and arguably more elegant way) by defining

$$\nabla u \cdot \hat{\mathbf{n}} \equiv \frac{\partial u}{\partial \hat{\mathbf{n}}}$$

and

$$\nabla g \cdot \hat{\mathbf{n}} \equiv \frac{\partial g}{\partial \hat{\mathbf{n}}}$$

so that we can write

$$\int_V (g\nabla^2 u - u\nabla^2 g)d^3\mathbf{r} = \oint_S \left(g\frac{\partial u}{\partial \hat{\mathbf{n}}} - u\frac{\partial g}{\partial \hat{\mathbf{n}}} \right) d^2\mathbf{r}.$$

This theorem provides a solution for the wavefield u at $\mathbf{r}_0$ of the form

$$u(\mathbf{r}_0, k) = \int_V f g d^3\mathbf{r} + \oint_S (g\nabla u - u\nabla g) \cdot \hat{\mathbf{n}} d^2\mathbf{r}.$$

We have shown that using a Green function and Green's theorem, the solution to the equation

$$(\nabla^2 + k^2)u(\mathbf{r}, k) = -f(\mathbf{r}), \quad \mathbf{r} \in V$$

is

$$u(\mathbf{r}_0, k) = \oint_S (g\nabla u - u\nabla g) \cdot \hat{\mathbf{n}} d^2\mathbf{r} + \int_V f g d^3\mathbf{r}.$$

It is important to appreciate that this solution is entirely general with no conditions being placed on any of the analysis at any point other than that u are g are piecewise continuous. However, as discussed before, it is not a 'solution' as such because the field variable u occurs on both the left hand and right hand sides of the 'solution'. It is therefore better to consider this 'solution' to be a transform from a partial differential equation to an integral equation. From a mathematical point of view, a Green function is that function which allows any linear inhomogeneous PDE to be transformed to an integral equation. Finally, note that the homogeneous equation

$$(\nabla^2 + k^2)u(\mathbf{r}, k) = 0$$

also has a Green function solution given by

$$u(\mathbf{r}_0, k) = \oint_S (g\nabla u - u\nabla g) \cdot \hat{\mathbf{n}} d^2\mathbf{r}.$$

5.4.2 Dirichlet and Neumann Boundary Conditions

Although Green's theorem allows us to simplify the solution for the wavefield u derived in the previous Section (in the sense that we now have a two dimensional instead of a three dimensional integral), we still do not have a proper solution for u since this field variable is present on both the left and right hand sides of the integral equation for u. However, as a result of applying Green's theorem, we now only need to specify u and ∇u on the surface S. Therefore, if we know, *a priori*, the behaviour of u and ∇u on S, then we can compute u at any other observation point $\mathbf{r}_0$. Clearly, a statement about the nature of u and ∇u on S is required, i.e. the boundary conditions need to be specified.

In general, the type of conditions that may be applied depends on the applications that are involved. In practice, two types of boundary conditions are commonly considered. The first one, known as the homogeneous Dirichlet boundary condition, states that u is zero on S. The second one, known as the homogeneous Neumann condition, states that ∇u is zero on S. Taken together, these boundary conditions are known as the 'homogeneous conditions' and are referred to as such throughout the rest of this work. When u satisfies these homogeneous boundary conditions, the solution for u is given by

$$u(\mathbf{r}_0, k) = \int_V f(\mathbf{r}) g(\mathbf{r} \mid \mathbf{r}_0, k) d^3\mathbf{r}$$

because

$$\oint_S (g\nabla u - u\nabla g)\cdot\hat{\mathbf{n}}d^2\mathbf{r} = 0.$$

If the wavefield generated by a source is measured a long distance away from the location of the source, then by using the far field approximation for the Green function, we have

$$u(\hat{\mathbf{n}}_0, k) = \frac{1}{4\pi r_0}\exp(ikr_0)\int_V f(\mathbf{r})\exp(-ik\hat{\mathbf{n}}_0\cdot\mathbf{r})d^3\mathbf{r}.$$

In this case, the field generated by the source is given by the 3D Fourier transform of the source function f. By measuring the radiation pattern produced by a source denoted by $f(\mathbf{r})$, the structure or spatial distribution of the source may be recovered through a processes of inversion. In the far field, the source function can be recovered by taking the inverse Fourier transform of the observed field. This is an example of a solution to a class of problem known as an inverse source problem.

5.4.3 The Reciprocity Theorem

The reciprocity theorem applies to all Green functions associated with any linear partial differential equation. Here, the theorem will be proved for the 3D Green function corresponding to the time-independent wave equation. The theorem states that if $\mathbf{r}_1$ and $\mathbf{r}_2$ are two points in space then

$$g(\mathbf{r}_1 \mid \mathbf{r}_2, k) = g(\mathbf{r}_2 \mid \mathbf{r}_1, k).$$

The proof of this result which can be obtained by considering the equations

$$(\nabla^2 + k^2)g(\mathbf{r} \mid \mathbf{r}_1, k) = -\delta^3(\mathbf{r} - \mathbf{r}_1), \quad r \in V$$

and

$$(\nabla^2 + k^2)g(\mathbf{r} \mid \mathbf{r}_2, k) = -\delta^3(\mathbf{r} - \mathbf{r}_2) \quad r \in V.$$

Then

$$\begin{aligned} &g(\mathbf{r} \mid \mathbf{r}_2, k)\nabla^2 g(\mathbf{r} \mid \mathbf{r}_1, k) - g(\mathbf{r} \mid \mathbf{r}_1, k)\nabla^2 g(\mathbf{r} \mid \mathbf{r}_2, k) \\ &= g(\mathbf{r} \mid \mathbf{r}_1, k)\delta^3(\mathbf{r} - \mathbf{r}_2) - g(\mathbf{r} \mid \mathbf{r}_2, k)\delta^3(\mathbf{r} - \mathbf{r}_1) \end{aligned}$$

Integrating over V and using Green's theorem, for homogeneous boundary conditions on the surface of V, we have

$$\int_V g(\mathbf{r} \mid \mathbf{r}_1, k)\delta^3(\mathbf{r} - \mathbf{r}_2)d^3\mathbf{r} - \int_V g(\mathbf{r} \mid \mathbf{r}_2, k)\delta^3(\mathbf{r} - \mathbf{r}_1)d^3\mathbf{r} = 0$$

or

$$g(\mathbf{r}_2 \mid \mathbf{r}_1, k) = g(\mathbf{r}_1 \mid \mathbf{r}_2, k).$$

Thus, the propagation of a wave from a point at $\mathbf{r}_1$ to $\mathbf{r}_2$ is the same as the propagation of a wave from a point at $\mathbf{r}_2$ to $\mathbf{r}_1$.

5.4.4 Coherent and Incoherent Sources

Suppose we have an extended one-dimensional source function $f(x)$ and are able to measure the resulting wavefield generated by the emission of radiation from just two points x_A and x_B of this source which are at a distance X_A and X_B from the detector, respectively. The amplitudes of the wave field generated from points x_A and x_B will be given by $f(x_A)g(X_A, k)$ and $f(x_B)g(X_B, k)$, respectively, where g is the Green function. The total amplitude u will be the sum of these two wavefields, i.e.

$$u = A + B$$

where $A = f(x_A)g(X_A, k)$ and $B = f(x_B)g(X_B, k)$. The intensity is then given by

$$I = uu^* =\mid A \mid^2 + \mid B \mid^2 + AB^* + BA^*.$$

This is the situation when the source function describes a coherent source where the phase difference between A and B is a constant.

If the source is incoherent, then the phases associated with different parts of the source do not maintain a constant relationship. We can model this by placing a random phase function $\phi(x) = \exp[i\theta(x)]$ in the expression for the source term, i.e.

$$f(x) \to \phi(x)f(x).$$

The statistical properties of ϕ reflect the fact that wave phases at different points are uncorrelated, so that, for $x \neq x'$,

$$\langle \phi(x)\phi^*(x') \rangle = 0$$

where

$$\langle \phi(x) \rangle \equiv \frac{\int \phi(x)dx}{\int dx}$$

and where we note that the magnitude of any single phase factor is 1, i.e

$$\langle \phi(x)\phi^*(x) \rangle = 1$$

so that

$$\langle \phi(x)\phi^*(x') \rangle = \begin{cases} 1, & x = x'; \\ 0, & x \neq x'. \end{cases}$$

With this phase function in place, we can calculate the amplitude as before:

$$u = A\phi(x_A) + B\phi(x_B).$$

The intensity is then given by

$$I = uu^* =\mid A \mid^2 + \mid B \mid^2 + AB^*\phi(x_A)\phi^*(x_B) + BA^*\phi(x_B)\phi^*(x_A)$$

Because ϕ varies rapidly with time as the relative phases at different parts of the source change, the quantity that determines the observed intensity is the average intensity. Taking the average intensity of the last equation and

using the fact that the phases at different parts of the source are uncorrelated, eliminates the last two terms and leaves us with

$$\langle I \rangle = \mid A \mid^2 + \mid B \mid^2$$

This is the same as the expression for the intensity of the coherent source, except for the last two cross-terms. These terms represent interference which average to zero in the incoherent case, leaving the sum of the intensities coming from the two different parts of the source.

Now consider the Green function solution to the inhomogeneous Helmholtz equation for the source function $f(x)$ given by

$$u(x,k) = \int g(x \mid x_0, k) f(x_0) dx_0$$

With coherent illumination, the phase relationships between different parts of the source are maintained and the intensity is

$$I(x,k) = \mid u(x,k) \mid^2 = \int dx_1 g(x \mid x_1, k) f(x_1) \int dx_2 g^*(x \mid x_2, k) f^*(x_2)$$

$$= \int \int dx_1 dx_2 g(x \mid x_1, k) g^*(x \mid x_2, k) f(x_1) f^*(x_2).$$

When the source is incoherent we introduce a random phase function $\phi(x')$ with statistical properties that reflect the fact that the phases at different points of the source are uncorrelated, or

$$\langle \phi(x_1) \phi^*(x_2) \rangle = \delta(x_1 - x_2) = \begin{cases} \infty, & x_1 = x_2; \\ 0, & x_1 \neq x_2. \end{cases}$$

Upon calculating the average intensity $\langle I(x) \rangle$, the expression simplifies as before to

$$\langle I(x,k) \rangle = \int \int dx_1 dx_2 g(x \mid x_1, k) g^*(x \mid x_2, k) f(x_1) f^*(x_2) \langle \phi(x_1) \phi^*(x_2) \rangle$$

$$= \int \int dx_1 dx_2 g(x \mid x_1, k) g^*(x \mid x_2, k) f(x_1) f^*(x_2) \delta(x_1 - x_2)$$

$$= \int dx_1 \mid g(x \mid x_1, k) \mid^2 \mid f(x_1) \mid^2 .$$

Now, $\mid f(x) \mid^2$ is the intensity $I_f(x)$ of the source function $f(x)$ and thus we have

$$\langle I(x,k) \rangle = \mid g(\mid x \mid, k) \mid^2 \otimes I_f(x)$$

where $\otimes$ denotes the one-dimensional convolution operation.

For homogeneous boundary conditions, in two- or three-dimensions, we can derive the same basic result. Thus, for a 2D coherent source,

$$I(\mathbf{r}, k) = \mid g(\mid \mathbf{r} \mid, k) \otimes \otimes f(\mathbf{r}) \mid^2$$

and for a 2D incoherent source,

$$\langle I(\mathbf{r},k)\rangle = \mid g(\mid \mathbf{r} \mid,k) \mid^2 \otimes\otimes I_f(\mathbf{r}).$$

The results above are basic to imaging science in terms of the differentiation between a coherent and an incoherent image in which g is replaced by the so-called point spread function p. Thus, if p is the amplitude point spread function for a coherent system, then the intensity point spread function for the corresponding incoherent system is $\mid p \mid^2$.

5.5 Time Dependent Green Function

We have studied the Green function for the time independent wave equation. In this section, we investigate the time dependent case.

As an introduction to the time dependent Green function, let us first consider the case where we have a homogeneous source of scalar radiation a long distance away from an observer at $\mathbf{r}$. Here, the scalar wavefield u as a function of space $\mathbf{r}$ and time t is described by the homogeneous equation

$$\left(\nabla^2 + \frac{1}{c^2}\frac{\partial^2}{\partial t^2}\right) U(\mathbf{r},t) = 0 \tag{5.7}$$

where c is the velocity at which the radiation propagates from the source to the observer.

5.5.1 Continuous Wave Sources

Let us assume that the source emits a continuous wave which oscillates at a fixed frequency. In this case, the source is known as a continuous wave (CW) or monochromatic source as used earlier in Chapter 4 to investigate the solutions to the Maxwell's equations for a linear isotropic medium. The time dependence of the radiation field is described by the complex exponential function $\exp(i\omega t)$ where ω is the angular frequency ($= 2\pi\times$frequency). The time dependent field u can therefore be written as

$$U(\mathbf{r},t) = u(\mathbf{r},\omega)\exp(i\omega t).$$

Substituting this expression into equation (5.7), we obtain

$$(\nabla^2 + k^2)u(\mathbf{r},k) = 0$$

where

$$k = \frac{\omega}{c} = \frac{2\pi}{\lambda}$$

is the wavenumber and λ is the wavelength of the wavefield described by the function u. A solution to this equation is

$$u(\mathbf{r},k) = \exp(i\mathbf{k}\cdot\mathbf{r})$$

where the wave vector

$$\mathbf{k} = k\hat{\mathbf{n}}$$

and it is assumed that the amplitude of the wave is 1. The unit vector $\hat{\mathbf{n}}$ points along the direction in which the wave propagates. Thus, the solution for the time dependent wavefield becomes

$$U(\mathbf{r}, t) = \exp[i(\mathbf{k} \cdot \mathbf{r} + \omega t)].$$

However, an equally valid solution is

$$U(\mathbf{r}, t) = \exp[i(\mathbf{k} \cdot \mathbf{r} - \omega t)]$$

which is obtained by using the $\exp(-i\omega t)$ to describe the time dependence of the wavefield. If we imagine a straight line along the direction of $\hat{\mathbf{n}}$, then the above solution for u represents a wave propagating to the right whereas the former solution represents a wave propagating to the left. The function

$$\exp[i(\mathbf{k} \cdot \mathbf{r} + \omega t)]$$

is said to describe a left-travelling wave and

$$\exp[i(\mathbf{k} \cdot \mathbf{r} - \omega t)]$$

is referred to as a right-travelling wave.

5.5.2 Pulsed Sources

If the source emits a pulse of radiation, then the time dependent field can be written as the sum of many different monochromatic waves of different frequencies ω and amplitudes u. If we consider all the different possible frequencies that can exist between $-\infty$ and ∞, then $U(\mathbf{r}, t)$ can be written in terms of its Fourier transform as,

$$U(\mathbf{r}, t) = \frac{1}{2\pi} \int_{-\infty}^{\infty} u(\mathbf{r}, \omega) \exp(i\omega t) d\omega.$$

Here, U describes a left-travelling pulse. We can also consider a solution for a right-travelling pulse by writing

$$U(\mathbf{r}, t) = \frac{1}{2\pi} \int_{-\infty}^{\infty} u(\mathbf{r}, \omega) \exp(-i\omega t) d\omega.$$

Substituting either of these expressions into equation (5.7), we obtain

$$(\nabla^2 + k^2) u(\mathbf{r}, k) = 0$$

where now k is not fixed but can take on any value between $-\infty$ and ∞. The time dependent field produced by a left-travelling pulse is therefore

$$U(\mathbf{r}, t) = \frac{1}{2\pi} \int_{-\infty}^{\infty} \exp[i(\mathbf{k} \cdot \mathbf{r} + \omega t)] d\omega.$$

If we now write $\mathbf{k}\cdot\mathbf{r}$ as $k\hat{\mathbf{n}}\cdot\mathbf{r} = (\omega/c)\hat{\mathbf{n}}\cdot\mathbf{r}$, then, using the integral representation for a delta function, the above equation can be written as

$$U(\mathbf{r},t) = \frac{1}{2\pi}\int_{-\infty}^{\infty} \exp[i\omega(t+\hat{\mathbf{n}}\cdot\mathbf{r}/c)]d\omega = \delta(t+\hat{\mathbf{n}}\cdot\mathbf{r}/c).$$

The expression for a right-travelling pulse is given by

$$U(\mathbf{r},t) = \delta(t-\hat{\mathbf{n}}\cdot\mathbf{r}/c).$$

5.6 Time Dependent Sources

Let us now turn our attention to the case when an inhomogeneous time varying source produces a wavefield $U(\mathbf{r},t)$. To describe this situation mathematically, we introduce a source function $f(\mathbf{r},t)$. The wavefield is then governed by the inhomogeneous equation

$$\left(\nabla^2 + \frac{1}{c^2}\frac{\partial^2}{\partial t^2}\right)U(\mathbf{r},t) = -f(\mathbf{r},t).$$

Now, as in the time dependent case, the Green function describes the wavefield that is produced when the source function is a delta function, i.e. when

$$S(\mathbf{r},t) = \delta^n(\mathbf{r}-\mathbf{r}_0)\delta(t-t_0)$$

where $n = 1, 2$ or 3 depending on whether we are considering a one-, two-, or three-dimensional wavefield respectively. Hence, the equation for the time dependent Green function (which is usually denoted by G) is given by

$$\left(\nabla^2 + \frac{1}{c^2}\frac{\partial^2}{\partial t^2}\right)G(\mathbf{r}\mid\mathbf{r}_0,t\mid t_0) = -\delta^n(\mathbf{r}-\mathbf{r}_0)\delta(t-t_0).$$

5.6.1 3D Time Dependent Green Function

We shall consider the three-dimensional time-dependent problem first which is based on an evaluation using the time-independent Green function. We write G and $\delta(t-t_0)$ as Fourier transforms,

$$G(\mathbf{r}\mid\mathbf{r}_0,t\mid t_0) = \frac{1}{2\pi}\int_{-\infty}^{\infty} g(\mathbf{r}\mid\mathbf{r}_0,\omega)\exp[i\omega(t-t_0)]d\omega$$

and

$$\delta(t-t_0) = \frac{1}{2\pi}\int_{-\infty}^{\infty} \exp[i\omega(t-t_0)]d\omega$$

where ω is the angular frequency. Substituting these equations into the equation for G we then have

$$(\nabla^2 + k^2)g(\mathbf{r}\mid\mathbf{r}_0,k) = -\delta^3(\mathbf{r}-\mathbf{r}_0)$$

which is the same equation as that used previously to define the time-independent Green function. Thus, once g has been obtained, the time dependent Green function can be derived by computing the Fourier integral given above. Using the expression for g derived earlier,

$$G(\mathbf{r} \mid \mathbf{r}_0, t \mid t_0) = \frac{1}{2\pi} \int_{-\infty}^{\infty} \frac{1}{4\pi \mid \mathbf{r} - \mathbf{r}_0 \mid} \exp(ik \mid \mathbf{r} - \mathbf{r}_0 \mid) \exp[i\omega(t - t_0)] d\omega$$

$$= \frac{1}{4\pi \mid \mathbf{r} - \mathbf{r}_0 \mid} \delta(t - t_0 + \mid \mathbf{r} - \mathbf{r}_0 \mid /c).$$

5.6.2 2D Time Dependent Green Function

In two dimensions, the point source (which depends on x and y) can be treated as a line source, that is a uniform source extending from $z_0 = -\infty$ to $z_0 = \infty$ along a line parallel to the z axis and passing through the point (x_0, y_0). Thus, a simple way of computing the two-dimensional Green function is to integrate the three-dimensional Green function from $z_0 = -\infty$ to $z_0 = \infty$, i.e.

$$G(\mathbf{s} \mid \mathbf{s}_0, t \mid t_0) = \int_{-\infty}^{\infty} \frac{\delta(t - t_0 + \mid \mathbf{r} - \mathbf{r}_0 \mid /c)}{4\pi \mid \mathbf{r} - \mathbf{r}_0 \mid} dz_0$$

where

$$\mathbf{s} = \hat{\mathbf{x}}x + \hat{\mathbf{y}}y$$

and

$$\mathbf{s}_0 = \hat{\mathbf{x}}x_0 + \hat{\mathbf{y}}y_0.$$

Writing $\tau = (t - t_0)c, \quad \xi = z_0 - z, \quad S = \mid \mathbf{s} - \mathbf{s}_0 \mid$ and $R = \mid \mathbf{r} - \mathbf{r}_0 \mid$ we have

$$R^2 = \xi^2 + S^2$$

and

$$\frac{dR}{dz_0} = \frac{\xi}{R}$$

and so the Green function can be written in the form

$$G(S, \tau) = \frac{1}{4\pi} \int_{-\infty}^{\infty} \frac{\delta(\tau + R)}{\sqrt{R^2 - S^2}} dR$$

$$= \begin{cases} \frac{1}{4\pi} \frac{1}{\sqrt{\tau^2 - S^2}}, & \tau > S; \\ 0, & \tau < S. \end{cases}$$

5.6.3 1D Time Dependent Green Function

In one dimension, the time-dependent Green function can be calculated by integrating the three dimensional Green function over z_0 and y_0. Alternatively, we can use the expression for $g(x \mid x_0, k)$ (right-travelling Green function) giving

$$G(x \mid x_0, t \mid t_0) = \frac{1}{2\pi} \int_{-\infty}^{\infty} \frac{i}{2k} \exp(ik \mid x - x_0 \mid) \exp[i\omega(t - t_0)] d\omega.$$

This equation is the inverse Fourier transform of the product of two functions (given that $k = \omega/c$), namely $i/2k$ and $\exp(ik \mid x - x_0 \mid)$. Thus, using the convolution theorem and noting that

$$\frac{1}{2\pi} \int_{-\infty}^{\infty} \frac{i}{2k} \exp[i\omega(t - t_0)] d\omega = \frac{c}{4} \operatorname{sgn}(t - t_0)$$

and

$$\frac{1}{2\pi} \int_{-\infty}^{\infty} \exp(ik \mid x - x_0 \mid) \exp[i\omega(t - t_0)] d\omega = \delta(t - t_0 + \mid x - x_0 \mid /c),$$

we obtain

$$\begin{aligned} G(x \mid x_0, t \mid t_0) &= \frac{c}{4} \operatorname{sgn}(t - t_0) \otimes \delta(t - t_0 + \mid x - x_0 \mid /c) \\ &= \frac{c}{4} \operatorname{sgn}[t - t_0 + \mid x - x_0 \mid /c] \end{aligned}$$

where $\otimes$ denotes the convolution integral and sgn is defined by

$$\operatorname{sgn}(x) = \begin{cases} 1, & x > 0; \\ -1, & x < 0. \end{cases}$$

5.6.4 Comparison of the Green Functions

There is a striking difference between the time dependent Green functions derived in the last Sections. In three dimensions, the effect of an impulse after a time $t - t_0$ is found concentrated on a sphere of radius $c(t - t_0)$ whose centre is the source point. The effect of the impulse can therefore only be experienced by an observer at one location over an infinitely short period of time. After the pulse has passed by an observer, the disturbance ceases. In two dimensions, the disturbance is spread over the entire plane $\mid \mathbf{s} - \mathbf{s}_0 \mid$. At $\mid \mathbf{s} - \mathbf{s}_0 \mid = c(t - t_0)$ there is a singularity which defines the position of the two dimensional wavefront as it propagates outwards from the source point at $\mathbf{s}_0$. For $\mid \mathbf{s} - \mathbf{s}_0 \mid < c(t - t_0)$ the Green function is still finite and therefore, unlike the three-dimensional case, the disturbance is still felt after the wavefront has passed by the observer. In one dimension, the disturbance is uniformly distributed over all points of

observation through which the wavefront has passed, since for all values of $\mid x - x_0 \mid$ and $c(t - t_0)$, the Green function is either $c/4$ or $-c/4$. This is illustrated in Figure 5.6.

Compared with the Green function in one and two dimensions, the three dimensional Green function possesses the strongest singularity. Compared to the delta function, the singularity of the two-dimensional Green function at $\mid \mathbf{s} - \mathbf{s}_0 \mid = c(t - t_0)$ is very weak. In one dimension, the time dependent Green function is not singular but discontinuous when $\mid x - x_0 \mid = c(t - t_0)$. An interesting example of a 3D time-dependent Green function is shown in Figure 5.4 (right). The almost spherical 'shell' is a picture of

$$G(\mathbf{r} \mid \mathbf{r}_0, t \mid t_0) = \frac{1}{4\pi \mid \mathbf{r} - \mathbf{r}_0 \mid} \delta(t - t_0 + \mid \mathbf{r} - \mathbf{r}_0 \mid /c)$$

at a snap-shot in time t in the very early stages of development of the explosion.

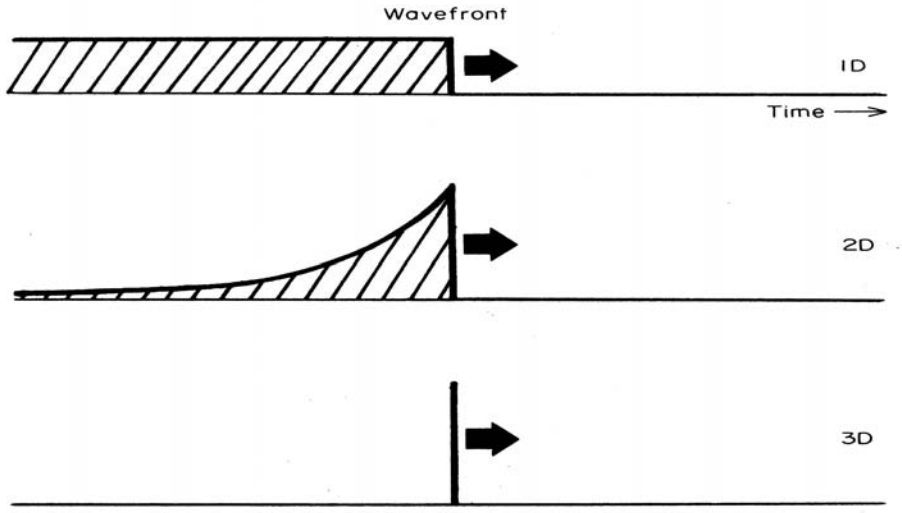

Figure 5.6: Time history of the Green function in one, two and three dimensions

5.7 Green Function Solution to Maxwell's Equation

In Chapter 4, a gauge transform, together with the Lorentz condition, was used to solve Maxwell's equations and reduce them to two independent time dependent wave equations given by

$$\nabla^2 U - \frac{1}{c^2} \frac{\partial^2 U}{\partial t^2} = -4\pi\rho$$

and

$$\nabla^2 \mathbf{A} - \frac{1}{c^2}\frac{\partial^2 \mathbf{A}}{\partial t^2} = -\frac{4\pi}{c}\mathbf{j}.$$

Having discussed the time dependent Green functions for the wave equation, we can now investigate the general solution to Maxwell's equations under the Lorentz condition. In particular, we consider the solution for the electric scalar potential U given ρ. The form of analysis is the same as used before, throughout this Chapter. Thus, solving for U, using Green's theorem (with homogeneous boundary conditions) and the conditions that u and $\partial u/\partial t$ are zero at $t = \pm\infty$ gives

$$U(\mathbf{r}_0, t_0) = \int_{-\infty}^{\infty} \int 4\pi\rho(\mathbf{r}, t) G(\mathbf{r} \mid \mathbf{r}_0, t \mid t_0) d^3\mathbf{r} dt = \int d^3\mathbf{r} \int_{-\infty}^{\infty} dt \frac{\rho(\mathbf{r}, t)}{R} \delta\left(\frac{R}{c} + t - t_0\right)$$

$$= \int d^3\mathbf{r} \frac{\rho\left(\mathbf{r}, t_0 - \frac{R}{c}\right)}{R}$$

where $R = \mid \mathbf{r} - \mathbf{r}_0 \mid$ or

$$U(\mathbf{r}_0, t_0) = \int \frac{\rho(\mathbf{r}, \tau)}{R} d^3\mathbf{r}$$

where

$$\tau = t_0 - \frac{R}{c}.$$

The solution for the Magnetic Vector Potential $\mathbf{A}$ can be found by solving for the components A_x, A_y and A_z separately. These are all scalar equations of exactly the same type and therefore have identical solutions and combine to give

$$\mathbf{A}(\mathbf{r}_0, t_0) = \int \frac{\mathbf{j}(\mathbf{r}, \tau)}{cR} d^3\mathbf{r}$$

The wavefields U and $\mathbf{A}$ are called the Retarded Potentials. The current value of U at $(\mathbf{r}_0, t_0)$ depends on ρ at earlier times $\tau = t_0 - R/c$. A change in ρ or $\mathbf{j}$ affects U and $\mathbf{A}$ (and hence $\mathbf{e}$ and $\mathbf{b}$) R/c seconds later - the change propagates outward at velocity c. This is the principle of electromagnetic wave propagation.

5.8 The Diffusion Equation

The homogeneous diffusion equation

$$\nabla^2 u(\mathbf{r}, t) = \sigma \frac{\partial}{\partial t} u(\mathbf{r}, t), \quad \sigma = \frac{1}{D}$$

where D is the 'Diffusivity' differs in many aspects from the scalar wave equation and the Green function exhibits these difference. The most important single feature is the asymmetry of the diffusion equation with respect to time.

For the wave equation, if $u(\mathbf{r},t)$ is a solution, so is $u(\mathbf{r},-t)$. However, if $u(\mathbf{r},t)$ is a solution of

$$\nabla^2 u = \sigma \frac{\partial u}{\partial t}$$

the function $u(\mathbf{r},-t)$ is not; it is a solution of the quite different equation,

$$\nabla^2 u(\mathbf{r},-t) = -\sigma \frac{\partial}{\partial t} u(\mathbf{r},-t).$$

Thus, unlike the wave equation, the diffusion equation differentiates between past and future. This is because the diffusing field u represents the behaviour of some average property of an ensemble of many particles which cannot in general go back to their original state. Thus, causality must be considered in the solution to the diffusion equation. This in turn leads to the use of the Laplace transform[3] for solving the equation with respect to t (compared to the Fourier transform used to solve the wave equation with respect to t).

As in the case of the scalar wave equation, it is possible to evaluate the Green function for the diffusion equation which satisfies homogeneous boundary conditions and the causality condition

$$G(\mathbf{r} \mid \mathbf{r}_0, t \mid t_0) = 0 \quad \text{if} \quad t < t_0.$$

This can be accomplished for one-, two- and three-dimensions simultaneously. Thus with $R = \mid \mathbf{r} - \mathbf{r}_0 \mid$ and $\tau = t - t_0$ we require the solution of the equation

$$\left(\nabla^2 - \sigma \frac{\partial}{\partial \tau}\right) G(R,\tau) = -\delta^n(R)\delta(\tau), \quad \tau > 0$$

where n is 1, 2 or 3 depending on the number of dimensions. One way of solving this equation is first to take the Laplace transform with respect to τ, then solve for G (in Laplace space) and then inverse Laplace transform the result. This requires an initial condition to be specified (the value of G at $\tau = 0$). Another way to solve this equation is to take its Fourier transform with respect to R, solve for G (in Fourier space) and then inverse Fourier transform the result. Here, we adopt the latter approach. Let

$$G(R,\tau) = \frac{1}{(2\pi)^n} \int_{-\infty}^{\infty} \widetilde{G}(\mathbf{k},\tau) \exp(i\mathbf{k}\cdot\mathbf{R}) d^n\mathbf{k}$$

and

$$\delta^n(R) = \frac{1}{(2\pi)^n} \int_{-\infty}^{\infty} \exp(i\mathbf{k}\cdot\mathbf{R}) d^n\mathbf{k}.$$

Then the equation for G reduces to

$$\sigma \frac{\partial \widetilde{G}}{\partial \tau} + k^2 \widetilde{G} = \delta(\tau)$$

[3] see Blackledge J M, Digital Signal Processing, Horwood, 2003.

which has the solution

$$\widetilde{G} = \frac{1}{\sigma}\exp(-k^2\tau/\sigma)H(\tau)$$

where $H(\tau)$ is the step function

$$H(\tau) = \begin{cases} 1, & \tau > 0; \\ 0, & \tau < 0. \end{cases}$$

Hence, the Green functions are given by

$$G(R,\tau) = \frac{1}{\sigma(2\pi)^n}H(\tau)\int_{-\infty}^{\infty}\exp(i\mathbf{k}\cdot\mathbf{R})\exp(-k^2\tau/\sigma)d^n\mathbf{k}$$

$$= \frac{1}{\sigma(2\pi)^n}H(\tau)\left(\int_{-\infty}^{\infty}\exp(ik_xR_x)\exp(-k_x^2\tau/\sigma)dk_x\right)...$$

By rearranging the exponent in the integral, it becomes possible to evaluate each integral exactly. Thus, with

$$ik_xR_x - k_x^2\frac{\tau}{\sigma} = -\left(k_x\sqrt{\frac{\tau}{\sigma}} - i\frac{R_x}{2}\sqrt{\frac{\sigma}{\tau}}\right)^2 - \left(\frac{\sigma R_x^2}{4\tau}\right) = -\frac{\tau}{\sigma}\xi^2 - \left(\frac{\sigma R_x^2}{4\tau}\right)$$

where

$$\xi = k_x - i\frac{\sigma R_x}{2\tau}.$$

the integral over k_x becomes

$$\int_{-\infty}^{\infty}\exp\left[-\left(\frac{\tau}{\sigma}\xi^2\right) - \left(\frac{\sigma R_x}{4\tau}\right)\right]d\xi = e^{-(\sigma R_x^2/4\tau)}\int_{-\infty}^{\infty}e^{-(\tau\xi^2/\sigma)}d\xi$$

$$= \sqrt{\frac{\pi\sigma}{\tau}}\exp\left[-\left(\frac{\sigma R_x^2}{4\tau}\right)\right]$$

with similar results for the integrals over k_y and k_z giving the result

$$G(R,\tau) = \frac{1}{\sigma}\left(\frac{\sigma}{4\pi\tau}\right)^{\frac{n}{2}}\exp\left[-\left(\frac{\sigma R^2}{4\tau}\right)\right]H(\tau).$$

The function G satisfies an important property which is valid for all n:

$$\int_{-\infty}^{\infty}g(R,\tau)d^n\mathbf{r} = \frac{1}{\sigma}; \quad \tau > 0.$$

This is the expression for the conservation of the Green function associated with the diffusion equation. For example, if we consider the diffusion of heat, then if at a time t_0 and at a point in space $\mathbf{r}_0$ a source of heat is introduced, then the heat diffuses out through the medium characterized by σ in such a way that the total flux of heat energy is unchanged.

5.9 Green Function Solution to the Diffusion Equation

Working in three dimensions, let us consider the general solution to the equation

$$\left(\nabla^2 - \sigma\frac{\partial}{\partial t}\right) u(\mathbf{r},t) = -f(\mathbf{r},t)$$

where f is a source of compact support ($\mathbf{r} \in V$) and define the Green function as the solution to the equation

$$\left(\nabla^2 - \sigma\frac{\partial}{\partial t}\right) G(\mathbf{r} \mid \mathbf{r}_0, t \mid t_0) = -\delta^3(\mathbf{r}-\mathbf{r}_0)\delta(t-t_0).$$

It is convenient to first take the Laplace transform of these equations with respect to $\tau = t - t_0$ to obtain

$$\nabla^2\bar{u} - \sigma[-u_0 + p\bar{u}] = -\bar{f}$$

and

$$\nabla^2\bar{G} + \sigma[-G_0 + p\bar{G}] = -\delta^3$$

where

$$\bar{u}(\mathbf{r},p) = \int_0^\infty u(\mathbf{r} \mid \mathbf{r}_0,\tau)\exp(-p\tau)d\tau,$$

$$\bar{G}(\mathbf{r},p) = \int_0^\infty G(\mathbf{r} \mid \mathbf{r}_0,\tau)\exp(-p\tau)d\tau,$$

$$\bar{f}(\mathbf{r},p) = \int_0^\infty f(\mathbf{r},\tau)\exp(-p\tau)d\tau$$

$$u_0 \equiv u(\mathbf{r},\tau=0) \quad \text{and} \quad G_0 \equiv G(\mathbf{r} \mid \mathbf{r}_0,\tau=0) = 0.$$

Pre-multiplying the equation for $\bar{u}$ by $\bar{G}$ and the equation for $\bar{G}$ by $\bar{u}$, subtracting the two results and integrating over V we obtain

$$\int_V (\bar{G}\nabla^2\bar{u} - \bar{u}\nabla^2\bar{G})d^3\mathbf{r} + \sigma\int_V u_0\bar{G}d^3\mathbf{r} = -\int_V \bar{f}\bar{G}d^3\mathbf{r} + \bar{u}(\mathbf{r}_0,\tau).$$

Using Green's theorem and rearranging the result gives

$$\bar{u}(\mathbf{r}_0,\tau) = \int_V \bar{f}(\mathbf{r},p)\bar{G}(\mathbf{r} \mid \mathbf{r}_0,p)d^3\mathbf{r} + \sigma\int_V u_0(\mathbf{r})\bar{G}(\mathbf{r} \mid \mathbf{r},p)d^3\mathbf{r} + \oint_S (\bar{g}\nabla\bar{u} - \bar{u}\nabla\bar{g})\cdot\hat{\mathbf{n}}d^2\mathbf{r}.$$

Finally, taking the inverse Laplace transform and using the convolution theorem for Laplace transforms, we can write

$$u(\mathbf{r}_0,\tau) = \int_0^\tau\int_V f(\mathbf{r},\tau')G(\mathbf{r} \mid \mathbf{r}_0,\tau-\tau')d^3\mathbf{r}d\tau' + \sigma\int_V u_0(\mathbf{r})G(\mathbf{r} \mid \mathbf{r}_0,\tau)d^3\mathbf{r}$$

$$+\int_0^\tau \oint_S [G(\mathbf{r} \mid \mathbf{r}_0, \tau')\nabla u(\mathbf{r}, \tau - \tau') - u(\mathbf{r}, \tau')\nabla G(\mathbf{r} \mid \mathbf{r}_0, \tau - \tau')] \cdot \hat{\mathbf{n}} d^2\mathbf{r} d\tau'.$$

The first two terms are convolutions of the Green function with the source function and the initial field $u(\mathbf{r}, \tau = 0)$, respectively.

As a simple case study which helps to investigate this solution further, suppose we consider the source term to be zero and the volume of interest is the infinite domain, so that the surface integral is zero. Then we have

$$u(\mathbf{r}_0, \tau) = \sigma \int_V u_0(\mathbf{r}) G(\mathbf{r} \mid \mathbf{r}_0, \tau) d^3\mathbf{r}.$$

In one dimension, this reduces to

$$u(x_0, \tau) = \sqrt{\frac{\sigma}{4\pi\tau}} \int_{-\infty}^{\infty} \exp\left[-\frac{\sigma(x_0 - x)^2}{4\tau}\right] u_0(x)\, dx, \quad t > 0.$$

Thus we see that the field u at a time $\tau > 0$ is given by the convolution of the field at time $t = 0$ with the Gaussian function

$$\sqrt{\frac{\sigma}{4\pi t}} \exp\left(-\frac{\sigma x^2}{4t}\right).$$

5.10 The Laplace and Poisson Equations

The Laplace and Poisson equations (in one- or two-dimensions) are given by

$$\nabla^2 u = 0$$

and

$$\nabla^2 u = -f$$

respectively. Let us consider the Poisson equation first. The general approach is identical to that used to derive a solution to the inhomogeneous wave equation. Thus, working in three dimensions and defining the Green function to be the solution of

$$\nabla^2 g(\mathbf{r} \mid \mathbf{r}_0) = -\delta^3(\mathbf{r} - \mathbf{r}_0)$$

from Poisson's equation, we obtain the following result

$$u = \oint_S (g\nabla u - u\nabla g) \cdot \hat{\mathbf{n}} d^2\mathbf{r} + \int_V g f d^3\mathbf{r}$$

where we have used Green's theorem to obtain the surface integral on the right hand side. The problem now is to find the Green function for this problem. Clearly, since the solution to the equation

$$(\nabla^2 + k^2)g = -\delta^3(\mathbf{r} - \mathbf{r}_0)$$

is

$$g(\mathbf{r} \mid \mathbf{r}_0, k) = \frac{1}{4\pi \mid \mathbf{r} - \mathbf{r}_0 \mid} \exp(ik \mid \mathbf{r} - \mathbf{r}_0 \mid)$$

we should expect the Green function for the three-dimensional Poisson equation (and the Laplace equation) to be of the form

$$g(\mathbf{r} \mid \mathbf{r}_0) = \frac{1}{4\pi \mid \mathbf{r} - \mathbf{r}_0 \mid}.$$

This can be shown by taking the Fourier transform of the equation for g which gives

$$k^2 G(k) = 1$$

where

$$G(k) = \int g(R) \exp(i\mathbf{k} \cdot \mathbf{R}) d^3\mathbf{R}, \quad R = \mid \mathbf{r} - \mathbf{r}_0 \mid .$$

Therefore

$$g(R) = \frac{1}{(2\pi)^3} \int \frac{\exp(i\mathbf{k} \cdot \mathbf{R})}{k^2} d^3\mathbf{k} = \frac{1}{(2\pi)^3} \int_0^{2\pi} d\phi \int_{-1}^{1} d(\cos\theta) \int_0^{\infty} dk \exp(ikR\cos\theta)$$

$$= \frac{1}{2\pi^2 R} \int_0^{\infty} \frac{\sin(kR)}{k} dk = \frac{1}{4\pi R}$$

using spherical polar coordinates and the result

$$\int_0^{\infty} \frac{\sin x}{x}\, dx = \frac{\pi}{2}.$$

Thus, we obtain the following fundamental result:

$$\nabla^2 \left(\frac{1}{4\pi R} \right) = -\delta^3(R).$$

With homogeneous boundary conditions, the solution to the Poisson equation is

$$u(\mathbf{r}_0) = \frac{1}{4\pi} \int_V \frac{f(\mathbf{r})}{\mid \mathbf{r} - \mathbf{r}_0 \mid} d^3\mathbf{r}.$$

In two dimensions the solution is of the same form, but with a Green function given by

$$g(\mathbf{r} \mid \mathbf{r}_0) = \frac{1}{2\pi} \ln \mid \mathbf{r} - \mathbf{r}_0 \mid .$$

Clearly, the general solution to Laplace's equation (in 3D) is

$$u = \oint_S (g\nabla u - u\nabla g) \cdot \hat{\mathbf{n}} d^2\mathbf{r}.$$

These solutions to the Laplace and Poisson equations are analogous to those for the homogeneous and inhomogeneous wave equations. The principle behind the method of solution is the same; what changes is the Green function.

5.11 Discussion

This Chapter has provided an introduction to the use of Green functions for solving partial differential equations in different dimensions and for time dependent and time independent problems. Moreover, the material presented has been based almost exclusively on the use of free space Green functions in which a solution is developed over the infinite domain to which boundary conditions can be applied. The focus has been on Green functions for wave equations as this is the principal basis for modelling imaging systems and image understanding.

There are a number of techniques for computing the Green function G for finite or bounded domain problems provided the geometry is simple enough. For example, we can consider

$$G(\mathbf{r} \mid \mathbf{r}_0) = g(\mathbf{r} \mid \mathbf{r}_0) + F(\mathbf{r} \mid \mathbf{r}_0)$$

where g is the free space Green function and F represents the boundary effects. F cannot have a singularity within the bounded domain and so as $r \rightarrow r_0$, $G(\mathbf{r} \mid \mathbf{r}_0) \rightarrow g(\mathbf{r} \mid \mathbf{r}_0)$. In the so called 'Imaging Method' F is determined by considering a mirror image of the source point $\mathbf{r}_0$ in the opposite side of the boundary at $\mathbf{r}_1$ say. F is then given by -$g(\mathbf{r} \mid \mathbf{r}_1)$ satisfying Dirichlet boundary conditions or $+g(\mathbf{r} \mid \mathbf{r}_1)$ satisfying Neumann boundary conditions. Application of this method for two or more boundaries leads naturally to expressions for G which involve infinite series as the effect of one boundary on another is taken into account in order to generate a complete solution on a bounded domain. Green functions are also used in certain numerical methods of solution to partial differential equations. These are the Boundary Element Methods in which a numerical solution is devised by discretizing the surface integral considered in this Chapter into surface patches, and computing the surface integral numerically.

With regard to this work, we are now in a position to consider Green function solutions to wave equations of the type

$$(\nabla^2 + k^2)\mathbf{u}(\mathbf{r}, k) = -\hat{L}\mathbf{u}(\mathbf{r}, k)$$

for a vector wavefield $\mathbf{u}$ or

$$(\nabla^2 + k^2)u(\mathbf{r}, k) = -\hat{L}u(\mathbf{r}, k)$$

for a scalar wavefield u as derived in Chapter 4. This is the basis for the material presented in Part II, starting with Chapter 6, which provides an introduction to scattering theory using the Helmholtz equation

$$(\nabla^2 + k^2)u(\mathbf{r}, k) = -k^2\gamma(\mathbf{r})u(\mathbf{r}, k)$$

where the 'scattering function' γ is of compact support (i.e. of finite spatial extent) and the Schrödinger equation

$$(\nabla^2 + k^2)u(\mathbf{r}, k) = \gamma(\mathbf{r})u(\mathbf{r}, k)$$

where γ is the 'scattering potential'.

5.12 Summary of Important Results

Time Independent Green functions for the wave equation

The time independent Green function g that is the solution to the equation

$$(\nabla^2 + k^2)g(\mathbf{r} \mid \mathbf{r}_0, k) = -\delta^n(\mathbf{r} - \mathbf{r}_0)$$

and is given by:

n=1

$$g(x \mid x_0, k) = \frac{i}{2k} \exp(ik \mid x - x_0 \mid)$$

n=2

$$g(\mathbf{r} \mid \mathbf{r}_0, k) = \frac{i}{4} H_0(k \mid \mathbf{r} - \mathbf{r}_0 \mid)$$

$$\simeq \frac{1}{\sqrt{8\pi}} \exp(i\pi/4) \frac{\exp(ik \mid \mathbf{r} - \mathbf{r}_0 \mid)}{\sqrt{k \mid \mathbf{r} - \mathbf{r}_0 \mid}}, \quad k \mid \mathbf{r} - \mathbf{r}_0 \mid >> 1$$

n=3

$$g(\mathbf{r} \mid \mathbf{r}_0, k) = \frac{1}{4\pi \mid \mathbf{r} - \mathbf{r}_0 \mid} \exp(ik \mid \mathbf{r} - \mathbf{r}_0 \mid)$$

Fresnel and Fraunhofer approximations

Fresnel approximation

$$\exp(ik \mid \mathbf{r} - \mathbf{r}_0 \mid) \simeq \exp(ikr_0) \exp(-ik\hat{\mathbf{n}}_0 \cdot \mathbf{r}) \exp(ir^2/2r_0), \quad \hat{\mathbf{n}}_0 = \mathbf{r}_0/r_0$$

Fraunhofer approximation

$$\exp(ik \mid \mathbf{r} - \mathbf{r}_0 \mid) \simeq \exp(ikr_0) \exp(-ik\hat{\mathbf{n}}_0 \cdot \mathbf{r})$$

Green's theorem

$$\int_V (g\nabla^2 u - u\nabla^2 g) d^3\mathbf{r} = \oint_S \left(g \frac{\partial u}{\partial \hat{\mathbf{n}}} - u \frac{\partial g}{\partial \hat{\mathbf{n}}} \right) d^2\mathbf{r}$$

Green function solution to the inhomogeneous wave equation

Given

$$(\nabla^2 + k^2)u(\mathbf{r}, k) = -f(\mathbf{r}), \quad \mathbf{r} \in V,$$

$$u(\mathbf{r}_0, k) = \oint_S (g\nabla u - u\nabla g) \cdot \hat{\mathbf{n}} d^2\mathbf{r} + \int_V f(r) g(\mathbf{r} \mid \mathbf{r}_0, k) d^3\mathbf{r}$$

Homogeneous Dirichlet condition

$u(\mathbf{r}) = 0$ on the surface defined by V

Homogeneous Neumann condition

$\nabla u(\mathbf{r}) = 0$ on the surface defined by V

Homogeneous conditions

Both $u(\mathbf{r})$ and $\nabla(\mathbf{r})$ are zero on the surface defined by V.

Reciprocity theorem

$$g(\mathbf{r}_2 \mid \mathbf{r}_1, k) = g(\mathbf{r}_1 \mid \mathbf{r}_2, k)$$

Intensity function for a coherent source function f

$$I(\mathbf{r}) = \mid g(\mid \mathbf{r} \mid, k) \otimes f(\mathbf{r}) \mid^2$$

Intensity function for an incoherent source function f

$$I(\mathbf{r}) = \mid g(\mid \mathbf{r} \mid, k) \mid^2 \otimes \mid f(\mathbf{r}) \mid^2$$

Green functions for the time dependent wave equation

The function G that is the solution to the equation

$$\left(\nabla^2 + \frac{1}{c^2}\frac{\partial^2}{\partial t^2}\right) G(\mathbf{r} \mid \mathbf{r}_0, t \mid t_0) = -\delta^n(\mathbf{r} - r_0)\delta(t - t_0)$$

and given by:

n=1

$$G(x \mid x_0, t \mid t_0) = \frac{c}{4}\,\mathrm{sgn}[t - t_0 + \mid x - x_0 \mid /c]$$

n=2

$$G(\mathbf{r} \mid \mathbf{r}_0, t \mid t_0) = \begin{cases} \frac{1}{4\pi}\frac{1}{\sqrt{|t-t_0|^2 - |\mathbf{r}-\mathbf{r}_0|^2}}, & \mid t - t_0 \mid > \mid \mathbf{r} - \mathbf{r}_0 \mid; \\ 0, & \mid t - t_0 \mid < \mid \mathbf{r} - \mathbf{r}_0 \mid . \end{cases}$$

n=3

$$G(\mathbf{r} \mid \mathbf{r}_0, t \mid t_0) = \frac{1}{4\pi \mid \mathbf{r} - \mathbf{r}_0 \mid}\delta(t - t_0 + \mid \mathbf{r} - \mathbf{r}_0 \mid /c)$$

Green function for the diffusion equation

For $n = 1$ (1D), $n = 2$ (2D) and $n = 3$ (3D),

$$G(\mid \mathbf{r}-\mathbf{r} \mid, \mid t-t_0 \mid) = \frac{1}{\sigma}\left(\frac{\sigma}{4\pi \mid t-t_0 \mid}\right)^{\frac{n}{2}} \exp\left[-\left(\frac{\sigma \mid \mathbf{r}-\mathbf{r}_0 \mid^2}{4 \mid t-t_0 \mid}\right)\right] H(\mid t-t_0 \mid).$$

Green function for the Laplace and Poisson equation

n=2

$$g(\mathbf{r} \mid \mathbf{r}_0) = \frac{1}{2\pi} \ln \mid \mathbf{r}-\mathbf{r}_0 \mid$$

n=3

$$g(\mathbf{r} \mid \mathbf{r}_0) = \frac{1}{4\pi \mid \mathbf{r}-\mathbf{r}_0 \mid}$$

Fundamental result

The solution to an equation of arbitrary dimensions and of the type

$$\hat{D}u = f$$

where $\hat{D}$ is a linear differential operator is, subject to homogeneous boundary conditions given by

$$u = g \otimes f$$

where g is the Green function.

5.13 Further Reading

- Morse P M and Feshbach H, *Methods of Theoretical Physics*, 1953, McGraw-Hill.
- Roach G F, *Green's Functions (Introductory Theory with Applications)*, Van Nostrand Reihold, 1970.
- Ferrers N M (Ed.), *Mathematical Papers of George Green*, Chelsea, 1970.
- Green H G, *A Biography of George Green*, in *Studies and Essays in the History of Science and Learning*, Montagu, M F A (Ed.), Arno Press, 1975.
- Economou E N, *Green's Functions in Quantum Physics*, Springer-Verlag, 1979.
- Stakgold I, *Green's Functions and Boundary Value Problems*, Wiley, 1979.
- Cannell D M, *George Green: Mathematician and Physicist 1793-1841: The Background to His Life and Work*, Society for Industrial and Applied Mathematics, Philadelphia, 2001.

Problems: Part I

I.1 Obtain the gradients of the following scalar fields: $x^3 + y^3 + z^3$, r^n, $\mathbf{a} \cdot \mathbf{r}$ (where $\mathbf{a}$ is a constant vector) and $\mathbf{r} \cdot \nabla(x + y + z)$.

I.2 Obtain the divergence of the following vector fields: $\mathbf{f}$ = constant vector, $\mathbf{r}$, $xyz(\hat{\mathbf{x}} + \hat{\mathbf{y}} + \hat{\mathbf{z}})$ and $\mathbf{r} \times [\hat{\mathbf{x}} f(x) + \hat{\mathbf{y}} g(y) + \hat{\mathbf{z}} h(z)]$.

I.3 Show that

$$\nabla^2(r^n) = n(n+1)r^{n-2}.$$

I.4 Show that

$$\nabla \times (\mathbf{A} + \mathbf{B}) = \nabla \cdot \mathbf{A} + \nabla \cdot \mathbf{B}$$

and

$$\nabla \cdot (u\mathbf{A}) = \nabla u \cdot \mathbf{A} + u \nabla \cdot \mathbf{A}$$

where $\mathbf{A}$ and $\mathbf{B}$ are vector fields and u is a sclar field.

I.5 Obtain the curls of the following vector fields: $\hat{\mathbf{x}} x$, $\hat{\mathbf{y}} y$, $\hat{\mathbf{x}} x \cos z + \hat{\mathbf{y}} y \log x + \hat{\mathbf{z}} z^2$ and $\mathbf{r} f(r)$.

I.6 Show that

$$\nabla \times (\mathbf{A} + \mathbf{B}) = \nabla \times \mathbf{A} + \nabla \times \mathbf{B}$$

and

$$\nabla \times (u\mathbf{f}) = u \nabla \times \mathbf{f} + (\nabla u) \times \mathbf{f}.$$

I.7 Show that

$$\nabla \times (\nabla u) = 0 \quad \text{and} \quad \nabla \cdot (\nabla \times \mathbf{f}) = 0.$$

I.8 Show that

$$\nabla \times \nabla \times \mathbf{f} = \nabla(\nabla \cdot \mathbf{f}) - \nabla^2 \mathbf{f}.$$

I.9 Given that $\mathbf{F} = \nabla u, \quad \nabla \cdot \mathbf{F} = 0$ and V is the volume enclosed by a surface S, use the divergence theorem to show that

$$\int_V F^2 d^3\mathbf{r} = \oint_S u\mathbf{F} \cdot \mathbf{n} d^2\mathbf{r}.$$

I.10 Use the divergence theorem to prove Green's first and second identities.

I.11 Show that

$$\nabla f(\mathbf{r}) \Longleftrightarrow i\mathbf{k}F(\mathbf{k})$$

and that

$$\nabla^2 f(\mathbf{r}) \Longleftrightarrow -k^2 F(\mathbf{k}).$$

I.12 Derive the 2D Fourier transform of the box-function

$$f(x,y) = \begin{cases} 1, & \mid x \mid \leq \frac{a}{2} \quad \text{and} \mid y \mid \leq \frac{b}{2}; \\ 0, & \text{otherwise.} \end{cases}$$

I.13 Derive the 2D Fourier transform of the Gaussian function

$$f(x,y) = \exp(-ar^2) \quad \text{where} \quad r^2 = x^2 + y^2,$$

noting that

$$\int_{-\infty}^{\infty} \exp(-x^2) dx = \sqrt{\pi}.$$

I.14 Prove the addition theorem, the similarity and the shift theorem for a 2D function $f(\mathbf{r})$.

I.15 Prove Parseval's theorem for a 2D function $f(\mathbf{r})$ and hence show that

$$\int_{-\infty}^{\infty} \mid f(\mathbf{r}) \mid^2 d^2\mathbf{r} = \frac{1}{(2\pi)^2)} \int_{-\infty}^{\infty} \mid F(\mathbf{k}) \mid^2 d^2\mathbf{k}.$$

(Rayleigh's theorem - also known as the energy theorem.)

I.16 Prove the convolution theorem, i.e.

$$f(\mathbf{r}) \otimes \otimes g(\mathbf{r}) \Longleftrightarrow F(\mathbf{k})G(\mathbf{k}).$$

I.17 Prove the product theorem, i.e.

$$f(\mathbf{r})g(\mathbf{r}) \Longleftrightarrow \frac{1}{(2\pi)^2} F(\mathbf{k}) \otimes \otimes G(\mathbf{k}).$$

I.18 Prove the correlation theorem, i.e.

$$f(\mathbf{r}) \odot \odot g(\mathbf{r}) \Longleftrightarrow F^*(\mathbf{k})G(\mathbf{k}).$$

I.19 Show that convolution is commutative, associative and distributive.

I.20 Prove that

$$\nabla(f \otimes \otimes g) = f \otimes \otimes \nabla g = g \otimes \otimes \nabla f$$

and that

$$\nabla^2(f \otimes \otimes g) = f \otimes \otimes \nabla^2 g = g \otimes \otimes \nabla^2 f.$$

In the questions that follow, the functions required should be void functions written in ANSI C. They should be compiled, tested and then added to a digital image processing object library. In each case, a simple I/O test procedure should be written, I/O being studied in terms of a digital image. Each function should be self-contained within the context of the algorithm to be coded. In each case, n (which is of type integer) is the size of the image (i.e. $n \times n$) which can be set to an upper limit of 512 pixels. I/O and display utilities are provided in Appendix D for development under a *unix/linux* operating environemnt with X-windows.

I.21 Write a function to compute the 2D FIR (convolution) filter of an image using a square window and zero padding.

```
void FIRCON(float **f, float **p, foat **s, int n, int w)
```

where f is the input image, p is the FIR (convolution) filter, s is the output and w is the window size.

I.22 Write a function to compute the 2D FIR (correlation) filter of an image using a square window and zero padding.

```
void FIRCOR(float **f, float **p, float **s, int n, int w)
```

where f is the input image, p is the FIR (correlation) filter, s is the output and w is the window size.

I.23 Test the FIR filters above by applying the following FIR filters to a test image.

1. $\frac{1}{9}\begin{pmatrix} 1 & 1 & 1 \\ 1 & 1 & 1 \\ 1 & 1 & 1 \end{pmatrix}$ 2. $\begin{pmatrix} 0 & 0 & 0 \\ -1 & 0 & 1 \\ 0 & 0 & 0 \end{pmatrix}$ 3. $\begin{pmatrix} 0 & -1 & 0 \\ 0 & 0 & 0 \\ 0 & 1 & 0 \end{pmatrix}$

4. $\begin{pmatrix} 0 & 1 & 0 \\ 1 & -4 & 1 \\ 0 & 1 & 0 \end{pmatrix}$ 5. $\begin{pmatrix} 0 & -1 & 0 \\ -1 & 5 & -1 \\ 0 & -1 & 0 \end{pmatrix}$

Display the output and interpret the results.

I.24 Write a function to compute an elliptical disc with given coordinates (in the image plane), major and minor axes and grey level.

```
void ELLIPSE(float **s,int nx,int ny,int maj,int min,int l,int n)
```

where s is the output, nx and ny are the x,y coordinates (in pixels) for the centre of the ellipse, maj and min are the major and minor axes and l is the gray level (amplitude).

I.25 Write a function to compute a solid rectangle with given coordinates (in the image plane), size and grey level.

```
void RECT(float **s, int nx, int ny, int lx, int ly, int l, int n)
```

where s is the output, nx and ny are the x,y coordinates (in pixels) for the centre of the rectangle, lx and ly are the length of sides in x and y direction respectively (in pixels) and l is the grey level (amplitude).

I.26 Write a function to compute a Gaussian point spread function of arbitrary width.

```
void GPSF(float **s, int n, int w)
```

where s is the output and w is the half width of function at $1/e$.

I.27 Write a function to compute the amplitude spectrum of an image using function *FFT1D* as given in Chapter 3.

```
void AMPSPEC(float **s, float **a, int n)
```

where s is the input image, a is the amplitude spectrum (output).

I.28 Write a function to compute the power spectrum of an image which provides an option for output on a logarithmic scale.

```
void POWSPEC(float **s, float **p, int n int opt)
```

where s is the image (input) and p is the power spectrum (output) and, if opt=1, then a logarithmic scale is used.

I.29 Write a main program to generate a complex of ellipses, circles, rectangles or squares with different grey levels using functions ELLIPSE and RECT. Compute the discrete amplitude spectrum of an elliptical disc, a rectangle (centered in the image plane) and a Gaussian point spread function using FFT2D. Study the effect of changing the width of these functions using a logarithmic scale to display the power spectrum.

I.30 Write a function to sinc interpolate an image from 2^k square to 2^l using FFT2D where $l > k$ and k and l are integers.

```
void SINCINT(float **x, int n, float **y, int m)
```

where x is the input, n is the size of the input, y is the output and m is the size of the output.

Use this function to interpolate an image from 128 square to 256 and 512 square.

I.31 By means of Laplace transforms, find the general Green function solution to the equation

$$\left(\frac{\partial^2}{\partial x^2} + k^2\right) u(x,k) = -f(x)$$

where k is a constant, the solution being required in the positive half space $x \in [0, \infty)$.

I.32 Find the Green function solution to the equation

$$\left(\frac{\partial^2}{\partial x^2} + k^2\right) u(x,k) = 0, \quad x \in [0, L],$$

subject to the boundary conditions $u(0, l) = 0$ and $u(L, k) = 0$ by first finding a Green function solution for the infinite domain and then adding a solution of the homogeneous equation to fit the boundary conditions.

I.33 By taking the Laplace transform with respect to x of the equation

$$\left(\frac{\partial^2}{\partial x^2} + k^2\right) g(x \mid x_0, k) = -\delta(x - x_0)$$

show that the Green function g on the interval $[0, 1]$ with the boundary conditions

$$g(0 \mid x_0, k) = 0 \quad \text{and} \quad \left[\frac{\partial g(x \mid x_0, k)}{\partial x}\right]_{x=0} = g(1 \mid x_0, k)$$

is

$$g(x \mid x_0, k) = \frac{\sin(kx)\sin[k(1-x_0)]}{k(\sin k - k)} - \frac{\sin[k(x-x_0)]}{k} H(x-x_0).$$

where $H(x)$ is the step function.

I.34 Use Fourier transforms to show that the solution of

$$\nabla^2 g(\mathbf{r} \mid \mathbf{r}_0, k) - \lambda g(\mathbf{r} \mid \mathbf{r}_0, k) = -\delta^3(\mathbf{r} - \mathbf{r}_0)$$

is

$$g(\mathbf{r} \mid \mathbf{r}_0, k) = \frac{\exp(-\sqrt{\lambda} \mid \mathbf{r} - \mathbf{r}_0 \mid)}{4\pi \mid \mathbf{r} - \mathbf{r}_0 \mid}.$$

I.35 Investigate the reciprocity theorem for the diffusion equation assuming homogeneous boundary conditions and, in particular, show that

$$G(\mathbf{r} \mid \mathbf{r}_0, t \mid t_0) = G(\mathbf{r}_0 \mid \mathbf{r}, -t_0 \mid -t).$$

Part II

Imaging Systems Modelling

Chapter 6

Scattering Theory

Unlike the field generated by a source, a scattered wavefield depends on both the nature of the scatterer and the type and properties of the radiation scattered by it. These properties are described by the characteristic inhomogeneous wave equations. In Chapter 4, the reader was introduced to the field equations and wave equations that form a basis for modelling electromagnetic and acoustic imaging systems. For scalar wavefields u, it was shown that we can derive inhomogeneous wave equations of the form

$$(\nabla^2 + k^2)u = -\hat{L}u$$

or

$$(\nabla^2 + k^2)\nabla^2 u = -\hat{L}u$$

or for vector fields $\mathbf{u}$ of the form

$$(\nabla^2 + k^2)\mathbf{u} = -\hat{L}\mathbf{u}.$$

For example, a non-viscous linear isotropic acoustic scatterer with variations in the compressibility γ_κ and density γ_ρ is characterized by

$$(\nabla^2 + k^2)P = -k^2\gamma_\kappa P + \nabla \cdot (\gamma_\rho \nabla P)$$

where P is the isotropic pressure. For a non-conductive linear isotropic electromagnetic scatterer with variations in the permittivity γ_ϵ and permeability γ_μ,

$$(\nabla^2 + k^2)\widetilde{\mathbf{E}} = -\hat{L}\widetilde{\mathbf{E}}$$

with

$$\hat{L}\widetilde{\mathbf{E}} = k^2\gamma_\epsilon\widetilde{\mathbf{E}} + \nabla(\widetilde{\mathbf{E}} \cdot \nabla \ln\epsilon) + \nabla \times (\gamma_\mu \nabla \times \widetilde{\mathbf{E}}).$$

Chapter 5 has introduced the Green function for operators of the form $(\nabla^2 + k^2)$ and considered the Green function solution for inhomogeneous wave equations of the form

$$(\nabla^2 + k^2)u = -f.$$

In this Chapter, we explore the use of the Green function for solving inhomogeneous wave equations of the type

$$(\nabla^2 + k^2)u = -k^2\gamma u$$

which is known as the inhomogeneous Helmholtz equation and

$$(\nabla^2 + k^2)u = \gamma u$$

which is the Schrödinger equation. These problems are related to volume scattering when $\gamma(\mathbf{r})$ is of compact support (i.e. $\mathbf{r} \in V$) and potential scattering theory when γ as given in Schrödinger's equation is a potential associated with the charge radiated by an elementary particle for example. We also study the solutions to the homogeneous Helmholtz equation

$$(\nabla^2 + k^2)u = 0$$

where u and ∇u are defined on a boundary defining a surface which generates surface scattering. The homogeneous and inhomogeneous Helmholtz equations provide the basis for developing a scattering theory that is of value in imaging science. We can then investigate scattering models that are based on physical models (inhomogeneous wave equations) that are more complete (i.e. models that describe a greater number of physical effects) when the right hand side of the wave equations considered here is of the form $-\hat{L}u$.

Much of the original work on scattering theory began in the 1930s and has been the product of mathematicians and physicists working on problems of theoretical physics including quantum mechanics and high energy nuclear physics, where the scattering of particles and the interpretation of their 'images' (particle tracking devices) has been fundamental to investigating the structure of matter.

6.1 The Schrödinger and Helmholtz Equations

The inhomogeneous Helmholtz and the Schrödinger equations have been studied for many years and have a wide range of applications in solid state physics, quantum mechanics, electromagnetic and acoustic wave propagation and scattering. In quantum mechanics, elementary particles of matter behave like waves called De Broglie or matter waves. The mechanics becomes that of wave motion and wave functions are used to describe the behaviour of quantum systems. If $\gamma(r)$ is taken to be an atomic (or nuclear) potential which is an elastic scatterer and the De Broglie waves describe non-relativistic particles then the (time independent) partial differential equation that describes this (scattering) effect is

$$(\nabla^2 + k^2)u(\mathbf{r}, k) = \gamma(\mathbf{r})u(\mathbf{r}, k)$$

where k is the wavenumber and u is the scattered field. This equation is known as the Schrödinger equation after the Austrian physicist Erwin Schrödinger who derived it in the 1920s. Comparing this equation with the partial differential equations derived in Chapter 4, it is clear that the equation for a De Broglie wavefield is produced by replacing the source function f with $-\gamma u$.

6.1.1 The Schrödinger Equation

The Schrödinger equation can be formulated using the equation

$$E = \frac{p^2}{2m} + E_p(\mathbf{r})$$

which states that the total energy E of a particle is the sum of the kinetic energy $p^2/2m$ plus the potential energy denoted by E_p and is taken to be a function of space. Here, p is the momentum and m is the mass of a fundamental particle. The basic postulates of quantum mechanics (first introduced by Max Planck in 1901 and De Broglie in 1924, respectively) are that

$$E = \hbar\omega \quad \text{and} \quad \mathbf{p} = \hbar\mathbf{k}$$

where

$$|\ \mathbf{p}\ | \equiv p, \quad |\ \mathbf{k}\ | \equiv k, \quad \text{and} \quad \hbar = \frac{h}{2\pi}.$$

Here $h = 6.6261 \times 10^{-34}$Js is Planck's constant. Now,

$$\frac{E}{p} = \frac{\omega}{k} = c$$

where c is the velocity of a wave and since we can write

$$p = \sqrt{2m(E - E_p)}$$

then

$$c^2 = \frac{E^2}{2m(E - E_p)}$$

and the wave equation

$$\left(\nabla^2 - \frac{1}{c^2}\frac{\partial^2}{\partial t^2}\right) U(\mathbf{r}, t) = 0$$

becomes

$$\left[\nabla^2 - \frac{2m(E - E_p)}{E^2}\frac{\partial^2}{\partial t^2}\right] U(\mathbf{r}, t) = 0.$$

With $U(\mathbf{r}, t) = u(\mathbf{r}, \omega)\exp(i\omega t)$, we can write

$$\left(\nabla^2 + \frac{2m(E - E_p)}{E^2}\omega^2\right) u(\mathbf{r}, k) = \left(\nabla^2 + \frac{2m(E - E_p)}{\hbar^2\omega^2}\omega^2\right) u(\mathbf{r}, k) = 0$$

or

$$(\nabla^2 + k^2)u(\mathbf{r}, k) = \gamma(\mathbf{r})u(\mathbf{r}, k)$$

where

$$k = \sqrt{\frac{2mE}{\hbar^2}} \quad \text{and} \quad \gamma(\mathbf{r}) = \frac{2m}{\hbar^2}E_p(\mathbf{r}).$$

Another approach is by way of introducing wave operators for the energy and the momentum given by

$$i\hbar\frac{\partial}{\partial t} \quad \text{and} \quad i\hbar\nabla$$

respectively. The energy equation

$$E = \frac{p^2}{2m} + E_p(\mathbf{r}),$$

which can be written as

$$EU(\mathbf{r},t) = \frac{p^2}{2m}U(\mathbf{r},t) + E_p(\mathbf{r})U(\mathbf{r},t)$$

then becomes

$$i\hbar\frac{\partial}{\partial t}U(\mathbf{r},t) = -\frac{\hbar^2}{2m}\nabla^2 U(\mathbf{r},t) + E_p U(\mathbf{r},t).$$

With $U(\mathbf{r},t) = u(\mathbf{r},\omega)\exp(-i\omega t)$, we then have

$$\hbar\omega u(\mathbf{r},\omega) = Eu(\mathbf{r},\omega) = -\frac{\hbar^2}{2m}\nabla^2 u(\mathbf{r},\omega) + E_p u(\mathbf{r},\omega)$$

or

$$\left(\nabla^2 + \frac{2m(E-E_p)}{\hbar^2}\right)u(\mathbf{r},k) = 0$$

which can be written in the form

$$(\nabla^2 + k^2)u(\mathbf{r},k) = \gamma(\mathbf{r})u(\mathbf{r},k)$$

as before. The wavefield u is a De Broglie or matter wave as it describes the behaviour of matter on the atomic scale. However, only the intensity $\mid u \mid^2$ is a measurable quantity. It can be interpreted in terms of the probability density function associated with the position of a particle in space. The probability of finding a particle described by the wave function u in the finite volume element $d^3\mathbf{r}$ around a point at $\mathbf{r}$ is $\mid u(\mathbf{r},k) \mid^2 d^3\mathbf{r}$. The probability of finding the particle within a finite volume V is then given by

$$\int\limits_V \mid u(\mathbf{r},k) \mid^2 d^3\mathbf{r}.$$

Since the particle must always be somewhere in space so, in extending the integral over all space, the probability becomes a certainty, i.e.

$$\int\limits_{-\infty}^{\infty} \mid u(\mathbf{r},k) \mid^2 d^3\mathbf{r} = 1$$

which gives the *normalization* condition. The postulates of quantum mechanics (i.e. $E = \hbar\omega$ and $\mathbf{p} = \hbar\mathbf{k}$) together with the sampling theorem discussed in

Part I, provide a fundamental limit to the ultimate precision with which we can (simultaneously) know the position of a particle and the component of its momentum. The sampling theorem states that

$$\Delta x \leq \frac{\pi}{K}$$

where K is the bandwidth of the analogue signal and Δx is the sampling interval. Let Δk denote the total bandwidth of the spectrum so that $\Delta k = 2K$, then the sampling theorem becomes

$$\Delta x \Delta k \leq 2\pi$$

Now, since $p = \hbar k$ and $p = E/c$ we have

$$\Delta x \Delta p \leq h \quad \text{and} \quad \Delta E \Delta t \leq h$$

which is Heisenberg's uncertainty principle. Unlike the Helmholtz equation that can be derived from Maxwell's equations for example, the Schrödinger cannot be derived in the same way. The equation is a direct consequence of the postulates $E = \hbar\omega$ and $\mathbf{p} = \hbar\mathbf{k}$ which in themselves can be justified experimentally. The validity of results that the Schrödinger equation predicts and which can be confirmed experimentally are ultimately the only justification for this equation. Thus, the Schrödinger equation is one of the most intriguing equations of physics in that it cannot be derived and its solution cannot be measured directly. Yet, to-date, it provides one of the most accurate models for characterizing the nature of matter. The success of quantum mechanics, which ranks as one of the greatest intellectual achievements of the Twentieth Century, points to the fact that matter, and physics in general, is best interpreted not in terms of particles but in terms of waves and the interaction of waves with waves and the scattering of waves by waves (e.g. electromagnetic waves scattering from matter waves, such as the reflection of light from material objects) over a broad frequency spectrum. Thus, for example (albeit a rather important one), instead of visualising of an electron as a particle with a negative charge that 'radiates' an electric field and is attracted to particles with a positive charge (which also 'radiate' an electric field), we should contemplate an electron in terms of a wave which is 'attracted' by the 'need' (through the principle of least energy) of becoming an eigenfunction (a standing wave with lower energy than a free wave) whose properties are determined by the functional form of the potential energy associated with any other physical entity such the atomic nucleus. Then, an electric field is, in effect, the field associated with the propensity for a free wavefield to become a standing wavefield and a magnetic field is a measure of the rate of change over which this propensity is satisfied. In this context, Schrödinger's equation provides the basis for modelling the atomic and molecular structure of matter in terms of discrete energy levels (eigenvalues) obtained when E_p is a potential well or for modelling the nuclear structure of matter. This includes, for example, the process of radioactive decay by the transmission of a wave through a potential barrier (the atomic nucleus). Clearly, the functional form of E_p (together with associated boundary

conditions) determines the nature and the characteristics of the solution for u. This includes interesting cases such as when $E_p = \mid U \mid^2$ and the (time-dependent) Schrödinger equation has the nonlinear form

$$\frac{\hbar^2}{2m}\nabla^2 U(\mathbf{r},t) + i\hbar\frac{\partial}{\partial t}U(\mathbf{r},t) = \mid U(\mathbf{r},t) \mid^2 U(\mathbf{r},t).$$

6.1.2 The Helmholtz Equation

Another fundamental wave equation of particular importance in electromagnetics and acoustics is the inhomogeneous Helmholtz equation given by

$$(\nabla^2 + k^2)u(\mathbf{r},k) = -k^2\gamma(\mathbf{r})u(\mathbf{r},k)$$

where γ is an inhomogeneity which is responsible for scattering the wavefield u and is therefore sometimes referred to as a scatterer - usually considered to be of compact support. Referring to the results discussed in Chapter 4, this equation is derived from the inhomogeneous acoustic wave equation for a non-viscous medium when we can assume that γ_ρ is constant. In EM imaging, the Helmholtz equation is obtained when we can assume that the medium is non conductive (i.e. $\sigma = 0$), γ_μ is a constant and the term $\nabla(\mathbf{E}\cdot\nabla \ln\epsilon)$ is ignored.

The Helmholtz equation can be derived quite generally from the time dependent wave equation

$$\left(\nabla^2 - \frac{1}{c^2}\frac{\partial^2}{\partial t^2}\right)U(\mathbf{r},t) = 0$$

by letting

$$\frac{1}{c^2} = \frac{1}{c_0^2}(1+\gamma)$$

where γ is a dimensionless quantity and c_0 is a constant (wave speed). Note that the form of the wave equation dictates that c must be of finite value. If a wavefield (whatever the field may be) was to convey information from one point in space to another instantaneously then the second term would be zero and the 'wave equation' would be reduced to 'Laplace's equation' and the indepednent variable t would become an irrelevance! The upper limit at which any wavefield can propagate is determined by the speed of an electromagnetic wave in a perfect vacuum. However, in a more general perspective, the rationale associated with the fact that c **must** be finite (as given above) means that the influence of any physical field (whether it be an electric, magnetic, gravitational, weak or strong force field) on any measurable entity can only occur in a finite period of time and that there can be no such thing as instantaneous 'action at a distance'. This is the essential difference between the 'universe' according to Isaac Newton and the 'universe' according to Albert Einstein, a difference that, given the wave equation, points to the 'physics' of a wavefield being more fundamental than the 'physics' of the field itself. This principle should be considered in light of the fact that the one property common to all the principal field equation of physics (i.e. Einstein's equations, Maxwell's equations and

Dirac's equations), is that they describe wave phenomena (i.e. gravity wave, electromagnetic wave and matter waves respectively).

With $U(\mathbf{r},t) = u(\mathbf{r},\omega)\exp(i\omega t)$ we have

$$(\nabla^2 + k^2)u(\mathbf{r},k) = -k^2\gamma(\mathbf{r})u(\mathbf{r},k)$$

where

$$k = \frac{\omega}{c_0}.$$

We can write the Schrödinger equation in terms of the Helmholtz equation since, from the postulates of quantum mechanics, we have

$$\frac{1}{c^2} = \frac{1}{c_0^2}(1+\gamma) = \frac{2m(E-E_p)}{E^2}$$

and thus the Schrödinger equation is

$$(\nabla^2 + k^2)u(\mathbf{r},k) = -k^2\gamma(\mathbf{r})u(\mathbf{r},k)$$

with

$$\gamma(\mathbf{r}) = 2mc_0^2\frac{[E-E_p(\mathbf{r})]}{E^2} - 1.$$

Note that since γ is dimensionless, this result implies that mc_0^2 is energy (i.e. Einstein's famous energy-mass equivalence formula, where c_0 is the speed of light and m is the rest mass). Thus, for a scalar electromagnetic wavefield interacting with a non-conductive dielectric - ignoring the term $\nabla(\mathbf{E}\cdot\nabla\ln\epsilon_r)$ - the Helmholtz equation is given by (see Chapter 4)

$$(\nabla^2 + k^2)u(\mathbf{r},k) = -k^2\gamma(\mathbf{r})u(\mathbf{r},k)$$

where $\gamma = \epsilon_r - 1$. We can therefore interpret the relative permittivity ϵ_r in terms of the function

$$2mc_0^2\frac{[E-E_p(\mathbf{r})]}{E^2}$$

on an entirely phenomenological basis.

In this Chapter, we consider solutions to the inhomogeneous Helmholtz and Schrödinger equations which, for k constant, are essentially the same. We start by investigating the Green function solution to the inhomogeneous Helmholtz equation.

6.2 Solution to the Helmholtz Equation

The same Green function method as presented in Chapter 5 can be used to solve the inhomogeneous Helmholtz equation. The basic solution is (under the assumption that γ is of compact support $\mathbf{r}\in V$)

$$u(\mathbf{r}_0,k) = k^2\int_V g\gamma u d^3\mathbf{r} + \oint_S (g\nabla u - u\nabla g)\cdot\hat{\mathbf{n}}d^2\mathbf{r}.$$

To compute the surface integral, a condition for the behaviour of u on the surface S of γ must be chosen. Consider the case where the incident wavefield u_i is a simple plane wave of unit amplitude

$$\exp(i\mathbf{k}\cdot\mathbf{r})$$

satisfying the homogeneous wave equation

$$(\nabla^2 + k^2)u_i(\mathbf{r}, k) = 0.$$

By choosing the condition $u(\mathbf{r}, k) = u_i(\mathbf{r}, k)$ on the surface of γ, we obtain the result

$$u(\mathbf{r}_0, k) = k^2 \int_V g\gamma u d^3\mathbf{r} + \oint_S (g\nabla u_i - u_i \nabla g)\cdot\hat{\mathbf{n}} d^2\mathbf{r}.$$

Now, using Green's theorem to convert the surface integral back into a volume integral, we have

$$\oint_S (g\nabla u_i - u_i\nabla g)\cdot\hat{\mathbf{n}} d^2\mathbf{r} = \int_V (g\nabla^2 u_i - u_i\nabla^2 g) d^3\mathbf{r}.$$

Noting that

$$\nabla^2 u_i = -k^2 u_i$$

and that

$$\nabla^2 g = -\delta^3 - k^2 g$$

we obtain

$$\int_V (g\nabla^2 u_i - u_i\nabla^2 g) d^3\mathbf{r} = \int \delta^3 u_i d^3\mathbf{r} = u_i.$$

Hence, by choosing the field u to be equal to the incident wavefield u_i on the surface of γ, we obtain a solution of the form

$$u = u_i + u_s$$

where

$$u_s = k^2 \int_V g\gamma u d^3\mathbf{r}.$$

The function u_s is the scattered wavefield.

6.2.1 The Born Approximation

From the last result it is clear that, in order to compute the scattered field u_s, we must define u inside the volume integral. Unlike the surface integral, a boundary condition will not help here because it is not sufficient to specify the behaviour of u at a boundary. In this case, the behaviour of u throughout V needs to be known. In general, it is not possible to do this (i.e. to compute the scattered wavefield exactly) and we are forced to choose a model for u inside V that is compatible with a particular physical problem in the same way that

an appropriate set of boundary conditions is required to evaluate the surface integral. The simplest model for the internal field is based on assuming that u behaves like u_i for $\mathbf{r} \in V$. The scattered field is then given by

$$u_s(\mathbf{r}_0, k) = k^2 \int_V g(\mathbf{r} \mid \mathbf{r}_0, k)\gamma(\mathbf{r})u_i(\mathbf{r}, k)d^3\mathbf{r}.$$

This assumption provides an approximate solution for the scattered field. It is known as the Born approximation after Max Born who first introduced it in his study of quantum mechanics in the 1930s.

There is another way of deriving this result that is instructive; it helps us to obtain a criterion for the validity of this approximation which will be considered shortly. We start with the inhomogeneous Helmholtz equation

$$(\nabla^2 + k^2)u = -k^2\gamma u$$

and consider a solution for u in terms of a sum of the incident and scattered fields, i.e.

$$u = u_i + u_s.$$

The wave equation then becomes

$$(\nabla^2 + k^2)u_s + (\nabla^2 + k^2)u_i = -k^2\gamma(u_i + u_s).$$

If the incident field satisfies

$$(\nabla^2 + k^2)u_i = 0,$$

then

$$(\nabla^2 + k^2)u_s = -k^2\gamma(u_i + u_s).$$

Assuming that

$$u_i + u_s \simeq u_i, \quad \mathbf{r} \in V$$

we obtain

$$(\nabla^2 + k^2)u_s \simeq -k^2\gamma u_i, \quad \mathbf{r} \in V.$$

Solving for u_s and using the homogeneous boundary conditions (i.e. $u_s = 0$ on S and $\nabla u_s = 0$ on S) we obtain

$$u_s = \oint_S (g\nabla u_s - u_s\nabla g) \cdot \hat{\mathbf{n}} d^2\mathbf{r} + k^2 \int_V g\gamma u_i d^3\mathbf{r} = k^2 \int_V g\gamma u_i d^3\mathbf{r}.$$

6.2.2 Validity of the Born Approximation

In general, the Born approximation requires that u_s is 'small' compared to u_i. What do we really mean by the term 'small' and how can we quantify it? One way to answer this question is to compute an appropriate measure for both the incident and scattered fields and compare the two results. Consider the case

where we compute the root mean square modulus (i.e. the L_2 norm) of each field. We then require that

$$\left(\int_V \mid u_s(\mathbf{r}_0, k) \mid^2 d^3\mathbf{r}_0 \right)^{\frac{1}{2}} << \left(\int_V \mid u_i(\mathbf{r}_0, k) \mid^2 d^3\mathbf{r}_0 \right)^{\frac{1}{2}}$$

or[1]

$$\frac{\|u_s\|}{\|u_i\|} << 1. \tag{6.1}$$

Essentially, this condition means that the overall intensity of u_s in V is small compared to that of u_i in V.

Let us now look in more detail at the nature of this condition. Ideally, what we want is a version of the condition that can be cast in terms of a set of physical parameters (such as the wavelength and the physical extent of γ for example). The Born scattered field at $\mathbf{r}_0$ is given by

$$u_s(\mathbf{r}_0, k) = k^2 \int_V g(\mathbf{r} \mid \mathbf{r}_0, k)\gamma(\mathbf{r})u_i(\mathbf{r}, k)d^3\mathbf{r}.$$

By taking the L_2 norm of this equation we can write

$$\|u_s(\mathbf{r}_0, k)\| = \|k^2 \int_V g(\mathbf{r} \mid \mathbf{r}_0, k)\gamma(\mathbf{r})u_i(\mathbf{r}, k)d^3\mathbf{r}\|$$

$$\leq k^2 \|u_i(\mathbf{r}_0, k)\| \times \| \int_V g(\mathbf{r} \mid \mathbf{r}_0, k)\gamma(\mathbf{r})d^3\mathbf{r}\|.$$

Using this result, the condition required for the Born approximation to hold [i.e. condition (6.1)] can be written as

$$k^2 \| \int_V g(\mathbf{r} \mid \mathbf{r}_0, k)\gamma(\mathbf{r})d^3\mathbf{r}\| << 1, \quad \mathbf{r}_0 \in V. \tag{6.2}$$

Here, the norm involves integration over the spatial variable $\mathbf{r}_0$ in the scattering volume V. To emphasize this we write $\mathbf{r}_0 \in V$.

Condition (6.2) can be written as

$$I(\mathbf{r}_0) << 1$$

where

$$I(\mathbf{r}_0) = k^2 \| \int_V g(\mathbf{r} \mid \mathbf{r}_0, k)\gamma(\mathbf{r})d^3\mathbf{r}\|$$

$$\leq k^2 \left(\int_V \mid g(\mathbf{r} \mid \mathbf{r}_0, k) \mid^2 d^3\mathbf{r} \right)^{\frac{1}{2}} \left(\int_V \mid \gamma(\mathbf{r}) \mid^2 d^3\mathbf{r} \right)^{\frac{1}{2}}.$$

[1] where $\| \bullet \|$ is taken to denote the L_2 norm, i.e. $\| \bullet \|_2$

Substituting the expression for the three-dimensional Green function into the above expression, we have

$$I(\mathbf{r}_0) \leq k^2 \left(\frac{1}{16\pi^2} \int\limits_V \frac{1}{\mid \mathbf{r} - \mathbf{r}_0 \mid^2} d^3\mathbf{r} \int\limits_V \mid \gamma(\mathbf{r}) \mid^2 d^3\mathbf{r} \right)^{\frac{1}{2}}.$$

A relatively simple calculation can now be performed, if we consider γ to be a sphere of volume V and radius R, and resort to calculating its least upper bound which occurs when $\mathbf{r}_0 = 0$. Using spherical polar coordinates (r, θ, ϕ), we have

$$\sup \int\limits_V \frac{1}{\mid \mathbf{r} - \mathbf{r}_0 \mid^2} d^3\mathbf{r} = \int\limits_V \frac{1}{r^2} d^3\mathbf{r} = \int\limits_0^{2\pi} \int\limits_{-1}^{1} \int\limits_0^R dr d(\cos\theta) d\phi = 4\pi R$$

where sup denotes the supremum. Using this result, we can write

$$\sup I(\mathbf{r}_0) \leq k^2 \left(\frac{R}{4\pi} \int\limits_V \mid \gamma(\mathbf{r}) \mid^2 d^3\mathbf{r} \right)^{\frac{1}{2}}$$

and noting that

$$V = \int\limits_V d^3\mathbf{r} = \frac{4}{3}\pi R^3$$

we obtain

$$\sup I(\mathbf{r}_0) \leq \frac{1}{\sqrt{3}} k^2 R^2 \bar{\gamma}$$

where

$$\bar{\gamma} = \sqrt{\frac{\int \mid \gamma \mid^2 d^3\mathbf{r}}{\int d^3\mathbf{r}}}.$$

Hence, the condition for the Born approximation to apply becomes (ignoring $\sqrt{3}$)

$$k^2 R^2 \bar{\gamma} << 1$$

or

$$\bar{\gamma} << \frac{1}{k^2 R^2}.$$

This condition demonstrates that, in principle, large values of γ can occur so long as its root mean square value over the volume V is small compared to $1/k^2R^2$. In scattering theory, γ is said to be a 'weak scatterer'. Note that when k or R approaches zero, this condition is easy to satisfy. Born scattering is thus, more likely to occur in situations when

$$\frac{\lambda}{R} >> 1$$

where λ is the wavelength (noting that $k = 2\pi/\lambda$). If

$$\frac{\lambda}{R} \sim 1$$

then the value of $\bar{\gamma}$ must be small for Born scattering to occur.

By repeating the method given above and using the two- and one-dimensional Green functions, respectively, it is easy to show that in two dimensions the condition required for the Born approximation to apply is given by

$$\bar{\gamma} << \frac{1}{(kR)^{3/2}}$$

where R is the radius of a disc of area A and $\bar{\gamma}$ is the root mean square over A.

In one dimension, the result is

$$\bar{\gamma} << \frac{1}{kL}$$

where L is the length of the scatterer and $\bar{\gamma}$ is the root mean square over L. In both cases we use the same Green function solution to solve the 2D and 1D inhomogeneous Helmholtz equations, respectively. In each case, we assume that the scattered field is, on average, weak compared to the incident field. We may consider the term 'weak' to imply that the total energy associated with u_s inside the inhomogeneity γ is small compared to u_i outside the scatterer.

6.2.3 Asymptotic Born Scattering

By measuring u_s, we can attempt to invert the relevant integral equation and hence recover or reconstruct γ. This type of problem is known as the inverse scattering problem, and solutions to this problem are called inverse scattering solutions. This subject is one of the most fundamental in mathematical physics and is the subject of continuing research. The simplest type of inverse scattering problem occurs when a Born scattered wavefield is measured in the far field or Fraunhofer zone (i.e. when the Green functions takes on its asymptotic form discussed in Chapter 5). From previous results, working in 3D, when the incident field is a (unit) plane wave

$$u_i = \exp(ik\hat{\mathbf{n}}_i \cdot \mathbf{r})$$

where $\hat{\mathbf{n}}_i$ points in the direction of the incident field, the Born scattered field observed at $\mathbf{r}_s$ is

$$u_s(\hat{\mathbf{n}}_s, \hat{\mathbf{n}}_i, k) = \frac{k^2}{4\pi r_s} \exp(ikr_s) \int_V \exp[-ik(\hat{\mathbf{n}}_s - \hat{\mathbf{n}}_i) \cdot \mathbf{r}]\gamma(\mathbf{r}) d^3\mathbf{r}, \quad \mathbf{r} \in V$$

where $\hat{\mathbf{n}}_s (= \mathbf{r}_s/r_s)$ denotes the direction in which u_s propagates. From this result, it is clear that the function γ can be recovered from u_s by

three-dimensional Fourier inversion. The scattered field produced by a two-dimensional Born scatterer in the far field is given by

$$u_s(\hat{\mathbf{n}}_i, \hat{\mathbf{n}}_s, k) = \frac{\exp(i\pi/4)}{\sqrt{8\pi}} \frac{k^2}{\sqrt{kr_s}} \exp(ikr_s) \int_A \exp[-ik(\hat{\mathbf{n}}_s - \hat{\mathbf{n}}_i)\cdot\mathbf{r}]\gamma(\mathbf{r}) d^2\mathbf{r}, \quad \mathbf{r} \in A.$$

In one dimension, the equivalent result is (for a right travelling wave)

$$u_s(x_s, k) = \frac{ik}{2} \exp(ikx_s) \int_L \gamma(x) dx, \quad x \in L.$$

When $\hat{\mathbf{n}}_s = \hat{\mathbf{n}}_i$, we see that

$$u_s = \frac{k^2}{4\pi r_s} \exp(ikr_s) \int_V \gamma(\mathbf{r}) d^3\mathbf{r}.$$

This is called the forward-scattered field. In terms of Fourier analysis, it represents the zero frequency or DC component of the spectrum of γ. Another special case arises when $\hat{\mathbf{n}}_s = -\hat{\mathbf{n}}_i$. The scattered field that is produced in this case is called the back-scattered field, and in three dimensions is given by

$$u_s(\hat{\mathbf{n}}_s, k) = \frac{k^2}{4\pi r_s} \exp(ikr_s) \int_V \exp(-2ik\hat{\mathbf{n}}_s \cdot \mathbf{r})\gamma(\mathbf{r}) d^3\mathbf{r}.$$

In one dimension, the result is (for a left travelling wave)

$$u_s(k) = \frac{ik}{2} \exp(ikx_s) \int_L \exp(-2ikx)\gamma(x) dx.$$

Note that, in one-dimension, the scattering function can only be recovered (via Fourier inversion) by measuring the back-scattered spectrum whereas in two and three dimensions, the scattering function can, in principle, be recovered by either keeping k fixed or varying k.

6.3 Examples of Born Scattering

By way of a short introduction to the applications and uses of the Born approximation, some well known examples are now presented in which it is used to derive expressions for the scattered intensity associated with two physically different scattering phenomena - Rayleigh scattering and Rutherford scattering.

6.3.1 Rutherford Scattering

Rutherford scattering ranks as one of the most important experiments of the Twentieth Century because it was the basis for developing the basic 'visual model' for the atom - a positively charged nucleus with negatively charged orbiting electrons.

In Rutherford's famous experiment (which dates from 1910), α-particles (or helium nuclei) were scattered by gold leaf. The differential cross-section denoted by $d\sigma/d\Omega$ (i.e. the number of particles scattered into a solid angle $d\Omega$ per unit time divided by the number of particles incident per unit area per unit time) was then measured at different scattering angles θ. By treating the α-particles as classical Newtonian particles, Rutherford showed that if the scattering potential (i.e. due to the nucleus of the atoms in the gold leaf) is a repulsive Coulomb potential, then

$$\frac{d\sigma}{d\Omega} \propto \frac{1}{\sin^4(\theta/2)}.$$

This was before the development of quantum mechanics and the emergence of Schrödinger's equation as a governing partial differential equation of quantum mechanics. In this Section, we shall derive Rutherford's result by solving Schrödinger's equation using a Green function.

In terms of quantum mechanics we can consider Rutherford's scattering experiment to consist of a source of plane waves (i.e. the de Broglie or probability waves associated with the α-particles), a scattering function γ (the potential associated with the nucleus of the atoms which make up the gold leaf) and a measuring device which allows us to record the intensity of the scattered radiation at different angles to the incident beam. The Green function solution to the 3D Schrödinger equation

$$(\nabla^2 + k^2)u(\mathbf{r}, k) = \gamma(\mathbf{r})u(\mathbf{r})$$

for an incident plane wave $u_i(\mathbf{r}, k) = \exp(i\mathbf{k} \cdot \mathbf{r})$ is given by

$$u(\mathbf{r}_0, k) = u_i(\mathbf{r}_0, k) + \int g(\mathbf{r} \mid \mathbf{r}_0, k)\gamma(\mathbf{r})u(\mathbf{r}, k)d^3\mathbf{r}.$$

This is the Lippmann-Schwinger equation. The limits of the integral are left 'open' because this equation applies to potentials that are finite (of compact support) or asymptotic (tend to zero at infinity). The inversion of this integral equation is the basis for inverse Schrödinger scattering in three-dimensions.

The Born scattered wave in the far field due to a scattering potential V which is influential over all space is given by

$$u_s(\hat{\mathbf{n}}_s, \hat{\mathbf{n}}_i, k) = -\frac{\exp(ikr_s)}{4\pi r_s} \int_{-\infty}^{\infty} \exp[-ik(\hat{\mathbf{n}}_s - \hat{\mathbf{n}}_i) \cdot \mathbf{r}]\gamma(\mathbf{r})d^3\mathbf{r}.$$

For fixed k and r_s (the distance at which the scattered wavefield is measured from the scattering event), the measured intensity I of the scattered wavefield is given by

$$I = u_s u_s^* = \frac{1}{16\pi^2 r_s^2} \mid A \mid^2$$

where A is the scattering amplitude,

$$A(\hat{\mathbf{n}}_s, \hat{\mathbf{n}}_i, k) = \int_{-\infty}^{\infty} \exp[-ik(\hat{\mathbf{n}}_s - \hat{\mathbf{n}}_i) \cdot \mathbf{r}]\gamma(\mathbf{r})d^3\mathbf{r}.$$

The differential cross section measures the flux of particles through a given area in specific period of time. It is thus a measure of the wavefield intensity, i.e.

$$\frac{d\sigma}{d\Omega} = I.$$

Hence, using quantum mechanics (i.e. Schrödinger's equation), the differential cross-section for Rutherford's scattering experiment can be obtained by evaluating the Fourier transform of the potential γ. For a radially symmetric potential $\gamma(r)$, the scattering amplitude becomes (switching to spherical polar coordinates r, ϕ, ψ)

$$A(\hat{\mathbf{n}}_s, \hat{\mathbf{n}}_i) = \int_0^{2\pi} d\psi \int_{-1}^{1} d(\cos\phi) \int_0^{\infty} dr \quad r^2 \exp(-ik \mid \hat{\mathbf{n}}_s - \hat{\mathbf{n}}_i \mid r\cos\phi)\gamma(r).$$

The modulus of $\hat{\mathbf{n}}_s - \hat{\mathbf{n}}_i$ is given by

$$\mid \hat{\mathbf{n}}_s - \hat{\mathbf{n}}_i \mid = \sqrt{(\hat{\mathbf{n}}_s - \hat{\mathbf{n}}_i) \cdot (\hat{\mathbf{n}}_s - \hat{\mathbf{n}}_i)} = \sqrt{2(1 - \cos\theta)}$$

where

$$\cos\theta = \hat{\mathbf{n}}_s \cdot \hat{\mathbf{n}}_i$$

and θ is the scattering angle (the angle between the incident and scattered fields). Using the half angle formula,

$$1 - \cos\theta = 2\sin^2(\theta/2)$$

we can write

$$\mid \hat{\mathbf{n}}_s - \hat{\mathbf{n}}_i \mid = 2\sin(\theta/2)$$

and integrating over ψ and $\cos\phi$ the scattering amplitude as a function θ can be written as

$$A(\theta) = \frac{2\pi}{k\sin(\theta/2)} \int_0^{\infty} \sin[2kr\sin(\theta/2)]\gamma(r) r dr.$$

All we need to do now is compute the remaining integral over r. If we use a simple Coulomb potential where $\gamma(r) \propto 1/r$, then we run into a problem because the integrand does not converge as $r \to \infty$. For this reason, another radially symmetric potential is introduced which is given by

$$\gamma(r) = \frac{\exp(-ar)}{r}$$

where $a > 0$ is a constant. This type of potential is known as a screened Coulomb potential, the parameter a determining the range over which the potential is influential. It allows us to evaluate the scattering amplitude analytically. We can then observe the behaviour of $\mid A \mid^2$ for a Coulomb potential by letting a approach zero. The scattering amplitude becomes

$$A(\theta) = \frac{2\pi}{k\sin(\theta/2)} \int_0^{\infty} \sin[2kr\sin(\theta/2)] \exp(-ar) dr.$$

This integral is given by

$$\frac{2k\sin(\theta/2)}{a^2+[2k\sin(\theta/2)]^2}$$

and we can write

$$A(\theta)=\frac{\pi}{k^2\sin^2(\theta/2)}\left(1+\frac{a^2}{[2k\sin(\theta/2)]^2}\right)^{-1}.$$

Hence, as $a\to 0$, we obtain

$$A(\theta)\simeq\frac{\pi}{k^2\sin^2(\theta/2)}$$

and the intensity of the scattered field is

$$I=\mid A(\theta)\mid^2\propto\frac{1}{\sin^4(\theta/2)}.$$

We may think of Rutherford's scattering experiment as an inverse scattering problem in the sense that he deduced the potential of the nucleus by recording the way in which it scattered α-particles. However, he did not actually solve the inverse problem directly because he assumed that the scattering potential acted like a repulsive Coulomb potential *a priori* and justified this hypothesis later by showing that the theoretical and experimental results were compatible. One final and interesting point to note is that in order to undertake the experiment Rutherford required a very thin foil which was only a few atoms thick. Gold leaf was the best possible technical solution to this problem at the time. The reason for this was that the α-particles needed (on average) to scatter only from one nucleus in order to investigate the repulsive Coulomb potential theory. If a thicker foil had been used, the α-particles may have scattered from a number of atoms as they passed through it. Multiple scattering would have led to an indeterminacy in the results. It is important to note that the Born approximation used here to verify Rutherford's results using a Green function solution to Schrödinger's equation is consistent with the concept of single, or weak, scattering.

6.3.2 Rayleigh Scattering

Rayleigh scattering is the scattering of electromagnetic radiation by small dielectric scatterers. It is named after the English scientist Lord Rayleigh who was one of the Nineteenth Century's most prolific scientists and made contributions in many areas in mathematics, physics and chemistry, including some of the earliest studies on the scattering of light following the development of James Clerk Maxwell's theory of electromagnetism.

If we consider a scalar electromagnetic wave theory, then we can consider a wave equation of the form

$$(\nabla^2+k^2)u(\mathbf{r},k)=-k^2\gamma(\mathbf{r})u(\mathbf{r},k),\quad \gamma=\epsilon_r-1;\quad \mathbf{r}\in V$$

to describe the behaviour of the electric field u, where ϵ_r is the relative permittivity of a dielectric of compact support V. This is of course a highly idealized case, but it helps to provide another demonstration of Born scattering in a form that is pertinent to the use of Green functions for solving physically significant problems.

In the context of electromagnetic scattering problems, the Born approximation is sometimes referred to as the Rayleigh-Gan approximation - just a different name for an identical mathematical technique. Using this approximation, the asymptotic form of the the scattered electric field is given by

$$u_s(\hat{\mathbf{n}}_s, \hat{\mathbf{n}}_i, k) = \frac{k^2}{4\pi r_s} \exp(ikr_s) \int_V \exp[-ik(\hat{\mathbf{n}}_s - \hat{\mathbf{n}}_i) \cdot \mathbf{r}] \gamma(\mathbf{r}) d^3\mathbf{r}.$$

There are two important differences between this equation and its counterpart in quantum mechanics (i.e. the Schrödinger equation). First, the coefficient in front of the integral possesses a factor k^2. Second, the integral itself is over a finite volume of space V which is determined by the spatial extent of γ. In quantum mechanics, the influence of a potential may be 'felt' over all space so that the integral is over $\pm\infty$. This is an important distinction between scattering problems in quantum mechanics which involve asymptotic potentials (potentials which go to zero at infinity) and classical scattering problems of the type considered here.

Let us consider a model where a plane electromagnetic wave is incident on a homogeneous spherical dielectric object of radius R and relative permittivity ϵ_r. The theory which describes this type of scattering (scattering of light from uniform spheres) is called Mie theory. In this case the Born scattered amplitude is given by (following the same methods as those used earlier)

$$A(\theta) = \frac{2\pi k\gamma}{\sin(\theta/2)} \int_0^R \sin[2kr\sin(\theta/2)] r dr. \tag{6.3}$$

If the dimensions of the scatterer are small compared to the wavelength, then

$$kR << 1$$

and

$$\sin[2kr\sin(\theta/2)] \simeq 2kr\sin(\theta/2), \quad 0 \leq r \leq R.$$

The scattering amplitude is then given by

$$A(\theta) \simeq 4\pi k^2 \gamma \int_0^R r^2 dr = k^2 \gamma V$$

where $V = 4\pi R^3/3$ is the volume of the scatterer. In this case, the scattering is entirely isotropic (i.e. the scattering amplitude is independent of the scattering angle). The intensity is proportional to k^4 or

$$\mid A(\theta) \mid^2 \ \propto \ \frac{1}{\lambda^4}.$$

Note the large inverse dependence on the wavelength. This result is characteristic of Rayleigh scattering and of the spectra produced by light scattering from small sub-wavelength structures. In the visible part of the spectrum, the intensity is greatest for blue light (the colour associated with the smallest wavelength of the visible spectrum). This is why the sky is blue, i.e. sunlight is scattered by the electrons in air molecules in the terrestial atmosphere generating blue light preferentially around in all directions. Further, as the Sun approaches the horizon, we have to look more and more diagonally through the Earth's atmosphere. Our line of sight through the atmosphere is then longer and most of the blue light is scattered out before it reaches us, especially as the Sun gets very near the horizon. Relatively more red light reaches us, accounting for the reddish colour of sunsets. In other words, the λ^{-4} dependence of the scattered intensity implies that the atmosphere scatters green, blue and violet light photons more effectively than yellow, orange, and red photons. As the Sun approaches the horizon, the path of light through the atmosphere increases, so more of the short-wavelength photons get scattered away leaving the longer-wavelength photons and the Sun look progressively redder.

When $kR \sim 1$, the scattering amplitude is obtained by evaluating the integral in equation (6.3), the scattering amplitude being given by

$$A(\theta) = 3V\gamma k^2 \frac{J_1[2kR\sin(\theta/2)]}{2kR\sin(\theta/2)}$$

where J_1 is the spherical Bessel function

$$J_1(x) = \frac{\sin(x)}{x^2} - \frac{\cos(x)}{x}.$$

In this case, the scattering is not isotropic but strongly dependent on the scattering angle.

6.4 Other Approximation Methods

So far in this Chapter, we have been concerned with the use of the Green function for solving two fundamental inhomogeneous partial differential equations (the Helmholtz and the Schrödinger equations). These have introduced the role that Green functions play in an important aspect of mathematical physics - scattering theory - which is fundamental to the field of image systems modelling and image understanding.

The solutions considered so far have been based on the application of the Born approximation (Born scattering theory) to Green function solutions of time-independent wave equations. In this section, we consider the Wentzel-Kramers-Brillouin (WKB) and the Rytov approximations for solving inhomogeneous wave equations, taking the inhomogeneous Helmholtz equation by way of an example (albeit an important one). The WKB method is based on the idea that if the wavelength of the wavefield u is very small compared to variations in γ then a suitable approximation can be introduced which provides an appropriate solution. A similar idea is used for the Rytov approximation. In both cases

the result is based on the use of an exponential type or 'eikonal' transformation where a solution of the type $A(\mathbf{r},k)\exp[\pm s(\mathbf{r},k)]$ or $A(\mathbf{r},k)\exp[\pm is(\mathbf{r},k)]$ is considered. This is analogous (in the latter case) to a plane wave solution of the type $A\exp(\mathbf{k}\cdot\mathbf{r})$. In this transform, the scalar field s is known as the 'eikonal' from the Greek meaning 'image' or 'icon'.

The WKB and Rytov approximations are based on a similar idea, one which has a long history dating back to Huygens. In his book *A Treatise on Light*, Huygens suggested that the reflection and refraction properties of light can be explained on the basis of a sequence of wavefronts which spreads out from a source much as ripples spread out from a stone thrown into water, and that each point on such a wavefront act as a new disturbance source. Although in 1678 Huygens did not specify exactly what is meant by a wavefront, he emphasized that the spacing between successive wavefronts need not to be uniform which is one way of considering the physical interpretation of the WKB approximation. Another example of the WKB approximation being used earlier was in a paper by George Green on *The Motion of Waves in a Variable Canal of Small Depth and Width* (published in the Transactions of the Cambridge Philosophical Society in 1837) who developed a solution for waves along a narrow (to make the problem one dimensional) but variable channel. His solution involves an approach which is essentially the same as the WKB method used in quantum mechanics. It is therefore arguable that the approximation should be called the Green approximation!

6.4.1 The WKB Approximation

To illustrate the idea behind the WKB approximation, let us consider a general solution to the 1D wave equation

$$\left(\frac{\partial^2}{\partial x^2}+k^2\right)u(x,k)=-k^2\gamma(x)u(x,k). \tag{6.4}$$

The Green function solution to this equation is given by

$$u=u_i+u_s$$

where u_i is the incident wavefield (typically a unit amplitude plane wave) and u_s is given by

$$u_s(x_0,k)=k^2\int\gamma(x)g(x\mid x_0,k)u(x,k)dx.$$

Instead of considering the solution to be the sum of two wavefields u_i and u_s, suppose we introduce the eikonal transform

$$u(x,k)=u_i(x,k)\exp[s(x,k)].$$

Substituting this result into equation (6.4) and differentiating, we obtain

$$\frac{\partial^2 u_i}{\partial x^2}+2\frac{\partial s}{\partial x}\frac{\partial u_i}{\partial x}+u_i\left(\frac{\partial s}{\partial x}\right)^2+u_i\frac{\partial^2 s}{\partial x^2}+k^2u_i=-k^2\gamma u_i.$$

Now if we consider u_i to be a solution to $\partial^2 u_i/\partial x^2 + k^2 u_i = 0$ [i.e. $u_i = \exp(ikx)$] then, after differentiating u_i and rearranging, we have

$$2ik\frac{\partial s}{\partial x} + \left(\frac{\partial s}{\partial x}\right)^2 + \frac{\partial^2 s}{\partial x^2} = -k^2\gamma. \tag{6.5}$$

This is a nonlinear Riccatian equation for s which at first sight, appears to be more complicated than the original. However, if we introduce the condition that the wavelength $\lambda = 2\pi/k$ is significantly smaller than the spatial extent over which s varies, then the nonlinear term and the second derivative can be ignored and we can write

$$2ik\frac{ds}{dx} = -k^2\gamma$$

whose general solution is (ignoring the constant of integration)

$$s(x) = \frac{ik}{2}\int^x \gamma(x)dx.$$

The solution for u is therefore given by

$$u(x,k) = u_i \exp\left(\frac{ik}{2}\int^x \gamma(x)dx\right) = \exp\left[ik\left(x + \frac{1}{2}\int^x \gamma(x)dx\right)\right].$$

This is an example of the WKB approximation. It is based on the idea that if k is large compared to the magnitudes of the terms $(\partial s/\partial x)^2$ and $\partial^2 s/\partial x^2$ then the only terms in equation (6.5) that matter are $2ik(\partial s/\partial x)$ and $-k^2\gamma$. In other words, if L is the characteristic scale length over which s varies, then

$$\frac{\lambda}{L} << 1.$$

The solution describes a plane wavefield whose phase kx is modified by $\frac{k}{2}\int \gamma dx$. A similar approach can be used in higher dimensions which leads to an interpretation of the solutions in terms of the characteristics or rays and the geometric properties associated with them.

The WKB approximation as illustrated here does not in itself make use of a Green function. We shall now consider the Rytov approximation which is based on a similar idea to the WKB approximation and which makes explicit use of the Green function.

6.4.2 The Rytov Approximation

Consider the 3D inhomogeneous Helmholtz equation

$$(\nabla^2 + k^2)u(\mathbf{r},k) = -k^2\gamma(\mathbf{r})u(\mathbf{r},k), \quad \mathbf{r} \in V.$$

If we substitute $u = u_i \exp(s)$ into this equation and differentiate, we obtain the nonlinear Riccatian equation

$$\nabla^2 s + 2\frac{\nabla u_i}{u_i}\cdot\nabla s + \nabla s\cdot\nabla s = -k^2\gamma$$

where u_i is taken to satisfy the equation

$$\nabla^2 u_i + k^2 u_i = 0, \quad \text{i.e.} \quad u_i = \exp(i\mathbf{k}\cdot\mathbf{r}).$$

Suppose we assume that s varies sufficiently slowly for the nonlinear term $\nabla s \cdot \nabla s$ to be neglected compared to the other terms, then we can write (approximately)

$$u_i \nabla^2 s + 2\nabla u_i \cdot \nabla s = -k^2 \gamma u_i. \tag{6.6}$$

This is the Rytov approximation. To facilitate a Green function solution, we substitute $s = w/u_i$ into equation (6.6). Differentiating, we have

$$u_i \nabla^2 s + 2\nabla u \cdot \nabla s$$

$$= \nabla^2 w + 2u_i \nabla w \cdot \nabla \left(\frac{1}{u_i}\right) + u_i w \nabla^2 \left(\frac{1}{u_i}\right) + 2\frac{\nabla u_i}{u_i} \cdot \nabla w + 2w\nabla u_i \cdot \nabla \left(\frac{1}{u_i}\right)$$

$$= \nabla^2 w + k^2 w$$

and thus, equation (6.6) reduces to

$$\nabla^2 w + k^2 w = -k^2 \gamma u_i.$$

The Green function solution to this equation (subject to homogeneous boundary conditions) is

$$w(\mathbf{r}_0, k) = k^2 \int_V u_i(\mathbf{r}, k)\gamma(\mathbf{r}) g(\mathbf{r} \mid \mathbf{r}_0, k) d^3\mathbf{r}$$

and we arrive at the solution

$$u(\mathbf{r}_0, k) = u_i(\mathbf{r}_0, k) \exp\left[\frac{k^2}{u_i(\mathbf{r}_0, k)} \int_V u_i(\mathbf{r}, k)\gamma(r) g(\mathbf{r} \mid \mathbf{r}_0, k) d^3\mathbf{r}\right].$$

We can write this result as

$$u = u_i \left(1 + \frac{k^2}{u_i} \int_V u_i \gamma g d^3\mathbf{r} + ...\right) \simeq u_i + k^2 \int_V u_i \gamma g d^3\mathbf{r}$$

which is the solution under the Born approximation.

6.4.3 Conditions for the Rytov Approximation

The condition required for the validity of the Rytov approximation can be investigated by considering a Green function solution with the nonlinear term $\nabla s \cdot \nabla s$ included. In this case, equation (6.6) becomes

$$u_i \nabla^2 s + 2\nabla u_i \cdot \nabla s = -k^2 \gamma u_i - u_i \nabla s \cdot \nabla s.$$

Substituting $s = w/u_i$ into this equation (except for the second term on the right hand side) we have

$$\nabla^2 w + k^2 w = -k^2 \gamma u_i - u_i \nabla s \cdot \nabla s$$

whose Green function solution is

$$w = k^2 \int_V u_i \gamma g d^3\mathbf{r} + \int_V u_i (\nabla s \cdot \nabla s) g d^3\mathbf{r}$$

so that we can write

$$s = \frac{k^2}{u_i} \int_V u_i \gamma g d^3\mathbf{r} + \frac{k^2}{u_i} \int_V u_i \gamma g \left(\frac{\nabla s \cdot \nabla s}{k^2 \gamma} \right) d^3\mathbf{r}.$$

In order for the second term on the right hand side to be neglected, we must introduce the condition

$$\frac{\nabla s \cdot \nabla s}{k^2 \gamma} << 1$$

or

$$\|k^2 \gamma\| >> \|\nabla s \cdot \nabla s\|.$$

The interpretation of this condition is not trivial. Clearly, the larger the value of k (i.e. the smaller the value of the wavelength) for a given magnitude of γ and ∇s, the more appropriate the condition becomes. Thus, the condition is valid if the wavelength of the field is small compared to γ. Since s can be taken to be the phase of the wavefield solution u, another physical interpretation of the condition is that the characteristic scale length over which a change in phase occurs ∇s is small compared to the wavelength for a given γ.

6.5 The Born Series

The Born approximation introduced earlier was used to solve some elementary scattering problems. We shall now consider a natural extension to the Born approximation which is based on generating a series solution to the problem, known generally as the Neumann series.

Consider the 3D Green function solution to the Helmholtz equation

$$(\nabla^2 + k^2) u(\mathbf{r}, k) = -k^2 \gamma u(\mathbf{r}, k)$$

which is given by

$$u(\mathbf{r}_0, k) = u_i(\mathbf{r}_0, k) + u_s(\mathbf{r}_0, k)$$

where

$$u_s(\mathbf{r}_0, k) = k^2 \int_V g(\mathbf{r} \mid \mathbf{r}_0, k) \gamma(\mathbf{r}) u(\mathbf{r}, k) d^3\mathbf{r},$$

u_i is the incident field satisfying the equation

$$(\nabla^2 + k^2) u_i(\mathbf{r}, k) = 0$$

and g is the outgoing Green function given by

$$g(\mathbf{r} \mid \mathbf{r}_0, k) = \frac{\exp(ik \mid \mathbf{r} - \mathbf{r}_0 \mid)}{4\pi \mid \mathbf{r} - \mathbf{r}_0 \mid}.$$

We have seen that the Born approximation to this equation is given by considering $u \sim u_i, \quad \mathbf{r} \in V$ which is valid provided $\|u_s\| << \|u_i\|$. We then obtain an approximate solution u_1, say, of the form

$$u_1(\mathbf{r}_0, k) = u_i(\mathbf{r}_0, k) + k^2 \int_V g(\mathbf{r} \mid \mathbf{r}_0, k)\gamma(\mathbf{r})u_i(\mathbf{r}, k)d^3\mathbf{r}.$$

This result can be considered to be the first approximation to a series solution, in which the second approximation u_2, say, is given by

$$u_2(\mathbf{r}_0, k) = u_i(\mathbf{r}_0, k) + k^2 \int_V g(\mathbf{r} \mid \mathbf{r}_0, k)\gamma(\mathbf{r})u_1(\mathbf{r}, k)d^3\mathbf{r}$$

and the third approximation u_3 is given by

$$u_3(\mathbf{r}_0, k) = k^2 u_i(\mathbf{r}_0, k) + \int_V g(\mathbf{r} \mid \mathbf{r}_0, k)\gamma(\mathbf{r})u_2(\mathbf{r}, k)d^3\mathbf{r}$$

and so on. In general, we can consider the iteration

$$u_{n+1}(\mathbf{r}_0, k) = u_i(\mathbf{r}_0, k) + k^2 \int_V g(\mathbf{r} \mid \mathbf{r}_0, k)\gamma(\mathbf{r})u_n(\mathbf{r}, k)d^3\mathbf{r}, \quad n = 0, 1, 2, 3, ..$$

where $u_0 = u_i$.

In principle, if this series converges, then it must converge to the solution. To investigate its convergence, it is convenient to use operator notation and write

$$u_{n+1} = u_i + \hat{I}u_n$$

where $\hat{I}$ is the integral operator

$$\hat{I} = \int_V d^3\mathbf{r} g\gamma.$$

At each iteration n we can consider the solution to be given by

$$u_n = u + \epsilon_n$$

where ϵ_n is the error associated with the solution at iteration n and u is the exact solution. A necessary condition for convergence is that $\epsilon_n \to 0$ as $n \to \infty$. Now,

$$u + \epsilon_{n+1} = u_i + \hat{I}(u + \epsilon_n) = u_i + \hat{I}u + \hat{I}\epsilon_n$$

and therefore we can write

$$\epsilon_{n+1} = \hat{I}\epsilon_n$$

since $u = u_i + \hat{I}u$. Thus

$$\epsilon_1 = \hat{I}\epsilon_0; \quad \epsilon_2 = \hat{I}\epsilon_1 = \hat{I}(\hat{I}\epsilon_0); \quad \epsilon_3 = \hat{I}\epsilon_2 = \hat{I}[\hat{I}(\hat{I}\epsilon_0)]; ...$$

or

$$\epsilon_n = \hat{I}^n \epsilon_0$$

from which it follows that

$$\|\epsilon_n\| = \|\hat{I}^n\epsilon_0\| \leq \|\hat{I}^n\| \times \|\epsilon_0\| \leq \|\hat{I}\|^n \|\epsilon_0\|.$$

The condition for convergence therefore becomes

$$\lim_{n\to\infty} \|\hat{I}\|^n = 0.$$

This is only possible if

$$\|\hat{I}\| < 1$$

or

$$k^2 \| \int_V g(\mathbf{r} \mid \mathbf{r}_0, k)\gamma(\mathbf{r}) d^3\mathbf{r} \| < 1.$$

Comparing this result with condition (6.2) and the analysis associated with it given in Section 6.2.2, it is clear that

$$\bar{\gamma} < \frac{1}{k^2 R^2}$$

must be satisfied for the series to converge where R is the radius of a sphere of volume V.

This series solution, which can be written out as

$$u(\mathbf{r}_0, k) = u_i(\mathbf{r}_0, k) + k^2 \int_V g(\mathbf{r} \mid \mathbf{r}_0, k)\gamma(\mathbf{r}) u_i(\mathbf{r}, k) d^3\mathbf{r} =$$

$$k^2 \int_V g(\mathbf{r} \mid \mathbf{r}_0, k)\gamma(\mathbf{r}) \left[k^2 \int_V g(\mathbf{r}_1 \mid \mathbf{r}, k)\gamma(\mathbf{r}_1) u_i(\mathbf{r}_1, k) d^3\mathbf{r}_1 \right] d^3\mathbf{r} + ...$$

$$= u_i(\mathbf{r}_0, k) + k^2 \int_V d^3\mathbf{r} g(\mathbf{r} \mid \mathbf{r}_0, k)\gamma(\mathbf{r}) u_i(\mathbf{r}, k)$$

$$+k^4 \int_V \int_V d^3\mathbf{r} d^3\mathbf{r}_1 g(\mathbf{r} \mid \mathbf{r}_0, k)\gamma(\mathbf{r}) g(\mathbf{r}_1 \mid \mathbf{r}, k)\gamma(\mathbf{r}_1) u_i(\mathbf{r}_1, k)$$

$$+k^6 \int_V \int_V \int_V d^3\mathbf{r} d^3\mathbf{r}_1 d^3\mathbf{r}_2 g(\mathbf{r} \mid \mathbf{r}_0, k)\gamma(\mathbf{r}) g(\mathbf{r}_1 \mid \mathbf{r}, k)\gamma(\mathbf{r}_1) g(\mathbf{r}_2 \mid \mathbf{r}_1, k)\gamma(\mathbf{r}_2) u_i(\mathbf{r}_2, k)$$

$$+ \quad ...$$

is an example of a Neumann series solution to a Fredholm integral equation and is known as the Born series. The scattered field can be written in the form

$$u_s(\mathbf{r},k) = k^2 g(r,k) \otimes \gamma(\mathbf{r}) u_i(\mathbf{r},k) + k^4 g(r,k) \otimes \gamma(\mathbf{r})[g(r) \otimes \gamma(\mathbf{r}) u_i(\mathbf{r},k)] + ...$$

where $\otimes$ denotes the three-dimensional convolution integral over V and $r \equiv \mid \mathbf{r} \mid$.

Another approach to deriving this result can be taken by considering the inverse operator. Writing

$$u = u_i + k^2 \hat{I} u$$

where

$$\hat{I} \equiv \int_V d^3\mathbf{r} \gamma(\mathbf{r}) g(\mathbf{r} \mid \mathbf{r}_0, k),$$

we have

$$(1 - k^2 \hat{I}) u = u_i$$

or

$$u = (1 - k^2 \hat{I})^{-1} u_i = (1 + k^2 \hat{I} + k^4 \hat{I}^2 + k^6 \hat{I}^3 + ...) u_i.$$

Either way, the Born series can be interpreted as follows:

$$\begin{gathered} u(\mathbf{r}_0, k) = \text{incident wavefield} \\ + \\ \text{wavefield generated by single scattering events} \\ + \\ \text{wavefield generated by double scattering events} \\ + \\ \text{wavefield generated by triple scattering events} \\ + \\ \vdots \end{gathered}$$

Each term in this series expresses the effects due to single, double, and triple, etc., scattering. Feynman diagrams can be used to represent these effects graphically, e.g. the propagation of a wavefield generated by one interaction with another. In particle physics, interparticle interactions are complicated multiple scattering events in which the forces are transmitted by quantum fields. The propagation of fields between points is precisely what Green functions describe. So Green functions, often called Feynman propagators in particle physics, are among the standard working tools of theoretical analysis in modern quantum physics.

For an incident plane wave $u_i(\mathbf{r},k) = \exp(i\mathbf{k}\cdot\mathbf{r})$ and with $R \equiv \mid \mathbf{r} - \mathbf{r}_0 \mid$ each term in the Born series scales as $\frac{1}{R}$, $\frac{1}{R^2}$, $\frac{1}{R^3}$, etc., so that multiple-scattering gets 'weaker by the term'. This is due to the form of the Green function in 3D which scales as $1/R$, the intensity of the field being $1/R^2$ - the inverse square law. Thus, if the scattering function is characterized by a number of scattering 'sites' (i.e. where γ is composed of a distribution of point-like scatterers that are of compact support) then, provided that the distance between these sites is large,

the effect of multiple scattering will be insignificant. However, if these sites are close together where the effect of the multiple scattering wavefield falling off as $1/R^2$, $1/R^3$, etc., is not appreciable, then multiple scattering events will contribute significantly to the scattered field. Hence, one way to interpret the meaning of 'weak' and 'strong' scattering is in terms of the 'density' of scattering sites over the volume V being low or high, respectively. For $\lambda \sim R$ where R is the characteristics size of the scatterer, the Born approximation holds provided the root mean square of the scattering function over the volume is much less than 1. This is a quantification of the principle that the density of scattering sites from which we can suppose the scattering function is composed is low.

Another important feature of the Born series for Helmholtz scattering is that the terms are scaled by k^2, k^4, k^6. Thus for a fixed $k << 1$ (long wavelength waves),

$$u(\mathbf{r}_0, k) = u_i(\mathbf{r}_0, k) + k^2 \int\limits_V g(\mathbf{r} \mid \mathbf{r}_0, k)\gamma(\mathbf{r})u_i(\mathbf{r}, k)d^3\mathbf{r}.$$

In 1D, the Green function scales as $1/k$, the Born series for Helmholtz scattering being given by

$$u(x_0, k) = u_i(x_0, k) + \frac{ik}{2}\int\limits_L dx \exp(ik \mid x - x_0 \mid)\gamma(x)u_i(x, k)$$

$$-\frac{k^2}{4}\int\limits_L\int\limits_L dxdx_1 \exp(ik \mid x - x_0 \mid)\gamma(x)\exp(ik \mid x_1 - x \mid)\gamma(x_1)u_i(x_1, k)$$

$$-\frac{ik^3}{8}\int\limits_L\int\limits_L\int\limits_L dxdx_1dx_2 \exp(ik \mid x - x_0)\gamma(x)\exp(ik \mid x_1 - x \mid)\gamma(x_1)$$

$$. \exp(ik \mid x_2 - x_1)\gamma(x_2)u_i(x_2, k)$$

$$+ \quad ...$$

In this case, the series does not get 'weaker by the term' according to $1/R^n$ but by $1/2^n$. Consequently, we should expect that multiple scattering is a more common occurrence when waves scatter (transmit/reflect) from layered materials. This is readily experienced when observing light reflecting from two glass plates - double glazing for example. Here, a number of faded 'ghost images' are seen in addition to the two primary images obtained from the partial reflection of light by the first plate and that from the second. As in the 3D case, the Born approximation 'improves' at larger wavelengths since for $k << 1$

$$u(x_0, k) = u_i(x_0, k) + \frac{ik}{2}\int\limits_L \exp(ik \mid x - x_0 \mid)\gamma(x)u_i(x, k)dx.$$

In quantum (Schrödinger) scattering, the Born series is of the same form but without the factors of k^2, k^4, k^6, etc., and in 1D is given by

$$u(x_0, k) = u_i(x_0, k) + \int dxg(x \mid x_0, k)\gamma(x)u_i(x, k)dx + ...$$

Now, the 1D Green function is given by

$$g(x \mid x_0, k) = \frac{i}{2k} \exp(ik \mid x - x_0 \mid)$$

and so for $k >> 1$

$$u(x_0, k) = u_i(x_0, k) + \frac{i}{2k} \int \exp(ik \mid x - x_0 \mid) V(x) \exp(ikx) dx$$

$$= u_i(x_0, k) + \exp(-ikx_0) \frac{i}{2k} \int V(x) \exp(2ikx) dx, \quad x_0 \to \infty.$$

Thus, for very high frequency quantum wavefields in 1D, the Fourier transform of the scattering potential γ is an exact scattering transform. This result can be applied to the 1D inhomogeneous Helmholtz equation by mapping it into the Schrödinger equation. Writing

$$\left(\frac{\partial^2}{\partial x^2} + k^2 \Gamma(x) \right) u(x, k) = 0$$

where

$$\Gamma(x) = 1 + \gamma(x),$$

application of the Liouville transformation

$$U(y, k) = g(x) u(x, k), \quad \frac{dx}{dy} = \frac{1}{[g(x)]^2}, \quad \text{and} \quad g(x) = \Gamma^{\frac{1}{2}}(x)$$

gives

$$\left(\frac{\partial^2}{\partial y^2} + k^2 \right) U(y, k) = f(y) U(y, k)$$

where

$$f(y) = \frac{1}{g(y)} \frac{\partial^2}{\partial y^2} g(y).$$

In imaging science, the fundamental imaging equation comes from assuming that the recorded data $d = u - u_i$ is of the form

$$d = k^2 \hat{I} u_i + n$$

where

$$n = (k^4 \hat{I}^2 + k^6 \hat{I}^3 + ...) u_i + \text{other} \quad \text{noise}$$

In other words, the multiple scattering events are assumed to be part of the noise inherent in the system recording.

One of the principal issues with using the Born approximation is that it is generally going to be valid for the case when $\lambda >> R$ where R is a measure of the characteristic size of the inhomogeneity. However, in imaging science, to obtain information on an object over a scale of R, we apply wavefields whose wavelength is of the same order, i.e. $\lambda \sim R$. Now, since the Born approximation requires that (in 3D)

$$\bar{\gamma} << \frac{1}{kR},$$

for $\lambda \sim R$,

$$\bar{\gamma} << 1.$$

In other words, to utilize the fundamental imaging equation (which is a product of applying the Born approximation) the material we are imaging should ideally have inhomogeneities whose root mean square value is much less than 1. Because this condition is not always satisfied, multiple scattering effects are inevitable. Nevertheless, the basic imaging model is, for better or worse, based on the Born scattering term plus noise for the case when $\lambda \sim R$. Asymptotic conditions such as $\lambda \to \infty$ or $\lambda \to 0$ may provide exact scattering solutions but they are inconsistent with imaging systems based on the use of radiation where $\lambda \sim R$.

When multiple scattering is a dominant feature of an image system, although it may be possible to construct a deterministic multiple scattering model, the application of such a model for the development of a practical image reconstruction and image processing algorithms is often intractable. Instead we can consider the wavefield generated by multiple scattering events to be a stochastic field and investigate its characteristics using statistical modelling and analysis. This approach is of course consistent with many areas of physics and engineering when the 'physics' that one is attempting to model becomes too complicated for a deterministic analysis to be of any practical value. In such cases we turn to statistical methods of modelling the data. This approach is discussed in Chapter 17.

It is worth mentioning that a Rytov series can be derived by extending the Rytov approximation in the same way that the Born series has been derived here by extending the Born approximation and considering higher order iterates subject to a condition for convergence being satisfied. However, the interpretation of the Rytov series is not trivial and the computational effort required to evaluate the series for a given scattering function can lead to the problem becoming a 'complete Rytov'!

The use of the Born series (and the Rytov series) leads to computational problems when evaluating a fully multiple scattered field. First is the issue over the converegence criterion for the series which may not always be satisfied; second is the issue of the singularities that arise when a multiple point scattering model (i.e. multiple delta functions located at different position in space) for the scattering function is introduced into the Born series. These problems necessitated the development of renormalization theory in the early 1960s which lies beyond the scope of this work. However, it is worth noting, that issues concerning the development of renormalization theory and the difficulties associated with its application helped to forge the foundations of string theory that, to this day, remains the most promising approach for the development of a unified field theory (a theory of everything!).

6.6 Inverse Scattering

Inverse scattering aims to reconstruct the scattering function from measurements of the data. The practicability of solving inverse scattering problems

analytically and implementing them experimentally varies considerably from one application to another. An inversion method is usually based on the approximation that has been applied to solve the forward scattering problem given the wave equation. For example, given the Helmholtz equation, then under the Born approximation, in the far field region, the scattering amplitude is given by

$$A(\hat{\mathbf{n}}_s, \hat{\mathbf{n}}_i, k) = k^2 \int_V \exp[-ik(\hat{\mathbf{n}}_s - \hat{\mathbf{n}}_i) \cdot \mathbf{r}]\gamma(\mathbf{r}) d^3\mathbf{r}.$$

The inverse solution to this problem is therefore compounded in the inverse Fourier transform. In 1D, the solution is, for a unit plane wave,

$$u(x_0, k) = \exp(ikx_0) + \exp(-ikx_0)r(k)$$

where r is the 'reflection coefficient' given by

$$r(k) = \frac{ik}{2} \int_L \gamma(x) \exp(2ikx) dx$$

which can be written as

$$r(k) = \frac{1}{4} \int dx \exp(ikx) \frac{d}{dx} \gamma(x/2).$$

Hence, inversion is achieved by taking the inverse Fourier transform and integrating the result.

The link between the application of the Born approximation in the far field and the Fourier transform should now be clear. This 'link' is essential in imaging science and is why the Fourier transform plays such an essential role. Inverse solutions under the Born approximation are in effect the same as implementing Fourier based reconstruction methods in imaging science, at least when the data collected are the result of a scattering event. In some cases, the scattering is not as weak as it should be to support application of the Born approximation. In such cases, Fourier based image reconstructions can become distorted. There is, however, a method of inverting a wavefield that is the result of multiple Born scattering; this is known as the Jost-Kohn method first published in 1952. A brief overview of this method follows.

Using operator notation, the Born series can be written as

$$u = u_i + \hat{I}_i\gamma + \hat{I}_i(\gamma\hat{I}\gamma) + I_i[\gamma\hat{I}(\gamma\hat{I}\gamma)] + ...$$

where γ is either the scattering potential (for Schrödinger scattering) or $k^2\gamma$ (for Helmholtz scattering) and

$$\hat{I}_i = \int d^3\mathbf{r} u_i g, \quad \hat{I} = \int d^3\mathbf{r} g.$$

Now, let $\epsilon U = u - u_i$ and

$$\gamma = \sum_{j=1}^{\infty} \epsilon^j \gamma_j.$$

Then

$$\epsilon U = \hat{I}_i[\epsilon\gamma_1 + \epsilon^2\gamma_2 + \epsilon^3\gamma_3 + ...]$$
$$+\hat{I}_i[(\epsilon\gamma_1 + \epsilon^2\gamma_2 + \epsilon^3\gamma_3 + ...)\hat{I}(\epsilon\gamma_1 + \epsilon^2\gamma_2 + \epsilon^3\gamma_3 + ...)]$$
$$+\hat{I}_i\{(\epsilon\gamma_1 + \epsilon^2\gamma_2 + \epsilon^3\gamma_3 + ...)\hat{I}[(\epsilon\gamma_1 + \epsilon^2\gamma_2 + \epsilon^3\gamma_3 + ...)$$
$$\hat{I}(\epsilon\gamma_1 + \epsilon^2\gamma_2 + \epsilon^3\gamma_3 + ...)]\} + ...$$

Equating terms with common coefficients ϵ, ϵ^2, etc., we have

For $j = 1$:

$$U = \hat{I}_i\gamma_1; \quad \gamma_1 = \hat{I}_i^{-1}U.$$

For $j = 2$:

$$0 = \hat{I}_i\gamma_2 + \hat{I}_i(\gamma_1\hat{I}\gamma_1); \quad \gamma_2 = -\hat{I}_i^{-1}[\hat{I}_i(\gamma_1\hat{I}\gamma_1)]$$

and so on. By computing the functions γ_j using this iterative method, the scattering function γ is obtained by summing γ_j for $\epsilon = 1$. This approach provides a formal exact inverse scattering solution but it is not unconditional, i.e. the inverse solution is only applicable when the Born series converges to the exact scattering solution and thus when

$$\| \int_V g(\mathbf{r} \mid \mathbf{r}_0, k)\gamma(\mathbf{r})d^3\mathbf{r}\| < 1$$

We note, that, for $j = 1$, the solution for γ_1 is that obtained under the Born approximation.

6.7 Surface Scattering Theory

The complete Green function solution to an equation of the form

$$(\nabla^2 + k^2)u = -k^2 fu, \quad \mathbf{r} \in V$$

is

$$u(\mathbf{r}_0, k) = \oint_S \left(g\frac{\partial u}{\partial \hat{\mathbf{n}}} - u\frac{\partial g}{\partial \hat{\mathbf{n}}} \right) d^2\mathbf{r} + k^2 \int_V g(\mathbf{r} \mid \mathbf{r}_0, k)f(\mathbf{r})u(\mathbf{r}, k)d^3\mathbf{r}$$

where

$$\frac{\partial u}{\partial \hat{\mathbf{n}}} \equiv \hat{\mathbf{n}} \cdot \nabla u \quad \text{and} \quad \frac{\partial g}{\partial \hat{\mathbf{n}}}\hat{\mathbf{n}} \cdot \nabla g,$$

the surface integral being obtained by application of Green's theorem. This surface integral has so far been discarded under the assumption of homogeneous boundary conditions or that $u = u_i$ (the incident field) on the surface S which encloses the volume V. We are then left with a volume integral and a volume scattering theory.

In general, both surface and volume scattering occur. However, if the incident field does not penetrate the object defined by V, then volume scattering will not occur. Instead, the scattering is determined by the way in which the

wavefield interacts with the surface alone and is thus determined by evaluating the surface integral alone. In this Section, we make explicit use of this surface integral to develop a solution to the homogeneous Helmholtz equation. This leads to the theory of surface scattering of which Kirchhoff's theory is a special (but very important) case. Kirchhoff developed a rigorous theory of diffraction in 1887 and demonstrated that previous results and ideas in optics could be obtained from the wave equation. This result is interesting in that it provided a well formulated theory of optics (i.e. one based on the solution to a partial differential equation) but it is also one of the first examples to make explicit use of Green's theorem and the Green function combined as a result of Lord Kelvin popularizing the work of George Green in the latter part of the Nineteenth Century.

6.7.1 Kirchhoff Diffraction Theory

Consider a scalar wavefield u described by the homogeneous Helmholtz equation

$$(\nabla^2 + k^2)u = 0.$$

Let u_i be the field incident on a (open) surface S and consider the following (Kirchhoff) boundary conditions

$$u = u_i, \quad \frac{\partial u}{\partial \hat{\mathbf{n}}} = \frac{\partial u_i}{\partial \hat{\mathbf{n}}} \quad \text{on} \quad \text{S}.$$

The results which derive from a solution to the Helmholtz equation based on these boundary conditions is called Kirchhoff diffraction theory. The theory can be applied to surfaces of different topology but is commonly associated with plane surfaces such as those representing a plane aperture in a screen.

The scalar diffraction theory used here should be regarded as a first approximation to optical diffraction. The observed intensity I (the observed quantity at optical frequencies) can be taken to be given by

$$I = \mid u \mid^2 .$$

Except in free space, u is not (in general) a Cartesian component of the vector electric or magnetic field, and scalar diffraction theory is accurate only if: (i) the diffracting aperture is large compared to the wavelength; (ii) the diffracted fields are observed at a reasonable distance from the screen.

In the following Section we solve the homogeneous Helmholtz equation using a Green function by implementing the Kirchhoff theory of diffraction - a theory which is fundamental to modern optics.

6.7.2 Green Function Solution

Consider the Green function g which is the solution to

$$(\nabla^2 + k^2)g = -\delta^3(\mathbf{r} - \mathbf{r}_0)$$

given by

$$g(\mathbf{r} \mid \mathbf{r}_0, k) = \frac{1}{4\pi \mid \mathbf{r} - \mathbf{r}_0 \mid} \exp(ik \mid \mathbf{r} - \mathbf{r}_0 \mid).$$

We can construct two equations:

$$g\nabla^2 u + k^2 g u = 0$$

and

$$u\nabla^2 g + k^2 u g = -u\delta^3.$$

Subtracting these equations and integrating over a volume V we obtain a solution for the field u at $\mathbf{r}_0$,

$$u(\mathbf{r}_0, k) = \oint_S \left(g\frac{\partial u}{\partial \hat{\mathbf{n}}} - u\frac{\partial g}{\partial \hat{\mathbf{n}}} \right) \cdot \hat{\mathbf{n}} d^2\mathbf{r}$$

where we have used Green's theorem to write the solution in terms of a (closed) surface integral. We must consider the surface integration carefully to obtain a sensible result for an aperture in a screen. Consider the case where the surface of integration is made up of the following three surface patches: (i) the surface covering the aperture S_1; (ii) a plane surface adjacent to the screen S_2 (not covering the aperture); (iii) a semi-spherical surface S_3 connected to S_2, where, in each case, the surfaces are considered to exist in the diffraction domain, i.e. the side of the screen which the incident field does not illuminate so that $S = S_1 + S_2 + S_3$. On S_2 (the screen itself) u and $\partial u/\partial \hat{\mathbf{n}}$ are identically zero. In the aperture (over the surface S_1) the values of u and $\partial u/\partial \hat{\mathbf{n}}$ will have the values they would have if the screen were not there (u_i and $\partial u_i/\partial \hat{\mathbf{n}}$). Evaluation of the behaviour of the field over S_3 requires some attention which is compounded in the computation of

$$\frac{\partial g}{\partial \hat{\mathbf{n}}} = \hat{\mathbf{n}} \cdot \nabla g.$$

Evaluating ∇g we have

$$\nabla g = \hat{\mathbf{x}} \frac{\partial}{\partial x} \frac{\exp(ik\sqrt{(x-x_0)^2 + ...})}{4\pi\sqrt{(x-x_0)^2 + ...}} + ...$$

$$= -\hat{\mathbf{x}} \frac{1}{4\pi} \exp(ik\sqrt{(x-x_0)^2 + ...})[(x-x_0)^2 + ...]^{-\frac{3}{2}}(x-x_0)$$

$$+\hat{\mathbf{x}} \frac{ik}{4\pi} \frac{(x-x_0)}{(x-x_0)^2 + ...} \exp(ik\sqrt{(x-x_0)^2 + ...}) + ...$$

$$= \hat{\mathbf{x}} \frac{\exp(ik\sqrt{(x-x_0)^2 + ...})}{4\pi\sqrt{(x-x_0)^2 + ...}} \frac{(x-x_0)}{\sqrt{(x-x_0)^2 + ...}} \times \left(ik - \frac{1}{\sqrt{(x-x_0)^2 + ...}} \right) + ...$$

$$= \hat{\mathbf{m}} \left(ik - \frac{1}{\mid \mathbf{r} - \mathbf{r}_0 \mid} \right) g$$

where

$$\hat{\mathbf{m}} = \frac{\mathbf{r} - \mathbf{r}_0}{\mid \mathbf{r} - \mathbf{r}_0 \mid}.$$

Therefore,

$$\frac{\partial g}{\partial \hat{\mathbf{n}}} = \hat{\mathbf{n}} \cdot \hat{\mathbf{m}} \left(ik - \frac{1}{\mid \mathbf{r} - \mathbf{r}_0 \mid} \right) g.$$

In most practical circumstances the diffracted field is observed at distances $\mid \mathbf{r} - \mathbf{r}_0 \mid$ where

$$\mid \mathbf{r} - \mathbf{r}_0 \mid >> \lambda.$$

This condition allows us to introduce the simplification

$$\nabla g \simeq ik\hat{\mathbf{m}} g$$

so that

$$\frac{\partial g}{\partial \hat{\mathbf{n}}} \simeq ik\hat{\mathbf{n}} \cdot \hat{\mathbf{m}} g.$$

The surface integral over S_3 can therefore be written as

$$\int_{S_3} g \left(\frac{\partial u}{\partial \hat{\mathbf{n}}} - ik\hat{\mathbf{n}} \cdot \hat{\mathbf{m}} u \right) d^2\mathbf{r}.$$

For simplicity, if we consider S_3 to be a hemisphere of radius $R =\mid \mathbf{r} - \mathbf{r}_0 \mid$ with the origin at O say, then we may write this integral in the form

$$\int_{\Omega} \frac{\exp(ikR)}{4\pi R} \left(\frac{\partial u}{\partial \hat{\mathbf{n}}} - ik\hat{\mathbf{n}} \cdot \hat{\mathbf{m}} u \right) R^2 d\Omega$$

where Ω is the solid angle subtended by S_3 at O. If we now assume that

$$\lim_{R \to \infty} R \left(\frac{\partial u}{\partial \hat{\mathbf{n}}} + ik\hat{\mathbf{n}} \cdot \hat{\mathbf{m}} u \right) = 0$$

uniformly with angle, then the surface integral over S_3 can be neglected. This limiting condition is called the Sommerfeld Radiation Condition and is satisfied if $u \to 0$ as fast as $\mid \mathbf{r} - \mathbf{r}_0 \mid^{-1} \to 0$. With this requirement met, the only contribution to the surface integral will be in the plane of the aperture. Using the Kirchhoff boundary conditions we have

$$u(\mathbf{r}_0, k) = \int_S \left(g \frac{\partial u_i}{\partial \hat{\mathbf{n}}} - u_i \frac{\partial g}{\partial \hat{\mathbf{n}}} \right) d^2\mathbf{r}$$

where S is taken to be S_1. This equation is referred to as the Kirchhoff integral. Note that this integral is not a closed surface integral and so Green's theorem will not apply. Also note that, in deriving this result we have failed to take into account the finite width of the aperture and therefore the effect of the edges of the aperture on the field within the aperture. Thus, the model can only apply to apertures much larger than the wavelength of the field and for apertures which are 'thin'.

To compute the diffracted field using the Kirchhoff integral, an expression for u_i must be introduced and the derivatives $\partial/\partial\hat{\mathbf{n}}$ with respect to u_i and g evaluated. Let us consider the case where the incident field is a plane wavefield of unit amplitude (with wavenumber $k \equiv \mid \mathbf{k} \mid$, $\hat{\mathbf{k}} = \mathbf{k}/k$). Then

$$u_i = \exp(i\mathbf{k}\cdot\mathbf{r}),$$

$$\frac{\partial u_i}{\partial\hat{\mathbf{n}}} = \hat{\mathbf{n}}\cdot\nabla\exp(i\mathbf{k}\cdot\mathbf{r}) = i\mathbf{k}\cdot\hat{\mathbf{n}}\exp(i\mathbf{k}\cdot\mathbf{r}) = ik\hat{\mathbf{n}}\cdot\hat{\mathbf{k}}\exp(i\mathbf{k}\cdot\mathbf{r})$$

and the Kirchhoff diffraction formula reduces to the form

$$u(\mathbf{r}_0,k) = ik\int_S \exp(i\mathbf{k}\cdot\mathbf{r})(\hat{\mathbf{n}}\cdot\hat{\mathbf{k}} - \hat{\mathbf{n}}\cdot\hat{\mathbf{m}})g(\mathbf{r}\mid\mathbf{r}_0,k)d^2\mathbf{r}.$$

6.7.3 Fraunhofer Diffraction

Fraunhofer diffraction assumes that the diffracted wavefield is observed a large distance away from the screen and, as in previous Sections, is based on the asymptotic form of the Green function. For this reason, Fraunhofer diffraction is sometimes called diffraction in the 'far field'. The basic idea is to exploit the simplifications that can be made to the Kirchhoff diffraction integral by considering the case when

$$r_0 >> r$$

where $r \equiv \mid \mathbf{r} \mid$ and $r_0 \equiv \mid \mathbf{r}_0 \mid$. In this case,

$$\frac{1}{\mid \mathbf{r}-\mathbf{r}_0 \mid} \simeq \frac{1}{r_0}$$

and

$$\hat{\mathbf{n}}\cdot\hat{\mathbf{k}} - \hat{\mathbf{n}}\cdot\hat{\mathbf{m}} \simeq \hat{\mathbf{n}}\cdot\hat{\mathbf{k}} + \hat{\mathbf{n}}\cdot\hat{\mathbf{r}}_0$$

where

$$\hat{\mathbf{r}}_0 = \frac{\mathbf{r}_0}{r_0}$$

With regard to the term $\exp(ik \mid \mathbf{r}-\mathbf{r}_0 \mid)$,

$$\mid \mathbf{r}-\mathbf{r}_0 \mid \simeq r_0 - \mathbf{r}\cdot\hat{\mathbf{r}}_0$$

and, hence, the Kirchhoff diffraction integral reduces to

$$u(\mathbf{r}_0,k) \simeq \frac{ik\alpha}{4\pi r_0}\exp(ikr_0)\int_S \exp(i\mathbf{k}\cdot\mathbf{r})\exp(-ik\hat{\mathbf{r}}_0\cdot\mathbf{r})d^2\mathbf{r}$$

where $\alpha = \hat{\mathbf{n}}\cdot\hat{\mathbf{k}} + \hat{\mathbf{n}}\cdot\hat{\mathbf{r}}_0$. This is the Fraunhofer diffraction integral.

6.7.4 Fresnel Diffraction

Fresnel diffraction is based on considering the binomial expansion of $\mid \mathbf{r} - \mathbf{r}_0 \mid$ in the function $\exp(ik \mid \mathbf{r} - \mathbf{r}_0 \mid)$ to second order and retaining the term $r^2/2r_0$;

$$\mid \mathbf{r} - \mathbf{r}_0 \mid = r_0 - \mathbf{r} \cdot \hat{\mathbf{r}}_0 + \frac{r^2}{2r_0} + ...$$

$$\simeq r_0 - \mathbf{r} \cdot \hat{\mathbf{r}}_0 + \frac{r^2}{2r_0}.$$

This approximation is necessary when the diffraction pattern is observed in what is called the intermediate field, or Fresnel zone, in which

$$u(\mathbf{r}_0, k) \simeq \frac{ik\alpha}{4\pi r_0} \exp(ikr_0) \int_S \exp(i\mathbf{k} \cdot \mathbf{r}) \exp(-ik\mathbf{r}_0 \cdot \mathbf{r}) \exp\left(ik\frac{r^2}{2r_0}\right) d^2\mathbf{r}.$$

This is the Fresnel diffraction formula.

6.8 Summary of Important Results

Green function solution

The general solution to the equation

$$(\nabla^2 + k^2)u(\mathbf{r}, k) = -k^2\gamma(\mathbf{r})u(\mathbf{r}, k), \quad \mathbf{r} \in V$$

is

$$u(\mathbf{r}_0, k) = \oint_S \left(g\frac{\partial u}{\partial \hat{\mathbf{n}}} - u\frac{\partial g}{\partial \hat{\mathbf{n}}}\right) d^2\mathbf{r} + k^2 \int_V g(\mathbf{r} \mid \mathbf{r}_0, k)\gamma(\mathbf{r})u(\mathbf{r}, k)d^3\mathbf{r}$$

where

$$\frac{\partial u}{\partial \hat{\mathbf{n}}} \equiv \hat{\mathbf{n}} \cdot \nabla u \quad \text{and} \quad \frac{\partial g}{\partial \hat{\mathbf{n}}} \equiv \hat{\mathbf{n}} \cdot \nabla g.$$

Boundary conditioning

If $u = u_i$ on S where u_i satisfies the equation

$$(\nabla^2 + k^2)u_i = 0$$

then

$$\oint_S \left(g\frac{\partial u}{\partial \hat{\mathbf{n}}} - u\frac{\partial g}{\partial \hat{\mathbf{n}}}\right) d^2\mathbf{r} = u_i$$

The Born approximation

$$u = u_i + u_s$$

where

$$u_s(\mathbf{r}_0,k) = k^2 \int g(\mathbf{r} \mid \mathbf{r}_0,k)\gamma(\mathbf{r})u_i(\mathbf{r},k)d^3\mathbf{r}$$

provided

$$\|u_s(\mathbf{r},k)\| << \|u_i(\mathbf{r},k)\| \implies \bar{\gamma} << \frac{1}{k^2R^2}$$

where u_i and u_s are the incident and scattered fields respectively and R is the characteristic scale of the scattering function γ, $\mathbf{r} \in V$.

The Born series

$$u(\mathbf{r}_0,k) = u_i(\mathbf{r}_0,k) + u_s(\mathbf{r},k)$$

where

$$u_s(\mathbf{r},k) = k^2 \int_V g(\mathbf{r} \mid \mathbf{r}_0,k)\gamma(\mathbf{r})u_i(\mathbf{r},k)d^3\mathbf{r} =$$

$$k^2 \int_V g(\mathbf{r} \mid \mathbf{r}_0,k)\gamma(\mathbf{r}) \left[k^2 \int_V g(\mathbf{r}_1 \mid \mathbf{r},k)\gamma(\mathbf{r}_1)u_i(\mathbf{r}_1,k)d^3\mathbf{r}_1 \right] d^3\mathbf{r} + ...$$

$$= u_i(\mathbf{r}_0,k) + k^2 \int_V d^3\mathbf{r} g(\mathbf{r} \mid \mathbf{r}_0,k)\gamma(\mathbf{r})u_i(\mathbf{r},k)$$

$$+k^4 \int_V \int_V d^3\mathbf{r}d^3\mathbf{r}_1 g(\mathbf{r} \mid \mathbf{r}_0,k)\gamma(\mathbf{r})g(\mathbf{r}_1 \mid \mathbf{r},k)\gamma(\mathbf{r}_1)u_i(\mathbf{r}_1,k)$$

$$+k^6 \int_V \int_V \int_V d^3\mathbf{r}d^3\mathbf{r}_1 d^3\mathbf{r}_2 g(\mathbf{r} \mid \mathbf{r}_0,k)\gamma(\mathbf{r})g(\mathbf{r}_1 \mid \mathbf{r},k)\gamma(\mathbf{r}_1)g(\mathbf{r}_2 \mid \mathbf{r}_1,k)\gamma(\mathbf{r}_2)u_i(\mathbf{r}_2,k)$$

$$+ \quad ...$$

under the condition that

$$\|u_s(\mathbf{r},k)\| \leq< u_i(\mathbf{r},k)\| \implies \bar{\gamma} < \frac{1}{k^2R^2}$$

The Rytov approximation

$$u(\mathbf{r}_0,k) = u_i(\mathbf{r}_0,k) \exp\left[\frac{k^2}{u_i(\mathbf{r}_0,k)} \int_V u_i(\mathbf{r},k)\gamma(r)g(\mathbf{r} \mid \mathbf{r}_0,k)d^3\mathbf{r} \right]$$

on the condition that

$$\|k^2\gamma\| >> \|\nabla s \cdot \nabla s\|$$

where

$$s = \ln(u/u_i)$$

.

The WKB approximation

The solution to the equation

$$\left(\frac{\partial^2}{\partial x^2} + k^2\right) u(x,k) = -k^2\gamma(x)u(x,k), \quad x \in L$$

given by

$$u(x,k) = \exp\left[ik\left(x + \frac{1}{2}\int^x \gamma(x)dx\right)\right], \quad \lambda << L$$

The Sommerfeld radiation condition

$$\lim_{R\to\infty} R\left(\frac{\partial u}{\partial \hat{\mathbf{n}}} + ik\hat{\mathbf{n}}\cdot\hat{\mathbf{m}}u\right) = 0$$

Kirchhoff boundary conditions

$$u = u_i, \quad \frac{\partial u}{\partial \hat{\mathbf{n}}} = \frac{\partial u_i}{\partial \hat{\mathbf{n}}} \quad \text{on S}$$

where S is an open surface.

Kirchhoff diffraction integral

$$u(\mathbf{r}_0,k) = ik\int_S \exp(i\mathbf{k}\cdot\mathbf{r})(\hat{\mathbf{n}}\cdot\hat{\mathbf{k}} - \hat{\mathbf{n}}\cdot\hat{\mathbf{m}})g(\mathbf{r}\mid\mathbf{r}_0,k)d^2\mathbf{r}$$

Fraunhofer diffraction integral

$$u(\mathbf{r}_0,k) = \frac{ik\alpha}{4\pi r_0}\exp(ikr_0)\int_S \exp(i\mathbf{k}\cdot\mathbf{r})\exp(-ik\hat{\mathbf{r}}_0\cdot\mathbf{r})d^2\mathbf{r}$$

where $\alpha = \hat{\mathbf{n}}\cdot\hat{\mathbf{k}} + \hat{\mathbf{n}}\cdot\hat{\mathbf{r}}_0$.

Fresnel diffraction integral

$$u(\mathbf{r}_0,k) = \frac{ik\alpha}{4\pi r_0}\exp(ikr_0)\int_S \exp(i\mathbf{k}\cdot\mathbf{r})\exp(-ik\hat{\mathbf{r}}_0\cdot\mathbf{r})\exp\left(ik\frac{r^2}{2r_0}\right)d^2\mathbf{r}$$

6.9 Further Reading

- Morse P M and Feshbach H, *Methods of Theoretical Physics*, McGraw-Hill, 1953.
- Newton R G, *Scattering Theory of Waves and Particles*, Springer-Verlag, 1967.

- Taylor J G, *Introduction to Quantum Mechanics*, George Allen and Unwin, 1970.
- Butkov E, *Mathematical Physics*, Addison-Wesley, 1973.
- Newton R G, *Inverse Schrödinger Scattering in Three Dimensions*, Springer, 1989.

Chapter 7

Imaging of Layered Media

Many imaging methods are based on the assumption that the scattering body is composed of layers. This highly idealized model reduces the dimension of a scattering problem to one dimension. In some special cases, this is consistent with the physical nature of the imaging system especially if: (i) the scattering function is a one-dimensional function; (ii) the incident wavefield is a 'pencil-line beam'.

Seismic imaging

The propagation and reflection of seismic waves through the Earth has been studied intensively in the context of the exploration of oil, coal and natural gas. In this case, an image is generated of the interior structure of the ground. This provides information on the geology of regions which are often stratified. Hence, seismic imaging can often be based on the theory of scattering from layered media. Seismic prospecting is conducted either on land or at sea. Seismic waves are generated by chemical explosions or vibrating impacts of short duration. By recording the time history of the reflected seismic waves, information on the nature and geological significance of the Earth's interior can be obtained.

An interesting example of a seismic image is given in Figure 7.1. This type of image is produced by collecting together and displaying side-by-side the seismic signals which are produced at different shot locations (the location of a small chemical explosion below the surface of the Earth) as shown in Figure 7.2. The seismic signals may be recorded over both sides of the shot or over just one side (the latter case being more common). Each signal or 'trace' is the sum of all those signals that have been detected by a linear array of geophones extending away from the shot location after they have been corrected for normal moveout, i.e. aligned to coincide with reflections from points at a common depth. This is called 'stacking' and a seismic image of this type is therefore usually known as a Common Depth Point (CDP) stack. It provides a set of seismic signals with an improved signal-to-noise ratio compared to the original pre-stacked data. It also reduces episodes in the data which are due to multiple scattering by enhancing the amplitudes of the primary or single scattering events. In effect, this process conditions the data in such a way as to make it conform better to

a Born scattering model.

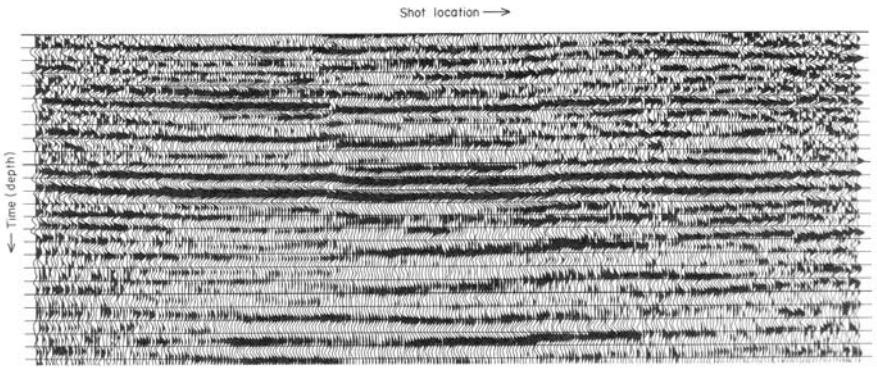

Figure 7.1: Example seismic image of a section of the South Yorkshire coal fiel

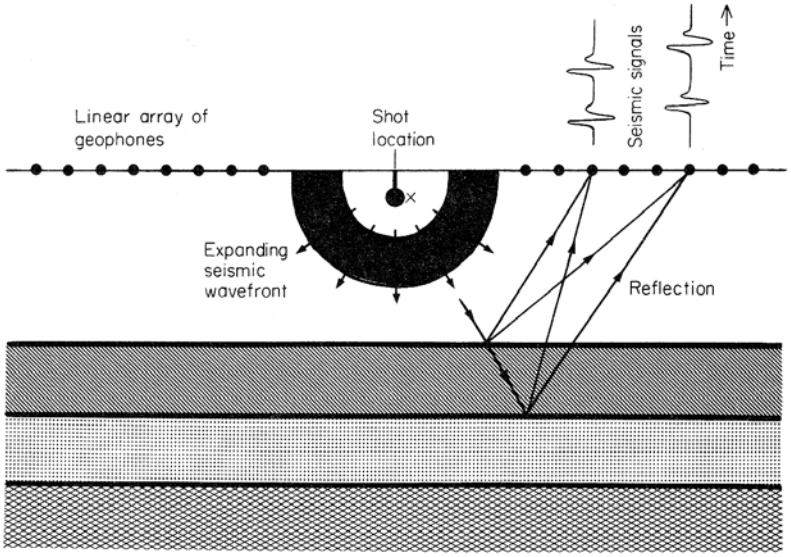

Figure 7.2: A small charge is placed below the surface of the earth at the point marked X. The explosion creates a seismic wave which travels through the earth and is reflected at interfaces between different rock strata. The seismic reflections travel back to the surface of the earth where they are recorded by a linear array of geophones either over both sides or more commonly, just one side of the shot. The recorded signals are corrected for normal moveout and added together to form a single trace improving the signal-to-noise ratio which, in effect, provides data on the scattered field that can be modelled using the Born approximation. By repeating this type of experiment for different shot locations, a seismic image can be built up of the type given in Figure 7.1.

The example given in Figure 7.1 shows a region of the South Yorkshire coal field. It is conventional to shade in the area under the positive lobes of each trace to emphasize the lateral correlation of the data. This makes it easier for a geologist to distinguish between layers of geological interest. In this image, the main event (which occurs approximately half way down the image) is due to seismic reflections from a coal seam.

Ultrasonic imaging

Another example where it is often assumed that the scattering object has a layered structure is in imaging with ultrasound. This is used extensively for the nondestructive evaluation of objects and for medical imaging. In the latter case, the layers are of different tissue types. Reflections of an ultrasonic pulse are generated at the interface between these layers. By moving the source of ultrasound (the transducer) and displaying the amplitude envelope of the ultrasonic signals on a visual display unit, an image can be generated which is known as a 'brightness' or B-scan as illustrated in Figure 7.3. In practice, an array of transducers is used which may be linear or curvilinear. This allows an experienced radiologist to judge the pathological state of the tissues. In some cases, a dramatic difference can be observed between healthy and unhealthy tissues. An example of this is provided in Figure 7.4. This shows two transverse B-scans of the thigh for a normal patient (left) and a patient suffering from muscular dystrophy (right) where the muscle wastes away, being replaced in part by fatty tissues. Figure 7.4 demonstrates that, in healthy tissue, the B-scan illustrates bulk anatomical features such as the skin (S), fascia lata (FL) and bone (B) which are clearly defined. In the case of muscular dystrophy, the B-scan demonstrates the striking differences in intensity and diffuseness of the scattered ultrasonic field in the muscle compared with normal muscle and the absence of scattering from bone.

Discussion

In addition to the examples discussed above, there are many other applications in acoustic imaging. Further, a variety of electromagnetic imaging systems can be 'cast' in terms of problems involving layered materials (e.g. the response of light, radio and microwaves to layered dielectric materials including the transmission of electromagnetic waves along transmission such as an optical fiber). Also, problems that involve radial symmetry may often be reduced to a form where one-dimensional scattering theory can be employed. One-dimensional scattering models may also be used effectively in cases when the probe is a narrow collimated beam - a so-called 'pencil' or 'pencil-line' beam although in reality all beams diverge. Ideally, all imaging theory should be fully three-dimensional. No arguments can then arise about the geometrical validity of the theory. However, it is often useful to reduce the dimension of a theoretical model for a physical problem when the opportunity arises, and this is the subject of this Chapter.

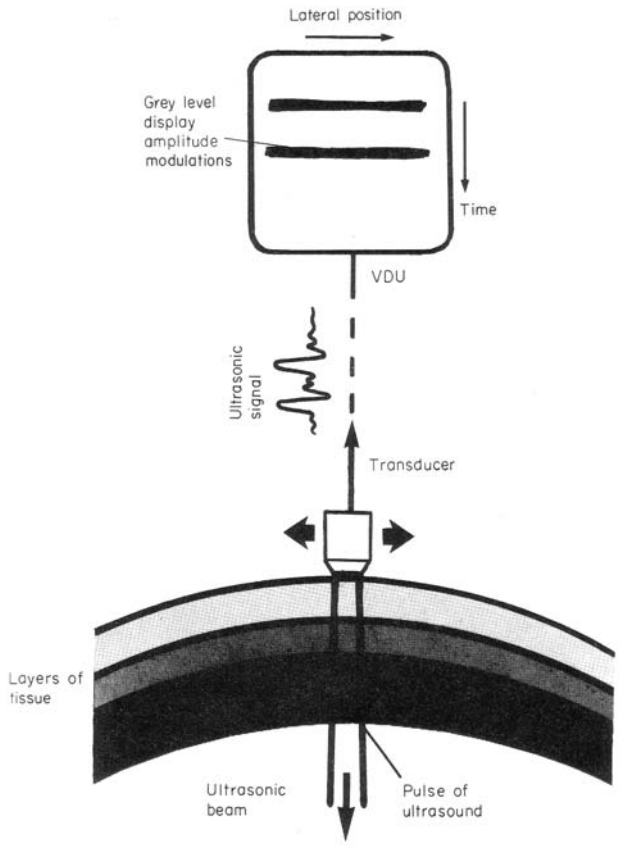

Figure 7.3: Medical imaging with ultrasound utilizes a short side-band pulse which is emitted by a transducer. The pulse is reflected by the tissue layers. The characteristic signal is recoded, demodulated and the amplitude modulations displayed on a visual display unit. Lateral movement of the transducer provides an ultrasonic image (a 'brightness' or B-scan).

7.1 Pulse-Echo Imaging

All the imaging methods that are discussed in this Chapter can be classified in terms of 'pulse-echo' imaging. This is where a short pulse of radiation is emitted from a source and the 'time history' of the scattered field is recorded by a receiver which is placed in the vicinity of the location of the source. By moving both the source and receiver and repeating this type of experiment, an image can be built up based on the nature of the reflected pulse at different source locations. The resolution that can be obtained with pulse-echo experiments of this type is determined by the length of the pulse that is used and the width of

the beam. To obtain high resolution, a short pulse and narrow 'pencil beam' are required. In some cases, the lateral resolution can be synthesized. This type of imaging is known as synthetic aperture imaging and is discussed later on in this work.

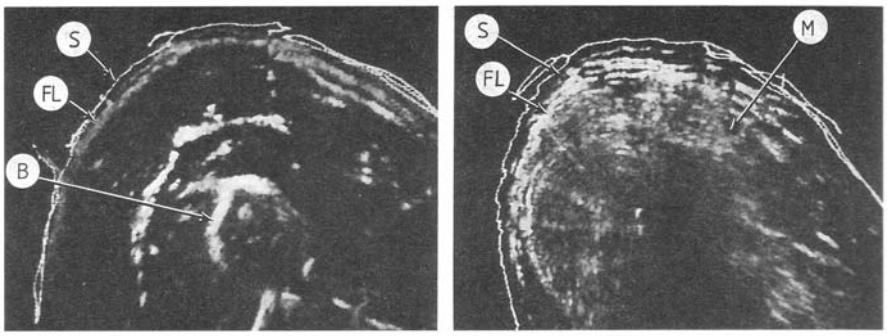

Figure 7.4: Transverse B-scans of a healthy thigh (left) and the thigh of a patient with Duchenne dystrophy (right). S-skin, FL-faccia lata, B-bone, M-muscle.

In a pulse-echo experiment, the receiver monitors the time history of the reflected waves (the echo). After a short delay (which depends on the distance of the source from the scatterer and the speed at which the pulse propagates), the first reflections are received followed by a series or 'train' of other reflections from the interior of the material. This process continues until all the energy of the pulse has been dissipated. In each case, the receiver produces a voltage trace which is proportional to the variations in time of the reflected waves. For example, in seismic imaging, the pulse is often produced by detonating a small charge which is placed in the ground. Seismic reflections are monitored by an array of instruments called geophones. A geophone consists of a thin wire coil which is free to move through a radial magnetic field induced by a bar magnet around which the coil is mounted. The geophone is weighted so that the coil moves in sympathy with the motion of the ground surface that is induced by the arrival of seismic reflections. The oscillation of the coil then produces a time varying voltage which can be amplified and recorded in analogue and then digitized. Thus, a record of the time history of the seismic waves is obtained. In ultrasonic imaging, the pulse is produced by an instrument known as a transducer. This instrument translates an electrical impulse into a mechanical impulse or visa versa. The reflected ultrasonic pressure waves induce motion of the transducer face which consequently produces a time varying voltage. As before, the time varying signal is amplified and digitized, providing data on the time history of the scattered field at a point in space. In electromagnetic imaging (time-history resolved), the scattered electric field is measured by the

way in which it induces a time varying voltage in an antenna.

Pulse-echo imaging is based on using wavefields at frequencies where the time variations of the wavefield can be recorded to produce a set of signals. In acoustics, the frequency range is from Hz - MHz. In electromagnetics, it is generally from kHz - GHz. Apart from synthetic aperture imaging systems, most pulse-echo based systems provide partially coherent (in time) images. There is one important difference between them, however, which is concerned with whether or not the pulse is a side-band of base-band wavefield. Baseband pulses are multi-frequency wavefields with a frequency range from 0-Ω Hz where Ω is the bandwidth of the pulse. Sideband pulses are fields with a bandwidth of Ω but with a central frequency of ω_0, the carrier frequency of the pulse, where typically, $\omega_0 >> \Omega$. In side-band systems, it is usual to demodulate back to base-band and then digitize the resulting signal(s). Sideband systems are a natural consequence of utilizing high frequency radiation sources where the pulse length is much longer than the wavelength. Thus, suppose a pulse of radiation denoted by $p(t)$ has a spectrum $P(\omega)$ where $\mid \omega \mid \leq \Omega$. Then, for a base-band system we have

$$p(t) \Longleftrightarrow P(\omega)$$

but for a side-band system

$$p(t)\exp(i\omega_0 t) \Longleftrightarrow P(\omega) \otimes \delta(\omega - \omega_0) = P(\omega - \omega_0).$$

In the latter case, there are many oscillations of the field over the duration of the pulse and hence we have $p(t)\exp(i\omega_0 t)$ rather than just $p(t)$.

Basic Equation

The signal produced in a pulse-echo experiment is described by the equation

$$s(t) = p(t) \otimes f(t) + n(t)$$

where p is the pulse, f is the object function and n is the noise. Here, p describes the profile in time of the pulse that is used to probe the material and f describes the response of the material to this probe. For this reason, f is called the impulse response function. It represents the signal that would be produced in the hypothetical case when p is an infinitely short pulse (an impulse or delta function) when

$$s(t) = \delta(t) \otimes f(t) + n(t) = f(t) + n(t).$$

The basic processing that is undertaken in pulse-echo imaging involves the reconstruction of f from s. This is known as deconvolution. The resolution in time that can be obtained in a pulse-echo experiment of this kind is determined by the length of the pulse - the shorter the pulse, the greater the resolution. In practice, the length of the pulse is limited by a number of technical and physical constraints such as the amount of energy that is required to penetrate the material. In the latter case, a major factor is the characteristic absorption of the material which tends to increase at higher frequencies in a manner that

is invariably nonlinear. For example, in acoustic imaging, the absorption coefficient (responsible for negative exponential decay) is proportional to the square of the frequency (in a viscous medium). In electromagnetism, the absorption is proportional to the square root of the frequency (in a conductive medium).

The pulse p depends upon the imaging system that is used, whereas the impulse response is a description for the material that is being imaged. A pulse-echo imaging system attempts to find out as much about the nature of the impulse response function as possible. To generate quantitative images of a layered material, expressions for the impulse response function must be derived in terms of an appropriate set of material parameters. In the following Sections, expressions for this function are derived for an electromagnetic and acoustic continuum with a layered structure. To do this, we employ the Born approximation. This approximation leads to an expression for the reflected field which is of the same form as $s = p \otimes f$. Here, the principal assumption is that multiple scattering does not contribute to the information in the signal.

7.2 EM Imaging of a Layered Dielectric

From Maxwell's equations, the wave equation for an electric field in a material composed of variations in the permittivity ϵ permeability μ and conductivity σ is given by (see Chapter 4)

$$\nabla \times \nabla \times \mathbf{E} + \epsilon\mu \frac{\partial^2 \mathbf{E}}{\partial t^2} + \mu\sigma \frac{\partial \mathbf{E}}{\partial t} = (\nabla \ln \mu) \times \nabla \times \mathbf{E} \tag{7.1}$$

We now introduce the following model:

1. A plane layered conductive dielectric

$$\epsilon = \epsilon(x); \quad \mu = \mu(x); \quad \sigma = \sigma(x) \tag{7.2}$$

2. A plane polarized **E**-field

$$\mathbf{E} = \hat{\mathbf{z}} E_z(x, y, t) \tag{7.3}$$

Our aim is to solve the inverse Born scattering problem posed by this model and reconstruct ϵ, μ and σ.

Substituting equations (7.2) and (7.3) into equation (7.1) we obtain

$$\left(\frac{\partial^2}{\partial x^2} + \frac{\partial^2}{\partial y^2} \right) E_z - \epsilon\mu \frac{\partial^2 E_z}{\partial t^2} - \mu\sigma \frac{\partial E_z}{\partial t} = \frac{d \ln \mu}{dx} \frac{\partial E_z}{\partial x}. \tag{7.4}$$

By introducing the Fourier transform

$$E_z(x, y, t) = \frac{1}{2\pi} \int_{-\infty}^{\infty} \widetilde{E}_z(x, y, \omega) \exp(i\omega t) d\omega$$

equation (7.4) can be written in the form

$$\left(\frac{\partial^2}{\partial x^2}+\frac{\partial^2}{\partial y^2}\right)\widetilde{E}+\omega^2\epsilon\mu\left(1-\frac{i}{\omega\tau}\right)\widetilde{E}_z=\frac{d\ln\mu}{dx}\frac{\partial\widetilde{E}_z}{\partial x}$$

where

$$\tau=\frac{\epsilon}{\sigma}.$$

The parameter τ is called the relaxation time. For one-dimensional scattering problems of this kind, it is convenient to separate the electric field into two components. Since the material is homogeneous in the y-direction, we can write the electric field as

$$\widetilde{E}_z(x,y,\omega)=u(x,\omega)\exp(-iky\sin\theta),\quad k=\frac{\omega}{c_0}$$

where θ is the angle of incidence and c_0 is the velocity of the electromagnetic waves in a vacuum. Using this result, the wave equation above can be reduced to the form

$$\left[\frac{\partial^2}{\partial x^2}+\omega^2\epsilon\mu\left(1-\frac{i}{\omega\tau}\right)\right]u=\frac{d\ln\mu}{dx}\frac{\partial u}{\partial x}+u\frac{\omega^2}{c_0^2}\sin^2\theta. \tag{7.5}$$

We see that this equation is inhomogeneous on both the left- and right-hand sides. The next thing to do is to write this equation in a form that enables us to use the appropriate Green function to solve it. This could be done using the methods discussed in Chapter 4. However, in one-dimensional (and only 1D) problems, it is more elegant to do this by introducing the transform

$$\frac{dx}{d\xi}=c(\xi). \tag{7.6}$$

This is known as the travel time transformation. The parameter ξ is the travel time and c is the velocity profile of the inhomogeneous dielectric given by

$$c=\frac{1}{\sqrt{\epsilon\mu}}.$$

Using the chain rule together and equation (7.6) we can write

$$\frac{\partial^2 u}{\partial x^2}=\frac{1}{c^2}\frac{\partial^2 u}{\partial\xi^2}-\frac{1}{c^3}\frac{dc}{d\xi}\frac{\partial u}{\partial\xi}$$

and

$$\frac{d\ln\mu}{dx}\frac{\partial u}{\partial x}=\frac{1}{c^2}\frac{d\ln\mu}{d\xi}\frac{\partial u}{\partial\xi}.$$

Noting that

$$\frac{1}{c}\frac{dc}{d\xi}=\frac{d\ln c}{d\xi}$$

equation (7.5) then becomes

$$\left(\frac{d^2}{d\xi^2}+\omega^2\right)u=-\hat{L}u$$

where

$$\hat{L}u = -\frac{d\ln Z}{d\xi}\frac{\partial u}{\partial \xi} - \frac{i\omega}{\tau}u - u\omega^2\frac{c^2}{c_0^2}\sin^2\theta$$

and

$$Z = \mu c.$$

The parameter Z is called the impedance. Using the Born approximation, the equation for the scattered field u_s becomes

$$\left(\frac{\partial^2}{\partial \xi^2} + \omega^2\right) u_s = -\hat{L}u_i$$

where u_i is the incident field. In a pulse-echo experiment, u_s is the reflected or back-scattered field that is produced by the emission of a pulse $p(t)$ with a spectrum $P(\omega)$ where

$$p(t) = \frac{1}{2\pi}\int_{-\infty}^{\infty} P(\omega)\exp(i\omega t)d\omega.$$

Consider a pulse-echo experiment which utilizes a right travelling pulse. In this case

$$u_i = P\exp(-i\omega\xi) \tag{7.7}$$

and so

$$\hat{L}u_i = i\omega P\exp(-i\omega\xi)\frac{d}{d\xi}\ln Z - \frac{i\omega}{\tau}P\exp(-i\omega\xi) - \omega^2 P\exp(-i\omega\xi)\frac{c^2}{c_0^2}\sin^2\theta. \tag{7.8}$$

The reflected field travels in the opposite direction to the incident field. Hence, in this case, we must use the Green function which represents a left-travelling wave, i.e.

$$g(\xi \mid \xi_0, \omega) = \frac{i}{2\omega}\exp(i\omega \mid \xi - \xi_0 \mid).$$

The back-scattered field at ξ_0 is then given by

$$u_s(\xi_0, \omega) = \frac{i}{2\omega}\int_{-\infty}^{\infty} \exp(i\omega \mid \xi - \xi_0 \mid)\hat{L}u_i d\xi.$$

In the far field, when $\xi_0 >> \xi$, $\mid \xi - \xi_0 \mid = \xi_0 - \xi$ and

$$u_s(\xi_0, \omega) = \exp(i\omega\xi_0)S(\omega)$$

where S is the reflection coefficient given by

$$S(\omega) = \frac{i}{2\omega}\int_{-\infty}^{\infty} \exp(-i\omega\xi)\hat{L}u_i d\xi. \tag{7.9}$$

Substituting equation (7.8) into equation (7.9) we obtain

$$S(\omega) = \frac{P}{2} \int_{-\infty}^{\infty} \left(-\frac{d}{dt} \ln Z + \frac{1}{2\tau} \right) \exp(-i\omega t) dt$$

$$-\frac{i\omega P \sin^2 \theta}{4c_0^2} \int_{-\infty}^{\infty} c^2 \exp(-i\omega t) dt$$

where $t = 2\xi$ (the two-way travel time). By taking the inverse Fourier transform of this equation, noting that

$$i\omega c^2 \Longleftrightarrow \frac{d}{dt} c^2$$

and using the convolution theorem, we obtain

$$s_\theta(t) = p(t) \otimes f_\theta(t) \tag{7.10}$$

where

$$f_\theta = -\frac{1}{2} \frac{d}{dt} \ln Z + \frac{1}{4\tau} - \frac{\sin^2 \theta}{4c_0^2} \frac{dc^2}{dt}.$$

The function $s_\theta(t)$ represents the time varying signal that is measured in an experiment of the type illustrated in Figure 7.5. In this example, the electromagnetic pulse is a right-travelling pulse. It travels through a homogeneous medium where the velocity of the wave is constant and the relaxation time is infinitely long (i.e. the conductivity is zero). The pulse is incident on the inhomogeneous region at an angle θ to the normal and the scattered field is observed at an angle 2θ to the path of the incident pulse. The receiver converts variations in the electric field as a function of the two-way travel time t into a voltage trace. The function $s_\theta(t)$ is taken to describe this voltage trace.

Equation (7.10) is based on a solution for a right-travelling incident pulse. To indicate this we write s_θ and f_θ with the superscript $^-$. Equation (7.10) then becomes

$$s_\theta^-(t) = p(t) \otimes f_\theta^-(t)$$

An equally valid solution can be constructed by considering the case when a left travelling pulse is incident on the material. In this case, equation (7.7) is replaced by

$$u_i = P \exp(i\omega\xi)$$

and we must use the Green function which represents a right-travelling wave, i.e.

$$g(\xi \mid \xi_0, \omega) = \frac{i}{2\omega} \exp(-i\omega \mid \xi - \xi_0 \mid)$$

$$= \frac{i}{2\omega} \exp(i\omega\xi) \exp(-i\omega\xi_0), \quad \xi_0 >> \xi.$$

In this case, the reflection coefficient becomes

$$S(\omega) = \frac{i}{2\omega} \int_{-\infty}^{\infty} \exp(i\omega\xi)\hat{L}u_i d\xi$$

where

$$\hat{L}u_i = -i\omega P \exp(i\omega\xi)\frac{d}{d\xi}\ln Z - \frac{i\omega}{\tau}P\exp(i\omega\xi) - \omega^2 P\exp(i\omega\xi)\frac{c^2}{c_0^2}\sin^2\theta.$$

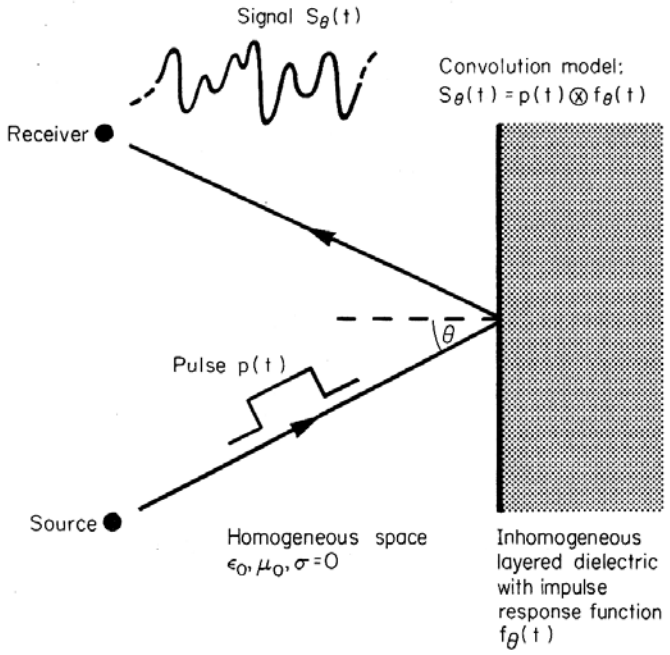

Figure 7.5: Illustration of the method for imaging an inhomogeneous layered dielectric with impulse response function $f_\theta(t)$ using a pulse $p(t)$ incident at an angle θ.

Evaluating this integral and taking the inverse Fourier transform, we then obtain an expression for the signal produced by a left-travelling incident pulse. This is given by

$$s_\theta^+(t) = p(t) \otimes f_\theta^+(t)$$

where

$$f_\theta^+ = \frac{1}{2}\frac{d}{dt}\ln Z + \frac{1}{4\tau} - \frac{\sin^2\theta}{4c_0^2}\frac{dc^2}{dt}.$$

Hence, we can write the general solution for a left (+) or right (−) travelling pulse as

$$s_\theta^\pm = p(t) \otimes f_\theta^\pm(t)$$

where

$$f_\theta^\pm(t) = \pm\frac{1}{2}\frac{d}{dt}\ln Z + \frac{1}{4\tau} - \frac{\sin^2\theta}{4c_0^2}\frac{dc^2}{dt}. \tag{7.11}$$

The calculations given above provide us with expressions for the signal, where the impulse response function is defined in terms of the material parameters ϵ, μ and σ. In addition to this, we know that a change in the direction of the incident pulse only effects the polarity of one term in the impulse response functions, namely $\frac{1}{2}d\ln Z/dt$. This result allows us to obtain a quantitative solution to the three-parameter problem (ϵ, μ, σ). By generating the data

$$s_0^+ = p \otimes f_0^+,$$

$$s_0^- = p \otimes f_0^-,$$

and

$$s_\theta^+ = p \otimes f_\theta^+$$

and deconvolving[1] each signal, we can construct the simultaneous equations

$$f_0^+ = \frac{1}{2}\frac{d}{dt}\ln Z + \frac{1}{4\tau},$$

$$f_0^- = -\frac{1}{2}\frac{d}{dt}\ln Z + \frac{1}{4\tau},$$

$$f_\theta^+ = \frac{1}{2}\frac{d}{dt}\ln Z + \frac{1}{4\tau} - \frac{\sin^2\theta}{4c_0^2}\frac{dc^2}{dt}.$$

Defining the functions

$$f_1 = f_0^+ - f_0^-,$$
$$f_2 = f_0^+ + f_0^-,$$
$$f_3 = f_0^+ - f_\theta^+,$$

the following equations are obtained,

$$f_1 = \frac{d}{dt}\ln Z,$$

$$f_2 = \frac{1}{2\tau},$$

$$f_3 = \frac{\sin^2\theta}{4c_0^2}\frac{dc^2}{dt}.$$

It is then a simple matter to solve each of these equations. Using the initial conditions,

$$Z(t) = Z_0, \quad t = 0;$$

[1]Deconvolution is discussed at length in *Digital Signal Processing*, Horwood, 2003.

$$c(t) = c_0, \quad t = 0;$$

$$\int^t f_1(t')dt' = 0, \quad t = 0,$$

and

$$\int^t f_3(t')dt' = 0, \quad t = 0$$

we obtain

$$Z(t) = Z_0 \exp\left(\int^t f_1(t')dt'\right),$$

$$\tau(t) = \frac{1}{2f_2(t)},$$

and

$$c(t) = c_0\left(1 + \frac{4}{\sin^2\theta}\int^t f_3(t')dt'\right)^{\frac{1}{2}}.$$

Using the definitions for Z, c and τ, the required set of parameters are given by

$$\epsilon = \frac{1}{Zc},$$

$$\mu = \frac{Z}{c},$$

and

$$\sigma = \frac{1}{Zc\tau}.$$

These solutions can be written as a function of the displacement x by inverting the travel time transform, i.e. equation (7.6). This gives

$$x(\xi) = \int^\xi c(\xi')d\xi'.$$

The method of quantitative imaging given here assumes that the deconvolution is ideal and that the impulse response functions can be recovered perfectly from the signal, i.e. some function $q(t)$ exists such that $q(t) \otimes p(t) = \delta(t)$. This of course is not possible because in reality each signal will be noisy, i.e.

$$s_0^+ = p \otimes f_0^+ + n^+,$$

$$s_0^- = p \otimes f_0^- + n^-,$$

and

$$s_\theta^+ = p \otimes f_\theta^+ + n_\theta^+.$$

However, we can still use the results under the assumption that f_0^+, f_0^- and f_θ^+ are band-limited spectral approximations to the ideal impulse response functions given.

Observe that at normal incidence (i.e. when $\theta = 0$), the impulse response function for a left-travelling incident pulse is

$$f_0^+(t) = \frac{1}{2}\frac{d}{dt}\ln Z + \frac{1}{4\tau}.$$

When the conductivity is zero, only the first term contributes to the result (since $1/\tau = \sigma/\epsilon$). The strength of the reflected signal is determined not by the value of the impedance but by the tie derivative of its logarithm. An everyday example of this is the reflection of light from a glass plate. If such a glass plate is then coated with a highly conductive material such as mercury, then the impulse response function is determined by the additional term $\frac{\sigma}{4\epsilon}$. In this case, the strength of the reflection is additionally determined by the value of the conductivity; what we have is a mirror!

7.3 Acoustic Imaging of a Layered Material

The same method as that used in the previous Section can be employed to study the reflection of an acoustic pulse from a layered acoustic continuum. The basic aim of the calculation is the same. However, because the wave equation for an acoustic field is more complicated, the calculations are a little more involved.

It was shown in Chapter 4 that the basic wave equation for the compressional velocity field $\mathbf{v}$ is given by

$$\rho\frac{\partial^2}{\partial t^2}\mathbf{v} = \nabla\left(\frac{1}{\kappa}\nabla\cdot\mathbf{v}\right) + \frac{\partial}{\partial t}\nabla\cdot(\alpha\mathbf{I}\nabla\cdot\mathbf{v} + 2\beta\nabla\mathbf{v}) \tag{7.11}$$

assuming that the shear wave component is negligible, or

$$\nabla\times\mathbf{v} = 0.$$

We now consider the following models:

1. A layered viscous continuum

$$\rho = \rho(x), \quad \kappa = \kappa(x), \quad \alpha = \alpha(x), \quad \beta = \beta(x). \tag{7.12}$$

2. A compressional velocity field

$$\mathbf{v} = \hat{\mathbf{x}}v_x(x, y, t). \tag{7.13}$$

Our problem is to solve the inverse acoustic Born scattering problem posed by this model.

Using the vector identity

$$\nabla\times\nabla\times\mathbf{v} = -\nabla^2\mathbf{v} + \nabla\nabla\cdot\mathbf{v}$$

we note that, if $\nabla\times\mathbf{v} = 0$, then

$$\nabla^2\mathbf{v} = \nabla\nabla\cdot\mathbf{v}.$$

Using this result, equation (7.11) becomes

$$\rho\frac{\partial^2}{\partial t^2}\mathbf{v} = \frac{1}{\kappa}\nabla^2\mathbf{v} - \frac{1}{\kappa^2}(\nabla\kappa)\nabla\cdot\mathbf{v}$$

$$+(\alpha+2\beta)\frac{\partial}{\partial t}\nabla^2\mathbf{v} + \frac{\partial}{\partial t}(\nabla\alpha)\nabla\cdot\mathbf{v} + 2\frac{\partial}{\partial t}(\nabla\beta)\cdot\nabla\mathbf{v}.$$

Substituting equations (7.12) and (7.13) into this equation and rearranging, we then obtain

$$\left(1+\tau\frac{\partial}{\partial t}\right)\left(\frac{\partial^2}{\partial x^2}+\frac{\partial^2}{\partial y^2}\right)v_x - \kappa\rho\frac{\partial^2 v_x}{\partial t^2} = \frac{1}{\kappa}\frac{d\kappa}{dx}\frac{\partial v_x}{\partial x}$$

$$-\kappa\frac{d}{dx}(\alpha+2\beta)\frac{\partial^2 v_x}{\partial x\partial t}$$

where τ is the relaxation time of the acoustic material given by

$$\tau = \kappa(\alpha+2\beta).$$

Introducing the Fourier transform,

$$v_x(x,y,t) = \frac{1}{2\pi}\int_{-\infty}^{\infty} V_x(x,y,\omega)\exp(i\omega t),$$

this equation becomes

$$(1+i\omega\tau)\left(\frac{\partial^2}{\partial x^2}+\frac{\partial^2}{\partial y^2}\right)V_x + \kappa\rho\omega^2 V_x$$

$$= \frac{1+i\omega\tau}{\kappa}\frac{d\kappa}{dx}\frac{\partial V_x}{\partial x} - i\omega\frac{d\tau}{dx}\frac{\partial V_x}{\partial x}. \tag{7.14}$$

In this case, our problem is to reconstruct the density ρ, the compressibility κ and the bulk viscosity $\alpha+2\beta$. To do this, exactly the same procedure as before can be used. Thus, we write

$$V_x(x,y,\omega) = u(x,\omega)\exp(-iky\sin\theta), \quad k = \frac{\omega}{c_0}$$

and introduce the travel time transformation

$$\frac{dx}{d\xi} = c(\xi)$$

where c is the acoustic velocity given by

$$c = \frac{1}{\sqrt{\rho\kappa}}.$$

From equation (7.14) we then obtain

$$\left(\frac{d^2}{d\xi^2}+\omega^2\right)u = -(1+i\omega\tau)\frac{d}{d\xi}\ln Z\frac{\partial u}{\partial\xi}$$

$$-i\omega\frac{d\tau}{d\xi}\frac{\partial u}{\partial \xi} - i\omega\tau\frac{\partial^2 u}{\partial \xi^2} + u(1+i\omega\tau)\omega^2\frac{c^2}{c_0^2}\sin^2\theta$$

where Z is the acoustic impedance given by

$$Z = \rho c = \sqrt{\rho/\kappa}.$$

Using the Born approximation and repeating the same type of calculation that was performed in Section 7.2, it can be shown that the signal produced by a right-travelling pulse is given by

$$s_\theta^-(t) = p(t) \otimes f_\theta^-(t)$$

where

$$f_\theta^- = \frac{1}{2}\frac{d}{dt}\ln Z + \frac{1}{2}\frac{d}{dt}\left(\tau\frac{d}{dt}\ln Z\right) + \frac{3}{4}\frac{d^2\tau}{dt^2} + \frac{\sin^2\theta}{4c_0^2}\frac{d}{dt}\left(c^2 + \frac{d}{dt}(\tau c^2)\right)$$

and, for a left-travelling pulse, is given by

$$s_\theta^+(t) = p(t) \otimes f_\theta^+(t)$$

where

$$f_\theta^+ = -\frac{1}{2}\frac{d}{dt}\ln Z + \frac{1}{2}\frac{d}{dt}\left(\tau\frac{d}{dt}\ln Z\right) + \frac{3}{4}\frac{d^2\tau}{dt^2} + \frac{\sin^2\theta}{4c_0^2}\frac{d}{dt}\left(c^2 + \frac{d}{dt}(\tau c^2)\right).$$

At this stage, it is interesting to compare the acoustic impulse response function with the electromagnetic impulse response function derived in Section 7.2. First of all, notice that, when $\theta = 0$ and $\tau = 0$, the impulse response functions for both the electromagnetic and acoustic models are the same. In this case, reflections are induced by variations in the impedance Z alone. The major difference between the two models occurs when variations in the relaxation time τ are present. Notice that the strength of the reflection of an electromagnetic wave induced by variations in τ is determined by the magnitude of $1/\tau$ which is proportional to the conductivity of the material. However, the strength of the reflection of an acoustic wave is determined by both the first and second derivatives of τ. This means that even if the average viscosity of the material is small, a sudden change in this parameter can still generate strong reflections of an acoustic wave.

By recording the signals s_0^+, s_0^- and s_θ^+ and deconvolving, we can, in principle, generate the functions

$$f_0^+ = -\frac{1}{2}\frac{d}{dt}\ln Z + \frac{1}{2}\frac{d}{dt}\left(\tau\frac{d}{dt}\ln Z\right) + \frac{3}{4}\frac{d^2\tau}{dt^2},$$

$$f_0^- = \frac{1}{2}\frac{d}{dt}\ln Z + \frac{1}{2}\frac{d}{dt}\left(\tau\frac{d}{dt}\ln Z\right) + \frac{3}{4}\frac{d^2\tau}{dt^2},$$

and

$$f_\theta^+ = -\frac{1}{2}\frac{d}{dt}\ln Z + \frac{1}{2}\frac{d}{dt}\left(\tau\frac{d}{dt}\ln Z\right) + \frac{3}{4}\frac{d^2\tau}{dt^2} + \frac{\sin^2\theta}{4c_0^2}\frac{d}{dt}\left(c^2 + \frac{d(\tau c^2)}{dt}\right).$$

We are then faced with the problem of solving these three simultaneous equations for the functions Z, τ and c. To do this we generate the data

$$f_1 = f_0^+ - f_0^-,$$

$$f_2 = f_0^+ + f_0^-,$$

and

$$f_3 = f_\theta^+ - f_0^+$$

so that we can write

$$f_1 = -\frac{d}{dt}\ln Z, \tag{7.15}$$

$$f_2 = \frac{d}{dt}\left(\tau\frac{d}{dt}\ln Z\right) + \frac{3}{2}\frac{d^2\tau}{dt^2} \tag{7.16}$$

and

$$f_3 = \frac{\sin^2\theta}{4c_0^2}\frac{d}{dt}\left(c^2 + \frac{d(\tau c^2)}{dt}\right). \tag{7.17}$$

Compared to the electromagnetic case, these equations are not as easy to solve except for equation (7.15) whose solution is

$$Z(t) = Z_0 \exp\left(-\int^t f_1(t')dt'\right)$$

where

$$Z = Z_0, \quad t = 0$$

and

$$\int^t f_1(t')dt' = 0, \quad t = 0.$$

This solution is often used in acoustic imaging when the angle of incidence of the pulse is zero ($\theta = 0$) under the assumption that the viscosity of the material is also zero ($\tau = 0$). The reconstruction of the impedance from a signal by deconvolution and application of the above formula is known as impediography which is discussed later.

Solution to Equation (7.16)

Using the initial conditions

$$\frac{dZ}{dt} = 0, \quad t = 0;$$

$$\frac{d\tau}{dt} = 0, \quad t = 0;$$

and

$$\int^t f_2(t')dt' = 0, \quad t = 0;$$

the solution to equation (7.16) can be obtained by first integrating directly to get

$$\tau \frac{d}{dt} \ln Z + \frac{3}{2} \frac{d\tau}{dt} = \int^t f_2(t')dt'.$$

Multiplying through by $2/3$ and noting that

$$\frac{2}{3} \ln Z = \ln Z^{2/3}$$

and

$$\frac{d}{dt} \ln Z^{2/3} = \frac{1}{Z^{2/3}} \frac{d}{dt} Z^{2/3}$$

we can write

$$\frac{1}{Z^{2/3}} \frac{d}{dt}(\tau Z^{2/3}) = \frac{2}{3} \int^t f_2(t')dt'.$$

Multiplying through by $Z^{2/3}$, integrating again and then using the initial conditions

$$Z = Z_0, \quad t = 0;$$

$$\tau = \tau_0, \quad t = 0;$$

and

$$\int^t dt' Z^{2/3}(t') \int^{t'} f_2(t'')dt'' = 0, \quad t = 0;$$

we get

$$\tau(t) = \tau_0 \left(\frac{Z_0}{Z(t)} \right)^{\frac{2}{3}} \left(1 + \frac{2}{3\tau_0 Z_0^{2/3}} \int^t dt' Z^{2/3}(t') \int^{t'} f_2(t'')dt'' \right).$$

Solution to Equation (7.17)

Writing equation (7.17) as

$$\frac{d}{dt} \left(c^2 + \frac{d(\tau c^2)}{dt} \right) = \frac{4c_0^2 f_3}{\sin^2 \theta}$$

and introducing the initial conditions

$$c = c_0, \quad t = 0;$$

$$\tau = \tau_0, \quad t = 0;$$

$$\frac{dc}{dt} = 0, \quad t = 0;$$

$$\frac{d\tau}{dt} = 0, \quad t = 0;$$

we can integrate directly to obtain

$$\frac{d}{dt}(\tau c^2) + c^2 = c_0^2 \left(1 + \frac{4}{\sin^2\theta} \int^t f_3(t')dt' \right).$$

We then use the relationship

$$\frac{d}{dt}(\tau c^2) + c^2 = \frac{d}{dt}\left[c^2 \tau \exp\left(\int^t \frac{dt'}{\tau} \right) \right] \exp\left(- \int^t \frac{dt'}{\tau} \right)$$

so that we can write

$$\frac{d}{dt}\left[c^2 \tau \exp\left(\int^t \frac{dt'}{\tau} \right) \right] = c_0^2 \left(1 + \frac{4}{\sin^2\theta} \int^t f_3 dt' \right) \exp\left(\int^t \frac{dt'}{\tau} \right).$$

Integrating this equation then yields the expression

$$c^2 \tau \exp\left(\int^t \frac{dt'}{\tau} \right) = \tau_0 c_0^2 + c_0^2 \int^t dt' \exp\left(\int^{t'} \frac{dt''}{\tau} \right) \left(1 + \frac{4}{\sin^2\theta} \int^{t'} f_3 dt'' \right)$$

where, in addition to the initial conditions given above, we have chosen that

$$\int^t \frac{dt'}{\tau} = 0, \quad t = 0$$

and

$$\int^t dt' \exp\left(\int^{t'} \frac{dt''}{\tau} \right) \left(1 + \frac{4}{\sin^2\theta} \int^{t'} f_3 dt'' \right) = 0, \quad t = 0.$$

The solution for the acoustic velocity can then be written in the form

$$c(t) = c_0 \left(\frac{\tau_0}{\tau(t)} \right)^{\frac{1}{2}} \exp\left(-\frac{1}{2} \int_0^t \frac{dt'}{\tau(t')} \right)$$

$$\times \left[1 + \frac{1}{\tau_0} \int^t dt' \exp\left(\int^{t'} \frac{dt''}{\tau(t'')} \right) \left(1 + \frac{4}{\sin^2\theta} \int^{t'} f_3(t'')dt'' \right) \right]^{\frac{1}{2}}.$$

Hence, using the definition for the impedance Z, velocity c and relaxation time τ of an acoustic material, we arrive at the quantitative solutions

$$\kappa = \frac{1}{Zc},$$

$$\rho = \frac{Z}{c},$$

and

$$\alpha + 2\beta = Zc\tau.$$

An illustration of the type of experiment that is required to obtain the relevant data is shown in Figure 7.6.

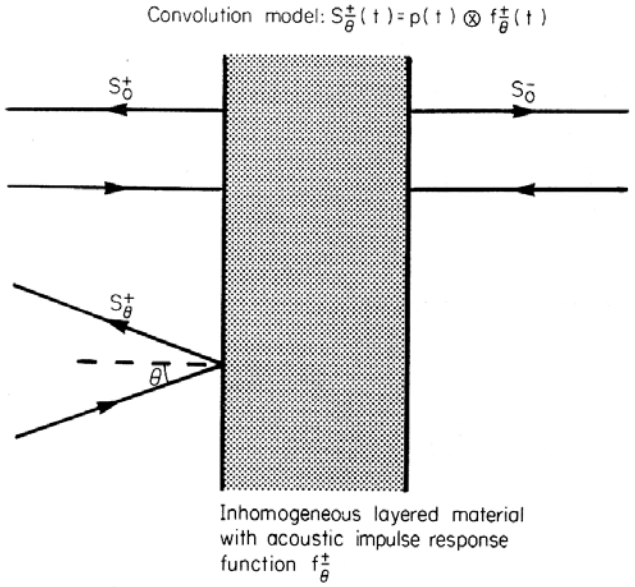

Figure 7.6: Experiment required to solve the three parameter reconstruction problem in electromagnetics (permittivity, permeability, conductivity) or acoustics (compressibility, density, viscosity).

A left travelling acoustic pulse is emitted at normal incidence to the material and at an angle θ to the normal. This provides the data s_0^+ and s_θ^+, respectively. Another experiment is then required where the material is interrogated by a right travelling pulse to provide the data s_0^-. By deconvolving these data to recover the impulse response functions, the density, compressibility and viscosity profiles of the layered material can be reconstructed using the formulae given above although, as mentioned before, deconvolution will only yield band-limited versions of the impulse response functions at best. The reconstruction formulae given here are under the theoretical assumption that some function exists q, such that $q \otimes s = \delta$.

7.4 Side-band Systems and Demodulation

In the previous Sections, we have considered the case when a layered material is interrogated with a pulse given by

$$p(t) = \frac{1}{2\pi} \int_{-\infty}^{\infty} P(\omega) \exp(i\omega t) d\omega$$

where $P(\omega)$ is the spectrum. We have then shown that the reflected signal(s) (are) is given by

$$s(t) = p(t) \otimes f(t)$$

where $f(t)$ is the impulse response function. This result is valid for any pulse $p(t)$. However, when side-band systems are used, the pulse is not of the form $p(t)$ but $p(t)\exp(i\omega_0 t)$ where ω_0 is the carrier frequency. In such systems, the signal received is usually demodulated by multiplying it with the complex conjugate of the carrier wave. We record and digitize not $s(t)$ but

$$S(t) = s(t)\exp(-i\omega_0 t).$$

What is the effect of this on the model for the impulse response function? Using the product and the convolution theorems,

$$S(t) = \exp(-i\omega_0 t)[p(t)\exp(i\omega_0 t) \otimes f(t)],$$

which in Fourier space becomes

$$S(\omega) = \delta(\omega + \omega_0) \otimes [P(\omega - \omega_0)F(\omega)]$$

$$= P(\omega)F(\omega + \omega_0) = P(\omega)[F(\omega) \otimes \delta(\omega + \omega_0)]$$

so that

$$S(t) = p(t) \otimes \exp(-i\omega_0 t) f(t).$$

For side-band systems (with demodulation), the basic convolution equation holds but the impulse response function is modulated by a wave oscillating at the same frequency as the modulated pulse. Thus, the impulse response function is given by

$$f(t) = \exp(i\omega_0 t)[q(t) \otimes S(t)]$$

where the filter $q(t)$ has the idealized property

$$q(t) \otimes p(t) = \delta(t).$$

7.5 Some Applications

The three parameter solutions given in Sections 7.2 and 7.3 are not always effective in practice. Nevertheless, the computation of the impulse response function provides a useful method of analysis and the basis for some applications.

7.5.1 Synthesis of Seismic Signals

The synthesis and analysis of signals and images using convolution models of the type presented in the previous Sections is a well established technique. In this Section, some examples are discussed.

Theoretical modelling of the propagation and interaction of acoustic radiation with different materials provides a vital input into the understanding of established acoustic imaging techniques and the development of new procedures. The synthesis of acoustic signals is important in a wide range of applications, especially when access to information on the relevant properties of the material is available. For example, in seismology it is common to have access to data which provides information on the vertical changes in the physical characteristics of the ground. These data can be obtained from a bore-hole and may include a log of the fluctuations in the density and acoustic velocity of the ground. From this information, a detailed account of the changes in impedance of the material as a function of depth can be obtained. From the velocity log, a time-dependent impedance log can be generated. Assuming that the viscosity of the material is negligible, the relaxation time can be set to zero. A single seismic trace can then be written as (after stacking)

$$s(t) = p(t) \otimes f(t)$$

where

$$f(t) = \frac{1}{2}\frac{d}{dt}\ln Z(t). \tag{7.18}$$

From the impedance log, the impulse response function for the ground can be computed from equation (7.18) (at the location of the bore hole). This result can be used to generate a synthetic seismic trace by convolving it with an appropriate wavelet[2] A detailed account of the precise nature of a seismic wavelet is difficult to obtain experimentally. It is therefore common practice to utilize appropriate models for the wavelet. A well known model used extensively in seismology is the Ricker wavelet (after N H Ricker, *Transient Waves in Visco-Elastic Media*, Developments in Solid Earth Geophysics 10, Elsevier, 1976). This is given by

$$p(t) = \sqrt{\frac{\pi}{2}}\left(u^2 - \frac{1}{2}\right)\exp(-u^2)$$

where

$$u = \frac{\omega_0 t}{2}.$$

Here, ω_0 is the centre frequency of the wavelet. By convolving the impulse response function with a suitable Ricker wavelet (i.e. a Ricker wavelet with an appropriate carrier frequency) a synthetic seismic trace can be obtained. An example of this is given in Figure 7.8. This figure compares a real seismic signal near to the location of the impedance log with a simulated signal which has been generated from the impedance log using a 200 Hz Ricker wavelet.

[2]The term 'wavelet' is traditionally used by seismologists to refer to the seismic pulse $p(t)$ or section of a seismic trace. It is not used here with reference to a wavelet as in a wavelet transform, although it is interesting to note that wavelet-based signal analysis originally developed from seismic signal analysis.

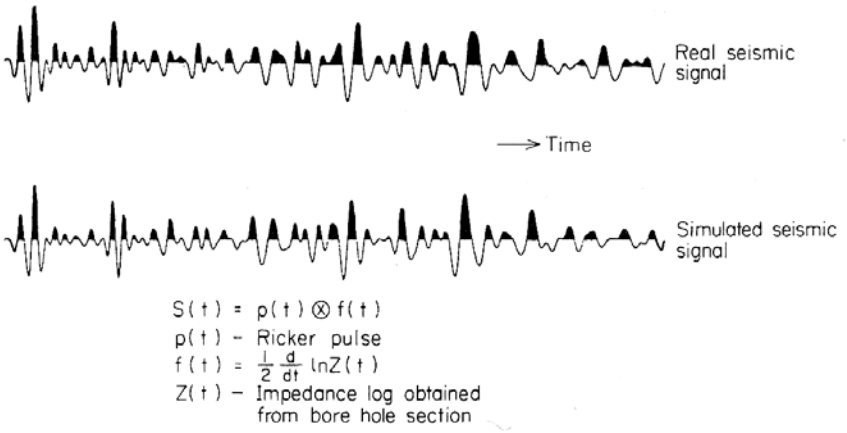

Figure 7.7: Comparison between a real seismic signal and a synthetic signal generated from the corresponding impedance log.

7.5.2 Impediography

Impediography is an inverse technique which seeks to reverse the process of deriving a synthetic signal from an impedance log. In other words, impediography attempts to reproduce the impedance variations (usually as a function of time) from a suitably processed signal. This technique is used in a wide variety of low frequency acoustic and some high frequency ultrasonic imaging techniques. Its success depends on the quality of the deconvolved signal. In seismology, the impedance profile can be compared with real impedance logs. Done on a trace-by-trace basis, this effectively replaces a seismic image composed from a stack of seismic signals with a seismic section made up of derived or pseudo impedance profiles. The wider the bandwidth of the original seismic trace, the more closely the derived impedance profile will match the real impedance log. This provides a technique which utilizes the processes inherent in broadband data to study, in detail, lateral and vertical changes in lithology. At normal incidence, impediography assumes that the relaxation time is zero. After deconvolution, we can then employ the equation

$$\frac{1}{2}\frac{d}{dt}\ln Z(t) = f(t) \tag{7.19}$$

where $f(t)$ is the deconvolved data (the impulse response function). The analytical solution for the impedance is

$$Z(t) = Z_0 \exp\left(\int^t f dt\right).$$

This inverse process is essentially integration which amplifies the low frequency components of the deconvolved data. Numerically, the integration can be be performed using a variety of techniques. One of the simplest methods utilized for fast display purposes is based on writing equation (7.19) as a difference equation. Noting that

$$\frac{d}{dt}\ln Z = \frac{1}{Z}\frac{dZ}{dt}$$

we have

$$\frac{dZ}{dt} = 2Zf$$

Differencing this equation we obtain the simple iterative process

$$Z_{n+1} = Z_n(1 + 2\Delta t f_n) \tag{7.20}$$

Once the impedance of the first layer Z_0 is known, the others follow from application of this formula. This assumes, however, that the processes are stationary and that no dispersion occurs. In practice, the pulse will, of course, decay in amplitude as it propagates as well as disperse, i.e. its bandwidth will decrease with travel time. Thus, impediography with deconvolution can usually only be practiced on segments of the data where, to a good approximation, the process is stationary (with respect to time).

7.5.3 Fuzzy and Quantitative Impediography

Conventional acoustic impediography assumes that a signal has been produced by single scattering from an inhomogeneous material with fluctuations in the impedance alone. When variations in the viscosity of the material are present, impediography can give rise to 'fuzzy images' of the impedance. A fuzzy image is an image which attempts to describe a single property of a material but fails to achieve this because the data are corrupted by some other interaction not included in the original model for the signal (i.e. the model for the impulse response function). This is a consequence of the fact that the reconstruction algorithm used to generate an image is ultimately determined by the type of wave equation which is used to describe the scattered field. A simple demonstration of this is given in Figure 7.8. Here, a hypothetical layered material is considered which consists of a simple impedance profile and a single mismatch in the relaxation time. If we consider the interaction of this material with an acoustic pulse $p(t)$ at normal incidence, then the reflected signal is given by (for a right-travelling wave)

$$s(t) = p(t) \otimes f(t)$$

where

$$f(t) = \frac{1}{2}\frac{d}{dt}\ln Z + \frac{1}{2}\frac{d}{dt}\left(\tau\frac{d}{dt}\ln Z\right) + \frac{3}{4}\frac{d^2\tau}{dt^2}. \tag{7.21}$$

In Figure 7.8, the signal has been computed by forward differencing equation (7.18) and convolving the result with a Ricker wavelet. Deconvolution recovers the impulse response function. If it is then assumed that the original signal

does not contain features that are due to changes in the relaxation time, then the impulse response function is given by equation (7.19) rather than equation (7.21). Integration then gives a fuzzy reconstruction because the impediography algorithm [which in this example is given by equation (7.20)] interprets the second echo (which arises from a mismatch in the relaxation time) as arising from an impedance mismatch. This is an example of image fuzziness (see Introduction).

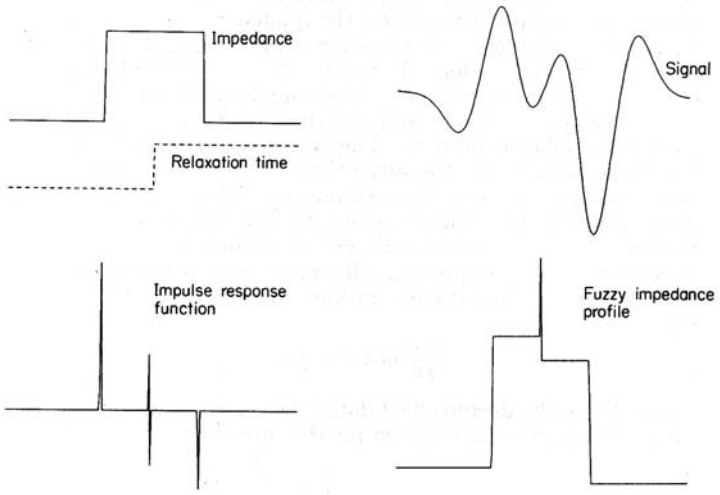

Figure 7.8: Fuzzy impedance profiles are obtained when features in the signal are due to variations of the relaxation time as well as of the impedance.

To avoid the production of fuzzy acoustic impedance profiles and therefore errors in the interpretation of the distribution of impedance, we must resort to normal incidence reflection experiments of the type illustrated in Figure 7.6. This requires access to both sides of the layered material which rules out a number applications, such as seismic imaging, where access is only available from the ground surface. In applications where the material can be scanned with an ultrasonic pulse from both sides, quantitative impediography may be utilized. This is illustrated in Figure 7.9. Each transducer emits a pulse and records the echo obtained at different lateral positions. Both signals are deconvolved and used to construct the functions given by equations (7.15) and (7.16). These equations are then solved to provide $Z(t)$ and $\tau(t)$, respectively. Ultrasonic inspection of this type provides two images, one of the impedance of the material and another of the relaxation time.

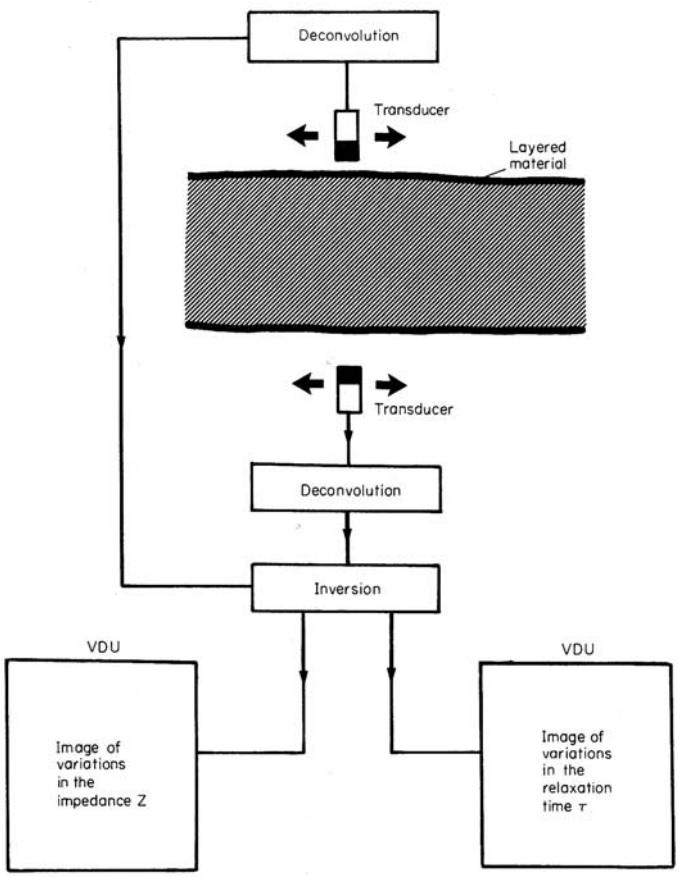

Figure 7.9: Quantitative ultrasonic impediography utilizes two transducers which provide data on the echoes generated from a material when it is insonified by a left- and right-travelling pulse. Deconvolution and inversion allow ultrasonic images of the variations in impedance and relaxation time of the material to be presented.

7.6 Case Study: Imaging the Ionosphere

The ionosphere is a weakly ionised gas which exists between the Earth's atmosphere and the magnetosphere. At long wavelengths the ionosphere behaves like a layered dielectric, and its ability to reflect radio waves is well known. This was the reason why Guglielmo Marconi was successful in being the first to transmit radio waves across the Atlantic ocean (from Cornwall in England to Newfoundland in Canada) in his famous experiment of 1901 although, at the time, he did not know it.

By observing the way in which radio waves are reflected we can determine

the structure and dielectric properties of the ionosphere using the methods discussed in Section 7.2. However, in order to apply this method we are required to make some reasonable assumptions about particle motions in the ionosphere. To a good approximation, the ionosphere is a three-component gas made up of ions, electrons and neutrals embedded in a magnetic field of uniform magnitude across its vertical extent (i.e. the Earth's magnetic field). If the component x is vertical, then the gyrofrequencies (the frequencies at which a charged particle gyrates about a magnetic field line) of ions and electrons (Ω_i, Ω_e) are roughly constant in x. However, the collision frequencies of ions, electrons and neutrals (ν_i, ν_e, ν_n) can change by five orders of magnitude as a function of x due to the change in neutral gas density as a function of altitude. As a consequence of this, charged particle motions at low altitudes are dominated by collisions $(\nu/\Omega >> 1)$ whereas, at high altitudes, the effects of the magnetic field are more important $(\nu/\Omega << 1)$, the collision frequencies being reduced by the low number densities that occur at high altitudes. In this type of model, it is assumed that thermal and viscous motions can be neglected. This is a reasonable assumption for a 'quiet' ionosphere where changes in its state are not abrupt but take place smoothly and over relatively long periods of time.

If an electric field is applied perpendicular to the Earth's magnetic field $\mathbf{H}$, current will flow in a parallel, intermediate and perpendicular direction for ν/Ω going from very large to very small values. The magnitude of the currents is a function of the anisotropic electrical conductivity. The conductivity is additionally anisotropic for electric field components parallel to $\mathbf{H}$. For the ionosphere, the current density $\mathbf{J}$ is related to the electric field $\mathbf{E}$ by the equation

$$\mathbf{J} = \sigma_1 \mathbf{E}_{\parallel} + \sigma_2 \mathbf{E}_{\perp} + \sigma_3 \mathbf{H} \times \mathbf{E} \tag{7.22}$$

where $\parallel$ and $\perp$ indicate the electric field components parallel and perpendicular to $\hat{\mathbf{h}} = \mathbf{H}/ \mid \mathbf{H} \mid$. Here, it is assumed that the conductivity is anisotropic in three different senses. The first term in equation (7.22) describes the current that is generated parallel to the magnetic field, namely the direct current with an associated conductivity σ_1. The second term identifies the current that is induced due to an electric field perpendicular to the magnetic field which represents the Ohmic current with an associated conductivity σ_2. Finally, there will exist a current known as the Hall current which is perpendicular to both the electric and magnetic fields and is described by the third term of equation (7.22). This term arises from the differential motion between the ions and electrons as a result of an $\mathbf{E} \times \mathbf{H}$ drift. The conductivity components σ_1, σ_2 and σ_3 are known as the direct, Pedersen and Hall conductivities, respectively.

If we now consider the ionosphere to be a continuum composed of different layers so that $\epsilon = \epsilon(x)$, $\mu = \mu(x)$ and $\sigma_i = \sigma_i(x); i = 1, 2, 3$, then, from Maxwell's equations, our basic time-dependent wave equation for the electric field $\mathbf{E}$ becomes

$$\nabla \times \nabla \times \mathbf{E} - \epsilon\mu \frac{\partial^2 \mathbf{E}}{\partial t^2} - \mu \frac{\partial \mathbf{J}}{\partial t} = \hat{\mathbf{x}} \frac{d}{dx} \ln \mu \times \nabla \times \mathbf{E}$$

where $\hat{\mathbf{x}}$ is the unit vector in the x-direction. Considerable simplification can be achieved by modelling the ionosphere at the equator where $\hat{\mathbf{h}}$ is to a good

approximation, horizontal over the extent of the ionosphere as shown in Figure 7.10.

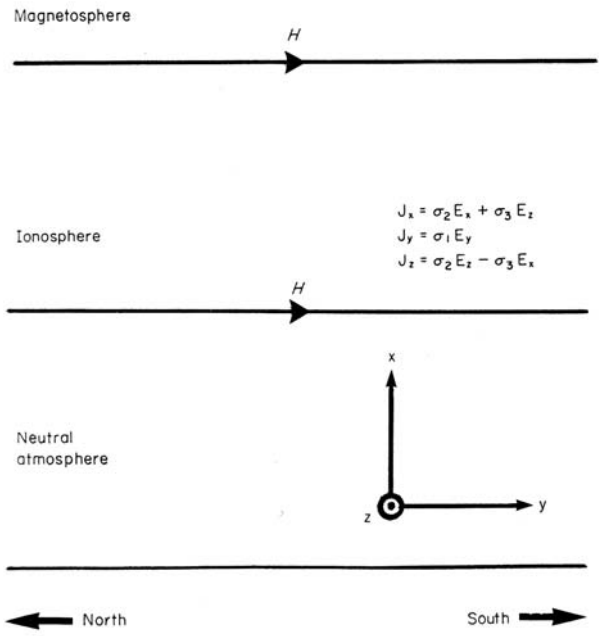

Figure 7.10: Model for the ionosphere at the Equator

At the equator (where $\hat{\mathbf{h}} = \hat{\mathbf{y}}$ and $\hat{\mathbf{h}} \times \mathbf{E} = \hat{\mathbf{x}}E_z - \hat{\mathbf{z}}E_x$), the components of the current density are from equation (7.22):

$$J_x = \sigma_2 E_x + \sigma_3 E_z,$$

$$J_y = \sigma_1 E_y,$$

and

$$J_z = \sigma_2 E_z - \sigma_3 E_x.$$

Using these results, the wave equation for the polarized electric field

$$\mathbf{E} = \hat{\mathbf{y}} E_y(x, y, t)$$

reduces to

$$\left(\frac{\partial^2}{\partial x^2} + \frac{\partial^2}{\partial y^2}\right) E_y - \epsilon\mu \frac{\partial^2 E_y}{\partial t^2} - \mu\sigma_1 \frac{\partial E_y}{\partial t} = \frac{d}{dx} \ln \mu \frac{\partial}{\partial x} E_y. \tag{7.23}$$

When a polarized electric field of the form

$$\mathbf{E} = \hat{\mathbf{z}} E_z(x, y, t)$$

is used, the wave equation reduces to

$$\left(\frac{\partial^2}{\partial x^2}+\frac{\partial^2}{\partial y^2}\right)E_z-\epsilon\mu\frac{\partial^2 E_z}{\partial t^2}-\mu\sigma_2\frac{\partial E_z}{\partial t}=\frac{d}{dx}\ln\mu\frac{\partial}{\partial x}E_z. \tag{7.24}$$

Both equations (7.23) and (7.24) are of the same form as equation (7.4) and, thus, by repeating the method presented in Section 7.2, we can obtain reconstructions for ϵ, μ and σ_1 using equation (7.23) and ϵ, μ and σ_2 using equation (7.24).

An illustration of the type of experiment required to reconstruct parameters ϵ, μ, σ_1 and σ_2 at the equator is shown in Figure 7.11.

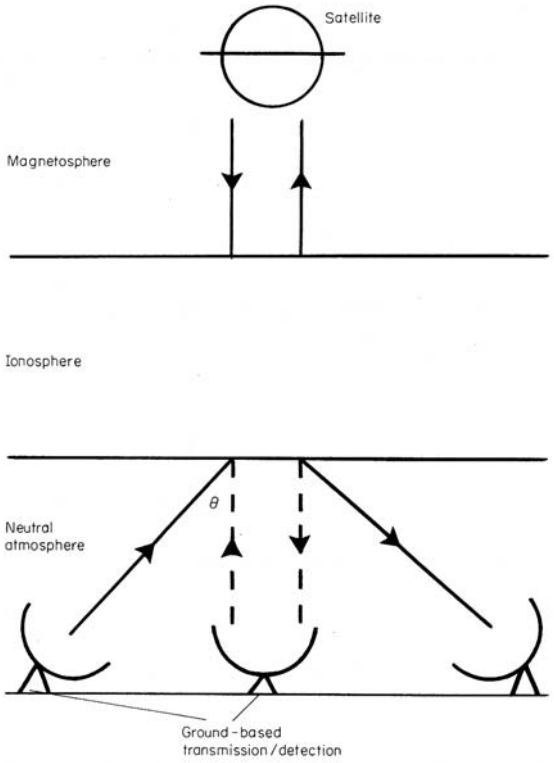

Figure 7.11: Illustration of the type of experiment required to recover the permittivity, permeability and anisotropic conductivity (the direct and Pedersen conductivities) of the ionosphere at the Equator using different polarized fields.

A ground-based emitter-detector sends out a known modulated pulse of radio waves with known polarization. The signal produced by the reflected electric field at normal incidence is then recorded. A second emitter generates

another and preferably identical pulse of radio waves at some known angle θ to the normal vertical component. The signal produced by the reflected electric field is then recorded as shown. These records are demodulated and deconvolved to recover the impulse response functions. A further experiment is then required to obtain information about the reflection of radio waves from the top of the ionosphere. These data may be obtained by a satellite in a geostationary orbit. By changing the polarization of the incident electric vector, reconstructions for two different types of conductivity can be obtained. This provides quantitative information about the anisotropic conductivity of the ionosphere.

7.7 Case Study: Radar Plasma Screening

Since its development in the late 1930s by the British, Radio Detection and Ranging or Radar has been used for many years to detect airborne objects using ground and/or airborne platforms.[3] The use of stealth technology for suppressing the detection of aerospace vehicles by Radar has been the subject of intensive research since the early 1970s following the development of radar guided surface-to-air missiles in the 1960s. One of the most notable current examples of the results of this research is the Lockhead-Martin F-117 stealth fighter and later the stealth bomber, first tested successfully under combat conditions in the Gulf war of 1991. Based on ideas first introduced by Denys Overholser in 1974 at Lockhead's advanced engineering laboratories, the technology is based on two principal aspects: (i) design features; (ii) radar absorbing materials and coatings. The geometry of the design is based on trying to minimize those features of an aerospace vehicle that are responsible for reflecting microwave radiation in such a way that the result can fly. Obvious features include embedding the gas turbine engines deep into the structure of the aircraft and introducing facets - diamond shaped flat surfaces - that reflect the microwave radiation away from the source. However, one of the principal factors for reducing the Radar Cross Section (RCS) is to minimize the profile of the aircraft while maximizing the 'smoothness' of the design. This effect was first noticed when a prototype 'flying wing' was developed in Germany by two Luftwaffe officers - the Horten brothers - and first tested in late 1944. This unique design was many years ahead of its time; it was investigated further in the 1950s by the USA (the Northrop flying wing), but limitations in control systems technology available at the time meant that the principle was not practically viable until significant improvements over the 1960s and 1970s in digital control processing had taken place.

Theoretically, the problem can be posed as follows: given that the aircraft can be assumed to be a Born scatterer and that

$$(\nabla^2 + k^2)\widetilde{\mathbf{E}}_s = -k^2\gamma\widetilde{\mathbf{E}}_i + ikz_0\sigma\widetilde{\mathbf{E}}_i - \nabla(\widetilde{\mathbf{E}}_i \cdot \nabla \ln \epsilon_r)$$

where

$$\gamma = \epsilon_r - 1,$$

[3]This case study is based on a research project undertaken by the author for MatraBAE dynamics Limited, Bristol, England, 2001

find 'flying functions' γ and σ which are of compact support such that $\widetilde{\mathbf{E}}_s = 0$.

In addition to investigating the RCS for different designs and materials, there is another approach to producing stealthy flying objects using a plasma, i.e. an ionised gas. The reduction of the RCS of an aerospace vehicle through the generation of a plasma is an effect that has been known about for some 50 years. The phenomenon has an obvious connection with the 'radio silence' phenomenon that occurs during re-entry of a spacecraft. This occurs when a plasma is formed around the spacecraft due to the 'friction' of the Earth's atmosphere such as the Space Shuttle.

A fundamental parameter of any plasma is the 'plasma (angular) frequency' ω_p given by

$$\omega_p = \left(\frac{4\pi n e^2}{m}\right)^{\frac{1}{2}}$$

where e is the charge of an electron (1.6×10^{-19} C), m is the mass of an electron (0.91×10^{-30}kg) and n is the number density of electrons in m^{-3}. For a plane EM wave incident on a plasma, Maxwell's equations (for transverse EM waves) yield the dispersion relation

$$k = \frac{1}{c_0}\sqrt{\omega^2 - \omega_p^2}$$

where k is the wavenumber ($= 2\pi/\lambda$) and c_0 is the velocity of light in a vacuum ($\simeq 3\times10^8$ m/sec). A cut-off occurs when $\omega = \omega_p$, i.e. when there is a critical number density

$$n_c = \frac{m\omega^2}{4\pi e^2}.$$

Radio waves can only propagate through a plasma when $\omega > \omega_p$. For a typical laboratory plasma with $n = 10^{12}\mathrm{cm}^{-3}$, a cut-off occurs when

$$f_p = \frac{\omega_p}{2\pi} \sim 10^4\sqrt{n} = 10\mathrm{GHz}$$

which is in the microwave range. This effect is used as method of measuring the density of laboratory plasmas. The idea of 'covering' an aerospace vehicle in a self-induced plasma with an appropriate critical number density is not a practical proposition. However, partial plasma screening of specific features which are good radar point-scatterers is possible, one example being the point on the 'nose-cone' of a missile.

In this case study, we derive a model for radar signals generated by a conductor that is screened by a plasma. We develop an electromagnetic scattering model to investigate the effect that a plasma has on a conventional radar system. Expressions for the Impulse Response Function generated by a scatterer with and without plasma screening are derived. For a weakly ionised plasma, we derive a result that shows that the screening of the scatterer by the plasma is characterized by a simple negative exponential whose decay rate is determined by the electron number density. We start with a model that is fully three dimensional but reduce the radar signal to a one-dimensional convolution equation that is consistent with the remit of this Chapter.

Basic Scattering Model

Our aim is to develop a suitable model for the plasma screening effect by developing some relatively simple analytical results that explain why, under certain conditions, it provides a near-zero RCS. The basic reason for this effect is assumed to be due to the following: (i) a plasma is a (good) conductor and will therefore absorb (and disperse) electromagnetic (microwave) radiation before it is reflected by a scatterer; (ii) the air/plasma boundary is continuous (on the scale of the wavelength) and will therefore not generate a strong reflection compared with that generated by the surface of the scatterer which represents a sharp discontinuity on the scale of a wavelength (of a microwave field).

Let us model the problem using the scalar wave equation (under the Born approximation)

$$(\nabla^2 + k^2)\widetilde{E}_s = -k^2\gamma(\mathbf{r})\widetilde{E}_i + ikz_0\sigma(\mathbf{r})\widetilde{E}_i, \quad \mathbf{r} \in V$$

where $\widetilde{E}_s$ is the scattered (scalar) electric field and $\widetilde{E}_i$ is the incident electric field. A general solution to this equation can now be obtained using the Green function method which, for homogeneous boundary conditions, gives

$$\widetilde{E}_s = \int g(ikz_0\sigma - k^2\gamma)\widetilde{E}_i d^3\mathbf{r}$$

where g is the 'out-going' Green function,

$$g(\mathbf{r} \mid \mathbf{r}_0) = \frac{\exp(ik \mid \mathbf{r} - \mathbf{r}_0 \mid)}{4\pi \mid \mathbf{r} - \mathbf{r}_0 \mid}$$

and the integral is taken over the volume V of the scatterer. Here, $\mathbf{r}$ and $\mathbf{r}_0$ are the spatial coordinates of the scatterer and the position at which the field is measured, respectively. The characteristics of the back-scattered field are dependent on ϵ_r, σ and their geometry (i.e. the shape of the scatterer over volume V). Note that, if $\epsilon_r = 1$ and $\sigma = 0$, then the scattered field is zero.

Let us assume that the scatterer is a good conductor, and that $\epsilon_r = 1$ so that $\gamma = 0$. This assumption is consistent with the application of a scalar wave equation since $\nabla(\widetilde{\mathbf{E}}_i \cdot \nabla \ln \epsilon_r) = 0$ with $\epsilon_r = 1$. The scattered field is now determined by the conductivity alone. Let us also assume that the incident field is described by the Green function g instead of a plane wave (the more usual case). This assumption helps to simplify slightly the analysis required in generating a model for the back-scattered field.

If the incident field propagates through a medium whose conductivity is effectively zero (i.e. air) then the solution for the back-scattered field will be given by

$$\widetilde{E}_s = \int ikz_0\sigma g^2 d^3\mathbf{r}.$$

The volume over which scattering is effective will be determined by the skin depth

$$\delta = \left(\frac{2}{kz_0\sigma}\right)^{\frac{1}{2}}$$

which, although very small for a good conductor, will be considered to be finite. This allows us to adopt a volume scattering approach instead of one based on surface scattering. The reason for this is that we can then consider the volume scattering effects introduced by a plasma screen. Note that the homogeneous boundary conditions used to produce this Green function solution yield a surface integral that is zero (i.e. $\widetilde{E}_s$ and $\nabla\widetilde{E}_s$ are considered to be zero on the surface of V).

The solution for $\widetilde{E}_s$ in the far field (i.e. when $r/r_0 << 1$) is (ignoring numerical scaling factors)

$$\widetilde{E}_s(\mathbf{r_0}, k) = \exp(2ikr_0)F$$

where F is the reflection coefficient given by

$$F(\mathbf{r}_0, k) = \int ik\sigma \exp(-2ik\hat{\mathbf{n}} \cdot \mathbf{r}) d^3\mathbf{r}$$

and $\hat{\mathbf{n}} = \mathbf{r}_0/r_0$. A relatively simple result can now be developed by considering the radar beam to be a narrow pencil-line beam oriented in the x-direction so that

$$r_0 \equiv \mid \mathbf{r}_0 \mid = x_0 \left(1 + \frac{y_0^2}{x_0^2} + \frac{z_0^2}{x_0^2}\right)^{\frac{1}{2}} \simeq x_0; \quad \frac{y_0}{x_0} << 1, \frac{z_0}{x_0} << 1.$$

This provides us with a solution for the reflection coefficient of the form

$$F(x_0, y_0, z_0, k) = \int ik\Omega \exp(-2ikx) dx$$

where

$$\Omega(x, x_0, y_0, z_0, k) = \int\int \sigma(x, y, z) \exp(-2iky_0 y/x_0) \exp(-2ikz_0 z/x_0) dydz.$$

If we now consider the case when the back-scattered field is measured at a fixed point $(x_0, 0, 0)$, we obtain

$$F(k) = \int ik\Omega \exp(-ikx) dx$$

where

$$\Omega(x) = \int\int \sigma(x/2, y, z) dydz.$$

Note that this result has been obtained by replacing x by $x/2$ and then ignoring scaling. If we assume that σ is a constant as a function of y and z, then

$$\Omega(x) = A\sigma(x/2)$$

where A is the area of the scatterer. Here, we see that the back-scattered field (i.e. the reflection coefficient) is given by the Fourier transform of $ik\Omega$. The time signature associated with the reflection coefficient (i.e. the temporal

Impulse Response Function or IRF) can now be obtained by taking the inverse Fourier transform giving

$$f(t) = -A\frac{d\sigma}{dt}$$

where we have ignored scaling and where t is the 'two-way' travel time (i.e. $x = 2c_0t$ where c_0 is the speed of light). This result illustrates that the strength of the return is determined by the following: (i) the area A of the scatterer that is illuminated by the radar beam; (ii) the gradient in the conductivity (from air to scatterer). Thus, assuming that the conductivity of air is zero, a scatterer, such as an aerospace vehicle composed of aluminium alloy with a conductivity of approximately 2.5×10^7 siemens/metre, represents a huge change in the conductivity across the air/scatterer boundary and so produces a very strong reflection. It is useful to consider a scatterer with unit area, so that $\Omega = \sigma$ which is assumed from now on.

Let us now consider the case when the scatterer is embedded in a plasma sheath which is taken to be a conductor with average conductivity σ_0. The sheath contributes to the volume V over which the scattered field is to be computed and is assumed to have a conductivity profile with no distinct air/plasma boundary. The average conductivity σ_0 is taken to be the volume integral of the plasma conductivity profile divided by the volume of the sheath over which the incident field is scattered. The effect of this sheath is of course to introduce absorption (and frequency dispersion) of the electric field before it is incident upon the scatterer.

We consider the conductivity profile of the plasma together with the scatterer over volume V to be described by $\sigma_0 + \sigma(x, y, z)$. Our wave equation then becomes

$$(\nabla^2 + k^2 - ikz_0\sigma_0)\widetilde{E}_s = ikz_0\sigma\widetilde{E}_i.$$

We can now repeat the calculation undertaken previously to obtain a far-field solution for the back-scattered field at $(x_0, 0, 0)$ produced by a narrow incident radar beam in the x-direction. In this case, the reflection coefficient is given by

$$F(k) = \int ik\sigma(x)\exp[-2i(k^2 - ikz_0\sigma_0)^{1/2}x]dx.$$

Note that an absorption effect has been introduced as a consequence of our model in which the electric field propagates through a plasma with an average conductivity σ_0 before incidence with the scatterer.

Impulse Respsonse Function for a Good Conductive Plasma: $k << z_0\sigma_0$

We can simplify the equation for $F(k)$ by noting that for a good conductor $k^2 - ikz_0\sigma_0 \sim -ikz_0\sigma_0$. Using the result $\sqrt{-i} = (1-i)/\sqrt{2}$ we can then write

$$F(k) = \int ik\sigma(x)\exp\left[-2i\left(\frac{kz_0\sigma_0}{2}\right)^{\frac{1}{2}}x\right]\exp\left[-2\left(\frac{kz_0\sigma_0}{2}\right)^{\frac{1}{2}}x\right]dx.$$

The form of this integral transform does not provide a simple Fourier-based relationship between σ and F. Nevertheless, the IRF $f(t)$ is given by the inverse

Fourier transform of $F(k)$ and it is clear that a major feature of this integral transform is the negative exponential which characterizes the absorption of electromagnetic energy in the plasma. The plasma is in effect producing a conductive shield that screens the scatterer from incident radiation.

For a given wavelength, the skin depth δ depends on the average conductivity of the sheath; the more conductive the plasma, the shorter the skin depth (i.e. $\delta \propto \sigma_0^{-1/2}$). For a fixed average conductivity, there is less penetration of radiation at higher frequencies. Since radar relies on high frequency sweeping (i.e. the emission of chirped and other coded pulse) to obtain high resolution, the dispersion introduced through this integral transform will yield a spectrum at the receiver in which the frequency components are attenuated according to a $\exp(-\alpha\sqrt{k})$ power law, where $\alpha = \sqrt{z_0\sigma_0/2}$.

Impulse Response Function for a Poor Conductive Plasma: $k >> z_0\sigma_0$

The equation for $F(k)$ above is a consequence of considering the case when $k << z_0\sigma_0$, and it is not possible to Fourier invert to give an analytical expression for the IRF. However, if we consider the condition

$$k >> z_0\sigma_0$$

which is valid for the case when the plasma is weakly conductive, then we can consider the approximation $\sqrt{k^2 - ikz_0\sigma_0} \simeq k - iz_0\sigma_0/2$, giving

$$F(k) = \int ik\sigma \exp(-2ikx) \exp(-z_0\sigma_0 x)dx.$$

Fourier inversion then allows us to establish the IRF, i.e.

$$f(t) = -\frac{d}{dt}[\sigma(t) \exp(-\sigma_0 t/\epsilon_0)]$$

where, as before, t is the 'two-way' travel time and scaling has been ignored. Assuming that the variations in conductivity are smooth and that the boundary between the atmosphere and the plasma (in terms of variations in conductivity) is continuous, the effect of the plasma sheath on the IRF is characterised by $\exp(-\sigma_0 t/\epsilon_0)$. On the other hand, if the air/plasma boundary is discontinuous, the IRF is dominated by the gradient in the conductivity across this boundary. In either case, there is no frequency dependence and the form of the negative exponential is the same as that describing the rate of decay of charge ρ in a conductor, i.e.

$$\rho = \rho_0 \exp(-\sigma_0 t/\epsilon_0).$$

Note that, since $\epsilon_0 \sim 10^{-11}$, only relatively low values of σ_0 are required to cause rapid decay in the IRF. If we consider a 1cm wavelength radar, then the condition that has been applied to achieve this simplification reduces to

$$\sigma_0 << 17.$$

The skin depth for this case is

$$\delta = \frac{10^{-3}}{\sqrt{\sigma_0}}$$

and, for a plasma with a very low conductivity of say 1 siemens/metre, the skin depth is 1 mm, i.e. the length over which the electric field strength has decayed by e^{-1} or by 63% .

The results obtained here are for the back-scattered field only; a special case has been considered where the field is measured at a fixed point $(x_0, 0, 0)$. For $k = k_0$ (i.e. the carrier wavenumber), the field strength as a function of $\theta \simeq y_0/x_0$ and $\phi \simeq z_0/x_0$ is determined by

$$\Omega(\theta, \phi) = \int\int \sigma(x, y, z) \exp(-2ik_0\theta y) \exp(-2ik_0\phi z) dxdy$$

and provides a Born estimate of the diffraction pattern produced by σ, i.e. a map of the back-scattered cross-section at small angles θ and ϕ.

7.7.1 The Radar Signal Equation

Assuming that the return has been demodulated with a carrier frequency ω_0, the radar signal $s(t)$ generated by a scatterer embedded in a weakly conductive plasma sheath is (ignoring scaling)

$$s(t) = p(t) \otimes f(t) + n(t)$$

where

$$f(t) = \exp(-i\omega_0 t) \frac{d}{dt} [\sigma(t) \exp(-\sigma_0 t/\epsilon_0)],$$

$p(t)$ is the outgoing pulse (typically a linear FM pulse) and $n(t)$ is the noise associated with the whole system.

The negative exponential component from which $f(t)$ is composed can be thought of as a Signal-to-Noise Ratio (SNR) control; as the conductivity increases, the SNR is reduced through negative exponential decay. In general, and in the practical application of using plasmas to screen aerospace vehicles, it is more likely that the plasma will be weakly ionised and weakly conductive. Hence, the equation above provides a useful initial model. For a weakly ionised plasma the electron number density determines its conductivity. In terms of this result, there are three principle factors affecting the performance of a practical radar plasma screening system: (i) maximizing the electron number density of the plasma; (ii) maximizing the thickness of the screen; (iii) maintaining continuity of the air/plasma interface. Points (i)-(iii) will depend on the power of the plasma generator, the stability of the plasma and its profile. Thus, a model is required for the electron number density profile of a plasma that we assume is generated by an electron beam which is discharged through an appropriate feature on a moving aerospace vehicle.

7.7.2 Model for an Electron-beam Induced Plasma

The conductivity of a plasma depends upon whether we consider it to be weakly or strongly ionised. A weakly ionised plasma is one in which the frequency of

collisions ν of electrons (e) and ions (i) with atoms (a) greatly exceeds that of collisions of these particle with one another, i.e.

$$\nu_{ea} >> \nu_{ee}, \nu_{ei}; \quad \nu_{ia} >> \nu_{ii}, \nu_{ie}.$$

A highly ionised plasma is described by the reverse of these inequalities.

The conductivity of a weakly ionised plasma is given by

$$\sigma = \frac{ne^2}{m_e \nu_{ea}} + \frac{2ne^2}{m_i \nu_{ia}}$$

where m_e and m_i are the masses of an electron and ion, respectively. This expression for the conductivity is dominated by the first term which describes the conductivity for the electron component of the plasma. The reason for this is that $m_i >> m_e$ always. Clearly, in this case, the conductivity is proportional to the electron number density n and the conductivity of a weakly ionised plasma can be approximated by

$$\sigma = \frac{ne^2}{m_e \nu_{ea}} \sim 10^{-9} \frac{n}{\nu_{ea}}$$

where ν_{ea} is the frequency of collisions between electrons and atoms. The ratio n/ν_{ea} will vary considerably from one regime (i.e. altitude and speed of flight) to another, although the values of n and ν_{ea} may tend to off-set each other. Assuming that the plasma is generated by e-beam breakdown of the atmosphere, at ambient atmospheric pressures, n will be large as will ν_{ea}. At higher altitudes, n will be less but so will ν_{ae}. Finally, above the atmosphere there will be relatively few atoms to break down and the collision frequency will be relatively small. However, if, for example, a hydrogen gas puff could be generated prior to ionization, then it would be possible to generate large electron densities with low collision frequencies leading to high and sustainable plasma conductivities and, therefore, more effective plasma screening systems.

Since the conductivity of the plasma screen is linearly proportional to the electron number density, a principal problem is to determine the number density distribution for a given configuration (of source and aerospace vehicle). Thus, we are required to obtain a model that predicts the generation and transport of electrons subject to a variety of processes such ionization, recombination, diffusion, radiative losses, air flow, etc. This can be accomplished by considering the macroscopic properties of the plasma which are governed by the dynamics of the growth process, a process that involves avalanche electron multiplication (an exponential process), i.e. the ionization rate per initial electron. A limiting mechanism for the growth of the cascade is taken to be due to the (ambipolar) diffusion of electrons out the volume of the e-beam. Away from the plasma source, the electron number density is taken to be determined primarily by the recombination rate, radiative losses or bremsstrahlung radiation and flow regime. The ionization mechanism is taken to include inverse bremsstrahlung processes.

Ionization

The ionization of a neutral gas by an electron beam, for example, is determined by a cascade process that produces an exponential growth in the electron density. In the absence of diffusion processes, this electron density is determined by the equation

$$\frac{dn}{dt} = In$$

where I is the ionization rate per initial electron and is assumed to be a constant. The solution is trivial, represents exponential growth and is given by

$$n = n_0 \exp(It)$$

where n_0 is the initial electron density. Suppose that for a given volume, we require the e-beam to produce 10^{13} electrons say and that this number should be produced from an initial value of 10 electrons that have been ionised by electrons from the e-beam alone, then

$$\ln\left(\frac{n}{n_0}\right) = \int I dt \sim 40.$$

In other words, the cascade process requires 40 generations to produce 10^{13} electrons from just 10 of them. This number is not strongly dependent on the assumed value of n_0 within reasonable bounds. The electron density becomes large only near the end of the cascade process; 99% of the ionisation is produced from the last 7 generations. Therefore, quantities such as the growth and losses from the cascade and the time to breakdown are determined by the conditions at times when the electron density is small.

The ionization rate will be determined by two principal processes: (i) the ionization rate I_b due to collisions of neutral atoms or molecules with electrons that have absorbed energy in the inverse bremsstrahlung process; (ii) the loss of potential ionizing electrons due to electron attachment with an ion which we denote by a rate coefficient I_a. Thus, in general

$$I = I_b - I_a.$$

The process of inverse bremsstrahlung involves raising a free electron to a higher energy state in the continuum of states available to it. The energy is a result of the absorption of a photon due to bremsstrahlung radiation which is itself produced by the acceleration of charged particles involved in elastic collisions. This absorption must occur with a simultaneous interaction with a heavy particle (atom, molecule or ion) in order that momentum is conserved.

Diffusion

The diffusion of electrons in a plasma is determined by the diffusion equation

$$\frac{\partial n}{\partial t} = D\nabla^2 n$$

where D is the (ambipolar) diffusion coefficient. In this equation, n represents the electron density of the plasma. With regard to ionization, the term In can be added to the diffusion equation to produce the inhomogeneous equation

$$\frac{\partial n}{\partial t} = D\nabla^2 n + In.$$

Note that, in general, I will be a function of both space and time. Another source term that is required is the multi-electron ionization rate due the e-beam alone which is responsible for the production of the initial electron density from which the cascade process develops. This ionization will also depend on both space and time and, in particular, on the distance of the beam away from the source. Thus, if we denote the e-beam ionisation rate by B (for beam), then the diffusion equation becomes

$$\frac{\partial n}{\partial t} = D\nabla^2 n + In + B$$

Recombination

Electron-ion collisions may lead to recombination, i.e. the production of a neutral atom as a result of the capture of an electron by an ion. The efficiency of the processes responsible for recombination is considerable at low electron energies at which the electron-ion interaction time is sufficiently large. Accordingly, at low electron temperatures (i.e. much less than the ionisation energy) these processes strongly affect the balance of the charged plasma particles. The rate of charged particle removal due to recombination in a volume is determined by the total recombination cross section and depends of the number densities of both ions n_i and electrons n_e. Thus the rate equation is given by

$$\frac{\partial n}{\partial t} = -Rn_i n_e = -Rn^2$$

where R is the recombination coefficient. The minus sign is introduced here because the process is lossy. This nonlinear equation has a simple analytical solution which can be obtained by inspection and is given by

$$\frac{1}{n} = \frac{1}{n_0} + Rt$$

where n_0 is the initial number density. After the density has fallen far below its initial value, it decays reciprocally with time, i.e.

$$n \propto \frac{1}{Rt}.$$

This is a fundamentally different behaviour from the exponential decay associated with diffusive processes and exponential growth associated with ionization processes. Since the recombination rate is proportional to n^2, for high values of n it can be expected to be the dominant process.

With regard to the diffusion equation, $-Rn^2$ is a source term and, thus, the diffusion equation must be modified again, this time to the nonlinear inhomogeneous form

$$\frac{\partial n}{\partial t} = D\nabla^2 n + In + B - Rn^2.$$

Note that, in general, it is expected that, like I and B, the recombination coefficient R will be a function of both space and time.

The rate equation above, has two source terms and two loss terms. The source terms are B and In which describe the initial population density of electrons produced by the e-beam alone and the population density generated by the cascade process. The loss terms $D\nabla^2 n$ and Rn^2 describe losses due to the processes of diffusion and recombination, respectively. Another effect that can be considered is loss through radiative processes. However, for weakly ionised plasmas, it reasonable to assume that this effect is relatively small compared to diffusion and recombination. These losses will also be proportional to n^2 since the total power P radiated per unit volume by a plasma is given by

$$P \sim 1.5 \times 10^{-38} Z^2 n_e n_i T_e^{\frac{1}{2}} \qquad (\text{Watts/m}^3)$$

where n is in m^{-3} and T_e is in eV. Because the radiated power is proportional to the square of the atomic number Z, a low Z plasma (e.g. a hydrogen plasma) will last longer.

Rate Equation Analysis

Analytical solutions to the rate equation

$$\frac{\partial n}{\partial t} = D\nabla^2 n + In + B - Rn^2$$

can be considered for different conditions compounded in the inclusion, or otherwise, of different terms.

In some practical cases, the diffusion loss will dominate over losses from recombination after initiation, and we can consider the electron density to be determined by the solution to

$$\frac{\partial n}{\partial t} = D\nabla^2 n + In.$$

For the characteristic diffusion length Λ of the breakdown, we may replace ∇^2 by $-1/\Lambda^2$ to obtain a solution of the form

$$n = n_0 \exp[(I - D/\Lambda^2)t].$$

This solution illustrates exponential growth of electrons, subject to exponential damping due to diffusion. Clearly, for a given coefficient of diffusion, the characteristic diffusion length should be low in order to achieve a high concentration of electrons.

Under conditions where, along with diffusion, the quadratic recombination term substantially affects the plasma decay, the rate equation takes the form

$$\frac{\partial n}{\partial t} = \nabla^2 n + In - Rn^2$$

or, in terms of the characteristic length of diffusion,

$$\frac{dn}{dt} = -\left(\frac{D}{\Lambda^2} - I\right) n - Rn^2.$$

The solution to this equation is

$$n(t) = \frac{\left(\frac{D}{\Lambda^2} - I\right) n_0 \exp\left(It - \frac{D}{\Lambda^2}t\right)}{\left(\frac{D}{\Lambda^2} - I\right) + Rn_0\left[1 - \exp\left(It - \frac{D}{\Lambda^2}t\right)\right]}.$$

Note that, when $D/\Lambda^2 - I >> Rn$, this solution changes into an exponential form that is characteristic of ionization growth and diffusion decay; alternatively, when $Rn >> D/\Lambda^2 - I$ the electron density is determined by the equation.

$$\frac{1}{n} = \frac{1}{n_0} + Rt.$$

Steady State Solutions

For steady state conditions

$$\frac{\partial n}{\partial t} = 0$$

and our rate equation reduces to

$$D\nabla^2 n + In + B - Rn^2 = 0.$$

Let us now consider some of the solutions available under different conditions.

If we consider the e-beam to produce ionization along the axis alone then the plasma source can be assumed to be axially symmetric. The electron density is then a function of the radius r and, using cylindrical coordinates, we have

$$\nabla^2 n = \frac{1}{r}\frac{\partial}{\partial r}\left(r\frac{\partial n}{\partial r}\right).$$

The simplest solution available to us in this case is obtained under the assumption that B, I and R are all zero. The plasma is therefore assumed to be a cylindrical plasma with losses due to diffusion alone. Except at $r = 0$, the density must satisfy

$$\frac{1}{r}\frac{\partial}{\partial r}\left(r\frac{\partial n}{\partial r}\right) = 0$$

which has the solution

$$n(r) = n_0 \ln r + c.$$

With the boundary condition $n(a) = 0$ (i.e. the electron density is zero some distance away from the source) we have $c = -n_0 \ln a$ and therefore

$$n(r) = n_0 \ln\left(\frac{a}{r}\right)$$

which is the fundamental solution to the 2D Laplace's equation.

Let us now consider the solution to the equation $D\nabla^2 n + In = 0$ in cylindrical coordinates. This requires that we solve the equation

$$\frac{1}{r}\frac{\partial}{\partial r}\left(r\frac{\partial n}{\partial r}\right) = -\frac{In}{D}$$

or

$$\frac{d^2n}{dr^2} + \frac{1}{r}\frac{dn}{dr} + \frac{I}{D}n = 0$$

which is Bessel's equation of order zero. This has the solution

$$n(r) = n_0 \mathrm{J}_0\left(r\sqrt{\frac{I}{D}}\right)$$

where J_0 is the Bessel function of order zero. The boundary condition that must be applied is that $n = 0$ at $r = a$. The Bessel function is zero for multiple values of $x = r\sqrt{I/D}$. However, the first zero occurs when $x \simeq 2.4$ or when

$$r = a = 2.4\sqrt{\frac{D}{I}}.$$

This solution describes the lowest diffusion mode in which a can be taken to define the boundary between the plasma and air. Although it is possible for higher diffusion modes to occur, they tend to decay rapidly in most plasmas and may therefore be ignored. Note that the radial extent of the electron density is proportional to the square root of the coefficient of diffusion.

Suppose we consider the case when the plasma source is in a steady state condition (i.e. the e-beam is operating in the continuous mode) and that the radial distribution of the electron density is described by J_0. For the case when the plasma source is moving through the atmosphere, it will be expected that the plasma streams away from the source (down wind) producing a decay of the electron density due to: (i) air flow effects, e.g. boundary layer thickening; (ii) recombination. Let us assume that the plasma forms a boundary layer with thickness

$$\Delta \sim \frac{L}{\sqrt{R}}$$

where R is the Reynolds number given by

$$R = \frac{Lv}{\eta},$$

L is the characteristic length scale of the flow, v is the velocity of the flow and η is the kinematic viscosity of air. For a 10 m long aerospace vehicle travelling at 100 m/s and with $\eta \sim 10^{-3} m^2/s$ for air,

$$\Delta = 1 \quad \text{mm}.$$

For a 1mm thick plasma sheath of 1 siemen/metre and considering the two-way travel path, the absorption of microwave radiation with a wavelength of 1cm (due to the skin depth effect) is 87%. Thus, relatively large absorption can occur over small boundary layers composed of low conductivity plasmas (i.e. plasmas with low electron number densities). As the plasma streams away from the source, the electron density will decrease due to an increase in the extent of the boundary layer (ignoring recombination). Since the initial radial extent of the plasma at source is given by a, we can expect the sheath thickness to be of the order of $a + \Delta$. The decay of the electron density as a function of r and L is therefore given by

$$n(r, L) = \frac{n_0 \mathrm{J}_0\left(r\sqrt{\frac{I}{D}}\right)}{2.4\sqrt{\frac{D}{I}} + \sqrt{\frac{L\eta}{v}}}.$$

This steady state solution neglects the effects of recombination but provides a qualitative estimate of the electron density profile produced by a continuous on-axis e-beam. In the following Section, we consider the equations required to compute the electron density accurately.

Steady State Equation with Flow

The rate equation for the electron density is given by

$$\frac{\partial n}{\partial t} = D\nabla^2 n + B + In - Rn^2.$$

If the plasma is generated in a flow of air then, to a good approximation, we can consider the electrons to flow with the air and thus conform to the conservation equation

$$\frac{\partial n}{\partial t} = \nabla \cdot (n\mathbf{v})$$

where $\mathbf{v}$ is the velocity of the flow. Hence, we are required to solve the equation

$$D\nabla^2 n + B + In - Rn^2 - \nabla \cdot (n\nabla u) = 0$$

where u is the velocity potential $\mathbf{v} = \nabla u$. Our problem is to find n given u which requires the velocity potential to be computed *a priori*. Suppose we compute the velocity potential for air (in the absence of a plasma). We can then consider a model in which the electron density is characterised by this potential alone. In other words, we consider the plasma to flow away from the source in a manner that is determined by the stream lines associated with the flow of air over the aerospace vehicle. For constant (air) density, the velocity potential is obtained by solving Laplace's equation

$$\nabla^2 u = 0$$

subject to appropriate boundary conditions. Noting that

$$\nabla u \cdot \nabla n = \nabla \cdot (u\nabla n) - u\nabla^2 n$$

we can write

$$(D+u)\nabla^2 n + B + In - Rn^2 - \nabla\cdot(u\nabla n) = 0.$$

This is the steady state equation for the electron density n subject to a flow regime characterized by velocity potential u. The 3D Green function solution to this equation is

$$n = \frac{1}{4\pi r} \otimes \left(\frac{B}{u+D} + \frac{In}{u+D} - \frac{Rn^2}{u+D} - \nabla\cdot(u\nabla n) \right)$$

where $\otimes$ denotes the 3D convolution. The order of iteration required to compute n can follow the order in which the physical mechanisms described by each of the terms occur. Thus:

Electron generation

$$n_1 = \frac{1}{4\pi r} \otimes \frac{B}{u+D}$$

Ionization

$$n_2 = n_1 + \frac{1}{4\pi r} \otimes \frac{In_1}{u+D}$$

Recombination

$$n_3 = n_1 + n_2 - \frac{1}{4\pi r} \otimes \frac{Rn_2^2}{u+D}$$

Flow

$$n_4 = n_1 + n_2 - n_3 - \frac{1}{4\pi r} \otimes \nabla\cdot(u\nabla n_3)$$

Figure 7.12 shows the effect of a plasma (specifically, the electron number density n_3) generated without ($u = 0$) and with ($\nabla^2 u = 0$) an air flow (from right to left) over a cone with a smooth point. This is achieved by implementing the equations above on a two-dimensional uniform grid of size 700×300, applying the convolution theorem and using the result

$$\frac{1}{\sqrt{x^2+y^2}} \Longleftrightarrow \frac{1}{\sqrt{k_x^2+k_y^2}}$$

with the boundary condition $n = 0$ (applied over the boundary and over the extent of the cone). The e-beam is taken to be a 'pencil line beam' (one pixel wide) emitted from the point of the cone with uniform intensity along its extent. The coefficients B, I, R and D are assumed constant with values: $B = 4\pi$, $I = 4\pi$, $R = 4\pi$ and $D = 1$. The velocity potential u is computed using the Successive-over-Relaxation method (see *Digital Signal Processing*, J M Blackledge, Horwood Publishing, 2003, Chapter 9) compounded in the following result (where $\omega = 1.1$ is the relaxation parameter)

$$u_{i,j}^{k+1} = u_{i,j}^{k} + \frac{\omega}{4}(u_{i+1,j}^{k} + u_{i-1,j}^{k+1} + u_{i,j+1}^{k} + u_{i,j-1}^{k+1} - 4u_{i,j}^{k})$$

for $i = 1, 2, ..., N$ and $j = 1, 2, ..., M$ with conditions $u_{ij} = 0$ on the boundary and over the extent of the cone, $u_{1,j} = u_0 \ \ \forall j$, $u_{N,j} = u_0 \ \ \forall j$, $u_{i,M} = u_0 \ \ \forall i$, $u_{i,1} = u_0 \ \ \forall i \notin C$ where C is the extent of the cone at the extreme left-hand edge of the grid (with $u_0 = 1$).

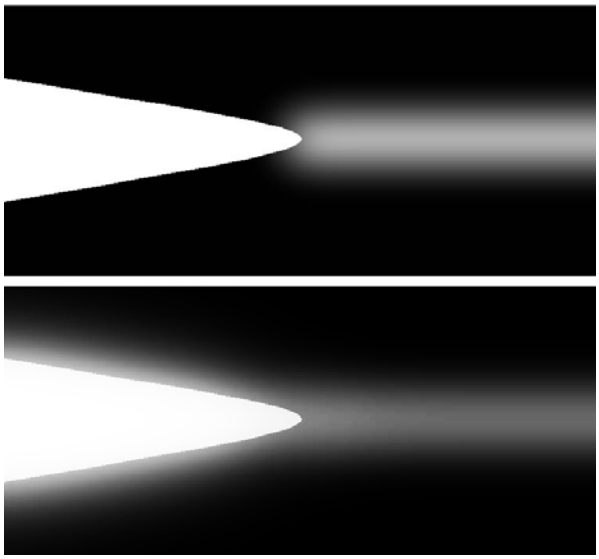

Figure 7.12: Plasma density profile generated by an electron beam without airflow (above) and with an airflow (below) from right to left over a 'smoothed cone'. The beam is taken to be of uniform intensity and emitted from the 'point' of the cone 'travelling' to the right.

The extent of the plasma sheath that forms over the boundary of the cone to provide a radar screen is quite noticeable when air flow is present, an extent that is strongly determined by the magnitude of the recombination coefficient and air flow for a given beam energy and coefficient of ionization. Actual values for R along with I, D and the beam profile B (which will not be uniform as in the idealized simulation presented here) and the flow rate will depend on the operating conditions that apply. These include the vehicle velocity, the plasma medium, additives (readily ionizable or reactive species), the electron beam energy, its diameter and profile. Typical parameters include an electron beam energy of 100keV, a (Gaussian) beam diameter of less than 5mm with a loss of 1keV per cm for an aerospace vehicle travelling at up to 100ms^{-1} operating in a plasma medium of air (over a range of atmospheric pressures) and with additives such as water vapour. Applications include the plasma screening of in-coming missiles, for example, against close proximity anti-missile systems that use radar for targeting and control.

Discussion

The idea of using a weakly ionized plasma to screen an aeropace vehicle is not new but interest in this effect and appraisal of the applications to which it can be practically applied are likely to grow. In this case study, we have developed a model for the radar signal generated with and without a plasma screen and illustrates that, for a weakly ionised plasma, the effect of such a screen is compounded in the function $\exp(-\sigma_0 t \epsilon_0)$ where t is the two-way travel time, σ_0 is the average conductivity of the plasma and ϵ_0 is the permittivity of free space. For a weakly ionised plasma, the conductivity is determined by the number density of electrons and qualitative results have been developed to estimate the number density of a plasma sheath enveloping a moving vehicle. A numerical procedure to simulate the number density of a plasma sheath has been developed and an example provided for the case when an e-beam induced plasma is generated from the front of a (sub-sonic) missile. This simulation is based on assuming cascade ionization with loss mechanisms due to diffusion and recombination. The simulator is not suitable for the super-sonic case when the airflow cannot by determined by the solution to Laplace's equation for the velocity potential. In this case, it may be expected that the plasma is partially distributed along the shock wave that is formed and thus, depending on the exact configuration of the aerospace vehicle, could provide a more extensive plasma screen.

7.8 Summary of Important Results

Stationary signals model

The signal $s(t)$ generated by the reflection of a pulse $p(t)$ from a layered inhomogeneous medium with an impulse response function $f(t)$ is given by

$$s(t) = p(t) \otimes f(t) + n(t)$$

where t is the two way travel time. This result assumes Born scattering, multiple scattering effects being assumed to be 'embedded' in the noise $n(t)$.

EM imaging

$$f(t) = \frac{1}{2}\frac{d}{dt}\ln Z(t) + \frac{1}{4\tau} - \frac{\sin^2\theta}{4c_0^2}\frac{d}{dt}c^2$$

Z - EM impedance $= \mu c$

c - EM wave velocity$= 1/\sqrt{\epsilon\mu}$

τ - Relaxation time $= \epsilon/\sigma$

θ - Angle of incidence

ϵ, μ and σ are the permittivity, permeability and conductivity respectively.

Acoustic imaging

$$f(t) = \frac{1}{2}\frac{d}{dt}\ln Z + \frac{1}{2}\frac{d}{dt}\left(\tau\frac{d}{dt}\ln Z\right) + \frac{3}{4}\frac{d^2\tau}{dt^2} + \frac{\sin^2\theta}{4c_0^2}\frac{d}{dt}\left(c^2 + \frac{d}{dt}(\tau c^2)\right)$$

Z - Acoustic impedance $= \rho c$

c - Acoustic wave velocity $= 1/\sqrt{\rho\kappa}$

τ - Relaxation time $= \kappa(\alpha + 2\beta)$

κ, ρ and $\alpha + 2\beta$ are the compressibility, density and bulk viscosity respectively.

Baseband systems

The pulse is given by

$$p(t), \quad t \in T \Longleftrightarrow P(\omega), \quad \mid \omega \mid \leq \Omega$$

where T is the pulse length and Ω is the bandwidth.

Sideband systems

The pulse is given by

$$p(t)\exp(i\omega_0 t) \Longleftrightarrow P(\omega - \omega_0)$$

where ω_0 is the carrier frequency.

7.9 Further Reading

- Rihaczek A W, *Principles of High Resolution Radar*, McGraw-Hill, 1969.
- Ricker N H, *Transient Waves in Visco-elestic Media*, Developments in Solid Earth Geophysics 10, Elsevier, 1976.
- Golant V E, Zhilinsky A P and Sakharov I E, *Fundamentals of Plasma Physics*, Wiley series in plasma physics, 1977.
- Aki K and Richards P, *Quantitative Seismology (Theory and Methods)*, Freeman and Company, 1980.
- Wells P N T (Editor), *Scientific Basis of Medical Imaging*, Churchill-Livingstone, 1982.
- Mitchell R L, *Radar Signal Simulation*, MARK Resources, 1985.
- Connor F R, *Waves*, Arnold, 1986.
- Bellman R and Vesudevan R, *Wave Propagation: An Invariant Embedding Approach*, Reidel, 1986.

- Wait J R, *Electromagnetic Wave Theory*, Wiley, 1987.
- Woolfson M M and Pert G J, *An Introduction to Computer Simulation*, Oxford University Press, 1999.
- Evans G A, Blackledge J M and Yardley P, *Analytical Methods for Partial Differential Equations*, Springer, 2000.
- Evans G A, Blackledge J M and Yardley P, *Numerical Methods for Partial Differential Equations*, Springer, 2000.

Chapter 8

Projection Tomography

The imaging of layered media discussed in the previous Chapter is based on utilizing a spectrum of waves through the application of a pulse of radiation in which the reflected or back-scattered waves are recorded. The models used are compounded in the calculation of the reflection coefficient. Whether the imaging system is based on a baseband pulse $p(t)$ or a sideband pulse $p(t)\exp(i\omega_0 t)$, the essential approximation that is used is the Born approximation which requires that

$$\bar{\gamma} << 1,$$

the information the images provide being on the scale of the (carrier) wavelength(s) used, i.e.

$$\lambda \sim D$$

where D is the characteristic dimension of the scatterer (reflector). In Chapter 6, the WKB and Rytov approximations were considered and it was shown that these approximations are most effective when

$$\lambda << D$$

with no condition having to be placed on the magnitude of $\bar{\gamma}$. When this condition is valid, imaging techniques can be developed that are based on considering the wavefield to be a field of 'rays', which propagate through the material, changing their properties cumulatively to give a projection at some point(s) in space. This is known as projection tomography. It is analogous to geometric optics and, like geometric optics, is based on assuming that the radiation field is composed of rays which can be described mathematically using geometric relationships.

In this Chapter, the principles and theoretical basis for projection tomography are discussed. This is for two reasons. First, projection tomography is used for imaging inhomogeneous materials for non-destructive analysis. Secondly, the theoretical basis of projection tomography has a wider range of applications. For example, it is used in diffraction tomography which is discussed in the following Chapter. Moreover, the theory of projection tomography, which is compounded in a transform known as the Radon transform, plays an important role in image processing and machine vision. Radon transform-based

computer vision and, in particular, the Hough transform (a special case of the Radon transform), is of value in pattern recognition when the image is composed of lines and curves (finger print identification, for example) obtained via the application of an edge detector. Further, it is sometimes of value to process a digital image in 'Radon space' through the application of various (Radon space) filters. In addition, the Radon transform provides a method of processing non-separable digital images using signal processing algorithms for which there is no directly equivalent image processing algorithm.

8.1 Basic Principles

The history of projection tomography is interesting in two respects. First, it is a good example of a scientific development where advances in technology (particularly in digital computer power) aided theoretical progress in the subject. Secondly, a large number of early investigators were entirely unaware of former contributions that had been made. Indeed, the theoretical basis for projection tomography was 're-discovered' many times before it was realized in the early 1970s that the Austrian mathematician Johannes Radon had studied the problem as early as 1917. It is now accepted that the theoretical basis for projection tomography is compounded in the analytical properties of the 'Radon transform' and its inverse.

8.1.1 X-ray CT

Although projection tomography now has a wide range of applications in many diverse areas, it originated as a problem in medical diagnosis using X-rays. The imaging technique and the transform(s) upon which it is now based grew rapidly as a result of the announcement in 1972 of the invention of Computer Tomography (CT) by G N Hounsfield using X-rays. It is therefore appropriate to introduce projection tomography in terms of an X-ray imaging technique.

X-rays have been used for many years in medical diagnosis. This involves recording the intensity of X-rays on a photographic plate as they emerge from a three-dimensional object after having been attenuated by an amount that is determined by the path followed by a particular ray through the object. This gives an image known as an X-ray radiograph. Each grey level (assuming the radiograph has been digitized) is determined by the combined effect of all the absorbing elements that lie along the path of an individual ray.

We can consider a three-dimensional object to be composed of a number of two-dimensional slices stacked one on top of the other. Instead of looking at the absorption of X-rays over a composite stack of these slices, we can choose to study the absorption of X-rays as they pass through an individual slice. To do this we must assume that the absorption properties over the finite thickness of the slice are constant. The type of image produced by looking at the material composition and properties of a slice is known as a tomogram. The absorption of X-rays as they pass through a slice provides a single profile of the X-ray intensity. This profile is characteristic of the distribution of material in the slice. This is illustrated in Figure 8.1.

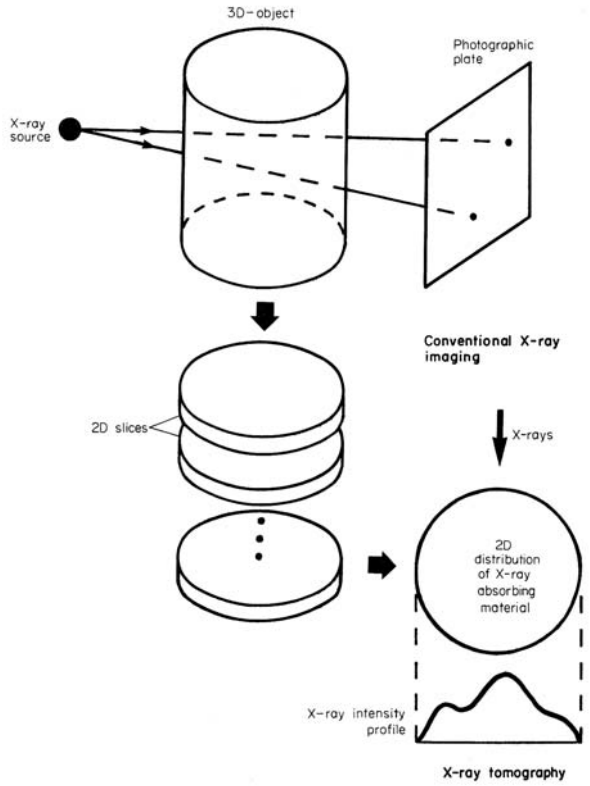

Figure 8.1: Conventional X-ray imaging (top) and X-ray tomography (bottom). By considering a three dimensional object to be composed of a stack of slices, we can investigate the distribution of X-ray absorbing material in a single slice by recording the corresponding X-ray intensity profile. This is known as X-ray tomography.

A single profile of the X-ray intensity associated with a particular slice only provides a qualitative account of the distribution of material in a slice. In other words, we only have one-dimensional information about a two-dimensional object just as in conventional X-ray radiography we only have two-dimensional information (i.e. an image) about a three-dimensional object. Further information can be obtained by changing the direction of the X-rays. This is determined by the angle of rotation θ of the slice relative to the source or, equivalently, by the location of the source relative to the slice. Either way, further information on the composition of the material may be obtained by observing how the X-ray intensity profile varies with the angle of rotation. The basic question then arises of how the two-dimensional structure of a slice can be reconstructed from information on the X-ray intensity profiles as a function

θ. One way is to use a computer-based arithmetic technique. This is where an initial estimate for the reconstruction is progressively updated until a sequence of simulated projections are obtained which are close to the experimental data. This is an iterative technique known as Arithmetic Reconstruction Tomography (ART). It can be used effectively when relatively small data fields are involved. However, ART is not an inverse solution to the problem. In other words, it is not an algorithm that reconstructs the distribution of material in a slice from the experimental data directly.

The addition of computer techniques to tomography has led to a method of X-ray imaging known a Computed Tomography (CT) or Computer Aided Tomography (CAT) and the so-called CAT-scan. Computer or computed tomography provides a quantitative image of the absorption coefficient for X-rays. To understand this, consider a single X-ray with initial intensity I_0. If it passes through a homogeneous material with an attenuation coefficient α over a length L, the resulting intensity is

$$I = I_0 \exp(-\alpha L).$$

If the material is inhomogeneous, we can consider the path along which the ray travels to consist of different attenuation coefficients α_i over elemental lengths $\Delta\ell_i$ (the length over which the attenuation coefficient is constant). The resulting intensity is then

$$I = I_0 \exp[-(\alpha_1 \Delta\ell_1 + \alpha_2 \Delta\ell_2 + ... + \alpha_N \Delta\ell_N)]$$

where

$$\sum_{i=1}^{N} \Delta\ell_i = L.$$

As $\Delta\ell_i \to 0$, we can consider the result

$$I = I_0 \exp\left(-\int_L \alpha d\ell\right).$$

By computing the natural logarithm of I/I_0, we obtain the data

$$P = \int_0^L \alpha d\ell$$

where

$$P = -\ln(I/I_0).$$

The value of the intensity and therefore P depends upon the point where the ray passes through the object, which shall be denoted by z. It also depends on the orientation of the object relative to the ray. This is determined by the angle of rotation of the object about its centre θ. Hence, by adjusting the orientation of the attenuating object to a linear X-ray field, a full sequence of projections can

be obtained which are related to the two-dimensional attenuation coefficient $\alpha(x, y)$ of a slice by the equation

$$P(z, \theta) = \int_{L(z,\theta)} \alpha(x, y) d\ell \tag{8.1}$$

where $d\ell$ is an element of a line passing through the function $\alpha(x, y)$ and L (as indicated in the equation above) depends on z and θ as shown in Figure 8.2.

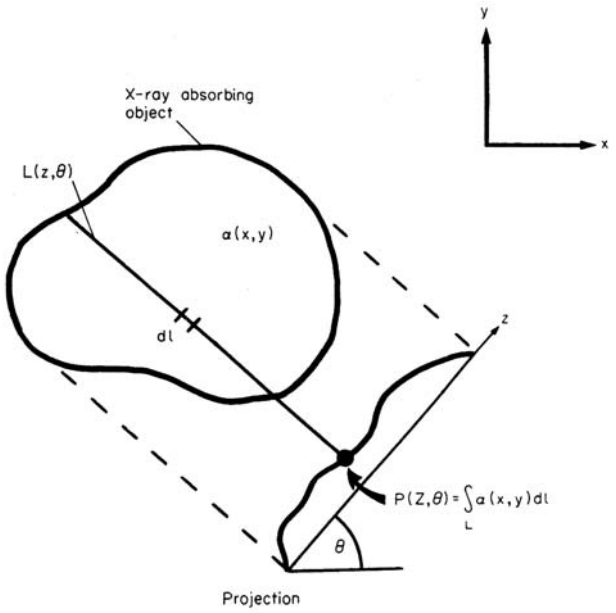

Figure 8.2: A projection is denoted by $P(z, \theta)$ where θ is the angle at which the projection is taken and z is the projection coordinate. This function is related to the variable X-ray absorption coefficient $\alpha(x, y)$ by the line integral shown. Projection tomography is based on measuring $P(z, \theta)$ for all values of z and θ and then inverting the line integral(s) to recover $\alpha(x, y)$.

The function P is a line integral through the two-dimensional X-ray absorption coefficient $\alpha(x, y)$. It is a projection of the function α that is characteristic of θ. The general name given to this type of imagery is therefore projection tomography. Here, the basic problem is to invert equation (8.1) to obtain $\alpha(x, y)$ when P is known for all values of z and θ. In Section 8.3, it is shown that equation (8.1) is just another way of writing the Radon transform of the function $\alpha(x, y)$ and how the inverse Radon transform can be used to reconstruct this function.

Recent advances in Dynamic Spatial Reconstructors (DSR) provide two very powerful features to CT: high resolution and synchronous (fully three di-

mensional) scanning. They have revolutionized medical imaging by providing dynamic studies of the anatomical structures and functional relationships of moving organ systems such as the heart, lungs and circulatory systems. Further, DSR are capable of simultaneous three-dimensional reconstructions of vascular anatomy and the dynamics of blood circulation in any region of the body.

8.1.2 Time-of-Flight CT

Although X-ray absorption CT is one of the main applications of projection tomography, it can of course be applied to any source/detector system where: (i) the probe can be assumed to pass through the material like a ray; (ii) a measurable property of the probe can be recorded that is associated with physical changes that take place along the path of the ray.

The term 'measurable property' includes the attenuation of X-rays or any other type of radiation that is attenuated by the object. However, there are properties of a field other than attenuation that may also be measured. For example, consider the case where a short pulse of radiation is emitted and the time taken for it to reach the detector recorded. If the material in which the pulse propagates is homogeneous, then the 'time-of-flight' for the pulse to traverse the distance between source and detector along a line L is given by the simple expression

$$t = \frac{L}{v}$$

where v is the velocity at which the pulse propagates through the material. Now, if the material is inhomogeneous along L, the time of flight becomes

$$t = \int_L \frac{dx}{v(x)}.$$

If we record the time of flight for all lines through a slice of material with an inhomogeneous velocity profile $v(x, y)$, then, by analogy with equation (8.1), we can write

$$P(z, \theta) = \int_L \frac{d\ell}{v(x, y)}.$$

In this case, a tomogram of the inhomogeneous velocity of the material can be found by inverting the above equation. This result is the basis for an imaging technique known as ultrasonic computer tomography (UCT). In this case, a short acoustic pulse is used as a probe. Alternatively, the decay in amplitude of the ultrasonic probe can be measured. This allows a tomogram of the acoustic attenuation to be obtained. Images of this kind may be interpreted as maps of the viscosity of the material since it is the viscous nature of a material that is responsible for attenuating acoustic radiation. By using electromagnetic probes, we can obtain information about the spatial distribution of the refractive index of a material using an appropriate time-of-flight experiment or the conductivity of a material by measuring the decay in amplitude of the EM field. Other tomographic imaging systems can be developed by measuring physical properties such as the capacitance, resistance and inductance, for example.

8.1.3 Emission CT

Emission Computed Tomography (ECT) refers to the use of radioactive isotopes as passive probes. This passive approach does not require external probes. There is a probe involved but it comes from the object itself. In the case of ECT, we determine the distribution (location and concentration) of some radioactive isotope inside an object by studying the emitted photons.

There are two basic types of ECT depending on whether the isotope utilized is a single photon emitter, such as iodine-131, or a positron (e^+ or β^+) emitter, such as carbon-11. When a β^+ emitter is used, the ejected positron loses most of its energy over a few millimetres. As it comes to rest, it annihilates with a nearby electron resulting in the formation of two γ-ray photons which travel in opposite directions along the same path. If a ring of detectors is placed around the object and two of the detectors simultaneously record γ-ray photons, then the radio-nuclide is known to lie somewhere along the line between the detectors.

The reconstruction problem can therefore be cast in terms of the Radon transform where a complete set of projections is a measure of the total radionucleide emission. The use of ECT has provided a dramatic advancement in nuclear medicine including investigations into brain and heart metabolisms. Other possibilities include new methods for cancer detection. Further, the method can be used in industry for imaging the distribution of isotope doped materials, e.g. imaging the distribution of oil in an internal combustion or gas turbine engine.

8.1.4 Diffraction Tomography

Diffraction tomography is a method of imaging based on reconstructing an object from measurements of the way in which it diffracts a probe signal. Unlike X-ray CT, this involves the use of a radiation field whose wavelength is the same order of magnitude as the object (e.g. ultrasound, with a wavelength $\sim 10^{-3}$m, and millimetric microwaves). Two methods are available based on (i) CW (Continuous Wave) fields and (ii) pulsed fields. In the latter case, the time history of the diffraction pattern set-up by a short pulse of radiation is related to the internal structure of the diffracting object by the Radon transform (see Chapter 9). Hence, in principle, the object can be reconstructed by employing algorithms for computing the inverse Radon transform.

8.1.5 Computer Vision

The Radon transform is used directly in computer vision which is concerned with the analysis and recognition of images. It is particularly important to manufacturing industry for automatic inspection and for military applications (e.g. guided weapons systems and automatic targeting).

The projection transform utilized in computer vision is the Hough transform. The Hough transform was derived independently from the Radon transform. However, the Hough transform is in fact just a special case of the Radon transform. The basic idea involves the identification of lines in digital images.

The Radon transform of a function concentrated at a point, described by the 2D delta function

$$\delta^2(x - x_0, y - y_0) = \delta(x - x_0)\delta(y - y_0),$$

yields a sinusoidal curve

$$p = x_0 \cos\theta + y_0 \sin\theta$$

in the $p\theta$-plane. All co-linear points in the xy-plane, along a line determined by fixed values of θ_0 and p_0, map to sinusoidal curves in the $p\theta$-plane and intersect at the same point. Thus, if we choose a suitable method for plotting the projections of a digital image as a function of θ and p, it follows that the Radon transform may be regarded as a line-to-point transformation. By utilizing the line detection properties of the Radon transform, the edges of manufactured objects for example can be analysed against their known characteristics. From these characteristics, the identification of faults can be realised. Other areas of imaging science which are based on the properties of the Radon transformation include the fields of astronomy, optics, and Magnetic Resonance (MR).

8.2 Projection Tomography and Scattering Theory

In general, projection tomography involves an experiment where the projections $P(z, \theta)$ of a two-dimensional object $O(x, y)$ are recorded at different angles θ. A computer algorithm is then designed to invert the equation

$$P(z, \theta) = \int_{L(z,\theta)} O(x, y) d\ell$$

numerically and reconstruct the object function O. The physical interpretation of the object function depends on the nature of the experiment, the type and frequency of the probe and the measurements that are made. The success of projection tomography as a useful imaging technique relies on how well the probe behaves like a ray. If the probe starts to diffract as a result of its interaction with the material, then projection tomography is inadequate and diffraction tomography must be applied, which, as discussed in the following Chapter, for pulsed systems, is based on an application of the Radon transform.

In Chapter 6, the WKB approximation was introduced as a method for solving the 1D inhomogeneous Helmholtz equation under the condition that

$$\lambda << L$$

where L is the characteristic length of the inhomogeneity. In particular, it was shown that the solution to

$$\left(\frac{\partial^2}{\partial x^2} + k^2\right) u(x, k) = -k^2 \gamma(x) u(x, k)$$

under this condition is given by

$$u(x,k) = \exp\left[ik\left(x + \frac{1}{2}\int^{x} \gamma(x)dx\right)\right]$$

using the eikonal transform

$$u(x,k) = \exp(ikx)\exp[s(x,k)].$$

Suppose we consider a pulse of radiation with spectrum $P(\omega)$ so that with $k = \omega/c_0$, where c_0 is the constant wave speed, we can write

$$u(x,\omega) = P(\omega)\exp\left[i\omega\left(t + \frac{1}{2}\int^{x} \frac{dx}{v(x)}\right)\right]$$

where $v(x) = c/\gamma(x)$. Inverse Fourier transforming, the time-dependent wavefield U associated with the time taken for this pulse to propagate from a source (taken to be at $x = 0$) to a receiver at x_0, say, is

$$U(x_0,t) = p(t) \otimes \delta\left(t + \frac{1}{2}\int_0^{x_0} \frac{dx}{v(x)}\right) = p(t+T)$$

where

$$T = \frac{1}{2}\int_0^{x_0} \frac{dx}{v(x)}.$$

However, in order for the WKB approximation to apply, a high frequency wavefield is required which dictates the need for a sideband system so that the spectrum becomes $P(\omega + \omega_0)$ where $\omega_0 >> \omega$ and $\mid \omega \mid \leq \Omega$ (the bandwidth of the pulse). In this case,

$$U(x_0,t) = \exp[i\omega_0(t+T)]p(t+T),$$

the demodulated signal being given by

$$\exp(-i\omega_0 t)U(x_0,t) = \exp(i\omega_0 T)p(t+T)$$

whose amplitude envelope is $p(t+T)$. The arrival of the pulse at the detector is then determined by the time of flight T.

In the case of attenuation-based tomography using EM waves for example, let us rework the WKB approximation using the 1D scalar wave equation

$$\left(\frac{\partial^2}{\partial x^2} + k^2\right)u(x,k) = -k^2\gamma_\epsilon u(x,k) + ikz_0\sigma u(x,k)$$

where

$$\gamma_\epsilon = \frac{\epsilon - \epsilon_0}{\epsilon_0},$$

σ is the conductivity, z_0 is the impedance of free space, and it is assumed that $\mu = \mu_0$. Using the eikonal transform $u = Au_i \exp(-s)$ where A is the amplitude of the incident field, the WKB approximation yields the equation

$$-2ik\frac{ds}{dx} = -k^2\gamma_\epsilon + ikz_0\sigma$$

whose solution is (ignoring the constant of integration)

$$s(x) = -\frac{ik}{2}\int^x \gamma_\epsilon(x)dx - \frac{z_0}{2}\int^x \sigma(x)dx.$$

Thus, the rayfield is given by

$$u(x,k) = A\exp\left[ik\left(x - \frac{1}{2}\int^x \gamma_\epsilon(x)dx\right)\right]\exp\left(-\frac{z_0}{2}\int^x \sigma(x)dx\right).$$

With X-ray tomography, we measure the intensity of the rayfield which in this case is given by (with $I_0 =\mid A \mid^2$)

$$I =\mid u(x,k) \mid^2 = I_0\exp\left(-\int^x \alpha(x)dx\right)$$

where $\alpha = z_0\sigma/2$.

The results above demonstrate that the principles of projection tomography discussed earlier are based on a WKB approximation to the scattering problem in which $\lambda >> L$ where the wavefield becomes a rayfield. Application of a multiple rayfield through a two-dimensional object at different angles then yields a set of projections from which we are required to reconstruct the object function. The basis for this is the Radon transform which provides one of the most successful theoretical foundations for imaging both the two- and three-dimensional internal structure of inhomogeneous objects. Consequently, it has a wide range of applications. The mathematical principles of projection tomography considers continuous functions. The inverse problem therefore involves the reconstruction of an object function from an infinite set of projections. In practice, only a finite number of projections can be obtained by computing the inverse Radon transform digitally. The accuracy of this approximation can be improved by increasing the number of projections used and employing suitable image enhancement techniques.

8.3 The Radon Transform

We have already seen in previous Chapters that a large proportion of the theory of imaging is closely related to the analytic properties of the delta function, in particular, the Fourier transform and the Green function. Another important example is the Radon transform which has a variety of applications and which is the mathematical basis for projection tomography. In this Section, the Radon transform is derived entirely from the analytic properties of the two-dimensional delta function.

8.3.1 Derivation of the Radon transform

Consider the two-dimensional delta function

$$\delta^2(\mathbf{r}-\mathbf{r}_0) = \delta(x-x_0)\delta(y-y_0).$$

Let us write this function in terms of its integral representation, i.e.

$$\delta^2(\mathbf{r}-\mathbf{r}_0) = \frac{1}{(2\pi)^2}\int_{-\infty}^{\infty} \exp[-i\mathbf{k}\cdot(\mathbf{r}-\mathbf{r}_0)]d^2\mathbf{k}.$$

Next, writing

$$\mathbf{k} = \hat{\mathbf{n}}k$$

where

$$\hat{\mathbf{n}} = \frac{\mathbf{k}}{k}$$

we note that

$$\int_{-\infty}^{\infty} \delta(z-\hat{\mathbf{n}}\cdot\mathbf{r})\exp(-ikz)dz = \exp(-ik\hat{\mathbf{n}}\cdot\mathbf{r})$$

where δ is the one-dimensional delta function. This result allows us to write the two-dimensional delta function, as

$$\delta^2(\mathbf{r}-\mathbf{r}_0) = \frac{1}{(2\pi)^2}\int_{-\infty}^{\infty}\int_{-\infty}^{\infty} \exp(ik\hat{\mathbf{n}}\cdot\mathbf{r}_0)\exp(-ik\hat{\mathbf{n}}\cdot\mathbf{r})d^2\mathbf{k}$$

$$= \frac{1}{(2\pi)^2}\int_{-\infty}^{\infty}\int_{-\infty}^{\infty} d^2\mathbf{k}\exp(ik\hat{\mathbf{n}}\cdot\mathbf{r}_0)\int \delta(z-\hat{\mathbf{n}}\cdot\mathbf{r})\exp(-ikz)dz.$$

This result can now be written in polar coordinates (k,θ) giving

$$\delta^2(\mathbf{r}-\mathbf{r}_0) = \frac{1}{(2\pi)^2}\int_0^{2\pi} d\theta\int_0^{\infty} dk k\int_{-\infty}^{\infty} dz\exp[ik(\hat{\mathbf{n}}\cdot\mathbf{r}_0 - z)]\delta(z-\hat{\mathbf{n}}\cdot\mathbf{r})$$

$$= \frac{1}{(2\pi)^2}\int_0^{\pi} d\theta\int_{-\infty}^{\infty} dk \mid k \mid \int_{-\infty}^{\infty} dz\exp[ik(\hat{\mathbf{n}}\cdot\mathbf{r}_0 - z)]\delta(z-\hat{\mathbf{n}}\cdot\mathbf{r}).$$

The next task involves a couple of simple analytical tricks. Using the definition of the sgn function, i.e.

$$\mathrm{sgn}(k) = \begin{cases} 1, & k \geq 0; \\ -1, & k < 0. \end{cases}$$

$| k |$ can be re-written as $k\,\mathrm{sgn}(k)$ so that

$$\delta^2(\mathbf{r}-\mathbf{r}_0) = \frac{1}{(2\pi)^2}\int_0^{\pi} d\theta \int_{-\infty}^{\infty} dk k\,\mathrm{sgn}(k) \int_{-\infty}^{\infty} dz \exp[ik(\hat{\mathbf{n}}\cdot\mathbf{r}_0 - z)]\delta(z-\hat{\mathbf{n}}\cdot\mathbf{r}).$$

Re-writing the two-dimensional delta function in this form allows us to utilize the result

$$\int_{-\infty}^{\infty}\left(\frac{\partial}{\partial z}\delta(z-\hat{\mathbf{n}}\cdot\mathbf{r})\right)\exp(-ikz)dz = ik\int_{-\infty}^{\infty}\delta(z-\hat{\mathbf{n}}\cdot\mathbf{r})\exp(-ikz)dz$$

giving

$$\delta^2(\mathbf{r}-\mathbf{r}_0) = -\frac{i}{(2\pi)^2}\int_0^{\pi} d\theta \int_{-\infty}^{\infty} dz\left(\frac{\partial}{\partial z}\delta(z-\hat{\mathbf{n}}\cdot\mathbf{r})\right)$$
$$\times\int_{-\infty}^{\infty} dk\,\mathrm{sgn}(k)\exp[ik(\hat{\mathbf{n}}\cdot\mathbf{r}_0 - z)].$$

We can progress further by using the definition of the sgn function in terms of the Fourier transform of $1/u$ (u being a dummy variable), i.e.

$$\int_{-\infty}^{\infty}\frac{1}{u}\exp(-iku)du = -i\pi\,\mathrm{sgn}(k).$$

On taking the inverse Fourier transform we obtain

$$\frac{1}{u} = -\frac{i}{2}\int_{-\infty}^{\infty}\mathrm{sgn}(k)\exp(iku)dk$$

or, rearranging,

$$\int_{-\infty}^{\infty}\mathrm{sgn}(k)\exp(iku)dk = \frac{2i}{u}.$$

The two-dimensional delta function can then be written as

$$\delta^2(\mathbf{r}-\mathbf{r}_0) = \frac{1}{2\pi^2}\int_0^{\pi} d\theta \int_{-\infty}^{\infty} dz\frac{1}{\hat{\mathbf{n}}\cdot\mathbf{r}_0 - z}\frac{\partial}{\partial z}\delta(z-\hat{\mathbf{n}}\cdot\mathbf{r}).$$

All that has been done here is to utilize various analytical results to write δ^2 in a different form. The reason for this is that the definition of the forward and inverse Radon transforms is now very easy to derive via the sampling property of the delta function. Consider a continuous 2D function O, referred to as the object function. This function may be written as

$$O(\mathbf{r}_0) = \int_{-\infty}^{\infty} O(\mathbf{r})\delta^2(\mathbf{r}-\mathbf{r}_0)d^2\mathbf{r}.$$

Substituting our definition for δ^2 into the above equation leads to the expression

$$O(\mathbf{r}_0) = \int_{-\infty}^{\infty} O(\mathbf{r}) \frac{1}{2\pi^2} \int_0^{\pi} d\theta \int_{-\infty}^{\infty} dz \frac{1}{\hat{\mathbf{n}} \cdot \mathbf{r}_0 - z} \frac{\partial}{\partial z} \delta(z - \hat{\mathbf{n}} \cdot \mathbf{r}) d^2\mathbf{r}$$

or, alternatively, after interchanging the order of integration,

$$O(\mathbf{r}_0) = \frac{1}{2\pi^2} \int_0^{\pi} \int_{-\infty}^{\infty} dz \frac{1}{\hat{\mathbf{n}} \cdot \mathbf{r}_0 - z} \frac{\partial}{\partial z} P(\hat{\mathbf{n}}, z) \tag{8.2}$$

where

$$P(\hat{\mathbf{n}}, z) = \int_{-\infty}^{\infty} O(\mathbf{r}) \delta(z - \hat{\mathbf{n}} \cdot \mathbf{r}) d^2\mathbf{r}.$$

The function P is defined as the Radon transform of O, and we can write

$$P(\hat{\mathbf{n}}, z) = \hat{R}O(\mathbf{r}) = \int O(\mathbf{r}) \delta(z - \hat{\mathbf{n}} \cdot \mathbf{r}) d^2\mathbf{r} \tag{8.3}$$

where $\hat{R}$ denotes the the Radon transform operator. The object function can be recovered or reconstructed from P using equation (8.2). By writing

$$O(\mathbf{r}_0) = \hat{R}^{-1} P(\hat{\mathbf{n}}, z) = \frac{1}{2\pi^2} \int_0^{\pi} d\theta \int_{-\infty}^{\infty} dz \frac{1}{\hat{\mathbf{n}} \cdot \mathbf{r}_0 - z} \frac{\partial}{\partial z} P(\hat{\mathbf{n}}, z) \tag{8.4}$$

we may define $\hat{R}^{-1}$ as the inverse Radon transform operator. The function P denotes the projection or line integral of O onto a line perpendicular to the direction of $\hat{\mathbf{n}}$. The unit vector $\hat{\mathbf{n}}$ defines the angle of rotation of the object function and so we may write

$$P(\hat{\mathbf{n}}, z) \equiv P(\theta, z).$$

The variable z may be interpreted as defining the location of $\hat{\mathbf{n}}$ at which the rectilinear line integral through O is taken.

8.3.2 Operator Analysis

At this stage, it is useful to introduce two more operators, namely the Hilbert transform operator $\hat{H}$, defined by

$$\hat{H}f = \frac{1}{\pi} \int \frac{f(z)}{\hat{\mathbf{n}} \cdot \mathbf{r}_0 - z} dz$$

and the Back projection operator $\hat{B}$ given by

$$\hat{B}f = \frac{1}{2\pi} \int_0^{\pi} f(\hat{\mathbf{n}}, \hat{\mathbf{n}} \cdot \mathbf{r}_0) d\theta$$

where f is a continuous function. From equation (8.4) the inverse Radon transform can then be written in terms of operators as

$$O(\mathbf{r}) = \hat{R}^{-1}P(\theta, z) = \hat{B}\hat{H}\partial_z P(\theta, z), \quad \partial_z \equiv \frac{\partial}{\partial z}.$$

It is then clear that

$$\hat{R}^{-1} \equiv \hat{B}\hat{H}\partial_z.$$

In other words, to compute the inverse Radon transform we need to differentiate, Hilbert transform and then back-project. This is known as filtered back-projection, the filtering being a result of implementing the operator $\hat{H}\partial_z$. The type of filter that is produced by this operation can be found by transforming $\hat{H}\partial_z P$ into Fourier space. For a fixed value of $\hat{\mathbf{n}}$ this operation can be written as

$$\hat{H}\partial_z P = \frac{1}{\pi z} \otimes \frac{\partial P}{\partial z}.$$

By taking the Fourier transform of this equation and using the convolution theorem we obtain

$$\hat{H}\frac{\partial P}{\partial z} \Longleftrightarrow -i\,\mathrm{sgn}(k)ik\widetilde{P}$$

where $\widetilde{P}$ is the Fourier transform of P. Hence, we see that the filter produced by the operation $\hat{H}\partial_z$ is $\mathrm{sgn}(k)k$ or $\mid k \mid$.

8.3.3 Geometric Analysis

Now that the main mathematical results have been presented, let us look at the geometrical significance of both a projection and back-projection. Writing $\hat{\mathbf{n}} \cdot \mathbf{r}$ as $x\cos\theta + y\sin\theta$, the projection function given in equation (8.3) is

$$P(\theta, z) = \int\int O(x, y)\delta(z - x\cos\theta - y\sin\theta)dxdy. \tag{8.5}$$

The delta function is non-zero at the 'point' where

$$z = x\cos\theta + y\sin\theta.$$

We can think of a projection as being the family of line integrals through the object function when it is rotated by an angle θ. To illustrate this, consider the case when $\theta = 0$. The projection at this angle is given by

$$P(0, z) = \int\int O(x, y)\delta(z - x)dxdy = \int O(z, y)dy.$$

In this case, it is easy to see that the projection $P(0, z)$ is obtained by integrating the object over y for all values of the projection coordinate z. This is shown in Figure 8.3a. When $\theta = \pi/2$, the projection at this angle is

$$P(\pi/2, z) = \int\int O(x, y)\delta(z - y)dxdy = \int O(x, z)dx$$

and so, in this case, the projection is obtained by integrating along x as shown in Figure 8.3b. It should now be clear that, for arbitrary values of θ, the line integral through O is along a line L as shown in Figure 8.3c. Another way of writing the Radon transform is therefore

$$P(\theta, z) = \hat{R}O(x, y) = \int_L O(x, y) d\ell$$

where L depends on the value of θ and z. This equation is useful as a conceptual guide, showing that the Radon transform is just a collection of parallel line integrals at different angles.

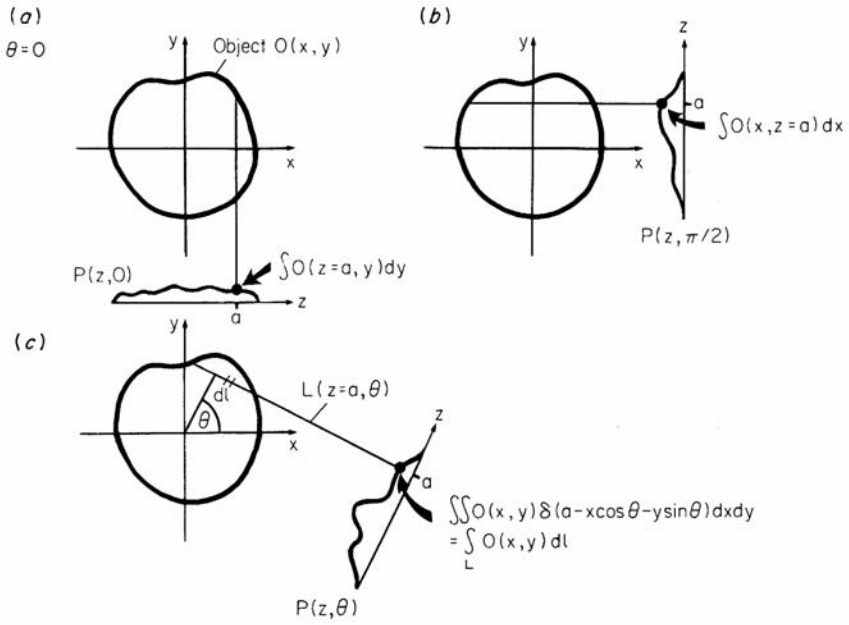

Figure 8.3: The projection of an object at three different angles.

Let us now turn our attention to back-projection. The result of back-projecting a sequence of projections

$$P(\theta, z), \quad z = x\cos\theta + y\sin\theta$$

may be written as

$$B(x, y) = \frac{1}{2\pi} \int_0^\pi P(x\cos\theta + y\sin\theta, \theta) d\theta.$$

The function $P(x\cos\theta + y\sin\theta, \theta)$ is the distribution of P along the family of lines L. In other words, for a fixed value of θ, $P(x\cos\theta+y\sin\theta,\theta)$ is constructed by assigning the value of the projection at z to all the points that lie along the line L. For example, referring to Figure 8.3c, we take the value of the projection at $z = a$ and let all points along the line L have the same value. By repeating this process for all values of z, the function $P(x\cos\theta + y\sin\theta, \theta)$ is obtained for a given value of θ. The whole process is then repeated for all values of θ between 0 and π. This provides the function $P(x\cos\theta+y\sin\theta,\theta)$ for all values of θ. By summing all these results, the back-projection function is obtained. This is how the inverse Radon transform is obtained, except that in this case we back project the filtered projections, i.e. we back-project $\hat{H}\partial_z P(\theta, z)$ rather than just $P(\theta, z)$.

8.4 Back-Projection PSF

The point spread function (PSF) associated with the back-projection function can be found by back-projecting the projections obtained from a single point and observing how the result is spread about this point. We can describe a 'perfect point' by a two-dimensional delta function. If we project a two-dimensional delta function, the result will be a sequence of one-dimensional delta functions at different angles. In terms of polar coordinates (r, θ_0) where $x = r\cos\theta_0$ and $y = r\sin\theta_0$, the back projection function becomes

$$B(r,\theta_0) = \frac{1}{2\pi}\int_0^{2\pi} \delta[r\cos(\theta_0 - \theta)]d\theta = \frac{1}{r}.$$

The point spread function of the back projection function is therefore given by

$$P(x,y) = \frac{1}{\sqrt{(x^2+y^2)}}.$$

Hence, the back projection function produced from an object $O(x, y)$ is given by

$$B(x,y) = P(x,y) \otimes\otimes O(x,y).$$

From this result, it is clear that we have another method of reconstructing the object function from its projections by inverting or deconvolving the above equation. From the convolution theorem, convolutions in real space are equivalent to multiplications in Fourier space. We can therefore write

$$\widetilde{B}(k_x,k_y) = \widetilde{P}(k_x,k_y)\widetilde{O}(k_x,k_y)$$

where

$$\widetilde{O} = \hat{F}_2 O, \quad \widetilde{P} = \hat{F}_2 P,$$

and

$$\widetilde{B} = \hat{F}_2 B.$$

Re-arranging

$$\widetilde{O}(k_x, k_y) = \frac{\widetilde{B}(k_x, k_y)}{\widetilde{P}(k_x, k_y)}.$$

The function $1/\widetilde{P}$ is the inverse filter and can be evaluated analytically since

$$\widetilde{P}(k_x, k_y) = \int_{-\infty}^{\infty}\int_{-\infty}^{\infty} \exp(-ik_x x)\exp(-ik_y y)\frac{1}{\sqrt{(x^2+y^2)}}dxdy$$

$$= \frac{1}{\sqrt{(k_x^2+k_y^2)}}.$$

Hence the object function is given by

$$O(x, y) = \hat{F}_2^{-1}[\sqrt{(k_x^2+k_y^2)}\widetilde{B}(k_x, k_y)].$$

One may think of the back-projection function as being a blurred image of the object because of the poor transmission of high spacial frequencies and the enhancement of low spacial frequencies. Any procedure that reverses this emphasis, helps to deblur the image. In other words, deconvolution amplifies the high spacial frequencies of the image which consequently enhances the resolution.

8.5 The Central Slice Theorem

It is always useful to know how various operations in image or real space are related to those in Fourier space. The central slice theorem gives the relationship between the Radon transform of an object and its two-dimensional Fourier transform. The theorem is as follows: The one-dimensional Fourier transform of a projection obtained at an angle θ is the same as the radial or central slice taken through the two-dimensional Fourier domain of the object at the same angle. To show this, consider the two-dimensional Fourier transform of $O(x, y)$ given by

$$\widetilde{O}(k\hat{\mathbf{n}}) = \hat{F}_2 O = \int_{-\infty}^{\infty} O(\mathbf{r})\exp(-ik\hat{\mathbf{n}}\cdot\mathbf{r})d^2\mathbf{r}.$$

We then use the result

$$\exp(-ik\hat{\mathbf{n}}\cdot\mathbf{r}) = \int \exp(-ikz)\delta(z-\hat{\mathbf{n}}\cdot\mathbf{r})dz$$

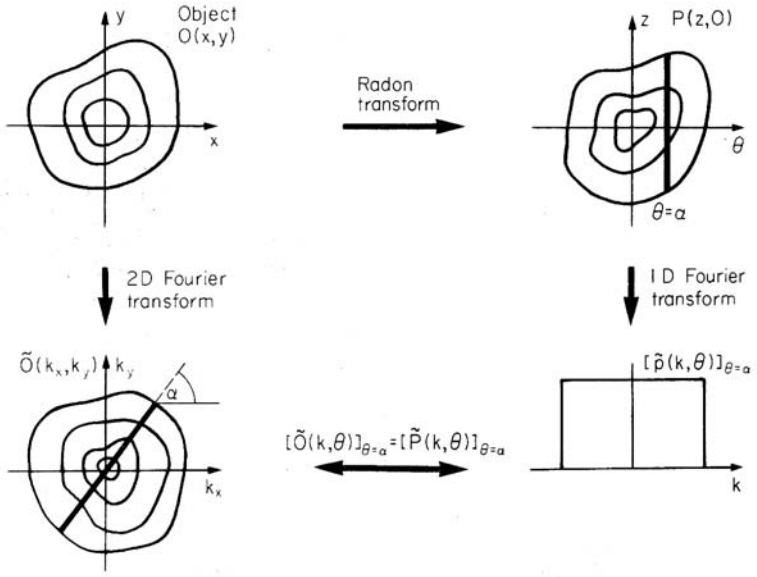

Figure 8.4: Illustration of the central slice theorem.

so that the Fourier transform may be written as

$$\widetilde{O}(k\hat{\mathbf{n}}) = \int_{-\infty}^{\infty} O(\mathbf{r}) \int_{-\infty}^{\infty} \exp(-ikz)\delta(z - \hat{\mathbf{n}} \cdot \mathbf{r}) dz d^2\mathbf{r}.$$

Interchanging the order of integration, we then have

$$\widetilde{O}(k\hat{\mathbf{n}}) = \int_{-\infty}^{\infty} dz \exp(-ikz) \int_{-\infty}^{\infty} O(\mathbf{r})\delta(z - \hat{\mathbf{n}} \cdot \mathbf{r}) d^2\mathbf{r}.$$

Hence, in terms of operators, we may write

$$\hat{F}_2 O(\mathbf{r}) = \hat{F}_1 \hat{R} O(\mathbf{r}).$$

Observe that the two-dimensional Fourier transform of the object function is the same as the one-dimensional Fourier transform operating on the Radon transform of the object. Using polar coordinates, this result can be written as

$$\widetilde{O}(k, \theta) = \int_{-\infty}^{\infty} \exp(-ikz) P(\theta, z) dz$$

where

$$\widetilde{O}(k,\theta) = \int_0^{2\pi}\int_0^{\infty} \exp[-ikr\cos(\phi-\theta)]O(r,\phi)rdrd\phi.$$

The relationship between $\widetilde{O}$ at a fixed value of θ and $P(\theta, z)$ at the same angle is shown in Figure 8.4 which is an illustration of the central slice theorem.

The central slice theorem gives us yet another way by which the object function can be reconstructed from its parallel projections. We take the Fourier transform of each projection and 'place it' along the appropriate radial slice. By repeating this process for all values of θ between 0 and π, Fourier inversion allows us to recover the object. In terms of the relevant operators, this result may be expressed in the form

$$O(\mathbf{r}) = \hat{F}_2^{-1}\hat{F}_1\hat{R}O(\mathbf{r}).$$

The projection slice theorem is widely used to design FFT-based reconstruction algorithms for commercial X-ray CT. An example of the type of result obtained using this method is given in Figure 8.5 which shows an X-ray tomogram of a normal abdomen after the application of a noise suppression filter (low-pass Gaussian filter).

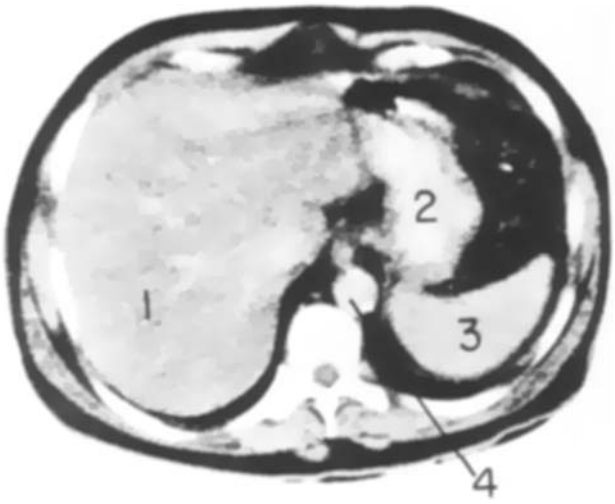

Figure 8.5: An X-ray tomogram of a normal abdomen showing the Liver (1), Stomach (2), Spleen (3) and Aorta (4).

8.6 Numerical Methods

Computing the Radon transform can be based on rotating an object about its centre and taking projections at regular steps in the angle of rotation. This is

an alternative but equivalent approach to that advocated in the proof of the Radon transform where, for a stationary object, the projection plane is rotated about the object through an angle θ. Two numerical functions are required to compute the Radon transform using this approach. The first is designed to rotate a Cartesian array of numbers (the object) about a fixed point (its centre). The second function computes the sum of all the pixels which lie along each column or row of the rotated array (i.e. it computes the family of discrete line sums associated with a specific angle of rotation - a projection).

8.6.1 Forward Radon Transform

The first problem encountered in designing an algorithm is that as the object is rotated, the size of the projection plane must be increased to accommodate the information contained in the corners of the array. The maximum length of the projection plane is reached when the object has been rotated through an angle of $\pi/4$ radians, when the diagonal vertex is parallel to the projection plane. In order to prevent 'corner clipping', the projection plane must be 'zero padded' providing an array size equal to the diagonal vertex of the object plane as shown in Figure 8.6. For example, if the original image contains 128×128 pixels, the new array length is given by

$$\text{int}(\text{sqrt}(128 * 128 + 128 * 128)) = \text{int}(128 * \text{sqrt}(2)) = 181 \quad \text{pixels}$$

Now, if the Radon transform is computed using angle increments of 1^o for all angles between 0^o and 180^o, then the data can be stored and displayed as a 181×181 square image.

The actual rotation of an object in the xy-plane can be accomplished via the co-ordinate transformation:

$$x' = x\cos\theta - y\sin\theta$$

and

$$y' = x\sin\theta + y\cos\theta$$

where x' and y' are the new co-ordinates. By applying this transformation to all pixels, the object can be rotated through any angle θ. However, one important problem remains: how to allocate the value of a co-ordinate transformed pixel (co-ordinates that will in general be floating point values) to the necessarily integer co-ordinate system of a Cartesian grid. One of the simplest solutions to this problem is to use a nearest neighbour approximation to generate integer co-ordinates (i.e. compute the nearest integer value of x' and y' at each step). This method produces an angle dependent distribution of 'holes', i.e. pixels that do not get assigned a value. The number of these holes increases as the angle of rotation approaches 45^o. They can be eliminated by interpolation or by the application of a Median filter. However, with regard to the computation of the Radon transform, nearest integer assignments can be used. This leads to predominantly high frequency digital noise being generated in the computation of the Radon transform and its inverse which can then be filtered using a lowpass filter as required. After rotating the Cartesian array through a given

angle θ via the method discussed above, a projection can be computed relatively easily by added together all the pixels which lie along each row.

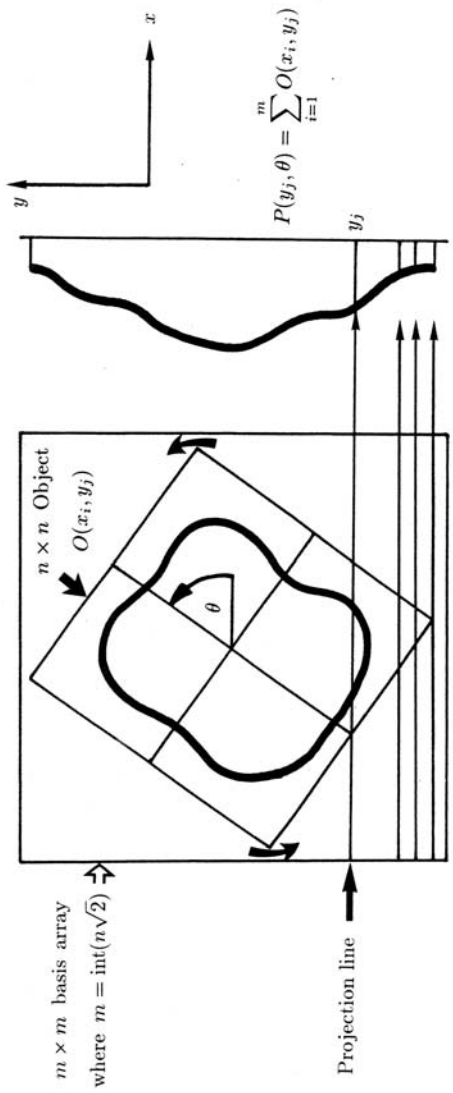

Figure 8.6: The rotation and projection of a square array.

8.6.2 Inverse Radon Transform

There are three possible methods of reconstructing an object from a complete set of its parallel projections: (i) back-projection and deconvolution, (ii) filtered back-projection and (iii) reconstruction via the central slice theorem.

Back-projection

The algorithm for back-projection is just a variation of that for rotating a Cartesian array. Each projection is back-projected onto the object plane. This plane is then rotated through the appropriate angle and the next projection back-projected. The results are added together and the process repeated. As before, computations are carried out on an array large enough to prevent 'corner clipping'. Finally, when all the projections have been back-projected, the reconstruction is extracted from the object plane, the algorithm used for the process of rotation being the same as before.

Deconvolution

The point spread function associated with the back-projection function is $\mid \mathbf{r} \mid^{-1}$ which has a Fourier transform of the same form, i.e. $\mid \mathbf{k} \mid^{-1}$. The inverse filter is therefore given by $\mid \mathbf{k} \mid$. Fortunately, this particular filter is non-singular and can therefore be used directly to deconvolve the back-projection function without recourse to optimization methods such as the Wiener filter. This is a rare and exceptional case. The process for deconvolving the back-projection function is relatively straightforward. The 2D Fourier transform of this function is taken and the real and imaginary parts multiplied by $\mid \mathbf{k} \mid$. The inverse Fourier transform is then computed, the reconstruction being given by the real part of the output.

8.7 The Hough Transform

The Hough transform dates from the early 1960s and was patented in 1963 well before the Radon transform was re-discovered. It evolved from a problem in high energy nuclear physics, in particular, the identification of particle tracks generated in a bubble chamber. If a magnetic field is applied perpendicular to the object plane, then neutral particles will travel in a straight line whereas charged particles will travel along a curve, the arc of a circle. The problem was to differentiate between a straight line and a curve in an image composed of both. Today, the Hough transform is used in pattern recognition to do the same whereby information in a digital image is quantified by processing it and/or analyzing it in Hough space. It is ironic that the application of the WKB approximation for predicting the interaction of high frequency de Broglie waves with slowly varying potentials should form the basis of an image processing method that can then be used to detect the results of these interactions.

The Hough transform is just a special case of the Radon transform; it is the result of considering the Radon transform of a point in the object plane at

(x_0, y_0) say described by

$$O(x, y) = \delta(x - x_0)\delta(y - y_0).$$

The Radon transform is then given by

$$P(z, \theta) = \int_{-\infty}^{\infty}\int_{-\infty}^{\infty} \delta(x - x_0)\delta(y - y_0)\delta(z - x\cos\theta - y\sin\theta)dxdy$$

$$= \delta(z - x_0\cos\theta - y_0\sin\theta)$$

which describes a curve in Radon space with the characteristic equation

$$z = x_0\cos\theta + y_0\sin\theta.$$

Consider a curve in the object plane which 'travels' through the set of points (x_i, y_i). Radon space will then consist of a set of curves with the characteristic equations

$$z = x_i\cos\theta + y_i\sin\theta.$$

In order to 'picture' the effect of this, it is easier to 'think' of this result in terms of a set of digital projections. For a line at the angle θ, the projection generated at this angle will be the sum of the pixel values of the line described by the set of points (x_i, y_i). For a line consisting of say 100 pixels each of value 1 and at an angle θ_0, the projection at θ_0 will be described by a single spike with a value of 100. At $\theta_0 + \pi/2$ radians, the projection will be a tophat function with an amplitude of one. Computing all the projections for $\theta \in [0, \pi]$ will give a function in Radon space, that is characterized by a maximum value (a point) occurring at θ_0, the amplitude of the point being determined by the length of the line, i.e. in this hypothetical example, 100. If the Radon transform is taken of a circle, each projection will have the same functional form and no single maximum value or point will be present in Radon space. This is illustrated in Figure 8.7.

If we take the Radon transform of a binary image composed of a line and a circle, for example and extract the maximum value in Radon space, then, by inverting, we can obtain an image of the line alone (except for its extent). Moreover, if we take the Radon transform of the Radon transform of a circle, then from Figure 8.7, we will obtain two points whose separation is determined by the diameter of the circle. This is an example of filtering in Radon space which processes information on the geometric features in an image. It should be compared with Fourier space processing which filters information on the spatial frequency content of these features. Line based features in the object plane can be transformed into Radon space and a point set generated, giving a relatively small numerical field that can be taken to be a unique description of the feature (a template). For example, suppose we want to generate a template for describing the symbols +, = and × in the object plane, all of which are composed of lines of equal length L. The Radon transform of + will produce two points of amplitude L at θ values of 0 and $\pi/2$ radians. The Radon transform of = will produce two points at θ values of 0 alone and the transform of ×, two points at $\theta = \pi/4$ and $\theta = \pi/4 + \pi/2$ radians.

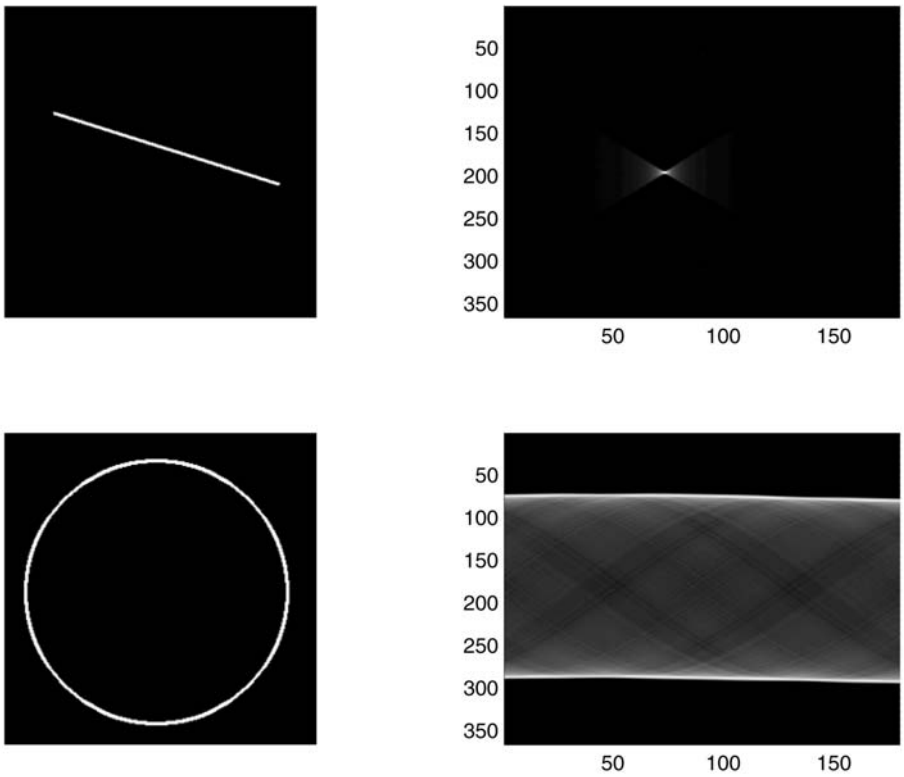

Figure 8.7: Radon transform (top-right) of a line (top-left) and the Radon transform (bottom-right) of a circle (bottom-left).

Point extraction in Radon space requires the application of numerical procedures that are designed to enhance the accuracy of their location which cannot be relied upon in practice via the application of a simple threshold alone (except in the simplest of cases). The template construction and identification of object plane features that are composed from lines of different lengths requires multiple amplitude point extraction. There are a number of methods available. For example, by correlating (i.e. matched filtering) the Radon space data with a kernel that has been designed to replicate the data fields that occur close to a point, a new 'clean' point set can be obtained from the correlation surface. Another method is to apply a median filter to eliminate isolated points and then subtract the output from the original.

From the computational point of view, two methods can be applied. The Radon transform can be computed directly by rotating and projecting where, given that the object plane is taken to by a binary image, only non-zero pixels

are processed. The other method is to compute the curves

$$z = x\cos\theta + y\sin\theta$$

for all non-zero pixels (x, y) in the object plane and add the results together in an 'accumulator'. The computational efficiency of this process can be enhanced by using a look-up table that stores the values of $\cos\theta$ and $\sin\theta$ for a given step change in θ.

8.8 Non-separable Image Processing

Many image processing methods originate from solutions for processing digital signals. In those cases, where the image can be considered to be separable, i.e. where $I(x, y) = I_x(x)I_y(y)$, any DSP algorithm can be applied directly. In those cases where the image is not separable but the process is, then it is usually possible to develop an equivalent 2D process from the 1D version that is required to be implemented. However, there are some cases where this is not possible and the image processing problem cannot be addressed by simply increasing the dimension of a signal processing method and/or algorithm. One method of solving this problem is to use the Radon transform to convert the image into a set of projections, apply the signal processing algorithm on a projection by projection basis and then inverse Radon transform the result, an idea that was first published in 1986 (Blackledge J M, *Digital image processing in Radon space and the inversion of limited Fourier data*, Optik 73(2): 74-82, 1986). This principle is entirely general but to be implemented in practice, requires the forward and inverse Radon transforms to be computed with high accuracy and resolution. The application of the Radon transform for this purpose is compounded in the equation

$$\hat{P}_2 O(x, y) \equiv \hat{R}^{-1}\hat{P}_1[\hat{R}O(x, y)]$$

where $\hat{P}_1$ is a 1D process for which there is no directly equivalent 2D process $\hat{P}_2$. For example, the Burg maximum entropy method (see *Digital Signal Processing*, J M Blackledge, Horwood, 2003 - Chapter 15) for which there is no closed form solution in two-dimensions can be applied to an image via application of the Radon transform. The inverse of this principle can also be applied in cases where an image processing method is available for which there is no directly equivalent signal processing algorithm. In this case, the signal is replicated to form a set of projections and the inverse Radon transform applied to form an image. Upon processing the image, the processed signal is derived by taking a single projection of the processed image. This approach can, for example, be used to solve the phase reconstruction problem for a signal by applying a phase retrieval algorithm (see Chapter 12) to the image that is formed via Radon inversion.

8.9 Summary of Important Results

Radon transform

$$P(z,\theta) = \hat{R}O(x,y) = \int\int O(x,y)\delta(z - x\cos\theta - y\sin\theta)dxdy$$

Inverse Radon transform

$$O(x,y) = \hat{R}^{-1}P(z,\theta) = \frac{1}{2\pi^2}\int\int \frac{1}{x\cos\theta + y\sin\theta - z}\frac{\partial}{\partial z}P(z,\theta)dzd\theta$$

Back-projection PSF

$$P(x,y) = \frac{1}{\sqrt{x^2+y^2}}$$

Projection slice theorem

$$\hat{F}_2O(x,y) = \hat{F}_1\hat{R}O(x,y)$$

The Hough transform

$$z = x\cos\theta + y\sin\theta$$

A General signal-to-image processing converter

If $\hat{P}_1$ is a 1D process for which there is no directly equivalent 2D process $\hat{P}_2$, then

$$\hat{P}_2O(x,y) \equiv \hat{R}^{-1}\hat{P}_1[\hat{R}O(x,y)]$$

8.10 Further Reading

- Herman G T, *Image Reconstruction for Projections*, Academic Press, 1980.
- Wells P N T, *Scientific Basis of Medical Imaging*, Churchill-Livingstone, 1982.
- Deans S R, *The Radon Transform and Some of Its Applications*, Wiley, 1983[1]
- Bates R H T and McDonnell M J, *Image Restoration and Reconstruction*, Clarendon Press, Oxford, 1986.

[1]Includes a translation of the original 1917 paper (written in German) by Johannes Radon.

- Natterer F, *The Mathematics of Computerized Tomography*, Wiley, 1986.
- Sanz J L C, Hinkle E B and Jain A K, *Radon and Projection Transform-Based Computer Vision (Algorithms, A Pipeline Architecture and Industrial Applications)*, Springer-Verlag (Series in Information Science), 1989.
- Blackledge J M and Turner M J (Eds.), *Image Processing III: Mathematical Methods, Algorithms and Applications*, Horwood Publishing Series: Mathematics and Applications, 2001.

Chapter 9

Diffraction Tomography

Diffraction tomography is an imaging method that attempts to reconstruct the internal structure of an inhomogeneous material by the way in which it diffracts radiation. This method of imaging is used when the wavelength of a probe λ is the same order of magnitude as the scatterer D, i.e. when

$$\lambda \sim D.$$

In this case, the reconstruction methods used for projection tomography (which rely on the condition $\lambda << D$) are inadequate.

In practice there is one very important difference between projection and diffraction tomography: whereas projection tomography is based on an exact reconstruction, diffraction tomography relies heavily on approximate solutions to the scattering problem. In other words, the inversion algorithm that enables us to recover the structure of an object from a sequence of projections is exact whereas, in diffraction tomography, the inversion algorithm is based on an approximate solution for the diffracted field. The type of approximation that is used has already been discussed in Chapter 6. It is known as the Born approximation and for $\lambda \sim D$ is valid when the root mean square of the scattering function is much less that 1.

The problems discussed in this Chapter are two-dimensional and, like projection tomography, are idealized in their concern with imaging a slice of material taken through a three-dimensional object. However, it should be stressed that the ideas and analytical techniques that are presented can be extended to three dimensions.

The principles of diffraction tomography are the same in both acoustic and electromagnetic imaging, but the theoretical details are different. In this Chapter, attention is focused on the diffraction of an acoustic wavefield from a slice of material by way of an introduction to the problem. The diffraction of a polarized electromagnetic field from a conductive dielectric is briefly discussed at the end of this Chapter.

9.1 Diffraction Tomography using CW Fields

Consider the 2D ultrasonic imaging system illustrated in Figure 9.1. A transducer emits a diverging wavefield at a fixed frequency which insonifies the scatterer completely. This field is transmitted through a homogeneous medium of uniform density ρ_0 and compressibility κ_0. The scatterer is assumed to be composed of variations in compressibility κ alone and confined to a finite region of space with area A. The inhomogeneous nature of this acoustic parameter causes diffraction to occur. The diffracted wavefield is detected by a second transducer (the receiver) which, like the acoustic source, is free to move around a circular frame which completely encloses the scatterer. As in projection tomography, the acoustic image obtained by this method is taken to be a cross section through a three-dimensional object. Our aim is to develop a scattering model for this system and obtain a suitable reconstruction algorithm.

9.1.1 Mathematical Model

By considering the acoustic source to be a point source, the diverging incident wavefield can be described by the appropriate Green function (in this case, the two-dimensional Green function). The 2D wave equation for the Born scattered pressure field P_s at $\mathbf{r}$ due to the presence of a point acoustic source at $\mathbf{r}_i$ is the solution of

$$(\nabla^2 + k^2)P_s(\mathbf{r}, \mathbf{r}_i, k) = -k^2\gamma_\kappa(\mathbf{r})g(\mathbf{r} \mid \mathbf{r}_i, k)$$

where

$$\gamma_\kappa = \frac{\kappa - \kappa_0}{\kappa_0}.$$

Here, it is assumed that there are no variations in the density and that the viscosity of the medium is negligible. Using the expression for the 2D Green function (see Chapter 5), the solution to this equation at $\mathbf{r}_s$ is then

$$P_s(\mathbf{r}_s, \mathbf{r}_i, k) = \frac{ik}{8\pi} \int_A \frac{\exp(ik \mid \mathbf{r} - \mathbf{r}_i \mid)}{\sqrt{\mid \mathbf{r} - \mathbf{r}_i \mid}} \frac{\exp(ik \mid \mathbf{r} - \mathbf{r}_s \mid)}{\sqrt{\mid \mathbf{r} - \mathbf{r}_s \mid}} \gamma_\kappa(\mathbf{r}) d^2\mathbf{r}.$$

Let us consider this solution under the far-field conditions

$$\frac{\mathbf{r}}{\mid \mathbf{r}_i \mid} << 1$$

and

$$\frac{\mathbf{r}}{\mid \mathbf{r}_s \mid} << 1$$

where

$$\mid \mathbf{r}_i \mid \simeq \mid \mathbf{r}_s \mid \simeq a,$$

the distance of the source and receiver from the centre of the scatterer as shown in Figure 9.1.

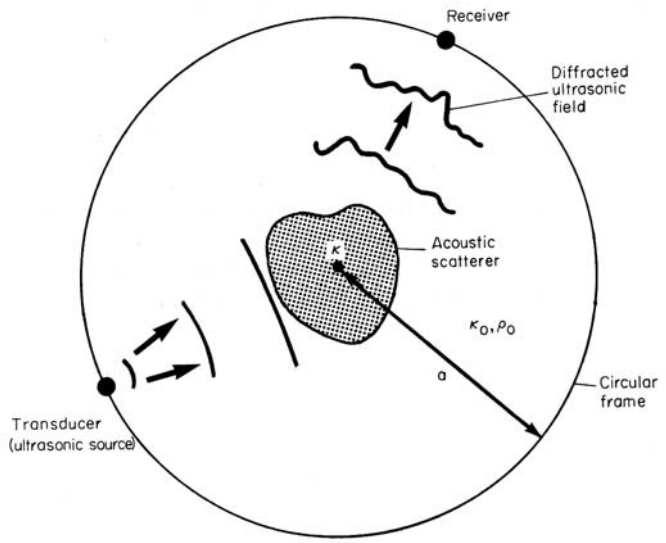

Figure 9.1: The type of experiment required to perform CW ultrasonic diffraction tomography using a circular source/receiver system. A transducer emits a wavefield oscillating at a fixed frequency through a homogeneous material with compressibility κ_0 and density ρ_0. The field is diffracted by an acoustic scatterer which is taken to be composed of variations in the compressibility κ alone. By measuring the diffracted field as a function of the position of the source and receiver on the frame, the variations in the compressibility can be recovered.

These conditions allow us to use a Fourier-based inversion scheme because the scattered pressure field can be written as

$$P_s(\hat{\mathbf{n}}_i, \hat{\mathbf{n}}_s, k) = \frac{ik}{8\pi a} \exp(2ika) \int_A \exp[-ik(\hat{\mathbf{n}}_s - \hat{\mathbf{n}}_i) \cdot \mathbf{r}] \gamma_\kappa(\mathbf{r}) d^2\mathbf{r}$$

where

$$\hat{\mathbf{n}}_i = -\frac{\mathbf{r}_i}{|\,\mathbf{r}_i\,|}$$

and

$$\hat{\mathbf{n}}_s = \frac{\mathbf{r}_s}{|\,\mathbf{r}_s\,|}.$$

This equation is essentially a two-dimensional Fourier integral of the compressibility variations where $\hat{\mathbf{n}}_i$ and $\hat{\mathbf{n}}_s$ represent the direction of the incident and scattered fields, respectively.

9.1.2 Geometric Model

If the scattered field is measured over a circular frame, then the appropriate co-ordinates to work with are polar co-ordinates. We therefore write

$$\hat{\mathbf{n}}_i = \hat{\mathbf{x}} \cos\phi_i + \hat{\mathbf{y}} \sin\phi_i$$

and

$$\hat{\mathbf{n}}_s = \hat{\mathbf{x}} \cos\phi_s + \hat{\mathbf{y}} \sin\phi_s$$

where ϕ_i and ϕ_s are the angles of incidence and scattering, respectively. The scattered pressure field can then be written as

$$P_s(k_x, k_y) = \frac{ik}{8\pi a} \exp(2ika) \int\int \exp(-ik_x x) \exp(-ik_y y) \gamma_\kappa(x, y) dx dy \quad (9.1)$$

where

$$k_x = k(\cos\phi_s - \cos\phi_i) \quad (9.2)$$

and

$$k_y = k(\sin\phi_s - \sin\phi_i) \quad (9.3)$$

Note that k is taken to be a constant and that k_x and k_y are functions of ϕ_i and ϕ_s.

9.1.3 Recording Model

Two basic parameters must be measured in an experiment of this kind: the amplitude of the scattered pressure field and its phase. In practice, the actual field that is measured in an imaging system of the type illustrated in Figure 9.1 is not just the scattered field but the sum of the incident P_i and scattered fields, i.e. the total pressure field

$$P(k_x, k_y) = P_i(k_x, k_y) + P_s(k_x, k_y).$$

To recover γ_κ from P_s, we require information on the amplitude A and phase θ of P_i and P_s as a function of ϕ_i and ϕ_s. The amplitude and phase of the incident pressure field can be obtained by measuring the total pressure field in the absence of the scatterer. The incident pressure field as a function of these angles is then given by

$$P_i(\phi_i, \phi_s) = A_i(\phi_i, \phi_s) \exp[i\theta_i(\phi_i, \phi_s)].$$

Exactly the same procedure must then be repeated with the scatterer present, producing the total pressure field

$$P(\phi_i, \phi_s) = A(\phi_i, \phi_s) \exp[i\theta(\phi_i, \phi_s)].$$

The scattered pressure field is then given by

$$P_s(\phi_i, \phi_s) = P(\phi_i, \phi_s) - P_i(\phi_i, \phi_s) = A\cos\theta - A_i\cos\theta_i + i(A\sin\theta - A_i\sin\theta_i).$$

The behaviour of the incident pressure field is ultimately a function of the design of the imaging system and must be known *a priori* before the scatterer is introduced. In other words, the system must be calibrated before conducting an experiment. It is then a relatively simple procedure to compute the complex scattered field by measuring the amplitude of the total field and its phase relative to the source (i.e. the phase shift)

9.1.4 Inversion

Having obtained the complex scattered pressure field, the compressibility fluctuations can be recovered by performing the appropriate Fourier inversion. Noting that γ_κ is a real function, we have from equation (9.1), by 2D Fourier inversion,

$$\gamma_\kappa(x,y) = \mathrm{Re}\left(\frac{2a}{\pi ik}\exp(-2ika)\int\int \exp(ik_x x)\exp(ik_y y)P_s(k_x,k_y)dk_x dk_y\right). \tag{9.4}$$

In this formula, P_s is a function of k_x and k_y and not the experimental parameters ϕ_i and ϕ_s. Hence, to use this inversion, we need to know how observations of the scattered field as a function of ϕ_i and ϕ_s are related to the spatial frequencies k_x and k_y.

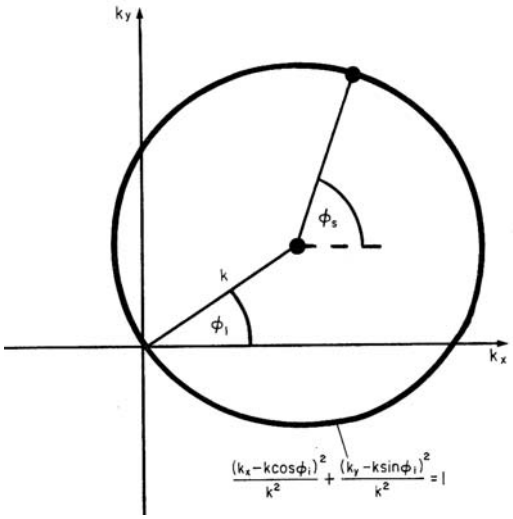

Figure 9.2: The geometric relationship between the spatial frequencies of the scatterer k_x and k_y and the incident and scattering angles (ϕ_i and ϕ_s respectively) is a circle of radius k (the wavenumber of the CW field used to insonify the scatterer) whose centre is at $(k\cos\phi_i, \quad k\sin\phi_i)$.

The relationship is provided by the parametric equations (9.2) and (9.3). Figure 6.2 shows the parametric curve in $k_x k_y$-space produced by changing ϕ_s from 0 to 2π when ϕ_i is fixed according to these parametric equations. This curve is a circle with an origin at $(k_x = k\cos\phi_i, \quad k_y = k\sin\phi_i)$. This can be shown by decoupling equations (9.2) and (9.3) for ϕ_s which gives the equation for a circle,

$$\frac{(k_x + k\cos\phi_i)^2}{k^2} + \frac{(k_y + k\sin\phi_i)^2}{k^2} = 1.$$

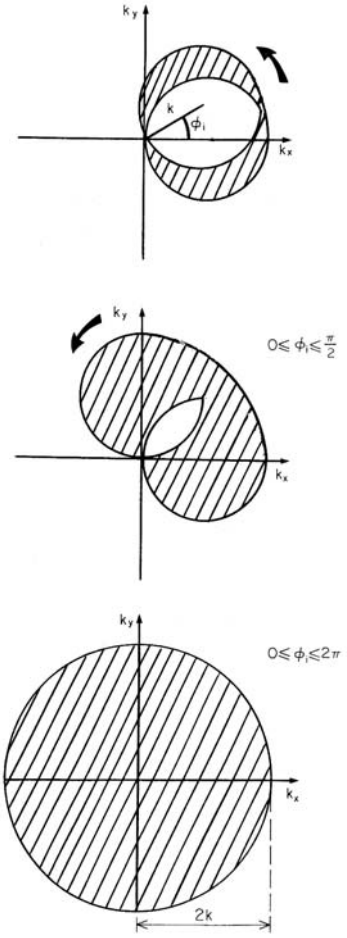

Figure 9.3: By changing the position of the source (determined by ϕ_i) and measuring the diffracted field as a function of ϕ_s, the spatial frequencies of the scatterer up to and including $2k$ can be determined. The scatterer can then be recovered by Fourier inversion.

This relationship demonstrates that, by changing the scattering angle, we are able to select the spatial frequencies of the scatterer which lie on a circle in Fourier space of radius k and origin $(k\cos\phi_i, k\sin\phi_i)$. By changing the value of ϕ_i (i.e. the position of the acoustic source), the origin of this circle is moved and a new set of spatial frequencies can be obtained by once again measuring the scattered field at different scattering angles ϕ_s. By repeating this process for all values of ϕ_i between 0 and 2π, all the spatial frequencies of the scatterer can be measured up to and including $2k$. In other words, by recording the behaviour of the complex scattered field for all values of ϕ_i and ϕ_s between 0 and 2π, the complex spectrum of the scatterer can be obtained. This is illustrated in Figure 9.3. The maximum spatial frequency that can be obtained in this way is $2k$. To emphasize this important point, equation (9.4) should be written in a form where the double integral is bounded by the condition

$$\sqrt{(k_x^2 + k_y^2)} \leq 2k.$$

Using vector notation, the inversion formula for the compressibility fluctuations can be written in the form

$$\gamma_\kappa(\mathbf{r}) = \mathrm{Re}\left(\frac{2a}{\pi ik}\exp(-2ika)\int\limits_{|\mathbf{k}|\leq 2k}\exp(i\mathbf{k}\cdot\mathbf{r})P_s(\mathbf{k})d^2\mathbf{k}\right).$$

9.2 Pulse Mode Diffraction Tomography

In the previous Section we examined how the compressibility fluctuations of an acoustic material can be recovered using a CW field and a scattering model that is based on the Helmholtz equation, the Born approximation and the far field approximation. Using exactly the same model we shall now examine how the compressibility fluctuations can be reconstructed using a pulsed acoustic (e.g. ultrasonic) field.

9.2.1 Basic Equations

To start with, let us see how the basic equations change when a pulse is introduced. Using a pulse is equivalent to using a spectrum of different CW frequencies. If we denote the pulse by $p(\tau)$ where τ =time×acoustic wave speed, then its characteristic spectrum can be written as

$$P(k) = \int\limits_{-\infty}^{\infty}\exp(-ik\tau)p(\tau)d\tau.$$

In this case the scattered pressure field at $\mathbf{r}$ induced by a pulsed acoustic point source at $\mathbf{r}_i$ is determined by the wave equation

$$(\nabla^2 + k^2)P_s(\mathbf{r}, \mathbf{r}_i, k) = -k^2P(k)\gamma_\kappa(\mathbf{r})g(\mathbf{r} \mid \mathbf{r}_i, k).$$

Following exactly the same procedure as before (i.e. for the CW case), the scattered pressure is given by

$$P_s(\hat{\mathbf{N}}, k) = \frac{ik}{8\pi a} P(k) \exp(2ika) \int_A \exp(-ik\hat{\mathbf{N}} \cdot \mathbf{r}) \gamma_\kappa(\mathbf{r}) d^2\mathbf{r}$$

where

$$\hat{\mathbf{N}} = \hat{\mathbf{n}}_s - \hat{\mathbf{n}}_i.$$

The function P_s describes the spectrum of the scattered pressure field. In practice, the spectrum of this field is not measured directly. What is actually measured is a time varying voltage (a signal with both positive and negative values) which is the time history of the scattered field. This is given by the inverse Fourier transform of P_s. Using the convolution theorem and remembering that ik in Fourier space yields a derivative in real space, we can write

$$\begin{aligned} p_s(\hat{\mathbf{N}}, \tau) &= \frac{1}{8\pi a} \frac{\partial}{\partial \tau} \left(p(\tau) \otimes \delta(\tau + 2a) \otimes \int_A \gamma_\kappa(\mathbf{r}) \delta(\tau - \hat{\mathbf{N}} \cdot \mathbf{r}) d^2\mathbf{r} \right) \\ &= \frac{1}{8\pi a} \frac{\partial}{\partial \tau} \left(p(\tau + 2a) \otimes \int_A \gamma_\kappa(\mathbf{r}) \delta(\tau - \hat{\mathbf{N}} \cdot \mathbf{r}) d^2\mathbf{r} \right) \end{aligned} \tag{9.5}$$

where

$$p_s(\hat{\mathbf{N}}, \tau) = \frac{1}{2\pi} \int_{-\infty}^{\infty} P_s(\hat{\mathbf{N}}, k) \exp(ik\tau) dk.$$

This is a rather nice result because the integral over γ_κ in the above expression is just the Radon transform of γ_κ. Hence, the techniques used to obtain the inverse Radon transform discussed in Chapter 8 can also be used here to reconstruct the compressibility fluctuations. The only additional problem that we have to contend with is the convolution of the integral with $\partial_\tau p$.

9.2.2 Inversion

To extract the Radon transform of γ_κ we need to deconvolve p_s. This can be done by transforming back into Fourier space and constructing the appropriate inverse filter. We can then write

$$D(\hat{\mathbf{N}}, \tau) = \int_A \gamma_\kappa \delta(\tau - \hat{\mathbf{N}} \cdot \mathbf{r}) d^2\mathbf{r}$$

where D is the deconvolved data given by

$$D(\hat{\mathbf{N}}, \tau) = 8\pi a \hat{F}_1^{-1} \left(\frac{P_s(\hat{\mathbf{N}}, k)}{ikP(k)} \exp(-2ika) \right). \tag{9.6}$$

Details of how to deconvolve signals in the presence of experimental noise and singular inverse filters such as this one, are given in *Digital Signal Processing*, J M Blackledge, Horwood, 2003.

Recalling the results of Chapter 8, D is completely equivalent to a projection, with the exception that γ_κ is not an object function but a scattering function and D is not a projection but a deconvolved time trace. To reconstruct γ_κ from D we need to know the characteristic time signals for all values of $\hat{\mathbf{N}}$. Because $\hat{\mathbf{N}}$ is the difference between the scattered and incident unit vectors, there are a number of ways of choosing $\hat{\mathbf{N}}$. We can choose to keep $\hat{\mathbf{n}}_i$ fixed and vary $\hat{\mathbf{n}}_s$ or vice versa. Alternatively, we may change both $\hat{\mathbf{n}}_i$ and $\hat{\mathbf{n}}_s$ keeping the angle between them fixed. This is equivalent to rotating the object by an angle ϕ while keeping the positions of the source and receiver fixed. Noting that

$$\begin{aligned} \mid \hat{\mathbf{N}} \mid = \mid \hat{\mathbf{n}}_s - \hat{\mathbf{n}}_i \mid &= \sqrt{[(\hat{\mathbf{n}}_s - \hat{\mathbf{n}}_i) \cdot (\hat{\mathbf{n}}_s - \hat{\mathbf{n}}_i)]} \\ &= 2\sin\frac{\theta}{2}, \quad \theta = \cos^{-1}(\hat{\mathbf{n}}_i \cdot \hat{\mathbf{n}}_s) \end{aligned}$$

where θ is the angle between the incident and scattered fields, we can write [with $\hat{\mathbf{N}} = \mid \hat{\mathbf{N}} \mid (\hat{\mathbf{x}}\cos\phi + \hat{\mathbf{y}}\sin\phi)$]

$$\hat{\mathbf{N}} \cdot \mathbf{r} = 2x\cos\phi\sin\frac{\theta}{2} + 2y\sin\phi\sin\frac{\theta}{2}.$$

For a fixed value of θ, the deconvolved data can then be written as

$$D(\phi,\tau) = \int\int \gamma_\kappa(x,y)\delta\left(\tau - 2x\cos\phi\sin\frac{\theta}{2} - 2y\sin\phi\sin\frac{\theta}{2}\right)dxdy.$$

This expression is identical to the formula for a projection except for the factor $2\sin(\theta/2)$. In this case, using the expression for the inverse Radon transform, the compressibility fluctuations are given by

$$\gamma_\kappa(x,y) = \hat{R}^{-1}D$$

$$= \frac{1}{2\pi^2}\int_0^\pi d\phi \int d\tau \frac{1}{2x\cos\phi\sin(\theta/2) + 2y\sin\phi\sin(\theta/2) - \tau}\frac{\partial}{\partial\tau}D(\phi,\tau).$$

9.3 The Diffraction Slice Theorem

We have shown that the deconvolved data generated by insonifying an acoustic scatterer with a pulse are related to the scattering function by the Radon transform. The spatial frequencies of the scattering function must therefore be related to the spectrum of these data in the same way that the spectrum of a projection is related to the spatial frequencies of the object function. In other words, the central slice theorem should apply. In this case, since we are dealing with a diffraction phenomenon, we refer to this theorem as the diffraction slice theorem. Its basic properties are the same as the projection slice theorem with one very important difference which arises from the presence of the additional

parameter θ. Following the same procedure as in Chapter 8 (for deriving the projection slice theorem) we write

$$\Gamma_\kappa(k\hat{\mathbf{N}}) = \int_A \gamma_\kappa(\mathbf{r}) \exp(-ik\hat{\mathbf{N}} \cdot \mathbf{r}) d^2\mathbf{r}$$

$$= \int_A d^2\mathbf{r}\gamma_\kappa(\mathbf{r}) \int_{-\infty}^{\infty} \exp(-ik\tau)\delta(\tau - \hat{\mathbf{N}} \cdot \mathbf{r}) d\tau = \int_A D(\hat{\mathbf{N}}, \tau) \exp(-ik\tau) d\tau.$$

In terms of the appropriate operators, this equation can be written as

$$\hat{F}_2\gamma_\kappa = \hat{F}_1\hat{R}\gamma_\kappa.$$

As in the projection slice theorem, the Fourier transform of $\hat{R}\gamma_\kappa$ at a given angle is equal to a slice through the Fourier domain of γ_κ at the same angle. The length of the slice is determined by the maximum value of

$$| \, k\hat{\mathbf{N}} \, | = 2k \sin(\theta/2).$$

This is illustrated in Figure 9.4.

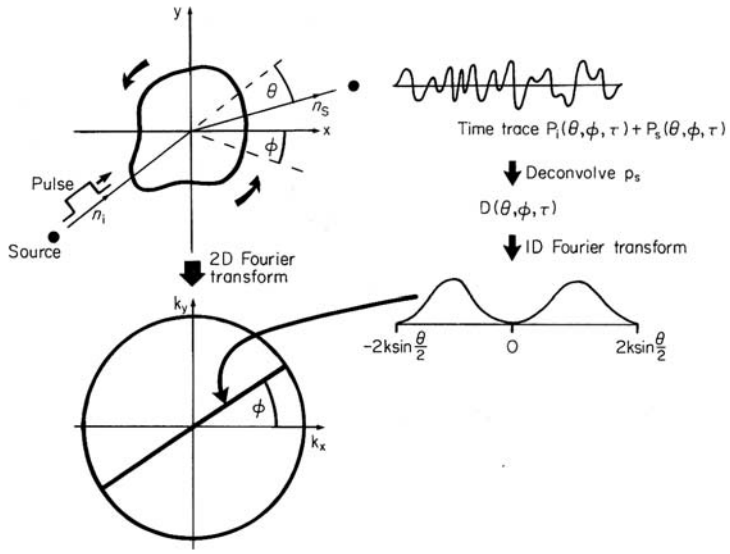

Figure 9.4: Illustration of the Diffraction Slice Theorem.

Using vector notation, the compressibility fluctuations can therefore be written in the form

$$\gamma_\kappa(\mathbf{r}) = \frac{1}{(2\pi)^2} \int_{|\mathbf{k}| \leq 2k \sin\frac{\theta}{2}} \Gamma_\kappa(\mathbf{k}) \exp(i\mathbf{k} \cdot \mathbf{r}) d^2\mathbf{k}.$$

Observe that the bandwidth of the reconstruction and therefore its resolution does not depend on the wavenumber alone but on the angle between the incident and scattered waves. Recall that the bandwidth of a CW reconstruction only depends on the magnitude of $2k$, whereas the value of the scattering angle plays a crucial role in defining the resolution of a reconstruction using pulsed fields. Note that maximum resolution will be obtained when $\theta = 180^0$, i.e. when the back-scattered field is recorded. Also note that when θ is zero, only the DC component of the spectrum can be recovered, i.e.

$$\Gamma_\kappa(0,0) = \int\int \gamma_\kappa(x,y)dxdy.$$

In addition to the scattering angle, the resolution also depends on the wavenumber k. With a pulsed system, the maximum value of k is determined by the bandwidth of the pulse. Hence, the larger the bandwidth of the pulse, the greater the resolution of the reconstruction. Since $\sqrt{k_x^2 + k_y^2} \leq 2k\sin(\theta/2)$, the maximum resolution available using an imaging system of this kind is obtained by measuring the back-scattered field. The resolution of the system is then determined by the bandwidth of the pulse alone. In this mode we may summarize the imaging method as follows:

(i) Insonify the acoustic scatterer with a pulse of acoustic radiation and record the time history of the back-scattered field.

(ii) Repeat this procedure for all angles by rotating the object or equivalently changing the position of the transducer.

(iii) Deconvolve each time trace.

(iv) Reconstruct the scattering function by taking the inverse Radon transform of the deconvolved data.

Another way of reconstructing γ_κ is first to back-project the time trace data without deconvolving. In this case, the back-projection function is given by

$$B(x,y) = P(x,y) \otimes\otimes \gamma_\kappa(x,y)$$

where

$$P(x,y) = \frac{1}{8\pi a r} \otimes \frac{\partial}{\partial r} p(r+2a), \quad r = \sqrt{x^2+y^2}.$$

We may then deconvolve the above equation by constructing the appropriate inverse filter. This is obtained by taking the Fourier transform of the point spread function which gives

$$\widetilde{P}(k_x,k_y) = \frac{1}{8\pi a k} ikP(k)\exp(2ika) = \frac{i}{8\pi a} P(k)\exp(2ika)$$

where

$$k = \sqrt{k_x^2 + k_y^2}.$$

The inverse filter is then given by $1/\widetilde{P}(k_x, k_y)$ and the scattering function can be reconstructed using the result

$$\gamma_\kappa(x,y) = 8\pi a \hat{F}_2^{-1}\left(\exp(-2ika)\frac{\hat{F}_2\widetilde{B}(k_x,k_y)}{iP(k)}\right).$$

9.4 Quantitative Diffraction Tomography

So far in this Chapter we have looked at two methods of reconstructing the compressibility fluctuations of an acoustic material using a CW or pulsed acoustic field. In both cases variations in only one acoustic parameter are assumed to generate the scattered field. This model was chosen because it produced a relatively simple wave equation (the Helmholtz equation) which allowed us to study inverse solutions using the Born and far field approximations without the analysis becoming unduly complicated.

9.4.1 Solution for a Non-viscous Medium

Now that the basic inversion method has been presented, let us go back and put some more 'physics' into the problem by considering a slightly more advanced scattering model where variations in the density of the acoustic material also contribute to the scattered field. In this case, the wave equation is (see Chapter 4)

$$(\nabla^2 + k^2)p = -k^2\gamma_\kappa p + \nabla\cdot(\gamma_\rho \nabla p)$$

where

$$\gamma_\rho = \frac{\rho - \rho_0}{\rho}.$$

Once again, we use the Born and far field approximations to produce the integral equation

$$p_s(\hat{\mathbf{n}}_i, \hat{\mathbf{n}}_s, k) = \frac{ik}{8\pi a}\exp(2ika)\Bigg(\int_A \exp[-ik(\hat{\mathbf{n}}_s - \hat{\mathbf{n}}_i)\cdot\mathbf{r}]\gamma_\kappa(\mathbf{r})d^2\mathbf{r}$$

$$-\frac{1}{k^2}\int_A \exp(-ik\hat{\mathbf{n}}_s\cdot\mathbf{r})\nabla\cdot[\gamma_\rho(\mathbf{r})\nabla\exp(ik\hat{\mathbf{n}}_i\cdot\mathbf{r})]d^2\mathbf{r}\Bigg).$$

It is clear that the behaviour of the scattered field due to density variations is compounded by one term which needs to be simplified. Our aim is to reduce this term to a form that is compatible with the first, so that we may adopt the same type of inversion scheme. Integrating by parts we can write

$$\int_A \exp(-ik\hat{\mathbf{n}}_s\cdot\mathbf{r})\nabla\cdot[\gamma_\rho\nabla\exp(ik\hat{\mathbf{n}}_i\cdot\mathbf{r})]d^2\mathbf{r}$$

$$= \int_A \nabla\cdot[\gamma_\rho\exp(-ik\hat{\mathbf{n}}_s\cdot\mathbf{r})\nabla\exp(ik\hat{\mathbf{n}}_i\cdot\mathbf{r})]d^2\mathbf{r}$$

$$-\int_A \gamma_\rho \nabla \exp(-ik\hat{\mathbf{n}}_s \cdot \mathbf{r}) \cdot \nabla \exp(ik\hat{\mathbf{n}}_i \cdot \mathbf{r}) d^2\mathbf{r}.$$

The second integral on the right hand side of the equation above can be evaluated directly, i.e.

$$\int_A \gamma_\rho \nabla \exp(-ik\hat{\mathbf{n}}_s \cdot \mathbf{r}) \cdot \nabla \exp(ik\hat{\mathbf{n}}_i \cdot \mathbf{r}) d^2\mathbf{r}$$

$$= k^2 \int_A \hat{\mathbf{n}}_i \cdot \hat{\mathbf{n}}_s \gamma_\rho \exp[-ik(\hat{\mathbf{n}}_s - \hat{\mathbf{n}}_i) \cdot \mathbf{r}] d^2\mathbf{r}.$$

Ideally, we now need a physical reason for neglecting (or otherwise) the integral over $\nabla \cdot [\bullet]$. To this end we can use Green's theorem in the plane to write

$$\int_A \nabla \cdot [\gamma_\rho \exp(-ik\hat{\mathbf{n}}_s \cdot \mathbf{r}) \nabla \exp(ik\hat{\mathbf{n}}_i \cdot \mathbf{r})] d^2\mathbf{r}$$

$$= \oint_C \gamma_\rho \exp(-ik\hat{\mathbf{n}}_s \cdot \mathbf{r}_c) \nabla \exp(ik\hat{\mathbf{n}}_i \cdot \mathbf{r}_c) \cdot \hat{\mathbf{n}} d\ell$$

where C is the contour enclosing A and $\mathbf{r}_c$ denotes the position vector on the contour C. We may now use one of two arguments. The first is to consider the contribution to the scattered field due to scattering at the boundary defined by C to be negligible compared to the scattering produced by the interior of the scatterer itself. Alternatively, we can introduce the boundary condition

$$\gamma_\rho(\mathbf{r}_c) = 0 \tag{9.7}$$

in which case the relevant integral vanishes completely. This condition implies that

$$\rho(\mathbf{r}_c) = \rho_0.$$

In this form it is clear that the density of the scatterer on the boundary defining A must be the same as the homogeneous support that surrounds the scatterer. In this case the expression for the scattered pressure field reduces to

$$p_s(\hat{\mathbf{n}}_i, \hat{\mathbf{n}}_s, k) = \frac{ik}{8\pi a} \exp(2ika) \int_A \exp[-ik(\hat{\mathbf{n}}_s - \hat{\mathbf{n}}_i) \cdot \mathbf{r}] f(\mathbf{r}, \theta) d^2\mathbf{r}$$

where

$$f(\mathbf{r}, \theta) = \gamma_\kappa(\mathbf{r}) + \gamma_\rho(\mathbf{r}) \cos\theta, \quad \cos\theta = \hat{\mathbf{n}}_i \cdot \hat{\mathbf{n}}_s.$$

Hence, by using the additional boundary condition (9.7), the scattered field generated by variations in both the compressibility and density is reduced to the Fourier transform of a scattering function with one extra term, namely, $\gamma_\rho \cos\theta$. This result shows that the scattering of an acoustic field due to density fluctuations is a source of dipole radiation whereas variations in the compressibility represents a monopole source of scattering. This is illustrated in Figure 9.5.

In order to develop a quantitative imaging system, we need to find a way of reconstructing γ_κ and γ_ρ independently. This is known as a two-parameter reconstruction problem and its solution is based on exploiting the angular dependence of the density variations. To see how this works, suppose that we can recover the function $f(\mathbf{r}, \theta)$ at any θ of our choice. If we choose two different angles θ_1 and θ_2 where $\theta_1 \neq \theta_2$, then we can write two simultaneous equations of the form

$$f(\mathbf{r}, \theta_1) = \gamma_\kappa(\mathbf{r}) + \gamma_\rho(\mathbf{r}) \cos\theta_1$$

and

$$f(\mathbf{r}, \theta_2) = \gamma_\kappa(\mathbf{r}) + \gamma_\rho(\mathbf{r}) \cos\theta_2.$$

Solving these equations, we then have

$$\gamma_\rho(\mathbf{r}) = \frac{f(\mathbf{r}, \theta_1) - f(\mathbf{r}, \theta_2)}{\cos\theta_1 - \cos\theta_2}$$

and

$$\gamma_\kappa(\mathbf{r}) = \frac{f(\mathbf{r}, \theta_1)\cos\theta_2 - f(\mathbf{r}, \theta_2)\cos\theta_1}{\cos\theta_2 - \cos\theta_1}.$$

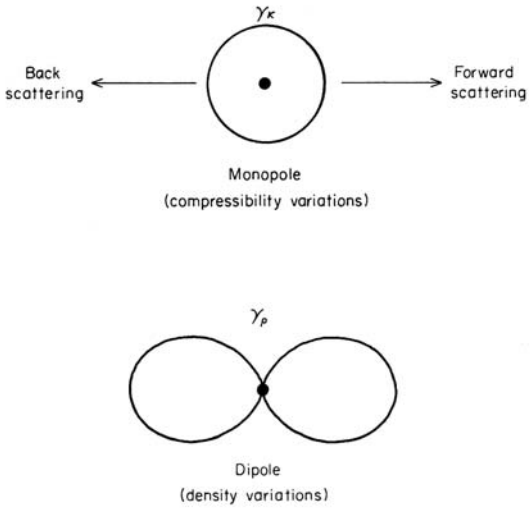

Figure 9.5: The directivity patterns produced by acoustic scattering from variations in the compressibility (monopole) and density (dipole). The difference in the directivity provides a method of recovering the density and compressibility variations independently. This is an example of quantitative acoustic diffraction tomography.

These solutions are quantitative reconstructions and this type of imagery is known as quantitative acoustic diffraction tomography. Let us examine how to

obtain $f(\mathbf{r},\theta)$. To do this, we introduce an experimental method which allows a two-dimensional function to be reconstructed but, at the same time, does not need the angle between the incident and scattered fields to be changed. In other words, we need a method of reconstructing the scattering function when the position of the receiver, relative to the source, is fixed. This rules out any reconstruction based on the use of a CW field because in this case the scattered field must be measured at all scattering angles ϕ_s. Since θ is related to ϕ_i and ϕ_s by

$$\theta = \phi_s - \phi_i$$

this means that θ is a necessary experimental variable. The only experiment where θ can remain fixed has already been discussed in Section 9.3, which examined a method of diffraction tomography using a pulsed field. Therefore, if we wish to conduct quantitative diffraction tomography based on a model where variations in the compressibility and density are responsible for the scattered field, we are forced to utilize a pulse mode system. Following Section 9.3, the scattered pressure field generated by a pulse $p(\tau)$ is given by

$$p_s(\hat{\mathbf{N}},\tau) = \frac{1}{8\pi a}\frac{\partial}{\partial\tau}p(\tau+2a) \otimes \int_A f(\mathbf{r},\theta)\delta(\tau-\hat{\mathbf{N}}\cdot\mathbf{r})d^2\mathbf{r}.$$

Radon inversion then gives

$$f(\mathbf{r},\theta) = \hat{R}^{-1}D(\phi,\tau,\theta)$$

where D is given by equation (9.6). By generating the data D at two different values of θ, γ_κ and γ_ρ can be recovered. Recall that for maximum resolution we need the value of θ to be as close to 180^0 as possible. It is therefore clear that one experiment should be based on measuring the back-scattered field when $\theta = 180^0$ where the reconstruction is for the function

$$f(\mathbf{r},\theta = 180^0) = \gamma_\kappa(\mathbf{r}) - \gamma_\rho(\mathbf{r}).$$

This function is a measure of the acoustic impedance.

9.4.2 Solution for a Viscous Medium

The solution to the two-parameter reconstruction problem given above assumes that the material is non-viscous. We shall now examine the type of inverse problem that occurs when a model is considered where, in addition to variations in the density and compressibility, scattering is also caused by variations in the bulk and shear viscosities which are related to the scattering functions γ_α and γ_β (see Chapter 4). In this case, the wave equation (as derived in Chapter 4) is given by

$$(\nabla^2+\xi^2)U = -\xi^2\nabla\cdot(\gamma_\rho\nabla u) + \frac{1}{1+ik\ell}\nabla^2(\gamma_\kappa\nabla^2 u)$$

$$-\frac{ik\ell}{1+ik\ell}\Big(\nabla^2(\gamma_\alpha\nabla^2 u) + 2\nabla\cdot[\nabla\cdot(\gamma_\beta\nabla\nabla u)]\Big)$$

where u is the longitudinal velocity potential, $U = \nabla^2 u$ is the acoustic dilatation, ℓ is the relaxation length and

$$\xi = \frac{k}{\sqrt{(1 + ik\ell)}}.$$

Once again, using the Born and far field approximations, the scattered acoustic dilatation can be written in the form

$$U_s(\hat{\mathbf{n}}_i, \hat{\mathbf{n}}_s, k) = \frac{i\xi}{8\pi a} \exp(2i\xi a)(I_1 + I_2 + I_3 + I_4)$$

where

$$I_1 = \int_A \exp(-i\xi \hat{\mathbf{n}}_s \cdot \mathbf{r}) \nabla \cdot [\gamma_\rho \nabla \exp(i\xi \hat{\mathbf{n}}_i \cdot \mathbf{r})] d^2\mathbf{r},$$

$$I_2 = -\frac{1}{\xi^2(1 + ik\ell)} \int_A \exp(-i\xi \hat{\mathbf{n}}_s \cdot \mathbf{r}) \nabla^2 [\gamma_\kappa \nabla^2 \exp(i\xi \hat{\mathbf{n}}_i \cdot \mathbf{r})] d^2\mathbf{r},$$

$$I_3 = \frac{ik\ell}{\xi^2(1 + ik\ell)} \int_A \exp(-i\xi \hat{\mathbf{n}}_s \cdot \mathbf{r}) \nabla^2 [\gamma_\alpha \nabla^2 \exp(i\xi \hat{\mathbf{n}}_i \cdot \mathbf{r})] d^2\mathbf{r}$$

and

$$I_4 = \frac{2ik\ell}{\xi^2(1 + ik\ell)}) \int_A \exp(-i\xi \hat{\mathbf{n}}_s \cdot \mathbf{r}) \nabla \cdot \Big(\nabla \cdot [\gamma_\beta \nabla \nabla \exp(i\xi \hat{\mathbf{n}}_i \cdot \mathbf{r})] \Big) d^2\mathbf{r}.$$

The above integrals can be simplified using the same method as before (i.e. the one used to solve the two-parameter problem). In each case, we integrate by parts and use Green's theorem in the plane to convert integrals over A to integrals around C where C is the contour that completely encloses A. Using the boundary conditions

$$\gamma_f(\mathbf{r}_c) = 0$$

and

$$\hat{\mathbf{n}} \cdot \nabla \gamma_f(\mathbf{r}_c) = 0$$

where $f = \rho, \kappa, \alpha$ or β, the scattered dilatation becomes

$$U_s(\hat{\mathbf{n}}_i, \hat{\mathbf{n}}_s, k) = -\frac{i\xi^3 \exp(2ika)}{8\pi a(1 + ik\ell)} \int_A \exp[-i\xi(\hat{\mathbf{n}}_s - \hat{\mathbf{n}}_i) \cdot \mathbf{r}] f(\mathbf{r}, \theta, k) d^2\mathbf{r} \qquad (9.8)$$

where

$$f = \gamma_\kappa + \gamma_\rho \cos\theta + ik\ell(\gamma_\rho \cos\theta + \gamma_\alpha + 2\gamma_\beta \cos^2\theta).$$

Note that the scattering function in this case depends on both the scattering angle θ and the wavenumber k. Also note that when the viscosity is zero so that $\ell = 0$, the scattering function reduces to

$$f = \gamma_\kappa + \gamma_\rho \cos\theta.$$

The directional properties of the scattering function γ_α are the same as scattering from variations in the compressibility. However, a $\cos^2\theta$ dependence characterizes scattering from the scattering function γ_β. When $k\ell$ is large, acoustic scattering is dominated by the composite scattering function

$$\gamma_\rho \cos\theta + \gamma_\alpha + 2\gamma_\beta \cos^2\theta.$$

Let us now look at a quantitative reconstruction method using CW fields. Recall that CW diffraction tomography requires the scattered field to be measured at all scattering angles. We therefore need a scattering function which is independent of θ. Suppose we consider a physical model where the scattering functions γ_α and γ_β are negligible so that the composite scattering function becomes

$$f = \gamma_\kappa + ik\ell\gamma_\alpha.$$

Fourier inversion of equation (9.8) then leads to the reconstruction

$$f(\mathbf{r}, k) = \frac{2ia(1+ik\ell)}{\pi\xi^3} \exp(-2ika) \int\limits_{|\mathbf{k}|\leq 2|\xi|} \exp(i\mathbf{k}\cdot\mathbf{r}) U_s(\mathbf{k}) d^2\mathbf{k}.$$

By equating real and imaginary parts, we then obtain the quantitative reconstructions

$$\gamma_\kappa(\mathbf{r}) = \frac{2a}{\pi} \operatorname{Re}\left(\frac{i(1+ik\ell)}{\xi^3} \exp(-2ika) \int\limits_{|\mathbf{k}|\leq 2|\xi|} \exp(i\mathbf{k}\cdot\mathbf{r}) u_s(\mathbf{k}) d^2\mathbf{k} \right)$$

and

$$\gamma_\alpha(\mathbf{r}) = \frac{2a}{\pi k\ell} \operatorname{Im}\left(\frac{i(1+ik\ell)}{\xi^3} \exp(-2ika) \int\limits_{|\mathbf{k}|\leq 2|\xi|} \exp(i\mathbf{k}\cdot\mathbf{r}) u_s(\mathbf{k}) d^2\mathbf{k} \right).$$

Observe that the bandwidth of these reconstructions is determined by

$$2 \mid \xi \mid = \frac{2k}{\sqrt{(1+k^2\ell^2)}}.$$

Hence, in this case, the resolution is governed by the magnitude of both the wavenumber and the relaxation length. As the viscosity of the material increases, the resolution of the reconstructions decreases. This result has an obvious physical explanation: as the viscosity increases, both the incident and scattered field are absorbed by a greater amount and so there is less penetration of acoustic energy into and out of the scatterer. The measured scattered field therefore becomes weaker. When the viscosity is very large, there is practically no penetration of acoustic radiation into the scatterer and therefore no information on the internal structure of the scatterer can be obtained.

9.5 EM Diffraction Tomography

Let us consider how the form of the electromagnetic scattering function compares with the acoustic scattering function using exactly the same type of model and approximations that have been presented in previous Sections. Consider a model where a body composed of two-dimensional variations in the permittivity, permeability and conductivity is illuminated by an electromagnetic field (such as a millimetric microwave field) where the polarization of the electric vector is perpendicular to the two-dimensional plane. With

$$\widetilde{\mathbf{E}}(\mathbf{r},k) = \hat{\mathbf{z}}u(\mathbf{r},k), \quad \mathbf{r} = \hat{\mathbf{x}}x + \hat{\mathbf{y}}y$$

the inhomogeneous wave equation (see Chapter 4)

$$(\nabla^2 + k^2)\widetilde{\mathbf{E}} = -k^2\gamma_\epsilon\widetilde{\mathbf{E}} + ikz_0\sigma\widetilde{\mathbf{E}} - \nabla(\widetilde{\mathbf{E}}\cdot\nabla\ln\epsilon) + \nabla\times(\gamma_\mu\nabla\times\widetilde{\mathbf{E}})$$

reduces to

$$(\nabla^2 + k^2)u = -k^2\gamma_\epsilon u + ikz_0\sigma u + \nabla\cdot(\gamma_\mu\nabla u).$$

Using the same method as before, the Born scattered field is given by

$$u_s(\hat{\mathbf{n}}_s,\hat{\mathbf{n}}_i,k) = \frac{ikP}{8\pi a}\exp(2ika)\int\limits_A \exp[-ik(\hat{\mathbf{n}}_s - \hat{\mathbf{n}}_i)\cdot\mathbf{r}]f(\mathbf{r},\theta,k)d^2\mathbf{r}$$

where

$$f = \gamma_\epsilon + \gamma_\mu\cos\theta - \frac{iz_0}{k}\sigma.$$

Here we see that γ_ϵ, γ_μ play an identical role to γ_κ and γ_ρ, respectively, and can thus be 'imaged' using the same methods as those discussed when u is an acoustic wavefield using a pulsed mode system with two different values of θ. Similarly, σ can be imaged using a CW system where k is a constant.

9.6 Case Study: Simulation of an Ultrasonic B-Scan

The B-scan, or Brightness-mode scan, provides a two-dimensional image which is generated by the diffraction (back-scattering) of an ultrasonic pulse from a cross section of the object that is scanned. In this sense a B-scan can be taken to be a form of ultrasonic diffraction tomography based on the back-scattered field generated by and recorded on a linear array of transducers, each of which emits a pulse and records the back-scattered signal on a transducer-by-transducer basis, one after the other. The received echoes are displayed in a way that bears correspondence between the displayed scan line and the direction of ultrasonic propagation.

9.6.1 Introduction

One of the most fundamental features of B-scan images is that one dimension of the image (axial) is inferred from the arrival time of echoes of a short ultrasonic pulse as they reflect from the object, assuming that the path of the signal is a straight line (the A-Scan). Features of the signal that have come from reflections off structures close to the source are received earlier than those reflected from structures deeper in the object.

The transverse dimension of the image is obtained by moving the transducer so that each pulse is transmitted through the object in a different straight line path. The transducer motion can be either mechanical or electronic and the process is repeated until the region of interest has been scanned. Alternatively a set of transducers can be employed, in which each transducer successively emits a pulse and detects the back-scatter. This is called a phased array.

In a B-scanner an electronic pulser is connected to a transducer and excites it so that a short pulse of ultrasound is generated. The pulse is considered to travel in a straight line path and part of its energy is lost through the processes of attenuation. The remaining energy is reflected from structures in the acoustic path; these reflected ultrasonic pressure waves impinge on the transducer and induce a motion of the receiver membrane, which is then translated into a voltage trace via the piezoelectric effect. The position and angular direction of the transducer are determined by position monitoring electronic circuits, which also determine the monitor co-ordinates for the signal display.

The time varying signals that are produced with the above process can be amplified, filtered, digitized and stored to provide data on the time history of the back-scattered field. By computing the amplitude envelope of the recorded signals and stacking them into columns a brightness mode (B-scan image) of the object can be constructed, which, after undergoing grey-level quantization, can be displayed on an appropriate VDU. The image that has been constructed in this way is a collection of signals rather than a proper image (in the photographic sense), but provides a perfectly valid representation of a scanned object.

9.6.2 B-scan Modalities

Different scan modalities can be used to construct a B-scan, the most widely used being linear, sector and arc modalities as illustrated in Figure 9.6.

Linear Scan

In a linear scan, the transducer moves in a straight line and, therefore, the transverse dimension of the image is limited by the transducer's length of travel, (or the size of the phased array employed) while the depth dimension (or time dimension) is limited by the penetration depth of the beam, or the size of the object being scanned. The main advantage with this technique is that the resulting image consists of a uniform line density which results in a constant spatial sampling rate of the scanned object.

Sector Scan

In a sector scan the transducer is fixed at a point on or above the object and is swept through an angular sector. In this case the field-of-view increases with the depth of penetration but, because of the beam divergence, the line density diminishes as the field-of-view expands. Because of its special field-of-view characteristics the sector scan is particularly well suited for imaging through narrow apertures.

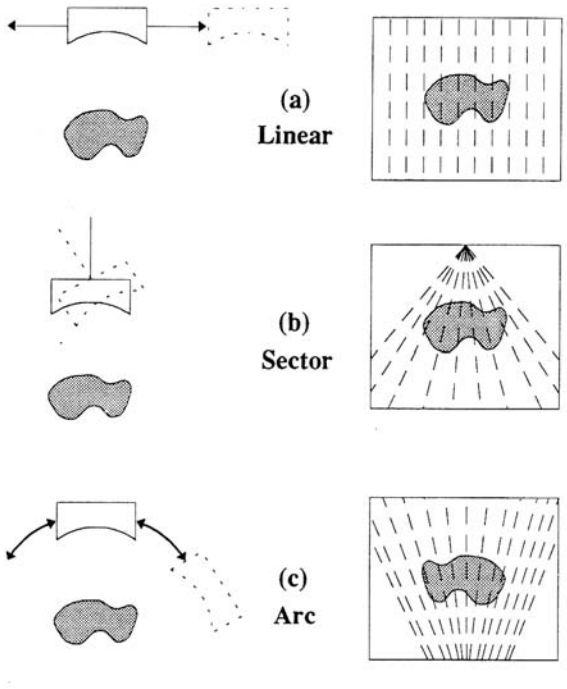

Figure 9.6: Motion and image format for linear (a), sector (b) and arc (c) B-scans.

Arc Scan

In the arc scan the transducer is moved along a circular arc which is situated on or above the object of interest, giving rise to an image which is the inverse of a sector format image. In this case the field-of-view is maximum near the transducer and decreases with depth of penetration.

Compound Linear Scan

In addition to the three scan modalities discussed above there is a fourth modality - the compound linear scan modality - which can be considered to be a combination of the sector scan with a linear scan. The major difference between a compound and a sector scan is that, in the latter case, the scanning angle can be as large as 45^o, while in the former case, much smaller angles are usually used. A compound linear scan is illustrated in Figure 9.7, where, for illustrative purposes, only two scanning positions of the transducer are shown. In compound scanning object points are imaged by more than one ultrasonic pulse along different paths.

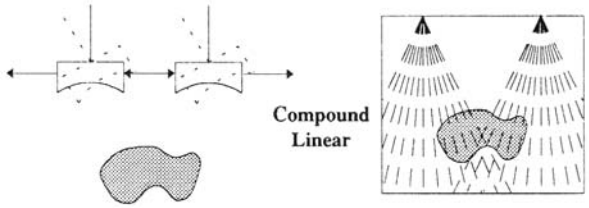

Figure 9.7: Motion and image format for a compound linear scan. Note that in the compound region, the object is imaged with more than one ultrasonic field.

One of the major difficulties with B-scanning is the detection of specular reflectors, which are objects whose reflection of ultrasound is direction dependent and determined by the orientation of the transducer. The major difficulty of imaging such objects stems from the fact that it is possible for a reflected beam not to reach the transducer and therefore the imaging system interprets this as an absence of reflective energy, even though a very strong reflection may have taken place. Because of its properties, a compound scan is often used in order to image specular reflections as well as to image objects which are positioned behind highly reflecting or attenuating structures.

In addition to the basic B-scanning method introduced here, there are numerous distinctions that can be applied to each of them. Most of the techniques operate in 'real time'. Another distinction often applied to B-scans is whether a system is a 'contact scanner' or based on a 'water-bath'. In the former case, the transducer is in direct contact with the object directly while, in the latter case, the ultrasonic field propagates in a liquid medium (usually water) before insonifying the object. Despite the differences that exist between the numerous B-scan techniques, it should be stressed that the basic concepts of B-mode imaging introduced here apply to all of them.

9.6.3 Coherence

The images produced by a linear B-scanning system are examples of partially coherent images; they provide a coherent record (i.e. a record of both amplitude and phase information) of the time history of the ultrasonic field. This type of imaging system is classified as a real aperture imaging system the resolution of the images obtained depending to first order on the pulse length and the beam width of the ultrasonic field.

Due to the coherent nature of the system, the images are characterized by speckle patterns from which information on the characteristics of the object can be inferred. Significant changes in the acoustic impedance at the interface of object features are clearly visible as are the shadows caused when the attenuation of the ultrasonic wavefield. However, in each case, speckle is a prominent feature of the images. Speckle patterns are a well known feature of coherent optics (e.g. the scattering of laser light from a rough surface). In general, any image obtained from the scattering of radiation (electromagnetic or acoustic) in which some measure of the phase of the radiation field is available provides a (partially) coherent image in which speckle is a primary characteristic. Speckle pattern characterization methods can be adopted from those developed to interpret speckle patterns in other fields of coherent imaging science (e.g. synthetic aperture radar imaging).

9.6.4 Resolution of B-scan Images

The two resolution factors in a B-scan are the 'lateral' or 'transverse' resolution and the 'axial' resolution, the former being the resolution in the direction of the transducer motion, while the latter is the resolution in the ultrasonic pulse propagation.

Lateral Resolution

In a focused optical system, the spacial resolution is given by $1.22\lambda f/D$ which is known as the Rayleigh criterion. This criterion describes the dependence of the resolution on the wavelength of light λ and the characteristics of the optical system, as described by the focal length f and the diameter D of the (circular) aperture (see Chapter 11). Historically, this resolution criterion was proposed in order to distinguish between two self-luminous point sources (stars), where the optical system is operating in a recording mode only. In such cases the impulse response or point spread function of the imaging system is given by the Airy pattern, $J_1^2(x)/x^2$ (ignoring scaling) where x is the transverse dimension and J_1 is the first order Bessel function.

With B-scans the imaging system operates on both transmitting and receiving mode and since, most of the time, the same transducer is used as both source and receiver, the impulse response function of the system is described by the square of the Airy pattern. These differences raise questions of how B-scan image resolution is affected, the answer depending on exactly how resolution is defined. If resolution is defined as the distance between the first zeros of the impulse response function, then the resolution remains unaffected since

the zeros of the two pattern coincide. However, it can be easily shown that for any other definition of resolution, such as that based on a 19% dip in the impulse response function as is sometimes used, then we have a significantly better resolution because of the steeper slopes of the intensity function (Airy pattern squared) as compared to the Airy pattern itself.

Another factor which affects lateral resolution is the fact that most B-scanners have fixed focus elements, the resolution being poorer for structures that do not lie within the focal length of the element. Resolution at the focal depth can be improved by increasing the aperture of the imaging system but, as a result, we get a decrease in the region over which the optimum resolution is obtained (depth-of-focus). This can be an undesirable compromise since the resolution improves with the size of the aperture while the depth-of-focus becomes smaller. To minimize this effect only weak focusing is used, but, even so, the resolution is rather poor for reflectors that lie far from the focal distance of a fixed focus element. However, it is possible to solve this problem by constructing electronically variable focusing devices which are based on the fact that ultrasonic imaging is a coherent technique - a transducer being sensitive to both amplitude and phase information. The transducer is subdivided into a number of independent units which process the signals before constructing the final image, the process involving a phase modification. Using these techniques, it is possible to increase lateral resolution but such devices are very complex.

Although on a theoretical basis image resolution is highly dependent on the definition employed, the question of which criterion should be used when defining resolution in a B-scan image is academic.

Axial Resolution

The axial resolution of a B-scan image is inferred from the time of arrival of the reflected signals and, therefore the resolution in this direction is not affected by the focusing elements, depending mainly on the transducer bandwidth. The larger the bandwidth, the shorter the ultrasonic pulse and, therefore, the finer the definition along the propagation axis.

The problem that arises when dealing with broadband transducers is that axial resolution cannot be defined anymore with the straightforward application of a simple Rayleigh criterion; instead of having just a single wavelength a wide spectrum of wavelengths is present.

9.6.5 Image Artifacts

Resolution improvement is a very important subject in ultrasonic imaging, the quality of images depending on many factors in addition to simple axial- and lateral-resolution parameters. Ultrasonic image artifacts can be the result of different transducer and instrumentation characteristics, or they can occur as a consequence of the physics of ultrasonic wave propagation.

Figure 9.8 illustrates a typical ultrasonic output function, the plot showing peak amplitude against distance value, the distance being either transverse or axial coordinates. The curve can be used in order to generate a B-mode display

and the grey levels of the image determined from the intersection points of the threshold values with the function. It should be noted that, for illustrative purposes, only one amplitude signal is shown, although additional amplitude could be added in order to obtain a more complete analysis of the imaging procedure in real ultrasonic experiments. The recording principle illustrated in Figure 9.8 is used to examine various ultrasonic artifacts associated with different instrumentation and physical limitations.

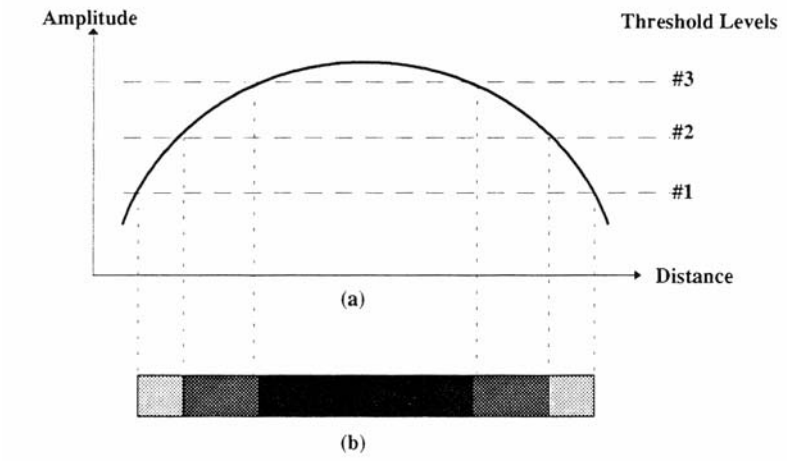

Figure 9.8: A sample recording of the 'information field' for a B-scan: (a) amplitude signal and (b) B-mode display.

Axial Resolution Artifacts

Axial resolution artifacts occur when the imaging system is not capable of resolving two point reflectors in an axial direction and will be discussed here because of its importance in ultrasonic imaging techniques. Consider the configuration illustrated in Figure 9.9, where an ultrasonic transducer is placed over the 'wire targets' (i.e. good reflectors) and a series of waveforms are produced on an A-mode display (i.e. a display of reflected signal itself). These waveforms are then used to produce a B-mode display, after applying an adequate recording threshold value, which in this example is considered to be just above zero, i.e. just above the noise level. Consideration of this setup shows that we have a rather poor B-mode display when the pulse duration is long, while a shorter duration pulse produces an improved B-mode image of the targets. From the above analysis, it is clear that the smaller the duration of the pulse, the better the axial resolution obtained.

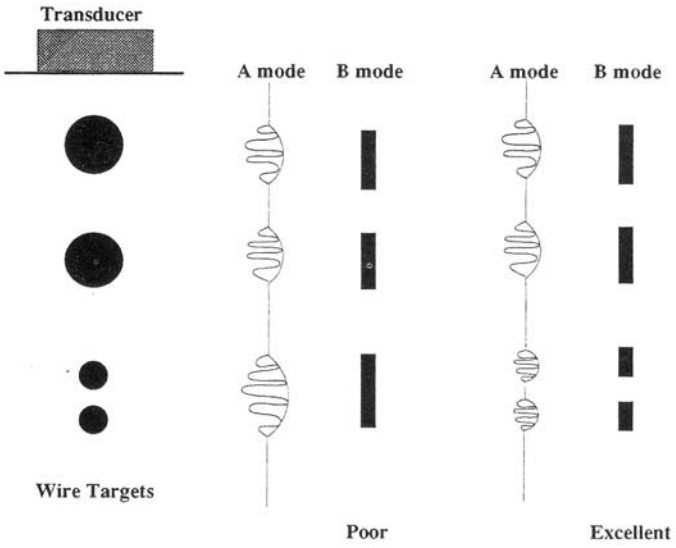

Figure 9.9: Axial resolution artifacts.

Lateral Resolution Artifacts

A second and very important factor that affects image resolution is lateral resolution which is proportional to the beam width. It can be defined in terms of the capability of resolving two point reflectors in a lateral (transverse) direction. Figure 9.10 illustrates two wire targets demonstrating that a beam consisting of a small width generates a better representation of the two wire targets.

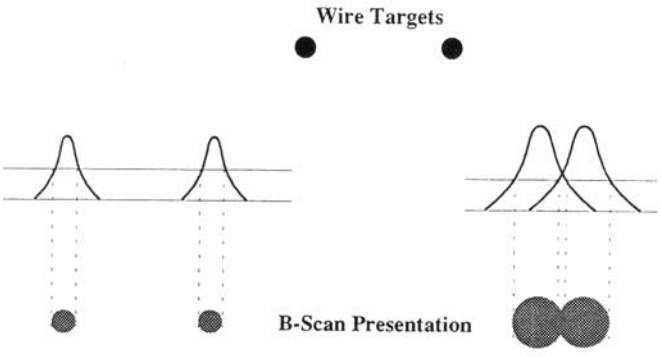

Figure 9.10: Lateral resolution artifacts.

Note that, in order to achieve maximum lateral resolution, the objects to be imaged have to be placed at the depth where the beam is focused - the depth at which the beamwidth is a minimum.

Side-Lobe Energy Artifacts

Ultrasonic transducers possess a side-lobe energy pressure component which is usually illustrated using a polar coordinate representation of pressure vs. angle, at a fixed radius from the transducer surface such as the one given in Figure 9.11. The circular arc illustrates the recording threshold of the instrument. Amplitudes which lie beyond the threshold value are used to construct the B-scan image, while amplitudes which have values less than the threshold are not taken into account.

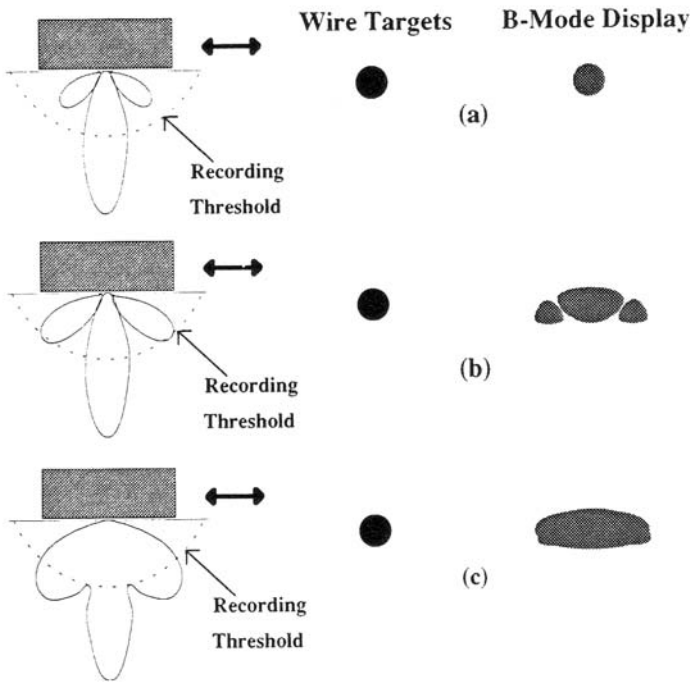

Figure 9.11: Sidelobe energy artifacts.

If we assume excellent axial-resolution characteristics, we obtain excellent imaging results when the side-lobe energy has values below the recording threshold level, as illustrated in Figure 9.11(a). When the side-lobe energy

component has values that extend beyond the threshold value (Figures 9.11(b) and 9.11(c)), ultrasonic artifacts begin to appear in the image, as the wire targets are not well defined any more and they seem to appear in different locations as the transducer is moved across them. The artifacts are more visible when the targets lie further away from the beam axis and are therefore mainly detected by the side-lobe energy components.

Gain-Control Effect Artifacts

The electrical voltages appearing on a transducer crystal as a result of the received echoes are rather small and extend over a high range of values. The pulses are in the range of $10^{-6} - 10^{-3}$ volts and are amplified in order to be displayed. The gain-control governs the amplification of the signals and the user may have to manipulate it in order to obtain a suitable number of echoes on the VDU. As illustrated in Figure 9.12 it is possible to influence the B-scan image formation be adjusting the gain-control settings of the recording instrument. From the different cases illustrated in Figure 9.12, it is clear that we can obtain significantly different images with different gain-settings, even though the lateral resolution is considered to be the same in all cases. If the gain is set too high, then the display will be overloaded and difficult to interpret, since the echoes will be over-emphasized. On the other hand, a gain that is too low may result in very few echoes being detected, again making the final image difficult to interpret.

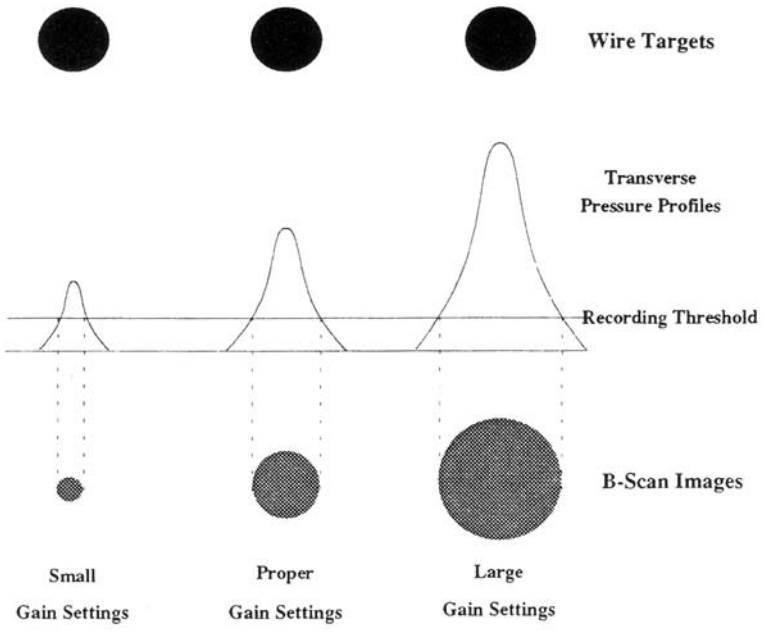

Figure 9.12: Sample B-scan recording, illustrating gain control artifacts.

Artifacts Associated with the Physics of Wave Propagation

In addition to the artifacts associated with instrumentation image artifacts may also occur even when we consider the hypothetical case of the 'perfect instrument'. These are due to the intrinsic physics of ultrasonic wave propagation, acoustic shadows and reverberations being two of the most common artifacts of this type, as illustrated in Figure 9.13.

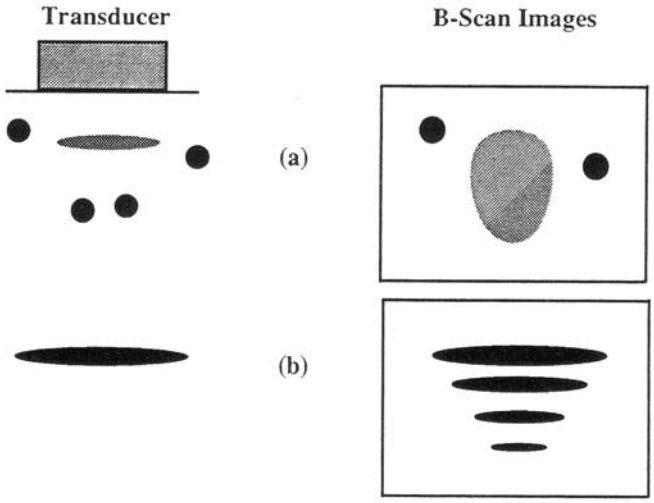

Figure 9.13: Image artifacts associated with the physical aspect of ultrasonic wave propagation; (a) acoustic shadows and (b) reverberation (due to multiple scattering).

Shadows occur in B-scan images because of the presence of a reflector that manifests itself in terms of a high differential acoustic impedance and does not allow sufficient energy to propagate and detect the structures that lie behind the reflector. This particular case is illustrated in Figure 9.13(a) where the two point scatterers that lie behind the high impedance reflector are not imaged in the B-scan image.

Another kind of artifact of this type is the phenomenon of reverberation as illustrated in Figure 9.13(b) where a reflector of intermediate acoustic impedance causes the appearance of several structures in the B-scan image which do not represent existing structures. This is due to multiple scattering effects which are particularly marked in cases were the object has a layered structure. However, with a number of B-scanners, the user can determine whether the structures

that appear in the image describe existing features in the object or whether they are artifacts due to multiple scattering. In many cases where the reverberation is relatively weak the gain control of the instrument can be used to eliminate this effect.

9.6.6 Theoretical Model for a B-scan Imaging System

Let us consider a model where the pressure wavefield $p(\mathbf{r}, k)$ is determined by the solution to the 3D inhomogeneous wave equation (see Chapter 4)

$$(\nabla^2 + k^2)u = -k^2\gamma_\kappa u + \nabla \cdot (\gamma_\rho \nabla u), \quad \mathbf{r} \in V$$

where

$$\gamma_\kappa = \frac{\kappa - \kappa_0}{\kappa_0}, \quad \text{and} \quad \gamma_\rho = \frac{\rho - \rho_0}{\rho}.$$

Here, κ and ρ are the scattering functions for the compressibility and density respectively and k is the wavenumber

$$k = \frac{\omega}{c_0}, \quad c_0 = \frac{1}{\sqrt{\kappa_0 \rho_0}},$$

ω being the angular frequency. This model does not include physical effects such as absorption and dispersion, i.e. the propagation and scattering of the acoustic field u is not influenced by the viscosity of the material, only its density and compressibility.

Consider a transducer to be a point source at $\mathbf{r}_0$ which emits a pulse of ultrasonic radiation with a spectrum given by $P(k)$. In this case the wave equation must be modified to include this source term and so we must write

$$(\nabla^2 + k^2)u(\mathbf{r} \mid \mathbf{r}_0, k) = -k^2\gamma_\kappa u(\mathbf{r} \mid \mathbf{r}_0, k) + \nabla \cdot (\gamma_\rho \nabla u(\mathbf{r} \mid \mathbf{r}_0, k) + P\delta^3(\mathbf{r} - \mathbf{r}_0).$$

The Green function solution for this equation at a point $\mathbf{r}_s$ is

$$u(\mathbf{r}_s \mid \mathbf{r}_0, k) = P(k)g(\mathbf{r}_s \mid \mathbf{r}_0, k)$$

$$+ \oint_S [g(\mathbf{r} \mid \mathbf{r}_s, k)\nabla u(\mathbf{r} \mid \mathbf{r}_0, k) - u(\mathbf{r} \mid \mathbf{r}_0, k)\nabla g(\mathbf{r} \mid \mathbf{r}_s, k)] \cdot \hat{\mathbf{n}} d^2\mathbf{r}$$

$$+ \int_V g(\mathbf{r} \mid \mathbf{r}_s, k)[k^2\gamma_\kappa u(\mathbf{r} \mid \mathbf{r}_0, k) - g(\mathbf{r} \mid \mathbf{r}_s, k)\nabla \cdot (\gamma_\rho \nabla u(\mathbf{r} \mid \mathbf{r}_0, k))]d^3\mathbf{r}$$

where g is the solution of

$$(\nabla^2 + k^2)g(\mathbf{r} \mid \mathbf{r}_s, k) = -\delta^3(\mathbf{r} - \mathbf{r}_0).$$

Let

$$u(\mathbf{r} \mid \mathbf{r}_0, k) = g(\mathbf{r} \mid \mathbf{r}_0, k), \quad \mathbf{r} \in S.$$

Then

$$\oint_S [g(\mathbf{r} \mid \mathbf{r}_s, k)\nabla g(\mathbf{r} \mid \mathbf{r}_0, k) - g(\mathbf{r} \mid \mathbf{r}_0, k)\nabla g(\mathbf{r} \mid \mathbf{r}_s, k)] \cdot \hat{\mathbf{n}} d^2\mathbf{r}$$

$$= \int_V [g(\mathbf{r} \mid \mathbf{r}_s, k)\nabla^2 g(\mathbf{r} \mid \mathbf{r}_0, k) - g(\mathbf{r} \mid \mathbf{r}_0, k)\nabla g(\mathbf{r} \mid \mathbf{r}_s, k)]d^3\mathbf{r}$$

$$= -g(\mathbf{r}_0 \mid \mathbf{r}_s, k) + g(\mathbf{r}_s \mid \mathbf{r}_0, k) = 0$$

from the reciprocity of theorem. Under the Born approximation, we have

$$u(\mathbf{r}_s \mid \mathbf{r}_0, k) = P(k)g(\mathbf{r}_s \mid \mathbf{r}_0, k)$$

$$+ \int_V g(\mathbf{r} \mid \mathbf{r}_s, k)[k^2\gamma_\kappa g(\mathbf{r} \mid \mathbf{r}_0, k) - \nabla \cdot (\gamma_\rho \nabla g(\mathbf{r} \mid \mathbf{r}_0, k))]d^3\mathbf{r}.$$

A B-scan measures the back-scattered field at $\mathbf{r}_0$ which we defined as

$$S(\mathbf{r}_0, k) = \lim_{\mathbf{r}_s \to \mathbf{r}_0} [u(\mathbf{r}_s \mid \mathbf{r}_0, k) - P(k)g(\mathbf{r}_s \mid \mathbf{r}_0, k)]$$

$$= k^2 P(k) \int_V g(\mathbf{r} \mid \mathbf{r}_0, k)[k^2\gamma_\kappa g(\mathbf{r} \mid \mathbf{r}_0, k) - g(\mathbf{r} \mid \mathbf{r}_0, k)\nabla \cdot (\gamma_\rho \nabla g(\mathbf{r} \mid \mathbf{r}_0, k))]d^3\mathbf{r}$$

Now,

$$\int_V g\nabla \cdot (\gamma_\rho \nabla g)d^3\mathbf{r} = \int_V \nabla \cdot (\gamma_\rho g \nabla g)d^3\mathbf{r} - \int_V \gamma_\rho(\nabla g \cdot \nabla g)d^3\mathbf{r}$$

$$= \oint_S \gamma_\rho g \nabla g \cdot \hat{\mathbf{n}} d^2\mathbf{r} - \int_V \gamma_\rho(\nabla g \cdot \nabla g)d^3\mathbf{r}.$$

Using the boundary condition

$$\rho(\mathbf{r}) = \rho_0, \quad \mathbf{r} \in S$$

the surface integral vanishes and noting that

$$\nabla g(\mathbf{r} \mid \mathbf{r}_0, k) = \hat{\mathbf{m}} \left(ik - \frac{1}{\mid \mathbf{r} - \mathbf{r}_0 \mid} \right) g(\mathbf{r} \mid \mathbf{r}_0, k) \simeq \hat{\mathbf{m}} ikg(\mathbf{r} \mid \mathbf{r}_0, k)$$

where

$$\hat{\mathbf{m}} = \frac{\mathbf{r} - \mathbf{r}_0}{\mid \mathbf{r} - \mathbf{r}_0 \mid}$$

we have

$$S(\mathbf{r}_0, k) = k^2 P(k) \int_V z(\mathbf{r}) g^2(\mathbf{r} \mid \mathbf{r}_0, k)d^3\mathbf{r}$$

where f is the acoustic impedance given by

$$z(\mathbf{r}) = \gamma_\kappa - \gamma_\rho.$$

In the far field, the back-scattered field is given by

$$S(\mathbf{r}_0, k) = k^2 P(k) \frac{\exp(ikr_0)}{4\pi r_0} \int_V z(\mathbf{r}) \exp(-2ik\hat{\mathbf{n}}_0 \cdot \mathbf{r})d^3\mathbf{r}$$

where

$$\hat{\mathbf{n}}_0 = \frac{\mathbf{r}_0}{r_0}.$$

This equation is the basic result from which we now derive a computer simulation of the B-scan. Consider the case, where the axial direction is x_0 and the lateral direction y_0 where $x_0 >> y_0$ and $x_0 >> z_0$ and where scattering occurs over a cube of length L. Using Cartesian coordinates,

$$r_0 = \sqrt{x_0^2 + y_0^2 + z_0^2} = x_0 \left(1 + \frac{y_0^2}{x_0} + \frac{z_0^2}{x_0^2}\right) \simeq z_0.$$

Thus,

$$\exp(-2i\hat{\mathbf{n}}_0 \cdot \mathbf{r}) = \exp[-2ik(xx_0 + yy_0 + zz_0)/x_0] \simeq \exp(-2ikx)$$

and

$$S(y_0, k) = k^2 P(k) \frac{\exp(2ikx_0)}{4\pi x_0} \int\limits_V \exp(-2ikx) z(x, y, z) dxdydz$$

$$= k^2 P(k) \exp(2ikz_0) \int\limits_{x_0 - L/2}^{x_0 + L/2} \exp(-2ikx) \left(\int\limits_{y_0 - L/2}^{y_0 + L/2} \int\limits_{-L/2}^{L/2} z(x, y, z) dzdy \right) dx.$$

Let

$$F(y_0, x) = \int\limits_{y_0 - L/2}^{y_0 + L/2} \int\limits_{-L/2}^{L/2} z(x, y, z) dzdy$$

and consider the case where we elongate the scattering volume in the x_0 direction (i.e. the contribution of the scattering volume over the path length of the beam). As the path length $\to \infty$ we can write

$$S(y_0, k) = k^2 P(k) \frac{\exp(ikx_0)}{4\pi x_0} \int\limits_{-\infty}^{\infty} F(y_0, x) \exp(-2ikx) dx.$$

Inverse Fourier transforming, we find

$$s(y_0, x) = \frac{1}{2\pi} \int\limits_{-\infty}^{\infty} S(y_0, k/2) \exp(ikx) dk = \frac{1}{16\pi x_0} \delta(x + x_0) \otimes p(x) \otimes \frac{\partial^2}{\partial x^2} F(y_0, x)$$

where

$$p(x) = \frac{1}{2\pi} \int\limits_{-\infty}^{\infty} P\left(\frac{k}{2}\right) \exp(ikx) dk$$

and $\otimes$ is the convolution operation. The convolution with the delta function (which introduces a x_0 shift) can be ignored together with the scaling by $1/16\pi x_0$ since it will not affect the appearance of the image. We can therefore

consider the back-scattered field that is recorded by the B-scanner to be of the form

$$s(x, y_0) = p(x) \otimes \frac{\partial^2}{\partial x^2} F(x, y_0).$$

If we then let

$$f(x, y) = \int_{-L/2}^{L/2} z(x, y, z) dz$$

then

$$F(x, y_0) = \int_{y_0 - L/2}^{y_0 + L/2} f(x, y) dy \equiv H(y_0) \otimes f(x, y_0)$$

where $H(y_0)$ is the tophat function given by

$$H(y_0) = \begin{cases} 1, & \mid y_0 \mid \leq L/2; \\ 0, & \mid y_0 \mid > L/2. \end{cases}$$

Hence, the model for the back-scattered field becomes (replacing y_0 with y for convenience)

$$s(x, y) = p(x) \otimes H(y) \otimes f(x, y) = H(y) \otimes p(x) \otimes f(x, y)$$

where

$$f(x, y) = \frac{\partial^2}{\partial x^2} \int_{-L/2}^{L/2} z(x, y, z) dz.$$

Finally, to simplify this result further, if we consider the impedance to be separable in z, then the integral over z is just a constant and, ignoring scaling, we can write

$$f(x, y) = \frac{\partial^2}{\partial x^2} z(x, y)$$

where z is the acoustic impedance function in the plane of the B-scan.

A linear B-scan displays the amplitude modulations of $s(x, y)$ for a given value of y - the location of a particular transducer in a linear array. This is equivalent to computing the analytic signal of $s(x, y)$ which is given by

$$a(x, y) = s(x, y) + iq(x, y)$$

where $q(z, y)$ is the Hilbert transform of $s(z, y)$, i.e.

$$q(x, y) = \frac{1}{\pi x} \otimes s(x, y).$$

The image that is displayed is then given by

$$I(z, y) = \mid a(z, y) \mid$$

The convolution of f with H is a result of considering the scattering volume to be finite in the y direction, which in turn is related to the fact that the ultrasonic beam is taken to be of finite width. If we consider the hypothetical case where the beam can be modeled as a pencil line beam then $H(y) \rightarrow \delta(y)$ and the effect of finite beam width is eliminated. However in reality the beam profile is not a constant as H would imply. The beam profile can vary from one application to the next and would ideally require careful experimentation in order to establish the profile and its variation (if any) with x. For the purpose of developing a simulator, if we assume that the beam profile generated close to the transducer, i.e. on the plane $z_0 = 0$ is Gaussian rather than a tophat, then provided that any physical variations of the beam are slow compared with $\exp(ikx)$ and that the energy of the beam is concentrated mainly around its axis, then the Gaussian profile can be taken to represent the beam profile at any point in x. This principle is the same as that used for modeling laser beams and is a consequence of the properties of the solution to the paraxial wave equation (see Chapter 11). Thus, we consider the case where (ignoring scaling)

$$H(y) = \exp(-y^2/\sigma_y^2)$$

the beam width being controlled by the standard deviation σ_y. Finally, in order to introduce the effect of beam divergence which is usually clearly visible in B-scan images obtained over large axial lengths (an effect that can be minimized only by windowing small portions of the image) we can consider the expression

$$H(y) = \exp[-y^2/\sigma_y^2(x)].$$

Here $\sigma_y(x)$ represents the beam divergence profile which to a first approximation can be taken to be of the linear form

$$\sigma_y(x) = \sigma_y + mx$$

where σ_y is the beam width at $x = 0$. By adjusting the value of m we can model a slowly diverging beam (small m) or a rapidly diverging beam (m large). The actual values of m used depends on the size of the B-scan image to be simulated and its resolution (i.e. nunber of pixels) and must be adjusted by the user to simulate a particular type of image.

The pulse profile $p(x)$ is characteristic of the impulse response of the transducer and may be obtained from suitable experimental measurements, i.e. recording the ultrasonic pulse profile near to the transducer as it propagates through a homogeneous medium and reflects from a point scatterer. In practice a B-scan utilizes a sideband pulse with a carrier frequency $\sim 10^6$ Hz and the recorded signals are demodulated. The effect of demodulation is to reproduce the pulse profile which will have a specific rise time, duration and decay time that depend on the characteristics of the B-scan. In order to facilitate a general simulation, we consider this profile to be Gaussian. The data are then given by

$$s(x, y) = \exp(-x^2/\sigma_x^2) \otimes \exp[-y^2/\sigma_y^2(x)] \otimes f(x, y)$$

9.6.7 Point Scattering Model

An example of a B-scan simulation for a point-scattering model where $f(x, y)$ is a distribution of points is given in Figure 9.14 using the example MATLAB code given below.

```
function BSCAN(sigma_x, sigma_y, m, n, threshold)
%
%Input:
%      sigma_x - standard deviation of pulse
%      sigma_y - standard dviation of beam width
%            m - beam divergence factor
%            n - size of image
%    threshold - threshold for computing point scatterers
%
%Compute a Gaussin noise field and normalize.
f=abs(randn(n,n));
f=f./max(max(f));
%Threshold noise field and binarize.
for i=1:n
    for j=1:n
        if f(i,j)>threshold
            f(i,j)=1.0;
        else
            f(i,j)=0.0;
        end
    end
end
f_image=f; %Image of point scatterers.
%Compute object function.
nn=1+n/2;
for i=1:n
    for j=1:n
    filter(i,j)=-abs(i-nn).^2;
end
end
f=real(fftshift(ifft2(filter.*fftshift(fft2(f)))));
%Compute axial IRF.
sgx=sigma_x.^2;
for i=1:n
    p(i)=exp(-((i-nn)^2)/sgx);
end
%Compute stationary axial response.
for j=1:n
   for i=1:n
    sx(i)=f(i,j);
   end
sx=real(fftshift(ifft(fft(p).*fft(sx))));
```

```
for i=1:n
s_x(i,j)=sx(i);
end
end
%Compute non-stationary lateral response.
for i=1:n
    sy=sigma_y+m*i/n;
    sgy=sy^2;
    for j=1:n
        p(j)=exp (-((j-nn)^2)/sgy);
    end
    for j=1:n
        sy(j)=s_x(i,j);
    end
    sy=real(fftshift(ifft(fft(p).*fft(sy))));
    for j=1:n
    s_y(i,j)=sy(j);
end
end
s_y=s_y/max(max(s_y));
%Compute Hilbert tranform and amplitude modulations.
for j=1:n
for i=1:n
    a(i)=s_y(i,j);
end
a=hilbert(a);
    for i=1:n
        s(i,j)=a(i);
    end
end
s=abs(s);
%Show output.
subplot(1,2,1), imshow(f_image);
subplot(1,2,2), imshow(s);
```

Here, a random distribution of point scatterers has been generated by applying a threshold to a random Gaussian noise field after normalization. The object function is computed using the appropriate Fourier filter, i.e.

$$\frac{\partial^2}{\partial x^2} f(x,y) \Longleftrightarrow -k_x^2 F(k_x, k_y).$$

The beam profile given in Figure 9.14 is obtained by executing function BSCAN for a uniform line of point scatterers in the axial direction.

The coherent nature of this real aperture ultrasonic imaging system is clearly evident (i.e. the speckle patterns) in the simulations provided as is the effect of beam divergence. However, although the simulator can be extended to introduce different pulse profiles (including modulation and demodulation as required), it does not include effects due to the dispersion and attenuation of an

ultrasonic pulse which lead to a non-stationary convolution of the pulse in the axial direction.

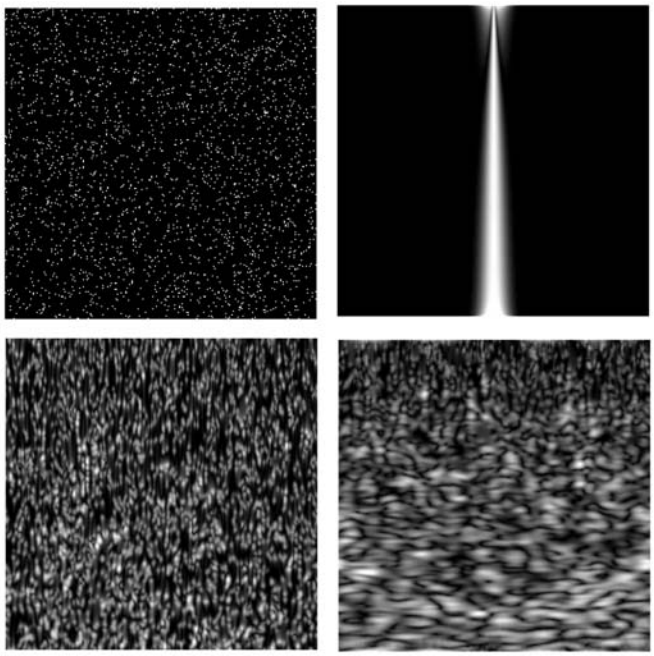

Figure 9.14: B-scan simulations for a distribution of point scatterers obtained using function BSCAN(1,1,1,256,0.5) and function BSCAN(1,1,10,256,0.5) - bottom-left and bottom-right, respectively. The top-left hand image shows the distribution of point scatterers and the top-right image shows the beam profile for the case when m=10.

9.7 Summary of Important Results

CW diffraction tomography

Data on diffraction pattern = Fourier transform of Born scattering function.

Resolution $\propto$ wavelength of CW field.

Pulsed mode diffraction tomography

Deconvolved Data on diffracted time trace = Radon transform of Born scattering function

Resolution $\propto$ Bandwidth of pulse $\times$ sin (half the scattering angle).

Born scattering functions

Non-viscous acoustic medium

$$f(\mathbf{r}) = \gamma_\kappa(\mathbf{r}) + \gamma_\rho(\mathbf{r})\cos\theta$$

Non-conductive dielectric

$$f(\mathbf{r}) = \gamma_\epsilon(\mathbf{r}) + \gamma_\mu(\mathbf{r})\cos\theta$$

Viscous acoustic medium

$$f(\mathbf{r},k) = \gamma_\kappa(\mathbf{r}) + \gamma_\rho(\mathbf{r})\cos\theta + ik\ell[(\gamma_\rho(\mathbf{r})\cos\theta + \gamma_\lambda(\mathbf{r}) + 2\gamma_\mu(\mathbf{r})\cos^2\theta]$$

Conductive dielectric

$$f(\mathbf{r},k) = \gamma_\epsilon(\mathbf{r}) + \gamma_\mu(\mathbf{r})\cos\theta - i\frac{z_0}{k}\sigma(\mathbf{r})$$

B-scan image

For a non-viscous medium, a non-dispersive pulse profile and Gaussian beam divergence

$$I(x,y) = \mid s(x,y) + iq(x,y) \mid$$

where

$$s(x,y) = p(x) \otimes \exp[-y^2/\sigma_y^2(x)] \otimes f(x,y),$$

$$f(x,y) = \frac{\partial^2}{\partial x^2} z(x,y),$$

q is the Hilbert transform of s, z is the acoustic impedance and $p(x)$ is the pulse profile.

9.8 Further Reading

- Morse P M and Ingard K U, *Theoretical acoustics*, McGraw-Hill, 1968.
- Devaney A J, *Diffraction Tomography, Inverse Methods in Electromagnetic Imaging, Reidel, 1985.*
- *Roach G F (Ed.), Inverse Problems and Imaging, Longman, 1991.*
- *Blackledge J M (Ed.), Image Processing: Mathematical Methods and Applications, Oxford University Press, 1997.*

Chapter 10

Synthetic Aperture Imaging

Aperture synthesis is used in a wide range of applications including radar, sonar, diagnostic ultrasound and radio astronomy. The basic principle is really very simple. In one form or another, the resolution of an image is determined by the size of the aperture that is used for observation. To improve the resolution the size of the aperture must be increased. In some cases, to achieve a given resolution, an aperture must be used which is impractical either to build or utilize effectively. However, if a smaller aperture (a real aperture) is used and its position changed while observations are being made, then in principle a much larger aperture can be synthesized, the size of which depends on how far the smaller or real aperture has been moved. The improvement in resolution that can be obtained using this principle is quite spectacular. For example, simple radio interferometers can be successfully operated using array lengths of up to tens of kilometres. This allows maps to be constructed of radio emissions from beyond our galaxy with resolutions of less than a minute of arc - better than the resolution of the human eye!

Although the principles of aperture synthesis is the same, the details vary according to the application. This chapter focuses on aperture synthesis using radar. This is an electromagnetic coherent imaging technique which is used for remote sensing from space and both civilian and military reconnaissance.

10.1 Synthetic Aperture Radar

Radar (**Ra**dio **d**etection **a**nd **r**anging) has been used for many years to detect airborne objects using ground based antennas and to image the 'ground truth' using airbourne platforms. The world's first ever Radar system was constructed in Britain in the late 1930s. It was originally based on using CW radio wavefields. When these radio waves were reflected from an object, a modulation in the amplitude of the return signal occurred providing a characteristic detection signature. The resolution of this Radar system was very poor due to the long

wavelength ($\sim$ 1km) radio waves that were available at the time but it was instrumental in tracking enemy aircraft and giving estimates of their direction and number during the 'Battle of Britain' in the late summer of 1940.

Research undertaken at Birmingham University in the early 1940s led to the development of the cavity magnetron. In a strong magnetic field electrons gyrate around the direction of the field-lines at a high frequency to produce radio waves with a much shorter wavelength ($\lambda \sim 10^{-3}$km). These are known today as microwaves. This technology was used almost immediately for navigation in the night bomber offensive of 1943-45. Microwave pulses were used to generate an image of the ground-truth by rotating the antenna (a microwave 'horn'). Major advances in microwave (Radar) technology occurred in Britain and Germany throughout the early 1940s, and a new research and development laboratory was established at the Massachusetts Institute of Technology, USA, to advance the systems provided to the Americans by the British as part of the lend-lease policy. The technology at the time was based on using sideband pulses. The range resolution was determined by the width of the pulse, and the lateral or azimuth resolution by the width of the beam at the range required. This was the basis for most of the Radar systems used up until the early 1960s when an American invention led to a radical improvement in the range resolution. This was achieved by linearly frequency modulating the pulse and then matched filtering the return 'echo' with its complex conjugate. The frequency modulation was achieved by linearly increasing the intensity of the magnetic field in the cavity magnetron over the duration of a pulse. Further developments in the 1960s and early 1970s paved the way for a new generation of high resolution Radar systems which helped lead to the development of Synthetic Aperture Radar in the mid 1970s (although it had been used covertly for military and some space programmes well before that time). SAR was developed to study the surface of the Earth (and other planets) from both spaceborne and airborne platforms. The basic difference between spaceborne and airborne SAR is the 'look-down' angle of the microwave beam that is used. Spaceborne SAR uses look-down angles of $\sim 70^0$ whereas airborne systems use look-down angles $\sim 10^0$. Both systems attempt to classify the inhomogeneous nature of the Earth's surface by repeatedly emitting a pulse of microwave radiation and recording the back-scattered field.

In this Chapter attention is focused on airborne SAR which is now used extensively for both civilian and military reconnaissance. The original spaceborne SAR - Seasat - became operational soon after its launch in June 1978 but only functioned for a limited period of time (from July to October of the same year) owing to malfunction. It was designed to carry out studies of the ocean surface using a range of microwave sensors and was equipped with a 24 cm wavelength SAR. Another satellite system - Earth Resources Satellite (ERS-1) was launched in the early 1990s and included a 5cm wavelength SAR.

A conventional side-looking radar (a real aperture radar) operating at many tens of kilometres is only able to obtain lateral resolutions of about a kilometre. By synthesizing the aperture of the radar, one can obtain resolutions of a few metres. This enhancement of resolution by three orders of magnitude, together with the fact that radar can be used in cloud or fog, means that SAR is ideal

for airborne reconnaissance. The quantity of data that must be recorded and processed is typically a million independent pixels (discrete picture elements) every second. This immense amount of data has to be examined and positions of interest (targets) identified and extracted, ideally, in near real time.

Another important aspect of SAR reconnaissance is that, in comparison with optical or infrared reconnaissance, radar can often pick out details on the ground which are either invisible or difficult to distinguish with the human eye. For example, it is possible to distinguish between different types of vegetation. In some cases it is even possible to observe sub-surface structures in regions where the skin depth of the ground is small and the radar can penetrate a short distance into the ground. Many ground-based objects are good reflectors of microwave radiation, particularly those objects that are composed from materials that are good conductors (i.e. metallic objects which have a relatively large radar cross-section). Objects of this kind can therefore be distinguished more easily using radar reconnaissance. This is why airborne SAR imaging is often used for the surveillance of military hardware.

SAR systems are usually classified in terms of the wavelength that is used. The two basic modes of operation are X-band, with a wavelength of 2.8 cm, and L-band, with a wavelength of 24 cm. In addition to different wavelengths, different polarizations can be used. One of the most commonly used types is vertical polarization. This is where an electric field is emitted which points in the vertical direction (relative to the orientation of the antenna). The back-scattered field that is produced with the same polarization is then measured. For this reason, the type of data produced is called vertical-vertical or VV polarization data. In addition to the vertically polarized return, scattering by the ground creates polarizations which differ from that of the incident electric vector, one component being along the direction of the horizontal axis. This is known as the depolarized return, and the type of data that is produced by measuring are known as vertical-horizontal or VH polarization data. Alternatively, an incident electric field can be produced where the electric vector points along the horizontal axis. The data produced by measuring the like polarized field is known as the horizontal-horizontal or HH polarization data. The data produced by measuring the cross-polarized return in this case is known as the horizontal-vertical or HV polarization data. Hence, in principle, there are four modes of operation that can be used. In practice VH and HV SAR images are not significantly different. However, the difference between VV, HH SAR images can be considerable.

An example of a SAR image and an optical photograph was given in the *Introduction* to this work (Figure 1). This is an airborne SAR image using a 2.8 cm (X-band) radar and VV polarization. This type of image is known as a VVX SAR image (VV for vertical-vertical polarization and X for X-band). Each resolution cell in this image corresponds to a real length of about 1.5m. The image was obtained at a range of approximately 50 km and an altitude of about 8 km. There are a number of interesting features in this SAR image. A close inspection reveals that there is a variety of textures which change from one region of the image to the next. These textures are related to physical changes in the terrain such as the type of vegetation that is present. There is a

particularly marked difference between rural and urban regions. An example of this is given in Figure 10.1 which shows two SAR and (approximately) matching optical images of a rural area consisting of a collection of fields and a small urban region. The latter SAR image consists of features which are related to the network of buildings, the large majority of these buildings being constructed from non-conductive materials (brick, concrete and wood, etc.).

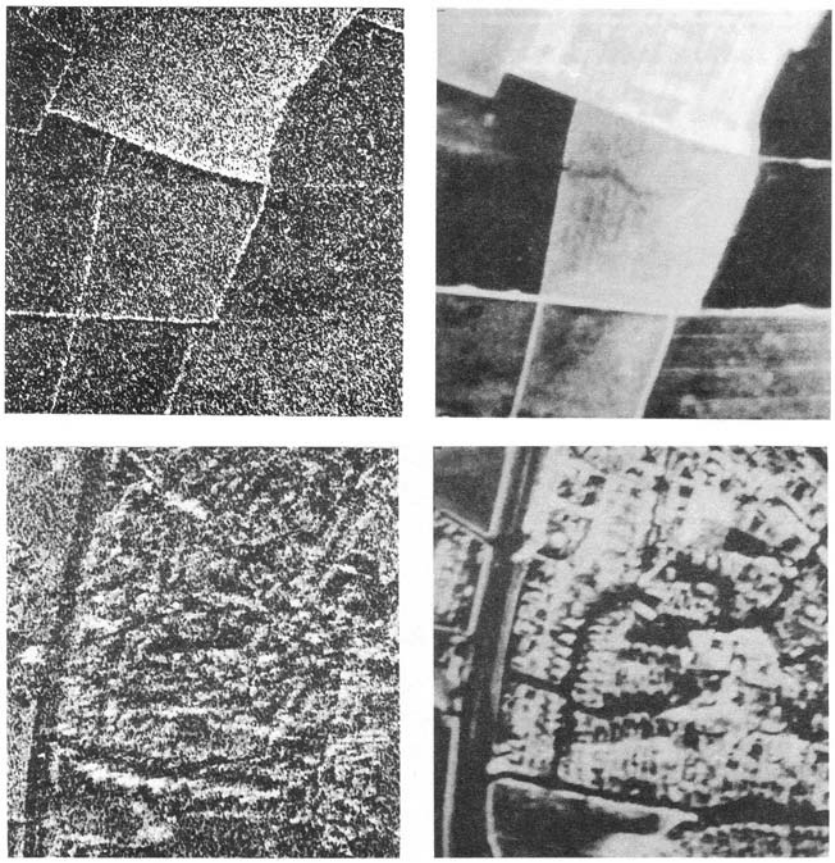

Figure 10.1: SAR (left) and optical (right) images of a rural (top) and urban (bottom) region.

Much stronger reflections occur from structures that are made from conductive materials. An example of this is given in Figure 10.2. which shows a SAR and optical image of a small factory. A large proportion of this object is constructed from metal panels which reflect a greater proportion of the incident microwaves than naturally occurring objects. Hence, this building has a relatively large radar cross-section.

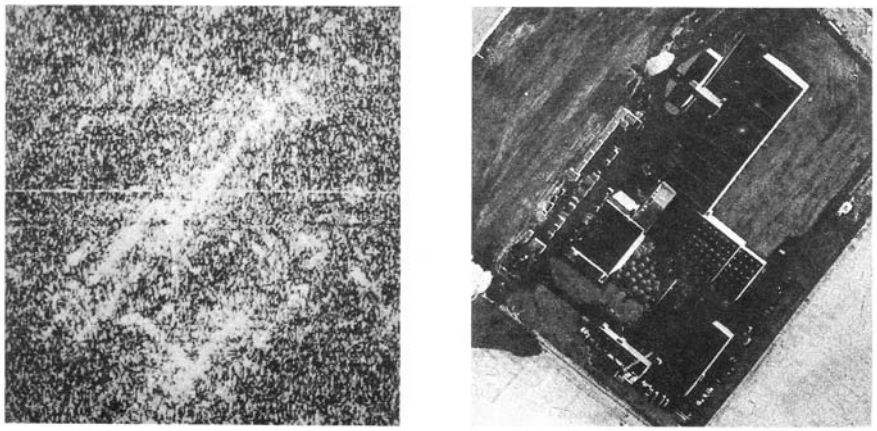

Figure 10.2: SAR (left) and optical (right) images of a small factory with a large radar cross-section due to its construction from metal panels.

10.2 Principles of SAR

Synthetic aperture radar is a pulse-echo system which utilizes the response of a scatterer as it passes through the beam to synthesize the lateral (azimuth) resolution. This allows relatively high resolution images to be obtained at a long range. The basic geometry of the system is given in Figure 10.3. Here, and throughout the rest of this chapter, the range coordinate is denoted by x and the tracking coordinate along the flight path is denoted by y. The latter coordinate is referred to as the azimuth direction. The antenna emits a pulse of microwave radiation and the return signal or echo is recorded at fixed time intervals along the flight path.

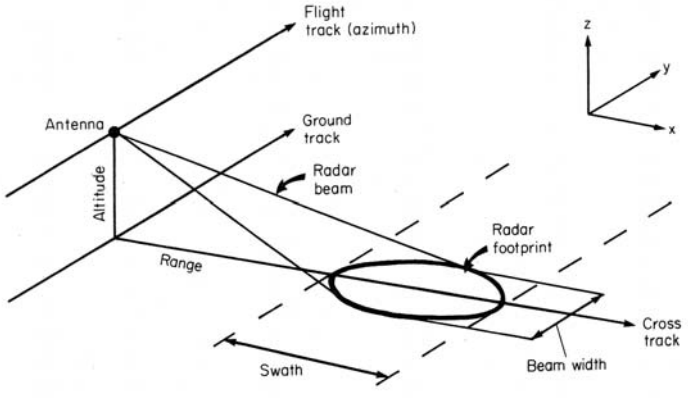

Figure 10.3: Basic geometry of an airborne SAR imaging system.

10.2.1 The Radar Pulse

SAR is a peak power limited system. In other words it operates at the maximum power available. The energy of the system is therefore given by

$$\text{Energy} = \text{Peak Power} \times \text{Time}.$$

In order to transmit a microwave field with enough energy to establish a measurable return, the duration of the pulse must be made relatively long. The length of this pulse is large compared to the wavelength and, hence the system is based on application of a side-band spectrum. If a simple on/off pulse is emitted then the characteristic spectrum is a narrow-band sinc function. The frequency content of this type of pulse is not usually broad enough to obtain adequate range resolution. For this reason, a frequency sweep or 'chirp' is applied over the duration of the pulse. Even with a frequency sweep applied to it, the pulse has a very narrow frequency band. In other words, the energy of the pulse is concentrated near to the carrier frequency. The type of pulse that is actually used is given by (complex form)

$$p(\tau) = \exp(ik_0\tau)\exp(i\alpha\tau^2), \quad -T/2 \leq \tau \leq T/2$$

where T is the pulse length, τ is time $\times$ speed of light, α is the quadratic chirp rate / (speed of light)^2 and k_0 is the carrier wave number (carrier frequency = $\frac{k_0}{2\pi}\times$ speed of light). Note that in reality the pulse is of course not a complex but a real valued function of time. It is given by the real part of p, i.e. $\cos(k_0\tau + \alpha\tau^2)$. This type of pulse is just one of a number of different types of coded pulses that can in principle be used. It is used extensively in radar systems because of its properties for generating range resolution and it can be implemented comparatively easily. The instantaneous phase of this pulse is $k_0\tau + \alpha\tau^2$. The rate of change of phase, or frequency modulation, is therefore $k_0 + 2\alpha\tau$ which is linear in τ. For this reason, the pulse is known as a linear frequency modulated (FM) chirp. In general, most SARs utilize values of k_0 and α where

$$k_0 >> 1$$

and

$$\alpha << 1.$$

For example, in the system used to produce the SAR images given in Figures 10.1 and 10.2,

$$k_0 \simeq 224\text{m}^{-1}$$

and the quadratic chirp rate was $2\pi \times 10^{13}\text{sec}^{-2}$ giving

$$\alpha \simeq 7 \times 10^{-4}\text{m}^{-2}.$$

10.2.2 The Range Spectrum

The spectrum of the FM chirp is obtained by evaluating the integral

$$P(k) = \int_{-T/2}^{T/2} \exp(ik_0\tau)\exp(-i\alpha\tau^2)\exp(-ik\tau)d\tau \tag{10.1}$$

This is given by

$$P(k) = \sqrt{\frac{\pi}{2\alpha}}\left[K\left(\frac{\alpha T + u}{\sqrt{2\pi\alpha}}\right) + K\left(\frac{\alpha T - u}{\sqrt{2\pi\alpha}}\right)\right]\exp(-iu^2/4\alpha)$$

where $u = k + k_0$ and

$$K(x) = \int_0^x \exp(i\pi x^2/2)dx = C(x) + iS(x)$$

with real and imaginary parts

$$C(x) = \int_0^x \cos\frac{\pi}{2}x^2 dx$$

and

$$S(x) = \int_0^x \sin\frac{\pi}{2}x^2 dx.$$

The integrals above are known as **Fresnel integrals**. Figure 10.4 is a sketch of the real valued pulse $\cos(k_0\tau + \alpha\tau^2)$ and its characteristic amplitude spectrum. Observe that the bandwidth of the pulse is determined by the value of αT. With microwave systems this is typically two to three orders of magnitude smaller than the carrier wavenumber k_0.

10.2.3 Range Processing

Consider a single point scatterer which reflects a replica of the transmitted pulse. At the receiver the return signal is coherently mixed down to base-band (i.e. frequency demodulated). In practice, the field that is actually measured is of course not a complex but a real valued signal. The imaginary part of this signal is obtained using a quadrature filter which demodulates the return signal using $\sin(k_0\tau)$ instead of $\cos(k_0\tau)$. This is equivalent to computing the Hilbert transform of the signal after demodulation to base-band. The complex or analytic signal that is obtained after demodulation is given by

$$\exp(i\alpha\tau^2), \quad -T/2 \le \tau \le T/2.$$

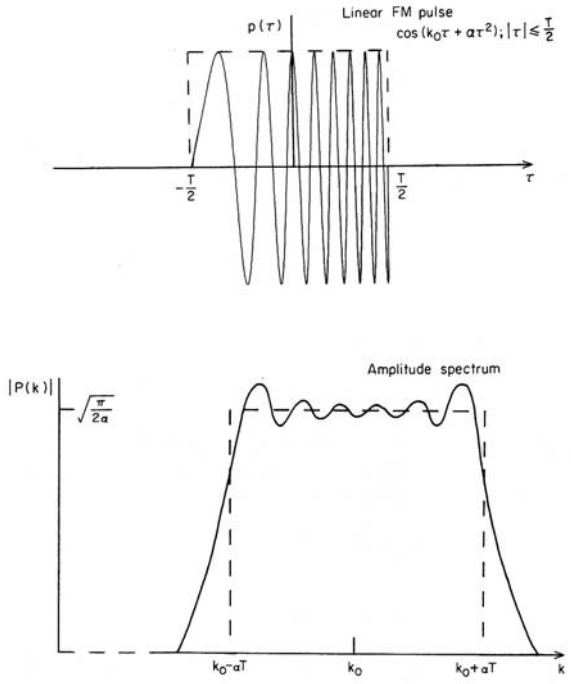

Figure 10.4: Sketch of a linear frequency modulated (chirped) pulse and its characteristic amplitude spectrum.

At this stage, the range resolution is determined by the pulse length T. By applying a suitable process to the return signal, we can enhance the range resolution and hence obtain a more accurate record of the position in range of the point scatterer. This is achieved by correlating the signal with its complex reference function $\exp(-i\alpha\tau^2)$. In SAR and other pulse-echo systems which utilize a linear FM pulse, this process is known as range compression. The range compressed data $R(\tau)$ can be written as (u being a dummy variable)

$$R(\tau) = \int_{-T/2}^{T/2} \exp[-i\alpha(\tau+u)^2]\exp(i\alpha u^2)du.$$

Expanding $(\tau+u)^2$, this equation becomes

$$R(\tau) = \exp(-i\alpha\tau^2) \int_{-T/2}^{T/2} \exp(-2i\alpha u\tau)du.$$

Evaluating the integral over u, we have

$$R(\tau) = T\exp(-i\alpha\tau^2)\,\mathrm{sinc}(\alpha T\tau).$$

The length of the pulse T is relatively large. As a consequence of this, the sinc function is very narrow compared with the complex exponential. For this reason we have

$$\cos(\alpha\tau^2)\,\mathrm{sinc}(\alpha T\tau) \simeq \mathrm{sinc}(\alpha T\tau)$$

and

$$\sin(\alpha\tau^2)\,\mathrm{sinc}(\alpha T\tau) \simeq 0.$$

The range compressed signal can therefore be written as

$$R(\tau) \simeq T\,\mathrm{sinc}(\alpha T\tau), \quad T >> 1.$$

By defining the range resolution to be the distance between the first two zeros of the sinc function which occur when $\alpha T\tau = \pm\pi$ the range resolution is given by

$$\text{Range resolution} = 2\pi/\alpha T \text{ metres} \quad .$$

Observe that, as the value of αT increases, the range resolution improves. For a 20 μs pulse, $T = 6$ km and, with $\alpha = 7 \times 10^{-4}$ m^{-2}, the range resolution is approximately 1.5 metres.

10.2.4 Azimuth Processing

As the radar travels along its flight path (repeatedly emitting a linear FM pulse and recording the back-scattered electric field that is scattered by the ground), the radar beam illuminates an area of the ground which depends upon the grazing angle, its angle of divergence and the range at which the radar operates. The width of the beam in azimuth is given by $R\tan(\beta/2)$ where R is the range and β is the angle of divergence of the beam. For a SAR system, this value corresponds to the maximum length of the synthetic aperture as shown in Figure 10.5. In practice, $\beta \sim 1^0$ and so the width of the beam is approximately given by $R\beta/2$. This value determines the resolution in azimuth of the so called Real Aperture Radar or RAR. At a range of of say 50 km with $\beta = 1^0$, this resolution is just under a kilometre which is very poor and of little practical use. Hence real aperture radar images are only useful when short ranges are involved. The whole point of SAR is to obtain high resolution at long ranges. By studying the response of the radar in azimuth as it passes by a scatterer, we can synthesize the resolution via the principle demonstrated in Figure 10.6. If we consider the radar to be a point source then the field that is produced may therefore be described by the three-dimensional Green function. At relatively large distances from the location of the source, the Green function can be simplified using the Fresnel approximation (see Chapter 5). This provides a description for the wavefield in the intermediate or Fresnel zone. The wavefronts in this zone have a curvature which is parabolic as illustrated in Figure 10.6.

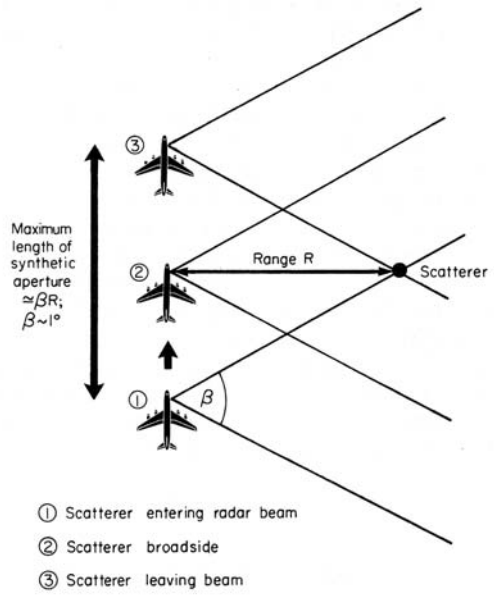

Figure 10.5: Plan view of a SAR showing the maximum length of the synthetic aperture.

Using the geometry shown in this figure, from Pythagoras' theorem we have

$$(R + \delta R)^2 + y^2 = R^2$$

or

$$2R\delta R + (\delta R)^2 + y^2 = 0.$$

If the angle of divergence of the beam is small, then δR is much less than 1. We can then ignore the nonlinear term $(\delta R)^2$ leaving the equation

$$2\delta R = -\frac{y^2}{R}. \tag{10.2}$$

A simple plane wave travelling along the two-way path length $2(R + \delta R)$ can therefore be written as

$$\exp[(-2ik_0(R + \delta R)] = \exp(-2ik_0 R)\exp(-2ik_0\delta R)$$

where k_0 is the wavenumber.

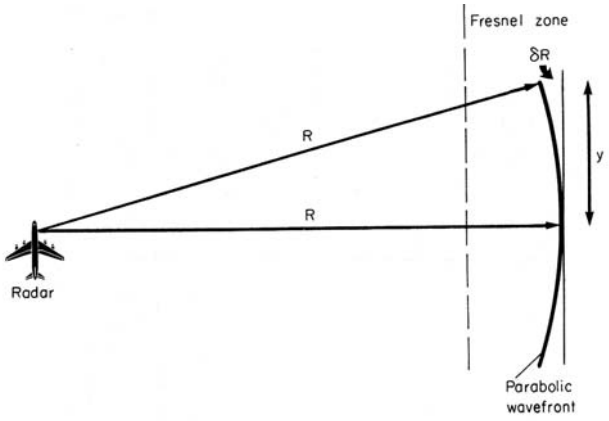

Figure 10.6: By the time the wavefield emitted by the radar has reached a point scatterer, the curvature of the wavefront is parabolic. Scattering occurs in the Fresnel zone. This gives a phase history that is proportional to the square of the distance moved in azimuth.

This wave has two phase factors. The first phase $2k_0R$ is constant but the second phase $2k_0\delta R$ is, from equation (10.2) a function of y and is given by k_0y^2/R. Hence, as the radar moves past the scatterer a quadratic phase shift takes place. If we denote the width of the beam at R by L, then the complex azimuth response of the radar can be written as

$$\exp(ik_0y^2/R), \quad -L/2 \leq y \leq L/2$$

where $-L/2$ is the point where the scatterer enters the beam and $L/2$ is the position where the scatterer leaves the beam. A plot of the azimuth response of a SAR is given in Figure 10.7. In some cases, this response can be clearly observed with real data when the radar passes by a strong scatterer with a large radar cross-section. An example of this is given in Figure 10.8. If the beamwidth is small, then this effect is not significant. Also, only if k_0 is sufficiently large will the effect be observed. In other words, the wavelength of the wavefield must be small compared with the range.

The analysis above demonstrates that the azimuth response of the radar is the same as the response in range to a linear FM pulse. Hence, by utilizing the principles of range compression, we can enhance the azimuth resolution. This is known as azimuth compression and, like range compression, is based on correlating the complex function $\exp(ik_0y^2/R)$ with its complex reference function $\exp(-ik_0y^2/R)$ over the beam width L. Hence, the azimuth compressed signal is given by

$$A(y) = \int_{-L/2}^{L/2} \exp[-ik_0(y+u)^2/R] \exp(ik_0u^2/R)du.$$

Expanding $(y+u)^2$ and evaluating the integral over u, we get

$$A(y) = L\exp(-ik_0y^2/R)\,\mathrm{sinc}(k_0Ly/R)$$
$$\simeq L\,\mathrm{sinc}(k_0Ly/R), \quad L >> 1.$$

For both azimuth compression and range compression, the correlation between the return signal and its reference may be computed in Fourier space using the correlation theorem and a FFT.

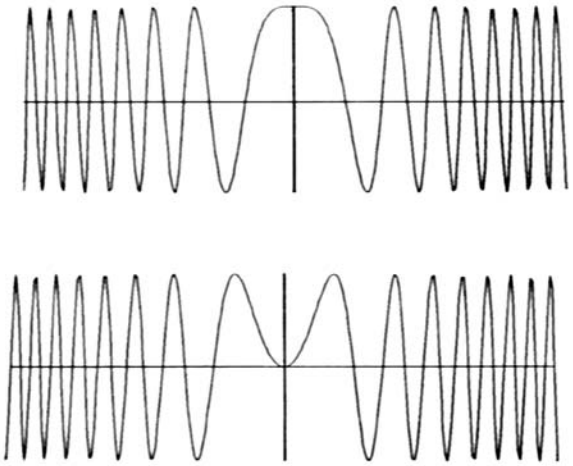

Figure 10.7: Real (top) and imaginary (bottom) components of the theoretical response in azimuth of a SAR to a single point scatterer, i.e. $\cos(k_0y^2/R)$ and $\sin(k_0y^2/R)$, respectively.

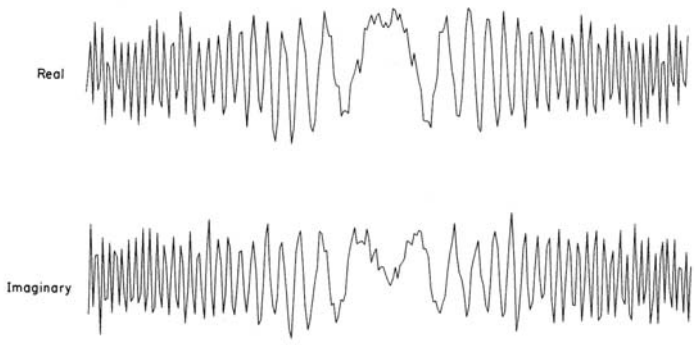

Figure 10.8: Example of the experimental response in azimuth of a SAR to a single point scatterer. It is clearly a noisy version of Figure 10.7.

By defining the azimuth resolution to be the distance between the first zeros of the sinc function which occur when $k_0 Ly/R = \pm\pi$, the azimuth resolution is given by

$$\text{Azimuth resolution} = 2\pi R/k_0 L = 2\pi/\beta k_0 \text{ metres} \quad .$$

The microwave antenna (i.e. essentially the horn at the end of the microwave transmission line) acts like a rectangular aperture which diffracts an otherwise collimated beam of microwaves. Now, the Kirchhoff diffraction integral for fixed $k = k_0$ is given by (see Chapter 6)

$$\int_S \exp(i\mathbf{k}\cdot\mathbf{r})\exp(-ik_0\hat{\mathbf{r}}_0\cdot\mathbf{r})d^2\mathbf{r}, \quad \hat{\mathbf{r}}_0 = \frac{\mathbf{r}_0}{|\,\mathbf{r}_0\,|}$$

which, for an aperture of width w, say, and an incident plane wave propagating in the z-direction (where $\mathbf{k} = \hat{\mathbf{z}}k_0$), becomes (with $r_0 \sim z_0$ and ignoring scaling)

$$\int_{-w/2}^{w/2}\int_{-w/2}^{w/2} \exp(-ik_0x_0x/z_0)\exp(-ik_0y_0y/z_0)dxdy$$

$$= 4\frac{\sin(k_0x_0w/2z_0)}{k_0x_0/z_0}\frac{\sin(k_0y_0w/2z_0)}{k_0y_0/z_0}.$$

The first zeros of this diffraction pattern in azimuth can be taken to determine the width of the radar beam (i.e. the first lobe). These zeros occur when

$$k_0\frac{w}{2}\sin\frac{\beta}{2} = \pm\pi$$

where $\beta/2 = y_0/z_0$. Hence, for small values of β,

$$\beta \simeq \frac{4\pi}{k_0 w}$$

and, hence,

$$\text{Azimuth resolution} \;\propto\; w.$$

The azimuth or synthetic resolution of the SAR is therefore independent of the wavelength!

10.2.5 Discussion

By studying the response of the radar to a point scatterer in range, and then in azimuth, we have established the form of the SAR point spread function. This is given by

$$P(x,y) = LT\,\text{sinc}(\alpha Tx)\,\text{sinc}(\beta k_0 y).$$

It is identical to the diffraction pattern produced by a rectangular aperture. Thus, the (post-processed) SAR image data $D(x,y)$ generated by scattering

from the ground is given by the convolution of the object function for the ground $O(x, y)$ with the appropriate point spread function, i.e.

$$D(x, y) = P(x, y) \otimes \otimes O(x, y). \tag{10.3}$$

A SAR image is a grey level display of the amplitude modulations in the data, i.e.

$$I_{SAR}(x, y) = \mid D(x, y) \mid .$$

The object function describes the imaged properties of the ground surface. The conventional model for this function is the point scattering model. This is where the object function is taken to be a distribution of point scatterers each of which reflects a replica of the emitted pulse and can be written in the form

$$O(x, y) = \sum_i \sum_j \delta(x - x_i)\delta(y - y_j).$$

Here, nothing is said about the true physical nature of the ground surface such as its shape and material (dielectric) properties. In the following Section this shortcoming is addressed.

10.3 Electromagnetic Scattering Model for SAR

By considering the response of the radar to a single point scatterer, the basic processing technique required to recover a SAR image can be established. However, this approach conveys no information about the possible physical interpretation of a SAR image. To do this the relationship between the object function and the physical properties of the ground surface such as its dielectric properties and height fluctuations must be established. In this Section approximate expressions for the object functions associated with different polarizations are derived.

10.3.1 A Physical Model for SAR

Consider the model illustrated in Figure 10.9. Here, x is the range coordinate, y is the azimuth coordinate and z is the vertical co-ordinate. Let the ground be composed of three-dimensional variations in the permittivity ϵ and conductivity σ with height variations h. We shall assume that the relative permeability of the ground is 1. Hence, the back-scattered field detected by the radar is produced by variations in $\epsilon(\mathbf{r})$ and $\sigma(\mathbf{r})$ over a region of space $\mathbf{r} = \hat{\mathbf{x}}x + \hat{\mathbf{y}}y + \hat{\mathbf{z}}z$ where $0 \leq z \leq h(x, y)$ and $\hat{\mathbf{x}}x + \hat{\mathbf{y}}y \in A$ - the area of the ground illuminated by the radar beam (i.e. the radar footprint). For $z > h(x, y)$, ϵ and σ are equal to the permittivity and conductivity of the atmosphere. The permittivity of the atmosphere is taken to be the same as for a vacuum and the conductivity of the atmosphere is assumed to be zero. Thus, if a denotes the altitude at which the radar operates, then for all values of z between h and a, $\epsilon = \epsilon_0$ and $\sigma = 0$. The field that is measured in a SAR is the electric field and so we can work

with equations for the electric field alone. From Maxwell's equations, we can write the basic wave equation for this field in the form (see Chapter 4)

$$(\nabla^2 + k^2)\widetilde{\mathbf{E}} = -k^2\gamma\widetilde{\mathbf{E}} + ikz_0\sigma\widetilde{\mathbf{E}} - \nabla(\widetilde{\mathbf{E}} \cdot \nabla \ln \epsilon)$$

where

$$\gamma = \frac{\epsilon - \epsilon_0}{\epsilon_0},$$

k is the wavenumber and z_0 is the impedance of free space ($\simeq 376.6$ ohms).

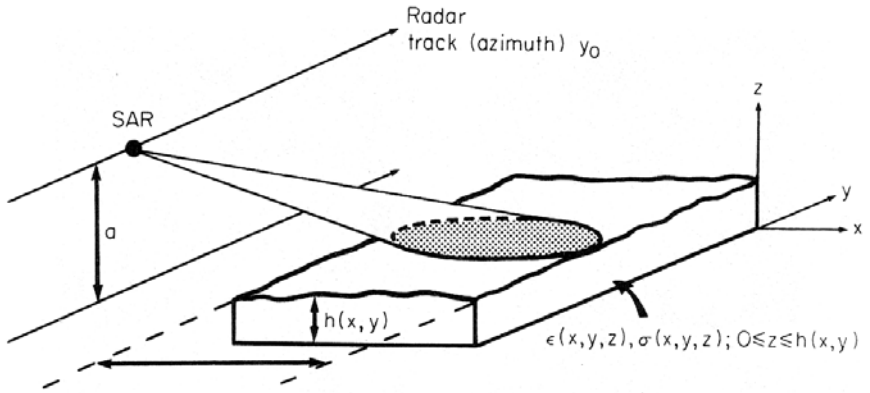

Figure 10.9: Physical model for an airborne SAR.

Assuming that the scattered field only weakly perturbs the incident field, i.e.

$$\|\widetilde{\mathbf{E}}_s\| << \|\widetilde{\mathbf{E}}_i\|$$

and writing $\epsilon = \epsilon_r\epsilon_0$ where ϵ_r is the relative permittivity, we obtain

$$(\nabla^2 + k^2)\widetilde{\mathbf{E}}_s = -k^2\gamma\widetilde{\mathbf{E}}_i + ikz_0\sigma\widetilde{\mathbf{E}}_i - \nabla(\widetilde{\mathbf{E}}_i \cdot \nabla \ln \epsilon_r) \tag{10.4}$$

where

$$\gamma = \epsilon_r - 1.$$

Note that, in this model, the effects of using different polarizations are determined entirely by the term $\nabla(\widetilde{\mathbf{E}}_i \cdot \nabla \ln \epsilon_r)$. If this term is neglected, then the behaviour of the electric field is independent of its polarization (i.e. the wave equation remains the same when the polarization of the electric field is changed). Our problem is to solve equation (10.4) for the scattered electric field $\widetilde{\mathbf{E}}_s$ and to write the solution in a form that is the same as equation (10.3) so that the object function can be defined in terms of the physical properties of the ground (ϵ_r, σ and h). To do this we need a suitable model for the incident field.

10.3.2 Green Function for Airborne SAR

Consider the radar to be a point source. We may then consider a model for the incident field of the form

$$\widetilde{\mathbf{E}}_i = \hat{n} P g$$

where P is the spectrum of the pulse that the radar emits given by equation (10.1) and g is the three-dimensional 'out-going' Green function given by

$$g(\mathbf{r} \mid \mathbf{r}_0, k) = \frac{\exp(ik \mid \mathbf{r} - \mathbf{r}_0 \mid)}{4\pi \mid \mathbf{r} - \mathbf{r}_0 \mid}.$$

The geometry of an airborne SAR allows us to approximate the Green function. Writing the path length $\mid \mathbf{r} - \mathbf{r}_0 \mid$ in Cartesian coordinates,

$$\mid \mathbf{r} - \mathbf{r}_0 \mid = (x - x_0) \left(1 + \frac{(y - y_0)^2}{(x - x_0)^2} + \frac{(z - z_0)^2}{(x - x_0)^2} \right)^{1/2}$$

and employing the conditions

$$\frac{(y - y_0)^2}{(x - x_0)^2} << 1$$

and

$$\frac{(z - z_0)^2}{(x - x_0)^2} << 1$$

a binomial expansion gives

$$\mid \mathbf{r} - \mathbf{r}_0 \mid \simeq x - x_0 + \frac{1}{2} \frac{(y - y_0)^2}{(x - x_0)} + \frac{1}{2} \frac{(z - z_0)^2}{(x - x_0)}.$$

This result yields an expression for the Green function in the Fresnel zone. In this case, we retain terms which are quadratic in both the azimuth and vertical directions. It is the inclusion of quadratic terms of this type which forms the theoretical basis for synthetic aperture imaging. Physically, we are assuming that the wavefront as a function of y and z has a curvature which is parabolic. The conditions required to do this place limits on the grazing angle θ and the angle of divergence of the radar beam β. In terms of θ and β, we may write these conditions in the form

$$\tan^2(\beta/2) << 1$$

and

$$\tan^2 \theta << 1.$$

It is reasonable to restrict values of θ and β to being less than or equal to 10^o when $\tan^2 \theta$ and $\tan^2(\beta/2)$ are two and three orders of magnitude less than 1, respectively. This upper limit for θ and β falls well within the values of these parameters that are used in airborne SAR systems, where θ is typically $5^o - 10^o$ and $\beta \sim 1^o$. The above expression for the path length can be further simplified by exploiting the fact that the range x_0 at which the radar operates is large

compared to the width of ground that is illuminated by the beam (the swath width), i.e. we can introduce the condition

$$\frac{\mid x \mid}{x_0} << 1.$$

This allows us to write

$$\mid \mathbf{r} - \mathbf{r}_0 \mid = x - x_0 - \frac{(y-y_0)^2}{2x_0} - \frac{(z-z_0)^2}{2x_0}.$$

The Green function is then given by

$$g = \frac{1}{4\pi r_0} \exp[ik(x-x_0)] \exp[-ik(y-y_0)^2/2x_0] \exp[-ik(z-z_0)^2/2x_0].$$

The parameter r_0 remains fixed throughout the operation of the SAR and is known as the slant range (i.e. the distance between the radar and the scattering region).

10.3.3 Wave Equations for SAR

Let us consider a SAR that can emit a vertically polarized electric field of the form

$$\widetilde{\mathbf{E}}_i = (\hat{\mathbf{z}} \cos\theta + \hat{\mathbf{x}} \sin\theta) Pg \tag{10.5}$$

or a horizontally polarized electric field where $\mathbf{E}_i$ is given by

$$\widetilde{\mathbf{E}}_i = \hat{\mathbf{y}} Pg. \tag{10.6}$$

Substituting equation (10.6) into equation (10.4) and taking the dot product of each term with $\hat{\mathbf{y}}$, the behaviour of the HH scattered field U_{HH} is determined by the wave equation

$$(\nabla^2 + k^2) U_{HH} = -k^2 \gamma Pg + ikz_0 \sigma Pg$$

$$-\frac{\partial}{\partial y}\left(Pg \frac{\partial}{\partial y} \ln \epsilon_r \right), \quad U_{HH} = \hat{\mathbf{y}} \cdot \widetilde{\mathbf{E}}_s. \tag{10.7}$$

The cross polarized scattered field in this case is obtained by taking the dot product of each term with $\hat{\mathbf{z}} \cos\theta + \hat{\mathbf{x}} \sin\theta$ giving

$$(\nabla^2 + k^2) U_{HV} = -\left(\cos\theta \frac{\partial}{\partial z} + \sin\theta \frac{\partial}{\partial x} \right) \left(Pg \frac{\partial}{\partial y} \ln \epsilon_r \right),$$

$$U_{HV} = (\hat{\mathbf{z}} cos\theta + \hat{\mathbf{x}} \sin\theta) \cdot \widetilde{\mathbf{E}}_s. \tag{10.8}$$

In a similar way, the wave equations for the VV and VH scattered fields are obtained by substituting equation (10.5) into equation (10.4) and taking the dot product of each term with $\hat{\mathbf{z}} \cos\theta + \hat{\mathbf{x}} \sin\theta$ and $\hat{\mathbf{y}}$, respectively. We then obtain

$$(\nabla^2 + k^2)U_{VV} = -k^2\gamma Pg + ikz_0\sigma Pg$$
$$-\left(\cos\theta\frac{\partial}{\partial z} + \sin\theta\frac{\partial}{\partial x}\right)\left(\cos\theta Pg\frac{\partial}{\partial z}\ln\epsilon_r + \sin\theta Pg\frac{\partial}{\partial x}\ln\epsilon_r\right),$$
$$U_{VV} = (\hat{\mathbf{z}}\cos\theta + \hat{\mathbf{x}}\sin\theta)\cdot\widetilde{\mathbf{E}}_s \tag{10.8}$$

and

$$(\nabla^2 + k^2)U_{VH} = -\frac{\partial}{\partial y}\left(\cos\theta Pg\frac{\partial}{\partial z}\ln\epsilon_r + \sin\theta Pg\frac{\partial}{\partial x}\ln\epsilon_r\right),$$
$$U_{VH} = \hat{\mathbf{y}}\cdot\widetilde{\mathbf{E}}_s. \tag{10.9}$$

Notice that the behaviour of the VV and HH fields is determined by variations in both the permittivity and conductivity whereas that of the HV and VH fields depends on variations in the permittivity alone. This result immediately suggests a method of quantitative imaging with SAR. By measuring U_{VH} we can in principle determine ϵ_r, and therefore $\gamma(=\epsilon_r - 1)$. Hence by measuring U_{VV}, with γ and ϵ_r known, we can determine σ.

In general, fluctuations in ϵ_r and therefore $\ln\epsilon_r$ (as a function x, y and z) occur on a scale that is much smaller than the wavelength. For this reason we can write

$$\frac{\partial}{\partial u}\left(g\frac{\partial}{\partial v}\ln\epsilon_r\right) \simeq g\frac{\partial^2}{\partial u\partial v}\ln\epsilon_r$$

where both u and v are equal to x, y or z. For example, from equation (10.7)

$$\frac{\partial}{\partial y}\left(g\frac{\partial}{\partial y}\ln\epsilon_r\right) = g\frac{\partial^2}{\partial y^2}\ln\epsilon_r + \frac{\partial g}{\partial y}\frac{\partial}{\partial y}\ln\epsilon_r$$
$$= g\left(\frac{\partial^2}{\partial y^2}\ln\epsilon_r - ik_0\frac{(y-y_0)}{x_0}\frac{\partial}{\partial y}\ln\epsilon_r\right)$$
$$\simeq g\frac{\partial^2}{\partial y^2}\ln\epsilon_r$$

provided

$$L_y << \frac{x_0}{k_0 \mid y - y_0 \mid}$$

where L_y is the characteristic scale length over which variations in $\ln\epsilon_r$ occur. For an X-band radar operating at a range of 50 km with a beamwidth of 1 km,

$$L_y << 22\text{cm}$$

which is physically reasonable. This result allows us to reduce equation (10.7) and write it in the form

$$(\nabla^2 + k^2)U_{HH} \simeq -k^2\gamma Pg + ikz_0\sigma Pg - Pg\frac{\partial^2}{\partial y^2}\ln\epsilon_r. \tag{10.10}$$

Similarly, equations (10.8)-(10.9) become

$$(\nabla^2 + k^2)U_{HV} \simeq -\cos\theta Pg\frac{\partial^2}{\partial z\partial y}\ln\epsilon_r - \sin\theta Pg\frac{\partial^2}{\partial x\partial y}\ln\epsilon_r \tag{10.11}$$

$$\begin{aligned}(\nabla^2 + k^2)U_{VV} \simeq &-k^2\gamma Pg + ikz_0\sigma Pg - \cos^2\theta Pg\frac{\partial^2}{\partial z^2}\ln\epsilon_r \\ &-2\cos\theta\sin\theta Pg\frac{\partial^2}{\partial z\partial x}\ln\epsilon_r - \sin^2\theta Pg\frac{\partial^2}{\partial x^2}\ln\epsilon_r\end{aligned} \tag{10.12}$$

$$(\nabla^2 + k^2)U_{VH} \simeq -\cos\theta Pg\frac{\partial^2}{\partial y\partial z}\ln\epsilon_r - \sin\theta Pg\frac{\partial^2}{\partial y\partial x}\ln\epsilon_r. \tag{10.13}$$

10.3.4 Determination of the Back-scattered Fields

Now that a set of wave equations has been derived, we can concentrate on developing a solution for the back-scattered field that is observed by the radar. To start with, we shall develop a solution for the HH field. For the time being, let us consider the reduced wave equation

$$(\nabla^2 + k^2)U = -k^2 Pg\gamma + ikz_0 Pg\sigma \tag{10.14}$$

After demonstrating the basic analytical method we shall return to equations (10.10)-(10.13). Remember, we are aiming at a solution for the processed SAR data which gives a mathematical expression for the object function in terms of ϵ_r, σ and h.

The Green function solution to equation (10.14) for the the back-scattered field is

$$U = P\int (k^2\gamma - ikz_0\sigma)g^2 d^3\mathbf{r}. \tag{10.15}$$

The radar measures the back-scattered field at a fixed range x_0 and altitude z_0 over a finite distance in azimuth. Denoting the fixed range and altitude by R and a, respectively, the kernel of equation (10.15) becomes

$$g^2 = \frac{1}{16\pi^2 r_0^2}\exp[2ik(x-R)]\exp[-ik(y-y_0)^2/R]\exp[-ik(z-a)^2/R].$$

Writing

$$X = x - R, \quad Y = y - y_0 \quad \text{and} \quad Z = z - a$$

the back-scattered field as a function of y_0 and k is given by

$$U(y_0,k) = \frac{P}{16\pi^2 r_0^2}\int\int\int \exp[ik(2X - Y^2/R - Z^2/R)](k^2\gamma - ikz_0\sigma)dxdydz.$$

Because the bandwidth of the pulse is so small compared to the carrier frequency we can write $k^2\gamma$ and $ikz_0\sigma$ as $k_0^2\gamma$ and $ik_0 z_0\sigma$, respectively. By taking the inverse Fourier transform of the integral equation above, the back-scattered

field can be written in terms of its measured time history $u(y_0, \tau)$ at different points in azimuth y_0. Using the convolution theorem we then obtain

$$u(y_0, \tau) = \frac{1}{16\pi^2 r_0^2} \int\int\int p(\tau + 2X - Y^2/R - Z^2/R)(k_0^2\gamma - ik_0 z_0 \sigma) dx dy dz$$

where

$$u(y_0, \tau) = \frac{1}{2\pi} \int_{-\infty}^{\infty} U(y_0, k) \exp(ik\tau) dk.$$

The pulse is of the form

$$p(\tau) = \exp(ik_0\tau) \exp(i\alpha\tau^2).$$

Noting that $k_0 >> 1$ and $\alpha << 1$, by comparing the magnitude of terms which make up the kernel p we obtain

$$p(\tau + 2X + Z^2/R - Y^2/R) \simeq p(\tau + 2X) \exp(-ik_0 Y^2/R) \exp(-ik_0 Z^2/R).$$

This simplification is a consequence of the result

$$k_0 - \alpha(Y^2 + Z^2)/R \simeq k_0$$

and allows the scattered field to be written as

$$U(y_0, \tau) = \int\int p(\tau + 2X) \exp(-ik_0 Y^2/R) f(x, y) dx dy$$

where f is the scattering function given by

$$f(x, y) = \frac{1}{16\pi^2 r_0^2} \int_0^h (k_0^2\gamma - ik_0 z_0 \sigma) \exp[-ik_0(z - a)^2/R] dz.$$

We now have an integral equation where our processing variables τ and y_0 have been separated into two different functions. This is why SAR data can be processed in range and azimuth separately. A further simplification can now be made to f by noting that

$$\frac{z}{a} << 1, \quad 0 \leq z \leq h$$

for an airborne SAR so that

$$(z - a)^2 = z^2 - 2za + a^2 \simeq -2za + a^2.$$

Hence, since $a/R = \tan\theta$, where θ is the grazing angle, the scattering function can be written as

$$f(x, y) = \frac{1}{16\pi^2 r_0^2} \exp(-ik_0 a \tan\theta) \int_0^h (k_0^2\gamma - ik_0 z_0 \sigma) \exp(2ik_0 z \tan\theta) dz.$$

We now introduce a couple of tricks which are designed entirely to write the scattered field in a more convenient form. First of all we use the properties of the delta function to write

$$\int\int p(\tau+2X)\exp(-ik_0Y^2/R)f(x,y)dxdy$$

$$=\int_{-\infty}^{\infty} d\tau' p(\tau')\int\int \delta(\tau'-\tau-2X)\exp(-ik_0Y^2/R)f(x,y)dxdy$$

$$=\int d\tau' p(\tau')\int f[\tau'/2-\tau/2+R,y]\exp(-ik_0Y^2/R)dy.$$

Next, we let $x=2R-\tau$ and $x'=\tau'+x$. Then, $\tau'=x'-x$, $\tau'/2-\tau/2+R=x'/2$ and $d\tau'=dx'$ and the scattered field can be written in the form

$$u(y_0,x)=\int dx' p(x'-x)\int f(x',y)\exp[-ik_0(y-y_0)^2/R]dy.$$

To be consistent with the notation now being used for the range variable we write y as y' and y_0 as y. The scattered field can then be written as

$$u(x,y)=\int\int \exp[ik_0(x'-x)]\exp[i\alpha(x'-x)^2]\exp[-ik_0(y'-y)^2/R]$$

$$\times f(x',y')dx'dy'.$$

At the receiver the scattered field, modelled by the above equation, is coherently mixed down to base-band. This is equivalent to multiplying it by $\exp(ik_0x)$ and provides the data

$$d(x,y)=\exp(ik_0x)u(x,y)$$

$$=\int\int \exp[i\alpha(x'-x)^2]\exp[-ik_0(y'-y)^2/R]\exp(ik_0x')f(x',y')dx'dy'.$$

This is a 2D convolution integral, and so we may write

$$d(x,y)=\exp(i\alpha x^2)\exp(-ik_0y^2/R)\otimes\otimes O(x,y)$$

where O is the object function given by

$$O(x,y)=\exp(ik_0x)f(x,y).$$

We can now apply the processing method which was explained in Section 10.2. Correlating these data with the functions $\exp(-i\alpha x^2)$ and $\exp(ik_0y^2/R)$ over the pulse length T and beam width L, respectively, we obtain

$$D(x,y)=\beta RT\,\mathrm{sinc}(\alpha Tx)\,\mathrm{sinc}(\beta k_0y)\otimes\otimes O(x,y) \tag{10.16}$$

where

$$D(x,y)=d(x,y)\odot\odot\exp(-i\alpha x^2)\exp(ik_0y^2/R)$$

and $\beta(= L/R)$ is the angle of divergence of the beam. The SAR image in then given by

$$I_{SAR}(x,y) =\mid D(x,y) \mid = \beta RT \mid \mathrm{sinc}(\alpha Tx)\,\mathrm{sinc}(\beta k_0 y) \otimes\otimes O(x,y) \mid .$$

Observe that this equation for D is the same as equation (10.3). However, in this case, the object function is defined in terms of a scattering function for the ground f.

By taking the two-dimensional Fourier transform of $D(x,y)$, equation (10.16) can then be written in k_xk_y-space as

$$\widetilde{D}(k_x,k_y) = \frac{\pi^2 R}{\alpha k_0} F(k_x - k_0, k_y); \quad -\alpha T \leq k_x \leq \alpha T, \quad -\beta k_0 \leq k_y \leq \beta k_0 \tag{10.17}$$

where

$$\widetilde{D}(k_x,k_y) = \int_{-\infty}^{\infty}\int_{-\infty}^{\infty} D(x,y)\exp(-ik_x x)\exp(-ik_y y)dxdy$$

and

$$F(k_x - k_0, k_y) = \int_{-\infty}^{\infty}\int_{-\infty}^{\infty} \exp(ik_0 x) f(x,y)\exp(-ik_x x)\exp(-ik_y y)dxdy.$$

From equation (10.17), it is clear that range compression provides a sample of the spectrum F of width $2\alpha T$ located at k_0. Unlike the range spectrum the azimuth spectrum is not the result of a spectral shift from GHz to MHz. The azimuth spectrum therefore gives base-band information on the nature of the scattering function f band limited by $2\beta k_0$. The spectral content of f that is acquired is therefore a rectangle of area $4\alpha\beta k_0 T$ centred on $(-k_0, 0)$ in k_xk_y space. This is shown in Figure 10.10 which illustrates that the spectral information (in contrast to resolution) on the ground depends on the wavelength of the microwaves. The wavelength determines the characteristic scale length over which scattering takes place. This leads to a marked difference between SAR images obtained at different wavelengths. An example of this is shown in Figure 10.11 which compares an XVV and LVV SAR image of the same region.

Let us now return to equations (10.10)-(10.13). Recall that we worked with the reduced wave equation (10.14) in order to demonstrate the basic analytic method. Now that this has been done we are in a position to go back and repeat the calculation for equations (10.10)-(10.13). From equation (10.10), the back-scattered HH field is

$$U_{HH} = P\int\int\int \left(k^2\gamma - ikz_0\sigma + \frac{\partial^2}{\partial y^2}\ln\epsilon_r\right) g^2 dxdydz.$$

This equation is identical in form to equation (10.15). The processed SAR data can therefore be written without further proof as

$$D_{HH}(x,y) = TR\beta\,\mathrm{sinc}(\alpha Tx)\,\mathrm{sinc}(\beta k_0 y) \otimes\otimes O_{HH}(x,y)$$

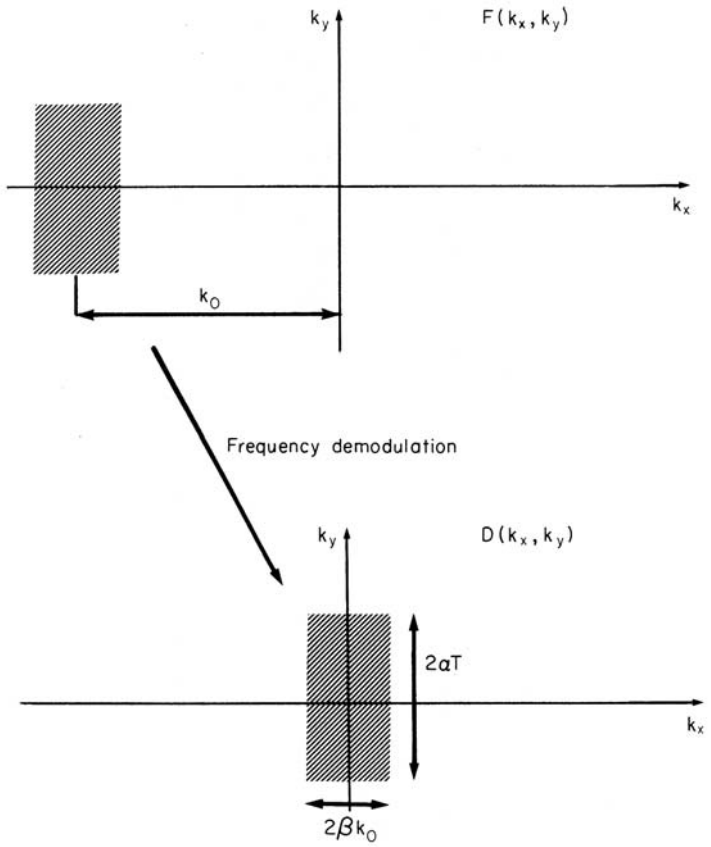

Figure 10.10: The shaded region represents the band of the spacial frequencies on the scattering function for the ground truth that is obtained with a SAR.

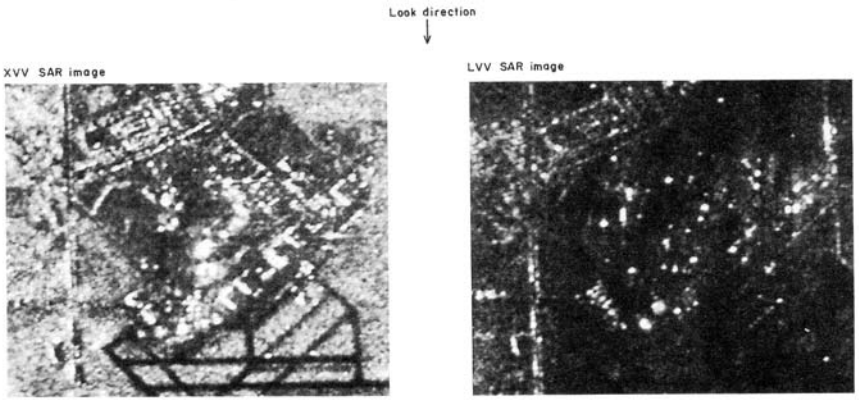

Figure 10.11: Comparison of two SAR images of the same region using different wavlengths: $\lambda = 2.8$ cm (left) and $\lambda = 24$cm (right).

where the HH object function is given by

$$O_{HH} = \frac{1}{16\pi^2 r_0^2} \exp(-ik_0 a \tan\theta) \exp(ik_0 x)$$

$$\times \int_0^h \left(k_0^2 \gamma - ik_0 z_0 \sigma + \frac{\partial^2}{\partial y^2} \ln \epsilon_r \right) \exp(2ik_0 z \tan\theta) dz. \tag{10.18}$$

A similar type of model can be generated for different polarization data. To begin with, we can evaluate the cross polarized scattered field. From equation (10.11), the back-scattered HV field is given by

$$U_{HV} = P \int\int\int \left(\cos\theta \frac{\partial^2}{\partial z \partial y} \ln \epsilon_r + \sin\theta \frac{\partial^2}{\partial x \partial y} \ln \epsilon_r \right) g^2 dx dy dz.$$

Once again the form of this equation is identical to that of equation (10.15). Hence the processed HV SAR data is

$$D_{HV}(x, y) = TR\beta \operatorname{sinc}(\alpha T x) \operatorname{sinc}(\beta k_0 y) \otimes\otimes O_{HV}(x, y)$$

where the HV object function is given by

$$O_{HV} = \frac{1}{16\pi^2 r_0^2} \exp(-ik_0 a \tan\theta) \exp(ik_0 x)$$

$$\times \int_0^h \left(\cos\theta \frac{\partial^2}{\partial z \partial y} \ln \epsilon_r + \sin\theta \frac{\partial^2}{\partial x \partial y} \ln \epsilon_r \right) \exp(2ik_0 z \tan\theta) dz. \tag{10.19}$$

From equation (10.12) it is easy to show that D_{VV} is given by

$$D_{VV}(x, y) = TR\beta \operatorname{sinc}(\alpha T x) \operatorname{sinc}(\beta k_0 y) \otimes\otimes O_{VV}(x, y)$$

where

$$O_{VV} = \frac{1}{16\pi^2 r_0^2} \exp(-ik_0 a \tan\theta) \exp(ik_0 x)$$

$$\times \int_0^h \left(k_0^2 \gamma - ik_0 z_0 \sigma + 2\cos\theta \sin\theta \frac{\partial^2}{\partial z \partial x} \ln \epsilon_r \right.$$

$$\left. + \sin^2\theta \frac{\partial^2}{\partial x^2} \ln \epsilon_r + \cos^2\theta \frac{\partial^2}{\partial z^2} \ln \epsilon_r \right) \exp(2ik_0 z \tan\theta) dz. \tag{10.20}$$

Finally, from equation (10.13), we get

$$D_{VH}(x, y) = TR\beta \operatorname{sinc}(\alpha T x) \operatorname{sinc}(\beta k_0 y) \otimes\otimes O_{VH}(x, y)$$

where

$$O_{VH} = \frac{1}{16\pi^2 r_0^2} \exp(-ik_0 z \tan\theta) \exp(ik_0 x)$$

$$\times \int_0^h \left(\cos\theta \frac{\partial^2}{\partial y \partial z} \ln \epsilon_r + \sin\theta \frac{\partial^2}{\partial y \partial x} \ln \epsilon_r \right) \exp(i2ik_0 z \tan\theta) dz. \tag{10.21}$$

10.4 Case Study: The 'Sea Spikes' Problem

SAR images are highly sensitive to the polarization of the field that is emitted or received. In principle, this result can be used to classify regions of an image when it is known, *a priori*, how certain types of terrain affect different polarized radiation. One of the most dramatic effects occurs when microwaves are scattered by the sea surface at low grazing incidence. An example of this is shown in Figure 10.12.

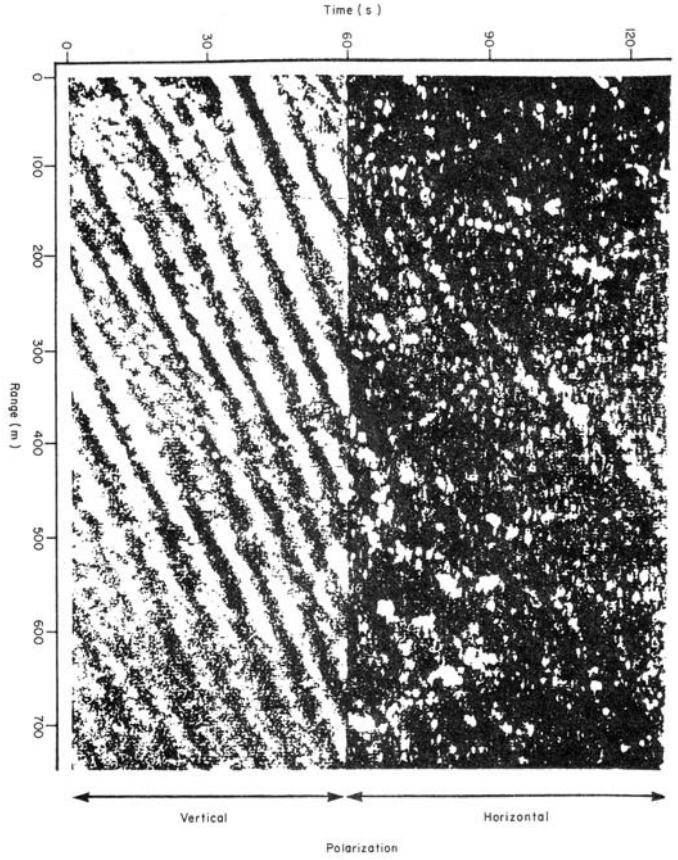

Figure 10.12: Real aperture radar images of the sea surface using vertical (left) and horizontal (right polarization).

This figure shows two real aperture radar or RAR images of the sea surface using X-band HH and VV polarization. In this example, a pulse is emitted in a fixed time interval and the VV return measured over a set period of time (approximately 60 seconds). The radar is then switched to HH mode. Clearly, there is a marked difference between the two images. The VV image shows features which are due to reflections from the crests of waves that are aligned

along the direction of the prevailing wind. These features are almost completely lost in the HH image, although it is just possible to observe the direction of wave motion. The HH image is dominated by a number of very intense reflections which are known as 'sea spikes'. This is a good example of a problem in image understanding. To explain this effect and solve the 'sea spikes' problem we need to establish the physics associated with polarization and establish a suitable model for the sea surface. From previous results, under the Born approximation, polarization effects are characterized by the term $\nabla(\ln\epsilon_r \cdot \mathbf{E}_i)$ in the wave equation for the electric field. Hence, a good starting point is to investigate the characteristics of this term subject to a simplified model of the sea surface.

To a good approximation, the sea is a homogeneous conductive dielectric of varying height $h(x, y)$. We may therefore consider a model where

$$\epsilon_r(x, y, z) = \epsilon_{ro}, \quad z \leq h(x, y);$$
$$\sigma(x, y, z) = \sigma_0, \quad z \leq h(x, y)$$

and where

$$\left[\frac{\partial \epsilon_r}{\partial x}\right]_{z<h} = \left[\frac{\partial \epsilon_r}{\partial y}\right]_{z<h} = \left[\frac{\partial \epsilon_r}{\partial z}\right]_{z<h} = 0.$$

Typical values for ϵ_{ro} and σ_0 are 81 and 4.3 siemens/metre, respectively. In this case, for an X-band radar ($k_0 \simeq 224m^{-1}$), $k_0^2\gamma_0 \simeq 4 \times 10^6 m^{-2}$ and $k_0 z_0 \sigma_0 \simeq 3.6 \times 10^5$ so that

$$k_0^2\gamma_0 - ik_0 z_0\sigma_0 \simeq k_0^2\gamma_0.$$

A simple mathematical model for the VV and HH RAR images given in Figure 10.12 can be obtained by letting the grazing angle θ approach zero. All terms involving $\sin\theta$ can then be neglected, giving

$$I_{RAR}^{ij}(x, y) = T \mid \mathrm{sinc}(\alpha T x) \exp(-ik_0 y^2/R) \otimes \otimes O_{ij}(x, y) \mid$$

where from equations (10.20) and (10.18),

$$O_{VV} = \frac{1}{16\pi^2 R^2} \exp(ik_0 x) \int_0^h \left(k_0^2\gamma_0 + \frac{\partial^2}{\partial z^2} \ln\epsilon_r\right) dz, \quad \gamma_0 = \epsilon_{ro} - 1$$

and

$$O_{HH} = \frac{1}{16\pi^2 R^2} \exp(ik_0 x) \int_0^h \left(k_0^2\gamma_0 + \frac{\partial^2}{\partial y^2} \ln\epsilon_r\right) dz$$

respectively. The VV object function is easy to evaluate, giving

$$O_{VV} = \frac{1}{16\pi^2 R^2} \exp(ik_0 x) \left(k_0^2\gamma_0 h + \frac{1}{\epsilon_{ro}} \left[\frac{\partial \epsilon_r}{\partial z}\right]_{z=h}\right).$$

The HH object function can be evaluated by using Leibniz' formula for the integral of a derivative, i.e.

$$\int_{a(x)}^{b(x)} \frac{\partial}{\partial x} f(x, y) dy = \frac{\partial}{\partial x} \int_{a(x)}^{b(x)} f(x, y) dy$$

$$+\Big[f(x,y)\Big]_{y=a(x)}\frac{da}{dx}-\Big[f(x,y)\Big]_{y=b(x)}\frac{db}{dx}.$$

We then obtain

$$O_{HH}=\frac{1}{16\pi^2R^2}\exp(ik_0x)\left(k_0^2\gamma_0h-\frac{1}{\epsilon_{ro}}\left[\frac{\partial\epsilon_r}{\partial y}\right]_{z=h}\frac{\partial h}{\partial y}\right).$$

Noting that

$$\int_0^h\frac{\partial}{\partial z}\left(\frac{\partial\ln\epsilon_r}{\partial y}\right)dz=\frac{1}{\epsilon_{ro}}\left[\frac{\partial\epsilon_r}{\partial y}\right]_{z=h}$$

and (using Leibniz's formula again)

$$\int_0^h\frac{\partial}{\partial y}\left(\frac{\partial\ln\epsilon_r}{\partial z}\right)dz=-\frac{1}{\epsilon_{ro}}\left[\frac{\partial\epsilon_r}{\partial z}\right]_{z=h}\frac{\partial h}{\partial y}$$

we have

$$\left[\frac{\partial\epsilon_r}{\partial y}\right]_{z=h}=-\left[\frac{\partial\epsilon_r}{\partial z}\right]_{z=h}\frac{\partial h}{\partial y}$$

since

$$\int_0^h\frac{\partial}{\partial z}\left(\frac{\partial}{\partial y}\ln\epsilon_r\right)dz=\int_0^h\frac{\partial}{\partial y}\left(\frac{\partial}{\partial z}\ln\epsilon_r\right)dz.$$

Hence, the HH object function becomes

$$O_{HH}=\frac{1}{16\pi^2R^2}\exp(ik_0x)\left[k_0^2\gamma_0h+\frac{1}{\epsilon_{ro}}\left[\frac{\partial\epsilon_r}{\partial z}\right]_{z=h}\left(\frac{\partial h}{\partial y}\right)^2\right].$$

A relatively simple expression for the VV and HH RAR images can then be obtained by letting

$$\frac{1}{\epsilon_{ro}}\left[\frac{\partial\epsilon_r}{\partial z}\right]_{z=h}=k_0\gamma_0\simeq1.8\times10^4\mathrm{m}^{-1}.$$

Here it is assumed that the gradient in the vertical direction due to a change in the permittivity across the interface between the sea and air is equal to $k_0\gamma_0\epsilon_{ro}\simeq1.3\times10^6\mathrm{m}^{-1}$ over the imaged scene. This allows us to write the VV and HH RAR images as

$$I_{RAR}^{VV}(x,y)=A\mid\mathrm{sinc}(\alpha Tx)\exp(-ik_0y^2/R)\otimes\otimes\exp(ik_0x)\left[1+k_0h(x,y)\right]\mid$$

and

$$I_{RAR}^{HH}(x,y)$$

$$=A\mid\mathrm{sinc}(\alpha Tx)\exp(-ik_0y^2/R)\otimes\otimes\exp(ik_0x)\left[k_0h(x,y)+\left(\frac{\partial}{\partial y}h(x,y)\right)^2\right]\mid$$

where A is given by

$$A = \frac{\gamma_0 k_0 T}{16\pi^2 R^2} \simeq \frac{114T}{R^2}.$$

In this form, it is clear that the VV RAR image is a map of the height variations h of the sea surface whereas the HH RAR image is a map of both h and $(\partial_y h)^2$. Compared to h, the nonlinear term $(\partial_y h)^2$ is very sensitive to the sea state. From this result we deduce that sea spikes are caused by rapid variations in the height of the sea surface as a function of the azimuth direction. In other words, the HH RAR image is dominated by features which map the location of points where

$$\left|\frac{\partial h}{\partial y}\right| >> k_0 h$$

on the scale of a wavelength. A simple illustration of this is given in Figure 10.13 which shows images of $\mid s_{ij} \mid$ and $\mid (s_{i(j+1)} - s_{ij})^2 \mid$, where s_{ij} is a 32×32 random Gaussian distributed array which is taken to represent a surface patch (without any deterministic patterns), each pixel being taken to be on the scale of a wavelength. A sequence of randomly distributed spikes occurs at locations where the difference between the $(j+1)^{th}$ and j^{th} elements of s_{ij} is relatively large so that the nonlinear term $(s_{i(j+1)} - s_{ij})^2$ produces a 'spike dominant' effect.

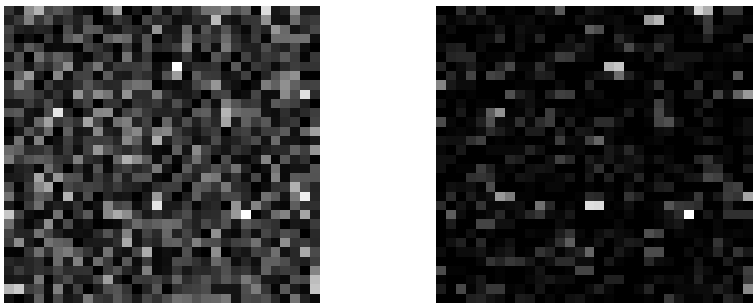

Figure 10.13: Simulation of sea spikes (right) using a low resolution rough surface patch model (left) for the sea surface.

10.5 Quantitative Imaging with SAR

The object functions for a SAR image show that the VV polarization data are related to both the permittivity and conductivity whereas the VH cross polarization data are related to the permittivity alone. This result provides a method of quantitative imaging using SAR. To illustrate the principle, consider a model where the grazing angle approaches zero and where the ground is

composed of conductors embedded in a homogeneous dielectric. Using this model, we can employ the following conditions

$$\epsilon_r(x,y,z) = \epsilon_{ro}, \quad 0 \le z \le h(x,y)$$

and

$$\left[\frac{\partial \epsilon_r}{\partial x}\right]_{z<h} = \left[\frac{\partial \epsilon_r}{\partial y}\right]_{z<h} = \left[\frac{\partial \epsilon_r}{\partial z}\right]_{z<h} = 0.$$

The problem is then reduced to that of processing and combining the VV and VH polarization data in such a way that the reflections from conductors are isolated. As $\theta \to 0$, the SAR data for ij polarization are given by

$$D_{ij}(x,y) = P(x,y) \otimes\otimes O_{ij}(x,y)$$

where

$$O_{VV} = \frac{1}{16\pi^2 R^2} \exp(ik_0 x) \left(k_0^2 \gamma_0 h + \frac{1}{\epsilon_{ro}} \left[\frac{\partial \epsilon_r}{\partial z}\right]_{z=h} - ik_0 z_0 \int_0^h \sigma dz \right)$$

and

$$O_{VH} = \frac{1}{16\pi^2 R^2} \exp(ik_0 x) \frac{1}{\epsilon_{ro}} \left(\left[\frac{\partial \epsilon_r}{\partial z}\right]_{z=h} \frac{\partial h}{\partial y} \right).$$

If we then consider the case when

$$\frac{1}{\epsilon_{ro}} \left[\frac{\partial \epsilon_{ro}}{\partial z}\right]_{z=h} = k_0 \gamma_0$$

the object functions reduce to

$$O_{VV} = \frac{k_0 \gamma_0}{16\pi^2 R^2} \exp(ik_0 x) \left(1 + k_0 h - \frac{iz_0}{\gamma_0} \int_0^h \sigma dz \right)$$

and

$$O_{VH}(x,y) = \frac{k_0 \gamma_0}{16\pi^2 R^2} \exp(ik_0 x) \frac{\partial h}{\partial y}.$$

The VV and HH processed SAR data are then given as

$$D_{VV} = \frac{k_0 \gamma_0}{16\pi^2 R^2} P \otimes\otimes \exp(ik_0 x) \left(1 + k_0 h - \frac{iz_0}{\gamma_0} \int_0^h \sigma dz \right)$$

and

$$D_{VH} = \frac{\gamma_0}{16\pi^2 R^2} P \otimes\otimes \exp(ik_0 x) \frac{\partial}{\partial y}(1 + k_0 h)$$

where P is the point spread function. The last equation can be integrated directly giving

$$\frac{k_0 \gamma_0}{16\pi^2 R^2} P \otimes\otimes \exp(ik_0 x)(1 + k_0 h) = k_0 \int^y D_{VH} dy$$

and, hence, the VV polarization data can be written as

$$D_{VV} = k_0 \int^{y} D_{VH} dy - \frac{ik_0 z_0}{16\pi^2 R^2} P \otimes\otimes \exp(ik_0 x) \int_0^h \sigma dz.$$

By defining the SAR image of the conductivity variations as

$$I^{\sigma}_{SAR}(x,y) = \frac{k_0 \gamma_0}{16\pi^2 R^2} \mid P(x,y) \otimes\otimes \exp(ik_0 x) \int_0^{h(x,y)} \sigma(x,y,z) dz \mid$$

we then obtain

$$I^{\sigma}_{SAR}(x,y) = \mid D_{VV}(x,y) - k_0 \int^{y} D_{VH}(x,y) dy \mid .$$

According to the result above, a quantitative SAR image of the conductivity of the ground may be obtained by a relatively simple procedure. All that is required is a suitable method of integrating the cross polarization data D_{VH}.

10.6 Synthetic Aperture Sonar

Sonar is divided into two classes: passive sonar and active sonar. Passive sonar is used for detecting objects in the sea by analysing the sound that they make using short time Fourier analysis, for example. The time signature is divided into equal segments and the amplitude spectrum of each segment is computed. An image is then generated of the amplitude modulations as a function of frequency and time. This reveals any dominant frequency components in the signal and hence a possible acoustic source. If the source moves, then a frequency shift occurs due to the Doppler effect which can be observed in the image. This effect can be used to detect moving acoustic sources such as submarines.

Active sonar uses acoustic waves to detect and locate objects or image regions of the seabed. The principles of active sonar are very similar to those of radar. They include sideways looking sonars which are used to produce surveys of the seabed and sub-bottom profiling where high resolution information regarding the sub-bottom of the sea bed is obtained to a depth of about ten metres. Compared to radar, the environment (i.e. the sea) in which a sonar must operate is much noisier due to the wide range of physical effects that can occur. For example, turbulence in the sea (caused by temperature gradients) generates random density fluctuations which may refract or even diffract the sonar beam. Another important difference between radar and sonar is that the absorption and dispersion of acoustic waves in the sea are much greater than the absorption and dispersion of microwaves in the atmosphere. The absorption of acoustic radiation is proportional to the square of the frequency. Hence, unlike radar, the resolution of a sonar image (i.e. its high frequency content) is, by comparison, severely limited by the range at which it operates.

Sideways looking sonars are usually real aperture systems. They may utilize either amplitude coded or frequency coded pulses but more commonly resort to frequency modulated chirps with carrier frequencies of the order of 10 kHz. In such cases, the principle is identical to a real aperture radar. The range resolution is given by $2\pi/\alpha T$ metres where α is the quadratic chirp rate/(speed of sound in sea water)^2 and T is the length of the pulse. Also, as in real aperture radar, the lateral resolution is determined by the width of the beam.

The principle of aperture synthesis may also be applied to sonar. One of the major problems with this is due to the relatively low velocity of sound in water ($\sim 10^3 \text{ms}^{-1}$ compared with $\sim 3 \times 10^8 \text{ms}^{-1}$ for microwaves in air). This means that the pulse repetition frequency for synthetic aperture sonar or SAS is much lower than in SAR. In order to sample the synthetic aperture adequately, the position of the transducer must not change along the track by a distance greater than its length (the real aperture). This condition means that either the survey speed is very low or the real aperture is relatively large. For a maximum effective range R, the period between successive transmissions is of the order of $2R/c$ where c is the sound velocity in sea water. If the survey speed is v, then the transducer will have moved between consecutive emissions by a distance

$$d = \frac{2vR}{c}.$$

For a survey speed of 3ms^{-1}, a sonar operating at a range of say 10 km requires a real aperture length of 60 metres if aperture synthesis is to be utilized effectively. Clearly to generate a 60 metre real aperture, a single transducer must be replaced by a linear array of transducers. Practical problems then arise of how the overall length of the real aperture can be kept rigid to avoid ambiguities caused by the non-ideal behaviour of the systems platform. Nevertheless, in principle, SAS can be used to acquire detailed high resolution surveys. We can consider the same type of model for a SAS as the one presented for SAR. This is illustrated in Figure 10.14. Assuming that the sea is a lossless homogeneous medium with density ρ_0 and compressibility κ_0 and the seabed has height variations $h(x, y)$ and compressibility variations $\kappa(x, y, z)$, then it can be shown that the SAS image is given by

$$I_{SAS}(x, y) = \mid \beta T R \,\text{sinc}(\alpha T x)\,\text{sinc}(\beta k_0 y) \otimes\otimes O(x, y) \mid$$

where

$$O(x, y) = \frac{k_0^2}{16\pi^2 r_0^2} \exp(-ik_0 a \tan\theta) \exp(ik_0 x)$$
$$\times \int_0^{h(x,y)} \gamma_\kappa(x, y, z) \exp(2ik_0 z \tan\theta) dz,$$

$$\gamma_\kappa = \frac{\kappa - \kappa_0}{\kappa_0}.$$

The parameters in the above equations are: β - angle of divergence of the sonar beam; T - length of the sonar pulse; R - range; α - quadratic chirp rate/(velocity

of sound)^2; k_0 - carrier wavenumber of pulse; r_0 - slant range of sonar beam; θ - grazing angle of sonar; h - height variations of the seabed; κ - compressibility of seabed; κ_0 - compressibility of the sea. This result has been obtained by solving the wave equation

$$(\nabla^2 + k^2)p = -k^2\gamma_\kappa Pg$$

for the pressure field p using the analysis provided in Section 10.3. The model used to derive this result assumes that the sea and the sea and seabed are density matched. It also assumes that acoustic absorption by the sea is negligible which is highly idealized.

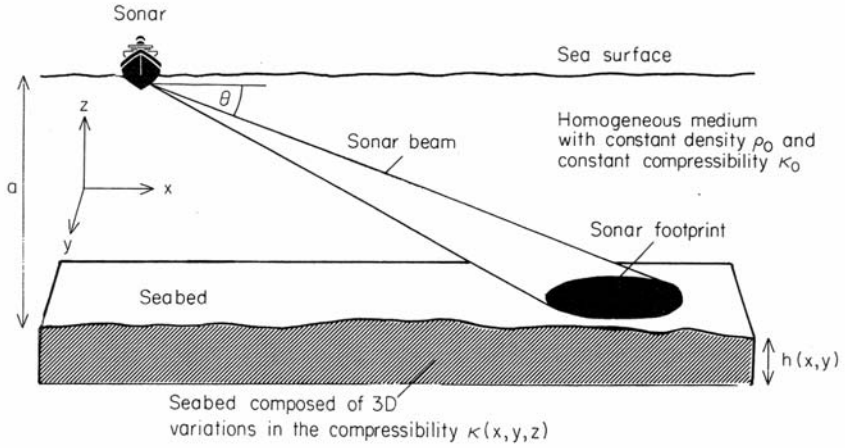

Figure 10.14: Basic geometry and physical model for synthetic aperture sonar.

10.7 Summary of Important Results

SAR point spread function

$$P(x, y) = \beta RT \,\mathrm{sinc}(\alpha T x)\,\mathrm{sinc}(\beta k_0 y)$$

Resolution

Range resolution $\propto 1/\alpha T$

where α is the chirp rate and T is the length of the pulse.

Azimuth resolution $\propto$ length of the real aperture.

SAR image

For ij polarization,

$$I^{ij}_{SAR}(x,y) =\mid P(x,y) \otimes \otimes O_{ij}(x,y) \mid$$

where O_{ij} is given by equations (10.18)-(10.21).

10.8 Further Reading

- Rihaczek A W, *Principles of High Resolution Radar*, McGraw-Hill, 1969.
- Harger R O, *Synthetic Aperture Radar Systems*, Academic Press, 1970.
- Kovaly J J, *Synthetic Aperture Radar*, Artech, 1976.
- Mitchell R L, *Radar Signal Simulation*; MARK Resources, 1985.
- Ulaby F T, Moore R K and Fung A K, *Microwave Remote Sensing (Active and Passive)*, Addison-Wesley, 1981 (Volume 1), 1982 (Volume 2) and 1986 (Volume 3).

Chapter 11

Optical Image Formation

In this Chapter we introduce the principles of optical imaging and discuss the theory of optical image formation. This is based on a linear systems theory approach which is introduced via scalar diffraction theory and forms the basis of Fourier optics. The principles of coherent and incoherent optical imaging are then addressed, and the characteristics of optical beams are considered through an analysis of the angular spectrum of plane waves and a model based on the paraxial wave equation. Finally, a case study is given on the use of incoherent imaging models for watermarking digital images in both soft- and hard-copy form.

11.1 Optical Diffraction

In Chapter 6, the Kirchhoff theory of scalar diffraction was introduced. By solving the 3D homogeneous Helmholtz equation

$$(\nabla^2 + k^2)u(\mathbf{r}, k) = 0$$

using the Green function and Green's theorem, it was shown that application of the Kirchhoff boundary conditions

$$u = u_i \quad \text{and} \quad \frac{\partial u}{\partial \hat{\mathbf{n}}} = \frac{\partial u_i}{\partial \hat{\mathbf{n}}}$$

on a surface S where u_i is the incident field, provides a solution of the form

$$u(\mathbf{r}_0, k) = \frac{ik\alpha}{4\pi r_0} \exp(ikr_0) \int_S \exp(i\mathbf{k} \cdot \mathbf{r}) \exp(-ik\hat{\mathbf{r}_0} \cdot \mathbf{r}) d^2\mathbf{r}, \hat{\mathbf{r}_0} = \frac{\mathbf{r}_0}{\mid \mathbf{r}_0 \mid}$$

in the far field (Fraunhofer diffraction) and

$$u(\mathbf{r}_0, k) = \frac{ik\alpha}{4\pi r_0} \exp(ikr_0) \int_S \exp(i\mathbf{k} \cdot \mathbf{r}) \exp(-ik\hat{\mathbf{r}_0} \cdot \mathbf{r}) \exp\left(ik\frac{r^2}{2r_0}\right) d^2\mathbf{r}$$

in the intermediate (Fresnel diffraction) where $\alpha = \hat{\mathbf{n}} \cdot \hat{\mathbf{k}} + \hat{\mathbf{n}} \cdot \hat{\mathbf{r}}_0$. We shall now use these results to develop a model for the diffraction of light by an aperture and discuss the Fourier transforming properties of a lens.

11.1.1 Fraunhofer Diffraction by an Aperture

The geometry of an 'aperture system' can be described using the Cartesian coordinates

$$\mathbf{r} = \hat{\mathbf{x}}x + \hat{\mathbf{y}}y + \hat{\mathbf{z}}z$$

and

$$\mathbf{r}_0 = \hat{\mathbf{x}}x_0 + \hat{\mathbf{y}}y_0 + \hat{\mathbf{z}}z_0.$$

Here, x_0 and y_0 are taken to describe the position on a flat screen at a distance z_0 from the diffracting aperture. Consider the following system:

(i) The aperture is illuminated by a plane wave with a fixed wavelength at normal incidence to the aperture, i.e.

$$\hat{\mathbf{k}} = \hat{\mathbf{z}}.$$

(ii) The diffraction pattern is observed only at small angles so that

$$\hat{\mathbf{r}}_0 \simeq \hat{\mathbf{z}}.$$

(iii) The aperture is 'infinitely thin' allowing us to consider a solution under the condition

$$kz \to 0.$$

Conditions (i) and (ii) give, with $\hat{\mathbf{n}} = \hat{\mathbf{z}}$,

$$\alpha \simeq \hat{\mathbf{n}} \cdot \hat{\mathbf{k}} + \hat{\mathbf{n}} \cdot \hat{\mathbf{r}}_0 = 2.$$

With condition (iii), we obtain

$$u(x_0, y_0, z_0) = \frac{i}{\lambda}\frac{\exp(ikr_0)}{r_0}\int\int \exp\left[-\frac{ik}{r_0}(xx_0 + yy_0)\right] dxdy$$

where the integrals are taken over the surface of the aperture. This equation gives the amplitude at (x_0, y_0, z_0) in the far field when the aperture is illuminated by a plane wave at normal incidence.

Since a point of observation lies in a plane (the observation screen) located at a fixed distance z_0 from the aperture

$$r_0 = \sqrt{x_0^2 + y_0^2 + z_0^2} = z_0\left(1 + \frac{x_0^2 + y_0^2}{z_0^2}\right)^{\frac{1}{2}} \simeq z_0 + \frac{x_0^2 + y_0^2}{2z_0}.$$

Using this expression for r_0 in the exponent $\exp(ikr_0)$ but using $r_0 \simeq z_0$ elsewhere, we have

$$u(x_0, y_0) = \frac{i}{\lambda}\frac{\exp(ikz_0)}{z_0}\exp\left(ik\frac{x_0^2 + y_0^2}{2z_0}\right)\int\int \exp\left(-\frac{ik}{z_0}(xx_0 + yy_0)\right) dxdy.$$

Finally, let the aperture be filled with an arbitrary distribution $f(x, y)$, that is zero outside S, then

$$u(x_0, y_0)$$

$$= \frac{i}{\lambda}\frac{\exp(ikz_0)}{z_0}\exp\left(ik\frac{x_0^2+y_0^2}{2z_0}\right)\int_{-\infty}^{\infty}\int_{-\infty}^{\infty} f(x,y)\exp\left(-\frac{ik}{z_0}(xx_0+yy_0)\right)dxdy.$$

Here, u is the amplitude of the Fraunhofer diffraction pattern produced by the aperture amplitude function f at a distance z_0 from the aperture. The aperture function f can be taken to describe the 'shape' of the aperture.

Apart from the factors in front of the integrals, u is given by the 2D Fourier transform of f evaluated at the coordinates (with $k = 2\pi/\lambda$)

$$k_x = \frac{2\pi x_0}{z_0\lambda}$$

and

$$k_y = \frac{2\pi y_0}{z_0\lambda}.$$

In practice, the observed quantity (at optical frequencies) is the intensity I given by $\mid u \mid^2$. We can therefore write

$$I(x_0, y_0) = \frac{1}{\lambda^2 z_0^2} \mid \hat{F}_2[f(x,y)] \mid^2$$

where $\hat{F}_2$ is the 2D Fourier transform operator:

$$\hat{F}_2[f(x,y)] = \int_{-\infty}^{\infty}\int_{-\infty}^{\infty} f(x,y)\exp[-i(k_x x + k_y y)]dxdy.$$

Examples of Fraunhofer Diffraction

Example 1: Diffraction by a rectangular aperture of size $a \times b$

In this case,

$$f(x,y) = \begin{cases} 1, & \mid x \mid \leq \frac{a}{2}, \quad \mid y \mid \leq \frac{b}{2}; \\ 0, & \text{otherwise.} \end{cases}$$

and

$$\hat{F}_2[f(x,y)] = \int_{-a/2}^{a/2}\int_{-b/2}^{b/2} \exp[-i(k_x x + k_y y)]dxdy = ab\,\mathrm{sinc}(k_x a/2)\,\mathrm{sinc}(k_y b/2).$$

The intensity pattern is therefore given by

$$I(x_0, y_0) = \frac{a^2 b^2}{\lambda^2 z_0^2}\,\mathrm{sinc}^2\left(\frac{\pi a x_0}{\lambda z_0}\right)\mathrm{sinc}^2\left(\frac{\pi b y_0}{\lambda z_0}\right).$$

The first minima in the x_0 and y_0 directions occur when

$$\frac{\pi a x_0}{\lambda z_0} = \pm\pi \quad \text{and} \quad \frac{\pi b y_0}{\lambda z_0} = \pm\pi$$

respectively, i.e. when

$$x_0 = \frac{\lambda z_0}{a}, \quad \text{and} \quad y_0 = \frac{\lambda z_0}{b}.$$

The distribution for a $a \times a/2$ aperture is given in Figure 11.1 using a logarithmic scale.

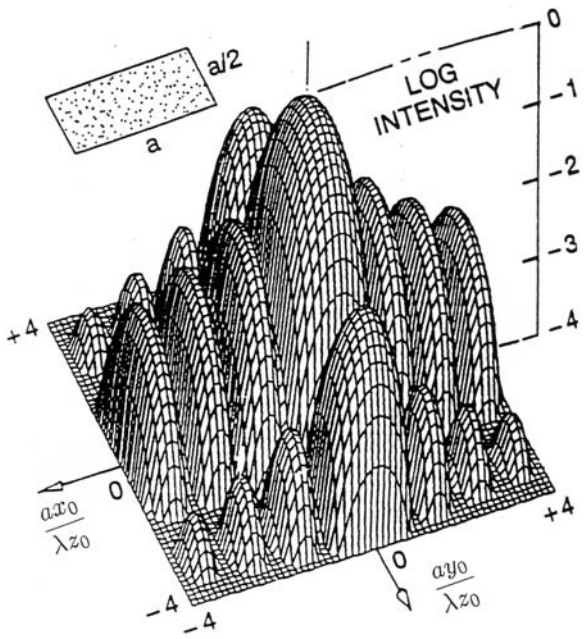

Figure 11.1: The intensity distribution for the Fraunhofer diffraction pattern produced by a rectangular aperture.

Example 2: Diffraction by a circular aperture with a radius of a

Here,

$$f(x,y) = \begin{cases} 1, & r \le a; \\ 0, & \text{otherwise} \end{cases}$$

where

$$r = \sqrt{x^2 + y^2}.$$

The Fourier transform is then given by (using polar coordinates)

$$\hat{F}_2[f(x,y)] = 2\pi \int_0^a J_0(kr) r dr = \pi a^2 \left(\frac{2J_1(ka)}{ka} \right)$$

where $k = \sqrt{k_x^2 + k_y^2}$.

The intensity is therefore given by

$$I(r_0) = \frac{\pi^2 a^4}{\lambda^2 z_0^2} \left(\frac{2J_1(z)}{z} \right)^2$$

where $z = 2\pi a r_0 / \lambda z_0$. The first minimum occurs when $z = 3.83$, i.e. when

$$r_{\min} = \frac{1.22 \lambda z_0}{a}.$$

The intensity distribution for this case is given in Figure 11.2 using a logarithmic scale.

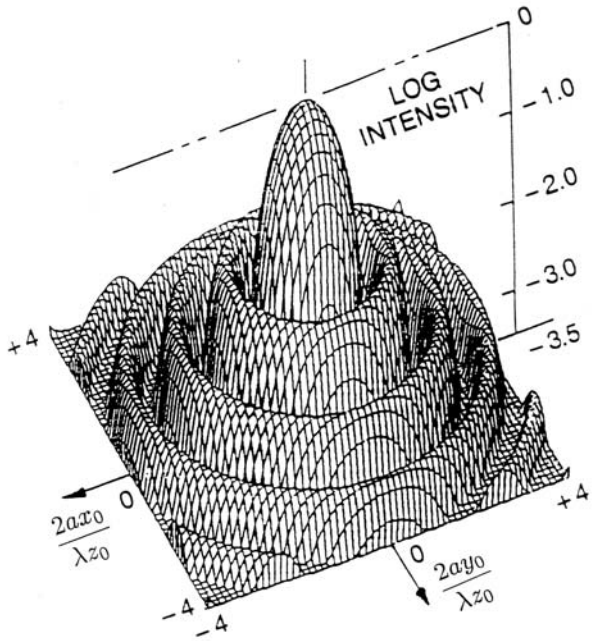

Figure 11.2: Distribution of the intensity for the Fraunhofer diffraction pattern produced by a circular aperture.

In addition to the diffraction pattern produced by a circular aperture, this pattern is also the distribution seen at the focus of a well-corrected lens when a point monochromatic source is imaged. For a distant source $z_0 \sim f$ where f is the focal length of the lens. Defining the 'F-number' as $F = f/a$, we get

$$r_{\min} = 1.22\lambda F.$$

For $\lambda = 500$ nm and some typical camera lens stops, we have:

F-Number	$r_{\min}$ in μm
22	13.4
11	6.7
5.6	3.3
2.8	1.7

11.1.2 Fresnel Diffraction by an Aperture

The Fresnel diffraction integral is given by (see Chapter 6)

$$u(\mathbf{r}_0, k) = \frac{ik\alpha}{4\pi r_0} \exp(ikr_0) \int_S \exp(i\mathbf{k} \cdot \mathbf{r}) \exp(-ik\hat{\mathbf{r}_0} \cdot \mathbf{r}) \exp\left(ik\frac{r^2}{2r_0}\right) d^2\mathbf{r}.$$

Consider a Cartesian coordinate system where

$$\mathbf{r} = \hat{\mathbf{x}}x + \hat{\mathbf{y}}y + \hat{\mathbf{z}}z,$$

$$\mathbf{r}_0 = \hat{\mathbf{x}}x_0 + \hat{\mathbf{y}}y_0 + \hat{\mathbf{z}}z_0$$

where x_0 and y_0 are taken to represent a position on a flat screen at a fixed distance z_0 from the aperture and let $\hat{\mathbf{k}} \simeq \hat{\mathbf{z}}$ (plane wave at normal incidence to the aperture), $\hat{\mathbf{r}}_0 \simeq \hat{\mathbf{z}}$ (observations at small angles only) and $kz \to 0$ ('infinitely thin' aperture). Then,

$$u(x_0, y_0) = \frac{i}{\lambda} \frac{\exp(ikr_0)}{4\pi r_0} \oint_S \exp\left[-\frac{ik}{r_0}(xx_0 + yy_0)\right] \exp\left[\frac{ik}{2r_0}(x^2 + y^2)\right] dxdy.$$

As with the analysis associated with Fraunhofer diffraction, we substitute

$$r_0 \simeq z_0 + \frac{x_0^2 + y_0^2}{2z_0}$$

into the exponent $\exp(ikr_0)$ but use $r_0 \simeq z_0$ elsewhere. Introducing the aperture function $f(x, y)$, the wavefield is then given by

$$u(x_0, y_0) = \frac{i}{\lambda} \frac{\exp(ikz_0)}{z_0} \exp\left(ik\frac{x_0^2 + y_0^2}{2z_0}\right)$$

$$\times \int_{-\infty}^{\infty} \int_{-\infty}^{\infty} f(x, y) \exp\left[-\frac{ik}{z_0}(xx_0 + yy_0)\right] \exp\left[\frac{ik}{2z_0}(x^2 + y^2)\right] dxdy.$$

Apart from the factors in front of this integral, u is equal to the 2D Fourier transform of

$$f(x,y)\exp\left[\frac{ik}{2z_0}(x^2+y^2)\right].$$

The term

$$\exp\left[\frac{ik}{2z_0}(x^2+y^2)\right]$$

is, in effect, a quadratic approximation to a spherical wave and thus

$$u \sim \text{spherical wave} \times \hat{F}_2[f \times \text{spherical wave}].$$

Noting that

$$\frac{ik}{2z_0}(x_0^2+y_0^2)+\frac{ik}{z_0}(-xx_0-yy_0)+\frac{ik}{2z_0}(x^2+y^2)$$

$$=\frac{ik}{2z_0}[x_0^2-2xx_0+x^2+y_0^2-2yy_0+y^2]=\frac{ik}{2z_0}[(x_0-x)^2+(y_0-y)^2],$$

we can write the Fresnel diffraction integral in the form

$$u(x_0,y_0)=\frac{i}{\lambda}\frac{\exp(ikz_0)}{z_0}\int_{-\infty}^{\infty}\int_{-\infty}^{\infty}f(x,y)\exp\left(\frac{ik}{2z_0}[(x_0-x)^2+(y_0-y)^2]\right)dxdy.$$

Here, we see that u is essentially (ignoring scaling constants) given by the convolution of

$$f(x,y) \quad \text{with} \quad \exp\left(\frac{ik}{2z_0}[x^2+y^2)]\right)$$

or

$$u(x,y)=\frac{i}{\lambda}\frac{\exp(ikz_0)}{z_0}f(x,y)\otimes\otimes\exp\left(\frac{ik}{2z_0}[x^2+y^2]\right)$$

where $\otimes\otimes$ denotes the 2D convolution integral.

Example of Fresnel Diffraction

As an example of Fresnel diffraction, consider using the last expression for u to evaluate the Fresnel diffraction pattern from a square aperture of width a:

$$f(x,y)=\begin{cases}1, & |\,x\,|\leq\frac{a}{2}, \quad |\,y\,|\leq\frac{a}{2};\\ 0, & \text{otherwise.}\end{cases}$$

In this case, u is given by

$$u(x_0,y_0)=\frac{i}{\lambda}\frac{\exp(ikz_0)}{z_0}\int_{-a/2}^{a/2}\int_{-a/2}^{a/2}\exp\left(\frac{i\pi}{\lambda z_0}[(x_0-x)^2+(y_0-y)^2]\right)dxdy$$

which can be written in the form of two integrals I_1 and I_2 as

$$u(x_0, y_0) = \frac{i}{\lambda}\frac{\exp(ikz_0)}{z_0} I_1(x_0) I_2(y_0).$$

Since the integrals are identical in form, we shall consider only I_1 given by

$$I_1(x_0) = \int_{-a/2}^{a/2} \exp\left[\frac{i\pi}{\lambda z_0}(x_0 - x)^2\right] dx.$$

Let

$$\xi = \sqrt{\frac{2}{\lambda z_0}}(x_0 - x)$$

so that

$$I_1(x_0) = \int_{\xi_1}^{\xi_2} \exp\left(i\frac{\pi}{2}\xi^2\right) d\xi \sqrt{\frac{\lambda z_0}{2}}$$

where

$$\xi_1 = \sqrt{\frac{2}{\lambda z_0}}\left(x + \frac{a}{2}\right) \quad \text{and} \quad \xi_2 = \sqrt{\frac{2}{\lambda z_0}}\left(x - \frac{a}{2}\right).$$

Defining the Fresnel integrals

$$C(z) = \int_0^z \cos\left(\frac{\pi t^2}{2}\right) dt, \quad S(z) = \int_0^z \sin\left(\frac{\pi t^2}{2}\right) dt$$

and noting that

$$\int_{\xi_1}^{\xi_2} = \int_0^{\xi_2} - \int_0^{\xi_1}$$

we can write

$$I_1(x_0) = \sqrt{\frac{\lambda z_0}{2}}([C(\xi_2) - C(\xi_1)] + i[S(\xi_2) - S(\xi_1)]).$$

The wavefield u is given by

$$U(x, y) = i\frac{\exp(ikz_0)}{2}$$

$$\times([C(\xi_2) - C(\xi_1)] + i[S(\xi_2) - S(\xi_2)])([C(\eta_2) - C(\eta_1)] + i[S(\eta_2) - S(\eta_1)])$$

where

$$\eta_1 = \sqrt{\frac{2}{\lambda z_0}}\left(y + \frac{a}{2}\right) \quad \text{and} \quad \eta_2 = \sqrt{\frac{2}{\lambda z_0}}\left(y - \frac{a}{2}\right).$$

The corresponding intensity pattern is

$$I(x_0, y_0) = \frac{1}{4}(\mid L_\xi \mid^2 \mid L_\eta \mid^2)$$

where $L(\xi)$ denotes the length of the vector

$$[C(\xi_2) - C(\xi_1)] + i[S(\xi_2) - S(\xi_1)].$$

The characteristic behaviour of this vector can be represented graphically by the Cornu Spiral, which is a plot of $S(z)$ vs. $C(z)$, and can be used to solve for the complex amplitude or intensity in a Fresnel diffraction problem. A three-dimensional representation of this spiral is given in Figure 11.3.

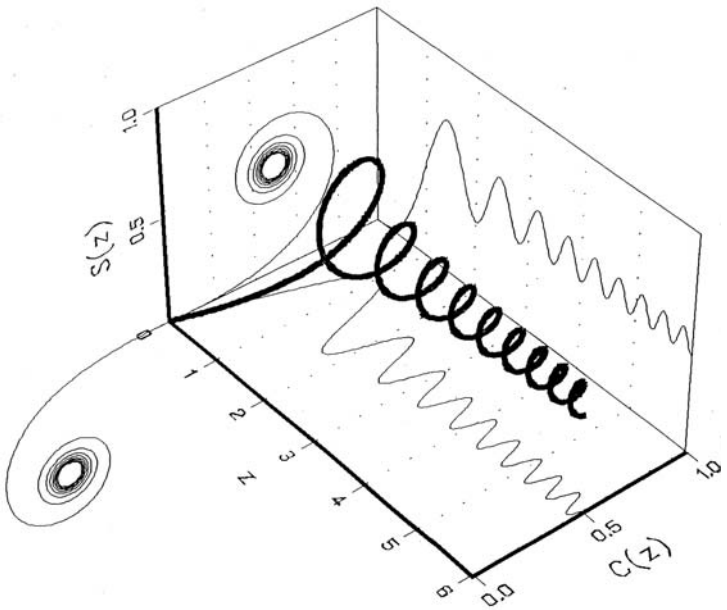

Figure 11.3: The Cornu spiral obtained by computing the Fresnel integrals that are obtained when a diffraction pattern is measured in the intermediate or Fresnel zone.

11.2 The Fourier Transforming Properties of a Lens

At the plane of focus of a well-corrected lens, the complex wavefield is (Fraunhofer condition)

$$u(x_0, y_0) = \frac{i}{\lambda} \frac{\exp(ikz_0)}{z_0} \exp\left(ik \frac{x_0^2 + y_0^2}{2z_0}\right) \hat{F}_2[f(x, y)].$$

If a transparency whose amplitude transmittance is $t(x, y)$ is placed just in front of a lens and then illuminated by a unit plane wave at normal incidence,

then the observed complex amplitude at the focal plane will be given by

$$u(x_0, y_0) = \frac{i}{\lambda}\frac{\exp(ikf)}{f}\exp\left(ik\frac{x_0^2 + y_0^2}{2f}\right)\hat{F}[t(x,y)]$$

where f is the focal length of the lens and

$$\hat{F}_2[t(x,y)] = \int_{-\infty}^{\infty}\int_{-\infty}^{\infty} t(x,y)\exp[i(k_x x + k_y y)]dxdy; \quad k_x = \frac{2\pi x_0}{\lambda f}, \quad k_y = \frac{2\pi y_0}{\lambda f}.$$

Thus, the amplitude is almost given by a Fourier transform; there is an additional quadratic phase factor, and the intensity is given by

$$I(x,y) = \frac{1}{\lambda^2 f^2} \mid \hat{F}[t(x,y)] \mid^2 .$$

Can a transparency be placed at a distance d in front of the lens so as to give an exact Fourier transform? Let the amplitude $T(x,y)$ generated by the transparency in front of the lens be given by the Fresnel diffraction formula

$$T(x,y) = \frac{i}{\lambda}\frac{\exp(ikd)}{d}t(x,y) \otimes\otimes \exp\left[\frac{i\pi}{\lambda d}(x^2 + y^2)\right].$$

The lens will then performs a Fourier transform on the field T and hence, in the focal plane,

$$u(x_0, y_0) = \frac{i}{\lambda}\frac{\exp(ikf)}{f}\exp\left(ik\frac{x_0^2 + y_0^2}{2f}\right)\hat{F}_2[T(x,y)].$$

Using the convolution theorem and noting that since

$$\exp(ax^2) \Longleftrightarrow \sqrt{\frac{\pi}{a}}\exp[k^2/(4a)]$$

then

$$\hat{F}_2\left(\exp\left[\frac{i\pi}{\lambda d}(x^2 + y^2)\right]\right) = -i\lambda d\exp[-i\lambda d(k_x^2 + k_y^2)/(4\pi)]$$

and we have

$$\hat{F}_2[T(x,y)] = \widetilde{T}(u,v) = \frac{\exp(ikd)}{d}\widetilde{t}(u,v)\exp[-i\lambda d(k_x^2 + k_y^2)/(4\pi)]$$

where $\widetilde{t} = \hat{F}_2[t]$. The wavefield is therefore given by

$$u(x_0, y_0) = i\frac{1}{\lambda f}\exp[ik(f+d)]\exp\left[\frac{i\pi}{f\lambda}(x_0^2 + y_0^2)\right]\exp\left[-i\pi\frac{\lambda d}{(\lambda f)^2}(x_0^2 + y_0^2)\right]\widetilde{t}(u,v)$$

$$= i\frac{1}{\lambda f}\exp[ik(f+d)]\exp\left[\frac{\pi i}{\lambda f}(x_0^2 + y_0^2)\left(1 - \frac{d}{f}\right)\right]\widetilde{t}(u,v).$$

Now, when $d = f$

$$u(x_0, y_0) = \frac{i}{\lambda f} \exp[2ikf]\widetilde{t}(u, v)$$

or, ignoring scaling constants, when $d = f$

$$u(x, y) = \hat{F}_2[t(x, y)].$$

Thus, there is an exact Fourier transform relationship between the front and back focal planes of a well corrected lens system. This analysis ignores the finite extent of the lens which causes vignetting.

11.2.1 Principles of Fourier Optics

Fourier optics is concerned with the applications which arise as a consequence of the Fourier transforming properties of a lens. In the light of this, let us now revisit the principles of optical imaging. Consider a 2D object function $f(x, y)$ which is placed at $z = 0$ say. Suppose we take this function to be a surface patch which is a surface scatterer of light. If we model the surface scattering using the Kirchhoff theory of diffraction then, in the far field, the scattered wavefield in the plane (x_0, y_0) at a point z_0 is essentially (i.e. ignoring scaling and constant phase factors) given by the Fourier transform of f, i.e.

$$F(k_x, k_y) = \hat{F}_2[f(x, y)]$$

where

$$k_x = \frac{2\pi x_0}{z_0\lambda}, \quad k_y = \frac{2\pi y_0}{z_0\lambda}.$$

Now, if the wavefield is passed through a well corrected lens, then at the focal point of the lens the inverse Fourier transform of that field is obtained. Let the spatial extent of the lens be given by K. Then, in the focal plane we measure

$$s(\mathbf{r}) = \frac{1}{(2\pi)^2} \int\limits_{|\mathbf{k}| \leq K} F(\mathbf{k}) \exp(i\mathbf{k} \cdot \mathbf{r}) d^2\mathbf{k}$$

or

$$s(x, y) = \frac{1}{4\pi^2} \int\limits_{-\infty}^{\infty} \int\limits_{-\infty}^{\infty} P(k_x, k_y) F(k_x, k_y) \exp(ik_x x) \exp(ik_y y) dk_x dk_y$$

$$= p(x, y) \otimes \otimes f(x, y)$$

where

$$P(k_x, k_y) = \begin{cases} 1, & \sqrt{k_x^2 + k_y^2} \leq K; \\ 0, & \text{otherwise} \end{cases}$$

and p is the inverse Fourier transform of P. This is the fundamental basis for optical imaging theory known as the Abbe theory of (optical) imaging. The lens must be 'ideal', i.e. free from all aberrations and the path lengths through the various regions of a lens must not depart from their ideal values by more than a very small fraction of a wavelength. The fraction that is allowable depends on how critical the application is, but varies typically from 1/10 to 1/100 of a wavelength. A lens of this perfection is called a diffraction-limited lens.

11.2.2 Optical Filtering

The Fourier transforming properties of a lens are invariant of the direction light propagates through the lens. If a mirror is placed at the focal plane of a lens the Fourier transform of the source distribution will be reflected back through the lens to reproduce the original distribution. Alternatively the Fourier transform of a source produced at the focus of lens can be reconstructed by employing a second lens. This provides a system which can be used to filter the spatial frequency components of a source distribution via the application of certain masks in the focal plane of the first lens - spatial filtering. Spatial filtering can be used to restore the quality of a collimated laser beam by blocking all spatial frequencies due to the interaction of the beam with dust particles for example. In general, any 'noise' induced by the (multiple) scattering of light with a complex of sub-wavelength objects (such as dust particles) modifies the spatial frequencies with high values and so can be removed by application of an optical lowpass filter (a mask placed at the focal plane of a lens). The use of a lens system to generate the Fourier transform of an image (forward Fourier transform) and to recover an image from this transform (inverse Fourier transform) provides an optical method of processing signals and images. This is known as optical signal processing. It exploits the Fourier transforming properties of a lens to process (optically filter) an image in the same way that a Fast Fourier Transform can be used to process (digitally filter) a digital image. This principle is illustrated in Figure 11.4

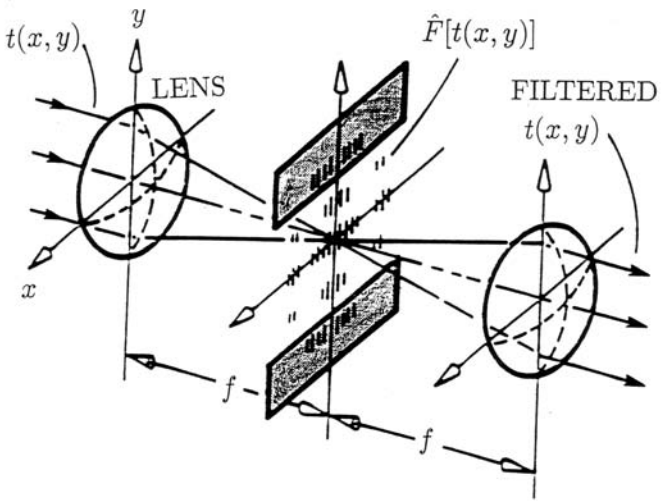

Figure 11.4: In the focal plane of a well corrected lens, the wavefield is given by the Fourier transform of the input field t (a transmittance function t), where it can be spatially filtered by placing an aperture in the focal plane. A second lens is then used to recover the filtered input field.

11.3 Linear Systems

A 'system' may be defined as that which produces a set of output functions from a set of input functions. Physically, it may be an electrical circuit (with input and output voltages for example) or an optical system where the inputs and outputs are either complex amplitudes or intensities. From the point of view of 'linear systems theory', the physical nature of the system is unimportant.

Let us represent a system via an operator $\hat{L}$ say in terms of the equation

$$s(x,y) = \hat{L}[f(x,y)]$$

where f is the input and s is the output. A linear system has the property that

$$\hat{L}[af_1(x,y) + bf_2(x,y)] = a\hat{L}[f_1(x,y)] + b\hat{L}[f_2(x,y)]$$

for all inputs f_1 and f_2 and all constants a and b. Linearity implies that an output function can be broken down into elementary functions, each of which can be separately passed through the system; the total output is then the sum of the 'elementary' outputs.

The 'sampling property' of the delta function allows us to consider any input function to be a linear combination of weighted and displaced delta functions:

$$f(x,y) = \int_{-\infty}^{\infty}\int_{-\infty}^{\infty} f(x',y')\delta(x-x')\delta(y-y')dx'dy'$$

giving an output

$$s(x,y) = \hat{L}[f(x,y)] = \int_{-\infty}^{\infty}\int_{-\infty}^{\infty} f(x',y')\hat{L}[\delta(x-x')\delta(y-y')]dx'dy'.$$

The system response at (x,y) due to a delta function input at (x',y') is called the Impulse Response Function (IRF) given by

$$p(x,y;x',y') = \hat{L}[\delta(x-x')\delta(y-y')].$$

In optical imaging systems, the quantity p is called the Point Spread Function (PSF). For a linear optical system,

$$s(x,y) = \int_{-\infty}^{\infty}\int_{-\infty}^{\infty} f(x',y')p(x,y;x',y')dx'dy'.$$

Note that the optical diffraction formulae are of the same form: for Fraunhofer diffraction

$$p(x,y;x',y') = \frac{i}{\lambda}\frac{\exp(ikz)}{z}\exp\left(ik\frac{(x^2+y^2)}{2z}\right)\exp\left[-\frac{ik}{z}(xx'+yy')\right]$$

and for Fresnel diffraction

$$p(x,y;x',y') = \frac{i}{\lambda}\frac{\exp(ikz)}{z}\exp\left(\frac{ik}{2z}[(x-x')^2+(y-y')^2]\right).$$

If the impulse response function of a linear system depends only on the coordinate differences $(x-x')$ and $(y-y')$, and not on each coordinate separately, i.e.

$$p(x,y;x',y') \equiv p(x-x',y-y'),$$

then we obtain an expression for p which involves the convolution relationship

$$s(x,y) = \int_{-\infty}^{\infty}\int_{-\infty}^{\infty} f(x',y')p(x-x',y-y')dx'dy'.$$

This is an example of a stationary linear system. In optical imaging, a stationary optical systems is called 'isoplanatic'. Isoplanacity requires that the point spread function is the same for all field angles and implies that the aberrations are independent of field angle. Many optical imaging systems are (to a good approximation) both linear and isoplanatic.

The convolution relationship between input and output suggests using Fourier transforms (FT) which, via the convolution theorem, gives

$$S(k_x,k_y) = F(k_x,k_y)P(k_x,k_y)$$

where

$$P(k_x,k_y) = \int_{-\infty}^{\infty}\int_{-\infty}^{\infty} p(x,y)\exp[-i(k_x x + k_y y)]dxdy$$

i.e.

FT of the output = (FT of the input)×(FT of the impulse response function).

The quantity P is called the system Transfer Function (TF). In optical imaging systems, P is called the Optical Transfer Function or OTF. The OTF is just the 2D FT of the point spread function. Note that: (i) the convolution relationship only applies to linear stationary optical systems; (ii) there is no unique OTF for an optical system with field-dependent aberrations (i.e. for the non-stationary case); (iii) there is no unique OTF for an optical system when an object is illuminated by spatially partially coherent light.

11.4 Images of Lines and Edges

Suppose we know that a particular system is linear and stationary in some particular quantity where the 'quantity' is either: (i) the complex amplitude for coherent illumination; (ii) the intensity (time averaged) for incoherent illumination. How are the images of lines and edges related to the point spread function?

11.4.1 Lines

The image of an infinitely narrow line in the object plane is called the line spread function. A line input can be represented by

$$f(x,y) = \delta(x).$$

Hence

$$s(x,y) = \int_{-\infty}^{\infty}\int_{-\infty}^{\infty} \delta(x-x')p(x',y')dx'dy'$$

or

$$\ell(x) = \int_{-\infty}^{\infty} p(x,y')dy'$$

where ℓ is the line spread function. The line spread function (the image of an infinitely narrow line) is an integration over one variable of the point spread function. In general, the input may be at some arbitrary angle to the y - axis and hence ℓ will also be a function of that angle. For the special case in which the point spread function is rotationally symmetrical, i.e.

$$p(r) = p(x,y); \quad r^2 = x^2 + y^2$$

the line spread function is given by the Abel transform of the point spread function,

$$\ell(x) = \int_{-\infty}^{\infty} p\left(\sqrt{x^2+y'^2}\right)dy' = 2\int_{x}^{\infty} \frac{p(r)rdr}{(r^2-x^2)^{\frac{1}{2}}}.$$

11.4.2 Edges

Consider the image of an opaque edge laying along the y-axis

$$f(x) = \begin{cases} 1, & x < 0; \\ 0, & x \geq 0. \end{cases}$$

The result is called the edge spread function e which is given by

$$e(x) = \int_{-\infty}^{\infty}\int_{-\infty}^{\infty} f(x-x')p(x',y')dx'dy' = \int_{-\infty}^{\infty} f(x-x')\ell(x')dx'$$

where

$$\ell(x') = \int_{-\infty}^{\infty} p(x',y')dy'$$

or

$$e(x) = \int_{-\infty}^{x} \ell(x')dx'.$$

The edge spread function is an integration over the line spread function. Thus, we can write

$$\ell(x) = \frac{d}{dx} e(x).$$

Clearly, the equation above indicates a way of measuring the line spread function from the image of an edge.

11.4.3 The Optical Transfer Function

Consider the response of a linear, stationary system to a 1D cosinusoidal input of the form

$$f(x, y) = a + b\cos(k_x x + \theta)$$

where k_x is the spatial frequency and θ is the phase. Define the modulation of this input M_{in} as

$$M_{\text{in}} = \frac{f_{\max} - f_{\min}}{f_{\max} + f_{\min}} = \frac{b}{a}.$$

The output s is given by

$$s(x) = \int_{-\infty}^{\infty} \int_{-\infty}^{\infty} [a + b\cos(k_x(x - x') + \theta)] p(x', y') dx' dy'.$$

Integrating with respect to y gives

$$s(x) = \int_{-\infty}^{\infty} \ell(x')[a + b\cos(k_x(x - x') + \theta)] dx'$$

where ℓ is the line spread function which, for convenience, can be considered to be normalized to unit area, i.e.

$$\int_{-\infty}^{\infty} \ell(x') dx' = 1.$$

Using the result

$$\cos(A - B) = \cos A \cos B + \sin A \sin B$$

the output s can be written in the form

$$s(x) = a + b\cos(k_x x + \theta) \int_{-\infty}^{\infty} \ell(x') \cos(k_x x') dx' + b\sin(k_x x + \theta) \int_{-\infty}^{\infty} \ell(x') \sin(k_x x') dx'$$

or

$$s(x) = a + b\cos(k_x x + \theta) C(k_x) + b\sin(k_x x + \theta) S(k_x)$$

where

$$C(k_x) - iS(k_x) = P(k_x) = \int_{-\infty}^{\infty} \ell(x') \exp(-ik_x x') dx'.$$

The function P is the 1D OTF and it is equal to the Fourier transform of the line spread function ℓ. Defining the modulus and phase of the OTF by

$$M(k_x) = \sqrt{C^2(k_x) + S^2(k_x)}, \quad \phi(k_x) = \tan^{-1}\left[\frac{-S(k_x)}{C(k_x)}\right]$$

so that

$$C(k_x) = M(k_x)\cos\phi(k_x), \quad S(k_x) = -M(k_x)\sin\phi(k_x)$$

the output s can be expressed as

$$s(x) = a + bM(k_x)\cos[k_x x + \theta + \phi(k_x)].$$

Like the input f, the output s is also cosinusoidal with the same frequency k_x.

The output modulation is

$$M_{\text{out}} = \frac{s_{\max} - s_{\min}}{s_{\max} + s_{\min}} = M(k_x)\frac{b}{a}$$

so that the ratio of the output modulation to the input modulation is equal to the modulus of the OTF. The Modulation Transfer Function or MTF is given by

$$M(k_x) = \frac{M_{\text{out}}}{M_{\text{in}}}.$$

The Phase Transfer Function (PTF) ϕ describes the shift in phase (or position) of the output frequency k_x relative to the input. The MTF can be found experimentally using sine wave objects or from the line spread function

$$M(k_x) = \left|\int \ell(x)\exp(-k_x x)dx\right|$$

which itself can be be found by differentiating the edge spread function.

11.4.4 Rotationally Symmetric Systems

An optical system is referred to as a rotationally symmetric system if the point spread function and OTF are rotationally symmetric, i.e.

$$p(x, y) = p(r), \quad r = \sqrt{x^2 + y^2}$$

and

$$P(k_x, k_y) = P(k), \quad k = \sqrt{k_x^2 + k_y^2}.$$

For a rotationally symmetric system, the line spread function is the same for all angles of the line input and is related to the point spread function by the Abel transform, i.e.

$$\ell \leftarrow \text{Abel} \quad \text{transform} \rightarrow p(r).$$

The OTF is the Fourier transform of the line spread function, i.e.

$$P(k) \leftarrow \text{1D} \quad \text{FT} \rightarrow \ell(x).$$

The rotational symmetry of the 2D OTF and point spread function means that, since they are 2D Fourier transform pairs, they are 1D Hankel transform pairs

$$P(k) \leftarrow \text{Hankel} \quad \text{transform} \rightarrow p(r).$$

11.5 Linearity of Optical Imaging Systems

Consider the case where the object plane is illuminated by a plane or spherical wave and by perfectly spatially coherent light. Let the complex amplitude immediately after the object be denoted by $U_{\text{in}}(x,y)$ and $U_{\text{out}}(x,y)$ be the complex amplitude at the image plane. Also, let the complex amplitude at (x,y) in the output due to a unit strength point input be $p(x,y;x',y')$. The total amplitude at (x,y) due to all such points in the object plane is then given by

$$U_{\text{out}}(x,y) = \int_{-\infty}^{\infty}\int_{-\infty}^{\infty} U_{\text{in}}(x',y')p(x,y;x',y')dx'dy'.$$

For an isoplanatic optical system, this reduces to

$$U_{\text{out}}(x,y) = \int_{-\infty}^{\infty}\int_{-\infty}^{\infty} U_{\text{in}}(x',y')p(x-x',y-y')dx'dy'.$$

A spatially coherent optical system is linear in the complex amplitude. Let us now consider the case of narrowband light that is not perfectly spatially coherent. The general complex representation of the time-varying scalar field is called the analytic signal $V(\mathbf{r},t)$; it is defined such that

$$\text{Real scalar field} = \text{Re}[V(\mathbf{r},t)].$$

For narrowband light, the analytic signal can be written in terms of a product of a slowly varying function; the time varying complex amplitude $U(\mathbf{r},t)$ times $\exp(-i\omega t)$. Thus,

$$V(\mathbf{r},t) = U(\mathbf{r},t)\exp(-i\omega t).$$

The instantaneous intensity is defined as

$$I(\mathbf{r},t) = \mid U(\mathbf{r},t) \mid^2$$

whereas the time-averaged intensity $\bar{I}(\mathbf{r})$ (i.e. that observed by an optical detector over a period of time T) is given by

$$\bar{I}(\mathbf{r}) = \frac{1}{2T}\int_{-T}^{T} I(\mathbf{r},t)dt.$$

In general, the time-varying complex amplitudes are related by

$$U_{\text{out}}(x,y,t) = \int_{-\infty}^{\infty}\int_{-\infty}^{\infty} U_{\text{in}}(x',y',t)p(x,y;x'y')dx'dy'.$$

Coherent illumination implies that $U(x,y,t) = U(x,y)$, i.e. the field does not vary in time. For incoherent light, however, the average intensity is given by

$$\bar{I}_{\text{out}}(x,y) = \frac{1}{2T}\int_{-T}^{T} \mid U_{\text{out}}(x,y,t) \mid^2 dt = \int_{-\infty}^{\infty}\int_{-\infty}^{\infty} p(x,y;x',y')p^*(x,y;x',y')$$

$$\times \left[\frac{1}{2T} \int_{-T}^{T} U_{\text{in}}(x', y', t) U_{\text{in}}^*(x'', y'', t) dt \right] dx' dy' dx'' dy''.$$

The term in [ ] is called the mutual intensity of narrow-band light and is given by

$$J_{\text{in}}(x', y'; x'', y'') = \frac{1}{2T} \int_{-T}^{T} U_{\text{in}}(x', y', t) U_{\text{in}}^*(x'', y'', t) dt$$

or

$$J_{\text{in}}(\mathbf{r}', \mathbf{r}'') = \langle U_{\text{in}}(\mathbf{r}', t) U_{\text{in}}^*(\mathbf{r}'', t) \rangle.$$

Incoherent light is defined to be such that

$$J(\mathbf{r}', \mathbf{r}'') = \bar{I}(\mathbf{r}') \delta(\mathbf{r}' - \mathbf{r}'').$$

That is, two neighbouring points $\mathbf{r}'$ and $\mathbf{r}''$ have uncorrelated fields, for any $\mathbf{r}' \neq \mathbf{r}''$. Using the definition for incoherent light above, the expression for $\bar{I}_{\text{out}}$ becomes

$$\bar{I}_{\text{out}}(x, y) = \int_{-\infty}^{\infty} \int_{-\infty}^{\infty} p(x, y; x', y') p^*(x, y; x', y')$$
$$\times \bar{I}_{\text{in}}(x', y') \delta(x' - x'') \delta(y' - y'') dx' dy' dx'' dy''$$

or

$$\bar{I}_{\text{out}}(x, y) = \int_{-\infty}^{\infty} \int_{-\infty}^{\infty} \mid p(x, y; x', y') \mid^2 \bar{I}_{\text{in}}(x', y') dx' dy'.$$

where the quantity $\mid p(x, y; x', y') \mid^2$ is the intensity point spread function. For an isoplanatic optical system, this result reduces to

$$\bar{I}_{\text{out}}(x, y) = \int_{-\infty}^{\infty} \int_{-\infty}^{\infty} \bar{I}_{\text{in}}(x', y') \mid p(x - x', y - y') \mid^2 dx' dy'.$$

where the bar over I is usually omitted when referring to the intensity because a time average is always assumed.

For perfectly incoherent illumination, an optical system is linear in intensity and, if isoplanicity holds, the output (image) intensity is equal to the input (object) intensity convolved with the intensity point spread function.

11.6 Coherent Image Formation

With coherent light, the complex amplitude of the image is equal to that at the object plane convolved with the amplitude point spread function (for an isoplanatic system), i.e.

$$U_{\text{out}}(x, y) = \int_{-\infty}^{\infty} \int_{-\infty}^{\infty} U_{\text{in}}(x', y') p(x - x', y - y') dx' dy'$$

where

$$p(x,y) = \int_{-\infty}^{\infty}\int_{-\infty}^{\infty} P(x',x')\exp\left[-\frac{ik}{z}(xx'+yy')\right]dx'dy'$$

and P is the pupil function of the optical system, i.e. the complex amplitude in the exit pupil. The pupil function P is, for a clear pupil, defined by

$$P(k_x,k_y) = \begin{cases}\exp[ikW(k_x,k_y)], & (k_x,k_y)\in \text{aperture};\\ 0, & \text{otherwise}\end{cases}$$

where the function W is called the Wave Aberration Function. A shaded or apodized pupil can be handled by introducing an absorption term A,

$$P(k_x,k_y) = A(k_x,k_y)\exp[ikW(k_x,k_y)].$$

Taking the Fourier transform of U_{out} and using the convolution theorem we can write

$$\widetilde{U}_{\text{out}}(k_x,k_y) = \widetilde{U}_{\text{in}}(k_x,k_y)T(k_x,k_y)$$

where $\widetilde{U}_{\text{out}}$ is the spectrum of the image amplitude, $\widetilde{U}_{\text{in}}$ is the spectrum of object amplitude and T is the Coherent Optical Transfer Function (COTF). Note that

$$T(k_x,k_y) = \int_{-\infty}^{\infty}\int_{-\infty}^{\infty} p(x,y)\exp[-i(k_xx+k_yy)]dxdy = P(\lambda z k_x/2\pi, \lambda z k_y/2\pi).$$

Thus, the COTF at spatial frequency (k_x,k_y) is simply equal to the pupil function at coordinates $(\lambda z k_x/2\pi, \lambda z k_y/2\pi)$.

Examples of Coherent Image Formation

Example 1: An aberration free, circular pupil of radius a. In this case

$$T(k) = \begin{cases}1, & k\le a;\\ 0, & k>a\end{cases}$$

where

$$k = \sqrt{k_x^2+k_y^2}$$

or

$$P(k_x,k_y) = \begin{cases}1, & k\le \frac{2\pi a}{\lambda z};\\ 0, & k>\frac{2\pi a}{\lambda z}.\end{cases}$$

Defining

$$\frac{2\pi a}{\lambda z} = \frac{1}{2\lambda F}$$

where F is the 'F-number' we get

$$\widetilde{U}_{\text{out}} = \begin{cases}\widetilde{U}_{\text{in}}, & (k_x,k_y)\le \frac{1}{2\lambda F};\\ 0, & (k_x,k_y)>\frac{1}{2\lambda F}.\end{cases}$$

In this case, there is a specific frequency cutoff at $\sqrt{k_x^2 + k_y^2} = 1/(2\lambda F)$ beyond which no frequencies pass. Spatial features associated with spatial frequencies greater than $1/(2\lambda F)$ are not imaged. Thus, for example, a 1D amplitude sinusoid of frequency $\leq 1/(2\lambda F)$ has an image amplitude exactly equal to the object amplitude but for a sinusoid of frequency $> 1/(2\lambda F)$ the image amplitude is zero.

Example 2: Find the image intensity when an object of amplitude transmittance

$$U_{\text{in}}(x) = 1 + \cos(k_0 x)$$

is imaged in an aberration free coherent optical system, with $k_0 < \frac{1}{2\lambda F}$, with and without a half-plane obstruction in the pupil.

Without the half-plane obstruction, since $k_0 < \frac{1}{2\lambda F}$

$$\widetilde{U}_{\text{out}}(k_x, k_y) = \widetilde{U}_{\text{in}}(k_x, k_y)$$

so

$$U_{\text{out}}(x, y) = U_{\text{in}}(x, y) = 1 + \cos(k_0 x)$$

and the intensity is given by

$$I_{\text{out}}(x, y) = \mid 1 + \cos(k_0 x) \mid^2 = [2\cos^2(k_0 x)]^2,$$

i.e. a periodic image of frequency k_0 equal to the original amplitude frequency. With the obstruction

$$\widetilde{U}_{\text{out}}(k_x, k_y) = \begin{cases} \widetilde{U}_{\text{in}}(k_x, k_y), & k_x > 0; \\ 0, k_x \leq 0. \end{cases}$$

Now

$$\widetilde{U}_{\text{in}} = \delta(k_x, k_y) + \pi\delta(k_x - k_0) + \pi\delta(k_x + k_0)$$

and therefore

$$\widetilde{U}_{\text{out}}(k_x, k_y) = \pi\delta(k_x - k_0), \quad U_{\text{out}}(x, y) = \pi \exp(-ik_0 x)$$

and

$$I_{\text{out}}(x, y) = \pi^2$$

giving uniform intensity.

Example 3: Effect of aberrations (for a clear pupil).

The COTF is given by

$$T(k_x, k_y) = \begin{cases} \exp[ikW(k_x, k_y)], & (k_x, k_y) \in \text{aperture}; \\ 0, & \text{otherwise} \end{cases}$$

which is unaffected by aberrations, i.e. each sine wave is transmitted without attenuation, provided $(k_x, k_y) < \frac{1}{2\lambda F}$. However, aberrations do give a phase

contribution to the COTF, yielding a shift of the spatial frequency components in the image. This shift can markedly affect the intensity distribution of the image. Consider a single cosinusoidal object with $k_0 < \frac{1}{2\lambda F}$ given by

$$U_{\text{in}}(x,y) = 2\cos(k_0 x).$$

Then

$$\widetilde{U}_{\text{in}}(k_x,k_y) = [\delta(k_x - k_0) + \delta(k_y + k_0)]\delta(k_y)$$

and

$$\widetilde{U}_{\text{out}}(k_x,k_y) = \exp[ikW(k_x,k_y)]\widetilde{U}_{\text{in}}(k_x,k_y)$$

$$= \exp[ikW(k_0,0)]\delta(k_x - k_0) + \exp[ikW(-k_0,0)]\delta(k_x + k_0).$$

For an even distribution $W(k_0,k_y) = W(-k_0,k_y)$. Thus

$$\widetilde{U}_{\text{out}}(k_x,k_y) = \exp[ikW(k_0,0)][\delta(k - k_0) + \delta(k + k_0)],$$

$$U_{\text{out}}(x,y) = \exp[ikW(k_0,0)]2\cos(k_0 x)$$

and

$$I_{\text{out}} = [2\cos(k_0 x)]^2.$$

Although the aberration does affect the image amplitude (as a phase term), there is no visible effect on the image (for this single sinusoid). For an odd aberration $W(k_0,k_x) = -W(-k_0,k_y)$,

$$U_{\text{out}}(x,y) = \exp[ikW(k_0,0)]\exp(-ik_0 x) + \exp[-ikW(k_0,0)]\exp(ik_0 x)$$

$$= 2\cos[k_0 x - kW(k_0,0)]$$

and

$$I_{\text{out}}(x,y) = 4\cos^2[k_0 x - kW(k_0,0)].$$

In this case, the periodic images are shifted by $kW(k_0,0)$; each frequency is shifted differently.

11.7 Phase Contrast Imaging

Imaging in coherent light is linear in the complex amplitude. In the special case of a weak phase object,

$$U_{\text{in}}(x,y) = \exp[i\theta(x,y)] \simeq 1 + i\theta(x,y), \quad \theta(x,y) << 1.$$

A linearity exists between the phase of the object and the intensity of the image, as the following analysis shows.

$$I_{\text{out}}(x,y) = \mid U_{\text{out}}(x,y) \mid^2 = \mid p(x,y) \otimes\otimes U_{\text{in}}(x,y) \mid^2$$

and therefore, using the correlation theorem (where $\odot\odot$ denotes the 2D correlation integral),

$$\widetilde{I}_{\text{out}}(k_x,k_y) = [\widetilde{U}_{\text{in}}(k_x,k_y)T(k_x,k_y)] \odot\odot [\widetilde{U}_{\text{in}}(k_x,k_y)T(k_x,k_y)]^*$$

or

$$\widetilde{I}_{\rm out}(k_x,k_y)=\int\limits_{-\infty}^{\infty}\int\limits_{-\infty}^{\infty}dk'_xdk'_y[\delta(k'_x,k'_y)-i\widetilde{\theta}^*(k'_x,k'_y)T^*(k'_x,k'_y)]$$

$$\times[\delta(k'_x+k_x,k'_y+k_y)+i\widetilde{\theta}(k'_x+k_x,k'_y+k_y)T(k'_x+k_x,k'_y+k_y)]$$

$$\simeq\delta(k_x,k_y)+i\widetilde{\theta}(k_x,k_y)T(k_x,k_y)-i\widetilde{\theta}^*(-k_x,-k_y)T^*(-k_x,-k_y).$$

Now, θ is real and therefore

$$\widetilde{\theta}^*(-k_x,-k_y)=\widetilde{\theta}(k_x,k_y)$$

and, thus, defining T_p as

$$T_p(k_x,k_y)=T(k_x,k_y)-T^*(-k_x,-k_y)$$

we get

$$\widetilde{I}_{\rm out}(k_x,k_y)\simeq[\delta(k_x,k_y)+i\widetilde{\theta}(k_x,k_y)]T_p(k_x,k_y)$$

i.e.

$$\text{FT of the output intensity} = \text{FT of the input phase}\times T_p.$$

The function T_p is called the Phase Contrast Transfer Function (PCTF) which can can be written as

$$T_p(k_x,k_y)=[T(k_x,k_y)-T^*(-u,-v)]=[P(\lambda zu,\lambda zv)-P^*(\lambda zk_x/2\pi,\lambda zk_y/2\pi)]$$

where the pupil function P is given by

$$P(\xi,\eta)=\begin{cases}\exp[ikW(\xi,\eta)], & (\xi,\eta)\in\text{aperture};\\ 0, & \text{otherwise}\end{cases}$$

and W is the aberration function. Note that if there are no aberrations then $W=0$ and $T_p=0$. In other words, some kind of aberration, or phase plate, is required to see the object phase. Suppose that a $\frac{\pi}{2}$ phase plate is placed in the pupil function so that

$$P=\exp(i\pi/2).$$

Then

$$T_p(k_x,k_y)=\exp(i\pi/2)-\exp(-i\pi/2)=2i\left(\frac{\exp(i\pi/2)-\exp(-i\pi/2)}{2i}\right)$$

$$=2i\sin(\pi/2)=2i$$

except at $(k_x,k_y)=(0,0)$ where $T_p(0,0)=1$. Hence,

$$\widetilde{I}_{\rm out}(k_x,k_y)=[\delta(k_x,k_y)+i\widetilde{\theta}(k_x,k_y)]T_p(k_x,k_y)=\delta(k_x,k_y)-2\widetilde{\theta}(k_x,k_y)$$

so that

$$I_{\rm out}(x,y)=1-2\theta(x,y),\quad\theta<<1.$$

This result is the basis for the phase contrast microscope. The intensity fluctuation is equal to twice the phase fluctuation, with the appropriate change in polarity. The phase contrast principle is also used in high resolution electron microscopy. In this application it is not technically possible to make a phase retarder, and the phase contrast is made possible by using even aberrations of the electron lens. Then

$$T_p(k_x, k_y) = (\exp[ikW(\lambda z k_x/2\pi, \lambda z k_y/2\pi)] - \exp[-ikW(\lambda z k_x/2\pi, \lambda z k_y/2\pi)])$$

for even aberrations $W(\xi, \eta) = W(-\xi, -\eta)$ and therefore

$$T_p = 2i \sin[kW(\lambda z k_x/2\pi, \lambda z k_y/2\pi)].$$

As before, if there are no aberrations and $W = 0$, then $T_p = 0$.

11.8 Incoherent Image Formation

In incoherent illumination, there is a linear relationship between the input I_{in} and output I_{out} (time-averaged) intensities. For an isoplanatic optical system,

$$I_{\text{out}}(x, y) = \int_{-\infty}^{\infty} \int_{-\infty}^{\infty} I_{\text{in}}(x', y') \mid p(x - x', y - y') \mid^2 dx' dy'.$$

If p is normalized to unit volume, $\mid p \mid^2$ is not and so we normalize it by dividing by its infinite integral, i.e.

$$\frac{\mid p(x, y) \mid^2}{\int_{-\infty}^{\infty} \int_{-\infty}^{\infty} \mid p(x, y) \mid^2 dxdy}.$$

The Incoherent Optical Transfer Function (IOTF) $T(k_x, k_y)$ is the Fourier transform of the (normalized) point spread function. Applying the autocorrelation theorem to the top line and Parseval's theorem to the bottom line,

$$T(k_x, k_y) = \frac{\int_{-\infty}^{\infty} \int_{-\infty}^{\infty} P(\xi, \eta) P^*(\xi + \lambda z k_x/2\pi, \eta + \lambda z k_y/2\pi) d\xi d\eta}{\int_{-\infty}^{\infty} \int_{-\infty}^{\infty} \mid P(\xi, \eta) \mid^2 d\xi d\eta}$$

where $P(\xi, \eta)$ - the pupil function - is the Fourier transform of $p(x, y)$,

$$P(\xi, \eta) = \int_{-\infty}^{\infty} \int_{-\infty}^{\infty} p(x, y) \exp\left[-i \frac{2\pi}{\lambda z}(\xi x + \eta y)\right] dxdy.$$

The equation above for T basically states that the IOTF is equal to the (normalized) spacial autocorrelation of the pupil function. The IOTF relates the input and output intensity spectra, i.e.

$$\widetilde{I}_{\text{out}}(k_x, k_y) = \widetilde{I}_{\text{in}}(k_x, k_y) T(k_x, k_y).$$

The spatial frequencies are intensity frequencies and are not the same as the amplitude frequencies produced in a coherent optical system. This expression for T can be written in the form

$$T(k_x, k_y) = \frac{\int_{-\infty}^{\infty}\int_{-\infty}^{\infty} P\left(\xi - \frac{\lambda z k_x}{4\pi}, \eta - \frac{\lambda z k_y}{4\pi}\right) P^*\left(\xi + \frac{\lambda z k_x}{4\pi}, \eta + \frac{\lambda z k_y}{4\pi}\right) d\xi d\eta}{\int_{-\infty}^{\infty}\int_{-\infty}^{\infty} \mid P(\xi, \eta) \mid^2 d\xi d\eta}.$$

From this result it follows that:

(i) normalization yields

$$T(0, 0) = 1;$$

(ii) the Fourier transform of a real quantity gives

$$T(-k_x, -k_y) = T^*(k_x, k_y);$$

(iii) from the Schwarz inequality,

$$T(k_x, k_y) \leq T(0, 0).$$

As with the coherent OTF, the modulus $\mid T \mid$, or Modulation Transfer Function (MTF) describes the transfer or modulation of sinusoidal components of the object. The phase of T describes spatial shifts of the sinusoidal components.

11.9 Coherent and Incoherent Optical Imaging

For an object function f and point spread function p, the coherent and incoherent images are given by

$$I_{\text{coherent}} = \mid p \otimes\otimes f \mid^2$$

and

$$I_{\text{incoherent}} = \mid p \mid^2 \otimes\otimes \mid f \mid^2 .$$

Figure 11.5 shows an example of a coherent and incoherent image generated by the coherent and incoherent point spread functions associated with a circular aperture (shown using a logarithmic scale).

If we consider the object function to be a rough surface (on the scale of a wavelength) then we can model this function in terms of a random distribution of amplitudes using a random number generator. An example of the result is given in Figure 11.6 which is based on the application of a Gaussian distributed random field. There is a striking difference between these images. The coherent image yields an effect called speckle which is a feature of all coherent and partially coherent images and is due to the 'phase mixing' of the functions p and f associated with the convolution operation given above.

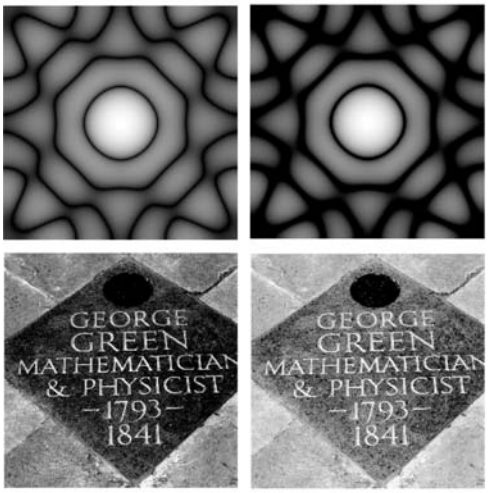

Figure 11.5: Simulation of the coherent (top-left) and incoherent (top-right) point spread function for optical instruments with a circular aperture and the memorial stone to George Green in Westminster Abbey viewed through these system (bottom-left and bottom-right, respectively). The absolute values of the point spread function are shown using a logarithmic grey-level scale.

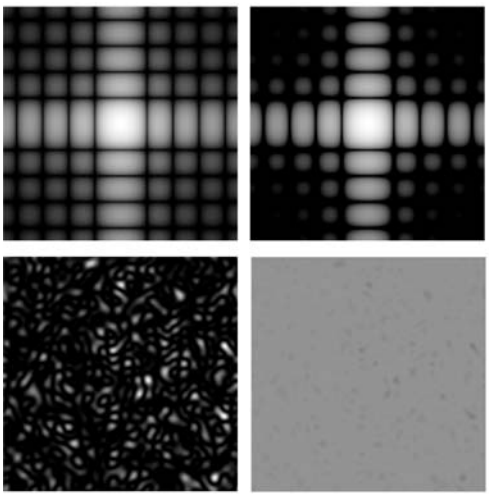

Figure 11.6: Simulation of the coherent (bottom-left) and incoherent (bottom-right) images obtained from rough surface scattering (Kirchhoff diffraction) imaged through a square aperture with coherent (top-left) and incoherent (top-right) point spread functions. The absolute values of the point spread functions are shown using a logarithmic grey-level scale.

11.10 Optical Beams

Coherent optical systems make use of laser light, some well known example being: (i) optical communications systems and optical computing; (ii) optical processing systems; (iii) laser diagnostic systems. One of the principal characteristics of coherent (laser) light is its 'beam forming' property. This property is used extensively in a wide range of applications and requires a suitable physical model to be established. In this Section we investigate the propagation of a beam by first considering the angular spectrum of plane waves and then investigating the solutions to the paraxial wave equation.

11.10.1 The Angular Spectrum of Plane Waves

The angular spectrum of planes waves is a way of representing a coherent optical field in a region of free space. In this representation, any field can be described by a sum (integral) of plane waves travelling in different directions where each plane wave is an elementary solution of the (homogeneous Helmholtz equation. Consider a scalar monochromatic field

$$u(\mathbf{r},t) = U(\mathbf{r})\exp(-i\omega t); \quad \mathbf{r} = \hat{\mathbf{x}}x + \hat{\mathbf{y}}y + \hat{\mathbf{z}}z$$

in a source free region $0 \leq z \leq Z$. In the free space domain, the complex amplitude U satisfies the Helmholtz equation

$$(\nabla^2 + k^2)U = 0; \quad k = \frac{\omega}{c}.$$

Let U have the following Fourier representation with respect to (x, y)

$$U(x,y,z) = \hat{F}_2[\widetilde{U}] = \int_{-\infty}^{\infty}\int_{-\infty}^{\infty} \widetilde{U}(k_x,k_y,z)\exp[i(k_x x + k_y y)]dk_x dk_y.$$

Using

$$\hat{F}_2[\nabla^2 U] = -(k_x^2 + k_y^2)\widetilde{U} + \frac{\partial^2 \widetilde{U}}{\partial z^2}$$

and substituting into the Helmholtz equation, we obtain

$$-(k_x^2 + k_y^2)\widetilde{U} + \frac{\partial^2 \widetilde{U}}{\partial z^2} + k^2\widetilde{U} = 0$$

or

$$\frac{\partial^2 \widetilde{U}}{\partial z^2} = -k^2\widetilde{U} + (k_x^2 + k_y^2)\widetilde{U} = -k_z^2\widetilde{U}$$

where

$$k_z^2 = k^2 - k_x^2 - k_y^2$$

or

$$k_z = \begin{cases} \sqrt{k^2 - k_x^2 - k_y^2}, & k_x^2 + k_y^2 \leq k^2; \\ i\sqrt{k_x^2 + k_y^2 - k^2}, & k_x^2 + k_y^2 > k^2. \end{cases}$$

The general solution to this equation is of the form

$$\widetilde{U}(k_x, k_y, z) = A(k_x, k_y)\exp(iwz) + B(k_x, k_y)\exp(-iwz)$$

where A and B are arbitrary functions (excluding the degenerate case when $w = 0$). The solution for U can now be written as

$$U(x, y, z) = \int_{-\infty}^{\infty}\int_{-\infty}^{\infty} A(k_x, k_y)\exp[i(k_x x + k_y y + k_z z)]dk_x dk_y$$

$$\int_{-\infty}^{\infty}\int_{-\infty}^{\infty} B(k_x, k_y)\exp[i(k_x x + k_y y - k_z z)]dk_x dk_y.$$

This is the angular spectrum representation of the field. The field U can be considered to be a linear combination of functions

$$\exp[i(k_x x + k_y y \pm k_z z)].$$

Each term in this solution for U represents a plane wave which is a solution of the same differential equation as the field itself (i.e. the Helmholtz equation). Each term is a mode of the Helmholtz equation and the angular representation is a mode expansion of the Helmholtz equation. The angular spectrum representation is not a Fourier representation, i.e. it is not a 3D Fourier transform of U, rather, it is a superposition of elementary solutions - plane waves - of the Helmholtz equation.

There are four different types of wave:

(i)

$$A(k_x, k_y)\exp[i(k_x x + k_y y + k_z z)]; \quad w = \sqrt{k^2 - k_x^2 - k_y^2}, \quad k_x^2 + k_y^2 \leq k^2$$

where k_z is real, positive or zero (a homogeneous wave propagating from $z = 0$ toward $z = Z$).

(ii)

$$A(k_x, k_y)\exp[i(k_x x + k_y y + k_z z)]; \quad k_x^2 + k_y^2 > k^2$$

where k_z is purely imaginary, i.e.

$$A(k_x, k_y)\exp[i(k_x x + k_y y)]\exp(- \mid k_z \mid z)$$

which describes an inhomogeneous or 'evanescent' wave.

(iii)

$$B(k_x, k_y)\exp[i(k_x x + k_y y - k_z z); \quad k_x^2 + k_y^2 \leq k^2$$

which describes a homogeneous wave propagating from Z to the origin.

(iv)

$$B(k_x, k_y)\exp[i(k_x x + k_y y - k_z z)]; \quad k_x^2 + k_y^2 > k^2$$

which describes an inhomogeneous wave propagating from Z to 0.

All four of these types of wave are, in general, necessary to represent the field U.

11.10.2 Half-Space Problems

Consider a half-space where a wave originating from $z = 0$ travels into the space for which $z > 0$ and has an outgoing behaviour. Since the waves are outgoing $B(k_x, k_y) = 0$ and thus in the half plane

$$U(x, y, z) = \int_{-\infty}^{\infty}\int_{-\infty}^{\infty} A(k_x, k_y) \exp[i(k_x x + k_y y + k_z z)] dk_x dk_y.$$

If we now let $k_x = kp$, $k_y = kq$ and $k_z = km$ where k is the wave number $(= \omega/c)$ then we can write

$$U(x, y, z) = \int_{-\infty}^{\infty}\int_{-\infty}^{\infty} a(p, q) \exp[ik(px + qy + mz)] dpdq$$

where

$$a(p, q) = k^2 A(kp, kq)$$

and

$$m = \begin{cases} \sqrt{1 - p^2 - q^2}, & p^2 + q^2 \leq 1; \\ \sqrt{p^2 + q^2 - 1}, & p^2 + q^2 > 1. \end{cases}$$

When $p^2+q^2 \leq 1$, the mode is a plane wave propagating in a direction whose 'direction cosines' are (p, q, m). Let us consider the relationship between $U(x, y, z)$ and this field at $z = 0$. Decomposing the boundary wave (i.e. the wave at $z = 0$) into a 2D Fourier integral,

$$U(x, y, 0) = \int_{-\infty}^{\infty}\int_{-\infty}^{\infty} \widetilde{U}_0(k_x, k_y) \exp[i(k_x x + k_y y)] dk_x dk_y.$$

According to the angular spectrum representation

$$U(x, y, 0) = \int_{-\infty}^{\infty}\int_{-\infty}^{\infty} a(p, q) \exp[ik(px + qy)] dpdq.$$

Substituting $k_x = kp$ and $k_y = kq$,

$$U(x, y, 0) = \frac{1}{k^2}\int_{-\infty}^{\infty}\int_{-\infty}^{\infty} a\left(\frac{k_x}{k}, \frac{k_y}{k}\right) \exp[i(k_x x + k_y y)] dk_x dk_y.$$

Thus,

$$\widetilde{U}_0(k_x, k_y) = \frac{1}{k^2} a\left(\frac{k_x}{k}, \frac{k_y}{k}\right)$$

or

$$a(p, q) = k^2 \widetilde{U}_0(kp, kq).$$

Hence,

$$U(x,y,z) = k^2 \int_{-\infty}^{\infty}\int_{-\infty}^{\infty} \widetilde{U}_0(kp,kq)\exp[ik(px+qy+mz)]dpdq$$

$$= \int_{-\infty}^{\infty}\int_{-\infty}^{\infty} \widetilde{U}_0(k_x,k_y)\exp[i(k_x x + k_y y + k_z z)dk_z dk_y.$$

Thus, the spectral amplitude $a(p,q)$ of each plane wave is completely specified by a single spatial frequency component of the boundary value of the field in the plane $z = 0$. The frequency of the spatial frequency components are

$$k_x = kp, \quad k_y = kq.$$

Homogeneous waves exist if

$$p^2 + q^2 \leq 1.$$

Hence, spatial frequencies in the boundary wave such that

$$\left(\frac{k_x}{k}\right)^2 + \left(\frac{k_y}{k}\right)^2 \leq 1$$

or

$$k_x^2 + k_y^2 \leq k^2$$

give rise to homogeneous waves. A spatial frequency k_x arises from a sinusoidal component of period $2\pi/\Delta x$ in the boundary wave. Therefore, periods in the boundary wave such that

$$\frac{1}{(\Delta x)^2} + \frac{1}{(\Delta y)^2} \leq \frac{1}{\lambda^2}$$

give rise to homogeneous waves. Periods such that

$$\frac{1}{(\Delta x)^2} + \frac{1}{(\Delta y)^2} > \frac{1}{\lambda^2}$$

give rise to evanescent waves. Since evanescent waves decay exponentially with distance it follows that detail in $U(x,y,0)$ smaller than a wavelength is inaccessible in the far field.

11.11 The Paraxial Wave Equation

A plane wave propagating along z can be represented by the field

$$U(x,y,z) = A\exp(ikz), \quad k = \frac{\omega}{c}$$

and is unidirectional. An optical beam, taken to be propagating in the z-direction, can be represented by the field

$$U(x,y,z) = \psi(x,y,z)\exp(ikz)$$

where it is assumed that: (i) $\psi(x, y, z)$ varies slowly in comparison with $\exp(ikz)$; (ii) $\psi(x, y, z)$ is concentrated mainly around the axis $(x, y) = (0, 0)$. With these assumptions, an approximate partial differential equation for ψ can be obtained called the Paraxial Wave Equation, whose solution provides a mathematical description for the propagation of an optical (laser) beam.

The field U satisfies the Helmholtz equation

$$\nabla^2 U + k^2 U = 0.$$

Now

$$\frac{\partial^2 U}{\partial x^2} = \frac{\partial^2 \psi}{\partial x^2} \exp(ikz), \quad \text{and} \quad \frac{\partial^2 U}{\partial y^2} = \frac{\partial^2 \psi}{\partial y^2} \exp(ikz).$$

Also,

$$\frac{\partial U}{\partial z} = \frac{\partial \psi}{\partial z} \exp(ikz) + ik\psi \exp(ikz)$$

and

$$\begin{aligned} \frac{\partial^2 U}{\partial z^2} &= \frac{\partial^2 \psi}{\partial z^2} \exp(ikz) + \frac{\partial \psi}{\partial z} ik \exp(ikz) \\ &\quad + ik \frac{\partial \psi}{\partial z} \exp(ikz) + (ik)^2 \psi \exp(ikz) \\ &= \exp(ikz) \left(\frac{\partial^2 \psi}{\partial z^2} + 2ik \frac{\partial \psi}{\partial z} - k^2 \psi \right). \end{aligned}$$

Assume that ψ varies so slowly with z that

$$\left| \frac{\partial^2 \psi}{\partial z^2} \right| << 2k \left| \frac{\partial \psi}{\partial z} \right|.$$

Under this condition

$$\frac{\partial^2 U}{\partial z^2} \simeq \exp(ikz) \left(2ik \frac{\partial \psi}{\partial z} - k^2 \psi \right)$$

and the Helmholtz equation reduces to

$$\frac{\partial^2 \psi}{\partial x^2} + \frac{\partial^2 \psi}{\partial y^2} + 2ik \frac{\partial \psi}{\partial z} = 0.$$

This equation is the paraxial wave equation or beam equation. It can be written in the form

$$\nabla_\perp^2 \psi + 2ik \frac{\partial \psi}{\partial z} = 0$$

where

$$\nabla_\perp^2 = \frac{\partial^2}{\partial x^2} + \frac{\partial^2}{\partial y^2}$$

is the transverse Laplacian. The condition

$$\left| \frac{\partial^2 \psi}{\partial z^2} \right| << 2k \left| \frac{\partial \psi}{\partial z} \right|$$

implies that

$$\left|\frac{\partial}{\partial z}\left(\frac{\partial \psi}{\partial z}\right)\right| << \frac{4\pi}{\lambda}\left|\frac{\partial \psi}{\partial z}\right|.$$

For small changes, the change $|\ \Delta(\partial\psi/\partial z)\ |$ in $|\ \partial\psi/\partial z\ |$ is such that

$$\left|\frac{\Delta\left(\frac{\partial \psi}{\partial z}\right)}{\Delta z}\right| << \frac{4\pi}{\lambda}\left|\frac{\partial \psi}{\partial z}\right|.$$

If we take $\Delta z = \lambda$, then

$$\left|\frac{\Delta\left(\frac{\partial \psi}{\partial z}\right)}{\frac{\partial \psi}{\partial z}}\right| << 4\pi.$$

Physically, this condition implies that the change in $\frac{\partial \psi}{\partial z}$ over a distance of the order of a wavelength λ is small compared to $\left|\frac{\partial \psi}{\partial z}\right|$ itself.

11.11.1 Solution to the Paraxial Wave Equation

The paraxial wave equation is given by

$$\frac{\partial^2 \psi}{\partial x^2} + \frac{\partial^2 \psi}{\partial y^2} + 2ik\frac{\partial \psi}{\partial z} = 0$$

where

$$U(x, y, z) = \psi(x, y, z)\exp(ikz).$$

Let us employ a Fourier integral representation for ψ, i.e.

$$\psi(x, y, z) = \int_{-\infty}^{\infty}\int_{-\infty}^{\infty} \widetilde{\psi}(k_x, k_y, z)\exp[i(k_x x + k_y y)]dk_x dk_y.$$

Substituting this expression into the paraxial wave equation, we get

$$\int_{-\infty}^{\infty}\int_{-\infty}^{\infty} dk_x dk_y \left(\widetilde{\psi}(k_x, k_y, z)[(ik_x)^2 + (ik_y)^2] + 2ik\frac{\partial \widetilde{\psi}(k_x, k_y, z)}{\partial z}\right)$$

$$\times \exp[i(k_x x + k_y y)] = 0$$

and, since this equality holds for all (x, y), it follows that

$$-(k_x^2 + k_y^2)\widetilde{\psi} + 2ik\frac{\partial \widetilde{\psi}}{\partial z} = 0.$$

Rearranging,

$$\frac{1}{\widetilde{\psi}}\frac{\partial \widetilde{\psi}}{\partial z} = \frac{1}{2ik}(k_x^2 + k_y^2)$$

or

$$\frac{d}{dz}\ln\widetilde{\psi} = \frac{1}{2ik}(k_x^2 + k_y^2)$$

which has the solution

$$\ln\widetilde{\psi} = \frac{1}{2ik}(k_x^2 + k_y^2)z + \text{constant}$$

or

$$\widetilde{\psi}(k_x, k_y, z) = \widetilde{\psi}(k_x, k_y, 0)\exp\left[\frac{1}{2ik}(k_x^2 + k_y^2)z\right].$$

Substituting this result into the Fourier integral representation for ψ, we obtain a general solution to the paraxial wave equation of the form

$$\psi(x, y, z) = \int_{-\infty}^{\infty}\int_{-\infty}^{\infty}\widetilde{\psi}(k_x, k_y, 0)\exp\left[-\frac{i}{2k}(k_x^2 + k_y^2)z\right]\exp[i(k_x x + k_y y)]dk_x dk_y.$$

Changing variables to $k_x = kp$ and $k_y = kq$, we can write the solution for the amplitude U as

$$U(x, y, z) = \exp(ikz)\int_{-\infty}^{\infty}\int_{-\infty}^{\infty}a(p, q)\exp[ik(px + qy)]\exp\left[-i\frac{k}{2}(p^2 + q^2)z\right]dpdq$$

where

$$a(p, q) = k^2\widetilde{\psi}(k_x, k_y, 0).$$

This is the solution to the Helmholtz equation in the 'beam approximation'.

11.11.2 Angular Spectrum Representation of a Beam

Consider a field $U(x, y, z)$ propagating into the half space $z > 0$ given by the Helmholtz equation

$$\nabla^2 U + k^2 U = 0.$$

We may represent the field as an angular spectrum

$$U(x, y, z) = \int_{-\infty}^{\infty}\int_{-\infty}^{\infty}a(p, q)\exp[ik(px + qy + mz)]dpdq$$

where

$$m = \begin{cases}\sqrt{1 - p^2 - q^2}, & p^2 + q^2 \leq 1;\\ i\sqrt{p^2 + q^2 - 1}, & p^2 + q^2 > 1,\end{cases}$$

$$a(p, q) = k^2\widetilde{U}_0(kp, kq)$$

and where $\widetilde{U}_0$ is the 2D spatial Fourier transform of the boundary value of U in the plane $z = 0$, i.e.

$$\widetilde{U}_0(k_x, k_y) = \frac{1}{(2\pi)^2}\int_{-\infty}^{\infty}\int_{-\infty}^{\infty}U(x, y, 0)\exp[-i(k_x x + k_y y)]dxdy.$$

For the field U to behave like a beam, we require that $\widetilde{U}_0$ must only contain low frequency components such that

$$k_x^2 + k_y^2 << k^2$$

or

$$p^2 + q^2 << 1.$$

The quantity m must therefore be real and positive; it is given approximately by

$$m = (1 - p^2 - q^2)^{\frac{1}{2}} \simeq 1 - \frac{1}{2}(p^2 + q^2).$$

Under this condition, U is given approximately by

$$U(x, y, z) \simeq \exp(ikz) \int_{-\infty}^{\infty} \int_{-\infty}^{\infty} a(p, q) \exp[ik(px + qy)] \exp\left[-i\frac{k}{2}(p^2 + q^2)z\right] dpdq.$$

This is the mathematical expression for a beam, subject to the constraint that $a(p, q)$ is appreciable only for values of p and q such that

$$p^2 + q^2 << 1.$$

Note that the field U is expressed in terms of its Fourier transform in the plane $z = 0$. Also note that this expression is identical to the general solution of the paraxial wave equation. The two approaches are mathematically equivalent.

11.11.3 Comparison with Fresnel Diffraction

The general solution to the paraxial wave equation can be written in the form

$$U(x, y, z) = \exp(ikz) \int_{-\infty}^{\infty} \int_{-\infty}^{\infty} \widetilde{U}_0(k_x, k_y) \exp[i(k_x x + k_y y)] \exp\left[-\frac{iz}{2k}(k_x^2 + k_y^2)\right] dk_x dk_y.$$

Substituting the expression for $\widetilde{U}_0$ into this equation,

$$U(x, y, z) = \exp(ikz) \int_{-\infty}^{\infty} \int_{-\infty}^{\infty} dx' dy' dk_x dk_y U(x, y, 0)$$

$$\times \left[\frac{1}{(2\pi)^2} \int_{-\infty}^{\infty} \int_{-\infty}^{\infty} \exp(i[k_x(x - x') + k_y(y - y')]) \exp\left(-\frac{iz}{2k}(k_x^2 + k_y^2)\right)\right].$$

The term in [ ] is just an inverse Fourier transform. In this form, we seek the inverse Fourier transform of

$$\exp\left[-\frac{iz}{k}(k_x^2 + k_y^2)\right] \quad \text{or} \quad \exp[-i\lambda z(k_x^2 + k_y^2)/2\pi]$$

which [evaluated at $(x-x', y-y')$] is equal to

$$\frac{i2\pi^2}{\lambda z}\exp\left[\frac{i\pi}{2\lambda z}([x-x']^2+[y-y']^2)\right]$$

using the result

$$\exp(-ak^2) \Longleftrightarrow \sqrt{\frac{\pi}{a}}\exp(-k^2/(4a)).$$

Hence,

$$U(x,y,z)=\frac{i}{\lambda}\frac{\exp(ikz)}{z}\int_{-\infty}^{\infty}\int_{-\infty}^{\infty}U(x',y',0)\exp\left[\frac{i\pi}{2\lambda z}([x-x']^2+[y-y']^2)\right]dx'dy'$$

which is essentially the same as the (convolution form) Fresnel diffraction formula. Note that this equation is valid everywhere for a beam. The Fresnel formula can thus be applied to beam propagation, even if the Fresnel approximation is apparently violated.

11.11.4 Gaussian Beams

Gaussian beams form the basis of Gaussian beam optics. A Gaussian beam remains Gaussian at every point along its path of propagation through an optical system. This makes it particularly easy to visualize the distribution of a field at any point in the system. Gaussian beams are not just of mathematical interest; they are the basis for modelling the propagation of a laser beam. Consequently, laser optics can be thought of in terms of a Gaussian beam of coherent light with a plane wave front, interacting with different optical components.

Consider the output of a laser at the plane $z=0$ which has a Gaussian beam profile of the form

$$U(x,y,0)=A\exp\left(-\frac{r^2}{w_0^2}\right)$$

where $r^2=x^2+y^2$ and w_0^2 is the amplitude spot size of the beam. The spectral amplitude of the plane waves in the angular spectrum representation is

$$a(p,q)=k^2\widetilde{U}_0(kp,kq)=\left(\frac{k}{2\pi}\right)^2 A\int_{-\infty}^{\infty}\int_{-\infty}^{\infty}\exp\left[-\frac{x^2+y^2}{w_0^2}\right]\exp[-ik(px+qy)]dxdy$$

$$=\frac{Aw_0^2k^2}{4\pi}\exp\left[-\frac{1}{4}(kw_0)^2(p^2+q^2)\right].$$

The width of this distribution at $1/e$ is equal to $2/(kw_0)$, i.e it is inversely proportional to the beam width w_0. The angular spectrum $a(p,q)$ is only a 'beam field' if $\mid a(p,q) \mid$ is appreciable for

$$p^2+q^2 << 1.$$

The amplitude of this spectrum $\mid a(p,q) \mid$ only has significant values when

$$\frac{1}{4}(kw_0)^2(p^2+q^2) \leq 1$$

or when

$$(p^2+q^2) \leq \frac{4}{(kw_0)^2}$$

so that the beam condition requires that

$$\frac{4}{(kw_0)^2} << 1 \quad \text{or} \quad \frac{\lambda^2}{\pi^2 w_0^2} << 1$$

i.e.

$$w_0 >> \frac{\lambda}{\pi}.$$

This result shows that the source distribution only gives a beam (in the defined sense of $p^2+q^2 << 1$) if its width is very much greater that a wavelength. This is true in physical lasers.

Given that the beam condition is satisfied, the amplitude in any plane z is (from previous results, i.e. the solution to the paraxial wave equation) given by

$$U(x,y,z) = \exp(ikz) \int_{-\infty}^{\infty} \int_{-\infty}^{\infty} a(p,q) \exp[ik(px+qy)] \exp\left[-ik\frac{z}{2}(p^2+q^2)\right] dpdq.$$

Substitution of the above expression for $a(p,q)$ into this result yields

$$U(x,y,z) = Ag(z) \exp\left(-\frac{r^2}{w_0^2}\right) \exp\left[i\left(k\left(z+\frac{r^2}{2R}\right)+\phi(z)\right)\right]$$

where

$$w(z) = w_0\sqrt{1+\left(\frac{2z}{kw_0^2}\right)^2}, \quad R(z) = z\left[1+\left(\frac{kw_0^2}{2z}\right)^2\right],$$

$$g(z) = \frac{w_0}{w(z)}, \quad \cos\phi(z) = \frac{w_0}{w(z)}$$

and

$$\sin\phi(z) = -\sqrt{1-\frac{w_0^2}{w^2(z)}}.$$

The function $w(z)$ describes the behaviour of the beam radius as a function of the distance of propagation z. The amplitude is given by

$$Ag(z) \exp\left(-\frac{r^2}{w_0^2}\right)$$

and the phase is given by

$$\left(z+\frac{r^2}{2R}\right)+\phi(z).$$

The function $w(z)$ determines the beam radius at distance z and the amplitude distribution remains Gaussian. The angular spread of the beam θ may be defined as

$$\theta = \lim_{z\to\infty}\left(\frac{w(z)}{z}\right) = \lim_{z\to\infty}\frac{1}{z}w_0\sqrt{1+\left(\frac{2z}{kw_0^2}\right)^2} = \frac{w_0}{z}\frac{2z}{kw_0^2} = \frac{2}{kw_0}$$

or

$$\theta = \frac{\lambda}{\pi w_0}.$$

For example, with

$$w_0 = 1\text{mm} \quad \text{and} \quad \lambda = 63\times 10^{-3} \quad \text{mm},$$

$$\theta \simeq 2\times 10^{-4}\text{rad} \simeq 40 \quad \text{arc} \quad \text{seconds}$$

As $kz \to \infty$,

$$W(z) \to \frac{2z}{kw_0}, \quad R \to z, \quad g(z) \to \frac{kw_0^2}{2z} = \frac{\pi w_0^2}{\lambda z}$$

$$\cos\phi(z) \to 0 \quad \text{and} \quad \sin\phi(z) \to -1 \quad \text{i.e.} \quad \exp[i\phi(z)] = -i$$

and

$$\frac{r^2}{w^2(z)} \simeq \frac{r^2(kw_0)^2}{(2z)^2} = \frac{1}{4}(kw_0)^2a^2$$

where

$$a = \frac{r}{z}$$

giving

$$U(z,a) = -\frac{i}{\lambda}A\frac{\exp(ikz)}{z}(\pi w_0^2)\exp\left[-\frac{1}{4}(kw_0)^2a^2\right], \quad kz\to\infty.$$

The beam spread in the far field is still $\frac{\lambda}{\pi w_0}$ and the intensity in the far-zone is $\mid U(z,a)\mid^2$.

11.12 Holographic Imaging

The principles of holographic imaging were invented in the late 1940s by the Hungarian born Dennis Gabor in England and, later, by Yuri Denisyuk in the USSR and Emmitt Leith in the USA in the 1950s. With the development of coherent laser light in the early 1960s, holographic imaging underwent a number of important developments over the following years, pioneered by Denisyuk in Russia, Nick Phillips at Loughborough University in England and Steve Benton at MIT, USA. More recent developments have involved the use of digital methods for generating holograms using high resolution print and full colour holography using red, green and blue laser light, pioneered by Hans Bjelkhagen in America and England. However, the original invention has been attributed to Gabor who won the Nobel prize in physics for his work in information science.

11.12.1 Fraunhofer Analysis

The basis for holography is to use a reference beam to generate and recover information on an object that is phase sensitive. In the far field, at a point z_0, the light wavefield scattered from a surface denoted by the object function $f(x, y)$ is, ignoring scaling and phase factors, given by the 2D Fourier transform, i.e.

$$u(k_x, k_y) = \hat{F}_2[f(x, y)] = \int_{-\infty}^{\infty}\int_{-\infty}^{\infty} f(x, y) \exp(-ik_x x) \exp(-ik_y y) dxdy$$

where the spatial frequencies are given by

$$k_x = \frac{kx_0}{z_0} \quad \text{and} \quad k_y = \frac{ky_0}{z_0}.$$

This result is based on the Fraunhofer approximation and the Kirchhoff boundary condition for surface scattering (or the Born approximation for volume scattering). We record the wavefield on a photographic plate to obtain a photograph, and then we take a measurement of the intensity of the wavefield $\mid u \mid^2$ over a period of time (the exposure time). Consider the case where a beam of coherent light (so that k is a constant) with a uniform spatial amplitude A illuminates the surface and the scattered light is measured in the far field together with the beam at normal incident to the photographic plate. Then, the recording is not of $\mid u \mid^2$ but of

$$\mid u + A \mid^2 = \mid u \mid^2 + \mid A \mid^2 + A^* u + A u^*.$$

The cross terms generated by the addition of a reference beam in the recording of the intensity distribution of $u + A$ (a hologram) instead of u (a photograph) is the fundamental basis for holographic imaging and, according to Gabor, was first conceived by him during a tennis match (which he was losing!).

If we illuminate the hologram with the reference beam, then, in the far field, the scattered wavefield will be given by the 2D (inverse) Fourier transform of (again ignoring scaling and phase factors) $A \mid u + A \mid^2$, i.e.

$$\hat{F}_2^{-1}[u(k_x, k_y)] = A \int_{-\infty}^{\infty}\int_{-\infty}^{\infty} [\mid u(k_x, k_y) \mid^2 + \mid A \mid^2 + A^* u(k_x, k_y) + A u^*(k_x, k_y)]$$

$$\times \exp(ik_x x) \exp(ik_y) dk_x dk_y = a(x, y) + A^2[f(x, y) + f(-x, -y)]$$

where

$$a(x, y) = \hat{F}_2^{-1}[A \mid u \mid^2 + A^3].$$

The function $A \mid u \mid^2 + A^3$ will vary slowly over large scales compared with the term $A^* u + A u^*$. Consequently, $a(x, y)$ will have a distribution which peaks around the origin because of the scaling property of the Fourier transform,

$$f(ax, by) \Longleftrightarrow F\left(\frac{k_x}{a}, \frac{k_y}{b}\right).$$

The pattern that is obtained when a hologram is illuminated by a plane wave is therefore the object function f together with a reversed copy of f and a peak at the origin. Apart from the peak, the hologram contains two images $f(x, y)$ and $f(-x, -y)$ which makes viewing difficult. If the hologram is generated using a reference beam at an angle θ to normal incidence, then the hologram will again contain two images: one is in the original location and one displaced by an angle of 2θ. This is the reason why an off-axis reference beam is used in holography.

11.12.2 Digital Holography

The analysis above refers to continuous functions taken to be recorded on a photographic plate. In digital holography, the hologram must be represented using a digital image. What is the resolution required in terms of the size of a pixel Δx in order to generate a digital hologram effectively? From the sampling theorem, the sampling frequency required to represent a continuous function accurately in digital form is the Nyquist frequency (i.e. twice the spatial frequency bandwidth W of the image) or

$$\Delta x = \frac{\pi}{K}$$

where $K = 2W$. Since $k_x = kx_0/z_0$, we have

$$\Delta x = \frac{\pi z_0}{kx_0} = \frac{\lambda z_0}{2x_0}.$$

For $\lambda \sim 10^{-7}$m, a 10cm×10cm digital hologram viewed at a distance of 1 metre, say, requires a pixel size ∼1 nm. Further, since $x_0/z_0 = \tan(\theta/2) \simeq \theta/2$ where θ is the total angle subtended by the holographic image, the pixel resolution required to obtain a viewing angle of θ is given by

$$\Delta x = \frac{\lambda}{\theta}.$$

For a fixed wavelength, the pixel resolution is inversely proportional to the viewing angle. A digital hologram of size 1cm×1cm must therefore be composed of $\sim 10^5 \times 10^5$ pixels to provide a viewing angle of just a few degrees. This currently severely limits the size and viewing capacity of a digital hologram that can be made compared to the normal hologram made by current optical methods.

11.12.3 Fresnel Holograms

In the Fresnel zone, the scattered wavefield is given by (ignoring scaling constants and phase factors)

$$u(x_0, y_0) = \int\int f(x, y) \exp\left(\frac{ik}{2z}[(x_0 - x)^2 + (y_0 - y)^2]\right) dxdy$$

which is just the convolution of the object function $f(x, y)$ with the Fresnel kernel

$$\exp\left(\frac{ik}{2z}[(x_0 - x)^2 + (y_0 - y)^2]\right)$$

and can therefore be computed using the convolution theorem. For fixed k the Fresnel kernel depends on the value of z, the distance from the object plane to the recoding plane. By computing the wavefield u_n for different values of $z = z_n$, $n = 1, 2, 3, ...$ and summing the result, we can generate the combined amplitude function

$$U(x, y) = \sum_n u_n(x, y).$$

The hologram is then given by

$$| U + A |^2 = | U |^2 + A^2 + AU^* + A^*U.$$

Holograms have a number of applications in science and engineering and the technology for generating high resolution holograms optically is well established. The use of digital holography is limited by the processing power required for their computation and the high resolution printing or other display facilities (e.g. liquid crystal displays) needed to obtain reasonable viewing angles. Foil holograms have been used very effectively as part of the print security features being used on a range of products (banknotes, credit/debit cards and personal identity cards, for example). However, this still relies on the use of optically generated holograms because of the high resolution microprinting required in order to generate holograms digitally. We conclude this chapter with a case study that approaches print security using an incoherent optical method based on the application of digital images that can be printed and recovered at relatively low resolution (e.g. 300 dots per inch, dpi).

11.13 Case Study: Digital Watermarking

The use of digital watermarking electronic and/or hardcopy documents is a area of growing importance in information technology security[1]. The principal model that underpins this technology is based on the fundamental imaging equation

$$s = \hat{P}f + n$$

where f is the information that is to embedded in the image (the watermark), $\hat{P}$ is some linear operator and s is the output image (the watermarked image). The function n, which is usually taken to be the noise, can indeed be a noise field, but in the context of watermarking it can be any other host image. The operation $\hat{P}f$ can be non-stationary or non-isoplanatic but, in most watermarking methods, an isoplanatic model is used. In such cases, the basic watermaking model is

$$s = p \otimes \otimes f + n$$

[1]This case study is based on the research thesis of Dr K W Mahmoud, *Low Resolution Watermarking for Print Security*, PhD Thesis, Loughborough University, England, December 2004

where p is any useful function that is of value to the watermarking process.

Watermarking is an area of cryptology that is related to the 'art' of hiding secret information in images, or Steganography. It has an advantage over cryptography in that, if information can be embedded in a data field that is fully covert, then it is not immediately clear to a potential attacker that there may be information in the data that is worth attacking. If we consider the case where this 'secrete information' is an encrypted field, then watermarking can provide a method of covert encryption.

In the field of cryptology, the operation $\hat{P}f$ is referred to as the processes of 'diffusion' and the process of adding noise (i.e. $\hat{P}f + n$) is referred to as the process of 'confusion'. One of the processes $\hat{P}f$ that can be used is to convolve f with the kernel

$$p(x, y) = \frac{1}{4\pi t} \exp\left[-\left(\frac{x^2 + y^2}{4Dt}\right)\right]$$

which is the Green function for the 2D diffusion equation with diffusivity D at time t (see Chapter 6), the process $p \otimes \otimes f$ being a solution to the 2D diffusion equation for a source $f(x, y)$ that starts to diffuse at $t = 0$.

In cryptography, the principal 'art' is to develop methods in which the processes of diffusion and confusion are maximized, a criterion being that the output s should ideally be dominated by the function n which in turn should be characterized by a maximum entropy (i.e. a uniform statistical distribution).

The ability to recover f from s provides a method of authentication. If, in addition, it is possible to determine that a copy of s has been made leading to some form of data degradation and/or corruption that can be conveyed through an appropriate analysis of f, then a scheme can be developed that provides a check on: (i) the authenticity of the data s; (ii) its fidelity.

Formally, the recovery of f from s is based on the inverse process

$$f = \hat{P}^{-1}(s - n)$$

where $\hat{P}^{-1}$ is the inverse operator. Clearly, this requires the field n to be known *a priori*. The data n can be any field that is appropriate for confusing the information $\hat{P}f$ including a pre-selected image. If the process of confusion is undertaken in which the signal-to-noise ratio is set to be very low (i.e. $\|n\| >> \|\hat{P}f\|$), then the watermark f can be hidden covertly in the data n provided the inverse process $\hat{P}^{-1}$ is well defined and computationally stable. In this case, it is clear that the host image n must be known in order to recover the watermark f, leading to a watermarking scheme in which the entire field n is the 'key'. In addition, the operator $\hat{P}$ (and its inverse $\hat{P}^{-1}$) can be key dependent (in terms of the characteristic numerical parameters and/or coefficients from which the operator is composed). For example, if we were to apply the Green function above, the values of the diffusivity D and the the time t represent the keys required to replicate the kernel in order to executed the inverse process. The value of this operator key dependency relies on the nature and properties of the operator that is used and whether it is compounded in an algorithm that is required to be in the public domain for example.

Another approach is to consider the case in which the field n is unknown and to consider the problem of extracting the watermark f in the absence of

this field. For this to be achieved, we require a process $\hat{P}$ where $P^{-1}n = 0$ so that we can construct the data field

$$s = \hat{P}f + n, \quad \|n\| >> \|\hat{P}f\|$$

such that

$$\hat{P}^{-1}s = \hat{P}^{-1}\hat{P}f + \hat{P}^{-1}n = f.$$

This approach does not rely on a knowledge of n *a priori*. The ability to recover the watermark only requires knowledge of the operator $\hat{P}$ (and its inverse). There are many operators $\hat{P}$ that may be considered. However, it is important that the inverse operator is not only well defined but computationally stable and easy to implement. If we consider a stationary process where

$$s = p \otimes \otimes f + n$$

then, to recover f, we need to deconvolve s. One of the simplest (possibly *the* simplest) ways of doing this is to correlate the data with p. In other words we require a kernel p such that

$$p(x, y) \odot \odot p(x, y) = \delta^2(x, y).$$

In this case, when n is not known *a priori*, a further condition on p is that

$$p(x, y) \odot \odot n(x, y) = 0.$$

There is one (and only one) function that has these idealized properties, i.e. the function (and 'variations on its theme')

$$p(x, y) = \exp[i\alpha(x^2 + y^2)]$$

which is the basis for imaging systems such as SAR (see Chapter 10) and is the 'central kernel' for Fresnel optics, a property that is compounded in the computation of the correlation integral

$$\int_{-X/2}^{X/2} \int_{-Y/2}^{Y/2} \exp(-i\alpha x^2) \exp(-i\alpha y^2) \exp[i\alpha(x + x_0)^2] \exp[i\alpha(y + y_0)^2] dxdy$$

$$= \exp[i\alpha(x_0^2 + y_0^2)] XY \text{sinc}(\alpha X x_0) \text{sinc}(\alpha Y y_0) \to \delta(x_0)\delta(y_0), \quad \text{as} \quad \begin{cases} X \to \infty; \\ Y \to \infty. \end{cases}$$

However, other kernels can be considered such that the recovery of the watermark is based on a correlation provided appropriate pre-processing of $p \otimes \otimes f$ is undertaken. Thus, since

$$p \otimes \otimes f \Longleftrightarrow PF$$

where P and F are the Fourier transforms of p and f, respectively, if we compute

$$Q = \frac{P}{\mid P \mid^2}$$

then

$$p \odot \odot q \otimes \otimes f \Longleftrightarrow P^* \frac{P}{\mid P \mid^2} F = F$$

and hence

$$p \odot \odot q \otimes \otimes f = f$$

where q is the inverse Fourier transform of Q. However, in order to compute Q, the denominator must be regularized. For this application, regularization can be achieved by replacing any zero that occurs in the power spectrum of p with 1. Moreover, p can be any function including a noise field. For applications in watermarking, the diffusion of an image with a noise field provides a better solution to the problem because: (i) a noise field provides uniform diffusion (analogous to an optical diffuser); (ii) noise fields can be generated using random number generators that depend on a single initial value or seed (i.e. a private key). An example of this is shown in Figure 11.7. Here an image i_1 (the 'host image') is watermarked by another image i_2 (the 'watermark image') using the result

$$s = r(q \otimes \otimes i_2) + i_1$$

where

$$\|q \otimes \otimes i_2\|_\infty = 1, \quad \|i_1\|_\infty = 1$$

and r, the signal-to-noise ratio, is 0.1. The function

$$q = \hat{F}_2^{-1} \left[\frac{N}{\mid N \mid^2} \right],$$

where N is the Fourier transform of the noise field n, is computed using the random number generator

$$x_{i+1} = a x_i \mathrm{mod}(P), \quad x_0 = \mathrm{seed}$$

with $P = 2^{31} - 1$ (a Mersenne prime number) and $a = 7^7$, the array $\mathbf{x}$ having been normalized so that $\|\mathbf{x}\|_\infty = 1$ and used to generate n on a row-by-row basis. Because $r = 0.1$, the output is 'dominated' by the image i_1. Here, the seed is any integer such as

$$187356287276635635...$$

which can be based on the application of a PIN (Personal Identity Number) or a password (e.g. 'Enigma', which in terms of an ASCII string - using binary to decimal conversion - is '216257556149'). This approach provides a method of watermarking one image with another. If the host image is distributed *a priori* to all recipients of the hidden information, then it can be considered to be a public key. Private keys (i.e. the seeds used to generate the noise field) can then be used to recover the watermark on a one-by-one basis. The effect of adding the diffused watermark image to the host image yields a different, slightly brighter image because of the perturbation of i_2 by $q \otimes \otimes i_1$. This effect can be minimized by introducing a smaller signal-to-noise ratio such that the perturbation is still recoverable by subtracting the host image from

the watermarked image. Pre-processing the noise field to generate q has a number of advantages: (i) it produces a relatively high-frequency and uniform output (in terms of the distribution of grey levels) when convolved with the watermark image; (ii) the watermark image can be recovered by correlation; (iii) high-fidelity reconstructions of the watermark are achievable with very low signal-to-noise ratios. This approach is based on a reversal of the roles that the noise and point spread function play in the fundamental isoplanatic imaging equation

$$s = p \otimes\otimes f + n.$$

In this application of the imaging equation, p is the noise and n is a deterministic function (the host image).

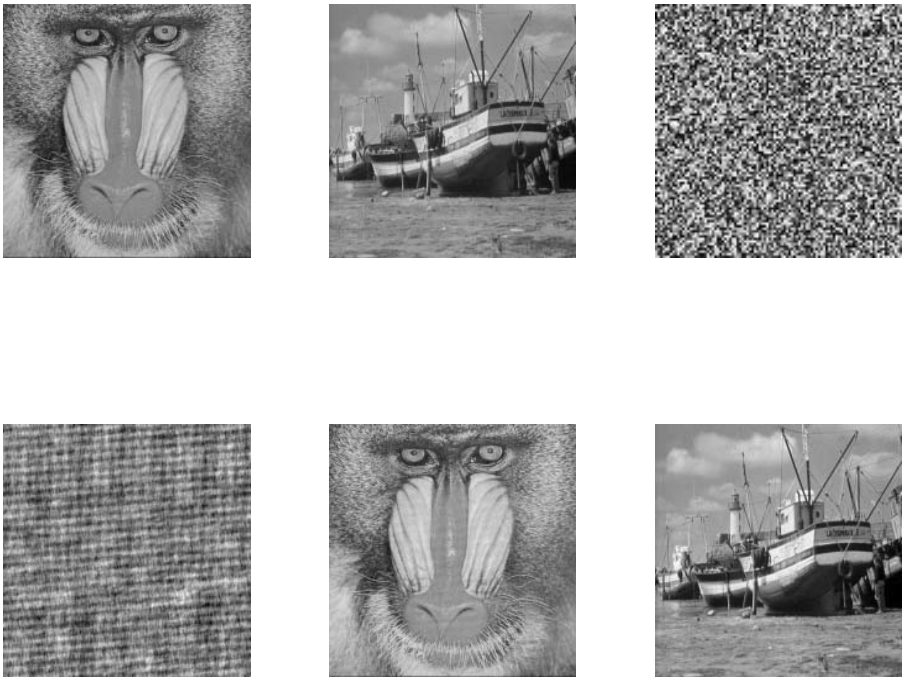

Figure 11.7: Example of watermarking an image with another image using noise based diffusion. The 'host image' i_1 (top-left) is watermarked with the 'watermark image' i_2 (top-centre) using the diffuser (top-right), i.e. a uniform noise field whose pixel-by-pixel values depend upon the seed used (the private key). The result of computing $q \otimes\otimes i_2$ (bottom-left) is added to the host image using a signal-to-noise ratio of 0.1 to obtain a watermarked image (bottom-centre). Recovery of the watermark image i_2 (bottom-right) is accomplished by subtracting the host image from the watermarked image and correlating the result with the noise field n. The correlation and convolution processes are undertaken using an FFT.

11.13.1 Low Resolution Hardcopy Watermarking

The methods discussed above provide an approach that is only effective for watermarking electronic images. If the watermarked image is printed and scanned back into electronic form, then the print/scan process will yield an array of pixels that will be significantly different from the original electronic image even though it might 'look' the same. These differences can include the size of the image, its orientation, brightness, contrast and so on. Of all the processes involved in the recovery of the watermark, the subtraction of the host image from the data s is critical. If this process is not accurate on a pixel-by-pixel basis and deregistered for any of many reasons, then recovery of the watermark by correlation will not work effectively. However, if we make use of the diffusion process alone, then the watermark can be recovered via a print/scan because of the compatibility of the processes involved. However, in this case, the 'watermark' is not covert but overt.

Depending on the printing process applied, a number of distortions will occur which diffuse the information being printed. Thus, in general, we can consider the printing process to introduce an effect that can be represented by the convolution equation

$$s_{\text{print}} = p_{\text{print}} \otimes \otimes s.$$

where s is the original electronic form of the diffused watermark image and p_{print} is the point spread function of the printer. An incoherent image of the data, obtained using a flat bed scanner for example (or any other incoherent optical imaging system) will also have a characteristic point spread function p_{scan}. Thus, we can consider a scanned image to be given by

$$s_{\text{scan}} = p_{\text{scan}} \otimes \otimes s_{\text{print}}$$

where s_{scan} is taken to be the digital image obtain from the scan. Now, because convolution is commutative, we can write

$$s_{\text{scan}} = p_{\text{scan}} \otimes \otimes p_{\text{print}} \otimes \otimes p \otimes \otimes f = p \otimes \otimes p_{\text{scan/print}} \otimes \otimes f$$

where

$$p_{\text{scan/print}} = p_{\text{scan}} \otimes \otimes p_{\text{print}}$$

which is the print/scan point spread function associated with the processing cycle of printing the image and then scanning it. By applying the method discussed earlier, we can obtain a reconstruction of the watermark whose fidelity is determined by the scan/print point spread function. However, in practice, the scanned image needs to be re-sized to that of the original. This is due to the scaling relationship

$$f(\alpha x, \beta y) \Longleftrightarrow \frac{1}{\alpha\beta} F\left(\frac{k_x}{\alpha}, \frac{k_y}{\beta}\right).$$

The size of any image captured by a scanner or other device will depend on the resolution used. The size of the image obtained will inevitably be different

from the original because of the resolution and window size used to print the watermark and the resolution used to scan the image. Since scaling in the spatial domain causes inverse scaling in the Fourier domain, the scaling effect must be 'inverted' before the watermark can be recovered by correlation since correlation is not a scale invariant process. Re-sizing the image (using an appropriate interpolation scheme such as the bi-cubic method, for example) requires a set of two numbers n and m (i.e. the $n \times m$ array used to generate the noise field and execute the diffusion process) that, along with the seed required to regenerate the noise field, provides the 'private keys' needed to recover the watermark from the diffused image. An example of this approach is given in Figure 11.8 which shows the result of reconstructing four different images (a photograph, finger-print, signature and text) used in the design of an impersonalized (HSBC) debit/credit card.

Figure 11.8: Example of the application of 'diffusion only' watermarking. In this example, four images of a face, finger-print, signature and text have been diffused using the same noise field (with pre-processing) and printed on the front (top-left) and back (bottom-left) of an impersonalized card using a 600 dpi printer. The reconstructions (bottom-left and bottom-right, respectively) are obtained using a conventional flat-bed scanner based on a 300 dpi grey-level scan.

The use of 'diffusion only' watermarking for print security can be undertaken in colour by applying exactly the same diffusion/reconstruction methods to the red, green and blue components independently. This provides two additional advantages: (i) the effect of using colour tends to yield better quality

reconstructions because of the colour combination process; (ii) for each colour component, it is possible to apply a noise field with a different seed. In this case, three keys are required to recover the watermark.

Because this method is based on a convolution (with pre-processing) and since

$$s_{\text{scan}} = q \otimes \otimes p_{\text{scan/print}} \otimes \otimes f$$

as discussed earlier, the recovery of the f will not be negated by the distortion of the point spread function associated with the print/scan process, just limited or otherwise by its characteristics. Thus, if an image is obtained of the printed data field $p \otimes \otimes f$ which is out of focus due to the characteristics of $p_{\text{scan/print}}$, then the reconstruction of f will be out of focus to the same degree. Decryption of images with this characteristic is only possible using an encryption scheme that is based a diffusion only approach. Figure 11.9 illustrates the recovery of a diffused watermark printed onto a personal ID card obtained using a flat bed scanner and then captured using mobile phone camera using colour (RGB-mode) but presented here in grey scale. In the latter case, the reconstruction is not in focus because of the wide-field nature of the lens used. However, the fact that recovery of the watermark is possible with a mobile phone means that the scrambled data can be transmitted securely and the card holders image (as in this example) recovered remotely and transmitted back to the same phone for authentication. This provides the necessary physical security needed to implement such a scheme in practice and means that specialist image capture devices are not required on site. Enhancement of the image can be undertaken as required using the methods discussed in Part III, for example.

The diffusion process can be carried out using a variety of different noise fields other than the uniform noise field considered here which is based on linear congruential random number generation. Changing the noise field can be of value in two respects: first, it allows a system to be designed that, in addition to specific keys, is based on specific algorithms which must be known *a priori*. These algorithms can be based on different pseudo uniform random number generators and/or different pseudo chaotic number generators that are post-processed to provide a uniform distribution of numbers. Second, the diffusion field depends on both the characteristics of the watermark image and the noise field. By utilizing different noise fields (e.g. Gaussian noise, Poisson noise and so on), the texture of the output field can be changed. This includes the application of fractal noise which is discussed in Part IV. The use of different noise fields is of value when different textures are required that are aesthetically pleasing and can be used to create a background that is printed over the entire document. In this sense, variable noise based diffusion fields can be used to replace complex print security features with the added advantage that, by de-diffusing them, information can be recovered. Further, these fields are very robust to data degradation created by soiling, for example. In the case of binary watermark images, data redundancy allows reconstructions to be generated from a binary output, i.e. after binarizing the diffusion field (with a threshold of 50% for example). This allows the output to be transmitted in a form that can tolerate low resolution and low contrast copying, e.g. a fax.

Figure 11.9: Original (top-left), diffused watermark (top-right), reconstruction using a flatbed scanner (bottom-left) and reconstruction using a mobile phone (bottom-right). These images have been scanned in grey scale from the original colour versions printed on to a personal ID card at 600dpi stamp-size (i.e. 2cm×1.5cm).

11.13.2 Covert Watermarking

Watermarking is usually considered to be a method in which the watermark is embedded into a host image in an unobtrusive way. Another approach is to consider the host image to be a data field that, when processed with another data field, generates new information.

Consider two images i_1 and i_2. Suppose we construct the following function

$$n = \hat{F}_2 \left(\frac{I_1}{\mid I_1 \mid^2} I_2 \right)$$

where $I_1 = \hat{F}_2[i_1]$ and $I_2 = \hat{F}_2[i_2]$. If we now correlate n with i_1, then from the

correlation theorem

$$i_1 \odot \odot n \Longleftrightarrow I_1^* \frac{I_1}{\mid I_1 \mid^2} I_2 \Longleftrightarrow i_2.$$

In other words, we can recover i_2 from i_1 with a knowledge of n. Because this process is based on convolution and correlation alone, it is compatible and robust to printing and scanning, i.e. incoherent optical imaging. An example of this is given in Figure 11.10. In this scheme, the noise field n is the private key required to reconstruct the watermark and the host image can be considered to be a public key. The tolerance of this method to printing and scanning is excellent provided the output is cropped and oriented correctly.

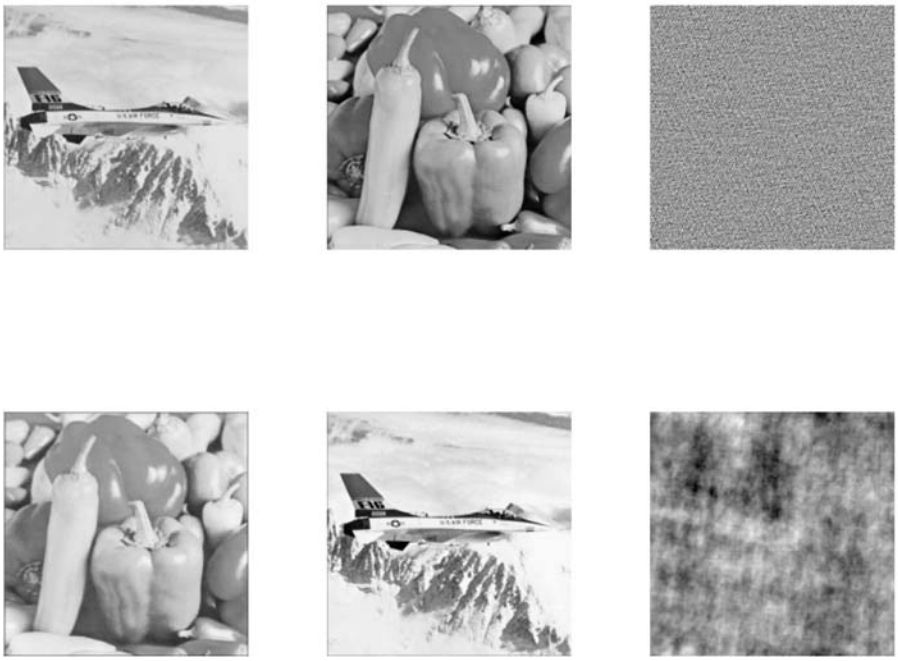

Figure 11.10: Example of a covert watermarking scheme. i_1 (top-left) is convolved (with pre-processing) with i_2 (top-middle) to produce the noise field (top-right). i_2 is printed at 600 dpi, scanned at 300 dpi and then re-sampled back to its original size (bottom-left). Correlating this image with the noise field generates the reconstruction (bottom-centre). The reconstruction depends on just the host image and noise field. If the noise field and/or the host image are different or corrupted, then a reconstruction is not achieved (bottom-right).

11.13.3 Application to Encryption

One of the principal components associated with the development of methods and algorithms to 'break' cyphertext is the analysis of the output generated by an attempted decrypt and its evaluation in terms of an expected type. The output type is normally assumed to be plain text, i.e. the output is assumed to be in the form of characters, words and phrases associated with a natural language such as English or German, for example. If a plain text document is converted into an image file then the method described in the previous Section on 'covert watermarking' can be used to diffuse the plain text image i_2 using any other image i_1 to produce the field n. If both i_1 and n are then encrypted, any attack on these data will not be able to make use of an 'analysis cycle' which is based on the assumption that the decrypted output is plain text. This approach provides the user with a relatively simple method of 'confusing' the cryptanalyst and invalidates attack strategies that have been designed and developed on the assumption that the encrypted data have been derived from plain text alone.

11.14 Summary of Important Results

Fraunhofer diffraction

$$u(x_0, y_0) = \frac{i}{\lambda}\frac{\exp(ikz_0)}{z_0}\exp\left(ik\frac{x_0^2+y_0^2}{2z_0}\right)\int_{-\infty}^{\infty}\int_{-\infty}^{\infty} f(x,y)\exp\left(-\frac{ik}{z_0}(xx_0+yy_0)\right)dxdy.$$

The intensity is given by

$$I(x_0, y_0) = \frac{1}{\lambda^2 z_0} \mid \hat{F}_2[f(x,y)] \mid^2$$

where

$$\hat{F}_2[f(x,y)] = \int_{-\infty}^{\infty}\int_{-\infty}^{\infty} f(x,y)\exp[-i(k_x x + k_y y)]dxdy$$

$$k_x = \frac{2\pi x_0}{z_0\lambda}, \quad k_y = \frac{2\pi y_0}{z_0\lambda}.$$

Fresnel diffraction

$$u(x,y) = \frac{i}{\lambda}\frac{\exp(ikz_0)}{z_0} f(x,y) \otimes\otimes \exp\left(\frac{ik}{2z_0}[x^2+y^2]\right)$$

Fourier transforming properties of a lens

There is an exact Fourier transform relationship between the front and back focal planes of a well corrected lens. If $t(x, y)$ is a transparency placed at the back focal plane of a well corrected lens with focal length f then, in the front focal plane, the distribution of the amplitude field is

$$u(x_0, y_0) = \frac{i}{\lambda f} \exp(2ikf)\hat{F}_2[t(x, y)].$$

Coherent image formation

$$U_{\text{out}}(x, y) = \int_{-\infty}^{\infty}\int_{-\infty}^{\infty} U_{\text{in}}(x', y')p(x - x', y - y')dx'dy'$$

where the point spread function p is given by

$$p(x, y) = \int_{-\infty}^{\infty}\int_{-\infty}^{\infty} P(x', x') \exp\left[-\frac{ik}{z}(xx' + yy')\right] dx'dy'$$

and P is the 'pupil function'.

Incoherent image formation

$$I_{\text{out}}(x, y) = \int_{-\infty}^{\infty}\int_{-\infty}^{\infty} I_{\text{in}}(x', y') \mid p(x - x', y - y') \mid^2 dx'dy'$$

where $\mid p \mid^2$ is the intensity point spread function.

Angular spectrum representation of plane waves

$$U(x, y, z) = \int_{-\infty}^{\infty}\int_{-\infty}^{\infty} A(k_x, k_y) \exp[i(k_x x + k_y y + k_z z)]dk_x dk_y$$

$$+ \int_{-\infty}^{\infty}\int_{-\infty}^{\infty} B(k_x, k_y) \exp[i(k_x x + k_y y - k_z z)]dk_x dk_y.$$

Paraxial wave equation

$$\nabla_\perp^2 \psi + 2ik\frac{\partial \psi}{\partial z} = 0$$

where

$$\nabla_\perp^2 = \frac{\partial^2}{\partial x^2} + \frac{\partial^2}{\partial y^2}$$

is the transverse Laplacean.

Solution to the paraxial wave equation

$$\psi(x,y,z) = \int_{-\infty}^{\infty}\int_{-\infty}^{\infty} \widetilde{\psi}(k_x,k_y,0)\exp\left[-\frac{i}{2k}(k_x^2+k_y^2)z\right]\exp[i(k_x x + k_y y)]dk_x dk_y.$$

11.15 Further Reading

- Goodman J W, *Introduction to Fourier Optics*, McGraw-Hill, 1968.
- Papoulis A, *Systems and Transforms with Applications in Optics*, McGraw-Hill, 1968.
- Lipson S G and Lipson H, *Optical Physics*, Cambridge University Press, 1969.
- Cathey T W, *Optical Information Processing and Holography*, Wiley, 1974.
- Born M and Wolf E, *Principles of Optics (6th Edition)*, Pergamon Press, Oxford, 1980.
- Klein M V and Furtak T E, *Optics*, Wiley, 1986.
- Hecht E, *Optics*, Addison-Wesley, 1987.
- Steward E G, *Fourier Optics: An Introduction*, Horwood Scientific Publishing, 1987.
- Cox I J, Miller M L and Bloom J A, *Digital Watermarking*, Morgan Kaufmann, 2002.

Problems: Part II

II.1 Show that if $u(\mathbf{r}, k)$ satisfies the partial differential equation

$$[\nabla^2 + k^2 + \gamma(\mathbf{r})]u(\mathbf{r}, k) = 0$$

then u also satisfies the integral equation

$$u(\mathbf{r}_0, k) = f(\mathbf{r}_0, k) + \int g(\mathbf{r} \mid \mathbf{r}_0, k)u(\mathbf{r}, k)\gamma(\mathbf{r})d^3\mathbf{r}$$

where $f(\mathbf{r}, k)$ is a solution to $(\nabla^2 + k^2)u(\mathbf{r}, k) = 0$ and $g(\mathbf{r} \mid \mathbf{r}_0, k)$ is a Green function.

II.2 The electric field potential U satisfies the equation

$$\nabla^2 U(\mathbf{r}, t) - \frac{1}{c^2}\frac{\partial^2}{\partial t^2}U(\mathbf{r}, t) = -4\pi\rho(\mathbf{r})\exp(i\omega t)$$

where ρ is the charge density, ω is the angular frequency and c is the speed of electromagnetic waves in a vacuum. Use a Green function to compute the amplitude of the electric field potential produced by a thin antenna radiating 10m wavelength electromagnetic radiation at a distance of 1000m from the antenna when $\rho(\mathbf{r}) = 1/(4\pi r^2)$.

[Hint: Compute the Green function solution to this equation in the far field and then use spherical polar coordinates (r, θ, ϕ) noting that $d^3\mathbf{r} = r^2 dr d(\cos\theta)d\phi$ in spherical polars and that $\int_0^\infty \frac{\sin x}{x}dx = \frac{\pi}{2}$]

II.3 By considering a plane wave solution of the form

$$u(\mathbf{r}, t) = \exp(-\alpha\hat{\mathbf{n}} \cdot \mathbf{r})\exp[i(k\hat{\mathbf{n}} \cdot \mathbf{r} - \omega t)]$$

to the following homogeneous wave equation operators, derive dispersion relations for the absorption α and the phase velocity $c_p = \omega/k$.

(i) Electromagnetic wave propagation in a conducting medium:

$$\nabla^2 - \frac{1}{c_0^2}\frac{\partial^2}{\partial t^2} - \tau_0\frac{\partial}{\partial t}$$

where c_0 and τ_0 are constants.

(ii) Acoustic waves propagation in a viscous medium:

$$\nabla^2 - \frac{1}{c_0^2}\frac{\partial^2}{\partial t^2} - \tau_0 \frac{\partial}{\partial t}\nabla^2$$

where c_0 and τ_0 are constants.

(iii) Ultrasonic wave propagation in a dispersive material (the Leeman operator):

$$\nabla^2 - \frac{1}{c_0^2}\frac{\partial^2}{\partial t^2} - \tau_0 \frac{\partial}{\partial t} - \tau_1 \frac{\partial}{\partial t} \mid \nabla \mid$$

where c_0, τ_0 and τ_1 are constants and $\mid \nabla \mid \Longleftrightarrow \mid \mathbf{k} \mid$.

II.4 Compute the 3D Green functions for the following time dependent wavefield operators (where τ_0 is a constant):

(i) The Klein-Gordon operator:

$$\nabla^2 - \frac{1}{c^2}\frac{\partial^2}{\partial t^2} - \tau_0^2$$

[Hint: The Laplace Transform of the function

$$f(x) = \begin{cases} J_0(a\sqrt{t^2 - b^2}), & t > b; \\ 0, & t < b \end{cases}$$

is

$$F(p) = \frac{\exp(-b\sqrt{p^2 + a^2})}{\sqrt{p^2 + a^2}}$$

where J_0 is the Bessel function (of order 0) and a and b are positive constants.]

(ii) Electromagnetic wave propagation in a conducting medium:

$$\nabla^2 - \frac{1}{c^2}\frac{\partial^2}{\partial t^2} - \tau_0 \frac{\partial}{\partial t}$$

[Hint: The Laplace Transform of the function

$$f(x) = \begin{cases} I_0(a\sqrt{t^2 - b^2}), & t > b; \\ 0, & t < b \end{cases}$$

is

$$F(p) = \frac{\exp(-b\sqrt{p^2 - a^2})}{\sqrt{p^2 - a^2}}$$

where I_0 is the modified Bessel function (of order zero) and a and b are positive constants.]

(iii) Acoustic wave propagation is a viscous medium:

$$\nabla^2 - \frac{1}{c^2}\frac{\partial^2}{\partial t^2} - \tau_0 \frac{\partial}{\partial t}\nabla^2$$

[Hint: Use the results

$$\exp(-ac\sqrt{p})\exp(abc/\sqrt{p}) = \exp[-a(1-b)c\sqrt{p}]\sum_{-\infty}^{\infty}(-1)^2 J_n(2abc)p^{\frac{n}{2}}$$

where J_n is the Bessel function and

$$\hat{L}^{-1}(p^n \exp(-a\sqrt{p}) = \frac{\exp[-a^2/(8t)]D_{2n+1}[a/\sqrt{2t}]}{2^{\frac{n+1}{2}}\sqrt{\pi}t^{1+n}}$$

where $\hat{L}^{-1}$ denotes the inverse Laplace transform and D_m is the Weber function.]

(iv) The Leeman operator for ultrasonic wave propagation in a dispersive material

$$\nabla^2 - \frac{1}{c^2}\frac{\partial^2}{\partial t^2} - \tau_0\frac{\partial}{\partial t} - \tau_1\frac{\partial}{\partial t} \mid \nabla \mid$$

where τ_0 and τ_1 are constants and $\mid \nabla \mid \Longleftrightarrow \mid \mathbf{k} \mid$.

[Hint: Use the Gegenbauer integral expression for a sinc function, i.e.

$$\frac{\sin\sqrt{x^2+y^2}t}{\sqrt{x^2+y^2}}$$

$$= \frac{1}{2\sqrt{1+\beta^2}}\int_{-\sqrt{1+\beta^2}t}^{\sqrt{1+\beta^2}t} J_0\left(\frac{\alpha}{1+\beta^2}\sqrt{s^2-(1+\beta^2)t^2}\right)\exp\left[-i\left(y - \frac{i\alpha}{1+\beta^2}t\right)\right]ds$$

where $x = \beta y - i\alpha$.

II.5 Find the Green function defined by the equation

$$\left(\nabla^2 + \sigma\frac{\partial}{\partial t}\right)G(\mathbf{r} \mid \mathbf{r}_0, t \mid t_0) = -\delta^3(\mathbf{r}-\mathbf{r}_0)\delta(t-t_0)$$

by first taking the Laplace transform with respect to t and using the initial condition

$$G \mid_{t=t_0} = 0$$

and the result

$$\int_0^{\infty} t^{-3/2}e^{a/t}e^{-pt}dt = \sqrt{\frac{\pi}{a}}e^{-2\sqrt{ap}}.$$

II.6 The propagation of a scalar wavefield u through a 1D inhomogeneous continuum with time-independent velocity profile $c(x)$ can be described by the equation

$$\left(\frac{\partial^2}{\partial x^2} + \frac{\omega^2}{c^2}\right) u(x,\omega) = 0$$

(i) Given that $c = c_0 + v$ where $v/c_0 << 1$ and c_0 is a constant and by writing u in the form $u = \exp(-ikx) + w(x,k)$ where $\mid w \mid << 1$, show that this equation can be reduced to the approximate form

$$\left(\frac{\partial^2}{\partial x^2} + k^2\right) w(x,k) = \frac{2k^2 v}{c_0} \exp(-ikx)$$

where $k = \omega/c_0$.

(ii) Solve the equation above using the appropriate Green function and asymptotic formulation. Hence show that

$$w(a,\tau) = -\frac{1}{2c_0}\frac{dv}{d\tau} \otimes \delta(\tau + a), \quad a \to \infty$$

where $\tau = 2t$ is the two-way travel time and $\otimes$ denotes the convolution integral. Explain the physical significance of the conditions $v/c_0 << 1$ and $\mid w \mid << 1$ use to derive this result.

(iii) Let $u(x,k) = \exp[iks(x)]$ where $k = \omega/c_0$ Show that if the continuum is characterised by a velocity profile given by $c = \alpha c_0/x$ where α is a constant, then as $\omega \to \infty$, the solution for u defined by the original equation is given by

$$u(x,k) = \exp\left[ik\left(\beta + \frac{x^2}{2\alpha}\right)\right]$$

where β is an arbitrary constant. Explain the physical significance of the limiting condition (on the frequency) used to derive this result.

II.7 Find the Green function solution to the equation

$$(\nabla^2 + k^2)u(\mathbf{r} \mid \mathbf{r}_0, k) = -k^2\gamma(\mathbf{r})u(\mathbf{r} \mid \mathbf{r}_0, k) - \delta^3(\mathbf{r} - \mathbf{r}_0)$$

using the eikonal transform

$$u(\mathbf{r} \mid \mathbf{r}_0, k) = g(\mathbf{r} \mid \mathbf{r}_0, k) \exp[s(\mathbf{r} \mid \mathbf{r}_0, k)]$$

and the Rytov approximation (with homogeneous boundary conditions) where g is the solution of

$$(\nabla^2 + k^2)g(\mathbf{r} \mid \mathbf{r}_0, k) = -\delta^3(\mathbf{r} - \mathbf{r}_0).$$

Compute the back-scattered field in this case.

II.8 Solve the following integral equation using: (i) Laplace transforms; (ii) the Neumann series

$$u(x) = x - \int_0^x (t - x)u(t)dt.$$

II.9 Consider the equation

$$(\nabla^2 + k^2)u(\mathbf{r} \mid \mathbf{r}_0, k) = -k^2\gamma(\mathbf{r})u(\mathbf{r} \mid \mathbf{r}_0, k) - \delta^3(\mathbf{r} - \mathbf{r}_0), \quad \mathbf{r} \in V$$

where $\mathbf{r}_0$ is the point of a source of radiation with constant wavelength $2\pi/k$. Calculate the scattered field at a point $\mathbf{r}_s$ when the field on the surface of V is taken to be the incident field. Hence, show that as $k \to 0$, we can derive an exact scattering transform given by

$$U(\mathbf{r}_s \mid \mathbf{r}_0) = \frac{1}{16\pi^2} \int_V \frac{\gamma(\mathbf{r})}{\mid \mathbf{r} - \mathbf{r}_0 \mid} \frac{d^3\mathbf{r}}{\mid \mathbf{r} - \mathbf{r}_s \mid}.$$

What information on the scatterer γ will the function U provide in the far fields?

II.10 Consider a dielectric screen with a constant relative permittivity which is of infinite extent but finite width Z in which a rectangular aperture with an area of XY is cut. Using a scalar wave theory, show that, under the Born approximation, the far field diffraction pattern observed in the forward image plane (x_0, y_0) at z_0 produced by the aperture (a 'thick slit') for a plane coherent light source (with wavelength λ) at normal incidence to the aperture is characterized by the function

$$\operatorname{sinc}\left(\frac{\pi x_0 X}{\lambda z_0}\right) \operatorname{sinc}\left(\frac{\pi y_0 Y}{\lambda z_0}\right).$$

Show that the diffraction pattern observed in the back image plane at $-z_0$ is characterized by the function

$$\operatorname{sinc}\left(\frac{\pi x_0 X}{\lambda z_0}\right) \operatorname{sinc}\left(\frac{\pi y_0 Y}{\lambda z_0}\right) \operatorname{sinc}(kZ).$$

II.11 Given that

$$u(\mathbf{r}, k) = u_i(\mathbf{r}, k) + k^2 g(\mid \mathbf{r} \mid, k) \otimes f(\mathbf{r})u(\mathbf{r}, k)$$

where $\otimes$ denotes the three dimensional convolution operation and g is the solution to the equation

$$(\nabla^2 + k^2)g = -\delta^3,$$

show that

$$f(\mathbf{r}) =$$

$$\frac{1}{u(\mathbf{r},k)}\nabla^2\left(q(\mathbf{r},k)\otimes g(\mid \mathbf{r}\mid,k)\otimes[u(\mathbf{r},k)-u_i(\mathbf{r},k)]-\frac{1}{k^2}[u(\mathbf{r},k)-u_i(\mathbf{r},k)]\right)$$

where q is the solution to the equation

$$q(\mid \mathbf{r}\mid,k)\otimes g(\mid \mathbf{r}\mid,k)=\frac{1}{4\pi\mid \mathbf{r}\mid}.$$

[Hint: Consider q to be a function such that $\nabla^2(q\otimes g)=-\delta^3$.]

II.12 For a CW incident spherical wave originating from a point $\mathbf{r}_0$, the three-dimensional Born scattered Helmholtz wavefield detected in the nearfield at a point $\mathbf{r}_s$ is given by

$$u_s(\mathbf{r}_s\mid \mathbf{r}_0,k)=k^2\int\limits_V g(\mathbf{r}\mid \mathbf{r}_0,k)g(\mathbf{r}\mid \mathbf{r}_s)\gamma(r)d^3\mathbf{r}$$

where γ is the scattering function, k is the wavenumber and g is the Green function given by

$$g(\mathbf{r}\mid \mathbf{r}',k)=\frac{\exp(ik\mid \mathbf{r}-\mathbf{r}'\mid)}{4\pi\mid \mathbf{r}-\mathbf{r}'\mid}.$$

By writing the Green functions in terms of a decomposition of plane waves, i.e. as

$$g(\mathbf{r}\mid \mathbf{r}',k)=\frac{1}{(2\pi)^3}\int\limits_{-\infty}^{\infty}d^3\mathbf{u}\frac{\exp[i\mathbf{u}\cdot(\mathbf{r}'-\mathbf{r})]}{u^2-k^2}$$

where $u=\mid \mathbf{u}\mid$, show that the inverse scattering solution is given by

$$\gamma(\mathbf{r})=\frac{1}{(2\pi)^3}\int\limits_{-\infty}^{\infty}d^3\mathbf{w}\exp(i\mathbf{w}\cdot\mathbf{r})\left(\frac{p^2}{k^2-1}\right)\left(\frac{q^2}{k^2-1}\right)$$

$$\times\int\limits_{-\infty}^{\infty}\int\limits_{-\infty}^{\infty}u_s(\mathbf{r}_s\mid \mathbf{r}_0,k)\exp(-i\mathbf{p}\cdot\mathbf{r}_0)\exp(-i\mathbf{q}\cdot\mathbf{r}_s)d^3\mathbf{r}_0d^3\mathbf{r}_s$$

where $\mathbf{w}=\mathbf{p}+\mathbf{q}$. If the incident field is a unit plane wave given by $\exp(ik\hat{\mathbf{n}}_i\cdot\mathbf{r})$ where $\hat{\mathbf{n}}_i$ is fixed, show that the inverse scattering solution is given by

$$\gamma(\mathbf{r})=\frac{\exp(-ik\hat{\mathbf{n}}_i\cdot\mathbf{r})}{(2\pi)^3}\int\limits_{-\infty}^{\infty}d^3\mathbf{p}\exp(i\mathbf{p}\cdot\mathbf{r})\left(\frac{p^2}{k^2}-1\right)\int\limits_{-\infty}^{\infty}\exp(-i\mathbf{p}\cdot\mathbf{r}_0)u_s(\mathbf{r}_0,k)d^3\mathbf{r}_0.$$

Interpret this result in terms of an experiment designed to generate a 3D image of γ using a square aperture. What are the factors affecting the resolution of the image in practice?

II.13 For a pulsed incident spherical wave originating from a point $\mathbf{r}_0$, the three-dimensional Born back-scattered Helmholtz wavefield detected in the nearfield at $\mathbf{r}_0$ is given by

$$u_{BS}(\mathbf{r}_0, k) = k^2 \int_V g^2(\mathbf{r} \mid \mathbf{r}_0, k)\gamma(r)d^3\mathbf{r}$$

where γ is the scattering function, $\mid k \mid < \infty$ is the wavenumber and g is the Green function given by

$$g(\mathbf{r} \mid \mathbf{r}_0, k) = \frac{\exp(ik \mid \mathbf{r} - \mathbf{r}_0 \mid)}{4\pi \mid \mathbf{r} - \mathbf{r}_0 \mid}.$$

(i) Show that this equation can be written as

$$w(\mathbf{r}_0, k) = \int_V g(\mathbf{r} \mid \mathbf{r}_0, k)\gamma(\mathbf{r})d^3\mathbf{r}$$

where

$$w(\mathbf{r}_0, k) = -16\pi i \frac{d}{dk}\left[\frac{u_{BS}(\mathbf{r}_0, k/2)}{k^2}\right].$$

(ii) By writing the Green function in terms of a decomposition of plane waves, i.e. as

$$g(\mathbf{r} \mid \mathbf{r}_0, k) = \frac{1}{(2\pi)^3} \int_{-\infty}^{\infty} d^3\mathbf{u} \frac{\exp[i\mathbf{u} \cdot (\mathbf{r}_0 - \mathbf{r})]}{u^2 - k^2}$$

where $u = \mid \mathbf{u} \mid$, show that the inverse scattering solution for a plane aperture at a fixed position z_0 is given by

$$\gamma(x, y, z) = \int_{-\infty}^{\infty}\int_{-\infty}^{\infty}\int_{-\infty}^{\infty} w(x_0, y_0, z_0, k)K(x - x_0, y - y_0, z - z_0, k)dkdx_0dy_0$$

where

$$K(x - x_0, y - y_0, z - z_0, k)$$

$$= -\frac{12i\pi^3}{(2\pi)^7} \int_0^{|k|} d\rho\rho e^{-i(z-z_0)\mathrm{sgn}(k)(k^2-\rho^2)^{\frac{1}{2}}} J_0(\rho[(x - x_0)^2 + (y - y_0)^2]^{\frac{1}{2}})$$

$$\mathrm{sgn}(k) = \begin{cases} +1, & k \geq 0; \\ -1, & k < 0. \end{cases}$$

Interpret this result in terms of an experiment designed to generate a 3D image of γ. What are the factors affecting the resolution of the image in practice?

In the programming problems that follow, n refers to the size of an image with $n \times n$ pixels.

II.14 Write a function to rotate a digital image (anti-clockwise) through a given angle (specified in degrees) using the nearest neighbour approximation (without corner clipping).

```
void ROTATE(float **s, float **r, int n, float theta)
```

where s is the input image, r is the output (rotated image) and theta is the angle of rotation.

II.15 Use function ROTATE to compute the Radon transform of an image.

```
void RADON(float **s, int n)
```

where s is the input/output.

II.16 Write a function to reconstruct an image from it projections - to compute the inverse Radon transform - using options for the following methods:

(i) back-projection and deconvolution.

(i) direct filtered back-projection (filtering each projection and back-projecting);

(iii) differentiation and the Hilbert transform method of filtered back-projection using a forward differencing method to differentiate each projection.

```
void IRADON(float **s, int n, int opt)
```

where s is the input/output and opt is a switch providing options on the method of reconstruction given above.

Generate a synthetic image consisting of a complex of rectangles, circles and lines, etc. Compute the Radon transform of this image and then study the result of computing its inverse using the options available. Observe the distortions that occur and account for their presence in terms of the computational methods used.

Part III

Digital Image Processing Methods

Chapter 12

Image Restoration and Reconstruction

Parts I and II have been concerned with the theoretical and computational foundations of imaging science and imaging systems. Part III of this work is concerned with methods for processing an image after is has been formed through the utilization of some image capture device or other imaging system.

In Part II it was shown that, for imaging systems that utilize a wavefield whose wavelength is the same order of magnitude as the scatterer, the Born approximation provides a solution for the measured field that is based on a Fourier transform, a result that is an inherent property of the linear systems approach to imaging science (see Chapter 11). This result yields the fundamental imaging equation

$$s = p \otimes \otimes f + n$$

which is a direct consequence of solving the single or Born scattering problem where f is the scattering function (the object function), p is the instrument function (the point spread function), s is the image and n is the noise which is taken to include all the non-ideal aspects of the imaging system that do not conform to the weak scattering condition, including multiple scattering, electronic noise, data error and so on. The problem then remains of how to recover f from s. This problem is known as deconvolution. It is the principal inverse problem in imaging science and for scatter-imaging system, is equivalent to solving the inverse scattering problem under the Born approximation. In previous chapters, we either ignored this problem or presented hypothetical solutions to this problem without discussing the variety of computational issues that can arise in practice. Deconvolution is now addressed within the context of being a general problem in digital imaging.

12.1 Introduction

All image formation systems are inherently resolution limited. Moreover, some images can be blurred and/or distorted due to a variety of physical effects that

determine the nature of the PSF, such as motion in the object or image planes, the effects of turbulence, light diffusion, limited aperture size and other physical effects. When an image is recorded that has been degraded in this manner, a number of digital image processing techniques can employed to 'de-blur' the image and enhance its information content. Nearly all of these techniques are either directly or indirectly based on a mathematical model for the blurred image which involves the convolution of two functions, i.e. the point spread function and the object function. Hence, 'de-blurring' an image amounts to solving the inverse problem posed by this model which is known as 'deconvolution'. Image restoration attempts to provide a resolution compatible with the bandwidth of the imaging system (a resolution limited system). Image reconstruction attempt to provide a resolution that is greater than the inherent resolution of the data (i.e. the resolution limit of the imaging system). This is often known as super resolution. In addition to this general inverse problem, there are specific deconvolution problems such as the reconstruction an image from a set of projections (see Chapter 8) and specialist problems such as the phase reconstruction problem which is addressed later on in this Chapter. The aim of this Chapter is to discuss: (i) basic methods of solution; (ii) essential algorithms; (iii) some applications.

Deconvolution is an inverse problem that is concerned with the restoration and/or reconstruction of information from known data. It depends critically on *a priori* knowledge of the way in which the data (the digital image) have been generated and recorded. Mathematically, the data obtained are usually related to some object function via an integral transform. In this sense deconvolution is concerned with inverting certain classes of integral equation, in particular, the convolution integral. In general, there is no exact or unique solution to the image restoration/ reconstruction problem because it is an ill-posed problem. We attempt to find a 'best estimate' based on some physically viable criterion subject to certain conditions.

The fundamental imaging equation is a stationary model for the image s in which the (blurring) effect of the PSF at any location in the 'object plane' is the same. For a coherent imaging system, p is the amplitude point spread function and, for an incoherent system, it is the intensity PSF (see Chapter 11). Using the convolution theorem we can write this equation in the form

$$S = PF + N$$

where S, P, F and N are the (2D) Fourier transforms of s, p, f and n, respectively. Assuming that F is a broadband spectrum, there are two cases we can consider:

(i) $P(k_x, k_y) \to 0$ as $(k_x, k_y) \to \infty$, where k_x and k_y are the spacial frequencies in the x and y directions, respectively. The image restoration problem can then be stated as 'recover F given S'.

(ii) $P(k_x, k_y)$ is band-limited, i.e. $P(k_x, k_y) = 0$ for certain values of k_x and/or k_y. The image reconstruction problem can then be stated as 'given S reconstruct F'. This typically requires the frequency components to be 'synthesized'

beyond the bandwidth of the data. This is a (spectral) extrapolation problem which is discussed in the following Chapter.

Consider an image restoration problem that involves finding a solution for f given that $s = p \otimes\otimes f + n$ where p is a Gaussian PSF given by (ignoring scaling)

$$p(x, y) = \exp[-(x^2 + y^2)/\sigma^2]$$

(σ being the standard deviation) which has a spectrum of the form (ignoring scaling)

$$P(k_x, k_y) = \exp[-\sigma^2(k_x^2 + k_y^2)].$$

This PSF is a piecewise continuous function as is its spectrum. An example of an image reconstruction problem is 'find f given that $s = p \otimes\otimes f + n$' where (ignoring scaling)

$$p(x, y) = \mathrm{sinc}(\alpha x)\,\mathrm{sinc}(\beta y).$$

This PSF has a spectrum of the form (ignoring scaling)

$$P(k_x, k_y) = H_\alpha(k_x)H_\beta(k_y)$$

where

$$H_\alpha(k_x) = \begin{cases} 1, & \mid k_x \mid \leq K_x; \\ 0, & \mid k_x \mid > K_x \end{cases} \quad \text{and} \quad H_\beta(k_y) = \begin{cases} 1, & \mid k_y \mid \leq K_y; \\ 0 & \mid k_y \mid > K_y. \end{cases}$$

This PSF is a piecewise continuous function but its spectrum is discontinuous, the bandwidth of $p \otimes\otimes f$ being given by K_x in the x-direction and K_y in the y-direction. In this Chapter we consider the problem of image restoration first and then consider how to extrapolate the spectrum of a band-limited image in the following Chapter.

12.2 Image Restoration

Let us consider a digital image that can be well-modelled using the discrete imaging equation

$$s_{ij} = p_{ij} \otimes\otimes f_{ij} + n_{ij}$$

where s_{ij} is the digital image. Suppose we neglect the term n_{ij}, then

$$s_{ij} = p_{ij} \otimes\otimes f_{ij}$$

or by the (discrete) convolution theorem

$$S_{ij} = P_{ij}F_{ij}$$

where S_{ij}, P_{ij} and F_{ij} and the DFTs of s_{ij}, p_{ij} and f_{ij}, respectively. Clearly,

$$F_{ij} = \frac{S_{ij}}{P_{ij}}$$

and therefore

$$f_{ij} = \hat{F}_2^{-1}\left(\frac{S_{ij}}{P_{ij}}\right)$$

where $\hat{F}_2^{-1}$ is taken to denote the discrete (inverse) Fourier transform. Note that

$$\frac{1}{P_{ij}} = \frac{P_{ij}^*}{\mid P_{ij} \mid^2}$$

which is called the Inverse Filter.

Suppose we were to implement this result on a digital computer. If P_{ij} approached zero (in practice a very small number) for any value of i and/or j then, depending on the compiler, the computer would respond with an output such as '... *arithmetic fault ... divide by zero*'. A simple solution would be to regularize the result, i.e. use

$$f_{ij} = \hat{F}_2^{-1}\left(\frac{P_{ij}^* S_{ij}}{\mid P_{ij} \mid^2 + \text{constant}}\right)$$

and 'play around' with the value of the constant until 'something sensible' was obtained which in turn would depend on the *a priori* information available on the form and support of f_{ij}. The regularization of the inverse filter is the basis for some of the methods which are discussed here. We start by considering the criterion associated with the inverse filter.

12.3 The Inverse Filter

The criterion for the inverse filter is that the mean square of the noise is a minimum. Since

$$s_{ij} = p_{ij} \otimes\otimes f_{ij} + n_{ij}$$

we can write

$$n_{ij} = s_{ij} - p_{ij} \otimes\otimes f_{ij}$$

and therefore

$$e = \|n_{ij}\|^2 = \|s_{ij} - p_{ij} \otimes\otimes f_{ij}\|^2$$

where

$$\|x_{ij}\| \equiv \left(\sum_i \sum_j x_{ij}^2\right)^{\frac{1}{2}}.$$

For the noise to be a minimum, we require

$$\frac{\partial e}{\partial f_{ij}} = 0.$$

Differentiating, we obtain

$$(s_{ij} - p_{ij} \otimes\otimes f_{ij}) \odot\odot p_{ij} = 0.$$

Using the (discrete) convolution and correlation theorems, in Fourier space, this equation becomes

$$(S_{ij} - P_{ij}F_{ij})P_{ij}^* = 0.$$

Hence, solving for F_{ij} we obtain the result

$$F_{ij} = \frac{P_{ij}^*}{\mid P_{ij} \mid^2} S_{ij}.$$

The inverse filter is therefore given by

$$\text{Inverse} \quad \text{Filter} = \frac{P_{ij}^*}{\mid P_{ij} \mid^2}$$

In principle, the inverse filter provides an exact solution to the problem when the noise term n_{ij} can be neglected. However, in practice, this solution is fraught with difficulties. First, the inverse filter is invariably a singular function. Equally bad is the fact that, even if the inverse filter is not singular, it is usually ill-conditioned. This is where the magnitude of P_{ij} goes to zero so quickly, as (i, j) increases, that $1/ \mid P_{ij} \mid^2$ rapidly acquires extremely large values. The effect of this is to amplify the (usually) noisy high frequency components of S_{ij}. This can lead to a restoration f_{ij} which is dominated by the noise in s_{ij}. The inverse filter can therefore only be used when:

(i) The filter is non-singular.

(ii) The signal-to-noise ratio (SNR) of the data is very large (i.e. $\|p_{ij} \otimes \otimes f_{ij}\| >> \|n_{ij}\|$).

Such conditions are rare. A notable exception occurs in computed tomography (see Chapter 8) in which the inverse filter associated with the 'Back-Project and Deconvolution' algorithm is non-singular and given by $\sqrt{k_x^2 + k_y^2}$.

The computational problems that arise from implementing the inverse filter can be avoided by using a variety of different filters whose individual properties and characteristics are suited to certain types of data. One of the most commonly used filters for image restoration is the Wiener filter which is considered next.

12.4 The Wiener Filter

An algorithm shall be derived for deconvolving images that have been blurred by some lowpass filtering process and corrupted by additive noise. In mathematical terms, given the imaging equation

$$s_{ij} = p_{ij} \otimes \otimes f_{ij} + n_{ij} \tag{12.1}$$

the problem is to solve for f_{ij} given s_{ij}, p_{ij} and some knowledge of the SNR. This problem is solved using the least squares principle which provides a filter known as the Wiener filter.

The Wiener filter is based on considering an estimate $\hat{f}_{ij}$ for f_{ij} of the form

$$\hat{f}_{ij} = q_{ij} \otimes \otimes s_{ij}. \tag{12.2}$$

Given this model our problem is reduced to computing q_{ij} or equivalently its Fourier transform Q_{ij}. To do this, we make use of the error function

$$e = \| f_{ij} - \hat{f}_{ij} \|^2 \equiv \sum_i \sum_j (f_{ij} - \hat{f}_{ij})^2 \tag{12.3}$$

and find q_{ij} such that e is a minimum, i.e.

$$\frac{\partial e}{\partial q_{ij}} = 0.$$

Substituting equation (12.2) into equation (12.3) and differentiating, we get

$$\frac{\partial e}{\partial q_{k\ell}} = -2 \sum_i \sum_j \left(f_{ij} - \sum_n \sum_m s_{i-n,j-m} q_{nm} \right) \frac{\partial}{\partial q_{k\ell}} \sum_n \sum_m s_{i-n,j-m} q_{nm}$$

$$= -2 \sum_i \sum_j \left(f_{ij} - \sum_n \sum_m s_{i-n,j-m} q_{nm} \right) s_{i-k,j-\ell} = 0.$$

Rearranging, we have

$$\sum_i \sum_j f_{ij} s_{i-k,j-\ell} = \sum_i \sum_j \left(\sum_n \sum_m s_{i-n,j-m} q_{nm} \right) s_{i-k,j-\ell}.$$

The left hand side of the above equation is a discrete correlation of f_{ij} with s_{ij} and the right hand side is a (discrete) correlation of s_{ij} with the convolution

$$\sum_n \sum_m s_{i-n,j-m} q_{nm}.$$

Using operator notation it is convenient to write this equation in the form

$$f_{ij} \odot \odot s_{ij} = (q_{ij} \otimes \otimes s_{ij}) \odot \odot s_{ij}.$$

Moreover, using the (discrete) correlation and convolution theorems, the equation above can be written in Fourier space as

$$F_{ij} S^*_{ij} = Q_{ij} S_{ij} S^*_{ij}$$

which, after rearranging, gives

$$Q_{ij} = \frac{S^*_{ij} F_{ij}}{| S_{ij} |^2}.$$

Now, in Fourier space, equation (12.1) becomes

$$S_{ij} = P_{ij} F_{ij} + N_{ij}$$

Using this result, we have

$$S_{ij}^* F_{ij} = (P_{ij}F_{ij} + N_{ij})^* F_{ij}$$

$$= P_{ij}^* \mid F_{ij} \mid^2 + N_{ij}^* F_{ij}$$

and

$$\mid S_{ij} \mid^2 = S_{ij}S_{ij}^* = (P_{ij}F_{ij} + N_{ij})(P_{ij}F_{ij} + N_{ij})^*$$

$$= \mid P_{ij} \mid^2 \mid F_{ij} \mid^2 + P_{ij}F_{ij}N_{ij}^* + N_{ij}P_{ij}^*F_{ij}^* + \mid N_{ij} \mid^2 .$$

Hence, the filter Q_{ij} can be written in the form

$$Q_{ij} = \frac{P_{ij}^* \mid F_{ij} \mid^2 + N_{ij}^* F_{ij}}{\mid P_{ij} \mid^2 \mid F_{ij} \mid^2 + D_{ij} + \mid N_{ij} \mid^2}$$

where

$$D_{ij} = P_{ij}F_{ij}N_{ij}^* + N_{ij}P_{ij}^*F_{ij}^*$$

12.4.1 Signal Independent Noise

At first sight the result above appears to be more complicated than the original one. However, this result can be simplified further by imposing a condition which is physically valid in the large majority of cases. The condition is that f_{ij} and n_{ij} are uncorrelated, i.e.

$$f_{ij} \odot \odot n_{ij} = 0$$

and

$$n_{ij} \odot \odot f_{ij} = 0.$$

In this case the noise is said to be 'signal independent' and it follows from the correlation theorem that

$$F_{ij}N_{ij}^* = 0$$

and

$$N_{ij}F_{ij}^* = 0.$$

These conditions allow us to cancel the cross terms present in the last expression for Q_{ij} (i.e. set $D_{ij} = 0$ and $N_{ij}^* F_{ij} = 0$), leaving us with the formula

$$Q_{ij} = \frac{P_{ij}^* \mid F_{ij} \mid^2}{\mid P_{ij} \mid^2 \mid F_{ij} \mid^2 + \mid N_{ij} \mid^2}.$$

Finally, rearranging, we obtain the expression for the least squares or Wiener filter,

$$Q_{ij} = \frac{P_{ij}^*}{\mid P_{ij} \mid^2 + \mid N_{ij} \mid^2 / \mid F_{ij} \mid^2}.$$

12.4.2 Estimation of the SNR

From the algebraic form of the Wiener filter derived above it is clear that this particular filter depends on: (i) the functional form of P_{ij} (e.g. the optical transfer function) that is used; (ii) the functional form of $\mid N_{ij} \mid^2 / \mid F_{ij} \mid^2$. The optical transfer function of an imaging system can be computed from the point spread function by literally imaging a single point source which leaves us with the problem of estimating the noise-to-signal power ratio $\mid N_{ij} \mid^2 / \mid F_{ij} \mid^2$. This problem can be solved if we have access to two successive images recorded under identical conditions.

Consider two digital images denoted by s_{ij} and s'_{ij} of the same object function f_{ij} recorded using the same PSF p_{ij} (i.e. imaging system) but at different times and hence with different noise fields n_{ij} and n'_{ij}. These images are given by

$$s_{ij} = p_{ij} \otimes \otimes f_{ij} + n_{ij}$$

and

$$s'_{ij} = p_{ij} \otimes \otimes f_{ij} + n'_{ij}$$

respectively, where the noise functions are uncorrelated and signal independent, i.e.

$$n_{ij} \odot \odot n'_{ij} = 0 \tag{12.4}$$

$$f_{ij} \odot n_{ij} = n_{ij} \odot \odot f_{ij} = 0 \tag{12.5}$$

and

$$f_{ij} \odot \odot n'_{ij} = n'_{ij} \odot \odot f_{ij} = 0. \tag{12.6}$$

We now proceed to compute the autocorrelation function of s_{ij} given by

$$c_{ij} = s_{ij} \odot \odot s_{ij}.$$

Using the correlation theorem and employing equation (12.5) we find

$$C_{ij} = S_{ij} S^*_{ij} = (P_{ij} F_{ij} + N_{ij})(P_{ij} F_{ij} + N_{ij})^*$$

$$= \mid P_{ij} \mid^2 \mid F_{ij} \mid^2 + \mid N_{ij} \mid^2$$

where C_{ij} is the DFT of c_{ij}. Next, we correlate s_{ij} with s'_{ij} giving the cross-correlation function

$$c'_{ij} = s_{ij} \odot \odot s'_{ij}.$$

Using the correlation theorem again and, this time, employing equations (12.4) and (12.6) we get

$$C'_{ij} = \mid P_{ij} \mid^2 \mid F_{ij} \mid^2 + P_{ij} F_{ij} N'^*_{ij} + N_{ij} P^*_{ij} F^*_{ij} + N_{ij} N'^*_{ij}$$

$$= \mid P_{ij} \mid^2 \mid F_{ij} \mid^2 .$$

The noise-to-signal ratio can now be obtained by dividing C_{ij} by C'_{ij} giving

$$\frac{C_{ij}}{C'_{ij}} = 1 + \frac{\mid N_{ij} \mid^2}{\mid P_{ij} \mid^2 \mid F_{ij} \mid^2}.$$

Re-arranging, we obtain the result

$$\frac{\mid N_{ij} \mid^2}{\mid F_{ij} \mid^2} = \left(\frac{C_{ij}}{C'_{ij}} - 1 \right) \mid P_{ij} \mid^2 .$$

Note that both C_{ij} and C'_{ij} can be obtained from the available data s_{ij} and s'_{ij}. Also, substituting this result into the formula for Q_{ij}, we obtain an expression for the Wiener filter in terms of C_{ij} and C'_{ij} given by

$$Q_{ij} = \frac{P^*_{ij}}{\mid P_{ij} \mid^2} \frac{C'_{ij}}{C_{ij}}.$$

In those cases where the user has access to successive recordings, the method of computing the noise-to-signal power ratio described above can be employed. The problem is that in many practical cases, we do not have access to successive images and, hence, the cross-correlation function c'_{ij} cannot be computed. In this case, we are forced to make an approximation and consider a Wiener filter of the form

$$\text{Wiener} \quad \text{Filter} = \frac{P^*_{ij}}{\mid P_{ij} \mid^2 + \text{constant}}.$$

The constant ideally reflects any available information on the average signal-to-noise ratio of the image. Typically, we consider an expression of the form

$$\text{constant} = \frac{1}{(\text{SNR})^2}$$

where SNR is the signal-to-noise ratio for the filter[1]. In practice, the exact value of this constant must be chosen by the user.

Before attempting to deconvolve an image the user must at least have some *a priori* knowledge on the functional form of the point spread function. Absence of this information leads to a method of approach known as 'Blind Deconvolution'. Suppose that the Point Spread Function is Gaussian, i.e.

$$p_{ij} = \exp[-(i^2 + j^2)/\sigma^2]$$

where σ is the standard deviation which must be defined by the user. In this case, the user has control of two parameters: (i) the standard deviation of the Gaussian PSF; (ii) the SNR. In practice, the user must adjust these parameters until a suitable 'user optimized' reconstruction is obtained. In other words, the Wiener filter must be 'tuned' to give a result which is acceptable based on the judgment and intuition of the user. This interactive approach to image restoration is just one of many practical problems associated with deconvolution which should ideally be executed in real time. Figure 12.1 gives an example of the application of the Wiener filter using a Gaussian PSF and the example MATLAB function given below.

[1] which is not necessarily the same as the SNR of the data!

```
function WIENER_FILTER(sigma,snr_filter)
%
%Input:
%      sigma- standard deviation of Gaussian IRF
%      snr_filter - signal-to-noise ratio for
%                   computing the Wiener filter
%
%Output:
%       f - Restored image.


%Read image (assumed to be .bmp file of size n x n)

s=imread('test','bmp');

n=size(s,1);   %Set size of array
nn=1+n/2; %Set mid point of array

%Convert to normalized floating point array
s=im2double(s);

%Display image
subplot(1,3,1), imshow(s);

%Compute Gaussian PSF
 for i=1:n
   x=i-nn;

    for j=1:n
      y=j-nn;
        p(i,j)=exp(-((x.*x)+(y.*y))/(sigma*sigma));
    end

end

%Display PSF
subplot(1,3,2), imshow(p);


%Restore image using Wiener filter:

%Transform image and PSF into Fourier space.
s=fftshift(fft2(s));
p=fftshift(fft2(p));

%Compute Wiener filter.
gamma=1./(snr_filter).^2;
```

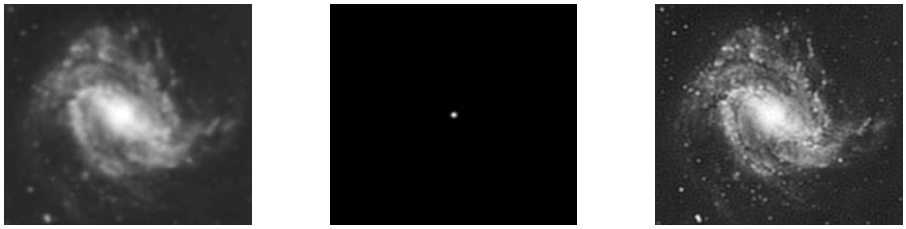

Figure 12.1: Example of the application of the Wiener filter. Original image (left), Gaussian point spread function (center) and restoration after application of the Wiener filter (right) using a standard deviation of 3 pixels and SNR=1.

```
f=(conj(p).*s)./((abs(p).*abs(p))+gamma);

%Transform back into imagfe space and
%computing the absolute value.
f=fftshift(ifft2(f));
f=abs(f);

%Normalize and display result
f=f./max(max(f));
subplot(1,3,3), imshow(f);
```

12.5 The Power Spectrum Equalization Filter

As the name implies the Power Spectrum Equalization (PSE) filter is based on finding an estimate $\hat{f}_{ij}$ whose power spectrum is equal to the power spectrum of the desired function f_{ij}. In other words, $\hat{f}_{ij}$ is obtained by employing the criterion

$$\mid F_{ij} \mid^2 = \mid \hat{F}_{ij} \mid^2$$

together with the linear convolution model

$$\hat{f}_{ij} = q_{ij} \otimes \otimes s_{ij}.$$

Like the Wiener filter the PSE filter also assumes that the noise is signal independent. Since

$$\hat{F}_{ij} = Q_{ij} S_{ij} = Q_{ij}(P_{ij} F_{ij} + N_{ij})$$

and given that $N_{ij}^* F_{ij} = 0$ and $F_{ij}^* N_{ij} = 0$, we have

$$\mid \hat{F}_{ij} \mid^2 = \hat{F}_{ij}\hat{F}_{ij}^* = \mid Q_{ij} \mid^2 (\mid P_{ij} \mid^2 \mid F_{ij} \mid^2 + \mid N_{ij} \mid^2).$$

Using the PSE criterion and solving for $\mid Q_{ij} \mid$, we obtain

$$\mid Q_{ij} \mid = \left(\frac{1}{\mid P_{ij} \mid^2 + \mid N_{ij} \mid^2 / \mid F_{ij} \mid^2} \right)^{\frac{1}{2}}.$$

In the absence of accurate estimates for the noise-to-signal power ratio (i.e. $\mid N_{ij} \mid^2 / \mid F_{ij} \mid^2$), we approximate the PSE filter by

$$\text{PSE filter} = \left(\frac{1}{\mid P_{ij} \mid^2 + \text{constant}} \right)^{\frac{1}{2}}$$

where

$$\text{constant} = \frac{1}{(\text{SNR})^2}.$$

Note that the criterion used to derive this filter can be written in the form

$$\sum_i \sum_j (\mid F_{ij} \mid^2 - \mid \hat{F}_{ij} \mid^2) = 0$$

or, using Parseval's theorem,

$$\sum_i \sum_j (\mid f_{ij} \mid^2 - \mid \hat{f}_{ij} \mid^2) = 0.$$

Compare this criterion with that use for the Wiener filter, i.e.

$$\text{Minimize} \quad \sum_i \sum_j (f_{ij} - \hat{f}_{ij})^2.$$

12.6 The Matched Filter

Matched filtering is based on correlating the image s_{ij} with the complex conjugate of the PSF p_{ij}. The estimate $\hat{f}_{ij}$ of f_{ij} can therefore be written as

$$\hat{f}_{ij} = p_{ij}^* \odot \odot s_{ij}.$$

Assuming that $n_{ij} = 0$, so that

$$s_{ij} = p_{ij} \otimes \otimes f_{ij}$$

we have

$$\hat{f}_{ij} = p_{ij}^* \odot \odot p_{ij} \otimes \otimes f_{ij}$$

which in Fourier space is

$$\hat{F}_{ij} = \mid P_{ij} \mid^2 F_{ij}.$$

Observe that the amplitude spectrum of $\hat{F}_{ij}$ is given by $\mid P_{ij} \mid^2 \mid F_{ij} \mid$ and that the phase information is determined by F_{ij} alone.

12.6.1 Criterion for the Matched Filter

The criterion for the matched filter is as follows. Given that

$$s_{ij} = p_{ij} \otimes \otimes f_{ij} + n_{ij}$$

the matched filter provides an estimate for f_{ij} of the form

$$\hat{f}_{ij} = q_{ij} \otimes \otimes s_{ij}$$

where q_{ij} is chosen in such a way that the ratio

$$R = \frac{|\sum_i \sum_j Q_{ij} P_{ij}|^2}{\sum_i \sum_j |N_{ij}|^2 |Q_{ij}|^2}$$

is a maximum.

The matched filter Q_{ij} is found by first writing

$$Q_{ij} P_{ij} = |N_{ij}| Q_{ij} \times \frac{P_{ij}}{|N_{ij}|}$$

and then using the (Schwarz) inequality

$$\left| \sum_i \sum_j Q_{ij} P_{ij} \right|^2 = \left| \sum_i \sum_j |N_{ij}| Q_{ij} \frac{P_{ij}}{|N_{ij}|} \right|^2$$

$$\leq \sum_i \sum_j |N_{ij}|^2 |Q_{ij}|^2 \sum_i \sum_j \frac{|P_{ij}|^2}{|N_{ij}|^2}.$$

From this result and the definition of R given above we get

$$R \leq \sum_i \sum_j \frac{|P_{ij}|^2}{|N_{ij}|^2}.$$

Now, recall that the criterion for the matched filter is that R is a maximum. If this is the case, then

$$R = \sum_i \sum_j \frac{|P_{ij}|^2}{|N_{ij}|^2}$$

or

$$\left| \sum_i \sum_j |N_{ij}| Q_{ij} \frac{P_{ij}}{|N_{ij}|} \right|^2 = \sum_i \sum_j |N_{ij}|^2 |Q_{ij}|^2 \sum_i \sum_j \frac{|P_{ij}|^2}{|N_{ij}|^2}.$$

But this is true if and only if

$$|N_{ij}| Q_{ij} = \frac{P_{ij}^*}{|N_{ij}|}$$

because we then have

$$\left| \sum_i \sum_j \frac{\mid P_{ij} \mid^2}{\mid N_{ij} \mid^2} \right|^2 = \sum_i \sum_j \frac{\mid P_{ij} \mid^2}{\mid N_{ij} \mid^2} \sum_i \sum_j \frac{\mid P_{ij} \mid^2}{\mid N_{ij} \mid^2}.$$

Thus, R is a maximum when

$$Q_{ij} = \frac{P_{ij}^*}{\mid N_{ij} \mid^2}.$$

12.6.2 The Matched Filter for White Noise

If the noise n_{ij} is white, then its power spectrum can be assumed to be a constant, i.e.

$$\mid N_{ij} \mid^2 = N_0^2.$$

In this case

$$Q_{ij} = \frac{P_{ij}^*}{N_0^2}$$

and

$$\hat{F}_{ij} = \frac{P_{ij}^*}{N_0^2} S_{ij}.$$

Hence, for white noise, the matched filter provides an estimate which may be written in the form

$$\hat{f}_{ij} = \frac{1}{N_0^2} p_{ij}^* \odot \odot s_{ij}.$$

12.6.3 Deconvolution of a Linear FM PSF

The matched filter is frequently used in coherent imaging systems whose PSF is characterized by a linear frequency modulated response. Two well known examples are Synthetic Aperture Radar (see Chapter 10) and imaging systems that use (Fresnel) zone plates. In this section we shall consider a separable linear FM PSF and also switch to a continuous noise free functional form which makes the analysis easier. Thus, consider the case when the PSF is given by

$$p(x, y) = \exp(i\alpha x^2) \exp(i\beta y^2); \quad \mid x \mid \leq X, \quad \mid y \mid \leq Y$$

where α and β are constants and X and Y determine the spatial support of the PSF. The phase of this PSF (in the x-direction say) is αx^2 and the instantaneous frequency is given by

$$\frac{d}{dx}(\alpha x^2) = 2\alpha x$$

which varies linearly with x. Hence, the frequency modulations (in both x and y) are linear which is why the PSF is referred to as a linear FM PSF. In this case the image that is obtained is given by (neglecting additive noise)

$$s(x, y) = \exp(i\alpha x^2) \exp(i\beta y^2) \otimes \otimes f(x, y); \quad \mid x \mid \leq X, \quad \mid y \mid \leq Y.$$

Matched filtering, we get

$$\hat{f}(x,y) = \exp(-i\alpha x^2)\exp(-i\beta y^2) \odot \odot \exp(i\alpha x^2)\exp(i\beta y^2) \otimes \otimes f(x,y).$$

Now,

$$\exp(-i\alpha x^2) \odot \exp(i\alpha x^2) = \int_{-X/2}^{X/2} \exp[-i\alpha(z+x)^2]\exp(i\alpha z^2)dz$$

$$= \exp(-i\alpha x^2) \int_{-X/2}^{X/2} \exp(2i\alpha zx)dz.$$

Evaluating the integral over z, we have

$$\exp(-i\alpha x^2) \odot \exp(i\alpha x^2) = X\exp(-i\alpha x^2)\operatorname{sinc}(\alpha X x).$$

Since the evaluation of the correlation integral over y is identical we can write

$$\hat{f}(x,y) = XY\exp(-i\alpha x^2)\exp(-i\beta y^2)\operatorname{sinc}(\alpha X x)\operatorname{sinc}(\beta Y y) \otimes \otimes f(x,y).$$

In many systems the spatial support of the linear FM PSF is relatively long. In this case,

$$\cos(\alpha x^2)\operatorname{sinc}(\alpha X x) \simeq \operatorname{sinc}(\alpha X x), \quad \cos(\beta y^2)\operatorname{sinc}(\beta Y y) \simeq \operatorname{sinc}(\beta Y y)$$

and

$$\sin(\alpha x^2)\operatorname{sinc}(\alpha X x) \simeq 0, \quad \sin(\beta y^2)\operatorname{sinc}(\beta Y y) \simeq 0$$

and so

$$\hat{f}(x,y) \simeq XY\operatorname{sinc}(\alpha X x)\operatorname{sinc}(\beta Y y) \otimes \otimes f(x,y).$$

In Fourier space this last equation can be written as

$$\hat{F}(k_x,k_y) = \begin{cases} \frac{\pi^2}{\alpha\beta}F(k_x,k_y), & \mid k \mid \leq \alpha X, \quad \mid k \mid \leq \beta Y; \\ 0, & \text{otherwise.} \end{cases}$$

The estimate $\hat{f}$ is therefore a band limited estimate of f whose bandwidth is determined by the product of the parameters α and β with the spatial supports X and Y, respectively. Note that the larger the values of αX and βY, the greater the bandwidth of the reconstruction.

An example of deconvolving an image by correlating it with a circularly symmetric linear FM PSF is given in Figure 12.2. In this example, an image has been convolved with the PSF

$$p(x,y) = \frac{1}{2} + \frac{1}{2}\cos[\alpha(x^2+y^2)]$$

and the reconstruction obtained by correlation alone. The result is excellent. The PSF here is an example of a zone plate that can be used to perform the same role as a lens in imaging systems where a conventional lens system is not available.

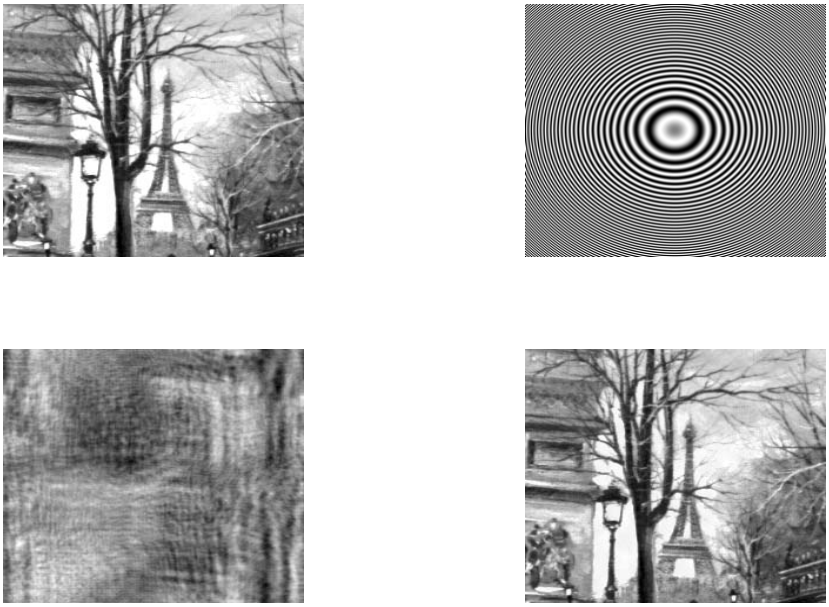

Figure 12.2: Original image of the Eiffel Tower in Paris (top-left), the PSF with distortions due to the effect of aliasing (top-right), convolution of the image with the PSF (bottom-left) and recovery of the image by correlating with the PSF (bottom-right).

12.7 Maximum Entropy Deconvolution

As before we are interested in solving the imaging equation

$$s_{ij} = p_{ij} \otimes \otimes f_{ij} + n_{ij}$$

for the object function f_{ij}. Instead of using a least squares error to constrain the solution for f_{ij}, we choose to find f_{ij} such that the entropy E, given by

$$E = -\sum_i \sum_j f_{ij} \ln f_{ij}$$

is a maximum. Note that because the ln function is used in defining the Entropy, the Maximum Entropy Method (MEM) must be restricted to cases where f_{ij} is real and positive.

From the imaging equation above, we can write

$$s_{ij} - \sum_n \sum_m p_{i-n,j-m} f_{nm} = n_{ij}$$

where we have just written the convolution operation out in full. Squaring both sides and summing over i and j we can write

$$\sum_i \sum_j \left(s_{ij} - \sum_n \sum_m p_{i-n,j-m} f_{nm} \right)^2 - \sum_i \sum_j n_{ij}^2 = 0.$$

But this equation is true for any constant λ multiplying both terms on the left hand side. We can therefore write the equation for E as

$$E = -\sum_i \sum_j f_{ij} \ln f_{ij}$$

$$+\lambda \left[\sum_i \sum_j \left(s_{ij} - \sum_n \sum_m p_{n-i,m-j} f_{nm} \right)^2 - \sum_i \sum_j n_{ij}^2 \right]$$

because the second term on the right hand side is zero anyway (for all values of the Lagrange multiplier λ). Given this equation, our problem is to find f_{ij} such that the entropy E is a maximum, i.e.

$$\frac{\partial E}{\partial f_{ij}} = 0.$$

Differentiating, and switching to the notation for 2D convolution $\otimes\otimes$ and 2D correlation $\odot\odot$, we find that E is a maximum when

$$1 + \ln f_{ij} - 2\lambda(s_{ij} \odot\odot p_{ij} - p_{ij} \otimes\otimes f_{ij} \odot\odot p_{ij}) = 0$$

or, after rearranging,

$$f_{ij} = \exp[-1 + 2\lambda(s_{ij} \odot\odot p_{ij} - p_{ij} \otimes\otimes f_{ij} \odot\odot p_{ij})].$$

This equation is transcendental in f_{ij} and, as such, requires that f_{ij} is evaluated iteratively, i.e.

$$f_{ij}^{k+1} = \exp[-1 + 2\lambda(s_{ij} \odot\odot p_{ij} - p_{ij} \otimes\otimes f_{ij}^k \odot\odot p_{ij})]; \quad k = 0, 1, 2, ..., N$$

where $f_{ij}^0 = 0 \ \ \forall \ \ i, j$, say. The rate of convergence of this solution is determined by the value of the Lagrange multiplier that is used.

In general, the iterative nature of this nonlinear estimation method is undesirable, primarily because it is time consuming and may require many iterations before a solution is achieved with a desired tolerance. We shall end this Section by demonstrating a rather interesting result which is based on linearizing the MEM. This is achieved by retaining the first two terms (i.e. the linear terms) in the series representation of the exponential function leaving us with the following equation

$$f_{ij} = 2\lambda(s_{ij} \odot\odot p_{ij} - p_{ij} \otimes\otimes f_{ij} \odot\odot p_{ij}).$$

Using the convolution and correlation theorems, in Fourier space, this equation becomes

$$F_{ij} = 2\lambda S_{ij} P_{ij}^* - 2\lambda \mid P_{ij} \mid^2 F_{ij}.$$

Rearranging, we get

$$F_{ij} = \frac{S_{ij}P_{ij}^*}{\mid P_{ij} \mid^2 + 1/2\lambda}.$$

Hence, we can define a linearized maximum entropy filter of the form

$$\frac{P_{ij}^*}{\mid P_{ij} \mid + 1/2\lambda}.$$

Notice that this filter is very similar to the Wiener filter. The only difference is that the Wiener filter is regularized by a constant determined by the SNR whereas this filter is regularized by a constant determined by the Lagrange multiplier.

12.8 Constrained Deconvolution

Constrained deconvolution provides a filter which gives the user additional control over the deconvolution process. This method is based on minimizing a linear operation on the object f_{ij} of the form $g_{ij} \otimes\otimes f_{ij}$ subject to some other constraint. Using the least squares approach, we find an estimate for f_{ij} by minimizing $\|g_{ij} \otimes\otimes f_{ij}\|^2$ subject to the constraint

$$\|s_{ij} - p_{ij} \otimes\otimes f_{ij}\|^2 = \|n_{ij}\|^2$$

where

$$\|x_{ij}\|^2 \equiv \sum_i \sum_j x_{ij}^2.$$

Using this result we can write

$$\|g_{ij} \otimes\otimes f_{ij}\|^2 = \|g_{ij} \otimes\otimes f_{ij}\|^2 + \lambda(\|s_{ij} - p_{ij} \otimes\otimes f_{ij}\|^2 - \|n_{ij}\|^2)$$

because the quantity inside the brackets on the right hand side is zero. The constant λ is called the Lagrange multiplier. The function $\|g_{ij} \otimes\otimes f_{ij}\|^2$ is a minimum when

$$(g_{ij} \otimes\otimes f_{ij}) \odot\odot g_{ij} - \lambda(s_{ij} - p_{ij} \otimes\otimes f_{ij}) \odot\odot p_{ij} = 0.$$

In Fourier space, this equation becomes

$$\mid G_{ij} \mid^2 F_{ij} - \lambda(S_{ij}P_{ij}^* - \mid P_{ij} \mid^2 F_{ij}) = 0.$$

Solving for F_{ij}, we obtain

$$F_{ij} = \frac{S_{ij}P_{ij}^*}{\mid P_{ij} \mid^2 + \gamma \mid G_{ij} \mid^2}$$

where γ is the reciprocal of the Lagrange multiplier ($= 1/\lambda$). Hence, the constrained least squares filter is given by

$$\text{Constrained Least Squares Filter} = \frac{P_{ij}^*}{\mid P_{ij} \mid^2 + \gamma \mid G_{ij} \mid^2}.$$

The important point about this filter is that it allows the user to change G_{ij} to suit a particular application. This filter can be thought of as a generalization of the other filters. For example, if $\gamma = 0$ then the inverse filter is obtained, if $\gamma = 1$ and $\mid G_{ij} \mid^2 = \mid N_{ij} \mid^2 / \mid F_{ij} \mid^2$ then the Wiener filter is obtained, and if $\gamma = 1$ and $\mid G_{ij} \mid^2 = \mid N_{ij} \mid^2 - \mid P_{ij} \mid^2$ then the matched filter is obtained.

The following table lists the filters discussed so far. In each case, the filter Q_{ij} provides a solution to the inversion of the following equation

$$s_{ij} = p_{ij} \otimes\otimes f_{ij} + n_{ij},$$

the solution for f_{ij} being given by

$$f_{ij} = \hat{F}_2^{-1}[Q_{ij} S_{ij}]$$

where $\hat{F}_2^{-1}$ stands for the 2D Discrete Inverse Fourier Transform and S_{ij} is the DFT of the digital image s_{ij}. In all cases, the DFT and inverse DFT can be computed using a FFT.

Name of Filter	Filter	Condition(s)
Inverse	$Q_{ij} = P_{ij}^* / \mid P_{ij} \mid^2$	Min $\|n_{ij}\|$
Wiener	$Q_{ij} = \frac{P_{ij}^*}{\|P_{ij}\|^2 + \|F_{ij}\|^2 / \|N_{ij}\|^2}$	Min $\|f_{ij} - q_{ij} \otimes\otimes s_{ij}\|^2$; $N_{ij}^* F_{ij} = 0, \quad F_{ij}^* N_{ij} = 0$
PSE	$Q_{ij} = \left(\frac{1}{\|P_{ij}\|^2 + \|F_{ij}\|^2 / \|N_{ij}\|^2} \right)^{\frac{1}{2}}$	$\mid F_{ij} \mid^2 = \mid Q_{ij} S_{ij} \mid^2$; $N_{ij}^* F_{ij} = 0, \quad F_{ij}^* N_{ij} = 0$
Matched	$Q_{ij} = P_{ij}^* / \mid N_{ij} \mid^2$	Max $\frac{\|\sum_i \sum_j Q_{ij} P_{ij}\|^2}{\sum_i \sum_j \|N_{ij}\|^2 \|Q_{ij}\|^2}$
Max Entropy	$Q_{ij} = \frac{P_{ij}^*}{\|P_{ij}\|^2 + 1/\lambda}$	Max $-\sum_i \sum_j f_{ij} \ln f_{ij}$
Constrained	$Q_{ij} = \frac{P_{ij}^*}{\|P_{ij}\|^2 + \gamma \|G_{ij}\|^2}$	Min $\|g_{ij} \otimes\otimes f_{ij}\|^2$

12.9 Phase Reconstruction and Phase Imaging

The phase reconstruction problem and phase imaging in general occurs in applications where:

(i) information on the phase is available from the recorded data and it is required to generate a phase image;

(ii) information on the phase is not available from the data and the phase needs to be reconstructed.

Consider an imaging system in which the Born scattered field generated by an object function $f(x, y)$ is measured in the far field. The recorded field in the image plane is then given by the Fourier transform of the object function (see Chapter 11), i.e.

$$F(k_x, k_y) = \int\int f(x, y) \exp(-ik_x x) \exp(-ik_y y) dxdy.$$

Now, for complex recorded data F, the object function can be obtained by Fourier inversion. Further, if the object function is a complex function involving data that have been generated using a time-resolved coherent system (e.g. diffraction tomography - see Chapter 9 - or real/synthetic aperture radar - see Chapter 10) in which the quadrature component of the recorded signals is available, then a phase image can be generated from the object function. This is the basis for phase imaging. However, with an incoherent imaging system, data are only available on the recorded intensity of the field. In this case, we do not measure

$$F(k_x, k_y) = A(k_x, k_y) \exp[i\theta(k_x, k_y)]$$

but

$$\mid F(k_x, k_y) \mid^2 = [A(k_x, k_y)]^2.$$

In order to reconstruct the object function $f(x, y)$ we are required to retrieve the (Fourier) phase function $\theta(k_x, k_y)$. This problem and its solution have a number of important applications, most notably in high frequency diffraction based imaging systems such as X-ray crystallography in which X-rays are diffracted by the atomic structure from which the solid is composed. The diffraction pattern that is recorded is, in effect, given by the power spectrum of the atomic structure of the crystal projected onto the image plane - the object function $f(x, y)$. This can be shown by considering the (Green function) solution to the inhomogeneous Helmholtz equation

$$(\nabla^2 + k^2) u(\mathbf{r}, k) = -k^2 \gamma(\mathbf{r}) u(\mathbf{r}, k), \quad \mathbf{r} \in V$$

which is given by the Lippmann-Schwinger equation (see Chapter 6)

$$u(\mathbf{r}_0, k) = u_i(\mathbf{r}_0, k) + k^2 \int_V \frac{\exp(ik \mid \mathbf{r} - \mathbf{r}_0 \mid)}{4\pi \mid \mathbf{r} - \mathbf{r}_0 \mid} \gamma(\mathbf{r}) u(\mathbf{r}, k) d^3\mathbf{r}$$

where u_i is the incident field. Under the Born approximation and in the far field,

$$u(\mathbf{r}_0, k) = u_i(\mathbf{r}_0, k) + k^2 \frac{\exp(ikr_0)}{4\pi r_0} \int_V \exp(-ik\hat{\mathbf{n}}_0 \cdot \mathbf{r}) \gamma(\mathbf{r}) u_i(\mathbf{r}, k) d^3\mathbf{r}, \quad r_0 \to \infty$$

where

$$\hat{\mathbf{n}}_0 = \frac{\mathbf{r}_0}{r_0}.$$

Let the field u be recorded in the plane defined by the coordinates x_0 and y_0 at a large distance z_0 from the scatterer γ and let the scatterer have a Cartesian volume of XYZ. Then

$$r_0 = (x_0^2 + y_0^2 + z_0^2)^{\frac{1}{2}} = z_0 \left(1 + \frac{x_0^2}{z_0^2} + \frac{y_0^2}{z_0^2}\right)^{\frac{1}{2}} \simeq z_0, \quad \frac{x_0}{z_0} << 1, \quad \frac{y_0}{z_0} << 1$$

$$\hat{\mathbf{n}}_0 \cdot \mathbf{r} = \frac{1}{r_0}(xx_0 + yy_0 + zz_0) \simeq \frac{1}{z_0}(xx_0 + yy_0 + zz_0)$$

and

$$u(x_0, y_0, z_0, k) = u_i(x_0, y_0, z_0, k) + \frac{\exp(ikz_0)}{4\pi z_0}$$

$$\times \int_{-X/2}^{X/2} \int_{-Y/2}^{Y/2} \int_{-Z/2}^{Z/2} \gamma(x, y, z) \exp\left[-\frac{ik}{z_0}(xx_0 + yy_0)\right] \exp(-ikz) u_i(x, y, z, k) dx dy dz.$$

Now, if u_i is a unit plane wave travelling along z, then, with $u_i = \exp(ikz)$, we have

$$u(x_0, y_0, z_0, k) = \exp(ikz_0)$$

$$+\frac{\exp(ikz_0)}{4\pi z_0} \int_{-X/2}^{X/2} \int_{-Y/2}^{Y/2} \int_{-Z/2}^{Z/2} \gamma(x, y, z) \exp(-ikxx_0/z_0) \exp(-ikyy_0/z_0) dx dy dz$$

$$= \exp(ikz_0) + \frac{\exp(ikz_0)}{4\pi z_0} F(k_x, k_y)$$

where

$$F(k_x, k_y) = \int_{-X/2}^{X/2} \int_{-Y/2}^{Y/2} f(x, y) \exp(-ik_x x) \exp(-ik_y y) dx dy,$$

$$f(x, y) = \int_{-Z/2}^{Z/2} \gamma(x, y, z) dz$$

and

$$k_x = \frac{kx_0}{z_0}, \quad k_y = \frac{ky_0}{z_0}.$$

Thus, ignoring scaling, the diffracted field in the plane at z_0 is given by the 2D Fourier transform of the object function f which is a projection along z of the scattering function γ.

The (Fourier) phase function is crucial in the reconstruction of the object function. Of the two functions that characterize a complex spectrum (i.e. the Fourier amplitude and the Fourier phase), the phase is more important in terms of defining the spatial features of an image. This is illustrated in Figure 12.3 which shows a Fourier amplitude and phase reconstruction of an original image, an amplitude only reconstruction and a phase only reconstruction. Clearly, the phase only reconstruction provides a recognizable 'measure' of the original image compared to the amplitude only reconstruction.

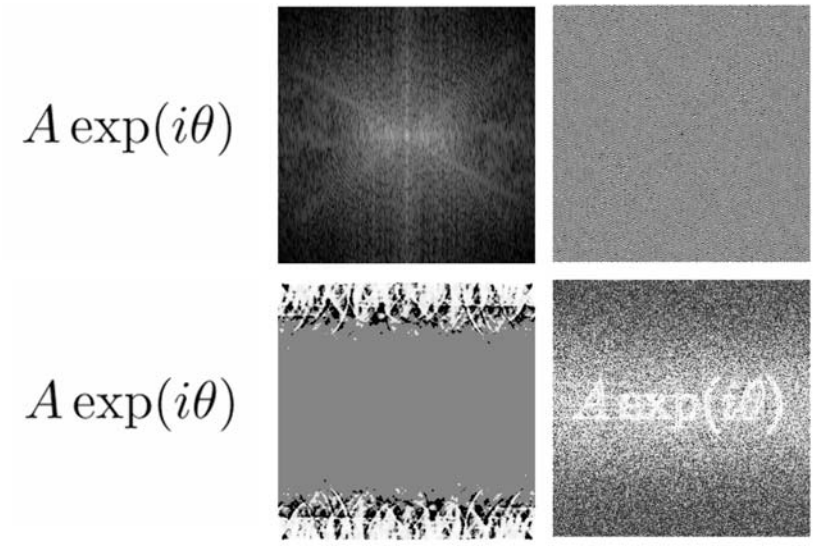

Figure 12.3: Original image (top-left), amplitude spectrum displayed using a logarithmic scale (top-centre), phase modulus spectrum (top-right), reconstruction using both the amplitude and phase spectra (bottom-left), amplitude only reconstruction (bottom-centre) and a phase only reconstruction (bottom-right).

12.9.1 Phase Retrieval

The phase retrieval problem is compounded as follows:

$$\text{Given } \mid F(k_x, k_y) \mid, \text{ find } f(x, y)$$

where

$$F(k_x, k_y) = \int_{-X/2}^{X/2} \int_{-Y/2}^{Y/2} f(x, y) \exp(-ik_x x) \exp(-ik_y y) dx dy$$

In order to solve this problem we consider an object function f that is real and of compact support A; a rectangle of size $X \times Y$. Outside the region A the data are zero giving an image of size, $2X \times 2Y$ say. The object function is taken to be at the centre of this 'zero padded' image. If we take an initial guess at the object function f, then, by taking the Fourier transform of the image, we can compute the amplitude and phase spectra which will both be of size $2X \times 2Y$. But the amplitude spectrum of f is known and so we can replace the amplitude spectrum obtained from the initial guess by the known spectrum $\mid F \mid$ which will be of size $X \times Y$. This provides us with a new complex spectrum that can be Fourier inverted to produce a new (real) image of size $2X \times 2Y$. However,

since the object function is of compact support A we can set all the data in the image outside A to zero. This provides a new object function which can be used to repeat the whole process on an iterative basis. In the absence of any *a priori* information on the object function, the initial guess can be a constant such as 1, i.e. a 'box-function'. This is an example of an error reduction algorithm which is based on applying a constraint in image space and a constraint in Fourier space given that the object function is real. It is commonly referred to as the Fienup phase reconstruction algorithm (e.g. Feinup J R, *Reconstruction of an Object from the Modulus of its Fourier Transform'*, Optics Letters 3(1), 1978) which in turn is based on the Gerchberg-Saxton algorithm (Gerchberg K and Saxton W O, *A Practical Algorithm for the Determination of Phase from Image and Diffraction Plane Pictures*, Optik, 35, 1972) designed to reconstruct a complex valued object function f when both the modulus $\mid f \mid$ and the Fourier modulus $\mid F \mid$ are known. This is a problem having applications in electron microscopy. The basic phase reconstruction process is given in the schematic diagram below, where $A(k_x, k_y)$ is the known Fourier amplitude and the initial object function $f(x, y)$ is a 'first guess' over the known region of support (the Feinup algorithm).

$$
\begin{array}{ccccc}
f(x,y) & \rightarrow & \hat{F}_2[f(x,y)] & \rightarrow & \mid F(k_x,k_y) \mid \exp[i\theta(k_x,k_y)] \\
\uparrow & & & & \downarrow \\
\text{Conform to region of support} & & & & \text{Satisfy amplitude constraint} \\
\uparrow & & & & \downarrow \\
f'(x,y) & \leftarrow & \mathrm{Re}\{\hat{F}_2^{-1}[F'(k_x,k_y)]\} & \leftarrow & F'(k_x,k_y) \\ & & & & = A(k_x,k_y)\exp[i\theta(k_x,k_y)]
\end{array}
$$

Similarly, the following diagram shows the error-reduction process for the case when both the Fourier amplitude A and the image amplitude a are known (the Gerchberg-Saxton algorithm)

$$
\begin{array}{ccccc}
f = a\exp(i\theta) & \rightarrow & \hat{F}_2[f] & \rightarrow & F = \mid F \mid \exp(i\phi) \\
\uparrow & & & & \downarrow \\
\text{Satisfy image amplitude constraint} & & & & \text{Satisfy Fourier amplitude constraint} \\
\uparrow & & & & \downarrow \\
f' = \mid f' \mid \exp(i\theta) & \leftarrow & \mathrm{Re}\{\hat{F}_2^{-1}[F']\} & \leftarrow & F' = A\exp(i\phi)
\end{array}
$$

Due to the large number of discrete Fourier transforms required, the convergence of these phase reconstruction algorithms can be slow. Moreover, the algorithm can stagnate and tend toward false solutions. Although there are a number of refinements and modifications to the basic process that can be applied, the critical issue with regard to generating a valid reconstruction for the object function is whether or not some form a *a priori* information on the object function is available. The use of *a priori* information for solving problems of this kind is essential. It is the basis for the material discussed in the following Chapter where it is used to construct a weighting function in order to extrapolate the spectrum of a band-limited image, a problem that can also be approached using an error reduction type process (e.g. Gerchberg R W, *Super-resolution Through Error Energy Reduction*, Optica Acta, 21(9), 1974).

12.9.2 Phase Imaging

Phase imaging is based on restoring the phase associated with an object function that is complex. This can occur when data have been generated using a time-resolved coherent system (e.g. diffraction tomography - see Chapter 9 - or real/synthetic aperture radar - see Chapter 10) in which the quadrature component (i.e. the Hilbert transform) of the recorded signals is available.

In order to recover a phase image from complex data the phase must be unwrapped. This is based on using a logarithmic transform. Thus, let the complex data be given by

$$s(x,y) = f(x,y) + iq(x,y) = A(x,y)\exp[i\theta(x,y) \pm 2\pi in], \quad n = 0, 1, 2, ...$$

then

$$\ln s(x,y) = \ln A(x,y) + i[\theta(x,y) \pm 2\pi n]$$

from which it follows that

$$\theta(x,y) = \mathrm{Im}[\ln s(x,y)] \mp 2\pi n$$

providing that $A(x,y) > 0$. The ambiguity in the value of the phase is then eliminated by differentiation since

$$\nabla\theta(x,y) = \mathrm{Im}[\nabla \ln s(x,y)] = \mathrm{Im}\left[\frac{1}{s(x,y)}\nabla s(x,y)\right]$$

$$= \mathrm{Im}\left[\frac{s^*(x,y)}{|\ s(x,y)\ |^2}\nabla s(x,y)\right] = \frac{1}{[A(x,y)]^2}\left[f(x,y)\nabla q(x,y) - q(x,y)\nabla f(x,y)\right].$$

In order to make the equation scalar, we can take the divergence of both sides to give

$$\nabla^2\theta(x,y) = h(x,y)$$

where

$$h(x,y) = \mathrm{Im}\left[\frac{1}{s(x,y)}\nabla^2 s(x,y) - \frac{1}{[s(x,y)]^2}\nabla s(x,y)\cdot\nabla s(x,y)\right]$$

$$= \frac{1}{[A(x,y)]^2}\mathrm{Im}\left[s^*(x,y)\nabla^2 s(x,y) - \frac{[s^*(x,y)]^2}{[A(x,y)]^2}\nabla s(x,y)\cdot\nabla s(x,y)\right].$$

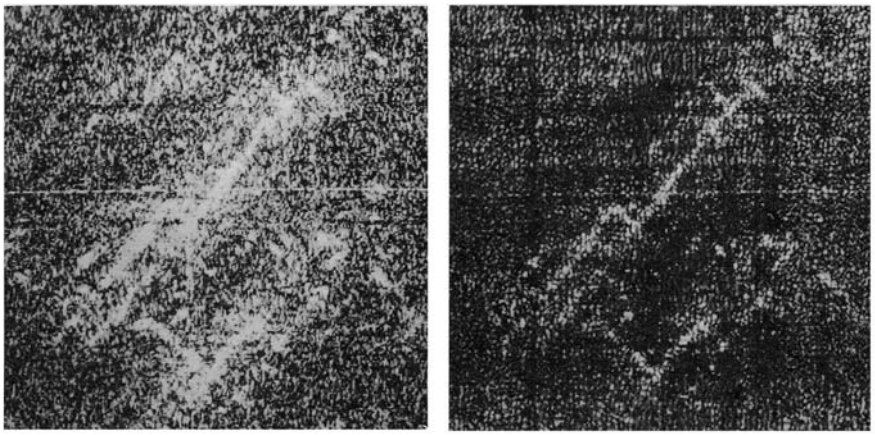

Figure 12.4: AM image (left) and an FM image (right) of a building (a factory) imaged using airbourne SAR.

The phase is then obtained by solving the Poisson equation given above. This can be achieved by applying the appropriate inverse filter, i.e.

$$\theta(x,y) = -\hat{F}_2^{-1}\left[\frac{H(k_x,k_y)}{k_x^2+k_y^2}\right]$$

where

$$H(k_x,k_y) = \hat{F}_2[h(x,y)].$$

Similarly, the terms $\nabla^2 s$ and ∇s can be computed through application of the filters $-(k_x^2+k_y^2)$ and $i(\hat{\mathbf{x}}k_x+\hat{\mathbf{y}}k_y)$, respectively. In practice, since the data s will be noisy, it is necessary to apply a low pass filter such as a Gaussian low pass filter to the function $s(x,y)$ prior to phase unwrapping .

In addition to generating an unwrapped phase image, another parameter that can be informative is the rate of change of phase and in particular the FM (Frequency Modulation) image which is given by $\mid \nabla\theta(x,y) \mid$. An example of such an image is given in Figure 12.4 which compares images of the amplitude modulations (i.e. $\mid s(x,y) \mid$) and the frequency modulations for complex data generated by a SAR. The FM image provides a significant improvement over the AM image in terms of clarifying the spatial location of the primary scatterer. This has been achieved using real zero conversion of the data (see *Digital Signal Processing*, J M Blackledge, Horwood, 2003 - Chapter 5).

12.10 Non-stationary Deconvolution

Convolution is an integral operation that associates an 'object function' f to another function s (the 'data function') via a given point spread function or

'instrument function') p. The usual form for describing a stationary convolution defined in one- and two-dimensions is

$$s(x) = \int_{-\infty}^{\infty} f(x - x')p(x')dx'dy'$$

and

$$s(x, y) = \int_{-\infty}^{\infty}\int_{-\infty}^{\infty} f(x - x', y - y')p(x', y')dx'$$

respectively. These equations assume that the instrument function is identical for all points over which the object function is convolved, i.e. that the process is stationary or isoplanatic. If the instrument function is not identical for all points over which the object function is convolved the problem becomes a non-stationary one. If we consider the convolution process in terms of the blurring of an image when it is acquired, the non-stationary form will result in portions of the image being less resolved (more blurred) than others.

Several types of non-stationary processes can occur which include:

(i) Amplitude variations that characterize an instrument function whose frequency content is constant but with a variable amplitude.

(ii) Frequency variations which characterize an instrument function whose amplitude is constant but with a variable spectrum.

(iii) Energy conservation in which the two types of non-stationarity processes given in (i) and (ii) above are combined such that the energy content of the instrument function remains constant.

(iv) Shape variation which arises when the basic shape (functional form) of the instrument function varies.

To model non-stationary convolution, the object function has been considered to be a function of dimension $2D$ where D is the dimension of the convolution operation. In the case of a 2D convolution, the object function can be written as

$$p(x', y', x, y)$$

where x' and y' are spatial variables over the support of the PSF at a particular point in the image and x and y are the coordinates of the point at which the PSF is to be applied. In other words, the instrument function can be seen as a collection of different PSFs, each of them applied at a singular point. Hence, non-stationary deconvolution is concerned with inverting the integral equations

$$s(x) = \int_{-\infty}^{\infty} f(x - x')p(x', x - x')dx'$$

and

$$s(x, y) = \int_{-\infty}^{\infty}\int_{-\infty}^{\infty} f(x - x', y - y')p(x', y', x - x', y - y')dx'dy'$$

for signal and image processing, respectively.

In this case, the convolution and correlation theorems are not valid. The instrument function gives the key as to why the convolution theorem fails in the non-stationary case: the dimensions of the spectra of the object function and of the instrument function are no longer compatible.

12.10.1 The Non-Stationary Convolution Operation

In discrete form the above integral equations have to be replaced by sums, giving

$$s[m] = \sum_{k=0}^{K-1} f[m-k]p[k][m-k]$$

and

$$s[m][n] = \sum_{k=0}^{K-1}\sum_{l=0}^{L-1} f[m-k][n-l]p[k][l][m-k][n-l]$$

respectively, where K is the length of the convolution mask and L is its width. If the kernel is non-stationary, it is not numerically optimal to have a convolution mask of constant size. To make the modelling easier, the optimum masks can be zero-padded so that they are of the same size.

Another issue arising with discrete deconvolution is the boundary conditions for the object function. If the convolution mask is of size $K \times L$, the value of the data function is affected by the value of the object function at the $K \times L$ points inside the mask. Hence, if the data function is to be defined on an array of size $M \times N$, the value of the object function has to be known for an array of size $(M + K - 1) \times (N + L - 1)$. In most cases, the extended array is obtained from an original $M \times N$ array by one of the following:

(i) Zero-padding where the object function takes on zeros outside its known support.

(ii) End-Point extension where the boundary values are extended over the necessary domain.

(iii) Wrapping where the known array is assumed to be one period of a periodic function.

12.10.2 Convolution as an Algebraic Operation

Any discrete convolution can be considered as the multiplication of a vector (the discrete object function) by a matrix (the discrete PSF). The resulting vector represents the discrete data function. In 1D, the equivalence is easy to see. For a convolution kernel of size N, the 1D non-stationary convolution is

$$s[m] = \sum_{k=0}^{N-1} f[m-k]p[k][m-k].$$

By constructing the matrix $P \equiv p_{ij}$ of size $N \times N$ and the vectors $\mathbf{f} \equiv f_i$ and $\mathbf{s} \equiv s_i$ of size N, as

$$p_{ij} = p[i-1][i-j],$$
$$f_i = f[i-1],$$
$$s_i = s[i-1],$$

the convolution sum is

$$s_i = \sum_{j=1}^{N} p_{ij} f_j.$$

or

$$P\mathbf{f} = \mathbf{s}.$$

The convolution matrix is constructed by reference to the instrument function only. Each of its columns describe the instrument function applied at a given point of the object function. The algebraic formulation of the convolution can take into account all three boundary conditions mentioned above. The chosen condition will also affect the structure of the matrix, but matrices are sparser if zero padding is adopted.

For convolution in higher dimensions, the object function has to be transformed into a 1D equivalent and the PSF can still be modelled by a matrix. The basic idea remains the same - each PSF is described by one column of the convolution matrix. The problem is then reduced to mapping a discrete function of dimension D into a discrete function of dimension 1. For the 2D case this is done by stacking up all the rows of the image to give a vector of size $N \times N$. For an image of size $N \times N$, the linear system (of size $N^2 \times N^2$) is constructed in the following way

$$p_{ij} = p[k][l][m-k][n-l]$$
$$s_i = s[k][l]$$
$$f_i = f[k][l]$$

with

$$i = kN + l + 1 \quad \text{and} \quad j = (m-k)N + (n-l) + 1.$$

For dimensions higher than one the convolution matrices can naturally be seen as sets of blocks, each block being similar to a 1D convolution matrix. In general, if D is the dimension of the convolution and N is the size of the object function support for all dimensions, then the size of the corresponding convolution matrix is $N^D \times N^D$.

In one dimension, if the convolution is stationary and wrapping is adopted as the boundary condition, the matrix is circulant. All the values of the columns are shifted with respect to one another. In two dimensions, under the same boundary conditions, the matrix is block circulant. For the non-stationary case, no regular pattern of the matrices can be exhibited. Circulant matrices can be diagonalized. It is interesting to note that the diagonalization is equivalent to taking the Fourier transform of the information conveyed in one of its rows (or columns). Hence, the convolution theorem, central in the theory of stationary

convolution (and deconvolution) can be obtained from an algebraic starting point. Likewise, the diagonalization of a block circulant matrix is equivalent to computing a 2D Fourier transform.

Once the convolution matrix is obtained, deconvolution is equivalent to the solution of a linear system of equation. However, these systems are very large for usual signals and images. For a 128×128 image, the convolution matrix has 268435456 entries. Clearly, numerical stability as well as computing time are important challenges to be overcome if algebraic deconvolution is to be of some value.

Solutions to this problem rely on three observations:

(i) Convolution matrices are often sparse, provided that the convolution masks are not too large compared to the support of the object functions.

(ii) Convolution matrices are very structured; the position of all non zero entries can be predicted from the PSF.

(iii) Point spread functions tend to have higher values at their origins, since the influence of the point where they are applied is nearly always predominant; hence the highest entries in the matrices will usually be found near the diagonals.

This suggests that the deconvolution problem should be approached using iterative methods of solution (see *Digital Signal Processing*, J M Blackledge, Horwood, 2003, Chapter 9).

12.10.3 Algebraic Deconvolution in 1D

Iterative methods for solving systems of linear equations are successful when applied to 1D non-stationary deconvolution even if the blur degradation is high (e.g. see Figure 12.5). Two algorithms are particularly efficient for this purpose: (i) the successive-under-relaxation method and (ii) the conjugate gradient method. Further, the performance of iterative methods applied to stationary processes are only marginally inferior to the usual restoration techniques (e.g. the Wiener filter, PSE filter and maximum entropy deconvolution), especially for broad convolution kernels. Moreover, signals restored using algebraic methods are qualitatively comparable to those obtained via Fourier space methods and, hence, iterative solutions do not introduce significant instability in one dimension. (Instability is rather caused by the nature of the problem.) Iterative methods are more efficient than segmentation for non-stationary deconvolution and the quality of the result obtained by algebraic deconvolution is conditioned by the extent to which the object image is degraded.

The most appropriate iterative method to use depends on the type of convolution kernel. If the kernel is smooth and wide (such as a Gaussian kernel), under-relaxation provides optimal solutions (in terms of accuracy and computational speed) with relatively few iterations ($\sim$32 for example), typically producing a good quality restoration for a low value of the relaxation parameter (typically 0.1). Conversely, if a discontinuous and narrow kernel is used

(such as a tophat kernel), the conjugate gradient method provides an optimal solution with relatively few iterations being required.

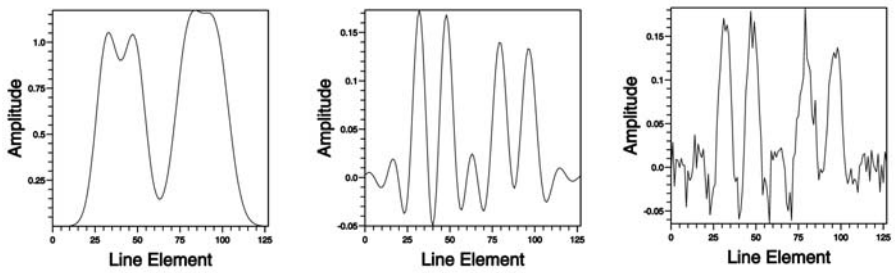

Figure 12.5: Non-stationary convolution of a set of 4 unit spikes for a Gaussian kernel with energy conservation (left); the result of applying algebraic deconvolution using successive-under-relaxation with a relaxation parameter of 0.11 and 32 iterations (centre) and the result of applying the same deconvolution method applied to data with additive Gaussian noise and an SNR of 100 (right).

The main drawback of algebraic methods, beside the computing and storage requirements, is the ill-conditioned characteristics of the matrices. For 1D deconvolution, for a signal of size 128, the condition number typically takes values as high as 10^{13}. Consequently, algebraic restoration is very sensitive to additive noise (e.g. see Figure 12.5). Signal-to-noise ratios defined by

$$\text{SNR} = \frac{\|p \otimes f\|_\infty}{\|n\|_\infty}$$

of around of 100 are sufficient to disrupt deconvolution especially in the case of Gaussian kernels. Fortunately, as the spectrum of the blurred data is by definition limited, the application of a low pass filter as a pre-processor provides much better restoration in the presence of (high frequency) noise. When the convolution kernel is space limited (such as a tophat function), the sensitivity to noise is less acute because of the broader spectrum of the data. The errors associated with algebraic non-stationary deconvolution are generally compatible with those obtained in the stationary case.

12.10.4 Algebraic Deconvolution in 2D

The extension of iterative algorithms to 2D deconvolution is not straightforward because the numerical stability, which is relatively sufficient in the case of signals, is less assured. This comes from the fact that the iterative methods make heavy use of the diagonal elements of the matrices. The ratio

$$\frac{a_{ii}}{\sum\limits_{\substack{j=1 \\ j \neq i}}^{n} a_{ij}}$$

where a_{ij} are the matrix elements has to be as large as possible to guarantee a stable solution. In 1D this ratio has small values (the order of 10^{-3}). In 2D, the number of terms in the sum over a_{ij}, which is given by the size of the convolution mask, jumps from N to $N \times N$. As a result, the ratio has much smaller values; stability is aften hindered. However, if restrictions are set as far as the extent to which the image is blurred, algebraic restoration can be successful and is certainly more appropriate than segmenting the image into regions where a stationary model can be applied (see Figure 12.6).

Figure 12.6: 128×128 test image (left); non-stationary convolution of test image using a tophat PSF with energy conservation where the average tophat half-width is 4 pixels (centre); restoration of the image using the conjugate gradient method (right).

We can take full advantage of the structure of the convolution matrices. Only the non zero entries are stored and used. Even so, the memory requirement is often very large. One side effect of this concerns the number of page faults. For instance, if each double (precision floating point value) is stored using 4 bytes, then, for a 128×128 images, with a convolution mask of size 16×16, the convolution matrix will occupy 1024 Mbytes of virtual memory if all entries are stored, and less than 16 Mbytes if only non zero entries are stored. In this last case, with 16 Mbytes of central memory available, 0.1% of the time is spent performing actual computations and 99.9% loading new memory pages. Thus, 2D algorithms need to be modified in order to reduce the number of page faults. The relaxation method can be modified to a block relaxation form while, for the conjugate gradient method the code for the computation of the product $A\mathbf{x}$, which is central to the method, needs to be written in such a way that each matrix block is referred to only once. It should be noted that iterative methods leave the characteristic matrix of the linear system unaltered. Given that convolution matrices are highly structured, it is possible to define them in terms of their matrix structure rather than in terms of the matrix itself in order to overcome memory issues. This comes at the price of more computing time since each entry needs to be evaluated each time it is referred to.

The complexity of the algebraic deconvolution problem, especially in 2D, is high, but the sparsity of the matrices involved allow iterative algorithms

to be partially (at least, depending on the sparsity of the matrices) stable. However, when the problem posed is based on a non-stationary model, algebraic solutions are required since the convolution theorem (which allows an FFT to be utilized) can only be applied for the stationary case. The choice of the best iterative algorithm depends on the characteristics of the convolution kernel. For broad smooth kernels, under-relaxation yields good results while the conjugate gradient method is to be preferred for sharp narrow (space-limited) kernels.

Algebraic methods suffer from two drawbacks: (i) the convolution matrices have a high condition number and therefore the restoration is sensitive to noise but its quality can be greatly improved by a low-pass filtering applied as a pre-processor; (ii) the algorithms are intensive both in terms of memory requirements as well as computing time. Further, they require that the non-stationary profile of the PSF is determined very accurately, which is not always possible. One well known example of this concerned the Hubble space telescope. Compensating optics had to be designed and installed in order to rectify the non-stationary de-focused images that were obtained when the telescope first came into operation; an error had been made during the telescope's manufacture.

12.11 Discussion

Deconvolution is concerned with the restoration of a signal or image from a recording which is resolution limited and corrupted by noise. This Chapter has been concerned with a class of solutions to this problem which are based on different criteria for solving ill-posed problems (e.g. the least squares principle) in the case when the noise is additive. We have considered the case when the object is convolved with a point spread function whose spectrum is continuous (e.g. a Gaussian point spread function). Solutions to the first problem have been discussed which are based on the Wiener filter, the Power Spectrum Equalization filter, the matched filter and constrained deconvolution. In all cases, knowledge of the characteristic function of the imaging system (i.e. the point spread function) is required together with an estimate of the signal to noise ratio (SNR). The success of the methods discussed depends on both the accuracy of the point spread function and the SNR value used. An optimum restoration is then obtained by experimenting with different values of SNR for a given PSF.

In some cases the PSF may be either difficult to obtain experimentally or simply not available. In such cases, it must be estimated from the data alone. This is known as 'Blind Deconvolution'. If it is known *a priori* that the spectrum of the object function is 'white' (i.e. the average value of each Fourier component is roughly the same over the entire frequency spectrum), then any large scale variations in the recorded spectrum should be due to the frequency distribution of the PSF. By smoothing the data spectrum, an estimate of the instrument function can be established. This estimate may then be used to deconvolve the data by employing an appropriate filter - an automatic gain control. The optimum value of the SNR when applied to the Wiener filter, for example, can be obtained by searching through a range of values and, for each

restored image, computing the ratio of the magnitude of the digital gradient to the number of zero crossings. This ratio is based on the idea that the optimum restoration is one which provides a well focused image with minimal 'ringing'.

The Fourier based approach to image restoration relies on the ability to implement the convolution and correlation theorems. This requires that the data has been recorded by an imaging system that is isoplanatic (i.e. the PSF is stationary). When a non-stationary process is involved algebraic deconvolution is required and the problem is reduced to finding optimal methods of solving large systems of algebraic equations.

In the following Chapter we consider the case when the object function is convolved with a sinc or jinc point spread function, for example, whose spectrum is discontinuous and consequently gives rise to a band-limited image.

12.12 Summary of Important Results

Wiener filter

Given that

$$s_{ij} = p_{ij} \otimes\otimes f_{ij} + n_{ij}$$

we find an estimate $\hat{f}$ of the object function f by minimizing the mean square error

$$e = \| f_{ij} - \hat{f}_{ij} \|^2$$

where

$$\hat{f}_{ij} = q_{ij} \otimes\otimes f_{ij}.$$

For signal independent noise, i.e.

$$f_{ij} \odot\odot n_{ij} = 0 \quad \text{and} \quad n_{ij} \odot\odot f_{ij} = 0$$

$$q_{ij} = \hat{F}_2^{-1} \left(\frac{P_{ij}^*}{\mid P_{ij} \mid^2 + \mid N_{ij} \mid^2 / \mid F_{ij} \mid^2} \right).$$

Power spectrum equalization filter

Given that

$$s_{ij} = p_{ij} \otimes\otimes f_{ij} + n_{ij},$$

and

$$\hat{f}_{ij} = q_{ij} \otimes\otimes s_{ij},$$

then if

$$\mid F_{ij} \mid^2 = \mid \hat{F}_{ij} \mid^2$$

and the noise is signal independent,

$$q_{ij} = \hat{F}_2^{-1} \left(\frac{1}{\mid P_{ij} \mid^2 + \mid N_{ij} \mid^2 / \mid F_{ij} \mid^2} \right)^{\frac{1}{2}}.$$

Matched filter

If

$$s_{ij} = p_{ij} \otimes \otimes f_{ij} + n_{ij},$$

and

$$\hat{f}_{ij} = q_{ij} \otimes \otimes s_{ij}$$

then

$$q_{ij} = \hat{F}_2^{-1}\left(\frac{P_{ij}^*}{\mid N_{ij} \mid^2}\right)$$

is that function that maximizes the ratio

$$R = \frac{\mid \sum_i \sum_j Q_{ij} P_{ij} \mid^2}{\sum_i \sum_j \mid N_{ij} \mid^2 \mid Q_{ij} \mid^2}.$$

For white normalized noise when $N_{ij} = 1, \quad \forall i, j$

$$q_{ij} = \hat{F}_2^{-1}[P_{ij}^*]$$

and

$$\hat{f}_{ij} = p_{ij} \odot \odot s_{ij}.$$

Maximum entropy filter

The solution for f_{ij}, given that

$$s_{ij} = p_{ij} \otimes \otimes f_{ij} + n_{ij}$$

which maximizes the entropy E defined by

$$E = -\sum_i \sum_j f_{ij} \ln f_{ij}$$

is obtained by solving the transcendental equation

$$f_{ij} = \exp[-1 + 2\lambda(s_{ij} \odot \odot p_{ij} - p_{ij} \otimes \otimes f_{ij} \odot \odot p_{ij})].$$

where λ is the Lagrange multiplier.

Constrained deconvolution

The solution for f_{ij}, given that

$$s_{ij} = p_{ij} \otimes \otimes f_{ij} + n_{ij}$$

which minimizes

$$\| g_{ij} \otimes \otimes f_{ij} \|$$

is given by

$$f_{ij} = \hat{F}_2^{-1}\left(\lambda \frac{S_{ij}P_{ij}^*}{\lambda \mid P_{ij} \mid^2 + \mid G_{ij} \mid^2}\right)$$

where λ is the Lagrange multiplier.

Phase reconstruction algorithm

An object function f which is exists over a finite region of support and is zero outside this region and whose amplitude spectrum $A(k_x, k_y)$ is known, can be reconstructed using the following algorithm (the Fienup algorithm):

$$\begin{array}{ccccc}
f(x,y) & \rightarrow & \hat{F}_2[f(x,y)] & \rightarrow & \mid F(k_x,k_y) \mid \exp[i\theta(k_x,k_y)] \\
\uparrow & & & & \downarrow \\
\text{Conform to region of support} & & & & \text{Satisfy amplitude constraint} \\
\uparrow & & & & \downarrow \\
f'(x,y) & \leftarrow & \mathrm{Re}\{\hat{F}_2^{-1}[F'(k_x,k_y)]\} & \leftarrow & F'(k_x,k_y) \\
 & & & & = A(k_x,k_y)\exp[i\theta(k_x,k_y)]
\end{array}$$

12.13 Further Reading

- Andrews H C and Hunt B R, *Digital Image Reconstruction*, Prentice-Hall, 1977.
- Rosenfeld A and Kak A C, *Digital Picture Processing*, Academic Press, 1980.
- Bates R H T and McDonnel M J, *Image Restoration and Reconstruction*, Oxford Science Publications, 1986.
- Katsaggelos A K (Ed.), *Digital Image Restoration*, Springer, 1991.
- Schulz T J, Snyder D L (Eds.), *Image Reconstruction and Restoration*, SPIE (Volume 2302), 1994.

Chapter 13

Reconstruction of Band-limited Images

A band-limited function is a function whose spectral bandwidth is finite. All real digital signals and images are band-limited functions. This leads us to consider the problem of how the bandwidth, and hence the resolution of a band-limited image can be increased synthetically using digital processing techniques. In other words, how can we extrapolate the spectrum of a band-limited function from an incomplete sample?

Solutions to this type of problem are important in image analysis where a resolution is needed that is not an intrinsic characteristic of the image provided and is difficult or even impossible to achieve experimentally. The type of resolution that is obtained by spectral extrapolation is referred to as super resolution.

Because sampled data are always insufficient to specify a unique solution and since no algorithm is able to reconstruct equally well all characteristics of an image, it is essential that the user is able to play a role in the design and execution of an algorithm and incorporate maximum knowledge of the expected features in the available data. Hence, an important aspect of practical solutions to the spectral extrapolation problem is the incorporation of *a priori* information on the structure of an object.

Here, an algorithm is discussed which combines *a priori* information with the least squares principle to reconstruct a two dimensional function from limited (i.e. incomplete) Fourier data. This algorithm is essentially a modified version of the Gerchberg-Papoulis algorithm to accommodate a user defined weighting function.

13.1 The Gerchberg-Papoulis Method

Let us consider the case where we have an image $f(x, y)$ characterized by a discrete spectrum F_{nm} which is composed of a finite number of samples:

$$-\frac{N}{2} \leq n \leq \frac{N}{2} \quad \text{and}$$

$$-\frac{M}{2} \leq m \leq \frac{M}{2}.$$

These data are related to the image by the equation

$$F_{nm} = \int_{-X}^{X} \int_{-Y}^{Y} f(x, y) e^{-i(k_n x + k_m y)} dxdy.$$

Here, f is assumed to be of finite support X and Y, i.e.

$$\mid x \mid \leq X \quad \text{and} \quad \mid y \mid \leq Y.$$

and k_n, k_m are discrete spatial frequencies. With this data, we can define the **B**and-**L**imited function

$$f_{BL}(x, y) = \sum_n \sum_m F_{nm} e^{i(k_n x + k_m y)}$$

which is related to F_{nm} by a two-dimensional Fourier series. Our problem is to reconstruct f given F_{nm} or, equivalently, f_{BL}. In this Section, a solution to this problem is presented using the least squares principle. First, we consider a model for an estimate $\hat{f}$ of f given by

$$\hat{f}(x, y) = \sum_n \sum_m A_{nm} e^{i(k_n x + k_m y)}. \tag{13.1}$$

This model is just a two-dimensional Fourier series representation of the object. Given this model, our problem is reduced to that of finding the coefficients A_{nm}. Using the least squares method, we compute A_{nm} by minimizing the mean square error

$$E = \int_{-X}^{X} \int_{-Y}^{Y} \mid f(x, y) - \hat{f}(x, y) \mid^2 dxdy.$$

This error is a minimum when

$$\frac{\partial E}{\partial A_{nm}} = 0.$$

Differentiating, we obtain

$$\frac{\partial E}{\partial A_{pq}} = \frac{\partial}{\partial A_{pq}} \int_{-X}^{X} \int_{-Y}^{Y} \left| f(x, y) - \sum_n \sum_m A_{nm} e^{i(k_n x + k_m y)} \right|^2 dxdy$$

$$= \int_{-X}^{X}\int_{-Y}^{Y} \left(f(x,y) - \sum_n \sum_m A_{nm} e^{i(k_n x + k_m y)} \right) e^{-i(k_p x + k_q y)} dxdy.$$

Thus, E is a minimum when

$$\int_{-X}^{X}\int_{-Y}^{Y} f(x,y) e^{-i(k_p x + k_q y)} dxdy$$

$$= \sum_n \sum_m A_{nm} \int_{-X}^{X}\int_{-Y}^{Y} e^{-i(k_p - k_n)x} e^{-i(k_q - k_m)y} dxdy.$$

The left hand side of the above equation is just the Fourier data F_{pq}. Hence, after evaluating the integrals on he right hand side, we get

$$F_{pq} = 4XY \sum_n \sum_m A_{nm} \operatorname{sinc}[(k_p - k_n)X] \operatorname{sinc}[(k_q - k_m)Y]. \tag{13.2}$$

The estimate $\hat{f}(x,y)$ can be computed by solving the equation above for the coefficients A_{nm}. This is a two-dimensional version of the Gerchberg-Papoulis method and is a least squares approximation of $f(x,y)$.

13.2 Incorporation of a Priori Information

Since we have considered an image f of finite support, we can write equation (13.1) in the following 'closed form':

$$\hat{f}(x,y) = w(x,y) \sum_n \sum_m A_{nm} e^{i(k_n x + k_m y)} \tag{13.3}$$

where

$$w(x,y) = \begin{cases} 1, & |\, x \,| \leq X, \quad |\, y \,| \leq Y; \\ 0, & |\, x \,| > X, \quad |\, y \,| > Y. \end{cases}$$

Writing it in this form, we observe that w (i.e. essentially the values of X and Y) represents a simple but crucial form of *a priori* information. This information is required to compute the sinc functions given in equation (13.2) and hence the coefficients A_{nm}. Note that the sinc functions (in particular the zero locations) are sensitive to the precise values of X and Y and hence small errors in X and Y can dramatically affect the computation of A_{nm}. In other words, equation (13.2) is ill-conditioned.

The algebraic form of equation (13.3) suggests incorporating further *a priori* information into the 'weighting function' w in addition to the support (spacial extent) of the object f. We therefore consider an estimate of the form

$$\hat{f}(x,y) = w(x,y) \sum_n \sum_m A_{nm} e^{i(k_n x + k_m y)}$$

where w is now a generalized weighting function composed of limited *a priori* information on the structure of f. If we now employ a least squares method to find A_{nm} based on the previous mean square error function, we obtain the following equation

$$\int_{-X}^{X}\int_{-Y}^{Y} f(x,y)w(x,y)e^{-i(k_p x+k_q y)}dxdy$$

$$= \sum_n \sum_m A_{nm} \int_{-X}^{X}\int_{-Y}^{Y} [w(x,y)]^2 e^{-i(k_p-k_n)x} e^{-i(k_q-k_m)y} dxdy.$$

The problem with this result is that the data on the left hand side are not the same as the Fourier data provided F_{pq}. In other words, the result is not 'data consistent'. To overcome this problem we introduce a modified version of the least squares method which involves minimizing the error

$$E = \int_{-X}^{X}\int_{-Y}^{Y} \mid f(x,y) - \hat{f}(x,y) \mid^2 \frac{1}{w(x,y)} dxdy. \tag{13.4}$$

In this case, we find that E is a minimum when

$$F_{pq} = \sum_n \sum_m A_{nm} W_{p-n,q-m} \tag{13.5}$$

where

$$W_{p-n,q-m} = \int_{-X}^{X}\int_{-Y}^{Y} w(x,y)e^{-i(k_p-k_n)x} e^{-i(k_q-k_m)y} dxdy.$$

Equation (13.5) is data consistent, the right hand side of this equation being a discrete convolution of A_{nm} with W_{nm}. Hence, using the notation for convolution, we may write this equation in the form

$$F_{nm} = A_{nm} \otimes\otimes W_{nm}.$$

Using the convolution theorem, in real space, this equation becomes

$$f_{BL}(x,y) = a(x,y)w_{BL}(x,y)$$

where

$$f_{BL}(x,y) = \sum_n \sum_m F_{nm} e^{i(k_n x+k_m y)},$$

$$w_{BL}(x,y) = \sum_n \sum_m W_{nm} e^{i(k_n x+k_m y)}$$

and

$$a(x,y) = \sum_n \sum_m A_{nm} e^{i(k_n x+k_m y)}.$$

Now, since

$$\hat{f}(x,y) = w(x,y) \sum_n \sum_m A_{nm} e^{i(k_n x + k_m y)} = w(x,y) a(x,y)$$

we obtain the simple algebraic result

$$\hat{f}(x,y) = \frac{w(x,y)}{w_{BL}(x,y)} f_{BL}(x,y).$$

Here w_{BL} is a band-limited weighting function, band-limited by the same extent as f_{BL}.

13.3 Example Demonstration and Applications

The algorithm presented above is based on an inverse weighted least squares error [i.e. equation (13.4)]. It is essentially an adaption of the Gerchberg-Papoulis method modified to: (i) accommodate a generalized weighting function $w(x,y)$; (ii) provide data consistency [i.e. equation (13.5)]. The weighting function $w(x,y)$ can be used to encode as much information as is available on the structural characteristics of $f(x,y)$. Since equation (13.4) involves $1/w(x,y)$, $w(x,y)$ must be confined to being a positive non-zero function. We can summarize this algorithm in the form

$$\text{reconstruction} = \frac{\text{band} - \text{limited} \quad \text{image} \times a \quad priori \quad \text{information}}{\text{band} - \text{limited} \quad a \quad priori \quad \text{information}}$$

Figure 13.1 provides an example of this reconstruction method using the example MATLAB code given below.

```
function SPECRTRAL_EXTRPOLATION(s,w,bw)
%
%Input:
%     s - Bandlimited image
%     w - a priori information
%     bw - bandwidth of image
%
%Output: Null

%Compute size of images;
%arrays s & w are taken to be the same size.
n=size(s);

%Float to double and normalize data.
s=im2double(s);
w=im2double(w);

%Compute Fourier transforms of s and w
```

```
%in optical form (using fftshift function).
s_spectrum=fftshift(fft2(s));
w_spectrum=fftshift(fft2(w));

%Compute ideal filter:
%Initialize array.
for i=1:n
    for j=1:n
        filter(i,j)=0;
    end
end

%Compute filter
nn=1+n/2; %DC value taken to be at 1+n/2.
bw=bw/2;
for i=nn-bw:nn+bw
    for j=nn-bw:nn+bw
        filter(i,j)=1;
    end
end

%Filter data, taking the real part of the absolute value.
s_bl=real(abs(ifft2(filter.*s_spectrum)));
w_bl=real(abs(ifft2(filter.*w_spectrum)));

%Reconstruct data.
f=w.*(s_bl./w_bl);

%Normalise data (for display).
s_bl=s_bl./max(max(s_bl)); f=f./max(max(f));

%Show images
subplot(2,2,1), imshow(s);
subplot(2,2,2), imshow(s_bl);
subplot(2,2,3), imshow(w);
subplot(2,2,4), imshow(f);
```

In this example, an object function has been chosen which consists of 512×512 pixels and is composed of a boundary in the form of a thin annular ring enclosing a region consisting of solid rectangles, circles, ellipses and a triangle. The bandwidth of this object has been reduced to 12 pixels using a square ideal low-pass filter giving the data shown (the Fourier data being composed of just 12×12 non-zero values - 0.6% of the original data). A weighting function is chosen which includes the support of the original object but does not reflect its internal structure (i.e. the internal solid objects). Application of the reconstruction method above provides the result shown.

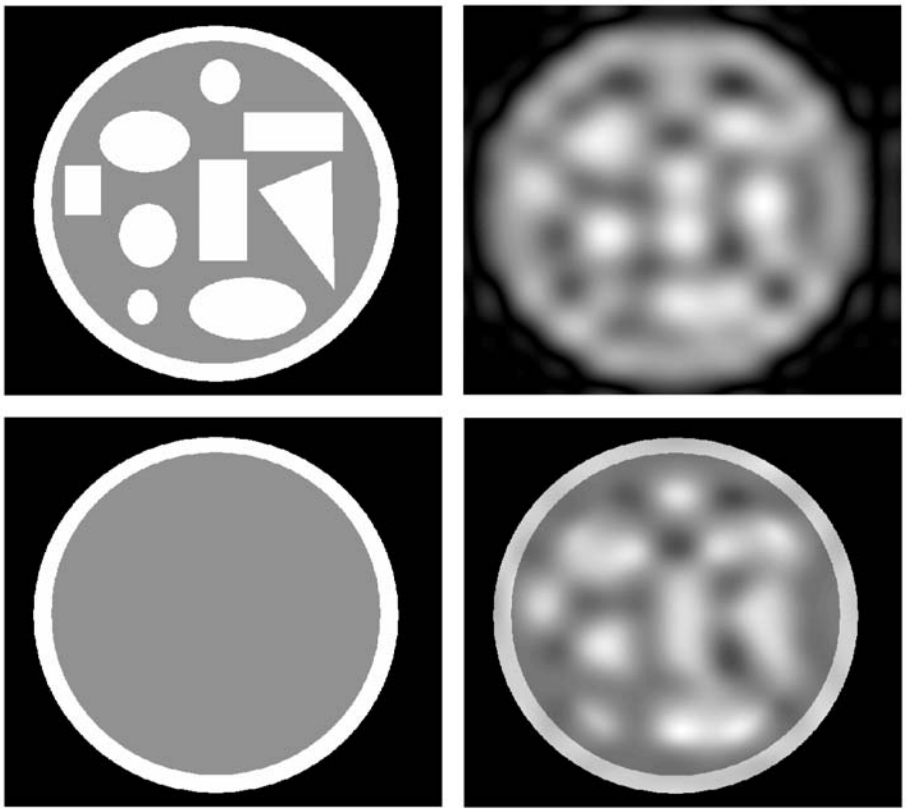

Figure 13.1: Reconstruction (bottom-right) of a test object (top-left) function from band-limited data (top-right) using prior information (bottom-left).

In the previous example it is assumed that the user has access to a limited but accurate form of information on the structure of the object including its (compact) support or spatial extent. In some applications this is a reasonable assumption especially in those cases where the object function has expected features. In other cases, however, no detailed or accurate *a priori* information may be available. In such cases, *a priori* information on the spatial support of the object must be estimated from the data alone. A simple way of doing this is to semi-threshold the data, i.e. apply the following process:

if $v_{ij}^{\text{in}} >$ threshold
then
$v_{ij}^{\text{out}} = v_{ij}^{\text{in}}$
else
$v_{ij}^{\text{out}} = 0$
endif

where v_{ij} is the value of a pixel at ij. An example of this approach is given in Figure 13.2 based on the following example MATLAB code.

```
function SRT(s,bw,threshold)
%Input:
%     s - Bandlimited image
%     w - a priori information
%     bw - bandwidth of image
%
%Output: Null
%
%Compute size of images;
%arrays s & w are taken to be the same size.
n=size(s);
%
%Normailze input array.
s=im2double(s);
%
%Compute Fourier transforms of s in
%optical form (using fftshift function).
%
s_spectrum=fftshift(fft2(s));
%
%Compute ideal filter:
%Initialize array.
for i=1:n
    for j=1:n
        filter(i,j)=0;
    end
end
%Compute
nn=1+n/2; %DC value taken to be at 1+n/2.
bw=bw/2;
for i=nn-bw:nn+bw
    for j=nn-bw:nn+bw
        filter(i,j)=1;
    end
end
%Filter data, taking the real part of the absolute value.
s_bl=real(abs(ifft2(filter.*s_spectrum)));
%Compute prior information by thresholding data.
s_bl=s_bl./max(max(s_bl));
w=s_bl;
for i=1:n
    for j=1:n
        if w(i,j)<threshold
            w(i,j)=0.0;
        end
```

```
    end
end
%Bandlimit data.
w_bl=real(abs(ifft2(filter.*(fftshift(fft2(w))))));
%Reconstruct data.
f=w.*(s_bl./w_bl);
%Normalize.
f=f./max(max(f));
%Show images.
subplot(2,2,1), imshow(s);
subplot(2,2,2), imshow(s_bl);
subplot(2,2,3), imshow(w);
subplot(2,2,4), imshow(f);
```

Here, an object function consisting of two points has been severely band-limited by applying a 9×9 square (ideal) low-pass filter. Thresholding these data provides an estimate of the support of the object (i.e. *a priori* information on the location of the two points in the image original object) which is then used to obtain the reconstruction shown.

Exactly the same technique has been used to obtain the reconstruction given in Figure 13.3 which is an example of a SAR image (see Chapter 10). The object at the centre of this image is a SAR image of a ship obtained using the Saesat satellite. The image is a display of the amplitude modulations after the bandwidth of the complex data has been reduced to remove the high frequency 'speckle' generate by coherent scattering of 24 cm microwaves from the sea surface. By thresholding the amplitude modulated image, *a priori* information on the location (support) of the object is obtained. Application of the reconstruction method provides the super-resolved image shown.

13.4 Error Reduction Algorithm

The error reduction algorithm has been discussed in Chapter 12 with regard to the Gerchberg-Saxton algorithm for reconstructing the object function f when both $\mid f \mid$ and $\mid F \mid$ are known. The same approach can be adopted to design an iterative approach to extrapolating the spectrum of a band-limited image. Suppose we have a band-limited image of size $X \times Y$ which is zero padded to produce an image of size $2X \times 2Y$. Let the complex spectrum of the original image be given by $F'_r + iF'_i$, which is of size $W_x \times W_y$ where W_x and W_y define the bandwidth of the image in the x- and y-directions, respectively. If we take the 2D DFT of the zero padded image, then a complex spectrum of size $2X \times 2Y$ will be generated whose central spectral components can be replaced with those of the original image satisfying the complex spectral constraint. Inverse Fourier transforming the result will give an output (the real part) which can be space limited to conform to the region of support. The processing cycle associated with this algorithm is as follows:

$$
\begin{array}{ccccc}
f(x,y) & \rightarrow & \hat{F}_2[f(x,y)] & \rightarrow & F_r(k_x,k_y)+iF_i(k_x,k_y)] \\
\uparrow & & & & \downarrow \\
\text{Conform to region of support} & & & & \text{Satisfy spectral constraint} \\
\uparrow & & & & \downarrow \\
f'(x,y) & \leftarrow & \mathrm{Re}\{\hat{F}_2^{-1}[F'(k_x,k_y)]\} & \leftarrow & \begin{array}{c} F'(k_x,k_y) \\ = F'_r(k_x,k_y)+iF'_i(k_x,k_y) \end{array}
\end{array}
$$

Clearly, any weighting function $w(x,y)$ can be incorporated by replacing f with fw in the cycle above.

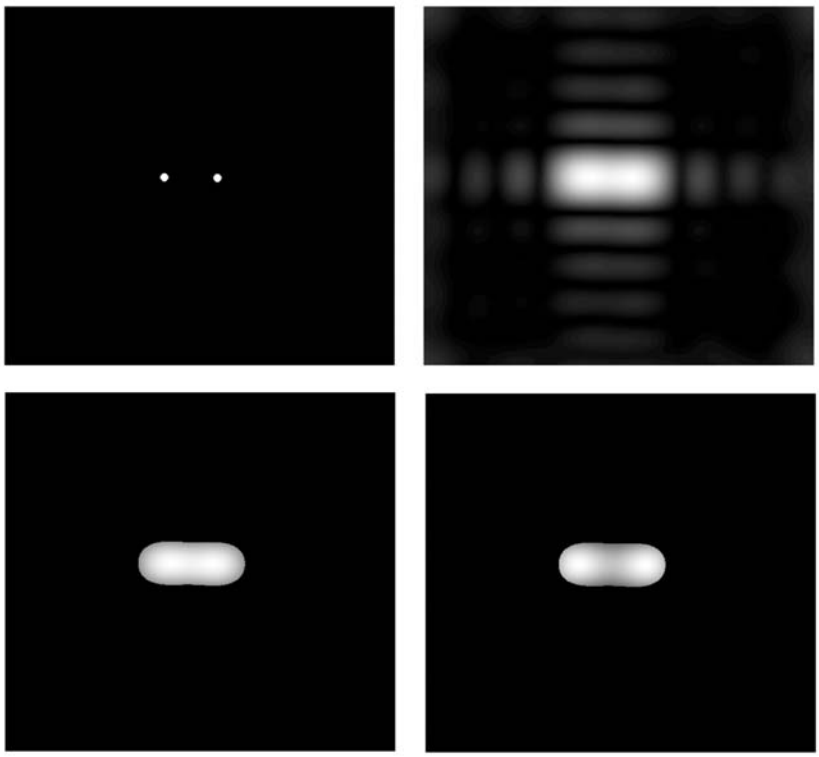

Figure 13.2: Reconstruction (bottom-right) of two points (top-left) from band-limited data (top-right). Here, the *a priori* information (bottom-left) on the support of the object (i.e. the approximate location of the two points in the object function) has been obtained by semi-thresholding the band-limited data using a threshold of 0.5.

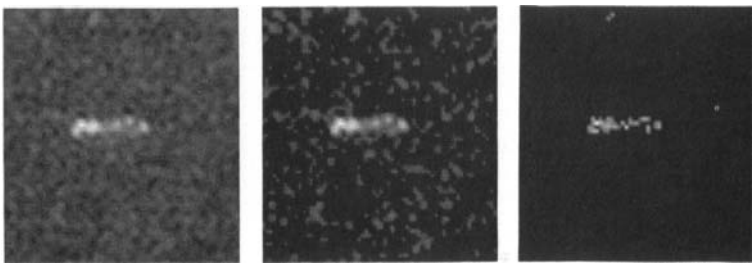

Figure 13.3: Super resolution of a SAR image. The complex data have been (ideal) low pass filtered to remove the speckle and the SAR image shown (far-left) is a display of the amplitude modulations of these data. The blurred object at the centre of this image is a ship obtained using the 24 cm Seasat radar satellite. By thresholding this image, an estimate of the spatial support of the object is acquired (see centre image which in this example has been obtained using a threshold of 0.5). This result is then used to extrapolate the spectrum of the band-limited (complex) data (far-right).

13.5 Discussion

The problem of reconstructing a band-limited function from limited Fourier data is an ill-posed problem. Hence, practical digital techniques for solving this problem tend to rely on the use of *a priori* information to limit the class of possible solutions. In this Chapter the least squares principle has been used as the basis for a solution and then modified to incorporate *a priori* information and provide a data consistent result. In this sense the algorithm derived belongs to the same class as the Wiener filter and, like the Wiener filter, ultimately relies on the experience and intuition of a user for optimization.

None of the approaches to solving the equation

$$s_{ij} = p_{ij} \otimes \otimes f_{ij} + n_{ij}$$

in this Chapter and Chapter 12 have made explicit use of the statistical properties of the digital noise function n_{ij}. However, in some practical cases, the probability density function of n_{ij} can be obtained experimentally (e.g. by applying a least squares fit to the histogram) or estimated theoretically. In this case we can develop a different approach to the deconvolution problem that is based on the application of Bayesian statistics.

13.6 Summary of Important Results

Spectral extrapolation of a band-limited image

$$\text{reconstruction} = \frac{\text{band}-\text{limited image} \times a \textit{ priori} \text{ information}}{\text{band}-\text{limited } a \textit{ priori} \text{ information}}$$

Error reduction algorithm

$$\begin{array}{ccccc}
f(x,y) & \rightarrow & \hat{F}_2[f(x,y)] & \rightarrow & F_r(k_x,k_y) + iF_i(k_x,k_y)] \\
\uparrow & & & & \downarrow \\
\text{Conform to region of support} & & & & \text{Satisfy spectral constraints} \\
\uparrow & & & & \downarrow \\
f'(x,y) & \leftarrow & \text{Re}\{\hat{F}_2^{-1}[F'(k_x,k_y)]\} & \leftarrow & \begin{array}{c} F'(k_x,k_y) \\ = F'_r(k_x,k_y) + iF'_i(k_x,k_y) \end{array}
\end{array}$$

13.7 Further Reading

- Andrews H C and Hunt B R, *Digital Image Reconstruction*, Prentice-Hall, 1977.
- Lim J S, *Two-dimensional Signal and Image Processing*, Prentice-Hall, 1990.
- Buck B B and Macaulay V A (Eds.), *Maximum Entropy in Action*, Clarendon Press, 1992.
- Jähne B, *Digital Image Processing: Concepts, Algorithms and Scientific Applications*, Springer, 1995.

Chapter 14

Bayesian Estimation Methods

The processing techniques discussed in Chapters 12 and 13 do not take into account the statistical nature of the noise inherent in an image. To do this, another type of approach must be taken which is based on a result in probability theory called Bayes rule named after the English mathematician Thomas Bayes.

14.1 Introduction to Probability and Bayes Rule

Suppose we toss a coin, observe whether we get heads or tails, and then repeat this process a number of times. As the number of trials increases, we expect that the number of times heads or tails occurs is half that of the number of trials. In other words, the probability of getting heads is 1/2 and the probability of getting tails is also 1/2. Similarly, if a dice with six faces is thrown repeatedly, then the probability of it landing on any one particular face is 1/6. In general, if an experiment is repeated N times and an event A occurs n times say, then the probability of this event $P(A)$ is defined as

$$P(A) = \lim_{N \to \infty} \left(\frac{n}{N} \right).$$

The probability is the relative frequency of an event as the number of trials tends to infinity. In practice, only a finite number of trials can be conducted and we therefore define the probability of an event A as

$$P(A) \simeq \frac{n}{N}$$

where it is assumed that N is large.

14.1.1 The Joint Probability

Suppose we have two coins which we label C_1 and C_2. We toss both coins simultaneously N times and record the number of times C_1 is heads, the number of times C_2 is heads and the number of times C_1 and C_2 are heads together. What is the probability that C_1 and C_2 are heads together? Clearly, if m is the number of times out of N trials that heads occurs simultaneously, then the probability of such an event must be given by

$$P(C_1 \text{ heads and } C_2 \text{ heads}) = \frac{m}{N}.$$

This is known as the joint probability of C_1 being heads when C_2 is heads. In general, if two events A and B are possible and m is the number of times both events occur simultaneously, then the joint probability is given by

$$P(A \text{ and } B) = \frac{m}{N}.$$

14.1.2 The Conditional Probability

Suppose we setup an experiment in which two events A and B can occur. We conduct N trials and record the number of times A occurs (which is n) and the number of times A and B occur simultaneously (which is m). In this case, the joint probability may written as

$$P(A \text{ and } B) = \frac{m}{N} = \frac{m}{n} \times \frac{n}{N}.$$

Now, the quotient n/N is the probability $P(A)$ that event A occurs. The quotient m/n is the probability that events A and B occur simultaneously given that event A has occurred. The latter probability is known as the conditional probability and is written as

$$P(B \mid A) = \frac{m}{n}$$

where the symbol $B \mid A$ means 'B given A'. Hence, the joint probability can be written as

$$P(A \text{ and } B) = P(A)P(B \mid A).$$

Suppose that we do a similar type of experiment but this time we record the number of times p that event B occurs and the number of times q that event A occurs simultaneously with event B. In this case, the joint probability of events B and A occurring together is given by

$$P(B \text{ and } A) = \frac{q}{N} = \frac{q}{p} \times \frac{p}{N}.$$

The quotient p/N is the probability $P(B)$ that event B occurs and the quotient q/p is the probability of getting events B and A occurring simultaneously given that event B has occurred. The latter probability is just the probability of getting 'A given B', i.e.

$$P(A \mid B) = \frac{q}{p}.$$

Hence, we have

$$P(B \text{ and } A) = P(B)P(A \mid B).$$

14.1.3 Bayes Rule

The probability of getting A and B occurring simultaneously is exactly the same as getting B and A occurring simultaneously, i.e.

$$P(A \text{ and } B) = P(B \text{ and } A).$$

Hence, by using the definition of these joint probabilities in terms of the conditional probabilities we arrive at the following formula

$$P(A)P(B \mid A) = P(B)P(A \mid B)$$

or alternatively

$$P(B \mid A) = \frac{P(B)P(A \mid B)}{P(A)}.$$

This result is known as Bayes rule. It relates the conditional probability of 'B given A' to that of 'A given B'.

14.1.4 Bayesian Estimation Methods

In signal and image analysis Bayes rule is written in the form

$$P(f \mid s) = \frac{P(f)P(s \mid f)}{P(s)}$$

where f is the object function that we want to recover from the signal

$$s(x) = p(x) \otimes f(x) + n(x)$$

or image

$$s(x, y) = p(x, y) \otimes \otimes f(x, y) + n(x, y).$$

This result is the basis for a class of restoration methods which are known collectively as Bayesian estimators.

Bayesian estimation attempts to recover f in such a way that the probability of getting f given s is a maximum. In practice, this is done by assuming that $P(f)$ and $P(s \mid f)$ obey certain statistical distributions which are consistent with the experiment in which s is measured. In other words, models are chosen for $P(f)$ and $P(s \mid f)$ and then f is computed at the point where $P(f \mid s)$ reaches its maximum value. This occurs when

$$\frac{\partial}{\partial f} P(f \mid s) = 0.$$

Here, the function P is the Probability Density Function (PDF) which is real and positive. The PDF $P(f \mid s)$ is called the *a posteriori* PDF. Since the

logarithm of a real positive function varies monotonically with that function, the *a posteriori* PDF is also a maximum when

$$\frac{\partial}{\partial f} \ln P(f \mid s) = 0.$$

Now, using Bayes rule, we can write this equation as

$$\frac{\partial}{\partial f} \ln P(s \mid f) + \frac{\partial}{\partial f} \ln P(f) = 0.$$

Because the solution to this equation for f maximizes the *a posteriori* PDF, this method is known as the Maximum *a Posteriori* or MAP method. To illustrate the principles of Bayesian estimation, we shall now present some simple examples of how this technique can be applied to data analysis.

Example 1

Suppose that we measure a single sample s (one real number) in an experiment where it is known *a priori* that

$$s = f + n$$

where n is noise (a single random number). Suppose that it is also known *a priori* that the noise is determined by a zero mean Gaussian distribution of the form (ignoring scaling)

$$P(n) = \exp(-n^2/\sigma_n^2)$$

where σ_n is the standard deviation of the noise. Now, the probability of measuring s given f - i.e. the conditional probability $P(s \mid f)$ - is determined by the noise since

$$n = s - f.$$

We can therefore write

$$P(s \mid f) = \exp[-(s-f)^2/\sigma_n^2].$$

To find the MAP estimate, the PDF for f must also be known. Suppose that f also has a zero-mean Gaussian distribution of the form

$$P(f) = \exp(-f^2/\sigma_f^2).$$

Then,

$$\frac{\partial}{\partial f} \ln P(s \mid f) + \frac{\partial}{\partial f} \ln P(f) = \frac{2(s-f)}{\sigma_n^2} - \frac{2f}{\sigma_f^2} = 0.$$

Solving this equation for f gives

$$f = \frac{s\Gamma^2}{1+\Gamma^2}$$

where Γ is the SNR defined by

$$\Gamma = \frac{\sigma_f}{\sigma_n}.$$

Notice that as $\sigma_n \to 0$, $f \to s$, which must be true since $s = f + n$ and n has a zero-mean Gaussian distribution. Also, note that the solution we acquire for f is entirely dependent on the *a priori* information we have on the PDF for f. A different PDF produces an entirely different solution. For example, suppose it is known, or we have good reason to assume that, f obeys a Rayleigh distribution of the form

$$P(f) = f \exp(-f^2/\sigma_f^2), \quad f \geq 0.$$

In this case,

$$\frac{\partial}{\partial f} \ln P(f) = \frac{1}{f} - \frac{2f}{\sigma_f^2}$$

and assuming that the noise obeys the same zero-mean Gaussian distribution

$$\frac{\partial}{\partial f} \ln P(s \mid f) + \frac{\partial}{\partial f} \ln P(f) = \frac{2(s-f)}{\sigma_n^2} + \frac{1}{f} - \frac{2f}{\sigma_f^2} = 0.$$

This equation is quadratic in f. Solving it, we obtain

$$f = \frac{s\Gamma^2}{2(1+\Gamma^2)} \left(1 \pm \sqrt{1 + \frac{2\sigma_n^2}{s^2} \left(1 + \frac{1}{\Gamma^2} \right)} \right).$$

The solution for f which maximizes the value of $P(f \mid s)$ can then be written in the form

$$f = \frac{s}{2a} \left(1 + \sqrt{1 + \frac{2a\sigma_n^2}{s^2}} \right)$$

where

$$a = 1 + \frac{1}{\Gamma^2}.$$

This is a nonlinear estimate for f. If

$$\frac{\sigma_n \sqrt{2a}}{s} << 1$$

then

$$f \simeq \frac{s}{a}.$$

In this case f is linearly related to s. In fact, this linearized estimate is identical to the MAP estimate obtained earlier where it was assumed that f had a Gaussian distribution.

From the example given above, it should now be clear that Bayesian estimation (i.e. the MAP method) is only as good as the *a priori* information on the statistical behaviour of f - the object for which we seek a solution. However, when $P(f)$ is broadly distributed compared with $P(s \mid f)$, the peak value of the *a posteriori* PDF will lie close to the peak value of $P(f)$. In particular, if $P(f)$ is roughly constant, then

$$\frac{\partial}{\partial f} \ln P(f)$$

is close to zero and therefore

$$\frac{\partial}{\partial f} \ln P(f \mid s) \simeq \frac{\partial}{\partial f} \ln P(s \mid f).$$

In this case, the *a posteriori* PDF is a maximum when

$$\frac{\partial}{\partial f} \ln P(s \mid f) = 0.$$

The estimate for f that is obtained by solving this equation for f is called the Maximum Likelihood or ML estimate. To obtain this estimate, only *a priori* knowledge on the statistical fluctuations of the conditional probability is required. If, as in the previous example, we assume that the noise is a zero-mean Gaussian distribution, then the ML estimate is given by

$$f = s.$$

Note that this is the same as the MAP estimate when the standard deviation of the noise is zero.

The basic and rather important difference between the MAP and ML estimates is that the ML estimate ignores *a priori* information about the statistical fluctuations of the object function f. It only requires a model for the statistical fluctuations of the noise. For this reason, the ML estimate is usually easier to compute. It is also the estimate to use in cases where there is a complete lack of knowledge about the statistical behaviour of the object function.

Example 2

To further illustrate the difference between the MAP and ML estimate and to show their use in signal analysis, consider the case where we measure N samples of a real signal s_i in the presence of additive noise n_i which is the result of transmitting a known signal f_i modified by a random amplitude factor a. The samples of the signal are given by

$$s_i = af_i + n_i, \quad i = 1, 2, ..., N.$$

The problem is to find an estimate for a. To solve problems of this type using Bayesian estimation, we must introduce multidimensional probability theory. In this case, the PDF is a function of not just one number s but a set of numbers $s_1, s_2, ..., s_N$. It is therefore a member of a vector space. To emphasize this, we use the vector notation

$$P(\mathbf{s}) \equiv P(s_i) \equiv P(s_1, s_2, s_3, ..., s_N).$$

The ML estimate is given by solving the equation

$$\frac{\partial}{\partial a} \ln P(\mathbf{s} \mid a) = 0$$

for a. Let us again assume that the noise is described by a zero-mean Gaussian distribution of the form

$$P(\mathbf{n}) \equiv P(n_1, n_2, ..., n_N) = \exp\left(-\frac{1}{\sigma_n^2}\sum_{i=1}^{N} n_i^2\right).$$

The conditional probability is then given by

$$P(\mathbf{s} \mid a) = \exp\left(-\frac{1}{\sigma_n^2}\sum_{i=1}^{N}(s_i - af_i)^2\right)$$

and

$$\frac{\partial}{\partial a}\ln P(\mathbf{s} \mid a) = \frac{2}{\sigma_n^2}\sum_{i=1}^{N}(s_i - af_i)f_i = 0.$$

Solving this last equation for a we obtain the ML estimate

$$a = \frac{\sum_{i=1}^{N} s_i f_i}{\sum_{i=1}^{N} f_i^2}.$$

The MAP estimate is obtained by solving the equation

$$\frac{\partial}{\partial a}\ln P(\mathbf{s} \mid a) + \frac{\partial}{\partial a}\ln P(a) = 0$$

for a. Using the same distribution for the conditional PDF, let us assume that a has a zero-mean Gaussian distribution of the form

$$P(a) = \exp(-a^2/\sigma_a^2)$$

where σ_a^2 is the standard deviation. In this case,

$$\frac{\partial}{\partial a}\ln P(a) = -\frac{2a}{\sigma_a^2}$$

and, hence, the MAP estimate is obtained by solving the equation

$$\frac{\partial}{\partial a}\ln P(\mathbf{s} \mid a) + \frac{\partial}{\partial a}\ln P(a)$$

$$= \frac{2}{\sigma_n^2}\sum_{i=1}^{N}(s_i - af_i)f_i - \frac{2a}{\sigma_a^2} = 0$$

for a. The solution to this equation is given by

$$a = \frac{\frac{\sigma_a^2}{\sigma_n^2}\sum_{i=1}^{N} s_i f_i}{1 + \frac{\sigma_a^2}{\sigma_n^2}\sum_{i=1}^{N} f_i^2}.$$

Note that if $\sigma_a >> \sigma_n$, then,

$$a \simeq \frac{\sum_{i=1}^{N} s_i f_i}{\sum_{i=1}^{N} f_i^2}$$

which is the same as the ML estimate.

14.2 The Maximum Likelihood Filter

In the last Section, the principles of Bayesian estimation were presented. We shall now use these principles to design deconvolution algorithms for digital images under the assumption that the statistics are Gaussian. The problem is as follows: given the real digital image

$$s_{ij} = \sum_n \sum_m p_{i-n,j-m} f_{nm} + n_{ij}$$

find an estimate for f_{ij} when p_{ij} is known together with the statistics for n_{ij}. In this Section, the ML estimate for f_{ij} is determined by solving the equation

$$\frac{\partial}{\partial f_{ij}} \ln P(s_{ij} \mid f_{ij}) = 0.$$

As before, the algebraic form of the estimate depends upon the model that is chosen for the PDF. Let us assume that the noise has a zero-mean Gaussian distribution. In this case, the conditional PDF is given by

$$P(s_{ij} \mid f_{ij}) = \exp\left[-\frac{1}{\sigma_n^2} \sum_i \sum_j \left(s_{ij} - \sum_n \sum_m p_{i-n,j-m} f_{nm}\right)^2\right]$$

where σ_n is the standard deviation of the noise. Substituting this result into the previous equation and differentiating, we get

$$\frac{2}{\sigma_n^2} \sum_i \sum_j \left(s_{ij} - \sum_n \sum_m p_{i-n,j-m} f_{nm}\right) p_{i-k,j-\ell} = 0$$

or

$$\sum_i \sum_j s_{ij} p_{i-k,j-\ell} = \sum_i \sum_j \left(\sum_n \sum_m p_{i-n,j-m} f_{nm}\right) p_{i-k,j-\ell}.$$

Using the appropriate symbols, we may write this equation in the form

$$s_{ij} \odot\odot p_{ij} = (p_{ij} \otimes\otimes f_{ij}) \odot\odot p_{ij}$$

where $\odot\odot$ and $\otimes\otimes$ denote the 2D correlation and convolution sums, respectively. The ML estimate is obtained by solving the equation above for f_{ij}. This

can be done by transforming it into Fourier space. Using the correlation and convolution theorems, in Fourier space this equation becomes

$$S_{ij}P_{ij}^{*} = (P_{ij}F_{ij})P_{ij}^{*}$$

and thus

$$f_{ij} = \hat{F}_2^{-1}[F_{ij}] = \hat{F}_2^{-1}\left[\frac{S_{ij}P_{ij}^{*}}{\mid P_{ij} \mid^2}\right]$$

where $\hat{F}_2^{-1}$ denotes the (2D) inverse discrete Fourier transform. Hence, for Gaussian statistics, the ML filter is given by

$$\text{ML Filter} = \frac{P_m^{*}}{\mid P_m \mid^2}$$

which is identical to the inverse filter.

14.3 The Maximum a Posteriori Filter

This filter is obtained by finding f_{ij} such that

$$\frac{\partial}{\partial f_{k\ell}} \ln P(s_{ij} \mid f_{ij}) + \frac{\partial}{\partial f_{k\ell}} \ln P(f_{ij}) = 0.$$

Consider the following models for the PDFs:

(i) Gaussian statistics for the noise

$$P(s_{ij} \mid f_{ij}) = \exp\left[-\frac{1}{\sigma_n^2}\sum_i\sum_j\left(s_{ij} - \sum_n\sum_m p_{i-n,j-m}f_{nm}\right)^2\right].$$

(ii) Gaussian statistics for the object

$$P(f_{ij}) = \exp\left(-\frac{1}{\sigma_f^2}\sum_i\sum_j f_{ij}^2\right).$$

By substituting these expressions for $P(s_{ij} \mid f_{ij})$ and $P(f_{ij})$ into the equation above, we obtain

$$\frac{2}{\sigma_n^2}\sum_i\sum_j\left(s_{ij} - \sum_n\sum_m p_{i-n,j-m}f_{nm}\right)p_{i-k,j-\ell} - \frac{2}{\sigma_f^2}f_{k\ell} = 0.$$

Rearranging, we may write this result in the form

$$s_{ij} \odot \odot p_{ij} = \frac{\sigma_n^2}{\sigma_f^2}f_{ij} + (p_{ij} \otimes \otimes f_{ij}) \odot \odot p_{ij}$$

In Fourier space this equation becomes

$$S_{ij}P^*_{ij} = \frac{1}{\Gamma^2}F_{ij} + \mid P_{ij} \mid^2 F_{ij}$$

where

$$\Gamma = \frac{\sigma_f}{\sigma_n}.$$

The MAP filter for Gaussian statistics is therefore given by

$$\text{MAP} \quad \text{Filter} = \frac{P^*_{ij}}{\mid P_{ij} \mid^2 + 1/\Gamma^2}.$$

Note that this filter is the same as the Wiener filter under the assumption that the power spectra of the noise and object are constant. Also, note that

$$\lim_{\sigma_n \to 0}(\text{MAP} \quad \text{Filter}) \quad = \quad \text{ML} \quad \text{Filter}.$$

14.4 Super Resolution using Bayesian Methods

In Chapter 13 we discussed the problem of extrapolating the spectrum of a band-limited image. The same problem can be tackled using a Bayesian method as discussed in this Section. The problem is given the data

$$S_{nm} \equiv S(k_n, k_m)$$

$$= \int_{-X}^{X}\int_{-Y}^{Y} s(x,y)\exp(-ik_n x)\exp(ik_m y)dxdy, \quad \mid k_n \mid \leq K_x, \quad \mid k_m \mid \leq K_y$$

where

$$s(x,y) = f(x,y) + n(x,y); \quad -X \leq x \leq X, \quad -Y \leq y \leq Y$$

obtain an estimate for f. This problem is equivalent to being given the band-limited data

$$s_{BL} = p \otimes\otimes s$$

where p is a band-limited point spread function such as a separable sinc or jinc function (i.e. the inverse Fourier transforms of a square and circular ideal low-pass filter respectively). As in Chapter 13, we consider a weighted linear polynomial model for f of the form

$$f(x,y) = w(x,y)\sum_n\sum_m A_{nm}\exp(ik_n x)\exp(ik_m y)$$

and find the discrete Fourier coefficients A_{nm} that satisfy the equation

$$\frac{\partial}{\partial A_{pq}}\ln P(s \mid f) + \frac{\partial}{\partial A_{pq}}\ln P(f) = 0$$

subject to appropriate and workable statistical models for $P(s \mid f)$ (i.e. the PDF of the noise field) and $P(f)$. For example, consider the distributions (ignoring normalization scaling)

$$P(s \mid f) \equiv P(n) = \exp\left[-\frac{1}{\sigma_n^2}\int_{-X}^{X}\int_{-Y}^{Y}\frac{\mid n(x,y)\mid^2}{w(x,y)}dxdy\right]$$

and

$$P(f) = \exp\left[-\frac{1}{\sigma_f^2}\int_{-X}^{X}\int_{-Y}^{Y}\frac{\mid f(x,y)\mid^2}{w(x,y)}dxdy\right].$$

The equation above is then satisfied if

$$-\frac{1}{\sigma_n^2}\frac{\partial}{\partial A_{pq}}\int_{-X}^{X}\int_{-Y}^{Y}\left|s(x,y) - w(x,y)\sum_n\sum_m A_{nm}\exp(ik_n x)\exp(ik_m y)\right|^2\frac{dxdy}{w(x,y)}$$

$$-\frac{1}{\sigma_f^2}\frac{\partial}{\partial A_{pq}}\int_{-X}^{X}\int_{-Y}^{Y}\left|w(x,y)\sum_n\sum_m A_{nm}\exp(ik_n x)\exp(ik_m y)\right|^2\frac{dxdy}{w(x,y)} = 0.$$

Differentiating, we obtain

$$\frac{1}{\sigma_n^2}S(k_p,k_q) - \frac{1}{\sigma_n^2}\sum_n\sum_m A_{nm}W(k_p-k_n,k_q-k_m)$$

$$+\frac{1}{\sigma_f^2}\sum_n\sum_m A_{nm}W(k_p-k_n,k_q-k_m) = 0.$$

Using the convolution theorem and rearranging the result, we get

$$f(x,y) = \frac{\Gamma^2}{1+\Gamma^2}\frac{w(x,y)}{w_{BL}(x,y)}s_{BL}(x,y)$$

where

$$\Gamma = \frac{\sigma_f}{\sigma_n}.$$

14.5 Summary of Important Results

Bayes rule

$$P(A)P(B \mid A) = P(B)P(A \mid B)$$

where $P(A)$ is the probability of A, $P(B)$ is the probability of B and $P(B \mid A)$ and $P(A \mid B)$ are the conditional probabilities of 'B given A' and 'A given B', respectively.

Principles of Bayesian estimation in image processing

Given that

$$s(x,y) = p(x,y) \otimes \otimes f(x,y) + n(x,y)$$

find f such that

$$\frac{\partial}{\partial f} \ln P(s \mid f) + \frac{\partial}{\partial f} \ln P(f) = 0$$

where $P(f)$ is the PDF of f and $P(s \mid f)$ is the PDF of n $(= s - p \otimes \otimes f)$.

MAP estimates

Based on knowledge (i.e. statistical models) for both $P(s \mid f)$ and $P(f)$.

ML estimates

Assume that

$$\frac{\partial}{\partial f} \ln P(f) \sim 0.$$

An estimate of f is then obtained based on the condition that

$$\frac{\partial}{\partial f} \ln P(s \mid f) = 0.$$

MAP and ML filters for Gaussian fields $P(f)$ and $P(s \mid f)$

Given that

$$s_{ij} = p_{ij} \otimes \otimes f_{ij} + n_{ij}$$

where n_{ij} and f_{ij} are Gaussian distributed with standard deviations σ_n and σ_f, respectively,

$$\text{ML} \quad \text{filter} = \frac{P_{ij}^*}{\mid P_{ij} \mid^2};$$

$$\text{MAP} \quad \text{Filter} = \frac{P_{ij}^*}{\mid P_{ij} \mid^2 + \frac{\sigma_f}{\sigma_n}}.$$

14.6 Further Reading

- Papoulis A, *Probability, Random Variables and Stochastic Processes*, McGraw-Hill, 1965.
- Van Trees H L, P*Detection, Estimation and Modulation Theory*, Wiley, 1968.
- Erickson G J and Smith C R (Eds.), *Maximum Entropy and Bayesian Methods in Science and Engineering*, Kluwer Academic Publishers, 1988.

- Lim J S, *Two-Dimensional Signal and Image Processing*, Prentice-Hall, 1990.
- Buck B B and Macaulay V A (Eds.), *Maximum Entropy in Action*, Clarendon Press, 1992.
- Lee P M, *Bayesian Statistics*, Arnold, 1997.

Chapter 15

Image Enhancement

One of the goals of image enhancement is to make the image look better. For this reason, image enhancement is a rather subjective matter because what 'looks better' depends on the type of details and contrasts in the image that the user is hoping to acquire which can include the application of resolution enhancing algorithms. In turn these properties depend on the physical characteristics of the image, the *a priori* knowledge that the user may have on certain features in the image, coupled with the user's experience, intuition and judgment. Hence, not surprisingly, there have evolved a wide variety of techniques for enhancing images which are based as much on the quality of the results that are achieved as on the criterion for enhancement. In this Chapter some of the more commonly used methods are discussed.

15.1 Basic Transforms

Basic transformations can be used to enhance details in an image which occur in the dark or light regions or 'fields' of the image. They are trivial to compute and in some cases have a physical significance.

15.1.1 Logarithmic Transform

The logarithmic transform is of the general form

$$v_{\text{out}}(i,j) = \ln v_{\text{in}}(i,j)$$

where v is the value of a pixel at a location (i,j). The portion of the logarithmic curve over which this transform is required can be adjusted by introducing a scaling parameter α and employing the transform

$$v_{\text{out}}(i,j) = \frac{1}{\alpha}\ln[1 + (e^{\alpha} - 1)v_{\text{in}}(i,j)].$$

The addition of 1 is included to prevent problems occurring if $v_{\text{in}} = 0$. The effect of this transform is to increase the dynamic range of dark fields in an image and decrease the dynamic range of the bright fields.

The logarithmic transform is a relatively simple method of adjusting the visual quality of an image in 'favour' of those features which have low grey level values. In some cases, using a logarithmic transform of this kind to enhance an image can be justified physically. For example, with X-ray images, the value of a pixel at (i, j) is given by the intensity of the X-rays I as they emerge from an object of varying thickness and density. The distribution in intensity is given by

$$I(i, j) = I_0 \exp[-f(i, j)]$$

where I_0 is the intensity of the X-ray source and f is a function of the X-ray attenuating properties of the material which in turn depend on the thickness and density of the material. If we apply the logarithmic transform to an X-ray image of this kind, we get

$$\ln I_{\text{out}}(i, j) = \ln I_0 - f(i, j).$$

In this case, the logarithmic transform provides an image which is a linear mapping of the X-ray attenuating properties of the material described by f.

15.1.2 Exponential Transform

The exponential transform is the inverse of the logarithmic transform and has an inverse effect on the image, i.e. it enhances detail in the bright fields of the image while decreasing the dynamic range of grey levels in dark fields. The basic transform is

$$v_{\text{out}}(i, j) = \exp[v_{\text{in}}(i, j)].$$

Bases other that the exponential can also be used for this purpose by employing the transform

$$v_{\text{out}}(i, j) = \frac{1}{\alpha}[(1 + \alpha)^{v_{\text{in}}(i,j)} - 1]$$

where α is a variable scaling parameter defined by the user.

15.2 Histogram Equalization

Another way of enhancing an image is to apply a transform which modifies the histogram of the image in a predetermined and desired fashion. A histogram is a plot of the number of times that a particular grey level occurs against the grey level. This provides a global description of the appearance of the image in terms of the characteristic (discrete) probability density function of grey levels. The profile or 'shape' of the histogram describes the density of grey levels in the image. If the histogram peaks at a low grey level, then the image is relatively dark and if the histogram has a concentration of pixels with a high grey level, then the image is relatively light.

Histogram equalization attempts to generate an image whose histogram is uniform (i.e. an image where each grey level occurs an equal number of times; hence the term, 'equalization'). The effect is to increase the dynamic range of grey levels. This has a considerable influence on the visual appearance of the image, enhancing the detail of many features in both the dark and light fields.

We can formulate the problem in the following way: Let v represent the value of a pixel which is confined to the range

$$0 \leq v \leq 1$$

where 0 represents black and 1 represents white. The pixels are quantized into L grey levels or 'bins' so that their range of values is now

$$0 \leq v_k \leq L, \quad k = 0, 1, 2, ..., L$$

where

$$v_0 = 0, \quad v_1 = 1, \quad v_2 = 2, \quad ...$$

The probability of a grey level occurring with value v_k is given by

$$P(v_k) = \frac{n_k}{N}$$

where n_k is the number of times a pixel occurs with value v_k in the image and N is the total number of pixels. The histogram is a plot of $P(v_k)$ against v_k. To equalize the histogram we require a transform $\hat{T}$ which produces a range of values

$$v_k^{\text{out}} = \hat{T}[v_k^{\text{in}}]$$

such that

$$P(v_k^{\text{out}}) = \begin{cases} 1, & \forall k > 1; \\ 0, & k = 0. \end{cases} \tag{15.1}$$

In these terms it is clear that the basic problem is to find $\hat{T}$. This is done by equating the cumulative histograms, i.e.

$$C(v_k^{\text{out}}) = C(v_k^{\text{in}}) \tag{15.2}$$

where $C(v_k^{\text{out}})$ and $C(v_k^{\text{in}})$ are given by

$$C(v_k^{\text{out}}) = \sum_{i=0}^{k} P(v_i^{\text{out}})$$

and

$$C(v_k^{\text{in}}) = \sum_{i=0}^{k} P(v_i^{\text{in}})$$

respectively.

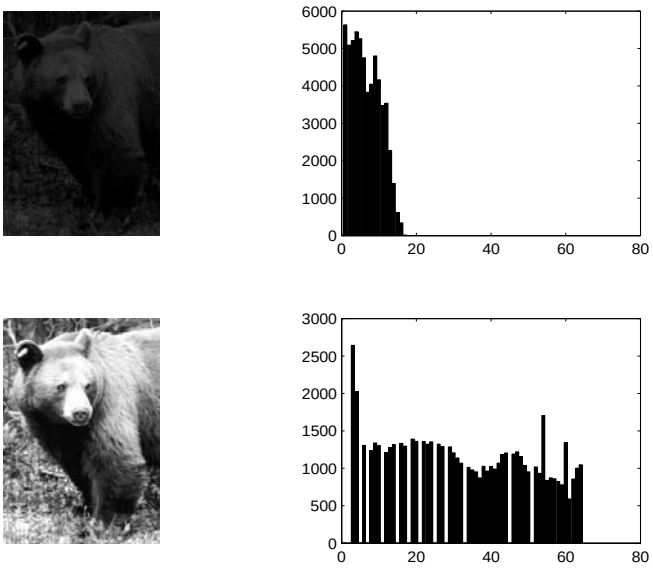

Figure 15.1: Original image before (top-left) and after (bottom-left) histogram equalization and the 64-bin histograms (top-right and bottom-right) respectively.

The transform is then obtained by noting that if equation (15.2) holds then

$$C(v_0^{\text{out}}) = \sum_{i=0}^{0} P(v_i^{\text{out}}) = P(v_0^{\text{out}}) = 0 = v_0^{\text{out}},$$

$$C(v_1^{\text{out}}) = \sum_{i=0}^{1} P(v_i^{\text{out}}) = P(v_0^{\text{out}}) + P(v_1^{\text{out}}) = 0 + 1 = 1 = v_1^{\text{out}},$$

$$C(v_2^{\text{out}}) = \sum_{i=0}^{2} P(v_i^{\text{out}}) = P(v_0^{\text{out}}) + P(v_1^{\text{out}}) + P(v_2^{\text{out}}) = 0 + 1 + 1 = 2 = v_2^{\text{out}},$$

and so on, i.e.

$$C(v_k^{\text{out}}) = \sum_{i=0}^{k} P(v_i^{\text{out}}) = v_k^{\text{out}}.$$

From equation (15.2), we then have,

$$v_k^{\text{out}} = C(v_k^{\text{in}})$$

which can computed directly from the original image. Thus, to enhance an image by histogram equalization we carry out the following procedure:

(i) normalize the image so that the largest pixel value is 1; (ii) quantize the pixels into L levels (defined by the user); compute the histogram of the image $P(v_k^{\text{in}})$; (iii) compute the cumulative histogram of the image

$$C(v_k^{\text{in}}) = \sum_{i=0}^{k} P(v_i^{\text{in}});$$

(iv) normalize this cumulative histogram and then quantize it into the same number of levels L; (v) assign the value of $C(v_k^{\text{in}})$ to all the pixels with an original grey level of v_k^{in}.

An example of histogram equalization is given in Figure 15.1. This process is very effective for images whose grey level distribution is narrow and shifted toward the origin leading to an image that is relative dark. The effect of histogram equalization is to redistribute the grey-levels over a the grey level range while maintaining the distribution as shown in Figure 15.1.

15.3 Homomorphic Filtering

Homomorphic filtering is based on using the properties of the logarithm to transform a multiplicative processes into an additive process. The method assumes a physical model for the object function that is based on an illumination-reflection equation of the form

$$f(x, y) = i(x, y)r(x, y)$$

where r is the reflection component, i is the illumination and f is the intensity distribution. In general, this model has two important features which homomorphic filtering relies upon. (i) the illumination component is composed of low spatial frequencies; (ii) the reflection component is composed of high spatial frequencies.

The objective of homomorphic filtering is to separate the reflection component from the illumination component. This is done by computing the logarithm of f, i.e.

$$\ln f(x, y) = \ln i(x, y) + \ln r(x, y).$$

The illumination and reflection components then become additive where:
(i) $\ln i$ is composed of low spatial frequencies; (ii) $\ln r$ is composed of high spatial frequencies. By applying a suitable high pass filter (HPF) to reduce the contribution of $\ln i$ to $\ln f$, $\ln r$ can be extracted, i.e.

$$\ln r(x, y) \simeq \text{HPF}[\ln f(x, y)].$$

Performing an exponentiation to convert the process back into an intensity distribution then provides the reflection component

$$r(x, y) \simeq \exp\left(\text{HPF}[\ln f(x, y)]\right).$$

This method of image enhancement is known as homomorphic filtering. It requires specification of the HPF. A variety of filters can be used for this purpose which include the following:

The Ideal High Pass Filter

The ideal high pass filter is given by

$$H(k_x, k_y) = \begin{cases} 0, & \sqrt{k_x^2 + k_y^2} \leq K \\ 1, & \sqrt{k_x^2 + k_y^2} > K. \end{cases}$$

where K is the cut-off frequency measured (in pixels) from the origin (the point in Fourier space where $k_x = k_y = 0$ assuming the optical form of the Fourier transform). This filter attenuates completely (i.e. sets to zero) all those spatial frequencies that are less than or equal to the cut-off frequency and passes without modification all those spatial frequencies that are greater than the cut-off frequency.

The Butterworth High Pass Filter

The Butterworth high pass filter (BHPF) is an approximation to the ideal filter. It is a continuous and circularly symmetric filter given by

$$B(k_x, k_y) = \frac{1}{1 + \left(\frac{K}{\sqrt{k_x^2 + k_y^2}} \right)^{2n}}.$$

The parameter n is a user-defined positive integer called the order of the filter. As the value of n increases, the BHPF approaches the ideal filter. Image enhancement by homomorphic filtering is usually carried out using the BHPF. In practice, a 2D FFT is used to carry out the filtering operation and the user may repeat this enhancing process for different values of K and n.

15.4 Light Diffusion and the High Emphasis Filter

High emphasis filtering is based on computing the Laplacian of an image and then subtracting the result from the image. This process provides a reconstruction which is particularly good at restoring the edges of a blurred image; it is an example of an image 'sharpening' filter.

The high emphasis filtered image (which shall be denoted by f_0) is related to the input image f by

$$f_0(x, y) = f(x, y) - \nabla^2 f(x, y).$$

The effect of the Laplacian is to amplify the high spatial frequencies in the image while leaving the low spatial frequencies relatively unchanged. This can be seen from the relationship

$$\nabla^2 f(x, y) \Longleftrightarrow (k_x^2 + k_y^2) F(k_x, k_y).$$

By subtracting $\nabla^2 f$ from f, the low frequencies are virtually canceled out while the high frequencies remain relatively unchanged.

15.4.1 Light Diffusion Model

High emphasis filtering is based on a physical model for an image that is assumed to have been degraded (i.e. blurred) through a process of diffusion[1]. Consider the 3D homogeneous time dependent wave equation

$$\nabla^2 u - \frac{1}{c^2}\frac{\partial^2}{\partial t^2}u = 0$$

where c is the speed of light. Let

$$u(x, y, z, t) = \phi(x, y, z, t)\exp(i\omega t)$$

where it is assumed that field ϕ varies significantly slowly in time compared with $\exp(i\omega t)$ and note that

$$u^*(x, y, z, t) = \phi^*(x, y, z, t)\exp(-i\omega t)$$

is also a solution to the wave equation. Differentiating

$$\nabla^2 u = \exp(i\omega t)\nabla^2\phi,$$

and

$$\frac{\partial^2}{\partial t^2}u = \exp(i\omega t)\left(\frac{\partial^2}{\partial t^2}\phi + 2i\omega\frac{\partial\phi}{\partial t} - \omega^2\phi\right) \simeq \exp(i\omega t)\left(2i\omega\frac{\partial\phi}{\partial t} - \omega^2\phi\right)$$

when

$$\left|\frac{\partial^2\phi}{\partial t^2}\right| << 2\omega\left|\frac{\partial\phi}{\partial t}\right|.$$

Under this condition, the wave equation reduces to

$$(\nabla^2 + k^2)\phi = \frac{2ik}{c}\frac{\partial\phi}{\partial t}$$

where $k = \omega/c$. However, since u^* is also a solution,

$$(\nabla^2 + k^2)\phi^* = -\frac{2ik}{c}\frac{\partial\phi^*}{\partial t}$$

and thus,

$$\phi^*\nabla^2\phi - \phi\nabla^2\phi^* = \frac{2ik}{c}\left(\phi^*\frac{\partial\phi}{\partial t} + \phi\frac{\partial\phi^*}{\partial t}\right)$$

which can be written in the form

$$\nabla^2 I - 2\nabla\cdot(\phi\nabla\phi^*) = \frac{2ik}{c}\frac{\partial I}{\partial t}$$

where $I = \phi\phi^* =\mid \phi \mid^2$. Let ϕ be given by

$$\phi(\mathbf{r}, t) = A(\mathbf{r}, t)\exp(ik\hat{\mathbf{n}}\cdot\mathbf{r})$$

[1]The author is grateful to Dr K I Hopcraft, Nottingham University, England for suggesting this approach.

where $\hat{\mathbf{n}}$ is a unit vector and A is the amplitude function. Differentiating, and noting that $I = A^2$, we obtain

$$\hat{\mathbf{n}} \cdot \nabla A = \frac{2}{c}\frac{\partial A}{\partial t}$$

or

$$\left(\frac{\partial}{\partial x} + \frac{\partial}{\partial y} + \frac{\partial}{\partial z}\right) A(x, y, z, t) = \frac{2}{c}\frac{\partial}{\partial t} A(x, y, z, t)$$

which is the unconditional continuity equation for the amplitude A of a wavefield

$$u(\mathbf{r}, t) = A(\mathbf{r}, t) \exp[i(k\hat{\mathbf{n}} \cdot \mathbf{r} + \omega t)]$$

where A varies slowly with time.

15.4.2 Diffusion Equation for the Intensity

The equation

$$\nabla^2 I - 2\nabla \cdot (\phi \nabla \phi^*) = \frac{2ik}{c}\frac{\partial I}{\partial t}$$

is valid for $k = k_0 - i\kappa$ (i.e. $\omega = \omega_0 - i\kappa c$) and so, by equating the and real and imaginary parts, we have

$$D\nabla^2 I + 2\mathrm{Re}[\nabla \cdot (\phi \nabla \phi^*)] = \frac{\partial I}{\partial t}$$

and

$$\mathrm{Im}[\nabla \cdot (\phi \nabla \phi^*)] = -\frac{k_0}{c}\frac{\partial I}{\partial t}$$

respectively, where $D = c/2\kappa$, so that under the condition

$$\mathrm{Re}[\nabla \cdot (\phi \nabla \phi^*)] = 0$$

we obtain

$$D\nabla^2 I = \frac{\partial I}{\partial t}.$$

This is the diffusion equation (see Chapter 5) for the intensity of light I. The condition required to obtain this result can be justified by applying a boundary condition on the surface S of a volume V over which the equation is taken to conform. Using the divergence theorem

$$\mathrm{Re} \int_V \nabla \cdot (\phi \nabla \phi^*) d^3\mathbf{r} = \mathrm{Re} \oint_S \phi \nabla \phi^* \cdot \hat{\mathbf{n}} d^2\mathbf{r} = \oint_S (\phi_r \nabla \phi_r + \phi_i \nabla \phi_i) \cdot \hat{\mathbf{n}} d^2\mathbf{r}.$$

Now, if

$$\phi_r(\mathbf{r}, t)\nabla\phi_r(\mathbf{r}, t) = -\phi_i(\mathbf{r}, t)\nabla\phi_i(\mathbf{r}, t), \quad \mathbf{r} \in S$$

then the surface integral is zero and

$$D\nabla^2 I(\mathbf{r}, t) = \frac{\partial}{\partial t} I(\mathbf{r}, t), \quad \mathbf{r} \in V.$$

This boundary condition can be written as

$$\frac{\nabla\phi_r}{\nabla\phi_i} = -\tan\theta$$

where θ is the phase of the field ϕ which implies that the amplitude A of ϕ is constant on the boundary (i.e. $A(\mathbf{r},t) = A_0, \quad \mathbf{r} \in S, \quad \forall t$), since

$$\frac{\nabla A_0 \cos\theta(\mathbf{r},t)}{\nabla A_0 \sin\theta(\mathbf{r},t)} = -\frac{A_0 \sin\theta(\mathbf{r},t)\nabla\theta(\mathbf{r},t)}{A_0 \cos\theta(\mathbf{r},t)\nabla\theta(\mathbf{r},t)} = -\tan\theta(\mathbf{r},t), \quad \mathbf{r} \in S.$$

15.4.3 Imaging a Diffused Intensity Field

Suppose we record the intensity I in the xy-plane for a fixed value of z. For $z = z_0$, let

$$f(x,y,t) = I(x,y,z_0,t)$$

so that

$$\frac{\partial}{\partial t} f(x,y,t) = D\nabla^2 f(x,y,t).$$

Let this two-dimensional diffusion equation be subject to the initial condition

$$f(x,y,0) = f_0(x,y).$$

Then, at any time $t > 0$, it is assumed that light diffusion is responsible for blurring the image f_0 and that, as time increases, the image becomes progressively blurred. The problem is to find f_0 from f at some time $t > 0$. High emphasis filtering is based on a solution to this problem that uses an approximation to the Taylor series expansion for f.

Suppose that we record the diffusion blurred image f at a time $t = T$. The Taylor series for f at $t = 0$ may then be written as

$$f(x,y,0) = f(x,y,T) - T\left[\frac{\partial}{\partial t} f(x,y,t)\right]_{t=T} + \frac{T^2}{2!}\left[\frac{\partial^2}{\partial t^2} f(x,y,t)\right]_{t=T} + ...$$

Let us approximate this function be neglecting all terms after the second term. Using the diffusion equation, we obtain

$$f(x,y,0) \simeq f(x,y,T) - T\left[\frac{\partial}{\partial t} f(x,y,t)\right]_{t=T} = f(x,y,T) - DT\nabla^2 f(x,y,T).$$

Now, since

$$f(x,y,0) = f_0(x,y)$$

we have

$$f_0(x,y) = f(x,y,T) - DT\nabla^2 f(x,y,T).$$

The equation for high emphasis filtering given earlier applies to the case when $DT = 1$ but the value of DT can be changed if the user requires control over the process. Introducing the coefficient $\alpha = DT$ we can use the equation

$$f_0(x,y) = f(x,y) - \alpha\nabla^2 f(x,y). \tag{15.3}$$

The effect of increasing the value of α is to amplify the high frequency content of f. By lowering the value of α, the influence of the high frequencies in f on f_0 is decreased.

15.4.4 Computational Method

Image enhancement by high emphasis filtering can be implemented by computing the digital Laplacian. This is achieved by applying a centre differencing scheme, i.e.

$$\nabla^2 f_{ij} = f_{(i+1)j} + f_{(i-1),j} + f_{i(j+1)} + f_{i(j-1)} - 4f_{ij}$$

for $\alpha = 1$ From this result, we have

$$f^0_{ij} = f_{ij} - \nabla^2 f_{ij} = 5f_{ij} - f_{(i+1)j} - f_{(i-1)j} - f_{i(j+1)} - f_{i(j-1)}$$

where

$$f^0_{ij} \equiv f_0(i,j).$$

The values of the pixels at the edges of the image (the boundary conditions) must be specified. For example, these pixels can be set to the value of their nearest neighbour, i.e.

$$f^0_{i1} = f^0_{i2}, \quad f^0_{iN} = f^0_{i(N-1)}$$

and

$$f^0_{1j} = f^0_{2j}, \quad f^0_{Nj} = f^0_{(N-1)j}.$$

The digital Laplacian is a shift invariant linear operation. Applying this operation to a digital image f_{ij} is the same as convolving the image with the two-dimensional array (the FIR filter)

$$\begin{pmatrix} 0 & 1 & 0 \\ 1 & -4 & 1 \\ 0 & 1 & 0 \end{pmatrix}.$$

Hence, computing f^0_{ij} is the same as convolving f_{ij} with the FIR filter

$$\begin{pmatrix} 0 & -1 & 0 \\ -1 & 5 & -1 \\ 0 & -1 & 0 \end{pmatrix}.$$

An example of the application of this filter is given in Figure 15.2. Given the simplicity of the process, the result can be remarkably good, provided that the degradation of the image conforms to a light diffusion model (i.e. to the diffusion equation).

15.4.5 Multiple Order Solution

If we record an image at a time $t = T$ then, by Taylor expanding f at $t = 0$, we can write

$$f(x,y,0) = f(x,y,T) + \sum_{n=1}^{\infty} \frac{(-1)^n}{n!} T^n \left[\frac{\partial^n}{\partial t^n} f(x,y,t) \right]_{t=T}$$

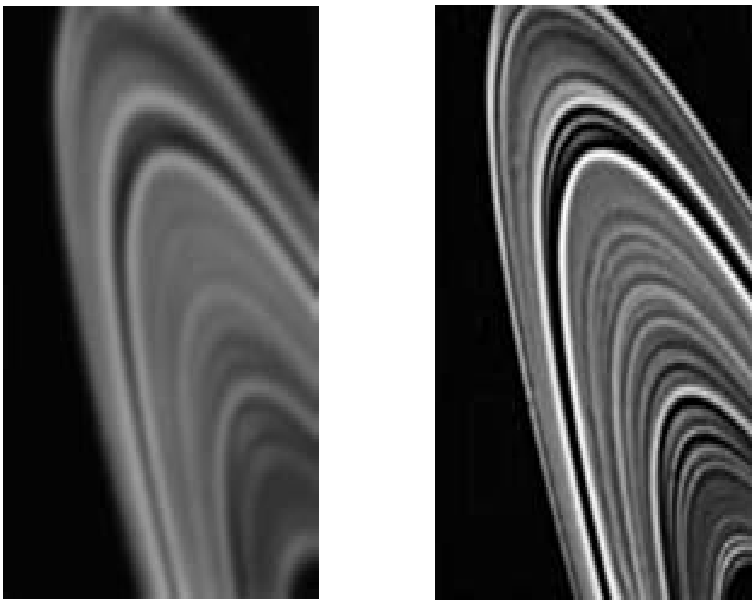

Figure 15.2: Original image (left) - rings of Saturn - and an enhanced image (right) using the high emphasis filter.

The high emphasis filter derived earlier is obtained by neglecting terms in the series above for $n > 1$ giving an approximate solution for the deblurred image f_0. If we include all the terms in this series, then an exact solution for f_0 can be obtained. This can be done by noting that (from the diffusion equation)

$$\frac{\partial^2 f}{\partial t^2} = D\nabla^2 \frac{\partial f}{\partial t} = D^2 \nabla^4 f$$

$$\frac{\partial^3 f}{\partial t^3} = D\nabla^2 \frac{\partial^2 f}{\partial t^2} = D^3 \nabla^6 f$$

and so on. In general we can write

$$\left[\frac{\partial^n}{\partial t^n} f(x,y,t)\right]_{t=T} = D^n \nabla^{2n} f(x,y,T).$$

Substituting this result into the series for f_0 given above, we get

$$f_0(x,y) = f(x,y,T) + \sum_{n=1}^{\infty} \frac{(-1)^n}{n!} (DT)^n \nabla^{2n} f(x,y,T)$$

and for $DT = 1$

$$f_0 = f - \nabla^2 f + \frac{1}{2!}\nabla^4 f - \frac{1}{3!}\nabla^6 f + ...$$

15.5 Noise Reduction

Noise refers to a variety of unwanted disturbances due to measuring and recording errors of all types and interference from external sources. All signals and images have some degree of noise present in them. The amplitude of the noise may vary considerably. Also, depending on the type of imaging system used, noise may be confined to a range of frequencies or exist over the entire spectrum of the image. In the latter case, the noise is referred to as white noise in analogy with white light which is composed of a range of different frequencies (in the visible part of the electromagnetic spectrum). Noise which is confined to a band of frequencies is sometimes referred to as coloured noise. The contamination of signals and images by noise has important consequences for all types of processing.

The aim of a noise reduction algorithm is primarily to enhance the visual quality of an image by eliminating features which are random and uncorrelated. In general, noise tends to corrupt the higher frequency content of most images where the energy of the data spectrum is usually low. Thus, one way of reducing noise is by attenuating the high frequency components of the data over a range of frequencies which can be selected and adjusted by the user to provide optimum results. This can be achieved by applying a low pass filter.

15.5.1 The Low Pass Filter

As the name suggests, the low pass filter passes the low frequencies of the data spectrum and attenuates the high frequencies.

The Ideal Low Pass Filter

The ideal low pass filter is given by

$$H(k_x, k_y) = \begin{cases} 1, & \sqrt{k_x^2 + k_y^2} \leq K; \\ 0, & \sqrt{k_x^2 + k_y^2} > K. \end{cases}$$

where K is the cut-off frequency. This type of filter attenuates (i.e. sets to zero) all the spatial frequencies above the cut-off frequency and retains without modification all those frequencies less than or equal to the cut-off frequency.

The Butterworth Low Pass Filter

The discontinuous nature of the ideal low pass filter causes ringing to occur in the filtered output. This phenomenon is known as the Gibbs effect and can be reduced by employing low pass filters which are continuous functions. A well known and widely used filter of this type is the Butterworth low pass filter (BLPF) which is given by

$$B(k_x, k_y) = \frac{1}{1 + \left(\frac{\sqrt{k_x^2 + k_y^2}}{K} \right)^{2n}}$$

where n is the order of the filter. This parameter is a positive integer and determines the rate at which the filter approaches zero.

15.5.2 The Neighbourhood Averaging Filter

The neighbourhood or moving averaging filter is a spatial domain technique. A window is chosen which encloses a predetermined neighbourhood of pixels. The average value of the pixels enclosed by this window is then computed and assigned to the pixel at the centre of the neighbourhood. By moving the window and repeating this process, a neighbourhood averaged image is obtained. The size of the window is defined by the user. Although different-shaped windows can be employed, a square window is easier to use in practice. The windows are typically 3×3, 7×7, 9×9, etc. The effect of computing the average of a neighbourhood of pixels is to eliminate any sudden jumps in the grey level which could be caused by some noise process. This is demonstrated in the following example: suppose we have the 3×3 neighbourhood

$$\begin{pmatrix} 2 & 2 & 3 \\ 3 & 30 & 2 \\ 1 & 3 & 2 \end{pmatrix}.$$

Compared with the numbers 1,2 and 3, the number 30 is relatively large and can be taken to be a digital representation of a noise spike. The average value of this group of numbers is 5.3. By assigning this value to the central pixel we obtain the neighbourhood

$$\begin{pmatrix} 2 & 2 & 3 \\ 3 & 5.3 & 2 \\ 1 & 3 & 2 \end{pmatrix}.$$

The value of the central pixel is now compatible with its neighbours. Hence, the noise spike is removed. We can express the neighbourhood averaging process as

$$s_{ij} = \frac{1}{M} \sum_{(n,m)\in S} f_{nm}$$

where S is the window enclosing $n \times m$ neighbours whose centre is located at (i, j) and M is the total number of pixels (enclosed by S). This process is the same as convolving the data with the kernel

$$p_{ij} = \frac{1}{M} \begin{pmatrix} 1 & 1 & \dots & 1 \\ 1 & 1 & \dots & 1 \\ \vdots & \vdots & \vdots & \vdots \\ 1 & 1 & \dots & 1 \end{pmatrix}.$$

The problem of computing the neighbourhood average of the pixels at the extreme edge of the image is overcome by zero padding, for example. For a 5×5 window the frame of zeros must be 2 pixels wide. The original image is then extracted after completing the neighbourhood averaging process.

The main problem with neighbourhood averaging is that it tends to blur the image. It therefore has a similar effect to the low pass filter in that high frequency noise is reduced at the expense of image sharpness. One way of reducing this effect is by using a thresholding process to leave unchanged those regions of an image with large variations in the grey level. This can be done by employing the following process:

if $\mid f_{ij} - s_{ij} \mid <$ threshold
$h_{ij} = s_{ij}$
else
$h_{ij} = f_{ij}$
endif

where

$$s_{ij} = p_{ij} \otimes \otimes f_{ij}$$

and h_{ij} is the output. If $\mid f_{ij} - g_{ij} \mid$ is greater or equal to the threshold, then the image remains unchanged. Regions of the image where $\mid f_{ij} - g_{ij} \mid$ is large correspond to places where there is an abrupt change in the value of the grey level. For this reason, application of the thresholding process given above helps to reduce high frequency noise while preserving the original sharpness of the image and, therefore, important features such as its edges.

15.6 The Median Filter

The aim of all noise-reducing processes is to suppress noise without blurring or degrading the original image. With low pass filters achieving optimum results often requires a considerable amount of trial and error. In the case of neighbourhood averaging, the application of a threshold can go some way to preserving image sharpness. However, once again, choosing the right threshold involves the user having to test a range of different values. These problems can be overcome to a limited extent be employing another filter known as the median filter. The basic idea is the same as the neighbourhood averaging filter except that, instead of computing the average of the neighbourhood we compute the median of the neighbourhood.

The median m of a set of numbers is such that half of the numbers in the set are less than m and half are greater than m. Thus, suppose we have a set of five numbers say

$$(1, 2, 3, 4, 5)$$

then the median of these numbers is 3. Similarly, the median of the numbers

$$(7, 19, 20, 30, 31, 49, 69, 72, 81)$$

is 31 because it is the fifth largest value of the set (there are four numbers less than 31 and four numbers greater than 31). As with neighbourhood averaging, the size of the neighbourhood is defined by the user - typically 3×3, 7×7, 9×9, etc. In a 3×3 neighbourhood, the median is the 5th largest value. In a 5×5 neighbourhood, the median is the 13th largest value and so on. In practice,

the median of a neighbourhood of pixels can be found by reordering them as a sequence of increasing numbers. For example, suppose we have the following 3×3 neighbourhood of pixels

$$\begin{pmatrix} 2 & 6 & 3 \\ 14 & 81 & 2 \\ 13 & 4 & 1 \end{pmatrix}.$$

First, we convert this 3×3 matrix into the row vector

$$(2, 6, 3, 14, 81, 12, 13, 4, 1).$$

Then, we reorder these numbers as a sequence of increasing values

$$(1, 2, 3, 4, 6, 12, 13, 14, 81).$$

The median of this sequence is then the fifth largest value which is 6. This example is a good illustration of why median filtering reduces noise spikes. In comparison with the other numbers in the neighbourhood above, 81 is relatively large and can be taken to represent a noise spike. The median filter replaces this value with the median of the neighbourhood, i.e. 81 is replaced by 6 and the neighbourhood becomes

$$\begin{pmatrix} 2 & 6 & 3 \\ 14 & 6 & 12 \\ 13 & 4 & 1 \end{pmatrix}.$$

If some of the numbers in the set are the same, then the equal values are grouped together. For example, suppose we have the set

$$(5, 6, 20, 10, 11, 10, 12, 13, 10)$$

where the number 10 occurs three times. Reordering these numbers in ascending values, the three 10's are grouped together, thus:

$$(5, 6, 10, 10, 10, 11, 12, 13, 20).$$

The median of this set is still the fifth largest value which in, this example, is 10.

The example given above demonstrates that the principal function of a median filter is to force pixels with very distinct values to be more like their neighbours. The problem of computing the median of those pixels at the extreme edge of the image is dealt with in exactly the same way as in the neighbourhood averaging filter, e.g. zero padding. An example of the application of a median filter is given in Figure 15.3. Compared with the neighbourhood averaging filter, it provides a superior result in the case when a the image has been corrupted by isolated noise spikes.

Figure 15.3: Original image (top-left); original image with additive noise spikes (top-right); noisy image after application of a 3×3 neighbourhood averaging filter (bottom-left) and after applying a 3×3 median filter (bottom-right).

15.7 Summary of Important Results

Histogram equalization

The basic process is

$$v_k^{out} = \sum_{i=0}^{k} P(v_k^{in})$$

where v is the value of a pixel located at (i, j) and P is the probability of a grey level occur with value v_k.

Homomorphic filtering

Basic problem is: Given

$$f(x, y) = i(x, y)r(x, y)$$

where f is the data, i is the illumination component and r is the reflection component, recover r. The solution to this problem is as follows:

(i) Apply the homomorphic process

$$\ln f = \ln i + \ln r.$$

(ii) Apply a high pass filter to recover $\ln r$

$$\ln r \simeq \text{HPF}[\ln f(x)].$$

(iii) Apply exponentiation to recover r

$$r = \exp(\ln r) \simeq \exp[\text{HPF}(\ln f)].$$

High emphasis filter

Assumes that the blur in an image is due to a process of light diffusion, i.e. convolution by a low-pass Gaussian filter. The restored image f_0 is given by

$$f_0(x, y) = f(x, y) - DT\nabla^2 f(x, y)$$

where f is the blurred image, D is the diffusivity and T is the period over which diffusion has occurred. The higher order solution (i.e. the solution to an order n) is given by

$$f_0(x, y) = f(x, y, T) + \sum_n \frac{(-1)^n}{n!}(DT)^n \nabla^{2n} f(x, y, T).$$

Butterworth low pass filter

$$B(k_x, k_y) = \frac{1}{1 + \left(\frac{\sqrt{k_x^2 + k_y^2}}{K}\right)^{2n}}$$

where K is the cut-off frequency and n is the order of the filter (a user-defined positive integer).

Neighbourhood averaging filter

$$s_{ij} = \frac{1}{M} \sum_{(n,m) \in S} f_{ij}$$

where S is the window containing $n \times m$ pixels whose centre is located at (i, j) and M is the total number of pixels in the image.

Median filter

The median m of a set of numbers is such that half the numbers are less than m and half the numbers are greater than m. The median filter operates in the same way as the neighbourhood averaging filter except that instead of computing the average of the neighbourhood, it computes the median of the neighbourhood.

15.8 Further Reading

- Niblack W, *An Introduction to Digital Image Processing*, Prentice-Hall, 1986.
- Lim J S, *Two-Dimensional Signal and Image Processing*, Prentice-Hall, 1990.
- Lewis R, *Practical Digital Image Processing*, Horwood, 1990.
- Pearson D (Ed.), *Image Procesing*, McGraw-Hill, 1991.
- Lindley C A, *Practical Image Processing in C*, Wiley Professional Computing, Wiley, 1991.
- Blackledge J M, *Image Processing: Mathematical Methods and Applications*, Oxford University Press, 1997.
- Blackledge J M and Turner M J, *Image Processing II: Mathematical Methods, Algorithms and Applications*, Horwood Publishing Series: Mathematics and Applications, 1999.
- Blackledge J M and Turner M J, *Image Processing III: Mathematical Methods, Algorithms and Applications*, Horwood Publishing Series: Mathematics and Applications, 2001.

Problems: Part III

In the questions that follow, n is the size of the input/output array.

III.1 Write a function to convolve a given object function with a point spread function using FFT2D.

```
void CONVOLVE(float **f, float **p, float **s, int n)
```

where f is the object function, p is the point spread function and s is the image.

Generate a digital image consisting of two discs of unit amplitude with a diameter of 10 pixels and with (x,y) coordinates of (54,64) and (74,64). Convolve this image with a Gaussian point spread function. Observe the effect of varying the width of the point spread function.

III.2 Write a function to autocorrelate an image using FFT2D.

```
void AUTOCOR(float **f, float **s, int n)
```

where f is the input image and s is the output image. Observe the result of autocorrelating different images.

III.3 Write a function to cross-correlate two digital images using FFT2D.

```
void CROSCOR(float **f, float **p, float **s, int n)
```

where f and p are the input images and s is the output.

III.4 Write a subroutine to restore an image using the Wiener filter.

```
float WIENER(float **s, float **p, float **f, int n, float snr)
```

where s is the digital image (input), p is the point spread function, f is the restored image (output) and snr is the signal-to-noise ratio.

III.5 Using function CONVOLVE, convolve the image and image with a Gaussian point spread function so that the features in the image become blurred. Attempt to restore this blurred image with function WIENER using a range of values for snr between 1 and 100. Repeat the restoration when a Gaussian noise field is added to the image before application of the Wiener filter and study the effect on the restoration.

III.6 Write a function to restore an image using the Power Spectrum Equalization Filter.

```
void PSE(float **s, float **p, float **f, int n, float snr)
```

where s is the digital image (input), p is the point spread function, f is the restored image (output) and snr is the signal-to-noise ratio. Repeat the question above using this filter.

III.7 Write two functions to lowpass filter an image using a rectangular window and an elliptical window.

```
void ILF_RECT(float **f, float **s, int x, int y, int n)

void ILF_ELLIPSE(float **f, float **s, int nx, int ny, int n)
```

where f is the input, s is the filtered output, x and y defines the (x,y) window size in pixels.

III.8 Write a function to process an image using the generalized logarithmic transform

```
void LOGTRAN(float **s, int n, float a)
```

where s is the input/output and a is the amplitude control.

III.9 Write a function to process an image using the generalized exponential transform

```
void EXPTRAN(float **s, int n, float a)
```

where s is the input/output and a is the amplitude control.

III.10 Write a function to 'histogram equalize' an image.

```
void HISTEQ(float **s, float **f, int n, int l)
```

where s is the input, f is the output and l is the number of grey levels.

Test this function using some 'dark field' images.

III.11 Write a function to highpass Butterworth filter a digital image.

```
void BHF(float **s, int n, int cut, int ord)
```

where s is the input/output, cut is the cutoff frequency (in pixels) and ord is the 'order' of the filter.

III.12 Write a function to homomorphic filter a digital image using the Butterworth highpass filter.

```
void HOMOFIL(float **s, int n, int cut, int ord)
```

where s is the input/output, cut is the cutoff frequency and ord is the 'order' of filter.

Working with ord=4, test this algorithm for on a range of image.

III.13 Write a function to high emphasis filter a digital image using an FIR filter with an appropriate kernel based on the result

$$O = I - \nabla^2 I$$

where I is the input image and O is the output.

```
void HEFIL(float **s, int n)
```

where s is the input/output.

III.14 By centre differencing of the Laplacian ∇^2, compute the FIR kernels for the second and third order high emphasis filters based on the results

$$O = I - \nabla^2 I + \frac{1}{2}\nabla^4 I$$

and

$$O = I - \nabla^2 I + \frac{1}{2}\nabla^4 I - \frac{1}{6}\nabla^6 I$$

respectively where I is the input image and O is the output image. Compare the result of applying the first and second order high emphasis filters to an image that has been 'diffused' via the application of a Gaussian lowpass filter.

III.15 Write a function to low-pass Butterworth filter an image

```
void BLF(float **s, int n, int cut, int ord)
```

where s is the input/output, cut is the cutoff frequency and ord is the order of filter.

Working with ord=4, evaluate this process using a range of images.

III.16 Write a function to filter a digital image using the moving average principle.

```
void MOVAV(float **s, int n, int w)
```

where s is the input/output and w is the window size.

III.17 Write a function to median filter a digital image.

```
void MEDIAN(float **s, int n, int w)
```

where s is the input/output and w is the window size

III.18 Study and compare the performance of the moving average and median filters by adding a random Gaussian noise field to an image. Repeat this study for the case when the noise field consists of some isolated noise spikes obtained by applying a threshold to a noise field with random Gaussian deviates.

Part IV

Pattern Recognition and Computer Vision

Chapter 16

Segmentation and Edge Detection

Image analysis and pattern recognition involves the use of image processing methods that are designed in an attempt to provide a machine interpretation of an image. Many of these 'methods' are based on models and computational procedures that are consistent with those that have already been covered in this work such as convolution, correlation, Fourier analysis and moving window-based data processing. In Part IV of this work, the principal themes of pattern recognition are considered, including methods of image segmentation as discussed in this Chapter.

Pattern recognition uses a range of techniques and image processing methods which are not necessarily based on any one particular theme or unified theoretical approach. The main problem is that, to date, there is no complete theoretical model for simulating the processes that take place when a human interprets an image generated by the eye. Hence, machine or computer vision remains a rather elusive subject area in which automatic inspection systems are advanced without having a fully operational theoretical framework as a guide. Vision can be thought of as a process of linking parts of the visual field (objects) with stored information or templates about their significance for the observer. There are a number of questions concerning vision such as: (i) what are the goals and constraints? (ii) what type of algorithm or set of algorithms is required to effect vision? (iii) what are the implications for the process given the types of hardware that might be available? (iv) what are the levels of representation required to achieve vision?

The levels of representation are dependent on what type of segmentation can and/or should be applied to an image. For example, we may be able to produce a primal sketch from an image via some measure of the intensity changes in a scene which are recorded as place tokens and stored in a database. This allows sets of raw components to be generated, e.g. regions of pixels with similar intensity values or sets of lines obtained by isolating the edges of an image scene and computed by locating regions where there is a significant difference in the intensity. However, such sets are subject to inherent ambiguities when

computed from a given input image and associated with those from which an existing data base has been constructed. Such ambiguities can only be overcome by the application of high-level rules, based on how humans interpret images, but the nature of this interpretation is not always clear. Nevertheless, parts of an image will tend to have an association if they share size, colour, figural similarity, continuity, shading and texture, for example. For this purpose, we are required to consider how best to segment an image and what form this segmentation should take.

The identification of the edges of an object in an image scene is an important aspect of the human visual system because it provides information on the basic topololgy of the object from which an interpretative match can be achieved. In other words, the segmentation of an image into a complex of edges is a useful pre-requisite for object identification. However, although many low-level processing methods can be applied for this purpose, the problem is to decide which object boundary each pixel in an image falls within and which high-level constraints are necessary. Figure 16.1 illustrates the problem. This is a binary image of a Dalmatian dog (which can be seen toward the centre of the image) under a tree casting shade. Clearly, it is difficult to imagine how, by segmenting the pixels in to sets (edge contours or otherwise), their overall organization into objects (such as 'tree' and 'dog') can be achieved. Thus, the question is, which comes first, recognition or segmentation?

Figure 16.1: Although this photograph is actually a composition of black shapes on a white surface, the mind organizes the elements, based on past experience, into the image of a Dalmatian dog.

Compared to image processing, computer vision (which incorporates machine vision) is more than automated image processing. It results in a conclu-

sion, based on a machine performing an inspection of its own. The machine must be programmed to be sensitive to the same aspects of the visual field as humans find meaningful.

Segmentation is concerned with the process of dividing an image into meaningful regions or segments. It is used in image analysis to separate features or regions of a pre-determined type from the background; it is the first step in automatic image analysis and pattern recognition. Segmentation is broadly based on one of two properties in an image: (i) similarity; (ii) discontinuity. The first property is used to segment an image into regions which have grey levels within a predetermined range. The second property segments the image into regions of discontinuity where there is a more or less abrupt change in the values of the grey levels. This is used to detect the boundaries or edges of features in the image, and is known as edge detection.

16.1 Correlation and the Auto-covariance Function

Correlation is one of the principal methods for recognizing a specific pattern in an image. Suppose we have an feature in an image f_{ij} which matches a template image t_{ij}. If we compute the correlation function given by

$$c_{ij} = t_{ij} \odot \odot f_{ij} \equiv \sum_n \sum_m t_{(i+n)(j+m)} f_{nm}$$

then the correlation image or surface c_{ij} will contain a maximum value (a 'peak' or 'point') at the position in the image f_{ij} which matches the template t_{ij}. A simple example is shown in Figure 16.2. Here, some text is used to illustrate the principle where the letter 'y' occurs just once in the image. By correlating the image with a template of this letter (i.e. the data obtained by cropping this feature from the image) a maximum or 'point' is obtained at the position where the template matches perfectly the image feature. By isolating this point and recording the coordinates in the image plane at which it occurs, the pattern and its location in the image can be 'recognized'. This method relies on a number of limiting conditions: (i) the orientation of the pattern must be the same as that of the template; (ii) the scale of the pattern must be the same; (iii) the template should be a good representation of the pattern. In practice, this is not always possible and several image processing methods are required to implement this method of pattern recognition in practice. Nevertheless, the correlation method introduced here is a principal approach in pattern recognition, once the pattern of interest has been decided upon and extracted from the image.

Given that f_{ij} is the pixel value at position ij in the image, for shift-invariant images (i.e. images that have been formed from a stationary or isoplanatic process), the normalized autocorrelation function is defined as

$$c_{ij} = \frac{1}{c_{00}}(f_{ij} \odot \odot f_{ij}).$$

This result can be derived from differences in the form of a normalized difference correlation function since

$$\sum_n \sum_m [f_{nm} - f_{(i+n)(j+m)}]^2 =$$

$$\sum_n \sum_m [f_{nm}^2 - 2f_{(i+n)(j+m)} f_{nm} + f_{(n+i)(m+j)}^2]^2 = 2 \sum_n \sum_m [f_{nm}^2 - f_{(i+n)(j+m)} f_{nm}]$$

$$= 2 \left(c_{00} - \sum_n \sum_m f_{(i+n)(j+m)} \right) = 2c_{00} \left(1 - \frac{1}{2} c_{ij} \right).$$

As most images are a mixture of deterministic and random processes (e.g. additive noise), it is useful to subtract the mean and then calculate the auto-correlation. This is termed the auto-covariance function which is defined as

$$C_{ij} = \sum_n \sum_m [f_{nm} - \langle f_{ij} \rangle][f_{(i+n)(j+m)} - \langle f_{ij} \rangle]$$

where $\langle f_{ij} \rangle$ is the mean value of f_{ij}.

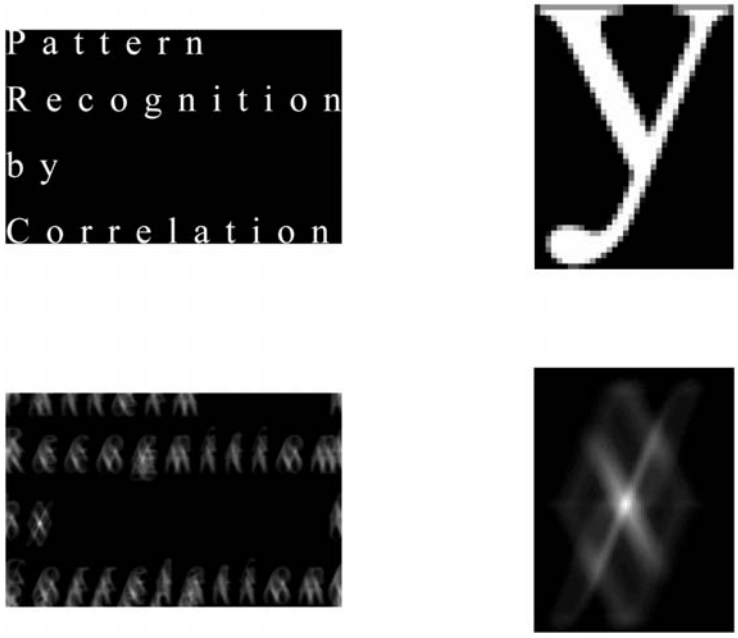

Figure 16.2: A text image (top-left) and a template of the letter 'y' (top-right enlarged) obtained from a crop of the text image. The result of correlating the text image with this template yields a point in the correlation surface (bottom-left) at the position in the image where the template and the feature match (bottom-right enlarged).

For a template t_{ij} the covariance function is given by

$$C_{ij} = \sum_n \sum_m [f_{nm} - \langle f_{ij} \rangle][t_{(i+n)(j+m)} - \langle t_{ij} \rangle]$$

where $\langle t_{ij} \rangle$ is the mean of t_{ij}.

The correlation function and the covariance function are two important metrics used in pattern recognition. The problem is to decide what feature(s) of an image to extract in order to generate a template that is robust and relatively insensitive to noise. The template is typically constructed be processing the image first in order to isolate features that may be based on pixel similarity, discontinuity, and statistical measures (including measures of the texture).

16.2 Thresholding

Thresholding is a relatively simple approach to segmenting an image into regions of similarity. The basic principle is to group pixels within a common range of grey levels into a pre-determined set. The simplest method is the single-band fixed threshold. This is based on first normalizing the image so the pixels have values which lie between 0 and 1, i.e.,

$$0 \leq v_{ij} \leq 1$$

where v is the value of the pixel at (i, j). Single-band fixed thresholding converts an image of this type into binary form consisting of just 0's and 1's by application of the following processes:

if $v_{ij}^{\text{in}} >$ threshold
$v_{ij}^{\text{out}} = 1$
else
$v_{ij}^{\text{out}} = 0$

where $0 <$ threshold < 1. This process can be used to isolate features in an image with a large intensity by applying a threshold which is close to 1. Examples where this technique is sometimes used include imaging with radar. Here, the image is composed of amplitude fluctuations caused by objects either in the air or on the ground which reflect microwaves. These modulations are related to the radar cross section (see Chapter 10). Radar operators are usually concerned with isolating targets with a large radar cross section from their surroundings which give rise to a feature known as clutter. By applying the process above, objects with a relatively large radar cross section can be isolated from the rest of the image.

In some cases, it is preferable to retain the grey level variations that occur above the threshold. This is known as semi-thresholding and is achieved by applying the following process:

if $v_{ij}^{\text{in}} >$ threshold
$v_{ij}^{\text{out}} = v_{ij}^{in}$

else
$v_{ij}^{\text{out}} = 0$

The thresholding principle can be extended to incorporate a number of different classes. This is known as multi-band fixed thresholding and is based on the following process:

$v_{ij}^{\text{out}} = 0$ if $0 \leq v_{ij}^{\text{in}} < t_1$;

$v_{ij}^{\text{out}} = 1$ if $t_1 \leq v_{ij}^{\text{in}} < t_2$;

$v_{ij}^{\text{out}} = 2$ if $t_2 \leq v_{ij}^{\text{in}} < t_3$

and so on where $t_1, t_2, t_3, ...$ are different thresholds.

16.3 Edge Detection

One of the most important expects of the human visual system is the way in which it appears to make use of the outlines or edges of objects for recognition and the perception of distance and orientation. This has led to a theory for the human visual system which is based on the idea that the visual cortex contains a complex of feature detectors that are tuned to edges and segments of various widths and orientations. For this reason, the detection of the edges in an image can play an important role in the analysis of an image.

Edge detection is basically a method of segmenting an image into regions of discontinuity. In other words, it allows the user to observe those features of an image where there is a more or less abrupt change in grey level or texture - indicating the end of one region in the image and the beginning of another. Like other methods of image analysis, edge detection is sensitive to noise. For this reason, detected edges can occur in places where the transition between regions is not abrupt enough or else edges can be detected in regions of an image where the texture is uniform.

In simple terms, edge detection makes use of differential operators to detect changes in the gradients of the grey levels. It is divided into two main categories: (i) first order edge detection; (ii) second order edge detection. As the name suggests, first order edge detection is based on the use of a first order derivative whereas second order edge detection is based on the use of a second order derivative, in particular, the Laplacian ∇^2.

To detect edges in an image we aim to highlight or emphasise changes in the value of the pixels. Mathematical derivative operations are ideally suited for this purpose. The first derivative, $\partial/\partial x$, shows extremes at an edge and the second derivative, $\partial^2/\partial x^2$, crosses the zero axis where the edge has its steepest gradient.

16.3.1 First Order Edge Detection

First order edge detection is based on computing the gradient of an image in x and y and observing the locations in the image where it changes abruptly. If

the image is denoted by the function $f(x, y)$ then the basic idea is to compute

$$\nabla f(x,y) = \hat{\mathbf{x}}\frac{\partial}{\partial x}f(x,y) + \hat{\mathbf{y}}\frac{\partial}{\partial y}f(x,y)$$

and then display the gradient magnitude defined by

$$\mid \nabla f \mid = \sqrt{\left(\frac{\partial f}{\partial x}\right)^2 + \left(\frac{\partial f}{\partial y}\right)^2}.$$

A threshold can be applied so that only a fraction of the gradients present in the image are retained. A binary image composed of 1's and 0's is then obtained which is a display of all the points in the image where its gradient is larger than the value of the threshold that is applied.

16.3.2 Digital Gradients

In many ways the different gradient methods used for edge detection result from attempts to find digital approximations to ∇f. The approximations available are compounded in a class of operators known as digital gradients. A continuous function $f(x)$ can be expanded about a point $x = \Delta x$, say, as a Taylor series

$$f(x + \Delta x) = f(x) + \Delta x \frac{d}{dx}f(x) + \frac{(\Delta x)^2}{2!}\frac{d^2}{dx^2}f(x) + ...$$

If we neglect all the terms which occur after the second term, then we obtain an approximation for the derivative of f at Δx, given by the difference equation

$$\frac{d}{dx}f(x) = \frac{f(x + \Delta x) - f(\Delta x)}{\Delta x}.$$

With partial derivatives we have

$$\frac{\partial}{\partial x}f(x,y) = \frac{f(x + \Delta x, y) - f(x,y)}{\Delta x}$$

and

$$\frac{\partial}{\partial y}f(x,y) = \frac{f(x, y + \Delta y) - f(x,y)}{\Delta y}.$$

Thus, with a digital image f_{ij}, we can replace the partial derivatives with the differences

$$D_x f_{ij} = f_{(i+1)j} - f_{ij}$$

and

$$D_y f_{ij} = f_{i(j+1)} - f_{ij}.$$

These operations are equivalent to convolving f_{ij} with the kernel $(-1, 1)$ in the x-direction to give $D_x f_{ij}$ and convolving f_{ij} with $(-1, 1)$ in the y-direction to give $D_y f_{ij}$. The kernels or (FIR) filters which are used to convolve a digital image in this way are called masks. They are shift invariant operators which allow us to write the former difference equations in the form

$$D_x f_{ij} = D_x \otimes f_{ij},$$

$$D_y f_{ij} = D_y \otimes f_{ij}$$

where

$$D_x = \begin{pmatrix} -1 & 1 \end{pmatrix}$$

and

$$D_y = \begin{pmatrix} -1 \\ 1 \end{pmatrix}.$$

The equivalence of digital gradient operations and discrete convolutions (i.e. FIR filters) with certain types of masks is an important result in the theory and practice of edge detection.

The differencing scheme derived above generates output values for the digital gradients centred at $(i+1/2, j)$ and $(i, j+1/2)$. This differencing is actually only one of a number of different arrangements that can be used. For example, to obtain digital gradients centred at (i, j), we use the differencing scheme

$$D_x f_{ij} = \frac{1}{2}[f_{(i+1)j} - f_{(i-1)j}],$$

$$D_y f_{ij} = \frac{1}{2}[f_{i(j+1)} - f_{i(j-1)}]$$

since

$$\frac{\partial}{\partial x} f(x,y) \simeq \frac{f(x,y) - f(x+\Delta x, y)}{\Delta x}; \quad \frac{\partial}{\partial x} f(x,y) \simeq \frac{f(x-\Delta x, y) - f(x,y)}{\Delta x}$$

and, hence,

$$\frac{\partial}{\partial x} f(x,y) \simeq \frac{f(x-\Delta x, y) - f(x+\Delta x, y)}{2\Delta x}.$$

In this case, the masks are given by

$$D_x = \frac{1}{2}\begin{pmatrix} -1 & 0 & 1 \end{pmatrix}$$

and

$$D_y = \frac{1}{2}\begin{pmatrix} -1 \\ 0 \\ 1 \end{pmatrix} \equiv \frac{1}{2}\begin{pmatrix} -1 & 0 & 1 \end{pmatrix}^T.$$

To detect edges independent of orientation, a gradient operator (a vector operator) is defined as

$$G = \sqrt{D_x \cdot D_x + D_y \cdot D_y}.$$

The gradient magnitude G is calculated with an operator $\cdot$ via the following procedure. The two values D_x and D_y are calculated separately and squared. The two values are then added and the square root of the sum provides the result. To simplify the calculations an alternative is sometimes used, namely

$$G = |D_x| + |D_y|.$$

The angle of gradient $\theta(G)$ is also a useful quantity and is given by

$$\theta(G) = \tan^{-1}\left(\frac{D_y}{D_x}\right).$$

There are a number of variants on this theme, that give different emphasis to detecting different types of edges which are discussed below.

16.3.3 The Roberts Edge Detector

The masks discussed so far provide a first approximation to computing the gradient of an image in the x- and y-directions which results in an emphasis on horizontal and vertical lines. Consequently, they are not good at detecting the edges at 45^o, for example. The Roberts gradient is based on approximating first order gradients using cross-differences, where the gradient magnitude is given by

$$G_{ij} = \sqrt{[f_{ij} - f_{(i+1)(j+1)}]^2 + [f_{(i+1)j} - f_{i(j+1)}]^2}$$

which is based on application of the masks

$$D_x = \frac{1}{2}\begin{pmatrix} 1 & 0 \\ 0 & -1 \end{pmatrix}$$

and

$$D_y = \frac{1}{2}\begin{pmatrix} 0 & -1 \\ 1 & 0 \end{pmatrix}.$$

However, these masks operate on a relatively small array of pixels and are consequently relatively sensitive to noise. Practical applications of digital gradients such as the Roberts operator usually require pre-processing to reduce the level of noise inherent in an image. Another approach is to consider digital gradients that operate on a larger pixel array.

16.3.4 The Sobel Edge Detector

The Sobel edge detector is an extension which includes a degree of smoothing to reduce automatically certain artefacts caused by noise. The larger the filter array the more noise reduction will occur with fewer edges being detected, but as the filter becomes too large useful edges may not be detected. The Sobel filter is based on the following digital gradients:

$$D_x = \frac{1}{8}\begin{pmatrix} -1 & 0 & 1 \\ -2 & 0 & 2 \\ -1 & 0 & 1 \end{pmatrix}, \quad D_y = \frac{1}{8}\begin{pmatrix} -1 & -2 & -1 \\ 0 & 0 & 0 \\ 1 & 2 & 1 \end{pmatrix}.$$

16.3.5 The Prewitt Edge Detector

The Prewitt edge detector is based on the following digital gradients:

$$D_x = \frac{1}{6}\begin{pmatrix} -1 & 0 & 1 \\ -1 & 0 & 1 \\ -1 & 0 & 1 \end{pmatrix}, \quad D_y = \frac{1}{6}\begin{pmatrix} -1 & -1 & -1 \\ 0 & 0 & 0 \\ 1 & 1 & 1 \end{pmatrix}.$$

16.3.6 The Compass Edge Detector

This detector is designed to avoid the sensitivity that a filter has for specific orientation of an edge. A set of different filters is employed detecting specific angles, for the gradient G_i. The resulting gradient is then computed as $G =$

$\max\{G_i : i = 1 \text{ to } n\}$. Various kernels can be used. As an example, the first two compass Sobel filters are:

$$0^o: \begin{pmatrix} -1 & 0 & 1 \\ -2 & 0 & 2 \\ -1 & 0 & 1 \end{pmatrix}, \quad 45^o: \begin{pmatrix} 0 & 1 & 2 \\ -1 & 0 & 1 \\ -2 & -1 & 0 \end{pmatrix}.$$

Any other filter can be used to create a set of compass filters. A few common ones include the Prewitt filter,

$$0^o: \begin{pmatrix} -1 & 1 & 1 \\ -1 & -2 & 1 \\ -1 & 1 & 1 \end{pmatrix}, \quad 45^o: \begin{pmatrix} 1 & 1 & 1 \\ -1 & -2 & 1 \\ -1 & -1 & 1 \end{pmatrix},$$

the Kirsch filter

$$0^o: \begin{pmatrix} -3 & -3 & 5 \\ -3 & 0 & 5 \\ -3 & -3 & 5 \end{pmatrix}, \quad 45^o: \begin{pmatrix} -3 & 5 & 5 \\ -3 & 0 & 5 \\ -3 & -3 & -3 \end{pmatrix},$$

and the Robinson filter

$$0^o: \begin{pmatrix} -1 & 0 & 1 \\ -1 & 0 & 1 \\ -1 & 0 & 1 \end{pmatrix}, \quad 45^o: \begin{pmatrix} 0 & 1 & 1 \\ -1 & 0 & 1 \\ -1 & -1 & 0 \end{pmatrix}.$$

16.3.7 Nine Dimensional Operators

Given a set of 3×3 filters, a complete basis is formed with nine orthogonal filters. There is obviously an infinite number of sets to choose from. For completeness, it is worth mentioning at this point one example, namely, a set containing four filters for edge detection (w_1–w_4), four filters for line detection (w_5–w_8) and the last filter, w_9, which is a simple averaging filter as defined below.

$$\underset{w_1}{\begin{pmatrix} 1 & \sqrt{2} & 1 \\ 0 & 0 & 0 \\ -1 & -\sqrt{2} & -1 \end{pmatrix}} \qquad \underset{w_2}{\begin{pmatrix} 1 & 0 & -1 \\ \sqrt{2} & 0 & -\sqrt{2} \\ 1 & 0 & -1 \end{pmatrix}} \qquad \underset{w_3}{\begin{pmatrix} 0 & -1 & -\sqrt{2} \\ 1 & 0 & -1 \\ \sqrt{2} & 1 & 0 \end{pmatrix}}$$

$$\underset{w_4}{\begin{pmatrix} -\sqrt{2} & -1 & 0 \\ -1 & 0 & 1 \\ 0 & 1 & \sqrt{2} \end{pmatrix}} \qquad \underset{w_5}{\begin{pmatrix} 0 & 1 & 0 \\ -1 & 0 & -1 \\ 0 & 1 & 0 \end{pmatrix}} \qquad \underset{w_6}{\begin{pmatrix} -1 & 0 & 1 \\ 0 & 0 & 0 \\ 1 & 0 & -1 \end{pmatrix}}$$

$$\underset{w_7}{\begin{pmatrix} 1 & -2 & 1 \\ -2 & 4 & -2 \\ 1 & -2 & 1 \end{pmatrix}} \qquad \underset{w_8}{\begin{pmatrix} -2 & 1 & -2 \\ 1 & 4 & 1 \\ -2 & 1 & -2 \end{pmatrix}} \qquad \underset{w_9}{\begin{pmatrix} 1 & 1 & 1 \\ 1 & 1 & 1 \\ 1 & 1 & 1 \end{pmatrix}}$$

16.3.8 The Canny Edge Detector

In developing the filters discussed above, two problems are encountered. As the data elements are discrete, it is not always obvious how to calculate a gradient value and, in the presence of noise, many spurious edges can become apparent. Increasing the size of the filter can alleviate these anomalies. The Canny edge detector is designed to combat some of these problems and consists of three main stages:

- Gaussian blur the image to reduce the amount of noise and remove speckles within the image. It is important to remove the very high frequency components that exceed those associated with the gradient filter used, otherwise, these can cause false edges to be detected.
- Gradient detect using one of the above filters, creating two images, one containing the gradient magnitudes G, and another containing the orientation $\theta(G)$. The most common implementations use a simple symmetric discrete first order derivative.
- Threshold the gradient magnitudes above a certain minimum threshold value so that only major edges are detected. As well as this minimum low threshold value, a high threshold value is also specified. On any connected line, at least one of the edge points has to exceed this high value. This removes small or insignificant line segments.

By controlling the standard deviation of the Gaussian blurring operation, and the high and low threshold values, most general edges can be detected. If it is known *a priori* what kind of edge is to be detected and the kind of noise that is present in the image, then an alternative filter can be applied instead of the Gaussian filter.

16.3.9 Programming Example: Sobel Edge Detection

As an example of edge detection in practice, the following MATLAB function is used to apply the Sobel edge detector which outputs of the following: D_x, D_y, $G =\mid D_x \mid + \mid D_y \mid$, $\tan^{-1}(D_y/D_x)$ and G after conversion to a binary image through application of a user defined threshold.

```
function Sobel(threshold)

%Input: threshold - threshold for binarization
%
%Output: None

%Read image (assumed to be .tif file)
f=imread('filename','tif');

%Convert to normalized floating point array
```

```
f=im2double(f);
f=f./max(max(f));

%Show image
figure(1)
subplot(2,3,1), imshow(f);

%Compute Sobel FIR filter Dx and Dy
Dx(1,1)=-1; Dx(1,2)= 0; Dx(1,3)= 1;
Dx(2,1)=-2; Dx(2,2)= 0; Dx(2,3)= 2;
Dx(3,1)=-1; Dx(3,2)= 0; Dx(3,3)= 1;
Dx=Dx/8;
Dy(1,1)= 1; Dy(1,2)= 2; Dy(1,3)= 1;
Dy(2,1)= 0; Dy(2,2)= 0; Dy(2,3)= 0;
Dy(3,1)=-1; Dy(3,2)=-2; Dy(3,3)=-1;
Dy=Dy/8;

%Apply filter using MATLAB conv2 'valid' option
Dx=conv2(f,Dx,'valid');
Dy=conv2(f,Dy,'valid');

%Display normalized absolute values of Dx and Dy
ADx=abs(Dx); ADx=ADx./max(max(ADx));
ADy=abs(Dy); ADy=ADy./max(max(ADy));
subplot(2,3,2), imshow(ADx);
subplot(2,3,3), imshow(ADy);

%Compute the gradient magnitude
G=ADx+ADy;

%Normalize and display result
G=G./max(max(G));
subplot(2,3,4), imshow(G);

%Compute the angle of gradient usin MATLAB angle function
c=complex(Dy,Dx);
theta=angle(c);

%Display normalized absolute value
theta=abs(theta); theta=theta./max(max(theta));
subplot(2,3,5), imshow(theta);

%Threshold gradient magnitude image using MATLAB im2bw function
TG=im2bw(G,threshold);
subplot(2,3,6), imshow(TG);
```

An example of the output produced by this function for a threshold value of 0.2 is given in Figure 16.3.

Figure 16.3: An image of Isaac Newton (top-left), D_x (top-centre), D_y (top-right), $G =\mid D_x \mid + \mid D_y \mid$ (bottom-left), $\tan^{-1}(D_y/D_x)$ (bottom-centre) and G after binarization with threshold = 0.2 (bottom-right).

16.4 Second Order Edge Detection

Second order edge detection is based on computing the second derivative in x and y and observing the locations in the image where zeros occur. The Laplacian of the image given by

$$\nabla^2 f(x,y) = \frac{\partial^2}{\partial x^2} f(x,y) + \frac{\partial^2}{\partial y^2} f(x,y)$$

is used for this purpose. A binary image is then generated by applying the following process:

If $\nabla^2 f_{\text{in}} \geq 0$ then
$f_{\text{out}} = 1$

else
$f_{\text{out}} = -1$

The positions where f_{out} changes from 1 to -1 or from -1 to 1 are then obtained and a binary grey level display presented. In other words, the value of any pixel where f_{out} changes from 1 to -1 or from -1 to 1 is set to 1 and all other pixels are set to zero.

The Digital Laplacian

Expanding the function $f(x + \Delta x)$ as a Taylor series, we have

$$f(x + \Delta x) = f(x) + \Delta x \frac{\partial}{\partial x} f(x) + \frac{(\Delta x)^2}{2!} \frac{\partial^2}{\partial x^2} f(x) + ... \tag{16.1}$$

If we express the function $f(x - \Delta x)$ in the same way, we get

$$f(x - \Delta x) = f(x) - \Delta x \frac{\partial}{\partial x} f(x) + \frac{(\Delta x)^2}{2!} \frac{\partial^2}{\partial x^2} f(x) + ... \tag{16.2}$$

Neglecting all terms of order $(\Delta x)^3$ and above, and then adding equations (16.1) and (16.2), we get

$$f(x + \Delta x) + f(x - \Delta x) = 2f(x) + (\Delta x)^2 \frac{\partial^2}{\partial x^2} f(x)$$

Rearranging, we have

$$\frac{\partial^2}{\partial x^2}(x) = \frac{f(x + \Delta x) - 2f(x) + f(x - \Delta x)}{(\Delta x)^2}.$$

For partial derivatives we have

$$\frac{\partial^2}{\partial x^2} f(x, y) = \frac{f(x + \Delta x, y) - 2f(x, y) + f(x - \Delta x, y)}{(\Delta x)^2}$$

and

$$\frac{\partial^2}{\partial y^2} f(x, y) = \frac{f(x, y + \Delta y) - 2f(x, y) + f(x, y - \Delta y)}{(\Delta y)^2}.$$

From these results the digital Laplacian ∇^2_{ij} operating on an image f_{ij} becomes

$$\nabla^2_{ij} f_{ij} = f_{(i+1)j} - 2f_{ij} + f_{(i-1)j} + f_{i(j+1)} - 2f_{ij} + f_{i(j-1)}$$

or, after collecting terms,

$$\nabla^2_{ij} f_{ij} = f_{(i+1)j} + f_{(i-1)j} + f_{i(j+1)} + f_{i(j-1)} - 4f_{ij}.$$

This operation can be written in terms of the convolution of f_{ij} with an appropriate mask, i.e.,

$$\nabla^2_{ij} f_{ij} = \text{mask}_{ij} \otimes \otimes f_{ij}$$

where

$$\text{mask}_{ij} = \begin{pmatrix} 0 & 1 & 0 \\ 1 & -4 & 1 \\ 0 & 1 & 0 \end{pmatrix}.$$

The digital Laplacian operator, ∇^2_{ij}, can be defined as, $\nabla^2_{ij} = D^2_x + D^2_y$ where

$$D^2_x = \begin{pmatrix} 1 & -2 & 1 \end{pmatrix}, \quad D^2_y = \begin{pmatrix} 1 & -2 & 1 \end{pmatrix}^T$$

since

$$\nabla^2_{ij} = \begin{pmatrix} 1 & -2 & 1 \end{pmatrix} + \begin{pmatrix} 1 \\ -2 \\ 1 \end{pmatrix} = \begin{pmatrix} 0 & 1 & 0 \\ 1 & -4 & 1 \\ 0 & 1 & 0 \end{pmatrix}.$$

The main advantage of the second derivative is that it is orientation independent. To detect an edge with the digital Laplacian, we looking for a position where the values cross zero. For this reason a 'signum operator' is often applied which creates a black and white image, with black representing positive values and white representing negative values.

16.5 The Marr-Hildreth Method

One of the major difficulties with real images is that changes in grey level can and do occur over a wide range of scales. For this reason, edges over a range of different scales cannot be obtained unless the image is filtered first. By applying a band-pass filter to an image, we can view separately the edges occurring at different scales. There are two physical considerations that, together, determine the appropriate smoothing process (i.e. the band-pass filter): (i) the motivation for band-pass filtering the image is to reduce the range of scales over which variations in grey level take place; (ii) the filtered output should be spatially localized. In other words, the contribution to each pixel in the filtered image should arise from a smooth average of nearby points. The filter should therefore be smooth and band-limited in the frequency domain with a small standard deviation. It should also be smooth and localized in the spatial domain (i.e. its spatial standard deviation should be small). There is only one distribution that optimizes both these conditions, namely, the Gaussian distribution (ignoring scaling)

$$g(x, y) = \exp[-(x^2 + y^2)/\sigma^2]$$

where σ is the standard deviation. An important property of this distribution is that its Fourier transform is of the same form, i.e. ignoring scaling,

$$G(k_x, k_y) = \exp[-\sigma^2(k_x^2 + k_y^2)].$$

By changing the value of σ the edges at different scales can be obtained by finding the zero crossings of the function

$$\nabla^2_{ij} \otimes\otimes g_{ij} \otimes\otimes f_{ij}.$$

Convolution of an image with a Gaussian function blurs the image, with a degree of blurring proportional to σ. This means that, in a single operation, we

have noise reduction and edge detection at the zero crossings. In fact the 3×3 matrix representation for the digital Laplacian described earlier uses a quantised Gaussian with $\sigma = 1/2$. A set of different scaled edge detection images can be created representing different Gaussian filters. This technique for edge detection is known as the Marr-Hildreth method after the authors important contribution to the subject (*On the theory of edge detection*, Proceedings of the Royal Society, London, B 207: 127-217, 1980). The Marr-Hildreth algorithm is not only an edge detector; it is the result of one of the first approaches in pattern recognition to be based on a model for the human visual system. The basic idea is that our ability to recognize and interpret different objects in an image scene is based on matching the edges of the scene over different frequency scales. Now, ignoring scaling

$$\exp[-r^2/\sigma^2] \otimes \otimes \nabla^2 f(x,y) \Longleftrightarrow -k^2 \exp[-\sigma^2 k^2]$$

where

$$r = \sqrt{x^2 + y^2} \quad \text{and} \quad k = \sqrt{k_x^2 + k_y^2}$$

which is a band-pass filter whose band depends on the value of σ. By varying σ, we can obtain the edges of an image at different frequency bands. Techniques using threshold values, similar to those used in the Canny edge detector, can be applied to remove possible small or insignificant edges. With zero crossing detection the Marr-Hildreth edge detector has the great advantage that regions are automatically defined as being totally enclosed. This can help immensely when we wish to cluster areas together.

16.6 Pixel Clustering

Detecting major edges in an image gives an indication as to how far away from any location there is a sharp change in image content. This does not necessarily define specific enclosed regions. Multiple line detections at different resolutions will also give possibly contradictory information as regards edge positions. It is often only by further definition of the type of segmentation required that useful segmentation decisions can be made. This further problem is solved to some extent by applying clustering algorithms. Application of a given filter merely indicates how likely pixels are to be included within a part of a structure. To represent these structures it is then required to group pixels together into separate regions. It is noted that certain images could inherently have no convenient dividing lines to segment images into regions; in such a case, further *a priori* information is required. A simple example of this is a smooth graduation. There are two techniques for grouping pixels together, either by region splitting, giving a top-down approach, or by region growing, giving a bottom-up approach.

16.6.1 Region Splitting

The basic concept is to look at the image as a whole and consider it as one region. If all the pixels within this region are in some way similar then keep

this as a single region, otherwise split the region into sub-areas and repeat the process.

The splitting strategy is often deterministic, and commonly consists of four equal quadrants. This means that, after the image has been completely defined as a large set of regions, many neighbouring regions may contain similar properties. A merging stage is required to re-group these regions together.

16.6.2 Region Growing

The alternative technique is to start with a known seed pixel within a region of interest, then grow the region from this pixel by adding neighbouring pixels that have some similarity. The filling algorithm can consider whole groups of pixels in any order as is convenient. To cover the whole of the image this process needs to be repeated with different seed pixels for each different region.

16.7 Clustering Tools

Many techniques are available for detecting specific edge features within an image. These include filters for the detection of lines, ellipsoids and other specific geometric shapes. In this section, a selection of the tools available to aid edge segmentation and the clustering process are presented.

16.7.1 The Hough Transform

The Hough transform was briefly mentioned in Chapter 8 in terms of its applications to computer vision and in relation to the Radon transform. The transform is a useful tool aimed at extracting the locations of regular curves such as lines or circles.

A line detecting Hough transform is calculated by considering all the detected edge points and representing all possible lines through these points. Consider a point (x_0, y_0), then the set of all lines through this point is represented as the set of all possible values of (r, θ) that satisfy

$$r = x_0 \cos\theta + y_0 \sin\theta.$$

By considering the sum of the sets of all lines through all edge points, we construct the Hough transform. To reconstruct these lines the inverse process, called de-Houghing (e.g. via application of the inverse Radon transform), is applied by selecting, often by thresholding, the main peaks and then creating the lines resulting from the values of (r, θ). As might be expected, the Hough transform is very resilient to noise and gaps in the edges. It has the disadvantage that the whole image is considered at once, which means that for accurate representation it is preferable for the object to fill the full field of view. The use of the gradient, $\theta(G)$, function can be used to emphasise the directional component.

By changing the parametric equation which constructs the Hough transform, other Euclidean objects other than lines can be detected, for example, circles

$\left[r^2 = (x_0 - a)^2 + (y_0 - b)^2\right]$ or ellipses $\left[(x_0 - a)^2/s + (y_0 - b)^2/t = 1\right]$. If there is no simple equation to define the surface a lookup table can be used to define the shape of the feature. This generalised Hough transform then specifies all possible scales and orientations.

16.7.2 Histogram Manipulation

If the image is considered homogeneous, that is, operations on the pixels do not depend on the position of the pixel in the image, then the intensity values can be visualised with a *histogram*. A first-order histogram of an image is a vector containing the number of occurrences of each intensity quantisation level, $H(v)$. Histograms are one of the first and simplest analytical tools available and often show the distortions in the acquisition hardware. The probability density function (PDF) is the proportion of each grey scale value within the image. If each pixel has unit area, this can be calculated from the histogram by normalisation, so

$$p(v) = \frac{1}{A}H(v)$$

where A is the area of the image. For an 8-bit image, the grey values vary from zero representing black to 255 representing white. The histogram can be simply extended to its second-order, which is a measure of the joint occurrence of pairs of pixels separated by a specific distance. The cumulative distribution function (CDF) is also sometimes used and given as

$$P(v) = \int_0^v p(x)dx = \frac{1}{A}\int_0^v H(x)dx$$

Using indirect operations that change the histogram is a very easy way of thresholding or highlighting certain features within an image.

Histogram equalization has been discussed in Chapter 15 and is a good method for modifying the dynamic range of an image to achieve automatic enhancement. Areas within the histogram that are very common are given a larger 'slice' of the available grey scale range, and areas that are uncommon have a reduced 'slice' of the range. The aim is for the final image to have a histogram with the property that its CDF has an equal fraction for all grey value levels. The transformation from an original image I through the histogram value to its equalised value is calculated simply from the CDF itself. Consider a grey value v within image I, then the final value is $q(v)$ given by

$$q(v) = g_{\max}P(v)$$

where g_{max} is the largest allowable grey level. A simpler operation, which often results in a less harsh enhancement, is the use of contrast stretching. This process involves scaling a range of the histogram to cover a larger range. Consider scaling the range $x \ldots y$ to a new range $p \ldots q$, then each pixel value d is scaled using

$$v' = \frac{(v - x)(q - p)}{(y - x)} + p$$

This method is ideal for expanding an image around a peak in the histogram. If we allow the $x \ldots y$ range to just cover all of the non-zero section of the histogram, and the range $p \ldots q$ to cover the whole range then the process is termed histogram normalization.

Another common modifying process is histogram gamma (γ) correction, which converts a linear interpolation of intensity values with an exponential law. This is designed to approximate to the logarithmic characteristics of the human visual system. In general, the formula for converting a grey value v to the gamma corrected version v' is

$$v' = a(v^{\gamma}) + b$$

where a and b bound the resulting values to some range. All these histogram operations may improve visibility for human inspection and aid the interactive image processing. Unfortunately, for many automated scientific processes a linear relationship between intensity and grey value is often essential.

16.7.3 Morphological Operations

Morphological operations combine an image with a structuring element, often a 3×3 matrix. They process an image pixel by pixel according to the neighbourhood pixel values. Morphological operations are often applied to binary images, although techniques are available for grey level images.

We present here the basic operations. The most common are used for highlighting or removing features, for example as edge detectors or for noise suppression. For all these operations we have an initial image, I and a structuring element S that is centred on pixel ij by shifting S to S^{ij}.

Dilation and Erosion

In dilation, position ij is included in the dilation of I by S if the intersection is non-zero which we define as

$$I \oplus S = \{(ij) : S^{ij} \vee I \neq 0\}$$

where $\vee$ denotes the logical AND operator. A process of region filling can be constructed using the dilation process. We can define the image X^0 to represent a single pixel within the region, and define E to represent the edge map of the region. Then by iterating

$$X^{i+1} = \left[X^i \oplus \begin{pmatrix} 1 & 1 & 1 \\ 1 & 1 & 1 \\ 1 & 1 & 1 \end{pmatrix} \right] \wedge E$$

where $\wedge$ denotes the logical OR operation, we converge to filling the entire region.

Erosion is the dual of dilation and position ij is included in the erosion of I by S whenever S is a subset of I, i.e.

$$I \ominus \mathcal{S} = \{(i, j) : S^{ij} \subseteq I\}.$$

The process is useful when detecting and separating objects that are slightly touching. Because erosion is the dual of dilation, each can be defined in terms of each other so that

$$I \ominus S = \overline{\overline{I} \oplus S}, \qquad I \oplus S = \overline{\overline{I} \ominus S}.$$

Opening and Closing

This operation is simply an erosion followed by a dilation operation that uses the same structuring element. Small minor elements of a structure are removed without increasing the size of the structure.

The dual of opening is closing and involves a dilation followed by an erosion. Closing has the property of filling in small holes. To achieve more severe opening or closing operations, the process can involve multiple erosions followed by the same number of dilations. For opening $\circ$ and closing $\bullet$ these can be defined as

$$I \circ^i S = (I \overbrace{\ominus S \ldots \ominus S}^{i}) \overbrace{\oplus S \ldots \oplus S}^{i}, \qquad I \bullet^i S = (I \overbrace{\oplus S \ldots \oplus S}^{i}) \overbrace{\ominus S \ldots \ominus S}^{i}.$$

Hit and Miss Transform

The most general operation is the hit and miss transform $\ominus$, which uses a structuring element that contains both 1's and 0's. These represent foreground and background pixels that in general can detect any feature. A position ij is included in the dilation of I by S^{ij} whenever there is an exact match. We can define this general operator by considering two structural elements S^1 and S^2 defined as

$$S^1 = \{(i,j) : S_{i,j} = 1\}, \quad S^2 = \{(i,j) : S_{i,j} = 0\}.$$

Then

$$I \oslash S = (I \ominus S^1) \vee \overline{(I \oplus S^2)}.$$

As an example, the following four structure elements can be used as corner detectors:

$$\begin{pmatrix} & 1 & \\ 0 & 1 & 1 \\ 0 & 0 & \end{pmatrix}, \quad \begin{pmatrix} & 1 & \\ 1 & 1 & 0 \\ & 0 & 0 \end{pmatrix}, \quad \begin{pmatrix} & 0 & 0 \\ 1 & 1 & 0 \\ & 1 & \end{pmatrix}, \quad \begin{pmatrix} 0 & 0 & \\ 0 & 1 & 1 \\ & 1 & \end{pmatrix}$$

and end points of a skeleton can be detected with the following:

$$\begin{pmatrix} & & \\ 0 & 1 & 0 \\ 0 & 0 & 0 \end{pmatrix}, \quad \begin{pmatrix} & 0 & 0 \\ & 1 & 0 \\ & 0 & 0 \end{pmatrix}, \quad \begin{pmatrix} 0 & 0 & 0 \\ 0 & 1 & 0 \\ & & \end{pmatrix}, \quad \begin{pmatrix} 0 & 0 & \\ 0 & 1 & \\ 0 & 0 & \end{pmatrix}$$

Thinning and Thickening

A process of thinning $\triangleright\!\triangleleft$ and thickening $\triangleleft\!\triangleright$, can be achieved via the hit and miss operator with the following definitions;

$$I \triangleright\!\triangleleft S = I \vee \overline{(I \oslash S)}, \qquad I \triangleleft\!\triangleright S = I \wedge (I \oslash S).$$

Examples of different structuring elements with regard to the thinning process are as follows:

$$\begin{pmatrix} 1 & 1 & 1 \\ 1 & 1 & 1 \\ 1 & 1 & 1 \end{pmatrix}$$

which deletes all those pixels that do not have a neighbouring background pixel and

$$\begin{pmatrix} 0 & 0 & 0 \\ 0 & 1 & 0 \\ 0 & & \end{pmatrix}, \quad \begin{pmatrix} 0 & 0 & 0 \\ 0 & 1 & 0 \\ & & 0 \end{pmatrix}$$

which, together with their rotational analogues, can be used to remove small spikes from a structure. For this reason they are termed 'pruning' operators. Continual use of pruning can be undertaken until convergence removes all elements except those that form closed loops.

Finally, an example of a set of structuring elements used within the thickening process is

$$\begin{pmatrix} 1 & 1 & \\ 1 & 0 & \\ 1 & & 0 \end{pmatrix}, \quad \begin{pmatrix} & 1 & 1 \\ & 0 & 1 \\ 0 & & 1 \end{pmatrix}.$$

Along with the related rotations, this set of structure elements converges to produce a convex hull approximation to any structure. However, this method does not necessarily have fast convergence rates.

16.8 Hierarchical Data Structures

Image information is often defined as multi-resolutional and can be described as having different classifications at different resolutions. This can be intuitively described by considering cartography where different scaled maps contain very different types of information and are used in many different ways dependent upon scale. Most of the filters described so far have fixed and finite sizes and, although it is possible to create a large set of filters for all possible resolutions, a favoured option is to modify the data structure holding the image. One strategy is to allow the image to hold automatically many different resolutions at the same time within a pyramid data structure. Two pyramid types are commonly used, a Gaussian pyramid and a Laplacian pyramid.

A Gaussian pyramid structure is defined to consist of a set of images each smaller by a factor of 2 in both the horizontal and vertical directions. The reduced image pixels are sampled with a blurring filter. For example, in the 2×2 case, a binomial filter simply requires averaging the four pixel values. Not all levels of the pyramid structure are required as the higher levels can become very small, yielding minimal information. For this reason the pyramid is cut

off at a certain stage to minimise the storage required. The high resolution level is often referred to as *fine* and the blurred levels are termed as *coarse*.

The total extra storage space requirement is minimal, as is the extra computational time required to apply filters at all levels rather than just at the very fine level. If the original image is an $n \times n$ array where $n = 2^k$ then the number of pixels N for the Gaussian pyramid is

$$\begin{aligned} N &= \left(2^k\right)^2 + \left(2^{k-1}\right)^2 + \left(2^{k-2}\right)^2 + \left(2^{k-3}\right)^2 + \cdots \\ &= \left(2^k\right)^2 \left[1 + 1/\left(2^2\right) + 1/\left(2^4\right) + 1/\left(2^6\right) + \cdots\right] \\ &\leq \left(2^k\right)^2 2^2/\left(2^2 - 1\right) = \left(2^k\right)^2 4/3 = (4/3)n^2. \end{aligned}$$

From the Gaussian pyramid, the Laplace pyramid can be derived very simply. Each Laplace level is created by subtracting the smoothed from the unsmoothed at each of the Gaussian levels. The top level is then a copy of the equivalent Gaussian level. Using similar inverse operations on the Laplacian pyramid we can reconstruct the original image.

To create the Gaussian pyramid we consider some averaging filter. In the simple case a 2×2 binomial filter,

$$G_x = B^1 = \frac{1}{2}\begin{pmatrix} 1 & 1 \end{pmatrix}$$

is sometimes sufficient. A recommendation is to use an even, separable and symmetric 5×5 smoothing filter, $G = G_x G_y$, where $G_x = \begin{pmatrix} \gamma & \beta & \alpha & \beta & \gamma \end{pmatrix}$. This gives a degree of overlapping for the results of each higher level pixel. Larger filters are usable but with a corresponding cost in computational time. The following two properties then need to hold:

- The average grey value should be conserved. This means that $\alpha + 2\beta + 2\gamma = 1$.
- Each point should contribute equally to the level above. The contribution from an even point is equal to $\alpha + 2\gamma$, and the contribution from an odd point is 2β. So $\alpha + 2\gamma = 2\beta$.

Thus $\beta = 1/4$ and $\alpha + 2\gamma = 1/2$ and the resulting set of filters are then of the form $\begin{pmatrix} 1/8 - x/2 & 1/4 & 1/4 + x & 1/4 & 1/8 - x/2 \end{pmatrix}$. Commonly used examples are:

$x = \frac{1}{2}$, gives negative end points, $\frac{1}{8}\begin{pmatrix} -1 & 2 & 6 & 2 & -1 \end{pmatrix}$.

$x = \frac{1}{4}$, gives the smaller binomial filter, $B^2 = \frac{1}{4}\begin{pmatrix} 0 & 1 & 2 & 1 & 0 \end{pmatrix}$.

$x = \frac{1}{8}$, gives the popular binomial filter, $B^3 = \frac{1}{16}\begin{pmatrix} 1 & 4 & 6 & 4 & 1 \end{pmatrix}$.

$x = \frac{1}{16}$, gives an alternative filter, $\frac{1}{32}\begin{pmatrix} 3 & 8 & 10 & 8 & 3 \end{pmatrix}$.

$x = 0$, gives a more square filter, $\frac{1}{8}\begin{pmatrix} 1 & 2 & 2 & 2 & 1 \end{pmatrix}$.

$x = -\frac{1}{4}$, gives an alternative filter, $\frac{1}{4}\begin{pmatrix} 1 & 1 & 0 & 1 & 1 \end{pmatrix}$.

The binomial filter has the disadvantage of not being a very sharp function. Binomial filters can be computed from the binomial distribution, in a similar

way to Pascal's triangle. They have the property that they balance kernel size with variance σ^2.

	Binomial Filter	σ^2
B^0	(1)	0
B^1	1/2 (1 1)	1/4
B^2	1/4 (1 2 1)	1/2
B^3	1/8 (1 3 3 1)	3/4
B^4	1/16 (1 4 6 4 1)	1
B^5	1/32 (1 5 10 10 5 1)	5/4
B^6	1/64 (1 6 15 20 15 6 1)	3/2
B^7	1/128 (1 7 21 35 35 21 7 1)	7/4
B^8	1/256 (1 8 28 56 70 56 28 8 1)	2
B^9	1/512 (1 9 36 84 126 126 84 36 9 1)	9/4
B^{10}	1/1024 (1 10 45 120 210 252 210 120 45 10 1)	5/2

This can mean that very large binomials are required for only moderate values for the standard deviation. For example, when $\sigma = 5$ the binomial B^{100} needs to be used that covers over 100 pixels. Alternative smoothing functions whose standard deviation is large compared with the kernel size can be used. For example, by slightly changing the binomial filter's rate of curvature we have

$$B^{a,b} = [I - (I - B^2)^a]^b.$$

Now a controls the steepness of the transition and b controls the cut-off position. A second alternative is to use the same averaging function but with pixels that are further spread out. Using the Jähne suffix naming scheme:

$$B_{x-y} = \begin{pmatrix} 1 & 0 \\ 0 & 1 \end{pmatrix}, \quad B_{x+y} = \begin{pmatrix} 0 & 1 \\ 1 & 0 \end{pmatrix},$$

$$B_{2x} = \begin{pmatrix} 1 & 0 & 1 \end{pmatrix}, \quad B_{2y} = \begin{pmatrix} 1 \\ 0 \\ 1 \end{pmatrix},$$

$$B_{x-2y} = \begin{pmatrix} 1 & 0 & 0 \\ 0 & 0 & 1 \end{pmatrix}, \quad B_{x+2y} = \begin{pmatrix} 0 & 1 \\ 0 & 0 \\ 1 & 0 \end{pmatrix},$$

$$B_{2x-y} = \begin{pmatrix} 1 & 0 \\ 0 & 0 \\ 0 & 1 \end{pmatrix}, \quad B_{2x+y} = \begin{pmatrix} 0 & 0 & 1 \\ 1 & 0 & 0 \end{pmatrix}.$$

16.9 Summary of Important Results

Correlation (matched filtering)

If t_{ij} is a feature (template) that is present somewhere in f_{ij} (with the same orientation and scale), then

$$s_{ij} = t_{ij} \odot \odot f_{ij}$$

has a maximum value at the (central) position in f_{ij} where this feature occurs.

Covariance function For a template t_{ij} the covariance function is given by

$$C_{ij} = \sum_n \sum_m [f_{nm} - \langle f_{ij} \rangle][t_{(i+n)(j+m)} - \langle t_{ij} \rangle]$$

where $\langle t_{ij} \rangle$ is the mean of t_{ij} and $\langle f_{ij} \rangle$ is the mean of f_{ij}.

Thresholding and binarization

Given that $0 \leq v_{ij} \leq 1$

if $v_{ij}^{\text{in}} >$ threshold

$v_{ij}^{\text{out}} = 1$

else

$v_{ij}^{\text{out}} = 0$

where $0 <$ threshold < 1

Example edge detecting filters

The Roberts edge detector

$$D_x = \frac{1}{2} \begin{pmatrix} 1 & 0 \\ 0 & -1 \end{pmatrix}, \quad D_y = \frac{1}{2} \begin{pmatrix} 0 & -1 \\ 1 & 0 \end{pmatrix}$$

The Sobel operator

$$D_x = \begin{pmatrix} -1 & 0 & 1 \\ -2 & 0 & 2 \\ -1 & 0 & 1 \end{pmatrix}, \quad D_y = \begin{pmatrix} -1 & -2 & -1 \\ 0 & 0 & 0 \\ 1 & 2 & 1 \end{pmatrix}$$

The Prewitt operator

$$D_x = \begin{pmatrix} -1 & 0 & 1 \\ -1 & 0 & 1 \\ -1 & 0 & 1 \end{pmatrix}, \quad D_y = \begin{pmatrix} -1 & -1 & -1 \\ 0 & 0 & 0 \\ 1 & 1 & 1 \end{pmatrix}$$

Mask for the digital Laplacian ∇^2_{ij}

$$\text{mask}_{ij} = \begin{pmatrix} 0 & 1 & 0 \\ 1 & -4 & 1 \\ 0 & 1 & 0 \end{pmatrix}$$

Marr-Hildreth algorithm

Locate the zero crossings associated the function

$$g_{ij} \otimes \otimes \nabla^2 f_{ij}$$

where g_{ij} is a Gaussian lowpass filter for different values of the filter's standard deviation.

16.10 Further Reading

- Beddow J and Meloy T, *Advanced Particulate Morphology*, CRC Press, 1980.
- Niblack W, *An Introduction to Digital Image Processing*, Prentice-Hall, 1985.
- Ballard D and Brown C, *Computer Vision*, Prentice-Hall, 1982.
- Levine M D, *Vision in Man and Machine*, McGraw-Hill, 1985.
- Gonzalez R C and Wintz P, *Digital Image Processing*, Addison-Wesley, 1987.
- James M, *Pattern Recognition*, BSP Professional Books, 1987.
- Fairhurst M C, *Computer Vision for Robotics Systems*, Prentice-Hall, 1988.
- De Valois R and De Valois K, *Spatial Vision*, Open University Press, 1988.
- Wilson R and Spann M, *Image Segmentation and Uncertainty*, Research Studies Press, 1988.
- Pau L F, *Computer Vision for Electronic Manufacturing*, Plenum Press, 1990.
- Wechsler H, *Computer Vision*, Academic Press, 1990.
- Low A, *Introductory Computer Vision and Image Processing*, McGraw-Hill, 1991.
- Jähne B, *Digital Image Processing: Concepts, Algorithms and Scientific Applications*, Springer, 1995.
- Stark J L, Murtagh F and Bijaoui A, *Image Processing and Data Analysis*, Cambridge University Press, 1998.

Chapter 17

Statistical Modelling and Analysis

Statistical imaging uses methods from stochastic field theory, statistical modelling techniques and information theory in an attempt to classify an image or regions of an image that are of statistical significance. It is an approach that is broadly based on an analysis of the Probability Density Function (PDF) of grey and/or colour levels just as Fourier based image processing is based on an analysis of the spectrum of an image. This includes developing approaches to modelling the PDF of an image from basic random walk principles.

The statistics of an image can be classified into two main types, those associated with a coherent and those of an incoherent image. The statistics of an incoherent image are variable, i.e. the PDF of an incoherent image varies considerably from one image to another. However, the statistics of a coherent image have a common form that is characterized by a PDF with a negative exponential of the type (ignoring scaling) $x^{\alpha}\exp(-\beta x)$. Thus, the PDF of a coherent image has a characteristic 'shape' whereas the shape of the PDF of an incoherent image is arbitrary. This is illustrated in Figure 17.1 which shows the intensity histograms of two incoherent images and Figure 17.2 which shows the histograms of two coherent images, a laser speckle pattern and a synthetic aperture radar image. In both cases, statistical methods can be used to process and/or analyse images by computing different statistical parameters for the image as a whole or by applying a moving window to segment the image statistically. In the latter case, information on the variations of a statistic across an image can provide a means for its classification.

Depending on the nature of a distribution, various image processing and transformation methods can be used to segment an image. A well known example is a method of automatic binerization that can be applied to an incoherent image when its distribution is bi-modal, i.e. has two distinct modes (two isolated maxima). In such cases, the threshold used for binarization can be taken to be the minimum value that occurs between the two modes which is a measure of the mid point between the dark and bright fields.

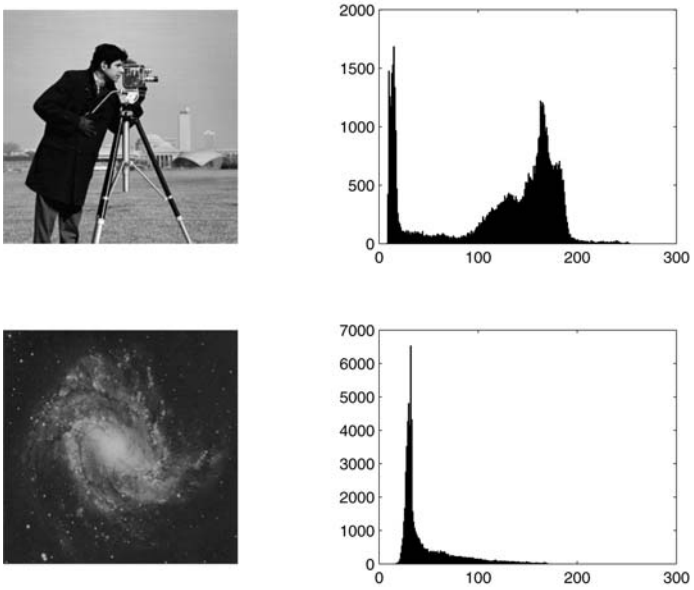

Figure 17.1: Two incoherent images (left) and their 256-bin histograms (right).

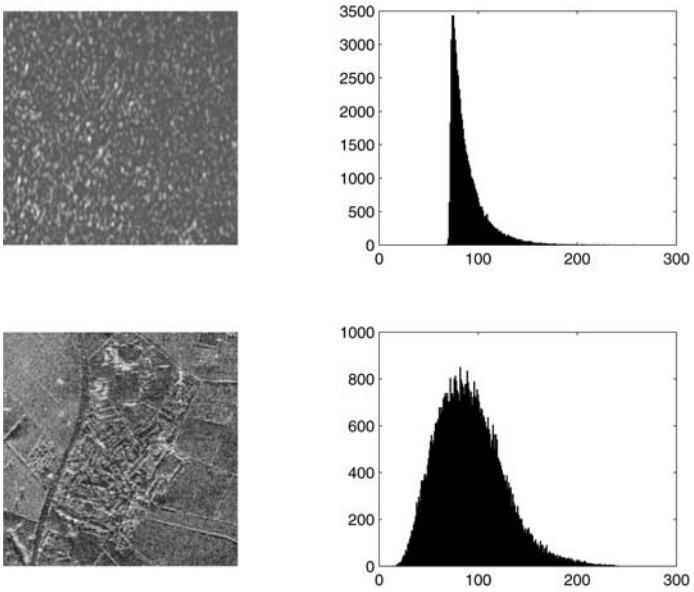

Figure 17.2: Two coherent images (a laser speckle pattern - top-left - and a synthetic aperture radar image - bottom-left) and their 256-bin histograms (right).

An example of this is given in Figure 17.3 which shows the binarization of an incoherent image after it has been quantized into a 5-bit image to obtain a gross statistical distribution compounded in a 32-bin distribution. This distribution is clearly bi-modal with a minimum value between the two modes occurring at the 17^{th} bin. This gives a threshold of $17/32 = 0.5313$, where it assumed that the original 8-bit image has been normalized to floating point values between 0 and 1 inclusively.

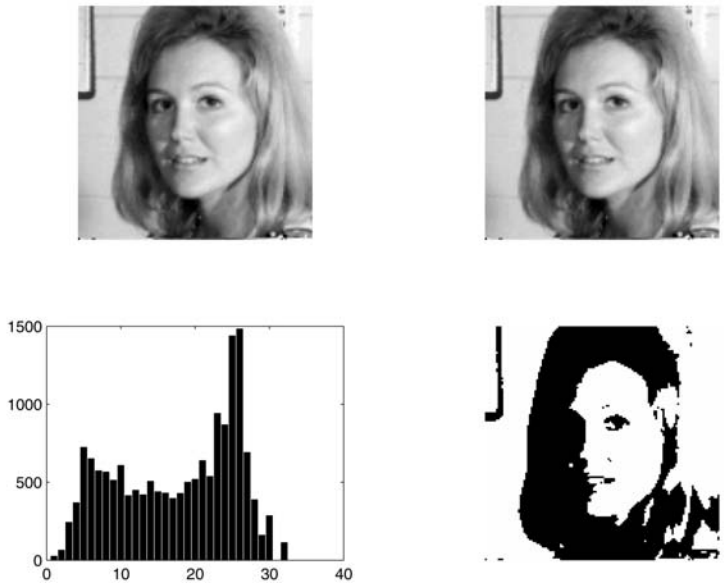

Figure 17.3: Binarization of an 8-bit image (top-left) after re-quantization to a 5-bit image (top-right) to provide a 32-bin histogram (bottom-left) from which a minimum value (in this case, the 17^{th} bin) can be acquired and applied as the threshold to give a binary image (bottom-right) - an optimal demarcation between the dark- and bright-fields.

17.1 Random Scattering Theory

Statistical analysis ideally requires a model for the physical behaviour of the random variable(s) that is derived from basic principles. In the case of statistical signal and image analysis, this typically involves modelling the scattered field in terms of its interaction with an ensemble of 'scattering sites' based on an assumed stochastic process. If the density of these scattering sites is low enough so that multiple scattering is minimal, then we can apply Born scattering to develop a model for the intensity of a wavefield interacting with a random Born scatterer.

In the far field, the Born scattered field (i.e. the scattering amplitude) is

given by the Fourier transform of the scattering function (see Chapter 6). If this function is known *a priori*, then the scattering amplitude can be determined. This is an example of a deterministic model. If the scattering function is stochastic (i.e. a randomly distributed scatterer) such that it can only be quantified in terms of a statistical distribution (i.e. the Probability Density Function - denoted by Pr) then we can simulate the (Born) scattered field by designing a random number generator whose output conforms to this distribution. The Fourier transform of this stochastic field then provides the Born scattering amplitude. Thus, given a three dimensional Helmholtz scattering function $\gamma(\mathbf{r}), \quad \mathbf{r} \in V$ with $\Pr[\gamma(\mathbf{r})]$ known *a priori*, the scattering amplitude A is given by

$$A(\hat{\mathbf{N}}, k) = k^2 \int_V \exp(-ik\hat{\mathbf{N}} \cdot \mathbf{r})\gamma(\mathbf{r}) d^3\mathbf{r}$$

where $\hat{\mathbf{N}} = \hat{\mathbf{n}}_s - \hat{\mathbf{n}}_i$ (the difference between the directions in which the scattered and incident wavefields propagate) and $\gamma(\mathbf{r})$ is a stochastic function whose deviates conform to the PDF $\Pr[\gamma(\mathbf{r})]$. This approach is the basis for the computation of the speckle patterns given in Figure 11.6.

17.1.1 Autocorrelation of the Scattering Function

The intensity of the scattering amplitude is given by

$$I(\hat{\mathbf{N}}, k) = \mid A(\hat{\mathbf{N}}, k) \mid^2 = A(\hat{\mathbf{N}}, k) A^*(\hat{\mathbf{N}}, k)$$

$$= k^4 \int_V \exp(-ik\hat{\mathbf{N}} \cdot \mathbf{r})\gamma(\mathbf{r}) d^3\mathbf{r} \int_V \exp(ik\hat{\mathbf{N}} \cdot \mathbf{r}')\gamma^*(\mathbf{r}') d^3\mathbf{r}'.$$

Using the autocorrelation theorem, we have

$$I(\hat{\mathbf{N}}, k) = k^4 \int_V \exp(-ik\hat{\mathbf{N}} \cdot \mathbf{r})\Gamma(\mathbf{r}) d^3\mathbf{r}$$

where Γ is the autocorrelation function given by

$$\Gamma(\mathbf{r}) = \int_V \gamma(\mathbf{r}')\gamma^*(\mathbf{r}' + \mathbf{r}) d^3\mathbf{r}'.$$

This result allows us to evaluate the intensity of the Born scattered amplitude by computing the Fourier transform of the autocorrelation function of the scattering function which is taken to be composed of a number of scatterers distributed at random throughout V. This requires the autocorrelation function to be defined for a particular type of random scatterer.

Consider the case when the scattering function is such that its autocorrelation function is radially symmetric and the intensity is given by [using spherical polar coordinates (r, ϕ, ψ)]

$$I(\hat{\mathbf{N}}, k) = k^4 \int_0^{2\pi} d\psi \int_{-1}^{1} d(\cos\phi) \int_0^R dr r^2 \exp(-ik \mid \hat{\mathbf{n}}_s - \hat{\mathbf{n}}_i \mid r\cos\phi)\Gamma(r).$$

Now,

$$\mid \hat{\mathbf{n}}_s - \hat{\mathbf{n}}_i \mid = \sqrt{(\hat{\mathbf{n}}_s - \hat{\mathbf{n}}_i) \cdot (\hat{\mathbf{n}}_s - \hat{\mathbf{n}}_i)} = \sqrt{2(1 - \cos\theta)}, \quad \cos\theta = \hat{\mathbf{n}}_s \cdot \hat{\mathbf{n}}_i$$

where θ is the scattering angle (i.e. the angle between the incident and scattered fields). Using the half angle formula

$$1 - \cos\theta = 2\sin^2(\theta/2)$$

we have

$$\mid \hat{\mathbf{n}}_s - \hat{\mathbf{n}}_i \mid = 2\sin(\theta/2)$$

and integrating over ψ and $\cos\phi$ we have

$$I(\theta, k) = \frac{2\pi k^3}{\sin(\theta/2)} \int_0^R \sin[2kr\sin(\theta/2)]\Gamma(r) r dr.$$

If we now consider the case when $kR << 1$ (i.e. the wavelength is large compared to the characteristic size of the scatterer - a condition that is consistent with the weak scattering approximation used to derive the result above), then we have

$$\sin[2kr\sin(\theta/2)] \simeq 2kr\sin(\theta/2)$$

and

$$I(\theta, k) = 4\pi k^4 \int_0^R \Gamma(r) r dr.$$

With regard to the autocorrelation function, the correlation of any function with itself produces a central peak at the point where the two functions match. We should therefore expect the autocorrelation function to consist of a peak with off-peak values that decay rapidly away from the position of the peak (i.e. its maximum value). In general, the maximum value will occur at $\mathbf{r} = \mathbf{0}$ where the value of the autocorrelation function is given by

$$\langle \gamma^2 \rangle = \int_V \mid \gamma(\mathbf{r}) \mid^2 d^3\mathbf{r}$$

Thus, if we let

$$\Gamma(r) = \langle \gamma^2 \rangle c(r)$$

where c is the normalized correlation function given by

$$c(r) = \frac{\Gamma(r)}{\langle \gamma^2 \rangle}$$

then we can write

$$I(\theta, k) = 4\pi k^4 \langle \gamma^2 \rangle f(R)$$

where

$$f(R) = \int_0^R c(r) r dr.$$

Note that the angular dependence of the intensity will depend on the characteristics of the Born scattering functions derived in Chapter 9, e.g. for a conductive dielectric

$$\langle\gamma^2\rangle = \langle(\gamma_\epsilon + \gamma_\mu\cos\theta)^2\rangle + \frac{z_0^2}{k^2}\langle\sigma^2\rangle \leq \langle\gamma_\epsilon^2\rangle + \langle\gamma_\mu^2\rangle\cos\theta + \frac{z_0^2}{k^2}\langle\sigma^2\rangle$$

and for a viscous acoustic medium,

$$\langle\gamma^2\rangle = \langle(\gamma_\kappa + \gamma_\rho\cos\theta)^2\rangle + (k\ell)^2\langle(\gamma_\rho\cos\theta + \gamma_\lambda + 2\gamma_\mu\cos^2\theta)^2\rangle$$

$$\leq \langle\gamma_\kappa^2\rangle + \langle\gamma_\rho^2\rangle\cos^2\theta + (k\ell)^2(\langle\gamma_\rho^2\rangle\cos\theta + \langle\gamma_\lambda^2\rangle + 4\langle\gamma_\mu^2\rangle\cos^4\theta).$$

17.1.2 Autocorrelation Function Models

Once the autocorrelation function is known, the Born scattered intensity can be computed by evaluating the Fourier transform of this function. Thus, a random medium can be characterized via its autocorrelation function by measuring the scattered intensity and inverse Fourier transforming the result. However, the characteristics of the autocorrelation function can formulated by considering its expected spectral properties since

$$\Gamma(\mathbf{r}) = \gamma(\mathbf{r}) \odot \gamma(\mathbf{r}) \Longleftrightarrow \mid \widetilde{\Gamma}(\mathbf{k}) \mid^2$$

where $\widetilde{\Gamma}$ is the Fourier transform of γ and $\mathbf{k}$ is the spatial frequency vector. Hence, in order to evaluate the most likely form of the autocorrelation function we need to consider the properties of the power spectrum of the scattering function. If this function is 'white' noise for example (i.e. its Power Spectral Density Function or PSDF is a constant), then the autocorrelation function is a delta function whose Fourier transform is a constant. However, in practice, we can expect that few scattering functions have a PSDF characterized by white noise, rather, the PSDF will tend to decay as the frequency increases. We can consider a model for the PSDF based on the Gaussian function

$$\mid \widetilde{\Gamma}(\mathbf{k}) \mid^2 = \Gamma_0^2 \exp\left(-\frac{k^2}{\ell_0^2}\right)$$

for example, where $\Gamma_0 = \widetilde{\Gamma}(0)$, $k = \mid \mathbf{k} \mid$ and ℓ_c defines the correlation length. This form yields an autocorrelation function which is of the same type, i.e. a Gaussian function. If the geometry of the scattering function is self-affine, then we can model the scattering function as a random scattering fractal whose PSDF is characterized by

$$\mid \widetilde{\Gamma}(\mathbf{k}) \mid^2 \sim \frac{1}{k^{2q}}$$

where $q > 0$ is the Fourier dimension (see Chapter 18). In this case, the autocorrelation function is characterized by (see Appendix C)

$$\Gamma(\mathbf{r}) \sim \frac{1}{r^{3-q}}$$

where $r = \mid \mathbf{r} \mid$. Other issues in determining the nature of the autocorrelation function are related to the physical conditions to which the scatterer should conform. For example, if the mean value of the scattering function over V is zero, then the integral of the autocorrelation function must also be zero. Thus, $\Gamma(\mathbf{r})$ cannot simply fall off exponentially to zero as r increases; it must be negative to a sufficient extent that its average value is zero. The simplest form of the autocorrelation function satisfying these requirements is

$$\Gamma(\mathbf{r}) = \langle \gamma^2 \rangle \left(1 - \frac{r^2}{r_0^2}\right) \exp\left[-\left(\frac{r^2}{r_0^2}\right)\right]$$

where r_0 is a scale factor approximately equal to the mean radius of the random distributed scatterers.

By way of an example, suppose we consider a scatterer that is characterized by a Gaussian autocorrelation function, i.e.

$$\Gamma(r) = \langle \gamma^2 \rangle \exp\left[-\left(\frac{r}{\ell_c}\right)^2\right].$$

The intensity is then given by

$$I(\theta, k) = k^4 \langle \gamma^2 \rangle \int_{-\infty}^{\infty} \exp(-ik\hat{\mathbf{N}} \cdot \mathbf{r}) \exp(-r^2/\ell_c^2) d^3\mathbf{r}.$$

Noting that

$$\int_{-\infty}^{\infty} \exp(-ikx) \exp(-ax^2) dx = \sqrt{\frac{\pi}{a}} \exp[-k^2/(4a)]$$

we have

$$I(\theta, k) = k^4 \ell_c^3 \pi^{\frac{3}{2}} \langle \gamma^2 \rangle \exp\left(-\frac{k^2 \ell_c^2}{2} \sin\frac{\theta}{2}\right).$$

Now, if $k\ell_c << 1$, then the intensity is given by

$$I(\theta, k) \sim \frac{(\ell_c k)^4}{\ell_c} \langle \gamma^2 \rangle$$

whose scale is determined by the size of the wavelength relative to the correlation length and whose PDF is determined by the PDF of $\langle \gamma^2 \rangle$.

The method discussed above can be used to model the (Born) scattered intensity from a random medium which requires an estimate of the autocorrelation of the scattering function to be known. However, this approach assumes that the density of scattering sites from which the scatterer is composed is low so that the Born approximation is valid. When the density of scattering sites increases and multiple scattering is present, the problem become progressively intractable. Then we resort to a purely stochastic approach which involves developing a statistical model, not for the scattering function, but for the scattered field itself. An introduction to this approach is provided in the following Section.

17.2 Statistical Modelling Methods

A signal $s(t)$ can, quite generally, be written in terms of the amplitude modulations $A(t)$ and the instantaneous phase $\Theta(t)$ as

$$s(t) = A(t)\exp[i\Theta(t)] = f(t) + iq(t)$$

where q is the quadrature component given by the Hilbert transform of f (see *Digital Signal Processing*, Horwood, 2003). Thus, at a given point in time t, we can consider the signal to be given by $A\exp(i\Theta)$. Let us suppose that A is the result of many interactions that can be viewed in terms of a random walk in the complex plane. From one point (a scattering site) to the next in this plane, we can consider each step, in general, to have a random amplitude a and a random phase θ. The amplitude A is then taken to be the resultant amplitude after many steps.

17.2.1 Random Phase Walks

Consider a random walk in the complex plane where the amplitude remains constant but where the phase changes, first by a constant factor and then by a random value between 0 and 2π.

Coherent Phase Walk

In the first case, let the amplitude taken from one step to the next be a and let the phase increase by a constant factor of θ at each step. After n steps, the resulting signal at a time t is given by

$$A\exp(i\Theta) = a + a\exp(i\theta) + a\exp(2i\theta) + ... + a\exp[i(n-1)\theta]$$

$$= a[1 + \exp(i\theta) + \exp(2i\theta) + ... + \exp[i(n-1)\theta]$$

$$= a\frac{[1-\exp(in\theta)]}{[1-\exp(i\theta)]} = a\frac{\exp(in\theta/2)[\exp(-in\theta/2) - \exp(in\theta/2)]}{\exp(i\theta/2)[\exp(-i\theta/2) - \exp(i\theta/2)]}$$

$$= a\exp[i(n-1)\theta/2)]\frac{\sin(n\theta/2)}{\sin\theta/2}.$$

Now, when n is large (i.e. for many steps),

$$\alpha = (n-1)\theta/2 \simeq n\theta/2$$

and when $\theta << 1$ (small phase changes only),

$$\sin(\theta/2) \simeq \frac{\theta}{2} \simeq \frac{\alpha}{n}$$

and hence

$$A\exp(i\Theta) = na\exp[i((n-1)/2)\theta]\text{sinc}\alpha \quad \text{where} \quad \text{sinc}\alpha = \frac{\sin\alpha}{\alpha}.$$

The amplitude is therefore given by (ignoring scaling by sincα)

$$A = na$$

which is proportional to the number of steps n. The intensity I is given by

$$I = n^2 a^2.$$

Incoherent Phase Walk

Let us now consider the case when the phase changes randomly between 0 and 2π. After n steps, the resulting signal at time t is given by

$$A\exp(i\Theta) = a\exp(i\theta_1) + a\exp(i\theta_2) + ... + a\exp(i\theta_n)$$

$$= a\sum_{m=1}^{n}\exp(i\theta_m).$$

The intensity is then given by

$$I = a^2\left|\sum_{m=1}^{n}\exp(i\theta_m)\right|^2 = a^2\sum_{m=1}^{n}\exp(i\theta_m)\sum_{m=1}^{n}\exp(-i\theta_m)$$

$$= a^2\left[n + \sum_{j=1,j\neq k}^{n}\exp(i\theta_j)\sum_{k=1}^{n}\exp(-i\theta_k)\right].$$

Now, in a typical term

$$\exp(i\theta_j)\exp(-i\theta_k) = \cos(\theta_j - \theta_k) + i\sin(\theta_i - \theta_k)$$

of the double summation, the functions $\cos(\theta_j - \theta_k)$ and $\sin(\theta_j - \theta_k)$ have random values between ± 1. Consequently, the double sum reduces to zero as n increases and the intensity is

$$I = na^2.$$

The resultant amplitude is therefore given by

$$A = \sqrt{n}a$$

which is proportional to the square root of the number of steps taken. The above results are directly applicable to coherence in optics and imaging in general. If the amplitude of a light source is given by the quantity a, then its intensity is proportional to a^2; n coherent sources yield a resulting amplitude na and a total intensity of n^2a^2. However, incoherent sources have random phases; n such sources, each of amplitude a, yield a resulting amplitude $\sqrt{n}a$ with intensity na^2.

17.2.2 Diffusion and Fractional Diffusion Processes

If we consider a to be the average distance a particle travels before it randomly interacts or collides with another particle (its mean free path) rather than the average amplitude of a scattered wave before it scatters from another scattering site, then after n collisions (where n is taken to be the average time interval between collisions) the particle will, on average, have travelled a distance of $a\sqrt{t}$ from its initial position at $t = 0$. Here, it is assumed that the direction in which a particle travels after a collision is determined by any value between 0 and 2π. The average distance travelled by the particle depends on the square root of time rather than time itself. This is not to say that all the particles in an ensemble of particles will have travelled a distance $\sqrt{t}a$ but that this distance is the most probable and represents a statistical average. This is a feature of all classical diffusion processes which can be described by the diffusion equation with a diffusivity D. The dimensions of diffusivity are length^2/time and must be interpreted in terms of a characteristic distance of the process which varies with the square root of time.

As shown in Chapter 5, the Green function to the 1D homogeneous diffusion equation

$$\left(\frac{\partial^2}{\partial x^2} - \frac{1}{D}\frac{\partial}{\partial t}\right) u(x,t) = 0$$

for a diffusivity D is given by

$$u(x,t) = p(x,t) \otimes u(x,0)$$

where $\otimes$ denotes the convolution over x, $u(x,0) = u(x,t)$ at $t = 0$ (i.e. the initial value of the diffusive field u) and

$$p(x,t) = \sqrt{\frac{1}{4\pi D t}} \exp\left(-\frac{x^2}{4Dt}\right).$$

Thus, for an initial (spatial) impulse $u(x,0) = \delta(x - x_0)$

$$u(x,t) = \sqrt{\frac{1}{4\pi D t}} \exp\left(-\frac{x_0^2}{4Dt}\right).$$

Now, if the time dependence of the diffusive field is measured at a fixed point in space close to the origin of the impulse, then we can consider the asymptotic result

$$u(t) \sim \frac{1}{\sqrt{Dt}}, \quad x_0 \to 0.$$

Based on the random phase walk analysis given in the previous Section, by induction we can interpret $\sqrt{D}$ as being a measure of the mean free path a.

The basic result of our random phase walk model, i.e.

$$A(t) = a\sqrt{t}$$

describes the process of Brownian motion (first considered by Albert Einstein in 1905). Fractional Brownian motion is a generalization of this result to

$$A(t) = at^H, \quad H \in (0,1]$$

where H is the Hurst exponent. By induction, this is equivalent to generalizing the homogeneous diffusion equation to

$$\left(\frac{\partial^2}{\partial x^2} - \frac{1}{D^q}\frac{\partial^q}{\partial t^q}\right) u(x,t) = 0, \quad q \in (0,2]$$

for a stationary process, or to

$$\left(\frac{\partial^2}{\partial x^2} - \frac{1}{D^{q(t)}}\frac{\partial^{q(t)}}{\partial t^{q(t)}}\right) u(x,t) = 0, \quad q \in (0,2]$$

for a non-stationary process which describes a field u generated by fractional diffusive processes. Fractional diffusive processes are, thus, intermediate between diffusive processes proper (random phase walks with $H = 0.5$) and 'propagative process' (coherent phase walks for $H = 1$). Solutions to equations of this type are explored in more detail in the following chapter.

17.3 Phase Distribution Analysis

The statistical characteristics of a digital signal/image may vary in time/space respectively. In such a case these non-stationary characteristics ideally require a suitable model to be formulated. Suppose we consider a hypothetical signal $s(t)$ whose amplitude $A(t)$ is determined by random phase walks over a finite period of time T_1. At the end of this period, we suppose that the signal switches instantaneously to one whose amplitude is determined by coherent phase walks over a period time T_2 say, i.e.

$$A(t) = \begin{cases} a\sqrt{t}, & t \in [0, T_1); \\ at, & t \in [T_1, T_1 + T_2). \end{cases}$$

We can extend this idea to one in which the signal continues to switch from one state to another, remaining in any given state for an arbitrary period of time. Now, taking a random or coherent phase walk to be a walk in the complex plane, we can describe the process in terms of the analytic signal

$$s(t) = \begin{cases} a\exp[i\theta_R(t)], & t \in [0, T_1); \\ a\exp[i\theta_C(t)], & t \in [T_1, T_1 + T_2); \\ a\exp[i\theta_R(t)], & t \in [T_1 + T_2, T_1 + T_2 + T_3); \\ \vdots \end{cases}$$

where θ_R denotes the random phase (i.e. for any time t over the interval in which a random phase walk occurs, θ_R has a randomly chosen value between 0 and 2π radians) and θ_C denotes the coherent phase (i.e. for any time t over the interval in which a coherent phase walk occurs, $\theta_C << 1$ has the same value) as illustrated (for the discrete case) in Figure 17.4.

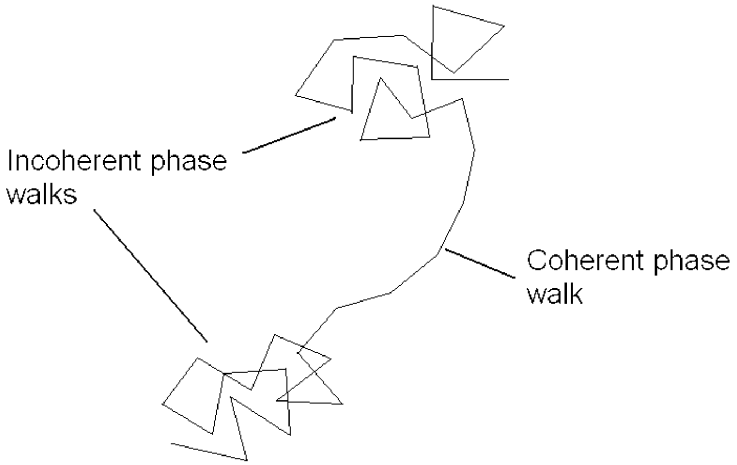

Figure 17.4: Example of a non-stationary (discrete) phase walk with instantaneous transitions for the random-coherent-random case.

What type of statistical analysis could we apply to such a signal in order to segment it into statistically significant intervals of time? Clearly, the PDF of the amplitude a of such a signal will be characterized by a delta function

$$\Pr[a(t)] = \delta(x - a)$$

but the PDF of the phase will change from one that is characterized by a delta function

$$\Pr[\theta_C(t)] = \delta(\theta - \theta_C)$$

for coherent phase walks to one that is characterized by a uniform distribution in which

$$\Pr[\theta_R(t)] = \frac{1}{2\pi} \quad \forall \theta_R \in [0, 2\pi]$$

for random phase walks. This is of course a highly idealized model and in reality we should expect that: (i) the amplitude a will not be a constant; (ii) the phase will not change instantaneously at a point in time from being determined by a constant value to a uniformly distributed deviate. Nevertheless, the argument above serves to highlight the importance of analyzing the phase distribution in addition to the amplitude distribution (conventional statistical analysis) of a signal for the purpose of segmenting it into regions of statistical significance with regard to the non-stationary model proposed.

Having established the rationale for a 'phase distribution analysis', we can generalize the idea further as follows. If a random phase walk is characterized by $A(t) = a\sqrt{t}$ and a coherent phase walk by $A(t) = at$, then the intermediate case should be characterized by

$$A(t) = at^H, \quad 0.5 < t < 1$$

But this relationship is the basis for the generalization of Brownian motion to fractional Brownian motion as discussed in the previous Section. We can interpret fractional Brownian motion is terms of a random phase walk in which the phase distribution changes from being a constant to a delta function as the Hurst exponent H changes from 0.5 to 1, respectively. In turn, this transitory behaviour can be cast in terms of the fractional diffusion equation

$$\left(\frac{\partial^2}{\partial x^2} - \frac{1}{D^{q(t)}}\frac{\partial^{q(t)}}{\partial t^{q(t)}}\right) u(x,t) = 0, \quad 1 \leq q(t) \leq 2, \quad \forall t$$

giving diffusive behaviour for the case when $q = 1$ (diffusion equation) and propagative behaviour for the case when $q = 2$ (wave equation). A general solution to this equation for an inhomogeneous stochastic source is developed in *Digital Signal Processing*, Horwood, 2003 which yields a method of segmenting a digital signal by computing the Fourier dimension q over a moving window.

Given that

$$\Pr[\theta(t)] = \begin{cases} \frac{1}{2\pi} \quad \forall\theta \in [0, 2\pi], & H = 0.5; \\ d(\theta), & H \in (0.5, 1); \\ \delta(\theta - \theta_C), & H = 1. \end{cases}$$

where $d(\theta)$ is the phase distribution for the intermediate case (fractional Brownian motion), another approach is to compute $d(\theta)$ over a moving window and look for a characteristic change in $d(\theta)$ (i.e. a robust statistical signature) as a function of time that proves to be of value in the segmentation process. This can include the computation of a range of statistical parameters such as the mean, the mode, the variance and other statistical moments (see Section 17.5) appropriate to the type of distribution associated with a given signal.

17.4 Fully Coherent Scattering Processes

The use of random walk methods of the type introduced in Section 17.2 can be used as the basis for generating a range of stochastic scattering models. The random phase walks considered so far are limited to the fact that the amplitude a is taken to be a constant (a measure of the mean free path). We shall now consider a model for the distribution of intensities observed in a fully coherent image when the scattering of a wavefield from one site to the next is taken to be a random walk in the plane with arbitrary amplitude and phase variations. In this case, we detect a coherent wavefield E (the electric field for example) given by

$$E = \sum_{j=1}^{N} r_j \exp(i\phi_j) = R\exp(i\Phi)$$

where r, ϕ and N are independent random variables. Both r and ϕ are assumed to be continuous random variables and N is discrete. We can write E as a vector, whose components are the real and imaginary parts of E, i.e.

$$\mathbf{E} = (E_{\text{real}}, E_{\text{imag}}).$$

It is useful to work in terms of the characteristic function of a complex random variable

$$\mathbf{U} = (U_{\text{real}}, U_{\text{imag}})$$

defined as (2D inverse Fourier transform)

$$C(\mathbf{U}) = \langle \exp(i\mathbf{E}\cdot\mathbf{U})\rangle = \int \exp(i\mathbf{E}\cdot\mathbf{U})P(\mathbf{E})d\mathbf{E}$$

where the integral is taken to over all $\mathbf{E}$ and where $P(\mathbf{E})$ is the Probability Density Function (PDF) of $\mathbf{E}$. Thus, P can be computed from C via the 2D Fourier transform, i.e.

$$P(\mathbf{E}) = \frac{1}{(2\pi)^2}\int \exp(-i\mathbf{E}\cdot\mathbf{U})C(\mathbf{U})d\mathbf{U}$$

where the integral is taken over all $\mathbf{U}$.

The aim of this calculation is to find an expression for P. This is done by first computing $C(\mathbf{U}) = \langle \exp(i\mathbf{E}\cdot\mathbf{U})\rangle$ and then taking the inverse Fourier transform to evaluate P. The calculation of the characteristic function will be based on the following assumptions:

(i) The phase is uniformly distributed which represents strong scattering.

(ii) The scattering events at each site are independent.

(iii) N conforms to a negative binomial distribution of the form

$$P_N = \left(\begin{array}{c} N+\alpha-1 \\ N \end{array}\right)\frac{(\bar{N}/\alpha)^N}{(1+\bar{N}/\alpha)^{N+\alpha}}$$

where $\bar{N}$ is the mean of the distribution and α is a 'bunching' parameter. Clearly $\alpha > \bar{N}$ for P_N to be a proper PDF. Assumption (iii) above is based on a birth-death-migration processes which is representative of the distribution of scatterers.

To find $\langle \exp(i\mathbf{E}\cdot\mathbf{U})\rangle$ we write $\mathbf{E}$ and $\mathbf{U}$ in terms of their real and imaginary components, i.e.

$$\mathbf{E} = (R\cos\Phi, R\sin\Phi), \quad \mathbf{U} = (U\cos\chi, U\sin\chi)$$

where $U \equiv |\,\mathbf{U}\,|$. Here R is the resultant amplitude and Φ is the resultant phase that is detected:

$$\mathbf{E}\cdot\mathbf{U} = R\cos\Phi U\cos\chi - R\sin\Phi U\sin\chi$$

$$= U\sum_{j=1}^{N} r_j(\cos\phi_j\cos\chi - \sin\phi_j\sin\chi) = U\sum_{j=1}^{N} r_j\cos(\phi_j+\chi).$$

Hence, the characteristic function for a random walk with N steps is

$$C_N(\mathbf{U}) = \langle \exp[iU\sum_{j=1}^{N} r_j\cos(\phi_j+\chi)]\rangle.$$

Since $\exp(x_1 + x_2 + ... + x_N) = \exp(x_1)\exp(x_2)\exp(x_3)...\exp(x_N)$,

$$C_N(\mathbf{U}) = \langle \prod_{j=1}^{N} \exp[iUr_j \cos(\phi_j + \chi)] \rangle.$$

The variables r, ϕ and N are independent. Assumption (ii) given above means that r_j is independent of r_k, i.e. a scattering event at site j is independent of a scattering event at site k. The net effect of this assumption is to eliminate conditional probabilities from the scattering process. In this case, the product can be taken outside the average, giving

$$C_N(\mathbf{U}) = \prod_{j=1}^{N} \langle \exp[iUr_j \cos(\phi_j + \chi)] \rangle.$$

The term $\langle \exp[iUr_j \cos(\phi_j + \chi)] \rangle$ is an average over both the amplitude distribution and the phase distribution. Assuming that the phases are uniformly distributed (strong scattering), the integral for the phase can be written as

$$\langle \exp[iUr_j \cos(\phi_j + \chi)] \rangle_\phi = \int_{\forall \phi} \exp(iUr_j \cos(\phi + \chi) P_j(\phi) d\phi$$

where P_j is the uniform phase distribution defined as

$$P_j(\phi) = \begin{cases} \frac{1}{2\pi}, & -\pi \leq \phi < \pi; \\ 0, & \text{otherwise.} \end{cases}$$

Consider the integral

$$I = \int_{-\pi}^{\pi} \exp[iUr_j \cos(\phi + \chi)] d\phi.$$

To evaluate this integral we use the following identity

$$\exp(i\alpha \cos\theta) = J_0(\alpha) + 2 \sum_{k=1}^{\infty} i^k J_k(\alpha) \cos k\theta$$

where J_k is the Bessel function of order k. Then

$$I = \int_{-\pi}^{\pi} \left[J_0(\alpha) + 2 \left(\sum_{k=1}^{\infty} i^k J_k(\alpha) \cos k\theta \right) \right] d\theta$$

$$= [J_0(\alpha)\theta]_{-\pi}^{\pi} + \left[2 \sum_{k=1}^{\infty} \frac{i^k}{k} J_k(\alpha) \sin k\theta \right]_{-\pi}^{\pi} = 2\pi J_0(\alpha).$$

Hence,

$$\langle \exp(i\mathbf{E} \cdot \mathbf{U}) \rangle_\phi = \langle \exp[iUr_j \cos(\phi_j + \chi)] \rangle_\phi = J_0(Ur_j)$$

where

$$U = \sqrt{U_{\text{real}}^2 + U_{\text{imag}}^2}$$

and

$$C_N(\mathbf{U}) = \prod_{j=1}^{N} \langle J_0(Ur_j)\rangle_r$$

where

$$\langle J_0(Ur_j)\rangle_r = \int_0^\infty J_0(Ur)P_j(r)dr.$$

Here $P_j(r)$ is the PDF for r. Now, if all the scattering processes are similar, then they will all have the same PDF and therefore

$$\prod_{j=1}^{N} \langle J_0(Ur_j)\rangle_r = \langle J_0(Ur)\rangle_r^N = \left(\int_0^\infty J_0(Ur)P(r)dr \right)^N.$$

This result depends on the number of steps N which is itself a random variable, and, in order to proceed further, we must consider a PDF for N. For this purpose we consider the negative binomial distribution - assumption (iii) - and develop an expression for the characteristic function for the mean $\bar{N}$ of N. This is given by

$$C_{\bar{N}}(\mathbf{U}) = \sum_{N=0}^{\infty} P_N C_N(\mathbf{U})$$

$$= \sum_{N=0}^{\infty} \begin{pmatrix} N+\alpha-1 \\ N \end{pmatrix} \frac{(\bar{N}/\alpha)^N}{(1+\bar{N}/\alpha)^{N+\alpha}} \langle J_0(Ur)\rangle_r^N$$

$$= \sum_{N=0}^{\infty} \frac{(N+\alpha-1)!}{N!(\alpha-1)!} \left(\frac{(\bar{N}/\alpha)\langle J_0(Ur)\rangle_r}{1+\bar{N}/\alpha} \right)^N \frac{1}{(1+\bar{N}/\alpha)^\alpha}$$

$$= \frac{1}{(\alpha-1)!(1+\bar{N}/\alpha)^\alpha} \sum_{N=0}^{\infty} \frac{(N+\alpha-1)!}{N!} \mu^N$$

where

$$\mu = \frac{(\bar{N}/\alpha)\langle J_0(Ur)\rangle_r}{1+\bar{N}/\alpha}.$$

Now,

$$\sum_{N=0}^{\infty} \frac{(N+\alpha-1)!}{N!}\mu^N = (\alpha-1)! \left(1 + \alpha\mu + \frac{\alpha(1+\alpha)}{2!}\mu^2 + ...\right) = (\alpha-1)!(1-\mu)^{-\alpha}$$

and therefore we can write

$$C_{\bar{N}}(\mathbf{U}) = \frac{(\alpha-1)!}{(\alpha-1)!(1+\bar{N}/\alpha)^\alpha} \frac{1}{(1-\mu)^\alpha}$$

$$= \frac{(1+\bar{N}/\alpha)^{\alpha}}{(1+\bar{N}/\alpha)^{\alpha}(1+\bar{N}/\alpha-(\bar{N}/\alpha)\langle J_0(Ur)\rangle_r)^{\alpha}}$$

$$= \left(1+\frac{\bar{N}}{\alpha}\left(1-\langle J_0(Ur)\rangle_r\right)\right)^{-\alpha}.$$

The calculation of $\langle J_0(Ur)\rangle_r$ is based on a small but important modification whereby we scale r according to $r \to r/\sqrt{\bar{N}}$. Thus, we consider

$$\langle J_0(Ur)\rangle_r = \int_0^{\infty} P(r)J_0(Ur/\sqrt{\bar{N}})dr.$$

As $\bar{N} \to \infty$, this modification of the definition of $\langle J_0(Ur)\rangle_r$ allows us to employ the Frobenius series for J_0, i.e.

$$J_0(x) = 1 - \frac{x^2}{4} + \frac{x^4}{2^6} - ...$$

then

$$\langle J_0(Ur)\rangle_r = \int_0^{\infty} P(r)dr - \frac{1}{4}\int_0^{\infty}\frac{U^2r^2}{\bar{N}}P(r)dr + \frac{1}{2^6}\int_0^{\infty}\frac{U^4r^4}{\bar{N}^2}P(r)dr - ...$$

$$= 1 - \frac{1}{4}\frac{U^2}{\bar{N}}\langle r^2\rangle + \frac{1}{2^6}\frac{U^4}{\bar{N}^2}\langle r^4\rangle - ...$$

where

$$\langle r^n\rangle = \int_0^{\infty} r^n P(r)dr.$$

Hence, we can write

$$C_{\bar{N}}(\mathbf{U}) = \left[1+\frac{\bar{N}}{\alpha}\left(1-\left(1-\frac{1}{4}\frac{U^2}{\bar{N}}\langle r^2\rangle + \frac{1}{2^6}\frac{U^4}{\bar{N}^2}\langle r^4\rangle - ...\right)\right)\right]$$

$$= \left(1+\frac{1}{4}\frac{U^2}{\alpha}\langle r^2\rangle - \frac{1}{2^6}\frac{U^4}{\bar{N}\alpha}\langle r^4\rangle + ...\right)^{-\alpha}$$

and

$$C(\mathbf{U}) = \lim_{\bar{N}\to\infty} C_{\bar{N}}(\mathbf{U}) = \left(1+\frac{1}{4}\frac{U^2}{\alpha}\langle r^2\rangle\right)^{-\alpha}.$$

This result allows us to compute the PDF of $\mathbf{E} = R\exp(i\Phi)$ which can be obtained by evaluating the Fourier integral of $C(\mathbf{U})$, i.e.

$$P(\mathbf{E}) = \frac{1}{(2\pi)^2}\int_{\forall\mathbf{U}} \exp(-i\mathbf{E}\cdot\mathbf{U})C(\mathbf{U})d\mathbf{U}$$

$$= \frac{1}{(2\pi)^2}\int_{-\pi}^{\pi}\int_0^{\infty}\frac{\exp(-i\mathbf{E}\cdot\mathbf{U})}{\left(1+\frac{1}{4}\frac{U^2}{\alpha}\langle r^2\rangle\right)^{\alpha}}UdUd\chi.$$

Integrating over χ generates a Bessel function as before

$$P(\mathbf{E}) = \frac{1}{2\pi} \int_0^\infty \frac{U J_0(UR)}{\left(1 + \frac{1}{4}\frac{U^2}{\alpha}\langle r^2 \rangle\right)^\alpha} dU.$$

Evaluating the final integral gives

$$P(\mathbf{E}) = \frac{1}{2\pi 2^{\alpha-1}} \frac{R^{\alpha-1}}{\Gamma(\alpha)} \left(\frac{4\alpha}{\langle r^2 \rangle}\right)^{\frac{1+\alpha}{2}} K_{\alpha-1}\left[R\left(\frac{4\alpha}{\langle r^2 \rangle}\right)^{\frac{1}{2}}\right]$$

where $K_{\alpha-1}$ is a modified Bessel function. The PDF of the amplitude follows by integrating $P(\mathbf{E})$ over all values of the phase Φ. However, $P(\mathbf{E})$ is independent of Φ and so this integral yield 2π, i.e.

$$P(R) = \int_{-\pi}^{\pi} P(\mathbf{E}) R d\Phi = 2\pi R P(\mathbf{E})$$

$P(R)$ can therefore be written as

$$P(R) = \frac{\beta^{1+\alpha}}{2^{\alpha-1}\Gamma(\alpha)} R^\alpha K_{\alpha-1}(\beta R)$$

where

$$\beta = \left(\frac{4\alpha}{\langle r^2 \rangle}\right)^{\frac{1}{2}}.$$

This is the so called 'K-distribution' which is a feature of most fully coherent images.

The calculation given above illustrates the way in which the PDF of an image can be derived subject to a model for the distribution of the phase (in this case, a uniform phase distribution representing strong scattering) and a statement of the characteristics of the random walk (in this case, a negative binomial distribution for the number of steps N). The PDF derived can then be used to characterize an image statistically by computing the parameters α, β and $\langle r^2 \rangle$. For a statistically stationary image, these values are computed from data obtained over the entire image. For a statistically non-stationary image, a moving window method can be applied to segment the image.

17.5 Statistical Moments

Statistical moments provide a measure of the statistical characteristics of an image which can be used to classify the image in its entirety or used to segment it using a moving window where the window is sufficiently large to provide a statistically significant result. For coherent images, in which a model for the PDF is derivable from first principles, classification can be undertaken using the model derived. However, with incoherent images, this is not always possible because of the arbitrary nature of their PDFs (see Figure 17.1). For

incoherent images there are a range of statistical classification methods that can be applied. The first of these are the statistical moments. Given an image f_{kl} we can calculate its local mean or expected value over a window W, centred in the image position ij as

$$\mu_{ij} = \langle f_{kl} \rangle_{ij} = \frac{1}{N} \sum_{k,l \in W} f_{i-k,j-l}.$$

The variance, σ^2, is a measure that characterizes how the values deviate from the mean value,

$$\sigma_{ij}^2 = \frac{1}{N} \sum_{k,l \in W} (f_{i-k,j-l} - \mu_{ij})^2$$

and a whole family of local moments can be calculated using

$$\mu_{ij}^n = [\langle (f_{i-k,j-l} - \mu_{ij})^n \rangle]^{\frac{1}{n}}$$

for $n = 1, 2, ...$ The standard deviation, σ, is equivalent to the second moment. Two other popular statistics are *skewness*,

$$s_{ij} = \frac{1}{\sigma_{ij}^3} \frac{1}{N-1} \sum_{k,l \in W} (f_{i-k,j-l} - \mu_{ij})^3$$

and the *kurtosis*,

$$\alpha_{ij} = \frac{\mu_{ij}^4}{\sigma_{ij}^2}.$$

A related measure calculated from the image derivatives is the total variance, V. This consists of the sum of gradient values throughout the window W. Any of the different gradient operators, G, as discussed in Chapter 16, can be used to compute

$$V_{ij} = \sum_{k,l \in W} G_{i-k,j-l}.$$

A commonly used indicator to describe the information content of any set of data is Shannon's formula for entropy. It is worth pointing out that Shannon's entropy was originally defined for all information streams. We will consider it here in terms of image data:

$$E_1 = -\sum_{n=0}^{N-1} p_n \log_2 \frac{1}{p_n}.$$

This gives order-1 entropy[1] where p_n is the probability of pixel value n, in the range $0 \ldots N-1$, of occurrence. This formula results in a single number that gives the minimum average code length if every pixel is encoded independently of the other pixels. Entropy is, in effect, a measure of the information content of the image.

[1]There is some disagreement in terminology and, although it is called first order entropy, it is often also written as order-0 entropy.

Order-m entropy can also be calculated by extending the formula. By defining $P_m(x_1, x_2, \ldots, x_m)$ as the probability of seeing the sequence of m pixels $x_1, x_2, \ldots, x_m$ we have

$$E_m = - \sum_{x_1, x_2, \ldots, x_m = 0}^{N-1} P_m(x_1, x_2, \ldots, x_m) \log_2 \frac{1}{P_m(x_1, x_2, \ldots, x_m)}.$$

Further, defining $\langle \cdot \rangle$ as the expected value, the full entropy of data is given by

$$E_{\max} = - \lim_{m \to \infty} \frac{1}{m} \left\langle \log_2 \frac{1}{P_m(x_1, x_2, \ldots, x_m)} \right\rangle.$$

This limit always exists if the data stream is stationary and ergodic. These numbers (i.e. $E_1, E_2, ..., E_m, E_{\max}$) can be calculated over a local moving window and used to segment an image into a multiplicity of information measures.

17.6 Noise and Statistical Tests

The simulation of noise holds a very important place in image synthesis, image processing and image analysis. Noise can be defined in terms of its PDF and/or its PSDF. In the latter case, many noise types can be classified in terms of a spectrum with the form k^{-q} as a function of the temporal or spatial frequency k. For example, *white* noise has a spectral exponent $q = 0$ and, like white light, has all frequencies equally represented. As q becomes larger the name for the noise changes from white to black.

Spectral exponent q	Colour
0	white
1	pink
2	brown
>2	black

White noise can be integrated over time to create *brown* noise, where $q = 2$. Brown noise can be used to model many kinds of statistical fluctuations, most prominently in the field of gambling. (*Brown* noise is named after the Scottish botanist Robert Brown who discovered it within the motion exhibited by a small particle that is totally immersed in a liquid or gas.) In between white and brown there is a whole range of alternatives including *pink* noise when $q = 1$. Pink noise has equal power in octave frequencies, which has made it popular as a hearing test signal, for example. This is because pink noise stimulates all parts of the auditory system within the human ear evenly, so it is the hearing equivalent of white noise. Pink noise occurs in other physical systems including resonance in semiconductor devices for example. At the other extreme, when $q > 2$, it is referred to as *black* noise. In statistics, black noise signals are associated with catastrophic events, including, for example, a financial market collapse, floods, earthquakes, extinctions, etc. This is because

it predicts events that come in groups. The temporal behaviour of these noise fields can be unified via the stochastic fractional partial differential equation

$$\left(\frac{\partial^2}{\partial x^2} - \tau^q \frac{\partial^q}{\partial t^q}\right) u(\mathbf{r}, t) = n(\mathbf{r}, t), \quad q \geq 0$$

where n is a white noise field (see *Digital Signal Processing*, Horwood Publishing, 2003, Chapter 17).

17.6.1 Computing Noise Fields

Most digital computers have methods for creating white noise via a *pseudo random number generator*. Methods of computing pseudo random numbers are covered *Digital Signal Processing*, Horwood Publishing, 2003, Chapter 14 which includes the generation of pseudo chaotic number streams. In this Section, we briefly revisit the basis for designing pseudo random number generating algorithms for reasons of completeness with regard to the remit of this Chapter.

Since a computer is a truly deterministic machine, it is rather perverse for it to be able to create random values. For this reason great care needs to be considered when creating noise of any type. This Section digresses with a discussion of a few algorithms to perform this task adequately.

Linear Congruence Method

Within most computers there is a system described as a pseudo random number generator. The first rule is to be very wary of using this operator as within the history of computer design there have been many poor implementations. The vast majority use a linear congruence method that is very simple but requires care in use. The algorithm produces a string of (integer) values $x_0, x_1, x_2, \ldots$ each calculated from the previous value, where

$$x_{j+1} = (ax_j + c) \text{mod } P.$$

The initial value, x_0, is often specified by the user as a seed value. The sequence is highly deterministic and has the property that it will always loop within a maximum of P different values. For example, if we assign $a = 7, c = 12, P = 30$ and $x_0 = 0$, we obtain the following sequence:

$$0, 12, 16, 4, 10, 22, 16, 4, 10, 22, \ldots$$

As in this example, the loop length can be very short. This limitation can cause very poor results, especially when considering a small range or using multiple dimensions. An inadequate choice for the constants a, c and P can lead to very limited and at times unusable ranges. The most famous case occurred in early IBM PCs within the inbuilt random number generator. It is noted that the longest sequence possible is equal to P, so a large P is recommended. The following conditions allow a linear congruence sequence to have a period of length P:

- c is relatively prime to P;
- $b = a - 1$ is a multiple of p, for every prime p dividing P;
- b is a multiple of 4 if P is a multiple of 4.

In addition to the standard linear congruential generator discussed so far, a number of 'variations on a theme' can be considered such as the iteration

$$x_i = (a_1 x_{i-1}^2 + a_2 x_{i-1} + a_3) \mathrm{mod} P$$

or

$$x_i = (a_1 x_{i-1}^3 + a_2 x_{i-1}^2 + a_3 x_{i-1} + a_4) \mathrm{mod} P$$

and so on, where a_n are predefined.

Shuffling

An extra stage which helps further randomise the values is to shuffle the values within a temporary storage. Unless a very poor choice of values for a, c, and P has been made, this approach can insure a consistent random number stream. The algorithm is very simple and can be applied to post filter any random number generator. First initialise an array $x[1..100]$ with random numbers from a random number generator RAND() say, and set y to the last random number calculated. To create the next random number, we use the following pseudo code

$j = 1 +$ Int$(100 * y)$
$y = x[j]$
$x[j] =$ RAND()
Output y

This simple indirection works as it frees the list of random numbers from sequential correlation. The exact size of the array, $x[\ldots]$, is most of the time irrelevant.

Additive Generators

Additive generators create very long cycles of values. A typical algorithm commences by initialising an array x_i with random numbers (not all of which are even) so that we can consider the initial state of the generator to be $x_1, x_2, x_3, \ldots$. We then apply

$$x_i = (x_{i-a} + x_{i-b} + \ldots + x_{i-m}) \mathrm{mod} 2^n$$

where $a, b, \ldots, m$ and n are assigned integers.

An example of this method is the 'Fish generator' in which

$$x_i = (x_{i-55} + x_{i-24}) \mathrm{mod} 2^{32}.$$

The algorithm commences by initialising an array $x[1..55]$ with random numbers, not all of which are even. Then two pointers are initialised, j is set to 24, and k is set to 55. To create the next random number we apply the following:

$x[k] = (x[k] + x[j]) \bmod 2^e$
decrease k and j by 1
if $j = 0$ then $j = 55$
if $k = 0$ then $k = 55$
Output $x[k]$

This algorithm has repeatedly proved itself to be very reliable, and universally popular. It is fast as no multiplication operations are required, and can work equally well with floating point numbers as with integers. The period of the sequence of random numbers is also very large, being of the order $2^f(2^{55} - 1)$, where $0 \leq f \leq e$. The initial choice of values 24 and 55 is very important to achieving a large loop length.

Further examples include the linear feedback shift register given by

$$x_n = (c_1 x_{n-1} + c_2 x_{n-2} + c_m x_{n-m}) \text{mod} 2^k$$

which, for specific values of $c_1, c_2, ...c_m$, has a cycle length of 2^k.

Gaussian Noise Generation

We now introduce an algorithm for creating random numbers which have a normal or Gaussian distribution. This probability distribution has zero mean and standard deviation of one, and is given by

$$p(y)dy = \frac{1}{\sqrt{2\pi}} \exp\left(-\frac{y^2}{2}\right).$$

The Box-Muller algorithm is used to create two independent normal distributed values, y_1 and y_2, using the Box-Muller transform.

repeat
$v_1 = \text{RAND}()$
$v_2 = \text{RAND}()$
$R^2 = v_1^2 + v_2^2$
until $R^2 \leq 1$
$y_1 = v_1 \sqrt{\frac{-2 \ln R^2}{R^2}}$
$y_2 = v_2 \sqrt{\frac{-2 \ln R^2}{R^2}}$

The basis for this method is as follows. Assume we wish to create two values y_1 and y_2; we first create two uniform random values, x_1, x_2 on $(0, 1)$. This can be written as

$$y_1 = \sqrt{-2 \ln x_1} \cos 2\pi x_2 \qquad \text{and} \qquad y_2 = \sqrt{-2 \ln x_1} \sin 2\pi x_2$$

or, equivalently,

$$x_1 = \exp\left(-\frac{1}{2}\left(y_1^2 + y_2^2\right)\right) \qquad \text{and} \qquad x_2 = \frac{1}{2\pi} \tan^{-1} \frac{y_2}{y_1}.$$

We can now calculate the joint probability distribution of the two y's, with the following:

$$p(y_1, y_2)dy_1dy_2 = p(x_1, x_2)\left|\frac{\partial(x_1, x_2)}{\partial(y_1, y_2)}\right| dy_1dy_2$$

where $|\partial(x_1, x_2/\partial(y_1, y_2|$ is the Jacobian determinant. Thus,

$$\left|\frac{\partial(x_1, x_2)}{\partial(y_1, y_2)}\right| = \begin{vmatrix} \frac{\partial x_1}{\partial y_1} & \frac{\partial x_1}{\partial y_2} \\ \frac{\partial x_2}{\partial y_1} & \frac{\partial x_2}{\partial y_2} \end{vmatrix} = -\left[\frac{1}{\sqrt{2\pi}}\exp\left(-\frac{y_1^2}{2}\right)\right]\left[\frac{1}{\sqrt{2\pi}}\exp\left(-\frac{y_2^2}{2}\right)\right].$$

This means that y_1 and y_2 are independent. So this method creates two Gaussian distributed values from two uniformally distributed random values as required. A further trick is to create v_1, v_2 as two points on a unit circle; then two simplifications can be made as

$$\sin 2\pi x_2 = v_1/R \qquad \text{and} \qquad \cos 2\pi x_2 = v_2/R$$

where $R = \sqrt{v_1^2 + v_2^2}$, and $x_1 = R^2$.

17.6.2 Statistical Tests

The preceding results allow us to choose the parameters for a deterministic random number generator that has a large cycle. Then begins the long series of tests essential before one can assert the suitability of these parameters to produce a random sequence. The most commonly applied initial tests are the Chi-squared and Kolmogorov-Smirnov tests. Such tests establish whether the numbers from the sequence are correctly distributed. We now present a brief overview of the procedures involved.

Chi-squared Test

Assume that observations can fall into one of n different outcomes, and the expected probability for the k^{th} outcome is p_k. If there are N independent observations, with Y_k of them falling into outcome k, the Chi-squared statistic is given by

$$\chi^2 = \sum_{1\le k\le n} \frac{(Y_k - Np_k)^2}{Np_k}$$

and is the measure of deviation from the expected.

Given n possible outcomes we need to be able to find out when χ^2 is too large or too small. The table below tells us how likely a value of χ^2 is. Consider the entry s found in row n, column p which states that *the probability that χ^2 is less than s is p if the number of samples is suitably large enough.* Thus, if, over a series of tests, χ^2 is often abnormally too large or too small, then that probability generator should be considered suspect.

	$p = 5\%$	$p = 25\%$	$p = 50\%$	$p = 75\%$	$p = 95\%$
$n = 5$	0.71	1.92	3.36	5.39	9.45
$n = 10$	3.33	5.90	8.34	11.39	16.92
$n = 20$	7.26	11.04	14.34	18.25	25.00

Kolmogorov-Smirnov Test

The Chi-squared test relies on the distribution giving n distinct outcomes. Often the outcomes cover a very large range. A similar procedure can be carried out by defining the empirical distribution function,

$$F_n(x) = \frac{\text{Number of } x_i \leq x, 1 \leq i \leq N}{N}.$$

This gives us two measures, K_n^+ that gives the greatest deviation from F when F_n is greater than F, and K_n^- that gives the greatest deviation when F_n is less than F, i.e.

$$K_n^+ = \sqrt{n} \max_x [F_n(x) - F(x)] \text{ and } K_n^- = \sqrt{n} \max_x [F(x) - F_n(x)].$$

Similarly to the Chi-squared test, there exists an equation to calculate how likely a series of tests are.

	$p = 5\%$	$p = 25\%$	$p = 50\%$	$p = 75\%$	$p = 95\%$
$n = 5$	0.0947	0.3249	0.5245	0.7674	1.1392
$n = 10$	0.1147	0.3297	0.5426	0.7845	1.1688
$n = 20$	0.1298	0.3461	0.5547	0.7975	1.1839
$n = 30$	0.1351	0.3509	0.5605	0.8036	1.1916
			$\approx \sqrt{\frac{1}{2} \ln \frac{1}{1-p}} - \frac{1}{6\sqrt{n}}$		

Alternative Tests

To be sure of the randomness of numbers, further tests may be necessary. We outline a few of the popular ones.

Serial independence looks at the independence one value has over the next. Pairs of numbers can then be considered as single values.

Gap analysis looks at the distance of the occurrence of one value to the next time it appears again.

The poker test considers the number of similar elements within a group of random numbers. The number of k-tuples with r different values, when there are n possible values, can be Chi-square tested with the probability,

$$p_r = \frac{n(n-1)\dots(n-r-1)}{n^k} \left(\begin{array}{c} k \\ r \end{array} \right).$$

The Coupon test is related to the poker test and looks at the length of segments required to get a complete set of all the integers 0 to d. The Chi-squared test can be applied to the set Y_i, $d \leq i \leq t$ for some arbitrary $t > d$. Y_i contains the number of occurrences where the complete set occurs within a segment of exactly i length, and Y_t includes the number of occurrences when the segment length is $\geq t$. The number of observations is then $N = t - d + 1$. Defining $k = t - d + 1$ the corresponding probability distribution is given by

$$p_k = \begin{cases} \frac{d!}{d^k} \left(\begin{array}{c} r-1 \\ d-1 \end{array} \right), & d \leq k < t; \\ 1 - \frac{d!}{d^{t-1}} \left(\begin{array}{c} t-1 \\ d \end{array} \right), & k = t. \end{cases}$$

The permutation test creates a sequence of groups each having t elements. There are $t!$ relative orderings in which the elements in each group can occur. Again a Chi-squared test can be applied to this sequence of permutations with $k = t!$ and $p_k = 1/t!$

The run test examines the length of monotonic sequences, either up or down. These length sequences are not independent as long as runs are likely to be followed by short ones and vice versa. To simplify the probabilities, a process of throwing away the element that follows a run makes them independent again. Then a Chi-squared test can be carried out.

Many other tests can be employed to deal with subsequences or correlations between elements and special tests for analysing test sets that are smaller than the possible number of categories can be developed. Special care also needs to be considered when dealing with algorithms that require a set of numbers at a time, for example within multidimensional sets.

Testing random number generators is useful for one main reason; to confirm to a third party that the random number generator being used is correct for their algorithm and will not cause spurious results. The simple recommendation is to always be prepared to look at the output of a random number generator and perform at least one test. It is important to remember that there are many poor pseudo random number generators that can sometimes only show their flaws under certain conditions. A sequence that passes one test may easily fail on another.

17.7 Texture Segmentation

No adequate definition of texture exists, because we have few insights into the detailed operation of the human visual system. A simple test as to whether a region contains a texture is to ask: if the region were expanded, would its contents be predictable from the original contents?

Segmentation is the process by which image sub-units are assigned to objects in a scene. There are three main types of segmentation in practice: pixel based methods, edge based methods and region based methods. Such techniques often require *a priori* knowledge of the types of texture present and are typically applied to rectangular regions which are iteratively reduced in size until internal homogeneity is achieved. Neighbouring regions are then tested in an attempt to form aggregations of uniform texture.

Three commonly used techniques for classifying texture are:

- Frequency space analysis.
- Spatial grey level dependence (co-occurrence) matrices. This technique computes a matrix of measures taken from the digitised image and then defines features (such as texture entropy, correlation, local homogeneity, etc.) as functions on this new matrix.
- Directional autocorrelations to determine periodicity. Here, an attempt is made to discover if there is any repeating pattern in a given direction. This technique involves taking pixels adjacent in some direction and correlating them with themselves after shifting them by one pixel, two pixels, etc.
- Fractal analysis. There is a fundamental relationship between texture and fractals which is explored in the following Chapter.

17.8 Summary of Important Results

Random Born scattering

The intensity of the scattering amplitude generated by a random Born scatterer is given by the Fourier transform of the autocorrelation function of the scattering function $\gamma(\mathbf{r})$:

$$I(\hat{\mathbf{N}}, k) = k^4 \int_V \exp(-ik\hat{\mathbf{N}} \cdot \mathbf{r})\Gamma(\mathbf{r}) d^3\mathbf{r}$$

where $\hat{\mathbf{N}} = \hat{\mathbf{n}}_s - \hat{\mathbf{n}}_i$ and $\Gamma(\mathbf{r})$, the autocorrelation function, is given by

$$\Gamma(\mathbf{r}) = \int_V \gamma(\mathbf{r}')\gamma^*(\mathbf{r}' + \mathbf{r}) d^3\mathbf{r}'$$

The autocorrelation function and the PSDF

$$\Gamma(\mathbf{r}) = \gamma(\mathbf{r}) \odot \gamma(\mathbf{r}) \Longleftrightarrow \mid \widetilde{\Gamma}(\mathbf{k}) \mid^2$$

Coherent phase walk

The resultant amplitude A of a coherent phase walk with amplitude a after time t is

$$A(t) = at$$

Random phase walk

The resultant amplitude A of a random phase walk with amplitude a after time t (Brownian motion) is

$$A(t) = a\sqrt{t}$$

Fractional random phase walk

The resultant amplitude A of a fractional random phase walk with amplitude a after time t (fractional Brownian motion) is

$$A(t) = at^H, \quad H \in (0, 1]$$

where H is the Hurst exponent.

Strong coherent scattering PDF - the K-distribution

$$P(R) = \frac{\beta^{1+\alpha}}{2^{\alpha-1}\Gamma(\alpha)} R^\alpha K_{\alpha-1}(\beta R)$$

where

$$\beta = \left(\frac{4\alpha}{\langle r^2 \rangle}\right)^{\frac{1}{2}}.$$

Segmentation with statistical moments

For an image f_{ij} that is segmented using a moving window W

$$\mu_{ij}^n = [\langle (f_{i-k,j-l} - \mu_{ij})^n \rangle]^{\frac{1}{n}}$$

where

$$\mu_{ij} = \langle f_{kl} \rangle_{ij} = \frac{1}{N} \sum_{k,l \in W} f_{i-k,j-l}$$

Order-m entropy

$$E_m = -\sum_{x_1, x_2, \ldots, x_m = 0}^{N-1} P_m(x_1, x_2, \ldots, x_m) \log_2 \frac{1}{P_m(x_1, x_2, \ldots, x_m)}$$

Noise types

For a noise field with a characteristic PSDF of the form k^{-q}:

Spectral exponent q	Colour
0	white
1	pink
2	brown
>2	black

Linear congruence method for pseudo random number generation

$$x_{j+1} = (ax_j + c) \mathrm{mod} P$$

17.9 Further Reading

- Knuth D E, *The Art of Computer Programming Volume 2: Seminumerical Algorithms*, Addison-Wesley, 1969.
- Cox D and Miller H, *The Theory of Stochastic Processes*, Chapman and Hall, 1972
- Johnson N L and Kotz S, *Distributions in Statistics: Continuous Univariate Distributions*, Houghton-Mifflin, 1980.
- Adler R J, *The Geometry of Random Fields*, Wiley, 1981.
- Press W H, Teukolsky S A, Vetterling W T and Flannery B P, *Numerical Recipes: The Art of Scientific Computing*, Cambridge University Press, 1986.
- Mortesen R E, *Random Signals and Systems*, Wiley, 1987.
- Dudewicz E J and Mishra S N, *Modern Mathematical Statistics*, Wiley, 1988.
- Wechsler H, *Computational Vision*, Academic Press, 1990.

Chapter 18

Fractal Images and Image Processing

Fractal signals were discussed in *Digital Signal Processing*, Horwood, 2003 (Chapter 17) and some case studies given on the applications of fractal geometry to signal analysis. In this Chapter, we extend the study of fractal geometry to include fractal images and consider applications on the synthesis of images, their segmentation (fractal dimension segmentation) and analysis.

18.1 Introduction

Fractal geometry is the the geometry of self-similarity in which an object appears to look similar at different scales - an obvious concept when observing naturally occurring features, but one that has only relatively recently started to be applied to various branches of science and engineering. This concept can be applied to systems of varying physical size depending on the complexity and diversity of the fractal model that is considered. It is of philosophical interest to view the Universe itself as a single fractal, the self-similar parts of which have yet to be fully categorized; those naturally occurring objects for which fractal models abound being smaller subsets of a larger whole. This view is closely related to the concept of chaotic systems in which the dynamical behavior of the system cannot necessarily be pre-determined. Such systems exhibit self-similarity when visualized and analyzed in an appropriate way (i.e. an appropriate phase space). In this sense, the geometry of a chaotic system may be considered to be fractal.

Self-similarity is a very general term. There are two distinct types of self-similarity: (i) deterministic self-similarity in which the fractal is composed of distinct features which resemble each other in some way at different scales (feature scale invariance); (ii) statistical self-similarity in which the features of the fractal may change at different scales but whose statistical properties at all scales are the same (statistical scale invariance).

Deterministic fractals associated with (i) above are usually generated

through some iterative process and are remarkable for the complexity that can be derived through the simplest of iterative procedures. The way in which the output from these systems is viewed graphically and interpreted geometrically changes from one fractal to another but the overall principle remains the same.

Statistically self-similar fractals are those used to model a variety of naturally occurring objects (background noise, clouds, landscapes, coastlines, etc.). They can be generated through a variety of different stochastic modelling techniques. They can also be considered to be the solution to certain classes of stochastic differential equations of fractional order.

Fractal geometry is a consequence of the computing revolution and its development has gone hand-in-hand with advances in digital data processing and computer graphics. However, the principles of fractal geometry have been studied for many years and began with the French School of mathematics in the late Nineteenth Century. This included French mathematicians such as Jules Henri Poincaré who was one of the first mathematicians in history to conceive the idea that a dynamical system (and a Newtonian one at that) could not be predicted deterministically. He was in effect describing the principles of chaos as a result of re-evaluating an award winning piece of work he had undertaken early in his career on the orbits of multiple interacting bodies.

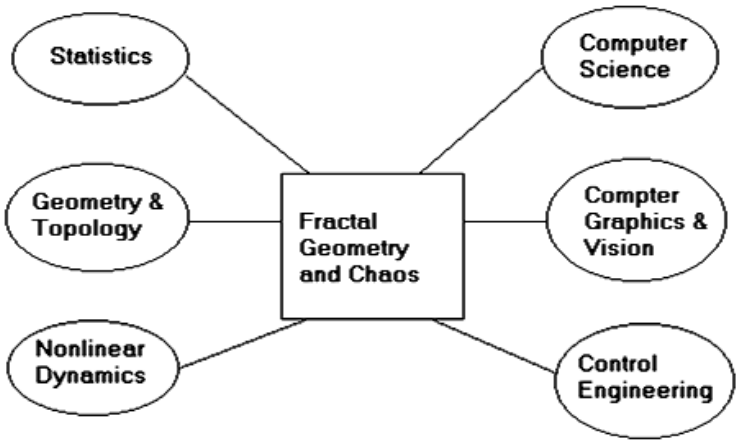

Figure 18.1: Fractal geometry and chaos and different fields of study.

Chaos is the study of functions which exhibit patterns or fields that are similar at different scales (see *Digital Signal Processing*, Horwood, 2003, Chapter 14). Today algorithms abound that are used to generate fractals and chaotic fields that ideally depend on: (i) an understanding of the physical (typically a nonlinear) system; (ii) a clear and concise mathematical definition of the field properties. Further, there are a range of applications based on fractals and

chaos that have been developed including time series analysis, speech processing, data compression, segmentation, terrain modeling, image synthesis, music, financial forecasting, biomedical engineering, digital communications and information technology security. The development of fractal geometry has been undertaken through many different fields of study and it now has an important contribution to make to these fields (see Figure 18.1)

Before the turn of the Nineteenth Century, it was believed that all continuous function must be differentiable in at least one location. It was well known that a continuous function may not be differentiable at a specific point, for example at $x = 0$ in the function $f(x) =\mid x \mid$. Having established a consistent approach to calculus by introducing the limiting condition for a derivative, i.e. defining a derivative as

$$\frac{df}{dx} = \lim_{\delta x \to 0} \frac{f(x + \delta x) - f(x)}{\delta x}$$

where $\delta x \neq 0$, Karl Wilhelm Weierstrass (1815-1879), was one of the first to create a function that was nowhere differentiable but still continuous. This is a function that has the property that the first derivative df/dx, and subsequently all higher order integer derivatives, cannot be found. A version of this function is based on an infinite sum of cosine curves, given by

$$f(x) = \sum_{n=1}^{\infty} a^n \cos(b^n \pi x)$$

where a is an odd integer, $b \in (0, 1)$ and $ab > 1 + 3\pi/2$. After the publication of this result, other mathematicians followed with slight alternatives. Giuseppe Peano (1858-1952), for example, introduced the first deterministic space filling function in 1890 which passes arbitrarily close to any point in the plane. The uses of these functions at the time was not apparent and many mathematicians were alarmed at the loss of differentiation as a 'constant'. Hermite defined them as a '*dreadful plague*', and Poincaré wrote in his collected works (Volume II, page 130), '*Yesterday, if a new function was invented it was to serve some practical end; today they are specially invented only to show up the arguments of our fathers, and they will never have any other use*'.

It was not until the 1920's, when nowhere differentiable functions were used to construct good models for Brownian motion, that such functions started to be appreciated for their practicability. By this time the idea of Weierstrass functions had gone from an interesting peculiarity to become the start of a new field within mathematics. The growing interest in random motion and stochastic field theory led, in the late 1930s, to Paul Lévy (1886-1971) asking a simple but profound question: *Under what circumstances does the distribution associated with a random walk of a few steps look the same as the distribution after many steps (except for scaling)?* This question is the same as asking under what circumstances do we obtain a random walk that is statistically the same at different scales. One of Paul Lévy's research students was Benoit Mandelbrot who later coined the phrase 'fractal' geometry (e.g. in his most famous book *The Fractal Geometry of Nature*, Freeman, 1982) as the study of

geometric objects, either deterministic or stochastic, that are self-similar, i.e. look the same at different scales. The term *fractal* is derived from the Latin adjective *fractus*. The corresponding Latin verb *frangere* means 'to break', to create irregular fragments. In addition to 'fragmented' *fractus* can also mean 'irregular', both meanings being preserved in *fragment*. The geometry of nature appears to have a fundamental feature which is that the shapes of things look the same at different scales (self-similarity) or at least have an affinity at different scales (self-affinity). This includes complex dynamical systems such as the structure of a society at a point in history and the evolution of society over time. The way in which we tend to perceive this 'geometry' is in terms of 'texture', '*an elusive notion which mathematicians and scientists tend to avoid because they can not grasp it... and... much of fractal geometry could pass as an implicit study of texture*' (B Mandelbrot).

Euclidean geometry (a term that derives from Euclid of Alexadra who publish his *Elements* around the year 300 BC and provided a systematic development of much of Greek mathematics up to that point) is based on ideas, axioms, theorems and results that are associated with simple objects - triangles, squares, circles, lines, etc. Some abstract concepts are required in order to maintain consistency such as defining two parallel lines as those that meet at infinity. However, the underlying philosophy of Euclidean geometry is that we can combine primitive objects to build-up and construct complex ones. To do this we first need to analyze a complex object in terms of its 'elements' to construct a simple set of primitives. This is the basis for the construction of most man-made objects and computational Euclidean geometry including computer aided design, solid geometry, etc. It is also the basis which we tend to use for analysing a complex problem. Fractal geometry is based on looking at things in terms of the 'big picture' and observing the fact that the 'smaller pictures' look similar. It uses ideas, axioms, theorems and so on associated with complex objects with repeating patterns, and includes abstract concepts such as infinite repeatability. Hence, unlike Euclidean geometry, the philosophy of fractal geometry is to construct an object by classifying it in terms of its repetitive underlying structure and repeating this structure again and again. This is the basis upon which many natural object and dynamical systems appear to be based. For example, consider Figure 18.2 which shows a number of grey scale images of natural objects and scenes - a tree, fern, rock, lava, etc. In each case, the image is of an object that, at first sight, appears relatively complex with different textures. However, if we 'look' at the object imaginatively enough in terms of its repeating patterns at different scales, then this complexity starts to be seen for what it is - self-similar simplicity! This principle is emphasized in Figure 18.3 which shows three images of a fern at different scales to illustrate the principle that '*self-similarity over limited ranges of scale is very common in nature'*.

While mathematicians and scientists may find texture 'hard to grasp', artists and musicians have understood it for many years. Impressionist paintings are studies in texture, initiated by English artists such as J M W Turner in the mid-Eighteenth Century, extended by the French school of impressionism by artists such as Claude Monet and developed further by modernists such as Jackson

Pollack (see Figure 18.4). Much of the music of composers such as Debussy, Ravel and Scriabin, for example, are studies of musical texture. Indeed, the art, music and languages of most cultures exhibit properties that are fractal, from the stylized versions of self-repeating patterns associated with Islamic art to Japanese art and the work of M C Escher (see Figure 18.5), for example.

Figure 18.2: Some example images of natural objects; from top to bottom and from left to right: a tree, rock, lava, a cloud, a forest, sage, a water fall and fern.

Figure 18.3: Three images of a Fern at different scales illustrating the principle of self-similarity.

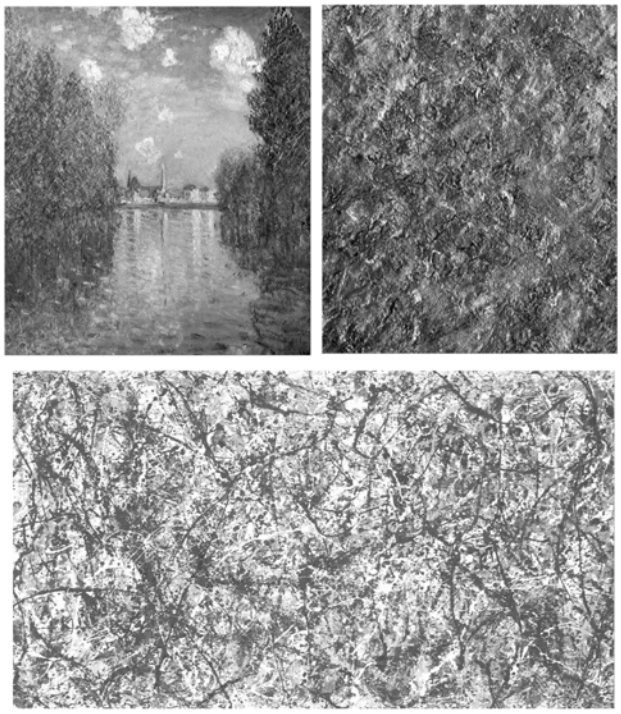

Figure 18.4: Texture by Claude Monet (top-right) taken from the painting shown (top-left) and texture by Jackson Pollock (bottom).

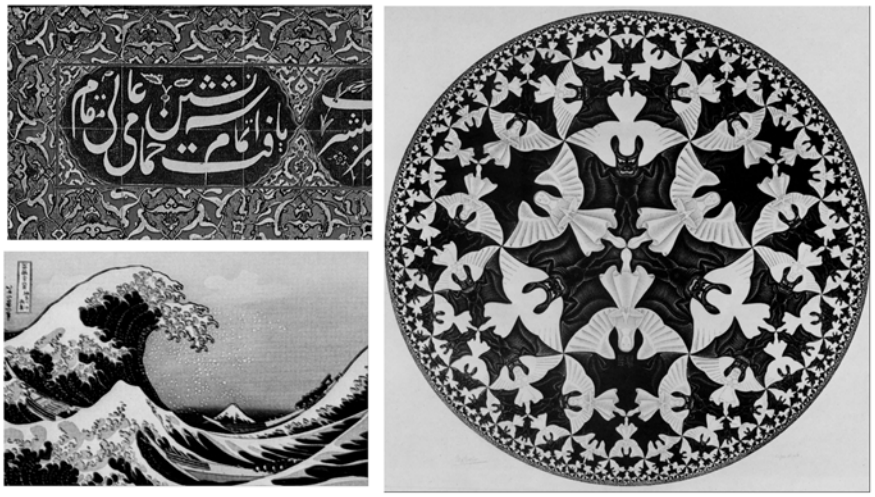

Figure 18.5: Examples of self-similarity in Islamic art (top-left), self-similarity by the Japanese artist K Hokusai from the 1800s (bottom-left), and an example of deterministic self-similarity by the Dutch graphic artist M C Escher (right).

The picture of the wave given in Figure 18.5 is an interesting 'reflection' on the perceptive Chinese proverb '*In every way one can sea the shape of the sea*'. Although very complex, the sea surface has dynamic structures (waves) which are similar at different scales, i.e. waves within waves. The images given in Figure 18.5 are different from those previously given in that the repeating patterns are deterministic, particularly the example of self-similarity by Escher. Deterministic fractals are fractals that have structures or shapes that are the same at different scales (such as the fern given in Figure 18.3), whereas random fractals are fractals whose structural distribution is similar at different scales. Self-similarity is not only a feature of nature, art, music, society and so on, it is also part of the way in which we imagine or 'image' physical concepts. For example, in the early fifteenth century (around 1505-1510), The Polish astronomer and cleric, Nicolaus Copernicus changed the way in which we imaged the solar system from the Ptolemaic theory where the planets and the Sun orbited the Earth to a heliocentric system in which all the planets, including the Earth, orbit the sun (*Concerning the Revolutions*, first published in 1543). In the early seventeenth century, Galileo Galilei introduced the concept of moons orbiting the planets when, in 1610, he discoved the moons of Jupiter. In 1913, following Ernest Rutherford's discovery of an atomic nucleus, Neils Bohr proposed a model for the hydrogen atom in which the electron orbits the nucleus, an orbit determined by a discrete energy level from which he provided a model that explained the hydrogen spectrum. This is the same basic idea (in terms of the 'images' of the physical system we use as a model) but at vastly different

scales. There is something intellectually and aesthetically pleasing about understanding things in terms of self-similar models, in addition to such models often providing a 'best fit' to the 'known data'. In physics, the model that would appear to be an underlying theme and a possibly unifier is the 'wave model'. In our models for the nucleus, the atom, for electromagnetism and gravity for example, the mechanics of waves as described by wave-type equations is a central theme (e.g. Schrödinger's equation in quantum mechanics, the wave equation for electromagnetic fields obtained by decoupling Maxwell's equations and the gravity wave equation obtained by decoupling Einstein's equations for a gravitational field). In this sense, physics is the study of 'waves within waves'.

18.2 Geometry and Dimension

Dimension is a concept and not necessarily a reality. We are all used to the concept of one-, two- and three-dimensions together with the fourth-dimension, time t, our four dimensional world being inter-related through Einstein's theory of relativity in which the speed of light c_0, which defines a length $c_0 t$, is taken to be a universal constant. Higher or hyper dimensions, i.e. 5, 6, 7, ... dimensions, are abstractions but are nevertheless of fundamental significance in modern theoretical physics. However, coming to terms with dimension in terms of 'imaging' has taken 'time'. For example, pre-Renaissance painting often exhibits a two-dimensional 'flatness' with distortions in perspective. During the Renaissance, new methods were developed to include perspective in paintings that 'reflected' the reality of imaging a three-dimensional world. Cubist art of the early Twentieth Century was an attempt to express four dimensions (or else an attempt to overcome a severe lack of talent!) - see Figure 18.6. Coming to terms with dimension has not only taken its time from the point of the evolution of art and the society which it reflects but is one of the most important aspects of our intellectual development, a point that is developed in the following (taken from Porter E and Gleik J, *Nature's Chaos*, Scribner, 1990):

'*When a child draws a tree, a green mass sits on top of a brown trunk, as if the basic shape were a Popsicle. A child's cloud is a smoothly rounded bulk, perhaps with a wavy or scalloped edge. These are not the clouds we see. They are lightly stylized forms, like the international symbols for Railrood Crossings or No Smoking. As children or adults we own a repertoire of such stylized images, like ideograms in Chinese painting. First they help us to see - for without such templates, our minds are powerless to shift the welter of sensations that bombard our eyes and ears. But they hinder our seeing too. The rivers, the clouds, the snowflakes of our perpetual toolkits miss much of nature's true complexity - the intricate recursion, the convoluted flows within flows within flows. Our mental lightning bolts are z's, our volcanoes are inverted and decapitated cones, our rivers are lines. Nature's are not so simple*'.

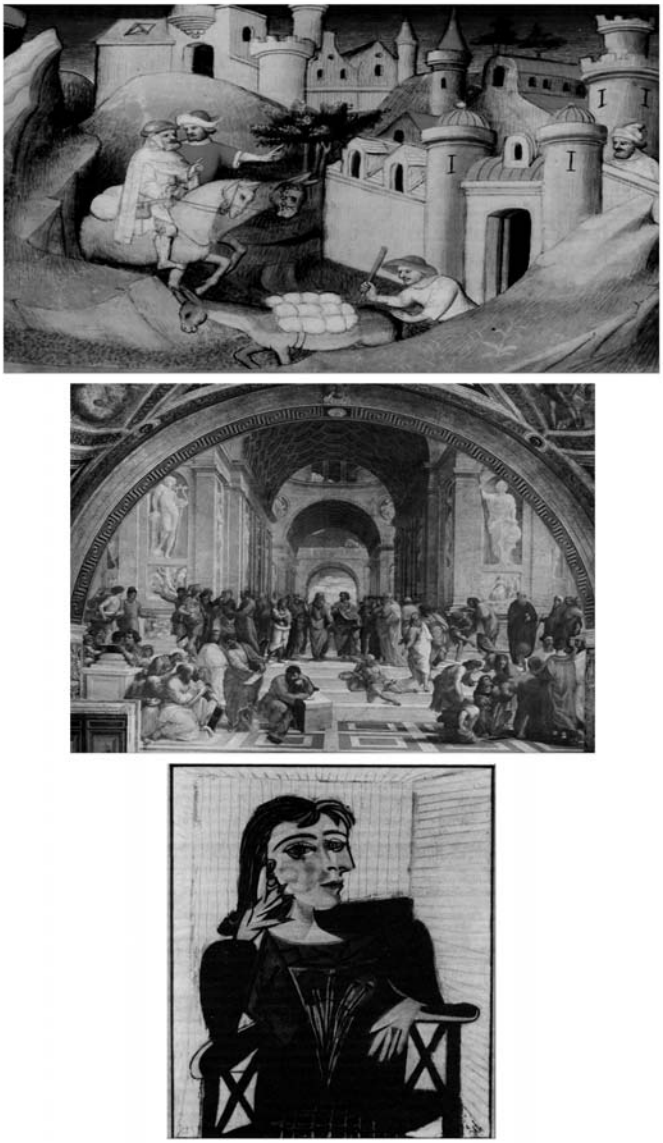

Figure 18.6: Examples of medieval art (top) high Renaissance art (centre) and Cubism (bottom).

Just as it takes some imagination and practice to 'think' in terms of multiple integer or topological dimensions, so it requires some further imagination to extend or generalize the idea of an integer dimension to a fractional dimension. After all, it took some 5000 years to generalize the concept of a whole number to a decimal number. (The Islamic world brought the decimal number system from India - where the concept of zero was first invented - in about 750 AD but it did not take hold in Europe for another 500 years after that.) Thus, the concept of a fractional or fractal dimension requires an appropriate introduction.

Suppose we cut up some simple 1D, 2D and 3D Euclidean objects (a line, a square surface and a cube, for example), make exact copies of them and then keep on repeating the copying process. Let N be the number of copies that we make at each stage and let r be the length of each of the copies, i.e. the scaling ratio. Then we have

$$Nr^D = 1, \quad D = 1, 2, 3, ...$$

The similarity or fractal dimension is that value of D which is usually (but not always) a non-integer dimension 'greater' that its topological dimension (i.e. 0,1,2,3,... where 0 is the dimension of a point on a line) and is given by

$$D = -\frac{\log(N)}{\log(r)}.$$

To illustrate this principle, let us consider the following examples.

Example 1: Cutting and copying lines with deletion

Suppose we cut up a line into lines of equal length, throw away one or more of the lines (deletion) and then keep on repeating or 'iterating' the process. At each iteration, $Nr^D = 1$ where $0 < D < 1$. For example, suppose we cut a line into three lines of equal length, delete one of the lines and continually repeat the process. At each stage of this process $N = 2$ and $r = 1/3$ and $D = -\log(2)/\log(1/3) = \log(2)/\log(3) = 0.6309297536....$ Suppose that we cut the line into four lines of equal length, delete two of them and repeat the process iteratively; then, $N = 2$, $r = 1/4$ and $D = \log(2)/\log(4) = 0.5$. The sets obtained at each stage of the process are examples of Cantor sets or fractal dust.

Example 2: Cutting and copy lines with addition

Suppose we cut up a line (an 'initiator') into smaller lines of equal length, add one (a 'generator') or a number of the lines (addition) and iterate. In this case, $Nr^D = 1$ where $1 < D < 2$. This process produces fractal curves of which there are many types. Suppose we iterate in such way that $N = 4$ and $r = 1/3$, as shown in Figure 18.7, which is an illustration of a curve known as the triadic von Koch curve. The fractal dimension of this curve is $D = \log(4)/\log(3) = 1.261859507....$ For the case when $N = 8$ and $r = 1/4$, we obtain the quadratic von Koch curve whose fractal dimension is $D = \log(8)/\log(4) = 1.5$ and that is also shown in Figure 18.7.

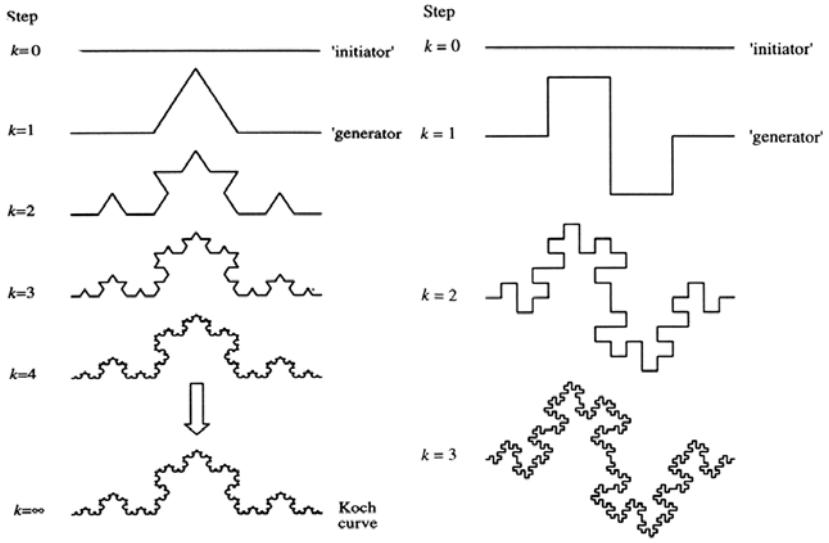

Figure 18.7: The triadic (left) and quadratic (right) von Koch curves.

Example 3: Cutting and copying surfaces with deletion

The previous example provided an illustration of some well known fractals with a fractal dimension $D \in (1, 2)$ based on cutting and copying lines with addition. However, fractals of this type can be generated by cutting and copying surfaces with deletion. Referring to Figure 18.8, this approach provides fractals with higher fractal dimensions such as the 'Sierpinski triangle', where $N = 3, r = 1/2$ at each step and $D = \log(3)/\log(2) = 1.584962501...$, and the 'Sierpinski carpet' where $N = 8, r = 1/3$ at each step and $D = \log(8)/\log(3) = 1.892789261...$ Observe in Figure 18.8 that the 'texture' of the Sierpinski carpet is greater than that of the Sierpinski triangle, a result that is reflected in the increased value of the fractal dimension D.

Example 4: Cutting and copying volumes with deletion

Just as fractal curves can be generated by either cutting and copying surfaces with deletion or cutting and copying lines with addition, so the same principle applies to generating fractal surfaces. As an example, and referring to Figure 18.9, suppose we cut up a cube into a set of cubes of equal length, delete one (or a number) and then keep on repeating the process. Then $Nr^D = 1$ where $2 < D < 3$. In Figure 18.9, $N = 20$, $r = 1/3$ and $D = \log(20)/\log(3) = 2.726833028....$ This produces a fractal surface known as a Menger sponge;

this is an object which, as $k \to \infty$, acquires an infinite surface area and zero volume. The Menger sponge after four iterations is shown in Figure 18.10.

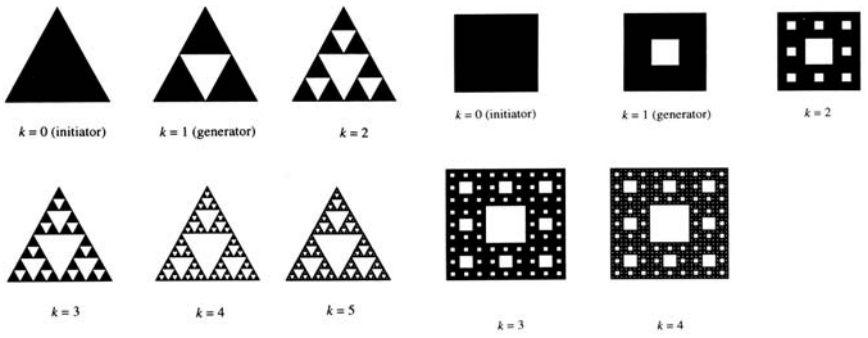

Figure 18.8: The Sierpinski triangle (left) and carpet (right).

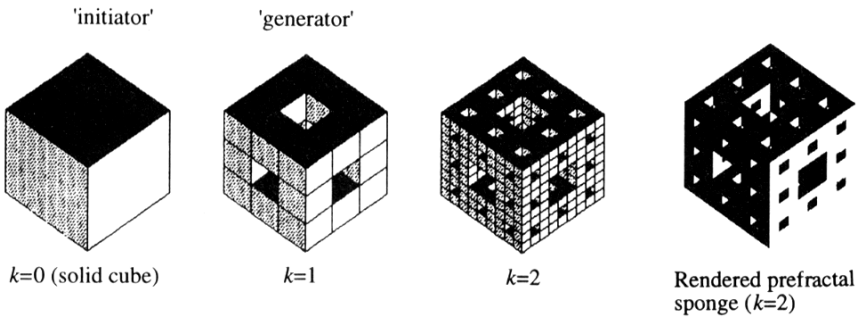

Figure 18.9: Generation of the Menger Sponge.

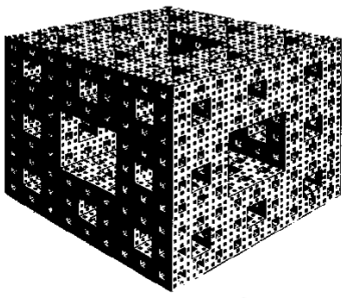

Figure 18.10: The Menger Sponge after four iterations.

18.3 Fractal Curves and Fractal Signals

The examples given in the previous Section are those for generating fractal dusts, curves and surfaces which can be undertaken by a process of deletion or addition. The principles given are general and provide the basis for generating an unlimited variety of fractals. However, we can theoretically extend the idea to include fractal volumes and fractal time where, in each case, the fractal dimension is greater than the topological dimension as given in the following table.

Fractal type	Fractal Dimension
Fractal Dust	$0 < D < 1$
Fractal Curve	$1 < D < 2$
Fractal Surface	$2 < D < 3$
Fractal Volume	$3 < D < 4$
Fractal Time	$4 < D < 5$
Hyper-fractals	$5 < D < 6$
$\vdots$	$\vdots$

In each case, as the value of the fractal dimension increases, the fractal becomes increasingly 'space-filling' in terms of the topological dimension which the fractal dimension is approaching. In each case, the fractal exhibits structures that are self-similar. A self-similar deterministic fractal is one where a change in the scale of a function $f(x)$ by a factor of a produces a smaller version, reduced in size by a, i.e.

$$f(ax) = af(x).$$

A self-affine deterministic fractal is one where a change in the scale of a function $f(x)$ by a factor a produces a smaller version reduced in size by a factor a^q, $q > 0$, i.e.

$$f(ax) = a^q f(x).$$

However, the regular fractal curves of the type discussed in the previous Section are not functions of the type $f(x)$. So how are they related to $f(x)$? The answer is through parametrization. Since the computation of a regular fractal curve, for example, is a discrete process, it can be taken to be given by a set of discrete point x_i, y_i in the xy-plane. Here, both x_i and y_i can be treated as independent digital signals. For a continuous fractal curve, these signals will be given by $x(t)$ and $y(t)$ and the fractal curve composed of an infinite set of coordinate points $[x(t), y(t)]$. Given these data and any point of origin in the plane, we can compute unique amplitude $A(t)$ and phase $\theta(t)$ signals given by

$$A(t) = \sqrt{x^2(t) + y^2(t)} \quad \text{and} \quad \theta(t) = \tan^{-1}\left[\frac{y(t)}{x(y)}\right].$$

The amplitude A for any value of t is the chord length from the origin to a point on the fractal curve. This signal will have properties that reflect the characteristics of the fractal curve, the most fundamental of which is a $1/k^q$

spectral power law as illustrated in Figure 18.11 for a Euclidean curve (a circle) and a hypothetical fractal curve enclosing the origin.

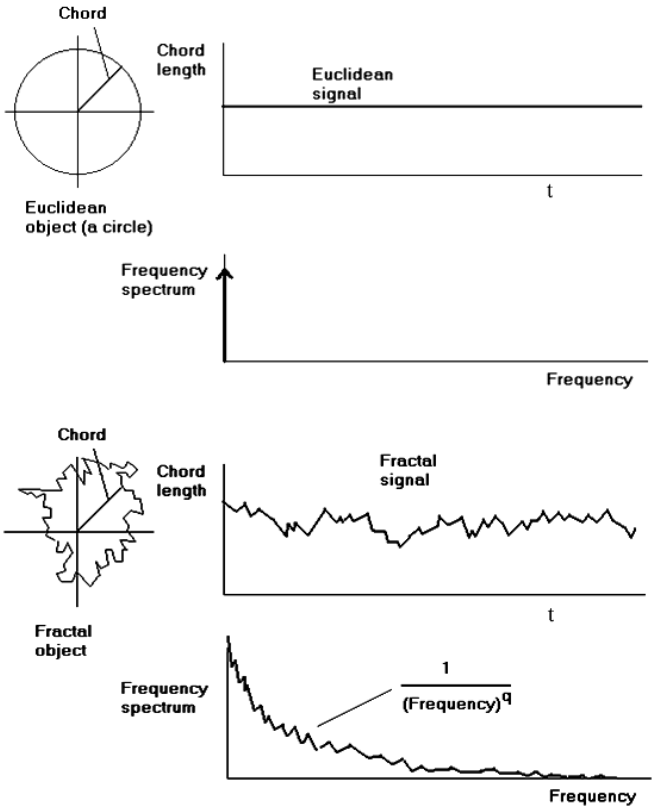

Figure 18.11: Chord length parametrization of a circle and its spectrum (top) and a chord length parametrization of a fractal curve and its spectrum (bottom).

If the spectrum $F(k)$ of a fractal $f(x)$ is proportional to k^{-q}, its Power Spectral Density Function (PSDF) will be given by

$$P(k) =\mid F(k) \mid^2 = \frac{c}{k^\beta}$$

where c is a constant and $\beta = 2q$. Taking logarithms, we obtain

$$\log(P) = C - \beta \log(k), \quad C = \log(C).$$

A plot of $\log(P)$ against $\log(k)$ will therefore produce a line with a gradient of $-\beta$. Consider the example fractals given in Figure 18.12 and Figure 18.13

for the 'Dragon curve' ($D = 1.3652...$) after 3 iterations and for the 'Peano curve' ($D = 1.8888...$) after 4 iterations, respectively. In each case, the discrete chord length signal $A_i = \sqrt{x_i^2 + y_i^2}$ is shown together with a bi-logarithmic plot (using natural logarithms - LN) of its power spectrum as a function of frequency. The broken line running through these bi-logarithmic spectra is a least squares fit to the data obtained by computing C and β using the least squares method in which the error function

$$e(C, \beta) = \sum_{i=1}^{N} (\ln P_i - \ln \hat{P}_i)^2 = \sum_{i=1}^{N} [\ln P_i - (C - \beta \ln k_i)]^2; \quad P_i > 0, \quad k_i > 0, \quad \forall i$$

is a minimum and where $P_i, \quad i = 1, 2, ..., N$ is the positive half-space data (excluding the DC), the solutions for q and C, respectively, being given by

$$\beta = \frac{N \sum_{i=1}^{N} (\ln P_i)(\ln k_i) - \left(\sum_{i=1}^{N} \ln k_i \right) \left(\sum_{i=1}^{N} \ln P_i \right)}{\left(\sum_{i=1}^{N} \ln k_i \right)^2 - N \sum_{i=1}^{N} (\ln k_i)^2}$$

and

$$C = \frac{1}{N} \sum_{i=1}^{N} \ln P_i + \frac{\beta}{N} \sum_{i=1}^{N} \ln k_i.$$

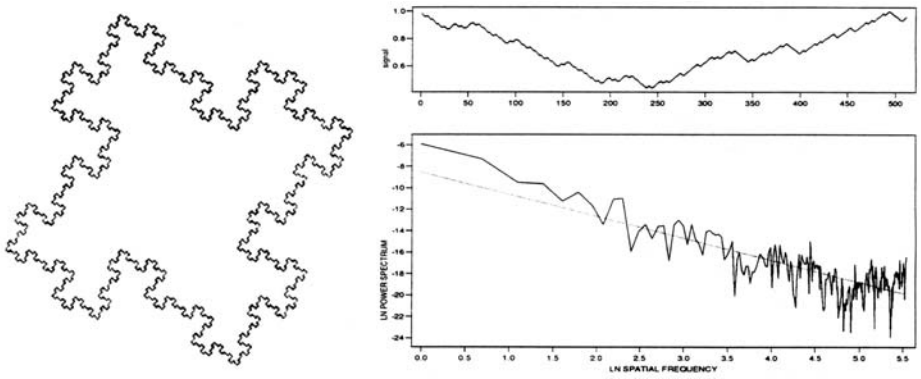

Figure 18.12: The 'Dragon curve' (left), the discrete chord length signal (top-right) and its bi-logarithmic PSDF showing a least squares fit to the data (bottom-right).

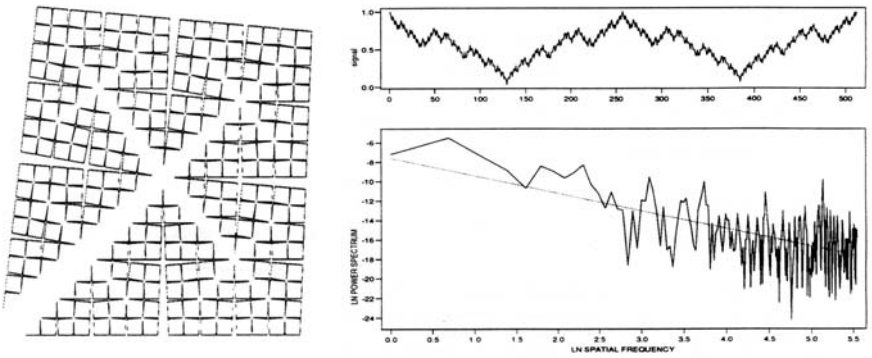

Figure 18.13: The 'Peano curve' (left), the discrete chord length signal (top-right) with its bi-logarithmic PSDF showing a least squares fit to the data (bottom-right).

Compared to the parametrization of a circle, for example, which is a smooth line with a dimension of 1, fractal curves have significantly more structure which is reflected in their frequency content. The spectrum of the chord length signal for the circle is composed of a DC component whose value is determined by the radius of the circle. The spectrum of the chord length of a fractal curve has components which decrease in amplitude as the frequency increases. This reflects the finer structure that exists over smaller scales. So what is the connection between a signal with a PSDF of the form

$$P(k) =\mid F(k) \mid^2 = \frac{c}{k^\beta}$$

and the equation for a self-affine curve, i.e.

$$f(ax) = a^q f(x)?$$

The connection comes from considering the spectrum of $f(x)$ to be a filtered version of a uniform or 'white' spectrum $N(k)$, so that

$$F(k) = \frac{N(k)}{(ik)^q}.$$

Now using the convolution theorem

$$f(x) = h(x) \otimes n(x) = \int_{-\infty}^{\infty} h(x-y)n(y)dy$$

where (see Appendix C)

$$h(x) = \frac{1}{2\pi}\int_{-\infty}^{\infty} \frac{1}{(ik)^q}\exp(ikx)dk = \frac{\alpha_1(q)}{x^{1-q}}, \quad \alpha_1(q) = \frac{1}{(2i)^q\sqrt{\pi}}\frac{\Gamma\left(\frac{1-q}{2}\right)}{\Gamma\left(\frac{q}{2}\right)}.$$

But, if $N(k)$ is a uniform spectrum, then

$$N(k) = \frac{1}{a} N\left(\frac{k}{a}\right)$$

or

$$n(x) = n(ax).$$

Hence,

$$f(x) = \alpha_1(q) \int_{-\infty}^{\infty} \frac{n(ay)}{(x-y)^{1-q}} dy = \frac{\alpha_1(q)}{a^q} \int_{-\infty}^{\infty} \frac{n(z)}{(ax-z)^{1-q}} dz = \frac{1}{a^q} f(ax)$$

or

$$a^q f(x) = f(ax).$$

The key point here is to note that

$$a^q f(x) = f(ax) \implies \mid F(k) \mid^2 \quad \text{scales as} \quad \frac{1}{\mid k \mid^{2q}}$$

where we defined q to be the 'Fourier dimension'. Further, if we define a fractional derivative using a generalization of the result

$$\frac{d^n}{dx^n} f(x) \Longleftrightarrow (ik)^n F(k), \quad n = 1, 2, 3$$

to

$$\frac{d^q}{dx^q} f(x) \Longleftrightarrow (ik)^q F(k), \quad q > 0$$

then we can define a (parametrized) fractal curve in terms of the solution to the fractional differential equation

$$\frac{d^q}{dx^q} f(x) = n(x).$$

18.4 Random Scaling Fractals and Texture

Texture is a word that is commonly used in a variety of contexts but is at best a qualitative description of a sensation. Visual texture can be associated with a wide range of signals and images, but the term cannot be taken to quantify any particular characteristic. How then can we quantify texture mathematically - is there a specific and unique definition for texture? To begin with, we can state that textural information is not well defined in terms of Euclidean geometry. Most objects can be divided into regions containing either: (i) deterministic information (where Euclidean geometry is usually applicable); (ii) textural information (which is not easily described by Euclidean geometry).

Whether a fractal is deterministic or random, its spectral characteristics obey the same basic scaling law. Figure 18.14 shows a randomized version of the triadic von Koch curve, for example, obtained by randomly changing the orientation of the 'amplitude' at each iteration. Although this randomized curve looks different from the regular curve given in Figure 18.7, its fractal and Fourier dimensions are the same.

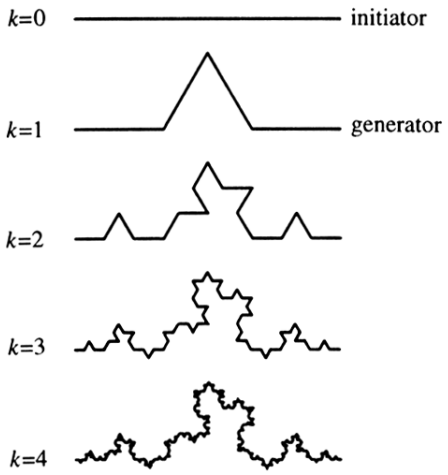

Figure 18.14: Randomization of the triadic von Koch curve.

The inverse-q power law is found throughout nature. It is a scaling law that is as universal as the inverse square law is in describing gravitational (Newton's law) and electric (Coulomb's law) fields. However, very few natural shapes are regular fractals, the majority are statistically self-affine, i.e. random scaling fractal curves or surfaces where, as we zoom into the fractal, the shape changes, but the distribution of lengths remains the same, i.e.

$$\Pr[f(ax)] = a^q \Pr[f(x)]$$

where Pr denotes the Probability Distribution Function or PDF. The value of q associated with this result provides a way of measuring the texture of an image. Typically one or more 'measures' for texture can be defined and a moving window applied to the data. For each window position, each of the texture measures is computed. If only one measure is defined then one 'measure image' is produced. If more than one measure is defined, then some sort of clustering algorithm (which converts a multiple numeric field into a single field) is needed to reduce the several measure images into one final image. In addition, scaling can be applied, whereby the window size is gradually decreased, giving rise to yet more measure-images at different scales.

Natural vision systems appear to be good at segmenting texture, i.e. at recognizing similarity between sub-patterns in an image. Texture gradients are important cues to 3D shape in the visual sense, and the role of texture may be primarily to help locate objects in visual space by analysis of texture gradients. When examining textures, we tend to look for deviations from uniform texture with a view to 'labelling' objects with a common textural property.

Finding suitable definitions for the texture of an image is important for developing an automatic means of extracting textural features that agrees with

human sensory perception. There are six measures of texture that are of value for classifying a given texture.

Coarseness: coarse versus fine. Coarseness is the most fundamental textural feature. In a narrow sense, coarseness is synonymous with texture. When two patterns differ only in scale, the magnified one is coarser. For patterns with different structures, the bigger its element size, and/or the less its elements are repeated, the coarser it is felt to be.

Coarseness is a measure of scale in microtexture within an image. A simple procedure that detects the largest size at which repetitive patterns are present is as follows:

- Take averages at every point in a digital image f_{ij} at different scales, k, which are a power of 2. This defines the arrays

$$A_k(x,y) = \sum_{i=x-2^{k-1}}^{x+2^{k-1}-1} \sum_{j=y-2^{k-1}}^{y+2^{k-1}-1} f_{ij}/2^{2k}.$$

- Calculate the differences between neighbouring averages which are non-overlapping. This is calculated in both horizontal h and vertical v directions,

$$E_{h,k}(x,y) = |A_k(x-2^{k-1},y) - A_k(x+2^{k-1},y)|,$$
$$E_{v,k}(x,y) = |A_k(x,y-2^{k-1}) - A_k(x,y+2^{k-1})|.$$

- Pick the largest size which gives the maximum value,

$$S(x,y) = 2^n, \text{ where } E_n = \max\{E_{h,1}, E_{v,1}, E_{h,2}, E_{v,2}, \ldots\}.$$

- Finally, take an average as the coarseness measure, $F_{crs} = \langle S(x,y)\rangle$.

Contrast: high contrast versus low contrast. The simplest method of varying signal or image contrast is by stretching or shrinking its amplitude or grey scale respectively. By changing the contrast of an image, we alter the image quality, not the image structure. When two patterns differ only in grey-level distribution, the difference in their contrast can be measured. However, more factors are supposed to influence the contrast difference between two texture patterns with different structures. The following factors are considered for a definition of contrast: (i) dynamic range; (ii) polarization of the distribution of dark-field and bright-field regions in the grey-level histogram or ratio of dark and bright areas; (iii) sharpness of edges (images with sharp edges have higher contrast); (iv) period of repeating patterns.

Two of the four factors discussed above have a major influence on the contrast within an image.

1. Dynamic range of grey levels, specified most commonly as the standard deviation σ.

2. Polarization of the distribution the grey level histogram (i.e. a bias toward the dark and bright field). The kurtosis, $\alpha_4 = \mu^4/\sigma^2$, is used where μ^4 is the fourth moment about the mean and σ^2 is the variance (see Chapter 17 - *Statistical Moments*).

Combining these two factors, we have a measure for contrast given by $F_{con} = \sigma/(\alpha_4)^n$.

Directionality: directional versus non-directional. This is a global property over a region. Directionality involves both element shape and placement rule. It can be divided into two groups, mono-directional and bi-directional. If only the total degree of directionality is considered then orientation of the texture pattern does not matter, i.e. patterns which differ only in orientation should have the same degree of directionality.

The values defined for the gradient angle $\theta(G)$ (see Chapter 16) can be quantized into a histogram, H. The position and number of peaks can be used to extract the type of directionality. To quantify this feature, the sharpness, or variance, of n_p peaks, positioned at angles θ_p can be calculated. By defining w_p as the range of angles between two valleys, we have, without normalization,

$$F_{\text{dir}} = n_p \sum_{1=p}^{n_p} \sum_{\theta \in w_p} (\theta - \theta_p)^2 H_d(\theta).$$

Line-likeness: line-like versus blob-like. This concept is concerned with the shape of a texture element. It is expected that this feature supplements the major ones previously mentioned, especially when two patterns cannot be distinguished by directionality.

Having calculated G and $\theta(G)$ for all locations, a definition of line-likeness considers how probable the direction, at a specific point, is similar to one at a certain distance away. A matrix, $P_d(i,j)$, is defined as the relative frequency with which two points on an edge, separated by a distance d, have direction codes i and j. A measure of line-likeness follows from

$$F_{\text{lin}} = \frac{\sum_{i=1}^{n} \sum_{j=1}^{n} P_d(i,j) \cos[(i-j)2\pi/n]}{\sum_{i=1}^{n} \sum_{j=1}^{n} P_d(i,j)}.$$

Regularity: regular versus irregular. This is a property concerning variations in the placement of pixel clusters. However, it can be supposed that variations of elements, especially in the case of natural textures, reduces the regularity on the whole. Additionally, a fine structure tends to be perceived as regular.

Four different features have been described so far, and regularity can be thought of as how much these features change over an image. The standard deviation σ of these four features can be used, so that

$$F_{\text{reg}} = 1 - (\sigma_{\text{crs}} + \sigma_{\text{con}} + \sigma_{\text{dir}} + \sigma_{\text{lin}}).$$

Roughness: rough versus smooth. This description was originally intended for tactile textures, not for visual textures. However, when we observe natural textures, we are usually able to compare them in terms of rough or smooth. It is debatable as to whether this subjective judgment is due to the total energy of changes in grey-level or due to our imaginary tactile sense.

The value of using fractal geometry for image analysis lies in its potential to classify an image into different regions of texture by using for example the fractal dimension or the Fourier dimension as a measure for texture. Take, for example, the images given in Figure 18.15 which shows sections of the histology of a patient with normal skin and a patient with chronic dermatitis. There is a significant difference in the texture between the two images; in such cases, the Fourier dimension can be used as a measure of this difference assuming that the Fourier dimension is constant over the entire image, i.e. that the image is both fractal and stationary.

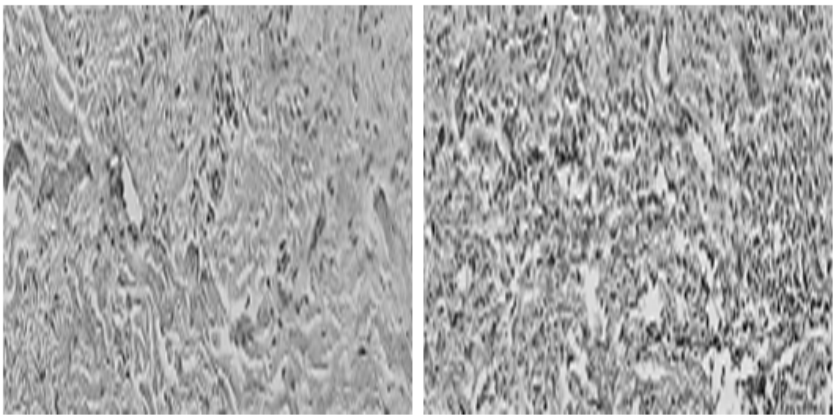

Figure 18.15: Histology of normal skin (left) and chronic dermatitis (right).

Naturally occurring fractals differ from the strictly mathematically defined fractals in that they do not display statistical or exact self-similarity over all scales. Rather, they display fractal properties over a limited range of scales. Given that natural surfaces can be approximated as fractals over a range of scales, it is necessary to examine how the imaging process maps fractal surfaces

into grey-level surfaces. The image of a fractal surface is itself a fractal surface under the following conditions: (i) the surface is Lambertian; (ii) the surface is illuminated by (possibly several) distant point sources; (iii) the surface is not self-shadowing. Under these conditions, we can use a range of 'fractal parameters' to segment images through the computation of fractal dimensions which give a measure of the 'roughness', or texture. For example, a high value fractal dimension indicates a rough image or surface whereas a low value indicates a smooth image or surface. Several methods have been developed to calculate the fractal dimension of signals and images which are discussed in the following Section.

18.5 Methods of Computing the Fractal Dimension

As with many other techniques of digital signal and image processing, the computation of the fractal dimension can be undertaken in 'real space' (processing the data directly) or in 'transform space' (processing the data after taking an appropriate integral transform). In the latter case, use can be made of the Fourier transform, as the Power Spectral Density Function (PSDF) of a fractal image has the expected inverse q-power scaling law.

In general, there is no unique and general rule for computing the fractal dimension. A number of algorithms exist to compute the fractal dimension which can be broadly categorized into two families: (i) size-measure relationships, based on recursive length or area measurements of a curve or surface using different measuring scales; (ii) application of relationships based on approximating or fitting a curve or surface to a known fractal function or statistical property, such as the variance.

By way of a brief introduction to the methods associated with (i) above, consider a simple Euclidean straight line ℓ of length $L(\ell)$ over which we 'walk' a shorter 'ruler' of length δ. The number of steps taken to cover the line $N[L(\ell), \delta]$ is then L/δ which is not always an integer for arbitrary L and δ. Since

$$N[L(\ell), \delta] = \frac{L(\ell)}{\delta} = L(\ell)\delta^{-1}$$

$$\Rightarrow 1 = \frac{\ln L(\ell) - \ln N[L(\ell), \delta]}{\ln \delta} = -\left(\frac{\ln N[L(\ell), \delta] - \ln L(\ell)}{\ln \delta}\right)$$

which expresses the topological dimension $D_T = 1$ of the line. In this case, $L(\ell)$ is the Lebesgue measure of the line and if we normalize by setting $L(\ell) = 1$, the latter equation can then be written as

$$1 = -\lim_{\delta \to 0}\left[\frac{\ln N(\delta)}{\ln \delta}\right]$$

since there is less error in counting $N(\delta)$ as δ becomes smaller. We also then have $N(\delta) = \delta^{-1}$. For extension to a fractal curve f, the essential point is that the fractal dimension should satisfy an equation of the form

$$N[F(f), \delta] = F(f)\delta^{-D}$$

where $N[F(f), \delta]$ is 'read' as the number of rulers of size δ needed to cover a fractal set f whose measure is $F(f)$ which can be any valid suitable measure of the curve. Again we may normalize, which amounts to defining a new measure F' as some constant multiplied by the old measure to get

$$D = -\lim_{\delta \to 0} \left[\frac{\ln N(\delta)}{\ln \delta} \right]$$

where $N(\delta)$ is taken to be $N[F'(f), \delta]$ for notational convenience. In practice, if we are dealing with a digital signal (a sampled curve) rather than an abstract continuous curve, which has precise fractal properties over all scales, then

$$D = -\left\langle \frac{\ln N(\delta)}{\ln \delta} \right\rangle \tag{18.1}$$

where we choose values δ_1 and δ_2 (i.e. the upper and lower bounds) satisfying $\delta_1 < \delta < \delta_2$ over which we do some sort of averaging processes denoted by $\langle \ \ \rangle$. The most common approach is to look at the bi-logarithmic plot of $\ln N(\delta)$ against $\ln \delta$, choose values δ_1 and δ_2 over which the plot appears to be straight and then apply a least squares fit to the straight line within these limits.

18.5.1 The Least Squares Approximation

All algorithms discussed in this section use a least squares approach to computing the fractal or Fourier dimension. It is therefore worth briefly reviewing this technique. Let $f_i, \quad i = 1, 2, ..., N$ be a real digital function consisting on N elements and let $\hat{f}_i$ be an approximation to this function. We assume that $\hat{f}_i$ is the expected form of the data f_i. The least squares error e is then defined as

$$e = \sum_{i=1}^{N} (f_i - \hat{f}_i)^2.$$

In most cases, algorithms for computing the fractal dimension use logarithmic or semi-logarithmic plots to fit the results of a given algorithm to a line. In these cases, we are interested in finding the slope m and in certain cases the constant c of the line

$$\hat{f}_i = mx_i + c.$$

To find the best fit, we are required to minimize the error e which is taken to be a function of m and c. This is achieved by finding the solutions to the equations

$$\frac{\partial e}{\partial m} = 0 \quad \text{and} \quad \frac{\partial e}{\partial c} = 0.$$

Differentiating with respect to m and c gives

$$\sum_{i=1}^{N} x_i (f_i - mx_i - c) = 0$$

and

$$\sum_{i=1}^{N}(f_i - mx_i - c) = 0.$$

Solving for m and c we obtain

$$m = \frac{N\sum_{i=1}^{N} f_i x_i - \left(\sum_{i=1}^{N} f_i\right)\left(\sum_{i=1}^{N} x_i\right)}{N\sum_{i=1}^{N} x_i^2 - \left(\sum_{i=1}^{N} x_i\right)^2}$$

and

$$c = \frac{\sum_{i=1}^{N} f_i - m\sum_{i=1}^{N} x_i}{N}.$$

This approach can also be used when the data is two-dimensional (a digital image or grey level surface) where we are required to approximate the data f_{ij} by a function

$$\hat{f}_{ij} = mx_{ij} + c.$$

The result (i.e. the expressions for m and c) is the same as above except that the summation is over i and j. In the following Sections, algorithms for computing the data used to calculate the fractal dimension with the least squares method are discussed. Some of these algorithms are based on the following relationship

$$Length = c(Step)^m$$

which can be linearized thus

$$\ln(Length) = \ln(c) + m\ln(Step).$$

Here, length represents the measurement of the curve or surface using a 'ruler' of size $Step$ and m is the slope of the log-log plot which has a simple algebraic relationship with the fractal dimension D, depending on the algorithm used.

18.5.2 The Walking-Divider Method

This method uses a chord length ($Step$) and measures the number of chord lengths ($Length$) needed to cover a fractal curve. The technique is based on the principle of taking smaller and smaller rulers of size ($Step$) to cover the curve and counting the number of rulers ($Length$) required in each case. This approach is based on a direct interpretation of equation (18.1) where $N(\delta) \equiv Length$ and $\delta \equiv Step$ are estimated in a systematic fashion. It is a recursive process in which the $Step$ is decreased (typically halved) and the new $Length$ calculated. Here, the input signals are taken to be of size N, where N is a power of 2 because of the recursive nature of the method. A least squares fit to the bi-logarithmic plot of $Length$ against $Step$ gives m, where $D = -m$. This part of the calculation essentially provides an estimate of the average gradient in equation (18.1) as illustrated in Figure 18.16.

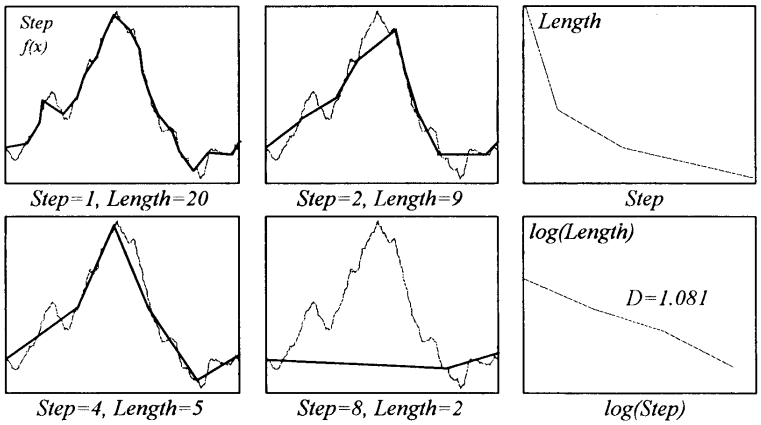

Figure 18.16: Illustration of the walking-divider method for computing the fractal dimension D of a signal showing four iterations and the least squares fit.

The walking-divider method suffers from a number of problems. First of all, the initial *Step* must be carefully chosen. An appropriate starting value is half of the average distance between the points. Clearly, the computation of the initial value, and the procedure required to count the number of *Steps*, makes this algorithm time consuming.

18.5.3 The Box Counting Method

Box counting involves covering a fractal with a grid of n-dimensional boxes or hyper-cubes with side length δ and counting the number of non-empty boxes $N(\delta)$. For signals, the grid is one of squares and, for images, a grid of cubes. Boxes of recursively different sizes are used to cover the fractal. Here again, an input signal with N elements or an image of size $N \times N$ is used as input, where N is a power of 2. The slope m obtained in a bi-logarithmic plot of the number of boxes used against their size then gives the fractal dimension (also known as the Box or Minkowski dimension) where $D = -m$. The principle is illustrated in Figure 18.17.

Successive divisions by a factor of two are used for the box $Size$ to give a regular spacing in the bi-logarithmic plot and least squares fit. In practice, a regular grid is usually applied (see Figure 18.18) to the data and the non-empty boxes counted.

The behaviour of this algorithm is such that the greater the number of points used for the least squares fit, the better the estimate of the fractal dimension. The optimum number of boxes for a given size required to compute an accurate fractal dimension can be obtained by mapping the entire image with boxes (cubes) and then identifying the lower box and higher box covering the surface.

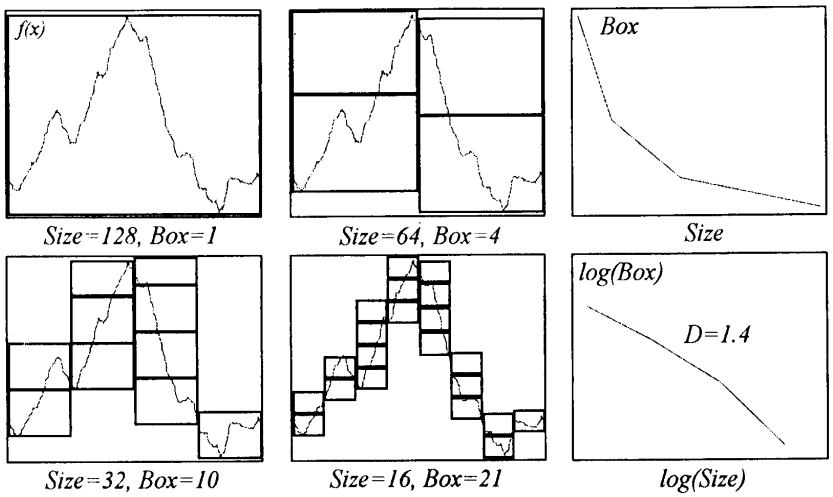

Figure 18.17: Illustration of the box counting method for computing the fractal dimension D of a signal showing 4 iterations and the least squares fit.

In general, box counting algorithms behave well and produce accurate estimates for fractal dimensions between 1 and 1.5 for digital signals and between 2 and 2.5 for digital images; they are easy to code and fast to compute. Outside this range (i.e. for higher fractal dimensions), they tend to give less accurate results, underestimating in most cases and saturating near 0.6 above the topological dimension.

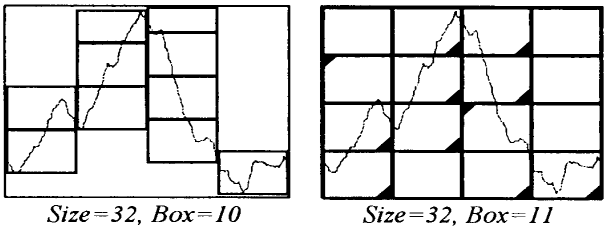

Figure 18.18: Illustration of irregular and regular grids used for the box counting algorithm.

For a smooth one-dimensional curve of unit length, we expect that

$$N(\delta) = \frac{1}{\delta}, \quad \delta \to 0.$$

The box counting measure is a generalization of this measure to

$$N(\delta) = \frac{1}{\delta^D}, \quad \delta \to 0$$

or, taking logarithms,

$$D = -\frac{\ln N(\delta)}{\ln \delta}.$$

18.5.4 The Prism Method

The prism method is based on the idea of box counting in which, instead of counting the number of boxes in a region for a given size, the area based on four triangles defined by the corner points is computed and summed over a grey level surface. The triangles define a prism based on the elevated corners and a central point computed in terms of the average of the four corners. A bi-logarithmic plot of the sum of the prisms' areas for a given base area gives a fit to a line whose slope is m in which $D = 2 - m$ The basic computational engine for this algorithm is similar to that for the box counting method, but is slower due to the number of multiplications implied by the calculation of the areas.

18.5.5 Hybrid Methods

Hybrid methods calculate the fractal dimension of 2D surfaces using 1D methods. This approach is based on the relationship between the fractal dimensions of a surface's contours (1D fractal curves), for example, and the fractal dimension of the surface itself, namely

$$D_2 = 1 + D_1$$

where D_1 is the average of the fractal dimensions of each contour line and D_2 is the fractal dimension of the surface. In principle, this result holds for any algorithm used to compute D_1.

Contour Lines Method

This algorithm is based on extracting the contour lines at a particular elevation in a grey-level surface, computing their fractal dimensions $D_{(1,n)}$ using the walking-divider method, for example, and then finding the general 2D fractal dimension D via the formula

$$D = 1 + \frac{1}{N} \sum_{n=1}^{N} D_{1n}.$$

The results are generally close to those computed using the box counting method for fractal dimensions between 2.1 and 2.4.

Vertical Slice Averaging

This approach considers the fractal dimension of the surface to be the normal average of all the vertical slices in the x- and y-directions plus 1. To add flexibility, this technique can be implemented with the possibility of computing either or both directions (rows and/or columns) and to consider only a limited number of slices. Another choice can be made with regard to the 1D algorithm used to compute the fractal dimensions.

Robust Fractal Estimator

This method improves the accuracy of computing the fractal dimension of a surface by computing the fractal dimension of the vertical slices in the x- and y-directions plus 1, and generating a new map of the fractal dimensions created where each point is defined by the average fractal dimensions of the two profiles intersecting at that position. The average value of the map is then taken to be the fractal dimension of the surface.

Perimeter-Area Relationship

For non-fractal closed curves in the plane, the perimeter ℓ is related to the enclosed area A by

$$\ell = c\sqrt{A}$$

where c is a constant for a given type of shape (e.g. for squares $c = 1$ and for circles $c = 2\sqrt{\pi}$). We can generalize this equation for the case of closed fractal curves to give

$$\ell = c\left(\sqrt{A}\right)^D, \quad 1 < D < 2.$$

This generalized perimeter-area relationship can be used to classify different objects in an image that are characterized by a closed contour.

18.5.6 Power Spectrum Method

The power spectrum method is based on the expected form of the PSDF of a fractal which is given by

$$\hat{P}_i = \frac{c}{k_i^\beta}$$

where c is a constant, $k_i \equiv \mid k_i \mid$ and $\beta = 2q$. Let $P_i, \quad i = 1, 2, 3, ..., N$ be the data obtained by taking the discrete Fourier transform of a digital fractal signal f_i and retaining the positive half space data (because the power spectrum is symmetric) excluding the DC value (because at $k_0 = 0$ a singularity occurs) and assume that $P_i > 0 \forall i$. We can then construct the error function

$$e(\beta, C) = \sum_{i=1}^{N} (\ln P_i - \ln \hat{P}_i) = \sum_i [\ln P_i - (C - \beta \ln k_i)]^2$$

where $C = \ln c$. The error function is a minimum when

$$\frac{\partial e}{\partial \beta} = 0 \quad \text{and} \quad \frac{\partial e}{\partial C} = 0.$$

Differentiating and solving the linear equations for β and C, we obtain

$$\beta = \frac{N\sum_{i=1}^{N}(\ln P_i)(\ln k_i) - \left(\sum_{i=1}^{N}\ln k_i\right)\left(\sum_{i=1}^{N}\ln P_i\right)}{\left(\sum_{i=1}^{N}\ln k_i\right)^2 - N\sum_{i=1}^{N}(\ln k_i)^2}$$

and

$$C = \frac{1}{N}\sum_{i=1}^{N}\ln P_i + \frac{\beta}{N}\sum_{i=1}^{N}\ln k_i.$$

Unlike the previous methods discussed, this method of computing the Fourier dimension $q = \beta/2$ is non-iterative and is immediately generalizable to fractal surfaces, when β and C are given by

$$\beta = \frac{N^2\sum_{i=1}^{N}\sum_{j=1}^{N}(\ln P_{ij})(\ln k_{ij}) - \left(\sum_{i=1}^{N}\sum_{j=1}^{N}\ln k_{ij}\right)\left(\sum_{i=1}^{N}\sum_{j=1}^{N}\ln P_{ij}\right)}{\left(\sum_{i=1}^{N}\sum_{j=1}^{N}\ln k_{ij}\right)^2 - N^2\sum_{i=1}^{N}\sum_{j=1}^{N}(\ln k_{ij})^2}$$

and

$$C = \frac{1}{N^2}\sum_{i=1}^{N}\sum_{j=1}^{N}\ln P_{ij} + \frac{\beta}{N^2}\sum_{i=1}^{N}\sum_{j=1}^{N}\ln k_{ij}$$

where it is assumed that P_{ij} is the data in the positive half space of the 2D power spectrum excluding the DC component. In either case, the power spectrum can be computed using a fast Fourier transform. The constant c provides a measure of the energy E of the fractal since from Parseval's theorem

$$E = \int_{-\infty}^{\infty} |\, f(x)\,|^2\, dx = \frac{1}{2\pi}\int_{-\infty}^{\infty} |\, F(k)\,|^2\, dk = \frac{c}{2\pi}\int_{-\infty}^{\infty}\frac{1}{|\, k\,|^{\beta}}dk.$$

The ratio c/q therefore provides a measure for an image that emphasizes regions where the intensity is high and the frequency content (texture) is low when computed on a moving window basis.

18.6 The Fourier and Fractal Dimensions

The relationship between the Fourier dimension q and the fractal dimension D can be determined by considering the box counting method for analysing a statistically self-affine signal, specifically, a fractional Brownian signal whose amplitude is given by (for unit step length)

$$A(t) = t^H, \quad H \in (0, 1]$$

where H is the Hurst dimension (see Chapter 17). Consider a fractal signal covering a time period $\Delta t = 1$ which is divided up into $N = 1/\Delta t$ equal intervals. The amplitude increments ΔA are then given by

$$\Delta A = \Delta t^H = \frac{1}{N^H} = N^{-H}.$$

Using the box counting method, with boxes of length $\delta = N^{-1}$, the number of boxes required to cover each interval is

$$\Delta A \Delta t = \frac{N^{-H}}{N^{-1}} = N^{1-H}$$

so that

$$N(\delta) = NN^{1-H} = N^{2-H}.$$

Now, since the box counting dimension D is related to $N(\delta)$ by

$$N(\delta) = \frac{1}{\delta^D}, \quad \delta \to 0,$$

then, by inspection,

$$D = 2 - H.$$

Thus, a Brownian signal, where $H = 1/2$, has a fractal dimension of 1.5. For higher topological dimensions D_T, using a similar box counting measure, we have

$$D = D_T + 1 - H.$$

This algebraic equation provides the relationship between the fractal dimension D, the topological dimension D_T and the Hurst dimension H. We can now determine the relationship between the Fourier dimension q and the fractal (box counting) dimension D.

Consider a fractal signal $f(x)$ over an infinite support with a finite sample $f_X(x)$, given by

$$f_X(x) = \begin{cases} f(x), & 0 < x < X; \\ 0, & \text{otherwise.} \end{cases}$$

A finite sample is essential as otherwise the power spectrum diverges. Furthermore, in reality $f(x)$ is a random function and for any experiment or computer simulation we must necessarily take a finite sample. Let $F_X(k)$ be the Fourier transform of $f_X(x)$, $P_X(k)$ be the power spectrum and $P(k)$ be the power spectrum of $f(x)$. Then

$$f_X(x) = \frac{1}{2\pi} \int_{-\infty}^{\infty} F_X(k) \exp(ikx) dk,$$

$$P_X(k) = \frac{1}{X} |F_X(k)|^2$$

and

$$P(k) = \lim_{X \to \infty} P_X(k).$$

The power spectrum gives an expression for the power of a signal for particular harmonics. $P(k)dk$ gives the power in the range k to $k + dk$. Consider a function $g(x)$, obtained from $f(x)$ by scaling the x-coordinate by some $a > 0$, the f-coordinate by $1/a^H$ and then taking a finite sample as before, i.e.

$$g_X(x) = \begin{cases} g(x) = \frac{1}{a^H} f(ax), & 0 < x < X; \\ 0, & \text{otherwise.} \end{cases}$$

Let $G_X(k)$ and $P'_X(k)$ be the Fourier transform and power spectrum of $g_X(x)$, respectively. We then obtain an expression for G_X in terms of F_X,

$$G_X(k) = \int_0^X g_X(x) \exp(-ikx) dx = \frac{1}{a^{H+1}} \int_0^X f(s) \exp\left(-\frac{iks}{a}\right) ds$$

where $s = ax$. Hence

$$G_X(k) = \frac{1}{a^{H+1}} F_X\left(\frac{k}{a}\right)$$

and the power spectrum of $g_X(x)$ is

$$P'_X(k) = \frac{1}{a^{2H+1}} \frac{1}{aX} \left| F_X\left(\frac{k}{a}\right) \right|^2$$

and, as $X \to \infty$,

$$P'(k) = \frac{1}{a^{2H+1}} P\left(\frac{k}{a}\right).$$

Since $g(x)$ is a scaled version of $f(x)$, their power spectra are equal, and so

$$P(k) = P'(k) = \frac{1}{a^{2H+1}} P\left(\frac{k}{a}\right).$$

If we now set $k = 1$ and then replace $1/a$ by k we get

$$P(k) \propto \frac{1}{k^{2H+1}} = \frac{1}{k^\beta}.$$

We have produced a signal that is statistically similar and is defined by the value H. Now since $\beta = 2H + 1$ and $D = 2 - H$, we have

$$D = 2 - \frac{\beta - 1}{2} = \frac{5 - \beta}{2}.$$

The fractal dimension of a fractal signal can be calculated directly from β using the above relationship. This method also generalizes to higher topological dimensions giving

$$\beta = 2H + D_T.$$

Thus, since

$$D = D_T + 1 - H,$$

we have that $\beta = 5 - 2D$ for a fractal signal and $\beta = 8 - 2D$ for a fractal surface or, more generally,

$$\beta = 2(D_T + 1 - D) + D_T = 3D_T + 2 - 2D$$

and

$$D = D_T + 1 - H = D_T + 1 - \frac{\beta - D_T}{2} = \frac{3D_T + 2 - \beta}{2},$$

the Fourier dimension being given by $q = \beta/2$.

18.7 Other Dimensions and Higher Order Fractals

In general, the fractal dimension alone is not sufficient to quantify a given texture. Many quite different fractals can have the same value of fractal dimension since

$$D = -\frac{\ln N}{\ln r} = -\frac{\ln N^\gamma}{\ln r^\gamma}$$

for all values of γ. For this reason, other fractal measures are required to supplement the fractal dimension in an attempt to uniquely define 'texture'.

18.7.1 The Fractal Signature

Many methods of computing the fractal dimension depend on the use of the equation

$$M(\epsilon) = c\epsilon^{D_T - D}$$

for some measured property M which is a function of scale ϵ, where c is a constant and D_T is the topological dimension. A single value of D can then be computed using a bi-logarithmic least squares fit. If, however, we use the fact that $M(1) = c$ we can compute D for $\epsilon = 2, 3, ...$ A plot of D against ϵ then gives the fractal signature. Natural imagery, such as a dense tree background gives a slowly changing, essentially constant signature. An image consisting of a single edge, for example, gives a low D at small ϵ rising to $D = 3$ at $\epsilon = 4$.

18.7.2 The Correlation Dimension and Signature

Each pixel in a grey-level image can be regarded as a point in a three dimensional space $X_k = [i, j, g_{ij}]$ where i and j are the spatial coordinates of a pixel and g_{ij} is the grey level at these coordinates. For each pixel, a cube of size $2\epsilon + 1$ is constructed centred on the pixel. The number of points X_ℓ that fall inside this cube is counted for various values of ϵ. The probability, $C(\epsilon)$, that at least one point lies within the cube can then be obtained by dividing the number of points by the cube volume:

$$C(\epsilon) = \frac{1}{N(2\epsilon + 1)^3} \sum_{k=1}^{N} \sum_{\substack{\ell=1 \\ \ell \neq k}} H(\epsilon - \mid X_k - X_\ell \mid)$$

where N is the number of pixels in the image (if we are considering the whole image or the number of pixels in a moving window - for the purpose of segmentation) and

$$H(\xi) = \begin{cases} 1, & \xi \geq 0; \\ 0, & \xi < 0. \end{cases}$$

$C(\epsilon)$ conforms to the equation

$$C(\epsilon) = c(2\epsilon + 1)^{3-D_C}$$

where D_C is the correlation dimension. Here, a single value of D_C can be computed by the normal bi-logarithmic least squares fit, or we may compute $C(0) = c$ and then compute a value of $C(\epsilon)$ for $\epsilon = 1, 2, ...$ In the latter case, we obtain the correlation signature as a plot of D_C against ϵ. For an image, the values of D_C range from two to three. A highly correlated surface gives a correlation dimension close to two whereas a highly uncorrelated surface gives a value close to three.

18.8 The Information Dimension

Given that p_i is the probability that an element i is populated, we can define an information function to be of the form

$$I = -\sum_{i=0}^{N-1} p_i(\delta) \ln p_i(\delta).$$

The information or Rényi dimension is then given by

$$D_I = -\lim_{\delta \to 0} \frac{I}{\ln \delta} = \lim_{\delta \to 0} \frac{\sum\limits_{i=0}^{N-1} p_i(\delta) \ln p_i(\delta)}{\ln \delta}.$$

When every element i is equally likely, then we have the property that,

$$\sum_{i=0}^{N-1} p_i(\delta) = N p_i(\delta) = 1, \quad p_i = \frac{1}{N}$$

and therefore, in this specific case, the relationship

$$D_I = \lim_{\delta \to 0} \frac{\sum\limits_{i=0}^{N_1} \frac{1}{N} \ln \frac{1}{N}}{\ln \delta} = \lim_{\delta \to 0} \frac{\ln N^{-1}}{\ln \delta} = -\lim_{\delta \to 0} \frac{\ln N}{\ln \delta} = D,$$

and it follows that if

$$I \leq -\sum_{i=0}^{N-1} \frac{1}{N} \ln \frac{1}{N}$$

then

$$D_I \leq D.$$

18.9 The Lyapunov Dimension

Consider the iterative system

$$f_{n+1} = F(f_n) = f + \epsilon_n$$

where ϵ_n is a perturbation to the value of f at an iterate n which is independent of the value of f_0. If the system converges to f as $n \to \infty$ then $\epsilon_n \to 0$ as $n \to \infty$ and the system is stable. If this is not the case, then the system may be divergent or chaotic. Suppose we model ϵ_n in terms of an exponential growth ($\sigma > 0$) or decay ($\sigma < 0$) so that

$$\epsilon_{n+1} = c \exp(n\sigma)$$

where c is an arbitrary constant. Then $\epsilon_1 = c$, $\epsilon_2 = \epsilon_1 \exp(\sigma)$, $\epsilon_3 = \epsilon_1 \exp(2\sigma) = \epsilon_2 \exp(\sigma)$ and thus, in general, we can write

$$\epsilon_{n+1} = \epsilon_n \exp(\sigma).$$

Noting that

$$\ln\left(\frac{\epsilon_{n+1}}{\epsilon_n}\right) = \sigma$$

we can write

$$\sum_{n=1}^{N} \ln\left(\frac{\epsilon_{n+1}}{\epsilon_n}\right) = N\sigma.$$

Thus, we can define σ as

$$\sigma = \lim_{N\to\infty} \frac{1}{N} \sum_{n=1}^{N} \ln\left(\frac{\epsilon_{n+1}}{\epsilon_n}\right).$$

The constant σ is known as the Lyapunov exponent. Since we can write

$$\sigma = \lim_{N\to\infty} \frac{1}{N} \sum_{n=1}^{N} (\ln \epsilon_{n+1} - \ln \epsilon_n)$$

and noting that (using forward differencing)

$$\frac{d}{dx} \ln \epsilon \simeq \frac{\ln \epsilon_{n+1} - \ln \epsilon_n}{\delta x} = \ln \epsilon_{n+1} - \ln \epsilon_n, \quad \delta x = 1$$

we see that σ is, in effect, given by the mean value of the derivatives of the natural logarithm of ϵ. Note that, if the value of σ is negative, then the iteration is stable and will approach f since we can expect that as $N \to \infty$, $\epsilon_{n+1}/\epsilon_n < 1$ and, thus, $\ln(\epsilon_{n+1}/\epsilon_n) < 0$. If σ is positive, then the iteration will not converge to f but will diverge or, depending on the characteristics of the mapping function F, will exhibit chaotic behaviour. The Lyapunov exponent is a parameter that is a characterization of the 'chaoticity' of the signal f_n which, in turn, can be taken to be a measure of its texture. In particular, if we compute σ_N using N elements of the signal f_n and then compute σ_M using M elements of the same signal, we can define the Lyapunuv dimension as

$$D_L = \begin{cases} 1 - \frac{\sigma_N}{\sigma_M}, & \sigma_M > \sigma_N; \\ 1 - \frac{\sigma_M}{\sigma_N}, & \sigma_M < \sigma_N. \end{cases}$$

18.9.1 Lacunarity

The term lacunarity comes from the Latin *lacuna* meaning gap. The most straightforward illustration comes from considering the class of Cantor dusts for which the fractal dimension (in this case, the similarity dimension) is given by $D = -\ln N / \ln r$ where N is the number of copies of a real line on the interval $[0, 1]$ and $r < 1$ is the scaling factor. Clearly, there is an infinite set of different $[N, r]$ which give the same D. For example the classic triadic Cantor set $[2, 1/3]$ gives the same D as $[4, 1/9]$, $[8, 1/27]$, etc. The appearance of these point-sets will, however, be quite different. The difference lies in the way the gaps are distributed. We can define the lacunarity of deterministic fractal sets such as the Cantor set discussed above. Such definitions are, however, unsuitable for random fractals and require suitable candidate definitions of lacunarity for the class of random fractals. These definitions are based on the idea of mass distribution. Consider, for example, a curve $f(x)$: (i) if the curve has negative values, then translate so that it is non-negative; (ii) consider the values of f as representing mass so that we regard f as a mass distribution over the support of f. We can consider definitions such as

$$L_1 = \left\langle \left| \frac{f}{\langle f \rangle} - 1 \right| \right\rangle$$

and

$$L_2 = \left\langle \left(\frac{f}{\langle f \rangle} - 1 \right)^2 \right\rangle = \frac{\langle f^2 \rangle}{\langle f \rangle^2} - 1$$

for the p^{th}-order lacunarity L_p, where $\langle\ \rangle$ denotes the mean. Note that the second definition can be expressed as the variance divided by the square of the mean. The definitions are not dissimilar to generalized statistical moments (see Chapter 17), and we can consider a general lacunarity measure such as

$$L_p = \left\langle \left| \frac{f}{\langle f \rangle} - 1 \right|^p \right\rangle^{\frac{1}{p}}.$$

This provides a 'key' to the higher order fractals approach which is discussed next.

18.9.2 Higher Order Fractals and Dimensions

In principle, there are an unlimited number of fractal or generalized dimensions. Further, the fractal dimension alone is not sufficient to characterize a fractal set and is only one of a number of generalized dimensions that can be considered. These generalized dimensions are defined via a measure theoretic analysis in 'real space'. The use of transforms and, in particular, the Fourier transform, applies principally to the Fourier dimension. This approach differentiates between regions in an image with different Fourier dimension, but not regions with the same Fourier dimension but differing correlation dimension, information dimension and so on. A good example follows from the result that

the fractal dimension D of the sum of two fractal curves C_1 and C_2, with fractal dimensions D_1 and D_2 is given by

$$D = \max[D_1, D_2].$$

Suppose, for example, that D_1 is significantly larger than D_2; C_2 could be a square wave for example, in which case $D_2 = 1$. Whilst it is clear to the eye that the merged curve is quite different from C_1 (or C_2), the same value of fractal dimension is found for the merged curve and C_1.

The need for multi-fractal measures can easily be grasped by considering the definition and calculation of the box dimension. Consider the case of a point-set with a large but finite number of points N embedded in fractal dimensional space where we cover the set with a uniform grid of hypercubes of size δ and count the number $M(\delta)$ of non-empty boxes. Such a strategy does not include information concerning the distribution of the number of points in the non-empty boxes.

Suppose there are N_k points in the k^{th} hypercube and let $p_k = N_k/N$. The similarity dimension (which takes account only of the total of non-empty boxes $M(\delta)$ and not the N_k) is then given by

$$D = -\lim_{\delta \to 0} \lim_{N \to \infty} \frac{\ln M(\delta)}{\ln \delta}.$$

The information (or Renyi) dimension is defined by

$$D_I = -\lim_{\delta \to 0} \lim_{N \to \infty} \frac{S(\delta)}{\ln \delta}$$

where

$$S(\delta) = -\sum_{k=1}^{M(\delta)} p_k \ln p_k.$$

The correlation dimension is

$$D_C = \lim_{\delta \to 0} \lim_{N \to \infty} \frac{\ln C(\delta)}{\ln \delta}$$

where

$$C(\delta) = \frac{1}{N^2} \sum_{i \neq j} H(\delta - \mid X_i - X_j \mid)$$

and H is the Heaviside step function. $C(\delta)$ counts the number of points whose distance $\mid X_i - X_j \mid$ is less than δ. D, D_I and D_C are the first three numbers of a hierarchy of generalized dimensions D_q for $q \geq 0$, i.e.

$$D = \lim_{q \to 0} D_q, \quad D_I = \lim_{q \to 1} D_q, \quad D_C = \lim_{q \to 2} D_q$$

and for $q = 3, 4, ..., n$ we have correlation dimensions associated with triplets, quadruplets and n-tuplets of points. Further, D_q forms a non-increasing series

$$D_q > D_{q'} \quad \text{for any} \quad q' > q$$

with the inequality replaced by an equality if and only if the fractal is homogeneous. Hence, various dimensions previously introduced quite independently form a general series. Moreover, a general expression for D_q can be obtained given by

$$D_q = \frac{1}{(q-1)} \lim_{\delta \to 0} \frac{\ln\left(\sum_i p_i^q\right)}{\ln \delta}.$$

18.10 Fractal Images and Mandelbrot Surfaces

The fractal geometry of nature is often associated with systems undergoing a phase transition. When a phase transition occurs, a system becomes characterized by the interconnectivity of its elements rather than by the elements themselves. The structures that are formed from this interconnectivity are governed by the universal power law

$$\text{System(size)} \quad \propto \quad \frac{1}{\text{size}^{\text{q}}}$$

where $q > 0$. Here, the term 'system' is a generic term representative of some definable parameter that can be measured over different scales of a certain size. With fractal images, the term 'size' relates to the level of detail that can be resolved which is determined by the frequency content of the spectrum. Fractal images are therefore characterized by a frequency distribution or spectrum given by

$$\text{Spectrum(frequency)} \quad \propto \quad \frac{1}{(\text{frequency})^q}$$

where q is the Fourier dimension. Why should this distribution produce an image that is self-similar? Suppose we have a complex spectrum $N(\mathbf{k})$ where $\mathbf{k} = \hat{\mathbf{x}}k_x + \hat{\mathbf{y}}k_y$ which is characteristic of white noise, i.e. has an amplitude spectrum that is a constant. Then, the (complex) spectrum of a fractal image is given by

$$U(\mathbf{k}) = \frac{N(\mathbf{k})}{(ik)^q}$$

and the fractal image $u(\mathbf{r})$ where $\mathbf{r} = \hat{\mathbf{x}}x + \hat{\mathbf{y}}y$ is given by the inverse Fourier transform

$$u(\mathbf{r}) = \hat{F}_2^{-1}\left[\frac{N(\mathbf{k})}{(ik)^q}\right] = \frac{1}{(2\pi)^2} \int_{-\infty}^{\infty}\int_{-\infty}^{\infty} \frac{N(\mathbf{k})}{(ik)^q} \exp(i\mathbf{k}\cdot\mathbf{r}) d^2\mathbf{k}.$$

Using the convolution theorem,

$$u(\mathbf{r}) = h(\mathbf{r}) \otimes \otimes n(\mathbf{r}) = \int_{-\infty}^{\infty}\int_{-\infty}^{\infty} h(\mathbf{r}-\mathbf{r}')n(\mathbf{r}')d^2\mathbf{r}'$$

where

$$n(\mathbf{r}) = \hat{F}_2^{-1}[N(\mathbf{k})]$$

and

$$h(\mathbf{r}) = \hat{F}_2^{-1}[(i\mathbf{k})^{-q}].$$

Now the n-dimensional Fourier transform of r^q is given by (see Appendix C)

$$\int_{-\infty}^{\infty} r^q \exp(-i\mathbf{k}\cdot\mathbf{r}) d^n\mathbf{r} = \frac{\left(\frac{q}{2}+\frac{n}{}-1\right)!}{\left(-\frac{q}{2}-1\right)!} 2^{q+n}\pi^{n/2}k^{-q-n}$$

and, hence, the function h is given by (for $n = 2$)

$$h(\mathbf{r}) = \alpha_2(q)\frac{1}{r^{2-q}}$$

where

$$\alpha_2(q) = \frac{i^q}{2^q\pi}\frac{\left[-\left(\frac{q-2}{2}\right)-1\right]!}{\left(\frac{q-2}{2}\right)!}.$$

Thus, we can write the fractal image as

$$u(\mathbf{r}) = \alpha_2(q)n(\mathbf{r}) \otimes\otimes \frac{1}{r^{2-q}}.$$

But this equation has a characteristic scaling property, i.e.

$$u(\mathbf{r}) = \alpha_2(q)\int_{-\infty}^{\infty}\int_{-\infty}^{\infty}\frac{n(a\mathbf{r}')}{\mid \mathbf{r}-\mathbf{r}' \mid^{2-q}}d^2\mathbf{r}' = \frac{\alpha_2(q)}{a^q}\int_{-\infty}^{\infty}\int_{-\infty}^{\infty}\frac{n(\mathbf{y})}{\mid a\mathbf{r}-\mathbf{y} \mid^{2-q}}d^2\mathbf{y} = \frac{1}{a^2}u(a\mathbf{r})$$

where $\mathbf{y} = a\mathbf{r}'$ and thus

$$\Pr[u'(\mathbf{r})] = \frac{1}{a^q}\Pr[u(a\mathbf{r})]$$

where Pr denotes the Probability Density Function (PDF). This equation is telling us that the PDF of the stochastic field $u(a\mathbf{r})$ at a scale $a > 0$ is the same as the PDF of the field $u(\mathbf{r})$ scaled by a^q which describes a statistically self-affine image or surface. A Mandelbrot surface is a fractal image where $q \in (1, 2)$. The range of values of q corresponds to fractal dimensions $D \in (3, 2)$, respectively. However, the self-affine nature of $u(\mathbf{r})$ is valid for all values of $q > 0$ and so q can take on values below and above the range $q \in (1, 2)$ which defines a Mandelbrot surface. Hence, we can define a statistically self-affine image as one in which

$$\Pr[u'(\mathbf{r})] = \frac{1}{a^q}\Pr[u(a\mathbf{r})], \quad q > 0$$

and a Mandelbrot surface as one where

$$\Pr[u'(\mathbf{r})] = \frac{1}{a^q}\Pr[u(a\mathbf{r})], \quad q \in (1, 2).$$

There is an interesting connection between this result and the solution to the fractional Poisson equation

$$\nabla^q u(\mathbf{r}) = n(\mathbf{r}).$$

If we use the n-dimensional fractional Riesz operator

$$\nabla^q \equiv \frac{1}{2\pi} \int_{-\infty}^{\infty} d^n\mathbf{k}(ik)^q \exp(i\mathbf{k}\cdot\mathbf{r}), \quad k \equiv \mid \mathbf{k} \mid$$

then, upon Fourier transforming the fractional Poisson equation, we have

$$(ik)^q U(\mathbf{k}) = N(\mathbf{k}) \quad \text{or} \quad U(\mathbf{k}) = \frac{N(\mathbf{k})}{(ik)^q}$$

giving (ignoring scaling by α_2)

$$u(\mathbf{r}) = \frac{1}{r^{2-q}} \otimes\otimes n(\mathbf{r}), \quad r \equiv \mid \mathbf{r} \mid .$$

Hence, a self-affine surface can be considered to be the solution to a 2D fractional Poisson equation with a white noise source term $n(\mathbf{r})$, i.e.

$$\nabla^q(\text{Fractal surface}) = \text{white noise}, \quad q > 0.$$

Note that a statistically self-affine volume can be defined as the solution to

$$\nabla^q u(\mathbf{r}) = n(\mathbf{r}), \quad \mathbf{r} = \hat{\mathbf{x}}x + \hat{\mathbf{y}}y + \hat{\mathbf{z}}z$$

which is given by (ignoring scaling)

$$u(\mathbf{r}) = \frac{1}{r^{3-q}}(\mathbf{r})$$

where $\otimes$ denotes the 3D convolution integral. This result is a direct consequence of the scaling law

$$\text{Spectrum} \propto \frac{1}{(\text{frequency})^q}$$

just as the Coulomb's inverse square law (in three dimensions)

$$\text{Electrostatic force} \propto \frac{1}{(\text{distance})^2}$$

yields the 3D Poisson equation

$$\nabla^2\phi(\mathbf{r}) = \rho(\mathbf{r})$$

where ϕ is the electric field potential and ρ is the charge density whose solution is (ignoring scaling)

$$\phi(\mathbf{r}) = \frac{1}{r} \otimes \rho(\mathbf{r}).$$

18.10.1 Computing a Self-affine Surface

Taking n to be a white Gaussian noise field, we can compute a fractal image $\mid u \mid$ say by using the convolution theorem and filtering the spectrum of n with k^{-q} where $k = \sqrt{k_x^2 + k_y^2}$ avoiding the singularity at $k = 0$ by setting the DC level of u to be that of n. This is this basis for the example MATLAB function that follows.

```
function FRACTAL_SURFACE(seed, q, size)

%
%Input:
%      seed - initiator for random number generator.
%         q - Fourier dimension.
%         n - image size
%

%Set state of random number generator using the randn function.
randn('state',seed);

%Compute a random Gaussian noise field using the randn function.
n=randn(size,size);

%Compute the Fourier transform using fft2 function with a shift.
n=fftshift(fft2(n));

%Filter the spectrum avoiding singularity at zero frequency.
s=1+size/2;
for i=1:size
    for j=1:size
        k=((i-s)^2+(j-s)^2)^0.5;
        if k > 0
            u(i,j)=n(i,j).*k^(-q);
        else
            u(i,j)=n(i,j); %DC of u = DC of n.
        end
    end
end

%Inverse Fourier tranform.
u=real(fftshift(ifft2(u)));

%Take absoute value, scale (normalize) and display.
u=abs(u);
u=u./max(max(u));
imshow(u);
```

The output of this function for seed=1, size=128 and values of q=1.1, 1.2, 1.3,..., 1.9 is shown in Figure 18.19. As the value of q increases, the texture becomes smoother as a result of the high frequency components of the Gaussian noise field being suppressed further.

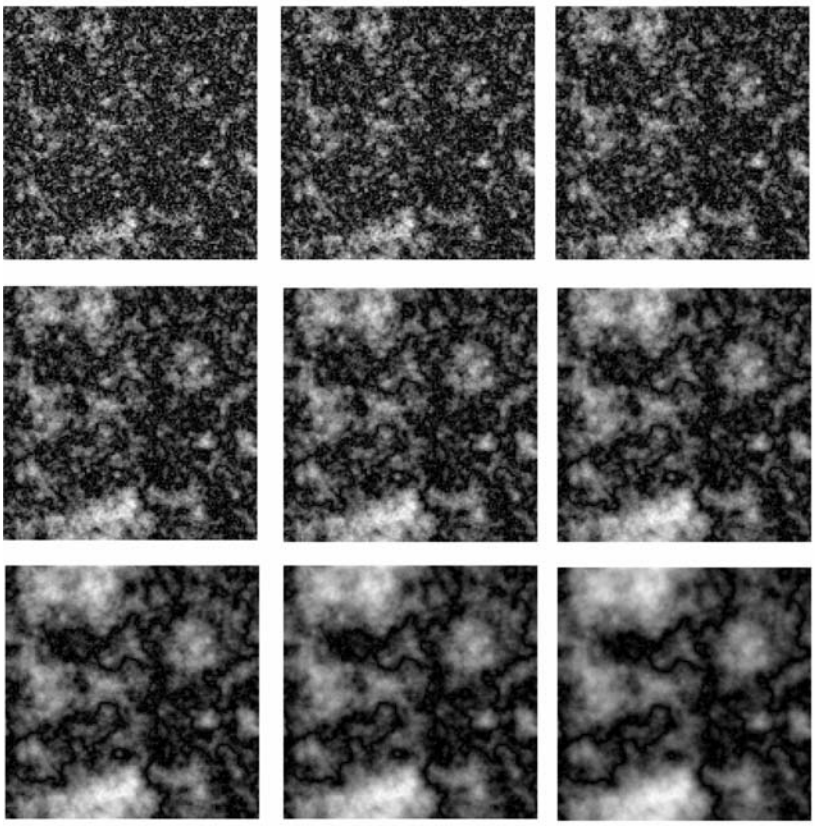

Figure 18.19: A random fractal image for (left-to-right and top-to-bottom) values of the Fourier dimension q between 1.1 and 1.9, in steps of 0.1.

Note that the PDF of the noise field used can vary provided that its spectrum is white. Thus, the mean value of a Gaussian noise field can be adjusted as required as can the type of noise (non-Gaussian) that is generated.

18.10.2 Tailoring a Fractal Surface

The smoothness of a fractal surface depends on the value of the Fourier dimension but its form (i.e. large scale shape or global topology) is determined by the random number generating algorithm and the seed used to generate the noise field n. Hence, we do not know the global topology of the surface until it has been computed using an algorithm of the type given in the previous Section.

How can we incorporate *a priori* information on the large scale structure of a fractal surface and thus tailor it accordingly. A solution to this problem is to replace the white noise field n by $(1-t)n + tf$, where f is some user defined function and $0 \leq t \leq 1$ is a 'transmission coefficient'. The fractal surface can then be considered to be a solution to the equation

$$\nabla^q u(\mathbf{r}) = (1-t)n(\mathbf{r}) + tf(\mathbf{r}), \quad t \in (0,1).$$

This solution requires that $F(k)$ does not approach zero as fast as k^{-q}. If this cannot be guaranteed then the *a priori* information can be encoded in the phase of the source function and the fractal computed by solving the equation

$$\nabla^q u(\mathbf{r}) = F_2^{-1}[\mid N(\mathbf{k}) \mid \exp(i(1-t)\theta_N + it\theta_F)], \quad t \in [0,1]$$

where θ_F and θ_F are the Fourier phase spectra of n and f, respectively.

In principle, any suitable algorithm developed for computational geometry can be used to compute the surface $f(x, y)$. For example, we can generate a smooth surface by applying an appropriate filter to a collection of user defined control points and/or patches. Smoothness is guaranteed if a filter is used that is a variation diminishing smoothing kernel, one such example being a Gaussian filter. An example is given in Figure 18.20 where the control surface has been hand sketched as shown, filtered using a Gaussian low-pass filter to obtain f and used to generate a fractal surface using the source term $(1-t)n + tf$ with $t = 0.3$, a Fourier dimension of 1.35 and where n and f have been normalized (i.e. $\|n(\mathbf{r})\|_\infty = 1$ and $\|f(\mathbf{r})\|_\infty = 1$).

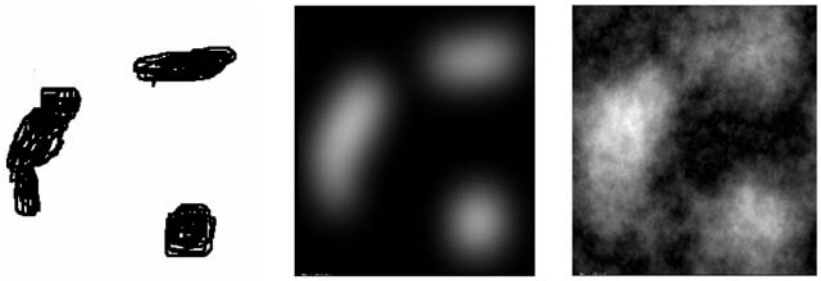

Figure 18.20: Control surface (left) based on hand sketched surface patches, the result of applying a Gaussian low-pass filter to the control surface (centre) and the fractal surface (left) for $q = 1.35$ and $t = 0.3$.

18.10.3 Fractal Flow, Divergent and Rotational Fields

If we model a fractal surface in terms of a solution to the equation

$$\nabla^q u(\mathbf{r}) = n(\mathbf{r})$$

where n can incorporate *a priori* information on the surface as discussed in the previous Section, then we can extend the principle under the Reisz operator for a fractional Laplacian to flow, divergent and rotational field.

Flow Fields

We consider a 2D flow field in terms of the solution to

$$\left(\frac{\partial^{q_x}}{\partial x^{q_x}} + \frac{\partial^{q_y}}{\partial y^{q_y}}\right) u(x,y) = n(x,y)$$

where for $q_x < q_y$ the flow is the the x-direction and for $q_y < q_x$ the flow is the y-direction, the values of q_x and q_y determining the 'flow rate'. The flow field is computed by applying the appropriate filter which, in this case, is given by $(k_x^{q_x} + k_y^{q_y})^{-1}$.

Divergent Fields

A divergent fractal field can be considered to be the solution to

$$\nabla^q \cdot \mathbf{u}(\mathbf{r}) = n(\mathbf{r}), \quad \mathbf{r} \in A$$

where $\mathbf{r} = \hat{\mathbf{x}}x + \hat{\mathbf{y}}y$ and n is taken to be of compact support A, i.e. confined to an area A. If we let $\mathbf{u} = \nabla\phi$ where ϕ is the field potential, then

$$\nabla^{1+q}\phi(\mathbf{r}) = n(\mathbf{r})$$

whose solution provides a scalar fractal field ϕ obtained by applying a $k^{-(1+q)}$ filter. The divergent field is then given by

$$\mathbf{u}(x,y) = \left(\hat{\mathbf{x}}\frac{\partial}{\partial x} + \hat{\mathbf{y}}\frac{\partial}{\partial y}\right)\phi(x,y)$$

where the partial differentials can be computed using the filters ik_x and ik_y, respectively.

Rotational Fields

A random scaling rotational field can be considered to be the solution to the equation

$$\nabla^q \times \mathbf{u}(\mathbf{r}) = \mathbf{n}(\mathbf{r}), \quad \mathbf{r} \in A.$$

Now let[1]

$$\nabla \times \nabla^q \times \mathbf{u} = -\nabla^{1+q}\mathbf{u} + \nabla(\nabla^q \cdot \mathbf{u})$$

and consider the case when the fractional divergent field is zero. We then have

$$\nabla^{1+q}\mathbf{u} = -\nabla \times \nabla^q \times \mathbf{u} = -\nabla \times \mathbf{n}$$

or

$$\nabla^{1+q}u(x,y) = \frac{\partial}{\partial y}n_x - \frac{\partial}{\partial x}n_y$$

[1] A generalization of the result $\nabla \times \nabla \times \mathbf{u} = -\nabla^2\mathbf{u} + \nabla(\nabla \cdot \mathbf{u})$ - see Chapter 1

where n_x and n_y are the components of the noise source in the x- and y-directions, respectively. By computing the terms $\partial_x n_y$ and $\partial_y n_x$ using the filters ik_x and ik_y, respectively, the rotational field can computed by using two different seeds to generate n_x and n_y and applying a $k^{-(1+q)}$ filter in the usual way. Examples of a flow, a divergent and a rotational fractal field are given in Figure 18.21. The flow field has been generated using Fourier dimensions of $q_x = 1.0001$ and $q_y = 1.9999$ and 256×256 pixels. The divergent and rotational fields have also been generated using 256×256 pixels for a Fourier dimension of 0.7 (i.e. $1 + q = 1.7$) and noise fields which are of compact support where

$$\sqrt{k_x^2 + k_y^2} \leq a^2$$

with $a = 32$ pixels. The rotational field has been generated by seeding n_y with the same seed plus 1 as that used to generate n_x.

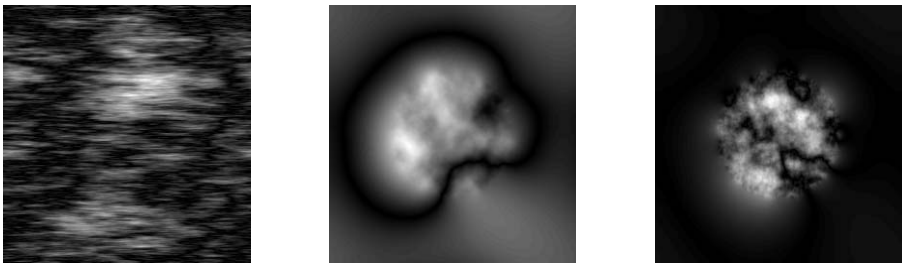

Figure 18.21: Examples of a random scaling flow field (left), divergent field (centre) and a rotational field (right).

Dynamic Fractal Images

Dynamic fractal simulation has value in the case when a time dependent model is required for the formation of a random scaling fractal. One approach is to consider a time varying Fourier dimension $q(t)$. In this case, we can consider the solution of the equation

$$\nabla^{q(t)} u(\mathbf{r}, t) = n(\mathbf{r}, t)$$

where the time dependent behaviours of q and n are taken to be slowly varying. Each time 'frame' at which u is computed for a given value of q is determined by the position of the window over which n is constructed from a larger noise field.

18.11 Generalized Random Scaling Fractal (RSF) Models

The PSDF associated with a fractal image (i.e. the k^{-2q} model) is not appropriate to all noise types and/or to the whole spectrum. Most images do have a high frequency decay but the complete power spectrum may have characteristics for which the $1/k^{2q}$ power law is not appropriate. Spectral partitioning can be used to extract the most appropriate part of the spectrum for which the $1/k^{2q}$ power law applies. Is there a more general model which can be used to characterize a wider variety of PSDFs of which the k^{-2q} law is a special case? Developing theoretically valid models for the spectral characteristics (PSDF) and/or the PDFs of stochastic fields is one of the principal aims of statistical mechanics. Ideally, what is required is a 'shape' for the PSDF which characterizes all possible cases. To this end, we consider a PSDF of the form

$$P(k) = \frac{ck^{2p}}{(k_0^2 + k^2)^q}$$

which is a generalization of the Bermann process

$$P(k) = \frac{ck^{2p}}{k_0^2 + k^2}$$

that is, in turn, a generalization of the Ornstein-Uhlenbeck process

$$P(k) = \frac{ck}{k_0^2 + k^2}$$

where c and k_0 are constants, $p > 0$ and $q > 0$. Here, both p and q can be considered to be Fourier dimensions which together with k_0 provides a way of 'shaping' the PSDF of a stochastic field. For $k > 0$, the function $P(k) > 0 \forall k$ has as maximum when

$$\frac{d}{dk} \ln P(k) = \frac{2p}{k} - \frac{2kq}{k_0^2 + k^2} = 0$$

or when

$$\frac{d}{dk} P(k) = \left(\frac{2p}{k} - \frac{2kq}{k_0^2 + k^2} \right) P(k) = 0.$$

This implies that the maximum value of $P(k)$ occurs at a value of $k = k_{\max}$ given by

$$k_{\max} = k_0 \sqrt{\frac{p}{q-p}}, \quad q > p.$$

The value of $P(k)$ at this point is therefore

$$P_{\max} \equiv P(k_{\max}) = \frac{ck_{\max}^{2p}}{(k_0^2 + k_{\max}^2)^q} = ck_0^{2(p-q)} \frac{p^p}{q^q} (q-p)^{q-p}.$$

Beyond this point, the PSDF decays and its asymptotic form is dominated by a k^{-2q} power law which is consistent with RSF signals and many noise types at

the high frequency end of their power spectra. At low frequencies, the power spectrum is characterized by the term k^{2p}. The 2D stochastic function that is characterized by this PSDF is given by (using the Riesz operator)

$$u(\mathbf{r}) = F_2^{-1}\left[\frac{(ik)^p}{(k-ik_0)^q}N(\mathbf{k})\right] = h(\mathbf{r}) \otimes \otimes \nabla^p N(\mathbf{r}), \quad k = \mid \mathbf{k} \mid$$

where

$$h(\mathbf{r}) = \hat{F}_2^{-1}\left[\frac{1}{(k-ik_0)^q}\right].$$

Now since (see Appendix C)

$$\int_{-\infty}^{\infty}\int_{-\infty}^{\infty} r^{q-2}\exp(-ik\hat{\mathbf{n}}\cdot\mathbf{r})d^2\mathbf{r} = \frac{\alpha_2}{k^q}$$

then

$$\int_{-\infty}^{\infty}\int_{-\infty}^{\infty} r^{q-2}\exp[-i(k-ik_0)\hat{\mathbf{n}}\cdot\mathbf{r}]d^2\mathbf{r} = \frac{\alpha_2}{(k-ik_0)^q}$$

and hence

$$\hat{F}_2^{-1}\left[\frac{1}{(k-ik_0)^q}\right] = \frac{1}{\alpha_2}\exp(-k_0\hat{\mathbf{n}}\cdot\mathbf{r})r^{q-2}.$$

Hence, ignoring scaling by α_2

$$u(\mathbf{r}) = \frac{\exp(-k_0\hat{\mathbf{n}}\cdot\mathbf{r})}{r^{2-q}} \otimes \otimes \nabla^p n(\mathbf{r})$$

whose scaling property is

$$\Pr[u(a\mathbf{r}, k_0/a)] = \frac{a^q}{a^p}\Pr[u(\mathbf{r}, k_0)].$$

Here, as we scale $\mathbf{r}$ by a, the characteristic frequency k_0 is scaled by $1/a$, a result that is analagous to the scaling property of the Fourier transform, i.e.

$$u(a\mathbf{r}) \Longleftrightarrow \frac{1}{a}U\left(\frac{\mathbf{k}}{a}\right).$$

The interpretation of this result is that, as we zoom into the image $u(\mathbf{r}, k_0)$, the distribution of amplitudes (i.e. the PDF) remains the same (subject to scaling by a^{p-q} and the characteristic frequency of the image increases by a factor of $1/a$. We can consider the equation

$$u(\mathbf{r}) = \frac{\exp(-k_0\hat{\mathbf{n}}\cdot\mathbf{r})}{r^{2-q}} \otimes \otimes \nabla^p n(\mathbf{r})$$

to be a solution to the fractional differential equation

$$\nabla^q u(\mathbf{r}) = \exp(k_0\hat{\mathbf{n}}\cdot\mathbf{r})\nabla^p n(\mathbf{r})$$

since

$$\exp(-k_0\mathbf{n}\cdot\mathbf{r})\nabla^q u(\mathbf{r}) \Longleftrightarrow (k-ik_0)^q$$

and

$$\nabla^p n(\mathbf{r}) \Longleftrightarrow (ik)^p N(\mathbf{k}).$$

Parameter Estimation

Clearly, all the results discussed above reduce to the 'normal' theory of RSF signals when $p=0$ and $k_0=0$, but this model provides a much greater degree of flexibility in terms of characterizing the PSDFs of many noise types, nearly all of which have some degree of statistical self-affinity and PSDFs with power laws of irrational form.

In terms of using this model to characterize texture, we consider the case where a suitable combination (some cluttering algorithm) of the parameters p, q, k_0 and c is taken to be a measure of texture, in particular, the parameters p and q - their product for example. In this case, we are required to obtain estimates for these parameters associated with the data u_{ij}; $\quad i=1,2,...N, \quad j=1,2,...,N$. The general four parameter problem is not easily solved, primarily because of difficulties in linearizing $P(k)$ with respect to k_0. However, suppose that a good estimate for k_0 can be obtained, then we can compute estimates for p, q and c using a standard least squares method by constructing a logarithmic least squares estimate in the usual way, i.e. consider (with $C=\ln c$)

$$e(g,q,C)=\sum_{i=1}^{N}\sum_{j=1}^{N}(\ln P_{ij}-\ln\hat{P}_{ij})^2$$

where P_{ij} is the discrete power spectrum (taken to be the positive half space data excluding the DC component) of u_{ij} and

$$\hat{P}_{ij}=ck_{ij}^{2g}/(k_0^2+k_{ij}^2)^q$$

is its expected form. In this case,

$$e(g,q,C)=\sum_{i=1}^{N}[\ln P_{ij}-2p\ln k_{ij}-C+q\ln(k_0^2+k_{ij}^2)]^2$$

which is a minimum when

$$\frac{\partial e}{\partial p}=0, \quad \frac{\partial e}{\partial q}=0, \quad \frac{\partial e}{\partial C}=0.$$

Differentiating, the set (p,q,C) is given by the solution to the following linear system of equations

$$\begin{pmatrix} a_{11} & a_{21} & a_{31} \\ a_{12} & a_{22} & a_{32} \\ a_{13} & a_{23} & a_{33} \end{pmatrix}\begin{pmatrix} p \\ q \\ C \end{pmatrix}=\begin{pmatrix} b_1 \\ b_2 \\ b_3 \end{pmatrix}$$

where

$$a_{11} = -2\sum_{i=1}^{N}\sum_{j=1}^{N}(\ln k_{ij})^2, \quad a_{21} = 2\sum_{i=1}^{N}\sum_{j=1}^{N}\ln(k_0^2 + k_{ij}^2)\ln k_{ij},$$

$$a_{31} = 2\sum_{i=1}^{N}\sum_{j=1}^{N}\ln k_{ij}, \quad a_{12} = -\sum_{i=1}^{N}\sum_{j=1}^{N}(\ln k_{ij})\ln(k_0^2 + k_{ij}^2),$$

$$a_{22} = -\sum_{i=1}^{N}\sum_{j=1}^{N}[\ln(k_0^2 + k_{ij}^2)]^2, \quad a_{32} = -\sum_{i=1}^{N}\sum_{j=1}^{N}\ln(k_0^2 + k_{ij}^2),$$

$$a_{13} = \sum_{i=1}^{N}\sum_{j=1}^{N}\ln k_{ij}, \quad a_{23} = \sum_{i=1}^{N}\sum_{j=1}^{N}\ln(k_0^2 + k_{ij}^2), \quad a_{33} = N$$

$$b_1 = \sum_{i=1}^{N}\sum_{j=1}^{N}(\ln P_{ij})(\ln k_{ij}), \quad b_2 = \sum_{i=1}^{N}\sum_{j=1}^{N}(\ln P_{ij})[\ln(k_0^2 + k_{ij}^2)]$$

and

$$b_3 = \sum_{i=1}^{N}\sum_{j=1}^{N}\ln P_{ij}.$$

An initial estimate for k_0 can be obtained from the result

$$k_0 = k_{\max}\sqrt{\frac{q-p}{p}}, \quad q > p$$

where $k_{\max}$ is the frequency corresponding to the maximum value of the power spectrum. The value of $k_{\max}$ can be estimated by applying a smoothing process to the power spectrum (a moving average filter for example) and then computing the mode of the resulting distribution. Having obtained an estimate for $k_{\max}$, we consider the case when $k_0 = k_{\max}$ which will give a first approximation to the parameter set (p, q, C). Iteration can then be used, where the initial estimates of p and q are used to compute a new value for k_0, and the linear system of equations given above solved to obtain a second estimate of the parameter set (p, q, C) and so on.

18.12 Multi-fractal Analysis

Defining and solving the image segmentation problem depends on both the classical Euclidean approach and the non-Euclidean fractal approach. Each has its advantages with regard to different image types. However, a 'route' between the two cases is possible that relies on the definition of the Hölder continuity.

The Hölder continuity defines a limit on the smoothness of a function and although it is not used as a form of fractal dimension it is strongly related. A function f has a Hölder continuous order, λ, when

$$|f(x) - f(y)| \leq k|x - y|^{\lambda} \qquad \forall x, y$$

where k is a constant. An alternative way of defining this is by using the modulus of continuity,

$$w(\delta) = \sup_{|x-y| \leq \delta} |f(x) - f(y)|$$

so

$$w(\delta) \leq k\delta^{\lambda}.$$

The exponent, λ, is thus given by

$$\lambda = \frac{-\ln k + \ln w(\delta)}{\ln \delta}.$$

If we ignore the constant term $\ln k$ and consider a two dimensional small neighbourhood around a point (x, y), then we can describe a digital 'coarse-grained' local Hölder order,

$$\lambda_{x,y}(i) = \frac{\ln c_{x,y}(i)}{\ln i}$$

where i is the size of the neighbourhood, and $c_{x,y}(i)$ is some capacity measure acting on the points within the neighbourhood

$$\lambda_{x,y} = \lim_{i \to 0} \lambda_{x,y}(i).$$

Next, we consider the two sets

$$E_{\lambda} = \left\{ (x, y) \quad \text{such} \quad \text{that} \quad \lim_{i \to 0} \lambda_{x,y}(i) = \lambda \right\}$$

$$N_{\epsilon}^{i}(\lambda) = \text{card} \left\{ (x, y) \quad \text{such} \quad \text{that} \quad \lambda_{x,y}(i) \in [\lambda - \epsilon, \lambda + \epsilon] \right\}.$$

We can now define $\varphi_h(\lambda)$ as the Hausdorff dimension (D_H) of E_{λ} and consider the double limit

$$\varphi_g(\lambda) = \lim_{\epsilon \to 0} \lim_{i \to 0} \frac{\ln N_{\epsilon}^{i}(\lambda)}{\ln i}.$$

Each point in an image can then be described by a pair of values $(\lambda, \varphi(\lambda))$. φ_h measures the Hausdorff dimension of the set of points that have a certain λ, which gives a geometric description of the singularities. φ_g approximately defines the probability distribution of the singularities. We now consider a process that estimates φ_g with the following algorithm:

for each i
  compute all $\lambda_{x,y}(i)$
end for
let $\lambda_{min} = \min \{\lambda_{x,y}(i)\}$
let $\lambda_{max} = \max \{\lambda_{x,y}(i)\}$
for each i
  create histogram with k cells of the $\lambda_{x,y}(i)$ values $\left[N_0^i, \ldots, N_{k-1}^i\right]$
end for
$\varphi_g(\lambda)$ calculated from a linear regression on $(\ln N_j^i, \ln i)$

The values λ_{min} and λ_{max} define the size of the i histograms so that they are comparable. The algorithm is only an approximation and for certain cases can yield unsatisfactory results. The number of cells in the histograms is arbitrary and does not take into account the ϵ limit in the definition of N_ϵ^i.

We have a choice of capacity measure $c_{x,y}(i)$; this can be related to the previously defined w_δ with the following, by considering W as the set of points within the neighbourhood around (x, y) that is defined by i:

$$c_{x,y}(i) = \sup_{m,n \in W \ k,l \in W} |f_{m,n} - f_{k,l}|$$

or, as an alternative, centreing it in the middle of the neighbourhood,

$$c_{x,y}(i) = \sup_{m,n \in W} |f_{m,n} - f_{x,y}|.$$

Further examples of different capacity measures include those that are designed to detect and analyse different kinds of singularities, such as

$$c_{x,y}(i) = \max_{m,n \in W} |f_{m,n}|$$

$$c_{x,y}(i) = \min_{m,n \in W} |f_{m,n}|$$

$$c_{x,y}(i) = \sum_{m,n \in W} |f_{m,n}|$$

and

$$c_{x,y}(i) = \text{card}\left\{(m,n) \ \text{ such that } \ f_{m,n} \equiv f_{x,y}, \ m,n \in W\right\}.$$

In practice, we can consider a series of square neighbourhoods, where i specifies the length of one side; then it is a simple process of creating the crude Hölder orders, $\lambda(i)$. The values of λ and φ_g are calculated via linear regression on the first few values of i. Different capacities detect different types of singularities; for example, the capacity given above is ideal for detecting lines hidden within lots of noise. In this case, a slight modification can be applied that counts the number of 'similar' values,

$$c_{x,y}(i) = \text{card}\left\{(m,n) \ \text{ such that } \ |f_{m,n} - f_{x,y}| < 3, \ m,n \in W\right\}.$$

All of these resulting images can be used as measure images that can be used within the segmentation and clustering algorithms. This provides a first order digital approximation to multi-fractal image analysis.

18.13 Case Study: Fractional Light Diffusion

In Chapter 15, a diffusion model for light was derived compounded in the diffusion equation for the intensity of light I given by

$$\left(\nabla^2 - \frac{1}{D}\frac{\partial}{\partial t}\right) I(\mathbf{r}, t) = 0$$

where D is the diffusivity. In terms of a random phase walk model (see Chapter 17), this equation represents the case when the intensity of light measured is the result of strong multiple scattering by an optical diffuser, the most likely resultant amplitude after a time t being given by $a\sqrt{t}$ where a is the mean free path (of propagation). For a deterministic or coherent phase walk, the resultant amplitude is given by at. This is equivalent to the case when scattering is a weak perturbation of the incident field, compounded in the use of a constant phase value $\theta << 1$. Physically, a deterministic phase walk describes a propagative rather than a diffusive process which is compounded in the solution to the wave equation

$$\left(\nabla^2 - \frac{1}{c^2}\frac{\partial^2}{\partial t^2}\right) u(\mathbf{r}, t) = 0$$

where c is the wave speed and $I =\mid u \mid^2$. It is therefore of value to consider a solution to the fractional diffusion equation given by

$$\left(\nabla^2 - \frac{1}{D^q}\frac{\partial^q}{\partial t^q}\right) I(\mathbf{r}, t) = 0, \quad 1 < q < 2$$

where D is the fractional diffusivity and q is the Fourier dimension, as a description for the case when the scattering processes are intemediate (neither strong nor weak scattering) - the case of a fractional diffuser. This is analagous to the case of fractional Brownian motion with scaling law at^H where $0.5 < H < 1$ is the Hurst exponent.

In this Section we consider the solution to the fractional diffusion equation above and derive a method of fractional de-diffusion (the inverse of diffusion) which is analagous to the high emphasis filter for the fully diffusive case. This provides another approach to computing the Fourier dimension that can be used to segment a fractal image.[2]

18.13.1 Green Function Solution to the Fractional Diffusion Equation

Consider the fractional diffusion equation for the intensity I given by

$$D^q \nabla^2 I(\mathbf{r}, t) = \frac{\partial^q}{\partial t^q} I(\mathbf{r}, t)$$

where D is the fractional diffusivity and $I_0(\mathbf{r}) = I(\mathbf{r}, t = 0)$ (the initial condition). For $q = 1$, the solution to this equation in the infinite domain (see Chapter 5) for dimensions $n = 1, 2$ and 3 is (with $\sigma = 1/D$)

$$I(\mathbf{r}_0, \tau) = \sigma \int I_0(\mathbf{r}) G(\mathbf{r} \mid \mathbf{r}_0, \tau) d^n \mathbf{r}.$$

Here,

$$G(R, \tau) = \frac{1}{\sigma}\left(\frac{\sigma}{4\pi\tau}\right)^{\frac{n}{2}} \exp\left[-\left(\frac{\sigma R^2}{4\tau}\right)\right] H(\tau)$$

[2]This case study is based on a research project undertaken by the author for Microsharp Corporation Limited, England

which is the solution to

$$\left(\nabla^2 - \sigma\frac{\partial}{\partial t}\right) G(R,\tau) = -\delta^n(R)\delta(\tau).$$

For the functional case, let us consider the same basic solution but where the Green function is given by the solution of

$$\left(\nabla^2 - \sigma^q\frac{\partial^q}{\partial t^q}\right) G(R,\tau) = -\delta^n(R)\delta(\tau)$$

where $\sigma^q = 1/D^q$. Using the Riesz operator for the time derivative (see Appendix A), we can transform this equation into the form

$$(\nabla^2 + \Omega_q^2) g(\mathbf{r} \mid \mathbf{r}_0, \omega) = -\delta^n(\mathbf{r} - \mathbf{r}_0)$$

where

$$g(\mathbf{r} \mid \mathbf{r}_0, \omega) = \int_{-\infty}^{\infty} G(\mathbf{r} \mid \mathbf{r}_0, \tau)\exp(i\omega\tau)d\tau,$$

$$\Omega_q^2 = -i\omega\sigma, \Omega_q = \pm i(i\omega\sigma)^{q/2}.$$

For $q = 2$, this equation becomes

$$(\nabla^2 + k^2) g(\mathbf{r} \mid \mathbf{r}_0, \omega) = \delta^n(\mathbf{r} - \mathbf{r}_0)$$

where $k = \pm\omega\sigma$. This equation defines the Green function for the time independent wave operator in n dimensions, the 'out going' Green functions being given by (see Part II, Chapter 6)

$n = 1$:

$$g(r \mid r_0, k) = \frac{i}{2k}\exp(ik \mid r - r_0 \mid);$$

$n = 2$:

$$g(\mathbf{r} \mid \mathbf{r}_0, k) = \frac{i}{4}H_0(k \mid \mathbf{r} - \mathbf{r}_0 \mid)$$

$$\simeq \frac{1}{\sqrt{8\pi}}\exp(i\pi/4)\frac{\exp(ik \mid \mathbf{r} - \mathbf{r}_0 \mid)}{\sqrt{k \mid \mathbf{r} - \mathbf{r}_0 \mid}}, \quad k \mid \mathbf{r} - \mathbf{r}_0 \mid >> 1$$

where H_0 is the Hankel function, and

$n = 3$:

$$g(\mathbf{r} \mid \mathbf{r}_0, k) = \frac{1}{4\pi \mid \mathbf{r} - \mathbf{r}_0 \mid}\exp(ik \mid \mathbf{r} - \mathbf{r}_0 \mid), \quad n = 3.$$

Generalizing these results, for $q \in [1, 2]$, by writing the exponential function in its series form, with $R = \mid \mathbf{r} - \mathbf{r}_0 \mid$ we have, for $\Omega_q = i(i\omega\sigma)^{q/2}$,

$n = 1$:

$$G(R,\tau) = \frac{1}{2\pi}\int_{-\infty}^{\infty}\frac{i}{2\Omega_q}\exp(i\Omega_q R)\exp(i\omega\tau)d\omega$$

$$= \frac{1}{2\pi}\int_{-\infty}^{\infty} d\omega \exp(i\omega\tau)\frac{i}{2(i\omega\sigma)^{q/2}}\left(1 - R(i\omega\sigma)^{q/2} + \frac{R^2}{2!}(i\omega\sigma)^q - ...\right)$$

$$= \frac{1}{2\sigma^{q/2}}\frac{1}{\tau^{1-(q/2)}} - \frac{1}{2}R\delta(\tau) + \sum_{n=1}^{\infty}\frac{(-1)^{n+1}}{2(n+1)!}R^{n+1}\sigma^{nq/2}\delta^{qn/2}(\tau);$$

$n = 2$:

$$G(R,\tau) = \frac{1}{2\pi}\int_{-\infty}^{\infty} d\omega \exp(i\omega\tau)\frac{\exp(i\pi/4)}{\sqrt{8\pi}}\frac{\exp[-(i\omega\sigma)^{q/2}R]}{\sqrt{iR}(i\omega\sigma)^{q/4}}$$

$$= \frac{1}{\sqrt{8\pi R}}\frac{1}{2\pi}\int_{-\infty}^{\infty} d\omega \exp(i\omega\tau)\left(\frac{1}{(i\omega\sigma)^{q/4}} - (i\omega\sigma)^{q/4}R + \frac{1}{2!}(i\omega\sigma)^{3q/4}R^2 - ...\right)$$

$$= \frac{1}{\sqrt{8\pi R}}\frac{1}{\sigma^{q/4}\tau^{1-q/4}} - \sqrt{\frac{R}{8\pi}}\sigma^{q/4}\delta^{q/4}(\tau)$$

$$+\frac{1}{\sqrt{8\pi}}\sum_{n=1}^{\infty}\frac{(-1)^{n+1}}{(n+1)!}R^{(2n+1)/2}\sigma^{3nq/4}\delta^{3nq/4}(\tau);$$

$n = 3$:

$$G(R,\tau) = \frac{1}{2\pi}\int_{-\infty}^{\infty} d\omega \exp(i\omega\tau)\frac{\exp[-(i\omega\sigma)^{q/2}R]}{4\pi R}$$

$$= \frac{1}{4\pi R}\frac{1}{2\pi}\int_{-\infty}^{\infty} d\omega \exp(i\omega\tau)[1 - (i\omega\sigma)^{q/2}R + \frac{1}{2!}(i\omega\sigma)^q R^2 - ...]$$

$$= \frac{\delta(\tau)}{4\pi R} - \frac{1}{4\pi}\sigma^{q/2}\delta^{q/2}(\tau) + \frac{1}{4\pi}\sum_{n=1}^{\infty}\frac{(-1)^{n+1}}{(n+1)!}R^n\sigma^{(n+1)q/2}\delta^{(n+1)q/2}.$$

These are the Green functions for the fractional diffusion equation in one-, two- and three-dimensions. Simplification of these infinite sums can be addressed be considering suitable asymptotics, the most significant of which (for arbitrary values of R) is the case when the (fractional) diffusivity D is large. In particular, we note that, as $\sigma \to 0$,

$$g(R,\tau) = \frac{1}{2\sigma^{q/2}\tau^{1-(q/2)}} - \frac{1}{2}R\delta(\tau), \quad n = 1;$$

$$g(R,\tau) = \frac{1}{\sqrt{8\pi R}\sigma^{q/4}\tau^{1-(q/4)}}, \quad n = 2;$$

$$g(R,\tau) = \frac{\delta(\tau)}{4\pi R}, \quad n = 3.$$

Thus, in 2D, we can consider a solution to the fractional diffusion equation

$$\left(D^q\nabla^2 - \frac{\partial^q}{\partial t^q}\right)I(\mathbf{r},t) = 0, \quad I(\mathbf{r},t=0) = I_0(\mathbf{r})$$

of the form (for $t_0 = 0$ and at time $t = T$)

$$I(x,y) = \frac{1}{2\sqrt{2\pi}} \frac{1}{(DT)^{1-q/4}} \frac{1}{(x^2+y^2)^{\frac{1}{4}}} \otimes\otimes I_0(x,y), \quad D \to \infty$$

which should be compared with the solution to the 2D diffusion equation, i.e. (see Chapter 5)

$$I(x,y) = \frac{1}{4\pi DT} \exp\left[-\left(\frac{x^2+y^2)}{4DT}\right)\right] \otimes\otimes I_0(x,y).$$

We see that when the diffusivity is large and the diffusion time $t = T$ is small such that $DT = 1$, the difference between an image obtained by a full 2D diffuser (see Chapter 15) and a fractional 2D diffuser is compounded in the difference between the convolution of the initial image with (ignoring scaling) the functions $\exp(-R^2/4)$ and $1/\sqrt{R}$. Compared with the Gaussian, the function $R^{-1/2}$ decays more rapidly and hence will have broader spectral characteristics. This leads to an output that is less blurred than that produced by the convolution of the input with a Gaussian which, in the context of the fractional diffusion model introduced, is to be expected.

Optical diffusers are used in a range of applications including the depixelation of Liquid Crystal Displays (LCDs). This becomes especially important when the LCD is composed of relatively few elements and is viewed at close range, e.g. LCD goggles. A common technique is to produce a thin film that is composed of a randomly distributed complex of scatterers (microspheroids whose relative permittivity is different from that of the body of the film) that is overlaid onto the LCD. The goal is to produce a diffuser that 'manages' the light in such a way that it depixelates the LCD while minimizing the angular distribution of light. This requires the manufacture of a fractional optical diffuser, an example of which is given in Figure 18.22. This shows the effect of a 'light management film' manufactured by Microsharp Corporation Limited (http://www.microsharp.co.uk).

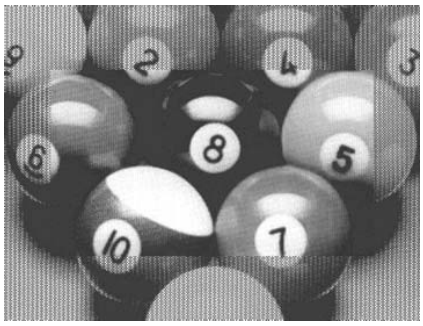

Figure 18.22: Illustration of the application of a fractional optical diffuser to a low resolution LCD. The effect of the diffuser is to eliminate the pixelation (central area) generated by the regular LCD lattice (edges) while minimizing the angular field of view.

18.13.2 Fractional De-Diffusion

Let I_0 be represented as a Taylor series at some time $T > 0$, i.e.

$$I(\mathbf{r},0) = I(\mathbf{r},T) + T\left[\frac{\partial}{\partial t}I(\mathbf{r},t)\right]_{t=T} - \frac{T^2}{2!}\left[\frac{\partial^2}{\partial t^2}I(\mathbf{r},t)\right]_{t=T} + ...$$

Now since

$$\frac{\partial u}{\partial t} = \frac{\partial^{1-q}}{\partial t^{1-q}}\frac{\partial^q}{\partial t^q}u$$

then from the fractional diffusion equation

$$\frac{\partial u}{\partial t} = D^q\frac{\partial^{1-q}}{\partial t^{1-q}}\nabla^2 u$$

and

$$\frac{\partial^2}{\partial t^2}u = \frac{\partial}{\partial t}\left(\frac{\partial u}{\partial t}\right) = \frac{\partial}{\partial t}\left(D^q\frac{\partial^{1-q}}{\partial t^{1-q}}\nabla^2 u\right) = D^q\frac{\partial^{1-q}}{\partial t^{1-q}}\nabla^2\frac{\partial u}{\partial t}$$

$$= D^q\frac{\partial^{1-q}}{\partial t^{1-q}}\nabla^2\left(D^q\frac{\partial^{1-q}}{\partial t^{1-q}}\nabla^2 u\right) = D^{2q}\frac{\partial^{1-q}}{\partial t^{1-q}}\left(\frac{\partial^{1-q}}{\partial t^{1-q}}\nabla^4 u\right)$$

so that, in general,

$$\frac{\partial^n u}{\partial t^n} = D^{nq}\frac{\partial^{n(1-q)}}{\partial t^{n(1-q)}}\nabla^{2n}u.$$

Now, the operator

$$\frac{\partial^{-q}}{\partial t^{-q}}$$

defines a fractional intgral. Using the Riemann-Liouville definition for a fractional integral[3],

$$\frac{\partial^{-q}}{\partial t^{-q}}I(\mathbf{r},t) = \frac{1}{\Gamma(q)t^{1-q}}\otimes I(\mathbf{r},t)$$

and we can write the Taylor series for the field at $t = 0$ in terms of the field at $t = T$ as

$$I(\mathbf{r},0) = I(\mathbf{r},T) + \frac{TD^q}{\Gamma(q)}\left[\frac{\partial}{\partial t}\left(\frac{1}{t^{1-q}}\otimes\nabla^2 I(\mathbf{r},t)\right)\right]_{t=T}$$

$$-\frac{T^2D^{2q}}{2!\Gamma(2q)}\left[\frac{\partial^2}{\partial t^2}\left(\frac{1}{t^{1-2q}}\otimes\nabla^4 I(\mathbf{r},t)\right)\right]_{t=T}$$

$$+\frac{T^3D^{3q}}{3!\Gamma(3q)}\left[\frac{\partial^3}{\partial t^3}\left(\frac{1}{t^{1-3q}}\otimes\nabla^6 I(\mathbf{r},t)\right)\right]_{t=T} - ...$$

For the case when $T << 1$,

$$I(\mathbf{r},0) = I(\mathbf{r},T) + \frac{TD^q}{\Gamma(q)}\left[\frac{\partial}{\partial t}\left(\frac{1}{t^{1-q}}\otimes\nabla^2 I(\mathbf{r},t)\right)\right]_{t=T}$$

[3]see Blackledge J M, *Digital Signal Processing* Horwood, 2003 - Chapter 17.

and under the condition that

$$\left[\frac{\partial}{\partial t}\left(\frac{1}{t^{1-q}} \otimes I(\mathbf{r},t)\right)\right]_{t=T} = I(\mathbf{r},T)$$

we can write

$$I(\mathbf{r},0) = I(\mathbf{r},T) + \frac{TD^q}{\Gamma(q)}\nabla^2 I(\mathbf{r},T).$$

Thus, for an image $I(x,y)$ recorded in the image plane at $z=0$, say, after the image I_0 has been fractionally diffused over a period of time T, we have

$$I_0(x,y) = I(x,y) + \frac{TD^q}{\Gamma(q)}\nabla^2 I(x,y).$$

18.13.3 Image Segmentation Metric

The result above provides us with an approach to estimating q given I and I_0 as follows: let

$$P(x,y) = \mid I_0(x,y) - I(x,y) \mid, \quad \text{and} \quad Q(x,y) = \mid \nabla^2 I(x,y) \mid$$

then, with $R(x,y) = P(x,y)/Q(x,y)$,

$$\langle R(x,y)\rangle = \frac{TD^q}{\Gamma(q)}$$

where

$$\langle R(x,y)\rangle = \frac{\int\int R(x,y)dxdy}{\int\int dxdy}.$$

Hence,

$$\ln T - \ln\Gamma(q) + q\ln D = M$$

where M is the metric (i.e. a measure of q) given by

$$M = \ln\langle R\rangle \leq \ln\left(\frac{\langle P\rangle}{\langle Q\rangle}\right).$$

For an image I which has been formed by the fractional diffusion of a uniform light source in which I_0 is a constant,

$$I - I_0 = \frac{TD^q}{\Gamma(q)}\nabla^2(I - I_0)$$

and with $J = I - I_0$

$$M = \ln\left(\frac{\langle J(x,y)\rangle}{\langle \mid \nabla^2 J(x,y) \mid\rangle}\right)$$

which can be applied on a moving window W basis in order to segment an image formed through short time fractional diffusion with variable q. The computation of $\langle I\rangle_{(x,y)\in W}$ (the moving average filter) and $\langle \mid \nabla^2 I \mid\rangle_{(x,y)\in W}$ (moving average of the second order edge detector) is relatively simple. The

averaging process is optional and, depending upon the application, M can be computed directly from an image I using the result

$$M(x,y) = \ln[I(x,y)] - \ln[\nabla^2 I(x,y)].$$

An application example is given in Figure 18.23 for an image generated by the scattering of a uniform laser light field incident on an aerosol obtained from the injection of fuel into the combustion chamber of a gas turbine engine.

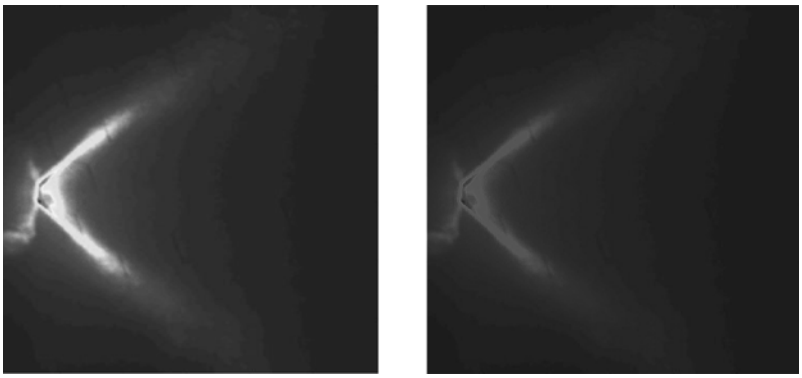

Figure 18.23: Image (left) generated by the scattering of a uniform laser light source from a fuel aerosol recorded in the plane and an image of $\mid M \mid$ (right).

18.13.4 Discussion

The use of a fully diffusive process for modelling strong (multiple) scattering has been extended to model intermediate scattering by generalizing the diffusion equation to fractional order $q \in (1,2)$. The rationale for this approach follows that of a random walk model in which diffusive processes characterized by a $t^{\frac{1}{2}}$ scaling law and propagative processes characterized by a t^1 scaling law are generalized to a scaling law of the form t^H, where $\frac{1}{2} < H < 1$ is the Hurst exponent. The homogeneous diffusion equation provides a series solution to the inverse problem in which a Gaussian blurred image can be restored using an appropriate FIR filter which depend on the order of the solution that is considered (i.e. the number of terms in the Taylor series). This approach can be extended to include fractional diffusion by computing the appropriate Green function in terms of an infinite series which, for the case when the (fractional) diffusivity D is large, reduces to the form $R^{-1/2}$ for the two-dimensional case. A FIR filter (a fractional high emphasis filter) can then be designed which scales as $TD^q/\Gamma(q)$ compared with TD for the fully diffusive case when $T << 1$. This leads to the proposition of a new algorithm for segmenting an image into regions of similarity based on a measure of the Fourier dimension q - the metric M.

18.14 Summary of Important Results

Basic fractal equation

$$Nr^D = 1, \quad D = -\frac{\ln N}{\ln r}$$

Basic fractal signature

$$\text{System(size)} \propto \frac{1}{(\text{size})^q}, \quad q > 0$$

Deterministic self-affinity

$$f(a\mathbf{r}) = a^q f(\mathbf{r})$$

Stochastic self-affinity

$$\Pr[f(a\mathbf{r})] = a^q \Pr[f(\mathbf{r})]$$

PSDF for a statistical self-affine fractal

$$P(k) = \frac{c}{k^\beta}, \quad \beta = 2q$$

where c is a constant

Measure theoretic estimation of the fractal dimension

$$D = -\left\langle \frac{\ln N(\delta)}{\ln \delta} \right\rangle$$

Bi-logarithmic least square estimate

For an n-dimensional fractal of size N^n

$$\beta = \frac{N^n \sum_i \sum_j \ldots (\ln P_{ij\ldots})(\ln k_{ij\ldots}) - \left(\sum_i \sum_j \ldots \ln k_{ij\ldots}\right)\left(\sum_i \sum_j \ldots \ln P_{ij\ldots}\right)}{\left(\sum_i \sum_j \ldots \ln k_{ij\ldots}\right)^2 - N^n \sum_i \sum_j \ldots (\ln k_{ij\ldots})^2}$$

and

$$C = \frac{1}{N^n} \sum_i \sum_j \ldots \ln P_{ij\ldots} + \frac{\beta}{N^n} \sum_i \sum_j \ldots \ln k_{ij\ldots}$$

Relationship between D, D_T, H and $\beta = 2q$

$$D = D_T + 1 - H = D_T + 1 - \frac{\beta - D_T}{2} = \frac{3D_T + 2 - \beta}{2},$$

Equation for an isotropic random scaling fractal

$$\nabla^q u(\mathbf{r}) = n(\mathbf{r})$$

Equation for a tailored RSF surface

$$\nabla^q u(\mathbf{r}) = (1-t)n(\mathbf{r}) + tf(\mathbf{r}), \quad t \in (0,1)$$

Equation for a divergent RSF surface

$$\nabla^q \cdot \mathbf{u}(\mathbf{r}) = n(\mathbf{r}), \quad \mathbf{r} \in A$$

Equation for a rotational RSF surface

$$\nabla^q \times \mathbf{u}(\mathbf{r}) = \mathbf{n}(\mathbf{r}), \quad \mathbf{r} \in A.$$

Equation for a generalized random scaling fractal

$$\nabla^2 u(\mathbf{r}) = \exp(k_0 \hat{\mathbf{n}} \cdot \mathbf{r}) \nabla^p n(\mathbf{r})$$

Fractional Diffusion Equation

$$\left(\nabla^2 - \frac{1}{D^q}\frac{\partial^q}{\partial t^q}\right) I(\mathbf{r}, t) = 0$$

Fractional Diffusion Segmentation Metric

$$M = \ln\left(\frac{\langle I \rangle}{\langle \mid \nabla^2 I \mid \rangle}\right)$$

18.15 Further Reading

- Mandelbrot B B, *Fractals: Form, Chance and Dimension*, Freeman, 1977.
- Mandelbrot B B, *The Fractal Geometry of Nature*, Freeman, 1983.
- Barnsley M F, Dalvaney R L, Mandelbrot B B, Peitgen H O, Saupe D and Mandelbrot R F, *The Science of Fractal Images*, Springer, 1988.

- Barnsley M F, *Fractals Everywhere*, Academic Press, 1988.
- Feder J, *Fractals*, Plenum Press, 1988.
- Kaye B, *A Random Walk Through Fractal Dimensions*, VCH Publishers, 1989.
- Falconer K J, *Fractal Geometry*, Wiley, 1990.
- Peitgen H O, Jürgens H and Saupe D, *Chaos and Fractals: New Frontiers of Science*, Springer, 1992.
- Turner M J, Blackledge J M and Andrews P R, *Fractal Geometry in Digital Imaging*, Academic Press, 1997
- Blackledge J M (Ed.), *Image Processing: Mathematical Methods and Applications*, Oxford University Press, 1998.
- Barnsely M F, Saupe D and Vrscay E R (Eds.) *Fractal in Multimedia*, IMA Volumes in Mathematics and its Applications, Springer, 2002.
- Blackledge J M, Evans A K and Turner M J (Eds.), *Fractal Geometry: Mathematical Methods, Algorithms and Applications*, Horwood Publishing Series in Mathematics and Applications, 2002.

Chapter 19

Coding and Compression

Image coding and compression is used mainly for data storage, the transmission of digital images over a network and in some cases for encryption. In this final Chapter[1] we discuss the current popular methods of coding images and compressing image data. First, we take a general look at why compression is important and then study some of the more popular compression techniques including the JPEG standard and, following the material discussed in the previous chapter, fractal image compression.

19.1 The Reasons for Compression

The first major practical uses of continuous tone digital images were on early telegraph lines, at the beginning of the Twentieth Century. The most common initial technique was to use specially created character sets that simulate a halftone pattern. This allowed an image to be transmitted by regular telegraph personnel. With the interest in news pictures, whose value is only high while the news is 'hot', cables were installed connecting the main capitals of the western world. Earlier, images crossing the Atlantic by ship took the better part of a week or more.

In 1921 publication of the first pictures transmitted between the *Daily Mirror* in London and the *Daily News* in New York established the Bartlane system. This was one of the first image coding schemes to be patented. The system reduced the transmission time across the Atlantic to a matter of two or three hours per picture. It remained in successful operation, dealing with nearly 500 pictures of important news events, prior to the outbreak of the Second World War in 1939. Then practical digital image compression techniques started to be used.

There are two main forms of compression; either lossless, where no information is lost and an exact copy of the image is reproduced, or lossy, where only an approximation to the original is created. For important data, including scientific and medical images, lossless coding has often been considered essential.

[1]Based on material from: Turner M J, Blackledge J M and Andrews P A, 'Fractal Geometry in Digital Imaging', Academic Press, 1998.

This is because the possible future uses of the data could easily be unknown and a degree of loss in fidelity might be unacceptable. Note that data resulting from any lossy method is often compressed itself with a lossless method.

19.2 Lossless Coding Methods

One of the first uses of digital image lossless compression was with the encoding and storage of Landsat Satellite images. Landsat 1, formerly known as ERTS-A (Earth Resources Technology Satellite-A), launched on July 23, 1972, was the first of a series of satellites designed to point toward the Earth. The resulting reliability, use and longevity of this satellite series caused a problem when the image data needed to be stored. The original Landsat 1 lasted six times longer than its designed life expectancy, creating, as a consequence, six times as much data. These satellites can produce megabytes a day, which is a reasonable amount of data today. Unfortunately, back in the 1970s, the data had to be stored on many large digital tapes in a carefully controlled environment. The resulting storage requirements were reflected in the cost of using expensive warehouse facilities. Lossless compression was required as the exact final use of the data was unknown and it was believed to be unacceptable to throw any piece of information away. Analysing the statistical nature of the images resulted in a reduction by a factor of two or three which relates directly to a saving of storage space and cost. Modern lossless coding methods are now used in all kinds of data transfer and storage, from simple modem links or facsimile machines to the general purpose archiving of data. Most of these methods use one of two main techniques, or possibly a combination:

Probability or statistical coding

Coding methods that exploit the fact that most digital information is not random and it is possible to predict values. These techniques code each input symbol into a variable length code determined by how likely it is to occur.

Dictionary or substitution coding

Methods that store either with explicit direction or by learning strings of symbols which are more likely to occur. These techniques code a sequence of input symbols into a fixed or variable length code.

19.2.1 Probability Coding

A probability coder is one which when given a probability of occurrence for each possible input symbol, p_i, produces a code for each symbol such that its length is inversely proportional to its probability. An optimal probability coder is one which produces an average code length equal to Shannon's entropy formula

$$E = -\sum_{i=0}^{N-1} p_i \log_2 \frac{1}{p_i}.$$

Shannon-Fano Coding

Shannon's coding scheme, which was discovered independently by R M Fano and C E Shannon, uses the simple algorithm:

- Divide the set into two almost equal halves based on the probabilities.
- Mark one half with a 0 and the other with a 1.
- Repeat the division until each half contains just one item.

This forms a binary tree that gives an average code length for the symbols which lie between $[E, E + 1]$. Note that Shannon-Fano coding does not necessarily produce optimal codes for any given set of symbols.

Huffman Coding

Shortly afterwards, D A Huffman developed the Huffman coder. Huffman codes are described as an optimal probability coder when all the probabilities are integral powers of $\frac{1}{2}$. For any set of symbols there are possibly many Huffman codes and an algorithm for deterministically creating one of these codes is as follows:

- List all symbols in order of probability.
- Successively combine the two symbols of the lowest probability to form a composite symbol with joint probability, marking one side with a 0 and the other with a 1.
- Once a complete binary tree is formed, the code representing each leaf symbol is the path to that leaf.

It is also possible to create a canonical Huffman tree, which has all its leaves at unique depths in the tree, with minimal loss of efficiency. This allows each leaf to be represented compactly as a single bit length. It should be noted that this code does not have any codeword as a prefix of another codeword. This is called a prefix-free or comma-free code.

Arithmetic Coding

As stated above, Huffman and Shannon-Fano codes are only optimal when probabilities are integral powers of $\frac{1}{2}$. When probabilities of actual symbols do not fit this criterion either a poor code is produced or joint probabilities of symbols have to be considered, which increases the complexity. AC (Arithmetic Coding) is a technique which codes the stream of input symbols into a real number in the range $[0, 1)$. Each input symbol is given a sub-range proportional to the size of its probability, and encoding a symbol is achieved by returning any number in its sub-range. To make the process iterative, the whole sub-range is returned and this is used as the new current range to encode the next

symbol. In practice, AC can be implemented for speed using scaled arithmetic on up to 256 symbols with up to 12 bits of information for probabilities. This slight approximation does not affect the performance, which for long coded sequences approaches Shannon's entropy.

The coder should be thought of and implemented separately from the *model*, which allows for adaptive models to exist. By adjusting the symbol probabilities as symbols arrive it is possible to have the model adjust as the input stream changes. The most common form of adaptation is simply to keep a frequency count of all symbols and divide this by the total number of frequencies to obtain the probability. When the sum of the frequencies is greater than a pre-defined maximum, all the frequencies are halved. Adaptive models out-perform static models for virtually all data streams.

Separating the model from the coder means that it is relatively easy to change the probabilities on the fly. This means that reducing the number of symbols to code is a simple matter of specifying the redundant symbols probabilities as zero. The arithmetic coder, as specified, caters for up to 256 symbols with a range from $[0, 1)$ specified using 12-bit fixed arithmetic. Versions which can handle 2^{16} symbols and up to 24-bit precision are used when extra flexibility is required.

19.2.2 Fractal Analysis of Arithmetic Coding

An alternative way of visualising arithmetic coding is as a fractal multi-lens photocopier. Consider that there is a lens for each symbol, i, with the two important properties that none of the resulting images overlap and the full image is covered by the sum of all the lenses. The scaling of the image for each lens is proportional to the probability that the symbol the lens represents occurs, p_i. Now, given a known seed position, consisting of a single dot, x_0, encoding a string of n symbols is then a process of iteratively choosing the lens that corresponds to the next character and transforming with this lens.

Given the number of characters in the input string, n, and the final position of the dot, x, the operations of an arithmetic coder have been performed and the original message can be retrieved without error. For this fractal photocopier machine to act like a perfect arithmetic coder the lenses should not only be non-overlapping but also need to cover the area fully.

If each of the lenses shrinks the image by a factor of $1/p_i$ then any value in a region $x_k \in I_k$ that is base 2 accurate will be sufficiently accurate to represent the dot, x. If we define that the input stream contains n_i occurrences of symbol i whose probability is p_i, the minimum number of bits required to represent x_k is

$$\text{Length of Output Stream} = -\log_2 \prod_{i=1}^{n} p_i^{n_i}.$$

The resulting compression ratio is then given by

$$\begin{aligned}\frac{\text{Length of Output Stream}}{\text{Length of Input Stream}} &= -\frac{1}{N}\log_2 \prod_{i=1}^{n} p_i^{n_i} \\ &= -\sum_{i=1}^{n} \frac{n_i}{N}\log_2 p_i\end{aligned}$$

where

$$N = \sum_{j=1}^{n} n_j$$

and for a large input string,

$$\frac{n_i}{N} = \frac{n_i}{\sum_{j=1}^{n} n_j} \approx p_i.$$

This means the compression ratio approaches first order Shannon's entropy, E.

19.2.3 Dictionary or Substitution Coding

The basic idea behind substitution coders is to replace an occurrence of a phrase or sequence of bytes by a reference to a previous occurrence of that phrase. There are two main families of coders named after Jakob Ziv and Abraham Lempel who first proposed them.

LZ77: Window Substitution Compression

LZ77 coders have a window of the last n bytes of data encountered. When a new phrase is in this window, it is encoded as a displacement and a length. The most common implementation is derived from the LZSS scheme. The LZSS maintains both an n byte *window* and a *lookahead buffer*. The coding algorithm is as follows:

```
loop until lookahead buffer empty
    get a pointer (position, match) to the longest match
    if length > MINIMUM MATCH LENGTH
      output a (position, length) pair
      shift the window length character along
    else
      output the first character in the lookahead buffer
      shift the window 1 character along
    end if
end loop
```

Variants of this method apply extra coding to the output stream; these have included simple variable-length code (LZB) and dynamic Huffman code (LZH). Most of the popular commercial archivers, including *pkzip*, are variants of the LZ77 algorithm.

LZ78: Dictionary Compression

LZ78 coders work by storing phrases into a dictionary and substituting phrases as dictionary entries. The most popular implementation is T Welch's LZW. In LZW a 4K dictionary is used, initially with the 256 individual bytes. The remaining 3840 entries refer to phrases. The coding algorithm is as follows:

S = NULL
loop until end of stream
    E = INPUT SYMBOL
    if S*E exists in the dictionary
        $S = S$*E
    else
        output dictionary code for phrase S
        store S*E in dictionary
        $S = E$
    end if
end loop
output dictionary code for phrase S

As the dictionary is built up during the coding process no entries need to be transmitted. A variant LZC, used in the UNIX *compress* program, have variable length dictionary pointers starting at 9 bits. Alternative versions include LZT, which uses a least-recently-used algorithm to discard and replace uncommon phrases once the dictionary becomes full, and LZMW, which concatenates the previous two phrases rather than just concatenating single characters.

19.3 Lossy Coding Methods

Different lossless coding techniques can be simply compared by measuring the compression ratios for different sources. Unfortunately, the compression ratios achievable are often fairly low. Heavily textured images are rarely compressed by more than a factor of two, if at all. To gain higher compression ratios a solution is to encode only an approximate representation of the image data. For images which are to be presented and analysed visually, the loss of quality or fidelity can be imperceptible with reasonable levels of compression ratio, up to 20-60 to 1.

The emphasis on lossless compression is understandable, but attitudes have changed as lossy compression methods are more clearly understood. Satellite images are now being distributed in a lossy form for speed of access with the original lossless data being made available when required. Many satellites now have a lossy compression mode on-board to speed up image transmission with, in certain cases, no uncompressed original data being transmitted at all. Another sector is medical imaging which for years has resisted lossy compression methods mainly for legal and liability reasons. However, the use of very well controlled lossy techniques within this sector is now being undertaken. This

has involved as much legal scrutiny as technical in order for this new standard to be usable within a hospital[2]

19.3.1 Joint Photographic Expert Group (JPEG)

The JPEG standard incorporates different modes of image compression. The most common method is baseline sequential compression using the discrete cosine transform. The compression system applies the following algorithm[3]

```
split the image up into 8 × 8 blocks
for each block
    transform using the Forward Discrete Cosine Transform and
    quantise the 64 coefficients according to a quality parameter
    output the DC term, as the difference from the previous DC
    for each of the other 63 coefficients
        if the coefficient is non-zero
          output the number of proceeding zeros
          output the coefficient value
        end if
    end for
end for
```

The output stream is entropy encoded using either an arithmetic or Huffman coder. Decompression is achieved by applying the reverse operations. It is the quantisation stage which results in a high compression ratio as well as reducing the quality of the image.

The discrete cosine transform is a variant on the Fourier transform and for a fixed size, in this case 64 elements, can be specified as a real matrix. The forward and inverse DCT for this specific case are given by

$$a_{kl} = \frac{1}{4} K_k K_l \sum_{i=0}^{7} \sum_{j=0}^{7} f_{ij} \cos \frac{(2i+1)k\pi}{16} \cos \frac{(2j+1)l\pi}{16}, \; 0 \leq k, \quad l \leq 7,$$

$$f_{ij} = \frac{1}{4} \sum_{k=0}^{7} \sum_{l=0}^{7} K_k K_l a_{kl} \cos \frac{(2i+1)k\pi}{16} \cos \frac{(2j+1)l\pi}{16}, \; 0 \leq k, \quad l \leq 7$$

where

$$K_n = \begin{cases} \frac{1}{\sqrt{2}}, & n = 0; \\ 1, & 1 \leq n \leq 7. \end{cases}$$

[2]The official algorithm involved in the lossless JPEG standard has never been popular and can be consistently surpassed with alternative compressors. The ISO JPEG committee did launch a new lossless standard JPEG-LS in the mid-1990s that has a highly controlled near lossless mode.

[3]The coefficient that scales the constant basis function is called the DC term and the other 63 coefficients are called AC terms. This relates historically to the use of the DCT for analysing electrical circuits that have both direct and alternating currents.

The coefficients a_{kl} are then quantised by a user definable array q_{kl}, giving

$$a'_{kl} = \text{Round}\left(\frac{a_{kl}}{q_{kl}}\right).$$

The coefficients in the quantisation array are based upon the human visual system with less emphasis given to higher frequencies to which it is less sensitive.

19.3.2 Segmentation Based Compression

We describe one of the many different segmentation techniques. The Contour Tree File Format (CTFF) is an image descriptor designed to store the two dimensional spatial structure of an image as a set of nodes. Each node consists of a homogeneous region, for example constant colour. Three parameters completely define a contour node: a colour value, an absolute location and a boundary description that describes the outside edge of the contour. A set of contour nodes then defines the whole image. The parameter information describing this set of contour nodes splits into three streams to be coded by a modified adaptive arithmetic coder. The contour tree format can easily deal with all different types of imagery, including continuous tone and colour images, within its structure.

For any particular image the list of contours can be very large. A hierarchical structure called a *contour tree* stores those contours totally enclosed by another contour as its children. The structure commences with an imaginary contour defining the image boundary and having all other contours as its children.

The structure defined is similar to a quadtree in the sense that nodes subdivide the image space, but all of its structure is dictated by the original image rather than by arbitrary division. This means that every single piece of information in the contour tree is related to the original image. In a similar way to the quadtree, the contour tree represents the entire image and for certain image types can provide an ideal lossless image compression system. This is one of the properties of the contour tree that makes it so useful for image representation. Other potential properties of the contour tree include using it as an intermediate format for doing fast spatial image operations on the tree directly rather than on a raster representation.

Once a contour tree has been created for the raster image, a simple algorithm can be developed to decide if two neighbouring contours should be merged together to form a larger single contour. Although this merging can result in a more complex contour, it is likely that the entropy of the whole contour tree is reduced. A single threshold value T is defined which may be increased to increase the amount of merging. There are four psychovisual based rules that govern the merging criteria:

(i) The size of the smaller contour is critical and its area is proportional to the possibility of being recognised as a separate region. The noticeability of an object to the human eye is proportional to its area.

(ii) The intensity ratio over background intensity is treated proportionally with the possibility of merger. Average light intensity follow Weber's rule, namely,

that there exists a value n under certain conditions such that a change in intensity δI is only noticed when it is greater than $n\%$ of the background intensity I. This is accurate only for average light intensities and short exposure times.

(iii) The Mach factor is considered for neighbouring intensities; this states that light objects appear lighter at the boundary with darker objects and vice-versa. The values of the overshoot of the response and its position are very subject dependent. Overshoot values of 50% the difference in intensity for bright edges, and 25% the difference in intensity for dark edges are considered. This means that intensity values brighter than the brightest and darker than the darkest have to be stored and dealt with within the contour structure.

(iv) The maximum 'historic' difference of contour intensity values is considered, not just the current value for each contour. This means that as a contour expands the intensities of its constituent contours are still considered.

Defining I_1 and I_2 to be the maximum 'historical' log intensity values for two contours, M to be the Mach adjusting function and S to specify the size of the smallest contour; then if $T > \text{Abs}[M(I_1) - M(I_2)] + S$ the contours should merge together. The algorithm used is iterative in operation:

```
sort the children of all nodes in order of size
flatten all contours in depth to first order
create a linked list of these semi-sorted contour nodes

for each contour I1 in linked list
    for all neighbouring contours I2
        select contour to minimise Abs[M(I1) − M(I2)]
    end for
    if T > Abs[M(I1) − M(I2)] + S
      merge contours together
      remove contours I1 and I2 from linked list
      add merged contour to end of linked list
    else
      remove contour I1 from linked list
    end if
end for
```

With careful choice of the above rules, it can be arranged so that the entropy for the combined contour node is less than the sum of the entropy of the two nodes. This provides a way of reducing the overall contour tree's entropy while increasing the compression ratio achieved during encoding.

19.4 Fractal Image Compression

Thus far, we have justified the use of compression techniques and discussed some of the popular algorithms used for image compression, in particular, the JPEG standard and the contour tree format. There are many different variants on all compression techniques such as the application of the wavelet transform (see *Digital Signal Processing*, Horwood, 2003, Chapter 5) instead of the cosine transform and continued improvements of vector quantization based methods.

We have seen that fractals can mimic other coders, for example within the arithmetic coder. This demonstrates the flexibility of the fractal transform. We now exploit the descriptive ability of fractal transforms and develop some techniques leading to a fractal image compressor.

An intriguing concept is that, if fractal geometry is so powerful at describing and creating a complex synthetic image, then inversely it should be an ideal candidate for representing and compressing natural images. To define a set of fractal transforms, we need to discuss the use of iterated function systems. This allows the conversion of an image into a set of simple transforms. A common metaphor to describe this process is the (hypothetical) creation of a multi-lens photocopier. This photocopier is similar to a normal photocopier with the following features:

- Each lens represents a copy of the original image which is transformed. This transformed image is allowed to overlap with any of the images of the other lenses.
- Each lens strictly reduces the size of the original image.
- The photocopier operates in an infinite loop, feeding back the output copy as the input to the next stage.

Each of the lenses acts as a transform code and the combination creates the Iterated Function System (IFS).

The main principle of fractal coding an image is the observation that self-similarity is found within images and is extractable. This employs an affine transform that has the following form:

$$w_i \begin{pmatrix} x \\ y \end{pmatrix} = \begin{pmatrix} a_i & b_i \\ c_i & d_i \end{pmatrix} \begin{pmatrix} x \\ y \end{pmatrix} + \begin{pmatrix} e_i \\ f_i \end{pmatrix} = \begin{pmatrix} a_i x + b_i y + e_i \\ c_i x + d_i y + f_i \end{pmatrix}.$$

The affine transform allows all possible two dimensional transformations, including rotation, shearing and translation as well as most the important issue of scaling to be performed. An IFS consists of a set of these transforms which in some way make up a whole image. Affine transforms are not the only kind of transform that can be used but they have proved themselves to be very convenient. The fundamental idea behind a fractal compression system is that if an image can be defined in terms of a self-similar set of transforms, and each transform can be described with an affine transform, then a complete

description of the image can be achieved within the numbers in the set of affine transforms.

Two properties need to be defined, that of *contractive mapping* which specifies that a final image is achievable and the *collage theorem* which shows how affine transforms can be combined.

19.4.1 The Contractive Mapping

The contractive mapping principle ensures that there exists a unique fixed point value. A transformation w is contractive on two points, x, y, if the distance, $d(\cdot)$, is of the form,

$$d(w(x), w(y)) < sd(x, y)$$

for some $s < 1$. This means that points will always be brought together, by a factor s. Thus, when a contractive transformation is repeated iteratively, the points will converge to a single point. This single point remains fixed and invariant with further transformations. Furthermore the Contractive Mapping Fixed Point Theorem states: 'If X is a complete metric space and $W : X \to X$ is contractive then W has a unique fixed point g'. To prove this we will use iteration. Given $x \in X$, create the sequence of points,

$$W^0(x) = x, W^1(x) = W(x), \ldots, W^i(x) = \overbrace{W(\ldots W}^{i}(x))\ldots).$$

Now, given the distance relation,

$$d(W^{i+1}(x), W^{i+2}(x)) < sd(W^i(x), W^{i+1}(x)).$$

So at each step the distance to the next point in the sequence is smaller than the distance from the previous point by a factor of $s < 1$. As we are taking geometric steps and the space has no gaps, being a metric space, we must converge onto a single point. Denote this fixed point

$$g = \lim_{i \to \infty} W^i(x)$$

which is unique. Consider that there are two fixed points, x_1 and x_2, so $W(x_1) = x_1$ and $W(x_2) = x_2$. As W is contractive, then

$$d(x_1, x_2) < sd(W(x_1), W(x_2)) = sd(x_1, x_2)$$

but as $s < 1$ this inequality cannot hold and therefore the fixed point $g = x_1 = x_2$ is unique for any initial value of x.

This means that we are looking for a contractive operator F whose fixed point $g = Fg$ is the best possible approximation of the original image.

The *IFS Theorem* expands on this to state that given a set of contractive transforms, $W = \{w_i : i = 1, \ldots, N\}$, with a transform defined as

$$W(x) = \bigcup_{i=1}^{N} w_i(x), \quad \forall x \in X$$

then the contractive factor is s,

$$d(W(x), W(y)) \leq sd(x, y)$$

which will have a unique fixed point, or attractor of the IFS, g, such that,

$$g = W(g) = \lim_{i \to \infty} W^i(x), \quad \forall x.$$

19.4.2 Hausdorff Distance Functions

For point sets, the normal distance functions have to be slightly modified and the Hausdorff function is a suitable representation. Given a complete metric space (X, d), we can define the Hausdorff space, $\mathcal{H}$ where $\mathcal{H}(X)$ represents the space whose points are the compact subsets of X, excluding the empty set. We can now define h, the Hausdorff metric that defines the distance between the sets A and $B \in \mathcal{H}(X)$, by

$$h(A, B) = \max\{d(A, B), d(B, A)\}$$

where

$$d(A, B) = \max\{d(x, B) : x \in A\}$$

and

$$d(x, B) = \min\{d(x, y) : y \in B\}$$

d, being the standard distance function. The set of standard Euclidean distance functions are commonly used. These are defined as

$$d^p(x, y) = (|x^p - y^p|)^{\frac{1}{p}}.$$

Absolute error (d^1) and mean squared error (d^2) are the most widely used parameters. We now have a measure that indicates, in a general sense, how similar two images are.

19.4.3 IFS and the Collage Theorem

An IFS code consists of $\{w_i, p_i : i = 1, 2, \ldots, N\}$, where the w_i are the affine transformation and each has an optional associated probability, p_i. We will discuss the use of the probability codes later. Previously, we have discussed the design of a multi-lens photocopier which recursively photocopied the same image. We can now define this machine with each lens being described with a single affine transform.

The best way of displaying these IFS codes is via a table which lists the components of the affine transforms, w_i, and the probabilities, p_i. The Sierpinski triangle, for example (see Chapter 18), requires three transforms each scaling the image by a half and translated in the appropriate manner as compounded in the following table:

i	a_i	b_i	c_i	d_i	e_i	f_i	p_i
1	0.5	0	0	0.5	0	0	0.33
2	0.5	0	0	0.5	100	0	0.33
3	0.5	0	0	0.5	50	50	0.33

The photocopy or deterministic algorithm takes any original image and applies all the transforms at the same time to the whole of the image, creating a new image. The process is repeated as many times as is required to create a final image as close as possible to the IFS attractor.

An alternative approach to creating the attractor is by using a random approach. The random approach uses the probability values and involves choosing an initial starting point and randomly transforming it by one of the w_i's according to the probability. Given N affine transforms, the probabilities are often calculated with regard to a measure theory, using the simple formulae

$$p_i \approx \frac{|\det\ w_i|}{\sum\limits_{j=1}^{N} |\det\ w_j|} = \frac{|a_i d_i - b_i c_i|}{\sum\limits_{j=1}^{N} |a_j d_j - b_j c_j|}$$

where det denotes the determinant. This means that the probability is proportional to the size of the transformed image. The set of points encountered will converge on the attractor of the IFS.

The two methods create the same attractor. Both versions are reasonably fast and are used to create very realistic images. The introduction of the probabilities for applying the transforms in the random process allow a technique to produce grey scale images. These enable certain areas to be visited more often and then have a corresponding increase in contrast. A way of visualising this process is to modify the photocopier so that each copy of the original image is modified with respect to contrast in accordance to the transform's probability.

To create large complex images from many transforms we can use the *collage theorem*. This states that given an IFS code $\{w_i, p_i : i = 1, 2, \ldots, N\}$, with contractive factor $0 \leq s < 1$, then

$$h\left(T, \bigcup_{i=1}^{N} w_i(T)\right) \leq \delta$$

where T is in the Hausdorff metric space. Then

$$h(T, g) \leq \frac{\delta}{1 - s}$$

where g is the attractor of the IFS. So, combining them we have

$$h(T, g) \leq \frac{1}{1 - s} h\left(T, \bigcup_{i=1}^{N} w_i(T)\right).$$

Given that we wish to find a set of transforms that have a specific attractor, the collage theorem tells us that if in order for T and g to be close it is sufficient

that

$$T \quad \text{and} \quad \bigcup_{i=1}^{N} w_i(T)$$

are close. If we consider a *collage* or *encoding error*,

$$\epsilon_c = h\left(T, \bigcup_{i=1}^{N} w_i(T)\right)$$

and a *decoding error*, $\epsilon_d = h(T, g)$ then we have an upper bound for ϵ_d as

$$\epsilon_d = \frac{1}{1-s}\epsilon_c.$$

For compression purposes, the requirement is such that we wish for the number of transforms, N, to be as small as possible with ϵ_d below a specified quality level. The solution to this very general problem is computationally intensive and is not trivial to solve automatically. It was originally called the 'Graduate Student Algorithm' and involved the following steps:

> acquire a graduate student
> place the student in a room with a picture and a computer
> lock the door
> and wait ...
> unlock when the picture has been reverse engineered

In other words, to create high quality images from a small set of transforms requires many hours of supervised operation.

19.4.4 PIFS Compression System

The PIFS compression system provides a more flexible transform with a partitioned IFS (PIFS), which solves some of the limitations of the standard IFS. A PIFS relates one area of an image to another which is similar. We define large areas called *domain blocks* that are associated with smaller areas called *range blocks*. Each range block is defined as being similar with respect to an affine transform with its associated domain block.

A compression system employing PIFS involves splitting the image into a non-overlapping set of range blocks and then allocating an affine transform from a domain block to each range block. Each domain block needs to be strictly larger than the range block to make the system contractive. The coding process then follows the following two stages:

(i) **The Encoding Process** The encoding process involves searching, for each range block, a domain block that is closest in similarity and then encoding a relevant transform and location.

(ii) **The Decoding Process** Starting with an initial image, possibly just a plain grey scale image, the set of PIFS transforms are repeatedly applied until the attractor is closely reached.

The collage theorem tells us that this set of transforms, one for each range block, will have an attractor that is similar to the original image.

19.4.5 Range-Domain Algorithm

We now wish to use this PIFS to encode grey scale images. The general algorithm for all range-domain fractal coding methods is given below. This creates the set $W = \bigcup_i w_i$.

```
divide the image into a set of non-overlapping ranges R_i
mark all ranges as uncovered
while there exists an uncovered R_i
        choose domain D_i and map w_i such that
                distance = min(R_i − w_i(D_i))
        if (distance < T (Threshold) or size R_i < minimum)
          mark R_i as covered
          output transformation w_i and location D_i
        else
          partition R_i into smaller regions
          remove R_i from the list
        end if
end while
```

There is an arbitrary choice of threshold value, T, which gives an indication of the quality or similarity required. The minimum size is included to stop detailed searching of very small range sizes which could reduce to a couple of pixels.

The key problem with the algorithm is the searching process, where the minimum domain is found. The order of complexity is multiplied by the number of possible domains, D_i, as well as the number of possible contractive affine transforms, w_i. Choosing a restrictive partitioning strategy and a simplified set of transforms reduces the complexity of the algorithm.

We now present a practical version of this system for encoding arbitrary grey scale images. The first point to consider is a slight modification to the affine transform to accommodate grey scale information. Two extra parameters, s_i and o_i, specify the contrast and brightness, respectively. The affine transform can then be considered as

$$w_i \begin{pmatrix} x \\ y \\ z \end{pmatrix} = \begin{pmatrix} a_i & b_i & 0 \\ c_i & d_i & 0 \\ 0 & 0 & s_i \end{pmatrix} \begin{pmatrix} x \\ y \\ z \end{pmatrix} + \begin{pmatrix} e_i \\ f_i \\ o_i \end{pmatrix} = \begin{pmatrix} a_i x + b_i y + e_i \\ c_i x + d_i y + f_i \\ s_i z + o_i \end{pmatrix}.$$

To extract the contrast and brightness values from a domain ($D_i = \{\bigcup_{j=1}^{m} d_j\}$) and a range ($R_i = \{\bigcup_{j=1}^{n} r_j\}$), we simply transform the domain block with the affine transformation, giving $D_i' = \{\bigcup_{j=1}^{n} d_j'\}$, and then minimise the result,

$$\delta_i = D_i' - R_i = \sum_{j=1}^{n} (s_i d_j' + o_i - r_j)$$

assuming there are n pixels in the range block. This can be calculated using the least squares approximation, and gives us

$$s_i = \frac{n^2 \sum_{j=1}^{n} d'_j r_j - \sum_{j=1}^{n} d'_j \sum_{j=1}^{n} r_j}{n^2 \sum_{j=1}^{n} d'_j - \left(\sum_{j=1}^{n} d'_j \right)^2}$$

and

$$o_i = \frac{\sum_{j=1}^{n} r_j - s_i \sum_{j=1}^{n} d'_j}{n^2}.$$

The distance δ_i can be calculated giving

$$\delta_i = \frac{\sum_{j=1}^{n} r_j^2 + s_i \left(s_i \sum_{j=1}^{n} (d'_j)^2 - 2 \sum_{j=1}^{n} d'_j r_j + 2 o_i \sum_{j=1}^{n} d'_j \right) + o_i \left(o_i n^2 - 2 \sum_{j=1}^{n} r_j \right)}{n^2}.$$

Different distance functions can be used and absolute error is a useful alternative to the mean squared error.

19.4.6 Partitioning Strategies

The choice of partitioning strategy is arbitrary, with any method that divides a range block R_i into a smaller non-overlapping set being acceptable. An obvious solution is to use a quadtree division which divides each range block into four smaller quads. Triangular range blocks can also be used which are not constrained to the restriction of having 90° edges. Such modifications allow more flexibility in the choice of domains and affine transforms, aiming to increase the compression ratio without reducing the quality.

19.4.7 Choice of Affine Transformations

In this specific case the range and domain regions are all square. The number of simple transforms that can be applied is limited to the following:

Type	Transformation matrix
Identity	$\begin{pmatrix} 1 & 0 \\ 0 & 1 \end{pmatrix}$
Rotation by 90^o	$\begin{pmatrix} 0 & -1 \\ 1 & 0 \end{pmatrix}$
Rotation by -90^o	$\begin{pmatrix} 0 & 1 \\ -1 & 0 \end{pmatrix}$
Rotation by 180^o	$\begin{pmatrix} -1 & 0 \\ 0 & -1 \end{pmatrix}$
Horizontal reflection	$\begin{pmatrix} 1 & 0 \\ 0 & -1 \end{pmatrix}$
Vertical reflection	$\begin{pmatrix} -1 & 0 \\ 0 & 1 \end{pmatrix}$
Reflection by 45^o	$\begin{pmatrix} 0 & 1 \\ 1 & 0 \end{pmatrix}$
Reflection by -45^o	$\begin{pmatrix} 0 & -1 \\ -1 & 0 \end{pmatrix}$

This restricts the coding for each of the transforms to simply representing one of eight choices, which can be encoded into just three bits. Two values have to be encoded that describe the contrast, s_i, and brightness, o_i.

19.4.8 Searching Strategies

For large images there are potentially many domain blocks that need to be searched for each iteration of the domain-range algorithm. As the required quality is increased, the number of iterations also increases and the encoding time can easily become very large. This is unlike the decoding time, which is dependent on the number of transforms and the resulting image size requested. As has been shown previously, the number of iterations required to reach an acceptable version of the attractor image is very small within this controlled environment. This means that the coding-decoding process is non-symmetrical, which for most practical purposes is acceptable. Often, almost all images are compressed once and decoded many times, so a fast decoder has to be developed.

The number of possible domain blocks is similar to the number of nodes in

a Gaussian pyramid, as described in Chapter 16. To speed up the searching process in the encoding stage, a helpful observation is that if the search is not totally exhaustive then the resulting PIFS may not be optimal but could be very close, with the result that only a minor loss of quality will occur. The simplest technique is only to look in a specific region, for example:

- Look at only a certain number of levels above the current range block and/or at a certain distance away.
- Consider only those domain blocks which partially overlap the range block to some extent. This can be visualised by having an inverted Gaussian pyramid with its peak at the range block.

Another idea is to categorise domain blocks depending on the edge types defined within their structure and then matching a range block with the set of possible domain blocks of similar type. The following four categories can be used: smooth, midrange, simple edge, and complex edge.

19.4.9 Low Level Coding Strategy

The final stage of any compression system lies in the design of the low level coding procedure. The following items need to be encoded:

Domain Block D_i, location and size, which can be encoded relative to the size of the range block in a few bits.

Affine Transform w_i, which requires three bits as there are eight possible transforms.

Contrast s_i and **Brightness** o_i values, e.g. quantizing the values so that s_i uses five bits and o_i has seven bits.

The set of contrast, s_i, and brightness, o_i, values are often correlated so it is worth encoding these values as separate streams through a probability or dictionary coder, as described in Section 19.2. It is also an easy process within the encoding operation to pass all the other values through a general lossless coder to gain an additional compression ratio advantage.

19.5 Properties and Features

To achieve a single value quality rating, for the degraded image, we need to devise a function F, such that if f_{ij} is the original and $\overline{f}_{ij}$ is the degraded image, the quality rating Q is defined as

$$Q = \sum_{j=0}^{N-1} \sum_{i=0}^{M-1} F(f_{ij}, \overline{f}_{ij}).$$

There are a number of possible functions F that can be used. A common set of error-measures is one based on the ℓ_p-norm. ℓ_1 is absolute error and ℓ_2 is root mean square error, i.e.

$$\ell_p = \left(\frac{1}{MN} \sum_{j=0}^{N-1} \sum_{i=0}^{M-1} \left| f_{ij} - \overline{f}_{ij} \right|^p \right)^{\frac{1}{p}}.$$

Other suggestions for this metric include the popular signal-to-noise ratio. This is defined by normalising the signal power by the error power and taking a scaled logarithm measured in decibels; one decibel (dB) is equal to one tenth of a logarithmic unit. It is assumed that the signal power is the same as the variance σ_f^2 of the signal samples, so

$$\begin{aligned} \text{SNR} &= 10 \log_{10} \frac{\left\langle f^2 \right\rangle}{\frac{1}{MN} \sum_{j=0}^{N-1} \sum_{i=0}^{M-1} \left| f_{ij} - \overline{f}_{ij} \right|^2} \\ &= 10 \log_{10} \frac{\sigma_f^2}{\sigma_{f-\overline{f}}^2}. \end{aligned}$$

A slight alternative is to consider the peak signal-to-noise ratio (PSNR),

$$\text{PSNR} = 10 \log_{10} \frac{\max f_{ij}^2}{\frac{1}{MN} \sum_{j=0}^{N-1} \sum_{i=0}^{M-1} \left| f_{ij} - \overline{f}_{ij} \right|^2}.$$

19.5.1 Knee Points

An idea for automatically finding an acceptable level of quality without having to resort to subjective experiments is to consider a numerical level of quality versus the compression ratio achieved which is termed the *rate distortion curve*. This should have a smooth almost linear curve with a knee point, before which the compression ratio steeply rises and after which it shallowly reduces. This is meant to represent the point at which all the redundant noise in the image has been removed or replaced. The idea is that, at this point, the compression method has reached its limit before the actual image signal is corrupted, and thus the quality should never be lowered beyond this point.

19.5.2 Stability of the Attractor

The contraction theorem gives a guarantee that the attractor will be reached irrespective of the starting point. This means that the initial image which is fed in to the PIFS is in theory irrelevant. With small scaling factors, $< 1/2$, the fixed point attractor is reached with only a few iterations.

A fast convergence strategy implies a fast decoding speed that allows fractal compressors to be used even with video sources. Also, the progressive nature of fractal compression means that a partial image can be viewed while the rest of the decoding takes place. This can be very useful for quickly browsing large numbers of images within a database, or viewing a high quality resolution image as soon as possible in a progressive form.

19.5.3 Resolution Independence and Enhancement

Due to self-similarity, images described within an IFS or a PIFS are not described at a fixed resolution or scale. This means the decoded image can be any arbitrary size. It is to be noted that this is purely a type of interpolation and, even if the created detail is appropriate, it is simply generated. Hence, zooming in on an image of a wheat field for example will not show the structure of individual grains or stalks of wheat. This is an important point and can lead to a slightly misleading claims with regard to high performance image compression.

Consider taking a grey scale image with resolution of 256×256, with one byte per pixel. This gives us an original image size of 65,536 bytes, before converting to a PIFS. If, after converting the image, the size of the PIFS is 6,554 bytes, the resulting compression ratio is 10:1. Now, if when decoding the PIFS, we magnify by a factor of 4 in both the horizontal and vertical direction, it will look like we started with a 1024×1024 image. This gives us a total compression ratio of $10 \times 16 = 160$. Unfortunately, this extra information has been synthetically generated and, as mentioned above, even if it is often appropriate there is no guarantee that it is correct.

The property of resolution independence gives us a process called resolution enhancement. It consists of converting the image to a very high quality PIFS, decoding the image to a higher resolution and then throwing away the PIFS. This is an advanced form of interpolation which is very useful when requiring higher resolutions, for example within the printing industry. The principle involves calculating a very complex PIFS which retains as high a quality as possible.

Alternative interpolation schemes do exist and a popular technique is to use either a quadratic or cubic interpolant which will give a smoother continuous image rather than the discrete nearest-neighbour method.

19.6 Improved Fractal Compression

There are two principal conditions for the inverse problem, fractal compression, to be feasible:

Nature is fractal with many scenes possessing this self-similar feature, and

A PIFS can be found that arbitrarily represents the image to any specified quality level.

Neither of these two conditions can be proved to be always true. Unlike a fern for example, a true fern does not branch indefinitely, and the background is very unlikely to be similar to the foreground. A further problem is that given an IFS for the foreground and one for the background there is no easy way of calculating the IFS for the composite image. There is considerbale scepticism regarding the general use of fractal compression since we can argue that a PIFS system is simply using a fractal transform; it is not a true fractal compression

but rather a form of self-vector quantization (VQ) that uses the image as the codebook.

In favour of PIFS, it offers a relatively simple method to approximate an image with respectable performance. The resulting decoded image also has pleasing properties that make it complementary to other compression techniques and the compression performance has frequently been shown to work as well as alternative methods.

Fractal compressors are useful tools but when considered for a specific purpose, for example, Internet image viewing or archiving photographic images of water-colour paintings, care must be taken.

There is a feature within the JPEG standard that allows the encoder to change the quantization table uniquely for each image. Although virtually all applications use the default quantization tables, significant improvement in quality can be gained by adjusting these tables on a per image basis without affecting the compression ratio. Likewise, there are many parameters which can be modified in the PIFS system and the development of a standard must take these into account. Fractal compression methods are often quoted as being within a factor of 2 better or worse than JPEG in terms of compression ratio with respect to quality for different images. Due to the fact that fractal coding is non-symmetrical, with encoding times often far larger than decoding times, it has gained popularity with the mass distribution of images and video sequences.

19.6.1 Colour Considerations

Since Isaac Newton's experiments with light and colour it has been well known that a wide range of colours can be generated from a choice of three primary colours. Modern displays generate their images by mixing light from three primaries: red, green and blue. In 1931 the CIE (Commission Internationale de L'Eclairage) developed the colour chart used in early television specifications based on defining the viewable colours for a display device in terms of a triangle with each of the primary colours at the endpoints. The colour space inside the triangle represents the possible colours available to the display and is called the gamut.

The CIE chart was partially used by the NTSC (National Television System Committee) to define a transmission format in terms of luminance and chrominance which was called YIQ, representing luminance, in-phase chrominance and quadrature chrominance coordinates. Later in Europe the PAL (Phase Alternation Line) format, for the UK, and the SECAM (Séquentiel Couleur à Mémoire) format, for France, were developed. These used a colour space called YUV or YC_rC_b, the difference between YIQ and YUV being a 33 degree rotation in UV space.

This system proved suitable for analogue transmission, but slight modifications were made to accommodate digital storage and transmission. Most digital systems store the three channels as 8-bit quantities allowing 256 values or quantisation levels. 10-bit, 12-bit or 16-bit quantities are also used in situations where higher resolution is required. Digital conversions between RGB

and YIQ or YC_rC_b commonly use the following matrices:

$$\begin{pmatrix} Y \\ I \\ Q \end{pmatrix} = \begin{pmatrix} 0.299 & 0.587 & 0.114 \\ 0.60 & -0.28 & -0.32 \\ 0.21 & -0.52 & 0.31 \end{pmatrix} \begin{pmatrix} R \\ G \\ B \end{pmatrix},$$

$$\begin{pmatrix} Y \\ C_r \\ C_b \end{pmatrix} = \begin{pmatrix} 0.299 & 0.587 & 0.114 \\ -0.1687 & -0.3313 & 0.5 \\ 0.5 & -0.4187 & -0.0813 \end{pmatrix} \begin{pmatrix} R \\ G \\ B \end{pmatrix}.$$

Due to the ease of calculation of the conversion in the digital world the YC_rC_b format is favoured over YIQ. It is worth noting that, while the Y values range from 0 to 255, the C_r and C_b values range from 0 to ± 128, which are often stored by adding 128 and forcing the range to 0-255. This defines a few values which do not map one-to-one and thus there is a very slight loss of information[4]. The YC_rC_b format is designed to concentrate as much of the image information into the luminance and less in the chrominance. This means that the three streams are less correlated and thus can be coded separately.

From physiological testing it is observed that the chrominance channels do not need to be specified as frequently as the luminance channel. Thus only every other C_r and C_b value is required to be stored. This means a 3:2 conversion takes place from RGB to YC_rC_b. In fractal terms this can relate to using varying threshold values for each of the three channels and/or using resolution enhancement to regain the full size image.

Colour in Printing

It is worth noting that other colour models exist, and the most popular alternative is that used by the printing industry. This uses the subtractive primary colours; cyan, magenta, yellow and black ($CMYK$). Black is used as a separate colour to achieve the best visual quality rather than combining equal quantities of C, M and Y. This makes the conversion from RGB to $CMYK$ a one-to-many mapping, and very device dependent. An image processed and printed in exactly the same way in Europe and the USA, for example, gives different results as printing inks and paper are different. Also the simple calibration system described above for visual displays fails for printing devices as mapping a specific colour is a highly non-linear process, and it is not sufficient to measure a set of points and interpolate. These problems are due to the lack of a model describing the printing process in sufficient detail. Colour management tools calibrate a set of devices together[5]. The defined set is normally small and often restricted to one manufacturer - normally the same as the one producing the colour management tool.

[4]This loss of information affects only a few values and at most changes the value of the least significant bit.

[5]Two examples are the Scanmatch colour calibration software which uses the TekColor Colour Management System, and is designed for matching and correcting a set of Pantone colours for scanners, and the Advanced Digital Control System which includes a ColorControl feature used in NEC MultiSync 5FG/6FG monitors to adjust monitor colours to printer colours.

Colour Compression

True-colour images are commonly represented as 24-bit RGB values, often captured images, containing a degree of noise. This means that they result in very low lossless compression ratios, but are ideal candidates for the lossy contour merging process. As 24-bit values are bulky to handle it is sensible to convert the values to YC_rC_b as recommended, and reduce the resolution of the C_r and C_b components by half in both vertical and horizontal dimensions. The reduction in resolution can be carried out using a cubic re-sampler which provided good reconstruction properties. This gives an automatic 2:1 conversion in image size. For lossy compression, each stream is sent through the fractal coding process, with varying threshold values. Quality of 'excellence', as previously defined, gives fairly high levels of compression ratio, up to 10:1.

19.6.2 Video Considerations

Image sequences can be fractal compressed with two techniques. The most common method is to consider each frame as a separate two dimensional image and encode it as such. Prediction from previous frames can help speed up the coder or alternatively provide a whole second set of domain blocks to transform from. Alternatively, it is possible to extend the domain and range blocks to three dimensional cubes.

Movie sequences can be very long with about 216000 35mm frames in a 2.5 hour film. If a fractal coder were to contain all the images in the sequence, then its size would become excessive, with approximately 432 billion pixels for a 2.5 hour high definition TV movie.[6] Fortunately, the pixels in the first frame are very unlikely to be correlated to the pixels in the last frame, and the coding efficiency involved is thus likely to be very small. This implies that splitting the movie into small sections is a sensible option. Attention has to be paid so that the join between any two sections does not cause serious artefacts in itself.

The digital broadcast media use versions of the MPEG (Motion Picture Experts Group) family of video compression standards (based upon the original JPEG). This is the basis for current technologies including white standard CD-ROMS and DVDs (Digital Versatile Discs). As the medium is digital, modifying the system to incorporate new coding techniques is not as fundamental a change as replacing the old analogue systems.

19.7 Compression Conscious Operations

The philosophy of compression conscious image operations is to define an image operation not just in terms of the final visual image, but also in terms of the compression performance achieved for this image. Two main advantages present themselves:

- operations continually have an idea of the final compression ratio achievable;

[6] High definition TV resolution of 1920×1152 (European standard) approaches that of standard 35mm quality film resolution which is quoted as being approximately 3000×2000.

- they can be carried out as the fractal compressed file is generated and are not proportional to the number of pixels in the full raster image.

This can then enable images which are extremely large to be manipulated. There is the potential for increased speed as the compressed size is smaller than the original.

To enable this, a *semi-compressed fractal description* that acts as an intermediate file format can be constructed. This format keeps a high level description of the elements within the fractal description, including a hierarchical structure of the partitioning strategy. If a low level encoded fractal image file is required then the low level coding operations need to be applied. Image operations are applied to this semi-compressed file format and at a reasonable compression ratio the size of this intermediate format will still be considerably smaller than the original. An operation that is ideally suitable for this technique to be applied is discussed in the following Section.

19.8 Fractal Texture Maps

We have seen how fractals can be used for a definition of texture (see Chapter 18). Let us now consider how the definition can be applied back on itself. Intuitively, a non-Euclidean, more texture oriented image is likely to fractal compress to a high level of compression retaining a high degree of quality. Also, the resolution enhancement technique is likely to prove quite accurate. We represent the process of texture mapping which, in its simplest form, applies a two dimensional image to the surface of a three dimensional shape. When viewed, the resolution of parts of the three dimensional surface often varies, being inversely proportional to the distance from the viewer. When the object is very close, a high resolution texture map is required and when further away the required resolution can be reduced. Most three dimensional rendering packages that create these images use a data structure called a MipMap. This consists of a two dimensional texture image which has been repeatedly scaled by a factor of 2 to form a hierarchy or pyramid of texture maps. The texture map of the required resolution is chosen as it is needed.

Consider using a fractal description of a single two dimensional texture as a replacement for the standard texture MipMap. As objects can be oriented in any direction the domain range blocks will need to accommodate all forms of rotation and scaling. A triangular description that replaces the square blocking strategy needs to be considered. During the decoding stage the range and domain blocks are calculated from the three dimensional transformations of the object to which they are to be applied. Then it is a simple matter of iterating the decoding algorithm to pixels within triangles. This also may suit the encoding stage as the number of extra choices to look at increases, which potentially allows for higher quality representations to be constructed by the range-domain algorithm.

A fractal texture map is inherently resolution independent so only one representation is needed and the image creation process is proportional to the number of pixels required, as well of course to the number of transforms. A

dynamic version of the fractal decoding algorithm would allow the three dimensional surface to be viewed over a very large range of distances, with minimal overheads. The progressive build up of the image also means that for interactive use, a crude image can be displayed while there is rapid movement and a detailed view created when the user stops moving and looks at the surface for a while. Over a period of time, the quality can be built up making efficient use of the processing engine. The rate of convergence to the attractor is less well defined and in certain cases may be slower, but this can be a minor problem given the increase in usability of the texture map. This technique has an ideal application within 3D visualisation and virtual reality type arcade games. When there is rapid movement, the quality of the texture mapping is less important but when the user wishes to spend time looking at an object in detail the quality of the texture mapping will improve.

19.9 Summary of Important Results

Algorithm for LZ77 substitution compressor

loop until *lookahead buffer* empty
    get a pointer *(position, match)* to the longest match
    if *length* > MINIMUM MATCH LENGTH
        output a *(position, length)* pair
        shift the window *length* character along
    else
        output the first character in the lookahead buffer
        shift the window *1* character along
    end if
end loop

Algorithm for LZ78 dictionary compressor

S = NULL
loop until end of stream
    E = INPUT SYMBOL
    if S*E exists in the dictionary
        $S = S$*E
    else
        output dictionary code for phrase S
        store S*E in dictionary
        $S = E$
    end if
end loop
output dictionary code for phrase S

Discrete cosine pair for JPEG compression

$$a_{kl} = \frac{1}{4} K_k K_l \sum_{i=0}^{7} \sum_{j=0}^{7} f_{ij} \cos \frac{(2i+1)k\pi}{16} \cos \frac{(2j+1)l\pi}{16}, \; 0 \leq k, \quad l \leq 7$$

$$f_{ij} = \frac{1}{4} \sum_{k=0}^{7} \sum_{l=0}^{7} K_k K_l a_{kl} \cos \frac{(2i+1)k\pi}{16} \cos \frac{(2j+1)l\pi}{16}, \; 0 \leq k, \quad l \leq 7$$

where

$$K_n = \begin{cases} \frac{1}{\sqrt{2}} & n = 0 \\ 1 & 1 \leq n \leq 7 \end{cases}$$

Algorithm for JPEG compression

split the image up into 8×8 blocks
for each block
    transform using the Forward Discrete Cosine Transform and
    quantise the 64 coefficients according to a quality parameter
    output the DC term, as the difference from the previous DC
    for each of the other 63 coefficients
        if the coefficient is non-zero
            output the number of proceeding zeros
            output the coefficient value
        end if
    end for
end for

Range Domain Algorithm

divide the image into a set of non-overlapping ranges R_i
mark all ranges as uncovered
while there exists an uncovered R_i
        choose domain D_i and map w_i such that
                $distance = \min(R_i - w_i(D_i))$
        if ($distance < T$ (Threshold) **or** size $R_i <$ minimum)
            mark R_i as covered
            output transformation w_i and location D_i
        else
            partition R_i into smaller regions
            remove R_i from the list
        end if
end while

19.10 Further Reading

- Rosenfeld A (Ed.), *Multi-resolution Image Processing and Analysis*, Springer, 1984.
- Storer J A, *Data Compression: Methods and Theory*, Computer Science Press, 1988.
- Bell T C, Cleary J G and Witten I H, *Text Compression*, Prentice-Hall, 1990.
- Barnsley M F and Hurd L P, *Fractal Image Compression*, A K Peters, 1993.
- Bell T C, Moffat A and Witten I H, *Managing Gigabytes: Compressing and Indexing Documents and Images*, Van Nostrand Rainhold, 1994.
- Blackledge J M (Ed.), *Image Processing: Mathematical Methods and Applications*, Oxford University Press, 1998.

Problems: Part IV

In the questions that follow, n is the size of the input/output array.

IV.1 Write a function to threshold a digital image at a fixed level.

```
void FLT(float **s, int n, float t)
```

where s is the input/output and t is the threshold ($0 < t < 1$).

IV.2 Write a function to semi-threshold a digital image at a fixed level.

```
void SLT(float **s, int n)
```

where s is the input/output and t is the threshold ($0 < t < 1$).

IV.3 Write a function to edge detect an image using the Roberts gradient and study its performance using some test images.

```
void ROBERTS(float **s, int n)
```

where s is the input/output.

IV.4. Write a function to edge detect an image using the Sobel gradient and study its performance using some test images.

```
void SOBEL(float **s, int n)
```

where s is the I/O.

IV.5. Write a function to edge detect an image using the Prewit gradient and study its performance using some example images.

```
void PREWIT(float **s, int n)
```

where s is the I/O.

IV.6. Write a function to edge detect an image using the Marr-Hildreth method and study its performance using some example images.

```
void MH(float **x, int n, float s, float **y)}
```

where x is the input image, y is the output image, and s is the standard deviation of the Gaussian function.

IV.7 Write a function to automatically threshold a bimodal image.

```
void AUTOTHRESHOLD( float **s, int n )
```

IV.8 The Γ-distribution can be considered to be an approximate model for the distribution of grey levels R associated with a coherent image given by

$$P(R) = \frac{1}{\beta^\alpha}\frac{1}{\Gamma(\alpha)}R^{\alpha-1}\exp(-R/\beta), \quad R \geq 0$$

By considering a discrete form of this distribution (i.e. an N-bin histogram), derive least squares estimates for the scaling factor

$$\frac{1}{\beta^\alpha}\frac{1}{\Gamma(\alpha)}$$

and the parameters α and β.

(i) Explain how this parameter estimation technique can be used to segment a coherent digital image using a moving window. What is the principal condition required for this technique to yield statistically significant results?

(ii) Derive expressions for the mode of the distribution in terms of α and β and the number of pixels that occur at the position of the mode?

Summary

The 'physics' associated with image formation and the engineering that has been, and continues to be, applied to develop various imaging systems is fundamental to the design of image processing and image analysis software. The goal of this book has been to introduce the reader to the mathematical techniques used for modelling imaging systems and show how such models can be used as a guide to the interpretation of the data captured by different imaging systems from which suitable image processing algorithms can be designed. There is an intimate relationship between the development of image processing systems and the 'physics' of waves and vibrations. Central to this relationship is the role of scattering theory and, in particular, the Green function solution (which is essentially a convolution) to an appropriate linear inhomogeneous wave equation that can be taken to describe (usually to a limited extent) the 'physics' associated with a particular type of wavefield. The model used for developing the basic imaging equation and its relationship to the properties of a detected scattered wavefield is almost exclusively based on application of the weak scattering or Born approximation which, in the far field, yields a Fourier transform relationship between the scattering function and the scattered field. All imaging systems can then be viewed in terms of some appropriate instrument that, by default, is only able to record the scattered field to a limited extent. Thus, the relationship between the object plane and the image plane is determined by the 'instrument function' which in turn, either directly or indirectly (i.e. after appropriate data processing has been applied), determines the characteristics of the image via the point spread function. This fundamental model is based on a weak scattering approximation (the Born approximation) which works best when the wavelength of the wavefield from which the image is obtained is large compared to the object function. This condition is at odds with the fact that most imaging systems are specifically designed to obtain information on the object function over scales that are of the same order as the wavelength. However, in most cases, the physical effects of strong scattering together with other incompatibilities and errors associated with the representation of a recorded image in terms of the fundamental imaging equation are combined to form a noise term, giving us the basic model

$$s(x, y) = p(x, y) \otimes \otimes f(x, y) + n(x, y)$$

where f is the object function, p is the point spread function, n is the noise and s is the image. Here, the point spread function is taken to be invariant of different

positions in the image plane and the process is stationary. This allows the convolution theorem to be applied providing us with a route to the analysis and processing of an image in Fourier space using the Fourier transform. However, if the point spread function varies in the image plane, the convolution process is non-stationary and the convolution theorem cannot be applied in the same way. This has important consequences for developing methods involved in solving the fundamental inverse problem: given s, p and a statistical model for n, find f. For the stationary case, Fourier based methods can be used to design a range of filters but, for non-stationary problems, deconvolution must be solved algebraically. This involves solving large systems of linear equations of size $n^2 \times m^2$ for digital images of size $n \times m$.

Ideally, by accurately modelling an imaging system, it is possible to derive a description of the relationship between the object and image plane, identify the nature of the inverse problem and, thus, develop an appropriate reconstruction method as required. However, the accuracy of the model has to be balanced with the simplicity of the results that can be derived from it in terms of providing a model that is of practical and 'engineering' value. Achieving the right balance is central to imaging systems modelling and image understanding.

Once an image has been acquired, there is a large number of processing methods that can be applied which depend on the type of image, its fidelity and application. Image processing algorithms can be used with a view to simply enhancing the display and/or extracting features within the data that are of value in terms of attempting to recognize meaningful patterns in an image and, ultimately, using such patterns to classify an image in some decision making process. The latter case is the basis for pattern recognition and computer vision which is, to some extent, model dependent but, in a broader sense, relies on a range of phenomenological paradigms, procedures and algorithms. This is because, to date, there is no known approach for developing a compound model of the human visual system and the interpretation of the image data that it uses. In other words, although we can develop an accurate physical model for the way in which the eye functions, the same cannot yet be said with regard to the functioning of the brain. Thus, whereas the methods for modelling an imaging system presented in this book can be applied generally (as discussed in Part II), the techniques associated with pattern recognition (as discussed in Part IV) are but a small selection of what is, as yet, an insoluble problem in general. Hence, there has evolved a multiplicity of solutions to pattern recognition problems that are highly idealized and applications specific. This is reflected in the material presented in Part IV of this work togther with the small chapter (i.e. Chapter 19) on image coding and compression that has been provided for completeness.

This book has attempted to help the reader to appreciate the underlying mathematical and numerical techniques required for designing imaging systems and for processing the data which they produce. Moreover, it has attempted to couple the role of imaging systems modelling with the principal methods for reconstructing an image, some of the routine image processing techniques that can be applied and how these techniques are converted into appropriate software. There is often a large 'gap' between the theoretical aspects of a

subject and 'engineering' practical solutions. Filling this 'gap' is often the most difficult part of the 'learning curve' and requires the engineer to come to terms with a diverse range of subjects. Imaging and image processing requires a unique blend of physics, mathematics, statistics, computing and electronics and a book of this type can only ever provide a brief glimpse of the role that these subjects play in imaging science. However, it is hoped that the reader will be able to approach new aspects of this subject and develop new and original ideas with a greater degree of understanding and confidence as a result of studying this book. If so, then its composition and publication, together with its companion volume *Digital Signal Processing*, has been worthwhile.

Appendix A

Solutions to Problems

Solutions to Problems: Part I

I.1

$$\nabla(x^3+y^3+z^3) = \left(\hat{\mathbf{x}}\frac{\partial}{\partial x}+\hat{\mathbf{y}}\frac{\partial}{\partial y}+\hat{\mathbf{z}}\frac{\partial}{\partial z}\right)(x^3+y^3+z^3)$$

$$= \hat{\mathbf{x}}\frac{\partial}{\partial x}x^3+\hat{\mathbf{y}}\frac{\partial}{\partial y}y^3+\hat{\mathbf{z}}\frac{\partial}{\partial z}z^3 = 3\hat{\mathbf{x}}x^2+3\hat{\mathbf{y}}y^2+3\hat{\mathbf{z}}z^2 = 3(\hat{\mathbf{x}}x^2+\hat{\mathbf{y}}y^2+\hat{\mathbf{z}}z^2).$$

$$\nabla r^n = \left(\hat{\mathbf{x}}\frac{\partial}{\partial x}+\hat{\mathbf{y}}\frac{\partial}{\partial y}+\hat{\mathbf{z}}\frac{\partial}{\partial z}\right)(x^2+y^2+z^2)^{\frac{n}{2}}$$

$$= \hat{\mathbf{x}}\frac{\partial}{\partial x}(x^2+y^2+z^2)^{\frac{n}{2}}+... = \hat{\mathbf{x}}\frac{n}{2}(x^2+y^2+z^2)^{\frac{n}{2}-1}2x+...$$

$$= n(x^2+y^2+z^2)^{\frac{n-2}{2}}(\hat{\mathbf{x}}x+\hat{\mathbf{y}}y+\hat{\mathbf{z}}z) = nr^{n-2}\mathbf{r}.$$

$$\nabla(\mathbf{a}\cdot\mathbf{r}) = \nabla(a_x x+a_y y+a_z z) = \hat{\mathbf{x}}a_x+\hat{\mathbf{y}}a_y+\hat{\mathbf{z}}a_z = \mathbf{a}.$$

$$\nabla[\mathbf{r}\cdot\nabla(x+y+z)] = \left(\hat{\mathbf{x}}\frac{\partial}{\partial x}+\hat{\mathbf{y}}\frac{\partial}{\partial y}+\hat{\mathbf{z}}\frac{\partial}{\partial z}\right)(x+y+z) = \hat{\mathbf{x}}+\hat{\mathbf{y}}+\hat{\mathbf{z}}.$$

I.2

$$\nabla\cdot\mathbf{F} = \left(\hat{\mathbf{x}}\frac{\partial}{\partial x}+\hat{\mathbf{y}}\frac{\partial}{\partial y}+\hat{\mathbf{z}}\frac{\partial}{\partial z}\right)\cdot(\hat{\mathbf{x}}F_x+\hat{\mathbf{y}}F_y+\hat{\mathbf{z}}F_z) = \frac{\partial}{\partial x}F_x+\frac{\partial}{\partial y}F_y+\frac{\partial}{\partial z}F_z = 0$$

if $\mathbf{F}$ is a constant vector.

$$\nabla\cdot\mathbf{r} = \frac{\partial}{\partial x}x+\frac{\partial}{\partial y}y+\frac{\partial}{\partial z}z = 1+1+1 = 3.$$

$$\nabla\cdot[xyz(\hat{\mathbf{x}}+\hat{\mathbf{y}}+\hat{\mathbf{z}})] = \frac{\partial}{\partial x}(xyz)+\frac{\partial}{\partial y}(xyz)+\frac{\partial}{\partial z}(xyz) = yz+xz+xy.$$

$$\mathbf{r}\times[\hat{\mathbf{x}}f(x)+\hat{\mathbf{y}}g(y)+\hat{\mathbf{z}}h(z)]=\begin{vmatrix}\hat{\mathbf{x}} & \hat{\mathbf{y}} & \hat{\mathbf{z}}\\ x & y & z\\ f(x) & g(y) & h(z)\end{vmatrix}$$

$$=\hat{\mathbf{x}}[yh(z)-zg(y)]-\hat{\mathbf{y}}[xh(x)-zf(x)]+\hat{\mathbf{z}}[xg(y)-yf(x)]$$

$$\therefore\ \ \nabla\cdot(\mathbf{r}\times[\hat{\mathbf{x}}f(x)+\hat{\mathbf{y}}g(y)+\hat{\mathbf{z}}h(z)])$$

$$=\frac{\partial}{\partial x}[yh(x)-zg(y)]-\frac{\partial}{\partial y}[xh(x)-zf(x)]+\frac{\partial}{\partial z}[xg(y)-yf(x)]=0.$$

I.3

$$\nabla^2 r^n=\frac{\partial^2}{\partial x^2}(x^2+y^2+z^2)^{\frac{n}{2}}+...=\frac{\partial}{\partial x}\left[\frac{n}{2}(x^2+y^2+z^2)^{\frac{n}{2}-1}2x\right]+...$$

$$n(x^2+y^2+z^2)^{\frac{n}{2}-1}+x\left(\frac{n}{2}-1\right)n2x(x^2+y^2+z^2)^{\frac{n}{2}-2}+...$$

$$=nr^{n-2}+2n\frac{(n-2)}{2}x^2r^{n-2}\frac{1}{x^2}+...=3nr^{n-2}+n(n-2)r^2r^{n-2}\frac{1}{r^2}$$

$$=3nr^{n-2}+n(n-2)r^{n-2}=n(n+1)r^{n-2}.$$

I.4 Let $\mathbf{A}=\hat{\mathbf{x}}A_x+\hat{\mathbf{y}}A_y+\hat{\mathbf{z}}A_z$ and $\mathbf{B}=\hat{\mathbf{x}}B_x+\hat{\mathbf{y}}B_y+\hat{\mathbf{z}}B_z$. Then,

$$\nabla\cdot(\mathbf{A}+\mathbf{B})=\left(\hat{\mathbf{x}}\frac{\partial}{\partial x}+\hat{\mathbf{y}}\frac{\partial}{\partial y}+\hat{\mathbf{z}}\frac{\partial}{\partial z}\right)\cdot[\hat{\mathbf{x}}(A_x+B_x)+\hat{\mathbf{y}}(A_y+B_y)+\hat{\mathbf{z}}(A_z+B_z)]$$

$$=\frac{\partial}{\partial x}(A_x+B_x)+\frac{\partial}{\partial y}(A_y+B_y)+\frac{\partial}{\partial z}(A_z+B_z)$$

$$=\frac{\partial}{\partial x}A_x+\frac{\partial}{\partial y}A_y+\frac{\partial}{\partial z}A_z+\frac{\partial}{\partial x}B_x+\frac{\partial}{\partial y}B_y+\frac{\partial}{\partial z}B_z$$

$$=\nabla\cdot\mathbf{A}+\nabla\cdot\mathbf{B}.$$

$$\nabla\cdot(u\mathbf{A})=\left(\hat{\mathbf{x}}\frac{\partial}{\partial x}+\hat{\mathbf{y}}\frac{\partial}{\partial y}+\hat{\mathbf{z}}\frac{\partial}{\partial z}\right)\cdot(u\hat{\mathbf{x}}A_x+u\hat{\mathbf{y}}A_y+u\hat{\mathbf{z}}A_z)$$

$$=\frac{\partial}{\partial x}(uA_x)+\frac{\partial}{\partial y}(uA_y)+\frac{\partial}{\partial z}(uA_z)$$

$$=A_x\frac{\partial}{\partial x}u+A_y\frac{\partial}{\partial y}u+A_z\frac{\partial}{\partial z}u+u\frac{\partial}{\partial x}A_x+u\frac{\partial}{\partial y}A_y+u\frac{\partial}{\partial z}A_z$$

$$=\left(\hat{\mathbf{x}}\frac{\partial}{\partial x}+\hat{\mathbf{y}}\frac{\partial}{\partial y}+\hat{\mathbf{z}}\frac{\partial}{\partial z}\right)u\cdot(\hat{\mathbf{x}}A_x+\hat{\mathbf{y}}A_y+\hat{\mathbf{z}}A_z)$$

$$+u\left(\hat{\mathbf{x}}\frac{\partial}{\partial x}+\hat{\mathbf{y}}\frac{\partial}{\partial y}+\hat{\mathbf{z}}\frac{\partial}{\partial z}\right)\cdot(\hat{\mathbf{x}}A_x+\hat{\mathbf{y}}A_y+\hat{\mathbf{z}}A_z)=\nabla u\cdot\mathbf{A}+u\nabla\cdot\mathbf{A}.$$

I.5

$$\nabla \times \hat{\mathbf{x}}x = \begin{vmatrix} \hat{\mathbf{x}} & \hat{\mathbf{y}} & \hat{\mathbf{z}} \\ \frac{\partial}{\partial x} & \frac{\partial}{\partial y} & \frac{\partial}{\partial z} \\ x & 0 & 0 \end{vmatrix} = 0.$$

$$\nabla \times \hat{\mathbf{x}}y = \begin{vmatrix} \hat{\mathbf{x}} & \hat{\mathbf{y}} & \hat{\mathbf{z}} \\ \frac{\partial}{\partial x} & \frac{\partial}{\partial y} & \frac{\partial}{\partial z} \\ y & 0 & 0 \end{vmatrix} = -\hat{\mathbf{z}}\frac{\partial}{\partial y}y = -\hat{\mathbf{z}}.$$

$$\nabla \times (\hat{\mathbf{x}}x\cos z + \hat{\mathbf{y}}y\log x - \hat{\mathbf{z}}z^2) = \begin{vmatrix} \hat{\mathbf{x}} & \hat{\mathbf{y}} & \hat{\mathbf{z}} \\ \frac{\partial}{\partial x} & \frac{\partial}{\partial y} & \frac{\partial}{\partial z} \\ x\cos z & y\log x & z^2 \end{vmatrix}$$

$$= -\hat{\mathbf{y}}\frac{\partial}{\partial z}(x\cos z) + \hat{\mathbf{z}}\frac{\partial}{\partial x}(y\log x) = \hat{\mathbf{z}}\frac{y}{x} - \hat{\mathbf{y}}x\sin z.$$

$$\nabla \times \mathbf{r}f(\mathbf{r}) = \begin{vmatrix} \hat{\mathbf{x}} & \hat{\mathbf{y}} & \hat{\mathbf{z}} \\ \frac{\partial}{\partial x} & \frac{\partial}{\partial y} & \frac{\partial}{\partial z} \\ xf(r) & yf(r) & zf(r) \end{vmatrix}$$

$$= \hat{\mathbf{x}}\left(z\frac{\partial}{\partial y}f - y\frac{\partial}{\partial z}f\right) - \hat{\mathbf{y}}\left(z\frac{\partial}{\partial x}f - x\frac{\partial}{\partial z}f\right) + \hat{\mathbf{z}}\left(y\frac{\partial}{\partial x}f - x\frac{\partial}{\partial y}f\right).$$

I.6

$$\nabla \times (\mathbf{A} + \mathbf{B}) = \begin{vmatrix} \hat{\mathbf{x}} & \hat{\mathbf{y}} & \hat{\mathbf{z}} \\ \frac{\partial}{\partial x} & \frac{\partial}{\partial y} & \frac{\partial}{\partial z} \\ A_x + B_x & A_y + B_y & A_z + B_z \end{vmatrix}$$

$$= \hat{\mathbf{x}}\left[\frac{\partial}{\partial y}(A_z + B_z) - \frac{\partial}{\partial z}(A_y + B_y)\right]$$

$$-\hat{\mathbf{y}}\left[\frac{\partial}{\partial x}(A_z + B_z) - \frac{\partial}{\partial z}(A_x + B_x)\right]$$

$$+\hat{\mathbf{z}}\left[\frac{\partial}{\partial x}(A_y + B_y) - \frac{\partial}{\partial y}(A_x + B_x)\right]$$

$$= \hat{\mathbf{x}}\left(\frac{\partial}{\partial y}A_z - \frac{\partial}{\partial z}A_y\right) + \hat{\mathbf{y}}\left(\frac{\partial}{\partial x}A_z - \frac{\partial}{\partial x}A_x\right) + \hat{\mathbf{z}}\left(\frac{\partial}{\partial x}A_y - \frac{\partial}{\partial y}A_x\right)$$

$$+\hat{\mathbf{x}}\left(\frac{\partial}{\partial y}B_z - \frac{\partial}{\partial z}B_y\right) + \hat{\mathbf{y}}\left(\frac{\partial}{\partial x}B_z - \frac{\partial}{\partial z}B_x\right) + \hat{\mathbf{z}}\left(\frac{\partial}{\partial x}B_y - \frac{\partial}{\partial y}B_x\right)$$

$$= \begin{vmatrix} \hat{\mathbf{x}} & \hat{\mathbf{y}} & \hat{\mathbf{z}} \\ \frac{\partial}{\partial x} & \frac{\partial}{\partial y} & \frac{\partial}{\partial z} \\ A_x & A_y & A_z \end{vmatrix} + \begin{vmatrix} \hat{\mathbf{x}} & \hat{\mathbf{y}} & \hat{\mathbf{z}} \\ \frac{\partial}{\partial x} & \frac{\partial}{\partial y} & \frac{\partial}{\partial z} \\ B_x & B_y & B_z \end{vmatrix} = \nabla \times \mathbf{A} + \nabla \times \mathbf{B}.$$

$$\nabla \times (u\mathbf{F}) = \begin{vmatrix} \hat{\mathbf{x}} & \hat{\mathbf{y}} & \hat{\mathbf{z}} \\ \frac{\partial}{\partial x} & \frac{\partial}{\partial y} & \frac{\partial}{\partial z} \\ uF_x & uF_y & uF_z \end{vmatrix}$$

$$= \hat{\mathbf{x}}\left(\frac{\partial}{\partial y}uF_z - \frac{\partial}{\partial z}uF_y\right) - y\left(\frac{\partial}{\partial x}uF_z - \frac{\partial}{\partial z}uF_x\right) + \hat{\mathbf{z}}\left(\frac{\partial}{\partial x}uF_y - \frac{\partial}{\partial y}uF_x\right)$$

$$= \hat{\mathbf{x}}\left(u\frac{\partial}{\partial y}F_z - u\frac{\partial}{\partial z}F_y\right) + \hat{\mathbf{x}}\left(F_z\frac{\partial}{\partial y}u - F_y\frac{\partial}{\partial z}u\right)$$

$$-\hat{\mathbf{y}}\left(u\frac{\partial}{\partial x}F_z - u\frac{\partial}{\partial z}F_x\right) - \hat{\mathbf{y}}\left(F_z\frac{\partial}{\partial x}u - F_x\frac{\partial}{\partial z}u\right)$$

$$+\hat{\mathbf{z}}\left(u\frac{\partial}{\partial z}F_y - u\frac{\partial}{\partial y}F_x\right) + \hat{\mathbf{z}}\left(F_y\frac{\partial}{\partial x}u - F_x\frac{\partial}{\partial y}u\right)$$

$$= u\begin{vmatrix} \hat{\mathbf{x}} & \hat{\mathbf{y}} & \hat{\mathbf{z}} \\ \frac{\partial}{\partial x} & \frac{\partial}{\partial y} & \frac{\partial}{\partial z} \\ F_x & F_y & F_z \end{vmatrix} + \begin{vmatrix} \hat{\mathbf{x}} & \hat{\mathbf{y}} & \hat{\mathbf{z}} \\ \frac{\partial}{\partial x}u & \frac{\partial}{\partial y}u & \frac{\partial}{\partial z}u \\ F_x & F_y & F_z \end{vmatrix} = u\nabla\times\mathbf{F} + \nabla u\times\mathbf{F}.$$

I.7

$$\nabla\times(\nabla u) = \begin{vmatrix} \hat{\mathbf{x}} & \hat{\mathbf{y}} & \hat{\mathbf{z}} \\ \frac{\partial}{\partial x} & \frac{\partial}{\partial y} & \frac{\partial}{\partial z} \\ \frac{\partial}{\partial x}u & \frac{\partial}{\partial y}u & \frac{\partial}{\partial z}u \end{vmatrix}$$

$$= \hat{\mathbf{x}}\left(\frac{\partial}{\partial y}\frac{\partial}{\partial z}u - \frac{\partial}{\partial z}\frac{\partial}{\partial y}u\right) - \hat{\mathbf{y}}\left(\frac{\partial}{\partial x}\frac{\partial}{\partial z}u - \frac{\partial}{\partial z}\frac{\partial}{\partial x}u\right) + \hat{\mathbf{z}}\left(\frac{\partial}{\partial x}\frac{\partial}{\partial y}u - \frac{\partial}{\partial y}\frac{\partial}{\partial x}u\right) = 0.$$

$$\nabla\times\mathbf{F} = \begin{vmatrix} \hat{\mathbf{x}} & \hat{\mathbf{y}} & \hat{\mathbf{z}} \\ \frac{\partial}{\partial x} & \frac{\partial}{\partial y} & \frac{\partial}{\partial z} \\ F_x & F_y & F_z \end{vmatrix}$$

$$= \hat{\mathbf{x}}\left(\frac{\partial}{\partial y}F_z - \frac{\partial}{\partial z}F_y\right) + \hat{\mathbf{y}}\left(\frac{\partial}{\partial z}F_x - \frac{\partial}{\partial x}F_z\right) + \hat{\mathbf{z}}\left(\frac{\partial}{\partial z}F_x - \frac{\partial}{\partial x}F_y\right)$$

$$\therefore\ \ \nabla\cdot(\nabla\times\mathbf{F})$$

$$= \frac{\partial}{\partial x}\left(\frac{\partial}{\partial y}F_z - \frac{\partial}{\partial z}F_y\right) + \frac{\partial}{\partial y}\left(\frac{\partial}{\partial z}F_x - \frac{\partial}{\partial x}F_z\right) + \frac{\partial}{\partial z}\left(\frac{\partial}{\partial x}F_y - \frac{\partial}{\partial y}F_x\right) = 0.$$

I.8 Using the notation

$$\partial_x \equiv \frac{\partial}{\partial x},\quad \partial_{xy} \equiv \frac{\partial}{\partial x\partial y},\quad \partial_y \equiv \frac{\partial}{\partial y},\quad \text{etc.}$$

we have

$$\nabla\times\nabla\times\mathbf{F} = \nabla\times\begin{vmatrix} \hat{\mathbf{x}} & \hat{\mathbf{y}} & \hat{\mathbf{z}} \\ \partial_x & \partial_y & \partial_z \\ F_x & F_y & F_z \end{vmatrix}$$

$$= \nabla\times[(\partial_y F_z - \partial_z F_y) + \hat{\mathbf{y}}(\partial_z F_x - \partial_x F_z) + \hat{\mathbf{z}}(\partial_x F_y - \partial_y F_x)]$$

$$= \begin{vmatrix} \hat{\mathbf{x}} & \hat{\mathbf{y}} & \hat{\mathbf{z}} \\ \partial_x & \partial_y & \partial_z \\ \partial_y F_z - \partial_z F_y & \partial_z F_x - \partial_x F_z & \partial_x F_y - \partial_y F_x \end{vmatrix}$$

$$
\begin{aligned}
&= \hat{\mathbf{x}}[\partial_y(\partial_x F_y - \partial_y F_x) - \partial_z(\partial_z F_x - \partial_x F_z)] \\
&+\hat{\mathbf{y}}[\partial_z(\partial_y F_z - \partial_z F_y) - \partial_x(\partial_z F_x - \partial_x F_z)] \\
&+\hat{\mathbf{z}}[\partial_x(\partial_z F_x - \partial_x F_z) - \partial_y(\partial_y F_z - \partial_z F_y)] \\
&= (-\partial_y^2 F_x - \partial_z^2 F_x)\hat{\mathbf{x}} + (-\partial_z^2 F_y - \partial_x^2 F_y)\hat{\mathbf{y}} + (-\partial_x^2 F_z - \partial_y^2 F_z)\hat{\mathbf{z}} \\
&+(\partial_{yx}^2 F_y + \partial_{zx}^2 F_z)\hat{\mathbf{x}} + (\partial_{zy}^2 F_z + \partial_{xy}^2 F_x)\hat{\mathbf{y}} + (\partial_{xz}^2 F_x + \partial_{yz}^2 F_y)\hat{\mathbf{z}} \\
&= (-\partial_x^2 F_x - \partial_y^2 F_x - \partial_z^2 F_x)\hat{\mathbf{x}} + (-\partial_x^2 F_y - \partial_y^2 F_y - \partial_z^2 F_y)\hat{\mathbf{y}} \\
&+(-\partial_x^2 F_z - \partial_y^2 F_z - \partial_z^2 F_z)\hat{\mathbf{z}} + (\partial_x^2 F_x + \partial_{yx}^2 F_y + \partial_{zx}^2 F_z)\hat{\mathbf{x}} \\
&+(\partial_{xy}^2 F_x + \partial_y^2 F_y + \partial_{zy}^2 F_z)\hat{\mathbf{y}} + (\partial_{xz}^2 F_x + \partial_{yz}^2 + \partial_z^2 F_z)\hat{\mathbf{z}} \\
&= -(\partial_x^2 + \partial_y^2 + \partial_z^2)(\hat{\mathbf{x}}F_x + \hat{\mathbf{y}}F_y + \hat{\mathbf{z}}F_z) \\
&+\hat{\mathbf{x}}\partial_x(\partial_x F_x + \partial_y F_y + \partial_z F_z) + \hat{\mathbf{y}}\partial_y(\partial_x F_x + \partial_y F_y + \partial_z F_z) + \hat{\mathbf{z}}\partial_z(\partial_x F_x + \partial_y F_y + \partial_z F_z) \\
&= -\nabla^2\mathbf{F} + \nabla(\partial_x F_x + \partial_y F_y + \partial_z F_z) = -\nabla^2\mathbf{F} + \nabla(\nabla\cdot\mathbf{F}).
\end{aligned}
$$

I.9 Noting that

$$\nabla\cdot(u\nabla u) = \nabla u\cdot\nabla u + u\nabla^2 u,$$

since $\mathbf{F} = \nabla u$, we can write

$$
\begin{aligned}
\nabla\cdot(u\mathbf{F}) &= \nabla u\cdot\nabla u + u\nabla\cdot(\nabla u) \\
&= \nabla u\cdot\nabla u + u\nabla\cdot\mathbf{F} = \nabla u\cdot\nabla u, \quad \text{with} \quad \nabla\cdot\mathbf{F} = 0. \\
\therefore \quad \int_V F^2 dV &= \int_V (\nabla u\cdot\nabla u)dV = \int_V \nabla\cdot(u\mathbf{F})dV = \oint_S u\mathbf{F}\cdot\hat{\mathbf{n}}dS
\end{aligned}
$$

from the divergence theorem.

1.10 Green's first identity is

$$\int_V (u\nabla^2 v + \nabla u\cdot\nabla v)dV = \oint_S u\nabla v\cdot\hat{\mathbf{n}}dS.$$

Proof:

$$
\begin{aligned}
\nabla\cdot(u\nabla v) &= u\nabla^2 v + \nabla u\cdot\nabla v \\
\therefore \quad \int_V (u\nabla^2 v + \nabla u\cdot\nabla v)dV &= \int_V \nabla\cdot(u\nabla v)dV = \oint_S u\nabla v\cdot\hat{\mathbf{n}}dS
\end{aligned}
$$

by the divergence theorem. To prove Green's second identity, we note that

$$\int_V (u\nabla^2 v + \nabla u\cdot\nabla v)dV = \oint_S u\nabla v\cdot\hat{\mathbf{n}}dS$$

and

$$\int_V (v\nabla^2 u + \nabla v\cdot\nabla u)dV = \oint_S v\nabla u\cdot\hat{\mathbf{n}}dS.$$

Subtracting the two equations above, we get

$$\int_V (u\nabla^2 v - v\nabla^2 u)dV = \oint_S (u\nabla v - v\nabla u)\cdot\hat{\mathbf{n}}dS.$$

I.11

$$\nabla f(\mathbf{r}) = \nabla\frac{1}{2\pi}\int_{-\infty}^{\infty} F(\mathbf{k})\exp(i\mathbf{k}\cdot\mathbf{r})d^2\mathbf{k}$$

$$= \left(\hat{\mathbf{x}}\frac{\partial}{\partial x} + \hat{\mathbf{y}}\frac{\partial}{\partial y}\right)\frac{1}{2\pi}\int_{-\infty}^{\infty}\int_{-\infty}^{\infty} F(k_x,k_y)\exp(ik_x x)\exp(ik_y y)dk_x dk_y$$

$$= \frac{1}{2\pi}\int_{-\infty}^{\infty}\int_{-\infty}^{\infty} F(k_x,k_y)(\hat{\mathbf{x}}ik_x + \hat{\mathbf{y}}ik_y)\exp(ik_x x)\exp(ik_y y)dk_x dk_y$$

$$= \frac{1}{2\pi}\int_{-\infty}^{\infty} F(\mathbf{k})i\mathbf{k}\exp(i\mathbf{k}\cdot\mathbf{r})d^2\mathbf{k}.$$

$$\left(\frac{\partial^2}{\partial x^2} + \frac{\partial^2}{\partial y^2}\right)\frac{1}{2\pi}\int_{-\infty}^{\infty}\int_{-\infty}^{\infty} F(k_x,k_y)\exp(ik_x x)\exp(ik_y y)dk_x dk_y$$

$$= \frac{1}{2\pi}\int_{-\infty}^{\infty}\int_{-\infty}^{\infty} F(k_x,k_y)(-k_x^2 - k_y^2)\exp(ik_x x)\exp(ik_y y)dk_x dk_y$$

$$= \frac{1}{2\pi}\int_{-\infty}^{\infty} F(\mathbf{k})(-k^2)\exp(i\mathbf{k}\cdot\mathbf{r})d^2\mathbf{k}.$$

I.12

$$\int_{-\infty}^{\infty} f(\mathbf{r})\exp(-i\mathbf{k}\cdot\mathbf{r})d^2\mathbf{r} = \int_{-a/2}^{a/2}\exp(-ik_x x)\int_{-b/2}^{b/2}\exp(-ik_y y)$$

$$= (ab)\text{sinc}(ak_x/2)\text{sinc}(bk_y/2)$$

where sinc(x) $\equiv \sin(x)/x$.

I.13

$$\int_{-\infty}^{\infty}\exp(-ar^2)\exp(-i\mathbf{k}\cdot\mathbf{r})d^2\mathbf{r}$$

$$= \int_{-\infty}^{\infty} \exp(-ax^2)\exp(-ik_x x)dx \int_{-\infty}^{\infty} \exp(-ay^2)\exp(ik_y y)dy.$$

Hence, we need to evaluate the integral

$$F(k) = \int_{-\infty}^{\infty} \exp(-ax^2)\exp(-ikx)dx$$

for both x and y. Noting that

$$\left(\sqrt{a}t + \frac{ik}{2\sqrt{a}}\right)^2 = ax^2 + ikx - \frac{k^2}{4a}$$

we can write

$$F(k) = \exp(-k^2/4a) \int_{-\infty}^{\infty} \exp\left[-\left(\sqrt{a}x + \frac{ik}{2\sqrt{a}}\right)^2\right] dx.$$

If we now let

$$y = \left(\sqrt{a}x + \frac{ik}{2\sqrt{a}}\right),$$

then $dy = \sqrt{a}dx$ and

$$F(k) = \frac{1}{\sqrt{a}}\exp(-k^2/4a) \int_{-\infty}^{\infty} \exp(-y^2)dy = \sqrt{\frac{\pi}{a}}\exp(-k^2/4a).$$

Combining the integrals over x and y, we get

$$\exp(-ar^2) \Longleftrightarrow \frac{\pi}{a}\exp(-k^2/4a)$$

where $k = \sqrt{k_x^2 + k_y^2}$.

I.14

$$\int_{-\infty}^{\infty} [f(\mathbf{r})+g(\mathbf{r})]\exp(-i\mathbf{k}\cdot\mathbf{r})d^2\mathbf{r} = \int_{-\infty}^{\infty} f(\mathbf{r})\exp(-i\mathbf{k}\cdot\mathbf{r})d^2\mathbf{r} \int_{-\infty}^{\infty} g(\mathbf{r})\exp(-i\mathbf{k}\cdot\mathbf{r})d^2\mathbf{r}$$
$$= f(\mathbf{k}) + g(\mathbf{k}).$$

$$\int_{-\infty}^{\infty} f(a\mathbf{r})\exp(-i\mathbf{k}\cdot\mathbf{r})d^2\mathbf{r} = \frac{1}{a}\int_{-\infty}^{\infty} f(a\mathbf{r})\exp\left(i\frac{\mathbf{k}}{a}\cdot a\mathbf{r}\right)d^2(a\mathbf{r})$$
$$= \frac{1}{a}F\left(\frac{\mathbf{k}}{a}\right).$$

$$\int_{-\infty}^{\infty} f(\mathbf{r}-\mathbf{a})\exp(-i\mathbf{k}\cdot\mathbf{r})d^2\mathbf{r} = \int_{-\infty}^{\infty} f(\mathbf{r}-\mathbf{a})\exp[-i\mathbf{k}\cdot(\mathbf{r}-\mathbf{a})]\exp(-i\mathbf{k}\cdot\mathbf{a})d^2(\mathbf{r}-\mathbf{a})$$
$$= \exp(-i\mathbf{k}\cdot\mathbf{a})F(\mathbf{k}).$$

I.15

$$\int_{-\infty}^{\infty} f(\mathbf{r})g^*(\mathbf{r})d^2\mathbf{r} = \int_{-\infty}^{\infty} g^*(\mathbf{r})\left(\frac{1}{2\pi}\int_{-\infty}^{\infty} F(\mathbf{k})\exp(i\mathbf{k}\cdot\mathbf{r})d^2\mathbf{k}\right)d^2\mathbf{r}.$$

$$= \frac{1}{2\pi}\int_{-\infty}^{\infty} F(\mathbf{k})\left(\int_{-\infty}^{\infty} g^*(\mathbf{r})\exp(i\mathbf{k}\cdot\mathbf{r})d^2\mathbf{r}\right)d^2\mathbf{k}$$

$$= \frac{1}{2\pi}\int_{-\infty}^{\infty} F(\mathbf{k})\left(\int_{-\infty}^{\infty} g(\mathbf{r})\exp(-i\mathbf{k}\cdot\mathbf{r})d^2\mathbf{r}\right)^* d^2\mathbf{k} = \frac{1}{2\pi}\int_{-\infty}^{\infty} F(\mathbf{k})G^*(\mathbf{k})d^2\mathbf{k}.$$

Now, if $g = f$, then it follows that

$$\int_{-\infty}^{\infty} \mid f(\mathbf{r}) \mid^2 d^2\mathbf{r} = \frac{1}{2\pi}\int_{-\infty}^{\infty} \mid F(\mathbf{k}) \mid^2 d^2\mathbf{k}.$$

I.16 With

$$f(\mathbf{r}) = \frac{1}{(2\pi)^2}\int_{-\infty}^{\infty} F(\mathbf{k})\exp(i\mathbf{k}\cdot\mathbf{r})d^2\mathbf{k},$$

$$g(\mathbf{r}) = \frac{1}{(2\pi)^2}\int_{-\infty}^{\infty} G(\mathbf{k})\exp(i\mathbf{k}\cdot\mathbf{r})d^2\mathbf{k}$$

we have

$$f \otimes \otimes g = \frac{1}{(2\pi)^4}\int_{-\infty}^{\infty} d^2\mathbf{r}\int_{-\infty}^{\infty} F(\mathbf{k})\exp(i\mathbf{k}\cdot\mathbf{r})d^2\mathbf{k}\int_{-\infty}^{\infty} G(\mathbf{k}')\exp[i\mathbf{k}'\cdot(\mathbf{r}'-\mathbf{r})]d^2\mathbf{k}'$$

$$= \frac{1}{(2\pi)^2}\int_{-\infty}^{\infty} d^2\mathbf{k}F(\mathbf{k})\int_{-\infty}^{\infty} d^2\mathbf{k}'G(\mathbf{k}')\exp(i\mathbf{k}'\cdot\mathbf{r}')\frac{1}{(2\pi)^2}\int_{-\infty}^{\infty}\exp[i\mathbf{r}\cdot(\mathbf{k}-\mathbf{k}')]d^2\mathbf{r}$$

$$= \frac{1}{(2\pi)^2}\int_{-\infty}^{\infty} d^2\mathbf{k}F(\mathbf{k})\int_{-\infty}^{\infty} d^2\mathbf{k}'G(\mathbf{k}')\exp(i\mathbf{k}'\cdot\mathbf{r}')\delta^2(\mathbf{k}-\mathbf{k}')$$

$$= \frac{1}{(2\pi)^2}\int_{-\infty}^{\infty} F(\mathbf{k})G(\mathbf{k})\exp(i\mathbf{k}\cdot\mathbf{r}')d^2\mathbf{k}$$

or

$$f(\mathbf{r}) \otimes \otimes g(\mathbf{r}) \Longleftrightarrow F(\mathbf{k})G(\mathbf{k}).$$

I.17 Let

$$F(\mathbf{k}) = \int_{-\infty}^{\infty} f(\mathbf{r}) \exp(-i\mathbf{k}\cdot\mathbf{r}) d^2\mathbf{r}$$

and

$$G(\mathbf{k}) = \int_{-\infty}^{\infty} g(\mathbf{r}) \exp(-i\mathbf{k}\cdot\mathbf{r}) d^2\mathbf{r}.$$

Then

$$F \otimes \otimes G = \int_{-\infty}^{\infty} d\mathbf{k} \int_{-\infty}^{\infty} f(\mathbf{r}) \exp(-i\mathbf{k}\cdot\mathbf{r}) d^2\mathbf{r} \int_{-\infty}^{\infty} g(\mathbf{r}') \exp[-i\mathbf{r}'\cdot(\mathbf{k}'-\mathbf{k})] d^2\mathbf{r}'$$

$$= \int_{-\infty}^{\infty} d^2\mathbf{r} f(\mathbf{r}) \int_{-\infty}^{\infty} d^2\mathbf{r}' g(\mathbf{r}') \exp(-i\mathbf{k}'\cdot\mathbf{r}') \int_{-\infty}^{\infty} \exp[-i\mathbf{k}\cdot(\mathbf{r}-\mathbf{r}')] d^2\mathbf{k}$$

$$= \int_{-\infty}^{\infty} d^2\mathbf{r} f(\mathbf{r}) \int_{-\infty}^{\infty} d^2\mathbf{r}' g(\mathbf{r}') \exp(-i\mathbf{k}'\cdot\mathbf{r}') (2\pi)^2 \delta^2(\mathbf{r}-\mathbf{r}')$$

$$= (2\pi)^2 \int_{-\infty}^{\infty} d^2\mathbf{r} f(\mathbf{r}) g(\mathbf{r}) \exp(-i\mathbf{k}'\cdot\mathbf{r})$$

or

$$\frac{1}{(2\pi)^2} F(\mathbf{k}) \otimes \otimes G(\mathbf{k}) \Longleftrightarrow f(\mathbf{r}) g(\mathbf{r}).$$

I.18

$$f \odot \odot g = \frac{1}{(2\pi)^4} \int_{-\infty}^{\infty} d^2\mathbf{r} \int_{-\infty}^{\infty} F(\mathbf{k}) \exp(i\mathbf{k}\cdot\mathbf{r}) d^2\mathbf{k} \int_{-\infty}^{\infty} G(\mathbf{k}') \exp[i\mathbf{k}'\cdot(\mathbf{r}-\mathbf{r}')] d^2\mathbf{k}'$$

$$= \frac{1}{(2\pi)^2} \int_{-\infty}^{\infty} d^2\mathbf{k} F(\mathbf{k}) \int_{-\infty}^{\infty} d^2\mathbf{k}' G(\mathbf{k}') \exp(-i\mathbf{k}'\cdot\mathbf{r}') \frac{1}{(2\pi)^2} \int_{-\infty}^{\infty} \exp[i\mathbf{r}\cdot(\mathbf{k}+\mathbf{k}')] d^2\mathbf{r}$$

$$= \frac{1}{(2\pi)^2} \int_{-\infty}^{\infty} d^2\mathbf{k} F(\mathbf{k}) \int_{-\infty}^{\infty} d^2\mathbf{k}' G(\mathbf{k}') \exp(-i\mathbf{k}'\cdot\mathbf{r}') \delta^2(\mathbf{k}+\mathbf{k}')$$

$$= \frac{1}{(2\pi)^2} \int_{-\infty}^{\infty} F(\mathbf{k}) G(-\mathbf{k}) \exp(i\mathbf{k}\cdot\mathbf{r}') d^2\mathbf{k}$$

or

$$f(\mathbf{r}) \odot \odot g(\mathbf{r}) \Longleftrightarrow F(\mathbf{k})G(-\mathbf{k}).$$

Now, for $g(\mathbf{r})$ real,

$$G(-\mathbf{k}) = \int_{-\infty}^{\infty} g(\mathbf{r}) \exp(i\mathbf{k}\cdot\mathbf{r}) d^2\mathbf{r} = \left(\int_{-\infty}^{\infty} g(\mathbf{r}) \exp(-i\mathbf{k}\cdot\mathbf{r}) d^2\mathbf{r} \right)^* = G^*(\mathbf{k}).$$

I.19 Using the convolution theorem:

$$F(\mathbf{k})G(\mathbf{k}) = G(\mathbf{k})F(\mathbf{k}), \quad \therefore \quad f(\mathbf{r}) \otimes \otimes g(\mathbf{r}) = g(\mathbf{r}) \otimes \otimes f(\mathbf{r}).$$

$$F(\mathbf{k})[G(\mathbf{k})H(\mathbf{k})] = [F(\mathbf{k})G(\mathbf{k})]H(\mathbf{k})$$
$$\therefore \quad f(\mathbf{r}) \otimes \otimes [g(\mathbf{r}) \otimes \otimes h(\mathbf{r})] = [f(\mathbf{r}) \otimes \otimes g(\mathbf{r})] \otimes \otimes h(\mathbf{r}).$$

$$F(\mathbf{k})[G(\mathbf{k}) + H(\mathbf{k})] = F(\mathbf{k})G(\mathbf{k}) + F(\mathbf{k})H(\mathbf{k})$$
$$\therefore \quad f(\mathbf{r}) \otimes \otimes [g(\mathbf{r}) + h(\mathbf{r})] = f(\mathbf{r}) \otimes \otimes g(\mathbf{r}) + f(\mathbf{r}) \otimes \otimes h(\mathbf{r}).$$

I.20

$$\nabla[f(\mathbf{r}) \otimes \otimes g(\mathbf{r})] \Longleftrightarrow i\mathbf{k}F(\mathbf{k})G(\mathbf{k})$$

and

$$i\mathbf{k}F(\mathbf{k})G(\mathbf{k}) = [i\mathbf{k}F(\mathbf{k})]G(\mathbf{k}) = F(\mathbf{k})[i\mathbf{k}G(\mathbf{k})]$$
$$\therefore \quad \nabla[f(\mathbf{r}) \otimes \otimes g(\mathbf{r})] = f(\mathbf{r}) \otimes \otimes \nabla g(\mathbf{r}) = g(\mathbf{r}) \otimes \otimes \nabla f(\mathbf{r}).$$

$$\nabla^2[f(\mathbf{r}) \otimes \otimes g(\mathbf{r})] \Longleftrightarrow -k^2 F(\mathbf{k})G(\mathbf{k})$$

and

$$-k^2 F(\mathbf{k})G(\mathbf{k}) = [-k^2 F(\mathbf{k})]G(\mathbf{k}) = F(\mathbf{k})[-k^2 G(\mathbf{k})]$$
$$\therefore \quad \nabla^2[f(\mathbf{r}) \otimes \otimes g(\mathbf{r})] = f(\mathbf{r}) \otimes \otimes \nabla^2 g(\mathbf{r}) = g(\mathbf{r}) \otimes \otimes \nabla^2 f(\mathbf{r}).$$

I.21

```
void FIRCON(float **f, float **p, float **s, int n, int w)
{
  int li, co, i, j, ii, jj, lm, cm, m=n+w-1, xx=w/2;
  float *temp[512], con;

/* Initialize the workspace */

 for (li=0; li<m; li++)
  temp[li]=(float *)malloc(m*sizeof(float));
```

```
 for (li=0; li<m; li++)
  for (co=0; co<m; co++)
   temp[li][co]=0.;


/* Invert the kernel */

 for (li=0; li<w; li++)
  for (co=0; co<w; co++)
  {
    i = xx - li;
    j = xx - co;
    temp[li][co] = p[xx+i][xx+j];  }


 for (li=0; li<w; li++)
  for (co=0; co<w; co++)
   p[li][co] = temp[li][co];

/* Input image into the workspace */

 for (li=0; li<m; li++)
  for (co=0; co<m; co++)
   temp[li][co]=0.;


 for (li=xx; li<n+xx; li++)
  for (co=xx; co<n+xx; co++)
   temp[li][co]=f[li-xx][co-xx];

/* Convolution */

for (li=xx; li<m-xx; li++)
  for (co=xx; co<m-xx; co++)
  {
    con = 0.;

     for (ii=li-xx, lm=0; ii<=li+xx, lm<w; ii++, lm++)
      for (jj=co-xx, cm=0; jj<=co+xx, cm<w; jj++, cm++)
con += temp[ii][jj]*p[lm][cm];

     s[li-xx][co-xx] = con;

  }

 for (li=0; li<m; li++)
```

```
  free(temp[li]);

}
```

I.22

```
void FIRCOR(float **f, float **p, float **s, int n, int w)
{
  int li, co, i, j, ii, jj, lm, cm, m=n+w-1, xx=w/2;
  float *temp[512], cor;

/* Initialize the workspace */

 for (li=0; li<m; li++)
  temp[li]=(float *)malloc(m*sizeof(float));


 for (li=0; li<m; li++)
  for (co=0; co<m; co++)
   temp[li][co]=0.;

/* Input image into the workspace */

 for (li=xx; li<n+xx; li++)
  for (co=xx; co<n+xx; co++)
   temp[li][co]=f[li-xx][co-xx];

/* Correlation */

for (li=xx; li<m-xx; li++)
  for (co=xx; co<m-xx; co++)
  {
    cor = 0.;

     for (ii=li-xx, lm=0; ii<=li+xx, lm<w; ii++, lm++)
      for (jj=co-xx, cm=0; jj<=co+xx, cm<w; jj++, cm++)
        cor += temp[ii][jj]*p[lm][cm];

     s[li-xx][co-xx] = cor;

  }

 for (li=0; li<m; li++)
  free(temp[li]);

}
```

I.23

```
/* FIR test program */

/* Performs an FIR convolution of an image with a kernel */

#include <stdio.h>

main()
{
float *f[512], *p[512], *s[512];
int n, w, i, j, iw1=1, iw2=2, ch;

xopen(); /* open X-windows imaging tool */

printf("\n\t Enter size of image: ");
scanf("%d",&n);

printf("\n\t Enter size of kernel: ");
scanf("%d",&w);

for(i=0; i<n;i++)
{ f[i] = (float *) malloc(n*sizeof(float));
  s[i] = (float *) malloc(n*sizeof(float));  }

for(i=0; i<w;i++)
 p[i] = (float *) malloc(w*sizeof(float));

printf("\n\t Object Function ");
rimage(f,n);
ximage(f, n, iw1); /* Display image */

printf("\n\t Input Elements of the kernel: ");

for(i=0; i<w; i++)
 for(j=0; j<w; j++)
  {
   printf("\n\t Input Element %d %d : ",i, j);
   scanf("%f",&p[i][j]);   }

printf("\n\t  Kernel ");

for(i=0; i<w; i++)
 for(j=0; j<w; j++)
   printf("\n\t  Element %d %d : %f",i, j, p[i][j]);
```

```
printf("\n\t 1. Correlation;  2. Convolution \n");
scanf("%d", &ch);

switch(ch)
{
  case 1:
printf("\n\t Computing the FIR Corelation...");
FIRCOR(f, p, s, n, w);
ximage(s,n,iw2); /* Display image */
printf("OK");
break;

  case 2:
printf("\n\t Computing the FIR Convolution...");
FIRCON(f, p, s, n, w);
ximage(s,n,iw2);
printf("OK");
break;

  default:
exit(1);

}


printf("\n\t Press Enter to exit");
getchar();
getchar();

xclose(); /* Close X-windows imaging tool */

for(i=0; i<n;i++)
{ free(s[i]);
  free(f[i]);  }

for(i=0; i<w;i++)
 free(p[i]);

}
```

An example of the application of these FIR filters is given in the accompanying figure below. Filter 1 is a 3×3 moving average filter and smooths the image; filter 2 is a horizontal gradient detector based on the process $f_{i(j+1)} - f_{i(j-1)}$, filter 2 is a vertical gradient detector based on the process $f_{(i+1)j} - f_{(i-1)j}$, filter 4 is a gradient detector based on centre differencing the Laplacian operator ∇^2, i.e. $f_{(i+1)j} + f_{(i-1)j} + f_{i(j+1)} + f_{i(j-1)} - 4f_{ij}$. Filter 5 is based on centre differencing the operator $1 - \nabla^2$ and is a high emphasis filter that can be derived by assuming that an image has been blurred by diffusion. It is a

processes that is good at restoring the edges of a blurred image as illustrated here.

Figure A.1: Original 128×128 test image (top left) and the result of applying filters 1 (top middle), 2 (top right), 3 (bottom left), 4 (bottom middle) and filter 5 (bottom right).

I.24

```
#include <math.h>

void ELLIPSE(float **s, int nx, int ny, int maj, int min, float l, int n)
{
 int i, j;
 float a=(float)min/2., b= (float)maj/2., test;

  for(i=0; i<n; i++)
   for(j=0; j<n; j++)
    {
     test= pow(((float)i-(float)ny)/a,2.) + pow(((float)j-(float)nx)/b,2.);
```

```
if(test <= 1.0)
 s[i][j]=l;        }

}
```

I.25

```
void RECT(float **s, int nx, int ny, int lx, int ly, float l, int n)

{
 int i, j;

  for(i=nx-lx/2; i<nx+lx/2; i++)
   for(j=ny-ly/2; j<ny+ly/2; j++)
 s[i][j]=l;

}
```

I.26

```
#include <math.h>

void GPSF(float **s, int n, int w)

{
 int i, j;
 float mid = (float)n / 2.;

for(i=0; i<n; i++)
 for(j=0; j<n; j++)
  s[i][j]=exp( -(pow((float)i-mid,2.)+pow((float)j-mid,2.))
             / pow((float)w,2.) ) ;

}
```

I.27

```
#include <math.h>

void AMPSPEC(float **s, float **a, int n)

{
 int i, j;
```

```
 float  *sr[512], *si[512];


/* Allocate Memory */

for(i=0; i<n;i++)
{
  sr[i] = (float *) malloc(n*sizeof(float));
  si[i] = (float *) malloc(n*sizeof(float));   }


/* Initialize real and imaginary parts */

for(i=0; i<n; i++)
 for(j=0; j<n; j++)
  { sr[i][j] = s[i][j];
    si[i][j] = 0.0;
     a[i][j] = 0.0;      }


/* Compute FFT2D */

 FFT2D(sr, si, n, -1);


/* Compute the amplitude spectrum */

for(i=0; i<n; i++)
 for(j=0; j<n; j++)
  a[i][j] =  sqrt(sr[i][j]*sr[i][j] + si[i][j]*si[i][j]) ;


/* Free the memory allocated */

for(i=0; i<n;i++)
{
  free(sr[i]);
  free(si[i]);   }

}
```

I.28

```
#include <math.h>

void POWSPEC(float **s, float **p, int n, int opt)
```

```
{
 int i, j;
 float  *sr[128], *si[128];

/*  Allocate  memory  */

for(i=0; i<n;i++)
{
  sr[i] = (float *) malloc(n*sizeof(float));
  si[i] = (float *) malloc(n*sizeof(float));   }

/* Initialize real and imaginary parts */

for(i=0; i<n; i++)
 for(j=0; j<n; j++)
  { sr[i][j] = s[i][j];
    si[i][j] = 0.0;
     p[i][j] = 0.0;      }

/* Compute the FFT2D */

 FFT2D(sr, si, n, -1);

/* Compute the power spectrum */

for(i=0; i<n; i++)
 for(j=0; j<n; j++)
  p[i][j] =  sr[i][j]*sr[i][j] + si[i][j]*si[i][j];

/* Option for logarithmic scale */

 if(opt == 1)
   for(i=0; i<n; i++)
    for(j=0; j<n; j++)
     p[i][j] =  log(1. + p[i][j]);;


/* Deallocate memory  */

for(i=0; i<n;i++)
{
  free(sr[i]);
  free(si[i]);   }

}
```

I.29

```
#include <stdio.h>

main()
{
float *s[128], *f[128], *a[128], *p[128], *fi[128], max=0., l;
int n, i, j, iw1=1, iw2=2;
int w,nx,ny,lx,ly,ch=0,maj,min;
char cc;


printf("\n\t Enter n  (<=128) : ");
scanf("%d",&n);

for(i=0; i<n;i++)
{ s[i]  = (float *) malloc(n*sizeof(float));
  f[i]  = (float *) malloc(n*sizeof(float));
  fi[i] = (float *) malloc(n*sizeof(float));
  a[i]  = (float *) malloc(n*sizeof(float));
  p[i]  = (float *) malloc(n*sizeof(float));  }


for(i=0; i<n; i++)
 for(j=0;j<n;j++)
  s[i][j]=0.;



while(ch != 4)
{

printf("\n\t Enter 1 (Square),  2 (Ellipse),
                  3 (Gaussian)  4 (Display) \n");
scanf("%d",&ch);

switch(ch)
{
case 1: printf("\n\t Enter centre (x,y): ");
scanf("%d",&nx);
scanf("%d",&ny);

printf("\n\t Enter length (lx,ly): ");
scanf("%d%d",&lx,&ly);

printf("\n\t Enter amplitude: ");
```

```
scanf("%f",&l);

printf("\n\t Computing square ...");

RECT(s,nx,ny,lx,ly,l,n);

printf(" OK");
break;

case 2: printf("\n\t Enter centre (x,y): ");
scanf("%d%d",&nx,&ny);

printf("\n\t Enter axes (maj,min): ");
scanf("%d%d",&maj,&min);


printf("\n\t Enter amplitude: ");
scanf("%f",&l);

printf("\n\t Computing ellipse ...");

ellipse_(s,nx,ny,maj,min,l,n);

printf(" OK");
break;


case 3: printf("\n\t Enter width: ");
scanf( "%d",&w);

printf("\n\t Computing Gaussian...");

GPSF(s,n,w);

printf(" OK");
break;

default:
break;

}    /* end of switch */

} /* end of while */


/* Display  Images */
```

```
xopen();

ximage(s, n, iw1);

printf("\n\t Press Enter to continue... ");
getchar();
getchar();

printf("\n\t Save it ? ");
if( (cc=getchar()) == 'y')
wimage(s,n);

/* Fourier Menu */

for(i=0;i<n;i++)
 for(j=0;j<n;j++)
  {  f[i][j] = s[i][j];
     fi[i][j] = 0.;   }

printf("\n\t Computing Fourier Transform...");
FFT2D(f, fi, n, -1);

ximage(f, n, iw2);
printf("OK");
printf("\n\t Press Enter to continue...");
getchar();

printf("\n\t Computing Amplitude Spectrum...");
AMPSPEC(s,a,n);
ximage(a, n, iw2);
printf("OK");
printf("\n\t Press Enter to continue...");
getchar();

printf("\n\t Computing Power Spectrum...");
POWSPEC(s, p, n, 1);
ximage(p, n, iw2);
printf("OK");
printf("\n\t Press Enter to continue...");
getchar();
getchar();

for(i=0; i<n;i++)
{ free(s[i]);
  free(f[i]);
  free(fi[i]);
  free(a[i]);
```

```
  free(p[i]);   }

printf("\n\t END \n");
xclose;
```

I.30

```
#include <math.h>


void SINCINT(float **x, int n, float **y, int m)

{
 int i, j, li, co, w=(m-n)/2;
 float  *xr[512], *xi[512], *yi[512];

/* Allocate Memory */

for(i=0; i<n; i++)
{
  xr[i] = (float *) malloc(n*sizeof(float));
  xi[i] = (float *) malloc(n*sizeof(float));  }

for(i=0; i<m; i++)
  yi[i] = (float *) malloc(m*sizeof(float));

/* Initialize real and imaginary parts */

for(i=0; i<n; i++)
 for(j=0; j<n; j++)
  { xr[i][j] = x[i][j];
    xi[i][j] = 0.0;     }


/* Compute FFT2D */

 FFT2D(xr, xi, n, -1);

/* Initialize the large image */

for(i=0; i<m; i++)
 for(j=0; j<m; j++)
  { y[i][j]  = 0.0;
    yi[i][j] = 0.0;     }

/* Interpolate */
```

```
li=0;

  for(i=w; i<n+w; i++)
  {
   co=0;

     for(j=w; j<n+w; j++)
     {   y[i][j]  = x[li][co];
         yi[i][j] = xi[li][co];
         co++;   }

   li++;
  }

/* Compute Inverse FFT2D */

 FFT2D(y, yi, m, 1);

/* Free Memory */

 for(i=0; i<n;i++)
 {
   free(xr[i]);
   free(xi[i]);   }

  for(i=0; i<m;i++)
   free(yi[i]);
}
```

Test unit.

```
/* Interpolates an image using sinc interpolation
   with function SINCINT. */

#include <stdio.h>

main()
{
float *x[512], *y[512];
int n, m, i, iw1=1, iw2=2;
char ch;

printf("\n\t Enter n (<=64) : ");
scanf("%d",&n);

for(i=0; i<n;i++)
```

```
 x[i] = (float *) malloc(n*sizeof(float));

rimage(x,n);

xopen();

ximage(x, n, iw1);

printf("\n\t Enter final size of image (<=512): ");
scanf("%d",&m);

for(i=0; i<m;i++)
 y[i] = (float *) malloc(m*sizeof(float));

SINCINT(x,n,y,m);

ximage(y,m,iw2);

printf("\n\t Print Enter to continue...");
getchar();
getchar();

printf("\n\t Do you want to save it ? ");

 if((ch=getchar()) == 'y')
  wimage(y,m);

xclose();

for(i=0; i<n;i++)
 free(x[i]);

for(i=0; i<m;i++)
 free(y[i]);
}
```

I.31 The Green function for the infinite space domain is, by definition, given by the solution of

$$\left(\frac{\partial^2}{\partial x^2} + k^2\right) g(x \mid x_0, k) = -\delta(x - x_0), \quad -\infty < x < \infty$$

where for a positive half space solution we require $0 \leq x < \infty$. Take the Laplace transform to obtain

$$p^2 \bar{g}(p \mid x_0, k) - pg(0 \mid x_0) - g'(0 \mid x_0, k) + k^2 \bar{g}(p \mid x_0, k) = e^{-px_0}$$

where

$$g'(0 \mid x_0, k) = \left[\frac{\partial}{\partial x} g(x \mid x_0, k)\right]_{x=0}.$$

Then,

$$\bar{g}(p \mid x_0, k) = \frac{p}{p^2+k^2} g(0 \mid x_0, k) + \frac{1}{p^2+k^2} g'(0 \mid x_0, k) + \frac{e^{-px_0}}{p^2+k^2}.$$

Inverting,

$$g(x \mid x_0, k) = g(0 \mid x_0, k)\cos(kx) + \frac{1}{k} g'(0 \mid x_0, k)\sin(kx) + \frac{1}{k}\sin[k(x-x_0)]H(x-x_0)$$

where $H(x)$ is the Heaviside step function. The solution is then given by

$$u(x_0, k) = \int_0^\infty g(x \mid x_0, k) f(x) dx$$

$$= \int_0^\infty g(0 \mid x, k)\cos(kx_0) dx + \frac{1}{k}\int_0^\infty g'(0 \mid x, k) f(x)\sin(kx_0) dx$$

$$+ \frac{1}{k}\int_0^\infty \sin[k(x_0 - x)]H(x - x_0) f(x) dx$$

$$= A(k)\cos(kx_0) + B(k)\sin(kx_0) + \frac{1}{k}\int_0^\infty \sin[k(x_0 - x)]H(x - x_0) f(x) dx$$

where

$$A(k) = \int_0^\infty g(0 \mid x, k) dx, \quad B(k) = \frac{1}{k}\int_0^\infty g'(0 \mid x, k) f(x) dx.$$

I.32 The Green function is

$$g(x \mid x_0, k) = -\frac{1}{k}\sin k \mid x - x_0 \mid$$

being the solution of

$$\left(\frac{\partial^2}{\partial x^2} + k^2\right) g(x \mid x_0, k) = -\delta(x - x_0)$$

for both left and right-travelling waves. The homogeneous equation has solutions $\sin(kx)$ and $\sin k(\ell - x)$ which vanish at $x = 0$ and $x = L$. Consider the linear combination

$$u(x, k) = -\frac{1}{k}\sin k \mid x - x_0 \mid + A\sin kx + B\sin k(\ell - x).$$

Then, using the boundary condition quoted,

$$-\frac{1}{k}\sin kx_0 + B\sin kL = 0$$

and

$$-\frac{1}{k}\sin k(L-x_0) + A\sin kL = 0.$$

Hence,

$$u(x \mid x_0) = -\frac{1}{k}\left[\sin k \mid x - x_0 \mid -\frac{\sin(kx_0)\sin k(L-x)}{\sin kL} - \frac{\sin(kx)\sin k(L-x_0)}{\sin kL}\right].$$

I.33 From I.32, $g(x \mid x_0, k)$ gives $g(0 \mid x_0, k) = 0, \quad g'(0 \mid x_0, k) = g(1 \mid x_0, k)$ and

$$g(1 \mid x_0, k) = \frac{1}{k}g(1 \mid x_0, k)\sin k + \frac{1}{k}\sin[k(1-x_0)]H(1-x_0).$$

Solving for g gives

$$g(1 \mid x_0, k) = \frac{\sin[k(1-x_0)]H(1-x_0)}{k - \sin k}$$

and hence

$$g(x \mid x_0, k) = \frac{\sin(kx)\sin[k(1-x_0)]}{k(k-\sin k)} + \frac{1}{k}\sin[k(x-x_0)]H(x-x_0)$$

for $0 \le x \le 1$ and $0 \le x_0 \le 1$.

I.34 Writing $\mathbf{R} = \mathbf{r} - \mathbf{r}_0$, with

$$g(R) = \frac{1}{(2\pi)^3}\int_{-\infty}^{\infty} G(\mathbf{k})e^{i\mathbf{k}\cdot\mathbf{R}}d^3\mathbf{k}$$

the equation for the Green function reduces to

$$G(\mathbf{k}) = \frac{1}{k^2 + \lambda}$$

where $k \equiv \mid \mathbf{k} \mid$. Thus, using spherical polar coordinates gives

$$G(R) = \frac{1}{(2\pi)^3}\int_{-\infty}^{\infty}\frac{e^{i\mathbf{k}\cdot\mathbf{R}}}{k^2+\lambda}d^3\mathbf{k}$$

$$= \frac{1}{(2\pi)^3}\int_0^{\infty} dk k^2 \int_{-1}^{1} d(\cos\theta)\int_0^{2\pi} d\phi \frac{e^{ikR\cos\theta}}{k^2+\lambda} = \frac{1}{4\pi^2R^2}\int_{-\infty}^{\infty}\frac{k\sin(kR)}{k^2+\lambda}dk.$$

Now, the contour integral

$$\oint_C \frac{ze^{izR}}{z^2+\lambda}dz$$

has two simple poles at $\pm i\sqrt{\lambda}$. Choosing the contour C in the upper half plane gives the residue

$$\lim_{z\to i\sqrt{\lambda}}\left[\frac{(z-i\sqrt{\lambda})ze^{izR}}{z^2+\lambda}\right]=\frac{1}{2}e^{-\sqrt{\lambda}R}$$

and hence, the solution

$$g(R)=\frac{e^{-\sqrt{\lambda}R}}{4\pi R}.$$

I.35 Consider

$$\left(\nabla^2-\sigma\frac{\partial}{\partial t}\right)G(\mathbf{r}\mid\mathbf{r}_0,t\mid t_0)=-\delta^3(\mathbf{r}-\mathbf{r}_0)\delta(t-t_0)$$

together with the time reversed equation

$$\left(\nabla^2+\sigma\frac{\partial}{\partial t}\right)G(\mathbf{r}\mid\mathbf{r}_1,-t\mid -t_1)=-\delta^3(\mathbf{r}-\mathbf{r}_1)\delta(t-t_1).$$

Pre-multiply the first equation by $G(\mathbf{r}\mid\mathbf{r}_1,-t\mid -t_1)$ and the second equation by $G(\mathbf{r}\mid\mathbf{r}_0,t\mid t_0)$ and subtract the results, integrating over the volume of interest and over t from $-\infty$ to t_0. Then, using Green's theorem, we get

$$\begin{aligned}
&\int_{-\infty}^{t_0}dt\oint_S[G(\mathbf{r}\mid\mathbf{r}_1,-t\mid t_1)\nabla G(\mathbf{r}\mid\mathbf{r}_0,t\mid t_0)\\
&-G(\mathbf{r}\mid\mathbf{r}_0,t\mid t_0)\nabla G(\mathbf{r}\mid\mathbf{r}_1,-t\mid -t_1)]\cdot d^2\mathbf{r}\\
&-\sigma\int_V d^3\mathbf{r}\int_{-\infty}^{t_0}\Big[G(\mathbf{r}\mid\mathbf{r}_1,-t\mid -t_1)\frac{\partial}{\partial t}G(\mathbf{r}\mid\mathbf{r}_0,t\mid t_0)\\
&+G(\mathbf{r}\mid\mathbf{r}_0,t\mid t_0)\frac{\partial}{\partial t}G(\mathbf{r}\mid\mathbf{r}_1,-t\mid -t_1)dt\\
&=G(\mathbf{r}_1\mid\mathbf{r}_0,t_1\mid t_0)-G(\mathbf{r}_0\mid\mathbf{r}_1,-t_0\mid -t_1).
\end{aligned}$$

The first integral vanishes under the assumption that G satisfies the homogeneous boundary conditions. The second integral is

$$\int_V d^3\mathbf{r}\left[G(\mathbf{r}\mid\mathbf{r}_1,-t\mid -t_1)G(\mathbf{r}\mid\mathbf{r}_0,t\mid t_0)\right]_{t=-\infty}^{t_0}$$

and since

$$G(\mathbf{r}\mid\mathbf{r}_0,t\mid t_0)=0,\quad t<t_0,\quad G(\mathbf{r}\mid\mathbf{r}_0,t\mid t_0\mid_{t=-\infty}=0$$

and

$$G(\mathbf{r} \mid \mathbf{r}_1, -t \mid -t_1) \mid_{t=t_0} = 0$$

for t in the range of integration. Hence,

$$G(\mathbf{r}_1 \mid \mathbf{r}_0, t_1 \mid t_0) = G(\mathbf{r} \mid \mathbf{r}_1, -t_0 \mid -t_1).$$

Solutions to Part II

II.1 Rewrite the equation as

$$(\nabla^2 + k^2)u(\mathbf{r}, k) = -\gamma(\mathbf{r})u(\mathbf{r}, k).$$

Then

$$(\nabla^2 + k^2)g(\mathbf{r} \mid \mathbf{r}_0, k) = -\delta^3(\mathbf{r} - \mathbf{r}_0)$$

and

$$\int_{-\infty}^{\infty} (g\nabla^2 u - u\nabla^2 g)d^3\mathbf{r} = -\int_{-\infty}^{\infty} g\gamma u d^3\mathbf{r} + \int_{-\infty}^{\infty} u(\mathbf{r}, k)\delta^3(\mathbf{r} - \mathbf{r}_0)d^3\mathbf{r}$$

$$= -\int_{-\infty}^{\infty} g\gamma u d^3\mathbf{r} + u(\mathbf{r}, k).$$

Hence,

$$u(\mathbf{r}_0, k) = f(\mathbf{r}_0, k) + \int_{-\infty}^{\infty} g(\mathbf{r} \mid \mathbf{r}_0, k)u(\mathbf{r}, k)V(\mathbf{r})d^3\mathbf{r}$$

where

$$f(\mathbf{r}_0) = \int_{-\infty}^{\infty} [g(\mathbf{r} \mid \mathbf{r}_0, k)\nabla^2 u(\mathbf{r}, k) - u(\mathbf{r}, k)\nabla^2 g(\mathbf{r} \mid \mathbf{r}_0, k)]d^3\mathbf{r}$$

which is a solution to

$$(\nabla^2 + k^2)u(\mathbf{r}, k) = 0.$$

II.2 Let $U(\mathbf{r}, t) = u(\mathbf{r}, \omega)\exp(i\omega t)$, then

$$\nabla^2 u + k^2 u = -4\pi\rho; \quad k = \frac{\omega}{c} = \frac{2\pi}{\lambda}$$

where λ is the wavelength. The Green function solution to this equation (at $\mathbf{r}_0$) is

$$u(\mathbf{r}_0, k) = \int_{-\infty}^{\infty} 4\pi\rho(\mathbf{r})g(\mathbf{r} \mid \mathbf{r}_0, k)d^3\mathbf{r}$$

where g (the outgoing Green function) is

$$g(\mathbf{r} \mid \mathbf{r}_0, k) = \frac{\exp(ik \mid \mathbf{r} - \mathbf{r}_0 \mid)}{4\pi \mid \mathbf{r} - \mathbf{r}_0 \mid}$$

whose asymptotic form is

$$\frac{\exp(ikr_0)}{4\pi r_0} \exp(-ik\hat{\mathbf{n}} \cdot \mathbf{r}); \quad \hat{\mathbf{n}} = \frac{\mathbf{r}_0}{r_0}, \quad r_0 >> r$$

which can be used in this problem because the antenna is 'thin'. Hence, in the far field

$$u(\mathbf{r}_0, k) = \frac{\exp(ikr_0)}{r_0} \int_{-\infty}^{\infty} \rho(\mathbf{r}) \exp(-ik\hat{\mathbf{n}} \cdot \mathbf{r}) d^3\mathbf{r}.$$

In spherical polar coordinates, for $\rho = 1/(4\pi r^2)$,

$$u(r_0, k) = \frac{\exp(ikr_0)}{4\pi r_0} \int_0^{2\pi} \int_{-1}^{-1} \int_0^{\infty} \frac{\exp(-ikr\cos\theta)}{r^2} r^2 dr d(\cos\theta) d\phi$$

$$= \frac{\exp(ikr_0)}{r_0} \int_0^{\infty} \frac{\sin(kr)}{kr} dr = \frac{\pi}{2kr_0} \exp(ikr_0).$$

Hence, $\mid u \mid = \lambda/4r_0$ and with $\lambda = 10$m and $r_0 = 1000$m has a value of 0.0025.

II.3

(i)

$$\left(\nabla^2 - \frac{1}{c_0^2}\frac{\partial^2}{\partial t^2} - \tau_0 \frac{\partial}{\partial t}\right) u(\mathbf{r}, t) = \left[-(k + i\alpha)^2 + \frac{\omega^2}{c_0^2} + i\omega\tau_0\right] u(\mathbf{r}, t) = 0$$

$$\Longrightarrow k^2 + 2i\alpha k - \alpha^2 - \frac{\omega^2}{c_0^2} - i\omega\tau_0 = 0$$

Equating real and imaginary parts, we have

$$2\alpha k - \omega\tau_0 = 0, \quad \Longrightarrow k = \frac{\omega\tau_0}{2\alpha}$$

and

$$k^2 - \alpha^2 - \frac{\omega^2}{c_0^2} = 0$$

giving

$$\frac{\omega^2\tau_0^2}{4\alpha^2} - \alpha^2 - \frac{\omega^2}{c_0^2} = 0$$

or

$$\alpha^4 + \frac{\omega^2}{c_0^2}\alpha^2 - \frac{\omega^2\tau_0^2}{4} = 0$$

whose solution (for α to be real and positive) is

$$\alpha = \frac{\omega}{c_0\sqrt{2}}\left[\left(1+\frac{c_0^4\tau_0^2}{\omega^2}\right)^{\frac{1}{2}}-1\right]^{\frac{1}{2}}.$$

The phase velocity is given by

$$c_p = \frac{2\alpha}{\tau_0}$$

Note that for large values of ω when $c_0^4\tau_0^2/\omega^2 << 1$,

$$\alpha \sim \frac{\omega}{c_0\sqrt{2}}\left(\frac{c_0^4\tau_0^2}{2\omega^2}\right)^{\frac{1}{2}} = \frac{c_0\tau_0}{2}$$

and the phase velocity is c_0.

(ii)

$$\left(\nabla^2 - \frac{1}{c_0^2}\frac{\partial^2}{\partial t^2} - \tau_0\frac{\partial}{\partial t}\nabla^2\right)u(\mathbf{r},t)$$

$$= \left[-(k+i\alpha)^2 + \frac{\omega^2}{c_0^2} - i\omega\tau_0(k+i\alpha)^2\right]u(\mathbf{r},t) = 0$$

$$\Longrightarrow k^2 + 2i\alpha k - \alpha^2 = \frac{\omega^2}{c_0^2}\frac{1-i\omega\tau_0}{1+\omega^2\tau_0^2}$$

Equating real and imaginary parts, we have

$$2\alpha k = \frac{\omega^2}{c_0^2}\frac{\omega\tau_0}{1+\omega^2\tau_0^2}, \quad \Longrightarrow \quad k = \frac{\omega^2}{2\alpha c_0^2}\frac{\omega\tau_0}{1+\omega^2\tau_0^2}$$

and

$$k^2 - \alpha^2 = \frac{\omega^2}{c_0^2}\frac{1}{1+^2\tau_0^2}$$

or

$$\alpha^4 + \frac{\omega^2}{c_0^2(1+\omega^2\tau_0^2)}\alpha^2 - \frac{\omega^6}{4c_0^2}\frac{\tau_0^2}{(1+\omega^2\tau_0^2)^2} = 0$$

whose solution (for α to be real and positive) is

$$\alpha = \frac{\omega}{c_0\sqrt{2}}\frac{[(1+\omega^2\tau_0^2)^{\frac{1}{2}}-1]^{\frac{1}{2}}}{(1+\omega^2\tau_0^2)^{\frac{1}{2}}}.$$

The phase velocity is then given by

$$c_p = \frac{\omega}{k} = \omega\frac{2\alpha c_0^2}{\omega^2}\frac{(1+\omega^2\tau_0^2)}{\omega\tau_0} = c\sqrt{2}(1+\omega^2\tau_0^2)^{\frac{1}{2}}\frac{[(1+\omega^2\tau_0^2)^{\frac{1}{2}}-1]^{\frac{1}{2}}}{\omega\tau_0}.$$

Noting that

$$[(1+\omega^2\tau_0^2)^{\frac{1}{2}}-1]^{\frac{1}{2}}[(1+\omega^2\tau_0^2)^{\frac{1}{2}}+1]^{\frac{1}{2}} = \omega\tau_0$$

we have

$$c_p = c_0\sqrt{2}\left[\frac{1+\omega^2\tau_0^2}{(1+\omega^2\tau_0^2)^{\frac{1}{2}}+1}\right]^{\frac{1}{2}}$$

and for $\omega\tau_0 << 1$,

$$\alpha(\omega) \simeq \frac{\omega^2\tau_0}{2c_0}$$

so that the absorption of acoustic radiation in a viscous medium is proportional to the square of the frequency. Low frequency acoustic radiation will therefore propagate much further through such a medium.

(iii) For

$$u(\mathbf{r},t) = \exp[i(\mathbf{K}\cdot\mathbf{r}-\omega t)]$$

where $\mathbf{K} = \hat{\mathbf{n}}(k+i\alpha)$, the Leeman operator gives

$$K^2 - \frac{\omega^2}{c_0^2} - i\omega\tau_0 - i\omega\tau_1 K = 0$$

where $K = \mid \mathbf{K} \mid$. Solving for K, we get

$$K = \frac{i\omega\tau_1}{2} \pm \frac{1}{2}\left[-\omega^2\tau_1^2 + 4\left(i\omega\tau_0 + \frac{\omega^2}{c_0^2}\right)\right]^{\frac{1}{2}} = \frac{i\omega\tau_1}{2} \pm \frac{\omega}{c_0}\left[\left(1-\frac{\tau_1^2c_0^2}{4}\right)+\frac{i\tau_0c_0^2}{\omega}\right]^{\frac{1}{2}}$$

$$= \frac{i\omega\tau_1}{2} \pm \omega\tau\left(1+\frac{i\tau_1}{\omega\tau_0}\right)^{\frac{1}{2}}$$

where

$$\tau = \left(\frac{1}{c_0^2} - \frac{\tau_1^2}{4}\right)^{\frac{1}{2}}.$$

For an ultrasonic field where the frequency is in the MHz range, we have (for $\omega\tau >> \tau_0$)

$$K \simeq \frac{i\omega\tau_1}{2} \pm \omega\tau\left(1+\frac{1}{2}\frac{i\tau_0}{\omega\tau}\right) = \pm\omega\tau + i\frac{\omega\tau_1}{2} \pm i\frac{\tau_0}{2}.$$

The absorption function is given by

$$\alpha(\omega) = \mathrm{Im}[K] = \frac{\omega\tau_1}{2} + \frac{\tau_0}{2}$$

and the phase velocity is given by

$$c_p = \frac{\omega}{k} = \frac{\omega}{\omega\tau} = \left(\frac{1}{c_0^2} - \frac{\tau_0^2}{4}\right)^{-\frac{1}{2}}.$$

In this case, the absorption of the wavefield varies linearly with the frequency.

II.4 (i) We require the Green function to the following equation:

$$\left(\nabla^2 - \frac{1}{c^2}\frac{\partial^2}{\partial t^2} - \tau_0^2\right) G(\mathbf{r} \mid \mathbf{r}_0, t \mid t_0) = -\delta^3(\mathbf{r}-\mathbf{r}_0)\delta(t-t_0).$$

Let

$$G(R,\tau) = \frac{1}{2\pi}\int\limits_{-\infty}^{\infty} g(R,\omega)\exp(i\omega\tau)d\omega$$

and

$$\delta(\tau) = \frac{1}{2\pi}\int\limits_{-\infty}^{\infty} \exp(i\omega\tau)d\omega$$

where $R = \mid \mathbf{r} - \mathbf{r}_0 \mid$ and $\tau = t - t_0$ so that the equation above becomes (in ω-space)

$$\left(\nabla^2 + \frac{\omega^2}{c^2} - \tau_0^2\right) g(R,\omega) = -\delta^3(\mathbf{r} - \mathbf{r}_0).$$

Further, let

$$g(R,\omega) = \frac{1}{(2\pi)^3}\int\limits_{-\infty}^{\infty} \widetilde{g}(\mathbf{k},\omega)\exp(i\mathbf{k}\cdot\mathbf{R})d^3\mathbf{k}$$

and

$$\delta^3(\mathbf{R}) = \frac{1}{(2\pi)^3}\int\limits_{-\infty}^{\infty} \exp(i\mathbf{k}\cdot\mathbf{R})d^3\mathbf{k}.$$

The equation then transforms to

$$\left(-k^2 + \frac{\omega^2}{c^2} - \tau_0^2\right)\widetilde{g} = -1$$

or

$$\widetilde{g}(k,\omega) = \frac{1}{k^2 - (\omega^2/c^2) + \tau_0^2}.$$

Fourier inverting, we obtain

$$G(R,\tau) = \frac{1}{(2\pi)^4}\int\limits_{-\infty}^{\infty}\int\limits_{-\infty}^{\infty} \frac{\exp(i\mathbf{k}\cdot\mathbf{R})\exp(i\omega\tau)}{k^2 - (\omega^2/c^2) + \tau_0^2} d^3\mathbf{k}d\omega.$$

Integrating over the angular components of $\mathbf{k}$ (using spherical polar coordinates) we have

$$G(R,\tau) = \frac{1}{2\pi}\frac{1}{4\pi^2 R}\int\limits_{-\infty}^{\infty}\int\limits_{-\infty}^{\infty} \frac{k\sin(kR)\exp(i\omega\tau)}{k^2 - (\omega^2/c^2) + \tau_0^2} dkd\omega.$$

The contour integral

$$\oint\limits_C \frac{z\exp(iRz)}{z^2 - (\omega^2/c^2) + \tau_0^2} dz$$

has simple poles at $z = \pm\sqrt{(\omega^2/c^2) - \tau_0^2}$. If we consider the contour to enclose the positive pole only, then contour integration (using the residue theorem) gives the outgoing Green function

$$G(R,\tau) = \frac{1}{2\pi}\frac{1}{4\pi R}\int_{-\infty}^{\infty} \exp\left(iR\sqrt{(\omega^2/c^2) - \tau_0^2}\right)\exp(i\omega\tau)d\omega.$$

The last part of the calculation is therefore to compute the integral above. Noting that $\sqrt{(\omega^2/c^2) - \tau_0^2} = i\sqrt{\tau_0^2 - (\omega^2/c^2)}$ and letting $i\omega = p$, we can write

$$G(R,\tau) = \frac{1}{4\pi R}\frac{1}{2\pi i}\int_{-i\infty}^{i\infty} \exp\left(-R\sqrt{\tau_0^2c^2 + p^2}/c\right)\exp(p\tau)dp$$

which expresses the problem in terms of the Bromwich integral. We are thus required to evaluate the inverse Laplace transform of $\exp(-R\sqrt{\tau_0^2c^2 + p^2}/c)$. Noting that

$$\exp\left(-R\sqrt{\tau_0^2c^2 + p^2}/c\right) = -c\frac{\partial}{\partial R}\left(\frac{\exp\left(-R\sqrt{\tau_0^2c^2 + p^2}/c\right)}{\sqrt{\tau_0^2c^2 + p^2}}\right)$$

we can write

$$G(R,\tau) = -\frac{c}{4\pi R}\frac{\partial}{\partial R}\left[J_0\tau_0^2c\sqrt{\tau^2 - (R^2/c^2)}\right], \quad \tau > \frac{R}{c}.$$

(ii) Using the same approach as that used in part (i) above, we can write the outgoing Green function as

$$G(R,\tau) = \frac{1}{2\pi}\frac{1}{4\pi R}\int_{-\infty}^{\infty} \exp\left(iR\sqrt{(\omega^2/c^2) - i\omega\tau_0}\right)\exp(i\omega\tau)d\omega$$

the term $i\omega\tau_0$ in the first integral being a direct result of the term $\tau_0\partial/\partial t$ present in this operator. Noting that

$$\sqrt{(\omega^2/c^2) - i\omega\tau_0} = i\sqrt{\left(\frac{i\omega}{c} + \frac{\tau_0 c}{2}\right)^2 - \frac{\tau_0^2c^2}{4}}$$

and letting $p = (i\omega/2) + (\tau_0 c/2)$, we obtain

$$G(R,\tau) = \frac{c}{4\pi R}\exp(-\tau_0c^2\tau/2)\frac{1}{2\pi i}\int_{-i\infty}^{i\infty} \exp(-R\sqrt{p^2 - \tau_0^2c^2/4}\exp(pc\tau)dp$$

$$= -\frac{c}{4\pi R}\exp(-\tau_0c^2\tau/2)\frac{\partial}{\partial R}\left[I_0\left(\frac{\tau_0 c}{2}\sqrt{c^2\tau^2 - R^2}\right)\right], \quad c\tau > R.$$

(iii) Using the Fourier technique, the Green function is given by

$$G(R,\tau) = \frac{1}{(4\pi)^2} \int_{-\infty}^{\infty} \frac{\exp(i\mathbf{k}\cdot\mathbf{R})\exp(i\omega\tau)}{(\omega^2/c^2) - k^2(1-i\omega\tau)}.$$

Integrating over $\mathbf{k}$, the outgoing Green function is then

$$G(R,\tau) = \frac{1}{4\pi R}\frac{1}{2\pi} \int_{-\infty}^{\infty} \exp(i\omega\tau)\exp\left(\frac{i\omega R}{c(1-i\omega\tau)^{\frac{1}{2}}}\right) d\omega.$$

We can write this result as

$$G(R,\tau) = \frac{\exp(-b\tau)}{4\pi R}\hat{L}^{-1}\left[\exp(-aR\sqrt{p})\exp(abR/\sqrt{p})\right]H(\tau - R/c)$$

where $a = 1/\sqrt{\tau c^2}$, $b = 1/\tau$ and $p = b + i\omega$; $\hat{L}^{-1}$ denotes the inverse Laplace transform and H denotes the step function. Using the results provided in the question, we have

$$G(R,\tau) = \frac{\exp(-b\tau)}{4\pi R}\frac{\exp(-a^2(1-b)^2R/8\tau)}{\sqrt{2\pi}\tau}$$

$$\times \sum_{n=-\infty}^{\infty}\Big[(-1/\sqrt{2\tau})^n J_n(2abR) D_{n+1}(a(1-b)R/\sqrt{2\tau})\Big]H(\tau - R/c).$$

(iv) Using the Fourier method,

$$G(\mathbf{R},\tau) = \frac{1}{(4\pi)^4} \int_{-\infty}^{\infty} \frac{\exp(i\mathbf{k}\cdot\mathbf{R})\exp(i\omega\tau)}{(k^2 - \omega^2/c^2) + \omega(i+\tau_1 k)} d^3\mathbf{k}d\omega$$

With $\gamma = i\alpha - \beta\kappa$ where $\alpha = \tau_0 c^2/2$, $\beta = \tau_1 c/2$ and $\kappa = kc$, this equation can be written as

$$G(R,\tau) = -\frac{c^2}{(2\pi)^4} \int_{-\infty}^{\infty} d^3\mathbf{k}\exp(i\mathbf{k}\cdot\mathbf{R}) \int_{-\infty}^{\infty} d\omega \frac{\exp(i\omega\tau)}{[(\omega-\gamma)^2 - (\gamma^2+\kappa^2)]}.$$

Integrating over ω and the angular components of $\mathbf{k}$, we obtain

$$G(R,\tau) = \frac{\exp(-\alpha\tau)}{2\pi^2 R} \int_0^{\infty} d\kappa\kappa \sin(\kappa R/c)\frac{\sin(\sqrt{\gamma^2+\kappa^2}\tau)}{\sqrt{\gamma^2+\kappa^2}}\exp(i\beta\tau\kappa).$$

Now, noting that

$$\gamma^2 + \kappa^2 = (1+\beta^2)\left(\kappa - \frac{i\alpha\beta}{1+\beta^2}\right)^2 - \frac{\alpha^2}{1+\beta^2},$$

using the Gegenbauer integral given in the question, we get

$$G(R,\tau)\frac{c}{4\pi^2 R}\frac{\exp(-\alpha\tau)}{\sqrt{1+\beta^2}}\frac{\partial}{\partial R}\int_0^\infty d\kappa\cos(R\kappa/c)\exp[-i(\beta\tau-s)\kappa]$$

$$\times\int_{-\sqrt{1+\beta^2}\tau}^{\sqrt{1+\beta^2}\tau} ds J_0\left(\frac{\alpha}{1+\beta^2}\sqrt{s^2-(1+\beta)^2\tau^2}\right)\exp\left(-\frac{\alpha\beta s}{1+\beta^2}\right).$$

On noting that

$$\int_{-\infty}^{\infty} d\kappa\cos(R\kappa/c)\exp[-i(\beta\tau-s)\kappa]=\pi\left[\delta\left(\frac{R}{c}-\beta\tau-s\right)+\delta\left(\frac{R}{c}+\beta\tau+s\right)\right]$$

we can write the Green function as

$$G(R,\tau)=\frac{c}{4\pi}\frac{\exp(-\alpha\tau)}{\sqrt{1+\beta^2}}\frac{1}{R}\frac{\partial}{\partial R}\left[J_0\left(\frac{\alpha}{1+\beta^2}\sqrt{\left(\frac{R}{c}-\beta\tau\right)^2-(1+\beta^2)\tau^2}\right)\right]$$

$$\times\exp\left[-\frac{\alpha\beta}{1+\beta^2}\left(\frac{R}{c}-\beta\tau\right)\right]H\left(\tau-\frac{R}{c_+}\right)$$

$$+\frac{c}{4\pi}\frac{\exp(-\alpha\tau)}{\sqrt{1+\beta^2}}\frac{1}{R}\frac{\partial}{\partial R}\left[J_0\left(\frac{\alpha}{1+\beta^2}\sqrt{\left(\frac{R}{c}+\beta\tau\right)^2-(1+\beta^2)\tau^2}\right)\right]$$

$$\times\exp\left[\frac{\alpha\beta}{1+\beta^2}\left(\frac{R}{c}+\beta\tau\right)\right]H\left(\tau-\frac{R}{c_-}\right)$$

where $c_\pm=c(\sqrt{1+\beta^2}\pm\beta)$.

II.5 With $\mathbf{R}=\mathbf{r}-\mathbf{r}_0$ and $\tau=t-t_0$, solve

$$\left(\nabla^2+\sigma\frac{\partial}{\partial\tau}\right)G(R,\tau)=-\delta^3(R)\delta(\tau),\quad \tau>0.$$

Take Laplace transforms to get

$$\nabla^2\bar{G}(R,p)+\sigma[p-G(R,0)]\bar{G}(R,p)=-\delta^3(R)$$

or

$$\nabla^2\bar{G}(R,p)+\sigma p\bar{G}(R,p)=-\delta^3(R),\quad G(R,0)=0$$

whose solution is

$$\bar{G}(R,p)=\frac{1}{4\pi R}\exp(-\sqrt{\sigma p}R).$$

Hence,

$$G(R,\tau)=\frac{1}{4\pi R}\hat{L}^{-1}\left[\exp(-\sqrt{\sigma p}R)\right].$$

Using the result provides in the question (i.e. the Laplace transform of the function $t^{-3/2}\exp(-a/t)$ we note that

$$\hat{L}^{-1}[\exp(-2\sqrt{ap})] = \sqrt{\frac{a}{\pi}}\tau^{-3/2}\exp(-a/\tau)$$

and thus, with $2\sqrt{a} = R\sqrt{\sigma}$ so that $a = R^2\sigma/4$ we have

$$G(R,\tau) = \frac{1}{4\pi R}\sqrt{\frac{R^2\sigma}{4\pi}}\tau^{-3/2}\exp\left(-\frac{R^2\sigma}{4\tau}\right)$$

$$= \frac{1}{\sigma}\left(\frac{\sigma}{4\pi\tau}\right)^{\frac{3}{2}}\exp\left(-\frac{\sigma R^2}{4\tau}\right), \quad \tau > 0.$$

II.6 (i) Since $c = c_0 + v$,

$$\frac{1}{c^2} = \frac{1}{(c_0+v)} = \frac{1}{c^2}\left(1+\frac{v}{c_0}\right)^{-2} = \frac{1}{c_0}\left(1-\frac{2v}{c_0}+...\right)$$

$$\frac{1}{c_0^2} - \frac{2v}{c_0^3}, \quad \frac{v}{c_0} << 1.$$

The equation then becomes

$$\left(\frac{\partial^2}{\partial x^2} + k^2 - 2k^2\frac{v}{c_0}\right)u(x,\omega) = 0.$$

With $u = w + \exp(-ikx)$ we have

$$\left(\frac{\partial^2}{\partial x^2} + k^2\right)\exp(-ikx) + \left(\frac{\partial^2}{\partial x^2} + k^2\right)w$$

$$-2k^2\frac{v}{c_0}\exp(-ikx) - 2k^2\frac{v}{c_0}w = 0$$

which reduces to

$$\left(\frac{\partial^2}{\partial x^2} + k^2\right)w(x,k) = 2k^2\frac{v}{c}\exp(-ikx)$$

because

$$\left(\frac{\partial^2}{\partial x^2} + k^2\right)\exp(-ikx) = 0$$

and since $v/c_0 << 1$ and $\mid w \mid << 1$, the term $2k^2vw/c_0$ can be neglected.

(ii) The outgoing Green function solution is

$$w(x_0,k) = \frac{2k^2}{c_0}\frac{i}{2k}\int_{-\infty}^{\infty}\exp(ik \mid x - x_0 \mid)v(x)\exp(-ikx)dx$$

$$= \frac{ik}{c_0} \exp(ikx_0) \int_{-\infty}^{\infty} v(x) \exp(-2ikx) dx, \quad x_0 \to \infty.$$

Now,

$$ik \int_{-\infty}^{\infty} v(x) \exp(-2ikx) dx = -\frac{1}{2} \int_{-\infty}^{\infty} \left(\frac{d}{dx} \exp(-2ikx) \right) v(x) dx$$

$$-\frac{1}{2} \int_{-\infty}^{\infty} \frac{dv}{dx} \exp(-2ikx) dx$$

assuming $v(x) \mid_{\pm\infty} = 0$. Thus,

$$w(x_0, k) = -\exp(ikx_0) \frac{1}{2c_0} \int_{-\infty}^{\infty} \frac{dv}{dx} \exp(-2ikx) dx.$$

Since $x = ct$ and $k = \omega/c$, we can write this result in the form

$$w(\tau_0, \omega) = -\exp(i\omega t_0/2) \int_{-\infty}^{\infty} \frac{1}{2c_0} \frac{dv}{d\tau} \exp(-i\omega\tau) d\tau$$

where $\tau = 2t$. Taking the inverse Fourier transform and using the convolution theorem we obtain

$$w(\tau) = -\frac{1}{2c_0} \frac{dv}{d\tau} \otimes \delta(\tau + t_0/2)$$

The condition $v/c_0 << $ implies that v is a small perturbation of c_0. The condition $\mid w \mid << 1$ implies weak or Born scattering. This expression for the impulse response function is obtained under the Born approximation.

(iii) With $u(x, k) = \exp[iks(x)]$,

$$\frac{\partial u}{\partial x} = ik \exp(iks) \frac{ds}{dx}$$

and

$$\frac{\partial^2 u}{\partial x^2} = (ik)^2 \exp(iks) \left(\frac{ds}{dx} \right)^2 + ik \exp(iks) \frac{d^2 s}{dx^2}$$

$$\simeq (ik)^2 \exp(iks) \left(\frac{ds}{dx} \right)^2, \quad \omega \to \infty$$

and the original equation transforms to

$$\frac{\omega^2}{c_0^2} \left(\frac{ds}{dx} \right)^2 = \frac{\omega^2}{c^2}, \quad \text{or} \quad \frac{ds}{dx} = \frac{c_0}{c}.$$

Hence, if $c = \alpha c_0/x$, then

$$\frac{ds}{dx} = \frac{x}{\alpha} \qquad s = \beta + \frac{x^2}{2\alpha}$$

where β is a constant of integration. The condition $\omega \to \infty$ implies that the wavelength is much smaller than the characteristic variations in s.

II.7 With $u = ge^s$, the equation becomes

$$\nabla^2 g + k^2 g + 2\nabla s \cdot \nabla g + g\nabla s \cdot \nabla s + g\nabla^2 s = -k^2\gamma g - \delta^3.$$

Under the Rytov approximation (i.e. neglecting the nonlinear term $g\nabla s \cdot \nabla s$), we have

$$g\nabla^2 s + 2\nabla s \cdot \nabla g = -k^2\gamma g$$

which, after the substitution of $s = w/g$, reduces to

$$\nabla^2 w + k^2 w = -k^2\gamma g - \frac{w}{g}\delta^3.$$

The Green function solution to this equation as a point $\mathbf{r}_s$ say (with homogeneous boundary conditions) is

$$w(\mathbf{r}_s \mid \mathbf{r}_0, k) = k^2 \int \gamma(\mathbf{r}) g(\mathbf{r} \mid \mathbf{r}_0, k) g(\mathbf{r} \mid \mathbf{r}_s, k) d^3\mathbf{r}$$

$$+ \int \frac{w(\mathbf{r}, k)}{g(\mathbf{r} \mid \mathbf{r}_0, k)} g(\mathbf{r} \mid \mathbf{r}_s, k)\delta^3(\mathbf{r} - \mathbf{r}_0) d^3\mathbf{r} = k^2 \int \gamma(\mathbf{r}) g(\mathbf{r} \mid \mathbf{r}_0, k) g(\mathbf{r} \mid \mathbf{r}_s, k) d^3\mathbf{r}$$

since $1/g(\mathbf{r}_0 \mid \mathbf{r}_0, k) = 0$. Hence the solution is

$$u(\mathbf{r}_s \mid \mathbf{r}_0, k) = g(\mathbf{r}_s \mid \mathbf{r}_0, k) \exp\left[\frac{k^2}{g(\mathbf{r}_s \mid \mathbf{r}_0, k)} \int \gamma(\mathbf{r}) g(\mathbf{r} \mid \mathbf{r}_0, k) g(\mathbf{r} \mid \mathbf{r}_s, k) d^3\mathbf{r}\right]$$

$$= g(\mathbf{r}_s \mid \mathbf{r}_0, k) + k^2 \int \gamma(\mathbf{r}) g(\mathbf{r} \mid \mathbf{r}_0, k) g(\mathbf{r} \mid \mathbf{r}_s, k) d^3\mathbf{r} + ...$$

The back-scattered field is given by

$$u(\mathbf{r}_0, k) = \lim_{\mathbf{r}_s \to \mathbf{r}_0} [u(\mathbf{r}_s \mid \mathbf{r}_0, k) - g(\mathbf{r}_s \mid \mathbf{r}_0, k)] = k^2 \int \gamma(\mathbf{r}) g^2(\mathbf{r} \mid \mathbf{r}_0, k) d^3\mathbf{r}.$$

II.8 (i) Taking the Laplace transform, the equation transforms (using the convolution theorem for Laplace transforms) to

$$U(p) = \frac{1}{p^2} - \frac{1}{p^2} U(p).$$

Thus,

$$U(p) = \frac{1}{1 + p^2} \quad \text{and} \quad u(x) = \sinh x.$$

(ii) The Neumann series for this equation is

$$u_n(x) = x - \int_0^x (t-x)u_{n-1}(t)dt, \quad n = 1, 2, 3, ...$$

Thus

$$u_0(x) = x;$$

$$u_1(x) = x - \int_0^x (t-x)tdt = x - \left[\frac{t^3}{3} - x\frac{t^2}{2}\right]_0^x = x - \frac{x^3}{3} + \frac{x^3}{2} = x + \frac{x^3}{6};$$

$$u_2(x) = x - \int_0^x (t-x)\left(t + \frac{t^3}{6}\right)dt = x - \left[\frac{t^3}{3} + \frac{t^5}{50} - x\frac{t^2}{2} - x\frac{t^4}{24}\right]_0^x = x + \frac{x^3}{6} + \frac{x^5}{120}$$

and by induction

$$x + \frac{x^3}{6} + \frac{x^5}{120} + ... = \sinh x.$$

II.9 The Green function solution to this equation at a point $\mathbf{r}_s$ is given by

$$u(\mathbf{r}_s \mid \mathbf{r}_0, k) = \oint_S [g(\mathbf{r} \mid \mathbf{r}_s, k)\nabla u(\mathbf{r} \mid \mathbf{r}_0, k) - u(\mathbf{r} \mid \mathbf{r}_0, k)\nabla g(\mathbf{r} \mid \mathbf{r}_s, k)].\hat{\mathbf{n}}d^2\mathbf{r}$$

$$+k^2 \int_V g(\mathbf{r} \mid \mathbf{r}_s, k)\gamma(\mathbf{r})u(\mathbf{r} \mid \mathbf{r}_0, k)d^3\mathbf{r} + g(\mathbf{r}_0 \mid \mathbf{r}_s, k)$$

where $g(\mathbf{r}_0 \mid \mathbf{r}_s, k)$ is the incident field (i.e. the field when $\mathbf{r} \notin V$) and $g(\mathbf{r} \mid \mathbf{r}_s, k)$ is the solution of

$$(\nabla^2 + k^2)g(\mathbf{r} \mid \mathbf{r}_s, k) = -\delta^3(\mathbf{r} - \mathbf{r}_s)$$

and given by

$$g(\mathbf{r} \mid \mathbf{r}_s, k) = \frac{1}{4\pi \mid \mathbf{r} - \mathbf{r}_s \mid} \exp(ik \mid \mathbf{r} - \mathbf{r}_s \mid).$$

If

$$u(\mathbf{r} \mid \mathbf{r}_0, k) = g(\mathbf{r} \mid \mathbf{r}_0, k)$$

on the surface of V, then using Green's theorem the surface integral becomes

$$\int_V [g(\mathbf{r} \mid \mathbf{r}_s, k)\nabla^2 g(\mathbf{r} \mid \mathbf{r}_0, k) - g(\mathbf{r} \mid \mathbf{r}_0, k)\nabla^2 g(\mathbf{r} \mid \mathbf{r}_s, k)]d^3\mathbf{r}$$

$$= \int_V g(\mathbf{r} \mid \mathbf{r}_s, k)[-k^2 g(\mathbf{r} \mid \mathbf{r}_0, k) - \delta^3(\mathbf{r} - \mathbf{r}_0)]d^3\mathbf{r}$$

$$- \int_V g(\mathbf{r} \mid \mathbf{r}_0)[-k^2 g(\mathbf{r} \mid \mathbf{r}_s, k) - \delta^3(\mathbf{r} - \mathbf{r}_s)]d^3\mathbf{r}$$

$$= -g(\mathbf{r}_0 \mid \mathbf{r}_s, k) + g(\mathbf{r}_s \mid \mathbf{r}_0, k) = 0$$

through the reciprocity theorem. Hence, the solution of the equation becomes

$$u(\mathbf{r}_s \mid \mathbf{r}_0, k) = g(\mathbf{r}_s \mid \mathbf{r}_0, k) + k^2 \int_V g(\mathbf{r} \mid \mathbf{r}_s, k)\gamma(\mathbf{r})u(\mathbf{r} \mid \mathbf{r}_0, k)d^3\mathbf{r}.$$

The Born series solution is now

$$u(\mathbf{r}_s \mid \mathbf{r}_0, k) = g(\mathbf{r}_s \mid \mathbf{r}_0, k) + k^2 \int_V g(\mathbf{r} \mid \mathbf{r}_s, k)\gamma(\mathbf{r})g(\mathbf{r} \mid \mathbf{r}_0, k)d^3\mathbf{r} + O(k^n)$$

where $n = 4, 6, 8, ...$ Hence, if we consider the limit

$$U(\mathbf{r}_s \mid \mathbf{r}_0) = \lim_{k\to 0}\left(\frac{u(\mathbf{r}_s \mid \mathbf{r}_0, k) - g(\mathbf{r}_s \mid \mathbf{r}_0, k)}{k^2}\right)$$

then we can write

$$U(\mathbf{r}_s \mid \mathbf{r}_0) = \frac{1}{16\pi^2}\int_V \frac{\gamma(\mathbf{r})}{\mid \mathbf{r} - \mathbf{r}_0 \mid}\frac{d^3\mathbf{r}}{\mid \mathbf{r} - \mathbf{r}_s \mid}.$$

In the far field, when $r_s \equiv \mid \mathbf{r}_s \mid >> \mid \mathbf{r} \mid$ say,

$$U(\mathbf{r}_s \mid \mathbf{r}_0) = \frac{1}{16\pi^2 r_s}\int_V \frac{\gamma(\mathbf{r})}{\mid \mathbf{r} - \mathbf{r}_0 \mid}d^3\mathbf{r}.$$

In the far fields when $r_s \equiv \mid \mathbf{r}_s \mid >> \mid \mathbf{r} \mid$ and $r_0 \equiv \mid \mathbf{r}_0 \mid >> \mid \mathbf{r} \mid$,

$$U(\mathbf{r}_s \mid \mathbf{r}_0) = \frac{1}{16\pi^2 r_s r_0}\int_V \gamma(\mathbf{r})d^3\mathbf{r}$$

which is the DC (zero frequency component) of the scatterer scaled by $1/(16\pi^2 r_s r_0)$. In this sense, using very low frequency radiation in the far fields provides an exact measure of the average value of the scatterer which is not the same as imaging it!

Remark: By considering a scalar Helmholtz scattering theory in the limit as the wavenumber approaches zero, we can derive some known characteristics of a gravitational field, namely, that gravity is a weak force, it obeys an inverse square law (Newton's law of gravity), it bends light (a consequence of Einstein's correction to Newton's law of gravity) and is an attractive only force.

Consider the Helmholtz equation

$$(\nabla^2 + k^2)u(\mathbf{r}, k) = -k^2\gamma(\mathbf{r})u(\mathbf{r}, k)$$

to be the result of transforming the inhomogeneous wave equation

$$\left(\nabla^2 - \frac{1}{c^2}\frac{\partial^2}{\partial t^2}\right)U(\mathbf{r}, t) = 0$$

using

$$U(\mathbf{r},t) = u(\mathbf{r},\omega)\exp(i\omega t), \quad \frac{1}{c^2} = \frac{1}{c_0^2}[1+\gamma(\mathbf{r})], \quad k = \frac{\omega}{c_0}$$

where ω is the angular frequency, c_0 is a constant and no physical significance is placed on the nature of the scalar wavefield u or the (dimensionless) scattering function γ other than it is taken to be of compact support $\mathbf{r} \in V$.

The general solution to this equation at a point $\mathbf{r}_0$ is given by the Lippmann-Schwinger equation

$$u(\mathbf{r}_0,k) = u_i(\mathbf{r}_0,k) + k^2 \int\limits_V g(\mathbf{r} \mid \mathbf{r}_0,k)\gamma(\mathbf{r})u(\mathbf{r},k)d^3\mathbf{r}$$

where u_i is the incident field and g is the Green function

$$g(\mathbf{r} \mid \mathbf{r}_0,k) = \frac{1}{4\pi \mid \mathbf{r}-\mathbf{r}_0 \mid} \exp(ik \mid \mathbf{r}-\mathbf{r}_0 \mid)$$

which is the solution of

$$(\nabla^2 + k^2)g(\mathbf{r} \mid \mathbf{r}_0,k) = -\delta^3(\mathbf{r}-\mathbf{r}_0).$$

Since the solution for u is of the form

$$u = u_i + \hat{I}u$$

where $\hat{I}$ is the operator

$$\hat{I} = k^2 \int\limits_V d^3\mathbf{r} g(\mathbf{r} \mid \mathbf{r}_0,k)\gamma(\mathbf{r})$$

we can iterate to produce a solution of the form

$$u = u_i + \hat{I}u_i + \hat{I}(\hat{I}u_i) + ...$$

or

$$u(\mathbf{r}_0,k) = u_i(\mathbf{r}_0,k) + u_s(\mathbf{r}_0,k)$$

where u_s is the scattered field given by

$$u_s(\mathbf{r}_0,k) = k^2 \int\limits_V g(\mathbf{r} \mid \mathbf{r}_0,k)\gamma(\mathbf{r})u_i(\mathbf{r},k)d^3\mathbf{r}$$

$$+k^4 \int\limits_V \int\limits_V g(\mathbf{r} \mid \mathbf{r}_0,k)\gamma(\mathbf{r})g(\mathbf{r} \mid \mathbf{r}',k)\gamma(\mathbf{r}')u_i(\mathbf{r}',k)d^3\mathbf{r}d^3\mathbf{r}' + ...$$

Each term in this 'Born series' describes different order scattering events; the first term models single scattering events, the second term models double scattering, the third term triple scattering and so on. Note that each term in the

Born series scales in k as k^{2n} where $n = 1, 2, 3...$ If we ignore higher order scattering events and model the scattered field in terms of single scattering alone then

$$u_s(\mathbf{r}_0, k) = k^2 \int_V g(\mathbf{r} \mid \mathbf{r}_0, k)\gamma(\mathbf{r})u_i(\mathbf{r}, k)d^3\mathbf{r}$$

This is the weak scattering solution to the problem (the Born approximation) which is valid if

$$\frac{\|u_s\|}{\|u_i\|} << 1$$

or for a spherical scatterer of radius R, if

$$\bar{\gamma} << \frac{1}{k^2R^2}$$

where

$$\bar{\gamma} = \sqrt{\frac{\int \mid \gamma \mid^2 d^3\mathbf{r}}{\int d^3\mathbf{r}}}.$$

If a Helmholtz wavefield oscillates at very low frequencies, then we can consider an asymptotic solution of the form

$$u_s(\mathbf{r}_0, k) = \frac{k^2}{4\pi} \int_V \frac{\gamma(\mathbf{r})}{\mid \mathbf{r} - \mathbf{r}_0 \mid} u_i(\mathbf{r}, k)d^3\mathbf{r}, \quad k \to 0.$$

This is a consequence of the fact that the higher order terms in the Born series can be ignored leaving just the first term as $k \to 0$ and because

$$\frac{\exp(ik \mid \mathbf{r} - \mathbf{r}_0 \mid)}{4\pi \mid \mathbf{r} - \mathbf{r}_0 \mid} = \frac{1}{4\pi \mid \mathbf{r} - \mathbf{r}_0 \mid}, \quad k \to 0$$

giving an exact solution to the problem, i.e. the Born approximation provides us with an exact solution for a Helmholtz scattered field when $k \to 0$. Now, if the incident field is a unit plane wave,

$$u_i(\mathbf{r}, k) = \exp(ik\hat{\mathbf{n}}_i \cdot \mathbf{r})$$

where $\hat{\mathbf{n}}_i$ is the normal unit vector that defines the direction of the plane wave relative to the scattering function, then

$$u(\mathbf{r}_0, k) = 1 + u_s(\mathbf{r}_0, k)$$

where

$$u_s(\mathbf{r}_0, k) = \frac{k^2}{4\pi} \int_V \frac{\gamma(\mathbf{r})}{\mid \mathbf{r} - \mathbf{r}_0 \mid} d^3\mathbf{r}, \quad k \to 0.$$

Here, the wavelength of the incident plane wavefield is assumed to be much much larger than the spatial extent V of the scatterer. For a given scattering function $\gamma(\mathbf{r})$ the scattered field will be a 'weak field' because of the low values

of k required to produce this result. But this particular result is the general solution to Poisson's equation

$$\nabla^2 u_s(\mathbf{r}, k) = -k^2 \gamma(\mathbf{r})$$

which can be written as

$$\nabla \cdot \mathbf{U}(\mathbf{r}, k) = k^2 \gamma(\mathbf{r}), \quad \mathbf{U}(\mathbf{r}, k) = -\nabla u_s(\mathbf{r}, k).$$

Integrating over the volume of the scatterer V, we get

$$\int_V \nabla \cdot \mathbf{U}(\mathbf{r}, k) d^3\mathbf{r} = k^2 \int_V \gamma(\mathbf{r}) d^3\mathbf{r}$$

and using the divergence theorem we can write

$$\oint_S \mathbf{U}(\mathbf{r}, k) \cdot \hat{\mathbf{n}} d^2\mathbf{r} = k^2 \Gamma$$

where

$$\Gamma = \int_V \gamma(\mathbf{r}) d^3\mathbf{r}$$

and S is taken to be the surface enclosing V. For a radially symmetric field $\mathbf{U} = \hat{\mathbf{n}} U$, the surface integral becomes $4\pi r^2 U$ and we get

$$U = \frac{k^2 \Gamma}{4\pi r^2}, \quad k \to 0.$$

Hence, if the scalar wavefield u_s is taken to be the potential of the vector field $\mathbf{U}$ then $U \propto 1/r^2$. Very low frequency Helmholtz scattering thus provides an exact solution for the scattered field whose gradient (for the radially symmetric case) is characterized by a $1/r^2$ scaling law. Very low frequency scattering therefore generates a weak field between the volume integral of the scattering function $\gamma(\mathbf{r})$ and a (gradient) detector at a distance r from the scatterer that obeys an inverse square law.

We have shown that the solution to the Helmholtz equation

$$(\nabla^2 + k^2) u(\mathbf{r}, k) = -k^2 \gamma(\mathbf{r}) u(\mathbf{r}, k)$$

where $\gamma(\mathbf{r})$ is of compact support $\mathbf{r} \in V$ is

$$u(\mathbf{r}, k) = u_i(\mathbf{r}, k) + u_s(\mathbf{r}, k)$$

where, for $k \to 0$, $u_s(\mathbf{r}, k)$, which we shall write as $u_s^0(\mathbf{r}, k)$, is the solution to

$$\nabla^2 u_s^0(\mathbf{r}, k_0) = -k_0^2 \gamma(\mathbf{r}), \quad k_0 \to 0.$$

Consider a weakly scattered Helmholtz wavefield $u_s(\mathbf{r}, k)$ for $k >> 1$ given by

$$u_s(\mathbf{r}_0, k) = k^2 \int_V g(\mathbf{r} \mid \mathbf{r}_0, k) \gamma(\mathbf{r}) u_i(\mathbf{r}, k) d^3\mathbf{r}$$

where

$$\bar{\gamma} << \frac{1}{k^2 R^2}.$$

and since $k >> 1$ we consider the case where $R \to 0$ so that no condition needs to be placed upon the value of $\bar{\gamma}$. We can then write

$$u_s(\mathbf{r}_0, k) = -\frac{k^2}{k_0^2} \int\limits_V g(\mathbf{r} \mid \mathbf{r}_0, k)[\nabla^2 u_s^0(\mathbf{r}, k_0)] u_i(\mathbf{r}, k) d^3\mathbf{r}$$

$$= -\frac{k^2}{k_0^2} \int\limits_V g(\mathbf{r} \mid \mathbf{r}_0, k)[\nabla \cdot \mathbf{U}(\mathbf{r}, k)] u_i(\mathbf{r}, k) d^3\mathbf{r} = \frac{\exp(ikr_0)}{4\pi r_0} A(\hat{\mathbf{n}}_0, \hat{\mathbf{n}}_i), \quad \frac{r}{r_0} << 1$$

where, with $u_i(\mathbf{r}, k) = \exp(ik\hat{\mathbf{n}}_i \cdot \mathbf{r}), \quad \hat{\mathbf{n}}_0 = \mathbf{r}_0 / \mid \mathbf{r}_0 \mid$ and

$$\mathbf{U} = \hat{\mathbf{n}} U = \hat{\mathbf{n}} \frac{k_0^2 \Gamma}{4\pi r^2},$$

$$A(\hat{\mathbf{n}}_0, \hat{\mathbf{n}}_i) = -\frac{k^2 \Gamma}{4\pi} \int\limits_V \exp[-ik(\hat{\mathbf{n}}_0 - \hat{\mathbf{n}}_i) \cdot \mathbf{r}] \nabla \cdot \left(\frac{\hat{\mathbf{n}}}{r^2} \right) d^3\mathbf{r}.$$

Thus, given the Helmholtz equation

$$(\nabla^2 + k^2) u(\mathbf{r}, k) = -k^2 \gamma(\mathbf{r}) u(\mathbf{r}, k)$$

where

$$u(\mathbf{r}, k) = u_i(\mathbf{r}, k) + u_s(\mathbf{r}, k)$$

then the scattered field $u_s(\mathbf{r}, k)$ for $k >> 1$ from a scatterer that is simultaneously generating a scattered field $u_s(\mathbf{r}, k)$ for $k \to 0$ is, in the far field (under the Born approximation) determined by the Fourier transform of the scattering function (assuming radial symmetry)

$$\nabla \cdot \frac{\hat{\mathbf{n}}}{r^2}.$$

In other words, a weak Helmholtz field generated by very low frequency scattering will diffract a high frequency Helmholtz field, the diffraction pattern being determined by the function above.

Can such a low frequency scattered field satisfying the equation

$$\nabla^2 u_s(\mathbf{r}, k) = -k^2 \gamma(\mathbf{r}), \quad k \to 0$$

be detected ? Gravity wave scattering perhaps, in which an apple for example, detects the weak force generated by the gradient of a field whose divergence bends light! If so, suppose the weak force F generated by the field U on a mass m' say is proportional to Um' so that

$$F = v^2 U m'$$

where v^2 is a constant of proportionality. Then

$$F = v^2 k^2 \frac{\Gamma m'}{4\pi r^2}$$

where v has the dimensions of velocity (i.e. length.second^{-1}).

The scattering function $\gamma(\mathbf{r})$ must describe some appropriate property of matter. But matter is composed of matter waves which conform to the wave equation (Schrödinger's equation - see Chapter 6)

$$\left(\nabla^2 + \frac{2m[E - E_p(\mathbf{r})]}{E^2}\frac{\partial^2}{\partial t^2}\right) U(\mathbf{r}, t) = 0$$

where E is the energy of the matter wave that characterizes a particle of mass m and E_p is the potential energy. Now, suppose we generalize this equation and consider the case where the wavefield $U(\mathbf{r}, t)$ can oscillate at any frequency ω less than or significantly less than the frequency ω' associated with a matter wave of energy $E = \hbar\omega'$ where $\hbar$ is Planck's constant so that Schrödinger's equation proper is only obtained when $\omega \to \omega'$.[1] Then, given that

$$\frac{1}{c^2} = \frac{1}{c_0^2}(1 + \gamma) = \frac{2m[E - E_p(\mathbf{r})]}{E^2}$$

and with $U(\mathbf{r}, t) = u(\mathbf{r}, \omega)\exp(i\omega t)$, Schrödinger's equation can be written in terms of the Helmholtz equation

$$(\nabla^2 + k^2)u(\mathbf{r}, k) = -k^2\gamma(\mathbf{r})u(\mathbf{r}, k)$$

where

$$\gamma(\mathbf{r}) = \frac{2mc_0^2}{E^2}[E - E_p(\mathbf{r})] - 1.$$

Hence,

$$\Gamma = Mm$$

where

$$M = \frac{2c_0^2}{E^2}\int\limits_V [E - E_p(\mathbf{r})]d^3\mathbf{r} - \frac{V}{m}, \quad V = \int\limits_V d^3\mathbf{r}.$$

The force field F, then becomes

$$F = G\frac{mm'}{r^2}$$

where

$$G = \frac{Mv^2k_0^2}{4\pi}$$

which is Newton's law of gravity with gravitational constant G.

From the results above, we can derive an expression for the wavelength of the wavefield $u_s(\mathbf{r}, k)$ $k \to 0$ in terms of the gravitational constant for a free matter wave when $E_p = 0$. In this case,

$$M = \frac{V}{m}\left(\frac{2mc_0^2}{E} - 1\right)$$

[1] An entirely phenomenological argument (like Schrödinger's equation itself) but essential with regard to the consequences that follow.

and

$$\lambda = \frac{2\pi}{k} = \frac{c_0}{\nu}$$

where ν is the frequency of the wave given by

$$\nu = r\frac{c_0}{v}\sqrt{\frac{Gm}{\pi V}}, \quad r = \sqrt{\frac{E}{2mc_0^2 - E}}.$$

Note that for the frequency (and wavelength) of the wave to be a real positive quantity, we require that

$$2mc_0^2 > E.$$

Finally, given the Helmholtz scattering function for a matter wave, i.e.

$$\gamma(\mathbf{r}) = \frac{2mc_0^2}{E^2}[E - E_p(\mathbf{r})] - 1,$$

for an attractive force $\gamma > 0$ and for a repulsive force $\gamma < 0$. If we consider a free matter wave with $E_p = 0$, then $\gamma > 0$ if an only if

$$\frac{2mc_0^2}{E} - 1 > 0.$$

But $2mc_0^2 > E$ for λ_0 to be a real positive quantity and thus, γ must always be greater than zero and a gravitational force must therefore be attractive and only attractive.

The results of this wave-theoretic model allow us to contemplate a gravity as follows:

Two bodies are attracted to each other because each detects the gravity waves scattered by the other.

This is a consequence of taking an asymptotic solution in which $k \to 0$ and provides four important and observable characteristics of a gravitational field:

(i) gravitation is a weak force;

(ii) a gravitational field bends (i.e. diffracts) light;

(iii) a gravitational field is characterized by an inverse square law;

(iv) gravity is an attractive only force.

However, with regard to point (iv), we note that if a material (i.e. a matter wavefield) exists such that $E < E_p \ \ \forall \mathbf{r} \in V$ then the scattering function will be negative and the force will become repulsive.

The approach considered here leads to a phenomenological idea in which the Helmholtz equation is used in an attempt to develop a unified (scalar) wavefield theory of 'physics' where the wavefield u exists over a broad range of frequencies. At very high frequencies, u describes matter waves, at intermediate frequencies, u describes (scalar) electromagnetic waves and at low frequencies,

u describes (scalar) gravity waves. The structure of matter, the characteristics of light and other electromagnetic radiation and the properties of gravity become phenomenologically related via Helmholtz scattering over different frequency bands. Low frequency waves (i.e. gravity waves) are scattered from high frequency waves (matter waves) to produce a gravitational field; intermediate frequency waves (electromagnetic waves) are scattered by high frequency waves (e.g. a lens) but can also be scattered by a gravitational field to produce gravitational lensing and so on. 'Physics' becomes the study of waves interacting with waves at vastly different frequencies, the breadth of the spectrum being a consequence of the instantaneous nature of the birth of the Universe (i.e. the 'big-bang') since it requires (noting that the Fourier transform of a delta function is a constant over all frequency space) a short impulse to generate a broad frequency spectrum.

II.10 The scalar wave equation is given by

$$(\nabla^2 + k^2)u(\mathbf{r}, k) = -k^2\gamma(\mathbf{r})u(\mathbf{r}, k), \quad \mathbf{r} \in V$$

where k is the wavenumber ($= 2\pi/\lambda$), $\gamma(\mathbf{r}) = \epsilon_r(\mathbf{r}) - 1$ with relative permittivity ϵ_r and u is the wavefield. A Green function solution gives

$$u(\mathbf{r}_0, k) = u_i(\mathbf{r}_0, k) + u_s(\mathbf{r}_0, k)$$

where

$$u_s(\mathbf{r}_0, k) = k^2 \int_V g(\mathbf{r} \mid \mathbf{r}_0, k)\gamma(\mathbf{r})u(\mathbf{r}, k)d^3\mathbf{r}$$

which under the Born approximation becomes

$$u_s(\mathbf{r}_0, k) = k^2 \int_V g(\mathbf{r} \mid \mathbf{r}_0, k)\gamma(\mathbf{r})u_i(\mathbf{r}, k)d^3\mathbf{r}$$

where u_i is the incident wavefield. In the far field,

$$u_s(\mathbf{r}_0, k) = k^2 \frac{\exp(ikr_0)}{4\pi r_0} \int_V \exp(-ik\hat{\mathbf{n}}_0 \cdot \mathbf{r})\gamma(\mathbf{r})u_i(\mathbf{r}, k)d^3\mathbf{r}$$

where $\hat{\mathbf{n}}_0 = \mathbf{r}_0/r_0$ and

$$r_0 = (x_0^2 + y_0^2 + z_0^2)^{\frac{1}{2}} = z_0\left(1 + \frac{x_0^2}{z_0^2} + \frac{y_0^2}{z_0^2}\right)^{\frac{1}{2}} \simeq z_0, \quad \frac{x_0}{z_0} << 1, \quad \frac{y_0}{z_0} << 1.$$

For a unit plane wave at normal incidence to the aperture we have

$$u_i(\mathbf{r}, k) = \exp(ikz)$$

and noting that

$$\hat{\mathbf{n}}_0 \cdot \mathbf{r} = \frac{1}{r_0}(xx_0 + yy_0 + zz_0) \simeq \frac{1}{z_0}(xx_0 + yy_0 + zz_0)$$

the forward scattered field is given by

$$u_s(x_0, y_0, z_0, k) = k^2 \frac{\exp(ikz_0)}{4\pi z_0} \int\int\int \exp(-ikxx_0/z_0) \exp(-ikyy_0/z_0) dxdydz.$$

For a dielectric screen of infinite extent with an aperture of size XY and thickness Z, we have

$$u_s(x_0, y_0, z_0, k)$$

$$= k^2 \frac{\exp(ikz_0)}{4\pi z_0} \int_{-\infty}^{\infty}\int_{-\infty}^{\infty}\int_{-Z/2}^{Z/2} \exp(-ikxx_0/z_0) \exp(-ikyy_0/z_0) dxdydz$$

$$-k^2 \frac{\exp(ikz_0)}{4\pi z_0} \int_{-X/2}^{X/2}\int_{-Y/2}^{Y/2}\int_{-Z/2}^{Z/2} \exp(-ikxx_0/z_0) \exp(-ikyy_0/z_0) dxdydz$$

$$= Zk^2 \frac{\exp(ikz_0)}{4\pi z_0} \left[4\pi^2 \delta(kx_0/z_0)\delta(ky_0/z_0) - XY \mathrm{sinc}\left(\frac{kx_0X}{2z_0}\right) \mathrm{sinc}\left(\frac{ky_0Y}{2z_0}\right) \right].$$

Hence, the observed intensity of the wavefield u is given by

$$I = \mid u(x_0, y_0, z_0, k) \mid^2 = \mid \exp(ikz_0) + A \exp(ikz_0) \mid^2 = 1 + 2A + A^2$$

where

$$A = \frac{Z\pi k^2}{4\pi z_0} \left[4\pi^2 \delta(kx_0/z_0)\delta(ky_0/z_0) - XY \mathrm{sinc}\left(\frac{kx_0X}{2z_0}\right) \mathrm{sinc}\left(\frac{ky_0Y}{2z_0}\right) \right].$$

The diffraction pattern in the back image plane will be formed from the back-scattering generated by the aperture. In this case, the wavefield u will be the back-scattered field (obtained by replacing $\hat{\mathbf{n}}_0$ with $-\hat{\mathbf{n}}_0$) given by

$$u_s(x_0, y_0, z_0, k)$$

$$= k^2 \frac{\exp(ikz_0)}{4\pi z_0} \int_{-\infty}^{\infty}\int_{-\infty}^{\infty}\int_{-Z/2}^{Z/2} \exp(ikxx_0/z_0) \exp(ikyy_0/z_0) \exp(2ikz) dxdydz$$

$$-k^2 \frac{\exp(ikz_0)}{4\pi z_0} \int_{-X/2}^{X/2}\int_{-Y/2}^{Y/2}\int_{-Z/2}^{Z/2} \exp(ikxx_0/z_0) \exp(ikyy_0/z_0) \exp(2ikz) dxdydz$$

$$= k^2 \frac{\exp(ikz_0)}{4\pi z_0} \mathrm{sinc}(kZ)$$

$$\times \left[4\pi^2 \delta(kx_0/z_0)\delta(ky_0/z_0) - XYZ \mathrm{sinc}\left(\frac{kx_0X}{2z_0}\right) \mathrm{sinc}\left(\frac{ky_0Y}{2z_0}\right) \right].$$

Note that when $Z = n\lambda/2$ where n is an integer, $u_s = 0$.

II.11 The solution for u can be written as

$$(u - u_i) = k^2 g \otimes fu$$

and thus

$$q \otimes (u - u_i) = k^2 q \otimes g \otimes fu$$

and

$$\nabla^2[q \otimes (u - u_i)] = k^2 \nabla^2 (q \otimes g \otimes fu) = k^2 \nabla^2 (q \otimes g) \otimes fu = -k^2 \delta^3 \otimes fu = -k^2 fu$$

provided

$$\nabla^2 (q \otimes g) = -\delta^3.$$

But

$$\nabla^2 (q \otimes g) = q \otimes \nabla^2 g = q \otimes (-k^2 g - \delta^3) = -k^2 q \otimes g - q = -\delta^3$$

and hence

$$q = \delta^3 - k^2 q \otimes g$$

so that

$$\begin{aligned} \nabla^2[q \otimes (u - u_i)] &= \nabla^2[\delta^3 \otimes (u - u_i) - k^2 q \otimes g \otimes (u - u_i)] \\ &= \nabla^2[(u - u_i) - k^2 q \otimes g \otimes (u - u_i)] = -k^2 fu. \end{aligned}$$

Thus,

$$f = \frac{1}{u}\left[q \otimes g \otimes (u - u_i) - \frac{1}{k^2}(u - u_i)\right]$$

where q is given by the solution to

$$\nabla^2 (q \otimes g) = -\delta^3$$

or

$$q \otimes g = \frac{1}{4\pi \mid \mathbf{r} \mid}$$

giving

$$f = \frac{1}{u}\left[\frac{1}{4\pi \mathbf{r}} \otimes (u - u_i) - \frac{1}{k^2}(u - u_i)\right].$$

II.12 Decomposing the Green functions into plane waves, we can write

$$u_s(\mathbf{r}_s \mid \mathbf{r}_0, k) = \frac{k^2}{(2\pi)^6} \int_V \gamma(\mathbf{r}) \int_{-\infty}^{\infty} d^3\mathbf{u} \frac{\exp[i\mathbf{u} \cdot (\mathbf{r}_0 - \mathbf{r})]}{u^2 - k^2} \int_{-\infty}^{\infty} d^3\mathbf{v} \frac{\exp[i\mathbf{v} \cdot (\mathbf{r}_s - \mathbf{r})]}{v^2 - k^2}.$$

Multiplying both sides of his equation by $\exp(-i\mathbf{p} \cdot \mathbf{r}_0) \exp(-i\mathbf{q} \cdot \mathbf{r}_s)$ and integrating over $\mathbf{r}_0$ and $\mathbf{r}_s$ we have

$$\int_{-\infty}^{\infty} \int_{-\infty}^{\infty} u_s(\mathbf{r}_s \mid \mathbf{r}_0, k) \exp(-i\mathbf{p} \cdot \mathbf{r}_0) \exp(-i\mathbf{q} \cdot \mathbf{r}_s) d^3\mathbf{r}_0 d^3\mathbf{r}_s$$

$$= \frac{k^2}{(2\pi)^6} \int_V d^3\mathbf{r}\gamma(\mathbf{r}) \int_{-\infty}^{\infty}\int_{-\infty}^{\infty} d^3\mathbf{u}d^3\mathbf{v} \frac{\exp(-i\mathbf{u}\cdot\mathbf{r})}{u^2-k^2}\frac{\exp(-i\mathbf{v}\cdot\mathbf{r})}{v^2-k^2}$$

$$\times \int_{-\infty}^{\infty} \exp[i\mathbf{r}_0\cdot(\mathbf{u}-\mathbf{p})]d^3\mathbf{r}_0 \int_{-\infty}^{\infty} \exp[i\mathbf{r}_s\cdot(\mathbf{v}-\mathbf{q})]d^3\mathbf{r}_s$$

$$= k^2 \int_V d^3\mathbf{r}\gamma(\mathbf{r}) \int_{-\infty}^{\infty}\int_{-\infty}^{\infty} d^3\mathbf{u}d^3\mathbf{v} \frac{\exp(-i\mathbf{u}\cdot\mathbf{r})}{u^2-k^2}\frac{\exp(-i\mathbf{v}\cdot\mathbf{r})}{v^2-k^2}\delta^3(\mathbf{u}-\mathbf{p})\delta^3(\mathbf{v}-\mathbf{q})$$

$$= k^2 \int_V d^3\mathbf{r}\gamma(\mathbf{r})\frac{\exp(-i\mathbf{p}\cdot\mathbf{r})}{p^2-k^2}\frac{\exp(-i\mathbf{q}\cdot\mathbf{r})}{q^2-k^2}$$

where we have used the result

$$\delta^3(\mathbf{u}) = \frac{1}{(2\pi)^3}\int_{-\infty}^{\infty} \exp(i\mathbf{u}\cdot\mathbf{r})d^3\mathbf{r}.$$

Re-arranging and then inverse Fourier transforming, we have

$$\gamma(\mathbf{r}) = \frac{1}{(2\pi)^3}\int_{-\infty}^{\infty} d^3\mathbf{w}\exp(i\mathbf{w}\cdot\mathbf{r})\left(\frac{p^2}{k^2}-1\right)\left(\frac{q^2}{k^2}-1\right)$$

$$\times \int_{-\infty}^{\infty}\int_{-\infty}^{\infty} u_s(\mathbf{r}_s \mid \mathbf{r}_0, k)\exp(-i\mathbf{p}\cdot\mathbf{r}_0)\exp(-i\mathbf{q}\cdot\mathbf{r}_s)d^3\mathbf{r}_0 d^3\mathbf{r}_s.$$

For an incident plane wave, the Born scattered field is given by

$$u_s(\mathbf{r}_0, k) = k^2 \int_V g(\mathbf{r} \mid \mathbf{r}_0, k)\gamma(\mathbf{r})\exp(ik\hat{\mathbf{n}}_i\cdot\mathbf{r})d^3\mathbf{r}.$$

Decomposing the Green function into plane waves, we have

$$\int_{-\infty}^{\infty} \exp(-i\mathbf{p}\cdot\mathbf{r})u_s(\mathbf{r}_0,k)d^3\mathbf{r}_0 = k^2\int_V d^3\mathbf{r}\gamma(\mathbf{r})\exp(ik\hat{\mathbf{n}}_i\cdot\mathbf{r})\frac{\exp(-i\mathbf{p}\cdot\mathbf{r})}{p^2-k^2}$$

or

$$\int_V \gamma(\mathbf{r})\exp[-i(\mathbf{p}-k\hat{\mathbf{n}}_i)\cdot\mathbf{r}]d^3\mathbf{r} = \left(\frac{p^2}{k^2}-1\right)\int_{-\infty}^{\infty} u_s(\mathbf{r}_0,k)\exp(-i\mathbf{p}\cdot\mathbf{r})d^3\mathbf{r}_0.$$

For $\hat{\mathbf{n}}_i$ fixed,

$$\gamma(\mathbf{r}) = \frac{\exp(-ik\hat{\mathbf{n}}_i\cdot\mathbf{r})}{(2\pi)^3}\int_{-\infty}^{\infty} d^3\mathbf{p}\exp(i\mathbf{p}\cdot\mathbf{r})\left(\frac{p^2}{k^2}-1\right)\int_{-\infty}^{\infty} u_s(\mathbf{r}_0,k)\exp(-i\mathbf{p}\cdot\mathbf{r})d^3\mathbf{r}_0.$$

Taking a square aperture to be the (x_0, y_0) plane, we record the scattered field on this plane for different values of z_0 (i.e. positions of the plane along the z_0 axis) to generate the 3D function $u_s(x_0, y_0, z_0, k)$. The result is then Fourier filtered using the filter

$$\left(\frac{p_x^2 + p_y^2 + p_z}{k^2} - 1\right)$$

where p_x, p_y and p_z are the spatial frequencies in the x_0, y_0 and z_0 directions respectively. Given that the field is Nyquist sampled over x_0, y_0 and z_0, the resolution of the image obtained will depend on the size of the aperture used and the extent in z_0 over which measurements are made.

II.13 The equation can be written as

$$\frac{4\pi}{k^2} u_s(\mathbf{r}_0, k) = \int_V \frac{\exp(2ik \mid \mathbf{r} - \mathbf{r}_0 \mid)}{4\pi \mid \mathbf{r} - \mathbf{r}_0 \mid^2} \gamma(\mathbf{r}) d^3\mathbf{r}.$$

Differentiating with respect to k and then replacing k by $k/2$, we have

$$w(\mathbf{r}_0, k) = \int_V \frac{\exp(ik \mid \mathbf{r} - \mathbf{r}_0 \mid)}{4\pi \mid \mathbf{r} - \mathbf{r}_0 \mid} \gamma(\mathbf{r}) d^3\mathbf{r}$$

where

$$w(\mathbf{r}_0, k) = -16\pi i \frac{d}{dk}\left[\frac{u_{BS}(\mathbf{r}_0, k/2)}{k^2}\right].$$

With the recording surface (i.e. the plane aperture) at a fixed position z_0

$$w(x_0, y_0, z_0, k) = \int_V dxdydz\gamma(x, y, z)$$

$$\times \frac{1}{(2\pi)^3} \int_{-\infty}^{\infty}\int_{-\infty}^{\infty}\int_{-\infty}^{\infty} du_x du_y du_z \frac{e^{i[u_x(x_0-x)+u_y(y_0-y)+u_z(z_0-z)]}}{u_x^2 + u_y^2 + u_z^2 - k^2}$$

Multiplying both sides by

$$\frac{1}{(2\pi)^2} e^{-i(U_x x_0 + U_y y_0)}$$

integrating over x_0 and y_0 and using the result

$$\frac{1}{(2\pi)^2} \int_{-\infty}^{\infty}\int_{-\infty}^{\infty} e^{i[(u_x - U_x)x_0 + (u_y - U_y)y_0]} dx_0 dy_0 = \delta(u_x - U_x)\delta(u_y - U_y)$$

we have

$$W(U_x, U_y, z_0, k) = \frac{1}{(2\pi)^3} \int dz\Gamma(U_x, U_y, z) \int_{-\infty}^{\infty} du_z \frac{e^{iu_z(z_0 - z)}}{U_x^2 + U_y^2 + u_z^2 - k^2}$$

where

$$W(U_x, U_y, z_0, k) = \frac{1}{(2\pi)^2} \int_{-\infty}^{\infty} \int_{-\infty}^{\infty} w(x_0, y_0, z_0, k) e^{-i(U_x x_0 + U_y y_0)} dx_0 dy_0$$

and

$$\Gamma(U_x, U_y, z) = \int \int \gamma(x, y, z) e^{-i(U_x x + U_y y)} dx dy.$$

Integrating over u_z, with $\rho^2 = U_x^2 + U_y^2$, we have

$$\int_{-\infty}^{\infty} du_z \frac{e^{iu_z(z-z_0)}}{u_z^2 + \rho^2 - k^2} = i\pi \text{sgn}(k) \frac{e^{i(z-z_0)\text{sgn}(k)(k^2-\rho^2)^{\frac{1}{2}}}}{(k^2-\rho^2)^{\frac{1}{2}}}; \quad |\, k \,| > \rho, \quad z > 0$$

where

$$\text{sgn}(k) = \begin{cases} +1, & k \geq 0; \\ -1, & k < 0. \end{cases}$$

and hence, we are required to invert the integral (writing U_x and U_y as u_x and u_y respectively)

$$\widetilde{W}(u_x, u_y, z_0, k) = \int dz \Gamma(u_x, u_y, z) \frac{e^{iz\text{sgn}(k)(k^2-\rho^2)^{\frac{1}{2}}}}{(k^2-\rho^2)^{\frac{1}{2}}}$$

where

$$\widetilde{W}(u_x, u_y, z_0, k) = -6\pi^2 i \text{sgn}(k) W(u_x, u_y, z_0, k) e^{iz_0 \text{sgn}(k)(k^2-\rho^2)^{\frac{1}{2}}}.$$

Multiplying both side of this equation by

$$k e^{-iZ\text{sgn}(k)(k^2-\rho^2)^{\frac{1}{2}}}$$

and integrating with respect to k between $-\infty$ and ∞ excluding those values of k for which $|\, k \,| < \rho$ (i.e. integrating k from $-\infty$ to $-\rho$ and from ρ to ∞) we have

$$\int_{-\infty}^{\infty} dk k \widetilde{W}(u_x, u_y, z_0, k) H(\rho/2k) e^{-iZ(k^2-\rho^2)^{\frac{1}{2}}}$$

$$= \int_0^{\infty} dz \Gamma(u_x, u_y, z) \left(\int_{\rho}^{\infty} dk k \frac{e^{i(z-Z)(k^2-\rho^2)^{\frac{1}{2}}}}{(k^2-\rho^2)^{\frac{1}{2}}} - \int_{-\infty}^{-\rho} dk k \frac{e^{-i(z-Z)(k^2-\rho^2)^{\frac{1}{2}}}}{(k^2-\rho^2)^{\frac{1}{2}}} \right)$$

where H is the step function defined by

$$H(\rho/2k) = \begin{cases} 1, & |\, \rho/2k \,| < \frac{1}{2}; \\ 0, & \text{otherwise.} \end{cases}$$

Changing variables, we now let $q = (k^2 - \rho^2)^{\frac{1}{2}}$ and $q = -(k^2 - \rho^2)^{\frac{1}{2}}$ in the first and second integrals over k respectively so that

$$\int_{\rho}^{\infty} dkk \frac{e^{i(z-Z)(k^2-\rho^2)^{\frac{1}{2}}}}{(k^2-\rho^2)^{\frac{1}{2}}} - \int_{-\infty}^{-\rho} dkk \frac{e^{-i(z-Z)(k^2-\rho^2)^{\frac{1}{2}}}}{(k^2-\rho^2)^{\frac{1}{2}}}$$

$$= \int_{0}^{\infty} dq e^{i(z-Z)q} + \int_{-\infty}^{0} dq e^{i(z-Z)q} = \int_{-\infty}^{\infty} dq e^{i(z-Z)q} = 2\pi\delta(z-Z).$$

Hence, we have

$$\Gamma(u_x, u_y, Z) = \frac{1}{2\pi} \int_{-\infty}^{\infty} dkk \widetilde{W}(u_x, u_y, z_0, k) H(\rho/2k) e^{-iz(k^2-\rho^2)^{\frac{1}{2}}}$$

the scattering function being given by the inverse Fourier transform of Γ, i.e. replacing Z with z,

$$\gamma(x, y, z) = \frac{1}{(2\pi)^2} \int_{-\infty}^{\infty} \int_{-\infty}^{\infty} \Gamma(u_x, u_y, z) \exp(iu_x x) \exp(iu_y y) du_x du_y.$$

Substituting the expression for Γ and $\widetilde{W}$ into the above integral and interchanging the order of integration, we can write

$$\gamma(x, y, z) = -\frac{6i\pi^2}{(2\pi)^7} \int dx_0 \int dy_0 \int_{-\infty}^{\infty} dkk w(x_0, y_0, z_0, k)$$

$$\times \int_{-\infty}^{\infty} \int_{-\infty}^{\infty} du_x du_y H(\rho/2k) e^{-i(z-z_0)\mathrm{sgn}(k)(k^2-\rho^2)^{\frac{1}{2}}} e^{iu_x(x-x_0)} e^{iu_y(y-y_0)}.$$

If we now change to polar coordinates and let $u_x = \rho\cos\theta, \quad u_y = \rho\sin\theta, \quad x - x_0 = R\cos\phi, \quad y - y_0 = R\cos\phi$ where $R = [(x-x_0)^2 + (y-y_0^2]^{\frac{1}{2}}$, then the integrals over u_x and u_y become

$$\int_{0}^{|k|} d\rho\rho e^{-i(z-z_0)\mathrm{sgn}(k)(k^2-\rho^2)^{\frac{1}{2}}} \int_{0}^{2\pi} d\theta e^{i\rho R\cos(\theta-\phi)}$$

$$= 2\pi \int_{0}^{|k|} d\rho\rho e^{-i(z-z_0)\mathrm{sgn}(k)(k^2-\rho^2)^{\frac{1}{2}}} J_0(\rho R)$$

where J_0 is the zero-order Bessel function. Hence, we can write the inverse solution as

$$\gamma(x, y, z) = \int_{-\infty}^{\infty} dx_0 \int_{-\infty}^{\infty} dy_0 \int_{-\infty}^{\infty} dk w(x_0, y_0, z_0, k) K(x - x_0, y - y_0, z - z_0, k)$$

where

$$K(x-x_0, y-y_0, z-z_0, k)$$

$$= -\frac{12i\pi^3}{(2\pi)^7} \int_0^{|k|} d\rho\rho e^{-i(z-z_0)\mathrm{sgn}(k)(k^2-\rho^2)^{\frac{1}{2}}} J_0(\rho[(x-x_0)^2 + (y-y_0^2]^{\frac{1}{2}}).$$

For a fixed position of the aperture at z_0, a pulse is emitted from each point (x_0, y_0) on the plane and the back-scattered spectrum (i.e. the Fourier transform of the signal received) at the same point recorded. The data $w(x_0, y_0, z_0, k)$ is then computed and γ reconstructed using the result above. The factors affecting the resolution of the reconstruction in practice are the size of the aperture that is practicable (which determines the range of the integrals over x_0 and y_0) and the band-width of the pulse that is emitted/received (which determines the range of the integral over k).

II.14

```
#include <math.h>

void ROTATE( float *s[], float *r[], int n, float theta )
{
  int i, j, nn, x1, y1, x2, y2;
  float pi, cos_t, sin_t, cos_i_t, sin_i_t, yd, xd;

/* FUNCTION: Compute a rotated digital image (anti-clockwise)
             through a specified angle (given in degrees).

   PARAMETERS:
        Input: s  - digital image
               n  - size of image (<=512)
           theta - angle of rotation (in degrees)
       Output: r - rotated image

   INTERNAL VARIABLES:
      nn - center position of matrix, offset right if necessary
      i,j  - matrix index variables
      pi - constant value of pi
      cos_t,sin_t - cosine and sine of angle
      cos_i_t,sin_i_t - cosine and sine of angle for i
      yd,xd - rotated point coordinate
      x1,y1 - nearest neighbour (below)
      x1,y1 - nearest neighbour (above)

   USED FUNCTIONS: INITMAT (Initialize a matrix)
                   CHECKXY (Check boundaries of X and Y) */

/* Determine mid point of matrix and convert theta into radians. */
```

```
  nn = n * 0.5;
  pi = 4.0 * atan( 1.0 );
  theta = theta * pi / 180.0;

/* Initialize the rotation matrix. */

  INITMAT( r, n, 0.0 );

/* Compute the cosine and sine terms of the angle. */

  cos_t = cos( theta );
  sin_t = sin( theta );

/* Start process of rotating non-zero values. */

  for ( i=0; i<n; i++ )
    {
    sin_i_t = nn + (i-nn)*sin_t;
    cos_i_t = nn + (i-nn)*cos_t;

    for ( j=0; j<n; j++ )
      {
      if (s[i][j] != 0)
        {
/* Rotate point through angle theta. */

        xd =  sin_i_t + (j-nn)*cos_t;
        yd =  cos_i_t - (j-nn)*sin_t;

/* Compute the coordinates of the nearest neighbour. */

        x1 = floor( xd );
        y1 = floor( yd );
        x2 = ceil( xd );
        y2 = ceil( yd );

/* Assign to each of the neighbours the value of s.  */

        if (CHECKXY( y1, x1, n ) != 0)
          r[y1][x1] = s[i][j];
        if (CHECKXY( y2, x2, n ) != 0)
          r[y2][x2] = s[i][j];
        if (CHECKXY( y2, x1, n ) != 0)
          r[y2][x1] = s[i][j];
        if (CHECKXY( y1, x2, n ) != 0)
          r[y1][x2] = s[i][j];
```

```
        }
      }
    }
}


void INITMAT( float *s[], int n, float value )

{
  int i, j;

  for ( i=0; i<n; i++ )
    {
    for ( j=0; j<n; j++ )
      {
      s[i][j] = value;
      }
    }
}


int CHECKXY( int x, int y, int max )
{
  if ((x>=0) && (x<max))
    {
    if ((y>=0) && (y<max))
      {
      return( 1 );
      }
    }

  return( 0 );
}
```

II.15

```
static float *sw[NMAX], *r[NMAX];

void RADON( float *s[], int n )
{
  int i, j, k;
  float temp, theta, sum;

/* FUNCTION: Compute the Radon transform of an image.

 PARAMETERS:
```

```
     Input: s  - digital image
            n  - size of image (<=512)
    Output: s - radon transform

INTERNAL VARIABLES:
   i,j,k  - matrix index variables
   theta - angle of rotation
   temp - temporary variable to reduce divisions
   sum - sum of the projection row
   sw - work matrix for image
   r - work matrix for rotated image

USED FUNCTIONS:   ROTATE  (Rotate an image)
                  XFERMAT (Matrix transfer)
                  alloc_matrix (allocate memory)
                  free_matrix (free memory) */


 /* Allocation Space for work matrix. */

 alloc_matrix( sw, n );
 alloc_matrix( r, n );

 /* Determine the scaling factor. */

 temp = 180.0 / n;

 /* Rotate the image n times. */

 for ( k=0; k<n; k++ )
   {
   theta = k * temp;

   /* Rotate the image. */

   ROTATE( s, r, n, theta );

   /* Compute the projection of the rotated image. */

   for ( i=0; i<n; i++ )
     {
     sum = 0.0;
     for ( j=0; j<n; j++ )
       {
       sum += r[i][j];
       }
     sw[i][k] = sum;
```

```
      }
    }

  /* Return work matrix. */

  XFERMAT( n, sw, 0, n, s, 0, n );

  /* Free space from work matrix. */

  free_matrix( r, n );
  free_matrix( sw, n );
}


void alloc_matrix( float *s[], int n )

/* FUNCTION: To allocate space for image matrix.

   PARAMETERS:
        Input: s  - digital image matrix
               n  - size of image (<=512)
       Output: s - digital image matrix */


{
  int i;

  for ( i=0; i<n; i++ )
    {
    s[i] = (float *) farcalloc( n, sizeof( float ) );
    }
}


void free_matrix( float *s[], int n )

/* FUNCTION: To free space allocated for image matrix.

 PARAMETERS:
       Input: s  - digital image matrix
              n  - size of image (<=512)
     Output: s - digital image matrix */



{
  int i;
```

```
  for ( i=0; i<n; i++ )
    {
    farfree ( s[i] );
    s[i] = NULL;
    }
}


void XFERMAT( int num, float *s1[], int nn1, int n1,
              float *s2[], int nn2, int n2 )

/* FUNCTION: To transfer digital image from one matrix to another.

   PARAMETERS:

        Input: s1 - digital image
               num - number of values to transfer
          n1, n2 - size of image (<=512)
         nn1, nn2 - midpoints of images

       Output: s2 - digital image */
{
  int i, j;

  for ( i=-nn1; i<num-nn1; i++ )
    {
    for ( j=-nn1; j<num-nn1; j++ )
      {
      s2[nn2+i][nn2+j] = s1[nn1+i][nn1+j];
      }
    }
}
```

II.16

```
#include <math.h>

void DIR_FILTER( float *s[], int n );
void DIF_FILTER( float *s[], int n );
void BP_DECONVOLUTION( float *s[], int n );

static float *r[NMAX], *x[NMAX], *sw[NMAX];

void IRADON( float *s[], int n, int opt )
{
  int i, j, k;
```

```
  float temp, theta, sum;

/* FUNCTION: Compute the Inverse Radon transform from projections.

 PARAMETERS
     Input: s  - radon transform
            n  - size of image (<=512)
           opt - options indicator

    Output: s - reconstructed image

 INTERNAL VARIABLES: None
    i,j,k - matrix index variables
    theta - angle of rotation
     temp - temporary variable to reduce divisions
       sw - work matrix for image
        r - work matrix for rotated image
        x - work matrix for rotated image

 USED EXTERNAL FUNCTIONS: ROTATE (Rotate an image)
                          FFT2D (2D Fast Fourier Transform)
                          INITMAT (Initialize a matrix)
                          XFERMAT (Move one matrix to another)
                          alloc_matrix (Allocation of a matrix)
                          free_matrix (Free matrix space)
                          FFT1D (1D Fast Fourier Transform)
                          HILBERT (Hilbert transform)

 USED INTERNAL FUNCTIONS: DIR_FILTER (Direct filtering)
                          DIF_FILTER (Diffentiation
                                      and Hilbert transform)
                          BP_DECONVOLUTION (Back-projection
                                            and deconvolution) */

/* Allocation Space for work matrix. */

  alloc_matrix( sw, n );
  alloc_matrix( r, n );
  alloc_matrix( x, n );

/* Apply direct filtering. */

  if (opt == 2)
    {
    DIR_FILTER( s, n );
    }
```

```
/* Apply Differentiation & Hilbert transform  */

  if (opt == 3)
    {
    DIF_FILTER( s, n );
    }

/* Initialize workspace. */

  INITMAT( sw, n, 0.0 );

/* Determine the scaling factor. */

  temp = -180.0 / n;

/* Back-project the image for n rotations. */

  for ( k=0; k<n; k++ )
    {
    theta = k * temp;

/* Save the image in the work matrix. */

    for ( i=0; i<n; i++ )
      {
      for ( j=0; j<n; j++ )
        {
        x[i][j] = s[j][k];
        }
      }

/* Rotate the image. */

    ROTATE( x, r, n, theta );

/* Backproject the image. */

    for ( i=0; i<n; i++ )
      {
      for ( j=0; j<n; j++ )
        {
        sw[i][j] += r[i][j];
        }
      }
    }

/* Return work matrix. */
```

```
  XFERMAT( n, sw, 0, n, s, 0, n );

/* Deconvolve back-projected data. */

  if (iopt == 1)
    {
    BP_DECONVOLUTION( s, n );
    }

/* Free space from work matrix. */

  free_matrix( x, n );
  free_matrix( r, n );
  free_matrix( sw, n );
}



void DIR_FILTER( float *s[], int n )
{
  int i, j, nn;
  float *sr, *si;

/* FUNCTION: Filters image using direct filtering.

 PARAMETERS
    Input: s  - radon transform
           n  - size of image (<=512)
   Output: s - filtered radon transform

 INTERNAL VARIABLES:
    nn - center position of matrix, offset right if necessary
    i,j - matrix index variables
    sr - work array for real slice of image
    si - work array for imaginary slice of image */


/* Determine mid point of matrix. */

  nn = n * 0.5;

/* Allocation Space for work array. */

  sr = (float *) calloc( 1+n, sizeof( float ) );
  si = (float *) calloc( 1+n, sizeof( float ) );

/* Filter the image for n rotations. */
```

```
  for ( i=0; i<n; i++ )
    {
/* Extract a projection. */

    for ( j=0; j<n; j++ )
      {
      sr[j+1]  = s[j][i];
      si[j+1] = 0.0;
      }

/* Compute the Discrete Fourier Transform of image s. */

    FFT1D( sr, si, n, -1);

/* Filter the projection. */

    for ( j=0; j<n; j++ )
      {
      sr[j+1] *= abs( j-nn );
      si[j+1] *= abs( j-nn );
      }

/* Compute the Inverse Discrete Fourier Transform of image s. */

    FFT1D( sr, si, n, 1 );

/* Write output.         */

    for ( j=0; j<n; j++ )
      {
      s[j][i] = sr[j+1];
      }
    }

/* Free space from work array. */

  free( sr );
  free( si );
}



void DIF_FILTER( float *s[], int n )
{
  int i, j;
  float *x;
```

```
/* FUNCTION: Filter each projection by differentiating
             and taking the the Hilbert transform.

    PARAMETERS
        Input: s  - radon transform
               n  - size of image (<=512)
       Output: s - filtered radon transform

 INTERNAL VARIABLES:
    i,j - matrix index variables
    x - work array for projection and forward differencing */

/* Allocation Space for work array. */

  x = (float *) calloc( 1+n, sizeof( float ) );

/* Filter the image for n rotations. */

  for ( i=0; i<n; i++ )
    {
/* Extract a projection. */

    for ( j=0; j<n; j++ )
      {
      x[j+1] = s[j][i];
      }

/* Differentiate projection using forward differencing. */

    for ( j=1; j<n; j++ )
      {
      x[j] = x[j+1]-x[j];
      }

/* Set ends of array to zero. */

    x[1] = 0.0;
    x[n] = 0.0;

/* Compute Hilbert transform of projection. */

    HILBERT( x, n );

/* Write output.     */

    for ( j=0; j<n; j++ )
```

```
      {
      s[j][i] = x[j+1];
      }
    }

/* Free space from work array. */

  free( x );
}



void BP_DECONVOLUTION( float *s[], int n )
{
  int i, j, nn;
  float temp;


/* FUNCTION: Compute the deconvolution of a reconstruction.

   PARAMETERS
        Input: s  - back-projected image
               n  - size of image (<=512)
       Output: s - deconvolved image

   INTERNAL VARIABLES:
      nn - center position of matrix, offset right if necessary
     i,j - matrix index variables
    temp - temporary variable to reduce calculations */



/* Determine mid point of matrix. */

  nn = n * 0.5;

/* Initialize array sw. */

  INITMAT( sw, n, 0.0 );

/* Compute the Discrete Fourier Transform of image s. */

  FFT2D( s, sw, n, -1 );

/* Apply Inverse Filter. */

  for ( i=0; i<n; i++ )
    {
```

```
    for ( j=0; j<n; j++ )
      {
      temp = sqrt( pow( i-nn, 2 ) + pow( j-nn, 2 ) );

      s[i][j]  *= temp;
      sw[i][j] *= temp;
      }
    }

/* Compute the Inverse Discrete Fourier Transform of image s. */

  FFT2D( s, sw, n, 1 );
}


void HILBERT(float s[], int n)
{
int i;
float *si;

/* FUNCTION: Returns the Hilbert transform of a signal s
             by computing the analytic signal. */

/* Allocate work space */

si=(float *) malloc((n+1) * sizeof (float));

/* Initialize si */

for(i=1; i<=n; i++) si[i]=0.0;

/* Compute Analysic signal */

ANASIG(s,si,n);

/* Overwrite s with its Hilbert transform si. */

for(i=1; i<=n; i++)s[i]=si[i];

/* Free memory */

free(si);
}


void ANASIG(float f[],float q[], int n)
{
```

```
int i,nn;

/* FUNCTION: Computes the analytic signal
             (see 'Digital Signal Processing',
             J M Blackledge, Horwood publishing, 2003). */

/* Determine mid point of array */

nn=1+(n/2);

/* Initialise q */

for(i=1; i<=n; i++)q[i]=0.0;

/* Take FFT */

FFT1D(f,q,n,-1);

/* Set the negative components of spectrum to zero */

for(i=1; i<=nn-1; i++)
{
f[i]=0.0;
q[i]=0.0;
}

/* Multiply DC and positive frequencies by 2 */

for(i=nn; i<=n; i++)
{
f[i]=2.0*f[i];
q[i]=2.0*q[i];
}
/* Compute the inverse FFT */

FFT1D(f,q,n,1);

}
```

Solutions to Problems: Part III

III.1

```
#include <math.h>

void CONVOLVE(float **f, float **p, float **s, int n)
```

```
{
 int i, j;
 float  *sr[512], *si[512], *pr[512], *pi[512], *fi[512];

/* Allocate memory */

for(i=0; i<n;i++)
{
  sr[i] = (float *) malloc(n*sizeof(float));
  si[i] = (float *) malloc(n*sizeof(float));
  pr[i] = (float *) malloc(n*sizeof(float));
  pi[i] = (float *) malloc(n*sizeof(float));
  fi[i] = (float *) malloc(n*sizeof(float));  }


/* Initialize real and imaginary parts */

for(i=0; i<n; i++)
 for(j=0; j<n; j++)
  { sr[i][j] = s[i][j];
    si[i][j] = 0.0;
    pr[i][j] = p[i][j];
    pi[i][j] = 0.0;
    fi[i][j] = 0.0;     }


/* Compute FFT2D */

 FFT2D(sr, si, n, -1);
 FFT2D(pr, pi, n, -1);


/* Convolve */

for(i=0; i<n; i++)
 for(j=0; j<n; j++)
  {  f[i][j]  = pr[i][j]*sr[i][j] - pi[i][j]*si[i][j] ;
     fi[i][j] = pr[i][j]*si[i][j] + pi[i][j]*sr[i][j] ;    }


/* Compute Inverse FFT2D */

 FFT2D(f, fi, n, 1);


/* Free memory */
```

```
for(i=0; i<n;i++)
  {
  free(sr[i]);
  free(si[i]);
  free(pr[i]);
  free(pi[i]);
  free(fi[i]);
  }
}
```

III.2

```
#include <math.h>

void AUTOCOR(float **f,float **s, int n)

{
 int i, j;
 float  *si[512], *fr[512], *fi[512];

/* Allocate Memory */

for(i=0; i<n;i++)
{
  si[i] = (float *) malloc(n*sizeof(float));
  fi[i] = (float *) malloc(n*sizeof(float));
  fr[i] = (float *) malloc(n*sizeof(float)); }


/* Initialize real and iamginary Parts */

for(i=0; i<n; i++)
 for(j=0; j<n; j++)
  { si[i][j] = 0.0;
    fr[i][j] = f[i][j];
    fi[i][j] = 0.0;     }


/* Compute FFT2D */

 FFT2D(fr, fi, n, -1);


/* Autocorrelation */

for(i=0; i<n; i++)
```

```
 for(j=0; j<n; j++)
  {  s[i][j]  = fr[i][j]*fr[i][j] + fi[i][j]*fi[i][j] ;
     si[i][j] = 0.0;    }


/* Compute Inverse FFT2D */

 FFT2D(s, si, n, 1);


/* Free Memory */

for(i=0; i<n;i++)
{
  free(si[i]);
  free(fr[i]);
  free(fi[i]);   }

}
```

III.3

```
#include <math.h>

void CROSCOR(float **f, float **p, float **s, int n)

{
 int i, j;
 float  *si[512], *pr[512], *pi[512], *fr[512], *fi[512];

/* Allocate Memory */

for(i=0; i<n;i++)
{
  si[i] = (float *) malloc(n*sizeof(float));
  pr[i] = (float *) malloc(n*sizeof(float));
  pi[i] = (float *) malloc(n*sizeof(float));
  fi[i] = (float *) malloc(n*sizeof(float));
  fr[i] = (float *) malloc(n*sizeof(float)); }

/* Initialize real and imaginary parts */

for(i=0; i<n; i++)
 for(j=0; j<n; j++)
  { si[i][j] = 0.0;
    pr[i][j] = p[i][j];
```

```
    pi[i][j] = 0.0;
    fr[i][j] = f[i][j];
    fi[i][j] = 0.0;     }


/* Compute FFT2D */

 FFT2D(fr, fi, n, -1);
 FFT2D(pr, pi, n, -1);

/* Cross correlation */

for(i=0; i<n; i++)
 for(j=0; j<n; j++)
  {  s[i][j]  = pr[i][j]*fr[i][j] + pi[i][j]*fi[i][j] ;
     si[i][j] = pr[i][j]*fi[i][j] - pi[i][j]*fr[i][j] ;    }


/* Compute Inverse FFT2D */

 FFT2D(s, si, n, 1);

/* Free Memory */

for(i=0; i<n;i++)
{
  free(si[i]);
  free(pr[i]);
  free(pi[i]);
  free(fr[i]);
  free(fi[i]);   }
}
```

III.4

```
#include <math.h>

void WIENER(float **s, float **p, float **f, int n, float snr)

{
 int i, j;
 float  *sr[512], *si[512], *pr[512], *pi[512], *fi[512], denom;

/* Allocate Memory */

for(i=0; i<n;i++)
```

```
{
  sr[i] = (float *) malloc(n*sizeof(float));
  si[i] = (float *) malloc(n*sizeof(float));
  pr[i] = (float *) malloc(n*sizeof(float));
  pi[i] = (float *) malloc(n*sizeof(float));
  fi[i] = (float *) malloc(n*sizeof(float));   }


/* Initialize real and imaginary parts */

for(i=0; i<n; i++)
 for(j=0; j<n; j++)
  { sr[i][j] = s[i][j];
    si[i][j] = 0.0;
    pr[i][j] = p[i][j];
    pi[i][j] = 0.0;
    fi[i][j] = 0.0;    }


/* Compute FFT2D */

 FFT2D(sr, si, n, -1);
 FFT2D(pr, pi, n, -1);


/* Wiener Filter */

for(i=0; i<n; i++)
 for(j=0; j<n; j++)
  {
    denom = pr[i][j]*pr[i][j] + pr[i][j]*pi[i][j] + 1./(snr*snr);

    f[i][j] = (pr[i][j]*sr[i][j]+pi[i][j]*si[i][j])/denom;

    fi[i][j] = (pr[i][j]*si[i][j]-pi[i][j]*sr[i][j])/denom;      }


/* Compute Inverse FFT2D */

 FFT2D(f, fi, n, -1);

/* Deallocate memory */

for(i=0; i<n;i++)
{
  free(sr[i]);
  free(si[i]);
```

```
  free(pr[i]);
  free(pi[i]);
  free(fi[i]); }
}
```

III.5 The restoration improves as the snr is decreased in the noise free case. When noise is present in the image, a larger value of the snr is required to obtain a noise free restoration.

III.6

```
#include <math.h>

void PSE(float **s, float **p, float **f, int n, float snr)

{
 int i, j;
 float  *sr[512], *si[512], *pr[512], *pi[512], *fi[512], denom;

/* Allocate Memory */

for(i=0; i<n;i++)
{
  sr[i] = (float *) malloc(n*sizeof(float));
  si[i] = (float *) malloc(n*sizeof(float));
  pr[i] = (float *) malloc(n*sizeof(float));
  pi[i] = (float *) malloc(n*sizeof(float));
  fi[i] = (float *) malloc(n*sizeof(float));   }

/* Initialize real and imaginary parts */

for(i=0; i<n; i++)
 for(j=0; j<n; j++)
  { sr[i][j] = s[i][j];
    si[i][j] = 0.0;
    pr[i][j] = p[i][j];
    pi[i][j] = 0.0;
    fi[i][j] = 0.0;    }


/* Compute FFT2D */

 FFT2D(sr, si, n, -1);
 FFT2D(pr, pi, n, -1);
```

```
/* Power Spectrum Equalization Filter */

for(i=0; i<n; i++)
 for(j=0; j<n; j++)
  {
    denom = sqrt( pr[i][j]*pr[i][j] + pr[i][j]*pi[i][j] + 1./(snr*snr) );

    f[i][j] = (pr[i][j]*sr[i][j]+pi[i][j]*si[i][j])/denom;

    fi[i][j] = (pr[i][j]*si[i][j]-pi[i][j]*sr[i][j])/denom;      }

/* Compute Inverse FFT2D */

 FFT2D(f, fi, n, -1);

/* Deallocate memory */

for(i=0; i<n;i++)
{
  free(sr[i]);
  free(si[i]);
  free(pr[i]);
  free(pi[i]);
  free(fi[i]); }
}
```

III.7

```
#include <math.h>

void ILF_RECT(float **f, float **s, int nx, int ny, int n )

{
 int i, j;
 float  *fr[512], *fi[512], *si[512], *filter[512];

/* Allocate Memory */

for(i=0; i<n;i++)
{
  fr[i] = (float *) malloc(n*sizeof(float));
  fi[i] = (float *) malloc(n*sizeof(float));
  si[i] = (float *) malloc(n*sizeof(float));
  filter[i] = (float *) malloc(n*sizeof(float));   }
```

```
/* Initialize real and imaginary parts */

for(i=0; i<n; i++)
 for(j=0; j<n; j++)
  { fr[i][j] = f[i][j];
    fi[i][j] = 0.0;
    si[i][j] = 0.0;
    filter[i][j] = 0.0;    }


/* Compute FFT2D */

 FFT2D(fr, fi, n, -1);


/* Construct the Filter */

for(i=n-nx; i<=n+nx; i++)
 for(j=n-ny; j<=n+ny; j++)
  filter[i][j]=1.;


/* Filter the Image */

for(i=0; i<n; i++)
 for(j=0; j<n; j++)
  {
   s[i][j] = fr[i][j]*filter[i][j];
   si[i][j] = fi[i][j]*filter[i][j];   }


/* Compute Inverse FFT2D */

 FFT2D(s, si, n, -1);

/* Deallocate memory */

for(i=0; i<n;i++)
{
  free(fr[i]);
  free(fi[i]);
  free(si[i]);
  free(filter[i]); }
}

/************************************************************/
```

```
#include <math.h>

void ILF_ELLIPSE(float **f, float **s, int nx, int ny, int n )

{
 int i, j;
 float  *fr[512], *fi[512], *si[512], *filter[512], test;

/* Allocate Memory */

for(i=0; i<n;i++)
{
  fr[i] = (float *) malloc(n*sizeof(float));
  fi[i] = (float *) malloc(n*sizeof(float));
  si[i] = (float *) malloc(n*sizeof(float));
  filter[i] = (float *) malloc(n*sizeof(float));   }

/* Initialize real and imaginary parts */

for(i=0; i<n; i++)
 for(j=0; j<n; j++)
  { fr[i][j] = f[i][j];
    fi[i][j] = 0.0;
    si[i][j] = 0.0;    }


/* Compute FFT2D */

 FFT2D(fr, fi, n, -1);


/* Construct the Filter */

for(i=n-nx; i<n+nx; i++)
 for(j=n-ny; j<n+ny; j++)
  {
    test = pow((float)(i-n/2)/(float)nx,2.)
         + pow((float)(j-n/2)/(float)ny,2.);

     if(test <= 1.)
filter[i][j]=1.;
     else
      filter[i][j]=0.;  }

/* Filter the Image */

for(i=0; i<n; i++)
```

```
 for(j=0; j<n; j++)
  {
   s[i][j] = fr[i][j]*filter[i][j];
   si[i][j] = fi[i][j]*filter[i][j];   }

/* Compute Inverse FFT2D */

 FFT2D(s, si, n, -1);

/* Deallocate memory */

for(i=0; i<n;i++)
{
  free(fr[i]);
  free(fi[i]);
  free(si[i]);
  free(filter[i]); }
}
```

III.8

```
#include <math.h>

void LOGTRAN( float **s, int n, float a )
{
  int i, j;

for(i=0; i<n; i++)
 for(j=0; j<n; j++)
  s[i][j] = (1./a) * log( 1.+s[i][j]*(-1.+exp(a)) );

}
```

III.9

```
#include <math.h>

void EXPTRAN( float **s, int n, float a )
{
  int i, j;

for(i=0; i<n; i++)
 for(j=0; j<n; j++)
  s[i][j] = (1./a) * (pow(1.+a , s[i][j]) - 1.);

}
```

III.10

```
#include <math.h>

void HISTEQ( float **s, float **f, int n, int l )
{
  int i, j, k;
  float *h, *c, sum, max=0.;

/* Allocate memory for the histograms */

 h=(float *)malloc(l*sizeof(float));
 c=(float *)malloc(l*sizeof(float));

/* Compute the histogram of s */

 HIST(s,n,h,l);

/* Compute the cumulative histogram  */

sum=0.;

 for(i=0; i<l; i++)
  { sum+=h[i];
    c[i]=sum;  }

/* Scale the cumulative histogram and
   quantize it into l grey levels */

 for(i=0; i<l; i++)
  c[i] *= ((float)(l-1)/((float)n*(float)n));

/* Scale the image and quantize it into l grey levels */

 for(i=0; i<n; i++)
  for(j=0; j<n; j++)
   if(s[i][j]>max)
    max=s[i][j];

 for(i=0; i<n; i++)
  for(j=0; j<n; j++)
   s[i][j] *= ((float)(l-1)/max);

/* Histogram Equalization */

 for(i=0; i<n; i++)
  for(j=0; j<n; j++)
```

```
   { k = (int)s[i][j];
     f[i][j] = c[k];  }

/* Free memory */

 free(h);
 free(c);
}



#include <math.h>

void HIST( float **s, int n, float *h, int lev )
{
  float *f[512], max=0.;
  int i, j, k;

/* Allocate memory  */

for(i=0; i<n; i++)
 f[i]=(float *)malloc(n*sizeof(float));

/* Initialize work space */

for(i=0; i<n; i++)
 for(j=0; j<n; j++)
   f[i][j] = s[i][j];

/*  Scale the image and quantize it into lev grey levels */

for(i=0; i<n; i++)
 for(j=0; j<n; j++)
  if(f[i][j] > max)
   max=f[i][j];

for(i=0; i<n; i++)
 for(j=0; j<n; j++)
  f[i][j] *= ((float)(lev-1)/max);

/* Initialize the histogram  */

for(i=0; i<lev; i++)
 h[i]=0.;

/* Compute the histogram  */

for(i=0; i<n;i++)
```

```
 for(j=0; j<n; j++)
  {  k=(int)f[i][j];
     h[k]++;  }

/* Deallocate memory space */

for(i=0; i<n; i++)
 free(f[i]);

}
```

III.11

```
#include <math.h>


void BHF(float **s, int n, float cut, float ord)

{
 int i, j;
 float  *si[512], but;

/* Allocate memory */

for(i=0; i<n;i++)
  si[i] = (float *) malloc(n*sizeof(float));


/* Initialize imaginary part */

for(i=0; i<n; i++)
 for(j=0; j<n; j++)
   si[i][j] = 0.0;


/* Compute FFT2D */

 FFT2D(s, si, n, -1);


/* Filter the image */

for(i=0; i<n; i++)
 for(j=0; j<n; j++)
  {
    but = 1. / (1. + pow(cut/sqrt((float)(i*i)
```

```
                  + (float)(j*j)) , 2.*ord));
    s[i][j] *= but;
    si[i][j] *= but;  }

/* Compute Inverse FFT2D */

 FFT2D(s, si, n, 1);


/* Free memory */

for(i=0; i<n;i++)
  free(si[i]);
}
```

III.12

```
#include <math.h>

void HOMOFIL(float **s, int n, float cut, float ord)

{
 int li, co, i;
 float  *si[512];

/* Allocate memory for imaginary part */

for(i=0; i<n;i++)
  si[i] = (float *) malloc(n*sizeof(float));

/* Initialize imaginary part */

for(li=0; li<n; li++)
 for(co=0; co<n; co++)
   si[li][co] = 0.0;

/* Compute the FFT */

 FFT2D(s, si, n, -1);


/* Butterworth highpass filter */

BHF(s, n, cut, ord);
BHF(si, n, cut, ord);
```

```
/* Compute the Inverse FFT */

 FFT2D(s, si, n, 1);

/* Homomorphic Filter */

for(li=0; li<n; li++)
 for(co=0; co<n; co++)
   s[li][co] = exp(s[li][co]);

/* Free memory */

for(i=0; i<n;i++)
  free(si[i]);
}
```

III.13

```
#include <math.h>

void HEFIL( float **s, int n)
{
  int i, j;
  float *temp[512], inter;

/*  Allocate memory for work space  */

for(i=0; i<n+2; i++)
 temp[i]=(float *)malloc((n+2)*sizeof(float));

/* Initialize the work space (zero pad) */

for(i=0; i<n+2; i++)
 for(j=0; j<n+2; j++)
   temp[i][j] = 0.;

/* Input the image into the work space */

for(i=1; i<n+1; i++)
 for(j=1; j<n+1; j++)
   temp[i][j] = s[i-1][j-1];

/*  High Emphasis Filter  */

for(i=1; i<n+1; i++)
 for(j=1; j<n+1; j++)
```

```
  {  inter= 5.*temp[i][j]-temp[i+1][j]-temp[i-1][j]
                         -temp[i][j+1]-temp[i][j-1];
     s[i-1][j-1] = inter ;   }

for(i=0; i<n+2; i++)
 free(temp[i]);
}
```

III.14 Center differencing, the Laplacean of a discrete function I_{ij} is

$$\nabla^2 I_{ij} = I_{(i+1)j} + I_{(i-1)j} + I_{i(j+1)} + I_{i(j-1)} - 4I_{ij} = J_{ij}$$

Hence,

$$\nabla^4 I_{ij} = \nabla^2 J_{ij} = J_{(i+1)j} + J_{(i-1)j} + J_{i(j+1)} + J_{i(j-1)} - 4J_{ij}$$

$$= I_{(i+2)j} + I_{ij} + I_{(i+1)(j+1)} + I_{(i+1)(j-1)} - 4I_{(i+1)j} + I_{ij} + I_{(i-2)j} + I_{(i-1)(j+1)}$$
$$+I_{(i-1)(j-1)} - 4I_{(i-1)j} + I_{(i+1)(j+1)} + I_{(i-1)(j+1)} + I_{i(j+2)} + I_{ij} - 4I_{i(j+1)} + I_{(i+1)(j-1)}$$
$$+I_{(i-1)(j-1)} + I_{ij} + I_{i(j-2)} - 4I_{i(j-1)} - 4I_{(i+1)j} - 4I_{(i-1)j} - 4I_{i(j+1)} + 4I_{i(j-1)}$$
$$+16I_{ij} = 20I_{ij} + I_{(i+2)j} + 2I_{(i+1)(j+1)} + 2I_{(i+1)(j-1)} - 8I_{(i+1)j} + I_{(i-2)j} + 2I_{(i-1)(j+1)}$$
$$+2I_{(i-1)(j-1)} - 8I_{(i-1)j} + I_{i(j+2)} - 8I_{i(j+1)} + I_{i(j-2)} - 8I_{i(j-1)}.$$

In terms of a convolution kernel, the result above can be written as

$$\begin{pmatrix} 0 & 0 & 1 & 0 & 0 \\ 0 & 2 & -8 & 2 & 0 \\ 1 & -8 & 20 & -8 & 1 \\ 0 & 2 & -8 & 2 & 0 \\ 0 & 0 & 1 & 0 & 0 \end{pmatrix}.$$

Hence, given that the convolution kernel associated with the first order solution $I - \nabla^2 I$ is given by

$$\begin{pmatrix} 0 & -1 & 0 \\ -1 & 5 & -1 \\ 0 & -1 & 0 \end{pmatrix}$$

the convolution kernel associated with the second order solution $I - \nabla^2 I + \frac{1}{2}\nabla^4 I$ is given by

$$\begin{pmatrix} 0 & 0 & 0 & 0 & 0 \\ 0 & 0 & -1 & 0 & 0 \\ 0 & -1 & 5 & -1 & 0 \\ 0 & 0 & -1 & 0 & 0 \\ 0 & 0 & 0 & 0 & 0 \end{pmatrix} + \begin{pmatrix} 0 & 0 & \frac{1}{2} & 0 & 0 \\ 0 & 1 & -4 & 1 & 0 \\ \frac{1}{2} & -4 & 10 & -4 & \frac{1}{2} \\ 0 & 1 & -4 & 1 & 0 \\ 0 & 0 & \frac{1}{2} & 0 & 0 \end{pmatrix}$$

$$= \begin{pmatrix} 0 & 0 & \frac{1}{2} & 0 & 0 \\ 0 & 1 & -5 & 1 & 0 \\ \frac{1}{2} & -5 & 15 & -5 & \frac{1}{2} \\ 0 & 1 & -5 & 1 & 0 \\ 0 & 0 & \frac{1}{2} & 0 & 0 \end{pmatrix} = \frac{1}{2}\begin{pmatrix} 0 & 0 & 1 & 0 & 0 \\ 0 & 2 & -10 & 2 & 0 \\ 1 & -10 & 30 & -10 & 1 \\ 0 & 2 & -10 & 2 & 0 \\ 0 & 0 & 1 & 0 & 0 \end{pmatrix}$$

To compute the convolution kernel associated with the third order solution $I - \nabla^2 I + \frac{1}{2}\nabla^4 I - \frac{1}{6}\nabla^6 I$, we use the same method as above to evaluate $\nabla^6 I_{ij}$ giving

$$\frac{1}{6}\begin{pmatrix} 0 & 0 & 0 & -1 & 0 & 0 & 0 \\ 0 & 0 & -3 & 15 & -3 & 0 & 0 \\ 0 & -3 & 24 & -87 & 24 & -3 & 0 \\ -1 & 15 & -87 & 202 & -87 & 15 & -1 \\ 0 & -3 & 24 & -87 & 24 & -3 & 0 \\ 0 & 0 & -3 & 15 & -3 & 0 & 0 \\ 0 & 0 & 0 & -1 & 0 & 0 & 0 \end{pmatrix}$$

The following MATLAB code 'diffuses' a grey level image (with file name 'image.bmp') using a Gaussian lowpass filter and applies the first and second order high emphasis filters using FIR filters *fir1* and *fir2* respectively.

```
function diffusion(sigma)

%Input: sigma - standard deviation of Gaussian PSF
%
%Output: None

%Read image (assumed to be .bmp file of size n x n)
f=imread('image','bmp');
n=size(f,1);   %Set size of array
nn=1+n/2; %Set mid point of array

%Convert to floating point array
f=im2double(f);

%Normalize
f=f./max(max(f));

%Show image
figure(1)
subplot(2,2,1), imshow(f);

%Compute the PSF - a unit Gaussian distribution
for i=1:n
   x=i-nn;
    for j=1:n
      y=j-nn;
        p(i,j)=exp(-((x.*x)+(y.*y))/(sigma*sigma));
    end
end

%Convolve f with p using the convolution theorem
%and normalize to unity.
```

```
f=fftshift(fft2(f)); p=fftshift(fft2(p));
          f=p.*f;
          f=fftshift(ifft2(f)); f=abs(f);
f=f./max(max(f)); %N.B. No check on case when f=0.

%Show filtered image
subplot(2,2,2), imshow(f);

%Compute first order FIR filter - fir1
fir1(1,1)=0;  fir1(1,2)=-1; fir1(1,3)=0;
fir1(2,1)=-1; fir1(2,2)=5;  fir1(2,3)=-1;
fir1(3,1)=0;  fir1(3,2)=-1; fir1(3,3)=0;

%Compute second order FIR filter - fir2
fir2(1,1)=0; fir2(1,2)=0;   fir2(1,3)=1;   fir2(1,4)=0;
fir2(1,5)=0;

fir2(2,1)=0; fir2(2,2)=2;   fir2(2,3)=-10; fir2(2,4)=2;
fir2(2,5)=0;

fir2(3,1)=1; fir2(3,2)=-10; fir2(3,3)=30;  fir2(3,4)=-10;
fir2(3,5)=1;

fir2(4,1)=0; fir2(4,2)=2;   fir2(4,3)=-10; fir2(4,4)=2;
fir2(4,5)=0;

fir2(5,1)=0; fir2(5,2)=0;   fir2(5,3)=1;   fir2(5,4)=0;
fir2(5,5)=0;

fir2=fir2/2;

%Convolve image with first order FIR filter
%returning only those parts of the convolution
%that are computed without the zero-padded edges
s1=conv2(f,fir1,'valid');
s1=abs(s1); %Compute absolute value
s1=s1./max(max(s1)); %Normalize

%Show image
subplot(2,2,3), imshow(s1);

%Convolve image with second order FIR filter
%returning only those parts of the convolution
%that are computed without the zero-padded edges
s2=conv2(f,fir2,'valid');
s2=abs(s2); %Compute absolute value
s2=s2./max(max(s2)); %Normalize
```

```
%Show image
subplot(2,2,4), imshow(s2);
```

An example of the output generated by the MATLAB code above is given below for the function *diffusion(1)*.

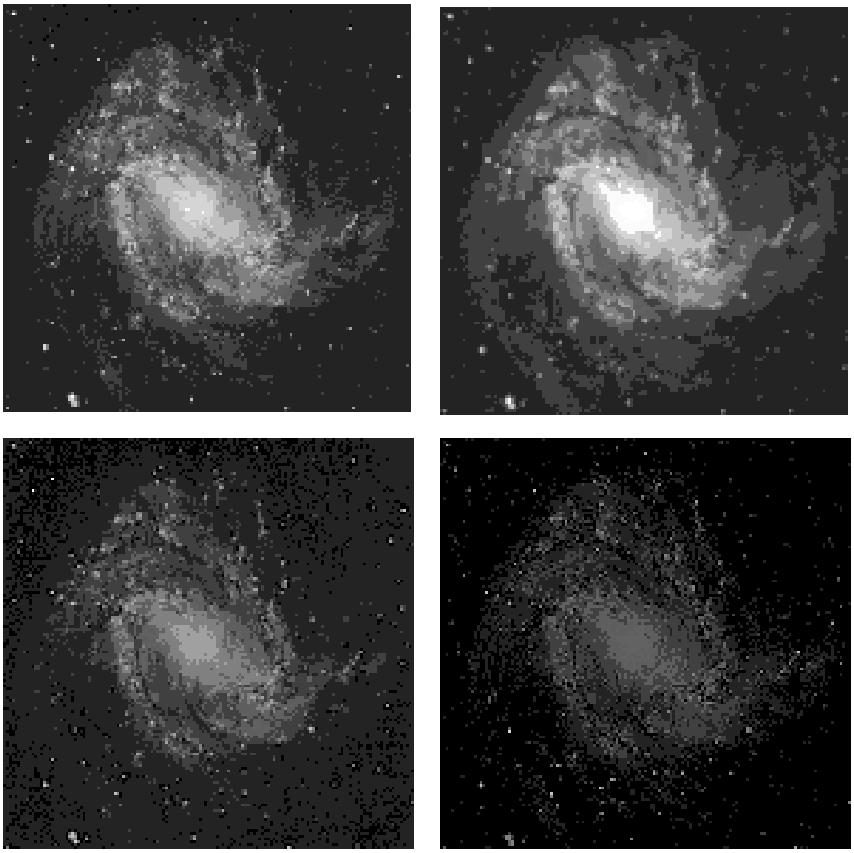

Figure A.2: Original 256×256 test image (top-left); result after applying a Gaussian lowpass filter (top-right); output after application of the first order high emphasis filter (bottom-left); output after application of the second order high emphasis filter (bottom-right).

III.15

```
#include <math.h>

void BLF(float **s, int n, float cut, float ord)

{
 int i, j;
 float  *si[512], but;

/* Allocate memory */

for(i=0; i<n;i++)
  si[i] = (float *) malloc(n*sizeof(float));


/* Initialize imaginary part */

for(i=0; i<n; i++)
 for(j=0; j<n; j++)
   si[i][j] = 0.0;


/* Compute FFT2D */

 FFT2D(s, si, n, -1);

/* Lowpass filter the image */

for(i=0; i<n; i++)
 for(j=0; j<n; j++)
  {
    but = 1./( 1.+ pow(sqrt((float)i*(float)i
                 +(float)j*(float)j)/cut,2.*ord ));
    s[i][j] *= but;
    si[i][j] *= but;  }

/* Compute inverse FFT2D */

 FFT2D(s, si, n, 1);


/* Free memory */

for(i=0; i<n;i++)
  free(si[i]);
```

```
}
```

III.16

```
#include <math.h>

void MOVAV( float **s, int n, int w)
{
  int li, co, i, j, ii, jj, m=n+w-1;
  float *temp[512], sum;

/*  Allocate memory for work space  */

for(i=0; i<m; i++)
 temp[i]=(float *)malloc(m*sizeof(float));

/* Initialize the work space (zero pad) */

for(li=0; li<m; li++)
 for(co=0; co<m; co++)
   temp[li][co] = 0.;


/* Input the image into the work space */

for(li=w/2; li<n+w/2; li++)
 for(co=w/2; co<n+w/2; co++)
   temp[li][co] = s[li-w/2][co-w/2];

/* Moving Average Filter */

i=0;

for(li=w/2; li<n+w/2; li++)
{
  j=0;

   for(co=w/2; co<n+w/2; co++)
   {
     sum=0.;

for(ii=li-w/2; ii<=li+w/2; ii++)
   for(jj=co-w/2; jj<=co+w/2; jj++)
  sum+=temp[ii][jj];

     s[i][j]=sum;
```

```
     j++;
    }

  i++;

}

/* Free memory */

for(i=0; i<m; i++)
 free(temp[i]);

}
```

III.17

```
#include <math.h>

void MEDIAN( float **s, int n, int w)
{
  int li, co, i, ii, jj, m=n+w-1;
  float *temp[512], *x;

/*  Allocate memory for work space  */

for(i=0; i<m; i++)
 temp[i]=(float *)malloc(m*sizeof(float));

 x=(float *)malloc(w*sizeof(float));

/* Initialize the work space (zero pad) */

for(li=0; li<m; li++)
 for(co=0; co<m; co++)
   temp[li][co] = 0.;

/* Input the image into the work space */

for(li=w/2; li<n+w/2; li++)
 for(co=w/2; co<n+w/2; co++)
   temp[li][co] = s[li-w/2][co-w/2];

/* Median Filter */

for(li=w/2; li<n+w/2; li++)
```

```
 for(co=w/2; co<n+w/2; co++)
 {
   i=0;

    for(ii=li-w/2; ii<=li+w/2; ii++)
     for(jj=co-w/2; jj<=co+w/2; jj++)
      {  x[i]=temp[ii][jj];
          i++;   }

    SORT(x,w);

    s[li-w/2][co-w/2]=x[1+w/2];
  }

/* Free allocated memory */

for(i=0; i<m; i++)
 free(temp[i]);

 free(x);

}



void SORT( float *x, int n)
{
  int i, j;
  float hold;

for(i=0; i<n-1; i++)
 for(j=0; j<n-i; j++)
   if(x[j]>x[j+1])
   { hold=x[j];
  x[j]=x[j+1];
  x[j+1]=hold; }

}
```

Solutions to Problems: Part IV

IV.1

```
void FLT( float **s, int n, float t )
{
  int i, j;
  float max = 0.;
```

```
/* Scale the image in the range 0 to 1 */

 for(i=0; i<n; i++)
  for(j=0; j<n; j++)
    if(s[i][j] > max)
     max=s[i][j];

 for(i=0; i<n; i++)
  for(j=0; j<n; j++)
   s[i][j] /= max;

/* Threshold the image */

 for(i=0; i<n; i++)
  for(j=0; j<n; j++)
   {
      if(s[i][j] > t)
       s[i][j] = 1.;
      else
s[i][j] = 0.;   }

}
```

IV.2

```
void SLT( float **s, int n, float t )
{
  int i, j;
  float max = 0.;

/* Scale the image in the range 0 to 1 */

 for(i=0; i<n; i++)
  for(j=0; j<n; j++)
    if(s[i][j] > max)
     max=s[i][j];

 for(i=0; i<n; i++)
  for(j=0; j<n; j++)
   s[i][j] /= max;

/* Semi-Threshold the image */

 for(i=0; i<n; i++)
  for(j=0; j<n; j++)
```

```
      if(s[i][j] <= t)
       s[i][j] = 0.;

}
```

IV.3

```
void ROBERTS( float **s, int n)
{
  int i, j;
  float *temp[512], sx, sy;

/*  Allocate memory for work space  */

for(i=0; i<n+1; i++)
 temp[i]=(float *)malloc((n+1)*sizeof(float));

/* Initialize the work space (zero pad) */

for(i=0; i<n+1; i++)
 for(j=0; j<n+1; j++)
   temp[i][j] = 0.;

/* Input the image into the work space */

for(i=0; i<n; i++)
 for(j=0; j<n; j++)
   temp[i][j] = s[i][j];

/*  Robert's Gradient  */

for(i=0; i<n; i++)
 for(j=0; j<n; j++)
  {  sx = temp[i+1][j+1]-temp[i][j];
     sy = temp[i][j+1]-temp[i+1][j];
     s[i][j] = sqrt(sx*sx + sy*sy) ;   }

/* Deallocate memory */

for(i=0; i<n+1; i++)
 free(temp[i]);
}
```

IV.4

```
void SOBEL( float **s, int n)
{
  int i, j;
  float *temp[512], sx, sy;

/*  Allocate memory for work space  */

for(i=0; i<n+2; i++)
 temp[i]=(float *)malloc((n+2)*sizeof(float));

/* Initialize the work space (zero pad) */

for(i=0; i<n+2; i++)
 for(j=0; j<n+2; j++)
   temp[i][j] = 0.;

/* Input the image into the work space */

for(i=1; i<n+1; i++)
 for(j=1; j<n+1; j++)
   temp[i][j] = s[i-1][j-1];

/*  Compute the Sobel gradient  */

for(i=1; i<n+1; i++)
 for(j=1; j<n+1; j++)
  {
     sx = temp[i-1][j+1]+2.*temp[i][j+1]+temp[i+1][j+1];
     sx -= (temp[i-1][j-1]+2.*temp[i][j-1]+temp[i+1][j-1]);

     sy = temp[i+1][j+1]+2.*temp[i+1][j]+temp[i+1][j-1];
     sy -= (temp[i-1][j+1]+2.*temp[i-1][j]+temp[i-1][j-1]);

     s[i-1][j-1] = sqrt(sx*sx + sy*sy) ;   }

/* Deallocate memory */

for(i=0; i<n+2; i++)
 free(temp[i]);
}
```

IV.5

```
void PREWIT( float **s, int n)
{
  int i, j;
```

```
  float *temp[512], sx, sy;

/*  Allocate memory for work space  */

for(i=0; i<n+2; i++)
 temp[i]=(float *)malloc((n+2)*sizeof(float));

/* Initialize the work space (zero pad) */

for(i=0; i<n+2; i++)
 for(j=0; j<n+2; j++)
   temp[i][j] = 0.;


/* Input the image into the work space */

for(i=1; i<n+1; i++)
 for(j=1; j<n+1; j++)
   temp[i][j] = s[i-1][j-1];

/*  Prewit's Gradient  */

for(i=1; i<n+1; i++)
 for(j=1; j<n+1; j++)
  {
     sx = temp[i-1][j+1] + temp[i][j+1] + temp[i+1][j+1];
     sx -= (temp[i-1][j-1]+temp[i][j-1]+temp[i+1][j-1]);

     sy = temp[i+1][j+1]+temp[i+1][j]+temp[i+1][j-1];
     sy -= (temp[i-1][j+1]+temp[i-1][j]+temp[i-1][j-1]);

     s[i-1][j-1] = sqrt(sx*sx + sy*sy) ;      }

/* Deallocate memory */

for(i=0; i<n+2; i++)
 free(temp[i]);
}
```

IV.6

```
#include <math.h>

void MH(float **x, int n, float s, float **y)

{
```

```
 int i, j;
 float  *xr[512], *xi[512], *yr[512], *yi[512], filter, test;

/* Allocate memory */

for(i=0; i<n;i++)
{
  xr[i] = (float *) malloc(n*sizeof(float));
  xi[i] = (float *) malloc(n*sizeof(float));
  yr[i] = (float *) malloc(n*sizeof(float));
  yi[i] = (float *) malloc(n*sizeof(float));   }


/* Initialize real and imaginary parts */

for(i=0; i<n; i++)
 for(j=0; j<n; j++)
  { xr[i][j] = x[i][j];
    xi[i][j] = 0.0;        }


/* Compute FFT2D */

 FFT2D(xr, xi, n, -1);


/* Construct the Marr-Hildreth Filter */

for(i=0; i<n; i++)
 for(j=0; j<n; j++)
 {
  filter = (float)i*(float)i + (float)j*(float)j;
  filter *= exp(-(pow((float)i,2.) + pow((float)j,2.)) /(2.*s*s));
  yr[i][j]=xr[i][j] * filter;
  yi[i][j]=xi[i][j] * filter;   }


/* Compute Inverse FFT2D */

 FFT2D(yr, yi, n, 1);


/* Construct the Image, detecting the zero crossings */

for(i=0; i<n; i++)
 for(j=0; j<n-1; j++)
 {
```

```
  test = yr[i][j] * yr[i][j+1];

if(test > 0.)
 y[i][j]=0.;
else
 y[i][j]=1.;
  }

for(i=0; i<n; i++)
 y[i][n-1] = y[i][n-2];


/* Free memory */

for(i=0; i<n;i++)
{
  free(xr[i]);
  free(xi[i]);
  free(yr[i]);
  free(yi[i]);   }

}
```

IV.7

```
void AUTOTHRESHOLD( float **s, int n )
{
  int i, j, *h, lev=256, mid=n/2, maxd, maxl, min, test;
  float thr;

/* FUNCTION: Automates the binarization of an image setting the
*            threshold at the minimum that occurs between the
*            two peaks in the histogram of the image.
*
*            The function works properly only with bimodal
*            histograms.
*
* Input: s - Data (digital image).
*        n - Size of image.
*
* Output: s - Binary image
*
*
* External Functions: HIST - Computes the histogram of an image */

/* Allocate memory for histogram  */
```

```
  h = (int *)malloc(lev*sizeof(int));


/* Compute the histogram */

 HIST(s,n,h,lev);

/* Search for the maximum in the dark field */

test = 0;

 for(i=0; i<mid; i++)
  if(h[i] > test)
   { test = h[i];
     maxd = i;   }

 /* Search for the maximum in the light field */

test = 0;

 for(i=mid; i<lev; i++)
  if(h[i] > test)
   { test = h[i];
     maxl = i;   }

/* Search for the minimum between the two peaks in the histogram */

test = h[maxd];

 for(i=maxd+1; i<maxl; i++)
  if(h[i] < test)
   { test = h[i];
     min = i;   }

/* Select the threshold and binarize the image */

thr = min;

 for (i=0; i<n; i++)
  for (j=0; j<n; j++)
  {
    if(s[i][j]>thr)
     s[i][j]=1.;
    else
     s[i][j]=0.; }
```

```
/* Free the memory */

free(h);
}



#include <math.h>

void HIST( float **s, int n, float *h, int lev )
{
  float *f[512], max=0.;
  int i, j, k;

/* Allocate memory  */

for(i=0; i<n; i++)
 f[i]=(float *)malloc(n*sizeof(float));

/* Initialize work space */

for(i=0; i<n; i++)
 for(j=0; j<n; j++)
   f[i][j] = s[i][j];

/*  Scale the image and quantize it into lev grey levels */

for(i=0; i<n; i++)
 for(j=0; j<n; j++)
  if(f[i][j] > max)
   max=f[i][j];

for(i=0; i<n; i++)
 for(j=0; j<n; j++)
  f[i][j] *= ((float)(lev-1)/max);

/* Initialize the histogram  */

for(i=0; i<lev; i++)
 h[i]=0.;

/* Compute the histogram  */

for(i=0; i<n;i++)
 for(j=0; j<n; j++)
  {  k=(int)f[i][j];
     h[k]++;  }
```

```
/* Deallocate memory space */

for(i=0; i<n; i++)
 free(f[i]);
}
```

IV.8 In practice, if we have a coherent digital image I_{ij} we can compute its histogram denoted by $H_k = P(I_{ij})$ which will normally have as many bins N as there are grey levels in the image, i.e. 256 bins for an 8-bit image. We then need to consider a discrete version of the PDF to which we require a best fit to the data. In such a case, the scaling factor

$$\frac{1}{\beta^\alpha}\frac{1}{\Gamma(\alpha)}$$

can be replaced by a constant C which will be a measure of the size of the digital image provided and we can consider developing a least squares fit to the data H_k based on a distribution (i.e. theoretical histogram) given by

$$\hat{H}_k = R_k^{x_2}\exp(x_1 - R_k x_3)$$

where $x_1 = \ln C$, $x_2 = \alpha - 1$ and $x_3 = 1/\beta$. Linearizing, we can find x_1, x_2 and x_3 such that the error function

$$e(x_1, x_2, x_3) = \| \ln H_k - \ln \hat{H}_k \|_2^2$$

$$= \sum_{k=1}^{N} (\ln H_k - x_1 - x_2 \ln R_k + x_3 R_k)^2$$

is minimum, i.e. when

$$\frac{\partial e}{\partial x_1} = 0, \quad \frac{\partial e}{\partial x_2} = 0 \quad \text{and} \quad \frac{\partial e}{\partial x_3} = 0.$$

The vector $\mathbf{x} \equiv (x_1, x_2, x_3)$ is then obtained by solving the following system of linear equations

$$\begin{pmatrix} a_{11} & a_{12} & a_{13} \\ a_{21} & a_{22} & a_{23} \\ a_{31} & a_{32} & a_{33} \end{pmatrix} \begin{pmatrix} x_1 \\ x_2 \\ x_3 \end{pmatrix} = \begin{pmatrix} b_1 \\ b_2 \\ b_3 \end{pmatrix}$$

where

$$a_{11} = N, \quad a_{12} = \sum_{k=1}^{N} \ln R_k, \quad a_{13} = -\sum_{k=1}^{N} R_k,$$

$$a_{21} \ln R_k, \quad a_{22} = \sum_{k=1}^{N} (\ln R_k)^2, \quad a_{23} = -\sum_{k=1}^{N} R_k \ln R_k,$$

$$a_{31} = \sum_{k=1}^{N} R_k, \quad a_{32} = \sum_{k=1}^{N} R_k \ln R_k, \quad a_{33} = -\sum_{k=1}^{N} R_k^2,$$

$$b_1 = \sum_{k=1}^{N} \ln H_k, \quad b_2 \sum_{k=1}^{N} (\ln H_k)(\ln R_k), \quad b_3 = \sum_{k=1}^{N} R_k \ln H_k.$$

Using Cramers rule, the solutions are

$$x_1 = \frac{\begin{vmatrix} b_1 & a_{12} & a_{13} \\ b_2 & a_{22} & a_{23} \\ b_3 & a_{32} & a_{33} \end{vmatrix}}{\begin{vmatrix} a_{11} & a_{12} & a_{13} \\ a_{21} & a_{22} & a_{23} \\ a_{31} & a_{32} & a_{33} \end{vmatrix}}, \quad x_2 = \frac{\begin{vmatrix} a_{11} & b_1 & a_{13} \\ a_{21} & b_2 & a_{23} \\ a_{31} & b_3 & a_{33} \end{vmatrix}}{\begin{vmatrix} a_{11} & a_{12} & a_{13} \\ a_{21} & a_{22} & a_{23} \\ a_{31} & a_{32} & a_{33} \end{vmatrix}}, \quad x_3 = \frac{\begin{vmatrix} a_{11} & a_{12} & b_1 \\ a_{21} & a_{22} & b_2 \\ a_{31} & a_{32} & b_3 \end{vmatrix}}{\begin{vmatrix} a_{11} & a_{12} & a_{13} \\ a_{21} & a_{22} & a_{23} \\ a_{31} & a_{32} & a_{33} \end{vmatrix}}.$$

This approach allows a Γ-distributed coherent image to be classified in terms of three statistical parameters C, α and β.

(i) By calculating these parameters over a moving square window W of size $M \times M$ say, centered in the image at a position (i, j), we can generate three statistically segmented images, namely α_{ij}, β_{ij} and C_{ij}, of size $(N - M) \times (N - M)$ where N is taken to be the size of the (square) image. The size of the window must be large enough for the windowed data to give a statistically significant result.

(ii) The mode of the Γ-distribution is that value (i.e. bin) at which the distribution

$$\hat{H}_k = CR_k^{\alpha} \exp(-\beta R_k)$$

is a maximum. This occurs when

$$\frac{\partial}{\partial R_k} H_k = \exp(-\beta R_k)\alpha R_k^{\alpha-1} - \beta R_k^{\alpha} \exp(-\beta R_k)$$

$$= \left(\frac{\alpha}{R_k} - \beta \right) R_k^{\alpha} \exp(-\beta R_k) = 0$$

or when

$$\left(\frac{\alpha}{R_k} - \beta \right) = 0$$

giving a mode value of

$$R_k = \frac{\alpha}{\beta}.$$

The number of pixels $H_{\max}$ occurring at this mode is then given by

$$H_{\max} = C \left(\frac{\alpha}{\beta} \right)^{\alpha} \exp \left[-\beta \left(\frac{\alpha}{\beta} \right) \right].$$

Appendix B

Supplementary Problems

The supplementary problems presented here are designed to test the readers general knowledge and programming skills associated with the subject area. Each question has been taken from the examination papers set by the author for students undertaking the MSc programme in *Digital Signal Processing*. Solutions to these questions are not provided.

1. (a) Use the 2D convolution theorem to obtain a solution to the equation

$$u(x,y) = \text{sinc}(\alpha x)\,\text{sinc}(\alpha y) - \int_{-\infty}^{\infty}\int_{-\infty}^{\infty} \text{sinc}[\beta(x-x')]\,\text{sinc}[\beta(y-y')]u(x',y')dx'dy'$$

for u when $\beta > \alpha$ and where $\text{sinc}(x) \equiv \sin(x)/x$.

(b) Consider a linear, position-invariant imaging system with a Gaussian Point Spread Function of the form

$$p(x,y) = \exp[-\alpha(x^2+y^2)]$$

in a noise free environment.

(i) Find an expression for the output $s(x,y)$ of this system when it is used to record an image of a line of infinitesimal width located at $x = a$ in the object plane.

(ii) By computing the 2D Fourier transform of the point spread function given above write down an expression for the inverse filter of this system. Hence, or otherwize show that if an image is obtained described by the equation

$$s(x,y) = \exp[-\beta(x^2+y^2)]$$

then the object function $f(x,y)$ is given by

$$f(x,y) = \frac{\alpha^2}{\pi(\beta-\alpha)}\exp[\alpha\beta(x^2+y^2)/(\beta-\alpha)], \quad \beta > \alpha$$

given that

$$\int_{-\infty}^{\infty} \exp(-z^2)dz = \sqrt{\pi}.$$

2. (i) Explain the differences between continuous wave and pulsed wave imaging systems providing some examples of both types and discussing some of their applications.

(ii) The Green function for a three dimensional wavefield detected at $\mathbf{r}$ originating from a continuous wave source located at $\mathbf{r}_0$ is given by

$$g(\mathbf{r} \mid \mathbf{r}_0; \omega) = \frac{1}{4\pi \mid \mathbf{r} - \mathbf{r}_0 \mid} \exp\left(i\frac{\omega}{c} \mid \mathbf{r} - \mathbf{r}_0 \mid\right)$$

where ω and c are the angular frequency and propagation velocity of the wavefield respectively.

By applying an appropriate expansion, derive an expression for g in the far field (Fraunhofer zone) and the intermediate field (Fresnel zone) explaining the physical basis for your results. Use your result to show that the time dependent Green's function for a pulsed source in the far field at a time t is given by

$$G(\mathbf{r} \mid \mathbf{r}_0; t) = \frac{1}{4\pi r_0}\delta\left(t + \frac{r_0}{c} - \frac{\hat{\mathbf{n}}_0 \cdot \mathbf{r}}{c}\right)$$

where $\hat{\mathbf{n}}_0 = \mathbf{r}_0/r_0$.

3. (i) Discuss how 'time-of-flight' experiments can be used to construct images of the acoustic velocity in a material using ultrasonic computed tomography. State the principle physical conditions which must be met for such an imaging system to be successful.

(ii) Consider the binary image given below (black=0, white=1) which consists of a small disc and a straight line.

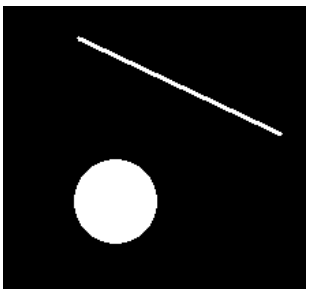

Sketch the parallel beam projections that would be obtained at angles of 0, 45 and 90 degrees to the horizontal.

(iii) By computing the Radon transform of the Gaussian function $e^{-\alpha(x^2+y^2)}$ show that the projection obtained at an angle of 0 degrees to the horizontal is given by $\sqrt{\pi/\alpha}e^{-\alpha z^2}$ where z is the projection coordinate and

$$\int_{-\infty}^{\infty} e^{-\alpha x^2} dx = \sqrt{\frac{\pi}{\alpha}}.$$

(iv) The back-projection function b of an object f can be written in the form

$$b(x,y) = \frac{1}{\sqrt{x^2+y^2}} \otimes\otimes f(x,y)$$

where $\otimes\otimes$ is the 2D convolution operation. It is known that the spectrum of b is given by

$$B(k_x,k_y) = \sqrt{k_x^2+k_y^2}G(k_x,k_y)$$

where k_x and k_y are the spatial frequencies in cycles per metre. Show that

$$f(x,y) = \nabla^2 g(x,y)$$

where g is the inverse Fourier transform of G given that

$$\frac{1}{\sqrt{x^2+y^2}} \frac{1}{\sqrt{k_x^2+k_y^2}}$$

4. A common method of estimating the point spread function of a Synthetic Aperture Radar (SAR) image is to image a single 'point scatterer' with a large radar cross section. The raw (complex) data s obtained from such an experiment after demodulation and quadrature detection can be approximated by

$$s(x,y) = \exp(i\alpha x^2)\exp(i2\pi y^2/\lambda R); \quad \mid x \mid \leq X/2, \quad \mid y \mid \leq Y/2$$

where α is the quadratic chirp rate/(speed of light)^2, R is the range at which the radar operates and λ is the wavelength of microwaves. The width of the beam (i.e. the width of the central lobe) can be taken to be equal to Y and the length of the pulse is X.

Consider a system which uses 3 cm microwaves operating at a range of 100km, has a $100\mu s$ pulse with $\alpha = 7 \times 10^{-4} m^{-2}$ and a beam divergence of 1^0.

(i) What is the resolution in range and azimuth that can be obtained using the raw data?

(ii) By matched filtering $s(x,y)$ first in range and then in azimuth show that the SAR image (i.e. a display of the amplitude modulations) is given by

$$XY \mid \mathrm{sinc}(\alpha X x)\,\mathrm{sinc}(2\pi Y y/\lambda R) \mid .$$

(iii) Taking the resolution of the image to be given by the distance between the zeros of the central lobe, calculate the resolution in range and azimuth of the SAR image. By what factor has the resolution of the image (in range and azimuth) been increased as a result of applying the matched filtering process?

(Note: The speed of light can be taken to be equal to $3 \times 10^8 ms^{-1}$)

5. (a) Briefly discuss the meaning of the following terms as applied to Fourier optics:

- Diffraction limited
- Intensity Point Spread Function
- Modulation Transfer Function

(b) Explain the principles of optical filtering giving some examples of its application and state the physical conditions which must exist for these principles to hold.

(c) A transparency with amplitude transmittance given by

$$\delta(x - x_1, y - y_1) + \delta(x - x_2, y - y_2) + \delta(x - x_3, y)$$

is placed in the object plane of a diffraction limited lens with focal length f. A square aperture of width $2a$ is placed in the image plane of the lens beyond which is a second identical lens at a distance $2f$ from the first. Use the theory of Fourier optics to derive an analytical expression for the image obtained in the image plane of the second lens when the transparency is illuminated with (i) coherent light and (ii) incoherent light.

6. (a) The Radon transform of a real function $f(x, y)$ is given by

$$g(z, \theta) = \int_{-\infty}^{\infty} \int_{-\infty}^{\infty} f(x, y)\delta(z - x\cos\theta - y\sin\theta)dxdy.$$

Show that in the case when f has circular symmetry, the Radon transform reduces to the Abel transform given by

$$g(z) = 2\int_{z}^{\infty} \frac{f(r)rdr}{\sqrt{r^2 - z^2}}.$$

By letting $\xi = r^2$, $\rho = z^2$, $G(z^2) = g(z)$ and $F(r^2) = f(r)$, write this transform in terms of a convolution integral. Hence, given that

$$\int_{-\infty}^{\infty} \frac{1}{\sqrt{x}} \exp(-ikx)dx = \sqrt{\frac{\pi}{ik}}$$

use the convolution theorem to show that the inverse Abel transform is

$$f(r) = -\frac{1}{\pi}\int_r^\infty \frac{1}{\sqrt{z^2 - r^2}}\left(\frac{dg(z)}{dz}\right) dz.$$

(b) Briefly discuss the basis of the following numerical techniques for reconstructing f given g:

- Back-projection and deconvolution
- Filtered back-projection
- Application of the central slice theorem

(c) Show that the Radon transform of a single point (described by a 2D delta function) located in the image plane at (x_0, y_0) yields a curve given by the equation

$$z = x_0 \cos\theta + y_0 \sin\theta.$$

Sketch the curves when: $(x_0, y_0) = (0, 0)$; $(x_0, y_0) = (a, a)$ and $(x_0, y_0) = (2a, 2a)$ for values of θ between $-\frac{\pi}{2}$ and $\frac{\pi}{2}$ radians. What are the coordinates in Radon space at which all three curves intersect.

7. Maxwell's (microscopic) equations (for Gaussian cgs units and with the speed of light $c \simeq 3 \times 10^8 ms^{-1}$) are:

$$\nabla \cdot \mathbf{e} = 4\pi\rho, \quad \nabla \cdot \mathbf{b} = 0,$$

$$\nabla \times \mathbf{e} = -\frac{1}{c}\frac{\partial \mathbf{b}}{\partial t}, \quad \nabla \times \mathbf{b} = \frac{1}{c}\frac{\partial \mathbf{e}}{\partial t} + \frac{4\pi}{c}\mathbf{j}$$

where $\mathbf{e}$ is the electric field, $\mathbf{b}$ is the magnetic field and ρ and $\mathbf{j}$ are the charge and current densities respectively.

(i) Discuss the physical significance of each of the equations above and show that

$$\frac{\partial \rho}{\partial t} + \nabla \cdot \mathbf{j} = 0.$$

(ii) By writing

$$\mathbf{b} = \nabla \times \mathbf{A}, \quad \mathbf{e} = -\nabla\phi - \frac{1}{c}\frac{\partial \mathbf{A}}{\partial t}$$

and using an appropriate gauge transformation, show that Maxwell's equations can be written in the decoupled form

$$\nabla^2\phi - \frac{1}{c^2}\frac{\partial^2\phi}{\partial t^2} = -4\pi\rho, \quad \nabla^2\mathbf{A} - \frac{1}{c^2}\frac{\partial^2 \mathbf{A}}{\partial t^2} = -\frac{4\pi}{c}\mathbf{j}.$$

Explain how this result can be used to calculate the electromagnetic field generated by a given source.

(iii) The electric field potential ϕ at a point $\mathbf{r}_0$ produced by a moving charge located at a point $\mathbf{r}$ oscillating at a fixed angular frequency ω is given by

$$\phi(\hat{\mathbf{n}}_0, \omega) = \frac{e^{ikr_0}}{r_0} \int \rho(\mathbf{r}) e^{-ik\hat{\mathbf{n}}_0 \cdot \mathbf{r}} d^3\mathbf{r}$$

where $\hat{\mathbf{n}}_0 = \mathbf{r}_0/r_0$ and $k = 2\pi/\lambda = \omega/c$, λ being the wavelength. Use this result to calculate the amplitude of the electric field potential produced by a 3cm wavelength microwave at a distance of 3m from the location of the emission when $\rho(\mathbf{r}) = 1/r^2$.

Note that

$$\int_0^\infty \frac{\sin x}{x} dx = \frac{\pi}{2}.$$

8. (i) Discuss the use of a scalar wave theory to describe optical diffraction phenomena and the conditions under which it can be used.

(ii) The diffracted wavefield U produced by a plane wave travelling in the z-direction with wavelength λ is, in the Fraunhofer zone, given by

$$U(x,y) = \frac{i}{\lambda}\frac{e^{ikz}}{z} \exp\left(ik\frac{(x^2+y^2)}{2z}\right) \int_{-\infty}^{\infty}\int_{-\infty}^{\infty} u(\xi,\eta) \exp\left(-\frac{2\pi i}{\lambda z}(x\xi + y\eta)\right) d\xi d\eta$$

where u is the aperture amplitude and $k = 2\pi/\lambda$.

(a) Using this result, compute the diffraction pattern (field intensity) produced by a square aperture of width $2a$ and sketch the result.

(b) Compute the area of the central lobe of this diffraction pattern when a=0.1mm at a distance of 1 cm from the aperture using an optical wavefield with a wavelength of 500nm.

9. Consider a stationary optical imaging system described by the convolution relationship

$$s(x,y) = \int_{-\infty}^{\infty}\int_{-\infty}^{\infty} p(x-x', y-y') f(x',y') dx' dy'$$

where f is the object function (input), p is the point spread function of the system and s is the optical image (output).

(i) In the context of this system, explain the meaning of the following terms:

- Isoplanicity

- Optical Transfer Function
- Phase Transfer Function

(ii) The Optical Transfer Function of this system is given by

$$P(k_x, k_y) = H_x(k_x)H_y(k_y)$$

where

$$H_x(k_x) = \begin{cases} 1, & \mid k_x \mid \leq K; \\ 0, & \mid k_x \mid > K. \end{cases}$$

$$H_y(k_y) = \begin{cases} 1, & \mid k_y \mid \leq K; \\ 0, & \mid k_y \mid > K. \end{cases}$$

and k_x, k_y are the spatial frequencies. Compute the point spread function of the system.

(iii) Derive an expression for the optical image produced when the system is used to image an infinitesimal narrow line parallel to the x-axis and passing through the origin of the object plane. Sketch the result.

Note that

$$\int_{-\infty}^{\infty} \frac{\sin x}{x} dx = \pi.$$

10. (a) Give brief explanations of the following terms (as applied to digital image processing):

- Point Spread Function
- Transfer Function
- Phase Spectrum
- Edge detection
- Aliasing

(b) The following row vector is to be correlated with the kernel (1 2 1):

$$(0 \quad 1 \quad 1 \quad 0 \quad 1 \quad 2 \quad 1 \quad 0)$$

(i) Compute the output.

(ii) Show that the process can be written as a matrix equation, defining the matrix and stating its bandwidth.

(iii) If the output obtained by correlating a row vector $\mathbf{x}$ consisting of 8 integer elements with the kernel $(0 \;\; 2 \;\; 1)$ using zero padding is given by

$$\left(0 \;\; \frac{2}{3} \;\; \frac{1}{3} \;\; \frac{1}{3} \;\; 0 \;\; \frac{1}{3} \;\; \frac{1}{3} \;\; 0\right)$$

use the matrix formulation of the problem to compute $\mathbf{x}$.

(c) The digital images given below show the original image together with three other images which are the result of applying certain FIR filters whose kernels are:

(i) $\frac{1}{9^2}\begin{pmatrix} 1 & \dots & 1 \\ \vdots & \ddots & \vdots \\ 1 & \dots & 1 \end{pmatrix}$ (ii) $\begin{pmatrix} 0 & -1 & 0 \\ -1 & 4 & -1 \\ 0 & -1 & 0 \end{pmatrix}$ (iii) $\begin{pmatrix} 1 & 1 & 1 \\ 1 & -8 & 1 \\ 1 & 1 & 1 \end{pmatrix}$

(iv) $\begin{pmatrix} 1 & 2 & 1 \\ 0 & 0 & 0 \\ -1 & -2 & -1 \end{pmatrix}$ (v) $\begin{pmatrix} 0 & -1 & 0 \\ -1 & 5 & -1 \\ 0 & -1 & 0 \end{pmatrix}$ (vi) $\begin{pmatrix} 0 & -2 & 0 \\ 1 & 2 & 1 \\ 0 & -2 & 0 \end{pmatrix}$

State which kernel in the list above has been used to obtain the images given providing reasons for your choice.

11. (a) The Fourier transform of an $n \times n$ image is an $n \times n$ complex valued array, or $2n^2$ values. For reasons of symmetry, only $n \times n$ values are independent. Nevertheless, storing the Fourier transform of an image takes much more computer memory. Why is this?

(b) Consider the following binary image

$$\begin{pmatrix} 0 & 0 & 1 & 1 & 0 & 0 \\ 0 & 0 & 1 & 1 & 0 & 0 \\ 1 & 1 & 1 & 1 & 1 & 1 \\ 1 & 1 & 1 & 1 & 1 & 1 \\ 0 & 0 & 1 & 1 & 0 & 0 \\ 0 & 0 & 1 & 1 & 0 & 0 \end{pmatrix}$$

(i) If this digital image was converted to analogue image described by a function $f(x, y)$ ahow that the 2D Fourier transform of this pattern is proportional to

$$4\,\mathrm{sinc}(u)\,\mathrm{sinc}(v)+2\,\mathrm{sinc}(v)[6\,\mathrm{sinc}(3u)-2\,\mathrm{sinc}(u)]+2\,\mathrm{sinc}(u)[6\,\mathrm{sinc}(3v)-2\,\mathrm{sinc}(v)]$$

where u and v are the spatial frequencies. (Hint: Decompose the pattern in to five blocks of equal size)

(ii) Compute the response of the digital Laplacian filter to the digital image above and show that the transfer function for this process is given by

$$2\cos(\pi n/3) + 2\cos(\pi m/3) - 4$$

where n and m are all integers with range 0 to 5.

12. The following 8×8 matrix is a binary image representation of the letter L.

$$\begin{pmatrix} 0 & 0 & 0 & 0 & 0 & 0 & 0 & 0 \\ 0 & 0 & 0 & 0 & 0 & 0 & 0 & 0 \\ 0 & 0 & 0 & 0 & 0 & 0 & 0 & 0 \\ 0 & 0 & 0 & 1 & 0 & 0 & 0 & 0 \\ 0 & 0 & 0 & 1 & 0 & 0 & 0 & 0 \\ 0 & 0 & 0 & 1 & 1 & 1 & 0 & 0 \\ 0 & 0 & 0 & 0 & 0 & 0 & 0 & 0 \\ 0 & 0 & 0 & 0 & 0 & 0 & 0 & 0 \end{pmatrix}$$

A pattern recognition algorithm is required to locate the position of this letter in the image.

(a)

(i) Write down the 3×3 kernel that should be used to solve this problem using a spatial correlation filter and compute the output.

(ii) Given that this letter is always of the same size and orientation in the image plane, explain how this filter can be used to determine the image plane coordinates of the letter.

(iii) Explain how the same problem can be solved using a least error approach. Compute the error function for the image above and compare the number of additions and multiplications required for this computation with those involved in computing the correlation filter.

(b) Write a C Void function to implement either of the two methods for the above image to output the coordinates of the position of the letter in the image plane.

13. The blurring of an image as a function of time t is known to be caused by a diffusion process governed by the 2D diffusion equation

$$\frac{\partial u}{\partial t} = D\nabla^2 u$$

where $u(x, y, t)$ is the time dependent image field and D is the Diffusivity.

(a)

(i) If $g(x, y)$ is the image at $t = 0$ and $f(x, y)$ is the blurred image obtained at some time t later, show that provided $t << 1$ and with $D = 1/t$, then g can be recovered from f using the result

$$g(x, y) = f(x, y) - \nabla^2 f(x, y).$$

(ii) Using a centre differencing scheme with unit step length, show that the equivalent digital output g_{ij} can be obtained by correlating the blurred digital image f_{ij} with the kernel

$$\begin{pmatrix} 0 & -1 & 0 \\ -1 & 5 & -1 \\ 0 & -1 & 0 \end{pmatrix}.$$

(iii) Assuming the image to be square, consisting of $N \times N$ pixels, show that this spatial filtering process can be computed using a digital Fourier filter of the form

$$5 - 2\cos(2\pi k/N) - 2\cos(2\pi \ell/N)$$

where k and ℓ are the spatial frequency components of the image.

(b) Assume that you have a 2D FFT (void) function written in C

```
FFT2D(a, b, N, sign)
```

which inputs/outputs real (a) and imaginary (b) arrays of size N and can be used to compute either the forward (sign=-1) or inverse (sign=1) DFT in 'optical form'.

Write a C void function to implement the Fourier filter given above for computing g_{ij} given f_{ij}.

14. (a)

(i) Define the mean, the median and the mode of a digital image.

(ii) Compute the probability function of the 3-bit image given below. Sketch the result and use it to determine the mean, the median and the mode of this image.

$$\begin{pmatrix} 0 & 3 & 7 & 1 & 3 & 1 & 3 & 5 \\ 4 & 4 & 4 & 3 & 3 & 1 & 5 & 3 \\ 2 & 2 & 0 & 5 & 1 & 2 & 2 & 5 \\ 4 & 3 & 5 & 5 & 3 & 5 & 0 & 6 \\ 6 & 4 & 2 & 0 & 7 & 2 & 6 & 6 \\ 6 & 2 & 2 & 1 & 7 & 1 & 4 & 4 \\ 1 & 6 & 1 & 2 & 3 & 1 & 3 & 3 \\ 4 & 1 & 4 & 7 & 7 & 2 & 2 & 2 \end{pmatrix}$$

(b) The histogram of a coherent image can be modelled by the distribution

$$P(x_i) = x_i^{\alpha} \exp(-\beta x_i); i = 1, 2, ..., N$$

where x_i are the pixel values and α and β are positive constants.

(i) Using a least squares method, show that the values of α and β which provide a best fit to a recorded distribution $Q_i \equiv Q(x_i)$ are given by

$$\beta = \frac{\left(\sum_{i=1}^{N} x_i \ln Q_i\right)\left(\sum_{i=1}^{N} (\ln x_i)^2\right) - \left(\sum_{i=1}^{N} \ln Q_i \ln x_i\right)\left(\sum_{i=1}^{N} x_i \ln x_i\right)}{\left(\sum_{i=1}^{N} (\ln x_i)^2\right)\left(\sum_{i=1}^{N} x_i \ln x_i\right) - \left(\sum_{i=1}^{N} (\ln x_i)^2\right)\left(\sum_{i=1}^{N} x_i^2\right)}$$

and

$$\alpha = \frac{\sum_{i=1}^{N} \ln Q_i \ln x_i + \beta \sum_{i=1}^{N} x_i \ln x_i}{\sum_{i=1}^{N} (\ln x_i)^2}.$$

(ii) Write a C void function to implement the formulae above for the case when $x_i = i$. The function should input the recorded distribution and its (array) size and output the values of α and β.

15. (a) Give brief explanations of the following terms (as applied to digital image processing):

- Pixel
- Spatial quantization
- Grey-level quantization
- Point Spread Function
- Signal-to-Noise ratio

(b) The illumination-reflection model for an image is compounded in the simple equation

$$f(x, y) = i(x, y)r(x, y)$$

where f is the image and i and r are the illumination and reflection components respectively.

(i) Suppose that a flat area with centre at (x_0, y_0) is illuminated by a light source with intensity distribution

$$i(x, y) = Ke^{-[(x-x_0)^2+(y-y_0)^2]}.$$

If the reflectance characteristic of the area is

$$r(x, y) = 10(x - x_0) + 10(y - y_0) + 20,$$

what is the value of K that would yield an image intensity of 100 at (x_0, y_0)?

(ii) Assume that the area in (i) above now has a constant reflectance of 1, and let $K = 255$. If the resulting image is digitized with n bits of intensity resolution (grey level quantization), and the eye can detect an abrupt change of eight shades of grey between adjacent pixels, what is the value of n that will cause visible false contouring?

(iii) Explain the principle of Homomorphic filtering and how it can be applied to recovering the reflection component in an image and the conditions upon which this technique is based.

16. (i) The Discrete Fourier Transform (DFT) of an array $f_0, f_1, f_2 ... f_{N-1}$ is given by

$$F_m = \frac{1}{N} \sum_{n=0}^{N-1} f_n \exp(-2\pi inm/N)$$

Writing $W_N = \exp(-2\pi i/N)$, decompose this result into two parts - a DFT of the odd values and a DFT of the even values of the array f_n. Explain how a decomposition of this type can be used to design a Fast Fourier Transform.

(ii) Calculate the DFT of the array (0,1,1,0) using the decomposition obtained in part (i) above. Hence, compute the discrete power spectrum and principal phase spectrum of this array.

(iii) Write down the form of the 2D DFT using a Cartesian coordinate system and explain how a 1D FFT can be used to compute a 2D FFT.

(iv) Explain the difference between the 'standard' and 'optical' forms of the 2D DFT and discuss some of the display techniques that can be used to assess the spectral information in a digital image.

17. (a)

(i) Explain the principle of the median filter for reducing 'salt and pepper' noise in a digital image.

(ii) By applying a frame of zero's, 1 pixel wide, write down the result of applying a median filter to the 4-bit image given below using a 3×3 window.

$$\begin{pmatrix} 2 & 1 & 3 & 5 \\ 1 & 2 & 15 & 7 \\ 3 & 2 & 5 & 6 \\ 8 & 7 & 3 & 0 \end{pmatrix}$$

(b) Consider the 8×8, 4-bit digital image given below

$$\begin{pmatrix} 1 & 0 & 5 & 6 & 5 & 6 & 1 & 0 \\ 2 & 5 & 1 & 3 & 1 & 2 & 5 & 4 \\ 1 & 3 & 11 & 15 & 14 & 14 & 6 & 5 \\ 2 & 1 & 14 & 10 & 9 & 12 & 1 & 2 \\ 0 & 1 & 8 & 14 & 11 & 11 & 5 & 1 \\ 2 & 4 & 8 & 9 & 11 & 15 & 4 & 1 \\ 4 & 6 & 5 & 1 & 5 & 2 & 6 & 3 \\ 0 & 1 & 5 & 0 & 5 & 2 & 2 & 4 \end{pmatrix}$$

(i) Write down the pixel values of the binary image produced by applying a threshold of 8 to the image above.

(ii) Taking the origin to be at the top left-hand corner, write down the pixel values produced by applying the Roberts gradient operator to detect the edges of this binary image.

18. (a) Give brief explanations of the following terms (as applied to digital image processing):

- Binarization
- Segmentation
- Spatial filtering
- Deconvolution
- Data Compression

(b) Explain how to compute a Finite Impulse Response filter and discuss some of the techniques available for implementing the filter at the extreme edges of an image.

(c) Consider the following 5×5 4-bit digital image

$$\begin{pmatrix} 0 & 1 & 2 & 1 & 1 \\ 1 & 3 & 2 & 2 & 3 \\ 3 & 2 & 3 & 15 & 2 \\ 1 & 2 & 2 & 3 & 4 \\ 2 & 0 & 2 & 2 & 0 \end{pmatrix}$$

Use 'zero padding' to filter this image with the kernel

$$\begin{pmatrix} -1 & -1 & -1 \\ -1 & 8 & -1 \\ -1 & -1 & -1 \end{pmatrix}$$

What is the effect of applying this kernel on the image and in what circumstances do you think it would be of value?

(d) Write a C void function to compute this filter directly for a square digital image of size n×n.

19. (a) The digital imaging equation for a stationary process is given by

$$s_{ij} = p_{ij} \otimes\otimes f_{ij} + n_{ij}$$

where s_{ij} is the digital image, p_{ij} is the point spread function, f_{ij} is the object function, n_{ij} is the noise and $\otimes\otimes$ is the discrete convolution operation. The functions p_{ij}, f_{ij} and n_{ij} all have discrete Fourier transforms denoted by P_{ij}, F_{ij} and N_{ij} respectively.

An estimate g_{ij} of the object function is to be derived given by

$$g_{ij} = q_{ij} \otimes\otimes s_{ij}$$

where q_{ij} is the restoring filter with Discrete Fourier Transform denoted by Q_{ij}.

Using the discrete convolution theorem, show that if a solution to this problem is attempted based on the premise of forcing the power spectrum of the restored image $\mid G_{ij} \mid^2$ to be equal to the power spectrum of the original image (i.e. the power spectrum of the object function $\mid F_{ij} \mid^2$) then, under the conditions

$$F_{ij}N_{ij}^* = 0 \quad \text{and} \quad N_{ij}F_{ij}^* = 0$$

the restoring filter is given by

$$Q_{ij} = \frac{1}{\sqrt{\mid P_{ij} \mid^2 + \frac{|N_{ij}|^2}{|F_{ij}|^2}}}.$$

In practical cases, where information on $\mid N_{ij} \mid^2$ and $\mid F_{ij} \mid^2$ is not available, it is common to approximate this filter by

$$Q_{ij} \sim \frac{1}{\sqrt{\mid P_{ij} \mid^2 + \Gamma}}$$

where

$$\Gamma = \frac{1}{(SNR)^2}$$

SNR being some estimate of the signal-to-noise ratio of the image.

Why is this approximated form usually required for the practical implementation of this filter and what are some of the likely effects?

(b) Assume that you have the 2D FFT function called *fft* which inputs/outputs real and imaginary arrays of size n and can be used to compute either the forward or inverse Fourier transform in 'optical form'.

Write a C void function to implement the approximated form of the restoration filter given above with input s, point spread function p, restoration f and signal-to-noise ratio snr.

20. (a) Consider the 4-bit grey level image (left) and associated histogram (right) given below.

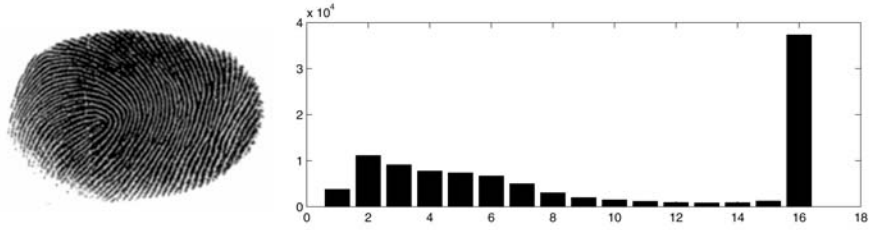

By studying the histogram provided determine the optimum threshold level that should be applied to binarize this image. Explain the reasons for you choice?

Explain how the process of binarization of a digital image (i.e. choosing a suitable threshold) could be automated assuming that its grey level histogram is bimodel.

Assuming that the two peaks always occur in the two halves of the histogram, write a C void function to implement this process (i.e. to compute an optimum threshold value).

Note: You may assume that the image is composed of integer numbers between 0 and 127 inclusive.

(b) The edges of the following 8×8 4-bit binary image are to be detected using the Roberts gradient operator

$$\begin{pmatrix} 0 & 0 & 0 & 0 & 0 & 0 & 0 & 0 \\ 0 & 15 & 15 & 15 & 15 & 15 & 15 & 0 \\ 0 & 0 & 15 & 15 & 15 & 15 & 15 & 0 \\ 0 & 0 & 0 & 15 & 15 & 15 & 15 & 0 \\ 0 & 0 & 0 & 0 & 15 & 15 & 15 & 0 \\ 0 & 0 & 0 & 0 & 0 & 15 & 15 & 0 \\ 0 & 0 & 15 & 0 & 0 & 0 & 15 & 0 \\ 0 & 0 & 0 & 0 & 0 & 0 & 0 & 0 \end{pmatrix}$$

What type of filter should be applied to this image before computing the Roberts gradient operator? Give reasons for your choice.

Compute the Roberts gradient for the above image with and without the application of this filter. Comment on the results.

21. (i) Give brief explanations of the following terms:

- Luminance quantization
- Coherence
- Image enhancement
- Image restoration
- Back-projection

(ii) Compute the response of the digital Laplacian filter ∇^2 (in real space) to the image patterns:

$$\begin{pmatrix} 0 & 0 & 0 & 0 & 0 \\ 0 & 0 & 0 & 0 & 0 \\ 0 & 0 & 1 & 0 & 0 \\ 0 & 0 & 0 & 0 & 0 \\ 0 & 0 & 0 & 0 & 0 \end{pmatrix} \quad \text{and} \quad \begin{pmatrix} 0 & 0 & 1 & 1 & 1 \\ 0 & 0 & 1 & 1 & 1 \\ 0 & 0 & 1 & 1 & 1 \\ 0 & 0 & 1 & 1 & 1 \\ 0 & 0 & 1 & 1 & 1 \end{pmatrix}.$$

Does it respond more strongly to isolated points or to edges?

(iii) The following algorithm is a selective highpass filter:

If $\nabla^2 v(i,j) <$threshold
$v(i,j) = v(i,j) + \alpha \nabla^2 v(i,j)$
Else
$v(i,j) =< v(i,j) >$
Endif

where α is a user-specified parameter and $< v(i,j) >$ is the mean in some neighbourhood of (i,j); $v(i,j)$ being the pixel value at (i,j).

What will be the effect of implementing a filter of this type?

Write an C (void) function to implement this filter. The I/O should be as follows:

Input: Image, image size (assume square images), α, neighbourhood of pixels.

Output: Processed image

22. An image s_{ij} can be described by the stationary process

$$s_{ij} = p_{ij} \otimes \otimes f_{ij} + n_{ij}$$

where p_{ij} is the point spread function, f_{ij} is the object function and n_{ij} is the noise function ($\otimes\otimes$ denotes the 2D convolution operation) . An estimate for the object function is required which maximizes its entropy E defined by

$$E = -\sum_i \sum_j f_{ij} \ln f_{ij}; \quad f_{ij} > 0$$

(i) Use the Lagrange multiplier method to show that the solution for f_{ij} is given by the iteration

$$f_{ij}^{k+1} = \exp[-1 + 2\lambda(s_{ij} \odot\odot p_{ij} - p_{ij} \otimes\otimes f_{ij}^k \odot\odot p_{ij})]; \quad k = 1, 2, ...$$

where $\odot\odot$ denotes the 2D correlation operation.

Explain how this algorithm could be implemented in practice.

(ii) By linearizing the result above, show that a filter of the type

$$\frac{P_{ij}^*}{\mid P_{ij} \mid^2 + 1/2\lambda}$$

can be constructed where P_{ij} is the DFT of p_{ij}.

(iii) An algorithm is required to estimate the Signal-to-Noise Ratio (SNR) of an image defined by

$$\text{SNR} = \sum_i \sum_j \mid F_{ij} \mid^2 / \mid N_{ij} \mid^2$$

where F_{ij} and N_{ij} are the DFT's of f_{ij} and n_{ij} respectively. Show that by recording two images s_{ij} and s'_{ij}, of the same object at different times and assuming that the noise is signal independent, then

$$\frac{\mid N_{ij} \mid^2}{\mid F_{ij} \mid^2} = \left(\frac{C_{ij}}{C'_{ij}} - 1 \right) \mid P_{ij} \mid^2$$

where C_{ij} and C'_{ij} are the DFT's of the correlation functions $s_{ij} \odot\odot s_{ij}$ and $s_{ij} \odot\odot s'_{ij}$ respectively.

(iv) Write an ANSI C (Void) function to compute the SNR defined above with the following I/O:

Input: Images s_{ij} and s'_{ij}, size of (square) images

Output: SNR as defined above.

Assume that you have a 2D FFT void function called

```
FFT2D(a,b,N,sign)
```

which inputs/outputs real (a) and imaginary (b) arrays of size N and can be used to compute either the forward (sign=-1) or inverse (sign=1) DFT in 'optical form'.

23. Consider the 4-bit image given below

$$\begin{pmatrix} 0 & 1 & 1 & 1 & 2 & 2 & 4 & 1 \\ 2 & 2 & 3 & 1 & 2 & 2 & 1 & 1 \\ 3 & 4 & 5 & 2 & 5 & 6 & 7 & 6 \\ 3 & 10 & 15 & 9 & 11 & 14 & 14 & 13 \\ 2 & 14 & 10 & 11 & 14 & 12 & 12 & 12 \\ 2 & 3 & 7 & 13 & 13 & 14 & 15 & 14 \\ 2 & 3 & 4 & 5 & 6 & 2 & 1 & 0 \\ 0 & 1 & 2 & 14 & 12 & 13 & 9 & 8 \end{pmatrix}$$

(a)

(i) Compute the probability density function of this image. Tabulate and sketch the result using a bar chart.

(ii) Use the tabulation to compute the mean, the median and the mode of this image.

(b) The image is to be classified by applying a 3×3 mode filter in which a pixel is replaced by its most common neighbour or else the lowest value in the neighbourhood. Compute the output.

(c)

(i) What threshold level should be used to binarize the original image; give reasons for your choice and use this value to compute the binary image.

(ii) Locate the edges of this binary image using the masks

$$\begin{pmatrix} 1 & -1 \end{pmatrix} \quad \text{and} \quad \begin{pmatrix} 1 \\ -1 \end{pmatrix}$$

and compute the magnitude.

(iii) Locate the edges of this binary image using a Sobel operator.

(iv) Write a C (Void) function to implement the Sobel operator directly with the following I/O:

Input: Digital Image, size of (square image)

Output: Processed image

24. (a) Give brief explanations on the following terms with respect to image enhancement:

- Logarithmic and exponential transforms
- Gamma correction
- Homomorphic filtering for dynamic range compression and contrast stretching with clipping
- Global and local histogram equalization
- Histogram normalization and contrast stretching with clipping

(b) Derive the transfer function T for histogram equalization, i.e. for each discrete value v_{in}, we obtain a new value

$$v_{\text{out}} = T[v_{\text{in}}]$$

such that the same number of pixels in the display show each of the possible intensity levels.

(c) Write a void function in C to histogram equalize a floating point image where the image is taken to be of size $n \times n$, i.e.

```
void HISTEQ(float **f, float **s, int n, int m)
```

where f is the input image, s is the output image, n defines the image size and m is the number of grey levels required. Explain the advantages of adding or reducing the required number of grey levels with respect to visualization and loss of information.

(d) The process of combining histogram equalization with a high emphasis filter is often used to achieve both enhancement and edge sharpening. Prove that it matters which process is applied first and give reasons as to which operation should be applied first.

(e) Describe any special problems that may occur if histogram equalization is applied to a Gaussian pyramid structure of an image. Give a reason as to whether the process should be applied to each level individually or to all the levels at the same time.

25. (a) Using first order derivatives, show how a gradient operator can be designed in terms of an FIR filter (i.e. the discrete convolution of an image with a convolution kernel). Consider the problems if the operator is non-symmetrical.

(b) With respect to the following filters, explain why each may be used as opposed to the others and their overall effectiveness in image segmentation

$$\begin{pmatrix} 0 & 1 \\ -1 & 0 \end{pmatrix}, \quad \frac{1}{15}\begin{pmatrix} -3 & 5 & 5 \\ -3 & 0 & 5 \\ -3 & -3 & -3 \end{pmatrix}$$

$$\frac{1}{8}\begin{pmatrix} -2 & 1 & -2 \\ 1 & 4 & 1 \\ -2 & 1 & -2 \end{pmatrix}, \quad \frac{1}{34}\begin{pmatrix} 1 & 1 & 1 & 0 & -1 & -1 & -1 \\ 1 & 2 & 2 & 0 & -2 & -2 & -1 \\ 1 & 2 & 3 & 0 & -3 & -2 & -1 \\ 1 & 2 & 3 & 0 & -3 & -2 & -1 \\ 1 & 2 & 3 & 0 & -3 & -2 & -1 \\ 1 & 2 & 2 & 0 & -2 & -2 & -1 \\ 1 & 1 & 1 & 0 & -1 & -1 & -1 \end{pmatrix}.$$

(c) Explain why noise may cause problems and instabilities within the digital Laplacian filter. Specify the use and give reasons as to why the Gaussian distribution is considered a suitable smoothing operator with regard to application of the digital Laplacian filter.

(d) Using appropriate pseudo-code, design a function to compute the filter

$$F_{ij} = \begin{pmatrix} 0 & 1 & 0 \\ 1 & -4 & 1 \\ 0 & 1 & 0 \end{pmatrix} \otimes\otimes G_{ij} \otimes\otimes I_{ij}$$

where I_{ij} is the input digital image, G_{ij} is a Gaussian function with standard deviation σ and $\otimes\otimes$ denotes discrete convolution.

(i) Design another function that computes the zero crossings of F_{ij}.

(ii) Justify your reason for using or otherwise an FFT for either the whole of the operation or just part of the operation for computing F_{ij}.

(iii) Consider any useful approximation when computing F_{ij} when it can be assumed that I_{ij} are a set of discrete levels.

(iv) State what happens in the algorithm as σ is varied from a high value to a low value and how the effect is related to a model for the human visual recognition system.

(e) Consider the application of detecting bubble chamber tracks in which the collisions and paths of high energy particles are recorded as pixel wide tracks. Particles whose tracks are longer than 100 pixels are considered to be relatively stable and need to be recorded. Tracks are allowed to have no more than five gaps that can be no more than 10 pixels long. Define a image segmentation process that detects all stable tracks that are at a user defined angle.

26. (a) Considering the reconstruction of tomographic images, write out the Radon transform for a projected intensity $P(r, \theta)$ in polar coordinates and define the terms used. From this result, define the Fourier slice theorem (the projection theorem) and explain its meaning graphically.

(b) The inverse Fourier transform for an object function $f(x_1, x_2)$ is given by

$$f(x_1, x_2) = \int_0^{2\pi} \int_0^{\infty} rF(r, \theta) \exp[ir(x_1 \cos\theta + x_2 \sin\theta)] dr d\theta$$

where $F(r, \theta)$ is the Fourier transform in polar coordinates. Using the Fourier slice theorem or otherwise, construct the continuous case method for Filtered Back Projection. Show how this relates to the digital version in which

$$f_{x_1 x_2} = \hat{B}\hat{H}\partial P_{r\theta}$$

where $\hat{B}$ is the back-projection operator, $\hat{H}$ is the Hilbert transform operator and ∂ is the differentiation operator. Describe some of the limitations the digital version has over the continuous method.

(c) Consider the process for the reconstruction of a simple object consisting of three points equally spaced. Sketch the projected intensity $P(r, \theta)$ profiles before and after filtering from at least two different directions. Sketch also the pixel shapes for the reconstructed object points when only four projections are used. Hence, discuss the problems of only having a finite number of projections.

(d) If an image is represented as a simple column vector, $\mathbf{c}$, consisting of $x \times y$ pixels, then k projections can be considered in terms of an array of weights W that has a dimension $k \times n$ (where $n = x \times y$). The projected intensity values can then be stored in $\mathbf{p}$ of size k which are related to $\mathbf{c}$ via the linear equation

$$\mathbf{P} = W\mathbf{c}.$$

Numerical methods for solving this equation for the unknown values $\mathbf{c}$ are well known. State some of the advantages and disadvantages of this method and give a brief outline of a practical solution.

27. The Green function for the three-dimensional inhomogeneous Helmholtz equation

$$\nabla^2 u(\mathbf{r}, k) + k^2 u(\mathbf{r}, k) = f(\mathbf{r})$$

is

$$g(\mathbf{r} \mid \mathbf{r}_0, k) = \frac{\exp(ik \mid \mathbf{r} - \mathbf{r}_0 \mid)}{4\pi \mid \mathbf{r} - \mathbf{r}_0 \mid}$$

where $\mathbf{r} = (x, y, z)$ is a three-dimensional position vector and k is the wavenumber.

(a) An optical experiment is setup where the wavefield u is stimulated by a coherent light source with amplitude function $f(\mathbf{r})$. Write down the equation for the wavefield u in terms of the Green function g and the driving field f.

(b) The experiment is arranged so that the source is in the plane $z = 0$ and depends only on x and the wavefield is measured only in the plane $z = z_0$

by a photographic plate. Draw a diagram and hence write an equation for the wavefield $w(x_0, k) = u(x_0, y, z_0, k)$ in terms of the source function $s(x) = f(x, y, 0)$.

(c) Under certain conditions, the integral obtained in part (b) above can be approximated by a Fourier transform of the source function s. Derive this approximation, stating clearly the conditions necessary for the approximation to be valid.

28. The operator $\hat{P}$ models a set of optical components that, given an image described by the optical amplitude function $f(x, y)$ as the input, outputs the Fourier transform image

$$F(u, v) = \int dx \int dy f(x, y) \exp[i(ux + vy)]$$

Thus $\hat{P}[f(x, y)] = F(x, y)$. The operator $\hat{Q}$ models a different set of optical components that, given an input image $f(x, y)$, gives an output image

$$\hat{Q}[f(x, y)] = f(x, y)q(x, y)$$

where q is the aperture function.

(a) Derive and state the effect of the composite system $\hat{P}\hat{Q}\hat{P}$, i.e. the system that takes the output of $\hat{P}$, sends it through $\hat{Q}$ and then through $\hat{P}$.

(b) If $q(x, y)$ describes a square hole of side $2a$ centered on the origin, calculate the coherent and incoherent point spread functions of the system $\hat{P}\hat{Q}\hat{P}$.

(c) If the input to the system is an incoherently illuminated picture of a newpaper's front page for example, describe how the appearance of the output varies with the value of a.

(d) Describe the effect on the output image of the fact that the hole has sharp edges. How could these effect be reduced?

Appendix C

Fourier Transform of a Fractal

Self-affine functions are characterised by an amplitude spectral density function of the type k^{-q} where $k =\mid \mathbf{k} \mid$ is the spatial frequency. This appendix provides detail on calculating the n-dimensional (inverse) Fourier transform of such a spectrum which is compounded in the following theorem:

Theorem If $q \neq 2m$ or $-n-2m$ where $m = 0, 1, 2, ...$, then

$$\hat{F}_n[r^q] = \int_{-\infty}^{\infty} r^q \exp(-i\mathbf{k}\cdot\mathbf{r}) d^n\mathbf{r} = \frac{(\frac{1}{2}q + \frac{1}{2}n - 1)!}{(-\frac{1}{2}q - 1)!} 2^{q+n}\pi^{n/2}k^{-q-n}$$

where $\mathbf{k}$ and $\mathbf{r}$ are the n-dimensional vectors $(k_1, k_2, ..., k_n)$ and $(r_1, r_2, ..., r_n)$ respectively, $r \equiv \mid \mathbf{r} \mid = \sqrt{r_1^2 + r_2^2 + ... + r_n^2}$ and $k \equiv \mid \mathbf{k} \mid = \sqrt{k_1^2 + k_2^2 + ... + k_n^2}$. Note that

$$\hat{F}_n[f(\mathbf{r})] = \int_{-\infty}^{\infty} f(\mathbf{r}) \exp(-i\mathbf{k}\cdot\mathbf{r}) d^n\mathbf{r}$$

is taken to mean

$$\int_{-\infty}^{\infty}\int_{-\infty}^{\infty}...\int_{-\infty}^{\infty} f(r_1, r_2, ..., r_n) \exp[-i(k_1r_1 + k_2r_2 + ... + k_nr_n)] dr_1 dr_2 ..., dr_n.$$

Proof The proof of this result is based two results:

(i) If f is a function of r only, then

$$F(\mathbf{k}) = \left(1 - \frac{\partial^2}{\partial k_1^2} - \frac{\partial^2}{\partial k_2^2} - ... - \frac{\partial^2}{\partial k_n^2}\right)^N (2\pi)^{n/2} \int_0^{\infty} \frac{f(r) r^{n-1}}{(1+r^2)^N} \frac{J_{\frac{n-2}{2}}(kr)}{(kr)^{(n/2)-1}} dr$$

where N is a positive integer and $J_{(n-2)/2}$ is the Bessel function (of order $(n-2)/2$).

(ii) For Bessel Functions,

$$\frac{(2\pi)^{n/2}}{k^{(n/2)-1}}\int_0^\infty \frac{r^{q+(n/2)}}{(1+r^2)^N}J_{\frac{n-2}{2}}(kr)dr$$

$$= \frac{\pi^{n/2}(\frac{1}{2}q+\frac{1}{2}n-1)!(N-\frac{1}{2}q-\frac{1}{2}n-1)!}{(N-1)!(\frac{1}{2}n-1)!}{}_1F_2(\tfrac{1}{2}q+\tfrac{1}{2}n;\tfrac{1}{2}q+\tfrac{1}{2}n-N+1,\tfrac{1}{2}n;\tfrac{1}{4}k^2)$$

$$+\frac{\pi^{n/2}k^{2N-q-n}(\frac{1}{2}q+\frac{1}{2}n-N-1)!}{(N-\frac{1}{2}q-1)!2^{2N-q-n}}{}_1F_2(N;N-\tfrac{1}{2}q,N+1-\tfrac{1}{2}q-\tfrac{1}{2}n;\tfrac{1}{4}k^2) \tag{C.1}$$

where

$${}_1F_2(a;b,c;x) = 1+\frac{a}{1!bc}x+\frac{a(a+1)}{2!b(b+1)c(c+1)}x^2+...$$

The first of these results can be obtained by choosing a polar axis to lie along the direction of $\mathbf{k}$ so that $\mathbf{k}\cdot\mathbf{r} = kr\cos\theta_1$ and

$$F(\mathbf{k}) = \int_{-\infty}^{\infty} f(r)\exp(-i\mathbf{k}\cdot\mathbf{r})d\mathbf{r} = \int_0^\infty f(r)r^{n-1}\int_0^\pi \exp(-ikr\cos\theta_1)\sin^{n-2}\theta_1 d\theta_1$$

$$\times\int_0^\pi ...\int_0^{2\pi}\sin^{n-3}\theta_2...\sin\theta_{n-2}d\theta_2...d\theta_{n-1}dr$$

$$= \int_0^\infty f(r)r^{n-1}\frac{2\pi^{(n-1)/2}}{(\frac{1}{2}n-\frac{3}{2})!}\int_0^\pi \exp(-ikr\cos\theta_1)\sin^{n-2}\theta_1 d\theta_1 dr$$

using

$$\int_0^\pi \sin^\nu d\theta = \frac{(\frac{1}{2}\nu-\frac{1}{2})!\pi^{1/2}}{(\frac{1}{2}\nu)!}.$$

Now,

$$-\left(\frac{\partial^2}{\partial k_1^2}+\frac{\partial^2}{\partial k_2^2}+...+\frac{\partial^2}{\partial k_n^2}\right) = \int_{-\infty}^{\infty} f(r)(r_1^2+r_2^2+...+r_n^2)\exp(-i\mathbf{k}\cdot\mathbf{r})d^n\mathbf{r}$$

and therefore

$$\left(1-\frac{\partial^2}{\partial k_1^2}-\frac{\partial^2}{\partial k_2^2}-...-\frac{\partial^2}{\partial k_n^2}\right)^N = \int_{-\infty}^{\infty} f(r)(1+r^2)^N\exp(-i\mathbf{k}\cdot\mathbf{r})d^n\mathbf{r}.$$

Hence, we can write

$$F(\mathbf{k}) = \left(1 - \frac{\partial^2}{\partial k_1^2} + \frac{\partial^2}{\partial k_2^2} - ... - \frac{\partial^2}{\partial k_n^2}\right)^N (2\pi)^{n/2} \int_0^\infty \frac{f(r) r^{n-1}}{(1+r^2)^N} \frac{J_{\frac{n-2}{2}}(kr)}{(kr)^{(n/2)-1}} dr. \tag{C.2}$$

The ratio of two successive terms u_{n+1}/u_n in the infinite series for ${}_1F_2$ is $(a+n)x/[(n+1)(b+n)(c+n)]$ which tends to zero as $n \to \infty$ for any finite x. Thus, the series for ${}_1F_2$ converges absolutely and uniformly with respect to x and the same is true of its derivatives (provided that neither b or c is a negative integer or zero when the series diverges). Therefore,

$$\left(\frac{\partial^2}{\partial k_1^2} + \frac{\partial^2}{\partial k_2^2} + ... + \frac{\partial^2}{\partial k_n^2}\right) {}_1F_2(a; b, \tfrac{1}{2}n; \tfrac{1}{4}k^2)$$

$$= \frac{(b-1)!(\frac{1}{2}-1)!}{(a-1)!} \left(\frac{\partial^2}{\partial k_1^2} + \frac{\partial^2}{\partial k_2^2} + ... + \frac{\partial^2}{\partial k_n^2}\right) \sum_{s=0}^\infty \frac{(a+s-1)!(\frac{1}{2}k)^{2s}}{(b+s-1)!(\frac{1}{2}n+s-1)!s!}$$

$$= \frac{(b-1)!(\frac{1}{2}n-1)!}{(a-1)!} \sum_{s=0}^\infty \frac{(a+s-1)!(\frac{1}{2}k)^{2s-2}}{(b+s-1)!(\frac{1}{2}n+s-2)!(s-1)!}.$$

The term for $s=0$ disappears so that, by replacing s by $s+1$ we obtain

$$\left(\frac{\partial^2}{\partial k_1^2} + \frac{\partial^2}{\partial k_2^2} + ... + \frac{\partial^2}{\partial k_n^2} - 1\right) {}_1F_2(a; b, \tfrac{1}{2}n; \tfrac{1}{4}k^2)$$

$$= \frac{(b-1)!(\frac{1}{2}n-1)!}{(a-1)!} \sum_{s=0}^\infty \frac{(a+s-1)!(\frac{1}{2}k)^{2s}}{(b+s)!(\frac{1}{2}n+s-1)!s!}(a+s-b-s)$$

$$= \frac{a-b}{b} {}_1F_2(a; b+1, \tfrac{1}{2}n; \tfrac{1}{4}k^2).$$

Hence,

$$\left(\frac{\partial^2}{\partial k_1^2} + \frac{\partial^2}{\partial k_2^2} + ... + \frac{\partial^2}{\partial k_n^2} - 1\right)^N {}_1F_2(a; b, \tfrac{1}{2}n; \tfrac{1}{4}k^2)$$

$$= \frac{(a-b)(a-b-1)...(a-b-N+1)}{b(b+1)...(b+N-1)} {}_1F_2(a; b+N, \tfrac{1}{2}n; \tfrac{1}{4}k^2). \tag{C.3}$$

In the first term of equation (C.1) $a = \frac{1}{2}(q+n), b = \frac{1}{2}(q+n) - N + 1$ so that $a - b = N + 1$ with the result that the right hand side of the equation vanishes. For the second term of equation (C.1), consider, with $b > 0$

$$\left(\frac{\partial^2}{\partial k_1^2} + \frac{\partial^2}{\partial k_2^2} + ... + \frac{\partial^2}{\partial k_n^2}\right) k^{2b} {}_1F_2(a; b+\tfrac{1}{2}n, b+1; \tfrac{1}{4}k^2)$$

$$= \frac{(b+\frac{1}{2}n-1)!b!}{(a-1)!} \sum_{s=0}^\infty \frac{(a+s-1)!k^{2b+2s-2}}{4^{s-1}(b+\frac{1}{2}n-2+s)!(b+s-1)!s!}$$

as above. Hence,

$$\left(\frac{\partial^2}{\partial k_1^2}+\frac{\partial^2}{\partial k_2^2}+...+\frac{\partial^2}{\partial k_n^2}-1\right)k^{2b}{}_1F_2(a;b+\tfrac{1}{2}n,b+1;\tfrac{1}{4}k^2)=\frac{(b+\frac{1}{2}n-1)!b!}{(a-1)!}$$

$$\times\left[\frac{(a-1)!4k^{2b-2}}{(b+\frac{1}{2}n-2)!(b-1)!}+\sum_{s=0}^{\infty}\frac{(a+s-2)!(a-1)k^{2b+2s-2}}{4^{s-1}(b+\frac{1}{2}n-2+s)!(b+s-1)!s!}\right]$$

from which is evident that

$$\left(\frac{\partial^2}{\partial k_1^2}+\frac{\partial^2}{\partial k_2^2}+...+\frac{\partial^2}{\partial k_n^2}-1\right)k^{2b}{}_1F_2(1;b+\tfrac{1}{2}n,b+1;\tfrac{1}{4}k^2)=(b+\tfrac{1}{2}n-1)4bk^{2b-2} \tag{C.4}$$

and

$$\left(\frac{\partial^2}{\partial k_1^2}+\frac{\partial^2}{\partial k_2^2}+...+\frac{\partial^2}{\partial k_n^2}-1\right)k^{2b}{}_1F_2(a;b+\tfrac{1}{2}n,b+1;\tfrac{1}{4}k^2)$$

$$=4b(b+\tfrac{1}{2}n-1)k^{2b-2}{}_1F_2(a-1;b+\tfrac{1}{2}n-1,b;\tfrac{1}{4}k^2),\quad a\neq 1.$$

Consequently, if $a\neq 1$ or 2, then since

$$\left(\frac{\partial^2}{\partial k_1^2}+\frac{\partial^2}{\partial k_2^2}+...+\frac{\partial^2}{\partial k_n^2}\right)k^q=q(q+n-2)k^{q-2}$$

for all q except those for which $q+n=2,0,-2,-4,...,$

$$\left(\frac{\partial^2}{\partial k_1^2}+\frac{\partial^2}{\partial k_2^2}+...+\frac{\partial^2}{\partial k_n^2}-1\right)k^{2b}{}_1F_2(a;b+\tfrac{1}{2}n,b+1;\tfrac{1}{4}k^2)$$

$$=4^2b(b-1)(b+\tfrac{1}{2}n-1)(b+\tfrac{1}{2}n-2)k^{2b-4}{}_1F_2(a-2;b+\tfrac{1}{2}n-2,b-1;\tfrac{1}{4}k^2)$$

where, in deriving this result, since it cannot be assumed that $b-1>0$, with $b=N-\frac{1}{2}q-\frac{1}{2}n$ we impose the condition $q=2m$ $(m=0,1,2,...)$. Thus, using equation (C.4) we can write

$$\left(\frac{\partial^2}{\partial k_1^2}+\frac{\partial^2}{\partial k_2^2}+...+\frac{\partial^2}{\partial k_n^2}-1\right)^N k^{2N-q-n}{}_1F_2(N;N-\tfrac{1}{2}q,N+1-\tfrac{1}{2}q-\tfrac{1}{2}n;\tfrac{1}{4}k^2)$$

$$=\left(\frac{\partial^2}{\partial k_1^2}+\frac{\partial^2}{\partial k_2^2}+...+\frac{\partial^2}{\partial k_n^2}-1\right)4^{N-1}\frac{(N-\frac{1}{2}q-\frac{1}{2}n)!(N-\frac{1}{2}q-1)!k^{-q-n+2}}{(-\frac{1}{2}q-\frac{1}{2}n+1)!(-\frac{1}{2}q)!}$$

$${}_1F_2(1;-\tfrac{1}{2}q+1,-\tfrac{1}{2}q-\tfrac{1}{2}n+2;\tfrac{1}{4}k^2)=\frac{(N-\frac{1}{2}q-\frac{1}{2}n)!(N-\frac{1}{2}q-1)!4^Nk^{-q-n}}{(-\frac{1}{2}q-\frac{1}{2}n)!(-\frac{1}{2}q-1)!}. \tag{C.5}$$

Using equations (C.5) and (C.3) in equations (C.1) and (C.2) we find that

$$F(\mathbf{k})=\frac{(N-\frac{1}{2}q-\frac{1}{2}n)!(\frac{1}{2}q+\frac{1}{2}n-N-1)!}{(-\frac{1}{2}q-\frac{1}{2}n)!(-\frac{1}{2}q-1)!}2^{q+n}(-1)^N\pi^{n/2}k^{-q-n}.$$

Finally, using the formula

$$z!(-z)!=\frac{\pi z}{\sin\pi z}$$

we have

$$(N-\tfrac{1}{2}q-\tfrac{1}{2}n)!(\tfrac{1}{2}q+\tfrac{1}{2}n-N-1)!=\frac{\pi}{\sin\pi(\frac{1}{2}q+\frac{1}{2}n-N)}$$

$$=\frac{(-1)^N\pi}{\sin\frac{1}{2}\pi(q+n)}=(\tfrac{1}{2}q+\tfrac{1}{2}n-1)!(-\tfrac{1}{2}q-\tfrac{1}{2}n)!(-1)^N$$

so that

$$F(\mathbf{k})=\frac{(\frac{1}{2}q+\frac{1}{2}n-1)!}{(-\frac{1}{2}q-1)!}2^{q+n}\pi^{n/2}k^{-q-n}.$$

We can write this result using the Gamma function notation where

$$m!=\Gamma(m+1)=\int_0^\infty t^m\exp(-pt)dt$$

which generalizes to values of m which are non-integer. Then,

$$F(\mathbf{k})=\frac{\Gamma\left(\frac{q+n}{2}\right)}{\Gamma\left(-\frac{q}{2}\right)}2^{q+n}\pi^{n/2}k^{-q-n}.$$

Hence, in the case when $n=1$,

$$F(k)=\hat{F}_1[r^q]=\frac{\Gamma\left(\frac{1+q}{2}\right)}{\Gamma\left(-\frac{q}{2}\right)}2^{1+q}\sqrt{\pi}k^{-q-1}$$

or

$$\hat{F}_1\left[\frac{1}{r^{1-q}}\right]=2^q\sqrt{\pi}\frac{\Gamma\left(\frac{q}{2}\right)}{\Gamma\left(\frac{1-q}{2}\right)}\frac{1}{k^q}$$

and thus,

$$\hat{F}_1^{-1}\left[\frac{1}{(ik)^q}\right]=\frac{\alpha_1(q)}{r^{1-q}}$$

where

$$\alpha_1(q)=\frac{1}{(2i)^q\sqrt{\pi}}\frac{\Gamma\left(\frac{1-q}{2}\right)}{\Gamma\left(\frac{q}{2}\right)}.$$

For $n=2$

$$\hat{F}_2\left[r^q\right]=\frac{\Gamma\left(\frac{q+2}{2}\right)}{\Gamma\left(-\frac{q}{2}\right)}2^{q+2}\pi k^{-q-2}$$

or

$$\hat{F}_2\left[\frac{1}{r^{2-q}}\right]=2^q\pi\frac{\Gamma\left(\frac{q}{2}\right)}{\Gamma\left(1-\frac{q}{2}\right)}\frac{1}{k^q}$$

and hence,

$$\hat{F}_2^{-1}\left[\frac{1}{(ik)^q}\right]=\frac{\alpha_2(q)}{r^{2-q}}$$

where

$$\alpha_2(q)=\frac{1}{(2i)^q\pi}\frac{\Gamma\left(1-\frac{q}{2}\right)}{\Gamma\left(\frac{q}{2}\right)}.$$

Thus, in general, ignoring scaling by $\alpha_1(q), \alpha_2(q), \alpha_3(q), ...,$

$$\hat{F}_n^{-1}\left[\frac{1}{(ik)^q}\right] \sim \frac{1}{r^{n-q}}, \quad n = 1, 2, 3, ...$$

Appendix D

I/O and Graphics Utilities

Reading and Writing Images to and From a Named Data File

Many different standard and some non-standard formats have been developed for writing and reading images to and from a file, respectively. A detailed analysis of these formats lies beyond the scope of this work. However, for completeness, code is provide for reading an image from a named file and writing an image to a named file. In both cases, the format is 'free'. These facilities are compounded in the void functions *rimage* and *wimage* as follows:

```
#include <stdio.h>
#include <string.h>

void rimage( float **s, int n )
{
  char  filename[80];
  int x, items;
  FILE *fp;

/* FUNCTION: Reads (free format) an image from a named data file.

   PARAMETERS

   Input:  n - Size of image.

   Output: s - Data (digital image). */


  /* Prompt user to input name of data file. */

  puts("INPUT FILE:");
```

```
  scanf("%s", filename);



   /* Open file. */

  if ((fp = fopen( filename, "r+b" )) == NULL)
    {
    puts( "OPEN ERROR" );
    fclose( fp );
    return;
    }

  /* Send message to user 'reading data...' */

  printf("\n\t READING DATA...");

  /* Read in array size and array s from data file. */

  for ( x=0; x<n; x++ )
    {
    if ((items = fread( s[x], sizeof( float ), n, fp )) != n)
      {
      puts( "READ ERROR" );
      fclose( fp );
      return;
      }
    }

  printf("OK");

  /* Close the file. */

  fclose( fp );
}



#include <stdio.h>
#include <string.h>

void wimage( float **s, int n )
{
  char filename[80];
  int x;
  FILE *fp;

/* FUNCTION: Writes (free format) an image to a named data file.
```

```
   PARAMETERS

   Input:  n - Size of image.

   Output: s - Data (digital image). */

  /* Prompt user to input name of data file. */

  puts( "OUTPUT FILE:" );
  scanf("%s", filename );



  /* Open file. */

  if ((fp = fopen( filename, "w+b" )) == NULL)
    {
    puts( "OPEN ERROR" );
    fclose( fp );
    return;
    }

  /* Send message to user */

  printf("\n\t WRITING DATA..." );


  /* Write out array to data file. */

  for ( x=0; x<n; x++ )
    {
    fwrite( s[x], sizeof( float ), n, fp );
    }

  printf("OK" );


  /* Close the file. */

  fclose( fp );
}
```

Displaying a Digital Image

There are a wide range of facilities available for displaying images that are system dependent or otherwise. These facilities can form part of an integrated

windows based package such as MATLAB which can of course be used for this purpose. A detailed discussion of the many graphics facilities currently available is beyond the scope of this book and it is left to the reader to apply the facilities best suited to his/her application and available software systems. However, for completeness, this appendix provides C code developed to display images using *X-windows* running under *unix* or *linux*. This was originally introduced for students undertaking an MSc programme in 'Digital Signal Processing' established by the author in the early 1990s and it may still be of value to those with limited access to a more advanced graphics system. This low level graphics facility follows the design of that given in *Digital Signal Processing*, J M Blackledge, Horwood, 2003 for plotting signals using Borland Turbo C++ and is based on the function *ximage* which is typically utilized as follows:

```
xopen();

...

option=1
ximage(s,n,option);

...

xclose();
```

Here, s in an image of size n×n which is taken to be a 2D array of floating point numbers. Two images can be displayed together: option=1 for the first image and option=2 for the second image. The image is automatically windowed and scaled but the size of the images that can be displayed is limited to 512×512 pixels. The function can be used in multiples to plot the progress of a process and for diagnostic purposes. Further, standard I/O can be used while the displays are 'open', the output being an overlay in standard format.

The code provides a number of other functions for:

(i) displaying a single 1024×1024 image;

(ii) displaying images with pre-defined colour maps;

(iii) displaying the histogram of an image.

The code has been designed to provide the reader with a 'platform' from which further graphics utilities can be developed as required operating in a unix or linux environment.

```
void xopen(void)
{

ipf_open_windows_();
```

```
ipf_install_lin_grey_cmap_();

}


void ximage(float **s, int n, int iw)
{

int i, j;
float max=0.;


for(i=0; i<n; i++)
for(j=0; j<n; j++)
if(s[i][j] > max)
  max=s[i][j];

for(i=0; i<n; i++)
for(j=0; j<n; j++)
s[i][j]*=(239./max);

ipf_display_image_(&iw, s, &n);

}



void xclose(void)
{

ipf_close_windows_();

}



#include <stdlib.h>
#include <stdio.h>
#include <string.h>

#include <X11/Xlib.h>
#include <X11/Xutil.h>

#define uchar unsigned char

#define WINDOW_1_PSN_X 0
#define WINDOW_2_PSN_X 512
#define WINDOWS_PSN_Y    100
```

```
#define BIG_WINDOW_PSN_X 0
#define BIG_WINDOW_PSN_Y 0

#define CHART_PSN_X 16
#define CHART_PSN_Y 450
#define CHART_MAX 400

#define BIG_CHART_PSN_X 32
#define BIG_CHART_PSN_Y 900
#define BIG_CHART_MAX 800

#define DEF_SCREEN DefaultScreen(display)
#define DEF_VISUAL DefaultVisual(display,DEF_SCREEN)
#define DEF_GC DefaultGC(display,DEF_SCREEN)
#define DEF_COLORMAP DefaultColormap(display, DEF_SCREEN)
#define ROOT_WINDOW RootWindow(display, DEF_SCREEN)
#define BLACK_PIX BlackPixel(display, DEF_SCREEN)
#define WHITE_PIX WhitePixel(display, DEF_SCREEN)


void ipf_open_windows_ ();
void ipf_open_big_window_ ();
void ipf_close_windows_ ();
void ipf_install_lin_grey_cmap_ ();
void ipf_install_user_def_cmap_ (int [], int [], int []);
void ipf_write_cmap_ (int [], int [], int[]);
void ipf_read_and_install_cmap_ ();
void ipf_display_image_ (int *, float **, int *);
void ipf_display_image_big_ (float [][512], int *);
void ipf_display_histogram_ (int *, float [], int *, int *);
void ipf_display_histogram_big_ (float [], int *, int *);


static void display_512_image (int, uchar *);
static void display_1024_image (uchar *);
static void
install_cmap (unsigned short int [], unsigned short int [],
      unsigned short int []);
static void     make_filename (char *, char *, char *, char *);
static void list_files (char *);

static Display *display;
static Window  window[3];


/*****************************************************************
```

```
IPF_OPEN_WINDOWS


Action:  Opens a pair of (512*512) "ip" windows on the display.

Note that only one set of windows (either a pair of 512*512
windows, or a single 1024*1024 window) may be open at any one
time.

*****************************************************************/


void ipf_open_windows_ ()


{


XSizeHints size_hints;


display = XOpenDisplay (0);


window[1] = XCreateSimpleWindow (display, ROOT_WINDOW,
         WINDOW_1_PSN_X, WINDOWS_PSN_Y, 512, 512, 0,
         BLACK_PIX, BLACK_PIX);

window[2] = XCreateSimpleWindow (display, ROOT_WINDOW,
         WINDOW_2_PSN_X, WINDOWS_PSN_Y, 512, 512, 0,
         BLACK_PIX, BLACK_PIX);


size_hints.flags = PPosition | PSize | PMinSize | PMaxSize;
size_hints.x = WINDOW_1_PSN_X;
size_hints.y = WINDOWS_PSN_Y;
size_hints.width = 512;
size_hints.height = 512;
size_hints.min_width = size_hints.max_width = 512;
size_hints.min_height = size_hints.max_height = 512;

XSetStandardProperties (display, window[1],
" ip1                                          DIP",
        "ip1", None, 0, 0, &size_hints);
```

```
size_hints.x = WINDOW_2_PSN_X;

XSetStandardProperties (display, window[2],
" ip2                                          DIP",
"ip2", None, 0, 0, &size_hints);



XMapWindow (display, window[1]);

XMapWindow (display, window[2]);

XFlush (display);


}


/*****************************************************************

IPF_OPEN_BIG_WINDOW


Action:  Opens a single (1024*1024) "ip" window on the display.


Note that only one set of windows (either a pair of 512*512
windows, or a single 1024*1024 window) may be open at any one
time.

*****************************************************************/


void ipf_open_big_window_ ()


{


XSizeHints size_hints;


display = XOpenDisplay (0);


window[1] = XCreateSimpleWindow (display, ROOT_WINDOW,
        BIG_WINDOW_PSN_X, BIG_WINDOW_PSN_Y,
```

```
1024, 1024, 0,
        BLACK_PIX, BLACK_PIX);


size_hints.flags = PPosition | PSize | PMinSize | PMaxSize;
size_hints.x = BIG_WINDOW_PSN_X;
size_hints.y = BIG_WINDOW_PSN_Y;
size_hints.width = 1024;
size_hints.height = 1024;
size_hints.min_width = size_hints.max_width = 1024;
size_hints.min_height = size_hints.max_height = 1024;

XSetStandardProperties (display, window[1],
" ip                                        DIP",
        "ip", None, 0, 0, &size_hints);


XMapWindow (display, window[1]);

XFlush (display);


}


/************************************************************

IPF_CLOSE_WINDOWS


Action:  Closes "ip" windows on the display.

This can be used to close either a pair of 512*512 windows,
or a single 1024*1024 window.


************************************************************/


void ipf_close_windows_ ()


{

XCloseDisplay (display);

}
```

```
/*****************************************************************

IPF_INSTALL_LIN_GREY_CMAP


Action:  Generates a linear grey-scale colour map, which is immediately
         installed as the current colour map for the display.



*****************************************************************/


void ipf_install_lin_grey_cmap_ ()


{

unsigned short int red[240], green[240], blue[240];
int v;


for (v = 0; v < 240; ++ v)
red[v] = green[v] = blue[v] = v * 274;

install_cmap (red, green, blue);

}

/*****************************************************************

IPF_INSTALL_USER_DEF_CMAP

Action Installs a user-defined colour map.

Parameters: in: "red", "green", "blue"

- arrays of 240 integers, defining the colour
  intensities to be used for each of the 240 pixel
  values.

Each value must be in the range 0 - 65535, where 0
represents zero intensity for that colour, and 65535
represents maximum intensity.
```

```
For array indexing starting with 1, since pixel
values start at 0, array element n will refer to pixel
value n-1 (e.g. red(15) defines the red intensity for
pixel value 14).


*************************************************************/


void ipf_install_user_def_cmap_ (red, green, blue)

int red[], green[], blue[];


{

unsigned short int red_out[240], green_out[240], blue_out[240];
int n;


for (n = 0; n < 240; ++ n)
{
red_out[n] = (unsigned short int) red[n];
green_out[n] = (unsigned short int) green[n];
blue_out[n] = (unsigned short int) blue[n];
}

install_cmap (red_out, green_out, blue_out);

}

/*************************************************************

IPF_WRITE_CMAP

Action:  Writes a colour map to a file, in a format that can be
         read by the "ipf_read_and_install_cmap" function.

The user is prompted for the name of the colour map, which
should be given without any extension. The extension ".cmp"
will be automatically added.

Colour maps are placed in a directory determined by the
environment variable IP_CMAPS_PATH, unless this has not been
set, in which case they are placed in the current working
directory.
```

```
Parameters: in: "red", "green", "blue"

- arrays of 240 integers, defining the colour map.
  See "ipf_install_user_def_cmap" for details.

*****************************************************************/


void ipf_write_cmap_ (red, green, blue)

int red[], green[], blue[];


{

int n;
unsigned short int red_out[240], green_out[240], blue_out[240];
char map_name[40];
char filename[80];
FILE        *fp;



for (n = 0; n < 240; ++ n)
{
red_out[n] = (unsigned short int) red[n];
green_out[n] = (unsigned short int) green[n];
blue_out[n] = (unsigned short int) blue[n];
}


printf ("(write colour map) give colour map name: ");
scanf ("%s", map_name);

make_filename (filename, "IP_CMAPS_PATH", map_name, ".cmp");

fp = fopen (filename, "wb");

fwrite (red_out, sizeof (unsigned short int), 240, fp);
fwrite (green_out, sizeof (unsigned short int), 240, fp);
fwrite (blue_out, sizeof (unsigned short int), 240, fp);

fclose (fp);

}
```

```
/*****************************************************************

IPF_READ_AND_INSTALL_CMAP

Action:  Reads a colour map from a file, and installs it as the
         current colour map for the display.

Colour maps must be in the format produced by the function
"ipf_write_cmap".

Colour maps are expected to be in a directory determined by
the environment variable IP_CMAPS_PATH, unless this has not been
set, in which case they are expected to be in the current
working directory. The contents of this directory are listed,
and the user is then prompted for the name of the colour map,
which should be given without the extension.

*****************************************************************/

void ipf_read_and_install_cmap_ ()


{

char map_name[40];
char filename[80];
FILE        *fp;
unsigned short int red[240], green[240], blue[240];


list_files ("IP_CMAPS_PATH");

printf ("(read colour map) give colour map name: ");
scanf ("%s", map_name);

make_filename (filename, "IP_CMAPS_PATH", map_name, ".cmp");

fp = fopen (filename, "rb");

fread (red, sizeof (unsigned short int), 240, fp);
fread (green, sizeof (unsigned short int), 240, fp);
fread (blue, sizeof (unsigned short int), 240, fp);

fclose (fp);

install_cmap (red, green, blue);
```

```
}


/*****************************************************************

IPF_DISPLAY_IMAGE


Action:  Displays an image in a 512*512 window.

Pixel values must be in the range 0 - 239.999... .  These are
truncated to integers before being displayed, but the original
array holding the image data is not affected. Pixel values in
the range 240 - 256 are reserved for the X-windows interface.

Images are automatically scaled to fill the window, but their
size must be an integer power of two (512, 256, 128 ....).

Input parameters:
"w" - an integer describing which window the image is to
      be displayed in (1 or 2).

"in_image" - the image, an array of 512 * 512 reals

"size" - an integer giving the size of the image.

*****************************************************************/


void ipf_display_image_ (w, in_image, size)

int        *w;
float        **in_image;
int        *size;



{

unsigned char disp_image[512][512];
int mag, x, y, q;

mag = 512 / *size;


for (y = 0; y < 512; ++ y)
{
```

```
q = (*size - 1) - (y / mag);
for (x = 0; x < 512; ++ x)
disp_image[y][x] = (unsigned char) in_image[x/mag][q] + 16;
}


display_512_image (*w, (unsigned char *) disp_image);

}


/*************************************************************

IPF_DISPLAY_IMAGE_BIG


Action:  Displays an image in a 1024*1024 window.

Pixel values must be in the range 0 - 239.999... .  These are
truncated to integers before being displayed, but the original
array holding the image data is not affected.

Images are automatically scaled to fill the window, but their
size must be an integer power of two (512, 256, 128 ....).

Parameters: in:
"in_image" - the image, an array of 512 * 512 reals.

"size" - the size of the image.


*************************************************************/


void ipf_display_image_big_ (in_image, size)

float in_image[][512];
int        *size;



{

unsigned char disp_image[1024][1024];
int mag, x, y, q;
```

```
mag = 1024 / *size;


for (y = 0; y < 1024; ++ y)
{
q = (*size - 1) - (y / mag);
for (x = 0; x < 1024; ++ x)
disp_image[y][x] = (unsigned char) in_image[x/mag][q] + 16;
}


display_1024_image ((unsigned char *) disp_image);

}


/*****************************************************************

IPF_DISPLAY_HISTOGRAM


Action:  Displays a histogram, of up to 480 levels, in a
         512*512 window.

If the scale factor argument is zero, a suitable vertical scale
factor will be calculated automatically on the basis of the
maximum value found in the range 1 - (levels-1), i.e. excluding
the very lowest and very highest bins.

If the scale factor argument is non-zero, the scale factor is
set to the value used in the most recent call to this function.
This is useful for comparing pairs of histograms.

Parameters: in:
"w" - an integer describing which window the histogram
                is to be displayed in (1 or 2).

"histogram" - the histogram, an array of up to 480
             reals.

"levels" - an integer giving the number of levels in
         the histogram.

"scale " - an integer which determines whether the
         vertical scale factor is calculated
         automatically (zero) or the scale factor
         from the previous call to this function
```

```
         is used (non-zero).

**************************************************************/


void ipf_display_histogram_ (w, histogram, levels, scale)

int *w;
float histogram[];
int *levels, *scale;



{

static double ysf;

int n, m, p, max, xsf;
XSegment chart[480];



xsf = 480 / *levels;

if ((*scale == 0) || (ysf == 0))
{
max = 0;

for (n = 1; n < (*levels - 1); ++ n)
if (histogram[n] > max)
max = histogram[n];

ysf = CHART_MAX / (double) (max * 2);
}


for (n = 0; n < *levels; ++ n)
      {
      if ((histogram[n] * ysf) > CHART_MAX)
histogram[n] = CHART_MAX / ysf;


      for (m = 0; m < xsf; ++ m)
{
p = (n * xsf) + m;

       chart[p].x1 = chart[p].x2 = CHART_PSN_X + p;
```

```
       chart[p].y1 = CHART_PSN_Y;
       chart[p].y2 = CHART_PSN_Y - (histogram[n] * ysf);
}

      }


XClearWindow (display, window[*w]);

XSetForeground (display, DEF_GC, WHITE_PIX);

XDrawLine (display, window[*w], DEF_GC, CHART_PSN_X, CHART_PSN_Y,
   CHART_PSN_X + (*levels * xsf), CHART_PSN_Y);

XDrawLine (display, window[*w], DEF_GC,
   CHART_PSN_X - 8, CHART_PSN_Y - CHART_MAX,
   CHART_PSN_X - 4, CHART_PSN_Y - CHART_MAX);

XDrawSegments (display, window[*w], DEF_GC, chart, *levels * xsf);

XFlush (display);


}


/*****************************************************************

IPF_DISPLAY_HISTOGRAM_BIG


Action:  Displays a histogram, of up to 960 levels, in a
         1024*1024 window.

If the scale factor argument is zero, a suitable vertical scale
factor will be calculated automatically on the basis of the
maximum value found in the range 1 - (levels-1), i.e. excluding
the very lowest and very highest bins.

If the scale factor argument is non-zero, the scale factor is
set to the value used in the most recent call to this function.
This is useful for comparing pairs of histograms.

Parameters: in:
"histogram" - the histogram, an array of up to 960
              reals.
```

```
"levels" - an integer giving the number of levels in
         the histogram.

"scale " - an integer which determines whether the
         vertical scale factor is calculated
         automatically (zero) or the scale factor
         from the previous call to this function
         is used (non-zero).

**********************************************************/



void ipf_display_histogram_big_ ( histogram, levels, scale)

float histogram[];
int *levels, *scale;

{

static double ysf;

int n, m, p, max, xsf;
XSegment chart[960];



xsf = 960 / *levels;

if ((*scale == 0) || (ysf == 0))
{
max = 0;

for (n = 1; n < (*levels - 1); ++ n)
if (histogram[n] > max)
max = histogram[n];

ysf = BIG_CHART_MAX / (double) (max * 2);
}


for (n = 0; n < *levels; ++ n)
      {
      if ((histogram[n] * ysf) > BIG_CHART_MAX)
histogram[n] = BIG_CHART_MAX / ysf;
```

```
      for (m = 0; m < xsf; ++ m)
{
p = (n * xsf) + m;

       chart[p].x1 = chart[p].x2 = BIG_CHART_PSN_X + p;
       chart[p].y1 = BIG_CHART_PSN_Y;
       chart[p].y2 = BIG_CHART_PSN_Y - (histogram[n] * ysf);
}

      }

XClearWindow (display, window[1]);

XSetForeground (display, DEF_GC, WHITE_PIX);

XDrawLine (display, window[1], DEF_GC,
   BIG_CHART_PSN_X, BIG_CHART_PSN_Y,
   BIG_CHART_PSN_X + (*levels * xsf), BIG_CHART_PSN_Y);

XDrawLine (display, window[1], DEF_GC,
   BIG_CHART_PSN_X - 8, BIG_CHART_PSN_Y - BIG_CHART_MAX,
   BIG_CHART_PSN_X - 4, BIG_CHART_PSN_Y - BIG_CHART_MAX);

XDrawSegments (display, window[1], DEF_GC, chart, *levels * xsf);

XFlush (display);


}


/*********** INTERNAL FUNCTION **************/


static void display_512_image (w, image)


int w;
uchar          *image;

{

XImage        *x_image;



x_image = XCreateImage (display, DEF_VISUAL, 8, ZPixmap,
```

```
        0, image, 512, 512, 8, 512);


XPutImage (display, window[w],
           DEF_GC, x_image, 0, 0, 0, 0, 512, 512);


XFlush (display);


}


/*************** INTERNAL FUNCTION *************/


static void display_1024_image (image)


uchar          *image;

{

XImage        *x_image;


x_image = XCreateImage (display, DEF_VISUAL, 8, ZPixmap,
        0, image, 1024, 1024, 8, 1024);

XPutImage (display, window[1],
          DEF_GC, x_image, 0, 0, 0, 0, 1024, 1024);


XFlush (display);


}

/*************** INTERNAL FUNCTION *****************/

static void install_cmap (red, green, blue)

unsigned short int red[], green[], blue[];


{
```

```
int v;
XColor map_defs[256];
Colormap x_colour_map;


for (v = 0; v < 256; ++ v)
map_defs[v].pixel = v;


XQueryColors (display, DEF_COLORMAP, map_defs, 16);


for (v = 16; v < 256; ++ v)
{
map_defs[v].red = red[v-16];
map_defs[v].green = green[v-16];
map_defs[v].blue = blue[v-16];
map_defs[v].flags = DoRed | DoGreen | DoBlue;
}

x_colour_map =

XCreateColormap (display, ROOT_WINDOW, DEF_VISUAL, AllocAll);


XStoreColors (display, x_colour_map, map_defs, 256);

XInstallColormap (display, x_colour_map);


XFlush (display);


}


/*************** INTERNAL FUNCTION *********************/


static void make_filename (filename, envar_path, file, def_ext)

char *filename, *envar_path, *file, *def_ext;


{

char *path;
```

```
if ((path = getenv(envar_path)) != NULL)
{
strcpy (filename, path);
strcat (filename, "/");
strcat (filename, file);
}
else
strcpy (filename, file);

if (strchr(file, '.') == NULL)
strcat (filename, def_ext);

}


/*************** INTERNAL FUNCTION ************/


static void list_files (envar_path)

char *envar_path;


{

char  command[80];
char *path;

strcpy (command, "ls ");

if ((path = getenv(envar_path)) != NULL)
strcat (command, path);

printf ("\n");
system (command);
printf ("\n");
}
```

Index